THE IMPERIAL VALLEY, CALIFORNIA, EARTHQUAKE OF OCTOBER 15, 1979

GEOLOGICAL SURVEY
PROFESSIONAL PAPER 1254

COVER

South-southeastward oblique aerial view of Imperial Valley and northern Baja California. Epicenter of October 15 earthquake (bull's-eye) is on Imperial fault about 5 km south of United States-Mexican border (note contrast in pattern of cultivated fields along border). During the earthquake, surface displacements formed along 30 km of the northern section of the Imperial fault in California (indicated by nearly continuous line from near center toward lower right-hand edge) and along strands of the Brawley fault zone (discontinuous lines on foreground side of Imperial fault trace). U.S. Air Force photograph, July 17, 1968.

The Imperial Valley, California, Earthquake of October 15, 1979

GEOLOGICAL SURVEY PROFESSIONAL PAPER 1254

Contributions from:
American Iron and Steel Institute
California Department of Transportation
California Division of Mines and Geology
California Institute of Technology
Centro de Investigación Científica y Educación Superior de Ensenada, Baja California
H. J. Degenkolb & Associates, Consulting Structural Engineers
Imperial College, London
J. D. Raggett & Associates, Inc., Structural Engineers
Scripps Institution of Oceanography
U.S. Department of the Interior, Geological Survey
Universidad Nacional Autónoma de México

UNITED STATES GOVERNMENT PRINTING OFFICE, WASHINGTON: 1982

UNITED STATES DEPARTMENT OF THE INTERIOR

JAMES G. WATT, *Secretary*

GEOLOGICAL SURVEY

Dallas L. Peck, *Director*

Library of Congress Cataloging in Publication Data

The Imperial Valley, California, earthquake of October 15, 1979.

(Geological Survey Professional Paper 1254)
Supt. of Docs. No.: I 19.16:1254
1. Imperial Valley (California and Mexico)—Earthquake, 1979. I. Johnson, Carl Edward, 1946– . II. Rojahn, Christopher. III. Sharp, Robert Victor, 1934– . IV. American Iron and Steel Institute. V. Series: United States. Geological Survey. Professional Paper 1254.

QE535.2.U6I46 1982 551.2'2'0979499 82-600245

For sale by the Superintendent of Documents, U.S. Government Printing Office
Washington, D.C. 20402

CONTENTS

ILLUSTRATIONS

[Plates are in separate case]

TABLES

THE IMPERIAL VALLEY, CALIFORNIA, EARTHQUAKE OF OCTOBER 15, 1979

INTRODUCTION

By CARL E. JOHNSON, CHRISTOPHER ROJAHN, and ROBERT V. SHARP,
U.S. GEOLOGICAL SURVEY

On October 15, 1979, the largest earthquake in California in the past decade occurred on the Imperial fault near the United States-Mexican border. The moment-magnitude (M) 6.5 event, whose epicenter was located in northern Mexico, damaged structures in and near the town of El Centro, Calif., was felt from Las Vegas, Nev., to the Pacific Ocean, and was accompanied by surface movement on four fault zones. The earthquake caused an estimated $21.1 million in damage and injured 73 people, but no deaths were reported in the United States. The small number of injuries is indeed fortunate and is no doubt related to the fact that the areas of greatest population and number of manmade structures were not situated in the most strongly shaken area.

The earthquake and its aftershocks occurred in a region that has undergone several similar-size earthquakes in the recent historical past, including the well-known $M=7.0$ earthquake near El Centro on May 18, 1940. Because of the frequent recurrence of moderately strong earthquakes, this region has been under intensive study for many years by seismologists, geologists, and engineers of the U.S. Geological Survey and other research institutions. Their efforts have included the design and installation of numerous types of seismologic, strong-motion, geodetic, and other earthquake-monitoring instruments as well as indepth studies of various earthquake-related topics. As a consequence of this preparatory work, the 1979 earthquake has provided the seismologic and geologic sciences and the field of earthquake engineering with a wealth of important information, much of it unprecedented.

This volume contains 35 technical papers on the following topics relating to the October 15 earthquake: seismologic investigations, surface-faulting and other geologic investigations, damage and shaking-intensity studies, and strong-motion data and analyses. Depending on their subject matter, several papers are preliminary in nature, whereas others reflect indepth studies of a particular topic or data set.

SEISMOLOGIC INVESTIGATIONS

The 1979 Imperial Valley earthquake occurred in the midst of a dense array of seismic instruments that includes short-period vertical and strong-motion seismometers on both sides of the border, and thus provided a unique opportunity for studying in detail the changes in seismicity both attending and preceding a moderately strong earthquake. Because of the locations of these data, their analysis necessarily took on an international character. Particularly important was the hypocentral control for the main shock, provided by data obtained in Mexico with the seismic array of the Centro de Investigación Científica y Educación Superior de Ensenada, as well as with five strong-motion instruments installed by the Universidad Nacional Autónoma de México and the University of California, San Diego.

The network of 22 short-period vertical seismometers operated jointly by the U.S. Geological Survey and the California Institute of Technology in the Imperial Valley since mid-1973 permitted a detailed analysis of the changes in seismicity leading up to the October 15 earthquake. Unlike many other areas of California, seismicity in the Imperial Valley manifests progressive changes in both style and level of activity. For example, a distinct and obvious decrease in the number of events was noted during the 3 months immediately before the main shock. A detailed analysis of such changes may provide important insight into the physical processes associated with potentially damaging earthquakes, as well as concomitantly increase our predictive capabilities.

The main-shock data were significantly augmented by data from a network of three-component wide-dynamic-range high-frequency-resolution digital triggered seismographs installed in the Imperial Valley soon after the main shock. The purpose of this array was to record large aftershocks and to obtain data that would aid in understanding physical processes near the north termination of fault rupture. Several of these instruments were later redeployed at stations near the strong-motion sites that recorded the main shock, in the hope that records of aftershocks would provide information useful in simulating the main-shock records and give insight into any effects due to local geologic features. Owing to the completeness of the events recorded and the quality of the data in terms of dynamic range and high-frequency resolution, these aftershock records are unprecedented.

By considerable good fortune, a detailed crustal-refraction study was also conducted in the Imperial Valley during the year before the 1979 earthquake. This study, together with the wealth of digital recordings and high-precision arrival-time data obtained from the Imperial Valley seismic network and the temporarily installed aftershock instruments, will undoubtedly prove to be one of the great contributions to understanding the 1979 event and active tectonic processes in the Imperial Valley. Teleseismic studies should also be greatly facilitated by detailed analysis of the local data.

SURFACE-FAULTING AND OTHER GEOLOGIC INVESTIGATIONS

In several respects, documentation of the faulting associated with the 1979 Imperial Valley earthquake has yielded important new and, in some cases, unique perspectives on the surface movement of faults. For example, careful recording of the traces of surface rupture and the growth of displacement have provided a much clearer picture of the complexities of the Imperial fault and the Brawley fault zone, and of the characteristics of postearthquake slip. Although investigations of earlier historical movements typically were less comprehensive than those of the 1979 event, the quality of earlier displacement measurements is sufficient to permit a comparison of surface movements for some pre-1979 slip events at several points on the fault traces. Up to this time, a comparison of the detailed behavior of faults at the ground surface during successive episodes of major displacement generally has not been possible for historical earthquakes elsewhere.

Surface faulting in this event has been observed and recorded by probably a larger number of different methods than in any previous earthquake. Creepmeters installed on the Imperial fault and the Brawley fault zone produced extraordinary data on coseismic slip and afterslip separately; one of the creepmeter records has yielded the first direct measure of the minimum rate of surface displacement. Alinement arrays, geodetic networks, leveling lines, and field documentation of offset manmade structures were employed to determine the components of fault displacement; repeated surveys using these methods for several months after the earthquake provide an unusually complete record of the afterslip. The results, which surpass in detail those of other earthquake investigations, show the irregularity of the approximately coseismic distribution of fault slip and the generally smooth but locally erratic growth of displacements during the afterslip period. Similar fault displacements elsewhere in the San Andreas system in California probably could not have been recorded in so great detail as were the 1979 movements in the Imperial Valley, owing in great part to the abundance of structures crossing the fault traces and to the preearthquake installation of monuments and instruments placed specifically to detect movements.

Ground failures generated by strong shaking of the earthquake rather than by tectonic faulting were widely distributed, especially near the main-shock epicenter. Through careful investigation, a zone of ground fractures that closely resembled fault ruptures in the southern Imperial Valley south of the 1979 surface breakage along the Imperial fault proved to be secondary ground failures along the margins of a buried stream channel that once drained northward from Mexico toward the Salton Sea.

In spite of the important new insights from studies of the geologic effects of this earthquake, some aspects of the 1979 event have presented unusually intriguing and as yet unsolved geologic problems. For example, although ground displacement was detected principally along the Imperial fault north of the United States-Mexican border, surface movement was not observed in the vicinity of the main-shock epicenter near the same fault in Mexico. Restriction of surface faulting to the area northwest of the main-shock epicenter was not the consequence of deficient searching in Mexico; a special check using a recent detailed map of the 1940 trace of the Imperial fault in Mexico failed to locate new movement anywhere on the fault trace south of the border.

The important question of why surface rupture appeared only beyond 10 km northwest of the main-shock epicenter is now the subject of continuing study, but as of this writing an unambiguous explanation is not available. A considerable literature undoubtedly will eventually address and satisfactorily explain the un-

usual relation of surface displacement to the main shock.

DAMAGE AND SHAKING-INTENSITY STUDIES

Although the Imperial Valley is not densely developed, shaking-intensity studies using manmade structures as primary indicators of the intensity of ground shaking yielded some interesting, if not controversial, findings. Results of a regional investigation of the distribution of intensity, for example, suggest some significant differences between the pattern of strong ground shaking during the 1940 and 1979 Imperial Valley earthquakes. One study, focused on the performance of structures very close to the fault trace, and another concerned with the performance of a specific class of buildings prevalent throughout the valley, suggest that the intensity of ground shaking was not so severe as might have been expected on the basis of previously obtained data. The second study also shows a correlation between observed shaking effects and peak ground accelerations obtained from nearby strong-motion stations.

One of the primary difficulties in assessing the results from such shaking-intensity studies is, of course, that they are biased by the type of regional construction. Most existing structures in the heavily shaken area of the Imperial Valley, for example, were low-rise stiff buildings that respond predominantly to high-frequency ground motion; by contrast, there were few long-period structures (for example, mid- and high-rise buildings) that respond predominantly to longer period ground motions. Although the results from such studies should not be indiscriminately applied, they are nevertheless extremely valuable because they document the shaking effects on particular classes of structures during particular types and magnitudes of earthquakes.

With regard to the performance of engineered structures, the partial collapse of the six-story reinforced-concrete Imperial County Services Building in El Centro and the complete collapse of an elevated steel water tank south of Brawley are particularly noteworthy. The fact that the 9-year-old Imperial County Services Building was designed to resist earthquakes and was damaged so severely that it had to be demolished makes it an especially important case study for the structural-engineering community.

STRONG-MOTION DATA AND ANALYSES

The October 15 earthquake generated the most comprehensive set of strong-motion-accelerograph data yet recorded from a damaging earthquake. These data are unprecedented because they include the first set of ground-motion records ever obtained close to fault traces that were activated during a moderately strong earthquake, as well as the first set of records from an extensive array in a severely damaged building and from an extensive array on a highway overpass bridge less than 1 km from the fault rupture.

Of particular importance to engineering seimology are the data obtained from the El Centro ground-motion array, a 13-accelerograph 45-km-long linear array oriented perpendicular to and crossing the Imperial fault near El Centro; and from the El Centro differential array, a six-accelerograph 300-m-long linear array designed to record differential ground motions due to horizontally propagating surface waves. Strong-motion data from the 45-km-long array provide information on the nature of shaking close to and at increasing distance from the fault rupture, whereas those from the differential array are particularly applicable to the study of earthquake-induced stresses in such extended structures as bridges, dams, pipelines, and large mat foundations for nuclear power stations. These data also include the largest ground accelerations yet recorded anywhere in the world.

From a structural-engineering point of view, the strong-motion data from the severely damaged six-story Imperial County Services Building in El Centro are undoubtedly the most significant obtained from this earthquake. Data from the building's 13-channel accelerograph system, designed specifically for acquiring information that could lead to improvements in engineering design practice, provide a complete description of building response before, during, and after the occurrence of severe structural damage. These data are exceptional because the time and mechanism of structural failure can be inferred directly from the recorded data. In conjunction with the records from a nearby free-field station, these data also provide important information on the extent of soil-structure interaction at the building site.

Overall, the strong-motion data recorded during the 1979 Imperial Valley earthquake and its aftershocks are expected to be of great value in many seismologic and earthquake-engineering studies. Such studies will undoubtedly provide more and better insights into the nature, causes, and effects of strong ground shaking. As a result, the world strides forward in the abatement of earthquake hazards.

TECTONIC SETTING OF THE IMPERIAL VALLEY REGION

By ROBERT V. SHARP,
U.S. GEOLOGICAL SURVEY

CONTENTS

ABSTRACT

The Imperial Valley region lies along the present axis of the Salton Trough, the northward extension of the linear topographic and structural depression of the Gulf of California. Active right-lateral faults of the San Andreas fault system have played dominant roles in the creation and evolution of the trough and gulf. Marine and nonmarine sedimentary deposits have accumulated within the trough since its precursor basin formed during Miocene time. Tectonic activity is continuing at present at a high rate, as indicated by deformation of young sedimentary deposits, high levels of seismicity, geomorphic evidence of recent fault displacements, and historical surface faulting. Earthquakes closely associated with historical surface faulting have occurred on the Imperial fault, the Brawley fault zone, and the Coyote Creek fault. The San Andreas, Imperial, and Superstition Hills faults have displayed surface rupture triggered by distant major seismic events on other faults within the trough.

INTRODUCTION

The earthquake of October 15, 1979, was centered within the Imperial Valley of California, a region of remarkably vigorous tectonic activity and seismicity. The Imperial Valley lies astride the present axis of a great linear structural and topographic depression that extends nearly 1,400 km through southern California and Mexico to the south end of the Gulf of California. The northern part of this linear depression, commonly referred to as the Salton Trough, is an extension of the Gulf of California physiographic province that has been isolated from the gulf by buildup of the deltaic cone of the Colorado River. The Salton Trough north of the Colorado delta was transformed into a sub-sea-level desert basin probably during late Pleistocene time, when the delta stood sufficiently high to restrict seawater from the gulf to the south. During Holocene time this basin was periodically inundated by floodwaters of the Colorado River to create former Lake Cahuilla, an ephemeral freshwater body whose highest level at times stood slightly above sea level. The latest flooding created the present-day Salton Sea in 1905 (Mendenhall, 1909), when the entire flow of the Colorado River was uncontrollably diverted into an irrigation canal.

In addition to the Imperial Valley and the East and West Mesas flanking it, the Coachella Valley and the Salton Sea in California and the Mexicali Valley and the Colorado River delta area in Mexico are the major geographic components of the Salton Trough (fig. 1). The geologic and tectonic framework of the region around the Imperial Valley was summarized by Dibblee (1954) and Sharp (1972), and the brief description of the tectonic setting presented here is derived substantially from those earlier works. The late Quaternary tectonic features and their relation to faults activated during the 1979 Imperial Valley earthquake are emphasized here.

REGIONAL TECTONICS OF THE SALTON TROUGH

The present geographic limits of the Salton Trough correspond approximately to the boundaries of a late Cenozoic marine and nonmarine depositional basin that has been downwarped, downfaulted, extended, and laterally translated between the bordering ranges along faults of the San Andreas system (fig. 2). The basin extends southward the length of Baja California and is filled with as much as 6 km of sedimentary deposits in the central Imperial Valley (Tarbet, 1951; Biehler and others, 1964, fig. 6; Fuis and others, this volume); most of these deposits may have accumulated during Quaternary time alone. In the axial part of the trough,

sedimentation under intermittently marine and nonmarine conditions may have been essentially continuous since late Miocene time.

In the Imperial Valley the basin is partly underlain and bounded by Mesozoic and older crystalline rocks, which on the west side of the trough consist predominantly of Cretaceous granitic rocks of the southern California batholith, as well as prebatholithic metasedimentary and metavolcanic rocks. East of the trough, diverse types of Precambrian crystalline rocks, as well as Mesozoic granitic rocks and other rocks of unknown age, are exposed. Basement rocks under the axial part of the trough beneath the central Imperial Valley may be more basic in composition, according to the seismic velocities recorded there (Fuis and others, this volume).

Active fault zones of the San Andreas system parallel the northeast margin of the Salton Trough and obliquely transect its southwest flank. Intermittent right-lateral movement on some members of the fault system has continued to deform the basin, and vertical components of offset on many of these faults have outlined dominant physiographic elements within the trough or bordering it.

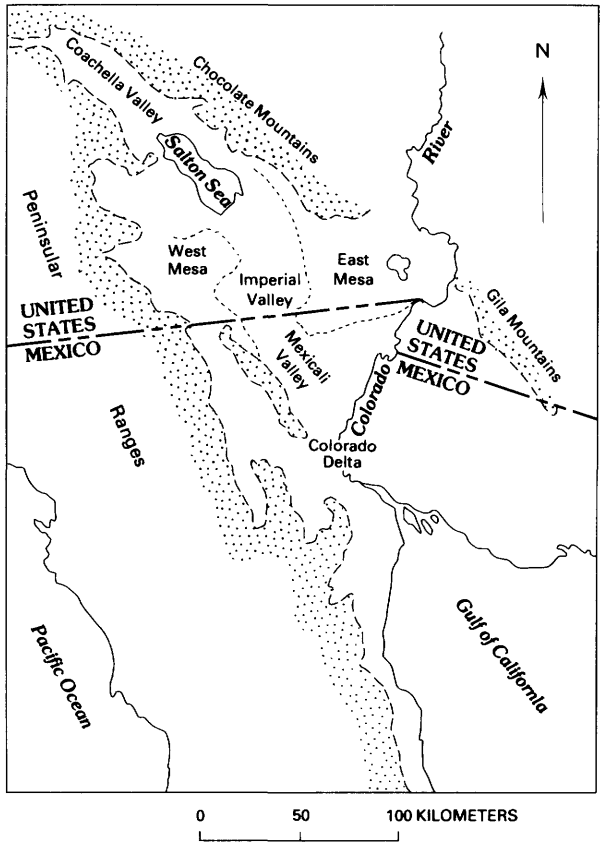

FIGURE 1.—Index map of Salton Trough and surrounding areas. Salton Trough lies between crystalline ranges (stippling). Dotted lines denote approximate boundaries of East and West Mesas of Imperial Valley.

Despite its overall northwest-trending linearity, the Salton Trough is not simply a narrow grabenlike structure. South of the Santa Rosa Mountains, for example, where it is relatively broad, the trough is actually a complexly folded and faulted crustal downwarp. Structural complexity within the southwest flank of the trough is reflected physiographically by the projection of several structurally high basement blocks from which the late Cenozoic strata have been stripped. Some of the irregularity of the west margin of the trough also is due to right-lateral offset on strike-slip fault zones that enter obliquely from the Peninsular Ranges to the west. For example, right-lateral translation amounting to 24 km on the Clark and Coyote Creek faults that make up the San Jacinto fault zone has created the jutting projections of the trough margin near the Borrego Valley (Sharp, 1967).

ORIGIN OF THE BASIN AND THE STRATIGRAPHIC SUCCESSION

From rates of sea-floor spreading at the junction of the Gulf of California and the East Pacific Rise near the tip of Baja California, Larson and others (1968) and Moore and Buffington (1968) estimated the age of the gulf and the Salton Trough at about 4 m.y. Although the sea-floor-spreading model suggests an origin during Pliocene time, a protogulf extending back into late Miocene time has also been postulated by these authors. Stratigraphic relations and a Miocene radiometric age on a volcanic unit (the Alverson Andesite of Woodard, 1974) in the western Imperial Valley confirm sedimentation of at least that age for the sedimentary mantle in the Salton Trough (Eberly and Stanley, 1978).

Late Cenozoic deposits in the Salton Trough, laid down under continental, freshwater and brackish-water lacustrine, and marine conditions, were derived from both distant and nearby sources. Although the mountainous areas bordering the trough on opposite sides contributed a large proportion of the detritus along the trough's flanks, much material within the sedimentary section in the central part of the trough was derived from the Colorado River drainage (Merriam and Bandy, 1965; Muffler and Doe, 1968). Figure 3 shows in diagrammatic form a composite stratigraphic column and approximate lateral relations of the stratal units as named by Tarbet and Holman (1944) and Dibblee (1954). Coarse clastic materials, including conglomerate, fanglomerate, and landslide deposits, are generally restricted to areas near the periphery of the basin and progressively grade into finer grained deposits toward the axis of the trough. In the central Imperial Valley, sediment coarser than sand has not been

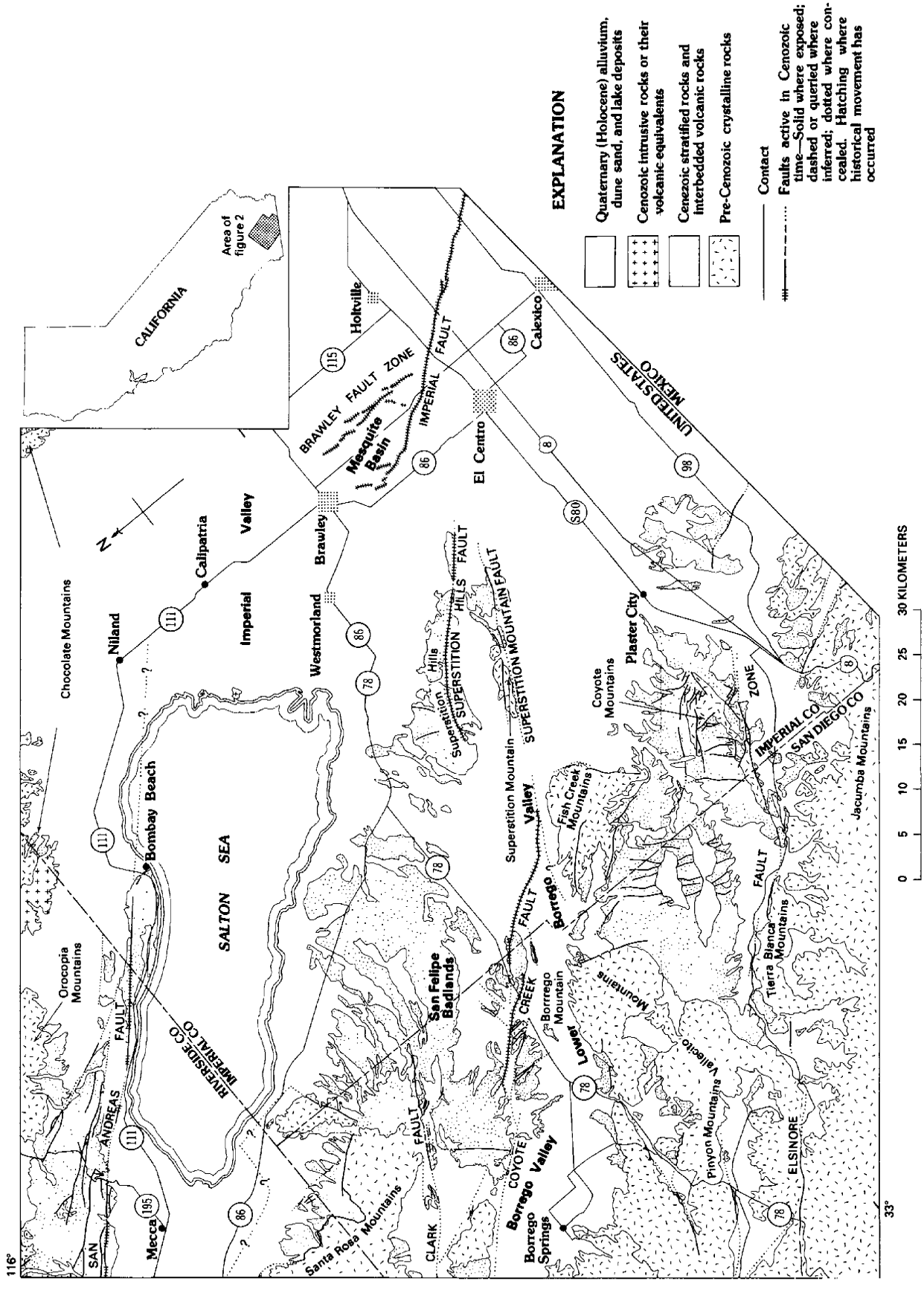

FIGURE 2.—Generalized geologic map of Imperial Valley region, southern California.

recognized in deep drill holes, and so the stratigraphic section under the central Imperial Valley and the sedimentary deposits exposed in the flanks of the basin generally cannot be correlated on a lithologic basis alone (Dibblee, 1954; Muffler and Doe, 1968, p. 388). Part of the Pliocene and Pleistocene sedimentary section in the western Imperial Valley has been placed tentatively in the absolute time scale by magnetostratigraphic correlation with dated rocks from outside the Salton Trough (Opdyke and others, 1975).

QUATERNARY VOLCANIC ROCKS

Late Quaternary volcanic or volcaniclastic rocks occur in several localities in the Salton Trough. Rhyolitic volcanic domes at the southeast corner of the Salton Sea protrude through Quaternary deposits in the floor of the northern Imperial Valley (Kelley and Soske, 1936; Elders and Robinson, 1970). These domes and the dacitic Cerro Prieto volcano in the southern Mexicali Valley, Baja California, constitute the only known late Quaternary volcanism closely associated with the San Andreas fault system north of the Gulf of California. The domes consist of rhyolite, obsidian, and pumice that have been dated at about 16,000 yr B.P. (Muffler and White, 1969, p. 162).

Rhyolitic tuff beds correlative with the basal part of the Bishop Tuff have been discovered on both the east and west sides of the Salton Trough (Merriam and Bischoff, 1975; Sarna-Wojcicki and others, 1980). The Bishop Tuff erupted about 500 km north of the Salton Trough in the eastern Sierra Nevada about 0.7 m.y. B.P., during the Pleistocene (Dalrymple and others, 1965). The tuffaceous beds in the Salton Trough and the magnetostratigraphically correlated beds described above are the only stratal units in the upper part of the sedimentary section in the Salton Trough whose ages have been determined by correlation with radiometrically dated rocks from outside the basin.

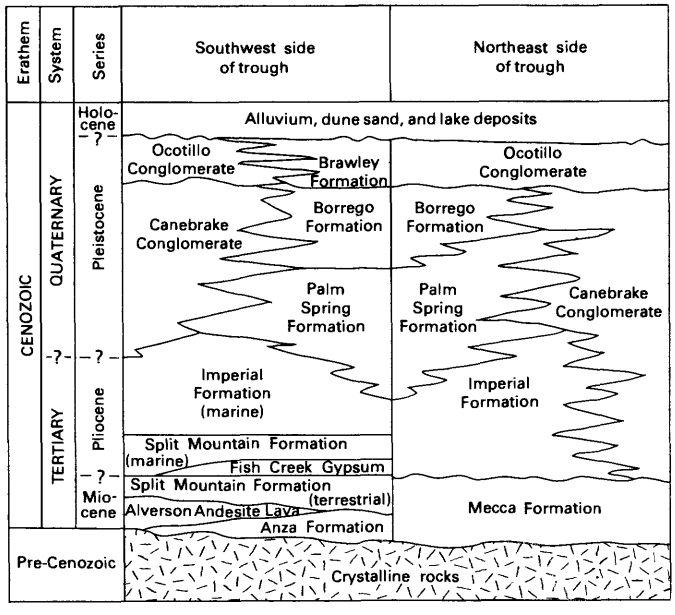

FIGURE 3.—Composite Cenozoic stratigraphic column along flanks of Salton Trough. Wavy lines, unconformable contacts; smooth lines, conformable contacts; queried lines, contacts not exposed. Nomenclature of Tarbet and Holman (1944) and Dibblee (1954), modified after more recent stratigraphic studies.

CENOZOIC DEFORMATION IN THE SALTON TROUGH

Late Cenozoic deposits of the Salton Trough are considerably folded and faulted, and this deformation appears to be continuing at the present time. Faulting is dominated by three active right-lateral strike-slip zones, parts of the broad and complex San Andreas fault system in southern California. Major faults within the trough, as well as those farther south under the Gulf of California, define an echelon pattern in which the separate strands trend more westerly than the axis of the depression (Biehler and others, 1964; Rusnak and others, 1964).

Folding of the Cenozoic deposits is evident throughout marginal areas of the Salton Trough. The intensity of deformation by folding is especially pronounced in, though not restricted to, certain belts bordering or bounded by active faults traversing the trough. The pattern of modern sedimentary accumulation and the incipient formation of anticlinal hills also reflect continuing diastrophism in the trough, particularly on the southwest side.

Many stratigraphic features of the Cenozoic deposits attest to regional crustal instability throughout the history of the basin. Although there was considerable initial relief on the basin floor, progressive diastrophism and erosion have allowed the youngest to oldest deposits to rest directly on basement. Regional unconformities also exist, although localized intraformational unconformities are far more common. Absence of lateral continuity, particularly in the coarser detritus and the lacustrine beds, is typical all along the margins of the trough. Widespread instability in the flanking area of the trough is evident from the marked erosional truncation of thick sections of Quaternary deposits. The eroded detritus has been redeposited elsewhere in the axial part of the basin. Such features suggest that the axial part of the trough may well have been continuously subsiding, whereas parts of the flanks have alternately received sediment and undergone erosion.

CENOZOIC FOLDING

Fault offsets outline the Salton Trough, but major crustal downwarping not directly attributable to fault-

ing has also taken place, particularly south of the middle of the Salton Sea, where the trough widens markedly. Downwarping in the axial part of the trough is demonstrated by emergence and erosional truncation of the late Pleistocene deposits on both flanks of the trough; this relation is confirmed by data from wells and by subsurface features under the Imperial Valley explored with geophysical techniques (Biehler and others, 1964; Fuis and others, this volume).

Late Cenozoic deposits throughout the trough display numerous intermediate- and small-scale folds, as well as homoclinal dips over large areas. Generally the older strata are more deformed than the younger; terrace gravel and alluvium, for example, show only local signs of folding. Some of the most pronounced folding, including overturning and isoclinal folding, is not restricted to older strata but occurs in belts adjacent to fault zones. Other zones of strongly folded strata resembling diapirs with clay cores appear to degenerate along strike into faults.

Present-day folding of the land surface is demonstrated by small hills that reflect anticlinal growth near at least one active fault zone, and by closed playa basins scattered throughout the southwest side of the Salton Trough (Sharp and Clark, 1972). Warped shorelines of several high stands of former Lake Cahuilla also indicate relatively recent large-scale diastrophic changes (Stanley, 1963, 1966).

LATE CENOZOIC FAULTING

The principal fault zones in the Imperial Valley region consists of the San Andreas zone, near the northeast margin; the Clark and Coyote Creek branches of the San Jacinto fault zone, which transects the southwest flank of the Salton Trough; and the Elsinore fault zone along the southwest edge of the trough (fig. 2). The Brawley fault zone, including the seismic zone that marks its northward extension, and the Imperial, Superstition Hills, and Superstition Mountain faults are situated on or near the axis of the trough. Although the relations of these structures to the major faults are incompletely known, some possibilities are outlined below.

With the exception of the Brawley fault zone, all the above-named faults display those surficial features characteristic of the San Andreas system throughout California: linearity, northwest-southeastward trend, and physiographic evidence of recent activity. Historical right-lateral movements on several of these faults and high levels of seismicity (Johnson and Hill, this volume) indicate that the Salton Trough area is one of the most active segments of the San Andreas system.

Larson and others (1968) and Moore and Buffington (1968) first discussed the significance of the San Andreas fault system in terms of a transformation of horizontal spreading movements near the tip of Baja California into strike-slip movement within the Gulf of California and the Salton Trough. According to their transform-faulting model, coastal Califonria and Baja California are drifting northwestward relative to the region east of the Salton Trough and the Gulf of California; movement occurs by a combination of right-lateral slip along northwest-trending faults and horizontal spreading between fault strands within the trough and gulf. Seismicity patterns in the Mesquite basin area and northward (Hill and other, 1975; Weaver and Hill, 1978/79) and in the Colorado River delta region (Lomnitz and others, 1970) have been interpreted in terms of transform faulting combined with spreading.

SAN ANDREAS FAULT ZONE

From about 30 km northwest of Mecca, Calif., the San Andreas fault zone is relatively straight and continuous to within about 5 km of Bombay Beach on the northeast shore of the Salton Sea (fig. 2). Although the San Andreas fault shows evidence of Holocene activity on this segment and moved historically in 1968 and again in 1979, the seismicity of this segment of the San Andreas fault zone is virtually nil. From the south terminus of the San Andreas fault trace near Bombay Beach, no surface evidence for recent faulting on strike with the fault zone to the southeast is known. Although a linear concealed extension of the San Andreas fault may exist under the Salton Sea or in the northern Imperial Valley, no convincing geologic or geophysical evidence yet supports such a projection. Babcock (1971) argued that photolineaments in cultivated fields and offset concrete canal liners southeast of Niland, Calif., represent possible active fault traces, but comparison of these photolineaments with earlier aerial photographs show them to be recessional shoreline features of former Lake Cahuilla. The offsets of canal liners are not convincing evidence of fault movement because of structional irregularities and because buckled and misalined liners are widespread throughout the Imperial Valley.

Near Bombay Beach, discontinuous faults approximately parallel the highly active seismic belt extending northward from the Imperial fault and the Brawley fault zone (Sharp, 1979; Johnson and Hill, this volume). The pattern of seismicity beneath and south of the Salton Sea, crustal-strain measurements (Savage and others, 1974), and these young faults near Bombay Beach all suggest but do not prove that a fault zone, perhaps the San Andreas, bends southward and either branches into or otherwise becomes part of the Imperial fault and the Brawley fault zone in the south-

central Imperial Valley. If the zone of major right-lateral dislocation that defines the San Andreas fault zone at depth curves southward, the fault traces near Bombay Beach indicate that this bending begins 3 to 5 km northwest of Bombay Beach.

IMPERIAL FAULT-BRAWLEY FAULT ZONE

The Imperial fault was first recognized from the displacement of the 1940 Imperial Valley $M=7.1$ earthquake (Buwalda and Richter, 1941; Richter, 1958). Until the 1979 earthquake, all post-1940 movements noted in 1966, 1968, 1971, and 1977 were relatively minor (Brune and Allen, 1967; Allen and others, 1972; Goulty and others, 1978). Aerial photographs taken before and after the earthquake of 1940, as well as the positions of offset cultural features identified in 1975–77, demonstrate a relatively smooth fault trace except for multiple complex branches near its north end (Sharp, 1977a). Downdip components of movement on the northern section of the Imperial fault define the west margin of a topographic basin once known as Mesquite Lake, which in turn is bounded on its east side by a complex set of fault scarps, now mostly destroyed by agricultural regrading, known as the Brawley fault zone (fig. 2). Although field observations revealed that surface faulting for a few kilometers along the Brawley fault zone occurred during the 1940 Imperial Valley earthquake (A. E. Sedgwick, unpub. data, 1940), the surface expression of this fault zone was generally unrecognized until new faulting occurred during a swarm of small earthquakes in 1975 (Johnson and Hadley, 1976; Sharp, 1976, 1977b). A comprehensive study of recent seismicity linking the Imperial fault and the Brawley fault zone by Johnson and Hill (this volume) defines subsurface-faulting patterns that are consistent with the transform-faulting and crustal-spreading model.

The traces of the Imperial fault and the Brawley fault zone cut Holocene alluvium and deposits of Lake Cahuilla (van de Camp, 1973), and so no data from the surface other than heights of scarps yet reveal much of the past history of movement. Displacement measurements on near-surface strata exposed in trenches cut into the Imperial fault near the United States-Mexican border demonstrate that if the Imperial fault had been active during one or both of two $M > 6$ earthquakes in 1915, surface displacement could have occurred only to the north or south of, but not at, the border (Sharp, 1980).

The surface faulting associated with the 1979 earthquake in the Imperial Valley confirmed the overall characteristics and revealed many new details of the traces of the Imperial fault and the Brawley fault zone. Surface faulting of 1979 and its comparison with earlier displacements are described more fully in other chapters of this volume.

SAN JACINTO FAULT ZONE

The two main branches of the San Jacinto fault zone, the Clark and Coyote Creek faults, enter the Salton Trough from the northwest at about the latitude of the Salton Sea and cut diagonally into the basin (fig. 2). Displacement across the San Jacinto fault zone in the Peninsular Ranges northwest of the Salton Trough is principally right lateral and has totaled about 24 km since movement began, probably during Pliocene time (Sharp, 1967).

Vertical components of displacement on various breaks along the Coyote Creek fault have created several topographically high welts, some of which show vertical separations of probably more than 1,000 m. Crystalline rocks and sedimentary deposits caught between separate strands of the Coyote Creek fault near Borrego Mountain have been squeezed up within the complex zone of faulting (Sharp and Clark, 1972).

Recent mapping of the Clark fault demonstrates that it is not traceable as a late Pleistocene or Holocene break as far east as the 116th meridian (Sharp, 1980). The dominant presently active strand of the San Jacinto fault zone at the latitude of the Vallecito Mountains and southeastward is the Coyote Creek fault (Sharp, 1975), which ruptured at the surface in 1968 at the time of the Borrego Mountain, Calif., $M = 6.7$ earthquake (Clark, 1972) and has continued to creep until the present along the southern part of the 1968 surface break (Burford, 1972; Clark, 1972; Harsh, 1982). Although the 1968 Borrego Mountain earthquake triggered visible surface displacement on the Imperial fault, the 1979 Imperial Valley earthquake, which was centered on the Imperial fault, apparently did not cause movement on the Clark fault.

Because the trace of the Coyote Creek fault is poorly delineated by physiographic and geologic features between the Fish Creek Mountains and Superstition Mountain, the 1968 surface rupture on the Coyote Creek fault represents the limit of present knowledge regarding its southeastward extent. A detailed gravity survey in the area west of Superstition Mountain confirms a possible continuity between the Coyote Creek fault and the Superstition Mountain fault to the southeast, but a concealed northeast-trending fault converges in the area of possible connection (Plouff, 1976, fig. 3). This concealed fault and other physiographically traceable faults of similar trend crossing the alluvial flat to the south indicate that the Coyote Creek fault does not connect in any simple manner with the

1969 surface fractures that broke across County Highway S–80, 4 km east of Plaster City, Calif.—a possibility mentioned by Sharp and Clark (1972). The remaining and most obvious structure that might represent a southeastward continuation of the Coyote Creek fault is the Superstition Mountain fault. Alined dunes covering mesquite trees southeast of the 1968 surface rupture and low hills of upwarped alluvium, all on the projection of the Coyote Creek fault, are collinear with the fault along the southwest side of Superstition Mountain (Sharp and Clark, 1972). Holocene scarps and other geomorphic features of Quaternary displacement occur along many parts of the Superstition Mountain fault, but slip in historical time has not been observed. No evidence of new movement was found after the 1979 Imperial Valley earthquake on this fault trace.

SUPERSTITION HILLS FAULT

The Superstition Hills fault cuts Quaternary deposits exposed in the badland area adjacent to the west side of the Imperial Valley (fig. 2). The fault forms the southwest boundary of the badland area over much of its length. Small historical displacement has been detected on this fault on several occasions, beginning in 1951 (Allen and others, 1965, p. 768). The displacements of 1968 and 1979 were triggered by the distant strong earthquakes at Borrego Mountain and in the Imperial Valley, respectively (Allen and others, 1972; Fuis, this volume). None of these historical displacements have extended beyond the Quaternary trace of the fault as originally mapped by Dibblee (1954).

ELSINORE FAULT ZONE

The Elsinore fault zone, a distinct, yet surficially discontinuous, zone of fractures, extends from the Peninsular Ranges into the Salton Trough near the Tierra Blanca Mountains (fig. 2). In the trough the zone is best defined and most continuous where it bounds the southwest sides of the Coyote Mountains and the Sierra de los Cucapás in Mexico. As with breaks on the San Jacinto fault zone that are concealed by alluvium in the floor of the mesa area west of the Imperial Valley, continuity between the many individual strands in the Elsinore fault zone cannot be demonstrated.

The total strike-slip offset on the Elsinore fault zone near the Salton Trough, about 2 to 3 km, is small relative to the estimated extent of displacement on the San Jacinto and San Andreas fault zones (Sharp, 1968; Baird and others, 1970; Todd and Hoggatt, 1979). Historical movement on the Elsinore fault zone has not been documented, and, indeed, within the Salton Trough only its section south of the United States-Mexican border has shown appreciable seismicity in recent times.

NEOTECTONICS OF THE IMPERIAL VALLEY REGION

The Imperial Valley and the Salton Sea are situated along the axis of the Salton Trough, defined here as the locus of topographically low points in the trough; however, early in Quaternary time the axis lay farther west than at present, as shown by mineralogic studies of detritus in the Palm Spring, Borrego, and Brawley Formations (fig. 3) that was derived from the Colorado River drainage (Merriam and Bandy, 1965; Muffler and Doe, 1968). The area where clastic detritus was laid down by the Colorado River extended nearly to the west margin of the Salton Trough and nearly to the north end of the Salton Sea (fig. 4). Although this distribution of sediment derived from the Colorado River implies that the axis, or low points, of the sedimentary basin probably lay even farther west or north, the structural axis of the subsiding trough may have been approximately at its present position under the Imperial Valley. If such was the case, then the rate of deposition of detritus from the Colorado River must have exceeded the rate of structural subsidence of the area under the present-day Imperial Valley. Alternatively, the entire width of the Salton Trough may have subsided as detritus borne by the Colorado River was deposited, and subsidence may not have been localized near the present axis.

During late Pleistocene and possibly early Holocene time, regional tectonic deformation vastly altered the geomorphology of the Imperial Valley region. Although crustal movement along major and minor fault zones and folding within the basin were proceeding vigorously throughout Quaternary time, regional relative uplift of approximately the west half of the trough raised the present mesa area west of the Imperial Valley until erosion rather than deposition dominated there. Part of the east flank of the trough next to the present-day Salton Sea also was similarly uplifted. The folded and faulted sedimentary deposits in these parts of the trough were vigorously incised by erosion as they emerged from the floor of the basin, and badlands and gravel-mantled terraces formed at various times and places. During this phase of emergence, as much as 3,500 m of Quaternary deposits was eroded from parts of the badland areas and redeposited in the newly defined depression along the present-day axis of the Salton Trough (Sharp, 1972). Sedimentation and, consequently, subsidence along the axis must have been extremely rapid, inasmuch as this strip of the trough received sedimentary detritus in great quantities from the flanks of the trough, as well as continuing contributions from the Colorado River, and yet maintained its low elevation relative to the flanking areas as well as sea level.

Faulting on the floor of the Imperial Valley along traces of the Imperial fault and the Brawley fault zone may have occurred throughout this period of the trough's history, although there is no direct evidence to confirm this interpretation. If the large horizontal slip on the San Andreas fault were continuously taken up by displacement on those faults near the axis of the trough rather than on now-concealed faults to the east, the evidence elsewhere for large late Quaternary slip on the San Andreas fault would indirectly support this conclusion. Growth of fault scarps at the north end of the Imperial fault and along the southern part of the Brawley fault zone, as well as formation of the Mesquite basin between them, is older than the last high stand of Lake Cahuilla, probably before A.D. 1700 (Sharp, 1981). The scarp of the Imperial fault had already been eroded subaerially to approximately its present rounded profile before being submerged under the last high stand of Lake Cahuilla and mantled by a thin layer of lakebeds. At present, no other geologic evidence for the antiquity of the Imperial fault or the Brawley fault zone before creation of the present scarps is known.

REFERENCES CITED

Allen, C. R., Saint Amand, Pierre, Richter, C. F., and Nordquist, J. M., 1965, Relationship between seismicity and geologic structure in the southern California region: Seismological Society of America Bulletin, v. 55, no. 4, p. 753–797.

Allen, C. R., Wyss, Max, Brune, J. N., Grantz, Arthur, and Wallace, R. E., 1972, Displacements on the Imperial, Superstition Hills, and San Andreas faults triggered by the Borrego Mountain earthquake, *in* The Borrego Mountain earthquake of April 9, 1968: U.S. Geological Survey Professional Paper 787, p. 87–104.

Babcock, E. A., 1971, Detection of active faulting using oblique infrared aerial photography in the Imperial Valley, California: Geological Society of America Bulletin, v. 82, no. 11, p. 3189–3196.

Baird, A. K., Welday, E. E., and Baird, K. W., 1970, Chemical variations in batholithic rocks of southern California [abs.]: Geological Society of America Abstracts with Programs, v. 2, no. 2, p. 69.

Biehler, Shawn, Kovach, R. L., and Allen, C. R., 1964, Geophysical framework of northern end of Gulf of California structural prov-

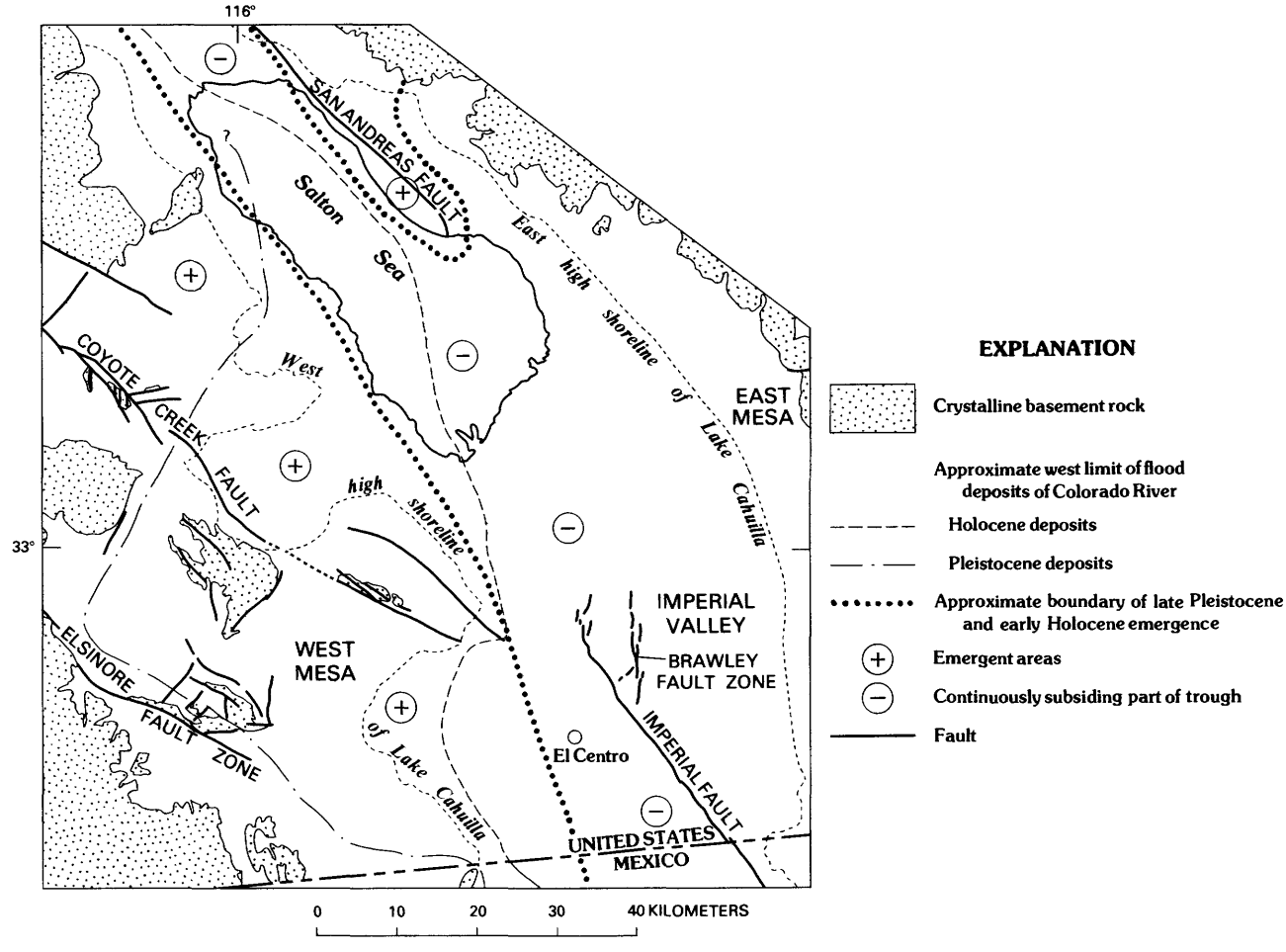

FIGURE 4.—Generalized map showing former extent of sedimentary deposits derived from Colorado River, and present geographic features in Imperial Valley region. After late Pleistocene and early Holocene emergence of present western part of Imperial Valley, flood deposits of Colorado River were restricted to area east of west high shoreline of Lake Cahuilla.

ince, *in* van Andel, T. H., and Shor, G. G., Jr., eds., Marine geology of the Gulf of California: American Association of Petroleum Geologists Memoir 3, p. 126–143.

Brune, J. N., and Allen, C. R., 1967, A low-stress-drop, low-magnitude earthquake with surface faulting: The Imperial, California, earthquake of March 5, 1966: Seismological Society of America Bulletin, v. 57, no. 3, p. 501–514.

Burford, R. O., 1972, Continued slip on the Coyote Creek fault after the Borrego Mountain earthquake, *in* The Borrego Mountain earthquake of April 9, 1968: U.S. Geological Survey Professional Paper 787, p. 105–111.

Buwalda, J. P., and Richter, C. F., 1941, Imperial Valley earthquake of May 18, 1940 [abs.]: Geological Society of America Bulletin, v. 52, no. 12, pt. 2, p. 1944–1945.

Clark, M. M., 1972, Surface rupture along the Coyote Creek fault, *in* The Borrego Mountain earthquake of April 9, 1968: U.S. Geological Survey Professional Paper 787, p. 55–86.

Dalrymple, G. B., Cox, Allan, and Doell, R. R., 1965, Potassium-argon age and paleomagnetism of the Bishop Tuff, California: Geological Society of America Bulletin, v. 76, no. 6, p. 665–673.

Dibblee, T. W., Jr., 1954, Geology of the Imperial Valley region, *in* Geology of the natural provinces, chap. 2 *of* Jahns, R. H., Geology of southern California: California Division of Mines Bulletin 170, v. 1, p. 21–28.

Eberly, L. D., and Stanley, T. B., Jr., 1978, Cenozoic stratigraphy and geologic history of southwestern Arizona: Geological Society of America Bulletin, v. 89, no. 6, p. 921–940.

Elders, W. A., and Robinson, P. T., 1970, Possible sea-floor spreading in the Imperial Valley of California IV: A model for magma generation [abs.]: Eos (American Geophysical Union Transactions), v. 51, no. 4, p. 422.

Goulty, N. R., Burford, R. O., Allen, C. R., Gilman, Ralph, Johnson, C. E., and Keller, R. P., 1978, Large creep events on the Imperial fault, California: Seismological Society of America Bulletin, v. 68, no. 2, p. 517–521.

Harsh, P. W., 1982, Continuing slip on the Coyote Creek fault, southern California: Seismological Society of America Bulletin [in press].

Hill, D. P., Mowinckel, Penelope, and Peake, L. G., 1975, Earthquakes, active faults, and geothermal areas in the Imperial Valley, California: Science, v. 188, no. 4195, p. 1306–1308.

Johnson, C. E., and Hadley, D. M., 1976, Tectonic implications of the Brawley earthquake swarm, Imperial Valley, California, January 1975: Seismological Society of America Bulletin, v. 66, no. 4, p. 1133–1144.

Kelley, V. C., and Soske, J. L., 1936, Origin of the Salton volcanic domes, Salton Sea, California: Journal of Geology, v. 44, no. 4, p. 496–509.

Larson, R. L., Menard, H. W., and Smith, S. M., 1968, Gulf of California: A result of ocean-floor spreading and transform faulting: Science, v. 161, no. 3843, p. 781–784.

Lomnitz, Cinna, Mooser, Federico, Allen, C. R., Brune, J. N., and Thatcher, Wayne, 1970, Seismicity and tectonics of northern Gulf of California region, Mexico. Preliminary results: Geofisica Internacional, v. 10, no. 2, p. 37–48.

Mendenhall, W. C., 1909, Groundwater of the Indio region, California: U.S. Geological Survey Water-Supply Paper 225, 56 p.

Merriam, Richard, and Bandy, O. L., 1965, Source of upper Cenozoic sediments in Colorado delta region: Journal of Sedimentary Petrology, v. 35, no. 4, p. 911–916.

Merriam, Richard, and Bischoff, J. L., 1975, Bishop ash: A widespread volcanic ash extended to southern California: Journal of Sedimentary Petrology, v. 45, no. 1, p. 207–211.

Moore, D. G., and Buffington, E. C., 1968, Transform faulting and growth of the Gulf of California since the late Pliocene: Science, v. 161, no. 3847, p. 1238-1241.

Muffler, L. J. P., and Doe, B. R., 1968, Composition and mean age of detritus of the Colorado River delta in the Salton Trough, southeastern California: Journal of Sedimentary Petrology, v. 38, no. 2, p. 384–399.

Muffler, L. J. P., and White, D. E., 1969, Active metamorphism of upper Cenozoic sediments in the Salton Sea geothermal field and the Salton Trough, southeastern California: Geological Society of America Bulletin, v. 80, no. 2, p. 157–181.

Opdyke, N. D., Lindsay, E. H., Johnson, N. M., and Downs, T., 1975, The paleomagnetism and magnetic polarity stratigraphy of the mammal-bearing section of Anza Borrego State Park, California: Quaternary Research, v. 7, no. 3, p. 316–329.

Plouff, Donald, 1976, Gravity and magnetic fields of polygonal prisms and application to magnetic terrain corrections: Geophysics, v. 41, no. 4, p. 727–741.

Richter, C. F., 1958, Elementary seismology: San Francisco, W. H. Freeman, 768 p.

Rusnak, G. A., Fisher, R. L., and Shepard, F. P., 1964, Bathymetry and faults of Gulf of California, *in* van Andel, T. H., and Shor, G. G., Jr., eds., Marine geology of Gulf of California: American Association of Petroleum Geologists Memoir 3, p. 59–75.

Sarna-Wojcicki, A. M., Bowman, H. R., Meyer, C. E., Russel, P. C., Asaro, Frank, Michael, Helen, Rowe, J. J., Baedecker, P. A., and McCoy, Gail, 1980, Chemical analyses, correlations, and ages of late Cenozoic tephra units of east-central and southern California, U.S. Geological Survey Open-File Report 80-231, 53 p.

Savage, J. C., Goodreau, D. D., and Prescott, W. H., 1974, Possible fault slip on the Brawley faults, Imperial Valley, California: Seismological Society of America Bulletin, v. 64, no. 3, p. 713–715.

Sharp, R. V., 1967, San Jacinto fault zone in the Peninsular Ranges of southern California: Geological Society of America Bulletin, v. 78, no. 6, p. 705–729.

———1968, Ancient mylonite zone and fault displacement in the Peninsular Ranges of southern California [abs.], *in* Abstracts for 1966: Geological Society of America Special Paper 101, p. 333.

———1972, Tectonic setting of the Salton Trough, *in* The Borrego Mountain earthquake of April 9, 1968: U.S. Geological Survey Professional Paper 787, p. 3–15.

———1975, En echelon fault patterns of the San Jacinto fault zone, *in* Crowell, J. C., ed., San Andreas fault in southern California: California Division of Mines and Geology Special Report 118, p. 147–152.

———1976, Surface faulting in Imperial Valley during the earthquake swarm of January–February 1975: Seismological Society of America Bulletin, v. 66, no. 4, p. 1145–1154.

———1977a, Holocene traces of the Imperial fault in south-central Imperial County, California: U.S. Geological Survey Open-File Report 77–815, 1 p.

———1977b, Map showing Holocene surface expression of the Brawley fault, Imperial County, California: U.S. Geological Survey Miscellaneous Field Studies Map MF–838, scale 1:24,000.

———1979, New geologic evidence relating the southernmost San Andreas fault to the seismic belt of central Imperial Valley [abs.]: Earthquake Notes, v. 49, no. 4, p. 97.

———1980, 1940 and prehistoric earthquake displacements on the Imperial fault, Imperial and Mexicali Valleys, California and Mexico, *in* Proceedings of California-Mexico Symposium; human settlements in the San Andreas fault zone: Sacramento, California Seismic Safety Commission, p. 68–81.

———1981, Variable rates of late Quaternary strike slip on the San Jacinto fault zone, southern California: Journal of Geophysical Research, v. 86, no. B3, p. 1754–1762.

Sharp, R. V., and Clark, M. M., 1972, Geologic evidence of previous

faulting near the 1968 rupture on the Coyote Creek fault, *in* The Borrego Mountain earthquake of April 9, 1968: U.S. Geological Survey Professional Paper 787, p. 131–140.

Stanley, G. M., 1963, Prehistoric lakes in Salton Sea basin [abs.], *in* Abstracts for 1962: Geological Society of America Special Paper 73, p. 249–250.

———1966, Deformation of Pleistocene Lake Cahuilla shore line, Salton Sea basin, California [abs.], *in* Abstracts for 1965: Geological Society of America Special Paper 87, p. 165.

Tarbet, L. A., 1951, Imperial Valley, California, [sec. 13] *of* Possible future petroleum provinces of North America: American Association of Petroleum Geologists Bulletin, v. 35, no. 2, p. 260–263.

Tarbet, L. A., and Holman, W. H., 1944, Stratigraphy and micropaleontology of the west side of Imperial Valley, California [abs.]: American Association of Petroleum Geologists Bulletin, v. 28, no. 12, p. 1781–1782.

Todd, V. R., and Hoggatt, W. C., 1979, Vertical tectonics in the Elsinore fault zone south of 33°7′30″ [abs.]: Geological Society of America Abstracts with Programs, v. 11, no. 7, p. 528.

van de Camp, P. C., 1973, Holocene continental sedimentation in the Salton Basin, California: A reconnaissance: Geological Society of America Bulletin, v. 84, no. 3, p. 827–848.

Weaver, C. S., and Hill, D. P., 1978/79, Earthquake swarm and local crustal spreading along major strike-slip faults in California: Pure and Applied Geophysics, v. 117, no. 1–2, p. 51–64.

Woodard, G. D., 1974, Redefinition of Cenozoic stratigraphic column in Split Mountain Gorge, Imperial Valley, California: American Association of Petroleum Geologists Bulletin, v. 58, no. 3, p. 521–526.

SEISMICITY OF THE IMPERIAL VALLEY

By CARL E. JOHNSON and DAVID P. HILL,
U.S. GEOLOGICAL SURVEY

CONTENTS

ABSTRACT

Earthquake activity in the Imperial Valley since 1900 has been characterized by clusters of swarm sequences along the Brawley fault zone, interspersed with magnitude 5 to 7 main-shock/aftershock sequences along the Imperial fault. The historical record, though incomplete before about 1940, suggests that changes in the spatiotemporal seismicity pattern evolve at a rate measured in tens of years. Spatiotemporal seismicity patterns observed since installation of a dense seismograph network in 1973 are consistent with models in which fluid phases in the crust are an important rate-controlling agent associated with the earthquake-swarm activity.

INTRODUCTION

In this chapter, we present a brief discussion of the historical seismicity in the Imperial Valley, emphasizing the long-term variations in seismotectonic phenomena leading to the damaging earthquake of October 15, 1979. This discussion serves as a background against which the detailed observations presented in this volume can be compared. We conclude with some speculation on processes governing the seismicity patterns. Much of this material represents the condensation of a discussion of recent seismic phenomena in the Imperial Valley by Johnson (1979).

Although the region of concentrated study with which this volume is concerned (fig. 5) makes up less than 4 percent of the principal coverage area of the southern California seismic network (bold outline, fig. 5), it contained 20 percent of all located events in the typical years 1977 and 1978. The importance of understanding the tectonics of the Imperial Valley (fig. 6) derives from the fact that this major structural trough is part of the transition zone between the oceanic-plate tectonics of the Gulf of California and the transform faulting represented by the San Andreas fault zone. Such an understanding should provide insight into the loading process of the San Andreas fault and is likely to be of major significance to the problem of earthquake prediction.

RECENT SEISMICITY

Coverage of small local events has been reasonably uniform only since the installation of the dense Imperial Valley network in mid-1973 (Hill and others, 1975b). Before that, the threshold magnitude for homogeneous coverage in the Imperial Valley exceeded 3.5, and location errors could be as large as 15 to 25 km because most

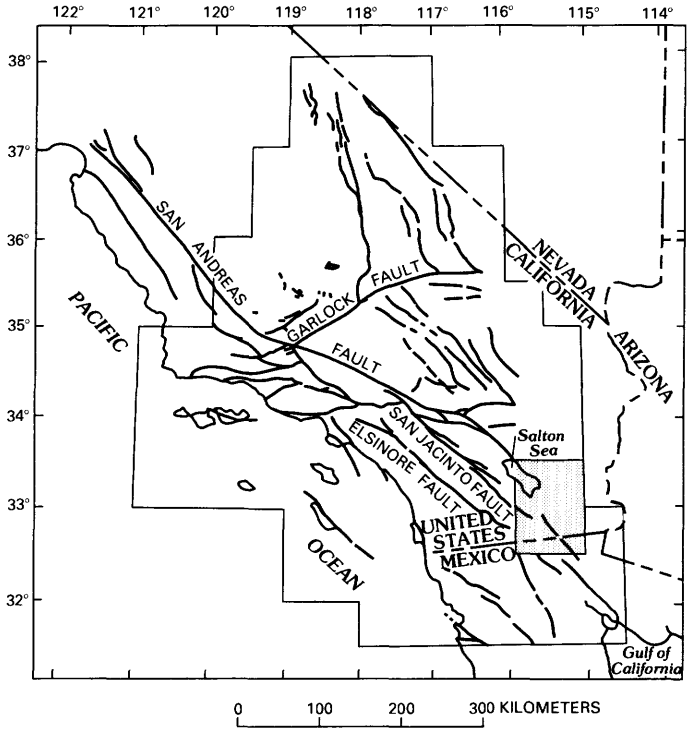

FIGURE 5.—Southern California, showing study area (shaded) and location of major faults. Outline denotes principal coverage area of southern California seismic network.

network stations lay beyond the P_n crossover distance. Many features of the seismicity distribution (fig. 7) were first observed and discussed by Hill and others (1975a) after the network's first year of operation. Specifically, these observations included the dense north-south-trending lineation of events (Brawley seismic zone of Johnson, 1979) connecting the Imperial and San Andreas faults, a weaker lineation trending northwest of El Centro, Calif., toward the San Jacinto fault zone, and a wedgelike intervening zone of low seismicity.

The most conspicuous zone of seismicity, termed the "Brawley seismic zone" by Johnson (1979), consists of earthquake swarms and clustered events in which what might be thought of as typical main-shock/aftershock sequences are notably absent. Two of the larger recent sequences within this zone were the January 1975 swarm (Johnson and Hadley, 1976) and the November 1976 swarm (Fuis and Schnapp, 1977), both of which comprised several spatially discrete clusters of events that became active progressively over time. These characteristics are also shared by five swarms that occurred along the trend of the Imperial fault, as discussed in considerable detail by Johnson (1979). We discuss below one example of this type of behavior on the Imperial fault—the October 1977 sequence. The presence of complex swarmlike seismicity and geothermal systems within the local spreading zone between two offset strike-slip faults (Weaver and Hill, 1978/79) resembles the observations of Reichle and Reid (1977) for the central part of the Gulf of California physiographic province.

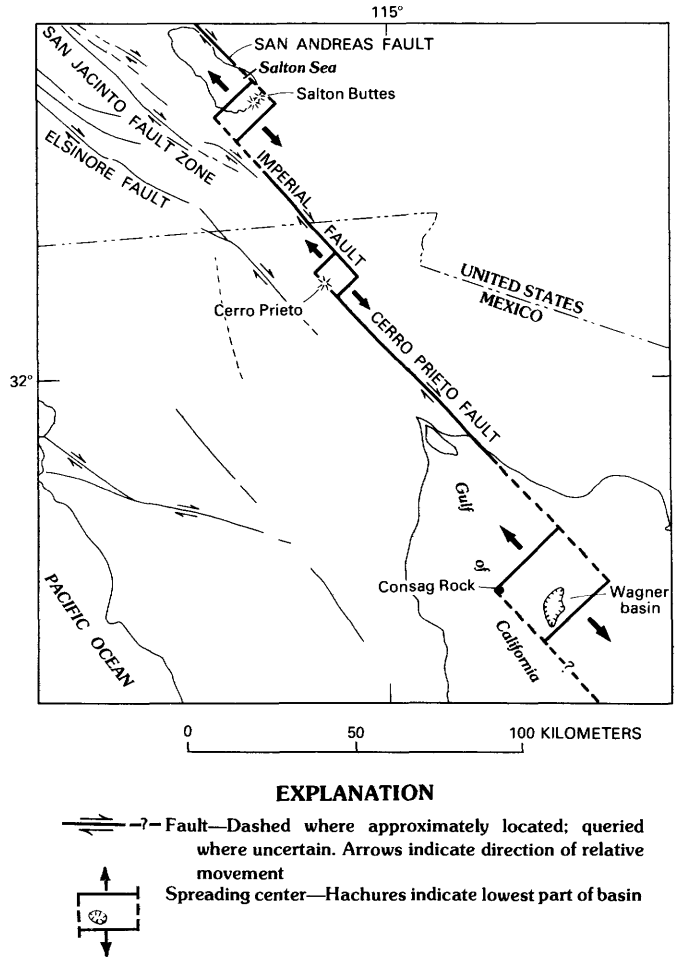

FIGURE 6.—Schematic relation between tectonics of Imperial Valley and northern Gulf of California. Adapted from Lomnitz and others (1970, fig. 3).

The sharp definition of the east and west boundaries of the Brawley seismic zone suggests an abrupt local change in physical properties. One possibility is that these boundaries are defined by faults paralleling the overall trend of the fault zone, although there is little other evidence to support such a conclusion. Another possibility involves an abrupt change in porosity. The Brawley seismic zone also marks a distinct change in the level of seismic activity from diffuse activity west of the zone to a near-absence of earthquakes east of the zone and throughout the eastern Imperial Valley.

The focal depths for earthquakes in the Imperial Valley are typically between 4 and 6 km, and the maximum depth of earthquake occurrence is about 8 km. The recently completed detailed seismic-refraction study of the Imperial Valley by Fuis and others (this volume) indicates that the crust beneath the central valley consists of 10 to 12 km of Miocene and younger deposits filling a profound structural trough floored by mafic rocks with P-wave velocities between 6.8 and 7.2 km/s. Fuis and others interpret the transition in P-wave velocities from 4.5 to 5.7 km/s at depths of 4 to 5 km to reflect a metamorphic transition to lower greenschist facies within the sedimentary pile. Accordingly, earthquakes in the Imperial Valley apparently occur entirely within sedimentary and metasedimentary rocks younger than 4 m.y.

MAIN-SHOCK SEQUENCES

The task of compiling a list of main-shock sequences on the Imperial fault since 1900 is complicated by the sporadicity of field reporting before 1940. Table 1 includes the most likely candidates for such a list, although surface breaks were observed only for the 1940 and 1970 events. More recent events suggest that surface breaks may well have been generated by the earlier events in the list, although none was reported. In the absence of such direct evidence, we have used instead the criterion that the maximum intensity—at least VIII (modified Mercalli) or IX (Rossi-Forel)—occurred at one of the communities immediately adjacent to the Imperial fault. We have excluded events for which a clear

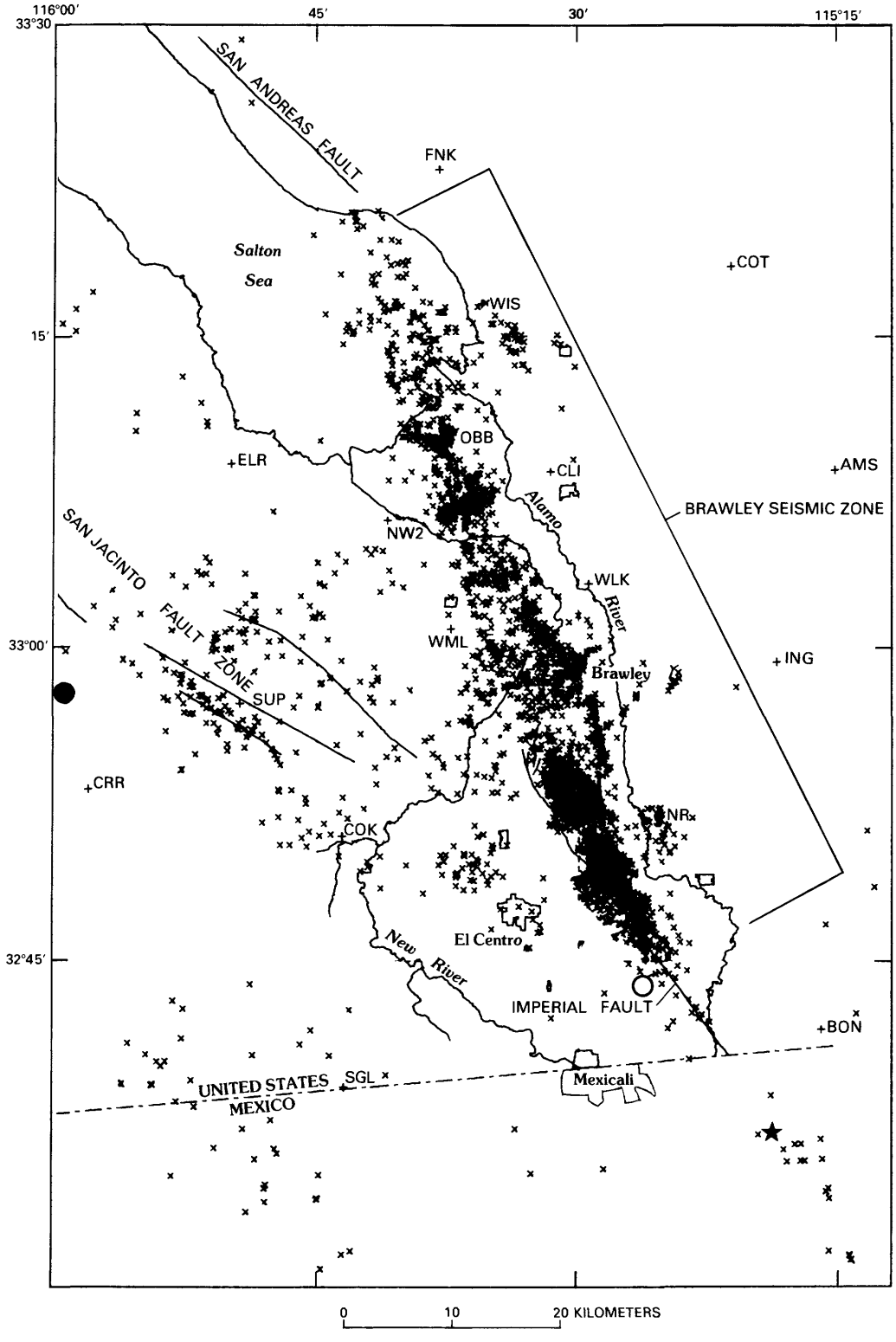

FIGURE 7.—Epicenter plot showing all epicenters with relative horizontal location errors less than 2.5 km (A- and B-quality solutions) for interval June 1973 through November 1978. Circle marks instrumental epicenter of 1940 Imperial Valley earthquake (M_L=7.1), dot of 1942 Superstition Mountain earthquake (M_L=6.5), and star of 1979 Imperial Valley earthquake. Letters refer to station localities in southern California seismic network.

TABLE 1.—*Earthquakes with intensities exceeding VIII (modified Mercalli) or IX (Rossi-Forel) at Brawley, Imperial, Holtville, and El Centro, Calif., and Mexicali, Mexico, since 1900*

Date	M	Time (G.m.t.)	References
April 19, 1906	6.0+	0030	Townley and Allen (1939), Toppozada and others (1978).
June 23, 1915	6.3	0359	Beal (1915).
June 23, 1915	6.3	0456	Do.
May 28, 1917	5.5	0606	Townley and Allen (1939), Toppozada and others (1978).
January 1, 1927	5.8	0816	Do.
January 1, 1927	5.5	0913	Do.
May 19, 1940	7.1	0436	Neumann (1942).
May 19, 1940	5.5	0635	Do.
October 15, 1979	6.6	2316	This study.
October 15, 1979	5.8	0658	Do.

association with faults other than the Imperial fault has been established.

It is a curious fact that main shocks in the Imperial Valley tend to occur in pairs of comparable size. This was particularly the case for the 1915 and 1927 sequences. For the 1940 and 1979 events, however, the second event in each year was nearly one magnitude unit smaller than the main shock, and the high reported intensity for both events (table 1) was due primarily to the proximity of the second event to Brawley, Calif.

The two events in 1915 were assigned by Beal (1915) to a fault that extends the San Jacinto fault as far southward as the Cerro Prieto fault. No field evidence in the form of surface breaks was found to support this conclusion, and, as yet, no major throughgoing structure is mapped where the San Jacinto extension is presumed to lie. Further, Beal knew nothing of the existence of the Imperial fault, although he was familiar with the San Jacinto fault and thus was not predisposed to look for faulting east of El Centro. The unexpectedly large intensities he reported at Holtville might otherwise have led to such an interpretation.

Almost nothing is known of the damaging earthquake of April 19, 1906, other than that it apparently had a magnitude of more than 6.0. The peculiar timing of this event—only about 12 hours after the great San Francisco earthquake, which occurred on the northern section of the San Andreas fault—evidently distracted attention from the Imperial Valley.

If all the events listed in table 1 actually did occur on the Imperial fault, we should apparently expect a recurrence time for damaging earthquakes on this structure of about 11 years, counting pairs as single occurrences. This interval, which is unusually short for California, suggests that the most recent interval (1940–79) was unusually long for the Imperial fault.

EARTHQUAKE SWARMS

Most earthquake sequences near the Imperial fault can be characterized as swarms that begin with a gradual buildup in activity over several days and in which the largest events occur well into the sequence. Although such sequences are typical throughout the Brawley seismic zone, only those that occurred immediately adjacent to the Imperial fault are considered here. Because most of these swarms are generally similar, we consider in detail only one, the October–November 1977 swarm.

The 1977 swarm comprised two discrete clusters along the trend of the Imperial fault (fig. 8). Actually, each cluster consisted of two temporally separate bursts of activity, and thus this sequence can be considered as four clusters. The northern cluster is clearly double, as shown on the distance-time plot (A, B, fig. 9). Unfortunately, the southern pair of clusters (C, D) occurred too close together in time to appear separated on the scale of this plot. The box in figure 9 marks the time-space window of an unsuccessful attempt to predict the occurrence of the southerly events on the basis of behavior observed in previous sequences along the Imperial fault.

Each burst of activity in the October–November 1977 swarm sequence appears to have been associated with the activation or formation of a planar fracture normal to the Imperial fault. In all four earthquake clusters, activity nucleated at depth along a planar projection of the Imperial fault under the Mesquite basin (fig. 10). This projection lies east of the surface trace of the fault, and the inferred direction of dip of the fault is largely consistent with the northeastward dip on the Imperial fault suggested by seismic-refraction measurements (Fuis and others, this volume). Subsequent activity in each cluster spreads progressively outward from the point of initiation. A series of stereopairs (figs. 10*A*–10*D*) illustrates this process for cluster C. Figure 10*A* shows the first few events in the cluster and their typically tight distribution. The cloud of points to the north marks the hypocenters of events in clusters A and B. Figure 10*B* shows the beginning of southward migration away from a plane inferred to represent the subsurface position of the Imperial fault; earlier events in cluster C are shown as points. Figures 10*C* and 10*D* show the continuation of this southward migration along an essentially vertical plane, and figure 11 presents a cross-sectional view of events plotted on the vertical plane, as inferred above (fig. 12). It is apparent that swarm activity migrated to the south at essentially a constant depth. Although lateral migration at constant depth is typical of other clusters as well, a change in hypocentral depth over time is also a common feature.

TEMPORAL VARIATIONS

Evidence is emerging that the spatiotemporal pattern of seismicity in the Imperial Valley may be somewhat repetitive. In particular, Richter (1958) observed that the rather high incidence of swarm activity in the years immediately before the 1940 earthquake declined afterward, and until 1950 few, if any, swarms were observed in the central Imperial Valley. This change in the level of activity is illustrated on a plot of seismic moment accumulated by year as inferred from magnitude (fig. 13), using the relation of Thatcher and Hanks (1973). The lull in activity after the 1940 earthquake was broken in 1950 by the largest swarm ever recorded in the Imperial Valley. Details of these changes in moment over time are better illustrated when we plot the accumulated moment on expanded scales (figs. 14*A*–14*C*). The large step for the 1940 earthquake (fig. 14*A*) is followed by a period of accelerated rate in the decade beginning 1950 (fig. 14*B*). More recently, an increase in moment rate beginning in 1975 (fig. 14*C*) is associated with an occurrence of swarm sequences along the Imperial fault beginning in 1973. Such sequences do not appear to have occurred before that time and may represent phenomena truly precursory to the 1979 event. The general increase in swarm activity led Johnson (1979) to speculate that conditions were once again similar to those before the 1940 earthquake.

The swarm-dominated seismicity pattern beginning in 1950 also has a migrational aspect. The large swarm in 1950 occurred near the north end of the Brawley

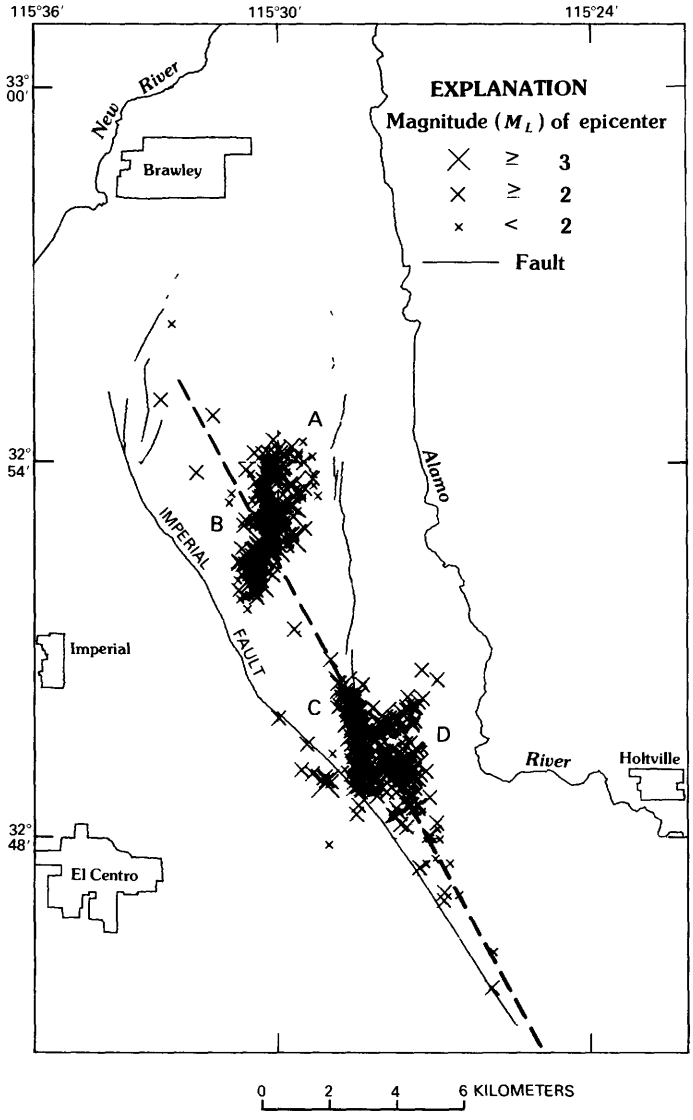

FIGURE 8.—Distribution of all epicenters with relative location errors less than 5 km (A-, B-, and C-quality solutions) for events associated with October 1977 swarm sequence along Imperial fault. Individual swarms in this sequence are labeled A through D in order of occurrence. Dashed line represents intersection with free surface of subsurface plane of Imperial fault, as suggested by hypocentral distributions of several swarm sequences.

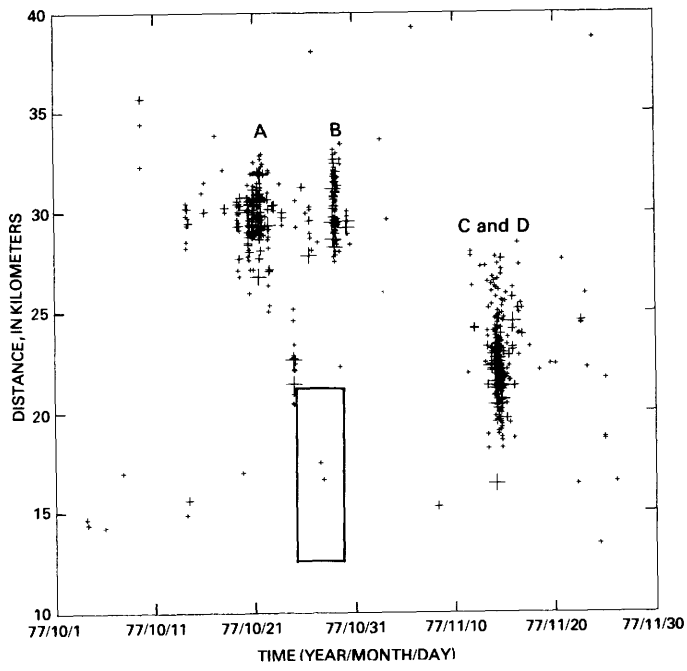

FIGURE 9.—Time-distance scatter plot, showing spatiotemporal relation among discrete events in October 1977 swarm sequence along Imperial fault trend; distance is measured from United States-Mexican border. Symbol size is proportional to magnitude. Individual swarms in this sequence are labeled A through D, as in figure 8. Rectangle represents location where second pair (C, D) was expected to occur on the basis of behavior of past sequences on Imperial fault.

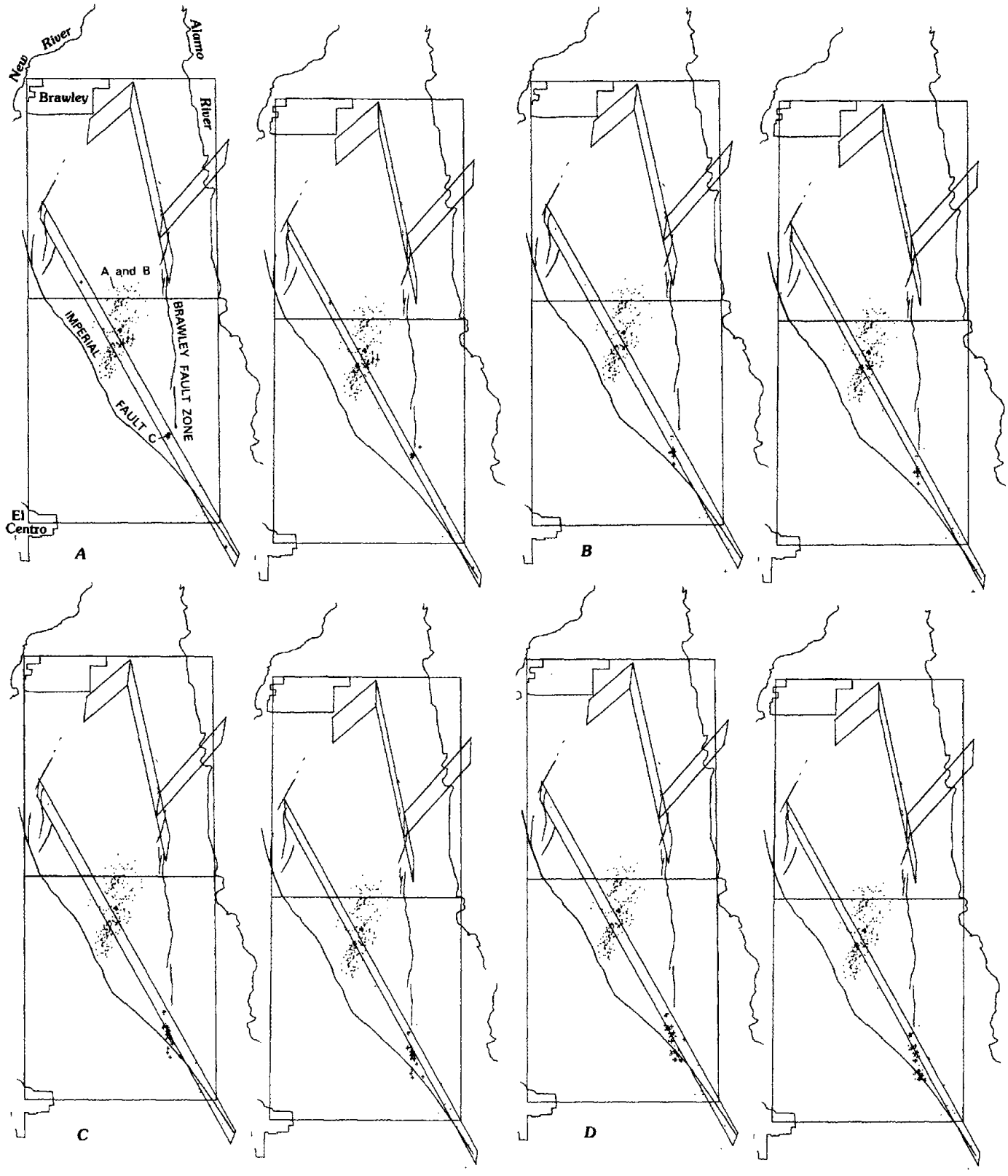

FIGURE 10.—Stereopairs showing all A-quality hypocenters of October 1977 swarm sequence under Mesquite basin. Reference grid, with sides of 0.1°, is plotted at depth of 6 km. View is from a point 275 km above lat 32°24′ N., long 115°33′ W. Both 1940 surface faulting and faulting associated with January 1975 Brawley-seismic-zone-trend sequence are shown. *A*, October 30 to midnight G.m.t. November 13, 1977 (336 hours). Note initiation of swarm C as a tight cluster on proposed subsurface plane of Imperial fault. *B*, Midnight to 0800 G.m.t. November 13 (8 hours). Note rapid development of swarm C to south. This development continues through figure 10*D*, although most of its extent is defined after 4 hours. We propose that this migration marks growth of vertical fracture. *C*, 0800 G.m.t. November 13 to 0100 G.m.t. November 14 (17 hours). *D*, 0100–0300 G.m.t. November 14 (2 hours).

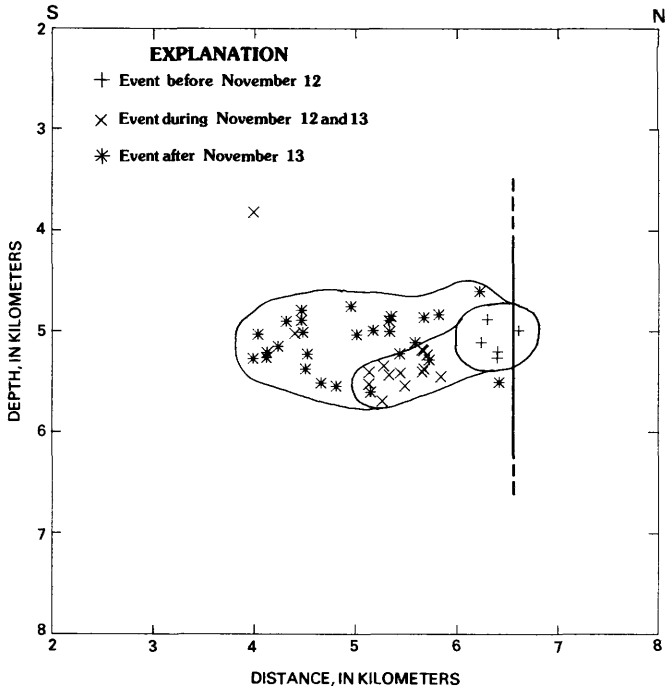

FIGURE 11.—Growth of swarm C on north-south-trending vertical plane. Line denotes proposed intersection of Imperial fault with this plane (dashed where uncertain).

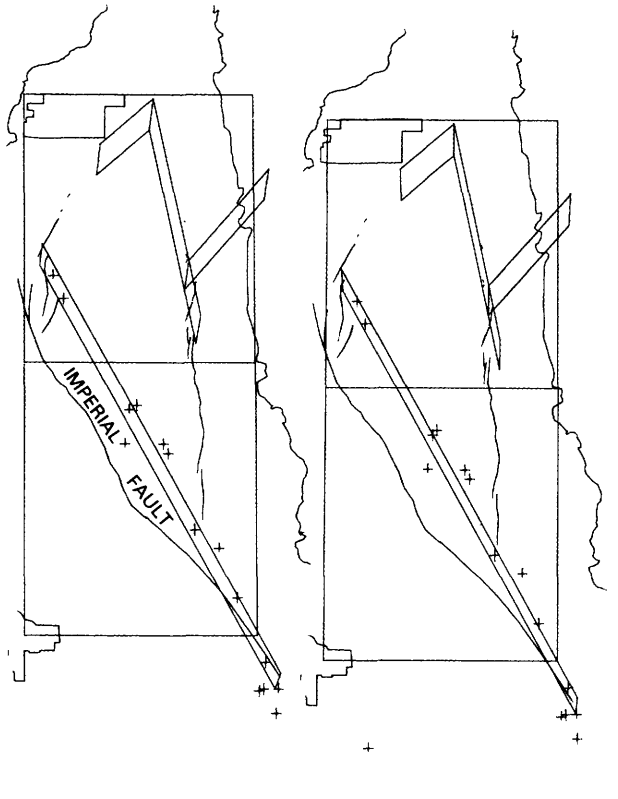

FIGURE 12.—Stereopair showing distribution of median initiation points for all significant swarms in five sequences from northwest to southeast along Imperial fault trend, as studied in detail by Johnson (1979). This distribution was used to define subsurface expression of Imperial fault (also shown). See figure 10 for details of stereopair.

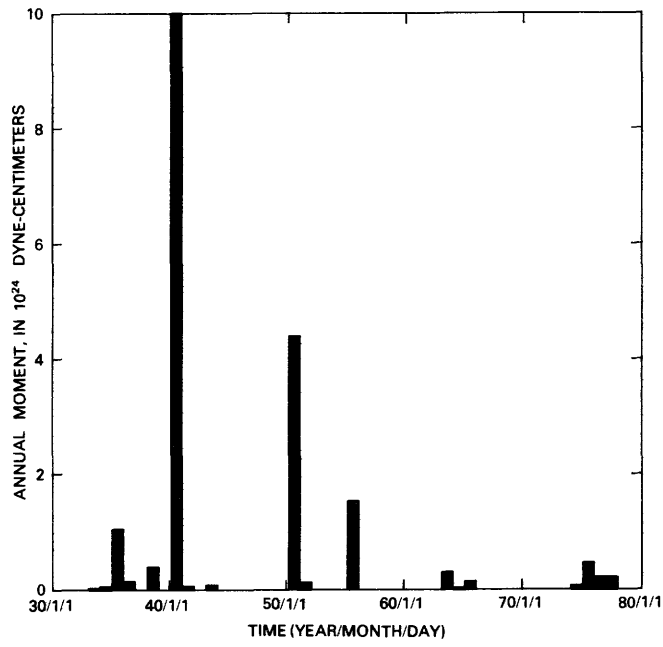

FIGURE 13.—Summed moment in Imperial Valley from 1932 to present. Seismic moment (M_0) is estimated from local magnitude (M_L), using relation $\log_{10} M_0 = 1.5M_L + 16$ (Thatcher and Hanks, 1973).

seismic zone, and subsequent activity moved progressively southward toward the epicentral region of the 1979 main shock. This movement is illustrated in a plot of effective slip (assuming a 5-km-thick seismogenic zone) along 10-km segments of the Brawley seismic zone for three consecutive periods of time (fig. 15). It is difficult to say whether the onset of paired swarms along the Imperial fault is related to southward migration of post-1940 seismicity or to seismicity precursory to the 1979 earthquake.

It seems reasonable to expect that the 1979 event should be followed by a period of quiet similar to that following the 1940 event. Because the seismic moment apparently is nearly tenfold smaller for the 1979 event, however, this quiet period may be substantially shorter than the 10 years that followed the 1940 event. As of early 1980, activity in the aftershock series appears to have fallen well below the level of activity before the 1979 earthquake, although it will be several more months before this decline can be verified.

PHYSICAL MODELS

Two physical models have been proposed for the earthquake swarm sequences in the Imperial Valley. The first, a kinematic model suggested by Hill (1977), holds that local spreading between offset strike-slip faults occurs on magma-filled dikes (or, more generally, fluid-filled cracks) penetrating brittle regions of the crust, and that the long axes of these dikes or cracks generally parallel the regional direction of maximum compression. (This direction in the Imperial Valley is

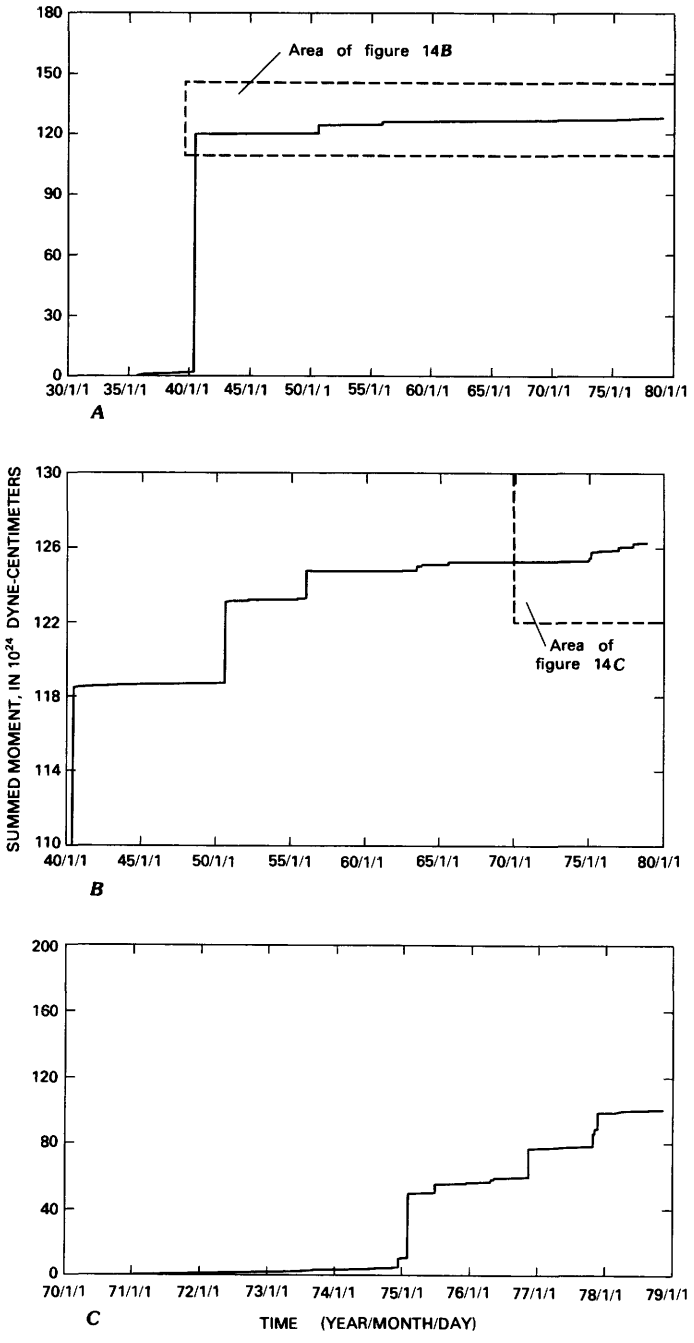

FIGURE 14.—Summed moment for Imperial Valley, calculated using relation of Thatcher and Hanks (1973). *A*, 1930 to 1979. *B*, 1940 to 1979. *C*, 1970 to 1979.

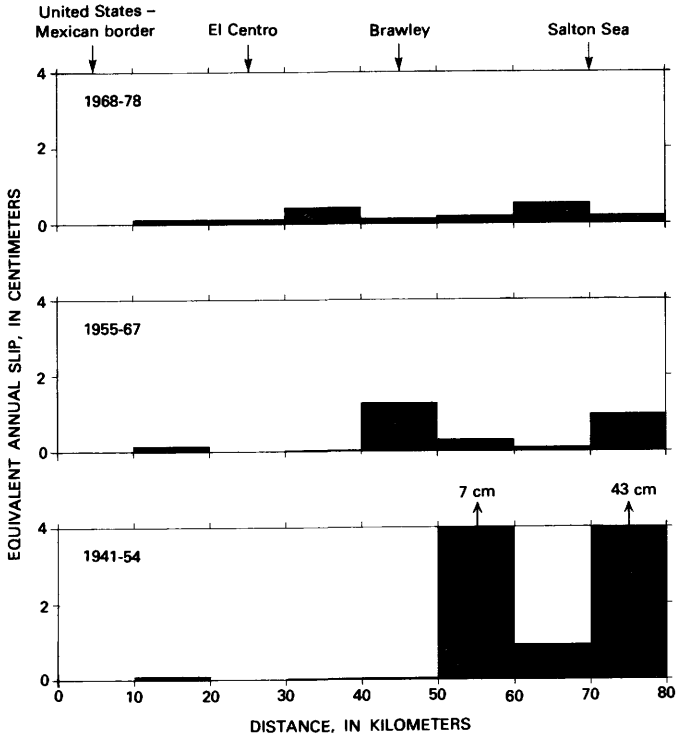

FIGURE 15.—Seismic moment summed in 10-km sections of Brawley seismic zone during three intervals bounded by triangulation surveys of geodetic network, as reported by Thatcher (1979). Seismic moment in each section is calculated from local magnitude, using relation of Thatcher and Hanks (1973), and plotted as equivalent slip on a fault surface 10 km long by 5 km deep. Distance is measured from lat 32.65° N., long 115.26° W.

presently slightly east of north.) Earthquake swarms occur as a result of series of shear failures along conjugate planes connecting adjacent tips of offset dikes (or cracks) as the fluid pressure within the dikes approaches the magnitude of least compressive stress in the brittle crust. This model is capable of accounting for many observed phenomena, including the podlike shape of the Brawley seismic zone (Weaver and Hill, 1978/79), the predominance of strike-slip fault-plane solutions, the occurrence of swarms on planes roughly perpendicular to the Imperial fault, and the tendency for events to cluster in time and space.

The second, a quasi-dynamic model proposed by Johnson (1979), holds that swarms are triggered by episodic creep events on the Imperial fault. Goulty and others (1978) have documented episodic creep on the Imperial fault at the surface in support of this model. A mechanism permitting both aseismic creep and earthquakes on the same fault was presented by Rice and Simons (1976) for a fluid-infiltrated elastic matrix. According to this mechanism, the magnitude of the driving stress determines whether creep or an earthquake will occur (lower driving stress favors creep). Thus, earthquake swarms are interpreted as due to creep episodes along the Imperial fault at depths of 3 to 6 km that induce a redistribution of interstitial-fluid pressure in the surrounding medium, which in turn induces a sequence of shear failures on faults within the regions of fluid-pressure increase. Thus, in some respects, swarms

can be thought of as aftershocks of aseismic creep, in much the same way that Nur and Booker (1972) related aftershocks to main-shock slip through pore pressure. In addition, this quasi-dynamic model can account for the nucleation of swarm clusters on the plane of the Imperial fault and the uniform progressive lateral expansion over time.

This model also appears able to explain the southward migration of swarm seismicity after the post-1940 quiet period. The Brawley seismic zone was in the dilatational-strain quadrant of the 1940 event, and a coseismic decrease in pore pressure should have occurred. This reduced pore pressure would have rendered the mechanism proposed by Rice and Simons (1976) ineffective until the pore pressure returned to nearly its previous levels. The return to elevated pore pressures would presumably be soonest where the coseismic static strains were lowest. Accordingly, the latest recovery would occur nearest the region of maximum fault slip.

We view these two models for swarm seismicity as, to a large extent, complementary. Both explain many aspects of Imperial Valley seismicity, and the time scales and spatial distributions of observed seismicity patterns argue for fluid-based processes common to both models.

CONCLUSION

Seismicity in the Imperial Valley since 1900 exhibits several intriguing characteristics that should facilitate an understanding of earthquake processes more generally. Tectonic changes in the Imperial Valley apparently are occurring at a rate measured in tens of years, and this pattern, if true, should provide a meaningful pattern of recurrence intervals, despite the brevity of the historical record. This relatively rapid pattern of change contrasts markedly with the slow changes in the gross seismicity of many other areas of southern California.

Recent observations of seismicity in the Imperial Valley have shown that earthquake swarms occur in bursts of activity that are discrete in both space and time. Migration of this activity can apparently be observed at many scales, from regional changes affecting much of the Imperial Valley to the growth of single planar features with dimensions of a few kilometers. The northern section of the Imperial fault appears to be capable of both surface rupture during major earthquakes and aseismic creep resulting in earthquake swarms.

Models proposed to explain the spatiotemporal aspects of Imperial Valley seismicity involve a fluid phase as the principal rate-controlling agent associated with the readjustment of stress. This fluid may be in both magma-filled dikes in the deeper crust and water- or brine-filled cracks and pore spaces at shallower depths. Earthquake-swarm occurrence is tied to changes in fluid pressure associated with magma injection at depth or episodic fault creep. The accumulated observations on the 1979 earthquake, many of which are presented in this volume, should lead to a deeper understanding of the physical processes of earthquake generation in the Imperial Valley.

REFERENCES CITED

Beal, C. H., 1915, The earthquake in the Imperial Valley, California, June 22, 1915: Seismological Society of America Bulletin, v. 5, p. 130–149.

Fuis, G. S., and Schnapp, Madeline, 1977, The November–December 1976 earthquake swarms in northern Imperial Valley, California: Seismicity on the Brawley fault and related structures [abs.]: Eos (American Geophysical Union Transactions), v. 58, no. 12, p. 1188.

Goulty, N. R., Burford, R. O., Allen, C. R., Gilman, Ralph, Johnson, C. E., and Keller, R. P., 1978, Large creep events on the Imperial fault, California: Seismological Society of America Bulletin, v. 68, no. 2, p. 517–521.

Hill, D. P., 1977, A model for earthquake swarms: Journal of Geophysical Research, v. 82, no. 8, p. 1347–1352.

Hill, D. P., Mowinckel, Penelope, and Lahr, K. M., 1975a, Catalog of earthquakes in the Imperial Valley, California: June 1973–May 1974: U.S. Geological Survey Open-File Report 75–401, 29 p.

Hill, D. P., Mowinckel, Penelope, and Peake, L. G., 1975b, Earthquakes, active faults, and geothermal areas in the Imperial Valley, California: Science, v. 188, no. 4195, p. 1306–1308.

Johnson, C. E., 1979, CEDAR—an approach to the computer automation of short-period local seismic networks; seismotectonics of the Imperial Valley of southern California: Pasadena, California Institute of Technology, Ph. D. thesis, 343 p.

Johnson, C. E., and Hadley, D. M., 1976, Tectonic implications of the Brawley earthquake swarm, Imperial Valley, California, January 1975: Seismological Society of America Bulletin, v. 66, no. 4, p. 1133–1144.

Lomnitz, Cinna, Mooser, Federico, Allen, C. R., and Thatcher, Wayne, 1970, Seismicity and tectonics of the northern Gulf of California region, Mexico. Preliminary results: Geofisica Internacional, v. 10, no. 2, p. 27–48.

Neumann, Frank, 1942, United States earthquakes, 1940: U.S. Coast and Geodetic Survey Serial 647, 74 p.

Nur, Amos, and Booker, J. R., 1972, Aftershocks caused by pore fluid flow?: Science, v. 175, no. 4024, p. 885–887.

Reichle, Michael, and Reid, Ian, 1977, Detailed study of earthquake swarms from the Gulf of California: Seismological Society of America Bulletin, v. 67, no. 1, p. 159–171.

Rice, J. R., and Simons, D. A., 1976, The stabilization of spreading shear faults by coupled deformation-diffusion effects in fluid-infiltrated porous materials: Journal of Geophysical Research, v. 81, no. 29, p. 5322–5334.

Richter, C. F., 1958, Elementary seismology: San Francisco, W. H. Freeman and Co., 768 p.

Thatcher, Wayne, 1979, Horizontal crustal deformation from historic geodetic data in southern Califoria: Journal of Geophysical Research, v. 84, p. 2351–2370.

Thatcher, Wayne, and Hanks, T. C., 1973, Source parameters of southern California earthquakes: Journal of Geophysical Research, v. 78, no. 35, p. 8547–8576.

Toppozada, T. R., Parke, D. L., and Higgins, C. T., 1978, Seismicity of California 1900–1931: California Division of Mines and Geology Special Report 135, 39 p.

Townley, S. D., and Allen, M. W., 1939, Descriptive catalog of earthquakes of the Pacific coast of the United States, 1769 to 1928: Seismological Society of America Bulletin, v. 29, no. 1, p. 1–297.

Weaver, C. S., and Hill, D. P., 1978/79, Earthquake swarms and local crustal spreading along major strike-slip faults in California: Pure and Applied Geophysics, v. 117, no. 1–2, p. 51–64.

CRUSTAL STRUCTURE OF THE IMPERIAL VALLEY REGION

By GARY S. FUIS, WALTER D. MOONEY, JOHN H. HEALEY,
GEORGE A. MCMECHAN, and WILLIAM J. LUTTER,
U.S. GEOLOGICAL SURVEY

CONTENTS

ABSTRACT

The U.S. Geological Survey conducted an extensive seismic-refraction survey in the Imperial Valley region during 1979. A total of 40 shots, ranging in size from 400 to 900 kg, were fired at seven shotpoints. Each shot was recorded by 100 portable seismic instruments arranged in profiles and arrays, with a typical instrument spacing of 0.5 to 1 km. More than 1,300 recording locations were occupied, and more than 3,000 usable seismograms were obtained.

We analyzed the data with a standard ray-tracing program adapted for interactive computing. This program permits rapid computation of traveltimes, so that a "best fitting" model can be determined by trial and error; as many as 50 models were tried for each profile.

In this chapter we report on our analysis of five profiles and present a contour map of reduced traveltimes from one shotpoint that was widely recorded in the Imperial Valley and on bordering mesas (shotpoint 1). In addition, we present a gravity model based on our new seismic structure for the Imperial Valley region. Analysis of these data reveals a deep (10–16 km) trough of sedimentary and metasedimentary rocks whose configuration tends to be an exaggerated version of the present topography in the Salton Trough. The deepest part of this trough approximately coincides with the zone of highest seismicity in the center of the valley, which we infer to be the location of present-day rifting. The trough is bounded on the west by a buried scarp that coincides in places with mapped faults, including the Superstition Hills and Superstition Mountain faults. In other places the scarp is apparently the buried expression of the rift that initiated formation of the Imperial Valley. On the east side of the Imperial Valley the thinning of the sedimentary rocks is more gradual; this boundary of the trough appears to differ significantly from the west boundary.

The velocity-depth functions determined for the Imperial Valley and bordering mesas, together with gravity data and geologic inference, can be used to infer rock composition and important details of the process by which the Imperial Valley was formed. In the center of the valley, near the United States-Mexican border, the velocity increases from 1.8 km/s near the surface to 5.65 km/s at a depth of 5.8 km, according to the relation $v=1.8+0.67z$ (km/s). At 5.8-km depth the gradient changes and the velocity increases more slowly (to 5.85 km/s at 10-km depth). At 10-km depth there is a discontinuity in both velocity and velocity gradient: the velocity jumps to 6.6 km/s and then rapidly increases to 7.2 km/s in a 1-km interval, followed by a very gradual increase with depth. No refractions from the M discontinuity were observed or expected in the distance range covered in this survey. The velocity-depth function on West Mesa differs significantly from the velocity-depth functions determined for the central valley. Starting with a value of 1.8 km/s, the velocity increases to 2.4 km/s at a depth of about 1.4 km, where there is a discontinuity. Below this discontinuity the velocity increases rapidly from 5.1 to 5.9 km/s in a 0.7-km interval, and then increases slowly with depth.

The depth at which the velocity gradient first decreases abruptly we term the "top of basement." An upper-basement velocity of 5.9 km/s on West Mesa is appropriate for crystalline rocks of granitic composition under sufficient pressure to close most cracks and microfractures. An upper-basement velocity of 5.65 km/s in the central valley is not characteristic of crystalline rocks. Therefore, we conclude that the Imperial Valley region is underlain by two different types of basement. Several lines of evidence lead us to infer that the basement under the central valley is metamorphosed sedimentary rocks. First, a velocity of 5.65 km/s is consistent with velocities determined in the laboratory for metasedimentary rocks of lower greenschist facies. Second, measurements made in deep (4 km) wells indicate that temperatures at basement depths (greater than 5 km in most places) are expected to exceed 300°C, at which point greenschist-facies metamorphism begins. Third, there is no observed reflection from a sediment/basement interface in the valley. Fourth, deep wells in the valley penetrate only the upper part of the known Cenozoic section for the region, implying a great thickness of underlying sedimentary material. Thus, the central valley is apparently underlain by a 10- to 16-km-thick section of sedimentary rocks (v less than 5.65 km/s) and metasedimentary rocks (v less than 5.85 km/s in most places) overlying mafic intrusive rocks (v greater than 6.6 km/s).

On a map of reduced traveltimes from shotpoint 1, areas of relatively early arrivals in the Imperial Valley correlate with five of the six major geothermal areas having reservoir temperatures higher than 150°C. The areas with the relatively earliest arrivals correlate with those geothermal areas containing the largest estimated heat reservoirs. This correlation probably reflects the presence of thermally metamorphosed sedimentary rocks and igneous intrusions. The traveltime map shows apparent connections between the Salton and Westmorland geothermal areas and between the Heber and East Mesa areas; the latter two areas appear to be right laterally offset across the Imperial fault.

Using our proposed velocity structure for the Imperial Valley region to constrain a gravity model, we discover that the layer of mafic intrusive rocks (model density, 3.1 g/cm^3), also referred to as subbasement, largely compensates for the low-density sedimentary rocks (model densities, 2.3–2.55 g/cm^3). The relatively flat gravity profile across the Salton Trough requires that the rapid variations in thickness of the low-density sedimentary rocks be compensated by variations in thickness of the high-density layer of mafic rocks at intermediate depths (greater than 10 km). The negative gravity anomalies over the Peninsular Ranges and the Chocolate Mountains require that the mafic layer deepen and (or) pinch out in those directions.

The plate-tectonic model for southern California can be further elaborated on from our studies. By drawing in an inferred boundary between crystalline continental crust and sedimentary fill, we can correlate idealized elements of this model with actual geologic structures. In particular, the San Jacinto and Elsinore faults appear to be active fracture zones that are northwestward extensions of the Imperial and Cerro Prieto transform faults, respectively. Part of the prominent buried scarp on the west side of the Imperial Valley appears to be a rift boundary that originated 60 km to the south in the Cerro Prieto geothermal area, an inferred spreading center, and moved northwestward between the Imperial-San Jacinto and Cerro Prieto-Elsinore faults.

INTRODUCTION

The Imperial Valley region of southeastern California is the birthplace of the San Andreas fault system, in the sense that the Imperial fault appears to be the structure along which most plate-boundary strain is transferred northward into two of the major fault branches of the San Andreas system—the San Jacinto and San Andreas (Banning-Mission Creek) faults. These faults are demonstrably linked in creep and strain behavior to the Imperial fault (Allen and others, 1972; Thatcher, 1979).

Dibblee (1954) summarized the geology of the Imperial Valley region. Kovach and others (1962) and Biehler and others (1964) published results from several short (less than 12 km long) seismic-refraction profiles in geographically separate areas of the Imperial Valley region, as well as results from a network of gravity measurements; their work provided the first accurate picture of the crustal structure of the Imperial Valley region. Lomnitz and others (1970) studied the seismicity of the northern Gulf of California and proposed a plate-tectonic model for the region, involving crustal spreading from small ridge segments connected by transform faults. Elders and others (1972) interpreted all the geologic, geophysical, and geodetic data on the region and elaborated on the model of Lomnitz and others. More recent studies of seismicity in the Imperial Valley (Hill and others, 1975; Johnson and Hadley, 1976; Fuis and Schnapp, 1977; Johnson, 1979) have delineated in detail active faults in the Imperial Valley and have emphasized the interplay between right-lateral strike-slip movement on the Imperial fault and various senses of movement on faults in the central and northern Imperial Valley, where crustal spreading appears to be occurring. Hill (1977) proposed a model for crustal spreading and earthquake-swarm generation that promises to be testable with seismic-refraction techniques. His model involves the intrusion of clusters of dikes parallel to the regional compression axis and implies a velocity anisotropy for the valley.

In this chapter we report on the results of an extensive seismic-refraction survey of the Imperial Valley region. This survey was undertaken to refine the crustal model used to locate earthquakes in the valley, and to study the seismic properties of active fault zones. A combination of new instrumentation and improved methods of analysis expedited our survey. The recent development of 100 self-contained seismic recording units capable of programmable turn-on, rapid deployment, and rapid field playback allowed extensive coverage of the Imperial Valley region with dense profiles and arrays. In addition, the adaptation of a standard method of ray tracing to interactive computing permitted testing and analysis of numerous models.

We summarize here the results of modeling five seismic profiles crossing the Imperial Valley region at different azimuths, and present a contour map of reduced traveltimes from our most widely recorded shotpoint. We also model an existing gravity profile across the region, using our seismic structure to provide new constraints. We infer rock compositions from our velocity-depth functions at selected places and apply these inferences, together with our structural results, to the plate-tectonic model for the region proposed by Lomnitz and others (1970).

DATA COLLECTION AND ANALYSIS

We conducted our seismic-refraction survey primarily during the period January–March 1979, although we gathered some additional data after the October 15 earthquake. During the primary survey, 40 shots, ranging in yield from 400 to 900 kg of high explosive, were detonated at seven shotpoints (fig. 16); each shot was recorded by 100 portable seismic instruments (see Blank and others, 1979). On a typical night the instruments were arranged in a line or pattern with instrument spacings of 0.5 to 1 km, and three shots were detonated. In all, more than 1,300 recording locations were occupied, and more than 3,000 usable seismograms were obtains.

The ray-tracing method described by Červený and others (1977) was adapted for interactive computing (R. L. Nowack, written commun., 1979). This program made possible rapid testing of models for traveltime consistency with the data and, in addition, permitted qualitative use of amplitudes to further constrain the models. The traveltimes and the amplitude behavior of first arrivals, wide-angle reflections, and multiple re-

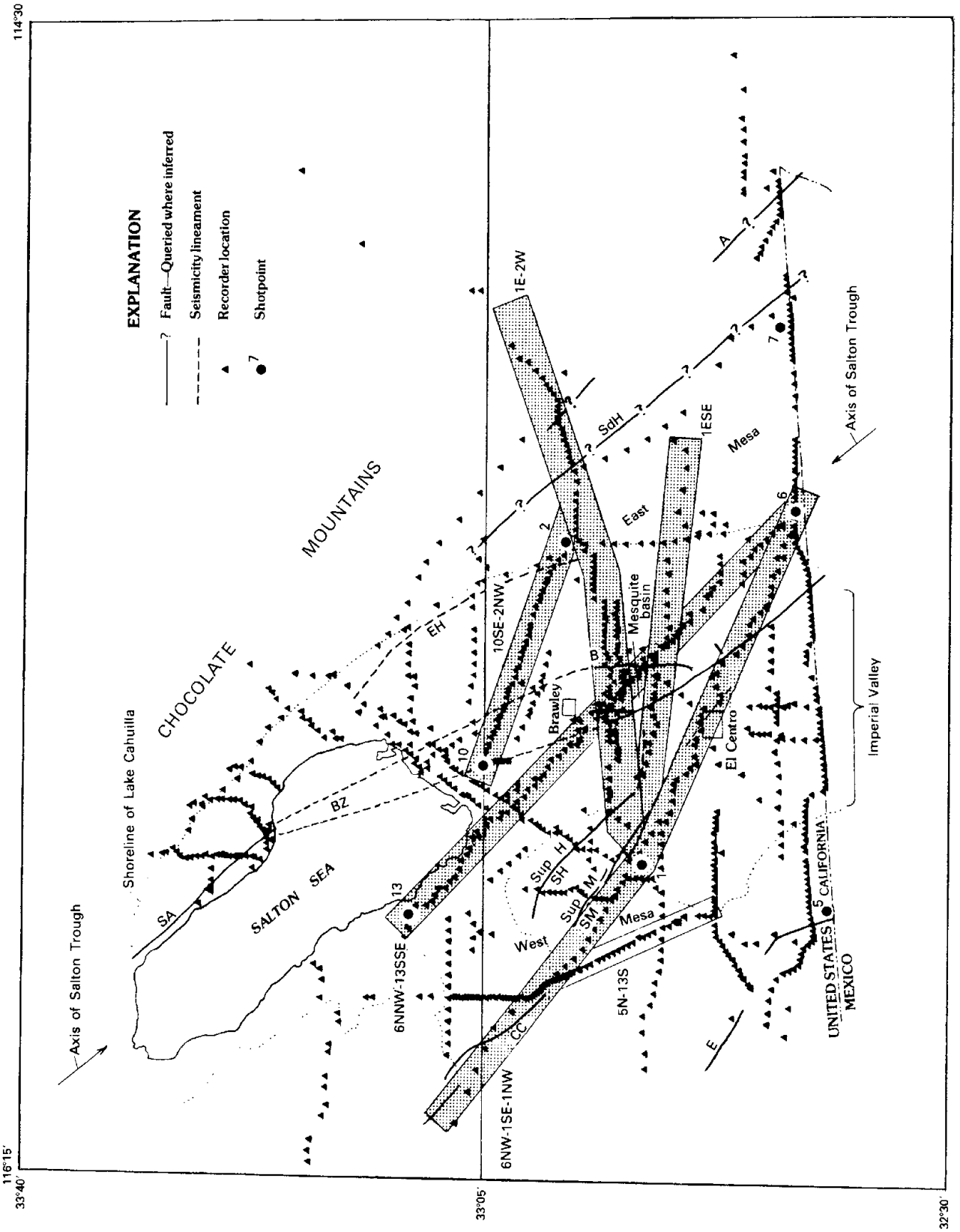

FIGURE 16.—Locations of shotpoints, recorders, and refraction profiles analyzed. Profiles modeled are indicated by outline and stipple; profile segment 5N–13S, indicated by outline only, is mentioned in text but not modeled. A, Algodones fault; B, Brawley fault zone; BZ, Brawley seismic zone (as defined by Johnson, 1979); CC, Coyote Creek fault; E, Elsinore fault; EH, East Highline Canal seismicity lineament; I, Imperial fault; SA, San Andreas fault; SdH, Sand Hills fault (?); SH, Superstition Hills fault; SM, Superstition Mountain fault; Sup H, Sup M, Superstition Hills, Sup M, Superstition Mountain.

fractions were fitted. The extra time constraints provided by the multiple refractions, and the sensitivity of these arrivals to lateral velocity changes, made them particularly useful in constraining the models.

Analysis of the five profiles reported here was split up among various combinations of the authors of this chapter. Except for agreement on the starting model at mutual shotpoints, the analyses were carried out more or less independently, although the models were largely patterned after that of Mooney and McMechan (this volume) for profile 6NNW–13SSE[1] (fig. 16), in which the structure is simple and amplitude ratios are used to provide additional constraints. As many as 50 models were tried for each profile. The final models are largely consistent with one another in places where consistency is expected, such as where they intersect or are adjacent. For example, where reversed profiles 6NNW–13SSE and 1E–2W intersect (figs. 17*A*, 17*C*), the velocity contours and structural boundaries to a depth of more than 5 km agree to within a few tenths of a kilometer, although deeper contours and boundaries diverge by as much as 1 km. The area of this intersection represents our best control on structure anywhere in the Imperial Valley region. We note that agreement between models near mutual shotpoints is not necessarily expected because these regions are unreversed, if sampled at all.

Several features of our models may reflect the specific capabilities of the computer program used to calculate ray paths through the models. A brief description of pertinent features of this program is needed here. The ray-tracing program permits us to construct two-dimensional models consisting of layers that vary laterally in velocity and thickness. The analyst may assign a linear vertical velocity gradient to each layer along arbitrary numbers of vertical gridlines (not shown). We note that if velocity gradients are assigned to a layer with an irregular horizontal variation, the boundaries between layers cannot be lines of constant velocity but rather lines at which the velocity gradient changes. We can envision changing these models by a tradeoff between the velocity gradient and the position of the layer boundaries. We believe that this tradeoff is not a serious ambiguity, although it certainly introduces some nonuniqueness.

Further uncertainties in a complex velocity structure may arise because the ray theory used does not include diffracted waves. This circumstance could present a problem in determining velocity gradients in the deeper horizons where the ray-theory approach demands a velocity increase with depth to bend the ray and return it to the surface, whereas a more complete wave theory might explain some arrivals as diffracted energy without requiring a velocity increase with depth. With these exceptions, we believe that the main features of our final models are approximately correct and will not be significantly changed by further work. Traveltimes generated by all models generally agree with the data to within 0.05 s and, in the worst case, to within 0.15 s. Both first arrivals and secondary phases are fitted by the models. (For a more complete description of the ray theory used here, see McMechan and Mooney, 1980.)

PROFILE MODELING

We modeled five profiles for the Imperial Valley region (fig. 16): one reversed profile along the axis of the Salton Trough[2] (profile 6NNW–13SSE; see also Mooney and McMechan, this volume), and four profiles across the Imperial Valley at various azimuths (profiles 6NW–1SE–1NW, 1ESE, 1E–2W, 10SE–2NW). We present here only the final models (figs. 17*A*–17*E*, 18); for a detailed description of the data and modeling procedures for these profiles, see the report by Fuis and others (1981). In the following discussion, we list and describe features of the models in the order of their occurrence from the surface downward.

1. All models have in common a section of sedimentary rocks (in one to three parts), a transition zone, a basement, and a subbasement.
2. The velocity in the sedimentary section increases continuously with depth without discontinuities but with changes in the velocity gradient. Velocity-depth curves also vary somewhat from place to place. In the Imperial Valley the velocity increases from 1.8 km/s at the surface to about 5 km/s at the base of the sedimentary rocks, at depths ranging from 2.5 to 4.8 km (figs. 17*A*–17*E*). The velocity gradient is generally lower (0.4–0.7 km/s/km) in the upper kilometer or so of these rocks, and steeper (0.7–1.8 km/s/km) in the lower part of the section. Along the axis of the Salton Trough, however, the gradient is more or less uniform (0.7 km/s/km) throughout the section (fig. 17*A*). One exception to this pattern occurs in the model for profile 1E–2W (fig. 17*C*) just east of shotpoint 1, where the velocity gradient is actually higher in the upper than in the lower part of the sedimentary section,

[1]Seismic lines constituting a profile are labeled from the shotpoints from which the lines originate and the azimuths of the lines: NNW, north-northwest; SSE, south-southeast; and so forth.

[2]We define the "axis of the Salton Trough" as the line that bisects the Salton Sea, projects southeastward on the same trend, and passes a few kilometers east of shotpoint 6 (fig. 16). We note that the topographic axis of the Imperial Valley diverges from the trough axis to the south; at the United States-Mexican border, it lies approximately 30 km west. We use the terms "Imperial Valley," "central Imperial Valley," and "central valley" to denote the cultivated lowlands south of the Salton Sea within the shorelines of ancient Lake Cahuilla. The term "Imperial Valley region" includes the Imperial Valley, the Salton Sea, East and West Mesas, and the flanking mountains.

possibly owing to structural complexity just east of the shotpoint. On West Mesa the velocity increases, with a gradient of 0.5 km/s/km, from 1.7 km/s at the surface to 2.4 km/s at the base of the sedimentary section (fig. 17*E*).

3. Contours of velocity generally dip toward the axis of the Salton Trough where they are well established in the regions between reversing shotpoints (figs. 17*B*, 17*C*, 17*E*).
4. The thickness of sedimentary rocks (velocity, less than about 5 km/s) along the axis of the Salton Trough ranges from about 4.8 km at the United States-Mexican border to 3.7 km along the southwest shore of the Salton Sea. An overall plunge of about 0.8° SE. is thus implied for the base of these rocks along the axis of the trough (fig. 17*A*). Across the trough between Brawley and El Centro, Calif., the sedimentary thickness changes rather abruptly from an average of about 1.4 km to West Mesa, through 4.5 km in the center of the Imperial Valley, to about 3 km on East Mesa. These changes in thickness occur at buried scarps near the shorelines of ancient Lake Cahuilla, which separate the valley from the mesas. The scarp on the west is sharp; the one on the east, gradual.
5. In the central Imperial Valley, smooth continuity of the traveltime curves from low (less than 5 km/s) to high (5.55–6.00 km/s) apparent velocities is modeled by a transition zone, 1 km thick, in which the velocity increases from about 5 km/s at the base of the sedimentary rocks to 5.65 km/s in most places in the upper part of the basement (see, for example, fig. 17*A*). The velocity gradient in this transition zone generally decreases slightly from that in the overlying rocks. On West Mesa and in other places where the sedimentary section is thinner than 2.5 km, a velocity discontinuity occurs at the top of this zone, and the zone is thinner (see, for example, fig. 17*E*).
6. The upper part of the basement has a velocity of about 5.65 km/s in the central Imperial Valley, on the basis of several reversed profiles; but on West Mesa its velocity is about 5.9–6.0 km/s, on the basis of a reversed-profile segment (5N–13S, fig. 16) and a time-term study by Hamilton (1970).
7. Several structures are evident that affect the basement and transition-zone boundaries as well as deeper velocity contours in the sedimentary rocks.

7(a). A scarp extends along the Imperial fault from at least 12 km southeast of El Centro to about 9 km

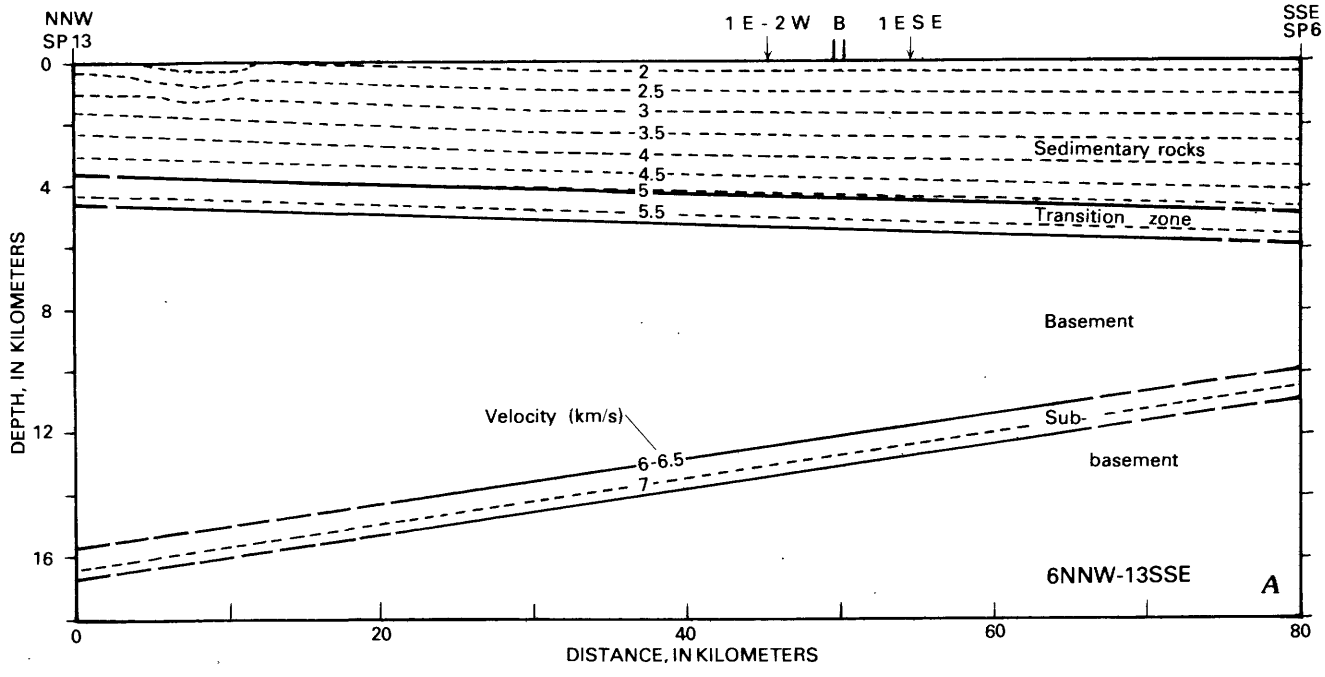

FIGURE 17.—Models for seismic-refraction profiles. *A*. 6NNW–13SSE (see also Mooney and McMechan, this volume); *B*, 10SE–2NW; *C*, 1E–2W; *D*, 1ESE; *E*, 6NW–1SE–1NW. Vertical exaggeration, ×2. Velocity boundaries (heavy lines; dashed where uncertain) are loci where velocity gradients can change but are not isovelocity contours (see text). Dashed lines are isovelocity contours (in kilometers per second); velocity-contour interval, 0.5 km/s. Shotpoints (SP) and geographic locations are indicated at top, as well as fault traces, seismicity lineaments, and points where other models intersect. See figure 16 for fault-name abbreviations. Profiles 10SE–2NW and 1E–2W intersect at shotpoint 2, profiles 1ESE and 6NW–1SE–1NW at shotpoint 1, and profiles 6NW–1SE–1NW and 6NNW–13SSE at shotpoint 6.

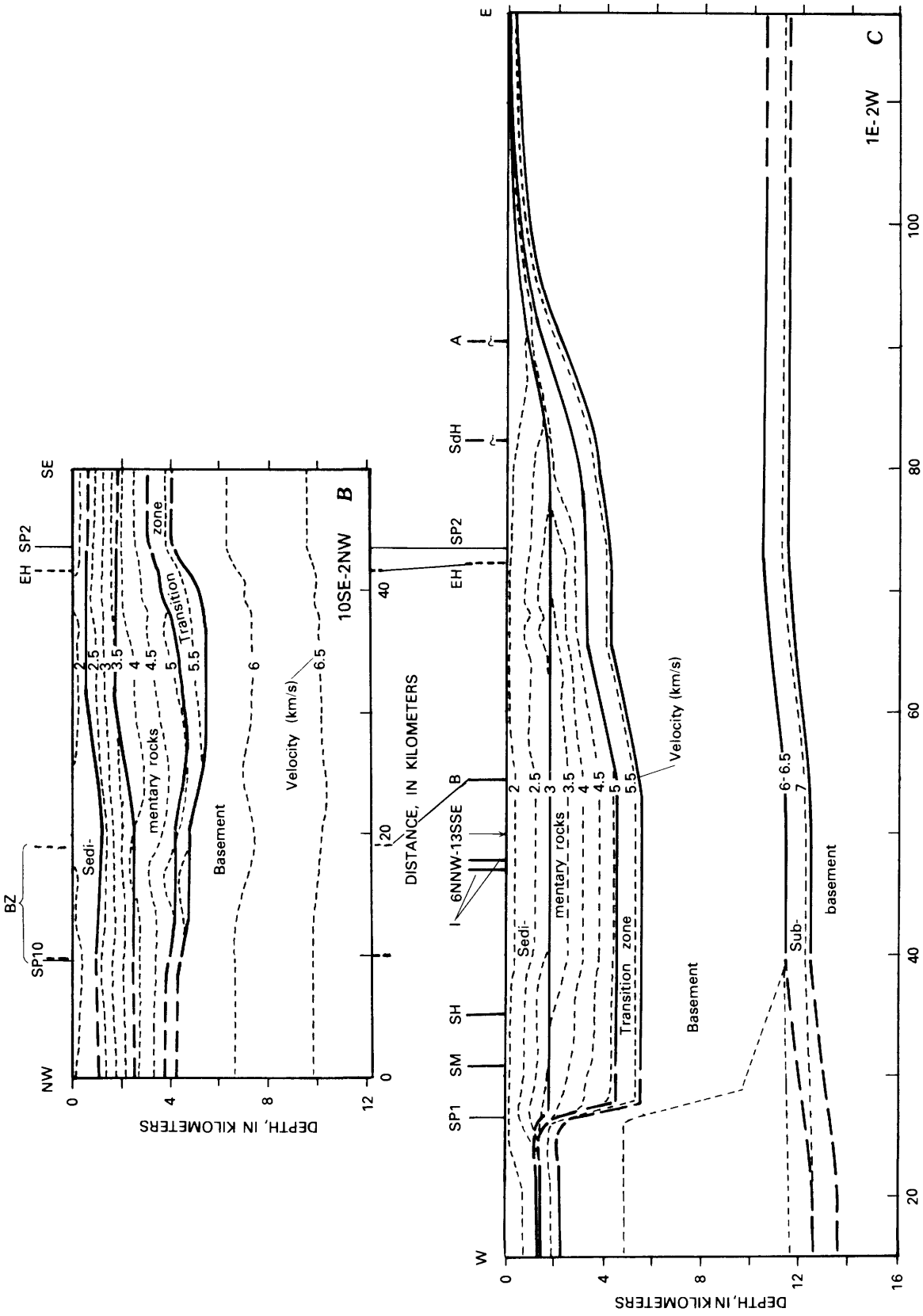

FIGURE 17.—Continued

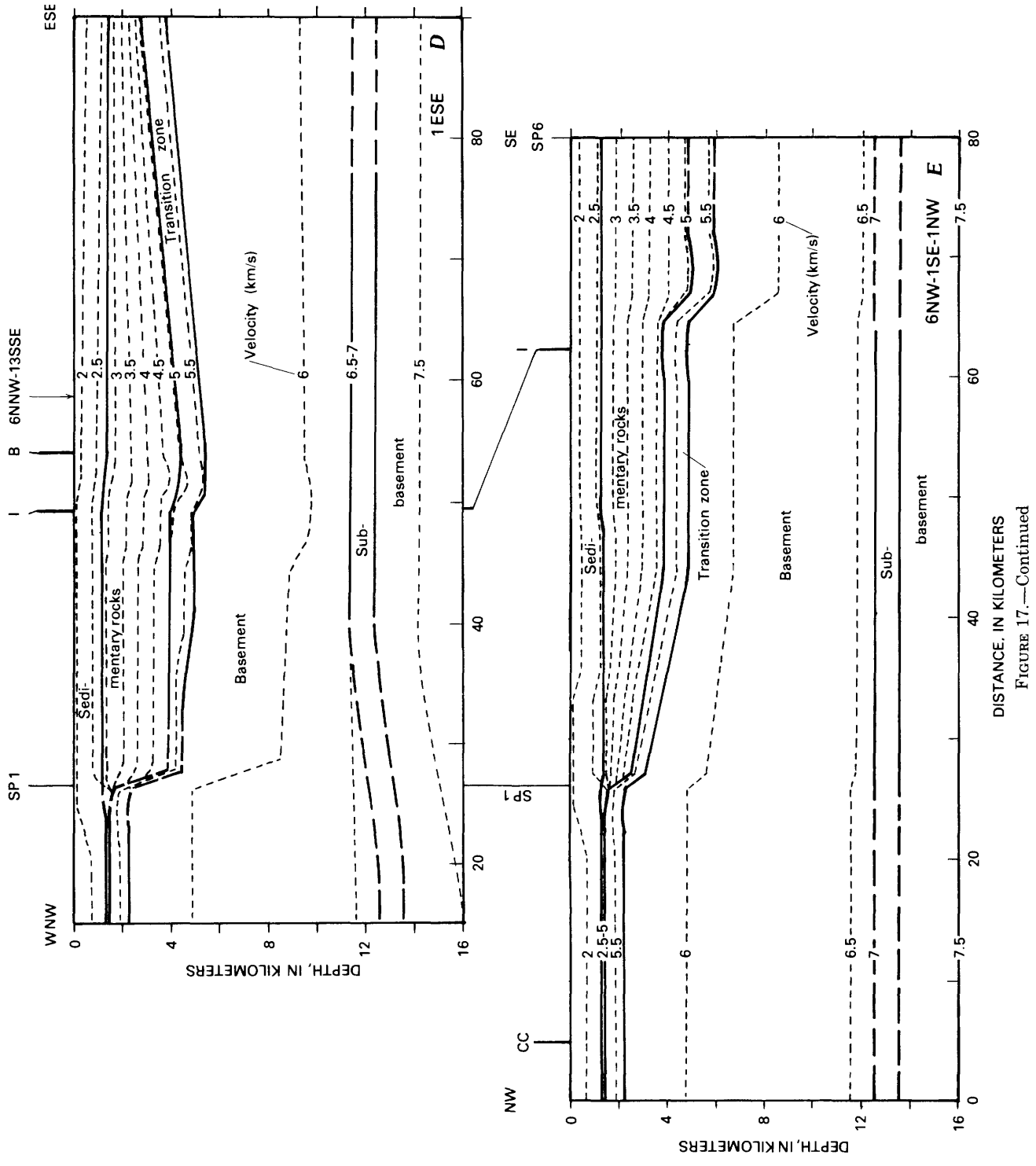

FIGURE 17.—Continued

north-northeast of El Centro (figs. 17*D*, 17*E*). Its height apparently decreases from about 1 km at the southeast end of this interval to less than 0.5 km at the northwest end. A dip on the fault of about 70° NE. fits the data at the southeast end, and a dip of 78° NE. fits the data at the northwest end; uncertainty in dip is estimated to be less than 10°. No scarp was detected across the fault where it splays out southwest of Brawley (fig. 17*C*). A decrease in velocity for waves passing through the fault zone was needed in the model for profile 1ESE (fig. 17*D*) and probably would have improved the fit in the

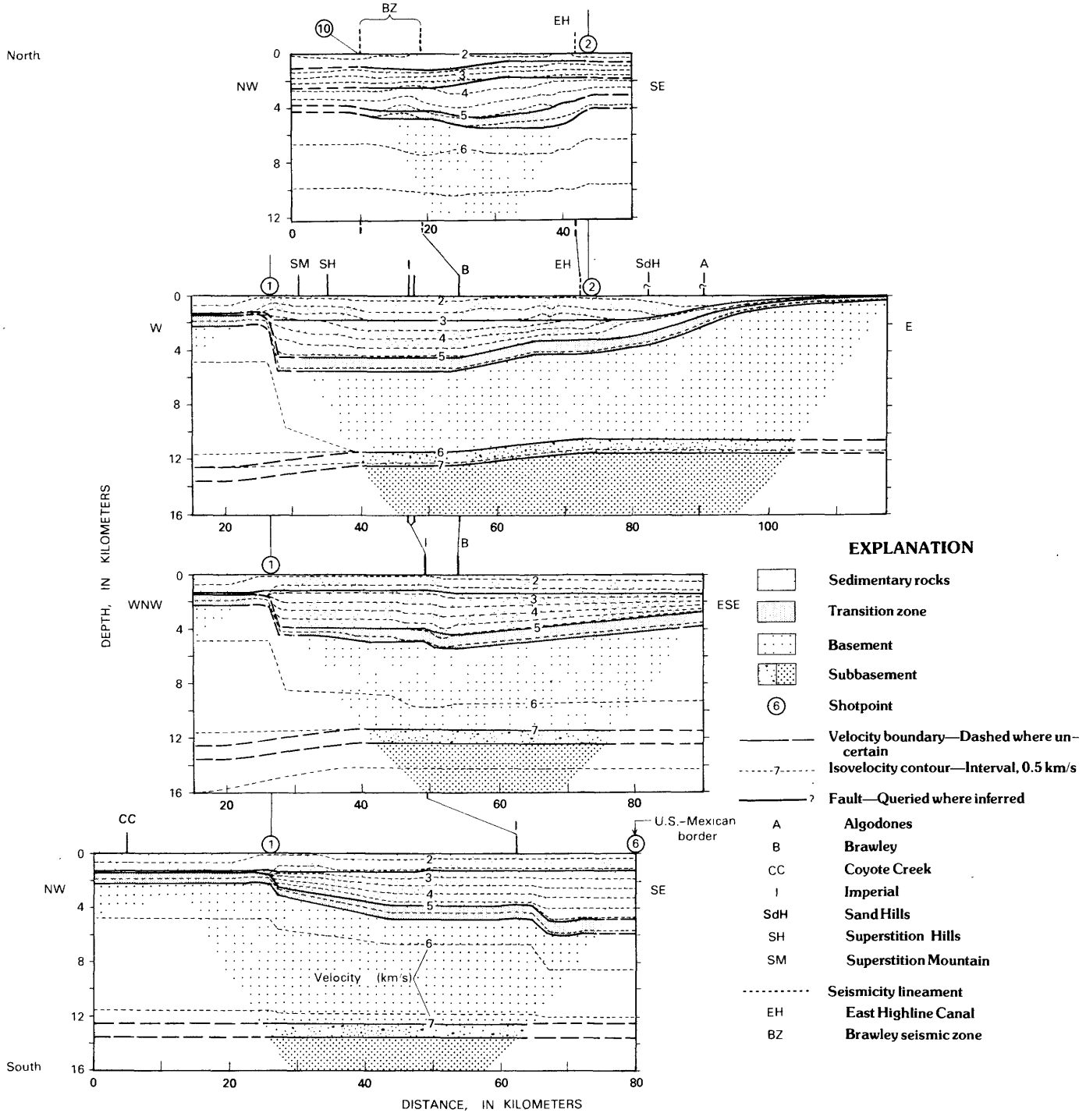

FIGURE 18.—Models for profiles across Imperial Valley (figs. 17*B*–17*E*), arranged to show integrated view of structure.

model for profile 6NW–1SE–1NW (fig. 17*E*).

7(b). In addition to the scarp along the Imperial fault, an anomalous "bump" in the velocity contours in the lower part of the sedimentary section 10 km north of Brawley (fig. 17*B*) correlates with the so-called Brawley seismic zone, defined by Johnson (1979) to include the band of seismicity connecting the Imperial and San Andreas faults.

7(c). A large scarp beneath shotpoint 1 is required because of the drastic difference in inferred depth to basement east and west of the shotpoint. The precise height, shape, and location of this scarp are more uncertain than most features in the models because, in the absence of any sharp reflection from the basement under shotpoint 1, no direct information on this feature is returned to the surface from this shotpoint. In fact, only shotpoint 6 (fig. 17*E*) samples this feature, and sparsely at that. Scarp height appears to increase from 1 km at an azimuth southeast of shotpoint 1 (fig. 17*E*), to 3.5 km at an azimuth east to northeast of shotpoint 1 (fig. 17*C*). East and northeast of the shotpoint, the scarp may be associated with the Superstition Mountain fault. Southeast of the shotpoint, the scarp appears to be part of a north-south-trending bench on basement and transition-zone rocks that does not correlate with any structure mappable at the surface (see discussion of traveltime-contour map below).

7(d). There are no conspicuous scarps in the models along other mapped faults, although the Brawley fault zone and the Sand Hills and Algodones faults(?) appear to correlate with changes in slope on basement and transition-zone rocks (figs. 17*C*, 17*D*).

8. An important discovery from our refraction survey is the existence of a subbasement with a velocity of 7.2 km/s near its top at depths ranging from 10 to 16 km under the Imperial Valley. Evidence for this subbasement appears on all profiles longer than about 40 km (figs. 17*A*, 17*C*–17*E*). Strong to weak second arrivals at distances beginning between 25 and 40 km are followed by crossovers at distances between 40 and 55 km to branches having apparent velocities of 7.2 to 8.5 km/s. This subbasement can be modeled by a velocity discontinuity separating the lower part of the basement (5.85–6.6 km/s) from the upper part of the subbasement (6.6–7.0 km/s). Below this discontinuity is a 1-km-thick zone of relatively rapid velocity increase to 7.2 km/s.

9. The topography of the subbasement, though of great importance to a tectonic framework for the Imperial Valley region, is difficult to resolve. An apparent dip of 4.5° NW. is indicated in the model for profile 6NNW–13SSE (fig. 17*A*), and the depth to subbasement is projected to be 10 km at the United States-Mexican border and nearly 16 km along the southwest shore of the Salton Sea. However, the depth to subbasement appears to decrease somewhat to the north in the models for profiles 6NW–1SE–1NW, 1ESE, and 1E–2W (figs. 17*C*–17*E*, 18). The greatest disagreement between the model for profile 6NNW–13SSE and other models where they intersect is about 1 km at the intersection of profiles 6NNW–13SSE and 1E–2W (figs. 17*A*, 17*C*). Thus, we estimate our uncertainty in resolving depth to subbasement at 1 km. Combining our best information on the depth to subbasement, we might plot only depths at the points for critical reflection on the different profiles. The picture that emerges is of a dome on the subbasement 11 km deep in the region between Brawley and El Centro. This dome has a relief on its south side of a little more than 1 km, an amount barely resolvable, and on its north side of 5 km. In addition, gravity modeling (see below) indicates an abrupt deepening of the subbasement under West Mesa and a more gradual deepening under East Mesa. Thus, the region of convergence of the Imperial and San Jacinto faults and the Brawley seismic zone would appear to be a subbasement high, although we emphasize that the south closure on this dome is barely resolvable.

TRAVELTIME-CONTOUR MAP

A contour map of reduced traveltimes from shotpoint 1 (fig. 19), our most widely recorded shotpoint, is roughly equivalent to a sediment-isopach map on which greater reduced traveltime correlates with greater sedimentary thickness. Although this map is difficult to interpret quantitatively because of structural complexity beneath shotpoint 1, qualitatively it reveals several intriguing features.

1. The map mirrors surficial topography, in that a "ridge" of high reduced traveltimes corresponds to the Imperial Valley and a "valley" of low reduced traveltimes corresponds to topographically higher West Mesa. The "ridge" reflects the trough of sedimentary rocks that underlie the valley. We note that an arrival at the surface corresponds to a ray leaving the basement several kilometers closer to the shotpoint. When we take into account this radial displacement (6–8 km in the center of the valley) of features on the map from basement features to which they might correspond, we see that the "ridgecrest," or locus of greatest sedimentary thickness, corresponds fairly accurately to the seismogenic belt in the valley, the Brawley seismic zone of Johnson (1979). The "valley" of low reduced

traveltimes on West Mesa corresponds to the relatively thin veneer of sedimentary rocks in that area.

2. A steep gradient in the contours separates the "ridge" from the "valley." Southeast of shotpoint 1 this steep gradient trends roughly north-south and is interpreted to correspond to a buried scarp with this same trend. This scarp is visible beneath shotpoint 1 in the model for profile 6NW–1SE–1NW (fig. 17*E*). North of shotpoint 1 this gradient is deflected successively along the Superstition Mountain and Superstition Hills faults, probably reflecting buried scarps along these faults. The inferred scarp along the Superstition Mountain fault is visible beneath shotpoint 1 in the model for profile 1E–2W (fig. 17*C*). Steep gradients are also associated with the Coyote Creek fault, the northwest margin of the Superstition Hills, and the Elsinore fault. In addition, northeast-trending lows and highs in reduced traveltimes that occur between the Elsinore and San Jacinto fault zones correspond to an inverse topography on the basement that probably represents northeast-trending horsts and grabens in that area (R. V. Sharp, oral commun., 1980).
3. Subtle "valleys" and "saddles," as long as 15 km and with relief as great as 0.3 s, indent the central "ridge" in northeasterly directions. These features correlate with five of the six known geothermal areas in the Imperial Valley having reservoir temperatures higher than 150°C (see Renner and others, 1975; Brook and others, 1978). The strongest features correlate with areas containing the largest estimated heat reservoirs. The traveltime map shows an apparent connection between the Salton and Westmorland areas and be-

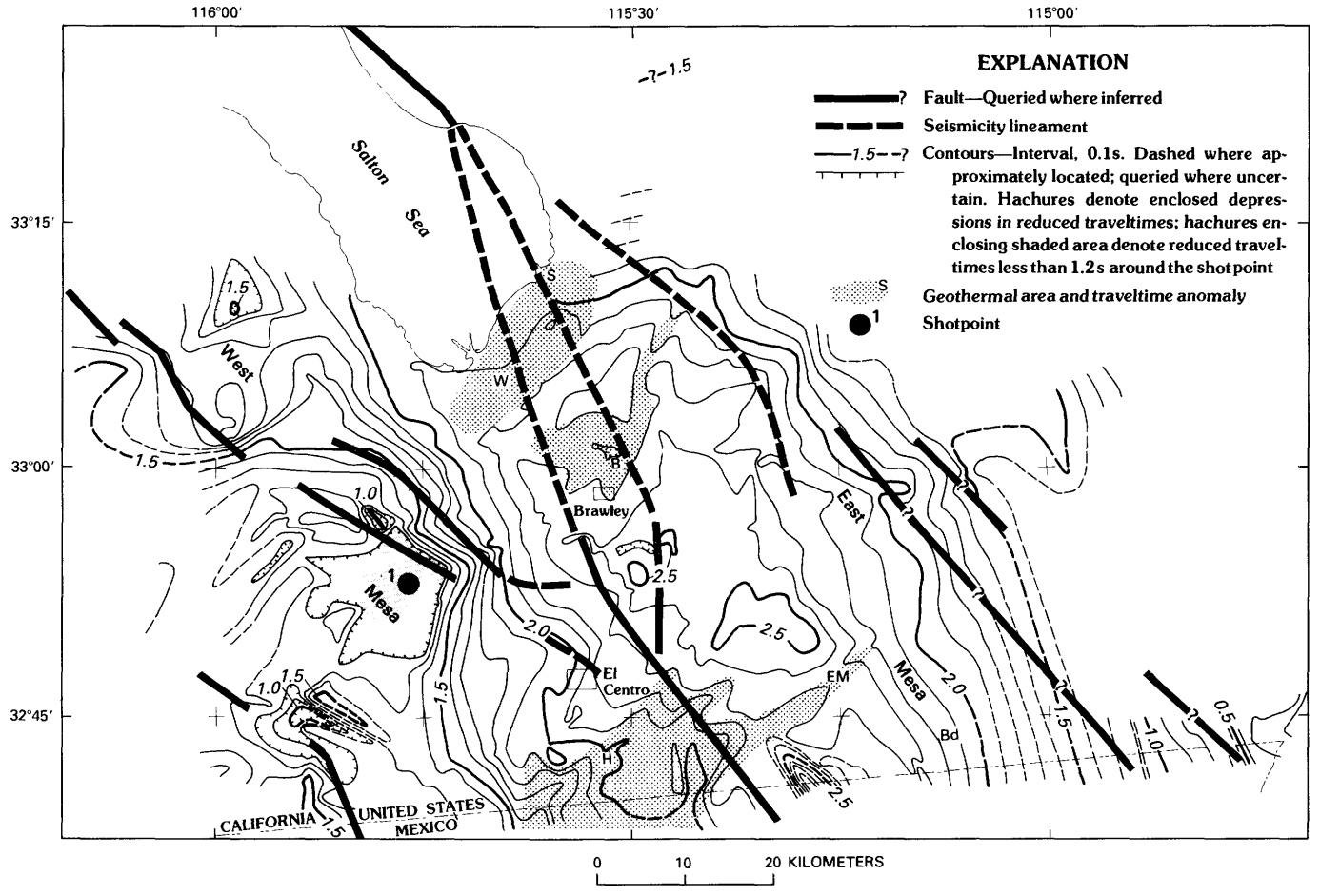

FIGURE 19.—Contour map of reduced traveltimes for first arrivals from shotpoint 1; reducing velocity, 6 km/s. Faults shown are same as in figure 16. Geothermal areas shown are those with reservoir temperatures greater than 150°C: B, Brawley; Bd, Border; EM, East Mesa; H, Heber; S, Salton Sea; W, Westmorland. Map is approximately similar to sediment-isopach map on which greater reduced traveltime correlates with greater sedimentary thickness.

tween the Heber and East Mesa areas; the latter two appear to be right laterally offset across the Imperial fault.

GRAVITY MODEL

Our velocity structure for the Imperial Valley region can be used to constrain an interpretation of the gravity data. To illustrate this point, we have made a preliminary interpretation of a gravity profile extending from the coast near San Diego, Calif., across the Peninsular Ranges and the Salton Trough, into the Chocolate Mountains. The data are from Oliver and others (1980), and the profile was selected to cross the Imperial Valley in an approximately east-westerly direction and pass approximately through shotpoint 1 (fig. 20).

The important new facts from our refraction data that bear on the gravity interpretation include a more detailed description of the distribution of sedimentary rocks, as well as evidence for a subbasement, a layer of probable basaltic composition (see below), at intermediate depths. An inspection of the gravity profile shows a marked anomaly associated with the Peninsular Ranges, probably caused by a thickening of the granitic crust. The gravity profile, however, is relatively flat across the Salton Trough, and there is no evidence for any anomaly associated with the thick sedimentary rocks (model densities, 2.3 and 2.55 g/cm^3) in the Imperial Valley. When we calculate the gravity effect of these sedimentary rocks and subtract it from the observed gravity, we obtain a pronounced anomaly of approximately 50 mGal with a steep gradient along the west margin of the Imperial Valley that is associated with the scarp revealed by the refraction data. This calculated gravity anomaly is difficult, if not impossible, to remove by varying the depth to the mantle (model density, 3.32 g/cm^3) but can be easily removed by varying the depth to the shallower subbasement, or intermediate layer (model density, 3.1 g/cm^3). We find that to match the observed gravity profile, the upper surface of this intermediate layer must largely mirror the contact between sedimentary rocks and basement (basement model densities, 2.75 g/cm^3 for crystalline rocks and 2.65 g/cm^3 for metasedimentary rocks); an abrupt deepening of this layer at the west margin of the Imperial Valley is required to compensate for the observed scarp on the basement above it (fig. 20*B*). In addition, the negative gravity anomalies over the Peninsular Ranges and the Chocolate Mountains require that the inter-

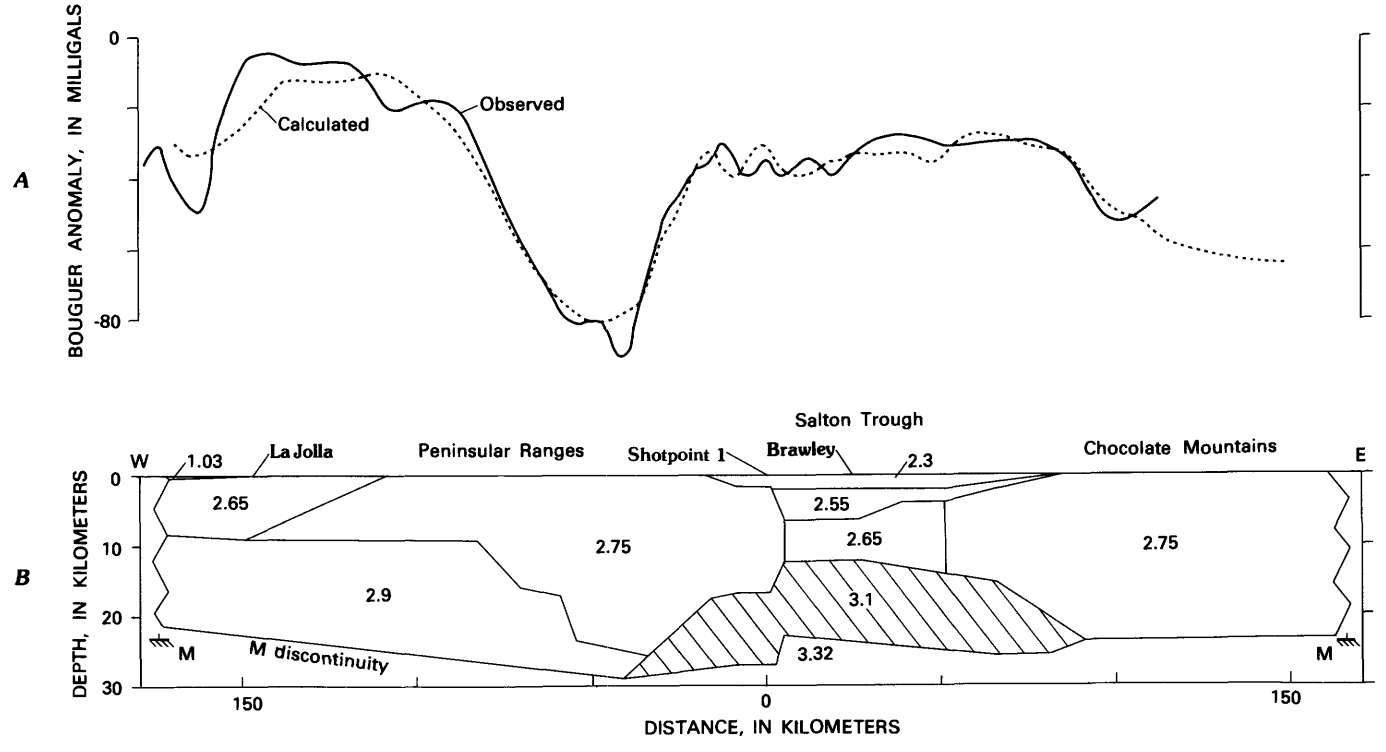

FIGURE 20.—Cross section east-northeastward across California from La Jolla to Chocolate Mountains. *A*, Gravity profile. *B*, Model, where numbers are densities (in grams per cubic centimeter). Subbasement (hachured area; density, 3.1 g/cm^3) beneath Salton Trough, a feature absent in previous gravity models for Imperial Valley region, provides most of gravitational compensation for sedimentary rocks (densities, 2.3 and 2.55 g/cm^3) and inferred metasedimentary rocks (density, 2.65 g/cm^3). Horizontal part of small rake symbol labeled "M" indicates Moho depth determined by seismic refraction.

mediate layer deepen and (or) pinch out in those directions.

In our model, we show the mantle at a minimum depth of 23 km under the Imperial Valley and some variation in the depth to mantle under the Salton Trough. These depths are not constrained by seismic data for the mantle, and the current interpretation of the gravity data is not unique regarding depth to mantle or structure of the crust-mantle boundary.

VELOCITY-DEPTH CURVES

Our models agree well with the earlier results of Kovach and others (1962), Biehler and others (1964), and Hamilton (1970) if we take into account that these researchers did not have interpretational tools to calculate models with velocity gradients or lateral velocity changes. Our observations of apparent velocities are similar to those of Kovach and others (1962) when compared on a histogram (fig. 21). Similar broad clusters of apparent velocities are seen to peak between 1.8 and 2.6 km/s and between 5.4 and 6.2 km/s on the histograms for both data sets, and there is no strong indication of grouping between these two clusters or beyond 6.2 km/s. In our models these two clusters are represented by layers of relatively low velocity gradient, namely, the uppermost part of the sedimentary section and the basement (fig. 22; table 2). Our interpretation of relatively high velocity gradients in the region between these two layers is certainly not contradicted by the relatively even spread in apparent velocities between the two clusters on the histograms. Comparing our interpretation for the central Imperial Valley with that of Biehler and others (1962), it is clear that our curve, showing a continuous increase in velocity with depth, is largely an average of their curve, showing a stepwise increase with depth (fig. 23). We note that the 6.4-km/s basement velocity in their model is an apparent velocity from an unreversed branch on a profile north of Brawley, Calif. The scatter in apparent velocities higher than 7.0 km/s (fig. 21*B*) is accounted for in our models by an irregular upper surface on the subbasement, of velocity 7.2 km/s, and considerable structure in the layers above.

Our velocity-depth curves (fig. 22; table 2) can, in principal, be checked against well velocity surveys, at least for the upper part of the sedimentary section. At present we have access to a velocity survey from only one well, the Grupe-Engebretson well (Kovach and others, 1962; Biehler and others, 1964), drilled 11 km northwest of shotpoint 6 to a depth of about 3.75 km. Referring to the nearest point on our profile, 6NNW–13SSE (fig. 17A), we see that this well penetrated below the calculated depth of the 4-km/s contour. The well was surveyed for velocity to 2.5 km and yielded a velocity-depth relation of $v(z)=1.80+0.67z$ (km/s), where z is the

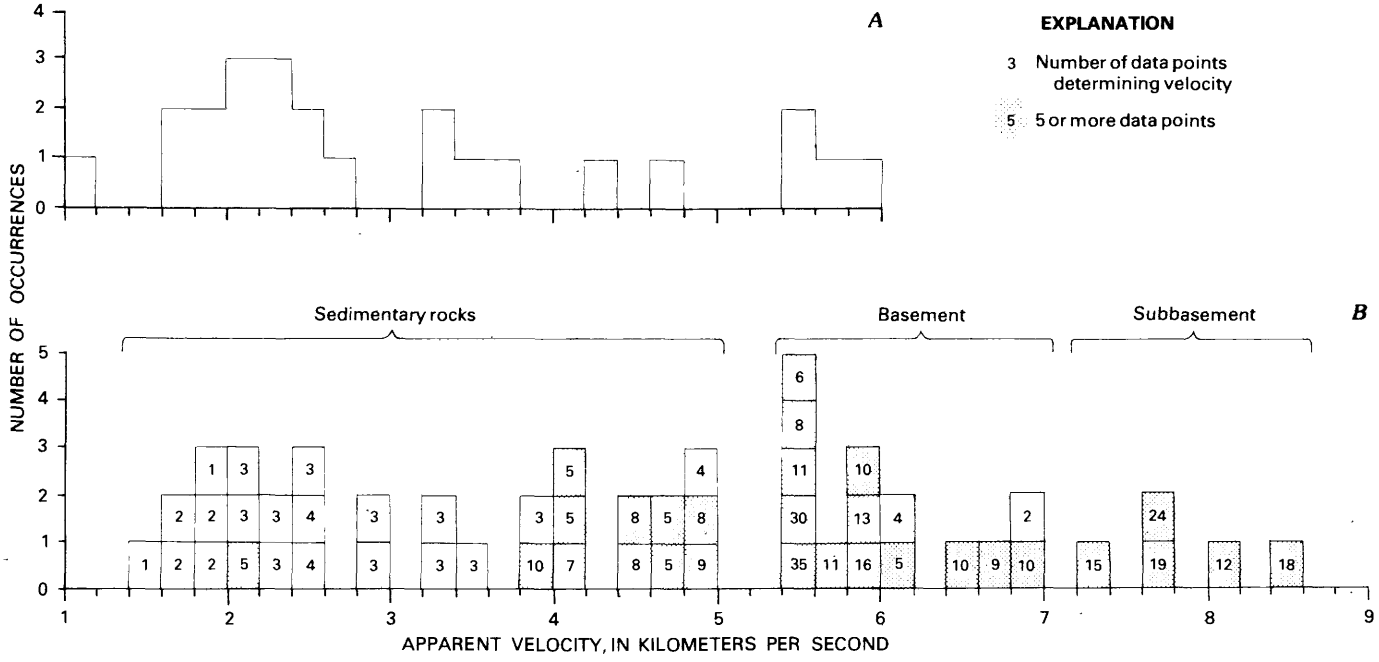

FIGURE 21.—Frequency distribution of apparent velocities. *A*, Data from Kovach and others (1962), shown for comparison. *B*, Data from this study. Geologic units to which intervals of apparent velocity generally apply are indicated above braces. Subbasement velocities, which are more interpretative than others shown, were determined from long average lines fitted through arrivals that were generally either difficult to pick (second arrivals) or emergent (first arrivals).

depth (in kilometers), which compares well with our relation at this point on the profile of $v(z)=1.80+0.67z$ (km/s).

The velocity-depth curves (fig. 22) are roughly similar to one another except for some locations along profile 6NW–1SE–1NW (SP1 to SP 6, fig. 22). In most places, a relatively high velocity gradient above a depth of 4–5 km is followed at greater depth by a relatively low velocity gradient, with a transitional region about 1 km thick in between within which the gradient is intermediate. This velocity structure reflects sedimentary rocks overlying basement, with an intervening transition zone. We note that the velocity of the upper part of the basement is considerably less than 6 km/s.

On profile 6NW–1SE–1NW on West Mesa, the velocity-depth curve is quite different (SP1 to SP6, −1, fig. 22). A sedimentary section 1½ km thick overlies the basement, and there is a marked velocity discontinuity between them; the upper part of the basement (below a thin transition zone) has a velocity of nearly 6 km/s. A basement velocity of nearly 6 km/s agrees with the results of Hamilton (1970), who studied a somewhat larger region than we did on the west flank of the Salton Trough. This velocity is also consistent with velocities determined in the laboratory for felsic igneous and metamorphic rocks (Birch, 1960) similar to those exposed on West Mesa and encountered in wells penetrating the sedimentary rocks in that area (Don Lande, oral commun., 1980). Along profile 6NW–1SE–1NW southeast of shotpoint 1 (SP1 to SP6, 1, 17, 53, fig. 22), a change in velocity-depth structure occurs, from the structure shown for West Mesa to a structure typified by most of the rest of the velocity-depth curves for the Imperial Valley. Most of this change appears to occur within a few kilometers of shotpoint 1, southeast of the major scarp evident in our model (fig. 17*E*) and on our traveltime-contour map (fig. 19). Importantly, the upper-basement velocity changes from 5.9–6.0 km/s on

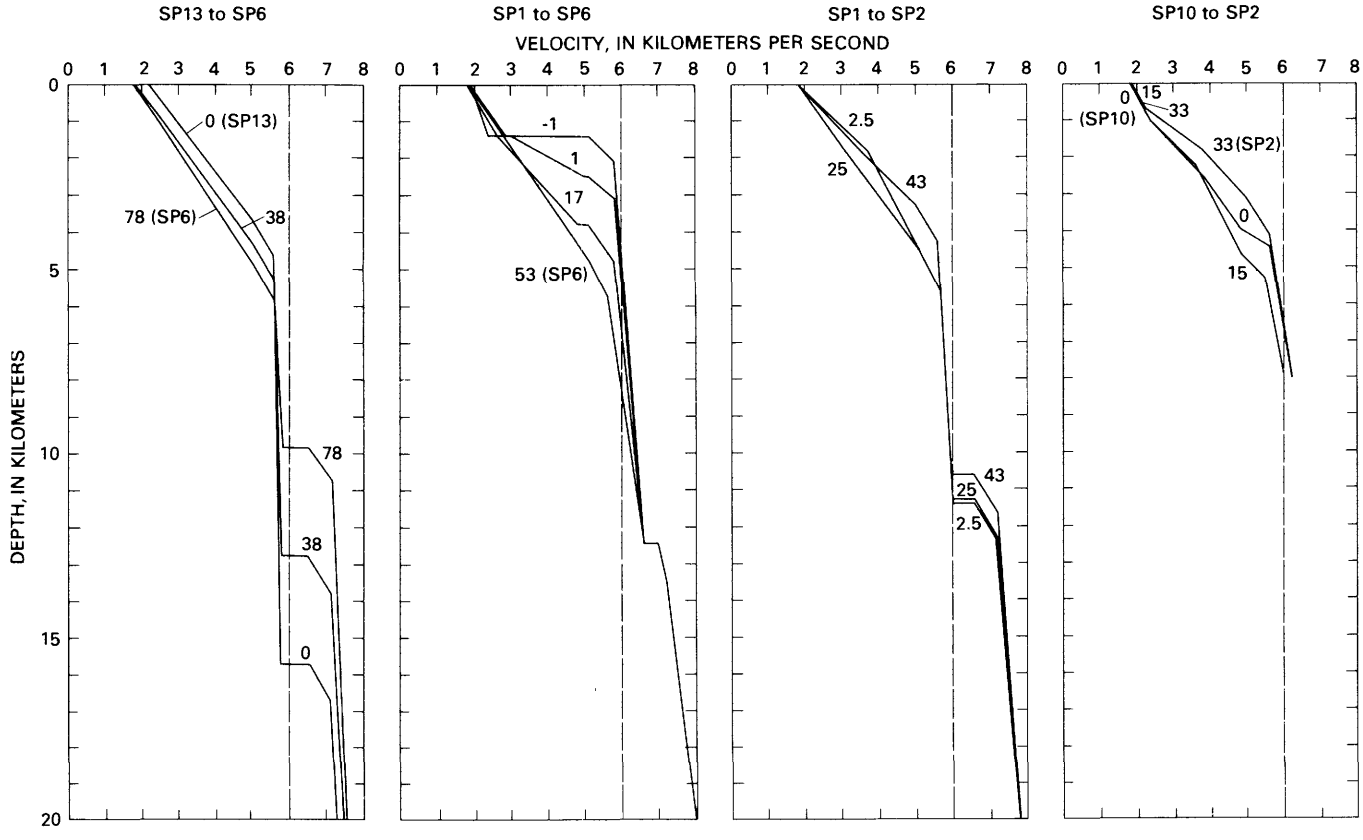

FIGURE 22.—Velocity as a function of depth at selected places along profiles modeled in figure 17. Numbers on curves indicate distance (in kilometers) southeast or east of first-named shotpoint (SP) on respective plot. Dashed vertical line at 6 km/s is for reference. Note that velocity at points where velocity gradients first decrease abruptly, which is uppermost part of basement, at depths of 4 to 6 km in most places, is considerably less than 6 km/s except at locations −1 and 1 on SP1 to SP6. We interpret these relatively low upper-basement velocities to correspond to metasedimentary rocks in Imperial Valley. Location −1 on SP1 to SP6 is on West Mesa, where evidence from outcrops and wells penetrating sedimentary rocks indicates that upper part of basement, corresponding to velocity greater than 5.8 km/s, is igneous and metamorphic (crystalline) rocks.

TABLE 2.—*Velocity above and below model boundaries at locations of velocity-depth curves in figure 22.*

[Velocity-depth curves in figure 22 were constructed from values listed here. Curve numbers, which are same as in that figure, indicate distance (in kilometers) southeast or east of first-named shotpoint (SP) in respective section of table. Double slant between two velocities indicates discontinuity; slant preceded or followed by dash indicates top or bottom of model, respectively.]

Depth to boundary (km)	Velocity above/below boundary (km/s)	Inferred geologic unit
SP13 TO SP6		
Curve 0 (SP13), lat. 33°10.6′ N., long 115°52.4′ W.		
0.0	—/2.2	
3.68	5.0/5.0	Sedimentary rocks.
4.68	5.65/5.65	Transition zone.
15.78	5.85//6.6	Basement.
16.68	7.2/7.2	
20.0	7.4/—	Subbasement.
Curve 38, lat 32°57.1′ N., long 115°34.0′ W.		
0.0	—/1.8	
4.33	5.05/5.05	Sedimentary rocks.
5.33	5.65/5.65	Transition zone.
12.82	5.85//6.60	Basement.
13.82	7.2/7.2	
20.0	7.51/—	Subbasement.
Curve 78 (SP6), lat 32°41.7′ N., long 115°15.1′ W.		
0.0	—/1.8	
4.95	5.1/5.1	Sedimentary rocks.
5.95	5.65/5.65	Transition zone.
9.84	5.85//6.60	Basement.
10.74	7.2/7.2	
20.0	7.58/—	Subbasement.
SP1 TO SP6		
Curve 1, lat 32°53.4′ N., long 115°46.8′ W.		
0.0	—/1.9	
1.2	2.3/2.3	Sedimentary rocks.
1.4	2.35//5.1	Transition zone.
2.1	5.8/5.8	Basement.
12.5	6.6//7.0	
13.5	7.2/7.2	
20.0	8.0/—	Subbasement.
Curve 1, lat 32°52.9′ N., long 115°45.7′ W.		
0.0	—/1.9	
1.3	2.8/2.8	Sedimentary rocks.
2.5	5.0//5.1	Transition zone.
3.1	5.8/5.8	Basement.
12.5	6.6//7.0	
13.5	7.2/7.2	
20.0	8.0/—	Subbasement.
Curve 17, lat 32 49.3′ N., long 115 37.1′ W.		
0.0	—/1.8	
1.3	2.6/2.6	Sedimentary rocks.
3.8	4.8//5.1	Transition zone.
4.8	5.8/5.8	Basement.
12.5	6.6//7.0	
13.5	7.2/7.2	
20.0	8.0/—	Subbasement.
Curve 53 (SP6), lat 32 41.7′ N., long 115°15.1′ W.		
0.0	—/1.8	
1.2	2.6/2.6	Sedimentary rocks.
4.75	5.1/5.1	Transition zone.
5.75	5.6/5.6	Basement.
12.5	6.6//7.0	
13.5	7.2/7.2	
20.0	8.0/—	Subbasement.

Depth to boundary (km)	Velocity above/below boundary (km/s)	Inferred geologic unit
SP1 TO SP2		
Curve 2.5, lat 32°53.6′ N., long 115°44.7′ W.		
0.0	—/1.8	
1.8	3.7/3.7	Sedimentary rocks.
4.55	5.1/5.1	Transition zone.
5.55	5.65/5.65	Basement.
11.4	5.95//6.6	
12.4	7.2/7.2	
20.0	7.76/—	Subbasement.
Curve 25, lat 32°55.3′ N., long 115°30.5′ W.		
0.0	—/1.8	
1.8	3.0/3.0	Sedimentary rocks.
4.55	5.1/5.1	Transition zone.
5.55	5.65/5.65	Basement.
11.3	5.95//6.60	
12.3	7.2/7.2	
20.0	7.76/—	Subbasement.
Curve 43, lat 32°57.1′ N., long 115°19.1′ W.		
0.0	—/1.8	
1.8	3.5/3.5	Sedimentary rocks.
3.3	5.0/5.0	Transition zone.
4.3	5.65/5.65	Basement.
10.63	5.95/6.6	
11.63	7.2/7.2	
20.0	7.76/—	Subbasement.
SP10 TO SP2		
Curve 0 (SP10), lat 33°05.2′ N., long 115°37.5′ W.		
0.0	—/1.8	
1.0	2.3/2.3	Sedimentary rocks.
2.5	3.8/3.8	
3.95	5.0/5.0	Transition zone.
4.45	5.65/5.65	Basement.
13.0	7.0/—	
Curve 15, lat 33°02.4′ N., long 115°28.5′ W.		
0.0	—/1.95	
1.0	2.3/2.3	Sedimentary rocks.
2.2	3.6/3.6	
4.6	4.8/4.8	Transition zone.
5.3	5.5/5.5	Basement.
13.0	7.0/—	
Curve 33 (SP2), lat 32°59.0′ N., long 115 17.6′ W.		
0.0	—/1.90	
.6	2.1/2.1	Sedimentary rocks.
1.8	3.8/3.8	
3.1	5.0/5.0	Transition zone.
4.1	5.65/5.65	Basement.
13.0	7.0/—	

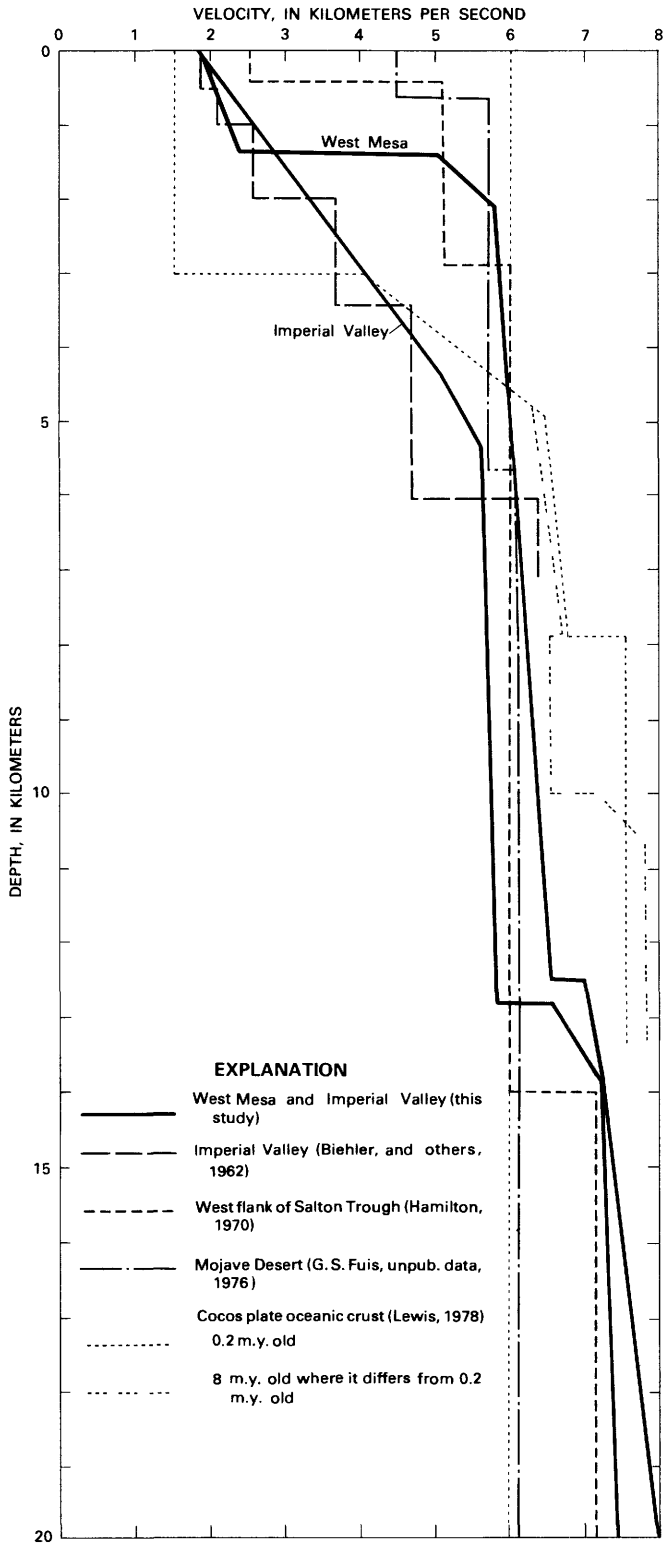

FIGURE 23.—Velocity as a function of depth from data of this study in comparison with those of other studies. Dotted vertical line at 6 km/s is for reference. Velocity-depth curve for West Mesa is that labeled "−1" on SP1 to SP6 in figure 22; curve for Imperial Valley is that labeled "38" on SP13 to SP6 in figure 22. Curve for West Mesa, which is underlain by crystalline igneous and metamorphic basement, agrees reasonably well (between 1.4- and 10-km depth) with curve of Hamilton (1970), which is average for somewhat larger area than we studied on west flank of Salton Trough, and also with curve for Mojave Desert region of California (G. S. Fuis, unpub. data, 1976), which is, likewise, underlain by crystalline igneous and metamorphic rocks. Curve for Imperial Valley indicates comparatively lower velocities for basement (between 5.5- and 13-km depth) that we infer to correspond to metasedimentary rocks. None of these curves resemble those for oceanic crust (Cocos plate, East Pacific Ocean) constructed by Lewis (1978). Upper oceanic crust (between 3- and 5-km depth) is largely made up of extrusive basalt; middle oceanic crust (between 5- and 8-km depth) is believed to be diabase at top and metagabbro below, on the basis of ophiolite studies. Middle oceanic crust probably resembles Imperial Valley subbasement, which is characterized by velocities higher than 6.6 km/s and occurs below 13-km depth on Imperial Valley curve.

West Mesa to 5.65 km/s near shotpoint 6. The implication of the 5.65-km/s velocity is discussed below.

BASEMENT IN THE IMPERIAL VALLEY

What is the composition of the basement in the Imperial Valley, which lies below depths of 5–6 km and is characterized by a relatively low velocity at its top of 5.65 km/s? The deepest wells in the valley bottom at about 4 km in Colorado River delta deposits of Pleistocene(?) age (Muffler and Doe, 1968). These deposits apparently represent only the upper part of the known Cenozoic section in the Salton Trough, which extends in age back to late Miocene (Sharp, 1972). It is thus geologically plausible that the rest of this sedimentary section is present in the Imperial Valley and constitutes the basement below depths of 5–6 km.

The shape of the velocity-depth curves down to 4–5 km is consistent with gradual closing of cracks and pores and with diagenetic processes in the sedimentary rocks. Such processes are described in rocks cored from the Wilson No. 1 well, drilled to a depth of 4 km at a site 10 km southeast of Brawley (Muffler and White, 1969). The temperature profile measured in this well, when extrapolated to greater depth, indicates that greenschist-facies metamorphism (at temperatures higher than 300° C) would begin at a depth of 5 km, the approximate depth of the top of our transition zone in this location. Thus, it appears likely that the basement, 1 km deeper yet at this site, is metamorphosed sedimentary rocks. This conclusion is supported by laboratory studies of velocity in sedimentary and metasedimentary rocks, discussed below.

In laboratory studies of Franciscan sedimentary and metasedimentary rocks at high temperatures and pressures, Stewart and Peselnick (1978) obtained a formula for the P-wave velocity:

$$v = v_0 + \left(\frac{\partial v}{\partial T}\right)T + \left(\frac{\partial v}{\partial P}\right)P + \left(\frac{\partial v}{\partial \rho_B}\right)\rho_B,$$

where $v_0 = -2.53$ km/s, $(\partial v/\partial T) = -8.6\times10^{-4}$ km/s/°C, $(\partial v/\partial P) = 4.1\times10^{-1}$ km/s/MPa, $(\partial v/\partial \rho_B) = 3.10$ km/s/g/cm^3, and ρ_B is the initial bulk density. This formula may need to be corrected for calcium content in a manner analogous to that described by Simmons (1964) for single minerals (Roger Stewart, oral commun., 1980). The correction term (in km/s) is $4.60[\mathrm{CaO}]$, where $[\mathrm{CaO}]$ is the weight fraction of calcium oxide. The Franciscan rocks analyzed by Stewart and Peselnick (1977) contained only a little more than 2 weight percent CaO, in comparison with about 7 weight percent CaO in rocks penetrated in the central Imperial Valley in the Wilson No. 1 well (Muffler and White, 1969). We use the difference of 5 weight percent as the weight fraction in the correction. To calculate the velocity of sedimentary or metasedimentary rocks at 6-km depth in the Imperial Valley, we use a temperature of about 300°C and a pressure of 145 MPa (1.45 kbars, assuming an average density of 2.45 g/cm^3—see fig. 20—in a column 6 km high). For bulk density, we use values between 2.60 and 2.65 g/cm^3, determined from sedimentary rocks in the Salton Sea geothermal area that have been metamorphosed to lower greenschist facies at temperatures higher than 300°C (W. A. Elders, oral commun., 1980). The calculated velocity ranges from 5.33 to 5.49 km/s, depending on the density. Correcting for calcium content, the velocity ranges from 5.56 to 5.72 km/s, in good agreement with the upper-basement velocity of 5.65 km/s determined in this study.

We note that these low velocities cannot be obtained from felsic igneous or metamorphic rocks (in which velocities range from 5.9 to 6.6 km/s at 200 MPa; Birch, 1960) by a thermal effect. Using a temperature coefficient for quartz monzonite (Lin and Wang, 1980) of -0.6×10^{-3} km/s/°C and a maximum temperature difference of 250°C at 6-km depth between the Imperial Valley and West Mesa (assuming that West Mesa could be as cool as the standard continental area of Lachenbruch and Sass, 1977), we obtain a velocity reduction of only 0.15 km/s for the Imperial Valley relative to West Mesa. We note also that the basement velocity in the central Imperial Valley differs considerably from laboratory velocities for intrusive basaltic rocks (6.5–6.8 km/s for diabase; Birch, 1960) and from velocities of oceanic crust at comparable pressures (fig. 23; Lewis, 1978).

Contradicting our conclusion that metasedimentary rocks overlie the subbasement, or intermediate crustal layer, in the Imperial Valley is evidence obtained from xenoliths in the Salton Buttes rhyolite extrusions. This evidence indicates that, at least in some places, remnants of granitic crust may underlie the metasedimentary rocks. The xenoliths are low-potassium tholeiitic basaltic rocks and soda granite in roughly equal proportions, and include sedimentary and metasedimentary rocks in much smaller amounts (Robinson and others, 1976). The granitic xenoliths are of particular interest in that they may indicate the presence of remnant continental basement at depth in this area. These granitic xenoliths apparently are not cognate xenoliths because they differ chemically from the enclosing rhyolite and their $^{87}Sr/^{86}Sr$ ratio is higher (0.72, in comparison with 0.705). However, the xenoliths are not clearly derived from granitic basement rocks of the Peninsular Ranges or the Chocolate Mountains, which tend to be granodioritic and quartz monzonitic in composition, respectively (Robinson and others, 1976). The granitic xenoliths display extensive recrystallization in their granophyric textures, as well as varying degrees of remelting, that must predate their inclusion within the rhyolite because the sedimentary and metasedimentary xenoliths show no such effects. We conclude that the granitic xenoliths came from greater depth than the sedimentary and metasedimentary xenoliths, where partial melting is occurring. If these xenoliths derive from arkosic sedimentary rocks at depth rather than granitic basement rocks, we must envision melting, crystallization, and remelting of the parent sediment. Furthermore, we would expect a spectrum of xenoliths intermediate in type between the granitic and sedimentary xenoliths, exhibiting all stages of partial melting, crystallization, and remelting, which is not the case.

INTERMEDIATE CRUSTAL LAYER

The most definitive evidence for the existence of an intermediate crustal layer, or subbasement, in the central Imperial Valley comes from profile 6NNW–13SSE (fig. 17*A*; Mooney and McMechan, this volume) along the axis of the Salton Trough. This is the only profile exhibiting reversing branches of arrivals from such a body, although phases from this crustal layer are evident on almost all the other profiles that we have examined.

A transition zone apparently exists at the top of the subbasement, where, after a velocity jump to 6.6–7.0 km/s, the velocity increases rapidly through this zone (1 km thick in our models) to 7.2 km/s. Velocities less than 7.2 km/s are required at the top of this zone to give the correct amplitude for reflections and the correct dis-

tance at which the critical reflection is seen (Mooney and McMechan, this volume).

A velocity of 7.2 km/s requires that the subbasement be mafic in composition, such as gabbro or amphibolite (see Birch, 1960). Basaltic xenoliths in the Salton Buttes rhyolite extrusions, and basaltic sills and dikes encountered in wells (Griscom and Muffler, 1971; Elders and others, 1972; Robinson and others, 1976; Browne, 1977), do indeed indicate the presence of mafic rocks at depth under the valley. Presumably the subbasement, like this basalt, intrudes the basement. We suggest that the transition zone at the top of the subbasement consists of sheeted dikes and sills of diabase, with velocities ranging from 6.6 to 6.8 km/s (see Birch, 1960), and the lower part of the subbasement consists of gabbro, with velocities of 7.2 km/s and higher. This inferred geology is similar to that of oceanic middle crust based on ophiolite studies (Clague and Straley, 1977; Lewis, 1978; see also comparison of velocity structures in fig. 23).

STRUCTURE AND TECTONICS

The seismic data reported here provide new insights into the structure and tectonics of the Imperial Valley region. In this section we incorporate this new evidence into a structural synthesis of the region (fig. 24). Mapped faults are generalized from geologic maps (Dibblee, 1954; Strand, 1962; Jennings, 1967; Gastil and others, 1971; Clark, 1972; Sharp, this volume). Buried (fault) scarps and geothermal traveltime anomalies are from the reduced traveltime-contour map (fig. 19). Seismicity lineaments are drawn on the basis of the epicenters compiled by Johnson (1979, p. 139). Focal mechanisms are those reported by Allen and Nordquist (1972), Hamilton (1972), Johnson and Hadley (1976), Fuis and Schnapp (1977), and Johnson and Hutton (this volume).

The inferred extent of crystalline igneous and metamorphic basement rocks (velocity greater than 5.9 km/s) on the map (fig. 24) is based on our interpretations of seismic-refraction data, on data from wells, and on the geology. On West Mesa, the boundary most likely corresponds to a prominent buried scarp (see figs. 17–19). We note an apparent left-lateral offset of this scarp along the (right lateral) Superstition Mountain fault (fig. 24). The queried bay in the crystalline basement northeast of the Coyote Creek fault (fig. 24) is inferred from the existence of a deep sedimentary basin indicated on the traveltime-contour map (fig. 19). The boundaries inferred along the southwest and northeast sides of the Salton Sea are based primarily on the prominent geologic boundaries between the crystalline massifs and Cenozoic sedimentary rocks. Data from one well control the boundary on the southwest side, but granitic basement could exist at depth beneath the Salton Sea. The boundary inferred on East Mesa is placed along the northwestern section of the East Highline Canal seismicity lineament and along the Sand Hills fault(?); these features are southward projections of the trend of the San Andreas fault. The shorelines of ancient Lake Cahuilla (see fig. 16) correspond in most places with the boundaries of crystalline crust on the map (fig. 24). These shorelines may reflect the boundaries of a region that is sinking owing to combined rifting and sediment compaction.

The major northwest-trending structural features on the map (fig. 24) include, from southwest to northeast: the Elsinore fault zone; the San Jacinto fault zone, which includes the Coyote Creek, Superstition Mountain, and Superstition Hills faults; the Imperial fault; the Brawley seismic zone, bounded at its south end by the northern section of the Imperial fault and the Brawley fault zone; the San Andreas fault; the East Highline Canal seismicity lineament; and the Sand Hills and Algodones faults(?). Subtler northeast-trending features include buried scarps on West Mesa and strong seismicity lineaments within the Brawley seismic zone.

Azimuthal discordances are evident among the northwest-trending features. The Imperial fault south of its junction with the Brawley fault zone trends N. 40° W., in comparison with trends on the Elsinore, San Jacinto, and San Andreas faults of N. 65° W., N. 45°–70° W., and N. 45° W., respectively (within area of fig. 24). Even more striking is the azimuthal discordance of the Brawley seismic zone, which trends, on the whole, N. 20° W. An angular discordance is also evident among the subtler northeast-trending features. The buried scarps on West Mesa trend N. 40° E., whereas the strong seismicity lineaments within the Brawley seismic zone trend N. 50°–60° E.

The angular discordances among both the northwest- and northeast-trending structures are associated with slight differences in the styles of displacement and deformation, as determined from geologic evidence and from modern ground breakage, leveling, and focal mechanisms. Along the Elsinore, San Jacinto, and San Andreas faults, uplift, folding, and reverse faulting are evident in addition to strike-slip. In contrast, no significant uplift is apparent along the Imperial fault south of its junction with the Brawley fault zone, and modern displacement indicates pure strike-slip. At the ends of the north-northwest-trending Brawley seismic zone, subsidence or graben formation is indicated both geologically, in the formation of the Mesquite basin and the Salton sink (now occupied by the Salton Sea), and from recent leveling-line surveys (Castle, 1978; Sharp and Lienkaemper, this volume). In addition, normal

dip-slip focal mechanisms are indicated under the Salton Sea (Fuis and Schnapp, 1977) and possibly also in the Mesquite basin (C. E. Johnson, oral commun., 1979). As for the northeast-trending structures, refraction data (fig. 19) indicate horsts and grabens along the faults striking N. 40° E. on West Mesa, whereas focal mechanisms indicate largely strike-slip along the seismicity lineaments striking N. 50°–60° W. in the Brawley seismic zone.

We can invoke a simple model of average stress directions during the recent geologic past to explain the various styles of displacement and deformation along the different trends. By "recent geologic past" we mean the time since the formation of the Imperial fault, the Brawley fault zone, the Brawley seismic zone, and the uplifts and folds along the Elsinore, San Jacinto, and San Andreas fault zones. A horizontal tension axis oriented slightly north of west (N. 85° W.) and a horizontal compression axis oriented slightly east of north (N. 5° E.) in most places would produce pure strike-slip on the Imperial fault and on the northeast-trending seismicity lineaments within the Brawley seismic zone.

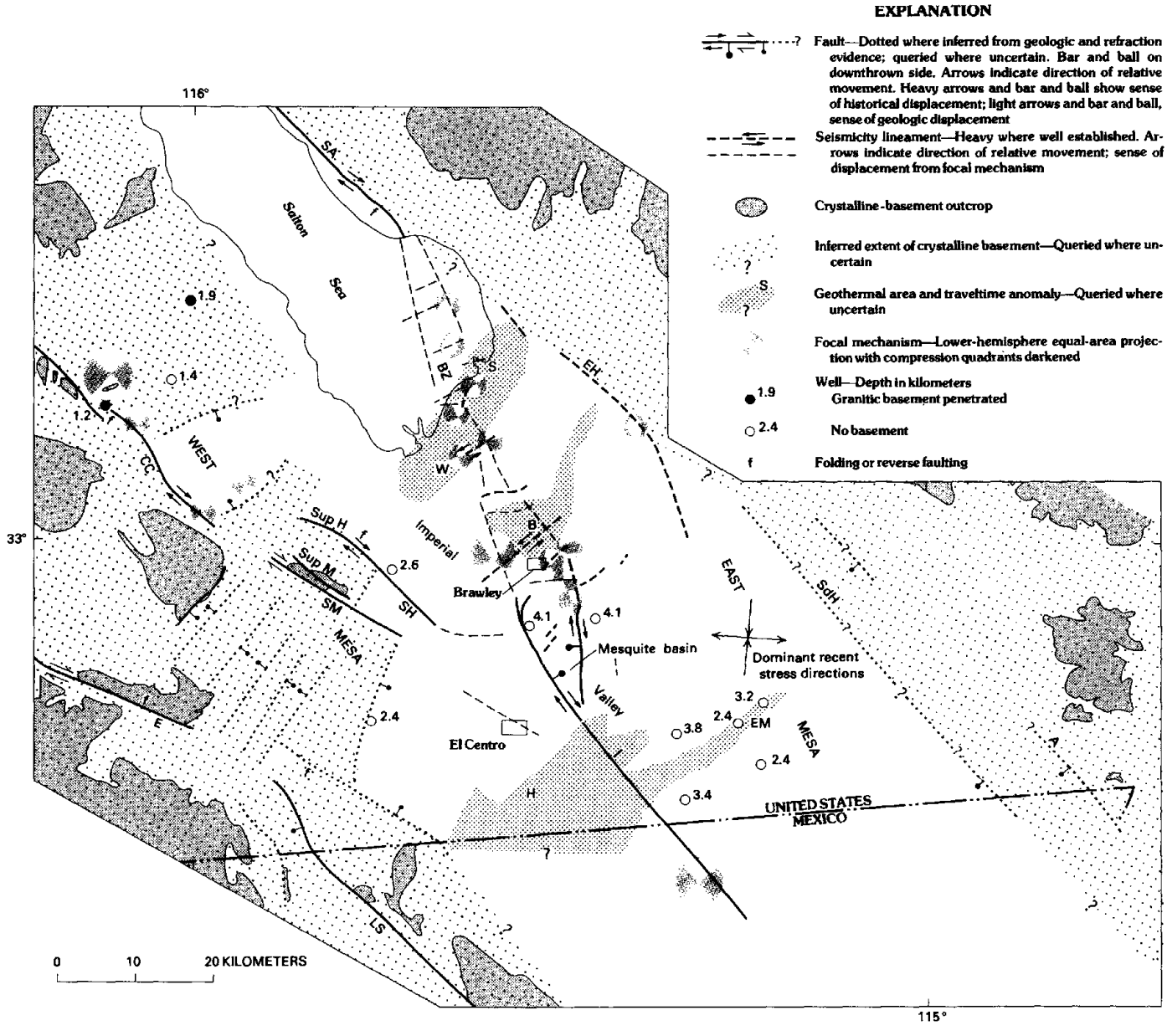

FIGURE 24.—Structure and tectonics of Imperial Valley region. Faults and geothermal areas abbreviated as in figures 16 and 19; LS, Laguna Salada fault; Sup H, Superstition Hills; Sup M, Superstition Mountain. Long arrows denote dominant recent stress directions inferred from this map.

This system would create compressional features across the Elsinore, San Jacinto, and San Andreas faults. A local change to a vertical compression axis would induce some component of graben formation along structures more nearly perpendicular to the tension axis, such as the northern section of the Imperial fault, the Brawley fault zone, certain north-northwest-trending lineaments within the Brawley seismic zone, and the north-northeast-trending structures on West Mesa. Similar ideas have been proposed by Hill (1978). This simple model implies that during the recent geologic past the Imperial fault and the northeast trending lineaments within the Brawley seismic zone have been, on the average, more favorably oriented to accommodate movement by pure strike-slip than have the Elsinore, San Jacinto, and San Andreas faults. Perhaps the Imperial fault and the Brawley seismic zone have formed more recently in virgin rocks—sedimentary and metasedimentary rocks—in response to a more modern stress direction than that associated with inception of movement on the Elsinore, San Jacinto, and San Andreas faults.

If the observed sedimentary (and metasedimentary) basin was formed by rifting and crustal thinning in the Imperial Valley region, then either normal dip-slip faulting or ductile necking of the crust, or a combination of these processes, must have occurred. Strike-slip faulting, the primary mode of deformation along the southern section of the Imperial fault and along the northeast-trending seismicity lineaments within the Brawley seismic zone, can cause only crustal shortening, not crustal thinning. Therefore, the faults that appear to be currently involved in rifting and thinning in the Imperial Valley region consist of: the northern section of the Imperial fault, the Brawley fault zone, certain north-northwest-trending lineaments in the Brawley seismic zone, and parts of the East Highline Canal seismicity lineament. In the past, the buried (fault) scarps on West Mesa may have been involved in rifting and crustal thinning, but there is no clear geologic or seismic evidence that these scarps outline currently active faults.

The structures on the map (fig. 24) are depicted in a block diagram (fig. 25) in which the sedimentary cover has been removed to reveal the upper surface of the basement. In addition, part of the basement east of the Brawley seismic zone has been cut away to reveal several structures in this zone. The postulated boundary between crystalline and metasedimentary basement is placed at the east edge of West Mesa. At this boundary the subbasement must dip beneath West Mesa because no pronounced gravity scarp is present. This block diagram lends itself to a relatively simple interpretation of how rifting and crustal thinning might be occurring in the Imperial Valley region. From a point of reference somewhere in the Brawley seismic zone, such as Obsidian Butte, we imagine block 1 being pulled away to the northwest and block 2 to the southeast. Rhombochasms (see Carey, 1958) and associated normal faults would form in the Brawley seismic zone, as are currently evident in the formation of the Mesquite basin and the Salton sink, at either end of the zone. In addition, ductile thinning of both blocks might occur. Such thinning could be accomplished, in effect, by numerous small-scale normal faults. Small-scale faults are, indeed, encountered in many wells in the Imperial Valley (Don Lande, oral commun., 1980). Ductile thinning of block 2 relative to block 1 southeast of the Brawley seismic zone might explain the buried scarp along the Imperial fault.

The scarp along the Imperial fault deserves some discussion at this point. If the sediment/basement transition in the central Imperial Valley is everywhere a metamorphic-facies change, a scarp could not occur in this transition zone without a scarp in isotherms, unless the rock near such a scarp had cooled down and the facies boundary was no longer an equilibrium feature. Perhaps the geothermal gradient is relatively high to the north, in the Brawley seismic zone, in keeping with the presence in this zone of the Salton Sea, Westmorland, and Brawley geothermal areas. Southeastward from this zone the geothermal gradient may decrease, and the metamorphic boundary may be out of equilibrium as block 2 is pulled to the southeast. Normal faulting and ductile thinning, as described above, could offset this boundary to create the observed scarp along the Imperial fault.

Crustal spreading northwestward from the Brawley seismic zone would cause left-lateral displacements along the San Jacinto fault zone, unless another spreading center existed to the southeast to drive the block southwest of that fault zone faster to the northwest than the block on the northeast. The Cerro Prieto geothermal area, 30 km south of the United States-Mexican border (fig. 26), is certainly a candidate for such a spreading center, as proposed by Lomnitz and others (1970) and Elders and others (1972). This geothermal area, which is characterized by volcanism, geothermal activity, and high seismicity, lies between the ends of two major right-stepping strike-slip faults, the Imperial and Cerro Prieto faults. Seismicity in this area resembles that in the Brawley seismic zone in showing an overall north-northwestward trend connecting these two strike-slip faults, and in showing both normal dip-slip and strike-slip focal mechanisms (Albores and others, 1977; Alfonso Reyes, oral commun., 1977; Johnson and Hutton, this volume.)

Lomnitz and others (1970) proposed a plate-tectonic model for the northern Gulf of California and the Salton

Trough that explains the basic relations among the major strike-slip faults and potential spreading centers. In addition, by postulating progressively lower spreading rates to the northwest, Lomnitz and others explained the numerous active right-lateral strike-slip faults diverging to the northwest. One consequence of their model, however, is a complementary set of active left-lateral strike-slip faults diverging to the southeast, for which no evidence exists. Elders and others (1972) pointed out that if these left-lateral faults do not exist, the spreading centers must be migrating northwestward at rates equivalent to half their total spreading rates.

In figure 26 we reproduce the model of Elders and others (1972, fig. 7), adding a stippled pattern to regions we believe to be underlain by continental igneous and metamorphic (crystalline) basement, on the basis of our studies (fig. 24), and attempting to correlate specific features in the idealized model (fig. 26*A*) with specific geologic structures (fig. 26*B*). These correlations meet with varying success. The Imperial and Cerro Prieto faults can be correlated straightforwardly with transform faults. The Brawley seismic zone, Cerro Prieto geothermal area, and Wagner basin appear to be spreading centers, but all three of these features trend north-northwest or north-south rather than northeast, if seismicity or topography is used to define them (see Johnson and Hutton, this volume, for a description of the seismicity of the Brawley seismic zone and Cerro Prieto geothermal area; and Fisher and others, 1964, for submarine topography of the Wagner basin). In this respect, all three spreading centers resemble "leaky" transform faults, as depicted in Hill (1977), or rhombochasms (compare with Carey, 1958). Fracture zones

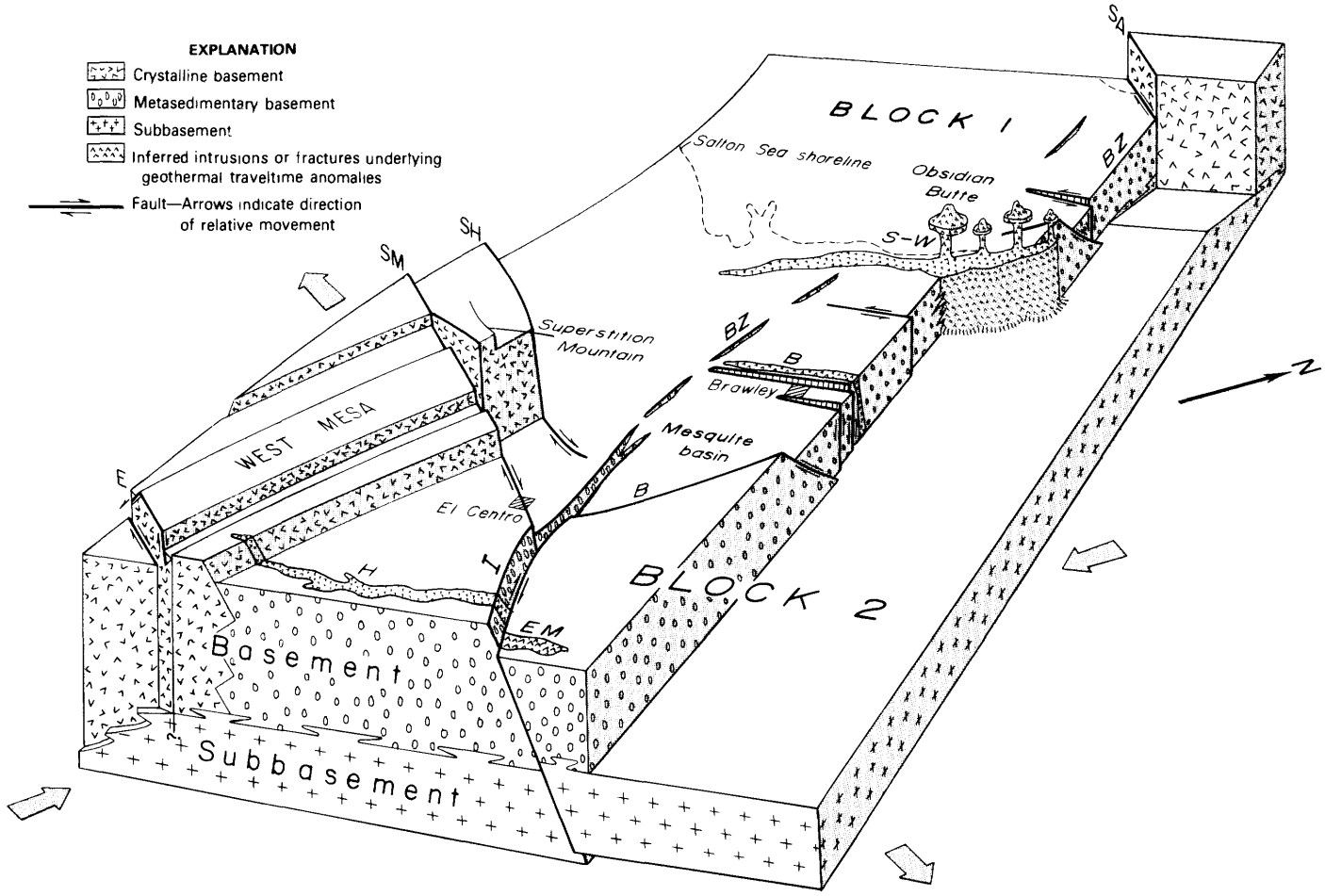

FIGURE 25.—Schematic block diagram of Imperial Valley region, with sedimentary rocks removed and basement cut away along a line roughly parallel to Brawley seismic zone. Geographic names are projected downward onto basement for reference. Structures same as in figure 24: B, Brawley fault zone; BZ, Brawley seismic zone; E, Elsinore fault; I, Imperial fault; SA, San Andreas fault; SH, Superstition Hills fault; SM, Superstition Mountain fault. Geothermal areas: B, Brawley; EM, East Mesa; H, Heber; S, Salton Sea; W, Westmorland. Shaded arrows indicate dominant tension and compression directions for recent geologic past. Blocks 1 and 2 are moving away from Brawley seismic zone, and inferred spreading center, in direction parallel to southern section of Imperial fault shown. Rhombochasms, or pullapart holes, are forming at Mesquite basin and Salton sink, which is presently occupied by Salton Sea. In addition, ductile thinning of both blocks may be occurring as they move away from Brawley seismic zone.

in the idealized model (fig. 26*A*) appear much more complex in the real picture (fig. 26*B*). The San Jacinto fault zone alines roughly with the Imperial fault, and its seismicity appears to merge with that of the Imperial fault (see Fuis and others, 1978; Fuis and Allen, 1979; Johnson and Hutton, this volume). Similarly, the Elsinore fault zone appears to aline roughly with the Cerro Prieto fault by way of a suture between crystalline and metasedimentary basement that we have inferred (fig. 24). There is some evidence for a weak seismic zone along this suture connecting the spotty seismicity along the Elsinore fault zone with seismicity on the Cerro

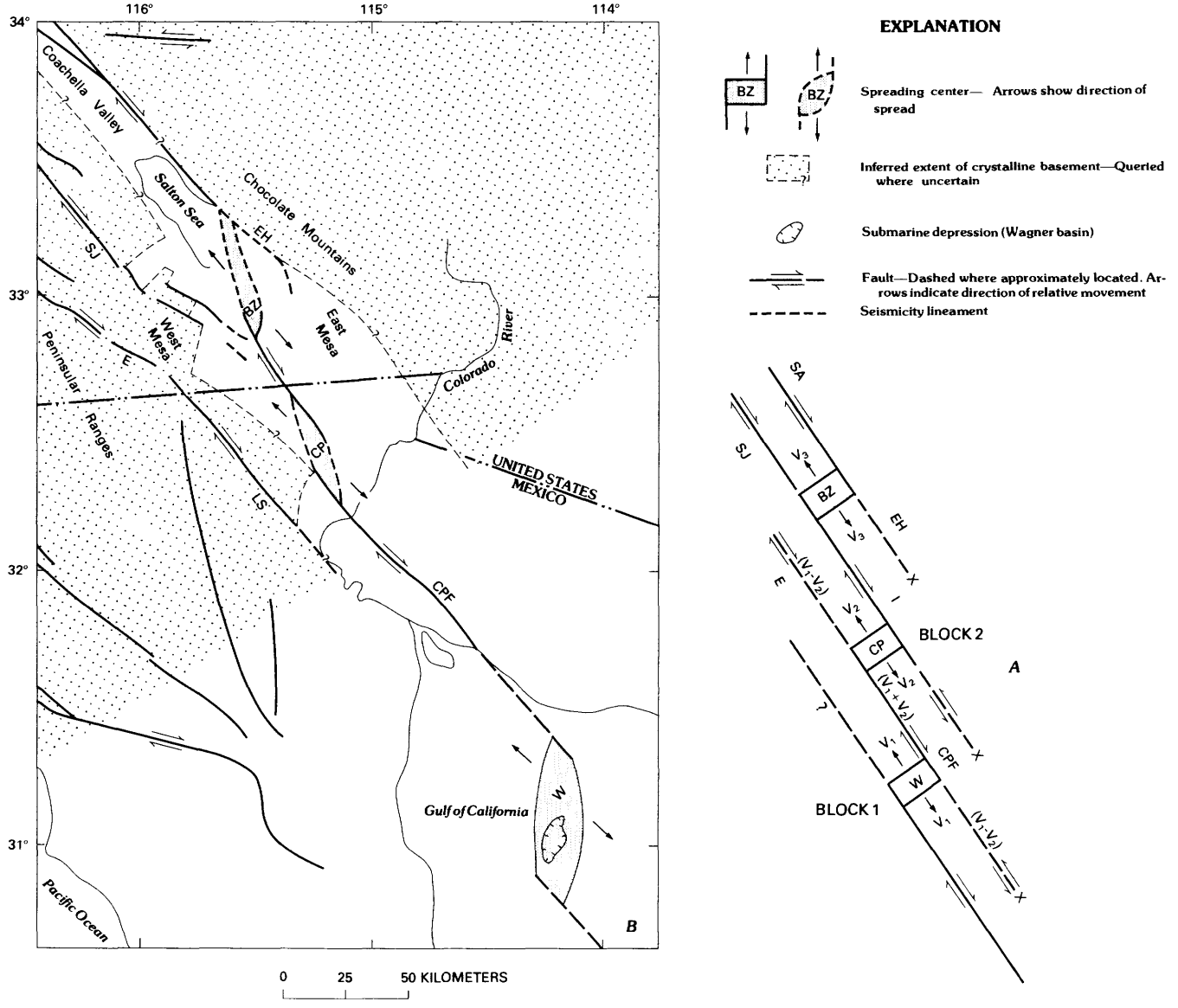

FIGURE 26.—Plate-tectonic model and map of northern Gulf of California and Salton Trough, modified from Elders and others (1972, fig. 7). Idealized model (*A*) of sketch map (*B*) illustrates interrelations of major spreading centers: Brawley seismic zone (BZ), Cerro Prieto geothermal area (CP), and Wagner basin (W); major transform faults: San Andreas fault (SA), Imperial fault (I), Cerro Prieto fault (CPF); and major fracture zones or sutures: San Jacinto fault zone (SJ), Elsinore fault (E), and East Highline Canal seismicity lineament (EH). Note that Laguna Salada fault (LS), which appears to be the seismically most active extension of Elsinore fault southeastward, does not appear to connect with any known transform fault. Such departures from idealized model (*A*) may reflect influence of North American Continent, with its preexisting weaknesses, on oceanic plate tectonics. X's denote fracture zones or sutures that are inactive in indicated left-lateral sense. East Highline Canal seismicity lineament appears to be associated with normal dip-slip motions (fig. 24); there is currently no seismic or geologic evidence for existence of other two proposed sutures. Inactivity along sutures on east side of Gulf of California and Salton Trough requires that spreading centers migrate northwestward from block 2 at their spreading half-rates. We assume that these half-rates decrease northwestward: $V_3 < V_2 < V_1$.

Prieto fault (see Fuis and others, 1978; Fuis and Allen, 1979; Johnson and Hutton, this volume). The Laguna Salada fault, however, which appears to be the seismically most active extension of the Elsinore fault zone into Mexico (see Fuis and others, 1977), cannot be clearly correlated with any fracture zone or suture in the idealized model (fig. 26*A*). We surmise that such departures from this model, which is based largely on observations from oceanic plate tectonics, reflect interference by the continental mass of North America, which has different mechanical properties from oceanic crust and preexisting weaknesses that might be readily utilized for fracture zones. Perhaps this continental interference also is responsible for the angular discordances noted above.

On the basis of this sketch map (fig. 26*B*), the inferred crystalline-crustal boundary along the east side of West Mesa appears to have been rifted northward from Cerro Prieto, a distance of more than 60 km. If the Cerro Prieto geothermal area was formed when Baja California was rifted from the North American Continent 4.5 m.y. B.P. (Larson and others, 1968), we calculate a spreading half-rate of about 1.3 cm/yr, considerably lower than the 2.75-cm/yr half-rate for the movement of North America past the Pacific plate (Atwater and Molnar, 1973). We might explain this discrepancy in either of at least two ways. First, uneven crustal spreading, as discussed above, is occurring: the Wagner basin and other spreading centers to the south are spreading faster than the Cerro Prieto geothermal area, and the differential motion is being accommodated along the Elsinore and other faults to the south. Second, the Cerro Prieto geothermal area may be younger than the opening of the Gulf of California.

The inferred boundary of crystalline crust northwest of the Brawley seismic zone is ragged as drawn; the pattern is not simple, as appears to be the case northwest of the Cerro Prieto geothermal area. Perhaps we have drawn the boundary incorrectly along the west side of the Salton Sea and the Coachella Valley, as well as along the San Andreas fault, where it is queried. If these boundaries are correct, however, the Brawley seismic zone apparently has operated in two sections: a northern section that rifted away the crystalline basement of the Salton Sea and the Coachella Valley, between the San Andreas fault and a now-dead fracture zone along the west side of the Coachella Valley; and a younger, southern section that rifted the Superstition Mountain block northwestward.

We note that the Superstition Mountain block appears to have moved approximately 25 km from the southern section of the Brawley seismic zone, or the Mesquite basin area (fig. 24), creating an apparent left-lateral offset across the (right lateral) Superstition Mountain fault. Because this movement is smaller than the postulated movement (60 km) of the adjacent block on the southwest, we infer that the southern section of the Brawley seismic zone is either younger or is spreading more slowly than the Cerro Prieto geothermal area. We note further that if the Superstition Mountain block moved 25 km northwest from the Mesquite basin area, there must be a symmetrical counterpart 25 km southeast of the Mesquite basin, near shotpoint 6, unless spreading is asymmetric. If such were the case, the crystalline-crustal boundary in the East Mesa area should be drawn through the vicinity of shotpoint 6, presumably along the east shoreline of ancient Lake Cahuilla, instead of along the Sand Hills fault(?) as shown (figs. 24, 26). Further analysis of our data in the East Mesa area and probably additional refraction work in this area will be necessary to resolve this question. The apparent embayment in the crystalline-basement distribution northwest of the Superstition Mountain block is not explainable in simple terms. Further work in this area will be necessary to document this feature.

SUMMARY

In summary, we have modeled five seismic-refraction profiles, contoured reduced traveltimes from our most widely recorded shotpoint, and modeled a gravity profile across the Salton Trough, using new crustal information. Our chief result is an integrated picture of the crustal structure of the Imperial Valley region that, though not unique, is consistent not only with refraction and gravity data but also with the geology and known tectonics of the region. The major elements of this picture include:

1. A trough of unmetamorphosed sedimentary rocks centered on the axis of the Salton Trough, with depths ranging from 3.7 km along the southwest shore of the Salton Sea to 4.8 km at the United States-Mexican border.
2. Two types of basement: one, with a velocity of 5.9–6.0 km/s at its top, on West Mesa; and the other, with a velocity of 5.65 km/s at its top, in the central Imperial Valley. We interpret the first type to be continental igneous and metamorphic (crystalline) rock, and the second to be metasedimentary rock. Onset of lower greenschist-facies metamorphism is expected at the calculated depths to the transition zone in the central valley, 1 km above the basement. According to this interpretation, the total thickness of the sedimentary section—unmetamorphosed and metamorphosed—in the central valley is 10 to 16 km. This interpretation explains the absence of any observed reflection from the sediment/basement interface in the center of the valley and also why deep (4 km) wells in the valley

penetrate only the upper part of the known Cenozoic section in this region.

3. A subbasement, with a velocity of 7.2 km/s near its top and a likely composition ranging from diabase at the top to gabbro farther down, at depths ranging from 16 km in the Salton Sea to 10 km at the United States-Mexican border. Gravity modeling indicates that this subbasement must be confined largely to the central Imperial Valley and that it compensates gravitationally for the great thickness of overlying metamorphosed and unmetamorphosed sedimentary rocks.
4. A buried basement scarp as high as 3 km along the east side of West Mesa. We interpret this scarp to be the suture, or rift boundary, between the crystalline and metasedimentary basements. A similar structure must exist near East Mesa, but it cannot be precisely located from our data.
5. A buried basement scarp along the Imperial fault. This scarp, dipping steeply northeast, increases in height from 0 km at the north end of the fault to 1 km at a location 12 km southeast of El Centro, Calif.
6. Steep scarps along some major mapped faults and along some structures not visible at the surface, revealed by a contour map of reduced traveltimes.
7. A good correlation between known geothermal-resource areas with reservoir temperatures higher than 150°C and subtle patches of relatively early arrivals in the central Imperial Valley, revealed on the contour map of reduced traveltimes. These patches of early arrivals are roughly linear, approximately 15 km long, and trend northeast.
8. Angular discordances among both northwest- and northeast-trending faults that, along with corresponding differences in the styles of displacement and deformation across the faults, point to an average stress orientation during the recent geologic past—since formation of the Imperial fault and the Brawley seismic zone—in which the tension axis is horizontal (N. 85° W.) and the compression axis is largely horizontal (N. 5° E.). The southern section of the Imperial fault and many structures within the Brawley seismic zone are adjusted in this stress field to deform by pure strike-slip, whereas other faults must accommodate these stresses by a combination of strike-slip and folding (the San Andreas, San Jacinto, and Elsinore faults) or by a combination of strike-slip and normal dip-slip (the northern section of the Imperial fault, the Brawley fault zone, and the buried faults on West Mesa).
9. A map of the distribution of continental crystalline basement in the Salton Trough that permits us to carry the existing tectonic model for the region a bit farther. In particular, it appears that a basement boundary on the east side of West Mesa has moved more than 60 km northwestward from the Cerro Prieto geothermal area, a spreading center. Likewise, a block underlying Superstition Mountain may have moved about 25 km from the south end of the Brawley seismic zone, another spreading center. These blocks are separated by the Superstition Mountain fault, part of the San Jacinto fault zone, which appears to be a fracture-zone extension of the Imperial fault. Differing spreading rates between the Brawley seismic zone and the Cerro Prieto geothermal area are taken up by movement on faults in this fracture zone. Likewise, the Elsinore fault zone appears to be a fracture-zone extension of the Cerro Prieto fault; however, the Laguna Salada fault appears to be its most active extension to the southeast, complicating the tectonic picture. Perhaps the influence of the North American Continent, with its preexisting weaknesses, on oceanic plate tectonics is responsible for such complications.

If basement in the Imperial Valley is metamorphosed sedimentary rocks and if the subbasement is intrusive basaltic rocks, as we have inferred, then the Imperial Valley is one location where we can study the generation of new continental crust. As old continental crust is rifted and rhombochasms are created, basaltic magma is intruded to fill the rhombochasms from below, forming an intermediate crustal layer, and sediment is deposited to fill the rhombochasms from above. Rifting and intrusion generates high heat flow and induces metamorphism of the sedimentary rocks at relatively shallow depths, consolidating the section into new continental crust.

ACKNOWLEDGMENTS

We estimate that data collection, analysis, and writing of this chapter have consumed more than 10 man-years of effort since early 1979. About half of this effort was expended by persons other than the authors, and without them this chapter could not have been written. We therefore wish to express our indebtedness to S. K. Gallanthine, L. R. Hoffman, Barry Keller, J. N. Roloff, and V. D. Sutton, who, together with W. J. Lutter (one of the authors), deployed the instruments; to W. M. Kohler and L. E. Leone, who digitized the data and kept the field computers and plotters running; to D. E. Taylor, who permitted the shotpoints; to Bruce Echols and S. S. Wegener, who managed the drilling and loading of shotholes; to R. D. Jones, Harry Tostado, and D. L. Styles, who drilled many of the shotholes; to P. T. German and Victor Lamanuzzi, who assisted with the surveying of instrument sites; to R. M. Kaderabek and

Robert McClearn, who kept the instruments running; and to K. B. Berg, N. C. Crossley, and Herbert Mills, who provided administrative assistance. In addition, several persons facilitated this survey in various ways. Landowners who permitted us to drill and shoot on their properties included R. E. Casey and Wendell Finley (shotpoint [3]8), and John Elmore (shotpoint 10). Permission to drill and shoot on Government land was granted or expedited by Lt. Comdr. W. F. Ellis of the U.S. National Parachute Test Range (shotpoints 1 and 13), S. L. Johnson of the U.S. Bureau of Land Management (shotpoints 2, [3]3, 5, 6, 7), and several employees of the U.S. Department of the Interior, Fish and Wildlife Service (shotpoint [3]4). Clifford Brown of the U.S. Department of Agriculture graciously allowed us to use a building at their Brawley, Calif., facility for our field headquarters. Sr. Chief C. W. Franklin of the U.S. National Parachute Test Facility kindly permitted us to store explosives at the facility. James Cantrell of the Southern Pacific Railroad Co. held up trains for one of our profiles. In addition, we express our appreciation to the many people, both public and private, of Imperial County who helped us in countless ways.

This report was improved by many discussions with W. A. Elders, D. P. Hill, L. J. P. Muffler, and P. A. Spudich. Don Lande of the California Division of Oil and Gas kindly provided information from wells in the Imperial Valley region. Vlastislav Červený of Karlova University, Prague, supplied the ray-tracing code used, and R. L. Nowack of the U.S. Geological Survey provided an interactive version of the code.

REFERENCES CITED

Albores, A., Reyes, Alfonso, Brune, J. N., Day, S., Gonzales, Javier, Nava, A., Garcilazo, L., and Vaillaro, I., 1977, Microearthquake study at the Cerro Prieto, Mexico, geothermal field [abs.]: Eos (American Geophysical Union Transactions), v. 58, no. 12, p. 1187–1188.

Allen, C. R., and Nordquist, J. M., 1972, Foreshock, main shock, and larger aftershocks of the Borrego Mountain earthquake, *in* The Borrego Mountain earthquake of April 9, 1968: U.S. Geological Survey Professional Paper 787, p. 16–23.

Allen, C. R., Wyss, Max, Brune, J. N., Grantz, Arthur, and Wallace, R. E., 1972, Displacements on the Imperial, Superstition Hills, and San Andreas faults triggered by the Borrego Mountain earthquake, *in* The Borrego Mountain earthquake of April 9, 1968: U.S. Geological Survey Professional Paper 787, p. 87–104.

Atwater, Tanya, and Molnar, Peter, 1973, Relative motion of the Pacific and North American plates deduced from sea-floor spreading in the Atlantic, Indian, and South Pacific Oceans, *in* Kovach, R. L., and Nur, Amos, eds., Proceedings of the conference on tectonic problems of the San Andreas fault system: Stanford University Publications in the Geological Sciences, v. 13, p. 136–148.

Biehler, Shawn, Kovach, R. L., and Allen, C. R., 1964, Geophysical framework of northern end of Gulf of California structural province, *in* van Andel, T. H., and Shor, G. G., Jr., eds., Marine geology of the Gulf of California: American Association of Petroleum Geologists Memoir 3, p. 126–143.

Birch, Francis, 1960, The velocity of compressional waves in rocks to 10 kilobars, part 1: Journal of Geophysical Research, v. 65, no. 4, p. 1083–1102.

Blank, H. R., Healy, J. H., Roller, John, Lamson, Ralph, Fisher, Fred, McClearn, Robert, and Allen, Steve, 1979, Seismic refraction profile, Kingdom of Saudi Arabia: Field operations, instrumentation, and initial results: U.S. Geological Survey Open-File Report 79–1568, 49 p.

Brook, C. A., Mariner, R. H., Mabey, D. R., Swanson, J. R., Guffanti, Marianne, and Muffler, L. J. P., 1978, Hydrothermal convection systems with reservoir temperatures ≥ 90°C, *in* Muffler, L. J. P., ed., Assessment of geothermal resources of the United States: U.S. Geological Survey Circular 790, p. 18–85.

Browne, P. R. L., 1977, Occurrence and hydrothermal alteration of diabase in the Heber geothermal field, Imperial Valley, California: University of California, Riverside, Institute of Geophysics and Planetary Physics Report 77/9, p. 1–61.

Carey, S. W., 1958, The tectonic approach to continental drift, *in* Continental drift: A symposium: Hobart, Australia, University of Tasmania, Geology Department, p. 177–355.

Castle, R. O., 1978, Leveling surveys and the southern California uplift: Earthquake Information Bulletin, v. 10, no. 3, p. 88–92.

Červený, Vlastislav, Molotkov, I. A., and Psenčík, Ivan, 1977, Ray method in seismology: Prague, Karlova University, 214 p.

Clague, D. A., and Straley, P. F., 1977, Petrologic nature of the oceanic Moho: Geology, v. 5, no. 3, p. 133–136.

Clark, M. M., 1972, Surface rupture along the Coyote Creek fault, *in* The Borrego Mountain earthquake of April 9, 1968: U.S. Geological Survey Professional Paper 787, p. 55–86.

Dibblee, T. W., Jr., 1954, Geology of the Imperial Valley region, California, *in* Geology of the natural provinces, chap. 2 *of* Jahns, R. H., ed., Geology of southern California: California Division of Mines Bulletin 170, v. 1, p. 21–28.

Elders, W. A., Rex, R. W., Meidav, Tsvi, Robinson, P. T., and Biehler, Shawn, 1972, Crustal spreading in southern California: Science, v. 178, no. 4056, p. 15–24.

Fisher, R. L., Rusnak, G. A., and Shepard, F. P., 1964, Submarine topography of Gulf of California, *in* van Andel, T. H., and Shor, G. G., Jr., eds., Marine geology of the Gulf of California: American Association of Petroleum Geologists Memoir 3, chart 1, 4 sheets.

Fuis, G. S., and Allen, C. R., 1979, The southern California cooperative seismic network: Earthquake Information Bulletin, v. 11, no. 6, p. 196–204.

Fuis, G. S., Friedman, M. E., and Hileman, J. A., 1977, Preliminary catalog of earthquakes in southern California, July 1974–September 1976: U.S. Geological Survey Open-File Report 77–181, 107 p.

Fuis, G. S., Mooney, W. D., Healy, J. H., McMechan, G. A., and Lutter, W. J., 1981, Seismic refraction studies of the Imperial Valley region, California—profile models, a traveltime contour map, and a gravity model: U.S. Geological Survey Open-File Report 81-270, 73 p.

Fuis, G. S., and Schnapp, M. R., 1977, The November–December 1976 earthquake swarms in northern Imperial Valley, California: Seismicity on the Brawley fault and related structures [abs.]: Eos (American Geophysical Union Transactions), v. 58, no. 12, p. 1188.

Fuis, G. S., Whitcomb, J. H., Johnson, C. E., Jenkins, D. J., Richter, K. J., Blanchard, A. C., Fischer, S. A., and Reed, B. A., 1978,

[3]Shotpoints 3, 4, and 8 were not used in our experiment.

Preliminary catalog of earthquakes in southern California, October 1976–September 1977: U.S. Geological Survey Open-File Report 78–672, 84 p.

Gastil, R. G., Phillips, R. P., and Allison, E. C., 1971,Reconnaissance geology map of the state of Baja California: Geological Society of America Memoir 140, 170 p.

Griscom, Andrew, and Muffler, L. J. P., 1971, Aeromagnetic map and interpretation of the Salton Sea geothermal area, California: U.S. Geological Survey Geophysical Investigations Map GP–754, 4 p., scale 1:62,500.

Hamilton, R. M., 1970, Time-term analysis of explosion data from the vicinity of the Borrego Mountain, California, earthquake of 9 April, 1968: Seismological Society of America Bulletin, v. 60, no. 2, p. 367–381.

Hamilton, R. M., 1972, Aftershocks of the Borrego Mountain earthquake from April 12 to June 12, 1968, *in* The Borrego Mountain earthquake of April 9, 1968: U.S. Geological Survey Professional Paper 787, p. 31–54.

Hill, D. P., Mowinckel, Penelope, and Peak, L. G., 1975, Earthquakes, active faults, and geothermal areas in the Imperial Valley, California: Science, v. 188, no. 4195, p. 1306–1308.

Hill, D. P., 1977, A model for earthquake swarms: Journal of Geophysical Research, v. 82, no. 8, p. 1347–1352.

——— 1978, A framework for block tectonics in California and Nevada [abs.]: Earthquake Notes, v. 49, no. 4, p. 96.

Jennings, C. W., compiler, 1967, Salton Sea sheet *of* Geologic map of California: California Division of Mines and Geology, scale 1:125,000.

Johnson, C. E., 1979, CEDAR—an approach to the computer automation of short-period local seismic networks; seismotectonics of the Imperial Valley of southern California: Pasadena, California Institute of Technology, Ph.D. thesis, 343 p.

Johnson, C. E., and Hadley, D. M., 1976, Tectonic implications of the Brawley earthquake swarm, Imperial Valley, California, January 1975: Seismological Society of America Bulletin, v. 66, no. 4, p. 1133–1144.

Kovach, R. L., Allen, C. R., and Press, Frank, 1962, Geophysical investigations in the Colorado delta region: Journal of Geophysical Research, v. 67, no. 7, p. 2845–2871.

Lachenbruch, A. H., and Sass, J. H., 1977, Heat flow in the United States and the thermal regime of the crust, *in* Heacock, J. G., ed., The Earth's crust: Its nature and physical properties: American Geophysical Union Geophysical Monograph 20, p. 626–675.

Larson, R. L., Menard, H. W., and Smith, S. M., 1968, Gulf of California: A result of ocean-floor spreading and transform faulting: Science, v. 161, no. 3843, p. 781–784.

Lewis, B. T. R., 1978, Evolution of ocean crust seismic velocities: Annual Review of Earth and Planetary Sciences, v. 6, p. 377–404.

Lin, Wunan, and Wang, C.-Y., 1980, P-wave velocities in rocks at high pressure and temperature and the constitution of the central California crust: Royal Astronomical Society Geophysical Journal, v. 61, no. 2, p. 379–400.

Lomnitz, Cinna, Mooser, C. R., Allen, C. R., Brune, J. N., and Thatcher, Wayne, 1970, Seismicity and tectonics of the northern Gulf of California region, Mexico. Preliminary results: Geofisica Internacional, v. 10, no. 2, p. 37–48.

McMechan, G. A., and Mooney, W. D., 1980, Asymptotic ray theory and synthetic seismograms for laterally varying structure: Theory and application to the Imperial Valley, California: Seismological Society of America Bulletin, v. 70, no. 6, p. 2021–2036.

Muffler, L. J. P. , and Doe, B. R., 1968, Composition and mean age of detritus of the Colorado River delta in the Salton Trough, southeastern California: Journal of Sedimentary Petrology, v. 38, no. 2, p. 384–399.

Muffler, L. J. P., and White, D. E., 1969, Active metamorphism of upper Cenozoic sediments in the Salton Sea geothermal field and the Salton Trough, southeastern California: Geological Society of America Bulletin, v. 80, no. 2, p. 157–181.

Oliver, H. W., Chapman, R. H., Biehler, Shawn, Robbins, S. L., Hanna, W. F., Griscom, Andrew, Beyer, L. A., and Silver, E. A., compilers, 1980, Gravity map of California and its continental margin: California Division of Mines and Geology Geologic Data Map 3, scale 1:750,000, 2 sheets.

Renner, J. L., White, D. E., and Williams, D. L., 1975, Hydrothermal convection systems, *in* White, D. E., and Williams, D. L., eds., Assessment of geothermal resources of the U.S.—1975: U.S. Geological Survey Circular 726 p. 5–57.

Robinson, P. T., Elders, W. A., and Muffler, L. J. P., 1976, Quaternary volcanism in the Salton Sea geothermal field, Imperial Valley, California: Geological Society of America Bulletin, v. 87, no. 3, p. 347–360.

Sharp, R. V., 1972, Tectonic setting of the Salton Trough, *in* The Borrego Mountain earthquake of April 9, 1968: U.S. Geological Survey Professional Paper 787, p. 3–15.

Simmons, Gene, 1964, Velocity of compressional waves in various minerals at pressures to 10 kilobars: Journal of Geophysical Research, v. 69, no. 6, p. 1117–1121.

Stewart, Roger, and Peselnick, Louis, 1977, Velocity of compressional waves in dry Franciscan rocks to 8 kbar and 300°C: Journal of Geophysical Research, v. 82, no. 14, p. 2027–2039.

——— 1978, Systematic behavior of compressional velocity in Franciscan rocks at high pressure and temperature: Journal of Geophysical Research, v. 83, no. B2, p. 831–839.

Strand, R. G., compiler, 1962, San Diego-El Centro sheet *of* Geologic map of California: California Division of Mines and Geology, scale 1:250,000.

Thatcher, Wayne, 1979, Horizontal crustal deformation from historic geodetic measurements in southern California: Journal of Geophysical Research, v. 84, no. B5, p. 2351–2370.

MAIN-SHOCK LOCATION AND MAGNITUDE DETERMINATION USING COMBINED U.S. AND MEXICAN DATA

By DAVE CHAVEZ, JAVIER GONZALES, ALFONSO REYES, MAURU MEDINA, and CARLOS DUARTE,
CENTRO DE INVESTIGACIÓN CIENTÍFICA Y EDUCACIÓN SUPERIOR DE ENSENADA, BAJA CALIFORNIA;

JAMES N. BRUNE, FRANK L. VERNON III, and RICHARD SIMONS,
SCRIPPS INSTITUTION OF OCEANOGRAPHY;

L. K. HUTTON,
CALIFORNIA INSTITUTE OF TECHNOLOGY;

and

PETER T. GERMAN and CARL E. JOHNSON,
U.S. GEOLOGICAL SURVEY

CONTENTS

ABSTRACT

We obtained a main-shock epicenter of lat 32°38.61′ N., long 115°18.53′ W., using combined U.S. and Mexican network and strong-motion data. A total of 31 *P*-wave and 4 *S*-wave arrival times within 30 km permit considerable confidence in a calculated focal depth of 10.0 km. We also determined a local magnitude of 6.6 on the basis of 14 amplitudes from torsion seismometers.

INTRODUCTION

The October 15, 1979, Imperial (Mexicali) Valley earthquake (M_L=6.6) occurred near several permanent seismic networks in the United States and Mexico. Because the epicenter lay outside the individual arrays, initial locations calculated using the data from any single group of stations were inaccurate. By pooling the arrival times from all networks, however, we have obtained almost complete azimuthal coverage and a reliable hypocentral solution.

DATA

In selecting the arrival-time data, we restricted ourselves to stations within 75 km of the probable epicenter. Most times are from 22 stations in the Imperial Valley seismic network, operated jointly by the U.S. Geological Survey (USGS) and the California Institute of Technology (CIT). These stations, as well as two additional strong-motion stations (Porcella and Matthiesen, 1979), are all within the United States. South of the epicenter, in Mexico, times were available from 10 stations in two permanent seismic networks; these stations include 5 of the Red Sismológica de Cerro Prieto (RESCEP), operated by the Centro de Investigación Científica y Educación Superior de Ensenada (CICESE), and five strong-motion instruments installed by the Universidad Nacional Autónoma de México (UNAM) and the University of California, San Diego (UCSD). The station coordinates and arrival times are listed in table 3, and their positions are shown on the map (fig. 27).

The CEDAR and RESCEP arrays are both short-period telemetry systems with radio WWVB time coding; arrival times at these stations were read with a precision of ±0.02 and ±0.10 s, respectively. The strong-motion instruments are film recorders with WWVB time coding that allow arrival times to be picked with an accuracy of ±0.10 s. The UNAM/UCSD strong-motion stations (with the exception of station SAHOP, fig. 27) record digitally on magnetic tape with timing by an internal clock. Time corrections for as-

TABLE 3.—*Stations used in locating the main shock*

[Arrival times in seconds after 2316 G.m.t. Residuals were calculated using model in table 4 and solution given in text]

Station		Epicentral distance (km)	Lat N.	Long W.	Correction (s)	*P*-arrival time 1		*S*-arrival time 2		Network
Name	Code					Observed	Residual	Observed	Residual	
Islas Agrarias	AG	2.6	32°37.25′	115°18.07′		56.88	+0.10	58.58	−0.15	UNAM/UCSD strong motion
Bond's Corner	5054	6.1	32°41.58′	115°20.28′		57.01	−0.07	59.51	+0.24	USGS strong motion
Bond's Corner	BON	6.8	32°41.67′	115°16.11′		56.97	−0.19			CEDAR
SAHOP, Mexicali	SAHOP	10.8	32°37.20′	115°25.20′		2.70	[1]+0.04			UNAM/UCSD strong motion
Calexico Fire Station	5053	17.2	32°40.20′	115°29.40′		58.77	+0.11	61.86	−0.21	USGS strong motion
Chihuahua	CH	19.0	32°29.00′	115°14.20′		59.32	[2]+0.41	61.52	−1.00	UNAM/UCSD strong motion
Cerro Prieto	CP	24.2	32°25.52′	115°18.34′	−0.80	58.84	0.00	62.34	−0.05	Do.
Tlaxcala	TLX	24.3	32°28.39′	115°08.71′		59.54	−0.12			RESCEP
Brock's Farm	BSC	26.4	32°43.49′	115°02.64′		59.87	−0.08			CEDAR
Schaffner Ranch	SNRV	27.0	32°51.71′	115°26.21′		60.04	+0.01			Do.
Schaffner Ranch	SNR	27.0	32°51.71′	115°26.21′		60.05	+0.02			Do.
Neuvo Leon	NVL	28.7	32°23.91′	115°12.66′		60.20	−0.06			RESCEP
Coachella	COA	30.0	32°51.81′	115°07.36′		60.45	+0.01			CEDAR
Delta	DT	33.6	32°21.37′	115°11.70′		61.39	[2]+0.44			UNAM/UCSD strong motion
Veracruz	VER	36.7	32°21.67′	115°06.32′		61.60	+0.23			RESCEP
Cucapah	QKP	37.6	32°18.30′	115°19.92′	−0.80	60.50	−0.20			Do.
Ingram Ranch	ING	38.2	32°59.30′	115°18.61′		61.60	+0.01			CEDAR
Signal Mountain	SGL	39.1	32°38.95′	115°43.52′	−0.80	60.81	−0.10			Do.
Sonora	SON	41.3	32°17.50′	115°09.83′		62.30	+0.28			RESCEP
Cook Ranch	COK	45.4	32°50.95′	115°43.61′		62.40	−0.18			CEDAR
Wiest Lake	WLK	48.3	33°03.08′	115°29.44′		63.18	+0.19			Do.
Westmorland	WML	50.6	33°00.91′	115°37.35′		63.49	+0.18			Do.
Pilot Knob	PLT	55.2	32°43.87′	114°43.76′	−0.80	63.65	+0.51			Do.
Amos	AMS	55.5	33°08.48′	115°15.25′		63.62	−0.36			Do.
Calipatria	CLI	58.8	33°08.45′	115°31.64′		64.54	+0.09			Do.
Superstition Mountain	SUP	59.4	32°57.31′	115°49.43′		63.99	+0.27			Do.
New River	NW2	61.2	33°05.43′	115°41.54′		64.81	+0.03			Do.
Obsidian Butte	OBB	65.7	33°10.04′	115°38.20′	−0.80	64.53	−0.07			Do.
Carrizo Mountain	CRR	67.4	32°53.20′	115°58.10′	−0.80	65.29	+0.45			Do.
Yuma Desert	YMD	72.4	32°33.28′	114°32.68′		66.14	−0.19			Do.
Chocolate Mountains	CH2	72.4	33°17.77′	115°20.17′		66.15	−0.19			Do.
Elmore Ranch	ELR	73.8	33°08.48′	115°49.95′		66.62	+0.09			Do.
Wister	WIS	75.0	33°16.56′	115°35.58′		66.49	−0.21			Do.
Ikopah	IKP	75.1	32°38.90′	116°06.50′	−0.80	66.39	+0.49			Do.

[1]$S-P$ time.
[2]Time was not used in calculations.

sumed linear clock drift over an average period of 1 week were approximately 2 s at each site. Arrival times were read with a precision of ±0.04 s. The strong-motion instrument at station SAHOP is a film recorder with no absolute timing; the $S-P$ time at station SAHOP is within ±0.10 s.

LOCATION PROCEDURE

We calculated the hypocenter and origin time using the HYPO71 computer program of Lee and Lahr (1975) with a velocity model from Mooney and McMechan (this volume) given in table 4. Several velocity models were tested, in each of which the resulting solution did not vary by more than a few hundred meters. We selected Mooney and McMechan's model because it gave the smallest traveltime residuals. Because their model includes a sedimentary cover, a correction of −0.80 s had to be applied to the times for all stations situated on bedrock; this value is the average traveltime residual at the bedrock sites, as calculated for a preliminary hypocentral location.

Arrival times at stations within 40 km of the epicenter were assigned distance weights of 1, and farther stations were assigned progressively lesser weights such that at 80 km the distance weight was 0. Standard Jeffreys' weighting of residuals was also applied.

The arrivals at strong-motion stations CH and DT (fig. 27) are inconsistent with the times at the surrounding stations, possibly owing to errors in the time correction, and so we did not use the data from these stations in our calculations. In all, a total of 31 P-wave arrivals, 4 S-wave arrivals (from the strong-motion records), and 1 $S-P$ time were used.

TABLE 4.—*Velocity model used in this study*

[Model from Mooney and McMechan (this volume). Velocities were computed assuming a V_p/V_s ratio of 1.78]

Depth to top of layer (km)	Compressional-wave velocity (km/s)
0.0	2.00
.5	2.40
1.0	2.80
2.0	3.45
3.0	4.10
4.0	4.75
5.0	5.45
6.0	5.80
10.0	6.75
10.5	7.05
11.0	7.20

The best solution obtained has an origin time of 2316:54.29 G.m.t. October 15, 1979, and a hypocentral location of lat 38°38.61′ N., long 115°18.53′ W., at a depth of 9.96 km (errors are ±0.4 km horizontal, ±0.2 km vertical). The traveltime residuals for this location are listed in table 3.

MAGNITUDE DETERMINATION

Magnitude (M_L) estimates for the main shock were determined using all available torsion seismometers in the southern California seismic network (table 5). The 2,800× instruments at station CWC are standard Wood-Anderson torsion seismometers recording photographically, and those at station ISA are telemetered with an electronically simulated Wood-Anderson response. All others (100× and 4×) are recorded photographically on film. Individual estimates of magnitude range from 6.2 to 7.1; both the mean and median magnitudes, however, are 6.6, a value that appears to be constrained to within ±0.1.

DISCUSSION

The main-shock epicenter was located 3 km south of the United States-Mexican border and approximately 10 km east of Mexicali, Mexico. This solution is well constrained by the broad azimuthal coverage (283°) and

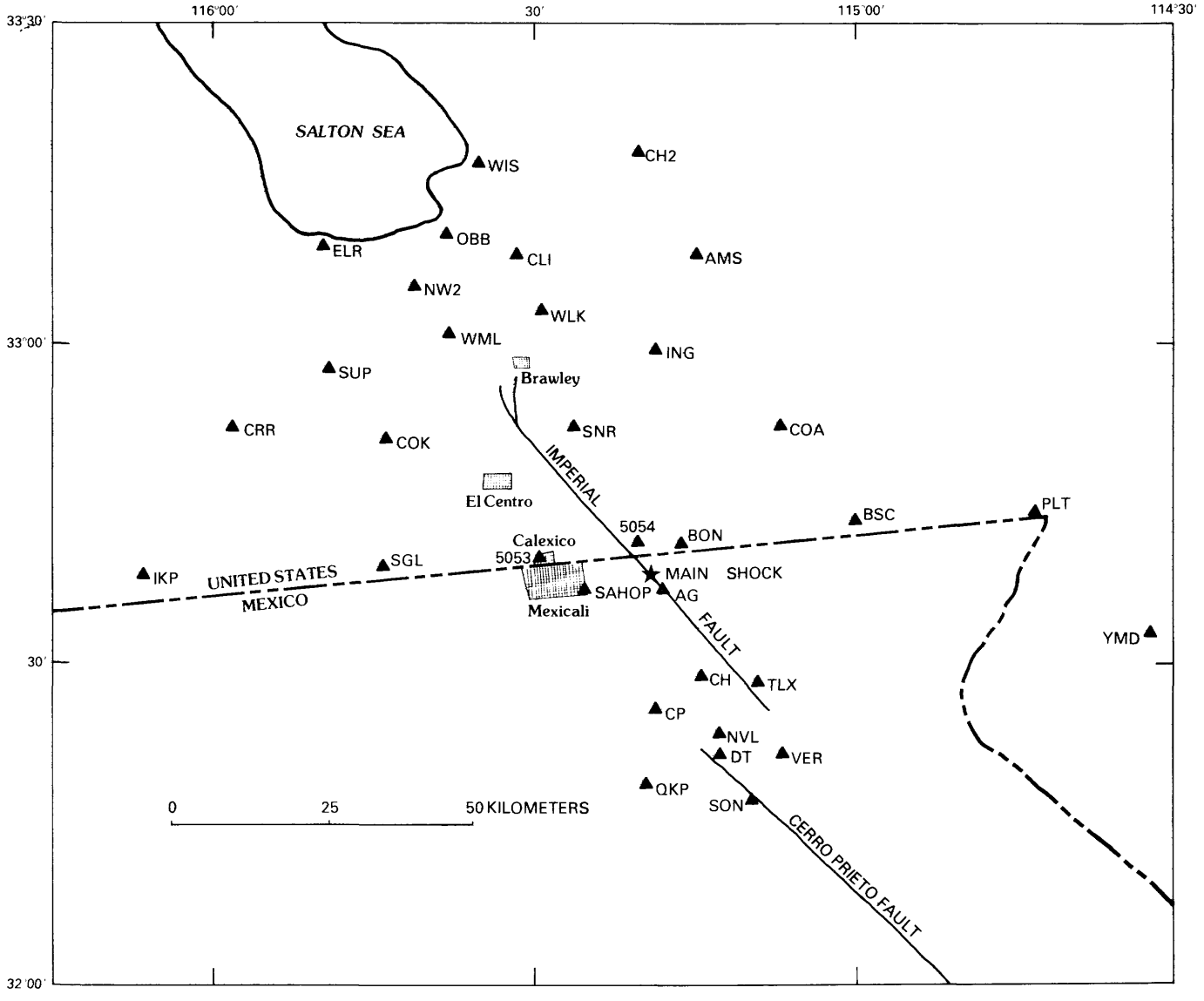

FIGURE 27.—Main-shock epicenter and seismic-network and strong-motion stations within 75 km.

TABLE 5.—*Individual station estimates and epicentral distances used in calculating local magnitude* (M_L)

Station	Epicentral distance (km)	Magnitude	
		Raw	Corrected
2,800× torsions			
CWCN	494	6.6	6.6
CWCE	494	6.8	6.8
ISAN	445	6.1	6.3
ISAE	445	6.2	6.4
100× torsions			
CWCN	494	6.9	6.9
CWCE	494	6.9	6.9
SBCN	445	7.2	7.1
SBCE	445	7.1	7.0
PASN	315	6.8	6.9
PASE	315	6.5	6.6
RVRN	244	6.1	6.2
RVRE	244	6.1	6.2
4× torsions			
PASN	315	6.4	6.5
RVRN	244	6.3	6.4
Median			6.6
Mean			6.63±0.08

by the data from three stations (AG, BON, 5054, fig. 27) that are within 7 km of the epicenter.

The 9.96-km depth we obtained is slightly greater than the 6- to 8-km average depth for Imperial Valley earthquakes (Johnson, 1979). The significance, if any, of this depth is not yet understood. This greater depth might explain, however, the fact that although the epicenter was in Mexico, the only surface rupture observed was north of the border.

REFERENCES CITED

Johnson, C. E., 1979, CEDAR—an approach to the computer automation of short-period local seismic networks; seismotectonics of the Imperial Valley of southern California: Pasadena, California Institute of Technology, Ph. D. thesis, 343 p.

Lee, W. H. K., and Lahr, J. C., 1975, HYPO71 (revised): A computer program for determining hypocenter, magnitude, and first motion pattern of local earthquakes: U.S. Geological Survey Open-File Report 75–311, 113 p.

Porcella, R. L., and Matthiesen, R. B., 1979, Preliminary summary of the U.S. Geological Survey strong-motion records from the October 15, 1979 Imperial Valley earthquake: U.S. Geological Survey Open-File Report 79–1654, 41 p.

LONG-PERIOD SURFACE WAVES[1]

By HIROO KANAMORI and JANICE REGAN,
CALIFORNIA INSTITUTE OF TECHNOLOGY

CONTENTS

ABSTRACT

The seismic moment of the 1979 Imperial Valley earthquake is determined to be 6×10^{18} N·m (that is, $M_w=6.5$) from long-period Love and Rayleigh waves. The ratio of local magnitude M_L to M_w for the event is 1.02, significantly larger than the value 0.90 for the 1940 Imperial Valley earthquake.

INTRODUCTION

Long-period surface waves (R_2, G_2, and G_3) generated by the 1979 Imperial Valley earthquake were recorded by the ultra-long-period seismographs at Pasadena and Berkeley, Calif. Here we present these data, determine the seismic moment, and compare this event with the 1940 Imperial Valley earthquake. Table 6 lists the location data for both stations.

Long-period (about 120 s) Rayleigh waves (R_2) were recorded with a peak-to-peak amplitude of 0.27 mm by the Pasadena (station PAS) ultra-long-period vertical seismograph (maximum magnification, 28× at $T=150$ s). Longer period (about 200 s) wave trains corresponding to the Airy phase (group velocity, 3.55 km/s) followed this wave train with a smaller amplitude (fig. 28).

TABLE 6.—*Data on ultra-long-period seismograph stations*

Station	Epicentral distance Δ	Azimuth ϕ_E	Backazimuth ϕ_s
PAS (Pasadena)	2.82°	303°	122°
BKS (Berkeley)	7.70°	315°	131°

[1]Contribution No. 3367, Division of Geological and Planetary Sciences, California Institute of Technology, Pasadena, CA 91125.

G waves (G_2 and G_3) were recorded by an ultra-long-period seismograph (NE-SW component) at Berkeley (station BKS) with peak-to-peak amplitudes of 10.5 and 7 mm, respectively (fig. 29). This seismograph has a peak magnification of 500× at a period of 100 s. Because the backazimuth at station BKS is S. 49° E., this component is almost transverse to the path and represents the *SH* component.

INTERPRETATION

We compared these seismograms with synthetic seismograms (figs. 28, 29) computed according to the method of Kanamori and Cipar (1974). The fault geometry was assumed to be vertical right-lateral strike-slip with a strike of N. 37° W. that coincides with the overall strike of the Imperial fault. For computing the synthetics, we used fundamental spheroidal and torsional modes with order numbers of from 2 to 100

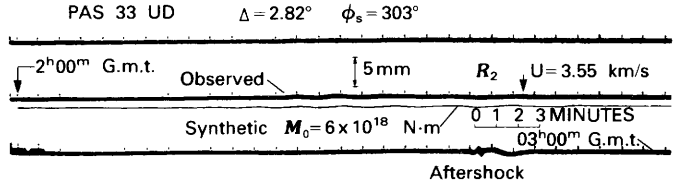

FIGURE 28.—Ultra-long-period record of Rayleigh waves (R_2) registered by station Pasadena (PAS) seismograph 33; UD denotes vertical component. Synthetic seismogram computed for seismic moment (M_0) of 6×10^{18} N·m is presented for comparison. Δ, epicentral distance; ϕ_s, backazimuth; U, group velocity.

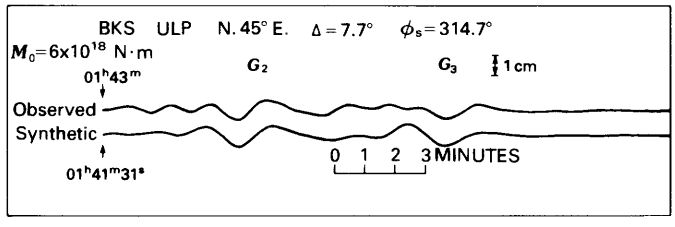

FIGURE 29.—Record of long-period Loves waves (G_2 and G_3) registered by station Berkeley (BKS) ultra-long-period (ULP) seismograph. Synthetic seismogram computed for a seismic moment (M_0) of 6×10^{18} N·m is presented for comparison. Δ, epicentral distance; ϕ_s, backazimuth.

computed for Earth model 5.08 M (Kanamori, 1970; Press, 1970). A point source was placed at a depth of 33 km. For vertical strike-slip, the excitation of long-period (100–300 s) surface waves does not vary significantly for a depth range of 0–50 km.

For the purpose of the present analysis, the choices of the Earth model and the depth are not critical. We obtain a seismic moment of 6×10^{18} N·m from comparison of the amplitude of the G_2 wave at station BKS. From the amplitude of the Rayleigh wave (R_2) at station PAS, we obtain a seismic moment of 5×10^{18} N·m. The azimuth of station BKS is in the loop direction (direction of maximum amplitude) of the G-wave radiation pattern for the assumed fault geometry (fig. 30), and so a small change in the strike direction of the fault results in an insignificant difference in the amplitude of the synthetic seismogram. On the other hand, station PAS is close to the nodal direction of the Rayleigh-wave radiation pattern, and so a small change in the fault geometry would significantly change our estimate of the seismic moment. For instance, a change in the fault strike of $\pm3°$ would change the seismic moment by about 30 percent. Thus, we prefer the value of 6×10^{18} N·m obtained from the station BKS record to that of 5×10^{18} N·m obtained from the station PAS record. The reasonably good agreement between these two estimates, however, suggests that the assumed fault geometry is a good approximation.

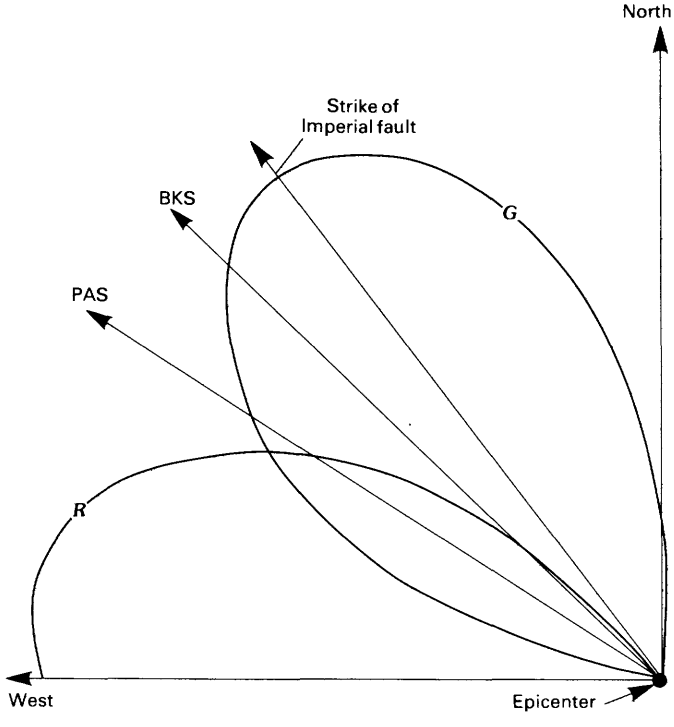

FIGURE 30.—Amplitude-radiation patterns of long-period Love (G) and Rayleigh (R) waves for a vertical strike-slip fault whose strike coincides with that of Imperial fault. Arrows indicate azimuths of seismograph stations PAS and BKS.

The assumed fault geometry (fig. 30) places station BKS almost in the nodal direction of the Rayleigh-wave radiation pattern, as substantiated by the absence of long-period (200 s) Rayleigh waves on the vertical component of the ultra-long-period seismogram from this station (not shown).

COMPARISON OF 1940 AND 1979 IMPERIAL VALLEY EARTHQUAKES

The seismic moment of the 1940 Imperial Valley earthquake has not been determined directly from long-period surface waves. On the basis of geodetic data and the amount of surface breaks, Byerly and DeNoyer (1958), Kasahara (1958), and Brune and Allen (1967) estimated the fault length, fault width, and amount of slip on the fault for the 1940 event. Kanamori and Anderson (1975) averaged these results and estimated a seismic moment of 56×10^{18} N·m, almost 10 times larger than that for the 1979 event. Converting the seismic moment to moment magnitude (M_w) (Kanamori, 1977), we calculate $M_w=6.5$ and 7.1 for the 1979 and 1940 events, respectively. The surface-wave magnitude (M_s) of 7.1 for the 1940 event (Gutenberg and Richter, 1949) agrees with this value of M_w.

The local magnitude (M_L) for the 1940 earthquake ranges from 6.3 to 6.5 (see Kanamori and Jennings, 1978). For the 1979 event, the average value of M_L obtained from the California Institute of Technology network is 6.6. These values can be used to compare the characteristics of the 1940 and 1979 events. Figure 31 plots M_L against M_s (or M_w) for major California events and for the 1976 Guatemala earthquake; the data points define a range of M_L at a given M_s for California earthquakes. Two important features are (1) the M_L scale appears to saturate at 7¼, and (2) for a given M_s the range of M_L is about 0.5. Because M_L represents the size of an earthquake at high frequencies, events that plot near the upper edge of the band are more likely to cause stronger ground shaking than events with the same M_s that plot near the lower edge of the band. We note that the 1940 and 1979 Imperial Valley earthquakes seem to represent the two extremes of California events. Because practically all M_L values have been determined from the data obtained at stations to the north of the epicenter, this contrast may be due to rupture propagation rather than to any intrinsic difference in the two events. Nevertheless, it is significant that two earthquakes originating from approximately the same source region could have such different spectral characteristics.

DISCUSSION AND CONCLUSIONS

The seismic moment (M_0) of 6×10^{18} N·m obtained for the 1979 event indicates that the average slip (offset) at depth was approximately 57 cm. This estimate assumes a fault length of 35 km, a fault width of 10 km, and rigidity of 30 GPa. The average surface displacement observed over a 35-km section of the Imperial fault was about 20 cm about 1 day after the earthquake; although this displacement nearly doubled during the subsequent 10-day period (K. E. Sieh, oral commun., 1979), it is still considerably smaller than the amount of slip inferred from the seismic data. The surface break probably represents a delayed anelastic response of the sedimentary and soil layers to slip at depth. If this interpretation is correct, we expect that the surface break will eventually equal the slip at depth (57 cm).

The nearly tenfold difference in the magnitude of the seismic moment between the 1940 and 1979 events suggests that the overall fault displacement of the 1979 event is only a small perturbation in comparison with that of the 1940 event. Nevertheless, in terms of the ratio of M_L to M_S (or M_W), the 1979 event appears to be unusually significant because it contained so much high-frequency energy (at least for paths to the north) for its relatively small overall size, as measured by M_W.

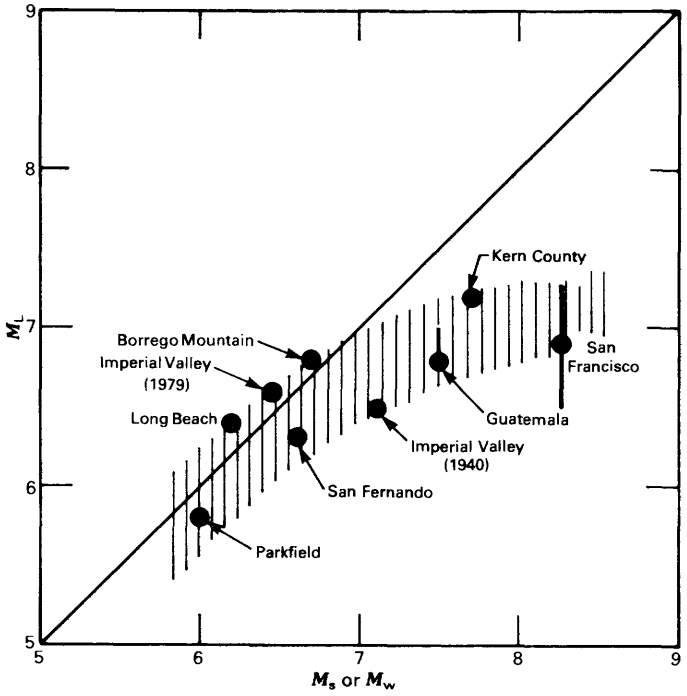

FIGURE 31.—Local magnitude (M_L) as a function of surface-wave magnitude (M_S) or moment magnitude (M_W) for California earthquakes and 1976 Guatemala earthquake (modified from Kanamori, 1979). Diagonal line represents M_L equivalent to M_S; band of vertical lines defines range of M_L at a given M_S for California earthquakes.

ACKNOWLEDGMENTS

The ultra-long-period seismograms from station BKS used in this report were made available to us through the courtesy of the director of the Seismographic Stations at the University of California, Berkeley. We thank Donald Michniuk for useful information on the instrumental constants, and Kerry E. Sieh for information on and discussion of the surface break. This research was supported by the Earth Sciences Section, National Science Foundation, under Grant EAR 78–12642, and by U.S. Geological Survey Contract 14–08–0001–18321.

Note added.—After our data were finalized, long-period seismograms from International Deployment of Accelerometers (IDA) stations (Agnew and others, 1976) became available to us by the courtesy of the IDA project team at the University of California, San Diego. To check the result reported in this chapter, we analyzed 14 Rayleigh-wave phases from 7 IDA stations and obtained the source parameters, according to the method of Kanamori and Given (1981). We constrained the mechanism to be either pure vertical strike-slip or 45° pure dip-slip, and obtained the following solution:

Fault type	Strike-slip
Fault strike	N. 34° W. (right lateral)
Seismic moment	7×10^{18} N·m at a period of 200 to 250 s, with a slight indication of increasing moment at longer periods (assuming a point source at a depth of 9.75 km).

This result agrees well with that reported in this chapter.

REFERENCES CITED

Agnew, D. C., Berger, Jonathan, Buland, R. P., Farrell, W. E., and Gilbert, Freeman, 1976, International Deployment of Accelerometers: A network for very long period seismology: Eos (American Geophysical Union Transactions), v. 57, no. 4, p. 180–188.

Brune, J. N., and Allen, C. R., 1967, A low-stress-drop, low-magnitude earthquake with surface faulting: The Imperial, California, earthquake of March 4, 1966: Seismological Society of America Bulletin, v. 57, no. 3, p. 501–514.

Byerly, Perry, and DeNoyer, John, 1958, Energy in earthquakes as computed from geodetic observations, *in* Benioff, Hugo, Ewing, Maurice, Howell, B. F., Jr., and Press, Frank, eds., Contributions in geophysics in honor of Beno Gutenberg: New York, Pergamon, p. 17–35.

Gutenberg, Beno, and Richter, C. F., 1949, Seismicity of the Earth and associated phenomena: Princeton, N.J., Princeton University Press, 273 p.

Kanamori, Hiroo, 1970, Velocity and Q of mantle waves: Physics of the Earth and Planetary Interiors, v. 2, no. 4, p. 259–275.

———1977, The energy release in great earthquakes: Journal of Geophysical Research, v. 82, no. 20, p. 2981–2987.

———1979, A semi-empirical approach to prediction of long-period ground motions from great earthquakes: Seismological Society of America Bulletin, v. 69, no. 6, p. 1645–1670.

Kanamori, Hiroo, and Anderson, D. L., 1975, Theoretical basis of some empirical relations in seismology: Seismological Society in America Bulletin, v. 65, no. 5, p. 1073–1095.

Kanamori, Hiroo, and Cipar, J. J., 1974, Focal process of the great Chilean earthquake May 22, 1960: Physics of the Earth and Planetary Interiors, v. 9, no. 2, p. 128–136.

Kanamori, Hiroo, and Given, J. W., 1981, Use of long-period surface waves for rapid determination of earthquake-source parameters: Physics of the Earth and Planetary Interiors, v. 27, no. 1, p. 8–31.

Kanamori, Hiroo, and Jennings, P. C., 1978, Determination of local magnitude, M_L, from strong-motion accelerograms: Seismological Society of America Bulletin, v. 68, no. 2, p. 471–485.

Kasahara, Keichi, 1958, Physical conditions of earthquake faults as deduced from geodetic data: University of Tokyo, Earthquake Research Institute Bulletin, v. 36, no. 4, p. 455–465.

Press, Frank, 1970, Earth models consistent with geophysical data, *in* Ringwood, A. E., and Green, D. H., eds., Phase transformations and the Earth's interior: Physics of the Earth and Planetary Interiors, v. 3 (special volume), p. 3–22.

AFTERSHOCKS AND PREEARTHQUAKE SEISMICITY[1]

By CARL E. JOHNSON,
U.S. GEOLOGICAL SURVEY;

and

L. K. HUTTON,
CALIFORNIA INSTITUTE OF TECHNOLOGY

CONTENTS

ABSTRACT

Although primary surface faulting was mapped for nearly 30 km, aftershocks extended in a complex pattern more than 100 km along the trend of the Imperial fault. A first-motion focal mechanism for the main shock is consistent with right-lateral motion on a vertical fault striking N. 42° W., in agreement with the strike of the Imperial fault within the limits of resolution. There is evidence that conjugate faulting on a buried complementary northeast-trending structure occurred at the north limit of displacement on the Imperial fault near Brawley, Calif. This faulting was apparently initiated at the time of a magnitude 5.8 aftershock 8 hours after the main shock. A line of epicenters extending along the trend of the San Andreas fault nearly 100 km into the eastern Imperial Valley was noted during the aftershock sequence, in an area recognized as notably aseismic during the preceding 5 years. The main shock was preceded by a 3-month period of significantly reduced seismicity affecting the central Imperial Valley. Although three small events near the incipient epicenter during this interval may be deemed foreshocks, no distinct foreshocks immediately before the main shock were observed.

INTRODUCTION

The Imperial Valley earthquake of October 15, 1979, was the largest in California since the installation of dense seismic networks and thus provides a unique opportunity for studying both the aftershocks and prior seismicity of a moderate earthquake in a detail never before possible. During the next few years we expect that the tens of thousands of digital seismograms for several thousand aftershocks, together with a large body of other geophysical data, will provide the basis for many inquiries into the physical processes attending major earthquakes. Here we provide only a preliminary and incomplete picture of the most conspicuous of these phenomena.

Our ideas are not presented chronologically. We first discuss gross aspects of the aftershock distribution and then place it within a context of seismicity during the preceding years. Having discussed what appears to have been normal background seismicity for the central Imperial Valley, we can then consider possibly unusual aspects of activity during the weeks immediately before the main shock.

ANALYSIS

Our data are from 150 short-period vertical instruments in the southern California seismic network operated jointly by the California Institute of Technology (CIT) and the U.S. Geological Survey (USGS). These data were telemetered in analog form to CIT, where they were digitized at 50 Hz. A real-time event detector recorded selected intervals of record on magnetic tape for subsequent offline analysis on an interactive cathode-ray-tube (CRT) display terminal.

Both the event locations and magnitudes reported here (table 7) are preliminary results from the first stage of routine processing, using the CEDAR system described by Johnson (1979). Final values will not be available until much more editing and analysis of the data have been completed. Processing of the more than 2,000 aftershocks that occurred during the first 20 days after the earthquake required the accurate timing of more than 40,000 discrete arrivals. Hypocenters were calculated using an unpublished program (QED1) de-

[1]Contribution No. 3459, Division of Geological and Planetary Sciences, California Institute of Technology, Pasadena, CA 91125.

TABLE 7.—*Preliminary origin times, epicentral coordinates, and local magnitudes for aftershocks of* $M_l \geq 4.0$

Date	Origin time (G.m.t.)	Epicentral coordinates		Local magnitude (M_l)
		Latitude N.	Longitude W.	
10/15	2316:53.44	32°36.82′	115°19.09′	6.6
	2319:29.98	32°45.94′	115°26.45′	5.0
	2325	----	----	4.0
	2355:03	32°55′	115°31′	[1]4.2
10/16	0022:14.20	32 57.46′	115°31.19′	4.2
	0100:13.86	32°57′	115°29′	[1]4.6
	0114:21.29	32°55.54′	115°31.38′	4.3
	0139:04	32°56.45′	115°31.45′	4.0
	0310	----	----	4.5
	0316:25.43	32°56.73′	115°32.56′	4.1
	0339	----	----	4.5
	0549:10.18	32°56.63′	115°32.38′	5.0
	0604:39.03	32°54.79′	115°32.07′	4.1
	0611:59.96	32°56.05′	115°30.88′	4.2
	0613:13.41	32°55.45′	115°31.60′	4.2
	0619:48.68	32°55.71′	115°32.36′	5.1
	0655	----	----	4.6
	0658:42.69	32°59.83′	115°34.41′	5.8
	0723:24.21	32°53.92′	115°31.12′	4.2
	0749	----	----	4.0
	0936:41.14	32°56.31′	115°30.87′	4.0
	1051:27.11	32°56.34′	115°33.02′	4.0
	1126:27.40	32°57.83′	115°35.19′	4.0
	1146	----	----	4.8
	1201:44.96	32°52.31′	115°31.07′	4.0
	1500	----	----	4.0
	2316	----	----	4.9
10/17	1914:37.72	32°54.39′	115°35.00′	4.2
	2052	----	----	4.2
	2245	----	----	4.6
10/19	1222	----	----	4.1

[1]Epicentral location in error by 5 km or more.

veloped at CIT, based on the generalized inverse method formalized by Wiggins (1972). The crustal model used for all hypocentral calculations (table 8) was obtained graphically from the models presented by Mooney and McMechan (this volume), using data obtained during the Imperial Valley seismic-refraction experiment discussed by Fuis and others (this volume). This model is representative of the central Imperial Valley south of Brawley, Calif. Most magnitudes greater than 3.0 are standard M_L's from peak amplitudes on Wood-Anderson torsion seismometers; the remaining magnitudes are M_{ca}'s calculated from coda amplitudes, using the method of Johnson (1979). Focal mechanisms were obtained using the computer program described by Whitcomb (1973).

TABLE 8.—*Crustal model used for locating aftershocks*

Depth to top of layer (km)	Layer velocity (km/s)
0	2.15
1	2.75
2	3.60
3	4.30
4	5.05
5	5.50
5.5	5.70
10.0	5.80
13.0	6.95
14.0	7.20
25.0	7.80

We selected events for analysis and graphic presentation solely on the basis of location quality (epicentral error, less than 5 km), a criterion that generally favors the largest events during a given period. Some events of magnitude larger than 4.0 have been ignored either because they were immediately preceded by others large enough to make accurate timing difficult or because they occurred during an interval for which digital data were not available.

AFTERSHOCK DISTRIBUTION

Figure 32 illustrates all well-located aftershocks that occurred during the first 20 days of the aftershock sequence (October 15 through November 5). The main shock, denoted by the star south of the United States-Mexican border, lies within a zone that remained surprisingly aseismic throughout the sequence. A more accurate epicenter for the main shock, obtained by Chavez and others (this volume) using a balanced suite of U.S. and Mexican data, plots about 2 km to the northeast, midway between the location shown on the map (fig. 32) and the United States-Mexican border.

The focal mechanism for the main shock (lower right, fig. 32) is consistent with right-lateral motion on a vertical fault striking N. 42° W., in general agreement with the trend of the southern section of the Imperial fault. Although surface breaks were limited to a zone 30 km long (heavy lines, fig. 33), aftershocks occurred within an area 110 km long, from the Cerro Prieto geothermal area to the Salton Sea. Except for one small group of events near the south terminus of surface rupture, most aftershocks were clustered within about 15 km of Brawley, particularly during the first 8 hours after the main shock (fig. 33).

A significant change in the aftershock distribution occurred after the largest aftershock (M_L=5.8) at 0658 G.m.t. October 16, approximately 8 hours after the main shock and immediately after the interval plotted in figure 33. The location of this event, here referred to as the Brawley aftershock, is marked by its focal mechanism, plotted west of Brawley on the map (center, fig. 32). The most distinctive change in the aftershock pattern was a strong northeast-trending line of epicenters from west of Brawley to just south of Wiest Lake (WLK, figs. 32, 33), in agreement with the left-lateral plane of the focal mechanism. Tectonically the local increase in strain at the north end of the Imperial fault break was apparently accommodated by left-lateral motion on a conjugate fault propagating from southwest to northeast. Independent support for this conclusion is provided by a coincident linear zone of ground disturbance, liquefaction, and cracking mapped by T. H. Heaton, J. G. Anderson, and P. T. German (unpub. data, 1980). Unfortunately, fieldwork was complicated by slumping

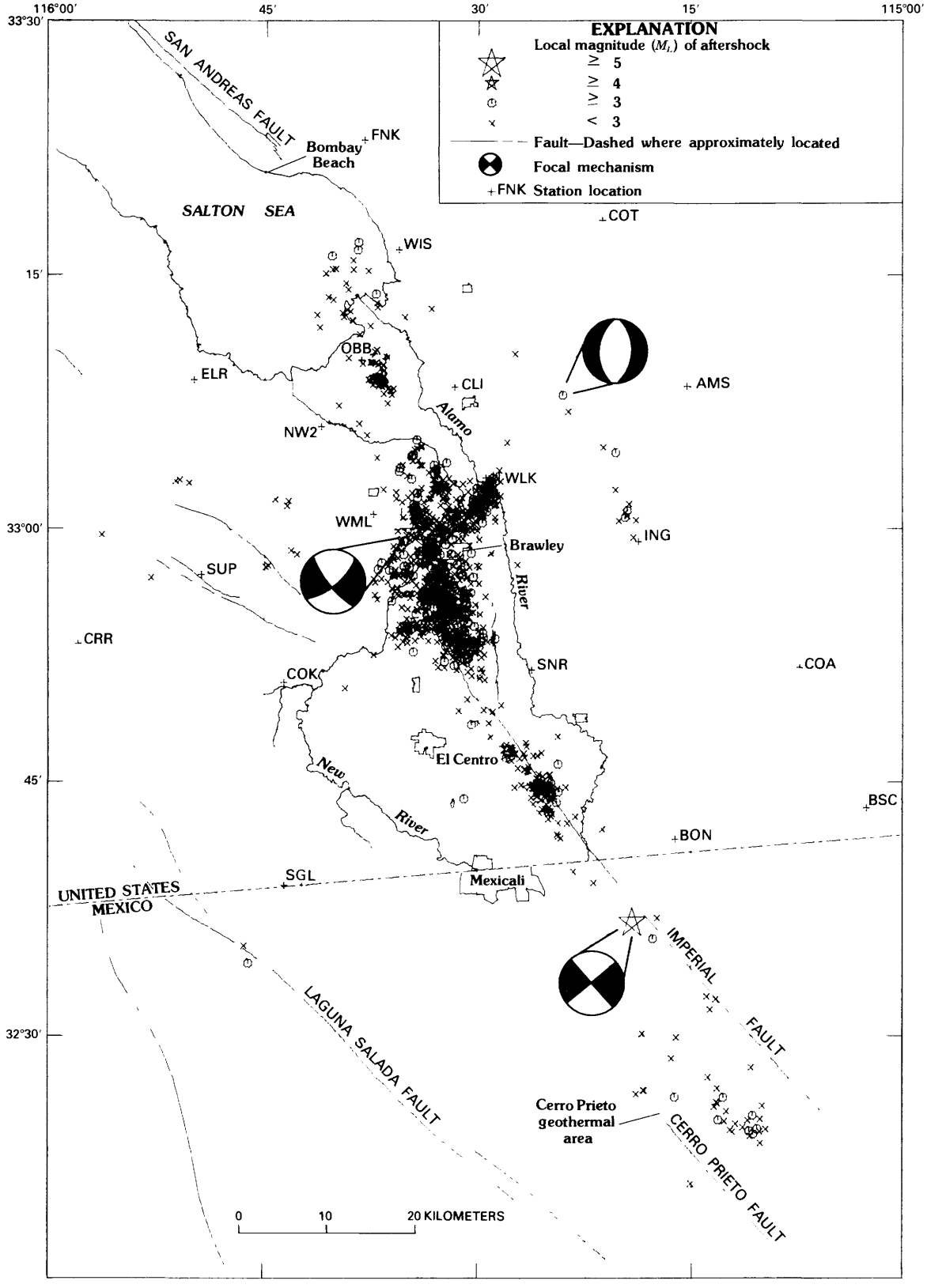

FIGURE 32.—Well-located aftershocks (epicentral error, less than 5 km) from October 15 through November 5, 1979. Focal mechanisms are lower-hemisphere equal-area projections with compressional quadrants darkened. Star denotes location of main shock.

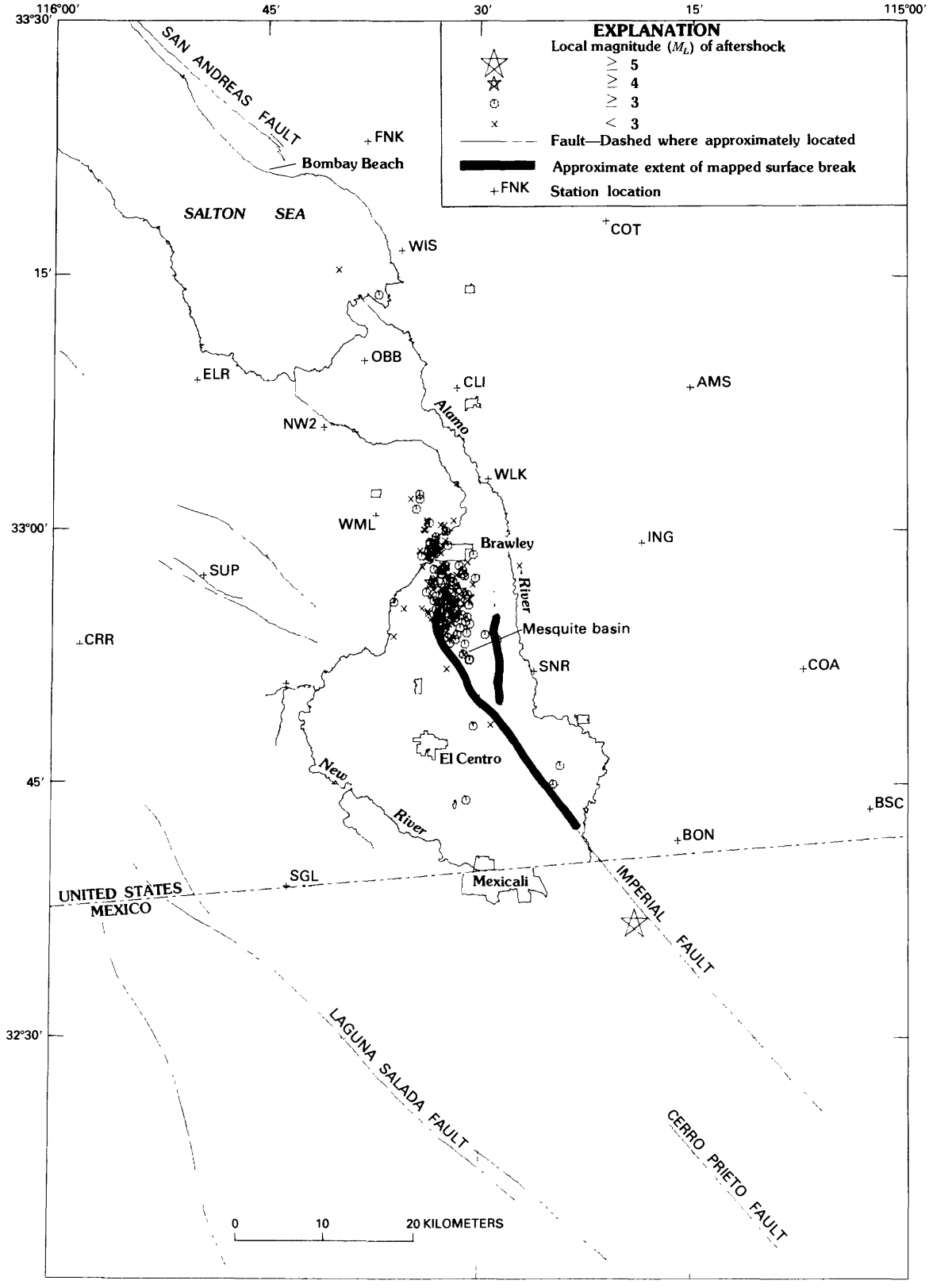

FIGURE 33.—Well-located aftershocks during first 8 hours of aftershock sequence.

of the south bank of the New River along much of the suggested structure.

Historically, conjugate faulting near Brawley does not appear to be unusual. A similar explanation was offered by Johnson and Hadley (1976) for arcuate northeast-trending breaks that were mapped along the northwest margin of the Mesquite basin after the 1940 earthquake. Their explanation was based primarily on lineations in seismicity and focal mechanisms from an earthquake swarm near Brawley during January 1975. The 1940 earthquake was also followed within several hours by an aftershock (M_L=5.5) that was more destructive at Brawley than was the 1940 main shock. This aftershock has generally been associated with delayed rupture on the Imperial fault unilaterally northward from the instrumental epicenter (see Trifunac and Brune, 1970; Johnson, 1979), following Richter (1958). However, in light of observations from the 1979 event, it appears that this earthquake may have occurred on a conjugate structure similar, if not identical, to that of the 1979 Brawley aftershock.

One of the most intriguing features apparent on the aftershock-distribution map (fig. 32) is a line of events that extends along the trend of the San Andreas fault 50 km into the Imperial Valley. As discussed by Johnson (1979), this part of the valley was virtually aseismic through 1978, since the installation of a dense seismograph network in mid-1973. The first events along this trend occurred in 1979 (discussed below) before the main shock. Although few of these events were large enough to provide well-constrained focal mechanisms, nevertheless, first motions are generally consistent with the normal focal mechanism shown in figure 32 for one of the largest events. An abrupt increase in activity along this trend after the main shock leaves little doubt that these events represent a response to the changes in stress associated with the main shock and thus can be considered aftershocks. Mechanically they may represent valley subsidence along an ancient strand of the San Andreas fault, particularly because they all occurred within the dilatational quadrant of the static-strain field associated with the main shock.

The development of the aftershock distribution over time is most clearly revealed by a series of time-distance plots (figs. 34–36) projected onto the Imperial fault. Events were selected from the solid parallelepiped shown in figure 37, with distances measured from its southeast corner. These three plots, covering 1, 3, and 23 days after the main shock, respectively, provide a reasonably complete picture of the temporal development of the aftershock pattern. A virtually aseismic zone separates the region of clusters of aftershocks during the first 12 hours (fig. 34) from the area of the main shock. After 12 hours an increase in activity outside the initial cluster seems to mark the beginning of a general expansion of the aftershock region both to the north and to the south (fig. 35). This expansion, which appears to be progressive over time, culminated in the north with a cluster of events near the south end of the Salton Sea, and in the south with a cluster centered near the Cerro Prieto geothermal area. Once it began, activity at each of several clusters along the Imperial fault tended to persist. If we associate a migration rate with the onset of activity at each cluster, based on a point of initiation near Brawley at the time of the main shock, a velocity of just less than 2 km would be appropriate. This rate is faster than the value of 0.2 to 1.0 km/d reported by Johnson (1979) for the characteristic velocity relating clusters with sequences of earthquake swarms along the same trend, but is much slower than the 12-km/d rate reported by Johnson and Hadley (1976) for the bilateral development of a large earthquake swarm on the Brawley fault zone (eastern branch of surface break, fig. 33) in January 1975. Migration at widely varying rates appears to be a general feature of earthquake sequences within the Imperial Valley.

HISTORICAL PERSPECTIVE

The phenomena accompanying recent faulting in the Imperial Valley can best be understood within a context of the historical seismicity of this region. In this section we touch briefly on the most important aspects of a more detailed discussion by Johnson (1979). Figures 37 and 38 provide an overview of the seismicity in the Imperial Valley during the 6 years since the installation of a dense seismic network in 1973. The most obvious feature on the seismicity map (fig. 37) is a pod-shaped area of seismicity connecting the Imperial fault north of Mexicali, Mexico, with the San Andreas fault near Bombay Beach. This area, termed the "Brawley seismic zone" by Johnson (1979), probably marks a zone of concentrated deformation associated with the transfer of displacement from the Imperial fault to the south end of the San Andreas fault. Its shape is identical to that of the pod-shaped intrusive zones in Hill's (1977) model for Imperial Valley tectonics as a manifestation of a leaky transform fault, although the zone is somewhat larger than he suggests. Another similar zone of seismicity connects the Imperial and Cerro Prieto faults at the lower part of figure 37. The sparseness of high-quality epicenters here is due to inadequate location capability rather than intrinsically lower activity. We note that the tectonic similarity between these two areas is strongly reflected in the seismicity patterns.

Both the 1940 and 1979 earthquakes originated near an apex of one of these two seismic zones (fig. 37). Because the site of maximum faulting was south of the instrumental epicenter, Richter (1958) and Trifunac

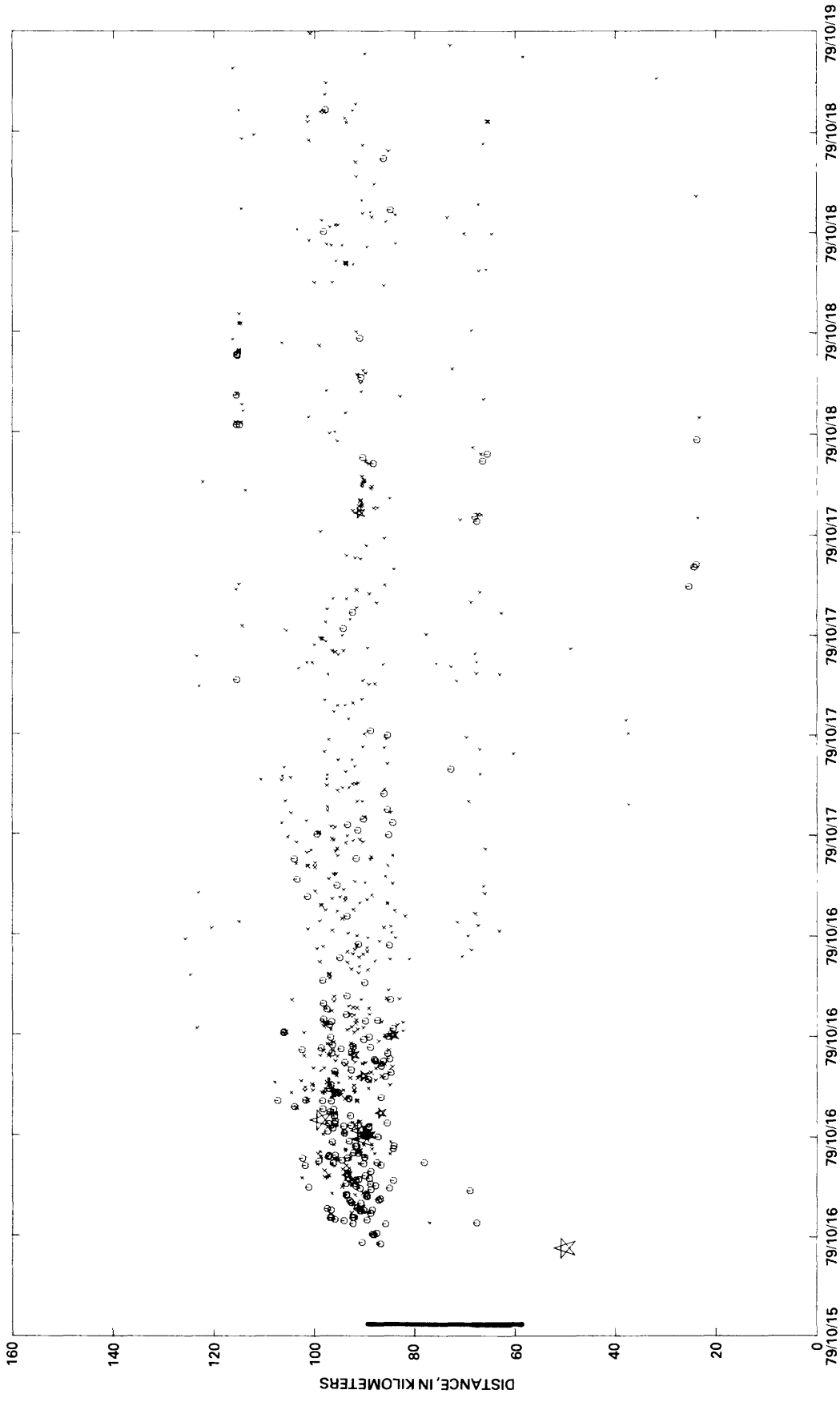

FIGURE 34.—Time as a function of distance for first 24 hours of aftershocks, projected onto trend of Imperial fault. Distance is measured from lat 32°15′ N., long 115°00′ W. (southeast corner, fig. 37). Line along distance axis of each graph shows extent of mapped surface breaks. Symbols for local magnitude same as in figure 32.

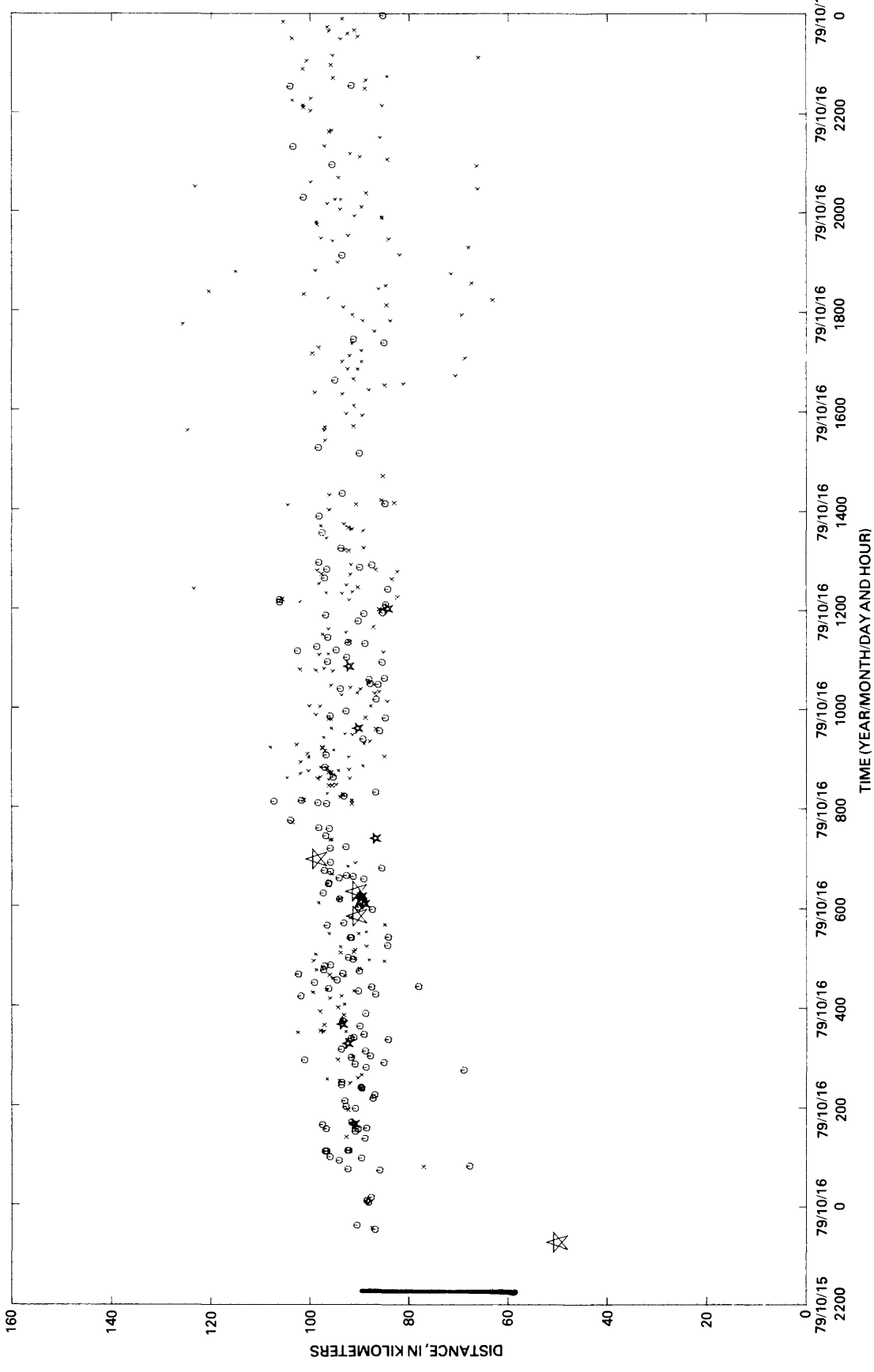

FIGURE 35.—Time as a function of distance for first 3 days of aftershocks, projected onto trend of Imperial fault. Distance is measured from lat 32°15′ N., long 115°00′ W. (southeast corner, fig. 37). Line along distance axis shows extent of mapped surface breaks. Symbols for local magnitude same as in figure 32.

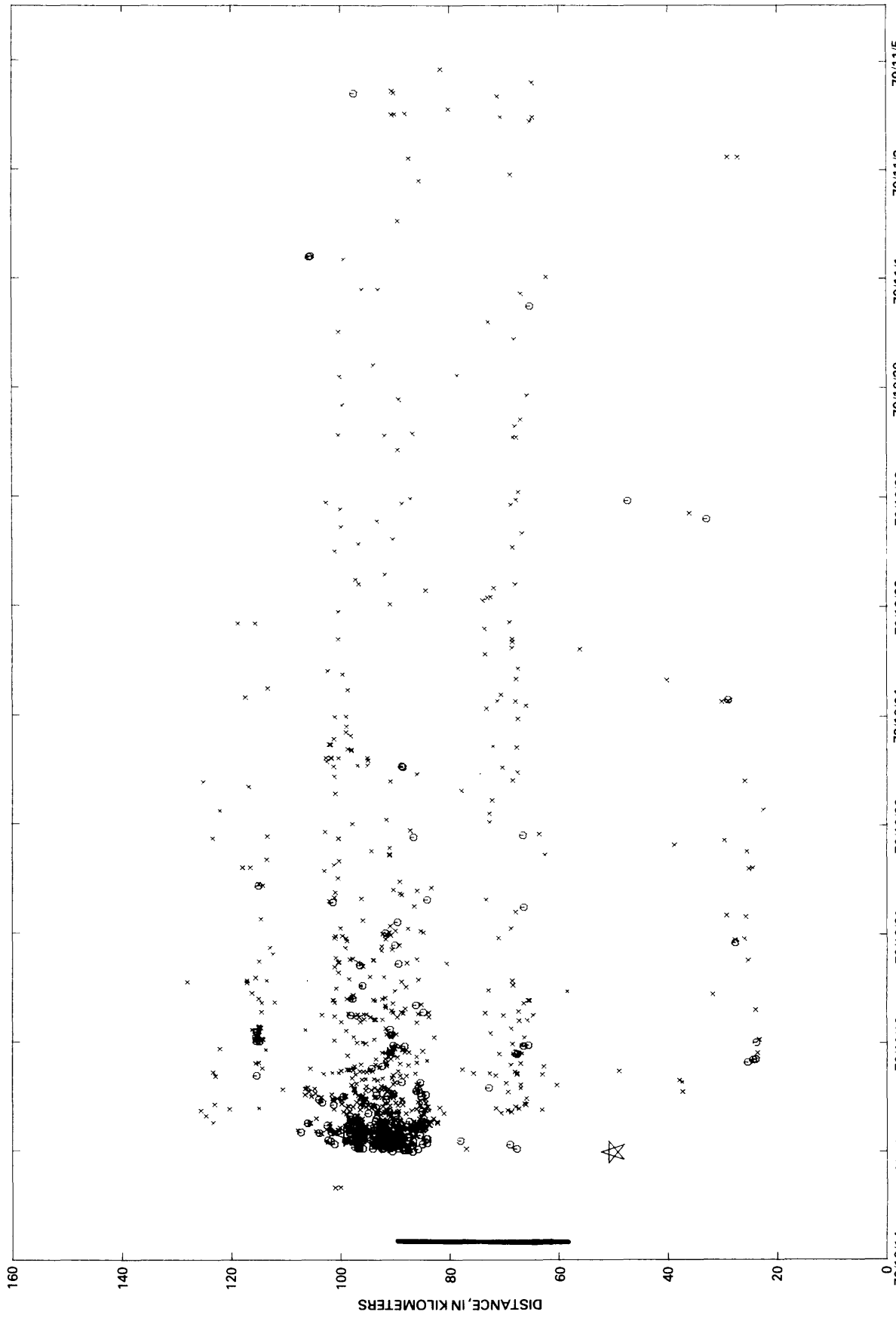

FIGURE 36.—Time as a function of distance for first 23 days of aftershocks, projected onto trend of Imperial fault. Distance is measured from lat 32°15′ N., long 115°00′ W. (southeast corner, fig. 37). Line along distance axis shows extent of mapped surface breaks. Symbols for local magnitude same as in figure 32.

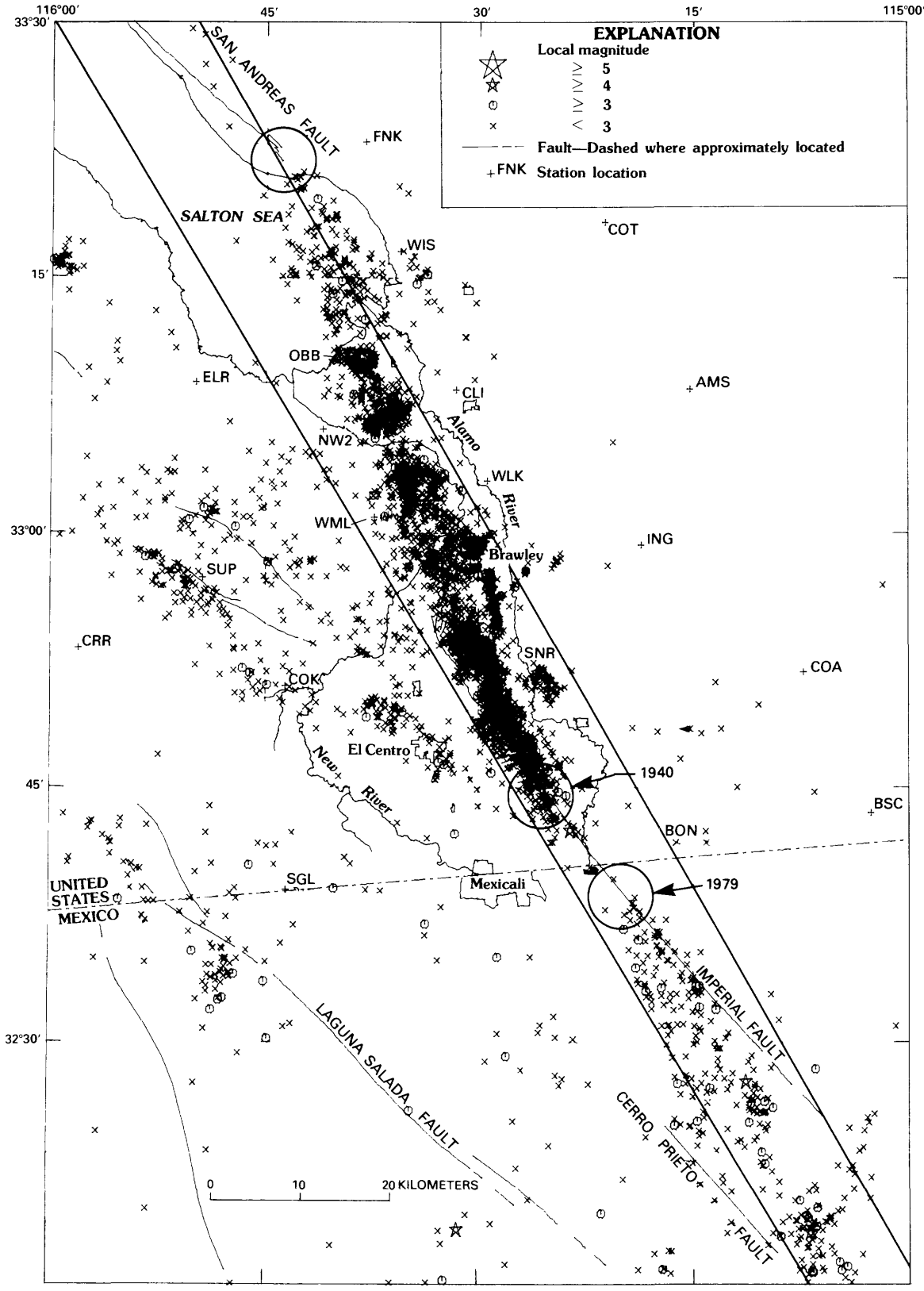

FIGURE 37.—Well-located earthquakes (epicentral error, less than 5 km) from installation of Imperial Valley seismic network in mid-1973 through September 1979. Southernmost circles denote epicentral regions of 1940 and 1979 Imperial Valley earthquakes; circle at north terminus of Brawley seismic zone indicates likely epicenter for major earthquakes on southern section of San Andreas fault. Area outlined in heavy lines defines section area for events shown in figures 34 through 36, 38, and 40.

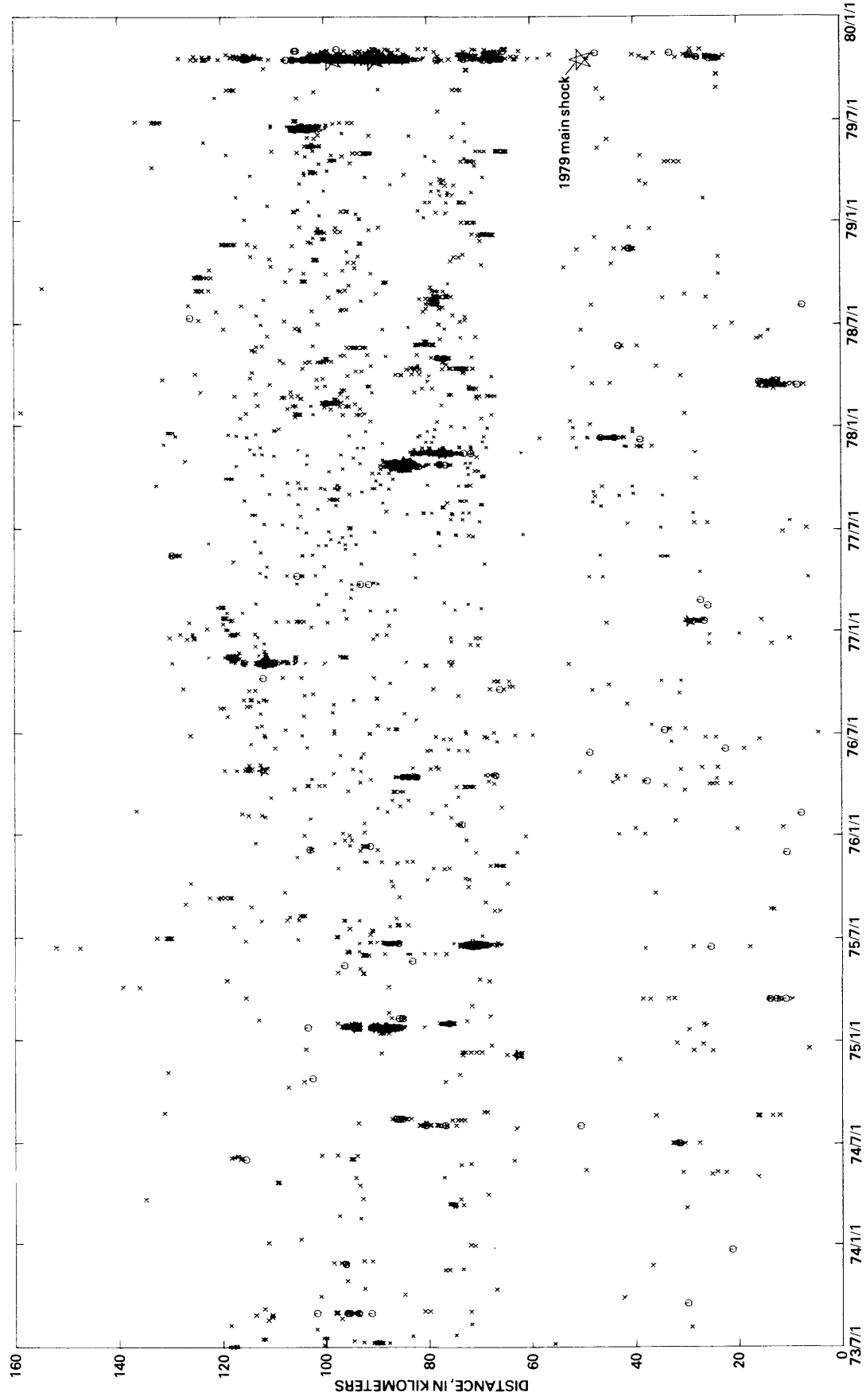

FIGURE 38.—Time as a function of distance for all well-located earthquakes along Imperial fault from mid-1973 through November 5, 1979. Distance is measured from lat 32°15′ N., long 115°00′ W. (southeast corner, fig. 37). Star denotes location of October 15 main shock. Symbols for local magnitude same as figure 37.

and Brune (1979) concluded that in 1940, rupture propagated southeastward across the aseismic zone straddling the United States-Mexican border. Similarly, the 1979 event apparently broke across the aseismic zone and this time propagated northward. If the two seismic zones represent regions of concentrated deformation, then their ends should represent points of concentrated loading on the major strike-slip faults. Strain energy stored in the "locked" aseismic section can be released periodically in moderate shocks. This concept is consistent with the observation by Johnson (1979) that episodic creep is confined to the seismic sections of the Imperial fault north of the border. There is no evidence for episodic creep within the aseismic sections, although continuously recording creepmeters have been in operation for several years at the Tuttle Ranch on the west bank of the Alamo River (Goulty and others, 1978). Nonepisodic creep rates of less than 2 mm/yr measured on an alinement array crossing the Imperial fault near the United States-Mexican border (reported by Goulty and others, 1978) are comparable to measurements for locked sections of the San Andreas fault near Indio, Calif., about 27 km northwest of the Salton Sea (Keller and others, 1978).

A similar tectonic relation exists at the north terminus of the Brawley seismic zone where it joins the San Andreas fault near Bombay Beach. This point (top circle, fig. 37) should be considered a likely epicenter for major earthquakes on the southern section of the San Andreas fault, in which rupture propagation would be to the northwest. More extensive tectonic instrumentation near this point seems prudent.

The correspondence between background seismicity and the intensity of aftershock activity along the Imperial fault can best be portrayed by a time-distance plot (fig. 38) covering the 6 years since the installation of the dense Imperial Valley network. Essentially, the spatial distribution of aftershocks mimics that of the preceding background: most events occur along previously seismogenic sections of the Imperial fault and avoid that section that was previously aseismic. The position of the main-shock epicenter at the south end of a persistent seismic gap and the predominance of aftershocks to the north are particularly clear on the plot. We note that this gap is not filled by the aftershock distribution.

The only event comparable to the 1979 main shock during the instrumental history of the Imperial Valley is the 1940 earthquake near El Centro. To facilitate a direct comparison, we reproduce here the Wood-Anderson seismograms recorded at Pasadena, Calif., for these two events (fig. 39). The main shock in 1979 appears relatively simple, and moderate aftershocks lasted throughout the first day; the initial shock in 1940 is considerably more complex, and all major aftershocks occurred within the first 1½ hours. This complexity was studied by Trifunac and Brune (1970), who concluded that substantial seismic energy was released at several discrete points along the Imperial fault as rupturing progressed southward. This conclusion implies that the energy release during the 1979 shock may have been more localized near the instrumental epicenter. The difference between the 1940 and 1979 events is also reflected in the difference in seismic moment: the 1940 event was about 10 times larger than the 1979 shock, although the local magnitude was somewhat smaller. Further analysis of the wealth of strong-motion data recorded during the 1979 main shock should greatly elucidate this comparison.

PREEARTHQUAKE SEISMICITY

One of the most important contributions from dense-seismic-network studies of moderate earthquakes is the determination of the presence or absence of phenomena that can be broadly classed as precursory. Possibly the most useful contribution to our study was evidence for a remarkable 40-percent decrease in seismicity during the 15 weeks immediately preceding the main shock. This decrease, apparently affecting seismicity all along the axis of the Imperial Valley, can be seen as a vertical swath of lower activity on the time-distance plot (fig. 38) and on the aftershock frequency distribution (fig. 40). Because the number of detected events is an objective measure of seismicity during the period in figure 40, the observed change is probably real. A change in the detection parameters toward the end of 1977 prevents a comparison with seismicity levels using the detectability criterion before this period.

The importance of this apparent seismicity change mandates considerable skepticism regarding its existence. A survey of the operational state of the stations in the Imperial Valley network did not reveal any problem that might increase the detection threshold sufficiently to account for the observed change. One possible problem concerns the implementaion of antialiasing filters affecting half of the Imperial Valley network on July 17, 1979. It was not anticipated that this change would reduce detectability—quite the contrary was intended. Similar changes throughout the rest of the southern California seismic network were not followed by a reduction in detection capability. In addition, the period of depressed seismicity appears to have commenced more than 2 weeks before the instrumentation change. To determine whether the remainder of this anomalous period could be related to properties of the instrumentation, a comparison was made with that part of routine processing dealing solely with the analysis of helicorder records for a subset of the network not affected by the

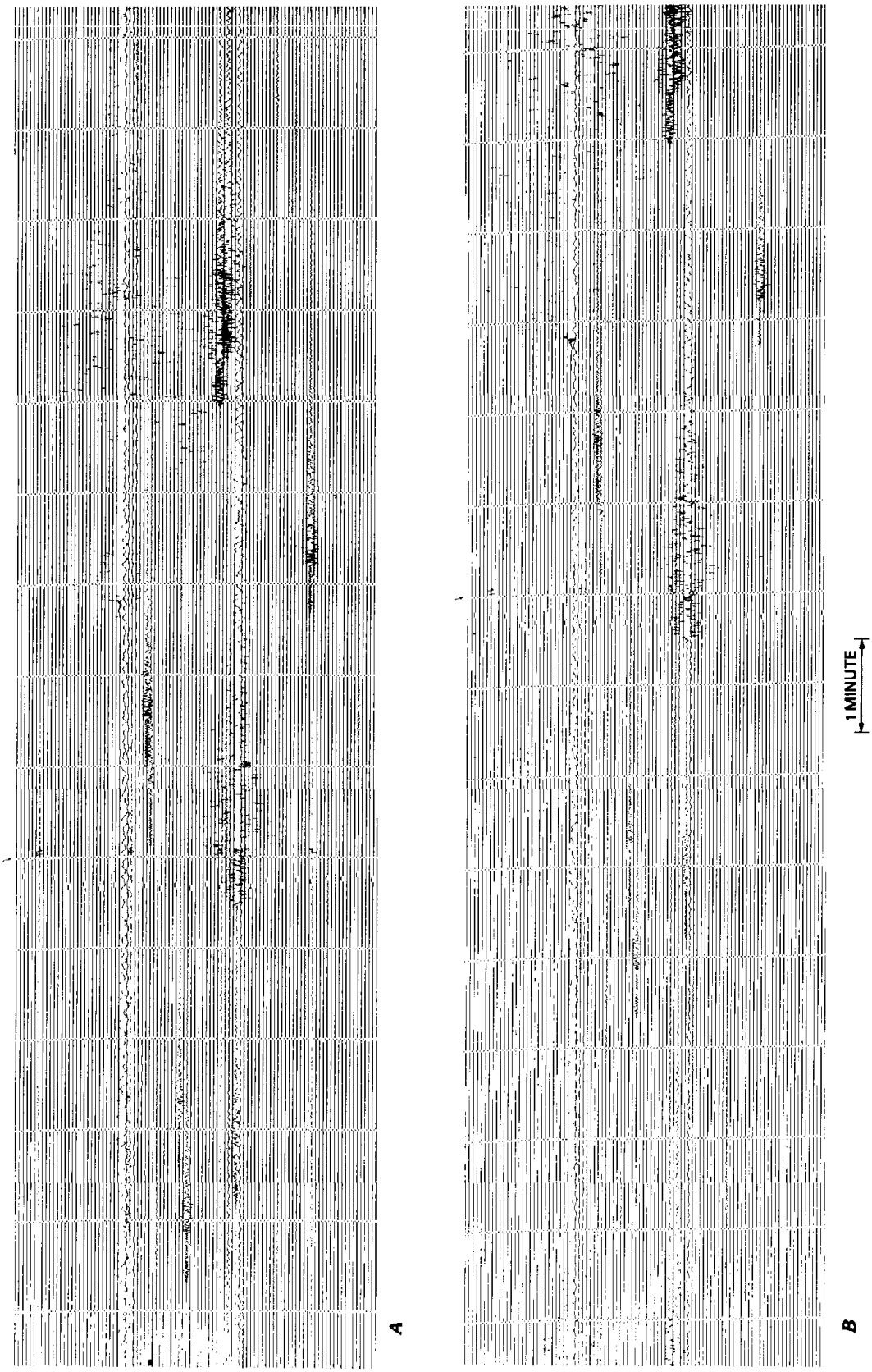

FIGURE 39.—Seismograms from Pasadena Wood-Anderson torsion seismometer. Marks and numbers on seismograms are made in routine record analysis. *A*, North-south component for 24-hour period beginning 1723 G.m.t. October 15, 1979. *B*, East-west component for 24-hour period beginning 1720 G.m.t. October 15, 1979. *C*, North-south component for 24-hour period beginning 1705 G.m.t. May 18, 1940. *D*, East-west component for 24-hour period beginning 1705 G.m.t. May 18, 1940.

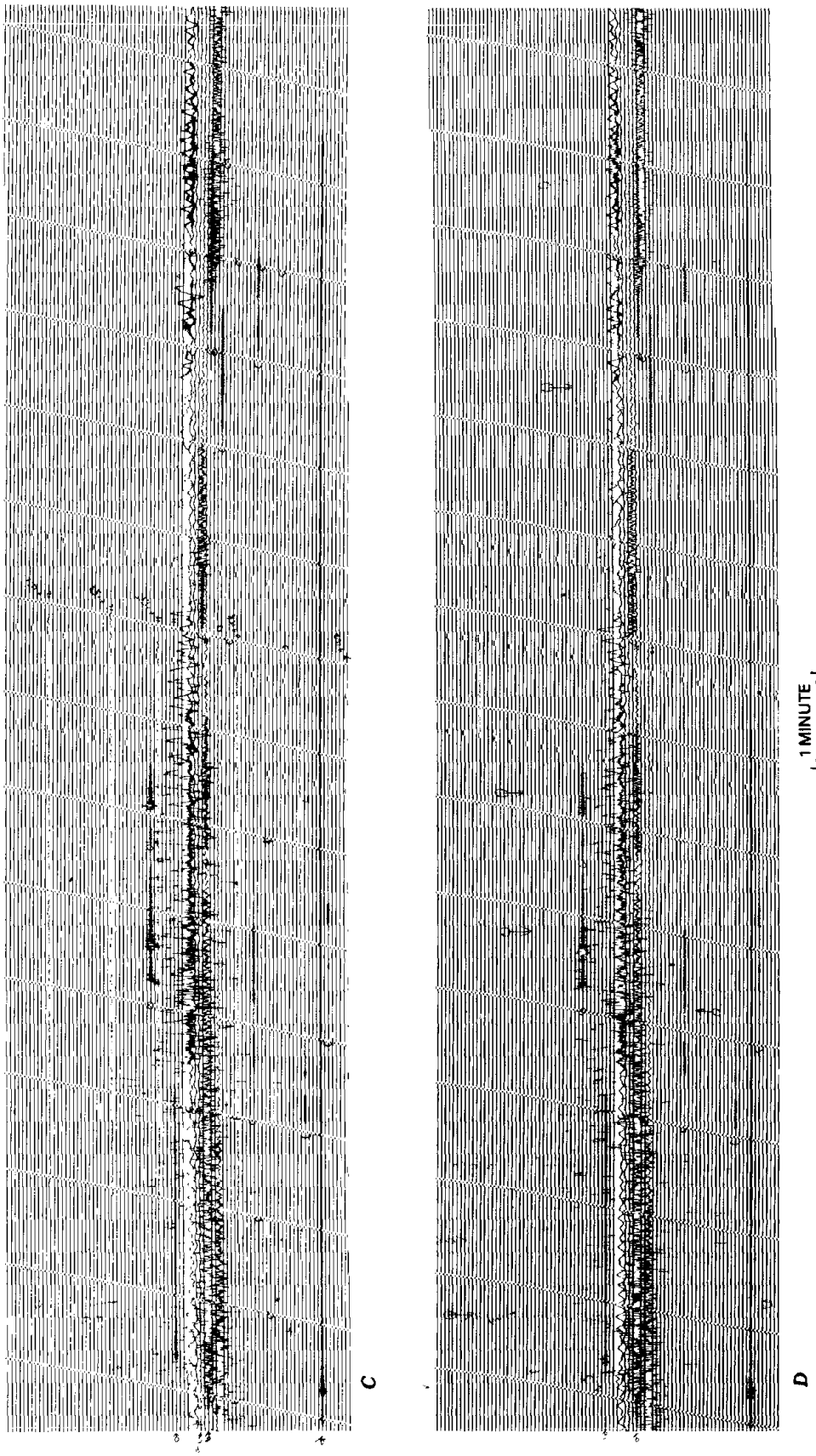

FIGURE 39.—Continued

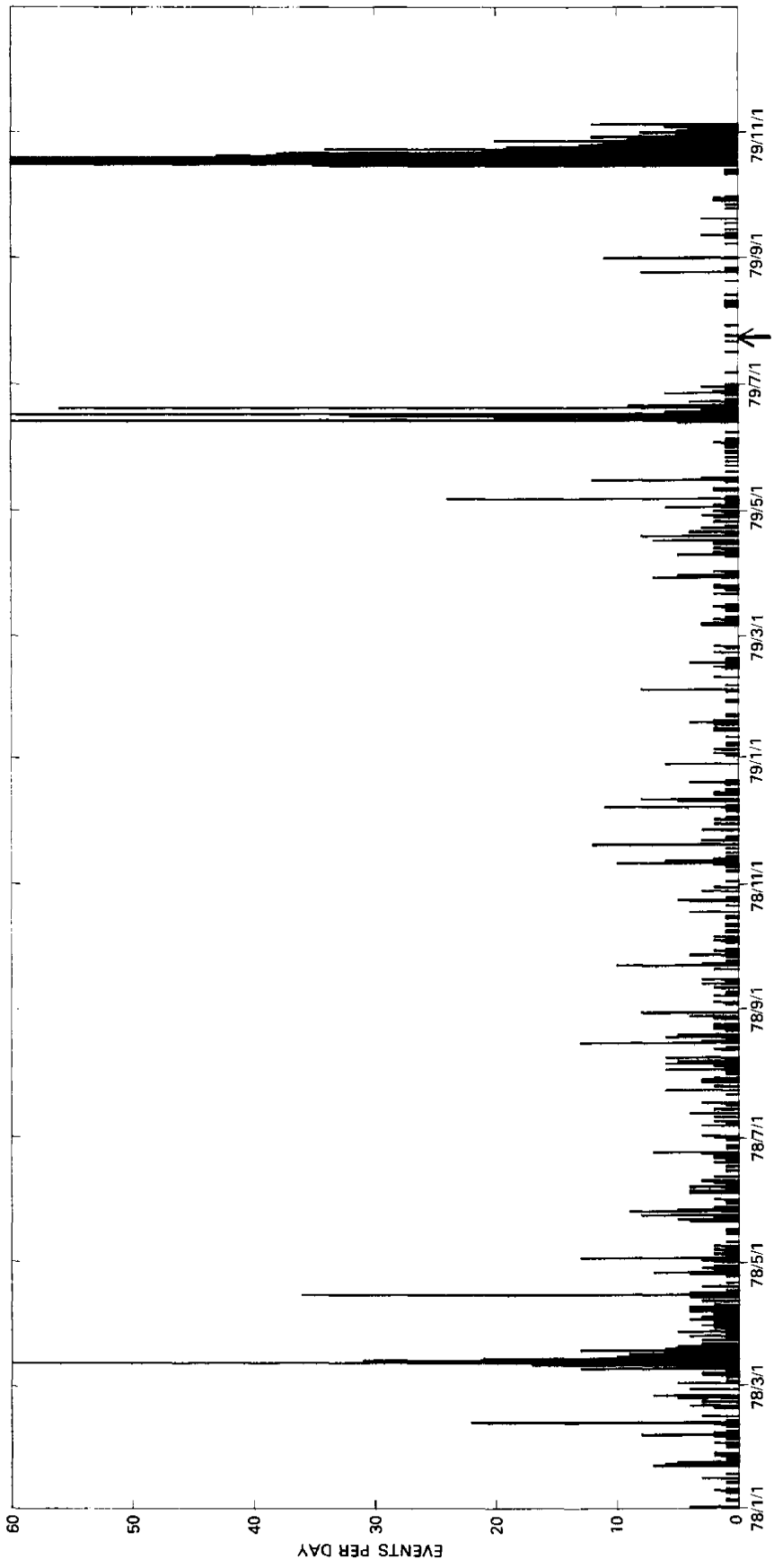

FIGURE 40.—Daily frequency of events detected by CEDAR system in area outlined in figure 37 from January 1, 1978, through November 5, 1979. Arrow marks change in instrumentation (see text).

above changes; these records are scanned independently of CEDAR system detection, and all events with coda lengths exceeding 25 s are timed and recorded. From this data set we compiled a list of all events with $S-P$ times at stations IKP and GLA of less than 12 s; the results agree with the existence of the period of low seismicity discussed above. At present, this quiet period appears to be real, although attempts to find an instrumental or procedural explanation will be continued.

If such a decrease in seismicity along the axis of the Imperial Valley did in fact occur, it would not be totally without precedent. Richter (1958) observed a decrease in swarm activity in the same area during the decade after the 1940 earthquake, and Johnson (1979) attributed this decrease to the dilatational quadrant of the 1940 earthquake, on the basis of a hydrologic model describing both episodic creep and swarm occurrence. Similarly, any dilatational component in the secular strain might be expected to decrease seismicity. For the interval 1973 through mid-1978 the geodetic results reported by Savage and others (1979) showed that dilatation in the northern Imperial Valley was negative (compression) and occurred at a constant rate. Beginning in late 1978 (Savage, 1979) this trend was reversed, 6 months before the sudden decrease in seismicity. Unfortunately, no data are available addressing the question whether an increase in extensional-strain rate may have accompanied the decrease in seismicity during mid-1979. Interestingly, it was during this period of apparent dilatation that the first normal events were observed on what has been suggested earlier as an extension of the San Andreas into the eastern Imperial Valley. Although these events are too small to provide focal mechanisms, first motions are generally compressive and agree with the normal mechanism (fig. 32) manifesting an east-west tension axis.

Figure 41 shows the spatial distribution of earthquakes during the quiet period. Seismicity seems to be more widely distributed than is generally apparent in a series of figures presented by Johnson (1979) covering comparable periods. A cluster of small earthquakes near the main-shock epicenter might be considered foreshocks, although they were uniformly distributed in time during this period and do not stand out as an obvious local increase in seismicity. Whether the records from these events are unusual in any respect is currently being studied.

The quiet period was immediately preceded by a swarm of earthquakes consisting of three discrete bursts of activity distributed over a 1-week interval during mid-June 1979. We do not know whether any special significance should be attributed to these events, although the epicentral distribution (fig. 42) lies just north of the area of most intense activity in the aftershock sequence near Brawley. This sequence also contrasts with previous swarms along the west margin of the Brawley seismic zone in being one of the most northerly during the preceding 6 years.

CONCLUSIONS

Aftershocks of the 1979 Imperial Valley earthquake were distributed in a complex pattern extending well beyond the zone of mapped surface rupture. The most intense activity was centered at the northwest end of surface faulting, and few aftershocks occurred near the main-shock epicenter. The largest aftershock ($M_L = 5.8$), which followed the main shock by nearly 8 hours, was apparently the result of sinistral motion on a conjugate northeast-trending fault north of Brawley, Calif. Thereafter, the aftershock clusters developed progressively over time along the Imperial fault trend at an apparent migration rate of approximately 2 km/d. A linear zone of events extending along the trend of the San Andreas fault south of the Salton Sea suggests sympathetic activation of a buried structure along the east margin of the Imperial Valley.

A remarkable 40-percent decrease in Imperial Valley seismicity that preceded the earthquake by 3½ months does not appear to be an artifact of either instrumentation or analysis. This decrease may in some way correlate with a change in east-west extension similar to that observed geodetically to the north during late 1978. Historical seismicity also suggests that an increase in the dilatational or possibly east-west extensional stress could have caused such a change in seismicity. Changes in the local secular-strain rate, which may ultimately have led to failure on the Imperial fault, may have preceded the main shock by several months and should have been observable had appropriate instrumentation been installed. Three small events clustered near the main-shock epicenter during the preceding months should be considered as candidate foreshocks, pending further investigation.

ACKNOWLEDGMENTS

We thank the CEDAR-system timers Anne Blanchard, Shirley Fisher, Peter German, Doug Given, Karen Richter, and Vic Lamanuzzi for their great diligence in the face of a seemingly endless task during the timing of initial aftershocks. Parts of the Imperial Valley base map were prepared by Peter T. German. This research was partly supported by U.S. Geological Survey Contract 14-08-0001-16719 and California Division of Mines and Geology Contract 5-0059.

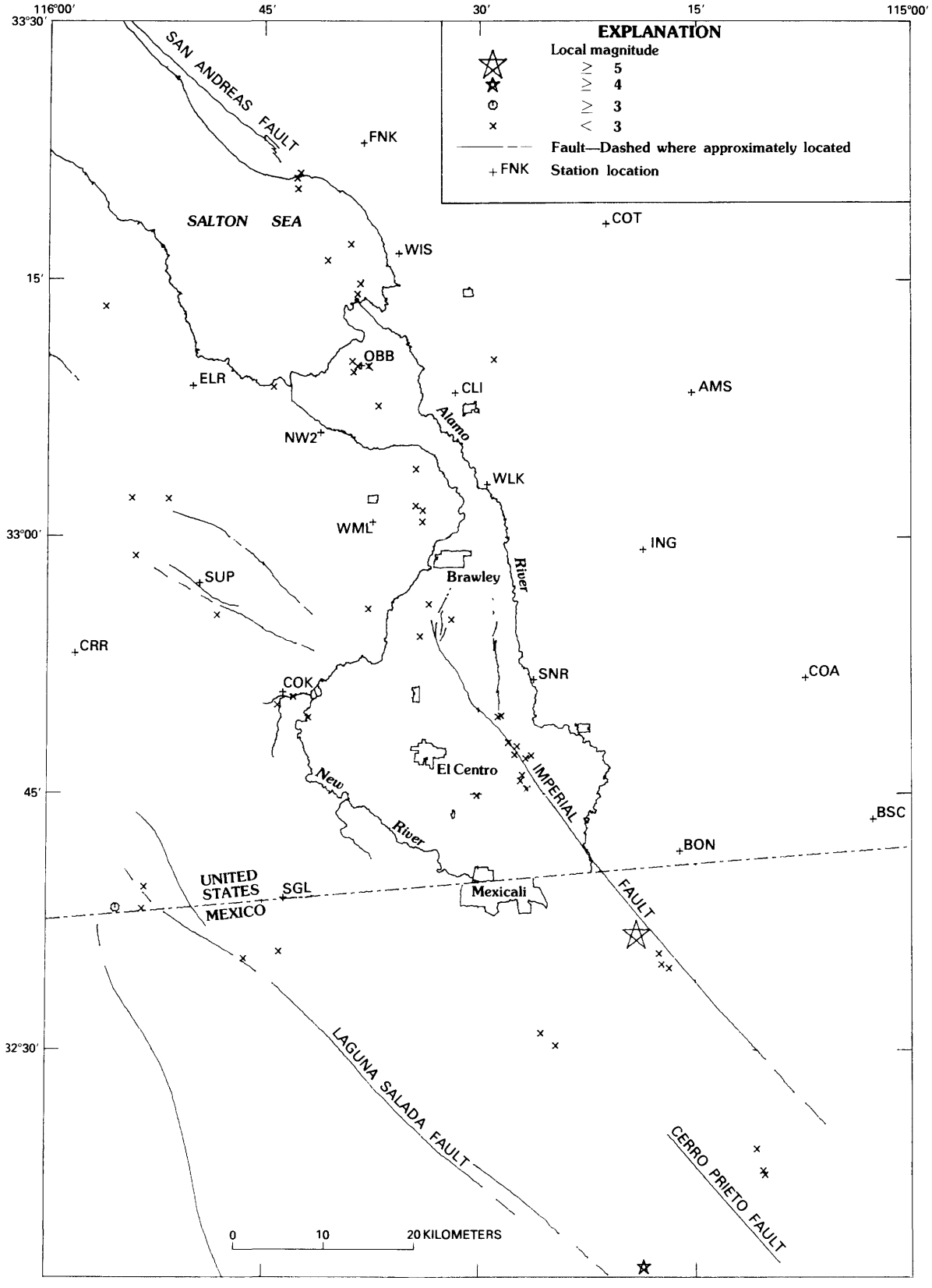

FIGURE 41.—Well-located earthquakes in Imperial Valley during 3½ months preceding October 15 main shock (large star), indicating quiet period in seismic activity.

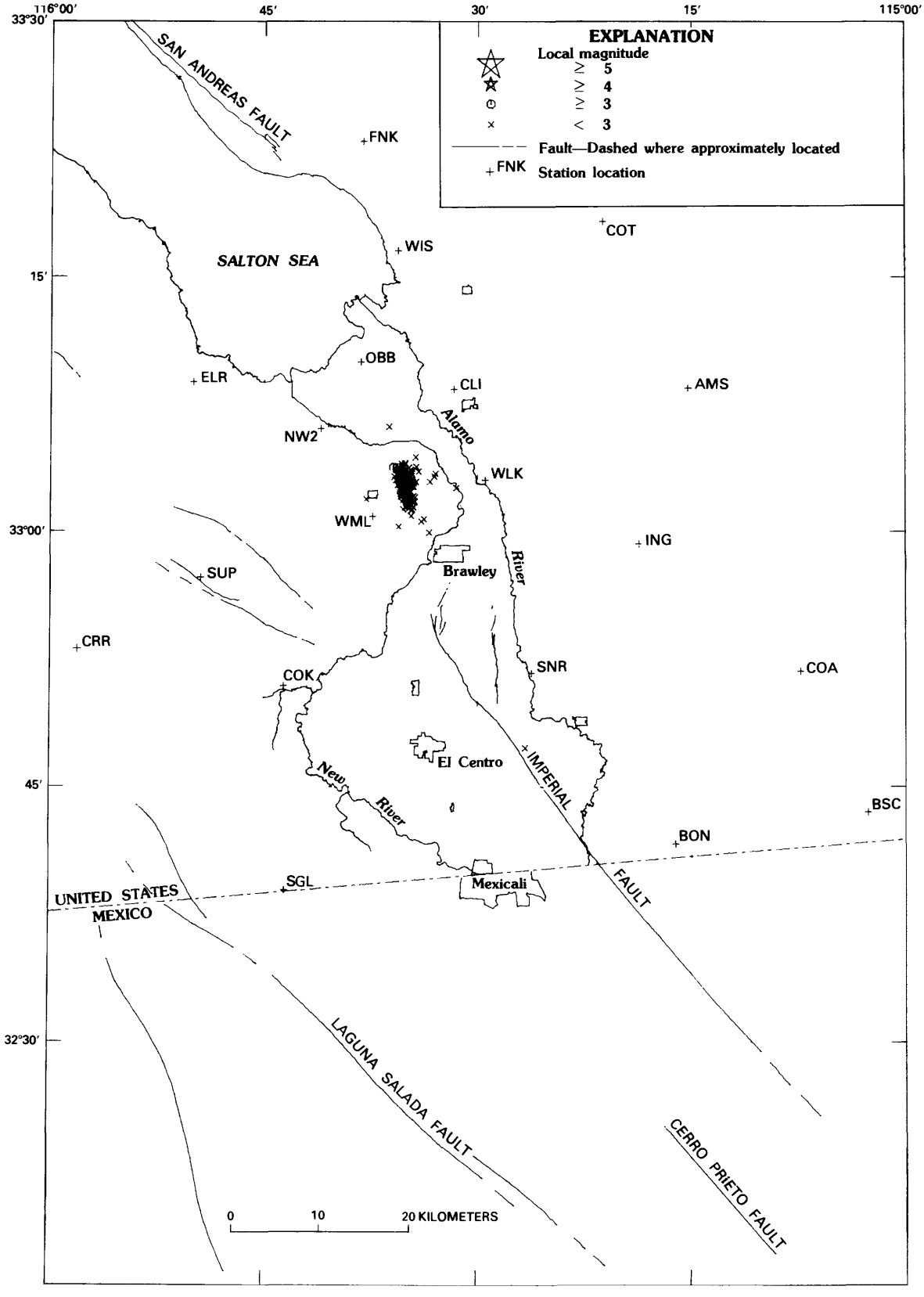

FIGURE 42.—Well-located earthquakes during an intense swarm near Brawley Calif., in mid-June 1979, immediately preceding quiet period shown in figure 41.

REFERENCES CITED

Goulty, N. R., Burford, R. O., Allen, C. R., Gilman, Ralph, Johnson, C. E., and Keller, R. P., 1978, Large creep events on the Imperial fault, California: Seismological Society of America Bulletin, v. 68, no. 2, p. 517–521.

Hill, D. P., 1977, A model for earthquake swarms: Journal of Geophysical Research, v. 82, no. 8, p. 1347–1352.

Johnson, C. E., 1979, CEDAR—an approach to the computer automation of short-period local seismic networks; seismotectonics of the Imperial Valley of southern California: Pasadena, California Institute of Technology, Ph. D. thesis, 343 p.

Johnson, C. E., and Hadley, D. M., 1976, Tectonic implications of the Brawley earthquakes swarm, Imperial Valley, California, January 1975: Seismological Society of America Bulletin, v. 66, no. 4, p. 1133–1144.

Keller, R. P., Allen, C. R., Gilman, Ralph, Goulty, N. R., and Hileman, J. A., 1978, Monitoring slip along major faults in southern California: Seismological Society of America Bulletin, v. 68, no. 4, p. 1187–1190.

Richter, C. F., 1958, Elementary seismology: San Francisco, W. H. Freeman, 768 p.

Savage, J. C., 1979, Crustal strain, *in* Seiders, W. H., compiler, Summaries of technical reports, volume 8: Menlo Park, Calif., U.S. Geological Survey, p. 317–319.

Savage, J. C., Prescott, W. H., Lisowski, M., and King, N., 1979, Deformation across the Salton Trough, California, 1973–1977: Journal of Geophysical Research, v. 84, no. B6, p. 3069–3079.

Trifunac, M. D., and Brune, J. N., 1970, Complexity of energy release during the Imperial Valley, California, earthquake of 1940: Seismological Society of America Bulletin, v. 60, no. 1, p. 137–160.

Whitcomb, J. H., 1973, A study of the velocity structure of the earth by the use of core phases (pt. 1); the 1971 San Fernando earthquake series focal mechanisms and tectonics (pt. 2): Pasadena, California Institute of Technology, Ph. D. thesis, 456 p.

Wiggins, R. A., 1972, The general linear inverse problem: Implication of surface waves and free oscillations for earth structure: Reviews of Geophysics and Space Physics, v. 10, no. 1, p. 251–285.

THE FOCAL MECHANISM FROM THE GLOBAL DIGITAL SEISMOGRAPH NETWORK

By BRUCE R. JULIAN, MADELEINE ZIRBES, and RUSSELL NEEDHAM,
U.S. GEOLOGICAL SURVEY

CONTENTS

ABSTRACT

We have estimated the focal mechanism of the main shock from the first motions of 18 long-period body waves (6 compressional waves and 12 horizontally polarized shear waves) recorded by the Global Digital Seismograph Network (GDSN). These data constrain the mechanism to be a nearly pure double couple, consistent with right-lateral strike-slip faulting on a nearly vertical plane with a strike of azimuth 315°–340°. *SH* polarities prove quite valuable; without them the mechanism would be almost totally undetermined.

INTRODUCTION

In this report we present an analysis of the source mechanism of the 1979 Imperial Valley earthquake, using the first motions of long-period body waves recorded by the Global Digital Seismograph Network (GDSN). Although this data set is sparse, it nevertheless strongly constrains the possible mechanism.

DATA SOURCES

We used digital data from 12 stations in the GDSN; detailed information about the GDSN is given by Zirbes and Julian (this volume). Data are not yet available from the stations in Ankara, Turkey (ANTO); Grafenberg, Germany (GRFO); Mashhad, Iran (MAIO); and Shillong, India (SHIO). The first three of these stations are very close to Kongsberg, Norway (KONO), on the focal sphere, and Shillong is near Chiang Mai, Thailand (CHTO), and so the missing stations would probably not contribute much additional information. Data from Kābul, Afghanistan (KAAO), are not used because first motions cannot be determined reliably from the recordings owing to microseismic noise. First motions can be determined from *P* waves at 6 stations and from horizontally polarized *S* waves at all 12 stations; figures 43 and 44 show the waveforms of these waves, and table 9 lists the first-motion data.

The first motions were mapped onto the focal sphere, using a preliminary hypocentral location supplied by the U.S. Geological Survey, National Earthquake Information Service (lat 32.641° N., long 115.325° W.; depth, 10 km), and continental Earth model PEMC (Dziewonski and others, 1975). The compressional- and shear-wave speeds at the focus in this model are 5.8 and 3.45 km/s, respectively. Figure 45 shows the observed first motions on the focal sphere.

The *SH* data proved to be particularly valuable. We could easily determine *SH* first motions from the numerically simulated transverse horizontal-component digital seismograms in figure 44. The *SH* first motions are much more reliable than such data as polarization angles, which involve vertically polarized motion, because they are free from contamination by compressional waves generated by mode conversion near the receiver. In addition, *SH* waves are efficiently diffracted around the Earth's core and thus are easily observed, even at great distances.

METHOD OF ANALYSIS

We analyzed the focal mechanism by using a new technique (Julian, 1978) that applies linear-programming methods to determine the moment-tensor representation of the source. This technique is computationally efficient and can be used to define the range of solutions consistent with a set of first-motion data by seeking solutions that extremize various physical parameters of the mechanism. The technique also identifies data that are not significant, in the sense that they do not affect the set of consistent solutions. In the solutions presented here, we constrain the trace of the moment tensor so that only solutions with no net volume change are considered.

RESULTS

In all, 11 of the first-motion data turn out to be significant (asterisks, table 9). Table 10 lists the principal moments and principal axes for three extreme focal mechanisms, and figure 46 compares the predicted polarities with those observed. Because we used no amplitude information in this analysis, the principal moments in table 10 are determined only within an arbitrary multiplier.

These three mechanisms have extreme values for the amplitude of the compressional wave radiated downward. The mechanism labeled "most thrustlike" has the largest (that is, most compressional) amplitude, the "most normal" mechanism has the smallest (most rarefactional) amplitude, and the "least dip-slip" mechanism has the smallest absolute amplitude (here, zero).

Because the mechanisms are not constrained to be double couples, the nodal curves are not orthogonal great circles on the focal sphere (although the least dip-slip mechanism is very nearly so). In fact, all the focal mechanisms are quite similar and are predomi-

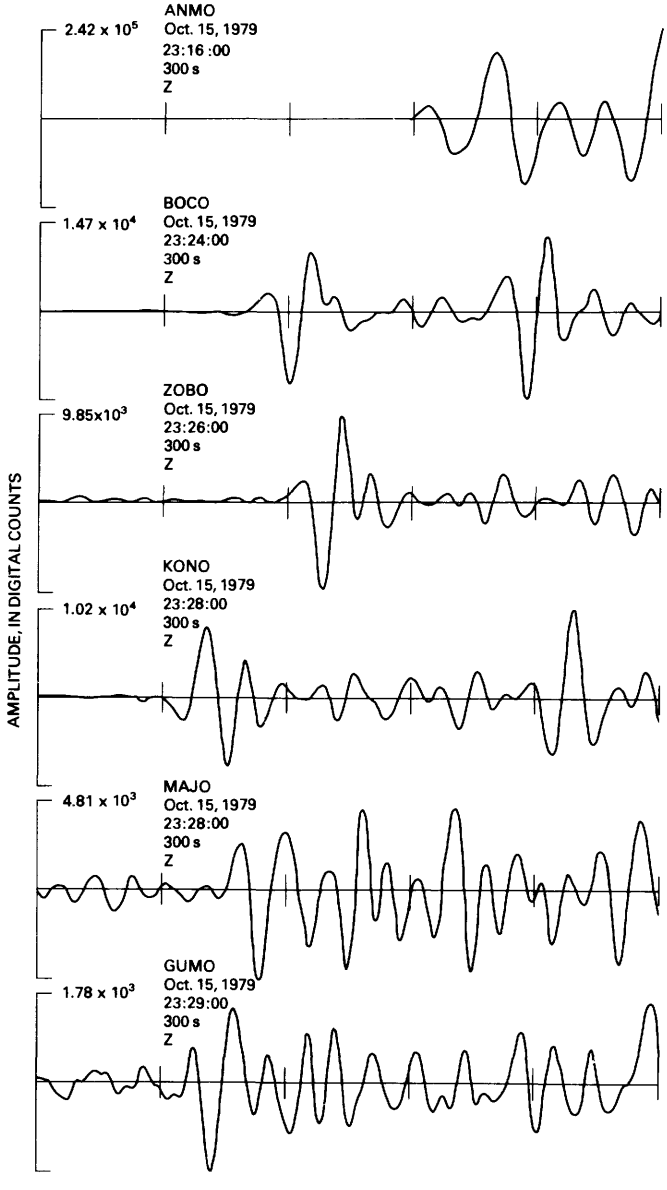

FIGURE 43.—*P* waveforms from main shock for which first motions are used in this study. Only vertical (*Z*) components is shown. Upward motion in plots corresponds to upward displacement. Ticks indicate 1-minute intervals. Codes from stations within GDSN (see Zirbes and Julian, this volume) are followed by date, starting time (G.m.t.), and duration of waveform.

TABLE 9.—*Long-period first motions of the 1979 Imperial Valley earthquake*

Station code	Epicentral distance (°)	Ep>sta azimuth (°)	Takeoff angle (°)	Phase	First motion
ANMO	7.73	70.28	45.82	P	+*
			45.82	SH	−
BOCO	47.57	117.00	23.98	P	+*
			23.98	SH	+*
ZOBO	66.35	129.71	19.45	P	+*
			19.45	SH	+*
KONO	77.46	25.25	16.95	P	−*
			16.95	SH	−*
MAJO	82.78	308.88	15.79	P	+*
			15.79	SH	+
GUMO	90.83	286.61	14.09	P	+
			14.09	SH	+*
SNZO	97.78	225.59	14.00	SH	−*
TATO	101.17	309.27	14.00	SH(dif)	+
CTATO	101.17	309.27	14.00	SH(dif)	−*
CTAO	107.42	257.03	14.00	SH(dif)	+
CHTO	119.24	322.28	14.00	SH(dif)	+
BCAO	122.87	58.82	14.00	SH(dif)	−
NWAO	136.20	254.76	14.00	SH(dif)	−

TABLE 10.—*Principal axes for extreme solutions*

Mechanism	Axis	Length	Plunge (°)	Trend (°)
Most thrustlike	T	0.366	23.42	267.85
	I	.052	65.17	108.40
	P	−.418	7.77	1.24
Most normal	T	.450	2.20	290.84
	I	−.036	86.54	161.25
	P	−.414	2.66	20.94
Least dip-slip	T	.450	2.26	291.76
	I	.000	86.40	163.01
	P	−.451	2.81	21.87

nantly double couples (as can be seen from the smallness of the intermediate principal axes of the moment tensors). They are consistent with right-lateral slip on a nearly vertical plane striking northwest, parallel to the San Andreas fault.

CONCLUSION

Long-period first motions of compressional and horizontally polarized shear waves are consistent with right-lateral motion on the San Andreas or a parallel fault.

REFERENCES CITED

Dziewonski, A. M., Hales, A. L., and Lapwood, E. R., 1975, Parametrically simple earth models consistent with geophysical data: Physics of the Earth and Planetary Interiors, v. 10, no. 1, p.12–48.

Julian, B. R., 1978, An inverse method for earthquake source mechanisms [abs.]: Tectonophysics, v. 49, no. 3–4, p. 223.

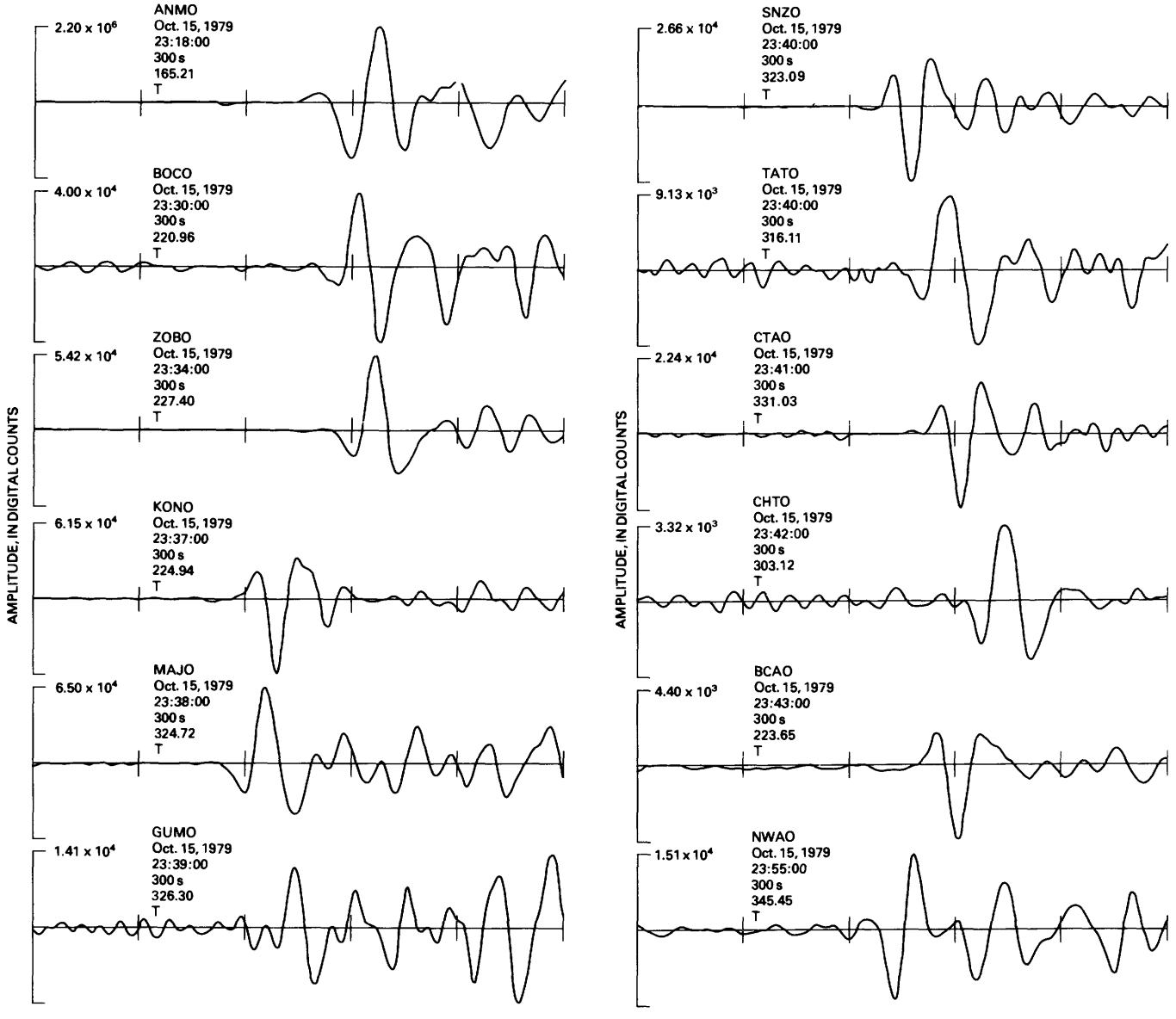

FIGURE 44.—*SH* waveforms for main shock for which first motions are used in this study. Only transverse (*T*) horizontal component is shown. Upward motion in plots corresponds to counterclockwise displacement in the Earth, where epicenter is viewed from above. Tick marks indicate 1-minute intervals. Codes for stations are followed by date, starting time (G.m.t.), duration of record, and azimuth corresponding to upward motion on seismogram.

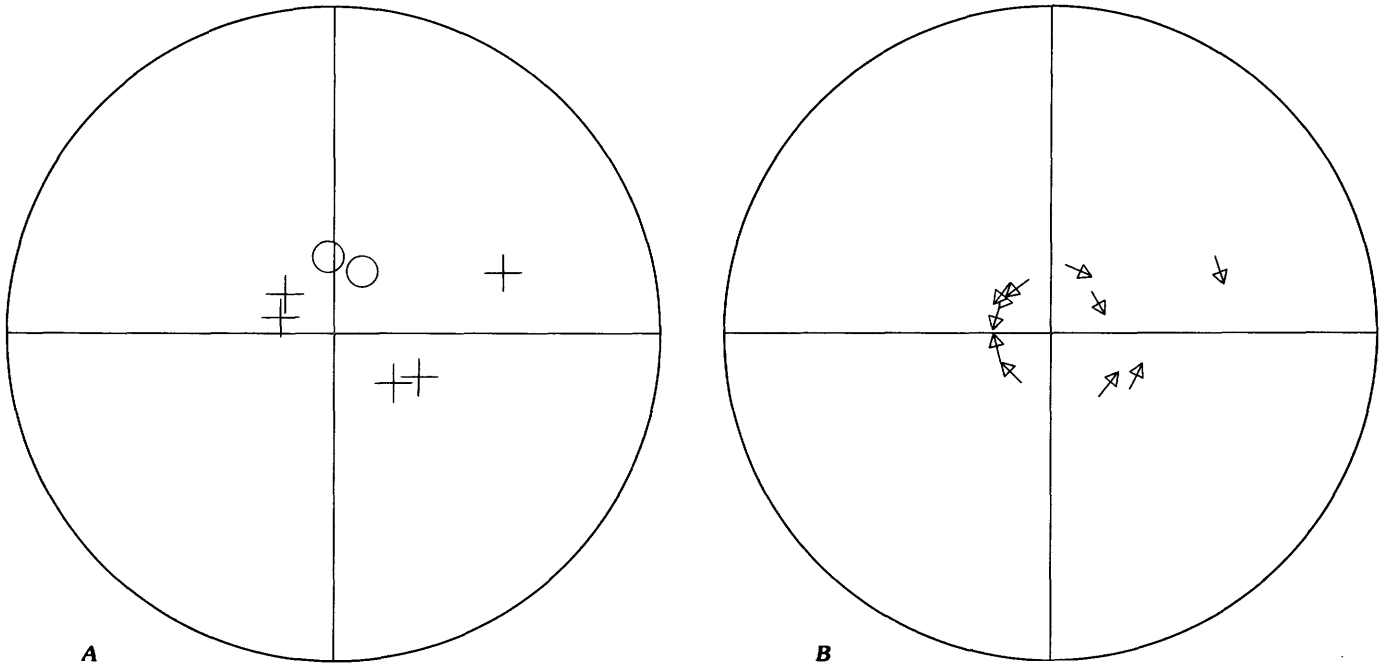

FIGURE 45.—Equal-area projection of lower focal hemisphere, illustrating first-motion data used in this study. *A*, Observed *P*-wave polarities. Cross, compression; circle, dilation. *B*, Observed *SH*-wave polarities (arrows).

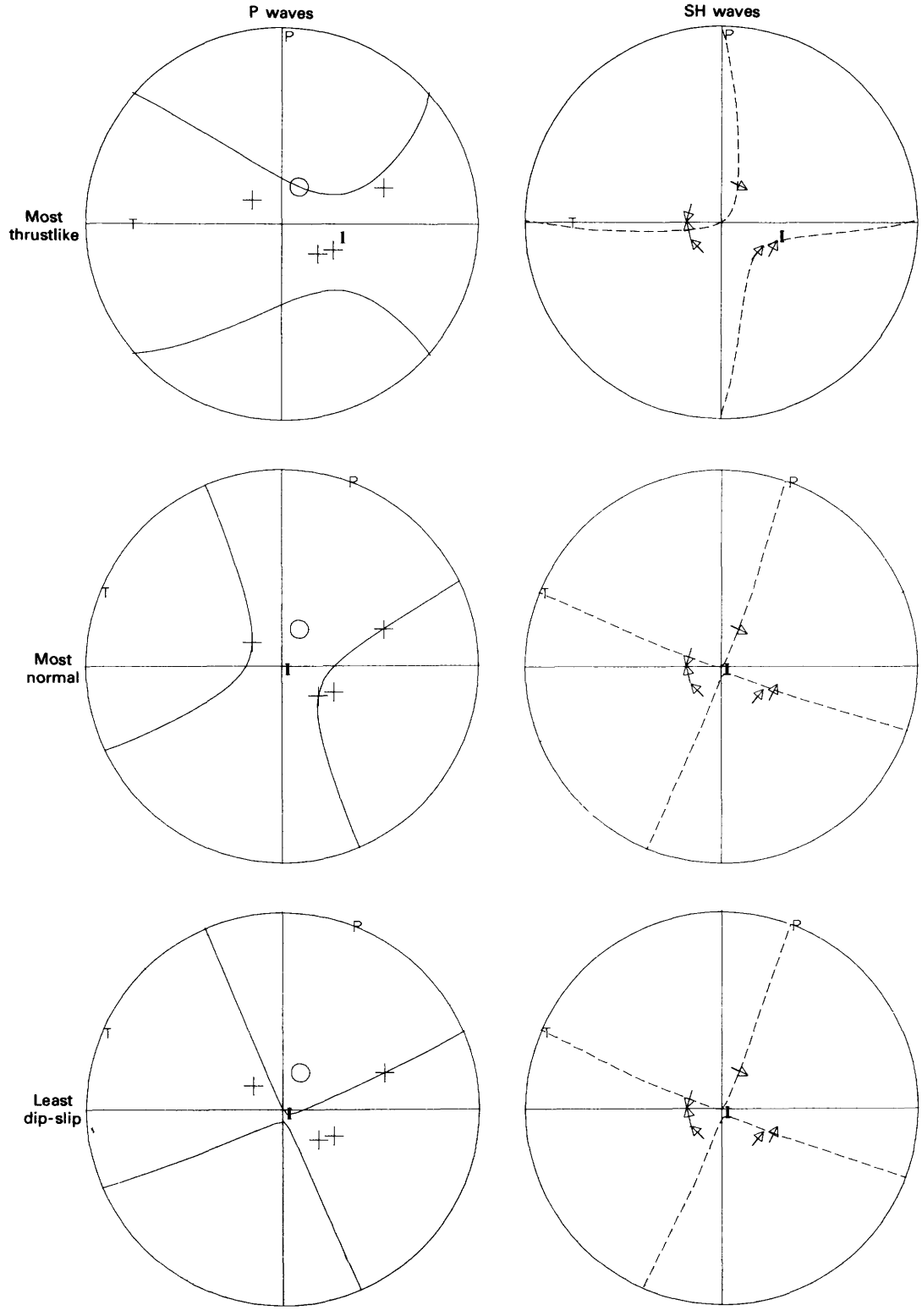

FIGURE 46.—Comparison of predicted and observed first motions for three extreme solutions listed in table 10. Only significant data are shown, using same symbols as in figure 45. Theoretical nodal curves are shown for *P* waves (solid) and *SH* waves (dashed). P, T, and I mark positions of respective principal axes for moment tensor.

DATA FROM THE GLOBAL DIGITAL SEISMOGRAPH NETWORK

By MADELEINE ZIRBES and BRUCE R. JULIAN
U.S. GEOLOGICAL SURVEY

In this chapter we present data obtained from the Global Digital Seismograph Network (GDSN) for the 1979 Imperial Valley earthquake. No interpretation of the data is given here; rather, our presentation is intended primarily for individuals who may wish to use these data in further studies of this earthquake. In the preceding chapter of this volume, Julian and others analyze the focal mechanism of the earthquake, using these data.

Figure 47 shows the locations of the Seismic Research Observatories (SRO) and modified high-gain long-period stations (ASRO) that make up the GDSN, and table 11 gives their coordinates and installation and closing dates, where applicable. Table 12 lists the fol-

TABLE 11.—*Global Digital Seismograph Network station information*

[South latitudes and west longitudes are listed as negative]

Station								
Code	Name	Type	Latitude	Longitude	Elevation	Burial	Date open	Date closed
ALQ	Albuquerque, N. Mex.	HGLP	34.942°	−106.458°	1853	10	----	July 78
ANMO	--do----------	SRO	34.946	−106.457	1740	100	Aug. 74	----
ANTO	Ankara, Turkey	SRO	39.900	32.783	1780	170	Aug. 78	----
BCAO	Bangui, Central African Empire	SRO	4.367	18.567	336	64	July 79	----
BOCO	Bogotá, Colombia	SRO	4.587	−74.043	3071	100	Dec. 77	----
CHG	Chiang Mai, Thailand	HGLP	18.790	98.977	416	0	----	Sep. 76
CHTO	--do----------	SRO	18.790	98.977	316	100	June 77	----
CTA	Charters Towers, Australia	HGLP	−20.088	146.256	357	30	----	Aug. 76
CTAO	--do----------	ASRO	−20.088	146.254	357	37	Oct. 76	----
ELA	Eilat, Israel----------	HGLP	38.683	39.233	200	200	----	Jan. 79
GRFO	Grafenberg, F.R. Germany	SRO	49.692	11.215	400	100	Oct. 78	----
GUMO	Guam, Mariana Is.	SRO	13.588	144.866	14	123	July 75	----
KAAO	Kābul, Afghanistan	ASRO	34.541	69.043	1920	7	May 77	----
KIP	Kipapa, Hawaii-----	HGLP	21.423	−158.015	70	37	----	Aug. 79
KON	Kongsberg, Norway	HGLP	59.649	9.598	216	340	----	July 78
KONO	--do----------	ASRO	59.649	9.598	216	340	Sept. 78	----
MAIO	Mashhad, Iran------	SRO	36.308	59.488	1000	100	Oct. 75	----
MAT	Matsushiro, Japan	HGLP	36.542	138.209	422	48	----	Apr. 77
MAJO	--do----------	ASRO	36.542	138.209	422	48	June 77	----
NWAO	Narrogin, Australia	SRO	−32.927	117.234	265	100	Apr. 76	----
OGD	Ogdensburg, N.J.	HGLP	41.087	−74.596	−373	543	----	Jan. 79
QUPO	Quetta, Pakistan----	SRO	----	----	----	----	----	----
SHIO	Shillong, India------	SRO	25.567	91.883	1600	100	May 78	----
SNZO	South Karori, New Zealand	SRO	−41.310	174.705	−12	100	Mar. 76	----
TATO	Taipei, Taiwan -----	SRO	24.975	121.488	53	100	May 76	----
TLO	Toledo, Spain -------	HGLP	39.860	−4.015	465	20	----	Jan. 79
ZLP	Zongo (La Paz), Bolivia	HGLP	−16.270	−68.125	4450	300	----	Aug. 76
ZOBO	--do----------	ASRO	−16.270	−68.125	4450	300	Sep. 76	----

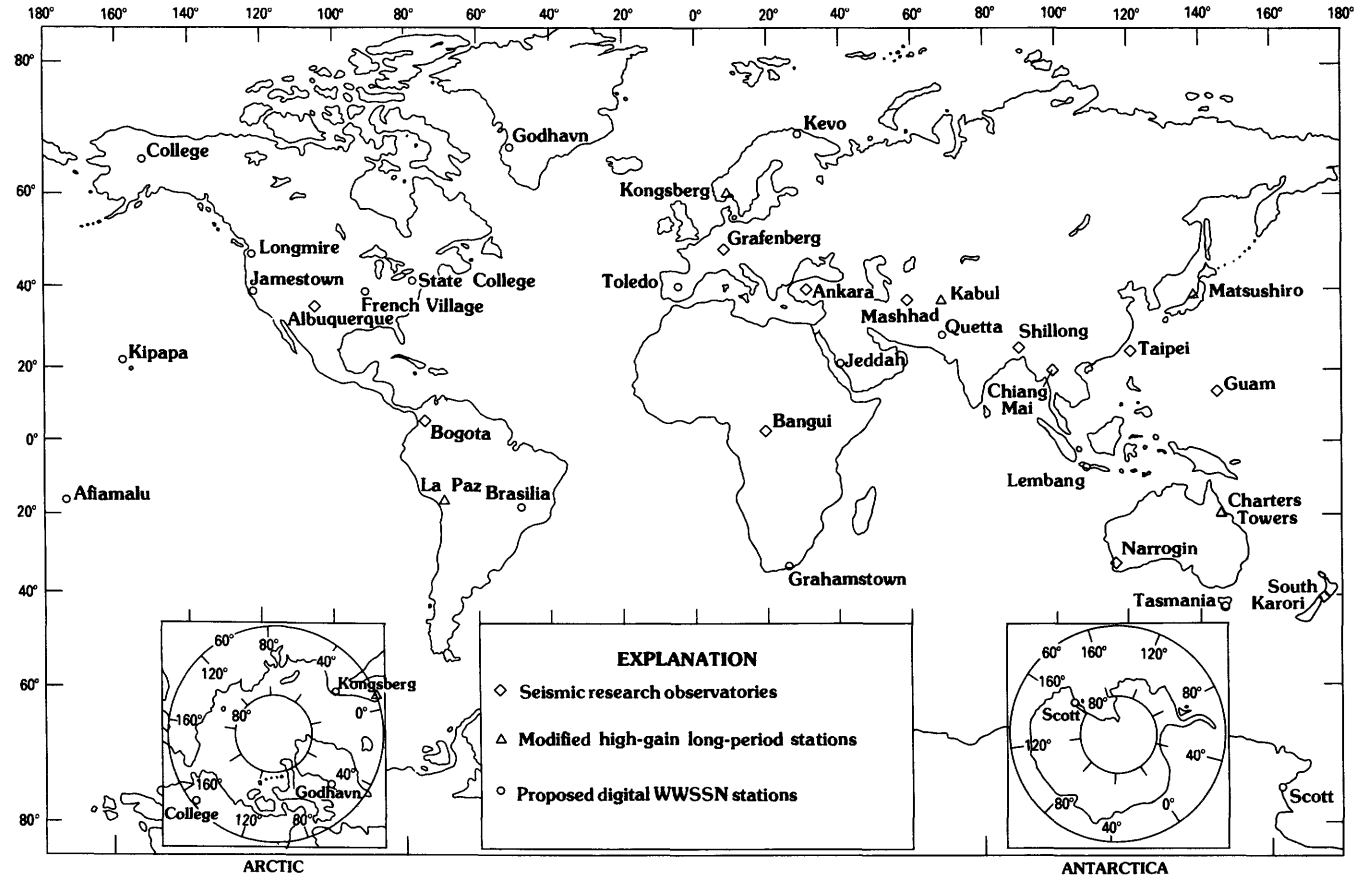

FIGURE 47.—Global Digital Seismograph Network (GDSN) in October 1979, including Seismic Research Observatories (SRO) and modified high-gain long-period stations (ASRO). All stations shown are now operating except Mashhad, whose status is unknown. Site locations for Digital World Wide Standardized Seismograph Network (DWNSSN) stations are tentative, and none are yet installed.

TABLE 12.—*Global Digital Seismograph Network data for the October 15 earthquake*

Station code	Epicentral distance (°)	Ep→sta azimuth (°)	Sta→ep azimuth (°)	SP gain (counts/nm)	LPZ gain (counts/nm)	LPN gain (counts/nm)	LPE gain (counts/nm)
ANMO	7.825	070.2	255.2	2,000	5	5	5
ANTO	102.076	024.5	333.0	2,000	5	5	5
BCAO	122.957	058.7	313.6	2,000	5	5	5
BOCO	47.637	116.9	311.0	2,000	5	5	5
CHTO	119.207	322.2	033.1	2,000	5	5	5
CTAO	107.329	257.0	061.0	1,000	10	10	10
ELA	105.258	020.3	338.0	----	1.01	.68	1.21
GRFO	85.370	031.5	317.2	2,000	5	5	5
GUMO	90.752	286.6	056.3	2	5	5	5
KAAO	113.071	356.0	004.1	1,000	10	10	10
KIP	39.307	264.4	064.4	----	1.09	.99	.94
KONO	77.524	025.2	314.9	1,000	10	10	10
MAJO	82.733	308.8	054.7	1,000	10	10	10
NWAO	136.109	254.7	075.5	2,000	5	5	5
OGD	33.505	063.6	268.7	----	1.83	1.31	1.36
SHIO	116.558	332.4	025.7	2,000	5	5	5
SNZO	97.692	225.5	053.1	2	5	5	5
TATO	101.121	309.2	046.1	2	5	5	5
TLO	83.962	046.1	307.8	----	1.02	1.06	1.05
ZOBO	66.401	129.6	317.4	1,000	10	10	10

lowing information relating to this event: epicentral distances, azimuths, and calibration factors. More detailed information about the GDSN may be found elsewhere (Peterson and others, 1976, 1980).

At the time of this writing, data were not yet available from Ankara, Turkey (ANTO); Grafenberg, Germany (GRFO); and Shillong, India (SHIO). The status of the SRO at Mashhad, Iran (MAIO), is unknown.

Figures 48 through 56 show short-period vertical seismograms for the stations that recorded such data. Short-period data are recorded only when an online processor at the observatory detects a signal, and so some stations are not represented. Figures 57 through 69 show three-component long-period seismograms. In most cases, two or three different plots are shown, with varying gains, to take advantage of the dynamic range of the data.

The horizontal traces for Taipei, Taiwan (TATO), and Bangui, Central African Empire (BCAO), appear, on the basis of Rayleigh-wave particle motion, to have been

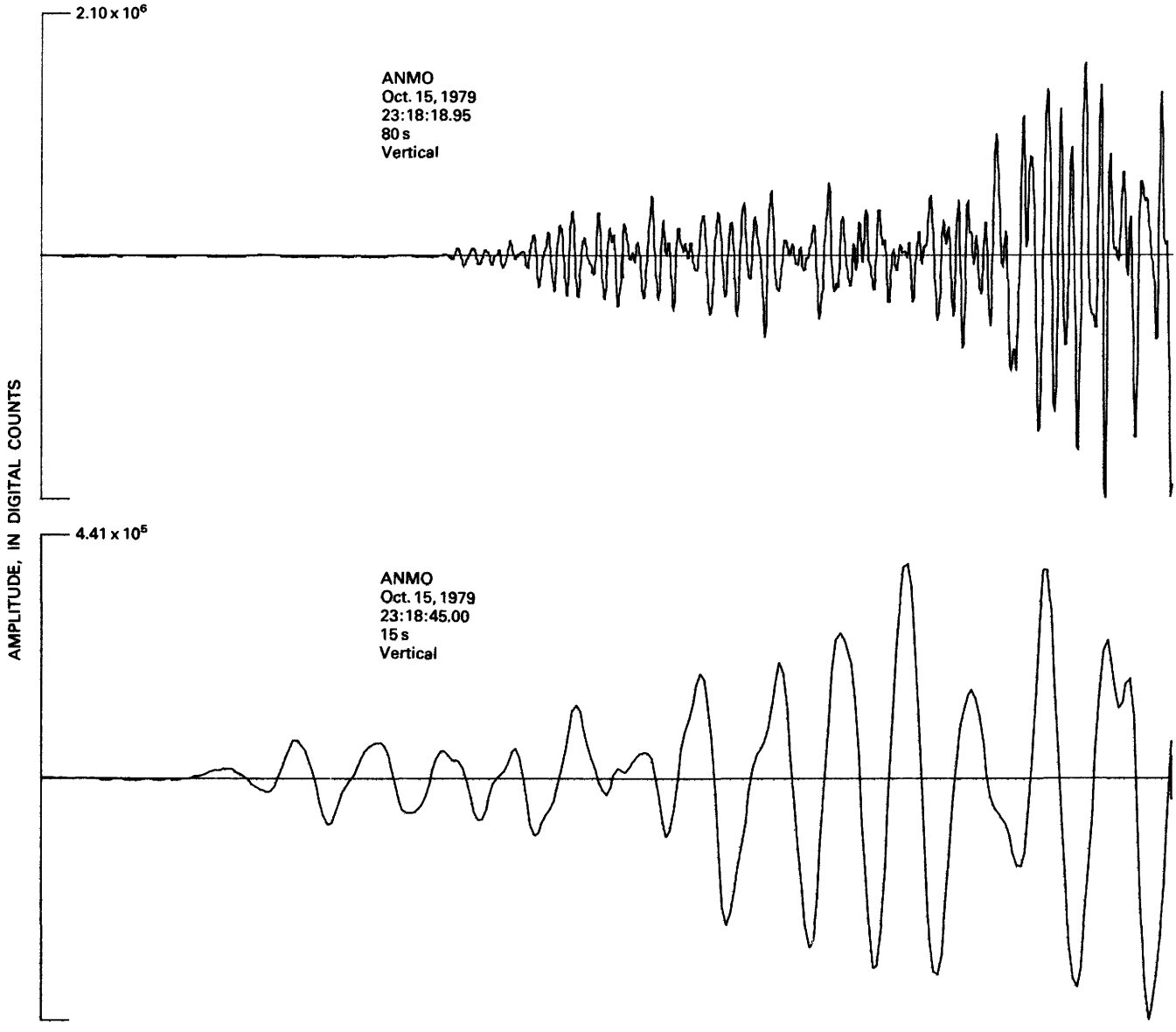

FIGURE 48.—Short-period seismograms from Albuquerque, N. Mex. Station code name, date, time (G.m.t.) of first sample, and total duration of each trace, respectively from top to bottom, are shown above each seismogram. Maximum amplitudes are in digital counts; see table 12 for calibration factors. Tick marks indicate 1-minute intervals.

recorded with reversed polarity. This error has not been corrected on the plots.

REFERENCES CITED

Peterson, Jon, Butler, H. M., Holcomb, L. G., and Hutt, C. R., 1976, The Seismic Research Observatory: Seismological Society of America Bulletin, v. 66, no. 6, p. 2049–2068.

Peterson, Jon, Hutt, C. R., and Holcomb, L. G., 1980, Test and calibration of the Seismic Research Observatory: U.S. Geological Survey Open-File Report 80–187, 86 p.

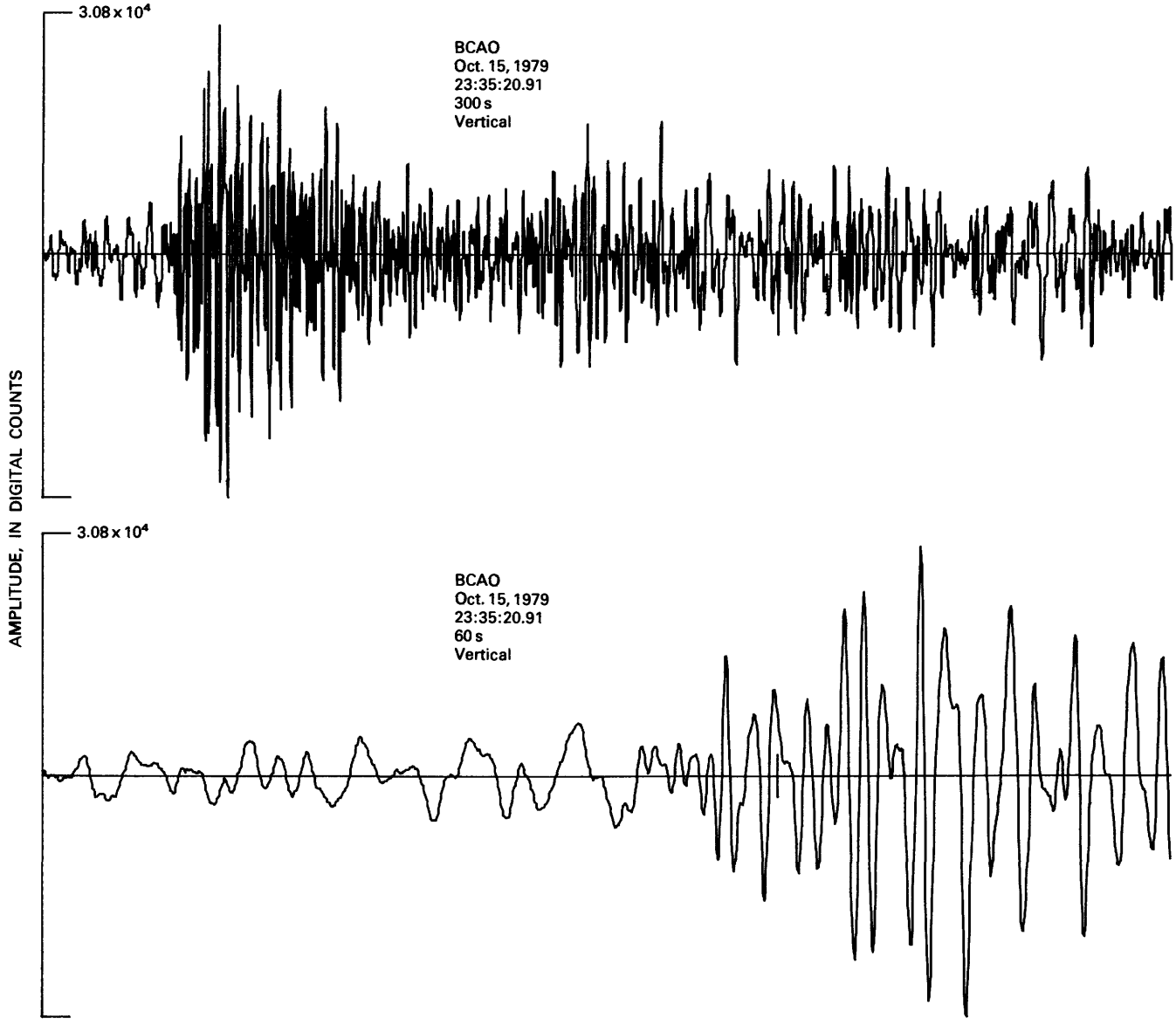

FIGURE 49.—Short-period seismograms from Banqui, Central African Empire. Conventions same as in figure 48.

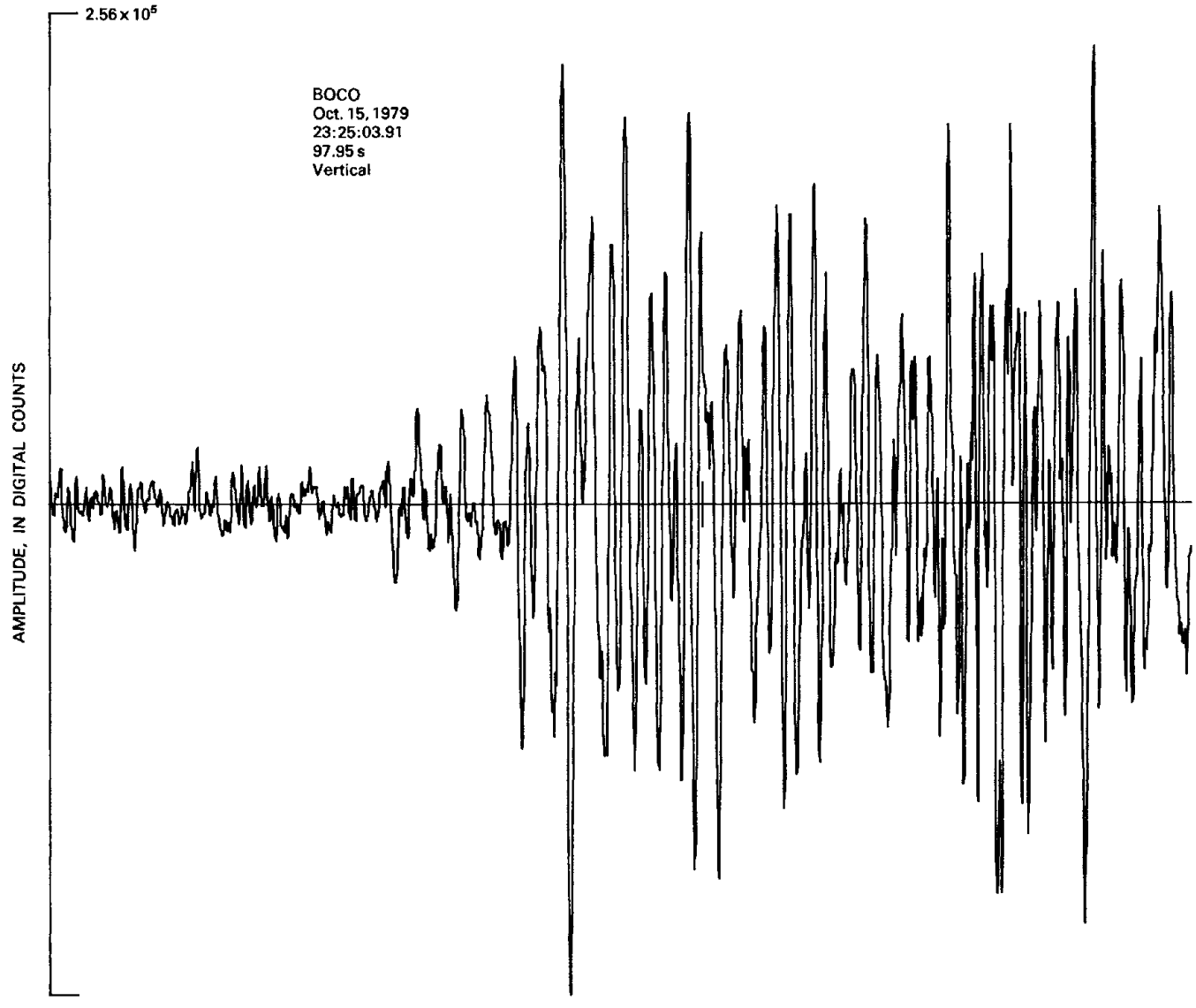

FIGURE 50.—Short-period seismogram from Bogotá, Colombia. Conventions same as in figure 48.

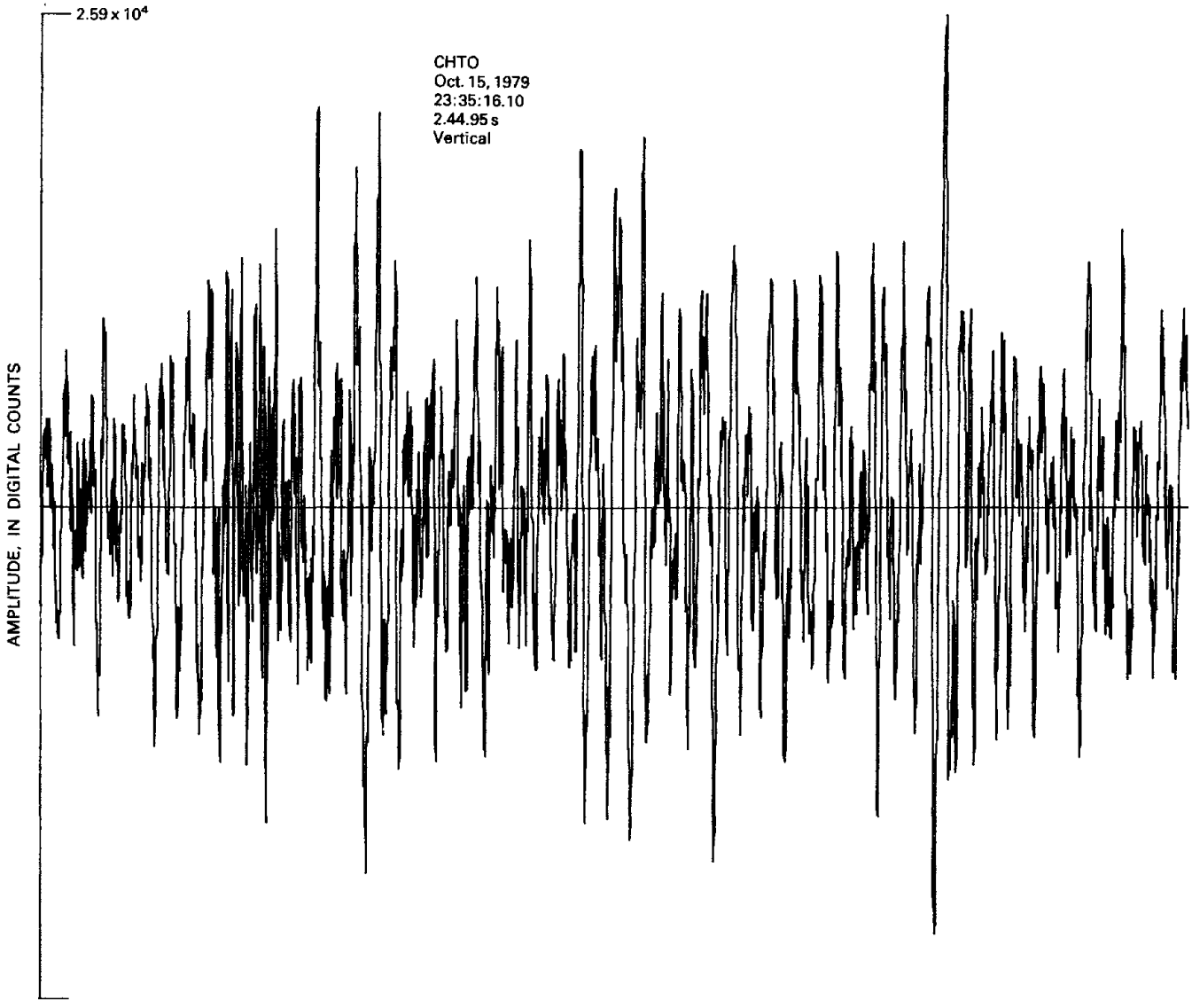

FIGURE 51.—Short-period seismogram from Chiang Mai, Thailand. Conventions same as in figure 48.

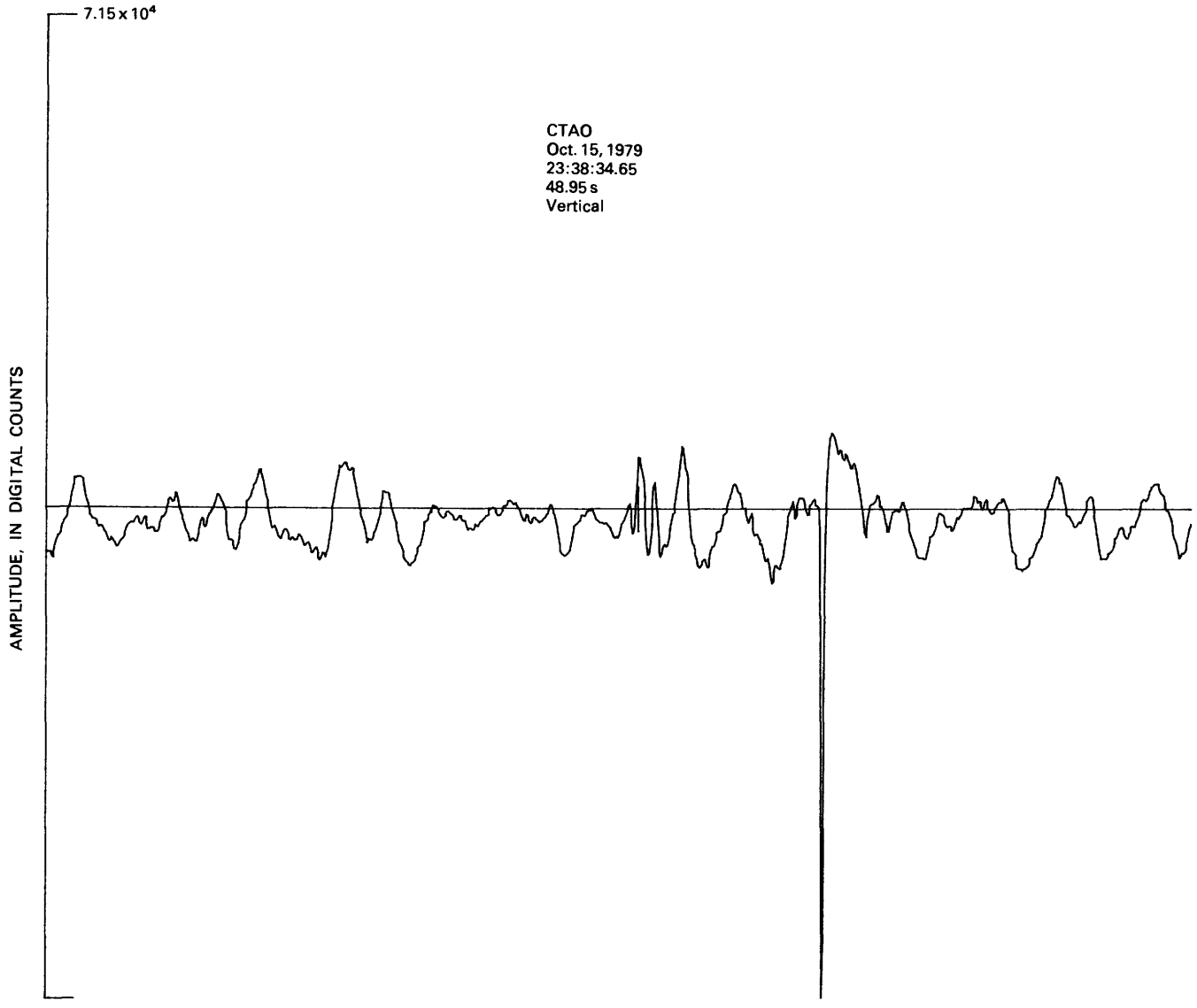

FIGURE 52.—Short-period seismogram from Charters Towers, Australia. Conventions same as in figure 48.

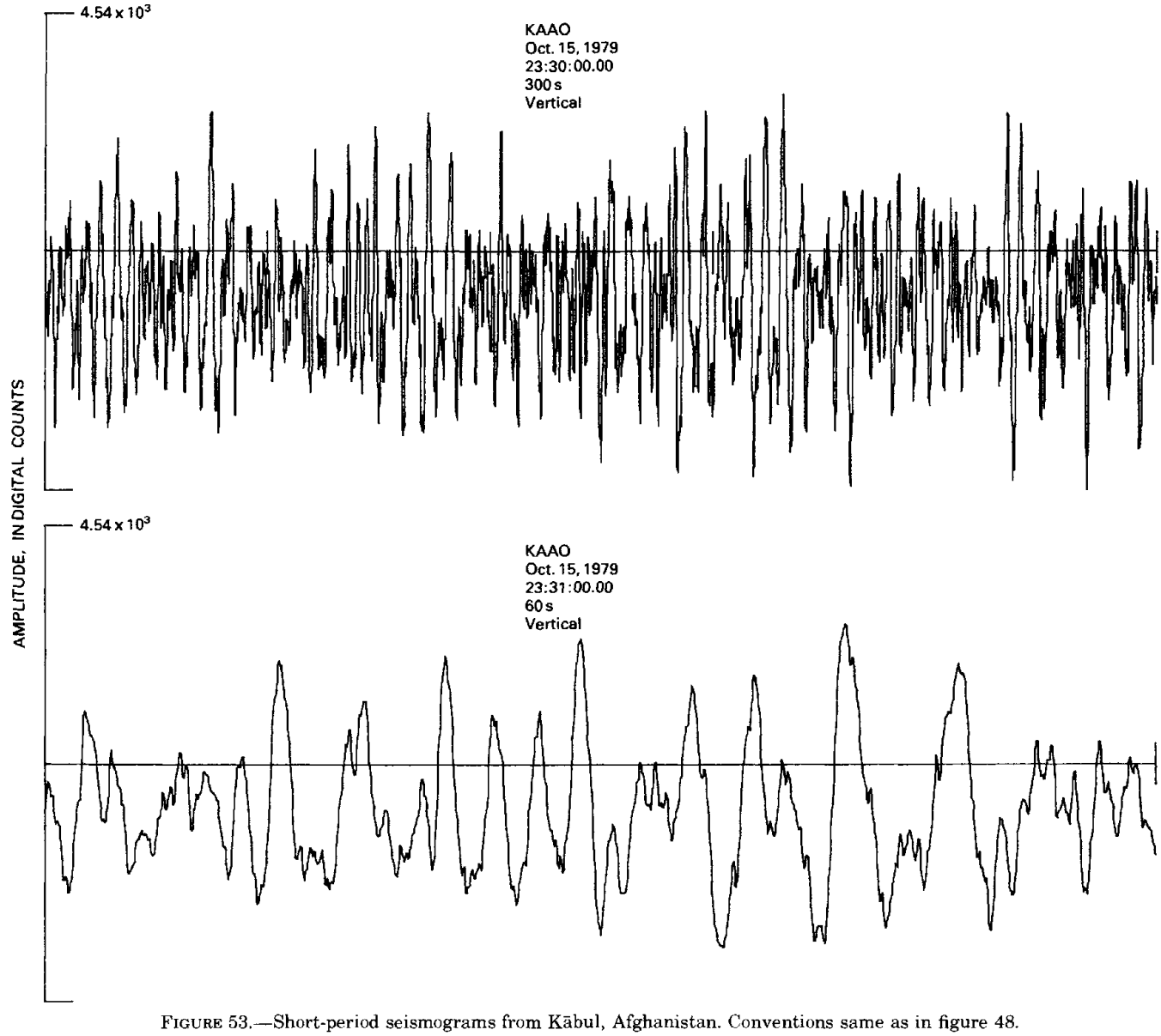

FIGURE 53.—Short-period seismograms from Kābul, Afghanistan. Conventions same as in figure 48.

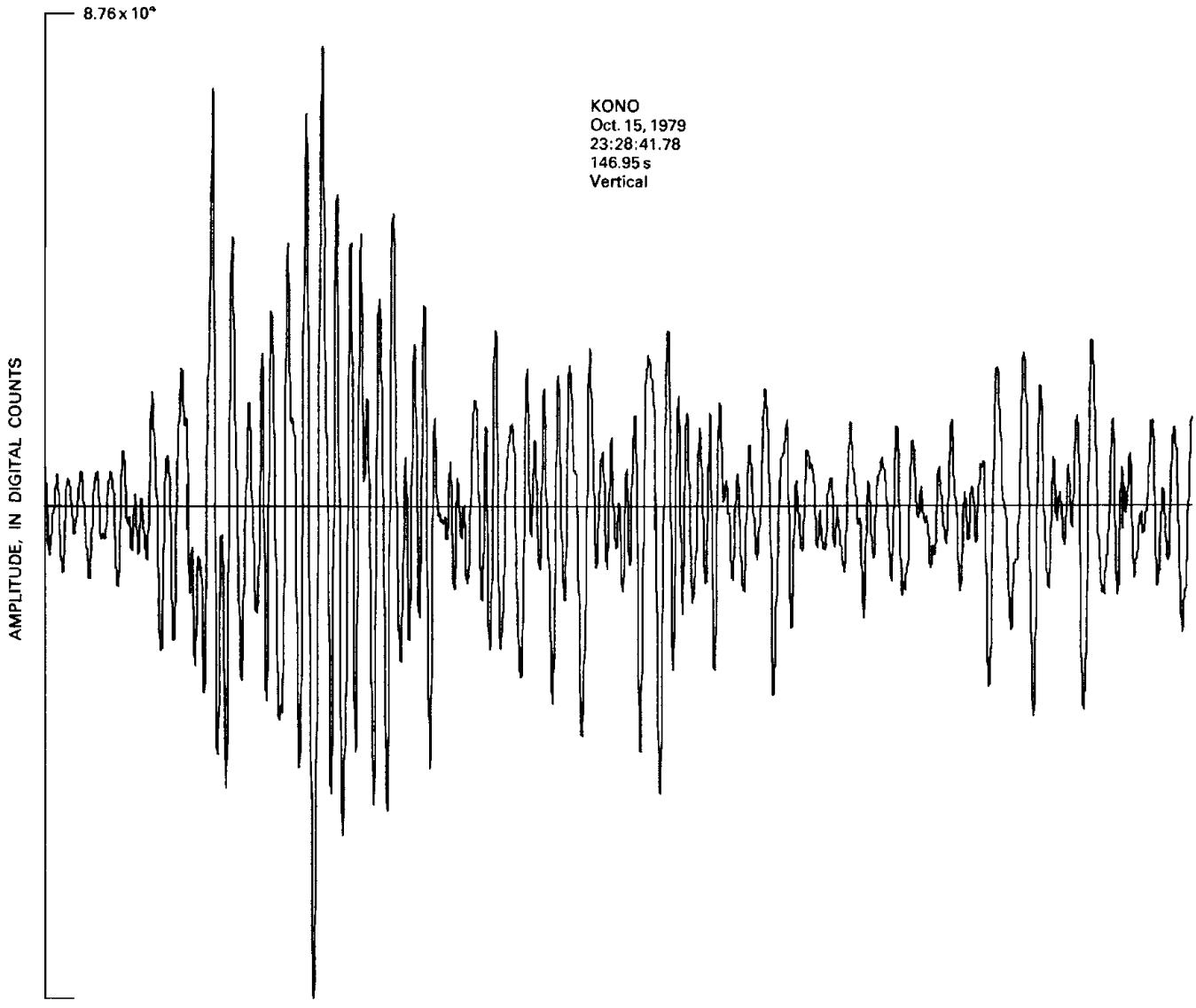

FIGURE 54.—Short-period seismogram from Kongsberg, Norway. Conventions same as in figure 48.

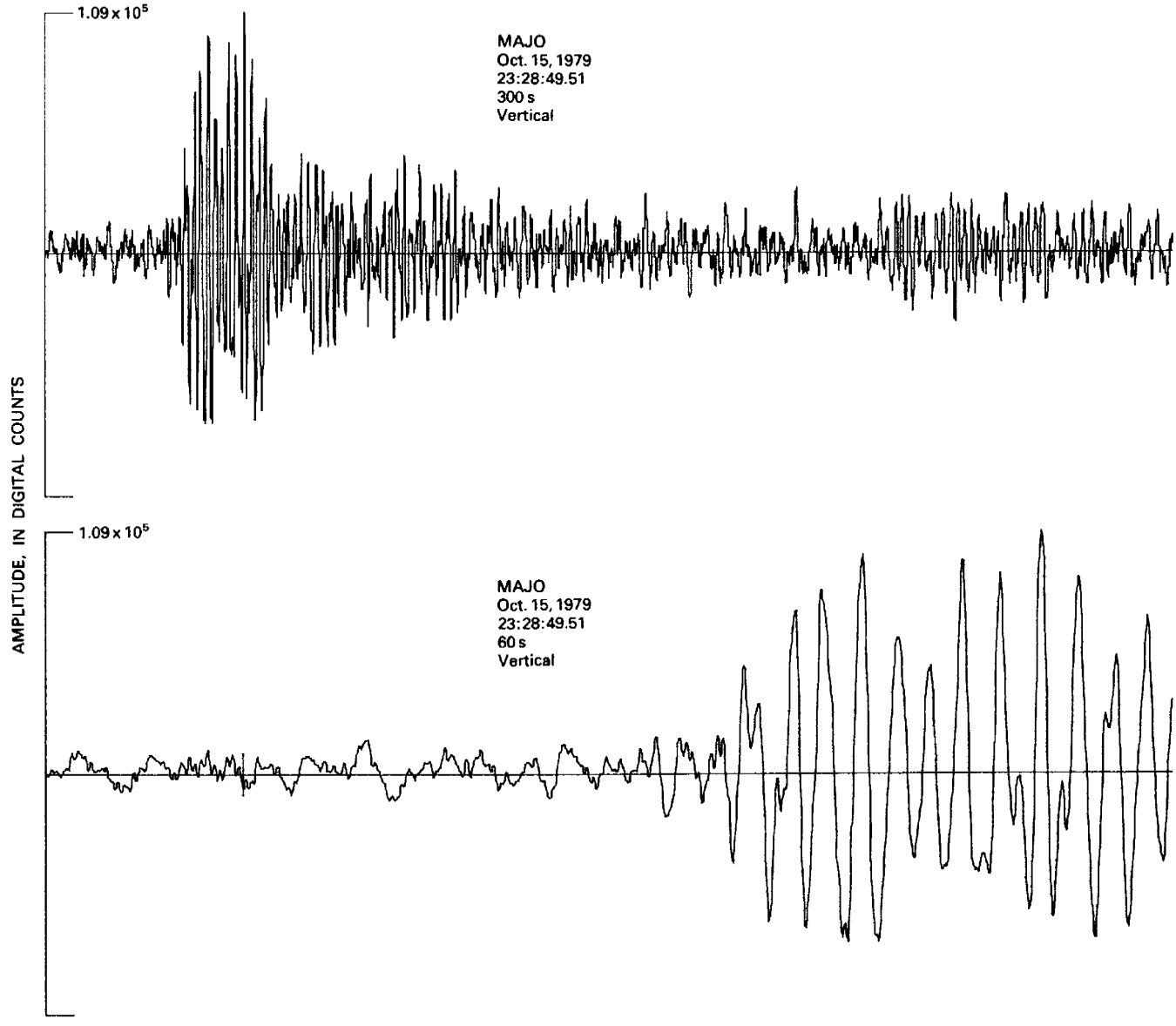

FIGURE 55.—Short-period seismograms from Matsushiro, Japan. Conventions same as in figure 48.

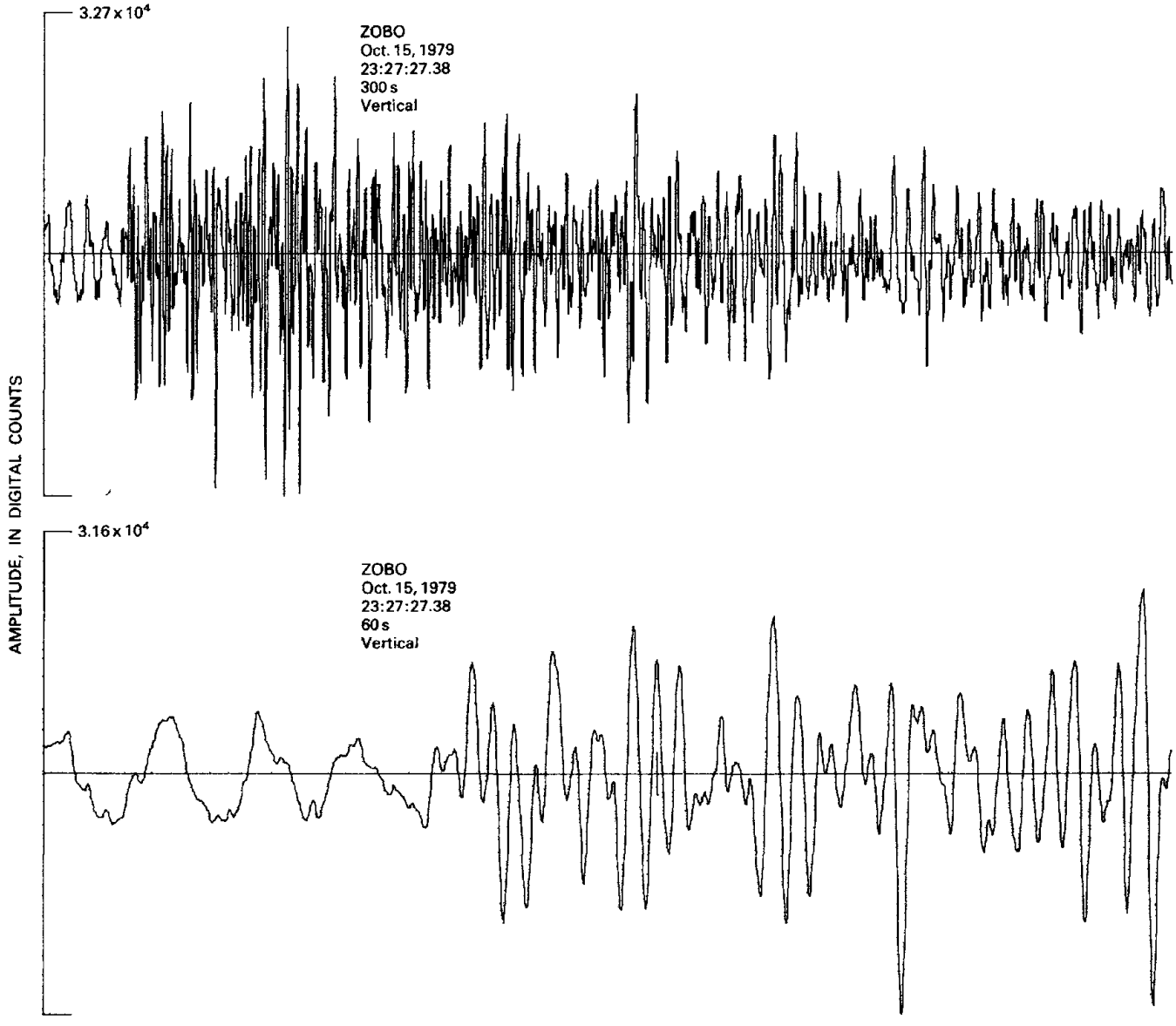

FIGURE 56.—Short-period seismograms from Zongo (La Paz), Bolivia. Conventions same as in figure 48.

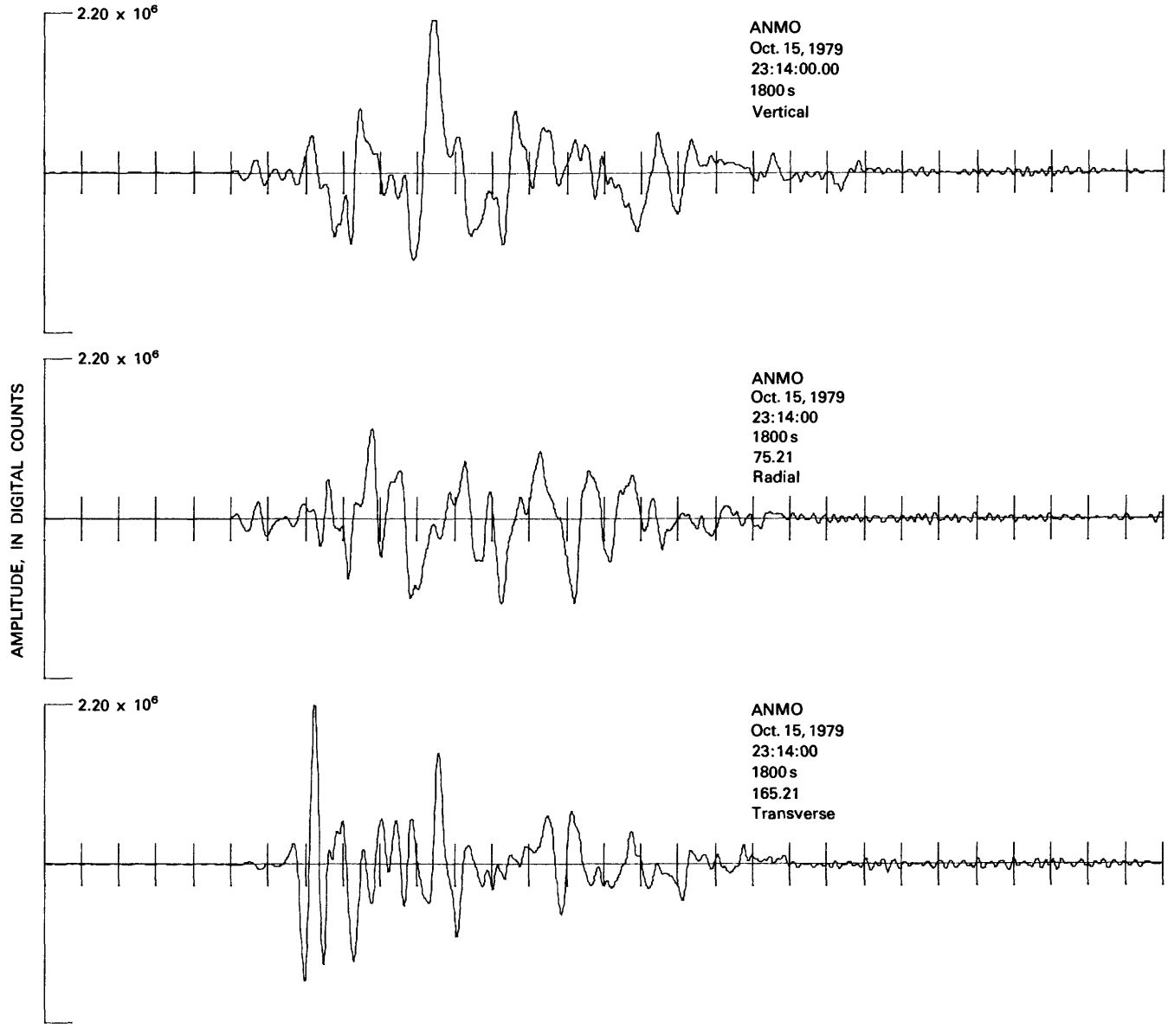

FIGURE 57.—Long-period seismograms from Albuquerque, N. Mex. Station code name, date, time (G.m.t.) of first sample, total duration of each trace, and azimuth corresponding to upward motion on seismogram, respectively from top to bottom, are shown above each seismogram. Tick marks indicate 1-minute intervals. Horizontal traces have been rotated numerically to generate synthetic radial and transverse components. See table 12 for calibration factors of amplitudes.

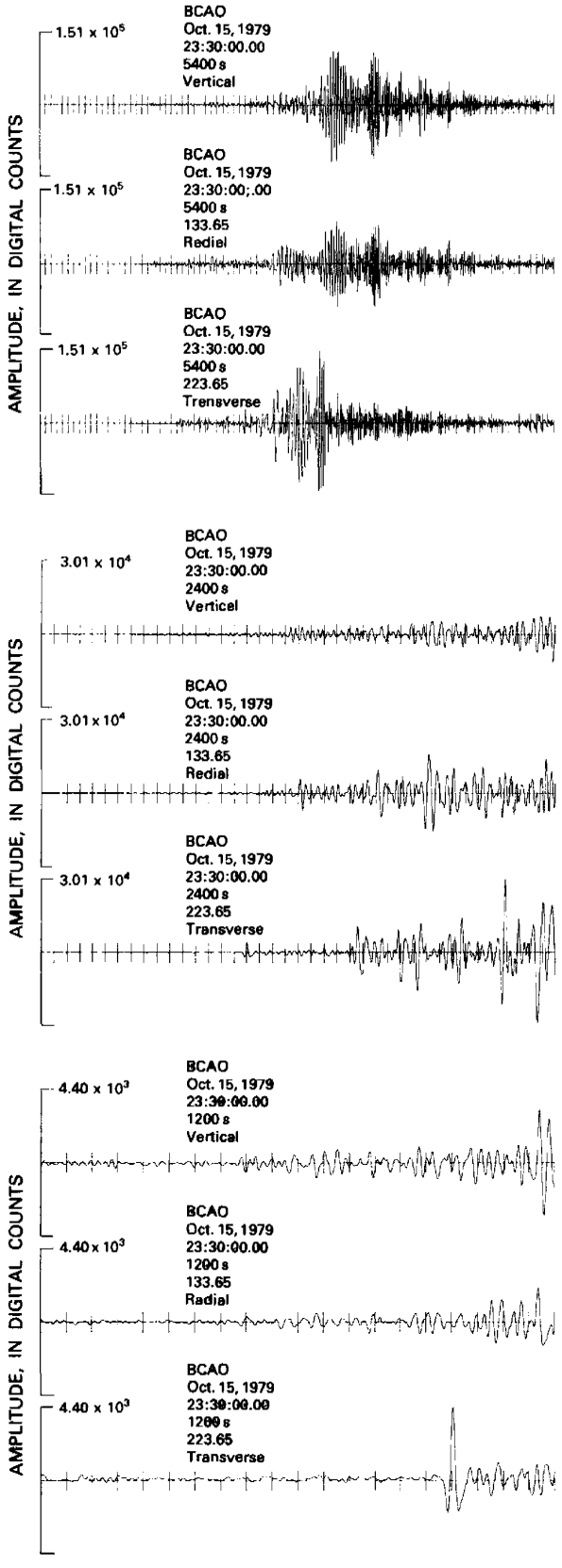

FIGURE 58.—Long-period seismograms from Bangui, Central African Empire. Conventions same as in figure 57.

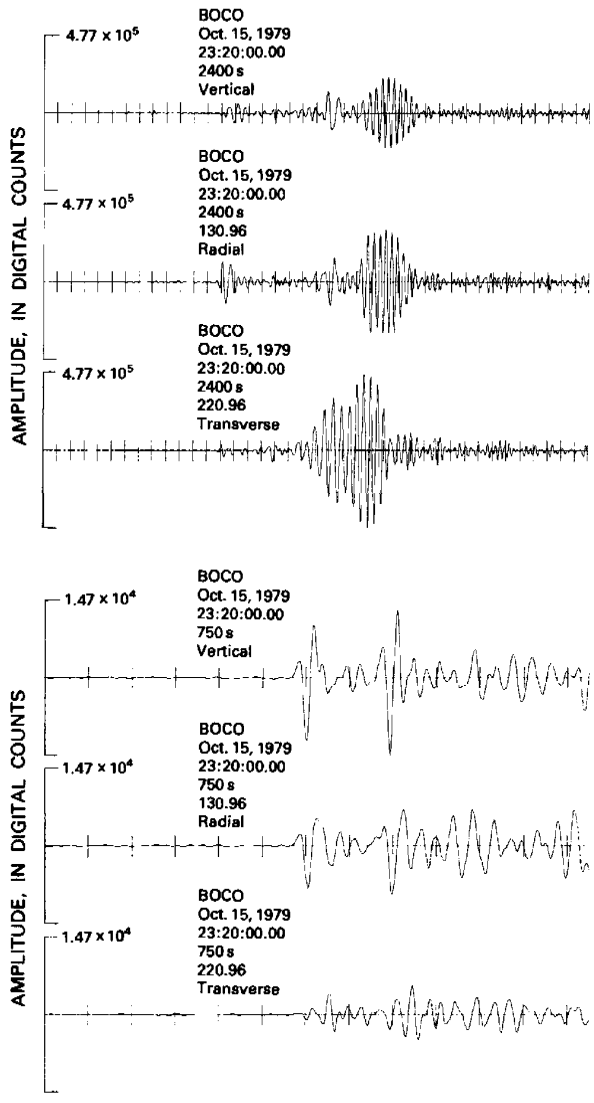

FIGURE 59.—Long-period seismograms from Bogotá, Colombia. Conventions same as in figure 57.

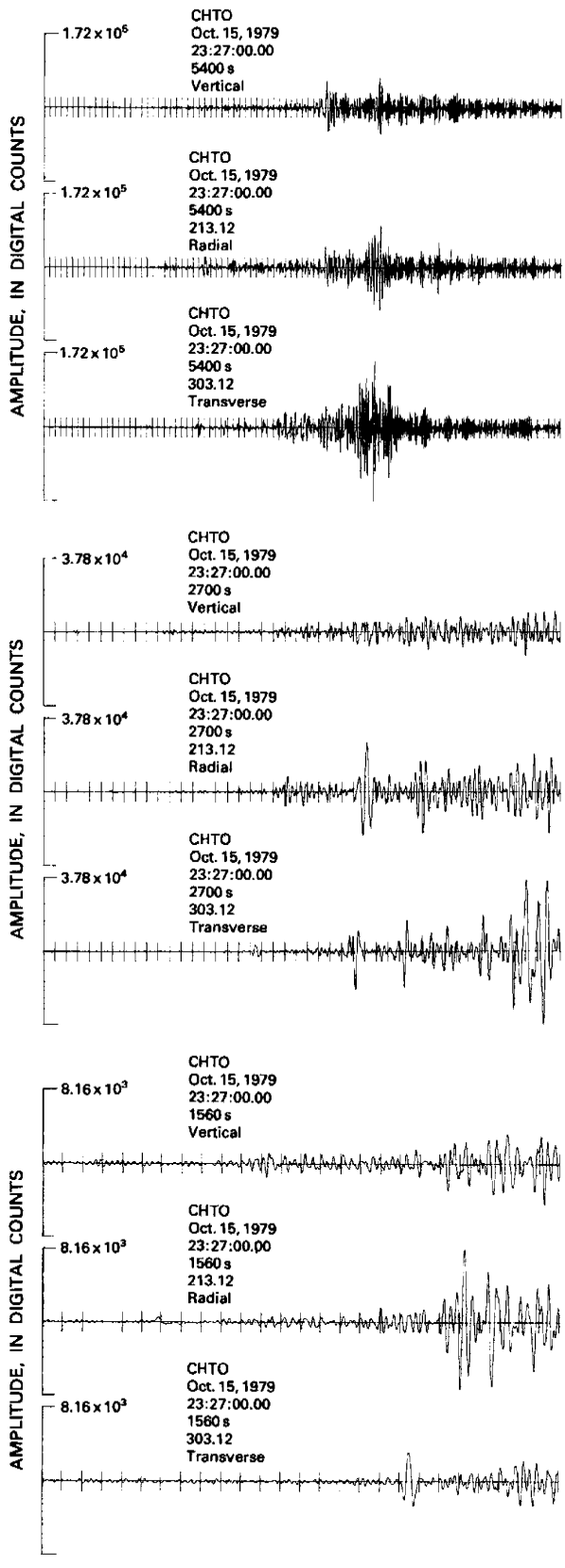

FIGURE 60.—Long-period seismograms from Chiang Mai, Thailand. Conventions same as in figure 57.

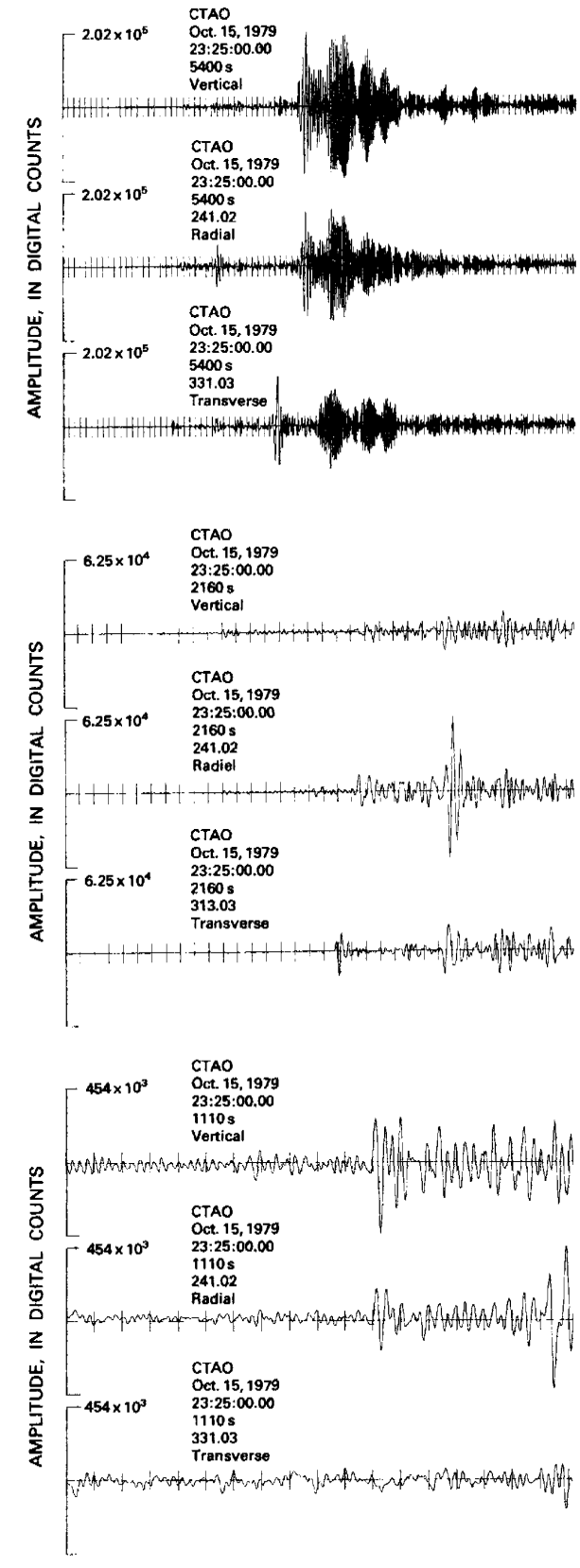

FIGURE 61.—Long-period seismograms from Charters Towers, Australia. Conventions same as in figure 57.

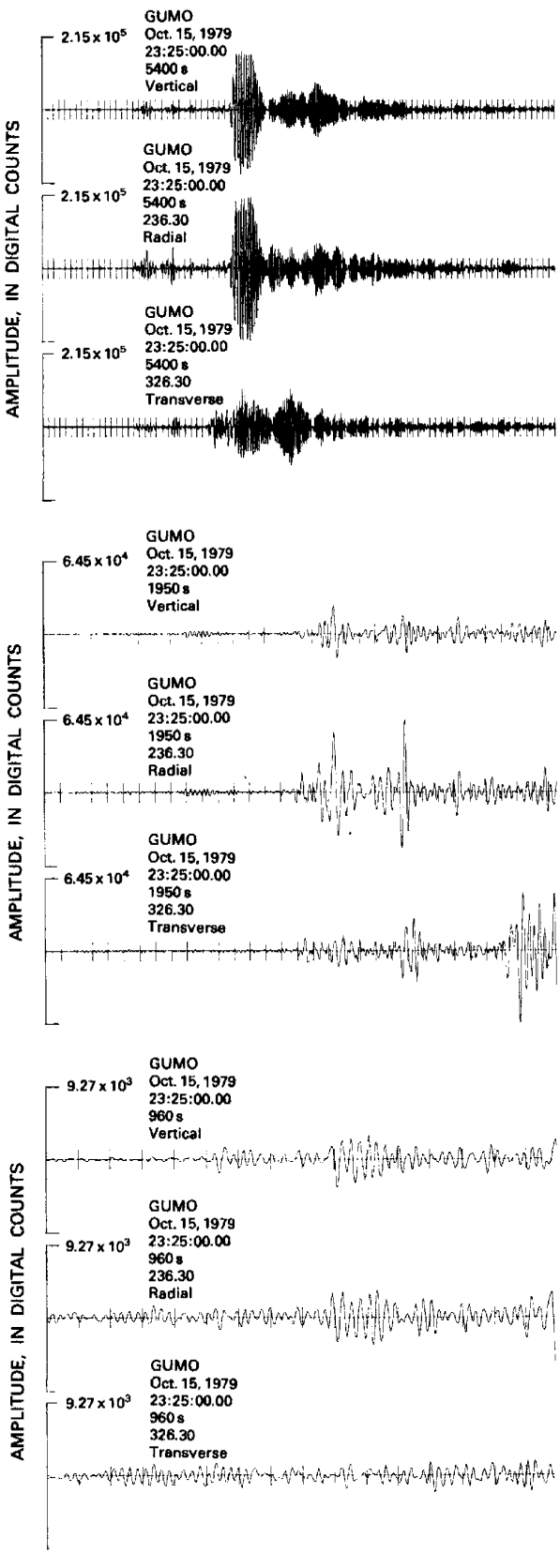

FIGURE 62.—Long-period seismograms from Guam, Marianas Islands. Conventions same as in figure 57.

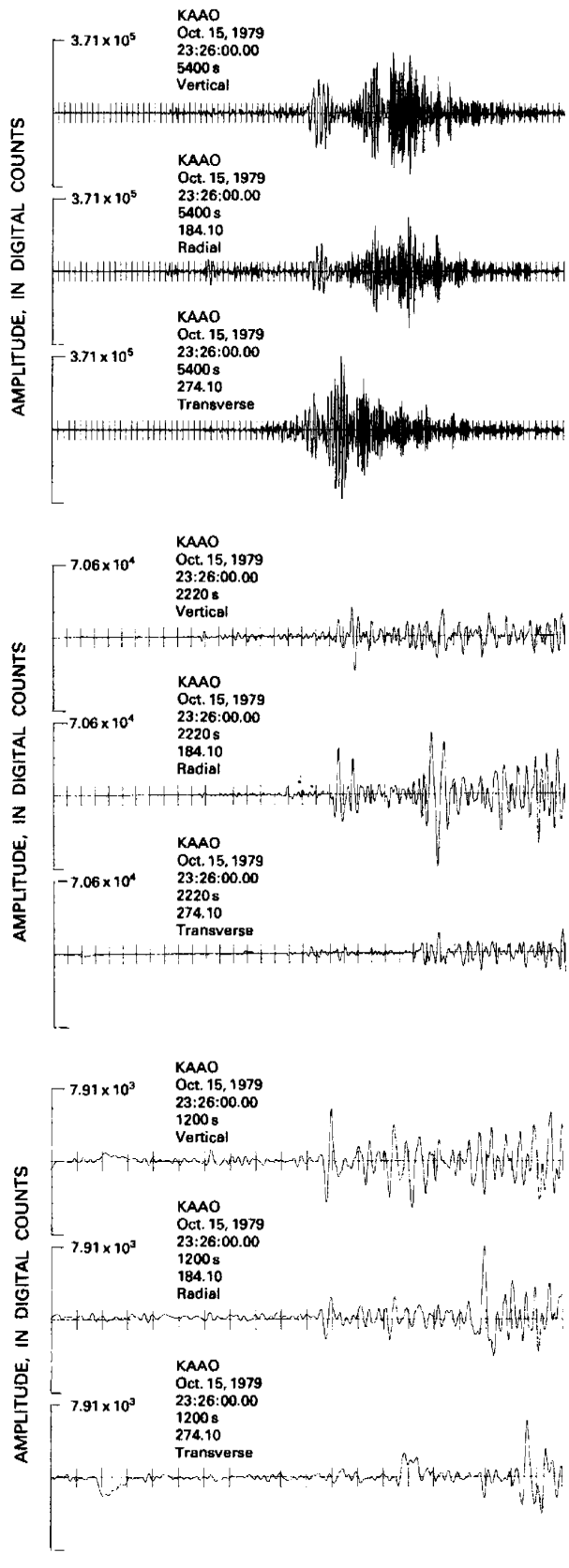

FIGURE 63.—Long-period seismograms from Kābul, Afghanistan. Conventions same as in figure 57.

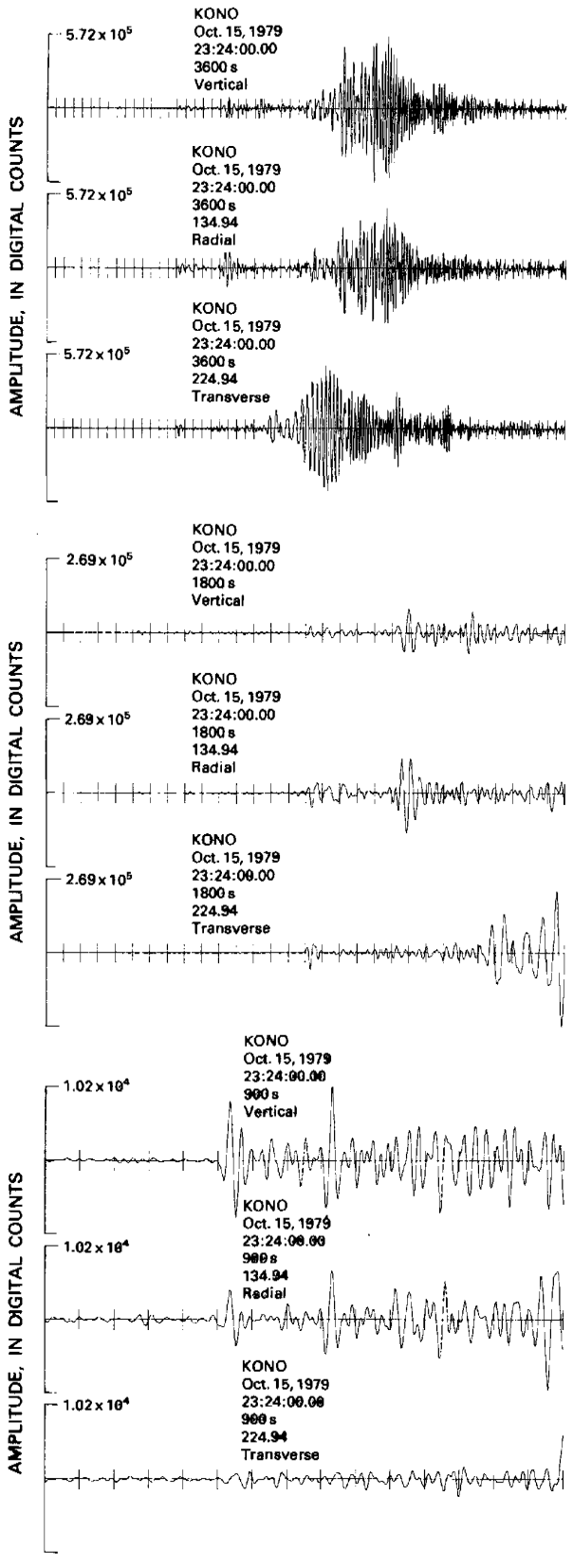

FIGURE 64.—Long-period seismograms from Kongsberg, Norway. Conventions same as in figure 57.

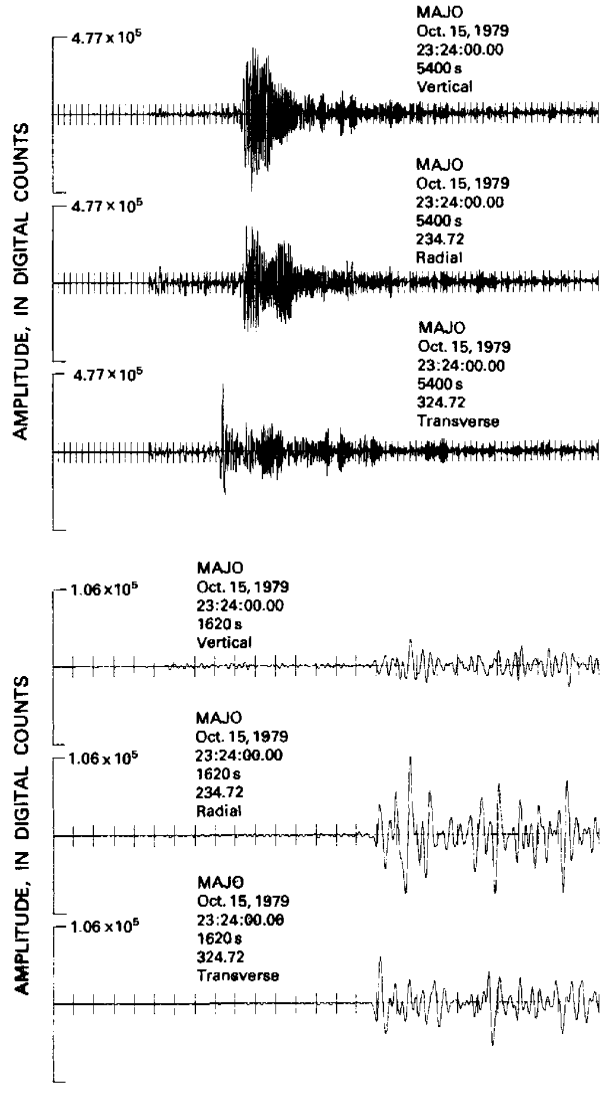

FIGURE 65.—Long-period seismograms from Matsushiro, Japan. Conventions same as in figure 57.

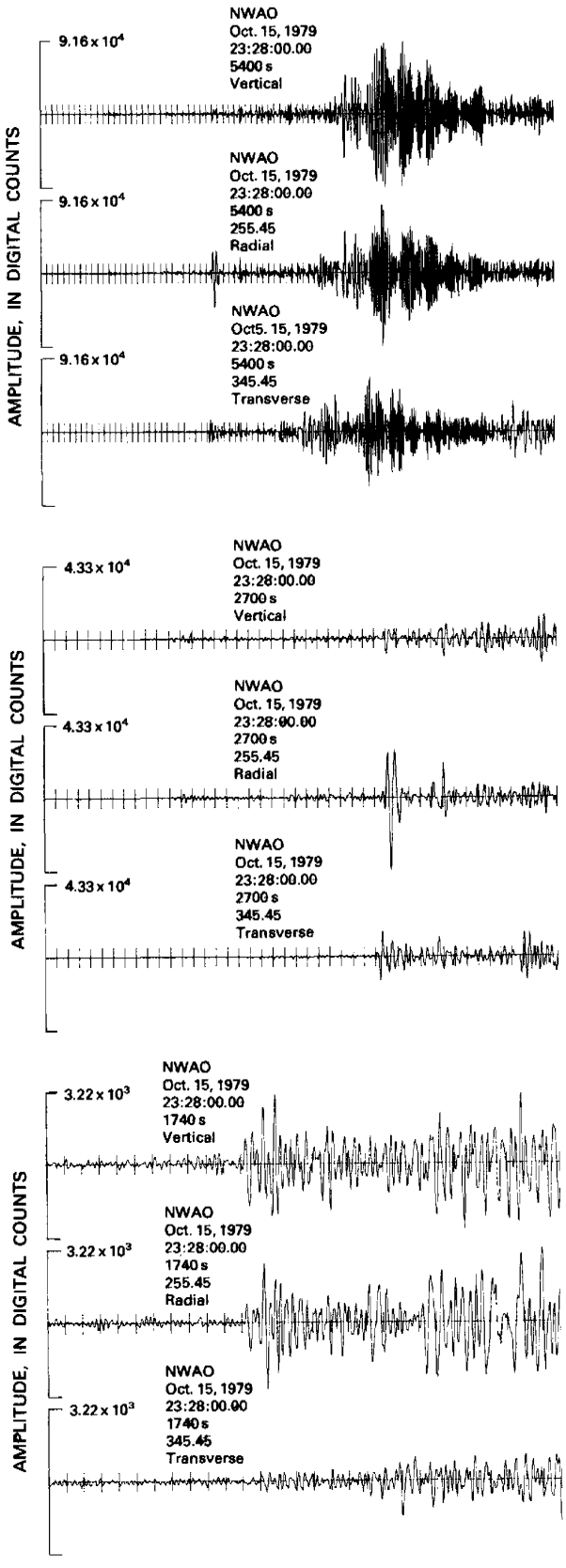

FIGURE 66.—Long-period seismograms from Narrogin, Australia. Conventions same as in figure 57.

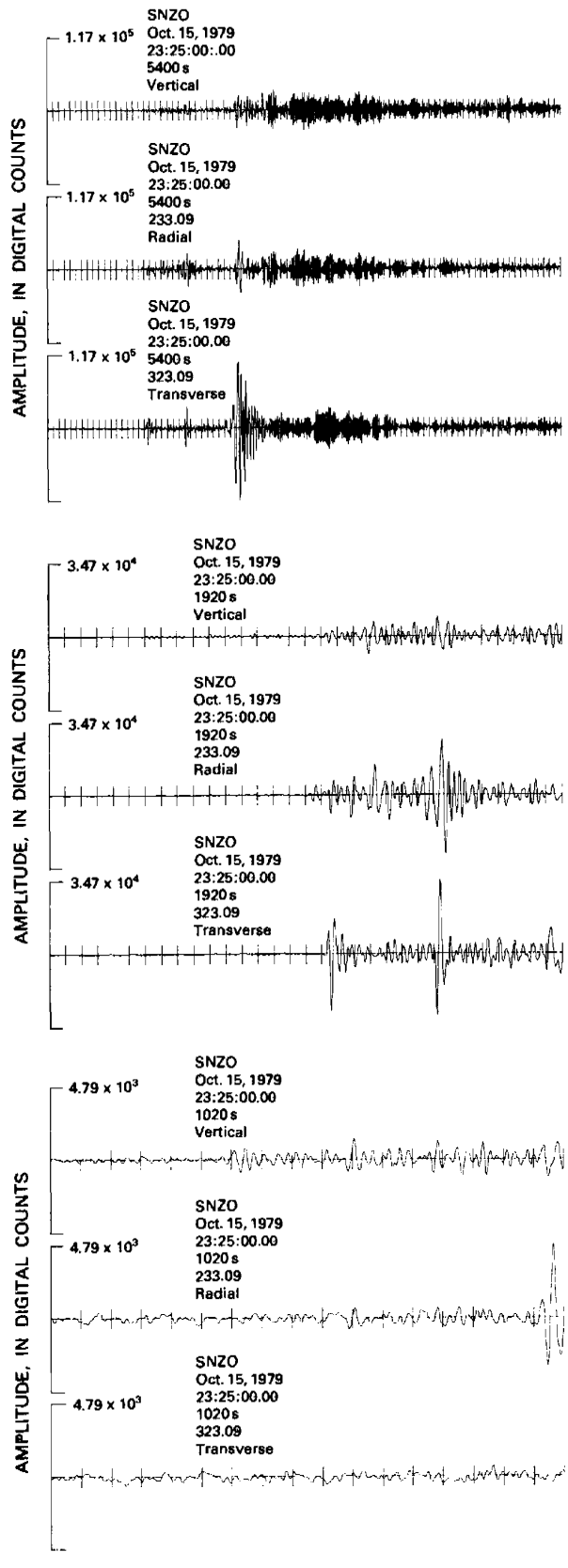

FIGURE 67.—Long-period seismograms from South Karori, New Zealand. Conventions same as in figure 57.

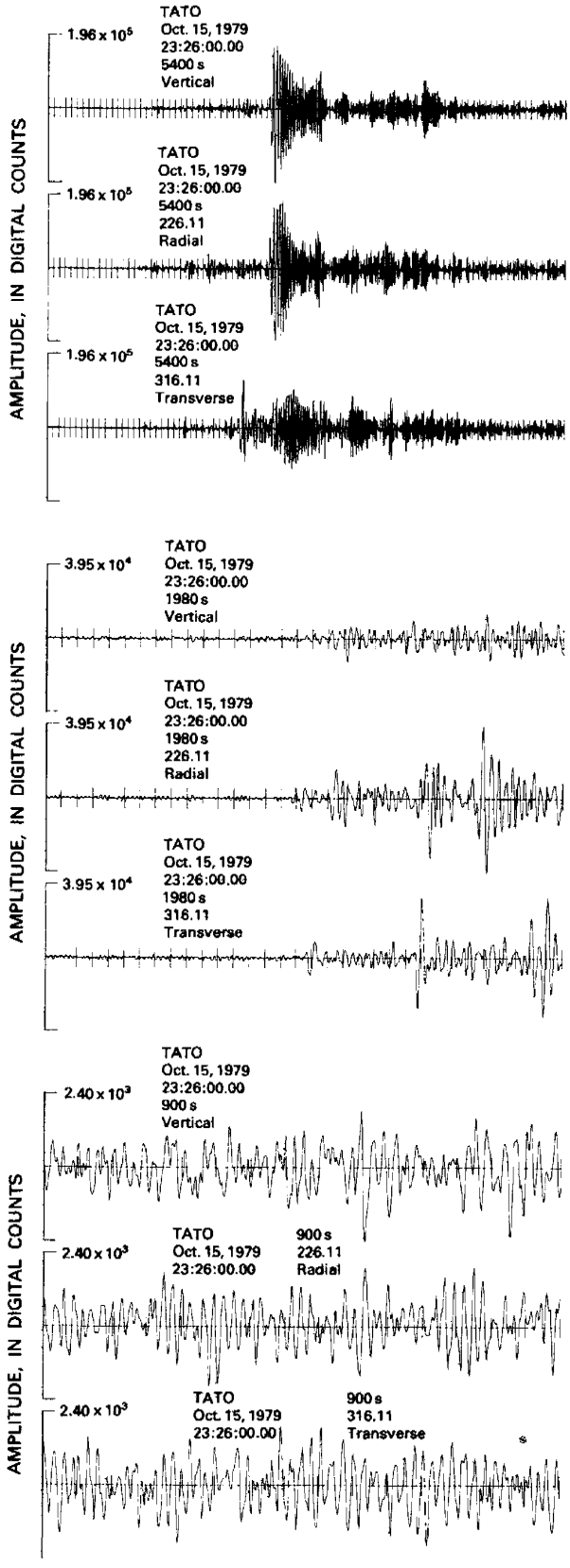

FIGURE 68.—Long-period seismograms from Taipei, Taiwan. Conventions same as in figure 57.

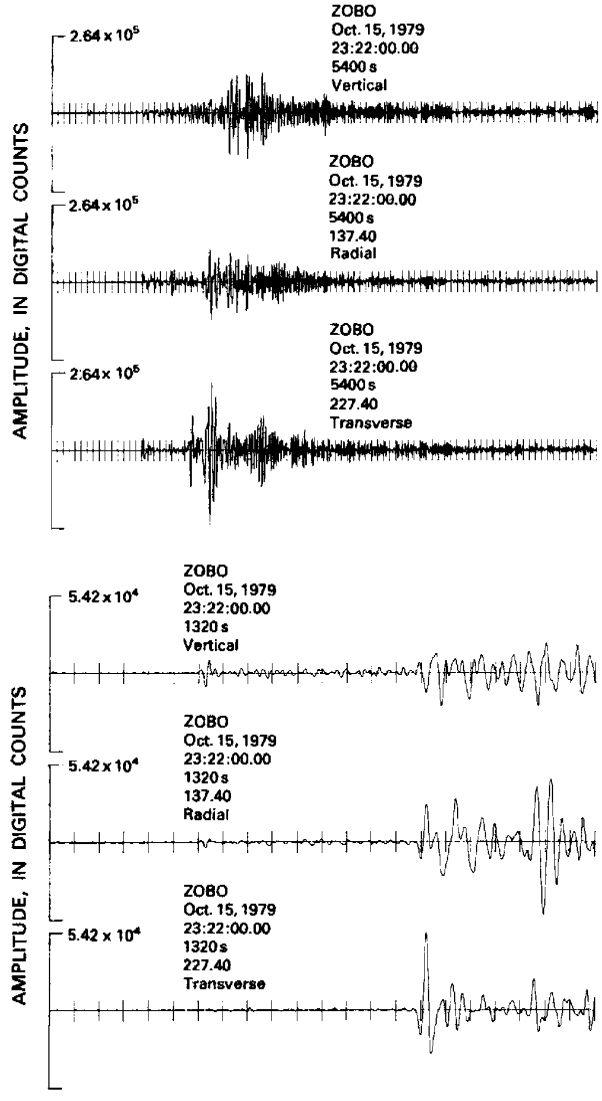

FIGURE 69.—Long-period seismograms from Zongo (La Paz), Bolivia. Conventions same as in figure 57.

SYNTHETIC SEISMOGRAM MODELING FOR THE LATERALLY VARYING STRUCTURE IN THE CENTRAL IMPERIAL VALLEY

By WALTER D. MOONEY and GEORGE A. MCMECHAN
U.S. GEOLOGICAL SURVEY

CONTENTS

INTRODUCTION

The U.S. Geological Survey conducted a detailed seismic-refraction experiment in the Imperial Valley during early 1979 (see fig. 70 for location). The goal of our investigation was to reveal the structural details of this tectonic province and to provide the velocity information necessary to better locate and model the numerous earthquakes that occur there. A description of the experiment and traveltime analysis of some of the data are given by Fuis and others (this volume). We present here a detailed amplitude and traveltime interpretation of a reversed profile obtained by a new method of computing synthetic seismograms for laterally varying structures.

ANALYTICAL METHODS

To maximize the amount of velocity information extracted from the profiles, we have considered the observed amplitude behavior as well as the traveltimes because the amplitudes are particularly sensitive to velocity gradients and discontinuities. Amplitude constraints are included by computing synthetic-seismogram profiles that can be compared with the observed profiles. Our analytical procedure consists of a series of iterative perturbations of the starting model, in which the perturbations are chosen to give increasing resemblance between the major features of the observed and computed seismograms.

Most presently available methods for constructing synthetic seismograms are not valid for laterally varying velocity structures. Asymptotic ray theory (Červený and others, 1977) provides one method that has been shown to be valid for such structures, but to our knowledge the present study is the first attempt to apply this theory to the interpretation of recorded refraction data. The method consists of tracing rays through the structure to obtain epicentral distances and traveltimes while computing complex reflection and transmission coefficients, the free-surface interaction, and geometric spreading to obtain amplitudes and pulse shapes. We chose the algorithm of Wesson (1970) to compute the geometric spreading because this algorithm is valid for arbitrary media and for turning rays (refractions) as well as for reflections. We have paid particular attention to including multiple-reflection phases (*PP* and *PPP*) because these phases are prominent in the Imperial Valley record sections. Details were given by McMechan and Mooney (1980).

DATA

The data used in this study are from a reversed profile between shotpoints 6 and 13 (fig. 70). This profile was selected for detailed interpretation because it provides, by virtue of its location and length, the best available information concerning the velocity-depth structure of the central Imperial Valley. Each of the two profiles was recorded by 100 identical instruments from a single shot; this procedure aids in correlating arrivals across the profiles. The recording sites were identical for both shots. All records are of vertical components. The total number of records available for profile 13–6 was 79, of which 62 are displayed in figure 71; the total number of records available for profile 6–13 was 83, of which 65 are displayed in figure 72. Where two records overlap on these plots, only the record with the highest signal-to-noise ratio is shown.

In addition to clear first arrivals, the profiles (figs. 71, 72) are characterized by distinct secondary arrivals that

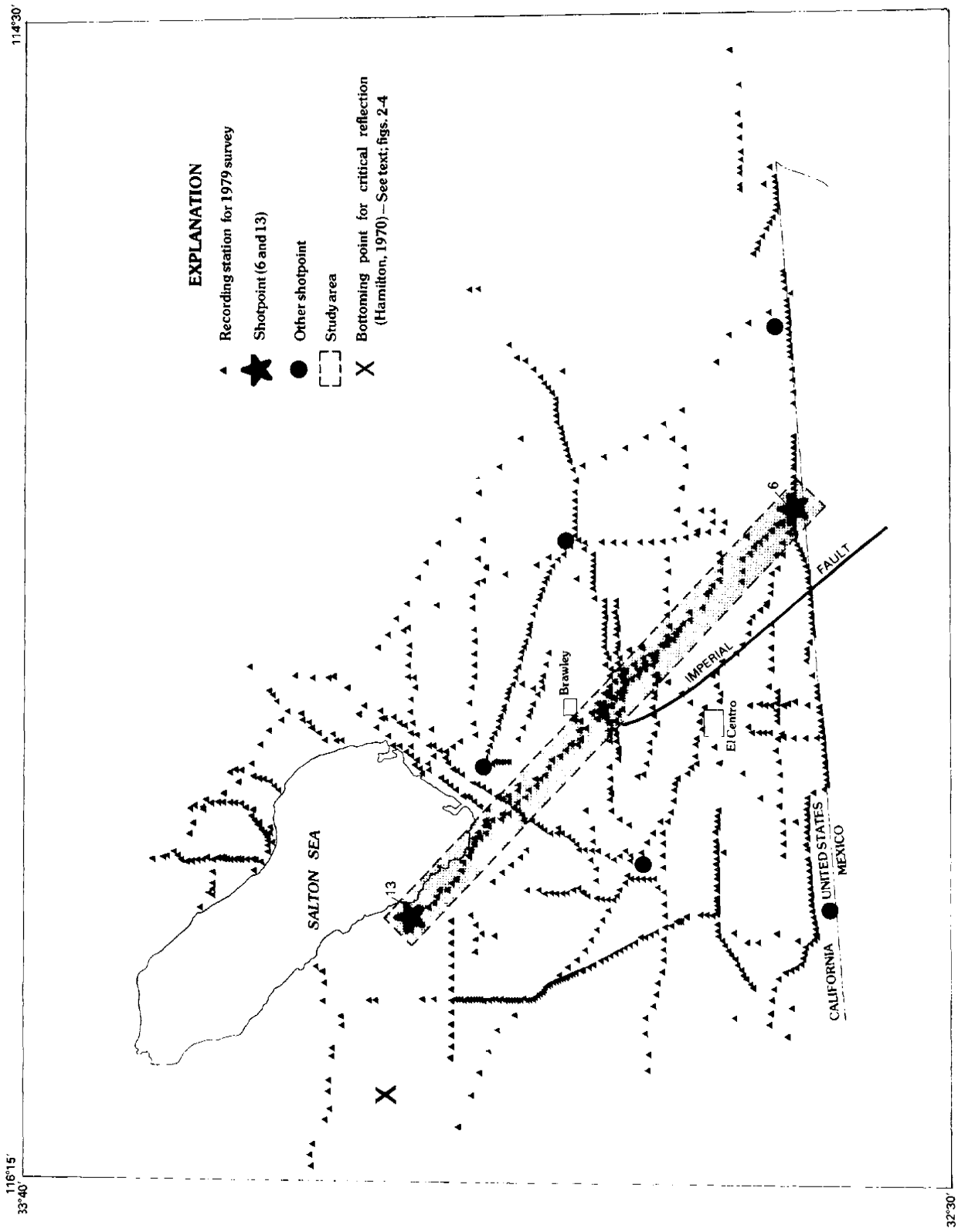

FIGURE 70.—Locations of Imperial Valley seismic-refraction experiment of 1979, showing relation of recording stations to Imperial fault. Only reversed profile between shotpoints 6 and 13 is considered in this study.

include subsurface reflections and free-surface multiples. Modeling of these secondary arrivals is an important aspect of our analysis and significantly constrains the model beyond what would be possible from an analysis of first arrivals alone.

Profile 6–13 (fig. 72) runs to the northwest from the Salton Sea southeastward to the United States-Mexican border (fig. 70). On this profile, the first arrivals between 3 and 17 km form a smooth curve (AB) that indicates a continuously increasing velocity with depth in the sedimentary column. Between 17 and 57 km the first arrivals, which represent refractions in the basement, form a relatively straight line (BC) with an apparent velocity of 5.55 km/s. Beyond 57 km the first arrivals represent a subbasement refraction (DE) with an apparent velocity of 7.7 km/s. The triplication (BCDE) evident beyond 40 km indicates either a velocity discontinuity or a high-velocity gradient in the region of transition from basement to subbasement. The traveltime curves of free-surface multiples (AF for *PP* arrivals and AH for *PPP* arrivals) are observed to be "stretched" in both time and distance relative to the

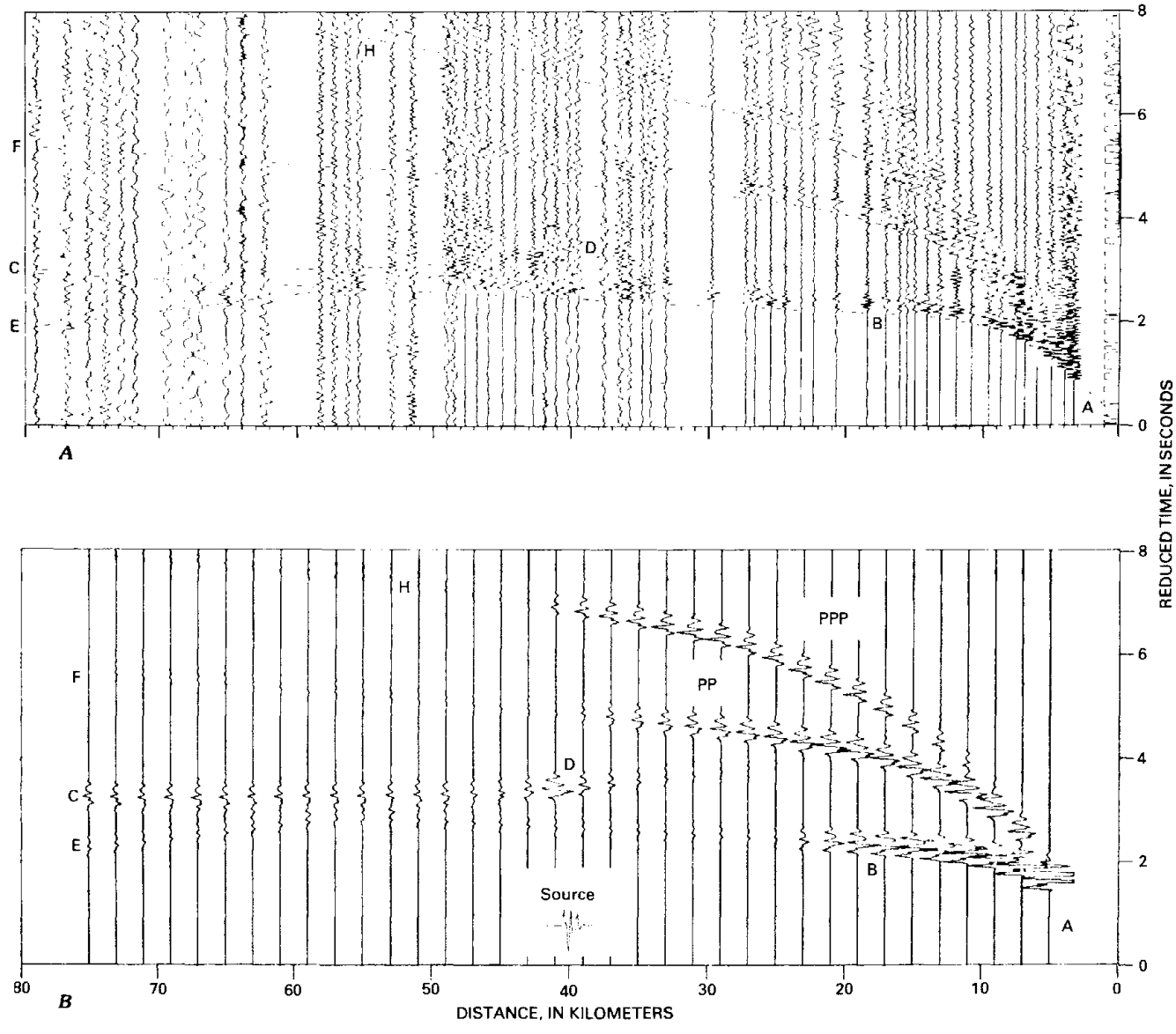

FIGURE 71.—Comparison of observed and synthetic record sections for profile 13–6. Specific refraction and reflection branches discussed in text are labeled by letters A through H on both profiles; phase G (fig. 72) is not evident in these sections (see text). *A*, Observed record section. Dashed line corresponds to theoretical arrival times in figure 71*B*. Observed traces are plotted so that each has approximately the same maximum amplitude as synthetic traces; no attempt was made to recover true amplitudes. *B*, Synthetic record section. Apparent source function used in synthetics is shown in inset. Wave groups labeled "*PP*" and "*PPP*" are free-surface multiples. Each synthetic trace is scaled by a factor proportional to square root of distance.

first-arrival curve by an amount proportional to their multiplicity (2 and 3, respectively).

Profile 6–13 (fig. 72) runs to the northeast from the border to the west side of the Salton Sea (fig. 70). The major features of this profile resemble those of its reverse. Proceeding outward from the shotpoint, the first arrivals again smoothly approach the basement velocity (ABC), a triplication (BCDE) occurs, a higher subbasement velocity is evident (DE), and free-surface multiples are present (AF and AH).

There are, however, significant differences between profiles 13–6 and 6–13. The traveltimes in profile 6–13 indicate a higher near-surface velocity than those in profile 13–6, although similar velocity gradients are present. The apparent velocity of the basement refraction in profile 6–13 is approximately 5.95 km/s, about 0.4 km/s higher than that observed in profile 13–6. The apparent velocity of the subbasement refraction in proile 6–13 is approximately 7.1 km/s, about 0.6 km/s lower than that in profile 13–6. The prominent triplication (BCDE) contains a high-amplitude cusp at about 30 km in profile 6–13 (fig. 72), in comparison with that at about 40 km in profile 13–6 (fig. 71).

All the major features of these two profiles (their dissimilarities as well as similarities) can be modeled by a two-dimensional (laterally as well as vertically vary-

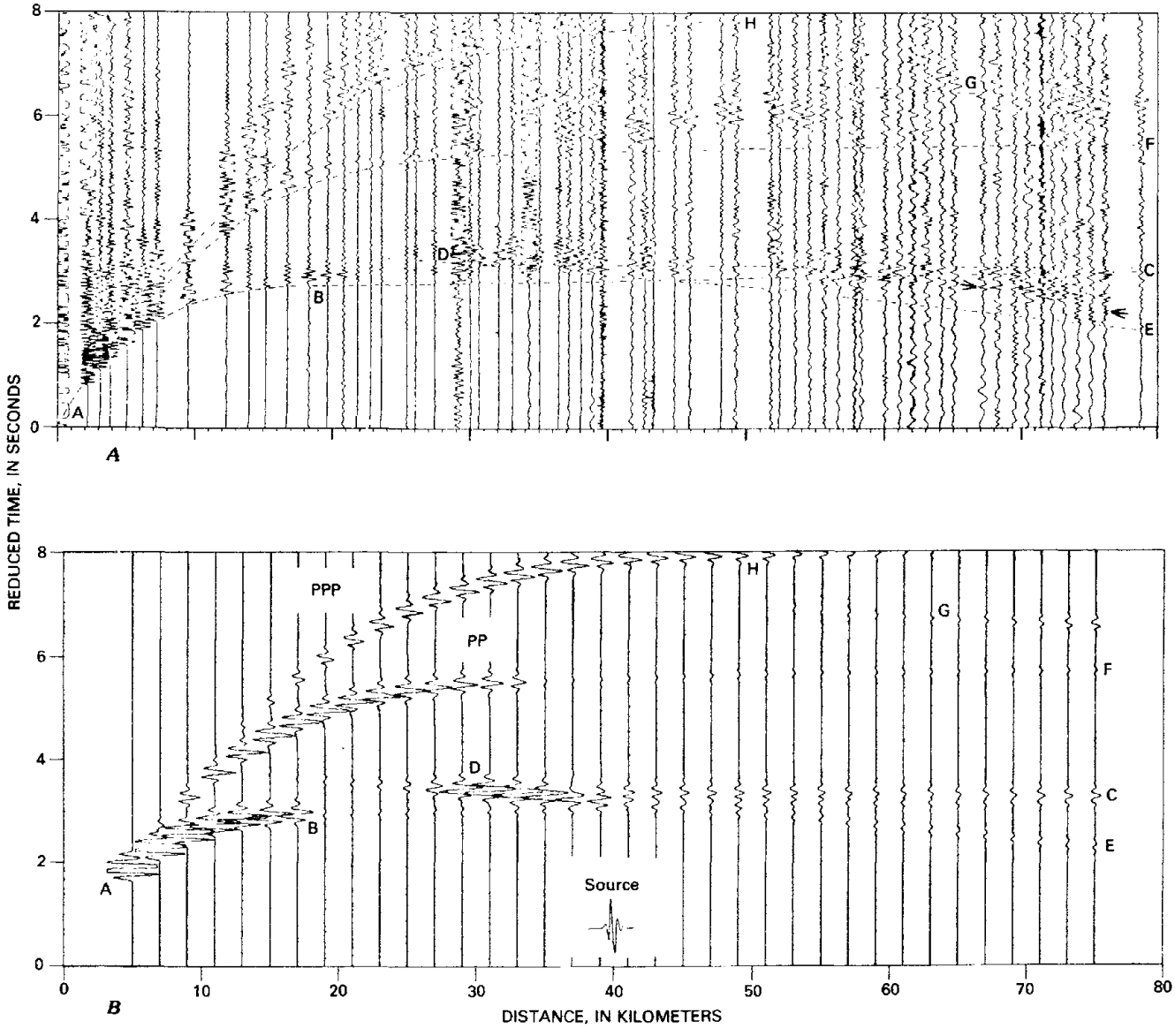

FIGURE 72.—Comparison of observed and synthetic record sections for profile 6–13. Labels and amplitude scaling same as in figure 71; phase G is critical reflection in branch *PP* (see text). *A*, Observed record section. Arrows between branches C and E indicate area with high apparent velocity that suggests possible existence of deeper layer. *B*, Synthetic record section.

ing) structure composed essentially of dipping (inhomogeneous) layers separated by transition zones. The modeling procedure is described below, from the surface downward.

INTERPRETATION

Interpretation began by fitting first-arrival traveltimes to straight lines to give a conventional solution consisting of dipping constant-velocity layers. The synthetic seismograms generated by this approximation inadequately represented the amplitudes and smoothly curving traveltime observations, particularly for those arrivals traveling predominantly in the sedimentary column. Far better agreement with the observations was achieved by modeling the sedimentary column as a region within which velocity increases with depth. Additionally, a lateral velocity gradient was required, in which the velocity at any depth increases from south to north (fig. 73*B*). These features are consistent with earlier models proposed by Kovach and others (1962) and by Biehler and others (1964).

To produce the observed smooth change from sedimentary velocities to the basement velocity, and to avoid producing a noticeable triplication, a 1.0-km-thick transition zone was placed in the model between the sediment and the basement (see fig. 73*A*). The velocity increases from 5.05 km/s at the top of the transition zone to 5.65 km/s at the bottom.

In the basement beneath the transition zone, the velocity gradient is much smaller than in either the transition zone or the overlying deposits. This change in gradient causes an abrupt drop in relative amplitude at about 20-km distance in the first arrivals, at about 35 km in branch PP, and at about 45 km in branch PPP (figs. 71, 72). Differences between the two profiles in the precise position of these features are due to the southward dip of the transition zone (fig. 73*A*).

The basement arrivals in both profiles were modeled by a velocity that increases linearly from 5.65 km/s at the top to 5.85 km/s at the bottom. Unlike the smooth sediment-to-basement transition, there is evidence (the prominent triplication BCDE) for a relatively abrupt increase from 5.85 to 7.2 km/s at a depth as shallow as 10 km. This triplication appears to be the same as that observed by Hamilton (1970) to the northeast of the present study area. This abrupt increase was modeled in two parts: a stepwise increase from 5.85 to 6.60 km/s, and a 0.9-km-thick transition zone in which the velocity increases smoothly from 6.6 to 7.2 km/s (fig. 73*B*). This combination was chosen to place the critical reflections

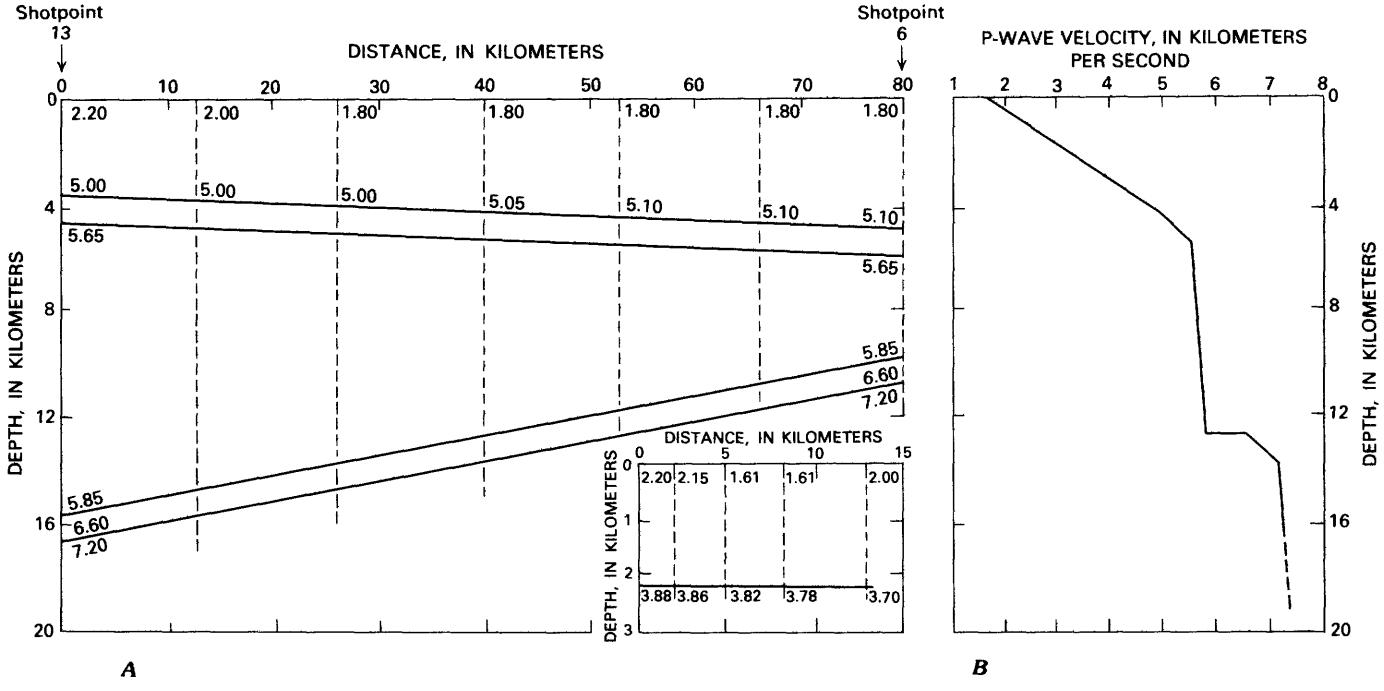

FIGURE 73.—Velocity models for study area in Imperial Valley. *A*, Two-dimensional *P*-wave-velocity model. Model approximates geologic structure in a vertical section through shotpoints 6 and 13 (fig. 70). Thin solid lines separate regions of differing velocity gradient. Intersections of dashed vertical lines with thin solid lines indicate points at which velocity was specified for synthetic traveltime and amplitude computations (figs. 71*B*, 72*B*). Numbers at intersections indicate *P*-wave velocities (in kilometers per second). Numbers at both ends of a given thin solid line indicate constant velocity along that line. Line labeled "5.85/6.60" indicates a velocity step. Inset shows details of model near shotpoint 13. Velocity at any point is determined by interpolation. *B*, Representative velocity-depth profile derived from figure 73*A* at a distance of 40 km.

(points D, figs. 71, 72) at their observed distances while including the large velocity increase required by the traveltimes of arrivals refracted in the lower medium (branches DE, figs. 71, 72). The relative amplitude of the critical reflection in profile 6–13 is larger than that in 13–6. This effect is reproduced in the model as a result of the northward dip of the lower part of the transition zone (fig. 73*A*). In addition, the corresponding critical reflection is observed in branch PP on profile 6–13 (near point G, fig. 72) but not in profile 13–6 because this reflection is off the end of the recorded profile. The large X in the center left of figure 70 indicates the approximate location of the bottoming point for the critical reflection observed by Hamilton (1970); the reflecting boundary is, therefore, not confined to the Imperial Valley.

One segment of an arrival branch observed on profile 6–13 between branches E and C beyond 65 km (arrows, fig. 72*A*) appears with a high apparent velocity (8.22 km/s). This segment may indicate the existence of a deeper layer; its high amplitude is consistent with a critical reflection, possibly from the Moho. A flat-layer solution yields a depth of 22.9 km for this reflector, and the method of Giese (1976) gives a maximum depth of 28.7 km.

One particularly important aspect of this modeling has been the generation of wave groups PP and PPP. Much of the energy propagating in these branches travels along paths that would not exist in a laterally homogeneous nondipping structure (fig. 74). The effects of the dipping structure, and the high velocity gradients in both the sedimentary column and the sediment-to-basement transition, combine to support the relatively energetic propagation of branches PP and PPP to extended ranges, as observed in figures 71 and 72.

DISCUSSION

We have performed a detailed analysis of the major features of a reversed seismic section consisting of the two profiles 13–6 and 6–13. The result is an accurate velocity model for the central Imperial Valley, the major features of which are a sedimentary column that thickens from the Salton Sea to the United States-Mexican border and a deep intracrustal transition that dips from south to north (fig. 73). To approximate the observed amplitude behavior, we found velocity gradients to be more appropriate than sharp boundaries throughout the model. Our model differs from that of Kovach and others (1962) and Biehler and others (1964), which

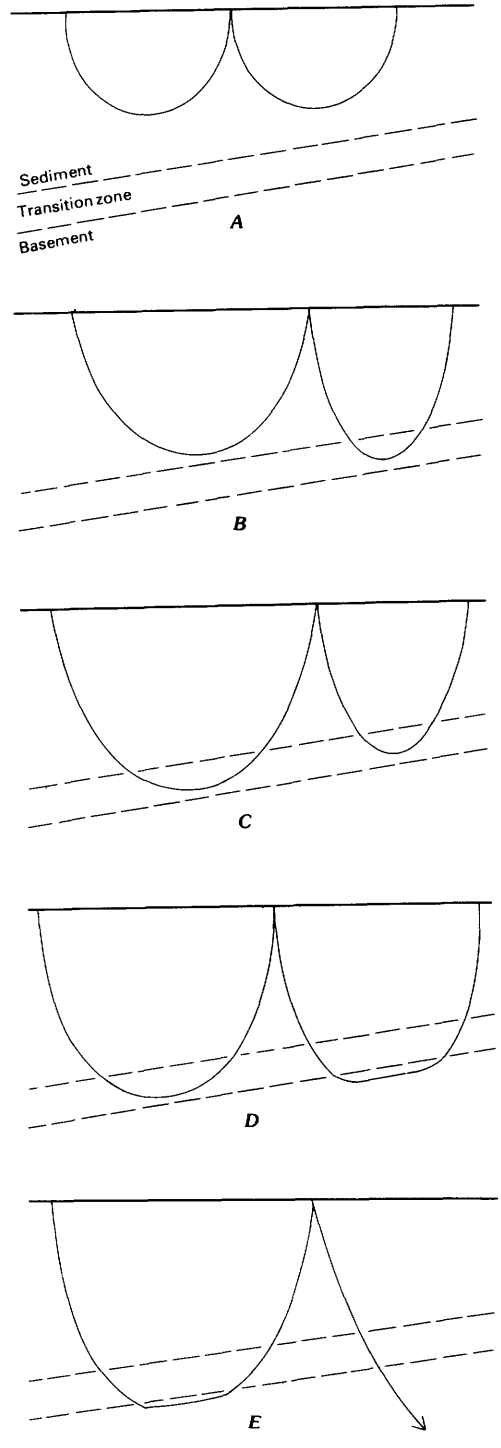

FIGURE 74.—Ray paths involved in propagation of *PP* phase in a laterally inhomogeneous medium. Each ray shown (dashed lines) is representative of a family of similar rays. Each family (*A–E*) contributes in turn to branch *PP* at successively greater distances. In velocity model (fig. 73), an abrupt decrease in amplitude is associated with progression from *C* to *D* (see figs. 71, 72). A similar progression is involved in propagation of branch *PPP*.

is composed of constant-velocity layers separated by sharp boundaries.

Although we cannot be precise regarding the resolution achieved by this method, we note that changes in the thickness of the transition zone of 0.1 km induce significant amplitude changes. Traveltimes are generally fitted to within approximately ± 0.05 s. Also, because we simultaneously modeled *PP* and *PPP* phases on both profiles, we had approximately 6 times the number of constraints available from a single unreversed profile. The least constrained aspect of our model is the structure beneath the basement-to-subbasement transition; because only the uppermost part of this region was sampled during this experiement, we do not know to what depth it extends.

This study demonstrates the feasibility of modeling refraction and wide-angle reflection data within two-dimensional velocity structures. The technique is general in the sense that synthetic seismograms can be computed for any structure through which rays can be traced.

REFERENCES

Biehler, Sean, Kovach, R. L., and Allen, C. R., 1964, Geophysical framework of northern end of Gulf of California structural province, *in* Van Andel, T. H., and Shor, G. G., Jr., eds., Marine geology of the Gulf of California: American Association of Petroleum Geologists Memoir 3, p. 126–143.

Červeny, Vlastislav, Molotkov, I. A., and Pšenčik, Ivan, 1977, Ray method in seismology: Prague, Univerzita Karlova, 214 p.

Giese, Peter, 1976, Depth calculation, *in* Giese, Peter, Prodehl, Claus, and Stein, Albert, eds., Explosion seismology in Central Europe: Data and results: New York, Springer-Verlag, p. 146–161.

Hamilton, R. M., 1970, Time-term analysis of explosion data from the vicinity of the Borrego Mountain, California, earthquake of 9 April 1968: Seismological Society of America Bulletin, v. 60, no. 2, p. 367–381.

Kovach, R. L., Allen, C. K., and Press, Frank, 1962, Geophysical investigations in the Colorado delta region: Journal of Geophysical Research, v. 67, no. 7, p. 2845–2871.

McMechan, G. A., and Mooney, W. D., 1980, Asymptotic ray theory and synthetic seismograms for laterally varying structure: Theory and application to the Imperial Valley, California: Seismological Society of America Bulletin, v. 70, no. 6, p. 2021–2035.

Wesson, R. L., 1970, A time integration method for computation of the intensities of seismic rays: Seismological Society of America Bulletin, v. 60, no. 2, p. 307–316.

PRELIMINARY STUDY OF SELECTED AFTERSHOCKS FROM DIGITAL ACCELERATION AND VELOCITY RECORDINGS

By D. M. BOORE and J. B. FLETCHER,
U.S. GEOLOGICAL SURVEY

CONTENTS

ABSTRACT

Beginning 28 hours after the main shock, we deployed 10 three-component digital triggered seismographs in an array about 18 km across, centered on the north terminus of the Imperial fault. About 30 aftershocks were recorded at three or more stations. Focal depths ranged from 3.5 to 9.0 km, and most events were near the bottom of the unmetamorphosed sedimentary deposits at 5.0-km depth. Most events clustered near the north terminus of surface traces of the Imperial fault, although no distinct lineaments of aftershocks were detected. Some events were several kilometers to the west of the mapped traces, and others between the Imperial fault and the Brawley fault zone. Focal mechanisms indicate primarily vertical strike-slip on northwest-southeast-striking planes, even though the earthquake occurred in a region where the mapped traces turn to the north and show significant dip-slip motion. Consistency of the mechanism for the shallowest event (normal on a north-south-striking plane) with surface faulting, however, suggests that the mode of faulting is depth dependent.

After about 10 days, we deployed five instruments at sites near the strong-motion instruments closest to the Imperial fault that had recorded the main shock. One aftershock recorded at all these sites showed that traveltimes, waveforms, and spectral amplitudes differ significantly at sites on either side of the Imperial fault. Relative to site 7 on the west side of the fault, the S-wave spectral amplitudes near site 6 in the region between the Imperial fault and the Brawley fault zone are increased in the range 2–5 Hz by as much as a factor of 10. The mainshock accelerograms at station 6 contain 3- to 5-Hz oscillations not present on the record from station 7. These observations suggest that digital velocity recordings of aftershocks can provide important information on the characteristics of strong-motion accelerograph sites.

DATA COLLECTION AND PROCESSING

We deployed an array of 10 Sprengnether DR100 digital-cassette seismographs at the north end of the surface trace of the Imperial fault (fig. 75), using five velocity transducers (natural frequency, 2 Hz; damping, 0.7 critical) and five force-balance accelerometers (natural frequency, 80 Hz). The intent of our experiment was twofold: To set a trap in hope of catching a large aftershock, and, failing that, to obtain data that would

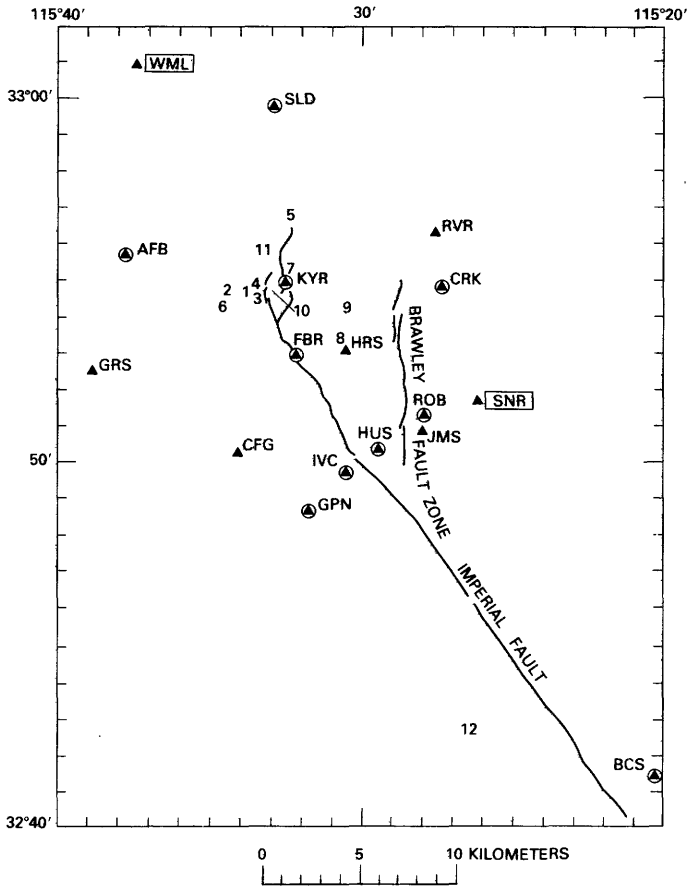

FIGURE 75.—Seismograph stations (triangles), epicenters (numbers), and surface faults (lines; from Sharp, 1977). Circled triangles denote positions after redeployment of stations CFG, GRS, HRS, JMS, and RVR. Boxed stations (SNR, WML) employed telemetered high-gain vertical-component seismographs operated by U.S. Geological Survey out of Pasadena, Calif.

aid in understanding the physical processes near the termination of the fault rupture. Unfortunately, no large aftershocks occurred after our instruments were installed. When the importance of the main-shock strong-motion data became clearer, we decided to redeploy five of the seismographs at stations near the strong-motion sites (fig. 75; tables 13, 14) in the hope that records of aftershocks would provide Green's functions useful in simulating the main-shock records and give insight into any effects from local geologic features. To avoid noise in our sensitive instruments, we did not locate our stations at the strong-motion sites (the sites differ in location by as much as 0.4 km). Although aftershock activity had decreased considerably by the time of redeployment, one event (12, fig. 75) was recorded at all the stations; we discuss this event below.

We transferred the digital field data from cassette to a diskpack connected to a Digital Equipment Corp. computer. The data from a given station were displayed on a video terminal, and the *P* and *S* waves were timed directly on the screen, using the movable crosshairs. These times were stored in files that were then used to locate the events. Figure 76 shows a typical suite of station records for one event (10, fig. 75).

TABLE 13.—*Data on stations in seismograph array*

Station	Location		Dates of operation (1979)
	Latitude N.	Longitude W.	
Velocity transducers			
AFB	32°55.70′	115°37.69′	Oct. 17–Nov. 14, Nov. 16–17
BCS	32°41.50′	115°20.31′	Oct. 26–Nov. 12
CRK	32°54.83′	115°27.36′	Oct. 17–Nov. 14, Nov. 16–17
FBR	32°52.92′	115°32.17′	Do
GPN	32°48.62′	115°31.75′	Oct. 25–Nov. 11, Nov. 16–17
GRS	32°52.46′	115°38.80′	Oct. 17–24
HUS	32°50.35′	115°29.37′	Oct. 24–Nov. 6; Nov. 9–12, 16–17
IVC	32°49.70′	115°30.51′	Oct. 24–Nov. 17
ROB	32°51.31′	115°27.92′	Oct. 25–Nov. 9; Nov. 12–14, 16–17
SLD	32°59.75′	115°32.85′	Oct. 18–Nov. 14, Nov. 16–17
Force-balance accelerometers			
CFG	32°50.24′	115°34.04′	Oct. 17–23
HRS	32°53.06′	115°30.49′	Oct. 18–25
JMS	32°50.88′	115°27.94′	Oct. 17–25
KYR	32°54.90′	115°32.49′	Oct. 17–Nov. 14, Nov. 16–17
RVR	32°56.30′	115°27.60′	Oct. 17–23

TABLE 14.—*Correspondence of seismograph stations to strong-motion sites*

Strong-motion site	Seismograph station	Remarks
5	ROB	ROB and 5 are almost colocated.
6	HUS	HUS is 0.3 km W. of 6.
7	IVC	IVC is 0.4 km SW. of 7.
8	GPN	GPN is 0.3 km E. of 8.
Bonds Corner	BCS	BCS and Bonds Corner are almost colocated.

EARTHQUAKE LOCATIONS

We have selected 12 well-recorded events for analysis here. These events were located using the HYPOINVERSE program, written by Klein (1978) and modified by J. M. Vinton to allow independent specification of the *P*- and *S*-wave velocity models. The *P*-wave velocity model used was based on interpretation of seismic-refraction data in the Imperial Valley (W. D. Mooney and G. A. McMechan, written comun., 1979). The *S*-wave velocity model was constructed by assuming a Poisson ratio of 0.25 in the lower part and constraining the velocities in the upper 0.1 km to those determined from a detailed study of velocities near a strong-motion site in El Centro, Calif. (Shannon & Wilson, Inc., and Agbabian Associates, 1976). A power law fitted to the surface velocities was extrapolated downward until the *S*-wave velocity reached one-half the *P*-wave velocity (see table 15 for velocity models, and fig. 75 and table 16 for aftershock locations). A few *P*-wave records from telemetered stations operated by the U.S. Geological Survey (USGS) were used for several events; excluding these records makes little difference in our results.

Because our seismograph array was small and was situated in the middle of a sedimentary basin showing

TABLE 15.—*S-wave velocity model*

Depth to top of layer (km)	Thickness of layer (km)	*P*-wave velocity (km/s)	*S*-wave velocity (km/s)
0.0	0.11	1.70	0.28
.11	.09	1.70	.53
.20	.10	1.80	.69
.30	.10	1.80	.85
.40	1.00	2.40	1.20
1.40	.90	3.00	1.50
2.30	.70	3.60	1.80
3.00	2.25	4.50	2.43
5.25	6.00	5.80	3.35
11.25	----	7.40	4.30

TABLE 16.—*Aftershock locations*

Event	Date (Oct.)	Origin time (h:m:s G.m.t.)	Location		Depth (km)
			Latitude (N.)	Longitude (W.)	
1	19	10:35:08.26	32°54.56′	115°33.46′	5.1
2	19	16:56:11.57	32°54.70′	115°34.37′	5.0
3	19	18:50:38.31	32°54.38′	115°33.52′	4.4
4	19	18:51:28.46	32°54.80′	115°33.34′	4.6
5	20	00:14:26.95	32°56.68′	115°32.36′	3.5
6	20	03:14:52.67	32°54.21′	115°34.56′	4.2
7	20	05:04:07.40	32°54.96′	115°32.43′	8.0
8	20	14:52:54.71	32°53.24′	115°30.67′	6.8
9	22	22:04:39.63	32°54.22′	115°30.41′	5.0
10	23	01:13:12.99	32°54.66′	115°32.75′	5.0
11	29	02:39:19.93	32°55.82′	115°33.24′	4.6
12	31	11:43:46.08	32°42.61′	115°26.39′	6.9

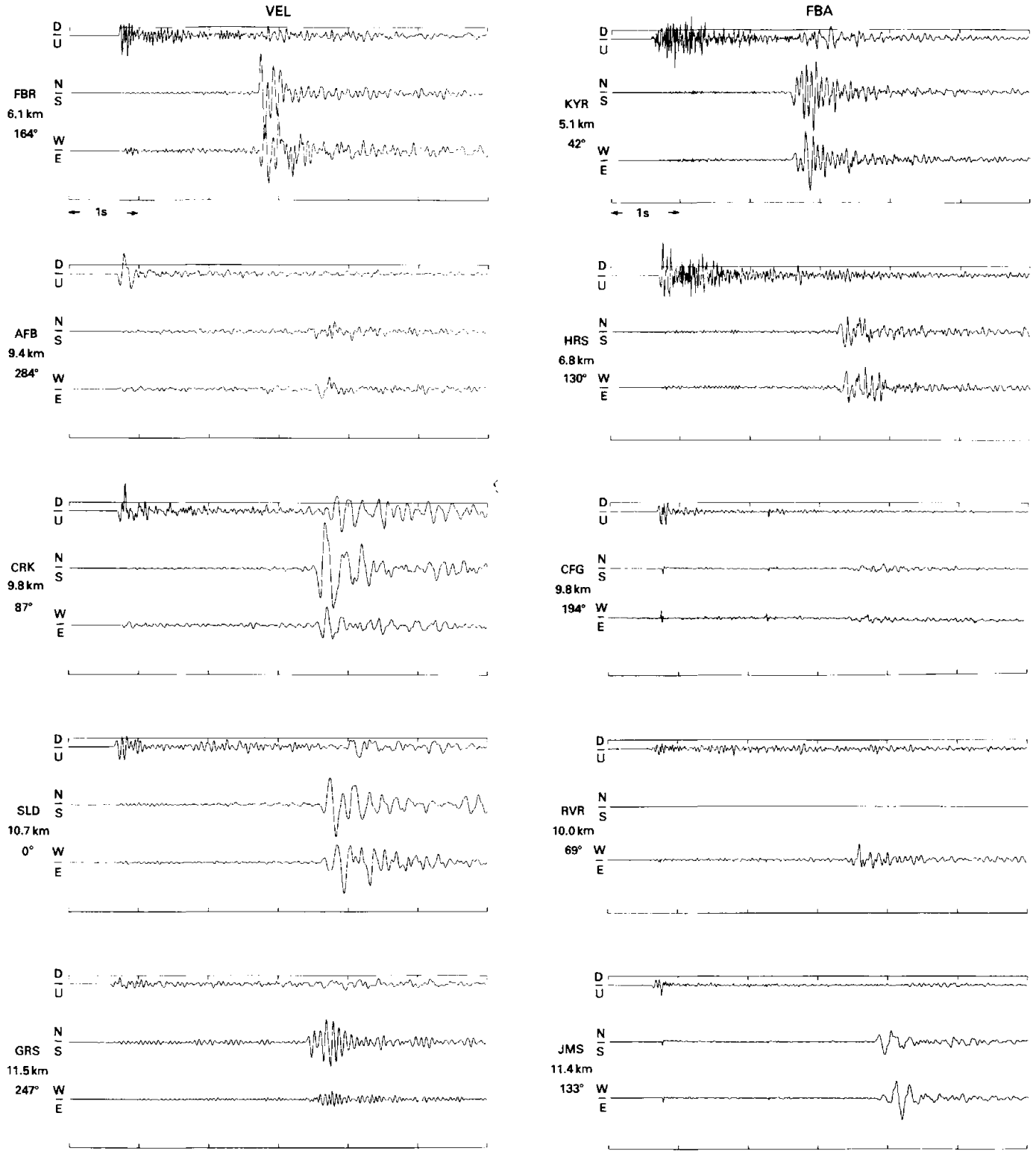

FIGURE 76.—Typical records (event 10, fig. 75) obtained from velocity (VEL) and force-balance-accelerometer (FBA) transducers, arranged by hypocentral distance and alined by *P*-wave arrival. Event-to-station azimuth, clockwise from north, is given on left of each record. D/U, down, up; N/S, north, south; W/E, west, east. Horizontal scale is in seconds; amplitude scale is arbitrary. Erratic spikes on some FBA traces (for example, CFG, JMS) are caused by weak d-c regulator in power supply. See figure 75 for locations of stations.

no significant lateral changes in geologic structure, no station corrections were used in the event locations, although we obtained systematic residuals as an output of the location program. Table 17 lists the mean and standard deviation of these residuals. Locations of aftershocks, after including these residuals, differ at most by 1.3 km in depth. Of course, there is some circularity in these determinations because the residuals were determined on the assumption that the original locations were correct. As a preliminary check on the residuals, we located the aftershocks without using the data from station FBR. Closeness of the mean residuals at station FBR (−0.17 and −0.36 for P and S waves, respectively) to those calculated previously (table 17) indicates that these residuals may, in fact, reflect differences in velocity structure near the fault.

Except for event 12 to the south, the pattern of aftershock locations is somewhat diffuse near the north end of mapped surface traces of the Imperial fault. We do not claim that event 12 should be located off the mapped trace of the fault, even though adding an S-wave arrival time from a temporary strong-motion station near the fault, north of the epicenter of event 12, does not change this location significantly. In addition to data from the temporary stations, we used the P-wave arrivals from USGS telemetered stations BON (16 km east of event 12) and SNR in locating event 12.

RECORD CHARACTERISTICS

Many of the records from certain stations had a characteristic signature (fig. 77). At station KYR the P waves commonly had a long-period beginning, and the S waves consisted of several distinct pulses. At station FBR many of the S waves on the north-south component preceded the arrival of the east-west component by several tenths of a second. At station GRS, many of the S waves were oscillatory, and the north-south component had larger amplitudes and longer periods than the east-west components (see also fig. 76). Interpretation of these features in terms of seismic source and structure is beyond the scope of this report.

TABLE 17.—*Preliminary station corrections*

[*N*, Number of residuals used in calculation of mean and standard deviation]

Station	Mean P-wave residual (s)	N	Mean S-wave residual (s)	N
AFB	0.17±0.03	10	0.00±0.06	9
CFG	.07±0.03	4	−.11±0.04	4
CRK	−.01±0.03	10	−.09	2
FBR	−.11±0.03	11	−.26±0.04	11
GRS	.17±0.03	9	−.12±0.03	5
HRS	.01±0.03	8	.17±0.02	7
JMS	.06±0.04	3	.19±0.13	3
KYR	−.08±0.01	9	.07±0.03	10
RVR	−.07±0.02	5	−.02±0.05	3
SLD	−.07±0.02	6	−.08±0.01	5

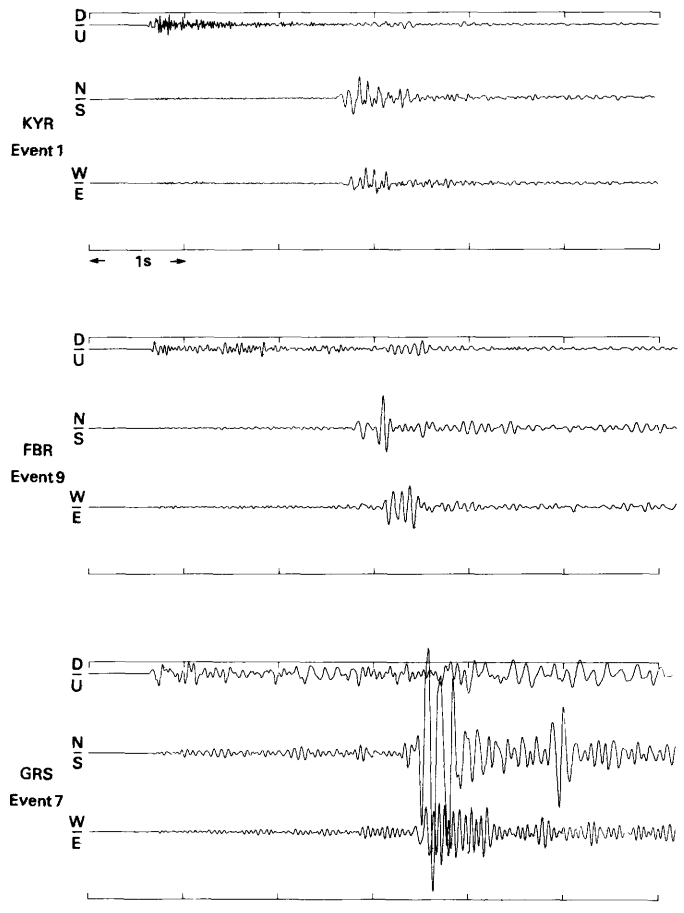

FIGURE 77.—Selected records, showing characteristic waveforms at stations KYR, FBR, and GRS for three separate events. See figure 76 for explanation of components and scales.

FOCAL MECHANISMS

We plotted P-wave first motions from our data and from the USGS telemetered stations on lower-hemisphere equal-area projections, and fitted possible fault planes to the data manually (fig. 78). Most events are well described by vertical right-lateral strike-slip faults trending about northwest-southeast, except for event 5, the shallowest event at the north end, which indicates a north-south-striking normal fault. The focal mechanism for event 12 requires a nonvertical fault plane if the northwest-southeast-striking plane corresponds to the fault, even if the epicenter of the earthquake is located on the fault trace (Ralph Archuleta, oral commun., 1980).

Northwest-southeast-trending strike-slip faulting seems at odds with the dominantly north-south trending dip-slip faults observed at the surface near the aftershock epicenters. Because the shallowest event in our data set (event 5) agreed in orientation with the surface faulting, the type and strike of the fault may be depth dependent. The deviation from north-south-trending

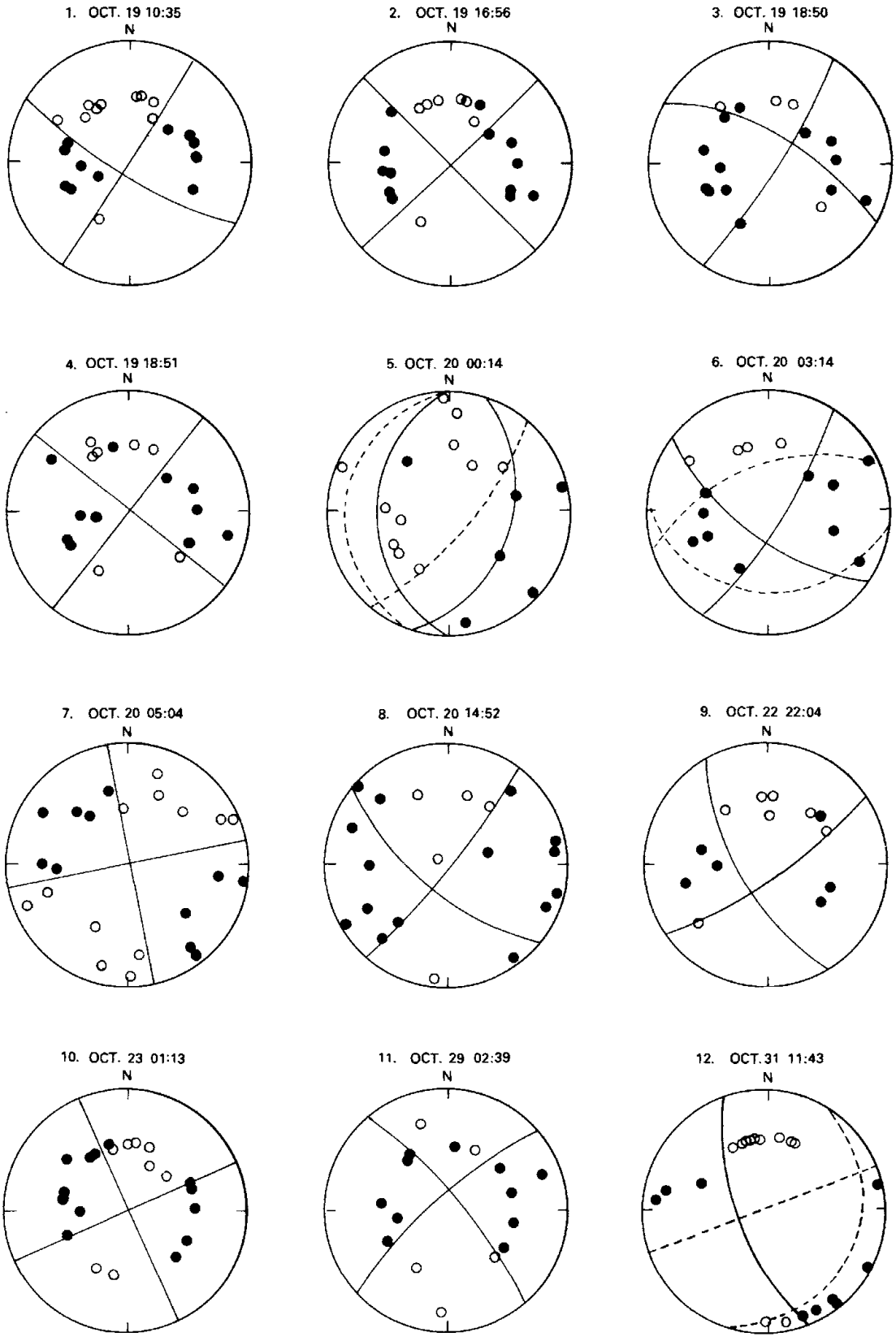

FIGURE 78.—Lower-hemisphere equal-area projections of *P*-wave first motions (circle, dilatation; dot, compression) for events 1–12, showing date and time of event. Dashed lines show other possible fault planes. See figure 75 for locations of epicenters.

normal faults at depth can occur without any change in the tension axes but involves a shift in the compression axes from near-vertical at the surface to horizontal at depth (fig. 79). Fuis and Lamanuzzi (1978) determined that the orientations of the tension axes for earthquakes in the eastern Transverse Ranges of southern California are similar to those that we measured.

BODY-WAVE SPECTRA AND SOURCE PARAMETERS

Our data provide an unusual opportunity to study the source characteristics from close-in recordings over a reasonably complete range of azimuths. We calculated body-wave spectra for event 7, which was particularly well recorded, from both the vertical and horizontal components with the largest pulse for P and S waves, respectively. We used a window with a cosine taper in the first and last 10 percent of the record, and obtained displacement spectra after correcting for instrument response and the effect of the 50-Hz antialiasing filter.

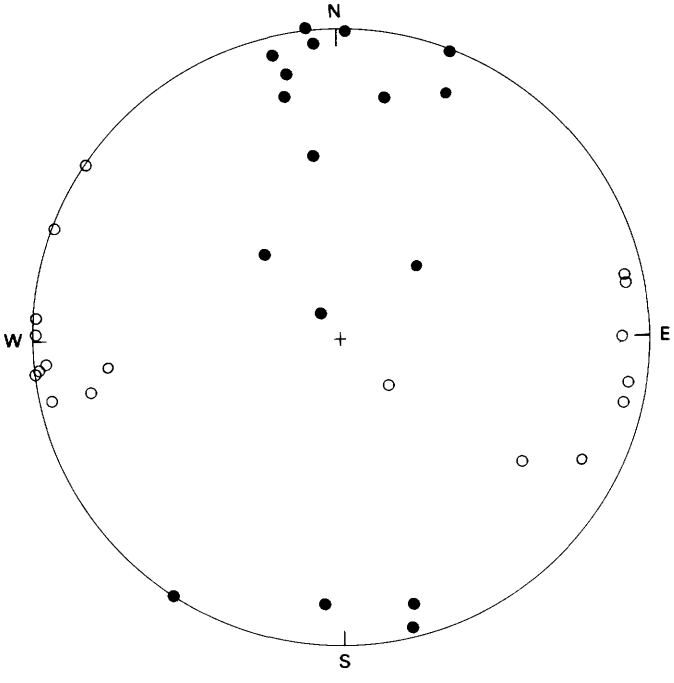

FIGURE 79.—Lower-hemisphere equal-area projection of compression (dots) and tension (circles) axes for focal mechanisms shown in figure 78.

The variation in displacement from station to station and the unusual shape of the spectra suggest that either the body waves were strongly altered along the ray path or the source was extremely complex. An exponential decay with increasing frequency in many of the spectra, in contrast to spectra of aftershocks of the Oroville, Calif., earthquake (Fletcher, 1980), suggests that anelastic attenuation is important over even these short distances. On several records the spectral decay is composed of a series of steps.

In spite of these complexities, we estimated source parameters from the spectra, using the model of Brune (1970) extended to P waves by Hanks and Wyss (1972). Each determination of moment has been corrected for the radiation pattern of a simple double couple. Table 18 lists the radiation pattern, moments, stress drop, and source radius for event 7. The spectra for the P waves give a moment of $260 \pm 40 \times 10^{12}$ N·m. The wide variation in movement for the S waves (110×10^{12} to $2{,}000 \times 10^{12}$ N·m) suggests that S waves are more strongly affected by geologic complexities than are P waves. The stress drop from the P-wave data is 2.9 ± 0.9 MPa. The range in stress drops for the S waves over almost three orders of magnitude again reflects variations in the amplitudes and corner frequencies of the S-wave spectra. The data listed in table 18, as well as a qualitative analysis of the seismograms, indicate that more detailed knowledge of the velocity and attenuation structure will be required to use these local data in source-parameter studies.

ANALYSIS OF EVENT 12

Event 12, which was registered over the reconfigured array (circled triangles, fig. 75), is significant because it

TABLE 18.—*Source parameters for event 7*

[Stations HRS, KYR, and RVR had force-balance accelerometers; other stations had velocity traneducers. Radiation-pattern correction was constrained to have a minimum value of 0.2 and includes a free-surface term; observed spectral amplitudes were corrected for radiation pattern by dividing by the values listed. R, source radius]

Station	P wave				S wave			
	Radiation-pattern correction	M_o (10^{12} N·m)	$\Delta\sigma$ (MPa)	R (m)	Radiation-pattern correction	M_o (10^{12} N·m)	$\Delta\sigma$ (MPa)	R (m)
AFB	0.83	410	5.5	320	0.86	260	3.4	320
CRK	.48	420	2.0	450	.48	400	28	180
FBR	.2	140	1.2	370	.2	210	.3	640
GRS	.70	170	.4	560	1.46	180	13	184
HRS	.76	270	5.4	280	1.0	910	12	320
KYR	--	--	--	--	.2	450	92	129
RVR	.35	140	5.5	220	1.5	110	11	181
SLD	.27	260	.3	750	.2	2,000	11	430

was recorded over a larger range of distances than the other aftershocks and thus contains unique information about the S-wave velocity structure (fig. 80). Perhaps even more important is that event 12 was recorded near accelerograph sites that recorded strong motions from the main shock, and thus this event can be used to calibrate those sites for the effects of lateral heterogeneities in geologic structure.

The Wadati diagram for event 12 (fig. 81) can be used to infer the ratio of P- to S-wave velocities, independently of the source location and averaged over various distance ranges. Ignoring the data from the distant stations AFB and SLD, the P- to S-wave velocity ratio is about 2.1, a reasonable value for waves traveling through the 5 km of sedimentary fill in the Salton Trough. Accepting this result, the average P- to S-wave velocity ratio at greater distances must decrease to a low of 1.6. If, on the other hand, the S waves at stations HUS and ROB were delayed by about 0.5 s, an average P- to S-wave velocity ratio of 1.7 would fit all the data.

An anomalous behavior of the S waves at station HUS compared with those at IVC is discernible on the records for event 12 from these two stations (fig. 82). The increased S–P interval at station HUS is evident, but even more remarkable are the differences in the

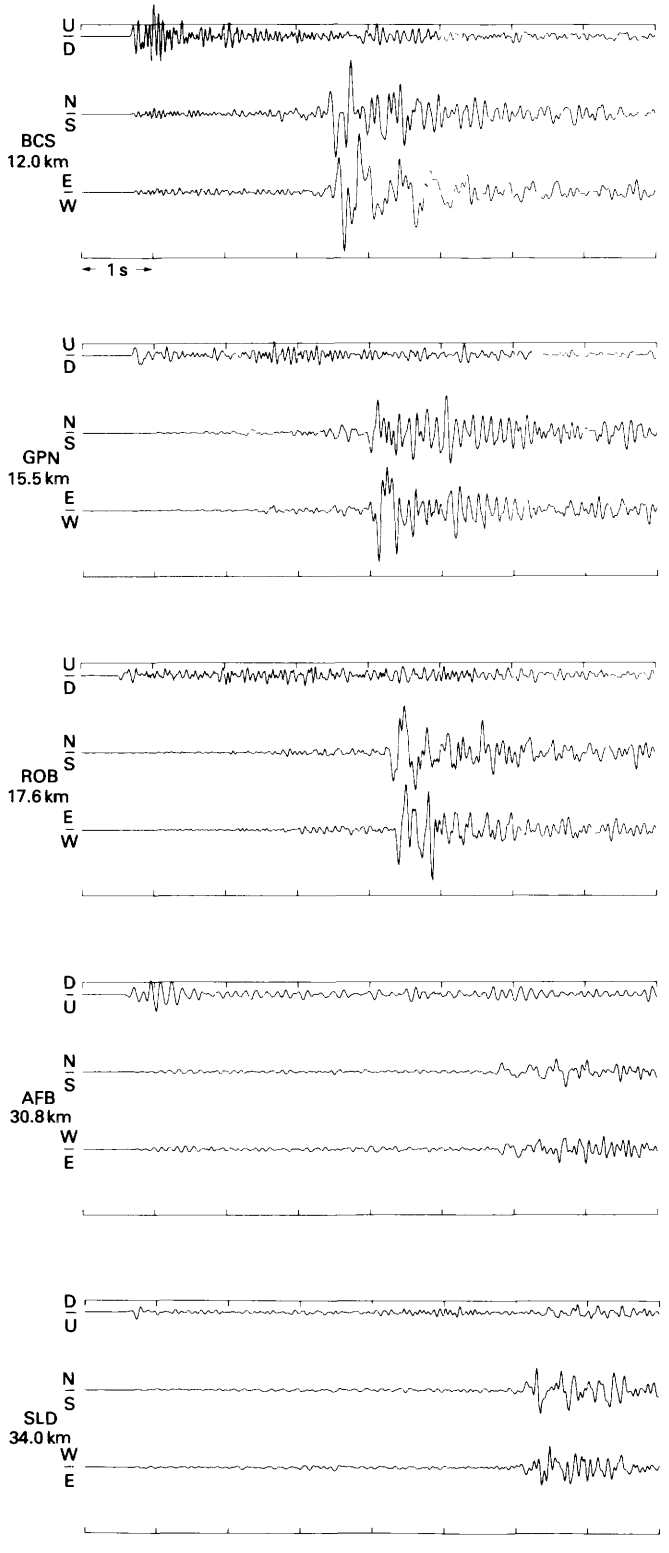

FIGURE 80.—Selected records for event 12, arranged by hypocentral distance and alined on P-wave arrival. See figure 76 for explanation of scales and component directions.

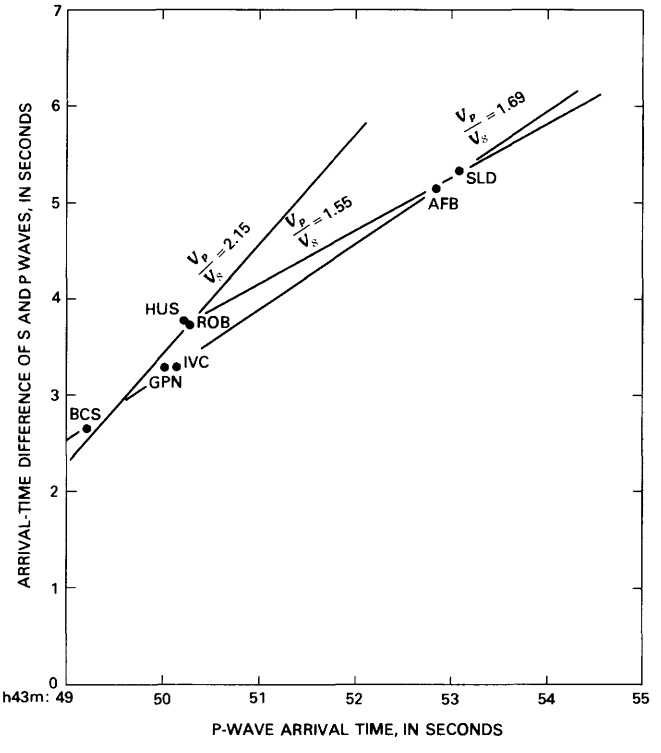

FIGURE 81.—Wadati diagram for event 12. Lines are manual fits to different subsets of data. Ratio for P-wave velocity (V_P) and S-wave velocity (V_S) is shown for each line. Dots indicate seismic stations. h, hours; m, minutes.

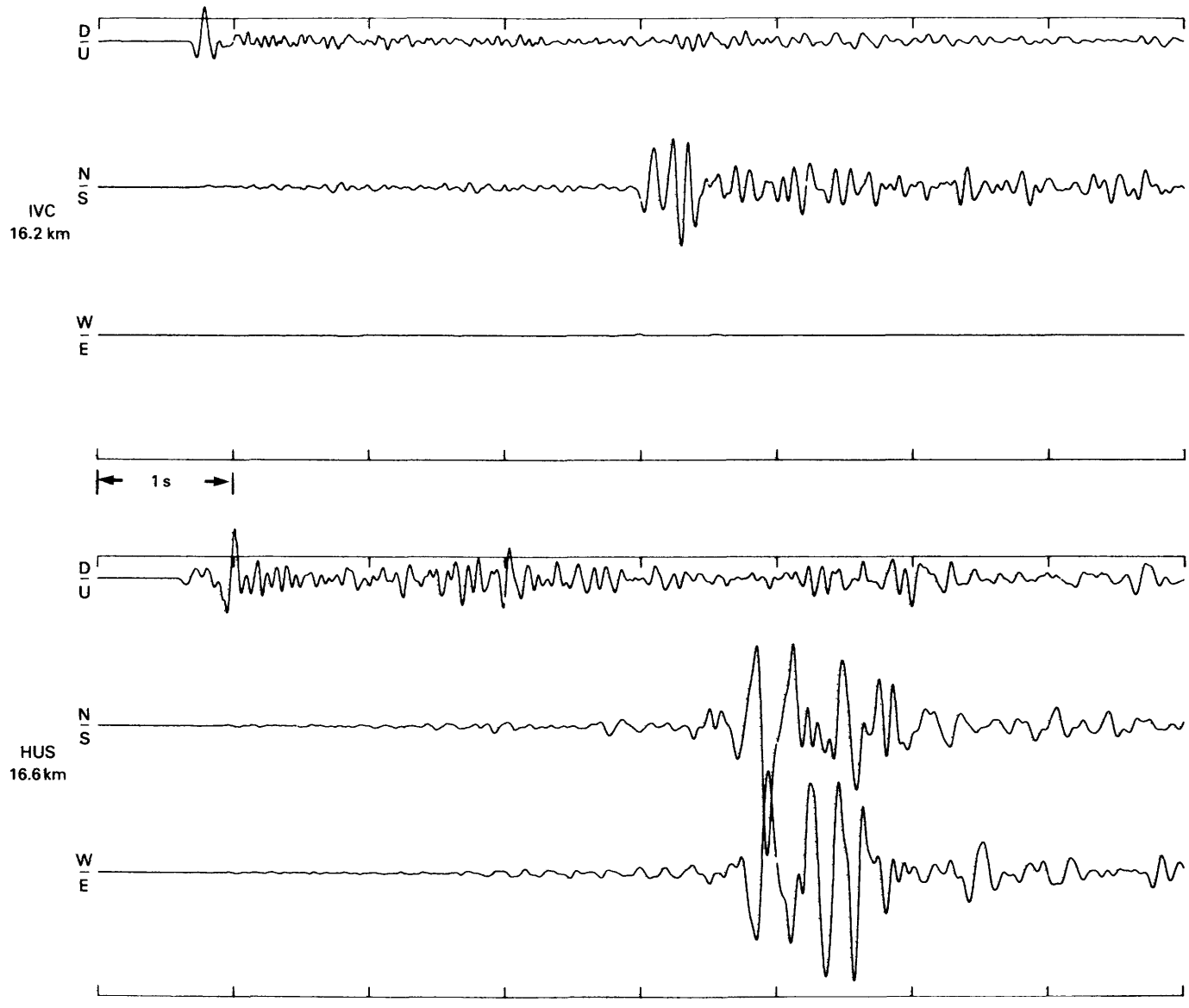

FIGURE 82.—Records from stations IVC and HUS for event 12, plotted with same vertical (arbitrary) and horizontal (seconds) scales, and alined on *P*-wave arrival. East-west component at station IVC malfunctioned. Distance given at left is hypocentral distance. D/U, down, up; N/S, north, south; W/E, west, east.

waveforms, even though these two stations were relatively close (about 2 km in absolute distance, and only 0.4 km in distance to the hypocenter). Nearness of the data points for two stations west of the Imperial fault (GPN, IVC), as well as for two stations east of the fault (ROB, HUS), on the Wadati diagram (fig. 81) suggests that the late arrivals at stations ROB and HUS, and the large amplitudes, long periods, and complicated arrivals at station HUS, may be due to propagation of waves from the west side of the fault into a lower velocity region east of the fault. This lower velocity region may correspond to a deformed and sheared zone between the Imperial fault and the Brawley fault zone (fig. 75), as well as to a region in which low-velocity sedimentary deposits were laid down in a expanding hole formed by the relative fault motions (C. E. Johnson, written commun., 1980). An anomalous pattern of wave propagation has also been observed along the San Andreas fault in central California (Boore and Hill, 1973). The Imperial Valley region differs in that its surface geology does not exhibit the striking lateral heterogeneities seen in central California. Our original expectation from geologic considerations and from small differences in the *P* waves evident from seismic-refraction surveys (W. D. Mooney, oral commun., 1979) was that the horizontal velocity structure would be reasonably uniform.

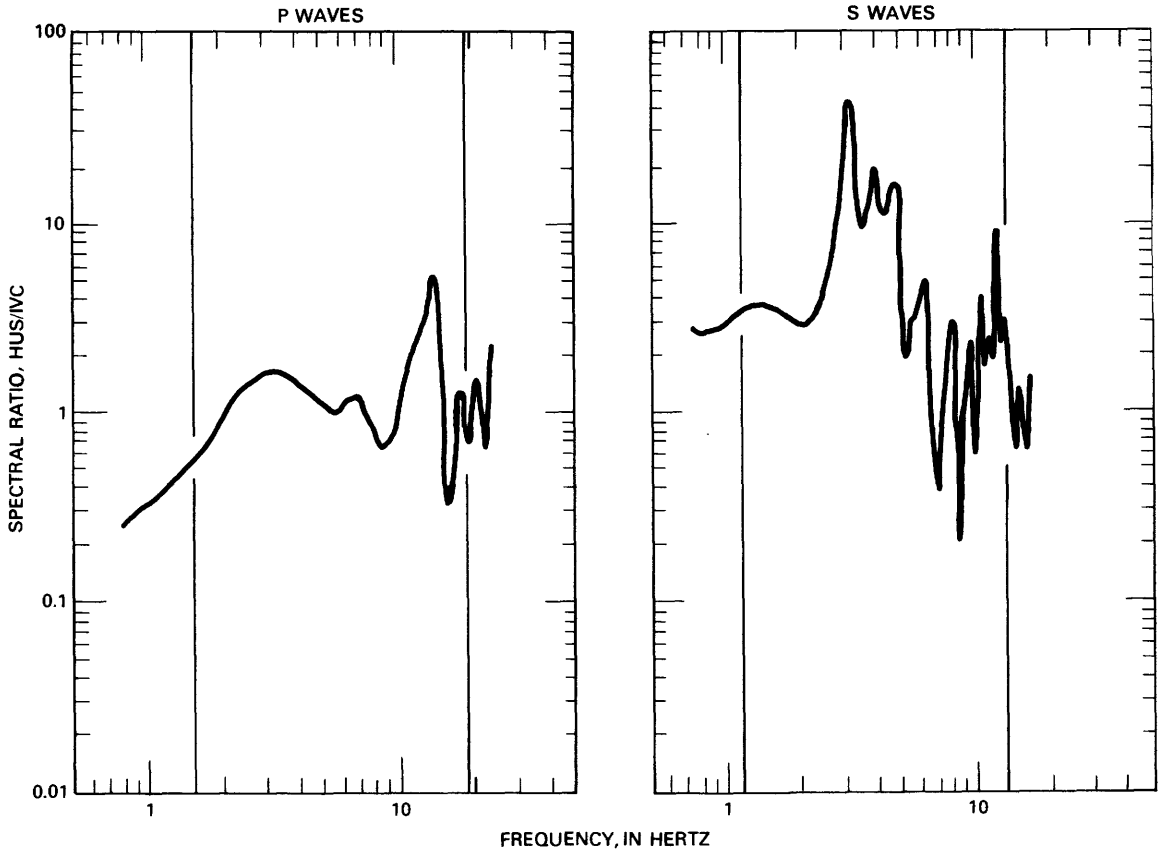

FIGURE 83.—Spectral ratios (station HUS value divided by station IVC value) for *P* and *S* waves of event 12. Narrow frequency bands of amplification near 12 and 4 Hz for *P* and *S* waves, respectively, are stable for changes in window length; increasing this length adds more oscillations to spectra. Vertical lines show frequencies inside of which spectral values from both stations IVC and HUS are within a factor of 10 of peak of each spectrum.

Clear evidence in the data set for lateral heterogeneity, however, is independent of the precise location of event 12—and, indeed, its location off the fault trace may be erroneous because our location program assumes lateral uniformity.

The spectral ratios at stations HUS and IVC (fig. 83) show that both the *P* and *S* waves are clearly amplified over a narrow frequency band at station HUS compared with IVC, and that the *S*-wave band occurs at lower frequencies than the *P*-wave band (as would be expected if amplification were due to a local-site effect). This amplification of both *P* and *S* waves occurs in frequency bands of concern to earthquake engineers, and therefore these results are relevant to any interpretation of the main-shock strong-motion records. A qualitative analysis of the main-shock records shows that the accelerogram at site 6 is much more energetic in the frequency range 3–5 Hz than at site 7, in agreement with our findings. If more detailed analysis shows a similar amplification for both the main shock and the aftershocks, this result will strongly constrain the amount of nonlinear soil behavior expected during strong shaking.

Further investigation of possible local-site amplification at station HUS can be based on an analysis of the accelerogram records obtained during previous small earthquakes. For example, accelerograms for several earthquakes from a swarm in 1977 north of these stations show that the peak accelerations at site 6, near station HUS, are consistently larger than at site 7, near station IVC (table 19; adapted from Porcella, 1978, p. 20–22). This observation is consistent with our results and is particularly significant because the waves arrive from a different azimuth. More detailed studies of these accelerogram records are in progress.

TABLE 19.—*Peak accelerations for November 14, 1977, events at El Centro accelerometer array*

[Most events were located near lat 32.83° N., long 115.47° W. Peak accelerations listed are maximum values, irrespective of component. From Porcella (1978)]

Time (G.m.t.)	Peak acceleration	
	Site 6	Site 7
0011	0.50	0.11
0205	.41	.14
0518	.13	.06

CONCLUSIONS

1. The faulting in the region of the north terminus of surface slip on the Imperial fault is predominantly strike-slip on planes oriented about ±45° from north, in contrast to the surface faulting, which is oriented north-south and displays a significant component of dip-slip motion.
2. A significant lateral variation in velocity structure, possibly related to an extensively sheared area between the Imperial fault and the Brawley fault zone, exists between El Centro accelerometer array sites 6 and 7. The *S* waves at site 6 were delayed and amplified relative to those at site 7. Future work will be directed at analyzing the source of this signal delay and site amplification and at evaluating its influence on the strong ground motions recorded during the main shock.

ACKNOWLEDGMENTS

We thank Ralph Archuleta, Roger Borcherdt, Shirley Marks, and particularly Gene Sembera for assistance with the fieldwork, and Joanne Vinton for help in computer processing of the data. Carl Johnson, who was monitoring aftershock activity from the telemetered stations, advised us on placement of our seismograph array. John Anderson provided an *S*-wave arrival time at a temporary strong-motion station for event 12.

REFERENCES CITED

Boore, D. M., and Hill, D. P., 1973, Wave propagation characteristics in the vicinity of the San Andreas fault, *in* Kovach, R. L., and Nur, Amos, eds., Proceedings of conference on tectonic problems of San Andreas fault system: Stanford University Publications in the Geological Sciences, v. 13, p. 215–224.

Brune, J. N., 1970, Tectonic stress and the spectra of seismic shear waves from earthquakes: Journal of Geophysical Research, v. 75, no. 26, p. 4997–5009.

Fletcher, J. B., 1980, Spectra from high-dynamic range digital recordings of Oroville, California aftershocks and their source parameters: Seismological Society of America Bulletin, v. 70, no. 3, p. 735–755.

Fuis, G. S., and Lamanuzzi, V., 1978, Seismicity of the eastern Transverse Ranges, southern California [abs.]: Eos (American Geophysical Union Transactions), v. 59, no. 12, p. 1051.

Hanks, T. C., and Wyss, Max, 1972, The use of body-wave spectra in the determination of seismic-source parameters: Seismological Society of America Bulletin, v. 62, no. 2, p. 561–589.

Klein, F. W., 1978, Hypocenter location program HYPOINVERSE. Part 1: Users guide to versions 1, 2, 3, and 4: U.S. Geological Survey Open-File Report 78–694, 113 p.

Porcella, R. L., ed., 1978, Seismic engineering program report, September–December 1977: U.S. Geological Survey Circular 762–C, 27 p.

Shannon & Wilson, Inc., and Agbabian Associates, 1976, Geotechnical and strong-motion earthquake data from U.S. accelerograph stations: U.S. Nuclear Regulatory Commission Report NUREG–0029, v. 1.

Sharp, R. V., 1977, Holocene traces of the Imperial fault in south-central Imperial County, California: U.S. Geological Survey Open-File Report 77–815, 1 p., scale 1:24,000, 5 sheets.

SURFACE FAULTING IN THE CENTRAL IMPERIAL VALLEY

By ROBERT V. SHARP, JAMES J. LIENKAEMPER, M. G. BONILLA, D. B. BURKE, B. F. FOX, D. G. HERD, D. M. MILLER, D. M. MORTON, D. J. PONTI, M. J. RYMER, J. C. TINSLEY, and J. C. YOUNT,
U.S. GEOLOGICAL SURVEY;

JAMES E. KAHLE and EARL W. HART,
CALIFORNIA DIVISION OF MINES AND GEOLOGY;

and

KERRY E. SIEH
CALIFORNIA INSTITUTE OF TECHNOLOGY

CONTENTS

ABSTRACT

In the central Imperial Valley, the October 15, 1979, earthquake generated displacements at the ground surface along the Imperial fault, the Brawley fault zone, parts of the Mesquite basin between these faults, and a minor structure here named the "Rico fault." The 30.5-km length of surface rupture on the Imperial fault included approximately the north half of the 1940 trace of surface faulting, which extended into Mexico. A maximum right-lateral displacement on the Imperial fault of 55 to 60 cm was measured during the first day after the earthquake about 1.4 km from the south terminus of surface faulting and about 10.5 km northwest of the earthquake epicenter. Although the point of maximum right-lateral slip has remained in the southernmost fifth of the surface rupture throughout the afterslip period, the point of maximum cumulative right-lateral slip has shifted northward. At 160 days after the earthquake, the maximum measured cumulative horizontal slip was about 78 cm (more than 29 cm of afterslip) at a point about 5.6 km from the south end of rupture. Average horizontal displacement on the Imperial fault grew from about 29 cm on the 4th day after the earthquake to about 43 cm on the 160th day.

Different segments of the Imperial fault varied considerably in the amount of horizontal afterslip. Some segments revealed a simple inverse relation of horizontal afterslip to coseismic displacement, and others with low initial slip increased only slightly in offset. Although at most localities on the fault, cumulative horizontal slip appeared to increase linearly as a function of the logarithm of postearthquake time, a few localities displayed distinctly nonlinear growth of displacement.

The Brawley fault zone east of the northern section of the Imperial fault ruptured discontinuously along multiple strands over a length of 13.1 km. The faulting extended about 0.9 km northward and 1.8 km southward beyond the previously known limits of faulting identified from an earthquake swarm in 1975. Displacement was dominantly vertical, similar to but smaller than and opposite in sense to that on the northern section of the Imperial fault. The Mesquite basin block between the two faults dropped relatively as much as 41 cm across the Imperial fault and no more than 15 cm across the Brawley fault zone. Horizontal slip in the Brawley fault zone was detected locally on the westernmost breaks within the zone; the largest dextral component of slip was about 7 cm at Keystone and Harris Roads. Horizontal and vertical afterslip in the Brawley fault zone were insignificant in comparison with that on the Imperial fault.

The Rico fault, a newly recognized structure near Holtville, Calif., is similar in orientation and sense of vertical displacement to the Brawley fault zone. Vertical offset was no greater than 20 cm, and no horizontal slip was detected; the rupture length was about 1 km. As in the Brawley fault zone, afterslip was insignificant on the Rico fault.

INTRODUCTION

During or after the October 15, 1979, earthquake in the Imperial Valley, four previously recognized faults or fault zones moved at the ground surface. Of these, only the Imperial fault and the Brawley fault zone in the central Imperial Valley were within the region of seismic-energy release. The Superstition Hills and San

Andreas faults, west and northwest of the central Imperial Valley, respectively, also ruptured at the ground surface as far as 100 km from the epicentral area (fig. 84). The principal movement, in terms of its close spatial association with the main shock and the length and amount of surface displacement, was along the Imperial fault, a mostly northwest-southwest trending dextral fault first recognized from field investigations after the Imperial Valley earthquake of 1940 (Buwalda and Richter, 1941; Ulrich, 1941; Richter, 1958). A complex zone of surface breaks that splay northward from the midpoint of 1979 surface rupture on the Imperial fault is here termed the "Brawley fault zone" (previously called the Brawley fault); several segments in this zone were first discovered in 1940 but were not documented in detail until surface movements were observed and mapped after a swarm of small earthquakes in 1975 (Sharp, 1976, 1977b). A fifth surface rupture along the Rico fault, a newly discovered minor fault that is similar in orientation and type of displacement to strands of the Brawley fault zone, lies southeast of the Brawley fault zone near Holtville, Calif. (fig. 84). Additional minor faulting occurred in the southeastern part of the Mesquite basin, a depression (the site of Mesquite Lake, now drained) formed by past subsidence between the northern section of the Imperial fault and the Brawley fault zone.

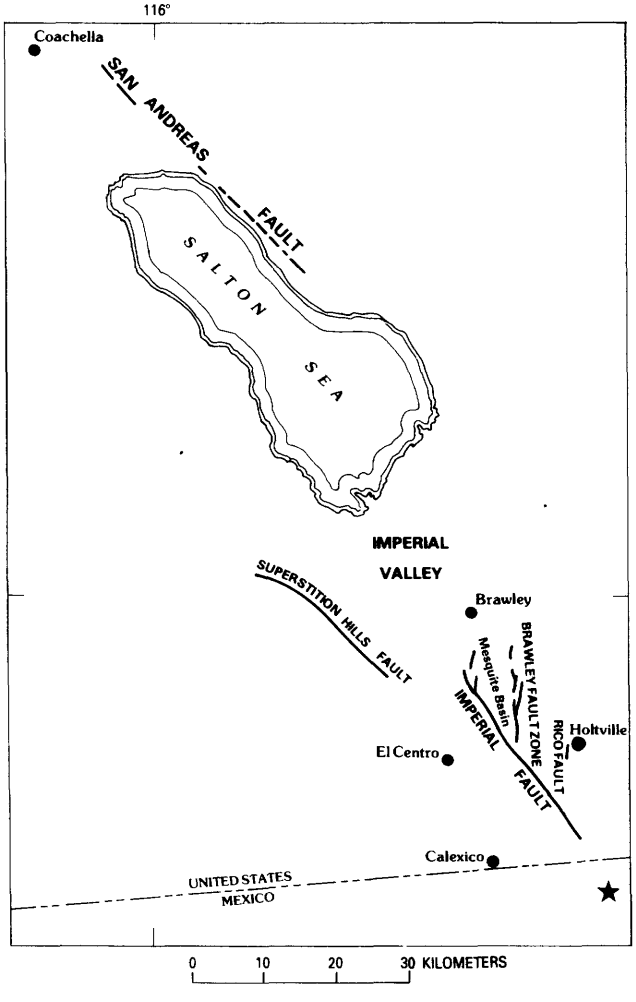

FIGURE 84.—Index map showing faults activated during 1979 Imperial Valley earthquake. Surface movements described here took place on faults south and east of Brawley, Calif. Star denotes epicenter.

The Superstition Hills fault and the activated segment of the San Andreas fault both were considerably distant from the epicentral area of the main shock and aftershock activity in the central Imperial Valley. The surface displacements on these two faults are described elsewhere in this volume by Fuis and Sieh.

Known historical movements on both the Imperial fault and the Brawley fault zone include aseismic-creep events, displacements associated with swarms of small earthquakes, slip triggered by the distant 1968 Borrego Mountain, Calif., earthquake, and the movements generated by the large earthquakes of 1940 and 1979. Together, historical movements have totaled six or seven slip events on the Imperial fault and at least four movements on the Brawley fault zone. Pre-1979 movements are discussed by Cohn and others (this volume) and Sharp (this volume).

REPRESENTATION OF SURFACE FAULTING

The accompanying map (pl. 1) illustrates all surface faulting discovered in our investigation after the 1979 earthquake, and tables 20 through 22 below summarize the measurements of slip components in different places, located on the map by: (1) numbered locality, (2) named roads and highways, and (3) distance along the kilometer reference lines for the Imperial fault (0–31 km) and the Brawley fault zone (0–15 km). The fault traces indicated on the map (pl. 1) are stylized representations of surface fractures that are too small to be shown individually at 1:24,000 scale; most rupture traces shown indicate average lines of surface faulting with small-scale complexities omitted.

IMPERIAL FAULT

A 30.5-km segment of the Imperial fault broke at the ground surface during the 1979 earthquake. This activated segment corresponds approximately to the north half of the known length of the fault, here taken to be the extent of 1940 surface rupturing observed by J. P. Buwalda (unpub. data, 1940), along with the 3 km of the fault trace north of the northernmost recorded 1940 breaks that are marked by well-defined Holocene scarps (Sharp, 1977a). Displacement in the south half of the 1979 rupture consisted dominantly of right-lateral slip,

and minor vertical components indicate that the movement was generally upward on the southwest side. Displacement in the north half of the 1979 rupture differed from that farther south in that the right-lateral component generally diminished northward and the vertical component of surface slip was commonly, though not everywhere, dominant. In the north half, the prominent east-facing scarp of the Imperial fault formed by earlier Holocene vertical offset defines the west margin of the Mesquite basin. The sense of relative vertical displacement for 1979 movement on the northern section of the Imperial fault was consistently the same as that along the preexisting scarp.

Subsidiary faulting, both as branches and as detached subparallel secondary breaks, occurred in several places on the Imperial fault. Although most branch faulting was concentrated in the north third of new surface breakage, important examples were observed in the south half, especially near and south of a discontinuity in the straightest strands of the fault near Interstate Highway 8 (loc. 15).

FIGURE 85.—Imperial fault trace 1.0 km south of County Highway S–80 (at 11.3 km). Echelon fissures (vertically oriented in this view) trend N. 20°–50° W.; fault trace trends between N. 30° and 40° W. Compressional features (dark horizontal bands) join ends of separate echelon fractures. Distance between manmade berms (wide dark diagonal bands) is about 9.1 m. Maximum width of obviously deformed zone is about 0.6 m. View southeastward. Photograph by M. J. Rymer, October 23, 1979.

DESCRIPTION OF SURFACE RUPTURE

The ground fracturing along much of the Imperial fault (figs. 85, 86) was identical to (or a mirror image of) strike-slip fault ruptures observed from past surface movements in other areas around the world. For that section of the Imperial fault where vertical components of slip were minor, the rupture trace (or "mole track") exhibited the characteristic succession of overlapping echelon fractures. Individual fractures were oriented more northerly than the average northwestward trend of the fault trace, and so the stepover direction from one fracture to the next was to the left—a common rupture pattern for right-lateral strike-slip.

The northern 40 percent of the Imperial fault rupture followed the trace of a late Holocene escarpment west of the Mesquite basin. In this segment of the fault, the vertical components of 1979 movement were relatively large and in most places were the dominant components

FIGURE 86.—Rupture (or "mole track") on Imperial fault in field south of Heber Road (at 2.4 km). Piled-up soil fragments are compressional mounds that formed between ends of echelon fractures in ground. View northwest. Photograph by J. C. Tinsley, who measured 45±3 cm of dextral displacement on offset crop rows in this field on October 17, 1979.

of surface displacement. The pattern of rupturing there also contrasted with that farther south, in that individual breaks tended to be singular and continuous rather than echelon, although many exceptions were observed (figs. 87–89). Other significant differences in the surface ruptures in places where the vertical components were large include: greater irregularity in the fault trend (fig. 90); branching, commonly, though not consistently, on the west side of the main trace; and, owing to this branching, increased width of the zone of ground rupturing. The maximum width across divergent branching breaks on the Imperial fault was about 1.5 km near Keystone Road (at 27 km).

Although southeast of the Mesquite basin the surface ruptures were generally restricted to a single echelon mole track, complexities involving branching, apparent discontinuity of the main fault strand, and multiple strands also appeared. The most notable of these complexities was near Interstate Highway 8 (loc. 15), where the principal fault strands, as judged by the linearity and amount of displacement, terminated and stepped to the right about 85 m. Subsidiary fractures south of this stepover lay 85 to 175 m southwest of and nearly parallel to the main rupture (fig. 91); these breaks are not connected on the map (pl. 1) between Chick Road (loc. 13) and Barbara Worth Road (at 6.3 km) because dense crops concealed them, although several breaks may have joined to form a second continuous strand. Aerial photographs of this segment of the fault after the 1940 displacement likewise indicated movement of the

FIGURE 87.—Imperial fault at Robinson Road (at 20.0 km). Vertical component of 1979 slip here created a low scarp (shadowed line) that has been smoothed at road surface by regrading. Vertical displacement at surface rupture is about 28 cm in this view. Surface rupture to right extends along line of bushes that conceal it. Vegetational lineaments of this type commonly mark fault trace along margin of Mesquite basin where some land has not been farmed or otherwise modified. View northwestward. Photograph by M. J. Rymer, October 23, 1979.

southwest strand at that time but also failed to prove its continuity.

The sense of vertical displacement varied only in an area of discontinuous surface rupturing near Interstate Highway 8 (loc. 15) and at stepovers to the right in areas farther southeast. The sketch map (fig. 92) indicates the reversals in sense along several breaks at Interstate Highway 8. Other stepovers to the right in the southeast half of the fault trace were smaller than those on the highway. One stepover, between McCabe and Anderholt Roads (at 4.8 km), illustrates the expectable relative sinking of the ground between echelon breaks in this configuration with respect to the surrounding land (fig. 93). Water leaking from a nearby broken canal flooded the area and proved that the depression between breaks was closed. This stepover also is unusual in that variations in the density of crop foliage coinciding with its outline clearly reveal the alinement of the fault traces on most aerial photographs taken since 1940. This was one of very few places where photolineaments accurately marked the trace of the Imperial fault in cultivated ground before the earthquake of 1979. Sags or sag ponds, fault-trace features common throughout the San Andreas system in California, are generated by repetitive movements on similarly configured fault strands in areas undisturbed by human activity.

One unusual discontinuity in the surface rupture of the Imperial fault was south of Huston Road (at 18 km). Before the 1979 slip event, probably less was known concerning the location and geometry of the trace in this segment than in any other part of the fault. The most unexpected geometric feature of the fault trace in this locality (fig. 94) is the conspicuous curvature of the separate echelon strands. The discontinuity near Huston Road is the southernmost such feature, although even more irregular curving and branching breaks were common farther north along the Imperial fault. All these discontinuities appear to be associated with local disappearance of the lateral component of displacement on the surface breaks.

FIGURE 88.—Imperial fault at Dogwood Road (at 23.1 km). Main fault trace crosses top horizontally (short arrows). Gullies are deeply incised on upthrown (southwest) side of fault. Secondary fault (long arrows) branches northward nearly parallel to Dogwood Road and eventually crosses pavement about 170 m north of point where main fracture crosses it. View southwestward. Photograph by D. G. Herd, October 22, 1979.

SUBSIDIARY FAULTING

North of the midpoint of the 1979 surface rupture on the Imperial fault, particularly north of Robinson Road (at 20 km), branching and secondary faulting were important features of 1979 ground displacement. The term "secondary faulting," as used here, includes surface breaks approximately parallel to the main rupture, though not connected with it; branch faults, in contrast, join the main break but project away on divergent traces. With two exceptions, all these subsidiary faults showed the same sense of vertical movement as the main fault trace (downward on the east side) where it traverses the west margin of the Mesquite basin. These two exceptions, exhibiting the opposite sense of vertical offset, include one short break subparallel to and about 0.1 to 0.2 km east of the main fault trace (loc. 47), and another break on the surface of Keystone Road (loc. 85). The break at Keystone Road with this sense could not be traced beyond the pavement. The break at locality 47 and the main fault define a narrow graben about 0.3 km long at the west margin of the larger graben represented by the Mesquite basin.

Most subsidiary breaks were within 0.6 km of the main trace of the Imperial fault and transected the slope of the erosionally degraded Quaternary escarpment of the main break. Although these traces resembled the main break in their irregularity and small-scale discontinuities, all had relatively minor vertical components of displacement and no significant right-lateral components. Figure 95 shows a vertical profile of two subsidiary breaks that cross Ralph Road (loc. 54); the sum of the vertical components of slip for the multiple breaks (about 0.3 m) is about the same as the maximum vertical offset measured at other points in the same section of the Imperial fault.

The main trace of the surface rupture on the Imperial

FIGURE 89.—Imperial fault 1.7 km south of Keystone Road (loc. 72). Canal liner near center was one site monitored for data on horizontal and vertical components of afterslip. Plunge of slip here is about 61° in fault surface, which is nearly vertical in a canal-bank exposure beyond left edge. View southwestward. Photograph by M. J. Rymer, October 23, 1979.

fault was clearly identifiable northward to a point about 1.5 km north of Harris Road (at 25.4 km). There, the fault bifurcated, and although one branch continued northward on the same trend as the trace to the south, both branches died out within about 1.5 km. Secondary fault breaks with relatively small displacements were found as far as 1.8 km west of the easternmost line of faulting, at about the latitude of Keystone Road (at 27.2 km), where combined branching and secondary faulting created the greatest width of any zone of surface rupturing activated during the 1979 earthquake.

Although at least five separate strands of subsidiary faulting make up the 1.8-km-wide zone near Keystone Road and three of these vertically offset the pavement, only one strand noticeably extended beyond the shoulder of the road (east break at loc. 86; fig. 96). Northward from Keystone Road the main fault strand appeared to be the easternmost break in the zone of fracturing, both for this event and for past faulting (fig. 97). The relation of this break to the Y-shaped branch faults south of Keystone Road is unclear because no evidence has been preserved of older fault traces in this section of the Imperial fault. Despite coincidence of the 1979 pattern of surface rupture with earlier Holocene fault traces in this area, the geometry or extent of continuity of the principal strand of subsurface faulting is unknown. At depth the faults could be simpler and more continuous than at the surface, although the small horizontal-displacement components near Keystone Road suggest that this need not be so.

FIGURE 90.—Imperial fault at Harris Road (loc. 67), which passes between utility poles on right. Sinuosity of fault trace is typical of much of northern segment of Imperial fault where vertical component of slip is large. Gullying of upthrown (southwest) side of fault has etched rounded late Holocene scarp. Note general but imperfect congruence of new surface rupture (dark narrow line) with base of older escarpment. View southwestward. Photograph by M. J. Rymer, October 23, 1979.

DISPLACEMENT

Coseismic slip on the Imperial fault caused nearly instantaneous surface displacement, according to one

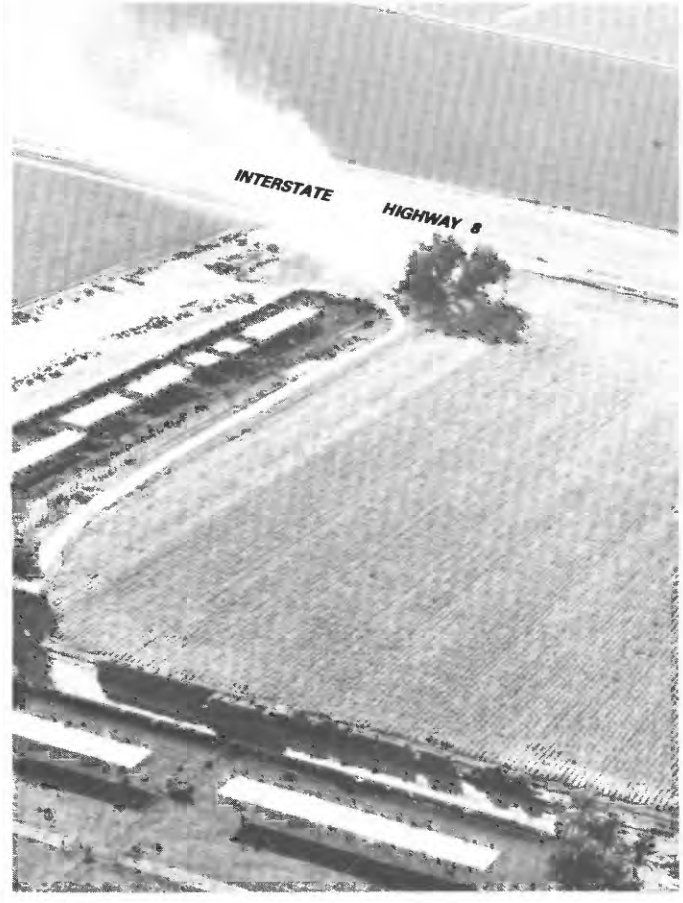

FIGURE 91.—Imperial fault at Interstate Highway 8 (loc. 15). Main fault trace, marked by offset rows of asparagus in foreground, dies out southeastward in field beyond highway. Subsidiary branching fault that crosses this field northwestward to highway probably joins main fault near palms in foreground. View southeastward. Photograph by M. J. Rymer, December 12, 1979.

creepmeter record of the event obtained at Heber Road (loc. 4) in the southern part of the fault rupture (Cohn and others, this volume). By the time direct measurements of displacement began at other points along the fault early in the day after the earthquake, afterslip had substantially increased these surface displacements. We continued to measure displacement sporadically until December 1979, and after a brief hiatus, the latest measurements reported here were made in March 1980.

Afterslip on the fault proceeded rapidly after the first recordings of displacement. Considering the time requirements and the few personnel involved in making measurements, we soon recognized that documentation of the growth of fault displacement over the entire length of surface rupture would be difficult. Fortunately, much of the Imperial fault trace traverses a grid of orthogonally arranged cultural features, including roads, a system of canals, and such cultivation lines in fields as crop rows and plowlines. These cultural features were nearly optimal for obtaining a well-distributed set of repeated displacement measurements.

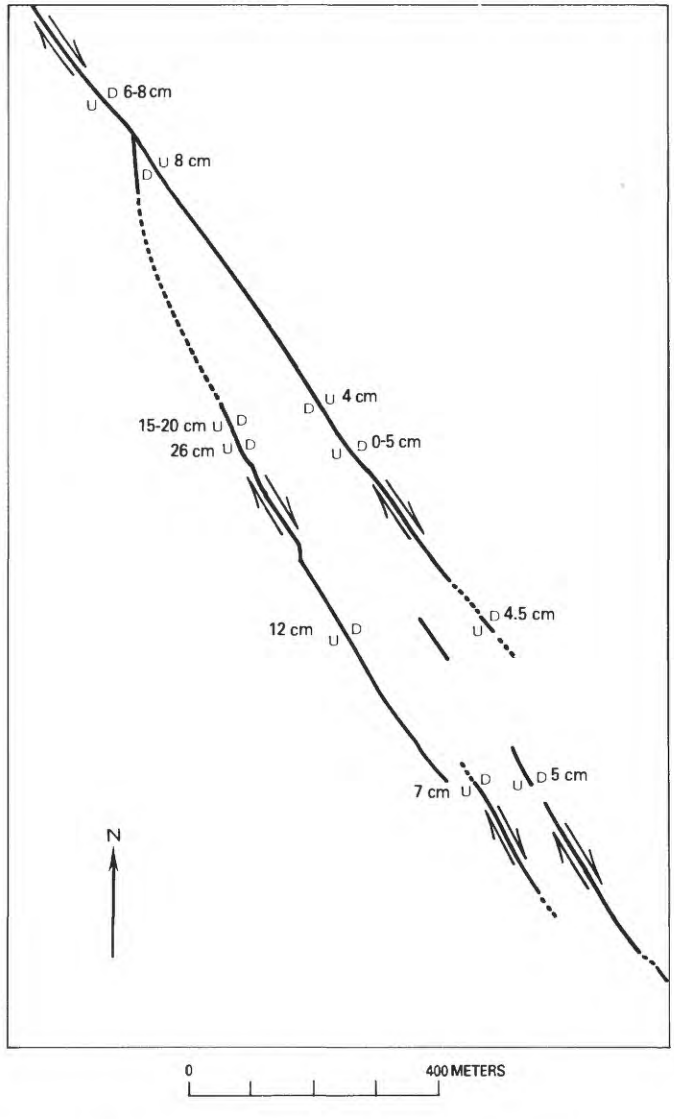

FIGURE 92.—Sketch map showing traces and direction and approximate amount of vertical displacement on branching and echelon strands of Imperial fault near Interstate Highway 8 (loc. 15). U, upthrown side; D, downthrown side; arrows, relative horizontal movement. See plate 1 for explanation of fault-trace symbols.

Our procedure for recording the accumulating slip was to measure repeatedly as many offset features as possible, obtain an approximate slip-rate function for each feature, and interpolate or extrapolate the data on plots of displacement against distance along the surface rupture for different times after the event. Although we made several measurements directly in the field at these times, to obtain an adequate density of points for each time on the plots we had to approximate the slip values from measurements at other times. Precise afterslip determinations on alinement arrays at several points along the fault trace all indicate a linear relation of cumulative slip to the logarithm of postearthquake time (Cohn and others, this volume; Crook and others, this volume; Harsh, this volume). Our data on cumulative slip, determined from less accurate measures of horizontal displacement, similarly confirm the generality of the relation of cumulative slip to the logarithm of time in many localities (see fig. 98), although the data also reveal important local departures from this relation. That the linear relation appeared to be generally valid for nearly the entire fault length during most of the sampled afterslip period justifies our method of interpolating slip in places where slip was not measured directly at the appropriate times. This technique—which, to our knowledge, has not previously been applied to measuring earthquake displacement—reveals or, at least, suggests several exceptionally interesting features of the afterslip history that might ordinarily have escaped detection. We describe these features in detail below.

We used two geometric methods to determine the horizontal components of displacement. Generally, we computed horizontal components from apparent offsets measured normal to cultural features that mostly were oriented east-west or north-south. Because direct measurements commonly were complicated by bending, buckling, or extensional opening at the fault intersections, these apparent offsets generally could be determined with greater precision than the true horizontal displacements. (Computation of true horizontal slip from apparent offset requires a trigonometric correction involving the angle between the azimuth of the fault trace and that of the cultural feature.) Otherwise, we measured horizontal slip directly from fissures in the ground surface by matching irregularities across the

cracks; such measurements were not used to determine afterslip because of uncertainty in relocating the same crack and because of the large variations in displacement over short distances. The azimuths of slip vectors and their lengths and inclinations from the horizontal could be measured directly on many cracks, and this azimuth could be compared with the fault trend recorded at the same point. Parallelism of these two measurements is consistent with, but does not require, a vertical dip of the fault surface, whereas nonparallelism suggests nonverticality, deformation in the ground materials not manifested as faulting, or both.

We determined the slip vectors, or their components or apparent components, by several techniques. Offsets on cultural features were in many places obtained by unaided visual projection of their alinement to the opposite side of the fault and measured by using a rule. We made similar measurements where visual projection was controlled by a vertical line, such as a plumb bob, to eliminate the possibility of obtaining a value for horizontal slip that might be affected by the vertical component of slip. In many places where the slip appeared to be horizontal, leveling across the fault trace revealed small vertical components of displacement on cultural features. To measure the apparent horizontal displacement of canals most accurately, we used a telescopic alidade to make many of the visual projections. Because many canals had already been offset slightly before the earthquake, we subtracted appropriate corrections to these measurements from the postearthquake displacements, using offsets scaled from photographs taken in the preceding 3 years.

The disagreements in the displacements measured at different times evidently stem from the different measurement or estimation techniques for determining the fault offset, as described above, and from subjective differences in their application. We have arbitrarily rejected a few measurements as unreliable; for example, we consider that measurements of offset on canals by telescopic alidade are more accurate than those by eye,

FIGURE 93.—Imperial fault 0.8 km south of McCabe Road (at 4.8 km). Double trace of fault here outlines depression between echelon strands that was flooded by leakage from canal liner (foreground) broken by October 15 displacement. Distance between berms is about 23 m. View northward. Photograph by M. J. Rymer, October 23, 1979.

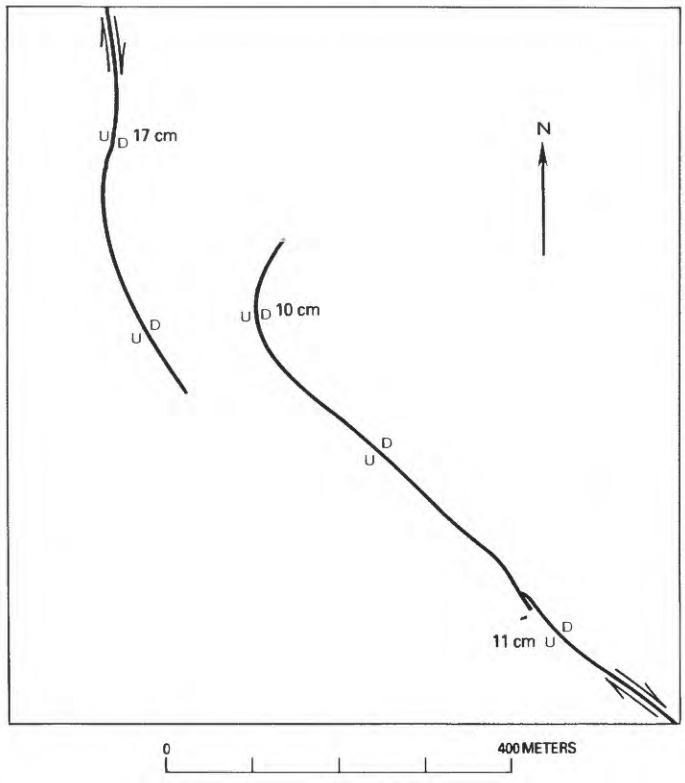

FIGURE 94.—Sketch map showing echelon traces and direction and approximate amount of vertical displacement on Imperial fault in field south of Huston Road (at 18 km). See figure 92 for explanation of symbols.

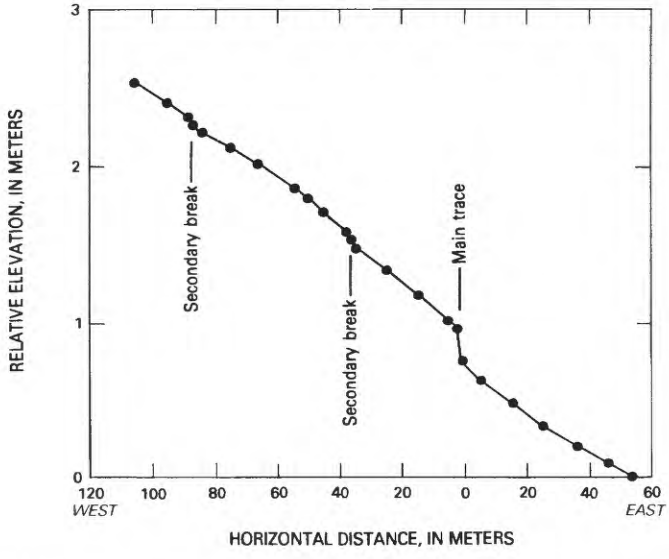

FIGURE 95.—Profile of elevations along Ralph Road (loc. 54) across main trace of Imperial fault and secondary breaks west of fault. Fourth break, measured separately but not shown here, crosses Ralph Road 0.45 km west of main fault (loc. 57). Fifth break, about 55 m east of main fracture, consists of extensional cracks with no detectable vertical displacement. Assuming a smooth slope for road surface before earthquake, vertical-displacement component for all five breaks was about 0.3 m on October 26, 1979 (6 cm of vertical displacement measured on westernmost break).

FIGURE 96.—Northern branch of Imperial fault 0.3 km north of Keystone Road (loc. 86). Of three breaks at Keystone Road, this was only strand of Imperial fault that extended away from pavement. Sinuous surface rupture is made up of left-stepping echelon breaks. 3 cm of vertical displacement (far side up) was measured near lower right corner on October 21, 1979. Rupture formed a single line of fractures; two dark bands paralleling trace are postearthquake footpaths worn by curious geologists and other confused visitors. Plowlines in field are spaced at 3.7-m intervals. View southwestward. Photograph by M. J. Rymer, October 23, 1979.

and that measurements of the misalinement of originally straight features are better than those across open cracks in the same features. Although displacements on echelon breaks in soil can be accurately determined in principle, in many places, particularly where nearly mature crops were growing in fields, determining whether the measured displacement represented the entire movement was difficult or impossible. We made many accurate measurements of displacement, however, in fields where the low density of crops permitted clear views of the ground surface or of the alinement of crop rows.

Table 20 summarizes the measured offsets used in reconstructing the horizontal-displacement and afterslip histories for surface rupturing along the Imperial fault. The right-lateral-displacement data in the table have been plotted as a function of the logarithm of postearthquake time for most localities; examples of the cumulative-horizontal-slip functions obtained in this way are shown for two locations on the fault in figure 98.

FIGURE 97.—Main branch of Imperial fault (at 29.2 km at bottom) 0.4 to 0.8 km north of Carey Road. Surface break (arrows) is dark line at base of low slightly gullied scarp in foreground. Trace generally follows curved edge of cultivated field in distance and converges with curved concrete canal liner at top. View northeastward.

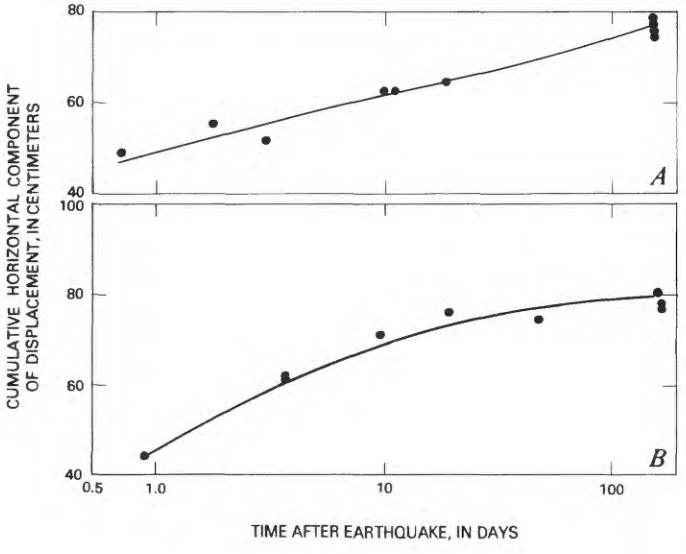

FIGURE 98.—Cumulative horizontal component of slip as a function of postearthquake time. *A*, Curve for canal on north side of McCabe Road (loc. 10); slope is relatively constant during entire period of measurement (160 days). *B*, Curve for canal about 200 m west of Anderholt Road (loc. 6); slope decreases markedly late in period of measurement.

The slopes of the curves relating cumulative horizontal displacement to the logarithm of postearthquake time (*b*, table 20) are shown as a function of distance along the surface rupture in Figure 99. These data provide a basis for plotting the variations in horizontal displacement along the Imperial fault at 4, 10, 20, and 160 days after the earthquake, times that maximize use of observations and minimize need for interpolation. Although these plots (fig. 100) necessarily are partly based on interpolation of the rates of afterslip in those places where direct measurements gave inadequate data, and therefore some error is possible, we regard the plots as generally reliable.

Figure 101, which summarizes the distributions of cumulative horizontal slip for the four postearthquake times mentioned above, illustrates the following major characteristics of surface movement along the Imperial fault. (1) For all the times shown, the largest displacements are skewed toward the main-shock epicenter and the south terminus of surface faulting, and the horizontal slip generally diminishes to the north. (2) The displacement curves show many spikes and troughs corresponding to local maxima and minima. (3) At 4 days after the earthquake, the largest dextral slip (about 60–65 cm) was at locality 3, within 1.7 km of the southeasternmost surface rupture detected at locality 1. (4) At 10 days after the earthquake, the maximum slip (about 70 cm) was at locality 6, 4 km from the southeast limit of surface faulting; the change in position of this maximum is not due to its progressive lateral migration but instead reflects the growth of an originally smaller, though apparently stationary, local maximum farther northwest. (5) At 20 days after the earthquake, the maximum cumulative horizontal slip was about 74 cm, still at locality 6. (6) At 160 days the maximum displacement increased to about 78 cm, and its position changed by relatively more rapid growth of the local maximum to the northwest at locality 10; by this time the maximum displacement had shifted about 4 km northwest of the position of the maximum at 4 days. (7) Cumulative horizontal afterslip, expressed as a percentage of the displacement at 4 days (coseismic displacement plus 4 days of afterslip) ranged from 0 to about 100 for the 160-day period at different points along the fault trace.

We emphasize that Figure 101 summarizes those

TABLE 20.—*Right-lateral components of slip along the Imperial fault*

[Features: C, concrete canal liner; K, crack in cultural feature; P, crack in ground surface; R, pavement of road; T, linear mark on ground surface; A, alinement-array data of Cohn and others (this volume) and Harsh (this volume). a and b are constants used in linear-regression best fit of measured slips to logarithm of time, according to equation $D=a+b\log_{10} t$, where D is horizontal displacement (in centimeters) and t is postearthquake time (in days). Methods of displacement estimation: E, extrapolated from b; G, crude field measurement; I, interpolated from measurements at other times; M, fairly accurate field measurement; U, not measurable. (0.4d), measured 0.4 d after earthquake, used in preference to slip interpolated for that date]

Locality	Feature	Distance along reference line (km)	a	b	Horizontal component of cumulative slip (cm)						
					Preearthquake	Days after earthquake					
						0-3	4	10	20	20-160	160
1	P	0.00	[1]4.0	0.00	0	4.0 (0.4d)(M)	4.0(E)	4.0(E)	4.0(E)	---	4.0(E)
2	T	.39	[1]54.1	1.19(I)	0	---	55.0 (2.9d)(M)	56.0(E)	56.6(E)	---	58.3(E)
3	C	1.60	[2]58.8	[2]7.85	---(U)	58.0 (0.9d)(M)	63.4(I)	66.80(M)	69.5(M)	---	75.6(152d)
4	R,P	2.55	[1]45.8	7.06(I)	0	47.5 (1.8d)(M)	50.0(I)	52.0(M)	54.9(E)	---	61.3(E)
5	A	3.70	[4]47.4	[3]6.10	0	---	[1]51.0	[3]53.5	[3]55.3	---	[3]60.8
6	C	4.03	[2]53.5	[2]12.81	2.4(M)	---	60.2(M)	69.6(M)	74.1(M)	---	76.2(M)
7	C	4.60	---	---	10(G)	---	56.0(M)	56.6(M)	59.0(I)	---	62.3(M)
8	C	5.04	[2]51.2	[2]8.40	12.9(M)	53.1 (2.9d)(M)	56.2(I)	62.6(M)	61.8(M)	---	68.9(M)
9	C	5.09	[2]51.3	[2]9.66	0	53.0 (2.9d)(M)	55.5(I)	63.4(M)	65.8(M)	---	71.8(M)
10	C	5.62	[2]49.3	[2]12.82	0	---	51.3(M)	62.3(M)	64.5 (18.5d)(M)	---	78.2(M)
11	C	6.44	[2]23.8	[2]13.68	0	28.0 (2.9d)(M)	30.9(I)	35.0(M)	48.8(M)	---	51.2 (159d)(M)
12	C	6.59	[2]34.2	[2]15.51	2.5(M)	36.5 (2.9d)(M)	40.9(I)	46.7(M)	56.5 (18.5d)(M)	---	64.7 (158d)(M)
13	C	7.65	[2]28.1	[2]11.12	0	---	33.0 (2.9d)(M)	32.8(M)	51.4(M)	---	51.5 (159d)(M)
14	C	8.07	[1]37.9	10.29(I)	---(U)	---	44.0(E)	48.1(E)	51.2(E)	---	60.5 (157d)(G)
15	R	8.48	[2]52.4	9.48(I)	---(U)	---	58.0(E)	61.8(E)	64.6(E)	---	73.2 (158d)(M)
16	C	9.02	[2]49.2	[2]8.42	4.4(M)	---	54.2(E)	57.7 (10.9d)(M)	60.6 (21d)(M)	---	67.7(M)
17	R	9.53	[2]36.3	[2]12.10	0	36.9 (2.0d)(M)	43.5(I)	48.3(I)	49.1 (24.9d)(M)	---	66.3 (158d)(M)
18	C	10.09	[2]25.0	13.10(I)	---(U)	---	32.7(E)	38.0(E)	41.9(E)	---	53.8 (158d)(M)
19	C	10.78	[1]27.8	14.33(I)	---(U)	---	36.3(E)	42.1(E)	46.3(E)	---	59.3 (158d)(M)
20	C	11.03	[2]23.0	[2]14.78	9(M)	---	31.6(E)	37.7 (10.9d)(M)	40.3(I)	49.9 (50d)(M)	54.4 (158d)(M)
21	C	11.52	[2]29.1	[2]13.85	10(M)	---	36.6(M)	43.1 (10.9d)(M)	48.7(M)	---	50.9(M)
22	C	11.53	[2]29.1	[2]14.36	0	---	36.6(M)	44.0 (10.9d)(M)	49.2(M)	---	60.0(M)
23	C	12.01	[2]24.6	[2]9.25	6.4(M)	---	30.0(E)	34.6 (10.9d)(M)	37.6 (23d)(M)	---	44.9(M)
24	R	12.53	[2]20.7	[2]12.93	0	---	27.5(M)	33.6(I)	37.4(I)	---	49.5(M)
25	C	13.59	[2]17.8	[2]9.17	0	---	23.3(E)	27.0 (7.8d)(G)	28.8 (23d)(M)	---	38.6(M)
26	C	14.14	22.6	1.7	7.4(M)	---	23.6(E)	24.1 (7.8d)	24.8(I)	---	26.3(M)
27	C	14.73	---	---	6.2(M)	---	33.4(M)	41.5 (7.9d)	43.0(I)	---	48.2(M)
28	R	14.89	[2]22.6	---	0	18.5 (0.5d)(M)	30.6(I)	36.1(M)	40.1(E)	---	52.5(E)
29	C	14.92	[2]19.4	[2]14.17	5.8(M)	---	27.7(E)	32.1 (7.9d)(M)	37.6(M)	---	50.6(M)
42	R	19.00	[2]14.2	[2]10.01	0	14.0 (0.9d)(M)	18.5 (4.9d)(M)	25.0(M)	27.1(I)	33.0 (75d)(M)	36.2(E)
54	A	21.71	[1]10.7	[4]7.80	0	---	[4]15.3(E)	18.5(M)	[4]20.8(E)	---	[4]27.9(E)
55	P										
61	R	23.15	[1]9.4	5.90(I)	0	---	12.9(E)	15.0 (8.9d)(M)	17.0(E)	---	22.4(E)
67	A	23.80	[1]11.2	[4]5.04	0	---	14.2(M)	[4]16.2(E)	[4]17.7(E)	---	[4]22.3(E)
68	P										
72	C	25.50	[2]6.5	[2]4.25	0	---	8.5(M)	11.8 (11.9d)(M)	12.0(I)	---	16.2 (159d)(M)
85	R	27.18	[1].0	.00	0	---	.0(E)	.0(E)	.0(E)	---	.0 (159d)(M)
95	C	29.70	[2]1.1	[2].66	0	---	1.5(E)	1.7 (6.9d)(M)	2.0(I)	---	2.6 (158d)(M)
96	K	30.53	.0	.00	0	---	.0(E)	.0 (8.9d)(M)	.0(I)	---	.0 (158d)(M)

[1]Slip extrapolated from single measured value, using b value from other data.
[2]Linear-regression best fit to data from 1 to generally 160 d after earthquake.
[3]Slip computed from alinement-array data of Cohn and others (this volume).
[4]Slip computed from b values of alinement-array data of Harsh (this volume) and best field measurement of slip.

measurements of displacement that were repeatable and thus are considered to be the most reliable determinants of afterslip. Had similar multiple measurements been possible in other places, we might have been able to follow the growth of additional local maxima and minima over time, and we might have measured an even greater maximum displacement somewhere else than at the localities shown in figure 101.

Figure 102 shows an even more irregular profile based on single measurements of maximum horizontal displacement within 1-km segments of the fault on manmade and ephemeral natural features offset by surface faulting (see table 21). These maximum displacement values have been adjusted according to their distance from the nearest localities in which measurements of right-lateral slip were repeated. These maxima were then extrapolated in time according to a model of the linear variation of displacement, interpolated over the distance between localities 27 and 96. Over this distance we made repeated measurements on permanent objects at the localities shown for the same segment of the fault as in figure 101. The afterslip functions for these localities were then interpolated for the places where displacement was measured only once. Thus, the relatively smooth profile of displacement in figure 101 between 14.7 and 25.5 km may actually have been as

rough on a small scale as the better documented part of the Imperial fault farther southeast.

This characteristic irregularity of the cumulative-displacement curves is about as pronounced on a scale of tens of meters as at distances of hundreds of meters along the fault trace. Measurements on individual crop rows in fields demonstrate that fairly large variations in slip are possible in alluvial materials along short segments of the fault and that these fluctuations are not simply due to the position of the measured points relative to stepovers of the echelon surface ruptures. Similar short-distance variations have been determined for displacements on the Superstition Hills and San Andreas faults that accompanied the Imperial Valley earthquake of 1979 (Fuis, this volume; Sieh, this volume). Moreover, other major fault displacements in the world—for example, the 1976 sinistral displacement on the Motagua fault in Guatemala—have shown the same short-range variability (Bucknam and others, 1977).

Figure 103 plots the maximum and average cumulative horizontal and vertical components of slip on the Imperial fault as a function of the logarithm of time after the earthquake. The data suggest that growth of the maximum displacement (curve A) is slowing on a logarithmic time scale and may not increase substantially in the future. In contrast, the bounds on the average slip (curves B, C) are more steeply sloped than the maximum slip at 160 days after the earthquake. For example, at 4 days after the earthquake the average horizontal displacement was about 40–45 percent of the maximum, but at 160 days it increased to 52–58 percent of the maximum.

The curves for cumulative horizontal displacement (figs. 100, 101) for the different postearthquake times indicate various styles of near-surface behavior for different segments of the fault trace. (1) Some segments with large initial displacements subsequently continued to move relatively slowly (for example, loc. 3). (2) Some segments with initial offsets that were smaller

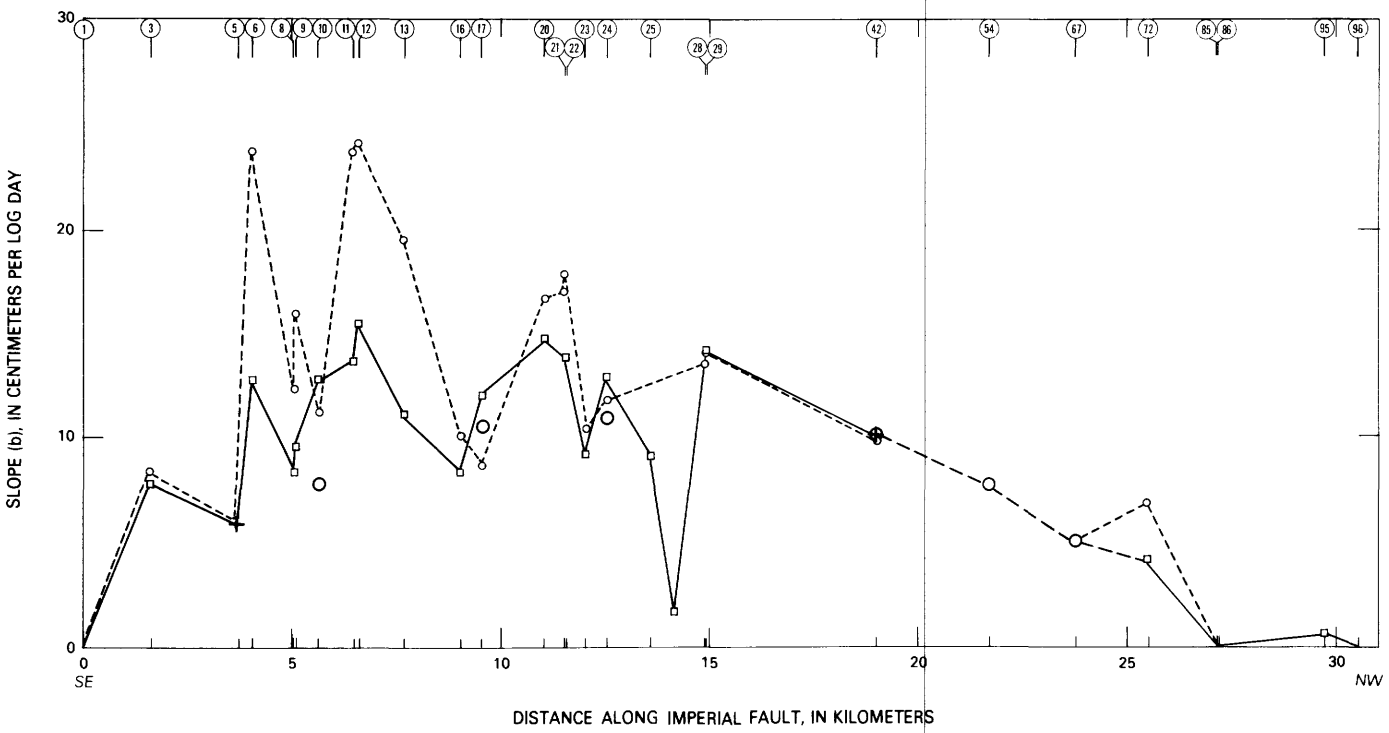

FIGURE 99.—Slope (b) of cumulative-slip curves as a function of distance along fault, according to equation $D=a+b\log_{10}t \geq 0.6$, where D is cumulative horizontal displacement (in centimeters), a and b are constants used in linear-regression best fit of measured slips, and t is postearthquake time (in days). Dotted line joins points (circles) based on displacements measured to March 1980; solid line joins data points (crosses) measured to November 1979. Squares represent b values from data of Cohn and others (this volume), and large circles those of Harsh (this volume). Table 20 lists a and b values, together with other data on displacement measurements. Locality numbers at top of plot are from plate 1.

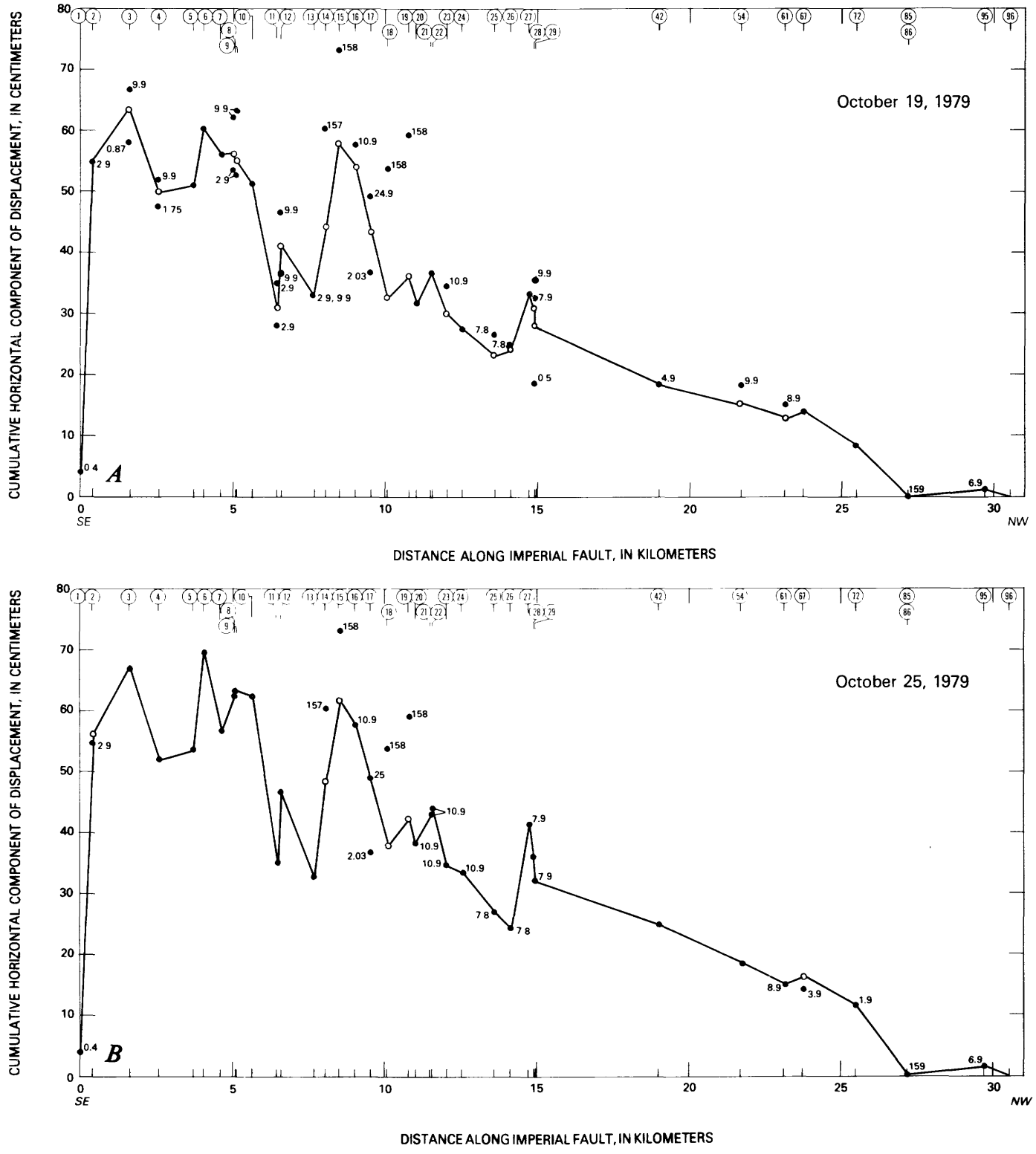

FIGURE 100.—Cumulative horizontal component of displacement along Imperial fault at four times after earthquake: 4 days (*A*), 10 days (*B*), 20 days (*C*), and 160 days (*D*). Dots represent horizontal-displacement measurements on day indicated. Circles on curves with a dot (dated) vertically above indicate data points extrapolated from displacements measured later, calculated from *b* value for that point or an interpolated *b* value from adjacent points. Circles on curves with dots (dated) vertically above and below indicate data points interpolated between given dates, calculated from *b* value for cumulative slip for that point. All values plotted on figure are from table 20. Locality numbers same as in figure 99.

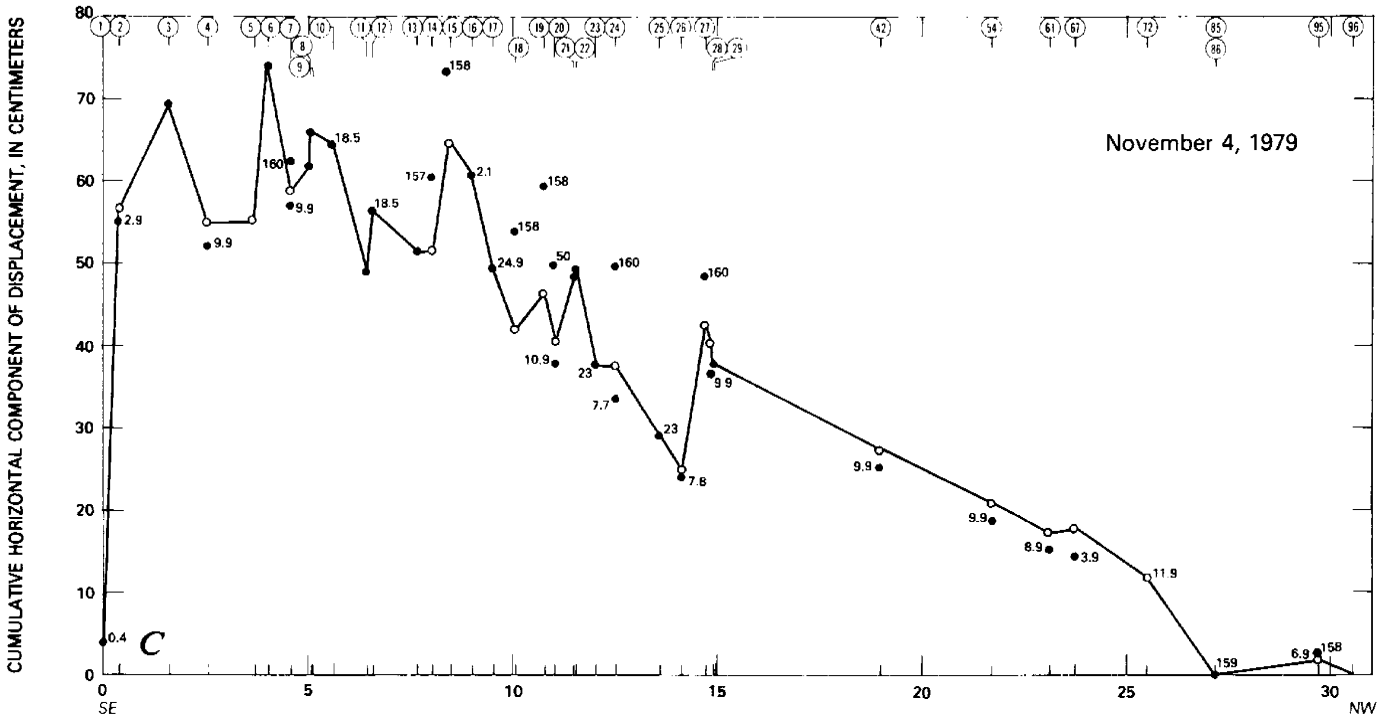

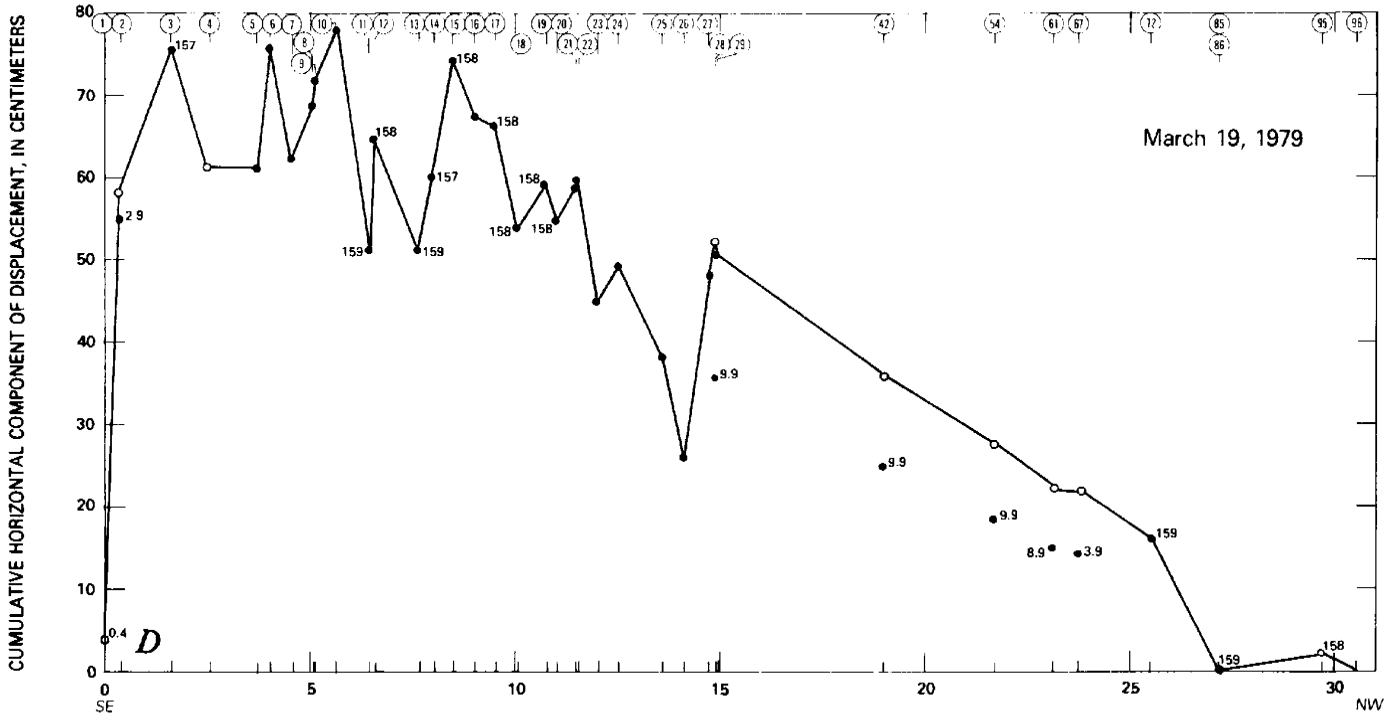

FIGURE 100.—Continued

than on adjacent sections of the fault showed large afterslip rates that reflect a steady postearthquake catching up with those adjacent sections (for example, loc. 12). (3) Some segments with initially small displacements thereafter continued to slip slowly and thus remained stuck (for example, loc. 17). (4) Some segments with relatively small initial afterslip rates later became the most rapidly moving parts of the fault, not only because of the progressively smaller slip rate of segments of the fault that earlier had moved more rapidly, but also because the afterslip function deviated locally from the typical linear relation (for example, loc. 10). At Chick Road (loc. 13) the slip was nearly constant from day 4 to day 10, then increased significantly by day 20, and has been nearly unchanged since that time.

The profiles of cumulative horizontal slip on the Imperial fault (fig. 101) provide more complete information on displacement than heretofore documented for other strike-slip movements. Although in some places a simple inverse relation between the initial coseismic slip and the amount of afterslip has been documented—similar to that found, for example, on the Motagua fault after the Guatemala earthquake of 1976 (Bucknam and others, 1978)—close spacing of the repeated measurements of displacement demonstrates other patterns of afterslip behavior that cannot readily be related to the local geologic setting. The nearly flat alluvial floor of the Imperial Valley and the deep sedimentary fill under that part of the valley transected by the fault suggests a relatively uniform environment that would expectably promote uniform surface afterslip. The significant local variations in afterslip behavior despite apparently uniform geologic conditions may reflect the abundance of our observations compared with those from investigations of other fault displacements. What appears as anomalous and erratic behavior for some segments of the Imperial fault may in fact represent the typical response of nearly uniform near-surface alluvial materials disturbed by more deep seated and presumably more uniform fault slippage. Closely spaced repeated measurements of displacement may demonstrate similar behavior for future movements on other faults, although a dense network of linear cultural features or rapid postearthquake construction of many alinement arrays would probably be required.

The markedly abrupt variations in horizontal displacement, and particularly the rapid dying out of measured displacements at the south end of the surface rupture, may be characteristic of the relatively shallow

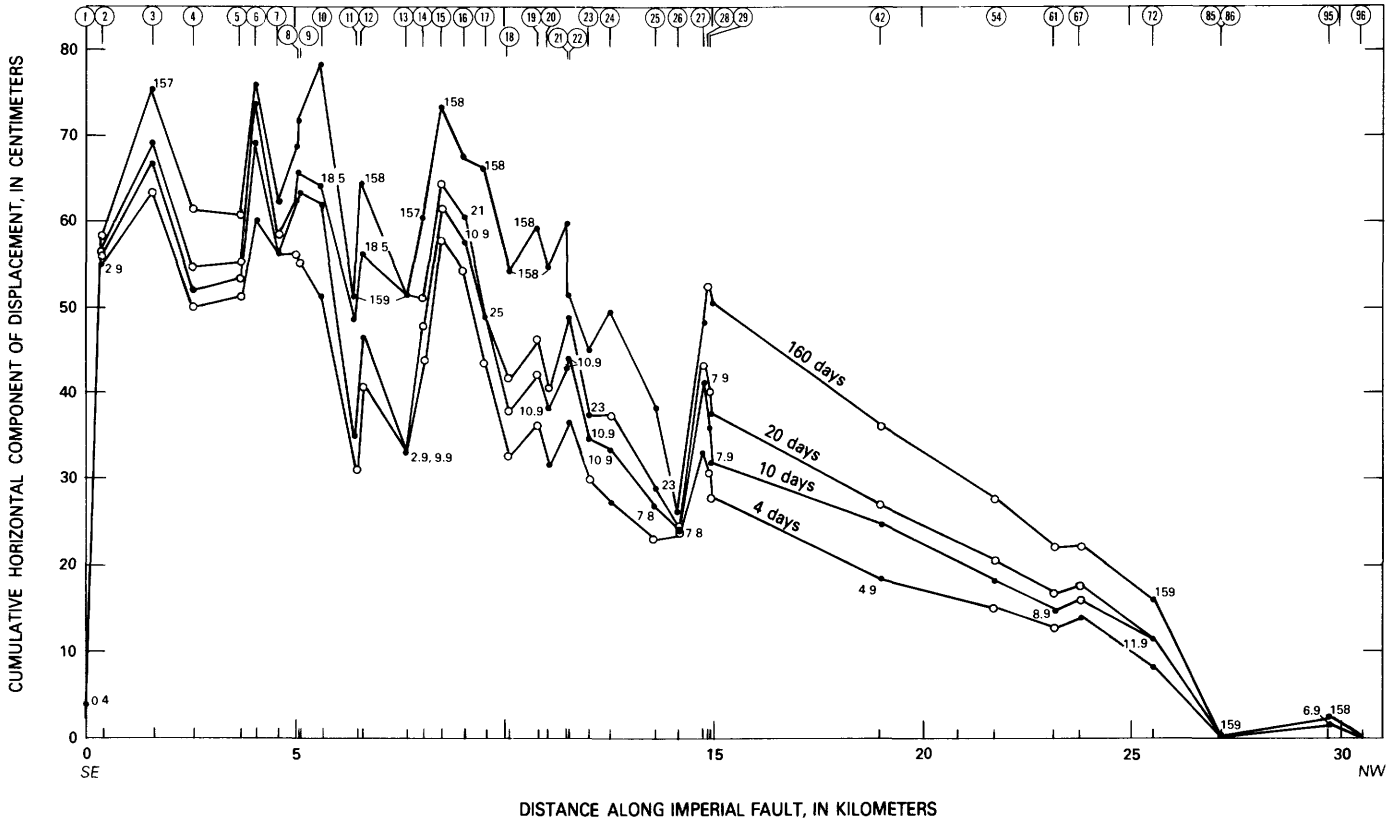

FIGURE 101.—Cumulative horizontal displacement as a function of distance along 1979 surface rupture on Imperial fault at 4, 10, 20, and 160 days after earthquake. Dots represent field measurements made on day indicated. Circles represent data determined by interpolation or extrapolation of a succession of measurements for which a logarithmic growth function was determined. Locality numbers same as in figure 99.

TABLE 21.—*Maximum vertical components of slip for segments of the Imperial fault*

[Features: C, concrete canal liner; L, releveling array on road surface; P, crack in ground surface; R, pavement of road; S, scarp at fault rupture. c and d are constants used in linear-regression best fit of measured slips to logarithm of time, according to equation $V=c+d\log_{10} t$, where V is vertical displacement (in centimeters) and t is postearthquake time (in days). (2.9d), measured 2.9 d after earthquake; M, measured in field; E, extrapolated from d; I, interpolated from measurements at other times]

Locality	Location on reference line (km)					Maximum vertical component of slip (cm)			
						Days after earthquake			
	Feature	End points of fault segment	Point of maximum slip	c	d	0-6	7	8-25	158
1	P	0.00-0.49	0.00	0	0.00	---	0	---	0
	---	0.50-1.49	---	---	---	---	---	---	
3	C	1.50-2.49	1.60	9	.00(I)	---	9(E)	9 (18.5d)	9(E)
---	---	2.50-3.49	---	---	---	---	---	---	---
6	C	3.50-4.49	4.03	0	.00	---	0(E)	0 (17.5d)	0(M)
7	C	4.50-5.49	4.60	9	.00(I)	---	9(E)	9 (18.5d)	9(E)
10	C	5.50-6.49	1.62	4	.00	---	4(E)	4 (18.5d)	4(M)
12	C	6.50-7.49	6.59	4 1/2	.00	---	4 1/2(E)	4 1/2(18.5d)	4 1/2 (M)
13	C	7.50-8.49	7.65	11 1/2	.55	---	12(E)	12 (19.5d)	12 1/2 (M)
16	C	8.50-9.49	9.02	9	.00	---	9(E)	9 (20.5d)	9(M)
---	---	9.50-10.49	---	---	---	---	---	---	---
---	---	10.50-11.49	---	---	---	---	---	---	---
23	C	11.50-12.49	12.01	4 1/2	1.15	---	5 1/2 (E)	6±3 (21.5d)	7±3 (M)
---	---	12.50-13.49	---	---	---	---	---	---	---
25	C	13.50-14.49	13.59	11	3.53	---	14(E)	16±3 (22.5d)	19±5(M)
27	C	14.50-15.49	14.73	10 1/2	2.59	---	12 1/2 (E)	14 (22.5d)	16(M)
34	P	15.50-16.49	16.44	7 1/2	5.35(I)	---	12(M)	---	19(E)
36	P	16.50-16.49	17.19	1	6.95(I)	4 (2.9d)	6 1/2 (E)	---	16(E)
40	P	17.50-18.49	18.24	15 1/2	9.20(I)	---	24± (M)	---	36(M)
43	R	18.50-19.49	19.00	21	8.04(I)	10 (~1d?)	26(I)	29 (9.9d)	38 1/2 (E)
48	P	19.50-20.49	20.15	22 1/2	6.28(I)	---	28.3(M)	---	36 1/2 (E)
50	P	20.50-21.49	20.79	~0	5.30(I)	---	1(M)	---	1 1/2 (E)
54	L	21.50-22.49	21.71	32 1/2	3.89	---	36(E)	36 1/2 (10.9d)	41(M)
63	R	22.50-23.49	23.32	11	6.48(I)	---	16 1/2 (E)	20 (25d)	25(E)
67	L	23.50-24.49	23.77	18 1/2	7.21(I)	---	24 1/2 (M)	---	34 1/2 (M)
71	S	24.50-25.49	25.40	16	4.60(I)	---	20(E)	21 (10.9d)	26 1/2
72	C	25.50-26.49	25.50	15	4.44	---	19(E)	20 (11.9d)	25(M)
82	P	26.50-27.49	26.49	16 1/2	4.81(I)	20 (5.9d)	20 1/2	---	27(E)
91	P	27.50-28.49	28.47	4	5.56(I)	---	8 1/2 (M)	---	16 1/2 (E)
93	P	28.50-29.49	29.20	5	5.84(I)	---	10(M)	---	18(E)
95	C	29.50-30.49	29.70	6	6.03	---	11(M)	---	19 1/2 (M)
---	---	30.50-31.49	---	---	---	---	---	---	---
96	P	31.50-37.49	30.53	0	0.00	---	0	---	---

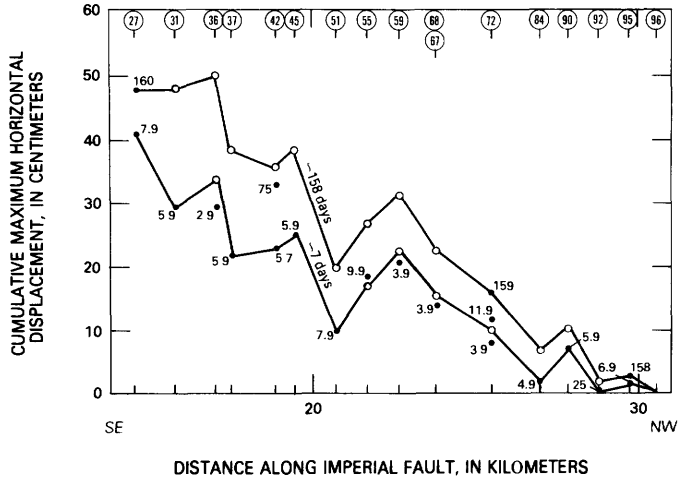

FIGURE 102.—Distribution of cumulative maximum horizontal displacement on Imperial fault northwest of area near McConnell Road at approximately 7 and 158 days after earthquake. Dots, maximum horizontal slip measured on day indicated for each 1-km segment of fault; circles, slips computed for other times, based on slip rates obtained by linear interpolation from adjacent b values in figure 99. Locality numbers same as in figure 99.

parts of the fault surfaces. At depth the displacement profile over the entire length of the fault may be much smoother and more closely modeled by a profile of horizontal slip constructed by connecting the largest surface-displacement maxima. Curve B in figure 103 shows that the cumulative growth of such an upper bound of the average horizontal displacement is only slightly larger than, but similar in slope to, the growth curve for the average displacement (curve C) and indicates that the upper-bound average lateral displacement is consistently about 4 to 5 cm larger than that obtained from the measured offsets. The upper-bound curve for cumulative horizontal displacement may be a more accurate estimate of fault offset at seismogenic depths (about 5–8 km) for this region.

Although the vertical component of displacement is greater than the horizontal component over much of the north half of the surface rupture on the Imperial fault and smaller for the south half, the vertical component generally has the same sense (upward on the southwest side) throughout its length (fig. 104; tables 21, 22)

TABLE 22.—*Lateral and vertical components of slip on the Imperial fault, the Brawley fault zone, unnamed intervening faults, and the Rico fault*

[Features: C, concrete canal liner; L, releveling array on pavement; K, crack in cultural feature; P, crack in ground surface; S, scarp at fault rupture; T, linear mark on ground surface. Positive values of lateral slip component are right lateral in sense, negative values are left lateral. Positive values of vertical slip component indicate west side up, negative values east side up]

Locality	Feature	Distance along reference line (km)	Slip component (cm)		Days after earthquake
			Lateral	Vertical	
Imperial fault					
30	T	15.9	28	10	4
31	P	15.9	30	---	6
32	S	16.0	---	4	6
33	S	16.1	---	11	6
34	P	16.4	21	12	8
35	S	16.8	---	5	6
36	T	17.2	29.5	4	3
37	T	17.6	22	---	6
38	S	17.8	---	~10	6
39	P	18.2	~0	17	6
40	P	18.2	~0, ~0	24, 36	8, 159
41	P	18.8	18±5	37	10
43	S	19.2	---	15	6
44	P	19.2	16	1	6
45	P	19.6	25	1	6
46	T	19.8	22	6.5	9
47	S	20.1	---	5-10	6
48	P	20.2	6½	28½	8
49	P	20.3	7	12	6
50	P	20.8	1½	1	9
51	P	20.8	9	~0	8
52	P	21.4	4	0	9
53	P	21.4	0	½	9
55	P	21.8	18½	6	10
56	P	21.9	16½	7½	9
57	S	21.9	~0	6	?
58	T	22.6	~15	~10	49
59	T	22.7	20½	---	4
60	P	22.9	23	18	25
61	T	23.2	~16½	9	---
62	P	23.3	7½	6½	9
64	P	23.4	4½	6	25
65	P	23.7	~0	16	4
66	P	23.7	~0	27½	25
68	P	23.8	14	10	4
69	P	24.2	8	3½	4
70	S	25.2	---	7½	5
73	S	25.8	---	11	158
74	P	25.9	1½	16	158
75	S	26.1	---	15	158
76	P	26.4	2.2	7½	158
77	S	26.5	---	11½	158
78	S	26.7	---	15	158
79	S	26.8	---	9	158
80	P	26.1	½	6½	5
81	P	26.3	~0	17	5
83	S	26.7	---	20	6
84	P	26.9	2.2	5	5
85	T	26.2	0	-6	159
86	T	27.2	0	13	159
87	S	27.7	---	1	25
88	P	27.9	~0	1½	6
89	P	28.2	~0	2	25
90	P	27.8	7	2½	6
91	P	28.5	~0	8½	6
92	P	28.8	~0	6½	25
94	P	29.6	~0	6	7
Brawley fault zone					
97	S	13.95	---	-2-7	6
98	K	13.4	~0	~0	6
99	K	11.9	~0	~0	6
100	C, L	10.7	7½	-9½	2
101	C, L	10.0	4	-12½	49, 23
102	T, S	9.9	~0	~-10	6
103	S	8.7	~0	~-10	10
104	S	8.1	~0	~-6	10
105	K	7.9	~0	~0	9
106	C, L	7.1	7½	-7½	49, 3
107	L	7.1	~0	-7	7
108	S	6.6	~0	-8	4
109	T	4.0	½	-1½	49
110	P	3.9	~0	-1	4
111	S	3.7	~0	~-10	49
112	S	3.4	~0	-15	49
113	S	3.3	~0	-20	49
114	S	3.3	~0	-24	49
115	L	3.0	---	-10	3
116	C	2.3	~0	-4½	4
117	P	1.28	3	-2	4
Unnamed faults between Imperial fault and Brawley fault zone					
118	C, L	---	-11	-4	50
119	C	---	-9	13½	5, 50
120	S	---	~0	~10	5
Rico fault					
121	L	---	~0	~20	7

BRAWLEY FAULT ZONE

Discontinuous and multiple-stranded fractures along a 13.1-km-long zone on the east side of the Mesquite basin formed at the ground surface at the time of the earthquake. Although pre-1979 surface faulting documented in parts of this approximately north-south oriented zone have been ascribed to structures termed the "Brawley fault" (Sharp, 1976), the number and distribution of 1979 surface ruptures make the term "Brawley fault zone" more appropriate.

Vertical displacement in the Brawley fault zone, wherever detectable, was uniformly downward on the west side for all surface breaks. In most places the vertical component apparently was dominant, although at several sites cultural features were also displaced right-laterally during the 1979 earthquake nearly as much as vertically. On the westernmost breaks in the Brawley fault zone, horizontal slip was detected at localities 100, 101, 106, and 117, although dextral components of slip may have been overlooked elsewhere in cultivated fields. Only at Robinson Road (loc. 109) did we measure a right-lateral-slip component on an east

break within the zone. Although the vertical component of slip throughout the length of the Brawley fault zone was smaller than the maximum vertical components measured along the Imperial fault rupture on the west side of the Mesquite basin, at some places the accompanying strike-slip components were larger along the Brawley fault zone than on the northern section of the Imperial fault (see tables 21, 22).

Some multiple strands in the Brawley fault zone were recognized from 1975 surface faulting (Sharp, 1976) and studies of Holocene scarps and photolineaments (Sharp, 1977b). The 1979 surface displacements, however, demonstrated both greater length of some fault strands than was previously known and reactivation of preexisting fault strands that were heretofore unrecognized. By combining the newly discovered fault strands with the pattern of earlier known Holocene and historical breaks, we obtain an overall picture of marked complexity for this zone of faulting.

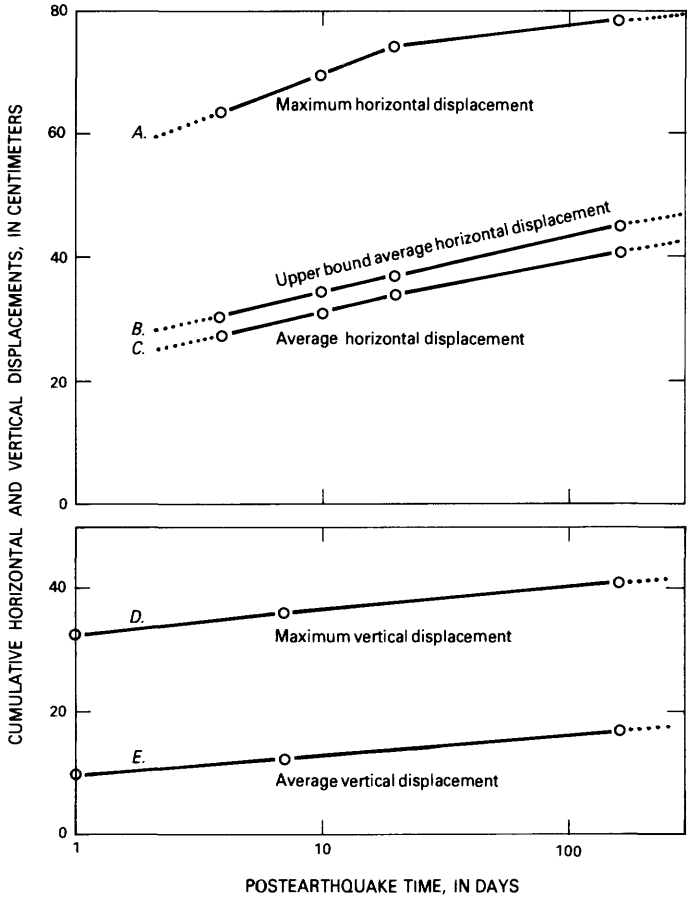

FIGURE 103.—Maximum and average cumulative horizontal and vertical components of displacement as a function of postearthquake time. Circles represent determined values of displacement components. *A*, Maximum cumulative horizontal displacement. *B*, Upper bound of average horizontal displacement, obtained by smoothing displacement profiles in figure 101 by considering only slip measurements that maximize area under curves. *C*, Average horizontal displacement, obtained by dividing area under profiles in figure 101 by length of fault trace. Plots of maximum (*D*) and average (*E*) cumulative vertical component of slip are derived from profiles in figure 104 in same way as for horizontal component, except for values at 1 postearthquake day, which were obtained from extrapolated vertical-displacement profile (not shown).

DESCRIPTION OF SURFACE RUPTURES

Surface breaks along the Brawley fault zone resemble those that formed in January 1975 in every respect. The ruptures commonly consisted of left-stepping echelon cracks that gaped a few millimeters to a few centimeters, although several longer and more continuous breaks were commonly made up of a single crack that only sporadically stepped over to an echelon fracture. With very few exceptions, the cracks formed near the rounded crest of a scarp that sloped westward into a linear sag paralleling the zone of cracks. Leveling profiles of the roads crossing the Brawley fault zone (fig. 105; Sharp and Lienkaemper, this volume) show that the scarps were typically rounded, both at their bases and at their crests, and this profile was easily seen in the fields of newly planted crops. The width of the sag was approximately proportional to the height of the associated scarp in many fields. Although accurate measurements were not possible, a few breaks appeared not to displace the surface of the field noticeably 10 m or more from the sag, even though erosional effects on several scarps after postearthquake irrigation of the fields suggested that real changes in level had distorted the uniform drainage gradients established before planting (fig. 106). Though relatively rare, a few surface ruptures formed abrupt escarpments that in profile were steplike instead of rounded.

Continuity of the surface rupture varied widely. At one extreme were echelon cracks in a zone perhaps only a few meters long, at scattered intervals as much as hundreds of meters apart along one strand of the fault. These widely spaced cracks can be assigned to one particular strand on the basis of the location either of the 1975 rupture or of prehistoric fault traces visible on earlier aerial photographs. At the other extreme were several remarkably continuous fault ruptures (figs. 107, 108) that generally formed single cracks with a few echelon stepovers. Within the longest (4 km) nearly continuous rupture in the Brawley fault zone, only a few echelon stepovers and discontinuities were recognized (partly owing to heavy crop cover in one field). This break (fig. 109) formed the easternmost of three ruptures that crossed Harris Road (loc. 107).

As in the northern part of the Imperial fault, irregularity in trend was common among breaks in the Brawley fault zone. The map trace of the longest nearly continuous rupture in the zone has relatively large irregularities, as well as small abrupt changes in trend (figs. 108–110), many too small to be adequately represented on the map (pl. 1).

DISPLACEMENT

Where vertical displacement was detectable on surface ruptures in the Brawley fault zone, its sense was downward on the west side. At localities where the rupturing appeared to be incipient, cracks commonly showed a small extensional opening only, with no obvious rounded scarp or vertical displacement.

Because the vertical and horizontal deformations across breaks in the Brawley fault zone typically were at least 5 m wide, accurate determinations of the amount of slip were possible only in a few places. We obtained the most complete measurements of displacement at Keystone Road (loc. 100), Harris Road (loc. 106), and Worthington Road (loc. 115), where leveling-survey lines were established before the earthquake (table 22). Table 22 also lists a few relatively crude measurements in newly plowed or crop-covered fields.

Keystone Road (loc. 100).—We determined horizontal and vertical components of slip at Keystone Road by measuring the misalinement of the previously straight canal liner on the north side of the road and by releveling the array of nails in the pavement of the road, respectively. The change of elevation across the fault was about 9 to 10 cm, spread across a zone as wide as 15 m (Sharp and Lienkaemper, this volume, fig. 133*B*). The right-lateral component of slip was measured by alidade sighting, which showed misalinement of the canal by about 7.3 cm. The canal was known to have been visually straight (approx ±1 cm) on January 17, 1979, before the earthquake, and so we attribute this misalinement to the displacement of October 15, 1979. Combining these measured components describes the slip only for a vertical fault surface. Leveling profiles of the 1979 displacement suggest that the fault dips west toward the Mesquite basin (Sharp and Lienkaemper, this volume); thus, an unknown amount of east-west extension may have occurred at Keystone Road. The plunge angle of slip at Keystone Road of about 51° to 54° for an assumed-vertical fault surface indicates right oblique displacement. If the fault surface actually departs from verticality, these plunges are maxima. Unfortunately, no geologic data from trenching or other sources are available from which to measure the fault dip directly, and the accuracy of location of earthquake foci probably is not yet sufficiently good for a reliable determination of dip. Nevertheless, the form of the vertical-displacement profiles suggests a steep dip toward the west.

Harris Road (loc. 106).—We measured the vertical and horizontal slip components at Harris Road in the same way as at Keystone Road. A concrete-lined canal was right-laterally offset about 7.3 cm, as measured by alidade, and the vertical component of displacement was about 5.1 cm on the westernmost break and about

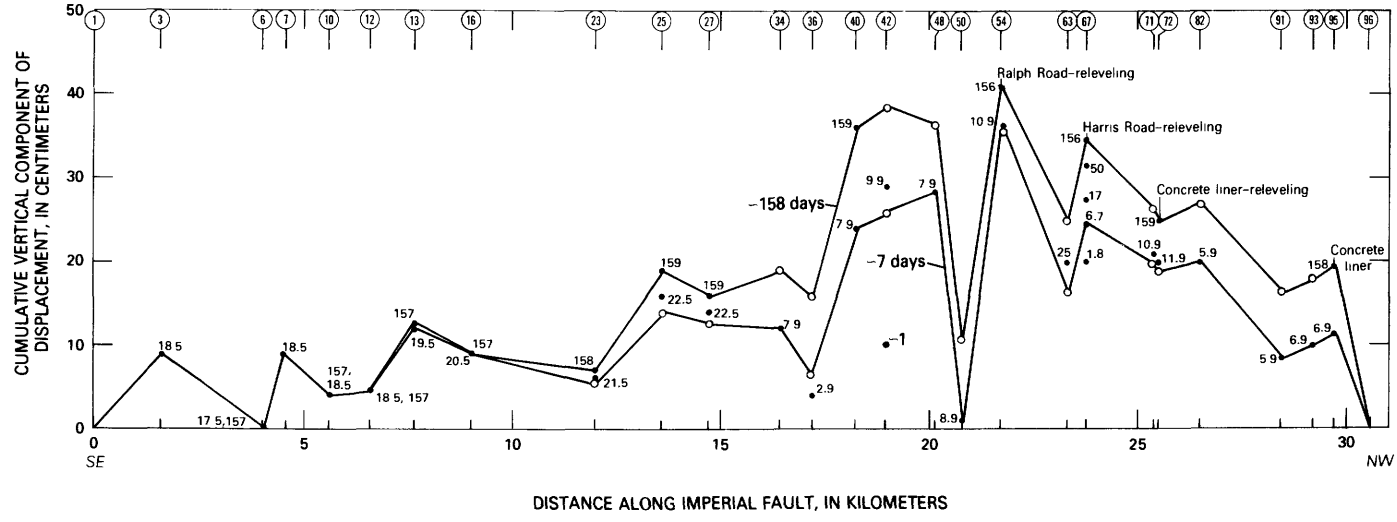

FIGURE 104.—Vertical component of displacement as a function of distance along Imperial fault (see tables 21, 22). Sense of displacement is upward on southwest side. Profiles at approximately 7 and 158 days after earthquake indicate that sense of net vertical component generally did not reverse along length of surface rupture (one local reversal is shown in fig. 92). Dots, vertical component of displacement measured on day indicated; circles, vertical component of displacement interpolated or extrapolated from measurements at other times. Data for localities 3 through 29 may include some preearthquake creep. Locality numbers same as in figure 99.

2.5 cm on a second break about 24.5 m to the east (Sharp and Lienkaemper, this volume, fig. 134*C*). The horizontal offset was measured on the westernmost break in the zone, and so by combining its components, displacement is described as right oblique slip with a plunge of about 35°, for an assumed vertical fault. No evidence of disturbance on the second break was detected on the canal liner; it either died out abruptly northward or caused only indiscernible deformation.

A third surface rupture in the Brawley fault zone crossed Harris Road about 0.4 km east of the breaks already discussed; this break had not been previously recognized, and consequently no preearthquake leveling was done. We made a leveling survey across the break on October 22, and the resulting profile of the pavement indicated a rounded scarp about 7 cm high (Sharp and Lienkaemper, this volume, fig. 135). This vertical uplift must have occurred since paving of the road in 1970, although most of it may have been associated with the 1979 earthquake.

Worthington Road (loc. 115).—Only the vertical component of displacement could be measured at Worthington Road because the canal liner crossing the surface rupture here was constructed with irregularities that made determination of the horizontal component impossible. Repeated leveling surveys before and after the earthquake indicated about 9.5 cm of relative vertical displacement. The displacement curve (Sharp and Lienkaemper, this volume, fig. 136*A*) shows that the base of the sag at the foot of the new scarp lay 15 to 20 m west of the surface fractures.

Other localities.—We made measurements of both horizontal and vertical components of displacement on surface ruptures in the Brawley fault zone at only two additional points (locs. 109 and 117), the second of which is at the southernmost extremity of rupture in the zone (fig. 106). All other measurements of individual components of slip are listed in table 22.

MAXIMUM DISPLACEMENT

Despite the difference between the 10- and 15-cm vertical components of displacement measured in the Brawley fault zone at Keystone and Harris Roads, the amount of oblique slip appears to be approximately equivalent at these two localities. Although substantially larger displacement may have occurred within fields where measurements could not be made, the largest recorded components of displacement on a single

FIGURE 105.—Scarp of Brawley fault zone at Keystone Road (loc. 100). Cracks (dark line) in pavement formed at crest of scarp where flexure of ground is maximum. Base of scarp generally is on west side of cracking for all strands of Brawley fault zone. This position of cracking with respect to base of scarp is generally present in fields as well as at road intercepts. Leveling of profile before and after earthquake indicated that about 9 cm of total relative uplift of about 16 cm at scarp was due to October 15 earthquake. Across an 80-m-wide zone centered on fault scarp, total relative uplift since road was paved in 1960 or 1961 is about 0.5 m. View eastward. Photograph by R. V. Sharp, October 17, 1979.

FIGURE 106.—Southernmost surface ruptures in Brawley fault zone (loc. 117). Two subparallel ruptures (arrows) curve southwest toward distant edge of field in center foreground. Although this field was newly plowed at time of earthquake and loose soil did not show fault rupture well, erosion on steepened slope of scarp caused by irrigation after earthquake enhanced visibility of disturbance of originally smooth sloped preearthquake surface. View westward. Photograph by M. J. Rymer, December 12, 1979.

break (at Keystone Road) indicate right-normal oblique slip (nomenclature of Bonilla and Buchanan, 1970) of about 12 cm at a plunge of less than 51° on a fault surface here interpreted to dip steeply west. Summing the components of slip for the three breaks at Harris Road, we obtain a composite maximum angle of right-normal oblique slip ranging from 11 to 16 cm and a plunge angle ranging from less than 46° to 63°. For the maximum displacement at Harris Road, the net right-lateral component used in the computation was that on the west break alone; we measured no lateral displacement on the two breaks farther east. The dip angles for breaks in the Brawley fault zone are mostly unknown, although the direction of dip is assumed to have a consistently westward component on the basis of similarity of the profiles of vertical displacement (W. R. Thatcher, oral commun., 1979).

AFTERSLIP

In contrast to the Imperial fault, surface ruptures in the Brawley fault zone showed little or no significant afterslip, at least at the three localities where repeated leveling was done. On the west breaks in the Brawley fault zone at Harris Road, however, minor westward tilting of the ground surface without vertical movement at the fault traces has been recorded (Sharp and Liendkaemper, this volume). This tilting, which apparently extends beyond the end points of the 0.25-km-long leveling profile, as of December 30, 1979, was proceeding at a calculated rate of about 13 microradians per month. Vertical afterslip at Keystone and Worthington Roads was negligible as of 156 days after the main shock.

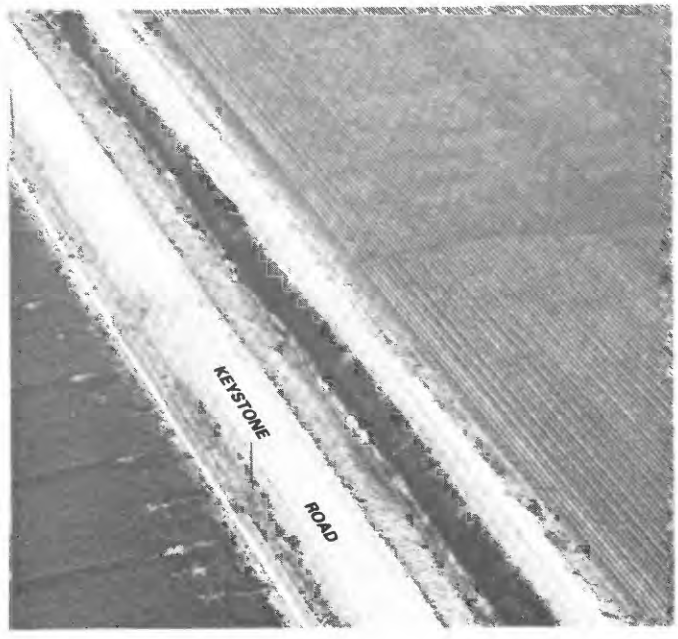

FIGURE 107.—Brawley fault zone at Keystone Road (loc. 100). Cracks in pavement and in field to right follow trace of 1975 surface displacement. Dark vegetation just east of trace formed abrupt lineament at fault trace before earthquake; part of darkness at trace is due to low-sun shadowing of scarp that faces west toward camera. Fracturing near crest of scarp generally forms single continuous break, although locally multiple echelon fractures also occur on this fault strand. View east-southeastward. Photograph by M. J. Rymer, October 23, 1979.

SUBSIDIARY FAULTING IN THE MESQUITE BASIN

We observed four surface ruptures in relatively isolated places in the Mesquite basin. The locations, orientations, and left-lateral sense of the horizontal component of displacement of these ruptures suggest that they should not be included with surface rupturing on the Imperial fault or in the Brawley fault zone. All the breaks trended northeast-southwest and were 5 to 6 km south of the center of the Mesquite basin. The three east breaks were roughly alined, though separated by gaps of nearly 1 km. The sense of the vertical component of movement reversed from downward on the northwest side at the easternmost break (loc. 118) to downward on the southeast side at the westernmost break (loc. 119). The central break was a zone of minor cracks crossing a

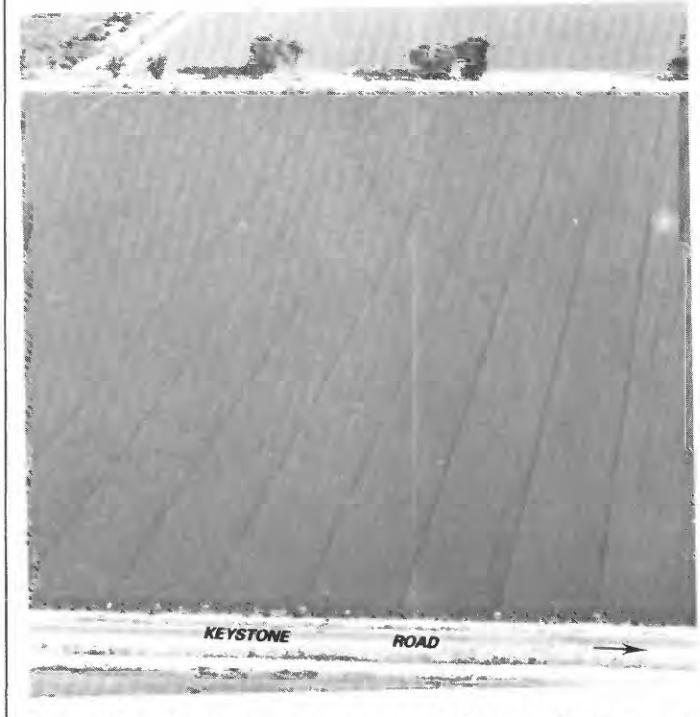

FIGURE 108.—Previously unknown strand of Brawley fault zone (at 11 km) near Keystone Road. Low sun from right (east) casts shadow of west-facing scarp, shown here on surface of an alfalfa crop. Long sinuous rupture dies out in each direction within field. Rupture that crosses Keystone Road in foreground (arrow) is only partly visible in alfalfa field. Vertical and horizontal components of displacement were measured on surface of Keystone Road by leveling and by sighting alinement of canal (white line) behind power pole, respectively. View northward. Photograph by M. J. Rymer, October 23, 1979.

canal, which may have been slightly offset laterally but not vertically. These three breaks may have represented discontinuous surface ruptures on a single preexisting fault strand. A photolineament that coincided with the easternmost break extends southwestward, but not as far as the more westerly breaks. The westernmost of these three breaks may coincide with a nearly parallel but more southerly fault. Vertical and horizontal components of displacement measured on the canal at the easternmost break (loc. 118), about 4 and 11 cm, respectively, combine to give an apparent left-oblique slip of nearly 12 cm and a slip plunge of 19° for a vertical fault. The dip of the fault at this locality is unknown, but if it is a normal fault (as suggested by the geologic environment of the Mesquite basin), some part of the left-lateral component of displacement could be an apparent horizontal offset due to the northwestward downdip component on a nonvertical fault. For example, the measured vertical component of slip would yield an apparent left-lateral offset of only 1.9 cm on a north-south-alined canal due to downdip slip on a fault surface dipping 70° NW. The fault surface at the west end of the three nearly alined breaks appeared to be vertical where it crossed a ditch on the south side of Robinson Road (loc. 119), and the slip there consisted of a left-lateral component of about 8 cm and a vertical component of 13 to 14 cm. The plunge angle of slip was about 60°.

Another subsidiary surface rupture broke the floor of the Mesquite basin about 0.5 km north of Robinson Road and 0.6 km east of State Highway 111 (loc. 120). Although the relative sense of vertical movement (downward on the east side) was easily seen in the crop-covered field, the height of the rounded scarp was

FIGURE 109.—Newly discovered east trace of Brawley fault zone at Harris Road (loc. 107). Sinuous break extends to foreground edge and beyond but is not entirely visible in this view. More nearly linear trace in mown alfalfa field north of Harris Road is marked by line of dark vegetation. View northeastward. Photograph by M. J. Rymer, October 23, 1979.

FIGURE 110.—Surface rupture of Brawley fault zone (loc. 114) in field north of Worthington Road (loc. 115). Wide dark spot on pavement (arrow) represents repairs to surface rupture at Worthington Road. Cracks in field, visible as erratic line extending through two excavations (dark areas), mark trace of fault strand. Cracks were traceable only after harvest of dense soybean crop more than a month after earthquake. View northeastward. Photograph by M. J. Rymer, December 12, 1979.

estimated at less than 10 cm. East-west-alined crop rows appeared to be consistently shifted to the left by a maximum of about 10 cm.

Subsidiary faulting in the southern part of the Mesquite basin is the only surface evidence to date that substantiates the existence of fractures conjugate to those making up the Imperial fault and the Brawley fault zone that bound the basin. Although northeast-trending structures have been suggested by the distribution of epicenters of swarms of small earthquakes in the Mesquite basin (Johnson and Hill, this volume), epicenters of seismic events both before and after the 1979 earthquake mostly lay north of the subsidiary breaks described here. No surface rupturing was observed near the center of the Mesquite basin, below which much of the aftershock activity was heavily concentrated.

RICO FAULT

Ground fractures and an apparently new scarp that formed along an approximately north-south trending line about 1.5 km west of Holtville, Calif., strongly resembled breaks within the Brawley fault zone. Because of heavy crop cover in fields along this break, we have characterized these fractures as indicating a fault from evidence in three places only: at the intersection with County Highway S–80 near the Rico railroad siding, at Holton Road 75 m farther north, and at Zenos Road (loc. 121). In each place the road surfaces were deformed to a rounded scarp, downward on the west side, similar to breaks in the Brawley fault zone. We observed no evidence of horizontal shifting of the ground surface at these localities.

We constructed a profile of the Rico fault rupture from leveling observations along Zenos Road (fig. 111); in form, this profile strongly resembles those across the Brawley fault zone (Sharp and Lienkaemper, this volume). Vertical displacement across a 20-m-wide zone was nearly 20 cm; part of this relative uplift, however, could have predated the earthquake. Although one resident near the fault trace at Zenos Road stated that the cracking and uplift became visible within a few minutes after the earthquake, evidence at Holton Road indicated that at least part of the uplift there was preearthquake. The graded but loosely graveled surface of Holton Road appeared to have been scraped only at the crest of the scarp to reveal its densely packed base. This scraping of the road base (noted on October 18), probably caused by passage of a grading machine before the earthquake, suggests that a scarp existed before the earthquake.

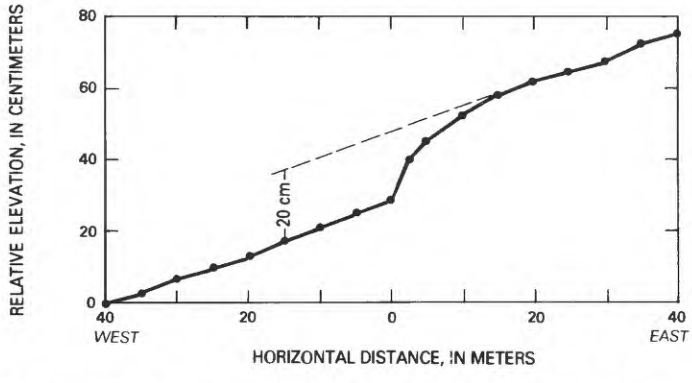

FIGURE 111.—Profile of relative elevation across Rico fault at Zenos Road (loc. 121). Dots joined by solid line indicate elevations across scarp measured on south edge of pavement. Dashed line denotes estimated original slope of pavement, with estimated vertical displacement shown.

Continuity of the surface rupture between Zenos and Holton Roads could not be proved because of dense crop cover in the intervening field. However, the alinement and continuity of the surface rupture from Holton Road southward across the track at the Rico railroad siding, the adjacent track connecting Holtville and El Centro, and both lanes of County Highway S–80 suggest that the break at Zenos Road was an extension of the same fault. Less is known about continuity of the fault south of the highway because a dense crop of cotton covered the trace at the time of investigation. Hairline extensional cracks on line with the surface ruptures on a dirt road parallel to and 0.2 km south of the highway may have marked the fault trace there, although vertical displacement was not apparent. Both the minuteness of cracking on the dirt road and the absence of any surface fracturing farther south suggest that the total length of the Rico fault rupture was about 1 km.

Other than the evidence for preearthquake disturbance at Holton Road, we observed no clear signs of either prehistoric movement or greater extent of an older fault structure beyond the limits of the 1979 surface rupture. Aerial photographs of the Imperial Valley taken in 1937 showed no obvious photolineaments or escarpments intact at that time. Such rupturing, locally conspicuous but limited in extent and remote relative to other known faulting, background seismicity, and aftershock activity in the central Imperial Valley, suggests that this displacement was triggered in the same way as that on the San Andreas and Superstition Hills faults. The Rico fault probably is not new, but at present we know little about its past history.

ACKNOWLEDGMENTS

The data on displacement included in the tables were collected by all the authors. J. J. Lienkaemper and R. V. Sharp assembled and interpreted the data, and Sharp wrote the text of this chapter.

REFERENCES CITED

Bonilla, M. G., and Buchanan, J. M., 1970, Interim report on worldwide historic surface faulting: Menlo Park, Calif., U.S. Geological Survey open-file report, 32 p.

Bucknam, R. C., Plafker, George, and Sharp, R. V., 1978, Fault movement (afterslip) following the Guatemala earthquake of February 4, 1976: Geology, v. 6, no. 3, p. 170–173.

Buwalda, J. P., and Richter, C. F., 1941, Imperial Valley earthquake of May 18, 1940 [abs.]: Geological Society of America Bulletin, v. 52, no. 12, pt. 2, p. 1944–1945.

Richter, C. F., 1958, Elementary seismology: San Francisco, W. H. Freeman, 768 p.

Sharp, R. V., 1976, Surface faulting in Imperial Valley during the earthquake swarm of January–February, 1975: Seismological Society of America Bulletin, v. 66, no. 4, p. 1145–1154.

———1977a, Holocene traces of the Imperial fault in south-central Imperial County, California: U.S. Geological Survey Open-File Report 77–815, 1 p., scale 1:24,000, 5 sheets.

———1977b, Map showing Holocene surface expression of the Brawley fault, Imperial County, California: U.S. Geological Survey Miscellaneous Field Studies Map MF–838, scale 1:24,000.

Ulrich, F. P., 1941, The Imperial Valley earthquake of 1940: Seismological Society of America Bulletin, v. 31, no. 1, p. 13–31.

DISPLACEMENT ON THE SUPERSTITION HILLS FAULT TRIGGERED BY THE EARTHQUAKE

By GARY S. FUIS,
U.S. GEOLOGICAL SURVEY

CONTENTS

ABSTRACT

Fresh surface breaks found along the Superstition Hills fault 4 days after the October 15, 1979, earthquake were mapped during the following month. These breaks occurred along the entire mapped length of the fault, a distance of 22.5 km. All clear horizontal displacements were right lateral and ranged from 1 to 22 mm in extent; minor vertical components of displacement were measured in some places. Displacement was irregular along the fault; maximum displacement was within 7 km of the northwest end of the fault.

The 1979 break had the same overall length and end points as the 1968 break. The maximum displacements are also similar but occur toward opposite ends of the fault, in each case away from the triggering earthquakes. Fewer than half of the more prominent mapped gaps in the breaks can be correlated.

Of the several possible triggering mechanism, shaking is consistent with most of the available information, whereas other mechanisms are inconsistent in part or unsupported by clear evidence. Oppositely skewed displacement curves for the 1968 and 1979 ruptures may represent, on one hand, complementary slip or, on the other hand, slip triggered in oppositely varying stress fields.

INTRODUCTION

After the Borrego Mountain, Calif., earthquake of April 9, 1968, geologists discovered displacements on three major faults at some distance from the zone of aftershocks and displacement associated with that earthquake (Allen and others, 1972). The Superstition Hills, Imperial, and San Andreas faults, at minimum distances of 30, 65, and 40 km, respectively, from the Borrego Mountain epicenter, showed consistent right-lateral displacements, ranging from 10 to 25 mm, along similar fault lengths, ranging from 20 to 30 km. These displacements are believed to have been triggered by the Borrego Mountain earthquake.

These triggered displacements are important to an understanding of fault mechanics in the Salton Trough. First, the displacements were apparently not associated with earthquakes in their immediate vicinity, although earthquakes of magnitude less than about 4.5 may have escaped detection during the first several minutes after the Borrego Mountain main shock. Certainly no aftershock zones developed along these distant breaks. Second, these displacements differ from coseismic displacements in their ratio of average offset to length of break; coseismic offsets in the range 0.1–1 m are expected (see Clark, 1972; Sharp and others, this volume). Third, although the time of occurrence of these breaks at the surface is uncertain, they may have appeared a few days after the Borrego Mountain main shock. Other examples of triggered displacement in the Salton Trough for which the timing is known indicate a lag of a few days (Allen and others, 1972; Sieh, this volume).

With the 1968 triggered displacements in mind, geologists searched the traces of several faults in the Salton Trough, including the Superstition Hills, Superstition Mountain, San Andreas, and Coyote Creek faults, for similar displacements after the 1979 Imperial Valley earthquake. Fresh ground breakage was observed along the Superstition Hills and San Andreas faults, and, although no surface breaks were discovered along the Coyote Creek fault, a resurvey of an alinement array across that fault revealed an unexpectedly large offset since the last measurement (P. W. Harsh, oral commun., 1979). No breaks were seen along the traces of the Superstition Mountain fault. Displacements on the Superstition Hills and San Andreas faults in 1979 are strikingly similar to those observed in 1968: virtually the same segments of both faults broke, and maximum crack displacement was similar both times on the Superstition Hills fault, although the 1979 displacement on the San Andreas fault was about half that of 1968 (Sieh, this volume).

STRUCTURAL SETTING

The Superstition Hills and Superstition Mountain faults appear to be the southeastward continuation of the San Jacinto fault zone into the Imperial Valley (Sharp and Clark, 1972). Although both these faults appear to be seismically active (Fuis and Allen, 1979), ground breakage has been observed historically only along the Superstition Hills fault. Features commonly associated with Holocene faults in this region, such as low scarps in soft sedimentary deposits, offset gullies, and sharp narrow lines of vegetation, are far more numerous along the Superstition Hills fault. Together with the Imperial fault to the southeast and the Coyote Creek fault to the northwest, both of which have broken historically, the Superstition Hills fault appears to be an echelon segment in a zone of left-stepping right-lateral strike-slip faults (fig. 112). In this fault zone, the magnitude of the left step between the faults is 5 to 7 km.

In the Superstition Hills, the Brawley Formation of Dibblee (1954), consisting of relatively fine grained clastic basin deposits of Pleistocene age, has been uplifted and strongly folded northeast of the Superstition Hills fault. In contrast, beds of this formation on the southwest side of the fault strike parallel to the fault and dip steeply to gently southwest. At its northwest end, where its strike becomes westerly, the fault appears to die out in an anticline. At its southeast end, structure is obscure owing to poor exposure; the fault appears to die out as it approaches cultivated fields near the New River. A search of the bluff deposits of the New River by R. V. Sharp (oral commun., 1980) yielded no evidence of the fault, although such evidence could be hidden by colluvium. A string of epicenters east-southeast of this end of the fault (Fuis and Allen, 1979) may, however, indicate continuation of the fault at depth.

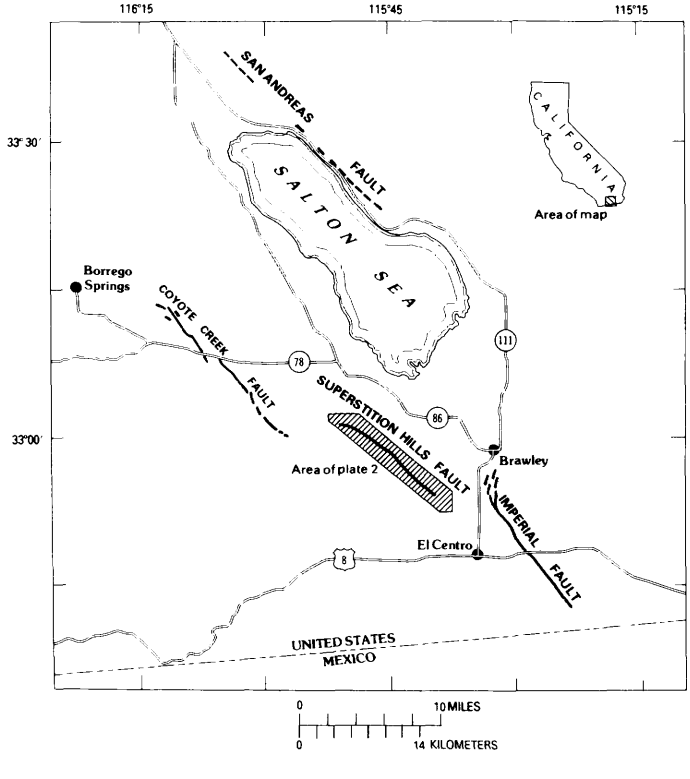

FIGURE 112.—Index map of Imperial Valley region.

1979 BREAK

I visited the Superstition Hills fault on the evening of October 19, 4 days after the main shock, and observed fresh cracks along the fault trace at the California Institute of Technology (CIT) creepmeter site (pl. 1) and also in the soil near a paved road that crosses the trace 4.1 km northwest of the creepmeter. No breaks were evident where the trace crosses Imler Road, 3.3 km southeast of the creepmeter. R. C. Gilman and D. C. Johnson, who had visited the creepmeter earlier (on October 18), measured 10.7 mm of right slip since the last measurement on August 23 (S. N. Cohn, oral commun., 1981). I proceeded to map the cracks between October 21 and November 15, during spare time between continuing seismic-refraction experiments (see Fuis and others, this volume). Two severe sandstorms that occurred on October 20 and 29 covered some cracks and eroded and filled many others, making them difficult to recognize. Surprisingly enough, most fault cracks remained fresh enough to be distinguished from other cracks in the area, including mud cracks and extensional cracks due to slumping of soil, and fresh enough to permit precise measurements of displacement. Even in places where the cracks were completely covered by sand, they could be traced as strings of sand dimples (created by draining of sand into the cracks).

As in 1968, breakage occurred along the entire mapped length of the Superstition Hills fault, from where it dies out in an anticline in the northwest Superstition Hills to where it is apparently buried by a thick sequence of young sedimentary deposits along the New River, a distance of 22.5 km (pl. 2). All clear horizontal displacements are right lateral and range from 1 to 22 mm in extent; minor vertical displacement occurs in some places.

The surface rupturing consists of two types of breaks: single straight breaks coinciding with the fault trace and showing right slip (fig. 113), and left-stepping echelon cracks trending individually more northerly than the fault trace but forming a narrow zone along the fault trace and showing opening in a direction parallel to the trace. These two types of breaks occur at many scales.

They occur next to each other along the fault trace and grade into one another. Where left-stepping echelon cracks are connected by crossbreaks in a zigzag pattern (fig. 114*A*), compressive features are seen; clods of delicately cemented soil are commonly thrust and folded along these crossbreaks (fig. 114*B*). The axes of these small folds generally trend west. Numerous thrust and folded clods give the appearance of a mole track (see Clark, 1972, fig. 29).

The single straight cracks occur in continuous segments that range from a few centimeters to more than 30 m and average approximately 1 m in length. The left-stepping echelon cracks range from a few centimeters to about 5 m and average 10 to 20 cm in length. The left step between cracks ranges from about 10 to more than 100 percent of the crack length and commonly is between 50 and 100 percent. Where the echelon cracks exceed about 3 m in length, they are shown schematically on the map (pl. 2). Although some echelon cracks as long as 100 m are shown, these features are actually zones consisting of shorter echelon cracks.

Where conspicuous, the fault is distinguished variously by: a low linear scarp several centimeters high, a sharp vegetation boundary or a line of vegetation, a lithologic boundary, vertical beds of resistant sandstone, gouge (rarely conspicuous), and linear drainage sumps as deep as 2 m but more commonly a few tens of centimeters deep (see Clark, 1972).

Displacements were determined along straight cracks by measuring the offsets between matching features and averaging the results of several measurements. In places where only echelon cracks were observed, the opening of these cracks in the direction of the fault trace was measured, and several measurements were averaged. Nearly all the horizontal displacements are right lateral and range from 1 to 22 mm

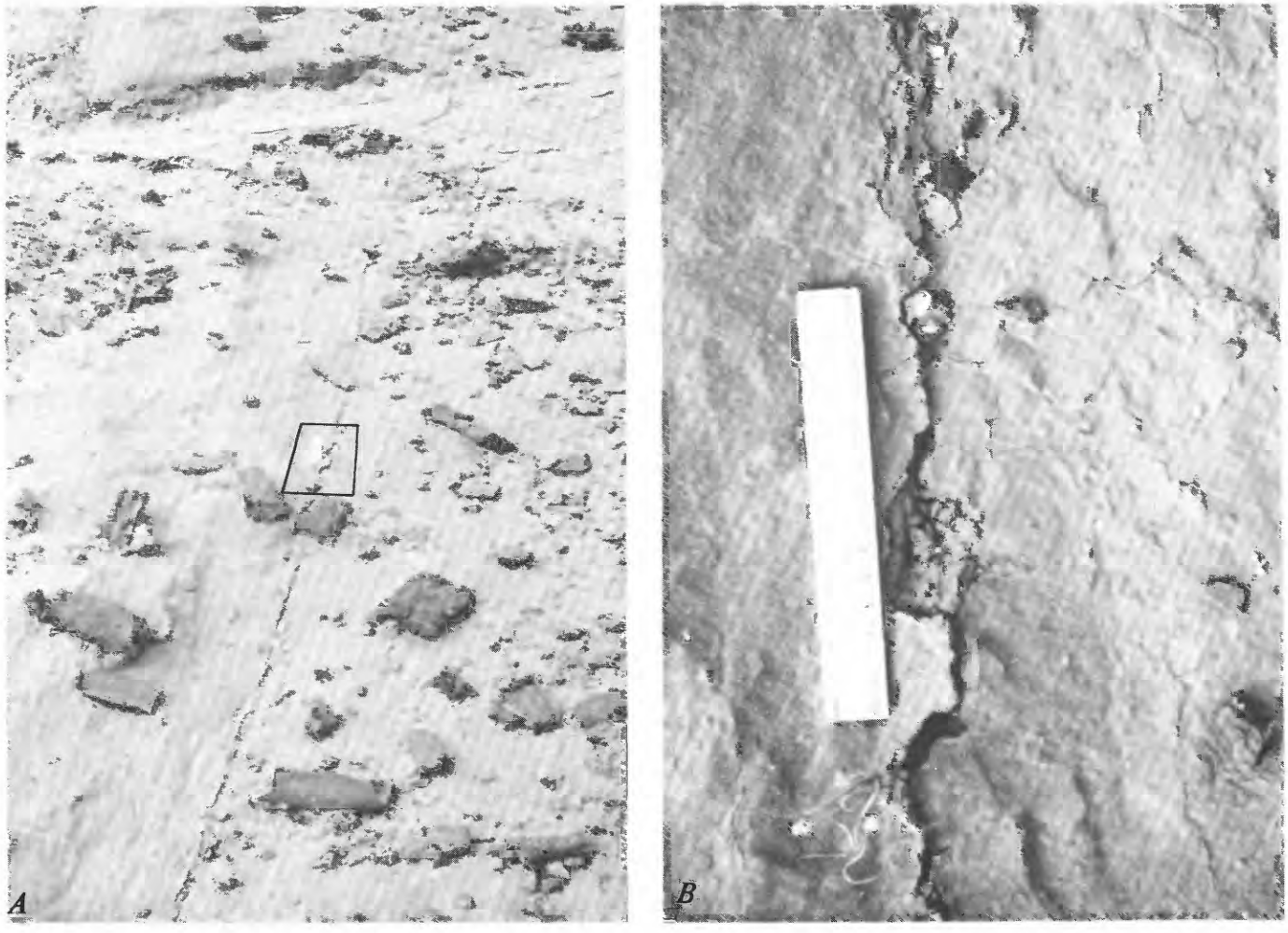

FIGURE 113.—Surface rupturing. *A*, Single straight break along Superstition Hills fault. *B*, Closeup of area in figure 113*A*, showing 7 mm of right slip. White ruler (circled) is 15 cm long.

in extent. In four localities, vertical components of displacement as large as 4 mm combined with right-lateral components to produce oblique slip (see pl. 2). All the vertical displacements are downward on the northeast side. In two of these localities, 1.4 km and 8.4 km northwest of the CIT creepmeter, vertical displacements occur along low scarps several centimeters high that are also downward on their northeast sides and are situated on the northeast sides of larger hills (or scarps). In the other two localities, 8.8 and 11.6 km northwest of the creepmeter, there are no conspicuous preexisting scarps, large or small, or else the area is hilly on both sides of the trace.

The plot of displacement against fault length (fig. 115) shows numerous spikes. Displacement is also irregular along the smallest crack observable. The displacements recorded on the map (pl. 2) are averages of the displacement maxima of individual cracks. Although cracks were covered by sand in some areas shown as gaps, most gaps are real, in that bare unbroken ground is observable for several meters on either side of the fault trace over much of a given gap. The longest continuous break is between about 3.5 and 11 km from the northwest end of the fault (pl. 2; fig. 115). The largest lateral displacements are seen along this break; they occur in several maxima as large as 22 mm. It may be significant that this interval is centered about 7 km from the northwest end of the fault and not at the geometric center of faulting, about 4 km farther southeast. The pattern of breaks both northwest and southeast of this interval includes, first, breaks about 1 km long separated by small gaps and characterized by twin peaks in displacement of as much as 10 mm; second, long gaps within the intervals 1.5–2.5 and 17–19 km (where distances are measured from the northwest end of the fault); and third, short breaks with displacement smaller than about 10 mm toward the ends of the fault. Thus, the pattern of ground rupturing is symmetrical in style but is skewed toward the northwest end of the fault.

COMPARISON WITH 1968 BREAK

The ground rupturing along the Superstition Hills fault in 1968 was mapped by Max Wyss and Arthur Grantz about a month after the Borrego Mountain

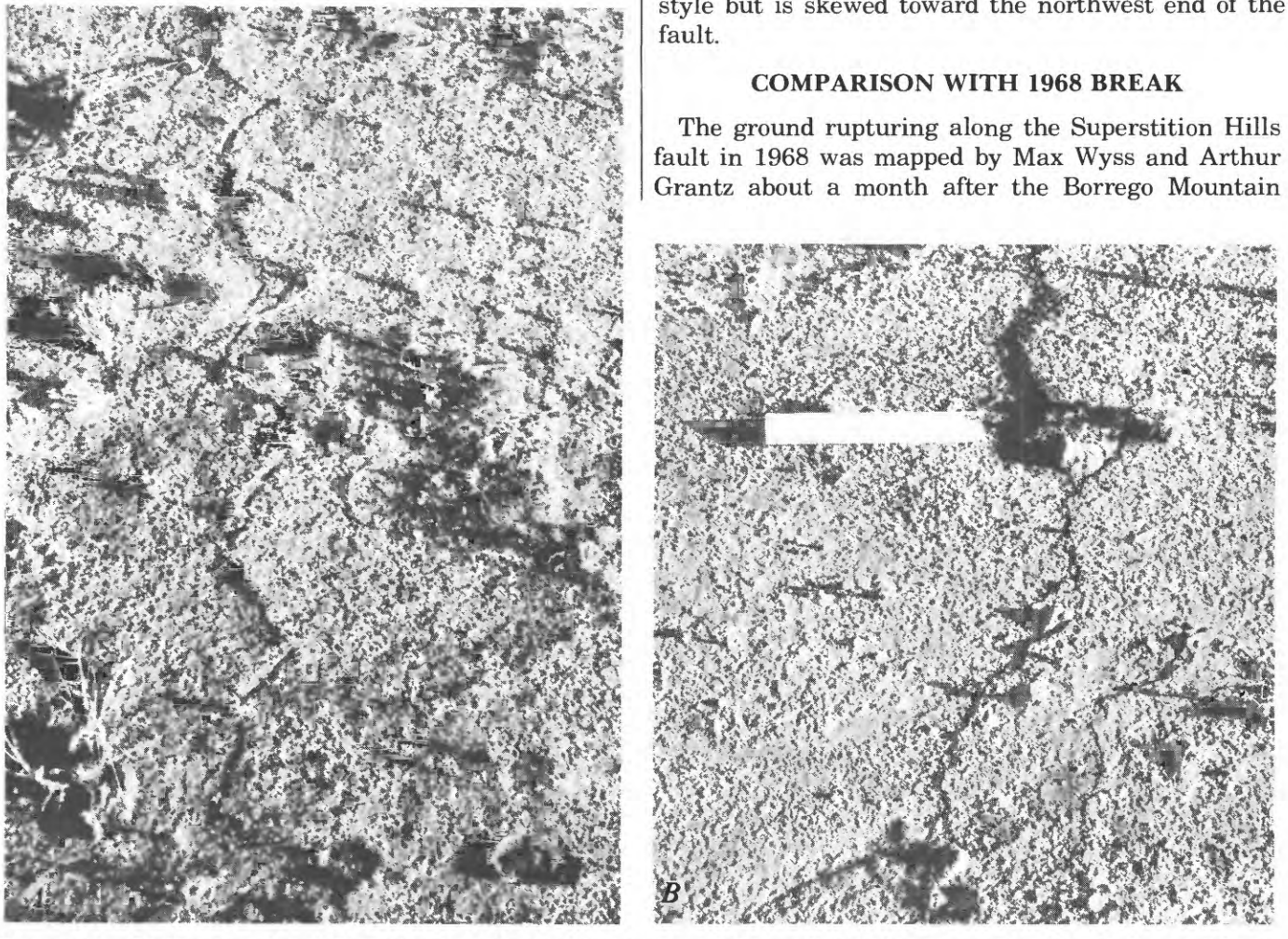

FIGURE 114.—Surface rupturing. *A*, Zigzag break consisting of left-stepping echelon cracks joined by compression ridges. Echelon cracks are about 20 cm long. *B*, Compression ridge connecting two left-stepping echelon cracks. Ridge consists of arched clod of delicately cemented soil a few millimeters thick. Axis of arch parallels ruler (15 cm long).

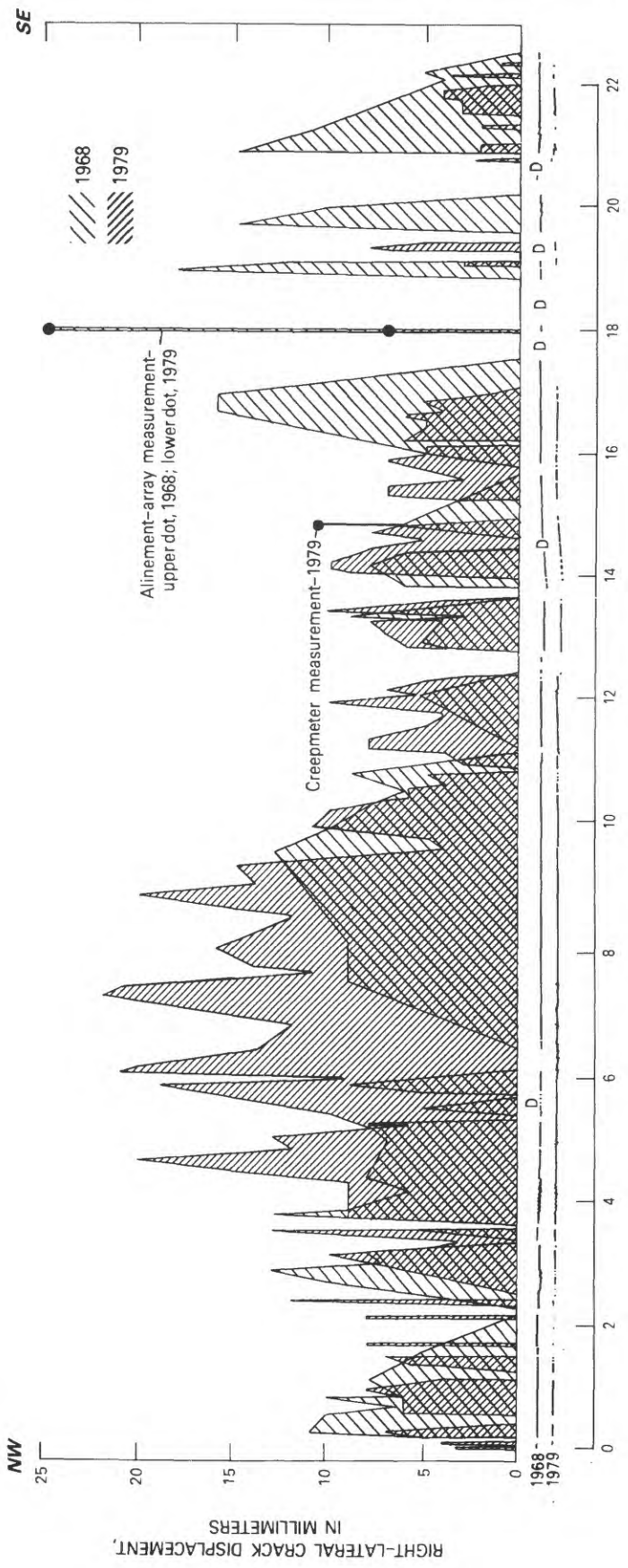

FIGURE 115.—Right-lateral displacement as a function of distance along Superstition Hills fault for 1968 and 1979 breaks. Actual breaks are plotted below diagram with general changes in strike removed, so that they appear as largely straight lines for ease of comparison. D, Dashed intervals on map of Allen and others (1972), representing intervals where evidence of surface rupturing was poorly preserved. Gaps greater than about 75 m on breaks are shown on displacement diagrams; dashed intervals on 1968 breaks are arbitrarily treated as gaps. Ranges in displacement reported by Allen and others (1972) in certain localities are averaged here. Alinement array was installed May 11, 1967; offset of 25 mm was measured between that date and April 19, 1968, spanning time of Borrego Mountain earthquake (Allen and others, 1972). Offset of about 7 mm was measured between May 24, 1979, and March 20, 1980, spanning time of October 15 earthquake (D. C. Johnson, written commun., 1980), but is queried because it may include left-lateral offset similar to that recorded on creepmeter several months after earthquake (see below). Creepmeter was installed after 1968 rupturing. Offset of 10.7 mm was measured between August 23 and October 18, 1979, spanning time of October 15 earthquake (S. N. Cohn, oral commun., 1981). This offset was followed by left-lateral offset of about 4.5 mm, which occurred between measurements on January 30 and March 20, 1981. Estimated measurement errors are ±1–2 mm for alinement array and ±1 mm for creepmeter.

earthquake (Allen and others, 1972). Their 1968 map is compared with the 1979 map at the bottom of the displacement plot (fig. 115).

The most striking similarity between the 1968 and 1979 ruptures is that both ruptures are nearly identical in overall length and end points. The 1968 break is slightly longer: 60 m longer in the northwest and 180 m longer in the southeast. In both ruptures the zone of ground breakage spans nearly the entire mapped length of the fault. Maximum right slip is also similar between the two ruptures: 18 mm for the 1968 break, and 22 mm for 1979. Where cracks occurred at the same point along the fault, they appear to have the same style and, as far as could be determined, the same location relative to the fault trace. For example, in the interval between 2.5 and 4.5 km from the northwest end of the fault the breaks step to the right at 2.5 km, become left-stepping echelons at 2.8 km, have small gaps or displacement minima at 3.3 and 3.6 km, become consistently left stepping echelons between 3.8 and 4.3 km, and thereafter are continuous (fig. 115). The gaps at 12.5 and 13.7 km also are similar. In addition, vertical components of displacements with the same sense are observed at about 13.5 km—the only place, however, where the vertical displacements agree. In 1968, a vertical displacement of as great as 25 mm was measured at the northwest end of the fault. No vertical displacement was seen there in 1979, although smaller vertical displacements were measured in several places within 7 km of the northwest end of the fault (pl. 2).

The most striking difference between the 1968 and 1979 ruptures is the location of the maximum displacement. The 1968 maximum is centered 19 km from the northwest end of the fault, whereas the 1979 maximum is centered 7 km from this end of the fault. Some gaps in the ruptures are similar—for example, at 2.2, 3.6, 12.5, 13.7, and possibly 20.3 km—but most differ. For example, prominent gaps in the 1968 break at 6.3, 11.1, 14.5, and 15.7 km are sites of displacement maxima on the 1979 break (fig. 115); the reverse is true at 17.3 and 19 km. It is, furthermore, not certain that a gap existed in the 1968 break between 17.5 and 18.8 km, matching the 1979 gap. The breaks in this interval were poorly preserved when mapped in 1968, and one alinement-array measurement in the middle of this gap indicated an offset of 25 mm (Allen and others, 1972).

In summary, the striking similarities between the 1968 and 1979 ruptures include nearly identical overall lengths and maximum displacements. An equally important difference, however, is the skewing of the displacement curves toward opposite ends of the fault. Fewer than half of the larger gaps in the ruptures can be correlated.

DISCUSSION

TRIGGERING MECHANISMS

This report brings at least one new bit of information to bear on the problem of triggering mechanism: displacement curves in two cases of triggered offset are skewed away from the triggering events. The report by Sieh (this volume) brings another new bit: surface breakage on the San Andreas fault occurred between about ¼ and 4½ days after the triggering event.

In their study of the 1968 triggered breaks, Allen and others (1972) discussed two mechanisms for triggering: static strain generated by displacement on the fault plane of the triggering earthquake, and dynamic strain (or shaking) generated by the triggering earthquake. Two other possible mechanisms might be added, although there is no positive evidence that these caused the 1979 triggered breaks; they are: creep migrating from the source region of the triggering event; and regional strain in the Imperial Valley causing slip at depth on numerous faults, followed by a seismic break on the Imperial fault and aseismic breaks on the Superstition Hills and San Andreas faults. Although the available evidence favors a dynamic-strain triggering mechanism, a brief discussion of all the above mechanisms is in order because they have all been used to explain strain in the Imperial Valley.

Allen and others (1972) calculated the dynamic strain in the Imperial Valley from the Borrego Mountain earthquake to be 11×10^{-6}, using strong-motion Wood-Anderson seismographs to measure the displacement (4.9 cm) and characteristic period (4.3 s). They calculated static strain in the Imperial Valley due to the earthquake, using the diagrams of Press (1965), to be 0.1×10^{-6}, or a hundred times smaller. Similar calculations for dynamic and static strains along the Superstition Hills fault due to the Imperial Valley earthquake give values that differ from each other by about a factor of 10. A value of 8×10^{-6} for dynamic strain is obtained using an integrated strong-motion accelerograph record on the Superstition Hills fault that shows a peak-to-peak displacement of 14.4 cm at a period of 4.9 s (Brady and others, 1968). For static strain at the same site, an upper limit of 0.6×10^{-6} can be obtained from Press's diagrams.

Creep migrating largely at depth has recently been interpreted as responsible for migrating seismicity in the Imperial Valley (Johnson and Hadley, 1976; Fuis and Schnapp, 1977) and for coupled earthquake swarms (Johnson, 1979), but there is no evidence in the seismicity after the Imperial Valley earthquake for creep migrating toward the San Andreas or Superstition Hills fault (see Johnson and Hutton, this volume). Seismicity

began under the southeast end of the Salton Sea, 40 km north of the Imperial and Brawley fault breaks and within 15 km of the triggered breaks on the San Andreas fault, as early as 2 hours after the main shock but did not progress northward more than a few kilometers during the next 10 days. Similarly, no seismicity was detected migrating toward the Superstition Hills fault, although earthquakes occurred as close as 8.5 km within 8 hours of the main shock.

No positive evidence exists of a significant regional strain event that might have caused simultaneous displacements on the Imperial, Superstition Hills, and San Andreas faults. Geodetic measurements, however, indicate a strain event in the region just north and northwest of the Imperial Valley during 1978. Between measurements in February 1978 and January 1979, J. C. Savage (oral commun., 1980) recorded a reversal in a trend toward increased uniaxial north-south compression that had been established since 1973. Significant east-westward extension was observed for the first time during this period, but no significant additional east-westward extension occurred between measurements in January and October 1979, spanning the time of the October 15 earthquake, and no anomalous changes occurred in other strain components. The Imperial fault slip and the triggered slip may have been a delayed response to the 1978 extension, but why these movements should occur more or less simultaneously after 10 months of quiescence is unclear.

Useful information on triggered displacements was provided in a study by King and others (1977) of fault slip recorded on creepmeters at the times of earthquakes in central California in the magnitude range 3.9–5.0. Coseismic slip of a fraction of a millimeter was measured over distances of tens of kilometers. Generally, the larger the earthquake, the larger the maximum displacement and the longer the interval affected. The maximum displacement (0.89 mm) and the longest slip interval (60 km) occurred at the time of a magnitude 5 earthquake. Strain steps calculated from these offsets are roughly symmetrical about the epicenter of the triggering earthquake when plotted against distance along the fault; a maximum occurs near the epicenter and tapers to zero at either end. These strain steps are a hundred times greater than those predicted from a static strain field due to seismic slip in the source region of the triggering earthquake, although this discrepancy could be reduced by a factor of 10 if a low-rigidity fault zone were allowed. For at least two earthquakes where the timing on a creepmeter record was highly accurate, coincidence of the recorded step with the seismic-wave arrivals (Bufe and Nason, 1973; R. O. Burford, oral commun., 1980) suggests a mechanism of triggering by shaking. In King and others' study, triggering by creep could be ruled out owing to the observed high velocity of slip propagation; creep events in this area generally propagate with velocities of 0.04 to 0.4 km/h (1–10 km/d) (King and others, 1973), and also generally produce larger offsets. For at least four earthquakes, however, the small coseismic offsets were followed within 40 minutes to 2 days by significant local creep events with offsets of several millimeters (Burford and others, 1973; King and others, 1977; R. O. Burford, oral commun., 1980). These creep events were measured only on the creepmeters recording the larger coseismic offsets.

These examples of small coseismic offsets followed by larger creep events may provide the best available analogies to the triggered displacements in the Imperial Valley region. An offset of a few centimeters triggered at depth during shaking along the Superstition Hills and San Andreas faults may have been followed by creep at the surface during the following day or so.

SKEWED DISPLACEMENT

The significance of the oppositely skewed curves for displacement on the Superstition Hills fault (fig. 4) is problematic. Two possible explanations are that (1) the slip during 1979 was complementary to that of 1968, or (2) slip adjustments were triggered in a stress field that varied oppositely along the fault in 1968 and 1979.

One example in which triggered slip apparently complemented an earlier creep offset was documented by Allen and others (1972). They recorded a creep offset of 11 mm on an alinement array across the Imperial fault at Worthington Road in late 1967. Two other alinement arrays across the fault at sites north and south of Worthington Road (Harris Road and County Highway S–80) showed no offset during that time. After the Borrego Mountain earthquake in April 1968, triggered offsets of 8 and 21 mm were observed at these two other sites, respectively, but no increased offset was measured at Worthington Road. In this example, the apparently complementary slip occurred after a period of several months. If the oppositely skewed curves for displacement on the Superstition Hills fault represent a similar type of complementary slip, then compensation occurred after a period of 11.5 years.

Skewed displacement curves have been observed for seismic breaks on strike-slip faults in a few places. Two longer breaks—the 1857 Fort Tejon, Calif., break (Sieh, 1978b) and the 1976 Guatemala break (Bucknam and others, 1978)—showed slightly skewed displacements. In the 1857 break the peak displacement was shifted toward the inferred point of initiation (Sieh, 1978a), and in the 1976 break, away from the point of initiation. Two

shorter breaks—the 1968 Borrego Mountain break (Clark, 1972) and the 1979 Imperial Valley break (Sharp and others, this volume)—show strongly skewed displacement with peaks at or toward the points of initiation. Structural complications along these breaks are probably responsible for the skewed and spiked nature of the displacement plots. On the other hand, laboratory and theoretical studies by Hartzell and Archuleta (1979) and Archuleta and Day (1980) indicate that on coherent breaks (with no structural complications), displacement is skewed in a direction away from the point of initiation, owing to focusing of stress in that direction during rupture propagation. This focusing and skewing is stronger at higher rupture velocities. Although the displacement on the Superstition Hills and San Andreas faults may have been triggered at depth at about the velocity of passing shear waves, these displacements probably did not result from a coherent rupture moving at that velocity. More likely, the shaking incoherently triggered offsets that were governed in size by the local stress field at different points along the fault. This hypothesis is developed further below.

In a study of historical geodetic measurements in southern California, Thatcher (1979) showed that during the interval 1934–41, spanning the 1940 Imperial Valley earthquake, the strain near the Imperial fault and the Brawley fault zone was right-lateral shear parallel to the faults, more or less northwest-southeast, whereas in adjacent areas the strain was right-lateral shear roughly perpendicular to the faults. This picture is expected for shallow fault slip. At greater distances from the faults, the strain should again be northwest-southeast right-lateral shear, the regional strain. Because one end of the Superstition Hills fault is within 7 km of the Imperial fault and the other more than 25 km away, the static-strain change produced by slip on the Imperial fault should differ from one end of that fault to the other; the greatest net right-lateral shear parallel to the fault might be expected at its northwest end, as observed in the 1979 displacement curve. A similar situation might have been expected after the Borrego Mountain earthquake, but the maximum right-lateral shear parallel to the fault should have occurred at its southeast end, as observed. Studies are currently underway to test this hypothesis in detail.

In summary, the oppositely skewed displacement curves for the 1968 and 1979 events could represent complementary slip, although the time scale for compensation exceeds by more than an order of magnitude that observed for compensating slip along the Imperial fault. These oppositely skewed displacement curves could also represent adjustment to stress fields that varied oppositely during 1968 and 1979.

MOMENT AND STRESS DROP

The moment and stress drop calculated from the 1979 triggered displacement on the Superstition Hills fault are, at best, conjectural, owing to ignorance of the depth of slip, but both quantities are much smaller than the moment and stress drop of the triggering event. In the following calculations, we use 100 m as the minimum depth of slip (compare with King and others, 1977). For the maximum depth of slip, it may be reasonable to use the maximum earthquake depth in this area of about 13 km (Hamilton, 1972; Fuis and others, 1978). Integrating the displacement curve (fig. 115) and dividing by a fault length of 22.5 km, we obtain an average displacement of 0.62 cm for 1979 (0.56 cm for 1968). Similarly, integrating the maximum-displacement curve (fig. 116) and dividing by the fault length gives a reasonable upper bound on the average displacement of 1.01 cm for 1979 (1.04 cm for 1968). The moment M is then calculated from

$$M=\mu dlw,$$

where μ is the rigidity, d is the average displacement, l is the fault length, and w is the fault width (or depth). Taking $\mu=30\times10^3$ MPa (0.3×10^{12} dynes/cm^2), we obtain a moment ranging from about 0.42×10^{15} to 88×10^{15} N·m ($4.2–880\times10^{21}$ dyne·cm), depending primarily on the depth of slip. The stress drop $\Delta\sigma$ is calculated from a formula by Knopoff (1958):

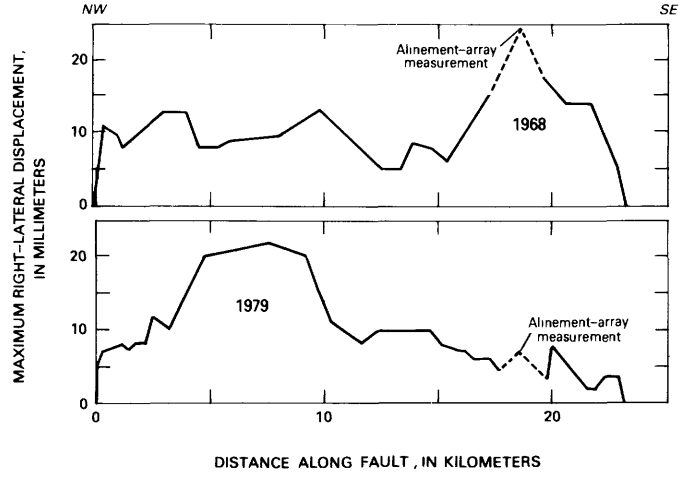

FIGURE 116.—Maximum right-lateral displacement as a function of distance along Superstition Hills fault for 1968 and 1979 breaks. Plots are derived from figure 115 by fitting curves through highest peaks of displacement. Dashed parts of plots are controlled by alinement-array measurements, one of which is queried (see fig. 115).

$$\Delta\sigma=(2/\pi)\mu d/w.$$

We obtain a stress drop ranging from about 0.01 to about 1.9 MPa (0.1–19 bars), depending primarily on the depth of slip.

By contrast, the moment and stress drop of the triggering event are known with greater certainty to be about 6×10^{18} N·m (60×10^{24} dyne·cm; Kanamori and Regan, this volume) and 0.54 MPa (5.4 bars; Archuleta and Sharp, 1980), respectively. Thus the moment of the triggered displacement is probably more than 100 times smaller than that of the triggering earthquake. The stress drop of the triggered displacement is probably also much smaller than that of the triggering event.

SUMMARY

Breaks were triggered along the entire mapped length of the Superstition Hills fault after both the 1968 Borrego Mountain earthquake and the 1979 Imperial Valley earthquake. The 1968 and 1979 breaks are similar in location, length, maximum displacement, and style of faulting. Important differences exist, however, most prominent of which are the positions of maximum displacement: the 1968 maximum displacement occurred near the southeast end of the fault, whereas the 1979 maximum displacement occurred toward the northwest end of the fault—in both cases, at the end most distant from the triggering earthquake.

Of several possible triggering mechanisms, shaking appears to be consistent with most of the available information, whereas other mechanisms are inconsistent in part or unsupported by clear evidence. Oppositely skewed displacement curves for the 1968 and 1979 events may represent, on the one hand, complementary slip or, on the other hand, slip triggered in oppositely varying stress fields.

REFERENCES CITED

Allen, C. R., Wyss, Max, Brune, J. N., Grantz, Arthur, and Wallace, R. E., 1972, Displacements on the Imperial, Superstition Hills, and San Andreas faults triggered by the Borrego Mountain earthquake, *in* The Borrego Mountain earthquake of April 9, 1968: U.S. Geological Survey Professional Paper 787, p. 87–104.

Archuleta, R. J., and Day, S. M., 1980, Dynamic rupture in a layered medium: An example, the 1966 Parkfield earthquake: Seismological Society of America Bulletin, v. 70, no. 3, p. 671–690.

Archuleta, R. J., and Sharp, R. V., 1980, Source parameters of the Oct. 15, 1979, Imperial Valley earthquake from nearfield observations [abs.]: Eos (American Geophysical Union Transactions), v. 61, no. 17, p. 297.

Brady, A. G., Perez, Virgilio, and Mork, P.N., 1980, The Imperial Valley earthquake, October 15, 1979: Digitization and processing of accelerograph records: U.S. Geological Survey Open-File Report 80–703, 309 p.

Bucknam, R. C., Plafker, George, and Sharp, R. V., 1978, Fault movement (afterslip) following the Guatemala earthquake of February 4, 1976: Geology, v. 6, no. 3, p. 170–173.

Bufe, C. G., and Nason, R. D., 1973, Creep, strain, and seismicity in the vicinity of Stone Canyon Observatory [Calif.], *in* Stepp, J. C., ed., Earthquake research in NOAA, 1971–1972: U.S. Department of Commerce, National Oceanic and Atmospheric Administration Technical Report ERL 256–ESL 28, p. 26–28.

Burford, R. O., Allen, S. S., Lamson, R. J., and Goodreau, D. D., 1973, Accelerated fault creep along the central San Andreas fault after moderate earthquakes during 1971–1973, *in* Kovach, R. L., and Nur, Amos, eds., Proceedings of the conference on tectonic problems of the San Andreas fault system: Stanford University Publications in the Geological Sciences, v. 13, p. 268–274.

Clark, M. M., 1972, Surface rupture along the Coyote Creek fault, *in* The Borrego Mountain earthquake of April 9, 1968: U.S. Geological Survey Professional Paper 787, p. 55–86.

Dibblee, T. W., Jr., 1954, Geology of the Imperial Valley region, California, *in* Geology of the natural provinces, chap. 2 *of* Jahns, R. H., ed., Geology of southern California: California Division of Mines Bulletin 170, p. 21–28.

Fuis, G. S., and Allen, C. R., 1979, The southern California cooperative seismic network: Earthquake Information Bulletin, v. 11, no. 6, p. 196–204.

Fuis, G. S., and Schnapp, M. R., 1977, The November–December 1976 earthquake swarms in northern Imperial Valley, California: Seismicity on the Brawley fault and related structures [abs.]: Eos (American Geophysical Union Transactions), v. 58, no. 12, p. 1188.

Fuis, G. S., Whitcomb, J. H., Johnson, C. E., Jenkins, D. J., Richter, K. J., Blanchard, A. C., Fischer, S. A., and Reed, B. A., 1978, Preliminary catalog of earthquakes in southern California, October 1976–September 1977: U.S. Geological Survey Open-File Report 78–672, 84 p.

Hamilton, R. M., 1972, Aftershocks of the Borrego Mountain earthquake from April 12 to June 12, 1968, *in* The Borrego Mountain earthquake of April 9, 1968: U.S. Geological Survey Professional Paper 787, p. 31–54.

Hartzell, S. H., and Archuleta, R. J., 1979, Rupture propagation and focusing of energy in a foam rubber model of a stick slip earthquake: Journal of Geophysical Research, v. 84, no. B7, p. 3623–3636.

Johnson, C. E., 1979, CEDAR—an approach to the computer automation of short-period local networks; seismotectonics of the Imperial Valley of southern California: Pasadena, California Institute of Technology, Ph. D. thesis, 343 p.

Johnson, C. E., and Hadley, D. M., 1976, Tectonic implications of the Brawley earthquake swarm, Imperial Valley, California, January 1975: Seismological Society of America Bulletin, v. 66, no. 4, p. 1133–1144.

King, C.-Y., Nason, R. D., and Burford, R. O., 1977, Coseismic steps recorded on creep meters along the San Andreas fault: Journal of Geophysical Research, v. 82, no. 11, p. 1655–1662.

King, C.-Y., Nason, R. D., and Tocher, Don, 1973, Kinematics of fault creep: Royal Society of London Philosophical Transactions, ser. A, v. 274, no. 1239, p. 355–360.

Knopoff, Leon, 1958, Energy release in earthquakes: Royal Astronomical Society Geophysical Journal, v. 1, no. 1, p. 44–52.

Press, Frank, 1965, Displacements, strains, and tilts at teleseismic distances: Journal of Geophysical Research, v. 70, no. 10, p. 2395–2412.

Sharp, R. V., and Clark, M. M., 1972, Geologic evidence of previous faulting near the 1968 rupture on the Coyote Creek fault, *in* The

Borrego Mountain earthquake of April 9, 1968: U.S. Geological Survey Professional Paper 787, p. 131–140.

Sieh, K. E., 1978a, Central California foreshocks of the great 1857 earthquake: Seismological Society of America Bulletin, v. 68, no. 6, p. 1731–1749.

———1978b, Prehistoric large earthquakes produced by slip on the San Andreas fault at Pallett Creek, California: Journal of Geophysical Research, v. 83, no. B8, p. 3907–3939.

Thatcher, Wayne, 1979, Horizontal crustal deformation from historic geodetic measurements in southern California: Journal of Geophysical Research, v. 84, no. B5, p. 2351–2370.

SLIP ALONG THE SAN ANDREAS FAULT ASSOCIATED WITH THE EARTHQUAKE[1]

By KERRY E. SIEH,
CALIFORNIA INSTITUTE OF TECHNOLOGY

CONTENTS

ABSTRACT

Some of the fault slip associated with the 1979 Imperial Valley earthquake occurred along other than the Imperial fault and the Brawley fault zone. More than 90 km to the north of the seismogenic fault, a 39-km-long section of the San Andreas fault developed a discontinuous set of surficial fractures soon after the earthquake. This set of fractures consisted of small left-stepping echelon cracks displaying extensional and dextral components of movement. Average dextral slip was about 4 mm, and slip reached 10 mm at one point along the fault. In one locality the cracks formed between ⅓ and 4½ days after the main shock, although slippage at depth may have been nearly simultaneous with the earthquake.

In general, this set of breaks duplicates the location, style, and slip magnitude of the set that was mapped in 1968 after the Borrego Mountain, Calif., earthquake. Such near-duplication indicates that this section of the San Andreas fault, in particular, is susceptible to small amounts of triggered slip. Although the reasons for such behavior are far from clear, similar behavior of the Imperial fault before 1979 suggests that this section of the San Andreas fault may generate a moderate earthquake within the next few decades.

INTRODUCTION

Soon after the Borrego Mountain, Calif., M_L = 6.4 earthquake of 1968, which was generated by slip along the Coyote Creek fault, fractures along parts of the surficial traces of the nearby Imperial, Superstition Hills, and San Andreas faults were detected (Allen and others, 1972) (fig. 117). The fractures displayed only a centimeter or so of dextral slip, but involved tens of kilometers of fault length. These fractures formed within a few days of the earthquake but did not appear to have been caused abruptly by seismic slip. Allen and others (1972) reasoned that the fractures were induced by seismic shaking and not by changes in the static-strain field that accompanied the earthquake.

At about the same time in the 1979 Imperial Valley earthquake, which was generated by slip along the Imperial fault, sets of fractures similar to those observed in 1968 again formed along the Superstition Hills and San Andreas faults. Fuis (this volume) discusses recent fracturing along the Superstition Hills fault; here, I discuss those fractures that formed along the San Andreas fault. A comparison of the 1968 and 1979 fracture sets raises intriguing new questions as to their significance, because the 1979 earthquake was generated by slip along the same section of the Imperial fault that displayed triggered slip in 1968 (fig. 117).

OBSERVATIONS

The cracks that formed along the trace of the San Andreas fault in 1979 were generally shorter than 1 m and displayed dextral movement of as much as 10 mm measured parallel to the main fault trace. These cracks were arranged in left-stepping echelon patterns within zones that only rarely exceeded half a meter in width (for example, at km 2.8, pl. 3) or were accompanied by adjacent sets of fractures (at km 26.0). Numerous photographs of this sort of fracturing were presented by Allen and others (1972).

Plate 3 compiles detailed observations on the location of observed fractures and the magnitude of dextral slip. Only those segments along which the fractures were unambiguously tectonic are represented on the map (pl. 3). The fracture sets were not continuous along the 39-km section of the fault shown but, instead, formed groups ranging in length from less than 1 m to 3.7 km. In most localities, dextral slip was between 2 and 4 mm; the maximum measured was 10 mm, at one point near the northwest terminus (at km 1.0, pl. 3). The amount of slip did not vary in any clearly systematic fashion along the fault.

[1]Contribution No. 3379, Division of Geological and Planetary Sciences, California Institute of Technology, Pasadena, CA 91125.

Knowledge of the time of formation of these fractures is important in understanding their cause. Near Mecca Beach Campground on the east shore of the Salton Sea, surficial fractures did not appear until more than 7 hours after the earthquake. An 80-m segment of the fault trace at this site (dot at km 26.2, pl. 3) was first visited between 11:10 and 11:14 p.m. P.d.t. October 15 by Ronald Miller, Michael Nelson, Gerald Roth, and myself, using a gasoline lantern and flashlights. The fault trace is particularly evident here because it is marked by a knee-high scarp in young alluvium. We walked along the scarp and carefully searched for fractures but found none. At about 7:30 a.m. P.d.t. October 20, I discovered echelon cracks at the same site. Our earlier footprints at two points crossed and in several other places were within a meter of the new set of fractures. Therefore, the origin time of these fractures may be placed with reasonable confidence between ⅓ and 4½ days after the earthquake. The records from a portable creepmeter that was designed, installed at the site, and monitored by Ralph Gilman indicate that no additional dextral fault slip occurred from the time of installation at 8 a.m. P.d.t. October 23 until November 9. Remeasurement of slip on several fractures at this site showed no appreciable further slip between October 20 and December 11.

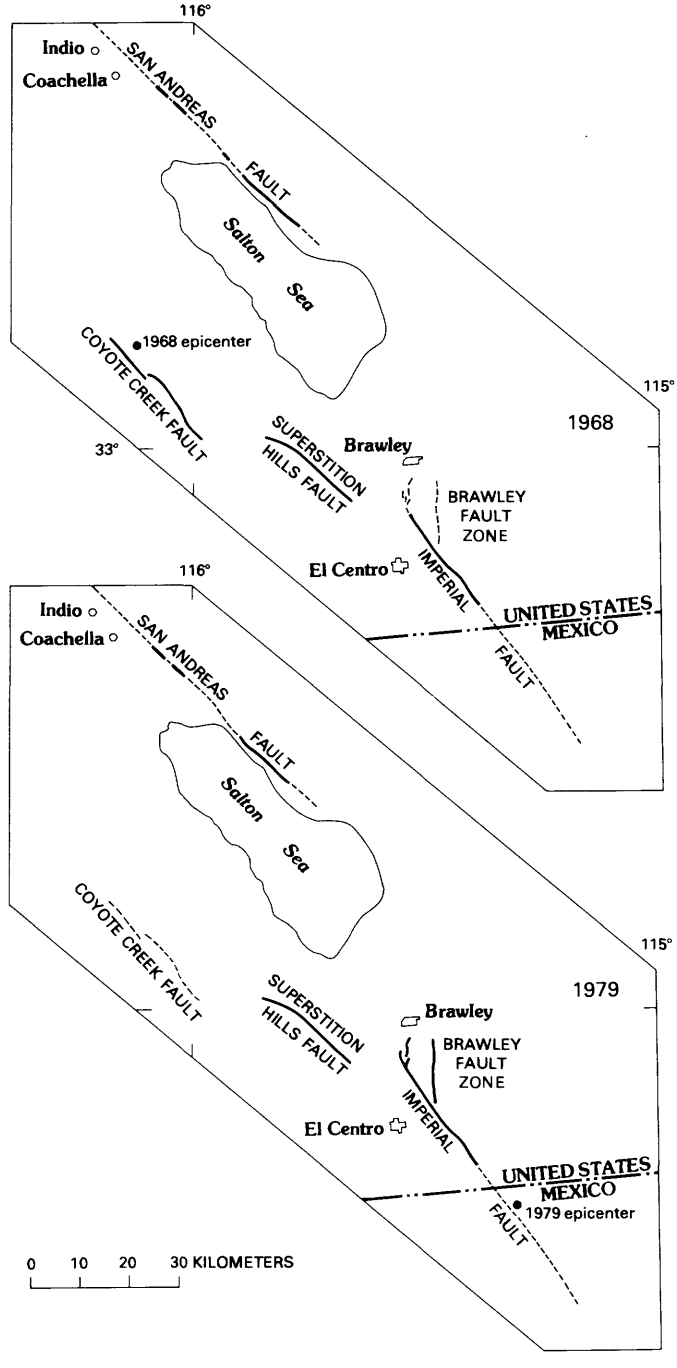

FIGURE 117.—Comparison of slip triggered in 1968 and 1979. In 1968, seismic movement along Coyote Creek fault triggered slip along parts of San Andreas, Superstition Hills, and Imperial faults (heavy lines). In 1979, triggered slip on heavy-lined sections of Superstition Hills and San Andreas faults was associated with seismic rupture on Imperial fault and in Brawley fault zone.

Whether or not the time of origin of these cracks is representative of the formation of cracks elsewhere along the fault trace or at depth is uncertain. Perhaps fault slip occurred simultaneously with the main shock at depth but required several hours or days to propagate to the surface. A similar time lag has been observed at least twice before: in association with the 1971 Imperial Valley M_L = 5.3 earthquake (Allen and others, 1972, p. 102), and during creep events on the San Andreas fault near Parkfield in central California (Goulty and Gilman, 1978). If rupturing at depth was simultaneous with the main shock, this rupturing must have been aseismic because reports from Coachella, a nearby community, indicated low intensities for the main shock (Nason, this volume).

The possibility that the rupturing coincided with aftershocks of the main event can probably be ruled out. No aftershocks have been located along the fractured section of the San Andreas fault, using either the seismic network or strong-motion records (C. E. Johnson and T. H. Heaton, oral commun., 1979). Any such aftershocks must also have been of rather low magnitude (M_L<4) to have gone unreported in nearby communities. Finally, if all the cracks originated seismically after the main shock, such an event must have produced 39 km of discontinuous fault rupture with very little slip. In the light of the above restrictions, it is reasonable—just as Allen and others (1972) concluded in analyzing 1968 fracturing—to exclude the possibility that the rupture was caused by seismic slip during one or more aftershocks.

A plausible alternative is that the ruptures formed in

association with postseismic creep events occurring at depth. Thatcher's (1979) interpretation of geodetic data is that very large amounts of aseismic dextral slip did occur at depth along this section of the San Andreas fault during the decade following the 1940 Imperial Valley earthquake. Perhaps further geodetic studies will allow selection of a suitable hypothesis for the formation of these fractures.

COMPARISON WITH 1968 SLIPPAGE

The fracturing of 1979 resembles that of 1968 (fig. 117). The most recent cracks formed in association with seismic rupture on the Imperial fault, tens of kilometers to the southeast. The 1968 cracks originated within a few days of the seismic rupture on the Coyote Creek fault, tens of kilometers to the southwest (Allen and others, 1972). In both events, the surficial breaks appear to have formed aseismically; both sets of fractures are characterized by discontinuity and a low ratio of dextral slip to rupture length.

Plate 3 compares in detail the locations of 1968 and 1979 fracturing. The 1968 breaks (dotted lines, pl. 3) were mapped on aerial photographs by R. E. Wallace and Max Wyss (Allen and others, 1972, pl. 2). To eliminate any inconsistencies in the 1968 and 1979 data sets due to tranference from photographic to topographic base, I inspected their annotated aerial photographs and plotted their data on my photographs; both sets of data were then transferred onto the topographic base.

SIMILARITIES

At only one locality where breaks occurred in both years could it be ascertained that the breaks occurred on different fault strands. Between kilometers 36.72 and 36.80 (pl. 3), a thorough search yielded only one zone of echelon cracks, about 10 to 15 m northeast of the small scarp that marks the main fault trace. The 1979 zone is probably the northeasternmost of the 10 to 12 subparallel zones observed there by R. E. Wallace and Max Wyss (Allen and others, 1972, pl. 2) over a 10-m width. Although more detailed and thorough study might have revealed other sites where the 1968 and 1979 fractures did not exactly coincide, in general the fractures seemed to be in the same places. Along much of the fault, for example, both sets of fractures appeared at the base of an older scarp or at a major fault in the sedimentary bedrock. In addition, in most places the fault locations plotted on the aerial photgraphs in 1968 by R. E. Wallace cannot be distinguished from those I plotted in 1979. Precision of locations on the photographs is a few meters.

The northwest and southeast limits of ground rupturing in 1968 and 1979 are nearly identical. One small set of fractures in 1979 was about 600 m farther northwest than the mapped limit of fractures in 1968 (at km 0, pl. 3). This isolated short northwesternmost set of recent fractures was so inconspicuous, however, that a similar set could easily have gone unnoticed in 1968. In 1968, fractures were found along a short reach of the fault 1 km southeast of the southeasternmost breaks of 1979 (at km 39.7, pl. 3). Thus, the northwest and southeast terminations of the two fracture sets were within 1 km of each other, and both sets were 39 km long.

In addition to sharing nearly identical termini and lengths, the 1968 and 1979 ruptures share two major unbroken segments between termini: a 1.7-km segment between kilometers 3.3 and 5.0, and a 17.1-km segment between kilometers 8.7 and 25.8. With two exceptions (km 20.2–21.4 in 1968, and at km 12.3 in 1979, pl. 3), surficial slip was not observed along these fault segments after either event. In addition, the 1968 and 1979 termini of these largely unbroken segments are everywhere within 100 m of each other (approx 60 m at km 25.8, approx 20 m at km 8.7, and approx 30 m at km 5.0 and 3.3, pl. 3).

DIFFERENCES

At almost every locality where cracks formed in both years, the magnitude of dextral slip in 1979 was less than that in 1968. In general, the 1979 slip values were about one-sixth to one-half those of 1968. Curiously, however, the maximum measured slip from both events was within a few kilometers of the northwest terminus of ground rupturing.

In addition to its smaller slip, the 1979 rupture clearly was less continuous than the 1968 break (see pl. 3), and only from kilometer 26.9 to 29.1 did a long zone of new cracks form in 1979 where none were reported in 1968. Total fracture length in 1979, excluding unbroken segments, was about 10.4 km, and in 1968 about 13.7 km. In many places, short sets of cracks formed in 1979 where none were observed in 1968; likewise, many short fractured segments of 1968 did not break again in 1979 (see pl. 3).

DISCUSSION

During their studies of the 1968 Borrego Mountain earthquake, Allen and others (1972) made the important discovery that the earthquake triggered aseismic fault slip outside the epicentral region. This phenomenon has now been observed again within the same region, and its repetition enables a better assessment of its significance.

Discontinuous minor surficial slip along a 39-km section of the San Andreas fault was triggered by both the

1968 and 1979 earthquakes. Although the gross similarity between the two sets of triggered fractures is remarkable, in detail neither the magnitude of slip nor the location of individual breaks along the fault is identical for these two events.

If, indeed, the passage of these two earthquakes through the fault zone in some manner enabled the fault to slip, a repeat performance should not be an identical performance. The amplitudes, times histories, and wavelengths of the seismic strains that passed through the fault zone in 1979 must certainly have differed from those in 1968. If the amount of triggered slip were a function of the amplitude of the dynamic seismic strains, the earthquake from the more distance source (the Imperial fault in 1979) might be expected to have triggered less slip than the nearer earthquake of 1968. The 1979 slip was, in fact, smaller and less continuous at most localities. If the specific location of a broken segment is determined by details of the seismic radiation passing through—its frequency content, amplitude variation, and time history—then the 1968 and 1979 distributions of fracture sets should differ both in detail (by tens of meters) and generally (by hundreds of meters to kilometers).

Although differences in the 1968 and 1979 seismic strains may have produced the differences in the two fracture sets, the similarities in the two sets are not so readily explained in terms of the seismic sources. It is unlikely that the northwest termini of the two 39-km-long zones would fall within a few hundred meters of each other if the fracture locations were entirely a function of seismic imput. It also is unplausible that the termini of the major faulted segments in 1979 would fall within a few meters of their locations in 1968 if the dynamics of each earthquake determined their placement.

Therefore, these and other similarities apparently indicate features or properties of the fault zone itself. Four static factors are plausible.

1. Young unfaulted sedimentary deposits may impede the propagation of subsurface fractures to the surface. In no locality, however, did cracking terminate at the edge of an alluvial cover. Near kilometer 39 (pl. 3) the cracks end, although clear exposures of Pleistocene semiconsolidated deposits continue to the southeast. Similar situations obtain from kilometers 33½ to 36½, 31 to 32, 20 to 21, 8¾ to 11¾, and 3½ to 5. Only between kilometers 0 and 1 and between kilometers 13 and 25½ can alluvial cover have hindered the 1968 and 1979 fractures from reaching the surface; because kilometers 14 to 20 was not searched in 1979 (nor, perhaps, in 1968), no strong case for sedimentary hindrance can be made there. Moreover, the presence of well-defined small scarps indicates that older faulting did break the surface along parts of both these alluviated segments.
2. Tectonic slip along segments of the fault that traverse expansive-clayey sedimentary bedrock may be completely obscured by larger expansion cracks. In several places the fault cuts such material, rife with polygonal cracks, typically with extensional separations of about a centimeter. In these localities (for example, km 4–5 and 9–9½), dextral slip of a few millimeters may have been obscured by the expansion cracks.
3. Tectonic slip along segments of the fault that consist of numerous branches or that have a substantial component of nonbrittle fracture (warping) may be too small to be visible or to propagate to the surface. Where the fault zone is diffuse and complex (km 3½–5 and 9–12), tectonic slip may have been spread over several traces or over a wide zone of deformation. If slip on individual traces was thereby reduced to less than about 1 mm, surficial cracks might not have formed or been recognized.
4. The various segments of the fault may be prestressed to different amounts or have different shear strengths, and only those near failure may be triggered to move. Differences in stress or strength may be related to bends or discontinuities in the fault or inhomogeneity of materials. Perhaps the fractured segments are weaker than the unfractured.

At kilometer 26½, the fault makes a leftward bend of about 30 m over a distance of about 80 m. Segments of dextral faults with this geometry are probably stronger than straight or right-stepping segments (Paul Segall and D. D. Pollard, written commun., 1979). Faulting in 1968 ended at this bend (pl. 3). In 1979, fractures were nearly continuous to the northwest and southeast of the bend but were nonexistent through the bend (except for the few very inconspicuous segments shown in pl. 3). Perhaps the fault is stronger at the bend than to the southeast or northwest.

At the 1968 and 1979 southeast termini, the fault trace traverses severely folded Pleistocene beds of the Borrego Formation of Babcock (1974), but no change in the nature of the bedrock is readily apparent along the several kilometers of fault trace nearby. The fault trace does, however, change in trend from N. 47½° W. (km 35–39) to N. 53½° W. (km 39–43). This bend at the 1968 and 1979 fracture termini may be equivalent to a leftward bend in the fault, inasmuch as it may give the fault greater resistance to dextral shear.

Between kilometers 0 and 1 are the northwest termini of both the 1968 and 1979 fractures. The fault is continuous and straight at this point, and alluvium and

sedimentary bedrock alike display scarps that indicate continuity of the fault to the surface. Perhaps at this point a change in strength or loading of the fault prohibited slip from continuing to the northwest in both 1968 and 1979.

One further comparison of the 1968 and 1979 faulting is valuable because it indicates that triggered slip may be a long-term precursor to seismic slip. In 1968, three fault segments in the Imperial Valley region showed triggered slip (fig. 117): (1) the entire known length of the Superstition Hills fault, (2) 39 km of the San Andreas fault, and (3) 22 to 30 km of the Imperial fault (Allen and others, 1972). Slip along this section of the Imperial fault generated the 1979 earthquake. This remarkable coincidence suggests that the exact location of both ruptures was controlled by more than the dynamics of the 1968 or 1979 earthquake; perhaps some property of this section of the fault or a peculiar state of stress across it brought about its failure both times.

The coincidence of the 1979 seismic rupture and 1968 triggered rupture is not the only distinctive feature of this section of the Imperial fault. Johnson (1979, ch. 4, figs. 4–27) showed that this section can be distinguished from the remainder of the Imperial fault on the basis of its high seismicity. J. P. Buwalda (unpub. data, 1940) reported that this section was characterized during the M_s=7.1 earthquake by much less slip than the section to the south. Allen and others (1972, p. 89) and Goulty and others (1978) showed that, in apparent contrast to the section to the south, this section of the Imperial fault occasionally undergoes creep.

Whatever the mechanics may be, the section of the Imperial fault that failed seismically in 1979 can be clearly distinguished from adjacent sections on the basis of its previous behavior: (1) triggered slip in 1968, (2) creep during the 1960's and 1970's, (3) moderate slip associated with the 1940 Imperial Valley earthquake, and (4) a high level of microearthquake activity. The Superstition Hills fault and the south 39-km section of the San Andreas fault are also characterized by triggered slip and perhaps by creep (Allen and others, 1972, p. 94; Keller and others, 1978); neither fault segment, however, is characterized by high levels of microearthquake activity. Nevertheless, these shared characteristics may indicate that the Superstition Hills fault and the south 39 km of the San Andreas fault will fail seismically within the next few decades.

ACKNOWLEDGMENTS

The ephemeral nature of evidence for triggered fault slip demanded rapid search and documentation that could not have been accomplished without the assistance of Stephen Cohn, James Conca, Ronald Miller, Michael Nelson, James and Judy Pechmann, Gerald Roth, and Ray Weldon—all of the Division of Geological and Planetary Sciences of the California Institute of Technology (CIT). C. R. Allen and R. V. Sharp substantially improved the manuscript. Fieldwork was supported by the Earthquake Research Affiliates of CIT and general Division funds.

REFERENCES CITED

Allen, C. R., Wyss, Max, Brune, J. N., Grantz, Arthur, and Wallace, R. E., 1972, Displacements on the Imperial, Superstition Hills, and San Andreas faults triggered by the Borrego Mountain earthquake, *in* The Borrego Mountain earthquake of April 9, 1968: U.S. Geological Survey Professional Paper 787, p. 87–104.

Babcock, E. A., 1974, Geology of the northeast margin of the Salton trough, Salton Sea, California: Geological Society of American Bulletin, v. 85, no. 3, p. 321–332.

Goulty, N. R., Burford, R. O., Allen, C. R., Gilman, Ralph, Johnson, C. E., and Keller, R. P., 1978, Large creep events on the Imperial fault, California: Seismological Society of America Bulletin, v. 68, no. 2, p. 517–521.

Goulty, N. R., and Gilman, Ralph, 1978, Repeated creep events on the San Andreas fault near Parkfield, California, recorded by a strainmeter array: Journal of Geophysical Research, v. 83, no. B11, p. 5415–5419.

Johnson, C. E., 1979, CEDAR—an approach to the computer automation of short-period seismic networks; seismotectonics of the Imperial Valley of southern California: Pasadena, California Institute of Technology, Ph. D. thesis, 343 p.

Keller, R. P., Allen, C. R., Gilman, Ralph, Goulty, N. R., and Hileman, J. A., 1978, Monitoring slip along major faults in southern California: Seismological Society of America Bulletin, v. 68, no. 4, p. 1187–1190.

Thatcher, Wayne, 1979, Horizontal crustal deformation from historic geodetic measurements in southern California: Journal of Geophysical Research, v. 84, no. B5, p. 2351–2370.

PREEARTHQUAKE AND POSTEARTHQUAKE CREEP ON THE IMPERIAL FAULT AND THE BRAWLEY FAULT ZONE[1]

By STEPHEN N. COHN, CLARENCE R. ALLEN, RALPH GILMAN, and NEIL R. GOULTY,
CALIFORNIA INSTITUTE OF TECHNOLOGY

CONTENTS

ABSTRACT

Taken together, 12 years of alinement-array data, 4 years of creepmeter records from four instruments, and 2 years of surveys from two nail files suggests that creep events on the Imperial fault 2 to 5 months before the October 15 earthquake are consistent with long-term trends and not indicative of any imminent event. No discernible creep occurred on the fault in the hours and days before the earthquake. Records of coseismic displacement imply that response of the soil to the fault slip at depth was brittle rather than plastic; they uniquely demonstrate that the minimum rate of surface fault displacement was 1.8 cm/s. Continuing measurements of afterslip show that all motion is due to discrete 0.2- to 1.5-cm creep events occurring less frequently over time. The accumulating displacement for the first 35 days after the earthquake is well approximated by linear logarithmic functions of time. Use of this accumulating displacement to predict future slip rates implies that for 6 years the afterslip rate from the 1979 earthquake should be greater than the 0.5-cm/yr average preearthquake creep rate. The maximum amount of slip on the surface trace of the Imperial fault associated with the 1979 earthquake, including afterslip, amounts to more than 60 cm.

INTRODUCTION

The earthquake of October 15, 1979, was associated with surface faulting along the Imperial fault for a distance of about 30 km. Surface faulting occurred simultaneously in the Brawley fault zone, and slip was triggered on the Superstition Hills fault and the southernmost segment of the San Andreas fault (Fuis, this volume; Sieh, this volume).

The Imperial fault and the Brawley fault zone together make up one of two segments of the San Andreas fault system where aseismic creep is known to occur regularly (Brune and Allen, 1967; Allen and others, 1972; Sharp, 1976; Goulty and others, 1978). The other segment is a 300-km-long zone in central California composed principally of the San Andreas, Calaveras, and Hayward faults (Nason, 1973). The first instrumentally observed creep on the Imperial fault was recorded at Worthington Road in 1967, where an alinement array had been installed across the fault in May 1967 and was repeatedly resurveyed (Allen and others, 1972; Goulty and others, 1978).

The Imperial fault has since been monitored for creep with a series of four fault-crossing alinement arrays. In 1975 three creepmeters were installed across the Imperial fault, and a fourth across the Brawley fault zone. These creepmeters have shown that the creep is episodic and occurs in 1- to 2-cm creep events at approximately 2-year intervals on the central segment of the Imperial fault in California (Goulty and others, 1978).

The 1979 Imperial Valley earthquake was associated with surface faulting primarily on the segment of the Imperial fault covered by the system of creepmeters and alinement arrays. This system provides a unique combination of observations of preearthquake creep, coseismic offsets, and continuing aftercreep.

Acknowledgment.—This research was supported by U.S. Geological Survey Contract 14-08-0001-16718.

INSTRUMENTATION

Slip on the Imperial fault and in the Brawley fault zone has been monitored since October 1975 by four continuously recording taut-wire creepmeters (fig. 118). Each of these instruments initially utilized an Invar wire suspended between an anchor on one side of the fault and a tensioning device anchored on the opposite side. The wire passes through a buried pipe and intersects the fault at 45°. Failure of the Invar wires due to corrosion led to their replacement in 1978 with durable, but thermally more sensitive, stainless steel. The

[1]Contribution No. 3369, Division of Geological and Planetary Sciences, California Institute of Technology, Pasadena, CA 91125.

creepmeters at Heber Road and the Tuttle Ranch, each spanning 20 m, use a micrometer screw to measure motion and a linearly variable differential transformer as a transducer for the continuous-strip-chart recording system, as described by Yamashita and Burford (1973). Those at Ross Road and Harris Road, spanning 20 m and 12 m, respectively, employ direct reading by a dial-gage micrometer and a continuous-rotation deposited-film potentiometer as the displacement transducer for the recording system, similar to the design described by Smith and Wyss (1968). Servicing and reading of these instruments typically has taken place at 3-month intervals.

All the instruments are limited to a maximum range of about 2.5 cm and, where possible, are installed so that dextral fault motion increases the separation between piers. Stretching of the wire thus appears as sinistral motion that is easily distinguished from dextral-creep signals. When the 2.5-cm range is exceeded, the wire may stretch, break, or slip in its clamp, and so the record of that and later events is lost. Such a breakdown occurred during the 1979 Imperial Valley earthquake at the Heber Road and Ross Road sites, where coseismic motion was probably several tens of centimeters, and once subsequently at Ross Road between service calls.

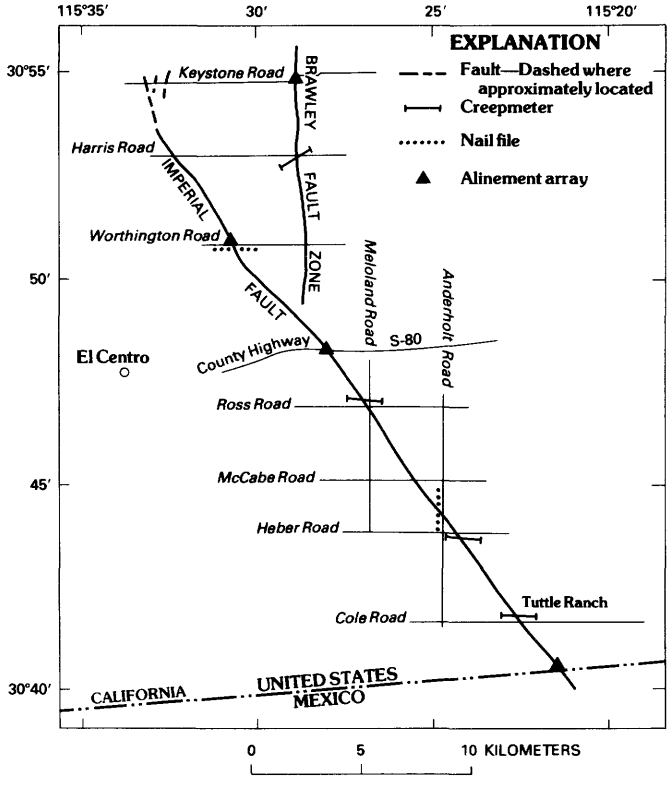

FIGURE 118.—Locations of creepmeters and nail files on Imperial fault and in Brawley fault zone in Imperial Valley.

At two other sites along the Imperial fault, nail files were installed in late 1977. Each nail file comprises seven steel studs embedded initially in a straight line at 4.6-m intervals along the edge of the pavement where the fault crosses the road; thus, roughly half the studs are on either side of the fault. The nail files are surveyed by measuring the deviations of intermediate studs from a line joining the end points. In our analysis of the nail-file measurements we assume that rigid motion between the end points of the nail file (approx 28 m) is taken up entirely on the fault surface. Uniform shear between end points, however, would not be detected and would make the measured offset values smaller than the actual relative motions of the end points.

The nail files were regularly resurveyed at 3-month intervals and beginning 8 hours after the 1979 earthquake, and have since been resurveyed much more frequently. At first, the nail files were resurveyed by stretching a fine wire between the end points and measuring the deviation of each intervening point with a rule. On calm days this technique gives reproducible readings to ±0.1 cm of resolved fault motion, although a moderate breeze may reduce the precision to ±0.3 cm. This difficulty has led to using a theodolite to measure deviations from the line defined by the wire in the previous method, thus avoiding wind contamination while retaining the ease and speed of measurement that initially made this method of monitoring fault slip attractive.

More cumbersome to resurvey and analyze, fault-crossing alinement arrays afford information on deformation that may be distributed outside the base line of a nail file. Several alinement arrays across the Imperial fault and the Brawley fault zone, with base lines of approximately 75 m, have been maintained and resurveyed at least once every year since 1968 (Goulty and others, 1978). Results from these arrays relevant to the 1979 earthquake will be reported at a future date.

PRESEISMIC CREEP

Creep records (fig. 119) for the 4 years preceding the 1979 earthquake show that creep was sporadic in the central part of that segment of the Imperial fault exhibiting earthquake-associated surface displacement. No slip was observed during the first 18 months of instrument observation; then, during several days in April 1977, 1 to 2 cm of dextral slip was observed on both the Ross Road and Heber Road creepmeters (Goulty and others, 1978). These events were followed by almost 2 years of quiescence, when the two nail files were added to the array. Then, between June 15 and November 27, 1978, 1.5 cm of dextral creep occurred at Worthington Road, followed by 1.3 cm at Ross Road on May 23, 1979; 0.6 cm at Anderholt Road between November 30, 1978,

and August 20, 1979; and two slip events at Heber Road, on May 27, 1979 (sinistral event discussed below), and August 2, 1979, that produced 0.4 cm of net dextral offset. Whereas the creep sequence in 1977 proceeded from south to north on the Imperial fault, this later sequence began in the north and apparently propagated southward, although the time of creep on the Anderholt Road nail file is not well constrained. In 4 years of creepmeter records, more than 90 percent of the total recorded creep is accounted for by discrete creep events, each of which exhibited several hours of accelerating displacement, 1 to 2 hours of fast creep producing 75 percent of the total slip, and a deceleration phase lasting as long as a day until it was buried in the thermal noise of the instrument. This pattern was empirically described by Crough and Burford (1977).

The creepmeter records show two well-defined episodes of motion on the Imperial fault. Although the second episode occurred 2 to 5 months before the earthquake (fig. 119), these motions cannot properly be construed as precursory indications of the imminent earthquake. The alinement array at County Highway S–80, which was installed in 1967 and has been resurveyed regularly, has shown four intervals of motion during the past years that range from 1 to 2 cm in amplitude and 2 to 4 years in separation (fig. 120). Thus, on the basis of this longer, though discontinuous, record, the recorded creep events in May and August 1979 are consistent with the observed frequency and amplitude of creep episodes on the Imperial fault for the 12 years before the earthquake.

The creepmeter records for the 10-day period immediately before the earthquake also preclude precursory surface motions. Figure 121 shows about 2 days of record from the Tuttle Ranch, Heber Road, and Harris Road creepmeters for the period beginning 30 hours before the earthquake; the record from the Ross Road instrument was lost owing to recorder malfunction. None of the records shows any unusual signals before the earthquake-induced offset, which starts instantaneously on each record.

The 0.12-cm sinistral signal on the record from the Heber Road creepmeter for May 27, 1979, mentioned above, occurred over a 16-hour period; displacement is

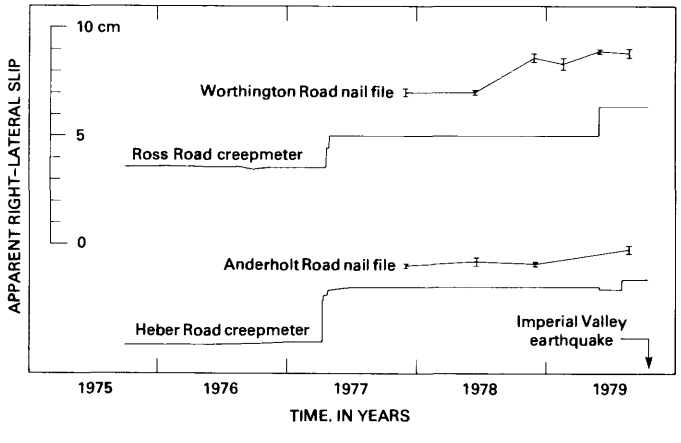

FIGURE 119.—Creep on Imperial fault before 1979 earthquake as a function of time at two creepmeter sites and along two nail files. All traces plotted on same scale; sequence of sites from north to south is displayed from top to bottom (see fig. 118 for location). Nail files show error bars.

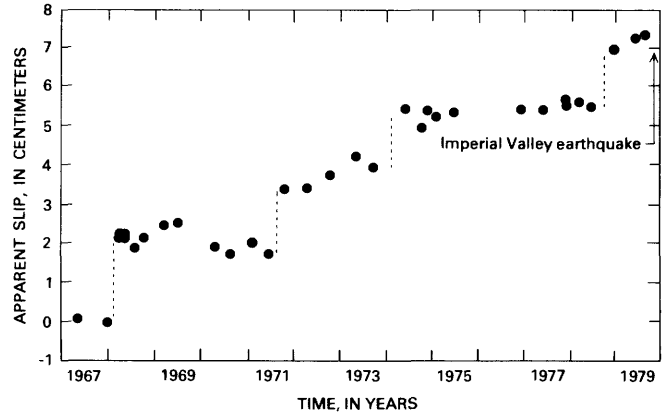

FIGURE 120.—Creep events between 1967 and 1979 at County Highway S–80 alinement array. Extended from Goulty and others (1978).

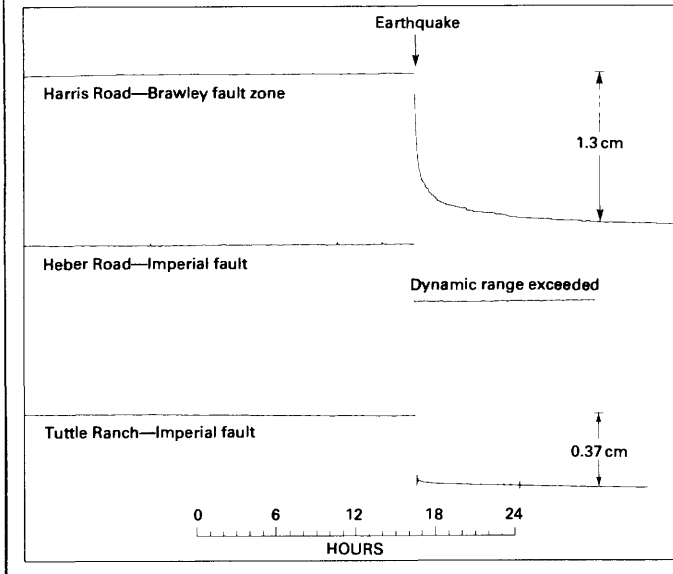

FIGURE 121.—Traced copies of records from creepmeters on Imperial fault and in Brawley fault zone, showing October 15, 1979, earthquake, displayed with same time scale. Records indicate quiescence on faults before event. Instruments on Imperial fault show that surface faulting was instantaneous, within resolution of instruments. Record for Brawley fault zone shows that slip behavior at surface resembled creep.

distributed more evenly over time than a typical dextral-creep signal. This event is probably real because nothing within the instrument has been known to produce such a signal, although it may represent a compressive strain of 6×10^{-5} rather than actual slip on the fault, because the effects would be instrumentally indistinguishable. This much strain is large but appears reasonable from initial studies, in which case the event may be related to deep-seated processes that also produced the 1.3-cm dextral event at Ross Road 4 days earlier.

Thus, although creep events occurred on the Imperial fault at no less than three sites within 6 months before the earthquake, we consider these events to be consistent with the observed long-term pattern of creep and not to be precursory indicators of the earthquake.

COSEISMIC DISPLACEMENT

Coseismic displacement of at least several centimeters occurred at the surface along most of the Imperial fault in California during the 1979 earthquake. Because the dynamic range of the creepmeters deployed along the fault is about 2.5 cm (3.5 cm of motion resolved on the fault), the instruments in the central segment of the fault were broken immediately by slip on the fault. However, the displacement at the Tuttle Ranch, near the southernmost extent of observed surface offset, was only 0.37 cm, and the instrument was able to continue in operation. We note in figure 121 that the Tuttle Ranch creepmeter record shows 12 minutes of shaking from seismic waves of the main event and first aftershocks, entirely confined to the period after the offset. The record was drawn by an Esterline Angus impact-type recorder on pressure-sensitive paper; an impact mark is made every 2 s. The presence on the original record (not shown in fig. 121) of only three impact marks that could have been made during the offset implies that the offset occurred in less than 8 s. The shaking observed from three subsequent aftershocks confirms that the creepmeters record strong surface waves. This behavior is important because the instruments have no other time base than the somewhat variable chart-recorder speed, and thus events can be precisely related in time only from the record of ground shaking.

The Heber Road creepmeter record displays an instantaneous offset without any intervening stray marks or evidence of shaking before the offset. Therefore, we conclude that at least 3.5 cm of motion occurred on the fault within 2 s at most before the arrival of strong shaking. This result is not surprising, in that particle velocities of many tens of centimeters per second would be expected and were in fact observed at the nearby Imperial Valley College (Thomas Heaton, oral commun., 1979). However, the record implies that the rupture propagated upward to the surface at about the shear-wave velocity and that the soil failure was brittle and in concert with the underlying rock, rather than plastic and delayed, as has been observed with creep (Goulty and Gilman, 1978). This record comes closer to measuring the actual rate of surface fault displacement than any other known observations.

No coseismic record was obtained from the Ross Road creepmeter owing to previous chart-recorder malfunction.

The creepmeter record at Harris Road, within the Brawley fault zone, is shown at the top of figure 121. The 1979 motion in the Brawley fault zone was principally vertical, downward on the west side. The Harris Road instrument is installed backward owing to siting restraints (see fig. 118), and dextral motion corresponds to contraction of the instrument. Thus, vertical motion on the fault would appear as sinistral motion on the record but would be recorded at much lower gain because the angle between the fault and the wire is close to 90° for that component of slip. The record shows contraction that represents primarily the dextral component of a principally vertical displacement. Fortuitously, the signal amounts to only 1.3 cm, and so the instrument remained on scale. Except for the instantaneous start of the event, again before the recording of ground shaking, the record is identical to that of creep events at other times at Ross Road (fig. 122; Goulty and others, 1978). This result suggests either that the soil did not accurately follow the motion of the rock at depth or that the motion at depth was actually a triggered creep process associated with the earthquake.

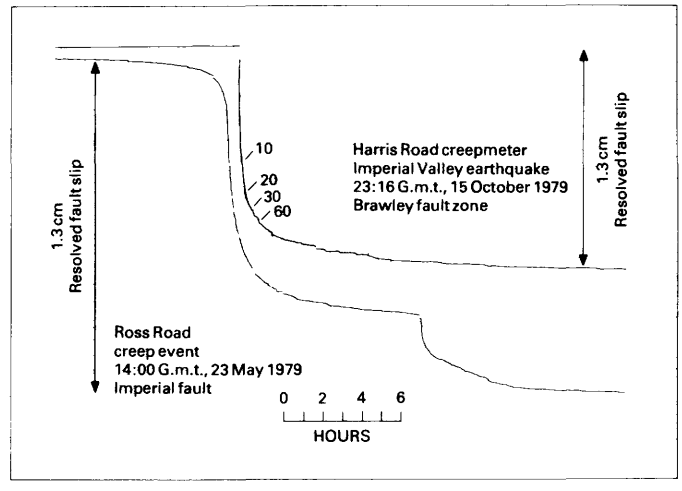

FIGURE 122.—Signal at Harris Road in Brawley fault zone, showing movement associated with earthquake (upper curve), in comparison with creep event recorded 5 months earlier at Ross Road on Imperial fault (lower curve), shown at same time scale. Numbers on upper curve indicate minutes after onset of displacement, determined from original record.

In summary, the recorded surface motions on the faults indicate several modes of behavior. At Heber Road the soil apparently failed by brittle fracture that suggests elastic response and presumably accurately reflects the underlying rock displacement. In contrast, all but 7 percent of the slip in the Brawley fault zone appears to be better characterized as creep triggered by the earthquake.

POSTSEISMIC CREEP

Afterslip on the Imperial fault from the 1979 Imperial Valley earthquake has been monitored by three techniques. Figure 123 shows the records from two creepmeters and two nail files, all in the aftercreep zone. Data from four fault-crossing alinement arrays, which should make a significant contribution to the other studies, are currently being studied.

The Worthington Road and Anderholt Road nail files were resurveyed 8 and 19.5 hours after the earthquake, respectively, and subsequently were resurveyed six more times in the month following the earthquake. Repair and resetting of the creepmeters at Heber Road and Ross Road was impractical during the first week after the earthquake because the creep rate was so high that the instruments would have required almost daily servicing, owing to their limited 2.5-cm range. The creepmeters were placed back in service on October 23 and 24, 1979, and have since been maintained as necessary.

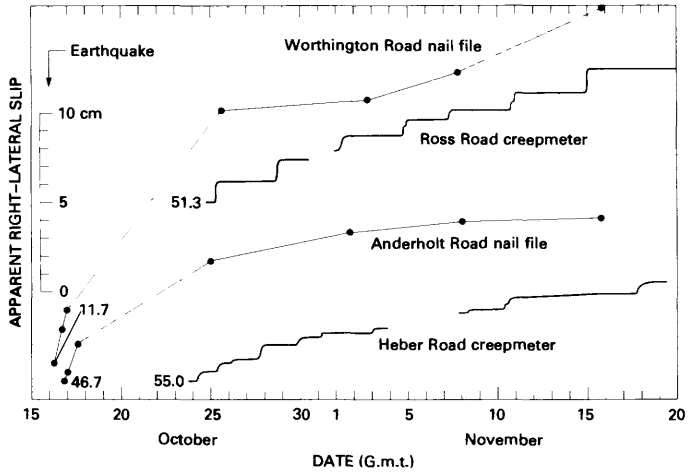

FIGURE 123.—Creep on Imperial fault after earthquake, recorded by creepmeters and nail-file surveys. All traces are shown on same scale; sequence of sites from north to south is displayed from top to bottom (see fig. 118 for locations). Numbers next to each trace indicate offset (in centimeters) accumulated between preearthquake period and time of first measurement after earthquake. For creepmeters, offset values are calculated from preliminary results of mekometer-network surveys (Chris Crook and Peter Wood, oral commun., 1979). Drafting of individual creep events is illustrative but does not necessarily accurately represent displacement histories.

Figure 123 illustrates the history of displacement as a result of creep on the Imperial fault for the first 35 days after the earthquake. The nail files permit an absolute determination of the total offset that occurred between August 20, 1979, and the postearthquake resurveys. Total-offset data were not available from the creepmeters because the range of each had been exceeded. We instead relied on preliminary data reductions of mekometer surveys (from trilateration networks across the fault) near the creepmeter sites to recover the extent of cumulative offset before restarting the instruments (Chris Crook and Peter Wood, oral commun., 1979). We also used these data reductions to recover the amount of offset between October 31 and November 1, 1979, when the range of the Ross Road creepmeter was exceeded between service trips. This procedure is justified by the close agreement between these two measurements where both data sets are complete. The hiatus in the Heber Road creepmeter record represents only a failure in the chart recorder. The amount of total motion was obtained from micrometer measurements made with the instrument itself.

Both creepmeter records show that virtually all the accumulating creep is due to discrete events, each lasting about 1 day, and that most of the displacement occurred during 1- to 2-hour periods. At Ross Road the events are all 1 ± 0.5 cm in amplitude and show no trend in size as a function of time; the events simply occur less frequently with increasing time. The same effect was observed at Heber Road, although the amplitude is smaller (0.5 ± 0.3 cm) and events are more frequent.

Displacement as a function of time for the two nail files, for which the longest span of observations is available, is well represented by linear functions of $\log_{10} t$, where t is the postearthquake time. A similar relation was observed for the 1966 Parkfield, Calif., earthquake by Smith and Wyss (1968). Figure 124 plots the displacement on the Anderholt Road and Worthington Road nail files as a function of the logarithm of postearthquake time (in hours). The two dashed lines, described by the equations

$$\text{Disp}=44+8.5\log_{10} t$$

and

$$\text{Disp}=3+8.7\log_{10} t,$$

approximate the observed displacements for Anderholt Road and Worthington Road, respectively, during the first 5 months after the earthquake. Interestingly, the coefficients of $\log_{10} t$ are very near the values observed by Scholz and others (1969) for displacements during the first 2 years after the 1966 Parkfield earthquake. This result suggests that we may use these equations to

predict crudely the average creep rate for at least the next few months. If these relations are projected far into the future, using the slower Anderholt Road creep rate and a background preearthquake creep rate of about 0.5 cm/yr (see fig. 120), then the projected aftercreep rate on the Imperial fault associated with the 1979 earthquake will take at least 6 years to fall below the average creep rate observed during the past 12 years.

Including the relatively small amount of projected afterslip, the 6-year total displacement associated with the 1979 earthquake on the surface trace of the Imperial fault has the following values:

Locality	*Displacement (cm)*
Worthington Road	50
Ross Road	72
Anderholt Road	80
Heber Road	79
Tuttle Ranch (Cole Road)	1

In the area where major slip occurred, the sites with the smallest offsets (Worthington Road and Ross Road) show the highest aftercreep rates (fig. 123). The offset values converge to approximately 50 to 80 cm; thus, the surface may be catching up with the more evenly distributed slip at depth.

In summary, we have documented the aftercreep from the 1979 Imperial Valley earthquake at these sites entirely as discrete events of rather uniform amplitude that occur with such decreasing frequency that the total displacement is presently well fitted by linear functions of $\log_{10} t$. Projecting the creep rate into the future suggests that afterslip from the earthquake should dominate creep processes on the Imperial fault for at least the next 6 years

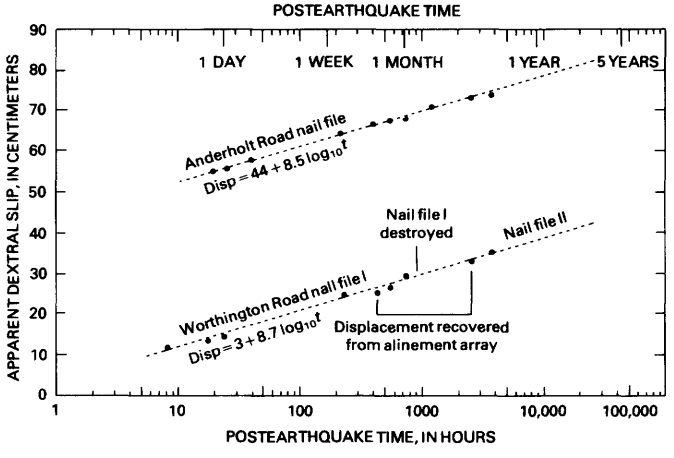

FIGURE 124.—Displacement (Disp) on Anderholt Road and Worthington Road nail files as a function of postearthquake time (t). Fix of regression lines suggests that approximate creep rates may be predicted at least several months in advance.

CONCLUSIONS

1. Creep events observed at three sites on the Imperial fault 2 to 5 months before the 1979 Imperial Valley earthquake are consistent with the long-term pattern of creep on the fault and do not qualify as anomalous behavior precursory to the earthquake.
2. No creep was observed at any of the sites on the Imperial fault or in the Brawley fault zone during the 10 days preceding the earthquake.
3. The coseismic surface displacements on the Imperial fault started at or before the arrival of heavy shaking and proceeded faster than 1.8 cm/s. The coseismic surface displacements in the Brawley fault zone started at or before the arrival of heavy shaking but proceeded at a slower, exponentially decaying rate. The displacement history several seconds after the initiation of motion is virtually identical to that seen in regular creep events.
4. Afterslip on the fault amounted to as much as 20 cm during the 35-day period beginning 8 hours after the earthquake. This aftercreep, where recorded by creepmeters, occurred in discrete creep events of 0.2- to 1.5-cm amplitude.
5. The total afterslip as a function of time is approximated well by linear functions of $\log_{10} t$. Projection of the observed creep rate into the future implies that the rate of aftercreep associated with the 1979 earthquake will be greater than the average preearthquake creep rate for the next 6 years.
6. The total surface slip on the Imperial fault associated with the earthquake, including projected afterslip, should accumulate to between 50 and 80 cm at Worthington Road, Anderholt Road, Ross Road, and Heber Road.

REFERENCES CITED

Allen, C. R., Wyss, Max, Brune, J. N., Grantz, Arthur, and Wallace, R. E., 1972, Displacements on the Imperial, Superstition Hills, and San Andreas faults triggered by the Borrego Mountain earthquake, *in* The Borrego Mountain earthquake of April 9, 1968: U.S. Geological Survey Professional Paper 787, p. 87–104.

Brune, J. N., and Allen, C. R., 1967, A low-stress-drop, low-magnitude earthquake with surface faulting: The Imperial, California, earthquake of March 4, 1966: Seismological Society of America Bulletin, v. 57, no. 3, p. 501–514.

Crough, S. T., and Burford, R. O., 1977, Empirical law for fault-creep events: Tectonophysics, v. 42, no. 1, p. T53–T59.

Goulty, N. R., Burford, R. O., Allen, C. R., Gilman, Ralph, Jotnson, C. E., and Keller, R. P., 1978, Large creep events on the Imperial fault, California: Seismological Society of America Bulletin, v. 68, no. 2, p. 517–521.

Goulty, N. R., and Gilman, Ralph, 1978, Repeated creep events on the San Andreas fault near Parkfield, California, recorded by a strainmeter array: Journal of Geophysical Research, v. 83, no. B11, p. 5415–5419.

Nason, R. D., 1973, Fault creep and earthquakes on the San Andreas fault, *in* Kovach, R. L., and Nur, Amos, Proceedings of the conference on tectonic problems of the San Andreas fault system: Stanford University Publications in the Geological Sciences, v. 13, p. 275–285.

Scholz, C. H., Wyss, Max, and Smith, S. W., 1969, Seismic and aseismic slip on the San Andreas fault: Journal of Geophysical Research, v. 74, no. 8, p. 2049–2069.

Sharp, R. V., 1976, Surface faulting in Imperial Valley during the earthquake swarm of January–February 1975: Seismological Society of America Bulletin, v. 66, no. 4, p. 1145–1154.

Smith, S. W., and Wyss, Max, 1968, Displacement on the San Andreas fault subsequent to the 1966 Parkfield earthquake: Seismological Society of America Bulletin, v. 58, no. 6, p. 1955–1973.

Yamashita, P. A., and Burford, R. O., 1973, Catalog of preliminary results from an 18-station creepmeter network along the San Andreas fault system in central California for the time interval June 1969 to June 1973: U.S. Geological Survey open-file report, 215 p.

PREEARTHQUAKE AND POSTEARTHQUAKE NEAR-FIELD LEVELING ACROSS THE IMPERIAL FAULT AND THE BRAWLEY FAULT ZONE

By ROBERT V. SHARP and JAMES J. LIENKAEMPER,
U.S. GEOLOGICAL SURVEY

CONTENTS

ABSTRACT

Three short (less than 250 m) leveling lines were installed across the Brawley fault zone at Keystone, Harris, and Worthington Roads after the January–February 1975 Imperial Valley earthquake swarm; in 1976 a line was also installed at Harris Road crossing the Imperial fault. Releveling was performed approximately annually, more frequently when deformation was observed. Postearthquake releveling began 43 hours after the October 15, 1979, earthquake and was repeated at 5-day intervals until November 1. Because of the diminishing rate of afterslip, surveying frequency was reduced thereafter.

Preearthquake vertical movement on the Imperial fault between January 1976 and April 1979 generally consisted of tilting toward the Mesquite basin; however, apparent discrete slip (3 cm) may have been a delayed effect of the October 1977 earthquake swarm (about 5 km distant; max $M_L = 4.3$). The largest tilt (54 microradians) was observed between January and April 1979. No significant tectonic deformation was detected from April through July 1979. Although the duration of the tilting period is not tightly constrained, it may agree approximately with the expected duration of precursory ground deformation for an earthquake of the magnitude of the 1979 event. Releveling on October 17, 1979, showed 16 cm of vertical displacement on the Imperial fault trace. The total vertical displacement (coseismic slip plus afterslip) increased logarithmically with time. By December 29, 1979, cumulative afterslip was 14 cm, about as much as the coseismic slip. An asymmetric profile of vertical deformation for all periods suggests an obliquely dipping fault.

The Brawley fault zone appeared relatively quiescent between January 1976 and April 1979 except for one small (0.8 cm) displacement that occurred at Harris Road between October 25, 1977, and January 1979, during which time the displacement on the Imperial fault also appeared. From north to south, the Brawley fault zone showed coseismic displacements of 9–10 cm at Keystone Road, 6.3 and about 7 cm on the west and east breaks, respectively, at Harris Road, and 9.5 cm at Worthington Road. No afterslip greater than 1 cm was measured on the Brawley fault zone.

The high level of background seismicity and infrequent fault displacement make the relation of the observed preearthquake vertical deformations to the 1979 earthquake unclear.

INTRODUCTION

The measurements of vertical deformation described in this chapter began after the Imperial Valley earthquake swarm of January–February 1975 but were expanded to incorporate new faults discovered after the October 15, 1979, earthquake. To determine the profiles of roads displaced vertically during the 1975 swarm, short-distance leveling-survey lines were established across the Brawley fault zone at Keystone, Harris, and Worthington Roads (Sharp, 1976); the longest of these lines was 240 m, and all were approximately centered on the fault trace. Because local residents and County road department personnel had noticed deformation before that earthquake swarm on Keystone Road where a fault strand intersected it, precise determinations of vertical surface displacement associated with those events were not possible, although the data did provide a measure of all deformation since paving of the roads.

In anticipation of future vertical movements on the Brawley fault zone and the Imperial fault—structures bounding the artificially drained basin of former Mesquite Lake—the three survey lines crossing the Brawley fault zone were remeasured annually, and one new line crossing the Imperial fault at Harris Road was constructed (fig. 125).

The high level of seismic activity in the Mesquite basin sector of the central Imperial Valley seismic belt (see Johnson and Hill, this volume) and the peculiar distribution of 1975 surface rupturing relative to earthquake epicenters suggested that frequent releveling of the survey lines was appropriate. Because our earlier experience led us to anticipate changes of elevation only after displacements happened, these lines were not designed to monitor the large-scale tilting that we began

to detect in October 1977, 2 years before the 1979 earthquake.

The possibility that deformation of the land surface in the Imperial Valley is due to periodic irrigation must be evaluated. Crops are grown in the Imperial Valley region on a year-round basis, and virtually all of them are irrigated with Colorado River water. Water has saturated the sediment under the valley, and so below the depths of the agricultural drainage system, generally just a few meters below the ground surface, the saturation is continuous. Consequently, fluctuations in the water content of the uppermost few meters of soil could contribute to minor changes in ground level, although we consider that the deformation reported here is largely tectonic in origin and that ground-water effects are minimal.

SURVEYING PROCEDURE

The leveling surveys were measured from nails driven into the pavement, approximately 0.3 m from the south edge on the roads crossing the Brawley fault zone and from the north edge of Harris Road where it crosses the Imperial fault. A Wild NAK–2 level was used with a Fiberglass rod and sighting distances generally shorter than 30 m. Maximum errors in the relative elevation determined at each station are estimated to be ±1.5 mm. Although the apparently erratic changes in relative elevation of a few millimeters in several relevelings probably are real rather than due to surveying errors, most of these changes probably reflect nontectonic processes affecting the road surface or the materials beneath the roadbed.

For nearly every survey, the leveling was repeated with the same rod and the same instrument, set up in the same places. The leveling data reported here are not fixed to any survey monuments beyond the limits of the lines. The end points of the lines on the downthrown sides of the faults (west ends for the Brawley fault zone, east end for the Imperial fault) were arbitrarily chosen as fixed datums.

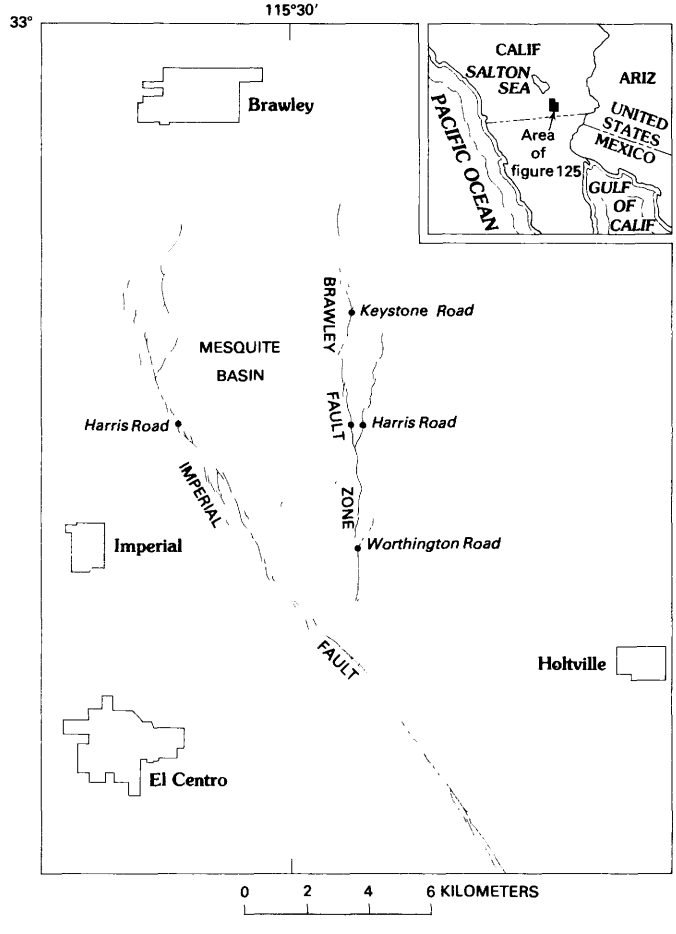

FIGURE 125.—Location map for leveling-survey lines across Imperial fault and Brawley fault zone.

ELEVATION CHANGES ACROSS THE IMPERIAL FAULT

The 210-m survey line centered on the Imperial fault at Harris Road was constructed on January 21, 1976. The profile of elevations along the survey line, after its extension to 390 m on July 6, 1979 (fig. 126*A*), depicts a total Quaternary vertical offset of the valley floor across the Imperial fault of more than 8 m. This offset is the consequence of cumulative vertical displacement of an unknown number of slip events during Holocene and possibly late Pleistocene time. The Harris Road survey line was subsequently releveled five times before the October 15, 1979, earthquake, and the cumulative changes in level through each survey relative to the initial survey are plotted in figure 126*B*. To emphasize the shape of the profiles of relative vertical displacement for the shorter intervals, the elevation differences recorded at the time of each survey are plotted separately (fig. 127).

PREEARTHQUAKE LEVELING DATA

January 21, 1976, to January 14, 1977.—The profile of elevation changes for this interval (fig. 127*A*), is irregular but suggests a slight upward movement on the west side of the fault as well as along a 30-m-long zone east of the trace. The irregularity of this profile, more pronounced during this interval than in any later period, may be related to the unusually heavy rainfall and runoff of September 10, 1976, that caused overflowing of drainage ditches and flooding in the Mesquite basin near Harris Road.

January 14 to October 25, 1977.—Figure 127*B* plots the observed elevation changes across the Imperial fault during this interval. The survey on October 25,

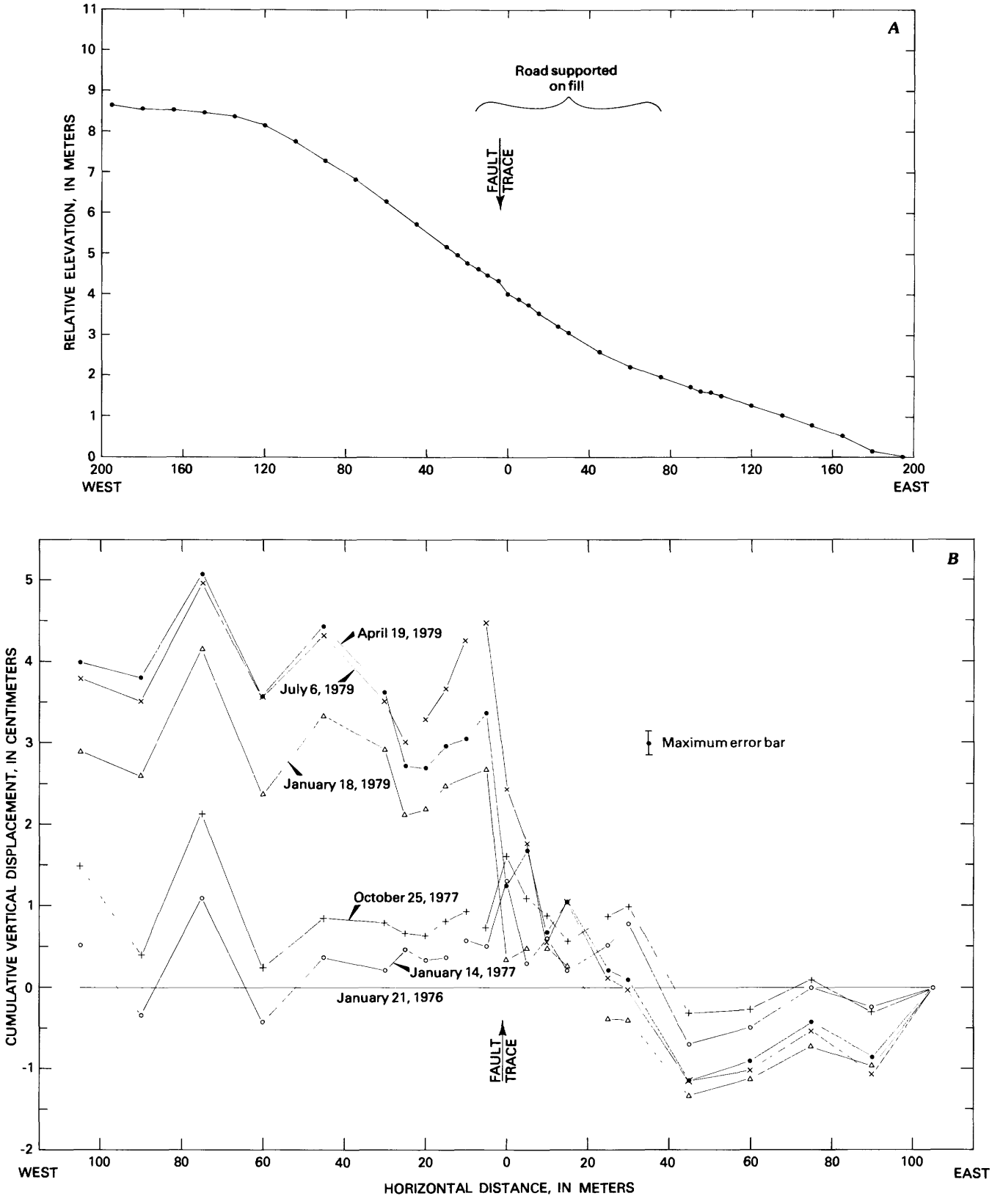

FIGURE 126.—Relative elevation and displacement on Imperial fault at Harris Road. *A*, Profile of relative elevation, indicating preearthquake slope in pavement and height of escarpment. *B*, Cumulative elevation changes for all surveys before October 15, 1979, earthquake; datum is initial survey of January 21, 1976, at station 105 m east. Maximum error for all stations shown by bar.

1977, was made after the first 5 days of a swarm of nearby small earthquakes that lasted about 3 weeks. The only apparent ground deformation for this 9-month period was a relatively smooth tilt downward to the east (toward the Mesquite basin) of about 48 microradians measured between end points of the survey line.

Although the survey was completed in the midst of an earthquake swarm that occurred to the east of the leveling line, inspection of the road surface revealed no clear evidence of vertical displacement on the fault trace from the early events of that swarm. From October 20 to 22, four events of magnitude 4.0 or larger occurred between

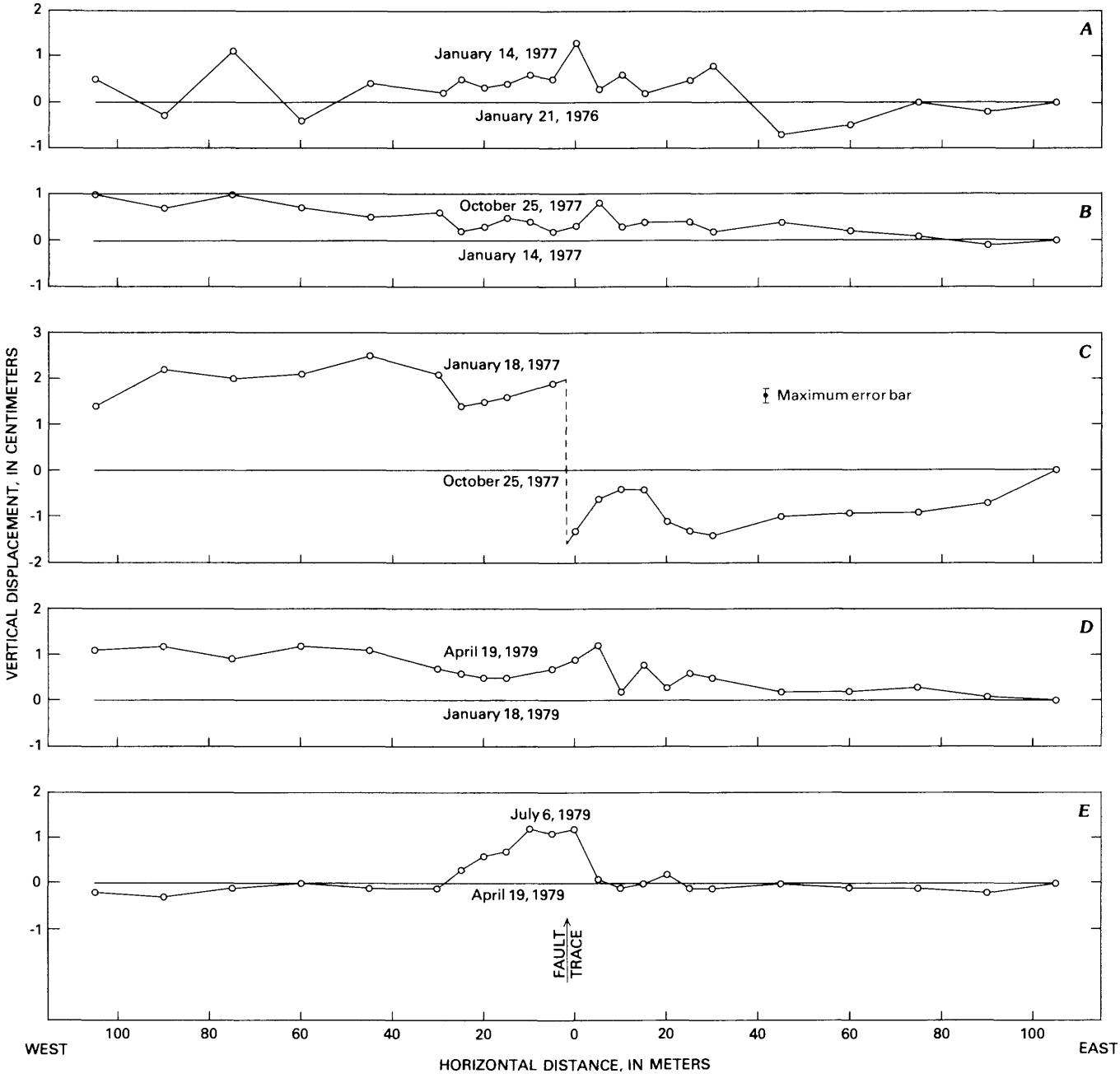

FIGURE 127.—Elevation changes across Imperial fault at Harris Road for different intervals before earthquake. Maximum error for all stations shown by bar. *A*, Changes for interval January 21, 1976–January 14, 1977. *B*, Changes for interval January 14–October 25, 1977. *C*, Changes for interval October 25, 1977–January 18, 1979. *D*, Changes for interval January 18–April 19, 1979. *E*, Changes for interval April 19–July 6, 1979.

2.4 and 4.2 km to the east of the line (Johnson, 1979). The relation of the eastward tilting observed at Harris Road during this interval to the earthquake-swarm activity is unclear.

October 25, 1977, to January 18, 1979.—Figure 127*C* plots the deformation measured during this interval. The releveling data indicate that the west side of the fault rose about 2 cm relative to the datum at the east end of the survey line, but that possibly 2 to 4 cm of relative uplift occurred on the fault trace. The form of the profile of elevation changes, especially the relatively flat uplift west of the fault and the subsidence between the fault and the east end of the leveling line, closely resembles that of coseismic displacement from the 1979 earthquake, as discussed below in this chapter. Upward tilting of the side west of the fault in conjunction with the fault displacement is not indicated by the shape of the elevation profile. Although new movement on the main fault trace was not recognized among the many old cracks that had formed in the pavement during earlier displacements (see Allen and others, 1972), the displacement may have been distributed across the 5-m survey interval that included the fault trace. In any case, the pavement showed no obvious evidence of an approximately 3 cm high scarp centered on the fault trace.

The 15-month interval between surveys included part of the earthquake swarm that began October 20 and continued into mid-November 1977 (fig. 128). Epicenters of most of these events were clustered about a north-northeast-trending line about 2 to 4 km east of where Harris Road crosses the Imperial fault. The possible fault displacement at Harris Road could reflect a creep event that, if already underway at depth, had not reached the surface by the time of the October 25 survey. No surface displacement is known to have occurred within the Mesquite basin on a fault that may have been more closely associated with the earthquakes of that swarm. Although the time of appearance of the vertical tilt or displacement on the Imperial fault at Harris Road is bracketed only by the leveling surveys and thus is not accurately known, this surface deformation and that at Harris Road in the Brawley fault zone (discussed below) appear to be the only significant movements documented near the Mesquite basin within the interval that includes the swarm.

January 18 to April 19, 1979.—Elevation changes at Harris Road during this interval (fig. 3*D*) resemble in profile those of the interval January 14–October 25, 1977, although the time elapsed was less than one-third that of the earlier interval. An approximately equal tilt downward to the east is spread fairly evenly across the length of the line. For this 3-month period the eastward tilt was about 54 microradians, the largest observed during all the releveling. Although a few irregularities were observed along a 20-m segment of the line just east of the fault trace, they did not appear to be fault offsets, and no signs of disturbance in the pavement were noted. The seismicity during this interval (fig. 129) indicates that the nearest event of $M_L \geq 2.0$ was farther than 9 km from Harris Road along the Imperial fault. The tilting is not clearly related to contemporaneous seismicity near the leveling site.

April 19 to July 6, 1979.—Because the tilt for the preceding interval was so large, monitoring over shorter periods was continued. In addition, the length of the survey line was extended to determine better whether the leveling fluctuations were due solely to near-surface deformation or reflected more deep seated strain. Although a very long line of first-order leveling could have provided data on the depth of activity, the quality of our leveling stations and instruments did not justify a large expansion of our existing line.

Figure 127*E* shows the leveling changes at the end of this interval. The tilting had apparently stopped, but an asymmetric bulge about 1 cm high formed between about 5 m east of the fault scarp and 30 m west of it. As during the previous surveys, no conspicuous changes were visible on the surface of the road during this releveling.

The seismicity during this interval (fig. 130) was slight; one event of $M_L > 2$ occurred on May 25, about 1.9 km southeast of the leveling array at Harris Road. Cessation of the earlier, most rapid tilting with no substantial change in the low level of seismicity implies that the earlier leveling changes may not have been related to the normal background seismicity but, instead, to an event yet to happen.

EARTHQUAKE DISPLACEMENT DATA

July 6 to October 17, 1979.—Releveling of the array 1½ days after the October 15, 1979, earthquake (fig. 131*A*) showed that many features of the fault displacement resembled those of the earlier displacement between October 1977 and January 1979. Perhaps the most important features were blocklike behavior of the upthrown (west) side of the fault and subsidence of the ground surface between the fault trace and the east end point of the leveling line on the downthrown side. The profile (fig. 131*A*) clearly shows that the deformation extended at least beyond the east end of the survey line and probably beyond the west end as well. The steepness of tilt at the east end of the line, if extrapolated farther eastward, suggests that the net vertical component of displacement relative to a point only 30 m farther east is substantially smaller than that recorded over the 390-m length of the survey line and, indeed, could approach zero.

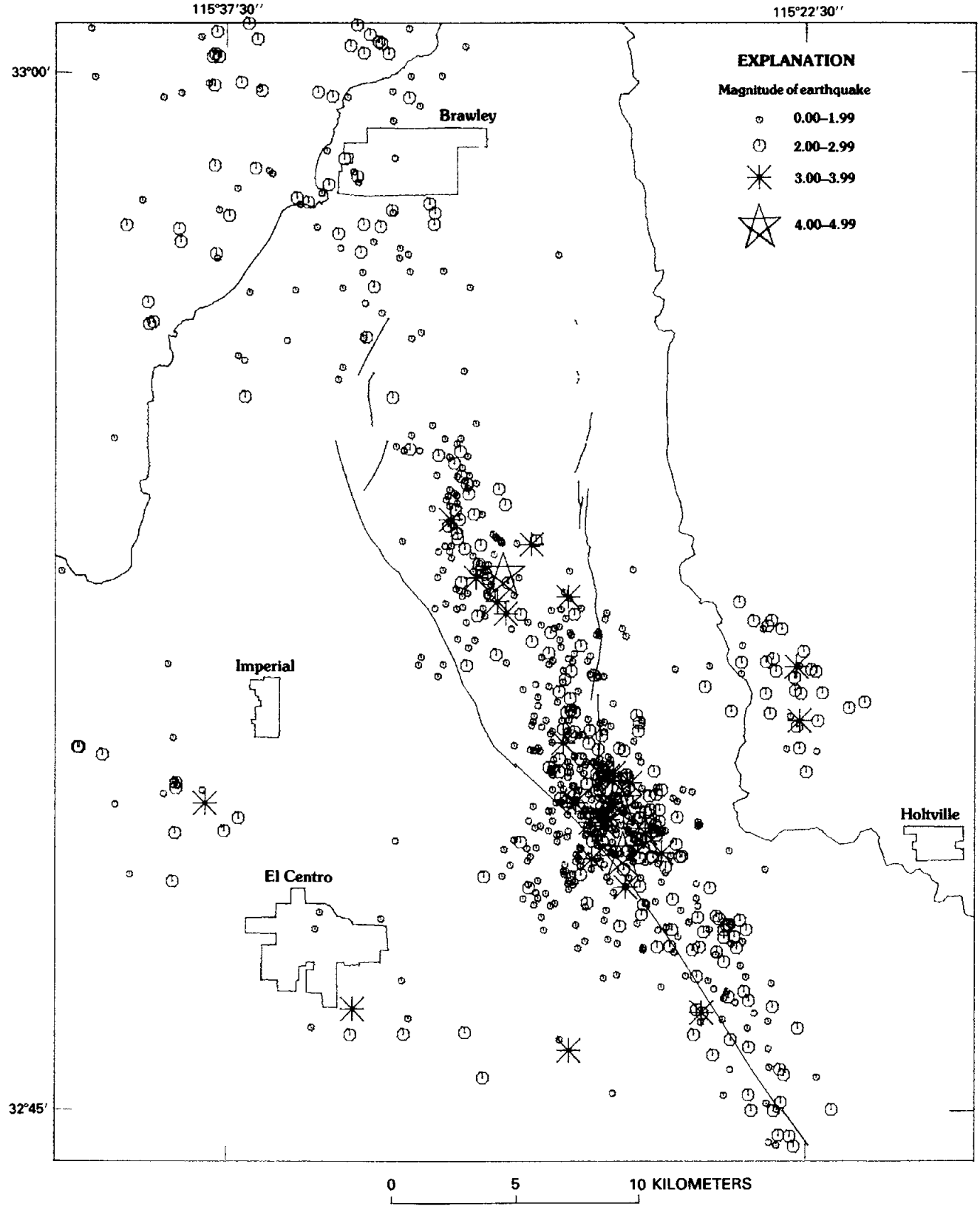

FIGURE 128.—Seismicity map for area around Mesquite basin for interval October 25, 1977–January 18, 1979. Map supplied by C. E. Johnson.

The relative depression centered about 30 m to the east of the fault trace appears, for several reasons, to be a real tectonic feature rather than the result of slumping or other surficial deformation within fill under that section of the road. Although no obvious settling or slope failure was observed along the margins of the fill ramp after the main shock, the most convincing facts arguing for a tectonic origin are that the slope of the tilt does not differ significantly within the filled section of the road from the slope farther east, and that a similar feature continued to form in the same place during the first 2 months of continuing postearthquake slip.

Station 0 (fig. 131*A*) probably was affected by surficial disturbance and consequently should be neglected in interpreting both the form and amount of deformation during the earthquake. In addition to the main fault trace about 2 m west of station 0, a secondary crack broke the pavement between stations 0 and 5 m east. This detached block containing station 0 may have settled or rotated during and after the main displacement. By disregarding station 0, we obtain a probably better measure of the relative vertical offset on the fault trace of about 16 cm, rather than the 19 cm of displacement recorded between stations 0 and 5 m west.

The first postearthquake profile of elevation differences (fig. 131*A*) includes about 42 hours of afterslip. On the basis of subsequent relevelings extrapolated logarithmically backward to the time of the earthquake, we attribute approximately 1.7 cm of this movement to afterslip, and we estimate that the extent of coseismic vertical displacement on the Imperial fault at Harris Road was about 14 cm.

A moderate (M_L=4.4) aftershock was felt at 12:14 p.m. P.s.t. October 17, just as the first postearthquake releveling was completed. A quick releveling between stations 0 and 5 m west, which bracket the fault trace, was completed within 7 minutes after the event; the results showed no changes in elevation from approximately 2 hours earlier. Although the aftershock epicenter was about 5 km west-northwest of the leveling line, it apparently did not trigger a measurable creep event that reached the surface at Harris Road within this brief period of releveling.

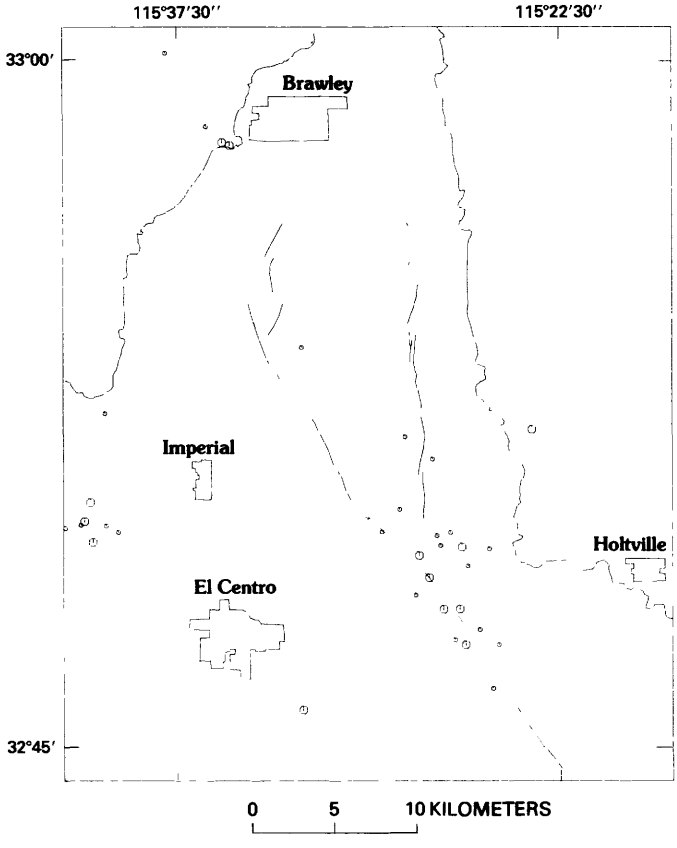

FIGURE 129.—Seismicity map for area around Mesquite basin for interval January 18–April 19, 1979. Magnitude symbols same as in figure 128. Map supplied by C. E. Johnson.

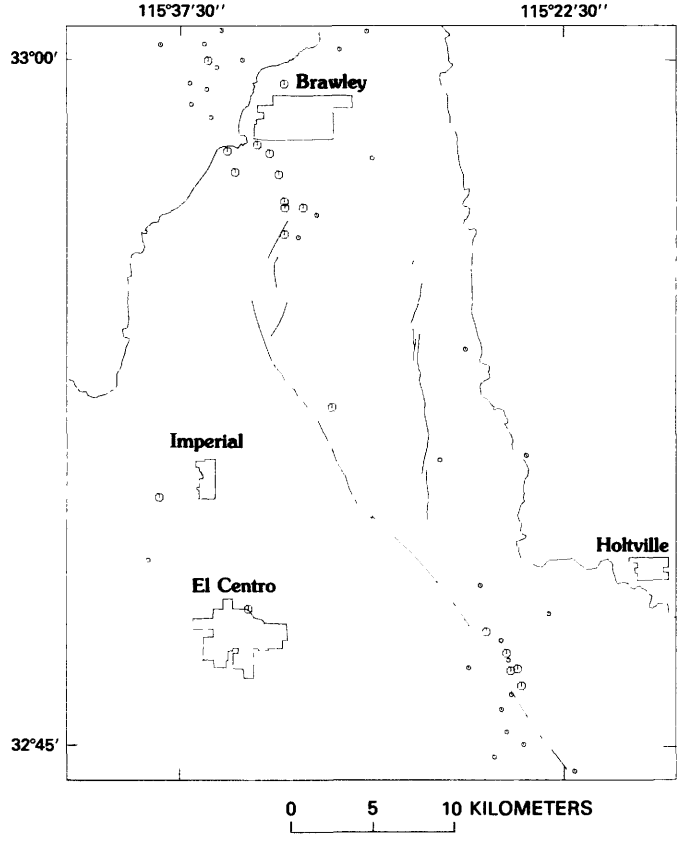

FIGURE 130.—Seismicity map for area around Mesquite basin for interval April 19–July 6, 1979. Magnitude symbols same as in figure 128. Map supplied by C. E. Johnson.

AFTERSLIP DATA

October 17 to December 29, 1979.—Relative changes in elevation during this interval were determined from eight sequential relevelings 5, 10, 15, 20, 25, 34, 48, and 73 days after October 17, 1979. The profiles of changes in relative elevation (fig. 131*B*) reveal a general logarithmic increase in vertical slip, plotted in figure 132.

Two characteristics of these afterslip profiles are especially noteworthy: (1) the shape of the profiles, including the approximately blocklike behavior of the upthrown side west of the fault and the tiltlike shape of the side east of and sloping toward the fault, resembles that of the profile for coseismic vertical slip; (2) the east limit of postearthquake deformation may have been contained within the length of the leveling line. Although the east end of this line was arbitrarily taken as a point of fixed elevation, the slope of the tilted part of the profile significantly decreases eastward to near zero at the easternmost station. These profiles imply that the vertical afterslip may be due to relatively shallow relaxation deformation, in contrast to the profile for coseismic elevation changes, which suggests more deep seated elastic rebound.

The total amount of afterslip on the fault trace could not be precisely determined after November 11 because repavement of the broken section of the road destroyed the survey stations close to the fault trace. By November 11, vertical afterslip on the fault trace totaled about 9.7 cm, if we correct for anomalous behavior of the two stations between the trace and the station 5 m east, and for afterslip incorporated into the elevation changes for the first postearthquake releveling (October 17). Thus, by November 11, vertical afterslip on the Imperial fault at Harris Road was two-thirds of the probable coseismic slip. By December 4 it had grown to about 84 percent, or more than 12 cm, although this value was extrapolated westward to the fault trace from the station 30 m east. Similarly, releveling on December 29 indicated about 14 cm of cumulative afterslip, about as much as the estimated coseismic slip.

Plotted on a logarithmic time scale (fig. 132), the data on cumulative vertical displacement relative to the last preearthquake survey through the period of afterslip measurement are closely fitted by a line whose equation is

$$D = 16.7 + 8.62 \log (1 + 1.052t),$$

where D is the cumulative vertical displacement (in centimeters) and t is the postearthquake time (in days). This equation represents the vertical movement of a point 32 m east of the fault relative to a point 3 m west of the fault. An accurate equation for slip on the fault trace could not be formulated because several leveling marks were destroyed during repaving of the road in the afterslip period. If we use the derivative of the above equation to estimate the vertical-slip rate of the fault, this rate would have been about 19 mm/d at $t=1$, 3.4 mm/d at $t=10$, and 0.4 mm/d at $t=100$.

ELEVATION CHANGES ACROSS THE BRAWLEY FAULT ZONE

Three leveling-survey lines crossing different breaks in the Brawley fault zone have been monitored at approximately annual intervals since the earthquake swarm of January–February 1975 (Johnson and Hadley, 1976; Sharp, 1976). In comparison with the large-scale changes already described for the Imperial fault at Harris Road, the Brawley fault zone was remarkably

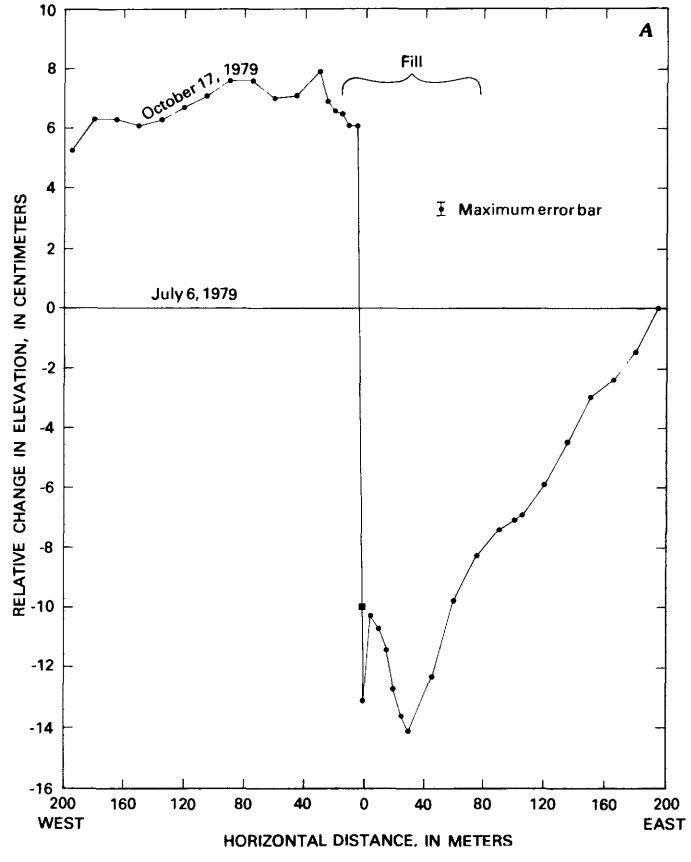

FIGURE 131.—Vertical displacement and afterslip on Imperial fault at Harris Road. Maximum error for all stations shown by bar. *A*, Profile of vertical displacement measured on October 17, 1979, relative to last preearthquake survey. Square denotes estimated elevation at station 0, extrapolated from stations east of fault. *B*, Profiles of cumulative afterslip for interval October 17–December 29, 1979.

stable; in fact, only one substantial change—a small steplike displacement at Harris Road—was measured between 1975 and October 15, 1979.

The characteristic surface expression of breaks within the Brawley fault zone (see Sharp and others, this volume) seldom permits accurate estimation of the vertical components of displacement unless a relatively smooth reference surface is available. Although some newly planted fields allowed direct visual estimation of these vertical components, more fully grown crops either concealed the breaks or, where traceable, made measurement of the vertical component difficult or impossible.

The leveling lines established before the October 15, 1979, earthquake provide the only accurate measures of relative vertical movements and, moreover, demonstrate the vast difference between the overall vertical displacement across a zone several meters wide and the generally much smaller vertical displacements at surface cracks near the points of maximum flexure on the upthrown sides of the traces. These cracks, however, which are the most conspicuous aspect of the faulting, were the features traced in mapping surface ruptures (see Sharp and others, this volume).

KEYSTONE ROAD

From January 1976, the Keystone Road leveling line was relatively stable until the 1979 earthquake. A small irregular bulge, at least 90 m long and mostly less than a centimeter high, centered over the fault trace, had formed by January 14, 1977. Subsequent changes in relative elevation were minor until January 17, 1979, the date of the last preearthquake releveling.

Relative elevations and vertical displacements at the time of the 1979 earthquake were determined by releveling on October 17. The form of the scarp is a step, rounded at both the base and the crest (fig. 133*A*). A slight rounding evident in the 1979 displacement profile

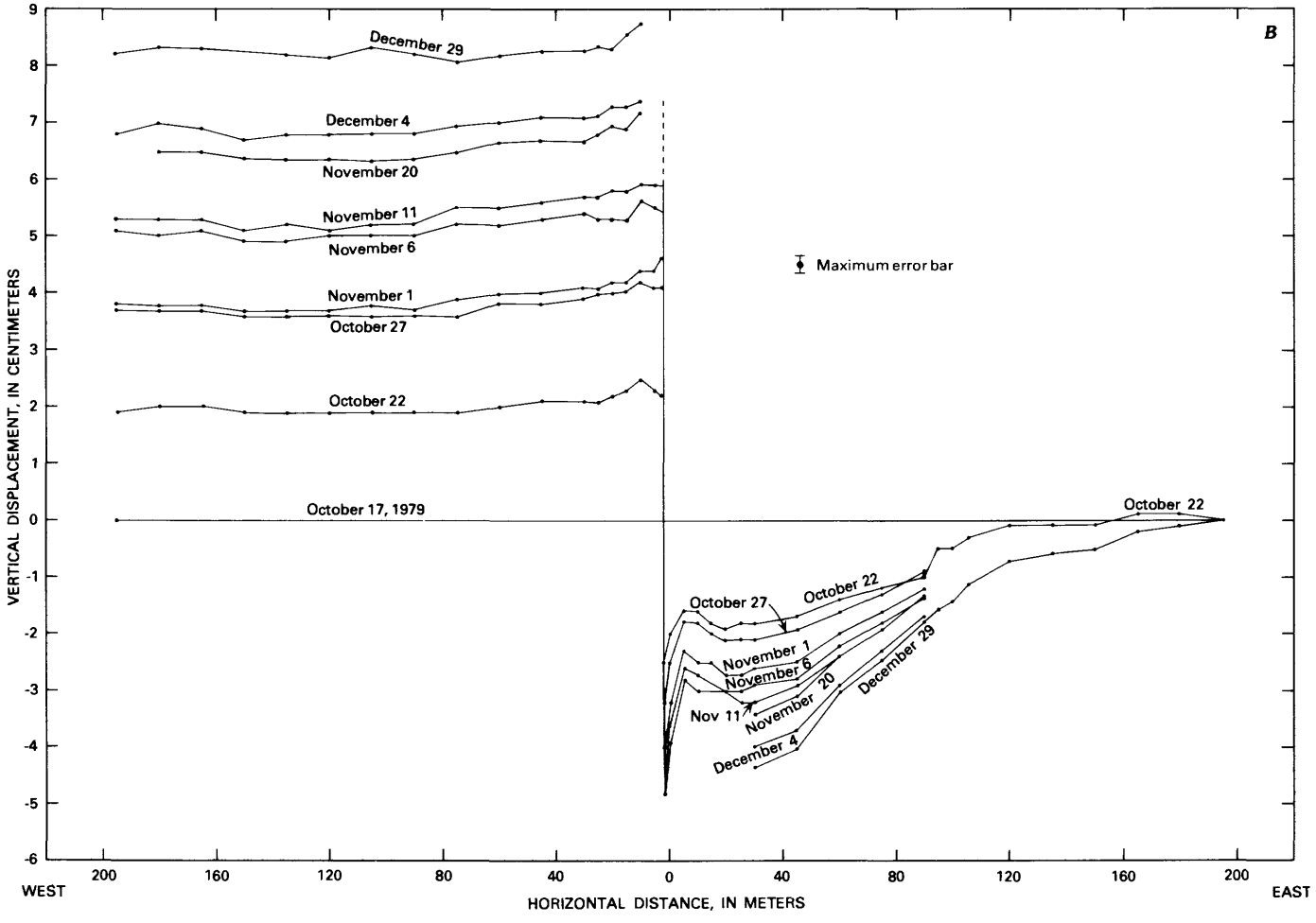

FIGURE 131.—Continued

(fig. 133*B*) indicates that most of the curvature was caused by earlier displacements in the pavement.

Vertical displacement at Keystone Road was about 9–10 cm, probably largely coseismic. A strainmeter measuring the right-lateral component on the Brawley fault zone at Harris Road established that the displacement there grew to about its full dimension over more than 12 hours (Cohn and others, this volume). Releveling of the line on October 22 indicated insignificant vertical afterslip since the first postearthquake survey.

On the basis of leveling across the Brawley fault zone at Keystone Road in 1975, Sharp (1976) estimated, from the size of the escarpment in the pavement and from statements by local residents and County road department employees, that the vertical displacement from the 1975 earthquake swarm was about 20 cm. The greater length of faulting within the Brawley fault zone during the 1979 event suggests that this estimated displacement for the 1975 swarm may be too large and possibly could be less than 10 cm.

HARRIS ROAD

Four leveling surveys at Harris Road between March 3, 1975, and October 25, 1977, revealed a mild bulgelike deformation similar to that formed contemporaneously at Keystone Road. The bulge profile (not illustrated), which reached a height of about 1.4 cm on the fault trace by January 14, 1977, and sloped down toward the east

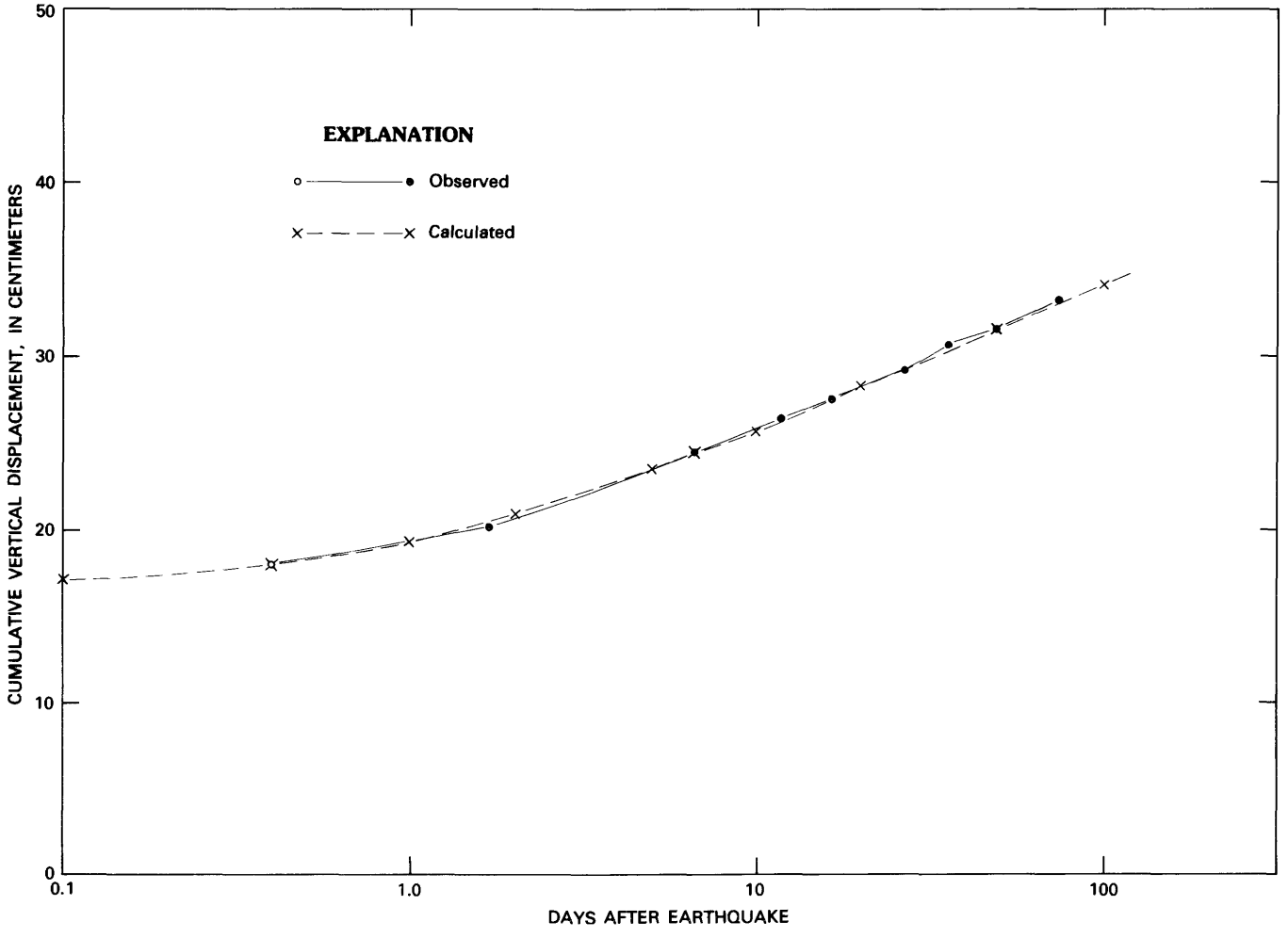

FIGURE 132.—Cumulative vertical displacement as a function of postearthquake time. Dots denote vertical elevation changes between stations 5 m west and 30 m east, which are closest surviving survey points to fault trace for all surveys. Circle denotes a data point obtained indirectly and adjusted from displacement on fault rupture measured by K. E. Sieh during night after earthquake. Solid line joins observed data points. Crosses denote vertical displacements calculated from equation given in text, and dashed line is curve of that equation.

and west end points of the profile, collapsed slightly between January 14 and October 15, 1977. During the 15-month period between October 1977 and January 1979, a vertical displacement of about 0.8 cm raised the east side of the fault relative to the west (fig. 134*B*). Whether this deformation was a warp or an offset on the fault is unknown. Part of the deformation appeared about 24.5 m east of the main trace on a fault trace that

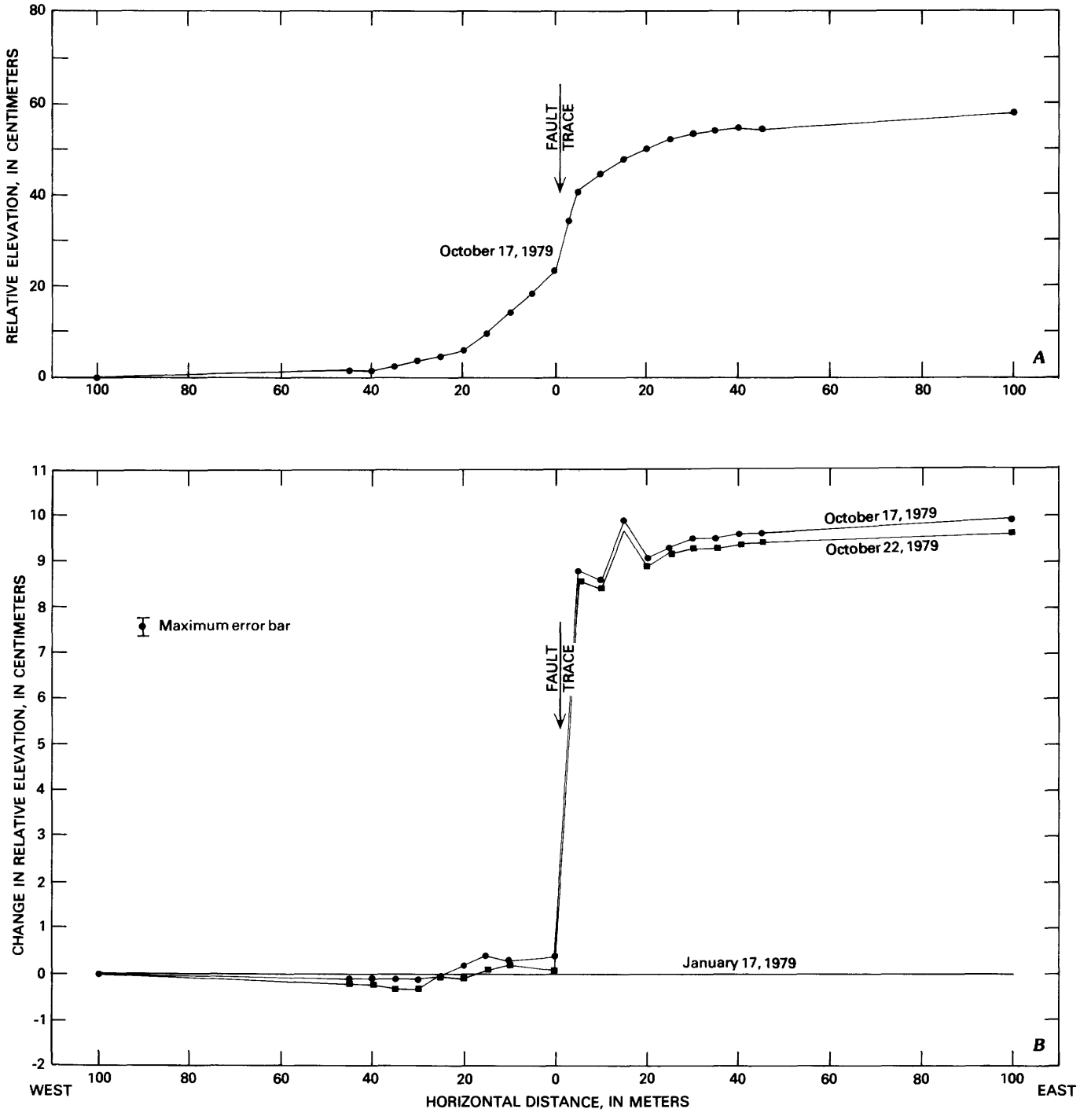

FIGURE 133.—Relative elevation and vertical displacement on Brawley fault zone at Keystone Road. *A*, Profile of relative elevation of road surface. *B*, Vertical displacement from October 15, 1979, earthquake, as shown by surveys on October 17 (dots) and October 22 (squares). Maximum error for all stations shown by bar.

had not been visible but that later created a scarp and caused surface fracturing during the 1979 earthquake. No net tilting of the leveling line toward the Mesquite basin was observed before this deformation, such as was observed on the Imperial fault before vertical movement there sometime between October 25, 1977, and January 17, 1979.

During the next 3 months (January 17–April 19, 1979), while the leveling array at the Imperial fault recorded a significant basinward tilt, releveling at Harris Road across the Brawley fault zone showed no deformation (fig. 134*B*).

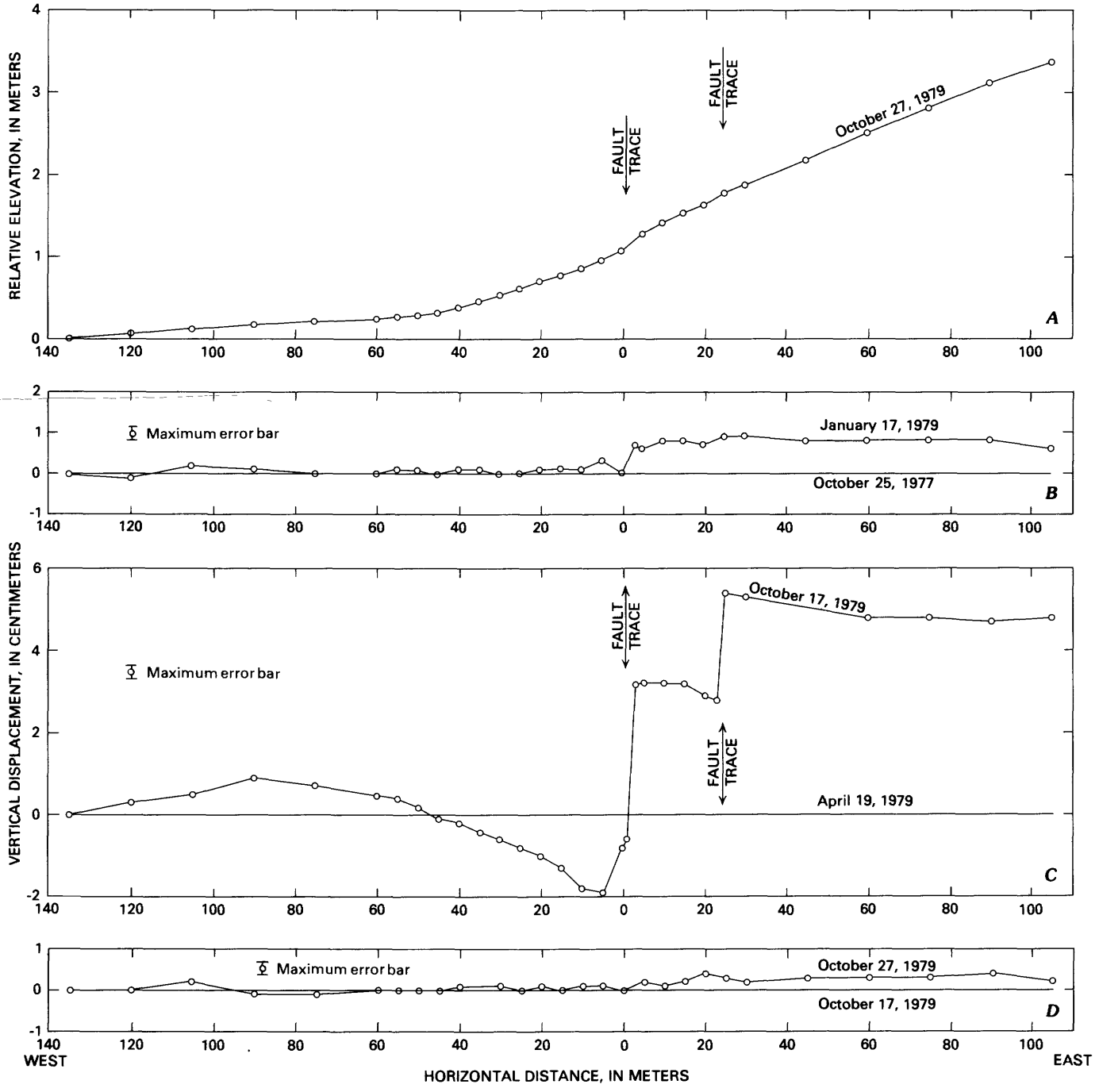

FIGURE 134.—Relative elevation, vertical displacement, and afterslip on Brawley fault zone (west breaks) at Harris Road. *A*, Profile of relative elevations along leveling array. *B*, Vertical displacement across fault traces from October 25, 1977, to January 17, 1979. *C*, Vertical displacement during October 15, 1979, earthquake. *D*, Afterslip for 2 to 12 days after earthquake.

We measured the vertical displacement generated coseismically with the October 15, 1979, earthquake by releveling the Harris Road line on October 17, using the April 19, 1979, survey as datum. The profile of vertical displacement (fig. 134*C*) shows several interesting features, some comparable to the profile for the Imperial fault but on a much smaller scale. The upthrown block east of the two breaks behaved nearly as a flat plate, similar to behavior on the Imperial fault. Immediately west of the main break, the profile of changed elevations slopes down toward the fault to a minimum at a point several meters west of the surface trace. An eastward slope west of the secondary fracture also is evident, although its scale is substantially smaller. The eastward tilt crests 90 m west of the main break as a positive feature, from which the profile slopes west to the end of the line at 135 m west. Figure 134*A* displays the profile of elevations of the road surface as of the last survey (October 27, 1979).

The vertical displacements measured at the fractures crossing the Brawley fault zone leveling line at Harris Road were 3.8 and 2.5 cm, or a total of 6.3 cm. These displacements are interpreted as approximately coseismic on the basis of the record of strike-slip there (Cohn and others, this volume). Releveling of the survey line on October 27, 1979, showed only slight tilting across the line but no clear vertical afterslip at the fault traces during this 10-day period (fig. 134*B*). By December 30, tilting had resumed, and the east end of the line had risen about 1 cm with respect to the west end. This aftertilting measured at Harris Road was unique for the Brawley fault zone; neither survey line at Keystone or Worthington Road showed significant postearthquake movement. Leveling after the earthquake swarm of 1975 showed that of the three survey lines, only that at Harris Road exhibited substantial continuing movement after the initial main surface faulting (Sharp, 1976).

Another major strand of the Brawley fault zone broke Harris Road about 0.4 km east of the survey line discussed above. Because this trace was not recognized earlier, no preearthquake leveling had been done. A survey line was constructed and measured on October 22; the profile of the road elevations (fig. 135) indicates an escarpment in the pavement of about 7 cm. The preearthquake configuration of the road is unknown, and so the amount of vertical displacement for the 1979 earthquake cannot be accurately determined. One week before the earthquake, a layer of seal coating was applied to the surface of Harris Road, and a County road department employee stated that no hump was noticeable in the road then. Much of the total height of the scarp may have formed at the time of the earthquake.

WORTHINGTON ROAD

Four relevelings at Worthington Road between January 21, 1976, and January 18, 1979, revealed no significant net changes in relative elevation. Figure 136*A* shows the differences in the relevelings on January 18 and October 18, 1979. The profile of elevation changes has the same shape as the profile for Harris

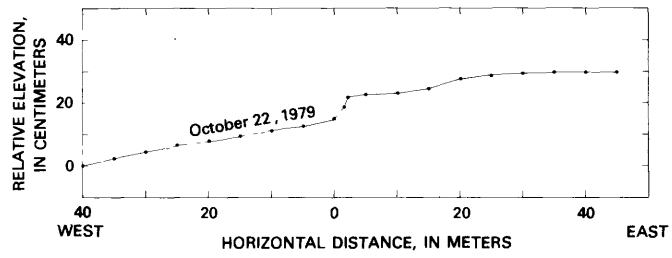

FIGURE 135.—Relative elevation across Brawley fault zone (east break) at Harris Road. Although about 7 cm of displacement must have occurred after road was paved in August 1970, most displacement may have occurred during 1979 earthquake.

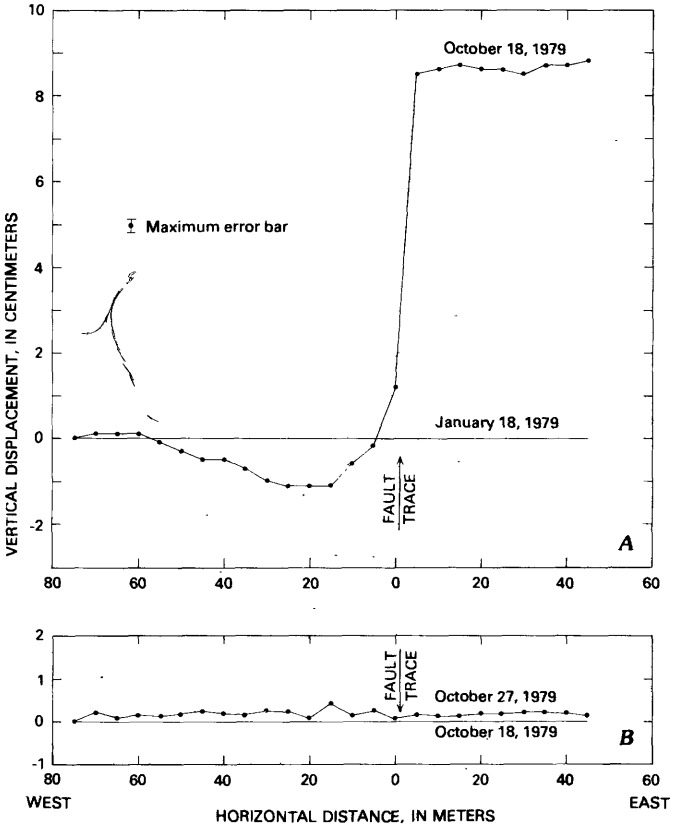

FIGURE 136.—Vertical displacement and postearthquake releveling on Brawley fault zone at Worthington Road. Maximum error for all stations shown by bar. *A*, Vertical displacement during October 15, 1979, earthquake. *B*, Releveling on October 27, which showed no significant afterslip.

Road in that, with respect to the west end of the survey line, progressively eastward a small positive bulge crests near the end of the line, and a tilt sloping toward the fault descends to a negative minimum west of the fault trace and rises eastward, in turn, to the fault trace. Here again, the upthrown block east of the fault behaved as a flat plate.

Vertical displacement measured between stations 15 m west and 10 m east is about 9.5 cm (fig. 136*A*). A releveling 9 days after the first postearthquake survey (fig. 136*B*) indicated only slight changes that do not correlate with the position of the fault trace.

CONCLUSIONS

Measurements of elevation changes across the Imperial fault and the Brawley fault zone reveal not only a relatively detailed picture of coseismic slip and afterslip at the fault traces, but also the distribution of elevation changes away from the fault for distances small relative to the focal depths of earthquakes in this region.

For the 1979 earthquake and its aftershocks (as of December 30), vertical displacement on the northern part of the Imperial fault totaled about 0.3 m at Harris Road. The largest vertical displacement measured on the Brawley fault zone was about 8 cm at Keystone Road, the same place where the largest scarp was measured after the 1975 earthquake swarm. The greater vertical displacement on the Imperial fault relative to the Brawley fault zone for this event is consistent with the geomorphic evidence for past dominance as well. The Holocene scarp on the Imperial fault is substantially higher than that along the Brawley fault zone.

The vertical component of afterslip on the Imperial fault at Harris Road (as of December 30, 1979) was approximately equal to the coseismic slip. In contrast, afterslip on the Brawley fault zone was minor at most and represented only a small fraction of the coseismic displacement.

Several features of the profiles of vertical coseismic and afterslip deformation across the Imperial fault are similar for the individual time intervals but differ significantly in scale. Deformation during coseismic slip was clearly wider than the nearly 0.2 km half-length of the survey line at the Imperial fault, but tilting of the downthrown block during the afterslip period may have been contained within the line's length. The coseismic relative changes in elevation of the end points of the survey line, as well as those throughout the afterslip period, reflect crustal movements at depths greater than the length of the line.

The general asymmetry of both the coseismic slip and afterslip deformations suggests nonvertical dip of the fault surfaces. The flatness of profiles of the uplifted sides of the faults and the downward tilt toward the fault traces apparent in most profiles on the Mesquite basin side of the faults imply that these structures dip toward the basin (W. R. Thatcher, oral commun., 1979). Langbein and others (this volume) combine the vertical component of afterslip for the interval October 27–December 29, 1979, with their data on the horizontal components of afterslip and compute an apparent dip of the Imperial fault along the alinement of Harris Road of $49° \pm 5°$ toward the Mesquite basin.

Whether the preearthquake tilting and its cessation that were observed across the Imperial fault at Harris Road signaled the likelihood of a major earthquake is unclear. We note, however, that the duration of precursory deformation expected for an earthquake of the magnitude of the October 15, 1979, earthquake could be some 3 years (10^3 days), according to Rikitake (1976, p. 295), although his analyses indicate that the leveling changes preceding earthquakes do not reveal a clear statistical relation of precursor time to magnitude. Although our leveling data cover that much time (surveys were done 1,363, 1,004, and 720 days before the earthquake), the general abundance of small earthquakes and the occurrence in 1977 of a swarm of nearby earthquakes and one small fault displacement during the period of tilting make the relation of the leveling data to the 1979 earthquake ambiguous. It may be that all the effects documented by our intermittent surveys are associated with high levels of background seismicity along faults that creep intermittently at depth and only occasionally at the surface. The data reported here constitute our entire base of experience in relating the vertical surface deformation near faults to the seismicity in this region; the deficiencies of the data and the ambiguities that arise largely from the long times between surveys clearly point to the need for more intensive future investigations.

REFERENCES CITED

Allen, C. R., Wyss, Max, Brune, J. N., Grantz, Arthur, and Wallace, R. E., 1972, Displacements on the Imperial, Superstition Hills, and San Andreas faults triggered by the Borrego Mountain earthquake, *in* The Borrego Mountain earthquake of April 9, 1968: U.S. Geological Survey Professional Paper 787, p. 87–104.

Johnson, C. E., 1979, CEDAR—an approach to the computer automation of short-period seismic networks; seismotectonics of the Imperial Valley of southern California: Pasadena, California Institute of Technology, Ph. D. thesis, 343 p.

Johnson, C. E., and Hadley, D. M., 1976, Tectonic implications of the Brawley earthquake swarm, Imperial Valley, California, January 1975: Seismological Society of America Bulletin, v. 66, no. 4, p. 1133–1144.

Rikitake, Tsuneji, 1976, Earthquake prediction: Amsterdam, Elsevier, 357 p.

Sharp, R. V., 1976, Surface faulting in Imperial Valley during the earthquake swarm of January–February 1975: Seismological Society of America Bulletin, v. 66, no. 4, p. 1145–1154.

GEODETIC MEASUREMENTS OF HORIZONTAL DEFORMATION ON THE IMPERIAL FAULT

By C. N. CROOK, R. G. MASON, and P. R. WOOD,
IMPERIAL COLLEGE, LONDON

CONTENTS

ABSTRACT

During the first 6 weeks after the earthquake, we resurveyed parts of a dense geodetic network spanning the Imperial fault near El Centro, Calif., for comparison with surveys conducted between 6 and 12 months earlier. Repeated measurements were made of five figures along 18 km of the fault and of two on each side, each consisting of 5 to 11 rays. A single resurvey was made of three chains of triangles, one along the fault and two normal to it.

Our measurements showed that the fault was still slipping at an exponentially decreasing rate during this period. Extrapolating back to the time of the earthquake, we estimate that the coseismic slip was about 37 cm right lateral at a point 2 km north of County Highway S–80 and that it increased steadily southward to about 62 cm at Heber Road, 13 km to the southeast and 1 km from the south end of the surface break. Six weeks after the event, when the slip had reached about 94 percent of its predicted final value, overall slip in these two places had increased to about 48 and 70 cm, respectively.

Coseismic strain, both linear and shear, which was strongly asymmetric about the fault, showed an extension of about 150 microstrain normal to the fault on its southwest side and a compression of about 200 microstrain on its northeast side, although shear strain parallel to the fault is dominantly right lateral on the southwest side and left lateral on the northeast side. Coseismic strains measured about 10 km from the fault on either side were generally less than 25 microstrain, consistent with left-lateral shear parallel to the fault. Little significant postearthquake strain was observed.

INTRODUCTION

In 1971, a trilateration network was established across the Imperial Valley near El Centro, Calif. Since then, the network has been remeasured and enlarged several times and now comprises 305 stations, most in an 8- by 10-km block on the Imperial fault (figs. 137, 138). Fortuitously, this network includes a 10-km length of the 1979 fault break. The most recent additions, made in April 1979, include three small-scale networks constructed around U.S. Geological Survey/California Institute of Technology creepmeter sites on the Imperial fault. One network (MD294 star), at Watermans Corner (intersection of Ross and Meloland Roads), lies inside the main network, and the other two, at the Heber Road and Tuttle Ranch creepmeter sites, lie outside it, about 3 and 8 km to the southeast, respectively (fig. 138). The first networks span the 1979 fault break, and the third lies beyond its south termination.

The most recent preearthquake measurements were made in May–December 1978 and April–May 1979. After the October 15, 1979, earthquake, we remeasured parts of the network to assess both coseismic and postseismic deformation. Our results, presented here, are based on a field reduction and analysis made within a few weeks of the earthquake. We plan to resurvey the entire network during 1980.

INSTRUMENTATION

Measurements were made with a Kern ME3000 mekometer, a high-precision short-range electro-optical distance-measuring instrument, and its associated retroreflector, both tripod mounted and centered over their respective stations with optical plummets. The stations consist of metal markers installed below ground level on an 800-m grid, as nearly regular as lines of sight and other local considerations permit. Measurement of a line takes about 15 minutes, including observation of the necessary atmospheric parameters. Most lines are between 700 and 1,200 m long, and the standard error of a measured length, after correction for atmospheric and instrumental factors, is about 1.5 mm.

MEASURING PROGRAM

We began our measurements 6 days after the earth-

quake and continued them for about 6 weeks. Because the fault was creeping initially at a rate of about 7 mm/d, our first objective was to monitor the changing deformation, both on and away from the fault. This objective was achieved by repeated surveys, each of which could be performed within about 2 hours, of the small Heber Road and Tuttle Ranch networks, and of the starlike patterns of as many as eight lines radiating from seven selected stations (fig. 138).

Three stars, centered on stations H33, MD294, and R27 (fig. 138), together with the two small networks, served to monitor deformation on the fault. Because of the possibility of a creep event during the course of a survey, we measured the line most sensitive to fault slip at the beginning and end of each survey but detected no significant changes. Deformation away from the fault was monitored by four stars, centered on stations Q33 and W41 about 3 and 10 km, respectively, from the fault on its southwest side; and on stations E30 and D21 at similar distances on its northeast side (fig. 138). The fault-crossing figures were measured four or five times during the 6 weeks, the close-in stars three times, and the more distant stars twice.

After establishing a deformation-monitoring scheme, we measured three chains of triangles, each between 9 and 10 km long: a north chain and a south chain, approximately normal to the fault, to provide profiles of deformation across it; and a fault chain, to measure the variation in deformation along the fault. We measured the first two chains during the third week after the earthquake and the last during the seventh week, by which time the fault was creeping more slowly than 1 mm/d.

ANALYSIS

Different approaches are necessary for analyzing the data from lines that cross the fault and from those that do not. For lines not crossing the fault, we assume that the changes in length derive only from a uniform infinitesimal strain. The most informative components are e_{11}, e_{22}, and γ_2 $(=e_{12}+e_{21})$, which can be calculated from the relation

$$e=e_{11}\cos^2\theta+e_{22}\sin^2\theta+\gamma_2\sin\theta\cos\theta,$$

where e is the extension of a line of bearing θ, measured anticlockwise from x_1. Solution for the three strain parameters requires a measurement of extension in at least three directions. In this report, strains are given in units of microstrain (10^{-6} strain).

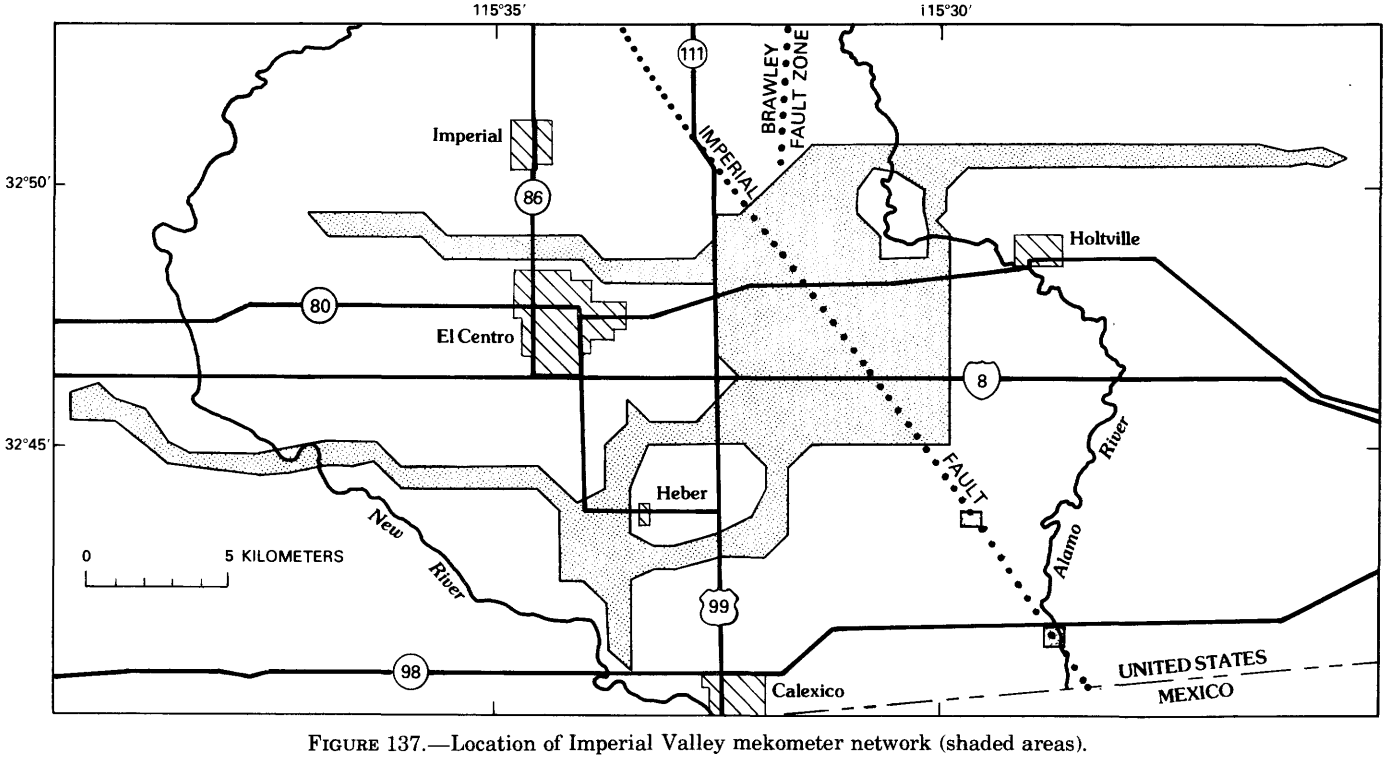

FIGURE 137.—Location of Imperial Valley mekometer network (shaded areas).

For lines that cross the fault, the changes in length include a component of fault displacement and a component of strain. For the fault-crossing figures, these components generally cannot be separated, and because the strain component is likely to be very much smaller than the displacement component, we have assumed that changes are due entirely to displacement on the fault. If the displacement is expressed as a vector (x_1, x_2), then a line at an angle θ to the x_1-direction will change in length by an amount Δl given to first order by

$$\Delta l = x_1 \cos\theta + x_2 \sin\theta.$$

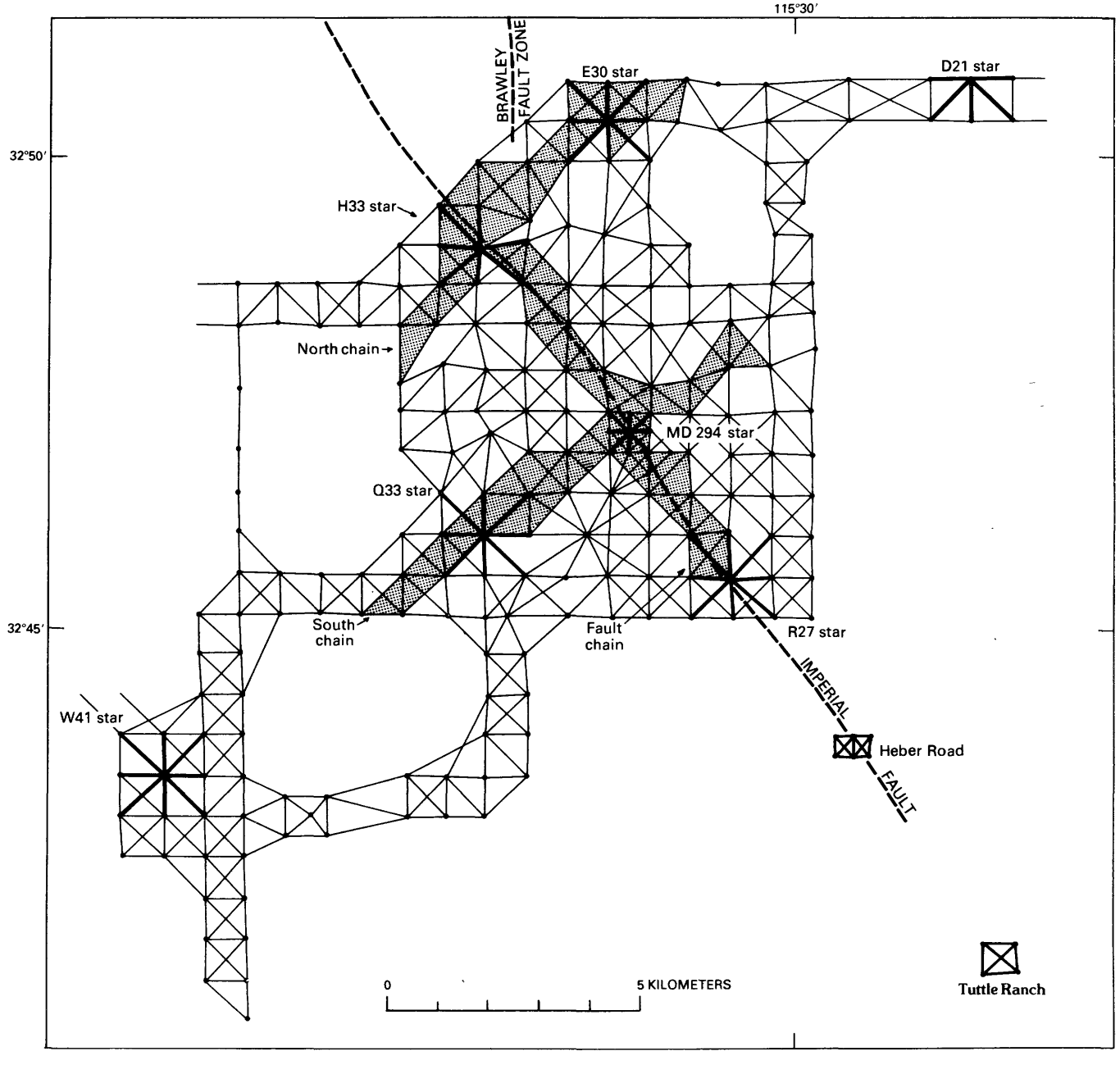

FIGURE 138.—Index map showing parts of network measured between October 21 and November 27, 1979. Repeated surveys to determine deformation were performed along radiating lines of starlike pattern at selected stations (labeled); shaded area indicates chains of triangles measured to determine deformation.

Solution of this equation for x_1 and x_2 requires measurements of Δl for two or more lines of different bearings. The direction defined by the vector (x_1, x_2) would be expected to correspond to the local direction of the fault.

For the fault chain, a more sophisticated approach is possible. If we assume that one station and one direction remained unchanged between the preearthquake and postearthquake surveys, then we may derive displacement vectors for each of the 17 stations by calculating their coordinates before and after the earthquake. Simple models that can then be fitted to the results permit strain and displacement to be separated.

If our assumptions of uniform strain and simple displacement are correct, then errors in measurement of about 1.5 microstrain would give rise to standard errors of less than 3 microstrain in the strain parameters and of less than 3 mm in the displacements. Much greater discrepancies, however, appear between the measured lengths and those calculated from the derived parameters.

DEFORMATION ALONG THE IMPERIAL FAULT

The principal sources of information about deformation along the fault are the five fault-crossing figures and the fault chain of triangles. The fault-crossing figures, measured several times between 1 and 6 weeks after the earthquake, thus served to monitor postearthquake slip at discrete points on the fault. By extrapolating backward from these data, we may estimate the amount of slip immediately after the earthquake. We measured the fault chain once only, about 6 weeks after the earthquake, by which time a considerable amount of postearthquake slip had occurred. Because the fault chain was a solid figure, however, we could obtain from it displacement vectors along about 8 km of the fault break, as well as strain parameters immediately adjacent to the fault.

The results of both sets of measurements concern deformation observed between surveys both before and after the earthquake, and thus contain components of preearthquake deformation. There is no way of determining from these observations what deformation may have taken place during the 6 months between the last preearthquake survey and the time of the earthquake. If deformation continued at the average rate observed between 1975 and 1978, strains would not have changed by more than 1 microstrain during this period, and the fault would not have slipped by more than about 5 mm. However, because fault creep on the Imperial fault is known to be episodic (Goulty and others, 1978) and creep events occasionally exceed 10 mm, very much larger changes might have occurred—even exceptionally large precursory changes.

POSTEARTHQUAKE FAULT SLIP

In analyzing our results from the fault-crossing figures, we assume that all length changes are due to slip and take no account of strain. Figure 139 plots the displacements calculated relative to the April 1979 survey data. Afterslip, which is in the same sense as displacement associated with the main event, over a period of 6 weeks will have contributed as much as 25 percent to the total fault slip.

The observations can be well fitted to an exponential-decay model:

$$\delta = a - be^{-ct},$$

where δ is the displacement at time t, t is the time (in days) after the event, a is the predicted total fault slip at a particular location, and b is the predicted postseismic slip. The time constant c has almost the same value in all four localities, and we adopted a common value of 0.06 for the final fit. Thus, half the predicted amount of postseismic slip would have occurred within about 12 days of the earthquake. Table 23 lists values of the estimated coseismic slip and the predicted postseismic and total slips. Unlike the coseismic fault slip, which

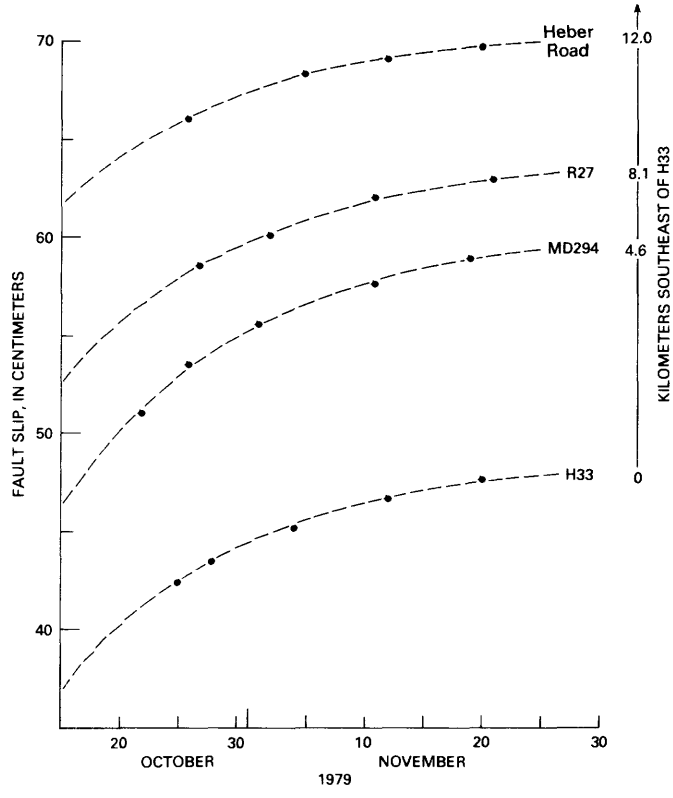

FIGURE 139.—Slip on Imperial fault since April 1979 survey. Note exponentially decreasing rate of slip over time. See figure 138 for locations of stations.

increased steadily from an estimated 37 cm at the north end of the network to about 62 cm at Heber Road 13 km to the southeast, the afterslip showed no pronounced trend. We note from figure 139 and table 23 that by 6 weeks after the earthquake, at the time of the fault-chain survey, at least 94 percent of the predicted total slip had already occurred.

FAULT-CHAIN SURVEY

We computed displacement vectors for stations in the fault chain on the assumption that the position of station H32, near the fault at one end of the line, and the direction of the line joining it and station P28, on the same side of the fault at the opposite end, did not change as a result of the earthquake. Our results are listed in table 24 and plotted in figure 140 ("balanced" about the fault by the addition of a common vector). The data show that displacements vary considerably along the fault, and their amplitudes tend to correlate with the distance from it.

TABLE 23.—*Coseismic and postseismic slip predicted from an exponential decay of slip rate over time*

[Error limits are one standard deviation, computed from fitting an exponential decay in slip rate to measured slips]

Station	Estimated coseismic fault slip (m)	Predicted postseismic fault slip (m)	Predicted total fault slip (m)
H33	0.368±0.005	0.122±0.005	0.490±0.007
MD294	.462±0.006	.145±0.004	.607±0.007
R27	.524±0.009	.119±0.007	.643±0.011
Heber Road	.616±0.007	.093±0.006	.709±0.009

TABLE 24.—*Displacements along the fault chain*

Station	Distance from fault (m)	Displacement vector		Component parallel to fault (m)	
		Length (m)	Bearing (az)	Observed	Corrected for strain
Southwest of fault					
J32	50	0.509	337°	0.498	0.483
K32	450	.654	334°	.646	.511
L31	300	.686	332°	.681	.591
M30	100	.728	329°	.726	.696
N30	450	.834	332°	.828	.693
P29	350	.799	331°	.794	.689
Q28	100	.757	330°	.754	.724
Northeast of fault					
H32	500	0	----	0	.030
J31	650	.034	285°	.026	.065
K31	200	.106	347°	.098	.065
L30	300	.166	304°	.155	.173
M29	550	.114	309°	.110	.143
N29	150	.114	324°	.114	.123
N28	800	.131	280°	.092	.140
P28	350	.056	326°	.056	.077
Q27	600	.150	274°	.095	.131
R27	150	.120	290°	.099	.108

To calculate the amount of slip on the fault, we assume that the computed displacement parallel to the fault varies linearly with distance along it, and that shear parallel to the fault is uniform on either side. The results indicate a right-lateral shear of about 300±100 microstrain adjacent to the fault on its southwest side and 60±64 microstrain on its northeast (error limits represent one standard deviation). Figure 141 plots the displacement on both sides of the fault (dashed curves), after correcting for shear; and the difference in displacement between both sides (solid curve), representing slip on the fault, as a function of distance along it. This difference, ranging from about 45 cm at the northwest end to about 60 cm at the southeast, agrees with values derived independently from the fault-crossing figures. At 3 km beyond the southeast end of the chain,

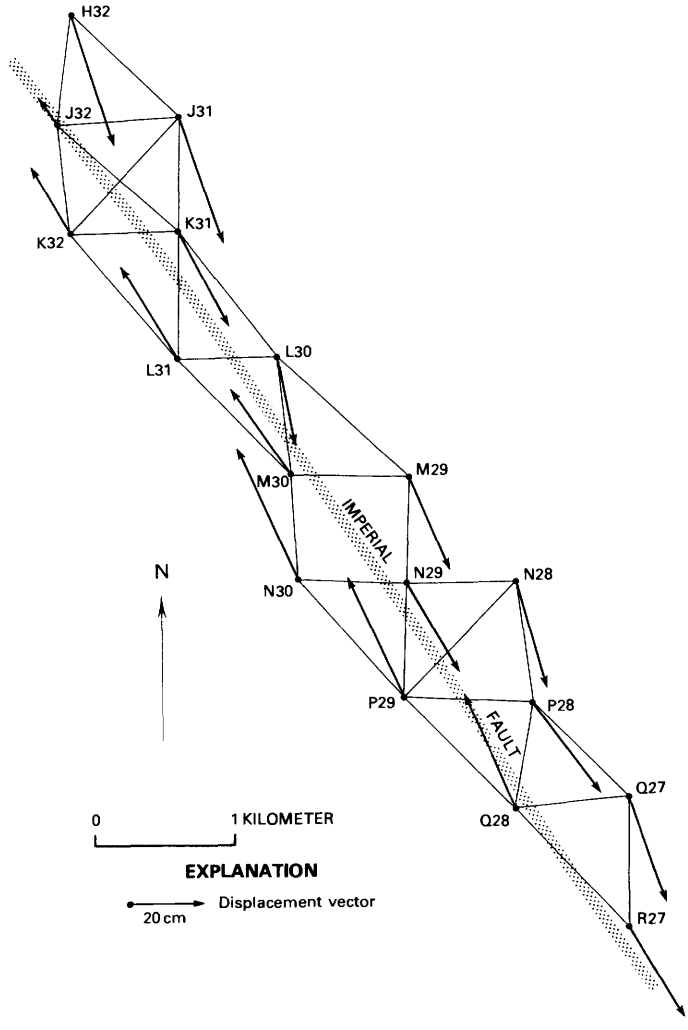

FIGURE 140.—Displacement of fault-chain stations between April and November 1979. Vectors have been "balanced" about fault by addition of a common vector. See figure 138 for location of fault chain.

at Heber Road, the observed displacement of about 70 cm confirms the general increase in displacement from north to south.

TUTTLE RANCH QUADRILATERAL

Although the Tuttle Ranch quadrilateral spans the 1940 trace of the Imperial fault, the 1979 break did not extend this far south. We observed changes of as much as 160 microstrain between preearthquake and postearthquake measurements, mainly of east-westward extension, but the pattern is neither uniform nor consistent with discrete fault movement. These changes can most adequately be described by westward movement of the northwestern station by about 10 cm and no movement of the other three stations, but there is no evidence on the ground to support such an interpretation. During the second week after the earthquake, we measured a dilation of −8 microstrain on the quadrilateral; during the following 2 weeks, however, this pattern reversed, and we determined a net dilatation of zero. During the same period the net change in shear strain was less than 4 microstrain.

DEFORMATION AWAY FROM THE IMPERIAL FAULT

Two sources of information provide data abou deformation away from the Imperial fault: the north and south chains, and the four stars (D21, E30, Q33, W41, fig. 138). The chains, surveyed once only (during the third week after the main shock), provide profiles of mainly coseismic strain changes normal to the fault, whereas the stars, measured two or three times between 1 and 6 weeks after the earthquake, permit an estimate of postearthquake strain adjustment.

NORTH AND SOUTH CHAINS

Figure 142 illustrates the principal strains along the north and south chains, and figure 143 plots the same information as profiles of the strain components e_{11}, e_{22}, and γ_2 ($=e_{12}+e_{21}$), calculated for axes orthogonal to the fault strike. At first sight, the lines appear to have little in common: (1) the principal axes on the south line are generally alined, whereas those on the north line rotate systematically clockwise from west to east; and (2) although significant changes occur on both lines at the fault, the pattern also changes abruptly about 2 km east

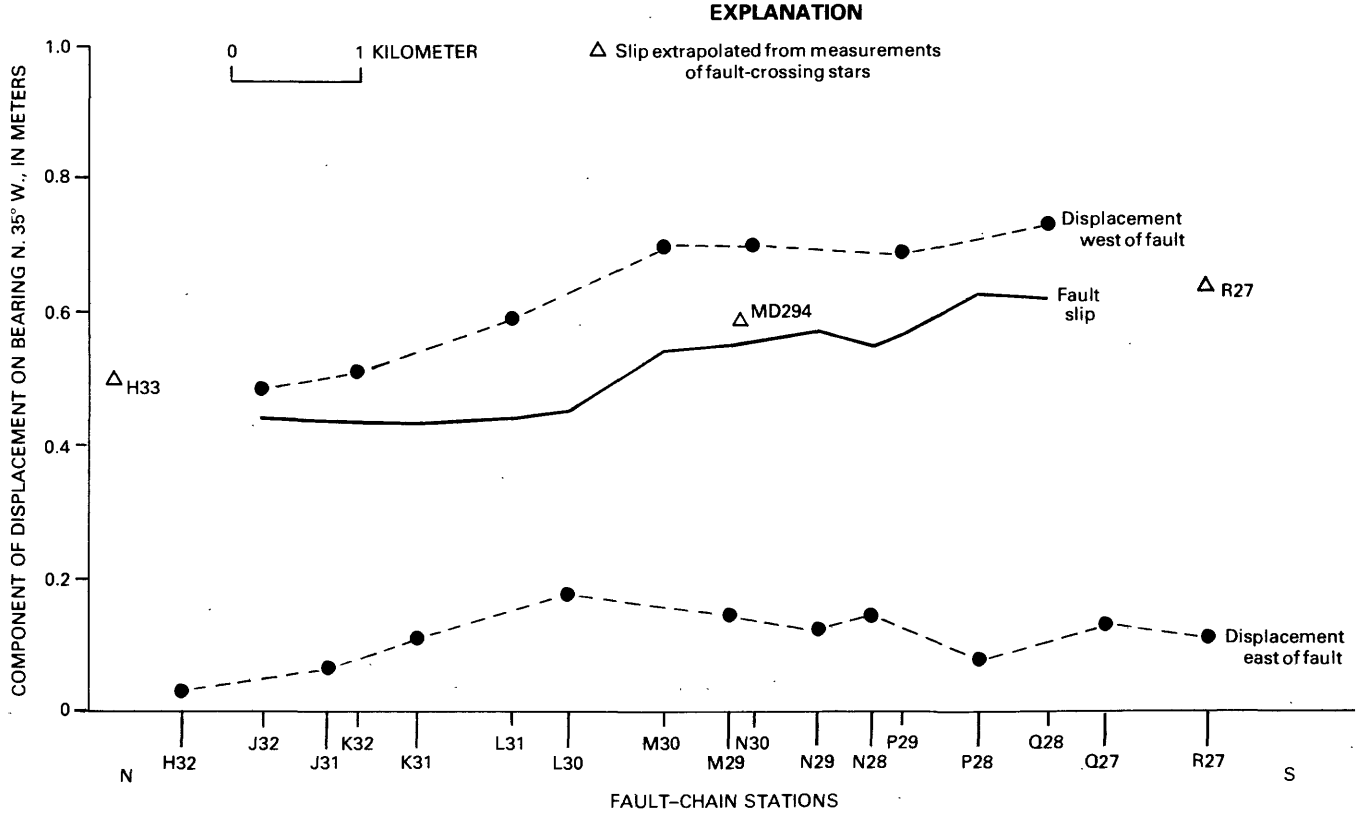

FIGURE 141.—Fault slip inferred from displacement of stations on opposite sides of Imperial fault, corrected for strain. See figure 140 for locations of fault-chain stations.

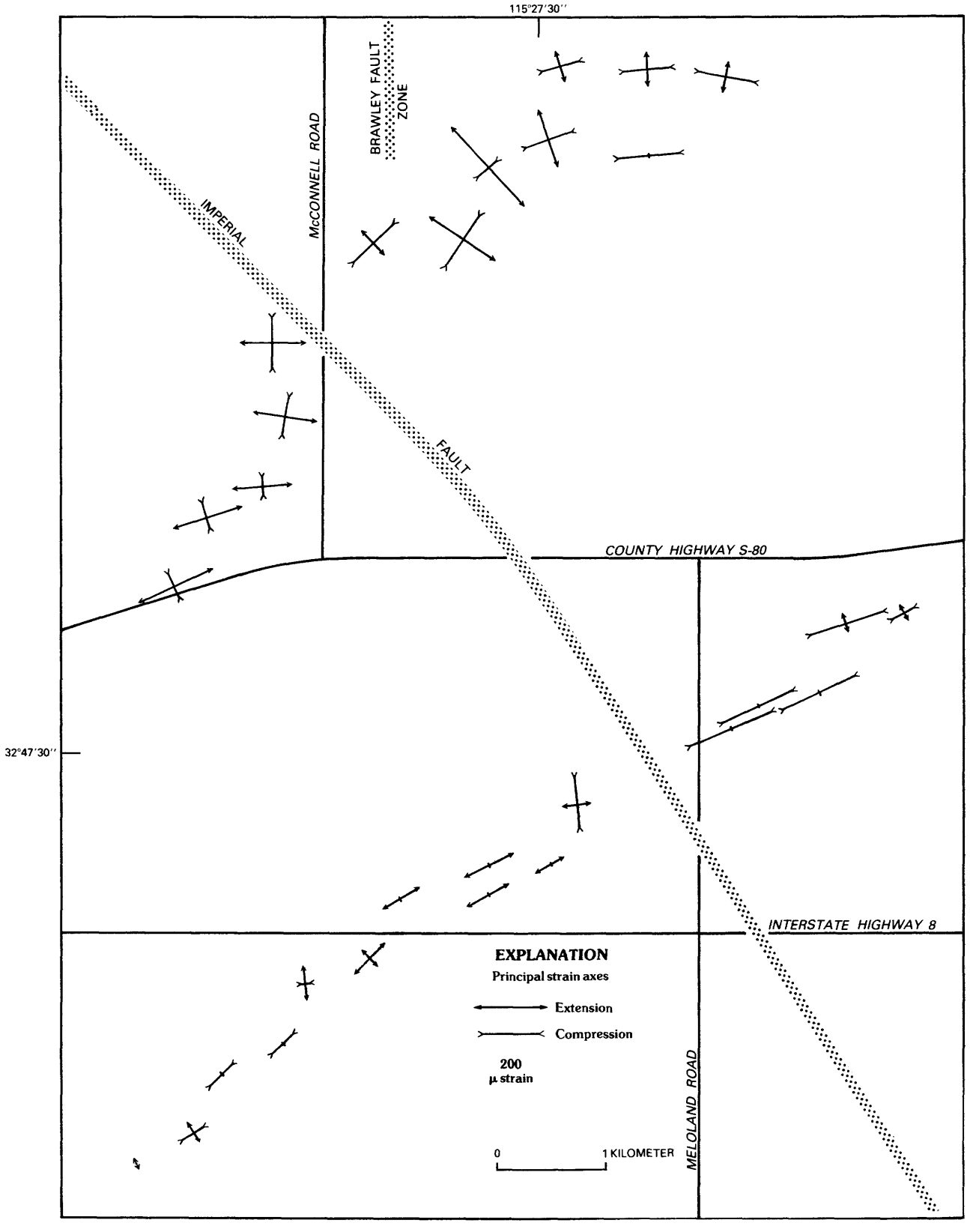

FIGURE 142.—Principal strain axes for north and south chains. Arrowheads omitted for values less than 25 microstrain.

of the fault on the north line, probably owing to the influence of the Brawley fault zone. The two lines, however, extend different distances on each side of the fault. Points of similarity between the two lines, as far as 2½ km on the southwest side of the fault and 3 km on the northeast, are: (1) the component of linear strain parallel to the fault (e_{11}) is relatively small except near the Brawley fault zone on the north line, where it increases to more than 300 microstrain; (2) the component of linear strain normal to the fault (e_{22}) is extensional on the southwest side of the fault and compressional on the northeast side; and (3) γ_2 is positive on the southwest

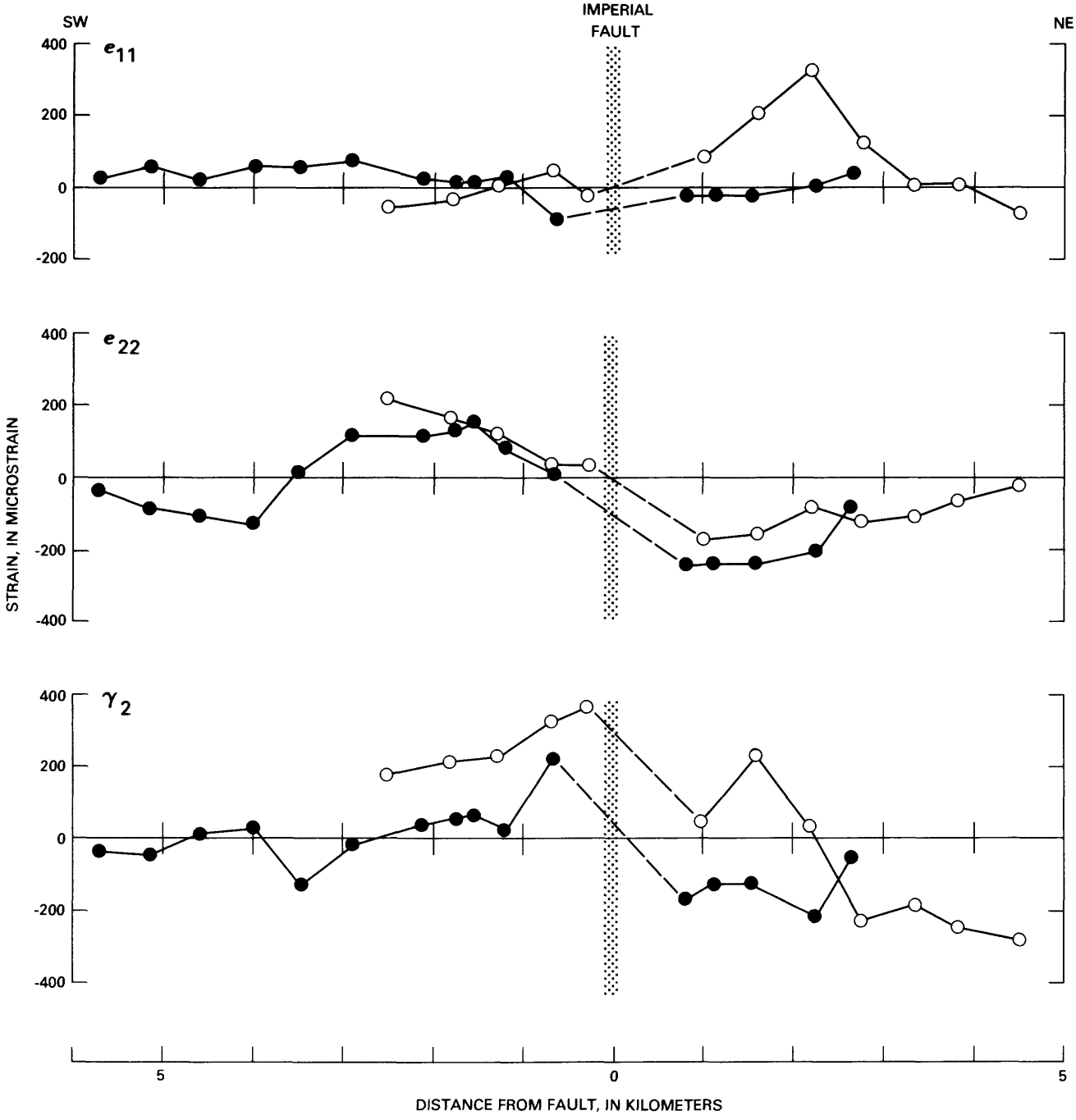

FIGURE 143.—Strain parameters (e_{11}, e_{22}, and γ_2; see text) calculated relative to axes orthogonal to fault strike (taken as N. 40° W.). x_1-axis is parallel to fault, positive to southeast; x_2-axis is normal to fault, positive to northeast. Circles, north chain; dots, south chain.

side of the fault and markedly large close to it, a configuration interpreted as right-lateral shear parallel to the fault.

STRAIN STARS

As might have been expected, the stars more distant from the fault show very much smaller changes between preearthquake and postearthquake surveys than those nearer to it. Thus at station D21, 9 km from the fault on its northeast side, the dominant strain change was a left-lateral shear of less than 25 microstrain parallel to the fault; and at station W41, 11 km from the fault on its southwest side, a left-lateral shear of less than 10 microstrain parallel to the fault. During the period of observation, changes on figures not crossing the fault were small, generally no more than 3 microstrain.

DISCUSSION

This small sample of the total information that can be extracted from the network reveals a complex pattern of coseismic strain changes, some of which almost certainly reflect the presence of unmapped faults, even of bifurcations of the Imperial fault itself. In particular, movement on the Brawley fault zone, whose mapped surface trace terminates just to the north of the network, has clearly affected strains on the north line.

One expected consequence of right-lateral slip on the Imperial fault is a relaxation of strain in a left-lateral sense on either side of the fault, which is evident on the northeast side except near the Brawley fault zone. On the southwest side, however, change has been in the opposite sense, and both lines indicate right-lateral shear parallel to the fault. We may interpret this result in terms of right-lateral slip parallel to the fault. Because the shear is more than 200 microstrain over the entire 2½-km length of the north line, a right-lateral slip of more than 50 cm over this length is implied.

ACKNOWLEDGMENTS

This work was supported by funds provided by the U.S. Geological Survey. Thanks are due also to the New Zealand Geological Survey and to Com-Rad Electronics for making mekometers available on very short notice.

REFERENCE CITED

Goulty, N. R., Burford, R. O., Allen, C. R., Gilman, Ralph, Johnson, C. E., and Keller, R. P., 1978, Large creep events on the Imperial fault, California: Seismological Society of America Bulletin, v. 68, no. 2, p. 517–521.

DISTRIBUTION OF AFTERSLIP ALONG THE IMPERIAL FAULT

By PHILIP W. HARSH,
U.S. GEOLOGICAL SURVEY

CONTENTS

ABSTRACT

Horizontal afterslip associated with the 1979 Imperial Valley earthquake occurred along the 30-km section of the Imperial fault where ground rupture was observed soon after the main shock. Six alinement arrays installed along the zone of ground rupture to monitor continuing fault displacements were measured several times, beginning from 2 to 19 days after the main shock.

Although the main-shock epicenter was located 10 km beyond the southeast end of surface rupture, the average rates of afterslip and the total measured afterslip during the interval of this study were greatest about 23 km northwest of the epicenter, near the midpoint of surface rupture. Both the total measured afterslip and the slip rates declined toward the ends of the surface rupture. Rates of slip a few days after the earthquake ranged from about 5 to 20 mm/d; 10 weeks later, the rates were generally about 1 mm/d. A least-squares fit to measured afterslip with respect to elapsed time since the main shock was calculated for data obtained at each alinement-array site. The curve chosen to represent the data, which has the form $U=-A+B\log(1+Ct)$, was fitted to the values of displacement and time by a finite-difference technique. The patterns and rates of afterslip resemble those observed after the 1966 Parkfield-Cholame, Calif., earthquakes. Previous hypotheses that the presence of a thick unconsolidated sedimentary cover is a major factor in delaying a large fraction of coseismic slip may not fully account for afterslip observations on the Imperial fault. The patterns and rates of afterslip observed along the 1979 surface rupture do not preclude continuing slip on the seismic zone at 5- to 10-km depth, and although similar slip patterns have been observed in regions of differing surficial lithology, these surface-slip data do not uniquely establish concurrent slip at seismic depths. The afterslip at County Highway S–80 may be similar to afterslip associated with the 1940 Imperial Valley earthquake insofar as information exists about fault slip at the highway from the 1940 event.

INTRODUCTION

Surface ruptures along a 30-km section of the Imperial fault from south of Heber Dunes to a point about 3 km south of Brawley, Calif. (fig. 144), were associated with the October 15, 1979, earthquake. Fault slip was also observed along this section of the Imperial fault in association with the 1940 Imperial Valley earthquake (Richter, 1958). Although the surface break in 1940 was much longer and the maximum slip greater, observed slip on the northwestern section of the Imperial fault in

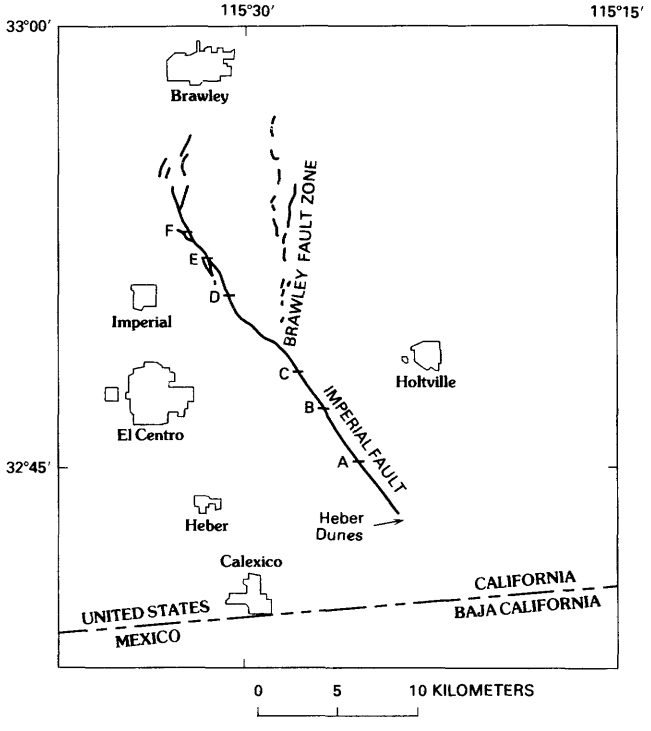

FIGURE 144.—Surface faulting in 1979 in Imperial Valley, showing locations of alinement-array sites. *A*, McCabe Road. *B*, Ross Road. *C*, County Highway S–80. *D*, Worthington Road. *E*, Ralph Road. *F*, Harris Road on Imperial fault.

1979 resembled that in 1940 (Sharp, this volume). Afterslip along the Imperial fault trace was initially observed by Richter (1958) soon after the 1940 earthquake. Continued measurements at several sites documented slip during the period 1940–79 (Brune and Allen, 1967; Goulty and others, 1978).

Results of the measurement of afterslip associated with the 1966 Parkfield-Cholame, 1968 Borrego Mountain, and 1976 Guatamala earthquakes have been previously reported in detail and thus provide a basis for comparison with the data of this study.

Six alinement arrays were installed on paved roads soon after the 1979 Imperial Valley earthquake: three during the second day, two during the third day, and one more during the third week after the main shock. All these arrays are located on the section of the Imperial fault that exhibited ground rupture. From southeast to northwest along the Imperial fault, the arrays are at McCabe Road, Ross Road, County Highway S–80, Worthington Road, Ralph Road, and Harris Road (see fig. 144 for locations). As of early 1980, all these arrays had been measured at least three times, and five had been measured more frequently; measurements were generally repeated every few days for a period of 3 weeks after the main shock, and again at 10 weeks after the earthquake. A linear pavement edge that predates the earthquake was also measured across the fault at the site of the County Highway S–80 alinement array to determine the total horizontal slip (sum of coseismic slip plus afterslip).

MEASUREMENT PROCEDURE

An alinement array comprises a line of monuments across the fault trace and a reference monument. All the alinement arrays were more than 250 m long by November 3, although the initial measurements on some arrays were obtained across a distance of only 100 m. Horizontal displacement of each monument is determined with respect to a reference position (the location of the theodolite monument, 50 m east of the fault trace at all arrays) and a reference direction (from the instrument station to the reference monument in a direction approximately perpendicular to the line of monuments); the position and orientation references are assumed to be fixed. This configuration of alinement arrays was more thoroughly discussed by Burford and Harsh (1980). Because measurement of the alinement arrays during the postearthquake period, which was characterized by a high rate of afterslip, did not warrant high precision, only a single measurement of each monument was made during each survey; without a basis for statistical evaluation, the standard error in determination of monument positions for each survey is estimated to be about 1 mm.

Monument positions were determined from measurements on the east-west roads and projected onto a line perpendicular to the fault. The component of horizontal afterslip parallel to the fault trace was calculated for each monument from the data of two surveys. The angle between the local fault strike and the direction of alinement arrays ranges from about 42° to 65°. This projection is straightforward from County Highway S–80 to the southeast because the fault generally consists of a single trace and is nearly linear; to the northwest, however, the fault trace exhibits significant local curvature and multiple strands. Thus, not only is the azimuth of local relative motion at many sites along the northwestern section of the fault uncertain, but also some deformation may occur within the fault blocks to accommodate changes in fault strike. The sinuosity of the main fault trace northwest of County Highway S–80, and the presence of a prominent vertical scarp and several subsidiary fault strands, complicate the pattern of fault geometry. Determination of the fault strike along the northwestern section of surface rupture is, therefore, somewhat subjective. The direction of fault strike for all alinement-array sites, taken from the map of Sharp and others (this volume), is averaged over a length of fault trace that is on the order of the length of the array. Fault strike for the sites northwest of County Highway S–80 was determined from a length of trace approximately equal to the array length.

Fault slip was estimated by two methods: measurements of relative displacement of the end points of each array, and estimated slip at the fault trace. The latter determination of fault slip is calculated by fitting a separate least-squares line to the displacement data from each side of the fault. Slip at the fault trace by this block-fit technique is determined from the separation of the projections of the two least-squares lines at the fault trace and is termed "trace-fit slip." Although an assumption that the fault blocks are rigid is generally reasonable to a first approximation, repeated measurements of alinement arrays at certain sites along the San Andreas fault in central California have provided evidence that apparent elastic distortion as well as distributed permanent strain can occur within blocks adjacent to the main fault trace (Burford and Harsh, 1980). For most array sites, there is a minor difference between relative movement of the end points of the array and slip determined at the fault trace; that is, some distributed distortion near the fault trace generally occurs, and it cannot be readily determined during a short period of monitoring whether the strain outside the main slip zone is elastic or permanent. The slip values discussed for comparison among sites are based on the ends of the

100-m length of closely spaced monuments. Subsidiary fault cracks outside the 100-m zone at some sites were evidence of permanent deformation, but at some sites, apertures larger than 100 m were not present until November 1979.

MCCABE ROAD

The southernmost array, at McCabe Road, is about 6 km from the southeast end of surface rupture. The initial measurement on November 3, 1979, sampled a 300-m array centered on the fault. As shown in figure 145*A*, 47.3 mm of the 53.0 mm of total slip that had accumulated by the time of the second survey (December 28, 1979) was concentrated within a zone about 100 m wide. Most (89 percent) of the slip across the 300-m array was contained within the 100-m zone of closely spaced monuments. The trace-fit slip value is between the wide-aperture values determined for the 300-m end points and across the 100-m zone (49 mm by least-squares fit to the displacements on each side of the fault).

No significant deviation from a constant strike is evident in the main fault trace within 1 km of McCabe Road. Considering the scale of the array and the displacement pattern, block motion is apparently an adequate description of the local-displacement distribution, at least during the period of observations.

ROSS ROAD

Ross Road is about 4 km northwest of the McCabe Road array (fig. 144). The Ross Road array was surveyed 19 times from October 17 to November 4 and then 52 days later on December 27, 1979.

The original array length at this site was 100 m, but the array was expanded just before the time of the 12th survey to 300 m. There is some indication of complexity in the slip zone within the 100-m array; 95 percent (166 mm) of the slip was contained within a 6-m-wide zone (fig. 145*B*), although a minor auxiliary zone of slip may also exist about 25 m west of the main slip zone where a few minor cracks were observed. A least-squares fit to the displacement data from each fault block has been calculated for two different models, one with fault slip attributed to only the main surface rupture, and the other that allows for additional offset on a minor subsidiary fault to the west of the main slip zone. The first model yields a total measured afterslip of 157 mm; the two-fault model, however, indicates a total of 166 mm summed across the two zones of cracking. The total end-point slip (166 mm) during the period of measurements across the 100-m length accumulated at a rate that apparently decreased over time, from 13.7 mm/d during the first interval (1 day) to an average of 1.2 mm/d for the interval of 55 days between November 2 and December 27 (fig. 146*B*). From November 2 to December 27, the time over which the 300-m array was measured, 8 percent of the measured afterslip (5.6 mm) occurred between 100 and 200 m to the west of the instrument station. If the original length of the array had been 300 m, the measured afterslip during the full time of this study might have been significantly greater.

COUNTY HIGHWAY S-80

The array along County Highway S–80 (fig. 144), which crosses the Imperial fault in an east-west direction 7 km northwest of McCabe Road, was the site of maximum measured afterslip. Afterslip across the original 100-m array grew to 175 mm during the period of measurement. There is no noticeable difference between the fault slip measured across the 100-m length of the array and the larger 260-m length (fig. 145*C*), but owing to late expansion of the aperture (just before the seventh survey on November 2, 1979), the record for this 260-m array is relatively incomplete. Although compressional features were observed along the road surface for about 1 km to the east, far beyond the alinement array, no clear evidence of subsidiary strike-slip fractures was detected on any of these features. A model of rigid block motion fits the data for the 100-m length of this array rather well, as determined from a comparison of the total slip calculated from displacement of 100-m end points and movement at the fault trace (175 mm of both end-point slip and trace-fit slip). This array was surveyed every few days during the first 3 weeks after the earthquake; the initial interval was 1 day. The slip rates determined for the first and last intervals were 14.3 and 1.2 mm/d, respectively, similar to the results for the site at Ross Road. The fault strike was obtained from measurement of a linear fault trace at the array position on the fault map of Sharp and others (pl. 1).

WORTHINGTON ROAD

Northwestward from County Highway S–80, the remarkably linear and relatively simple trace of the Imperial fault becomes progressively more complex, discontinuous, and curvilinear. The first alinement array northwest of County Highway S–80 is at Worthington Road, where measurements were begun on October 18 and were repeated, on the average, about every 4 days for the first 3 weeks after the main shock. A right-lateral offset of about 20 mm in the double yellow line of the highway was observed at each of two large cracks west of the 100-m array of closely spaced monuments, but only slight offsets have been observed across these

subsidiary cracks since the initial measurement. Internal deformation of fault blocks at this site is not unlikely because the fault is rather sinuous in the nearby area. (The fault strike used here is the tangent to the fault measured at Worthington Road.) With the possible exception of a small amount of coseismic slip that produced subsidiary cracks, only a slight departure from rigid block motion is evident in the data for the present array of 308-m length. Only 10 percent of the total measured afterslip of 144 mm occurs beyond the 100-m zone of closely spaced monuments. A block fit yields 126 mm of slip across the main zone of surface faulting during the period of measurements.

The initial slip rate was 6.4 mm/d, significantly less than the rates of 12.6 and 11.4 mm/d for the comparable period on the Ross Road and County Highway S–80 alinement arrays, respectively. The rate at Worthington Road for the most recent interval (1.1 mm/d) is similar to the rate of 1.2 mm/d obtained for Ross Road and County Highway S–80.

RALPH ROAD

Complex patterns of fault rupture were documented for the area northwest of Worthington Road (Sharp and others, this volume); the Ralph Road alinement array

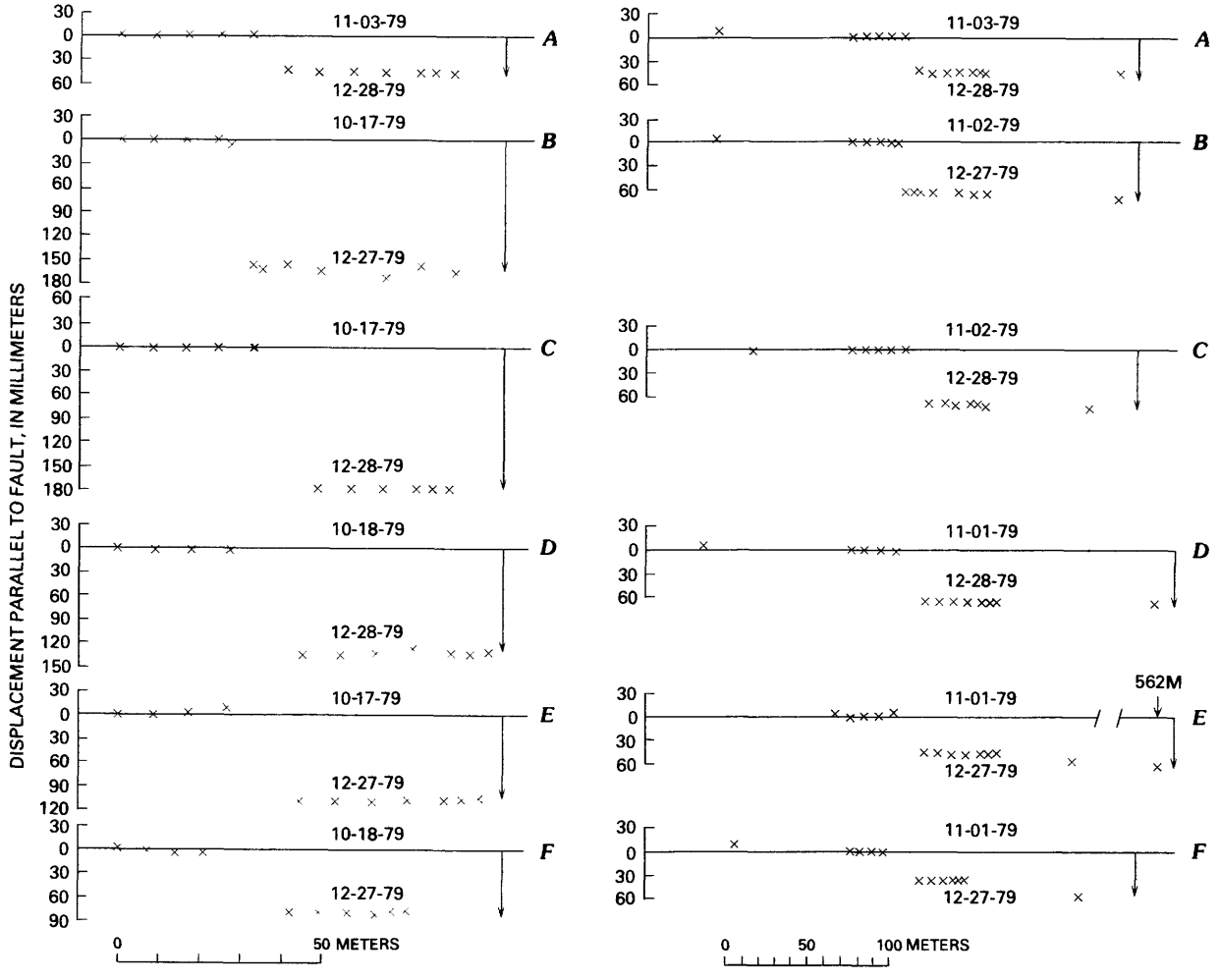

FIGURE 145.—Pattern of displacement at sites of alinement arrays (see fig. 144 for locations). Diagrams in left column show displacements for small-aperture arrays, and in right column for large-aperture arrays. Arrows represent relative direction of slip at each site. Date along horizontal line for each array indicates time of initial measurement; date near data points, time of last survey. *A*, McCabe Road. *B*, Ross Road. *C*, County Highway S–80. *D*, Worthington Road. *E*, Ralph Road. *F*, Harris Road.

crosses the Imperial fault in that area at a site where five zones of cracking were observed a few days after the earthquake. The main zone of cracking was also the location of maximum vertical slip at this site. A 1-km linear fit to the sinuous fault trace near Ralph Road was selected to obtain a representative fault strike. No linear features from which total slip (coseismic slip plus afterslip) could be measured were found at Ralph Road.

Most of the measured horizontal offset occurred across the main fault trace, similar to the pattern of displacement at Worthington Road. The initial measurement of horizontal afterslip (between October 17 and 18) at this site was across a 100-m length. Although the array was expanded to about 560 m on October 18 to cover the entire zone of observed surface faulting, only a minor difference in slip (118 mm across 560 m vs. 102 mm across 100 m) was detected across this larger aperture (standard error across this 560-m distance may be about 5 mm). The initial slip rate of 9.4 mm/d is less than rates during the same period at Ross Road and County Highway S–80. During the next interval, from October 18 to 21, the average rate (8.1 mm/d) is also less than those at Ross Road and County Highway S–80 (12.6 and 11.4 mm/d, respectively) but is greater than that determined for Worthington Road (6.4 mm/d) during the same period. The rate for the most recent interval, between December 29, 1979, and March 20, 1980, was 0.8 mm/d (fig. 146*E*). Both the total measured afterslip across the 100-m length (112 mm) and the slip inferred from a block-fit model (134 mm) are less than the corresponding afterslip measured at points to the southeast (fig. 146*E*) for a similar period.

HARRIS ROAD

The Harris Road alinement array is 28 km northwest of McCabe Road, within an area of marked fault curvature. Although the fault strike at Harris Road is N. 5° E., a regional average of N. 46° W. may better represent the fault trend over a length of about 0.5 km centered on Harris Road. The results given below represent apparent horizontal afterslip as projected from displacement measured on the east-west road onto a line perpendicular to the regional fault strike.

A significant departure from rigid-block motion is apparent in the pattern of displacement at this site; displacement of the east end point of the line (150 m east of the fault trace) with respect to the instrument station was 21 percent of the slip value of 86.5 mm measured across the 300-m length (fig. 145*F*) during the interval October 21–December 27, 1979. Although the absence of intermediate stations between the east end point and the instrument station precludes any determination of whether the eastern offset is due to a subsidiary fault trace or a warp, no evidence of fault rupture was found in that area (Sharp and others, this volume). Slight departures from the rigid-fault-block model are also in evidence outside the main slip zone west of the fault trace; 60 mm of right-lateral afterslip across a 100-m length is slightly less than the 69 mm of slip measured across a 200-m distance from the instrument station to the west end.

The Harris Road array site was surveyed at about 4-day intervals, on the average, for the first 3 weeks after the main shock, and then once again 10 weeks after the main shock. The afterslip rate of 6.4 mm/d during the first interval was relatively low in comparison with the rates determined for most other arrays during a comparable interval (October 18–21). By the time of the latest survey, the afterslip rate had decreased to 0.6 mm/d, about half the rate for the Ross Road, County Highway S–80, and Worthington Road arrays and slightly less than the rates at Ralph and McCabe Roads. The total afterslip of 94 mm for the 100-mm array also agrees closely with the value of 102 mm at Ralph Road for the comparable period (figs. 146*E*, 146*F*) and the same array length.

ANALYSIS OF AFTERSLIP

Several expressions have been used by different authors to describe afterslip data. The equation used here is

$$D = B \log (1 + Ct),$$

where D is the total slip, is a constant scaling factor, C is a constant that is the inverse of a time constant, and t is the postearthquake time. Allowing for an amount of afterslip A to have occurred at the time of the first observation, this equation becomes

$$U = D - A = -A + B \log (1 + Ct),$$

where U is the total measured afterslip. The constants A and C are mutually dependent for the accuracy allowed by the range of data in this study; thus, B is the constant that is definable from these data.

Afterslip from this study was fitted to the above equation by a finite-difference least-squares technique. The following afterslip data are presented in the order of location of the alinement arrays, beginning at the southeast end of the fault rupture. Values of the constant B determined for each site are:

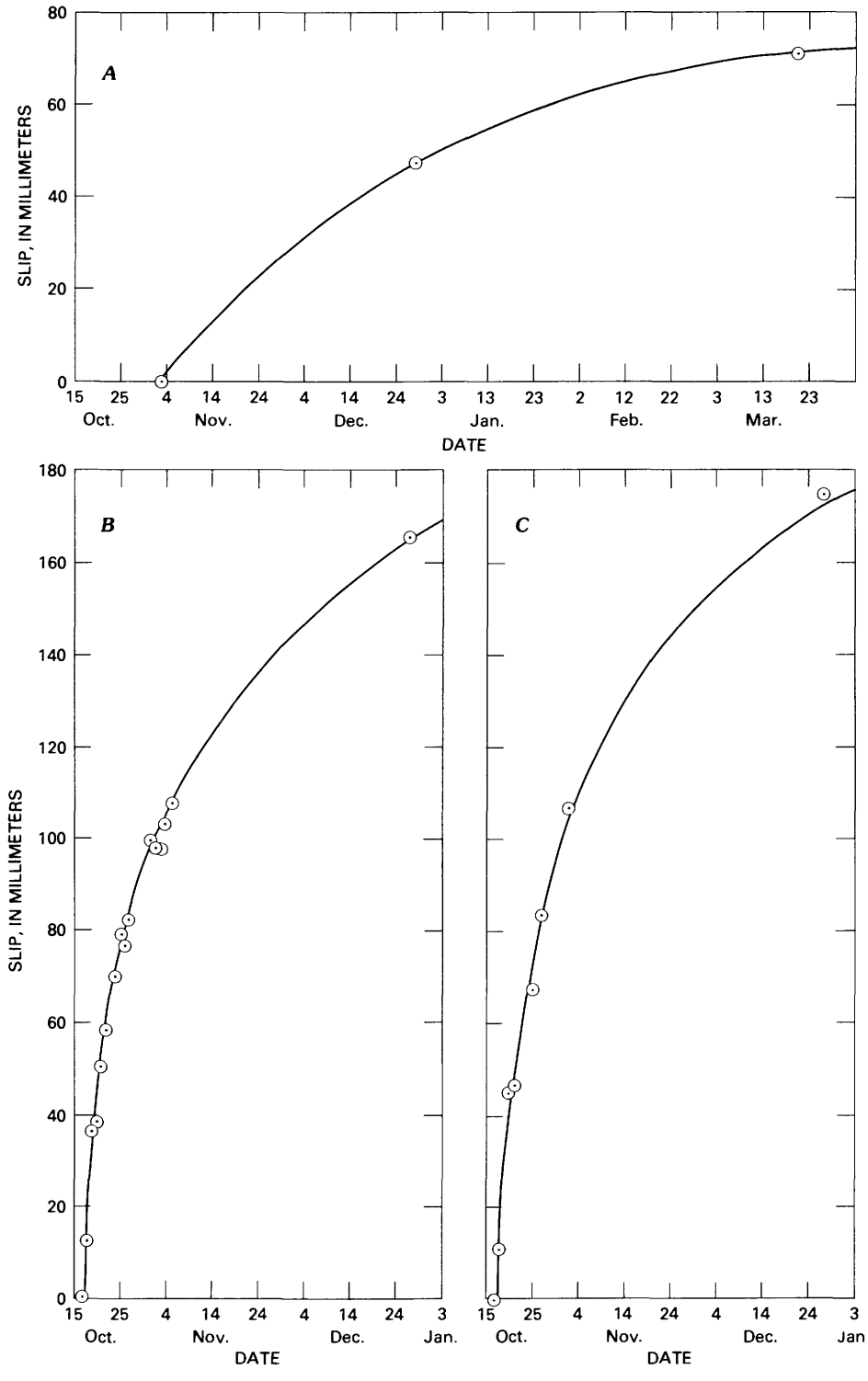

FIGURE 146.—Displacement as a function of time for each alinement array. Line is curve of equation $U = -A + B\log(1+Ct)$ fitted to data by iterative least-squares procedure. *A*, McCabe Road. *B*, Ross Road. *C*, County Highway S–80. *D*, Worthington Road. *E*, Ralph Road. *F*, Harris Road.

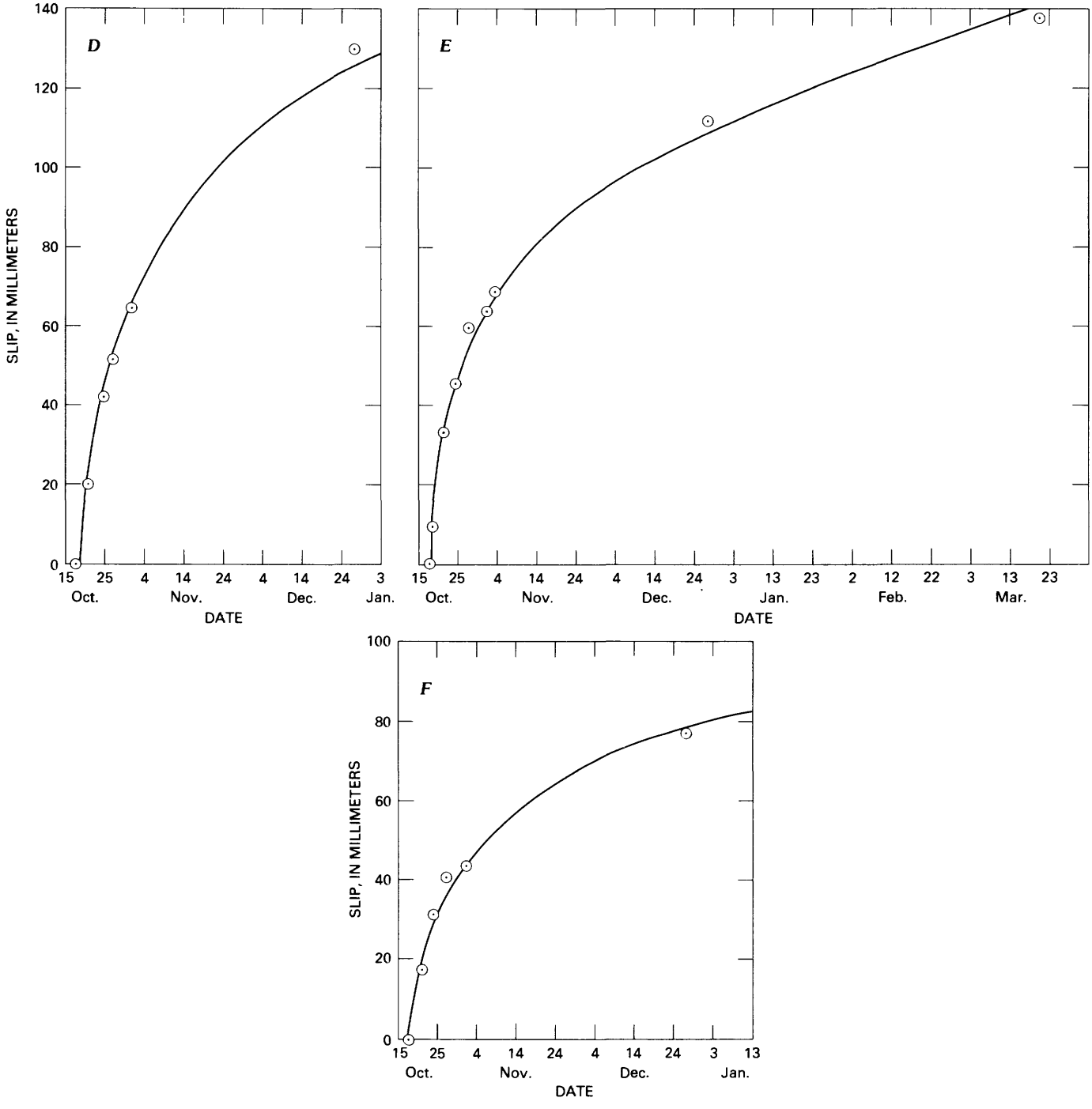

FIGURE 146.—Continued

Site	B
McCabe Road	78
Ross Road	103
County Highway S–80	111
Worthington Road	94
Ralph Road	69
Harris Road	55

DISTRIBUTION OF AFTERSLIP IN TIME AND SPACE

Initial measured slip rates from October 17 to 18 were similar from Ross Road northwestward to Ralph Road, a distance of 12 km. Between October 18 and 21, however, the slip rate differed significantly but inconsistently with position—from 13 mm/d near Ross Road to 6.4 mm/d at Harris Road. The rates at each site have continued to decline. An average slip rate of 0.9 mm/d obtained from the Ralph Road site is similar to the rate for the same period near the opposite end of surface rupture but is lower than the rates for similar intervals at sites more centrally located on the main fault break (1.1–1.2 mm/d). Total slip is also progressively less northwestward from Ross Road toward Harris Road (Sharp and others, this volume). This decrease in total slip and slip rate to the northwest is matched by a similar relation to the southeast of Ross Road, although the density of alinement-array sites is not so high and the measurements were less frequent. Northwest of County Highway S–80, this decrease is accompanied by a progressively greater scarp height of the main fault.

The changes in horizontal-afterslip scaling factor are not uniform along the Imperial fault. Figure 147 plots constant B of the equation against position along the fault. The maximum value of B was determined for the site near the center of ground rupture, and the value of B decreases to both the southeast and northwest. Decline in B to the northwest begins in the section of the Imperial fault that is nearest the Brawley fault zone, and although there is no major obvious structural analog of the Brawley fault to the southeast, the decline in B also appears to be related to the southeast end of surface rupture.

The constant B does not vary linearly with respect to apparent initial slip (the total of coseismic slip plus afterslip for the first few days after the earthquake before measurements began) at the array sites. For example, a displacement of 410 mm was reported at Ross Road (Sharp and others, this volume). Apparent initial displacement was higher at McCabe Road (658 mm; Sharp and others, this volume), and the coefficient B is comparatively small at this site. Although data from these two sites may indicate an inverse relation of initial slip to the value of B, the initial displacements near the northwest end of surface faulting were small, and B varies directly with initial slip.

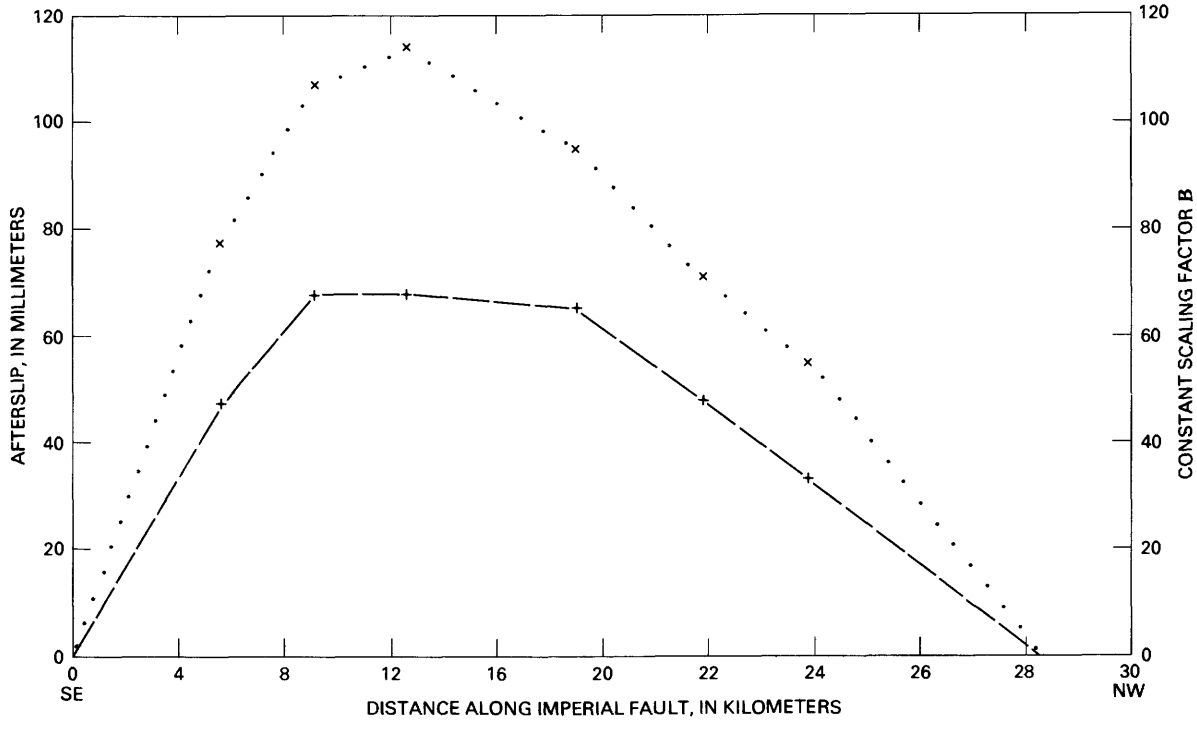

FIGURE 147.—Afterslip (dashed curve) and constant B (dotted curve) as a function of distance along fault from November 1 to December 28, 1979.

The relatively consistent relation on the plot of displacement against position (fig. 147) contrasts with that of Sharp and others (this volume), possibly because their measurements were made across smaller apertures. Displacement profiles for several alinement-array sites provide evidence of displacement outside the main fault trace, although subsidiary cracks were not observed at all these sites.

Some features of the afterslip pattern observed in the Imperial Valley may resemble those at some sites along the San Andreas fault. The patterns of displacement discussed by Burford and Harsh (1980) indicate small fluctuations in the distribution of shearing or slip activity within slip zones at several sites along the trace of the San Andreas fault. The relative amounts of slip at certain points in the displacement profiles for some sites of this study were also observed to vary. The distortion beyond the main slip zone in displacement profiles determined from alinement-array measurements in the Imperial Valley resembles that described for some sites by Burford and Harsh (1980).

The centerline between blocks of concrete pavement in the westbound lanes of County Highway S–80 was measured shortly after the 1940 Imperial Valley earthquake and again in 1966 (Brune and Allen, 1967). From the time of measurement in 1940, 6 days after the main shock, to July 1966, 380 mm of apparent offset accumulated. The correction for fault strike yields 470 mm of displacement parallel to the fault, comparable to the value of 360 mm modeled for a similar period from the data of this study. An offset of 15 mm was observed at this site after a swarm of earthquakes in March 1966 (Brune and Allen, 1967), and so the afterslip for the period discussed above was no more than 450 mm, considering the fault strike and the comparatively narrow zone over which the 1966 displacement was measured. The slip rate of 5.5 mm/yr in the decade before the 1979 event (Goulty and others, 1978) is higher than a rate predicted from the data of this study. The 1931 construction date (Herbert Hughes, oral commun., 1980) allows that the measured 1940 offset may include some pre-1940 creep. If the rate of creep for the decade before the 1979 event was similar to the pre-1940 rate at this site, the displacements (determined from Brune and Allen, 1967, and Sharp and others, this volume) for comparable times after the main shocks would be similar for the two events (380 vs. 490 mm, calculated for the 1979 and 1940 events, respectively).

Departures from the logarithmic slip-rate curve might occur owing to swarms of earthquakes during the 20 years or so before the 1979 event (Johnson and Hill, this volume). Slip was described as episodic in this region by Goulty and others (1978), and so the logarithmic fit is merely an envelope for the cumulative slip, not a precise description of the slip rate.

COMPARISON WITH THE 1966 PARKFIELD-CHOLAME EARTHQUAKE

Marked similarities in both the tectonic setting and patterns of displacement between the 1979 Imperial Valley earthquake and the 1966 Parkfield-Cholame, Calif., earthquake are evident in postearthquake observations from the two regions (fig. 148). The fault geometry is generally similar for both events: a relatively linear fault trace extends about 20 km from the end of surface rupture nearest the main-shock epicenter toward the end farthest away (Brown, 1970; Sharp and others, this volume). Sinuosity and complex patterns of multiple traces also are evident within about 10 km of the end of the surface rupture farthest from the main-shock epicenter, and a conspicuous right-echelon step occurs between two major faults in the zone of ground rupture in both areas. These echelon steps are associated with a local topographic basin that in both cases may reflect tectonic subsidence between the two faults.

Among the common elements in the seismotectonic history of both regions, the most obvious is that both these fault segments had previously broken during ear-

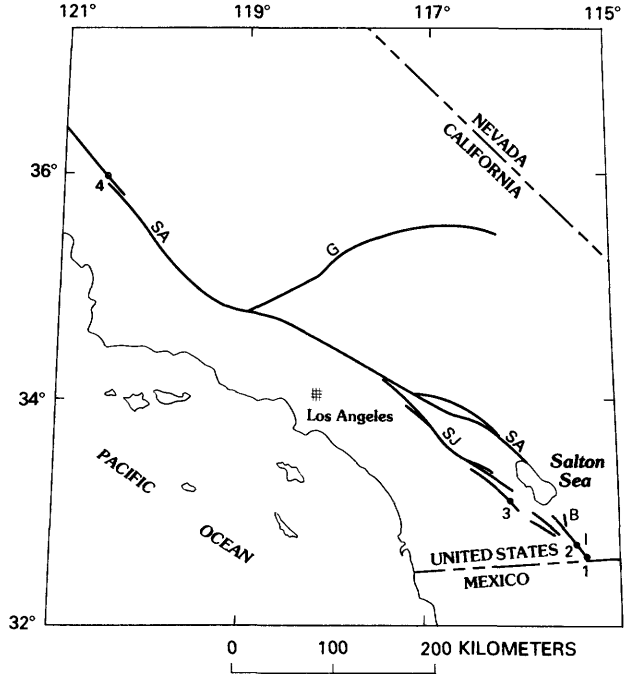

FIGURE 148.—Locations of major faults and epicenters for 1979 Imperial Valley earthquake and other moderate earthquakes discussed in text. I, Imperial fault; B, Brawley fault zone; SJ, San Jacinto fault zone; SA, San Andreas fault zone; G, Garlock fault zone. 1, epicenter of 1979 Imperial Valley earthquake; 2, epicenter of 1940 Imperial Valley earthquake; 3, epicenter of 1968 Borrego Mountain earthquake; 4, epicenter of 1966 Parkfield-Cholame earthquake.

lier historical earthquakes: the 1940 Imperial Valley and the 1934 Parkfield-Cholame (Wallace and Roth, 1967) earthquakes. Both regions are near the ends of segments of the San Andreas fault that have been quiescent for long periods; the northern segment apparently last ruptured during the great earthquake of 1857. Fault creep of a continuing mode has been measured, and microseismicity observed for several years, along both sections of ground rupture (Wesson and others, 1973; Johnson and Hill, this volume), and so both sections may be viewed as regions of at least temporary transition from relatively frequent moderate earthquakes, microseismicity, and fault creep to regions characterized by long periods of quiescence, as discussed previously for the San Andreas fault (Smith and Wyss, 1968; Burford and Harsh, 1980).

The patterns of displacement are similar for both sections of ground breakage (see Smith and Wyss, 1968, fig. 10). The length of surface cracking on the main fault was about 30 km for both events. Rupture also occurred along a length of 5 to 10 km of the Brawley fault zone that extends northward from near the end of the Imperial fault, along a branch of the San Andreas fault, for about 7 km on the west side of the Cholame Valley. Although the total displacements and magnitudes of the associated earthquakes are not closely comparable, the maximum total measured afterslip is about 20 cm for both events, and the plots of measured afterslip versus distance along the fault also closely match. The initial length of surface rupture in both places does not appear to have increased during the period of afterslip measurements, although significant afterslip occurred. Afterslip from the 1979 event apparently occurred most rapidly at a substantial distance (10 km; Johnson, this volume) from the epicenter, similar to the results obtained for the 1968 Borrego Mountain earthquake (Burford, 1972) and the 1966 Parkfield earthquake (Wallace and Roth, 1967; Smith and Wyss, 1968). An approximately logarithmic decrease in slip rate with time is apparently characteristic of all three sites, as is the characteristically narrow main zone of slip at many sites within the three regions.

The most evident difference in tectonic setting between the Imperial Valley and Parkfield-Cholame regions may be the great depths of sediment on both sides of the fault in the Imperial Valley. Because the thickness (4–5 km) of sediment is relatively constant along the activated section of the Imperial fault (Fuis and others, this volume), variations in depth to basement should not significantly affect the relative pattern of displacement. This pattern of displacement distribution contrasts with the results of other studies that have found afterslip rates corresponding to varying thicknesses of unconsolidated sediment (Smith and Wyss, 1968) or inversely related to initial displacement (Bucknam and others, 1978), or both (Burford, 1972). Although Smith and Wyss (1968) suggested a delay of fault slip by the alluvium for the State Highway 46 site of the Parkfield-Cholame earthquake study, they stated that end effects might be an alternative explanation for that site. Plots of displacement versus time for sites of the Parkfield-Cholame study also contained evidence for logarithmically decreasing slip rates at sites near the northwest end of ground rupture (Smith and Wyss, 1968), although very little alluvium occurs along the fault on a high-standing ridge in this area. Although delay of seismic slip by a deep unconsolidated sedimentary section may account for part of the observed afterslip, this pattern of logarithmic decrease in slip rate occurs along the entire length of apparent seismic rupture in both regions and may result from moderate earthquakes in regions of differing surficial lithology. Afterslip in the seismogenic zone at 5- to 10-km depth is not precluded as a primary factor, however, for the afterslip observed at the surface. The major changes in fault strike, though a possible influence on the distribution of coseismic slip and thus on potential afterslip and its rate, may be related to end effects of the fault structure itself, and so the variation in slip rate along the fault may be affected by both factors.

CONCLUSIONS

The similarities of pre-1979 slip measurements to 1979 afterslip at County Highway S–80 suggest that these features are not uniquely related to the October 15 earthquake but may represent typical behavior at this site on the Imperial fault, although data to test such a hypothesis adequately are unavailable.

The similarities between the Parkfield-Cholame and Imperial Valley regions may indicate a more than fortuitous resemblance between the slip-versus-distance relations for the two sites. Similarity of the amplitude of measured horizontal afterslip and its relation to distance along the fault for both regions provide additional evidence to support the conclusion that afterslip is not due primarily to poor consolidation of the overlying sediment. The pattern of afterslip along the Imperial fault may actually be controlled by fault geometry and seismic-rupture patterns. Similar afterslip-versus-distance and logarithmic-decrease-of-afterslip relations may occur in regions of differing surficial lithology, although the surficial lithology may somewhat influence afterslip.

ACKNOWLEDGMENTS

Several colleagues assisted in many helpful ways. Michael Rymer, Pat Vaughn, and James Lienkaemper assisted with the field measurements of afterslip, and

Robert V. Sharp and Robert O. Burford made many useful suggestions. I am also indebted to several officials of Imperial County, among them David Pierson, Director of Public Works, and Robert Estes, Robert Goff, and J. W. Luker.

REFERENCES CITED

Brown, R. D., Jr., 1970, Map showing recently active breaks along the San Andreas and related faults between the northern Gabilan Range and Cholame Valley, California: U.S. Geological Survey Miscellaneous Geologic Investigations Map I–575, scale 1:62,500.

Brune, J. N., and Allen, C. R., 1967, A low-stress-drop, low-magnitude earthquake with surface faulting: The Imperial, California, earthquake of March 4, 1966: Seismological Society of America Bulletin, V. 57, no. 3, p. 501–514.

Bucknam, R. G., Plafker, George, and Sharp, R. V., 1978, Fault movement (afterslip) following the Guatemala earthquake of February 4, 1976: Geology, v. 6, no. 3, p. 170–173.

Burford, R. O., 1972, Continued slip on the Coyote Creek fault after the Borrego Mountain earthquake, *in* the Borrego Mountain earthquake of April 9, 1968: U.S. Geological Survey Professional Paper 787, p. 105–111.

Burford, R. O., and Harsh, P. W., 1980, Slip on the San Andreas fault in central California from alinement array surveys: Seismological Society of America Bulletin, v. 70, no. 4, p. 1233–1261.

Clark, M. M., 1972, Surface displacement along the Coyote Creek fault, *in* The Borrego Mountain earthquake of April 9, 1968: U.S. Geological Survey Professional Paper 787, p. 55–86.

Goulty, N. R., Burford, R. O., Allen, C. R., Gilman, Ralph, Johnson, C. E., and Keller, R. P., 1978, Large creep events on the Imperial fault, California: Seismological Society of America Bulletin, v. 68, no. 2, p. 517–521.

Richter, C. F., 1958, Elementary seismology: San Francisco, W. H. Freeman, 768 p.

Smith, S. W. and Wyss, Max, 1968, Displacement on the San Andreas fault subsequent to the 1966 Parkfield earthquake: Seismological Society of America Bulletin, v. 58, no. 6, p. 1955–1973.

Wallace, R. E., and Roth, E. F., 1967, Rates and patterns of progressive deformation, *in* Brown, R. D., Jr., Vedder, J. G., Wallace, R. E., Roth, E. F., Yerkes, R. F., Castle, R. O., Waananen, A. O., Page, R. W., and Eaton, J. P., The Parkfield-Cholame, California, earthquakes of June–August 1966—surface geologic effects, water-resources aspects, and preliminary seismic data: U.S. Geological Survey Professional Paper 579, p. 23–40.

Wesson, R. L., Burford, R. O., and Ellsworth, W. L., 1970, Relationship between seismicity, fault creep, and crustal loading along the central San Andreas fault, *in* Kovach, R. L., and Nur, Amos, eds., Proceedings of the conference on tectonic problems of the San Andreas fault system: Stanford University Publications in the Geological Sciences, v. 13, p. 303–321.

GEODETIC OBSERVATIONS OF POSTSEISMIC DEFORMATION AROUND THE NORTH END OF SURFACE RUPTURE

By JOHN O. LANGBEIN, M. J. S. JOHNSTON, and A. MCGARR,
U.S. GEOLOGICAL SURVEY

CONTENTS

ABSTRACT

We have measured postseismic deformation, using an electronic distance-measuring instrument, in the area around the northern third of observed surface rupture from the 1979 Imperial Valley earthquake. Measurement of a geodetic network consisting of 54 base lines was initiated on October 27, 1979, and the lines were repeatedly measured during the next several months. We analyzed the line-length changes in terms of a simple model of uniform slip over a semi-infinite plane, corresponding to the Imperial fault, and homogeneous strain changes in the surrounding region. For the interval October 27–December 13, 1979, the average rate of fault slip was found to be 1.08±0.08 mm/d, and the most significant component of strain change was an east-westward contraction of 0.08±0.02 microstrain per day, with an uncertainty of 28.5° in the azimuth of this component of the principal strain. Generally, the rate of postseismic deformation decreased over time during the entire period of observation. For example, from October 27 to November 14 the average rate of fault displacement was 1.96±0.29 mm/d, whereas from November 12 to December 13 the rate was 0.80±0.13 mm/d. From October 27 to November 14 the strain change was correspondingly rapid, with northwest-southeastward compression occurring at a rate of 0.3±0.1 microstrain per day. Most of these observations can be tentatively explained in terms of strain release on either side of the fault due to postseismic slip.

INTRODUCTION

In this report we describe the preliminary results of a geodetic survey in the vicinity of the northern section of the Imperial fault after the main shock of October 15, 1979. On the basis of information of continuing postseismic fault motion of as much as 10 mm/d (P. W. Harsh, oral commun., 1979), we initiated a program of line-length measurements, using a Hewlett-Packard 3800A distance-measuring instrument and an array of 18 corner-cube reflectors. With this instrumentation, apparent strain changes along lines of about 2 km can be resolved at about the 2-microstrain level (Lisowski and Prescott, 1981).

Of particular interest with regard to questions of postseismic-strain redistribution was the area around the north end of the Imperial fault break. Most of the aftershocks tended to occur there and on the adjacent echelon Brawley fault zone and the Superstition Hills fault (Johnson and Hutton, this volume). Indications of displacements on the San Andreas fault (Sieh, this volume) and on the Superstition Hills fault (Fuis, this volume) also suggest continuing deformation in this northern area. In view of these displacements and because of the existence of excellent geodetic control across the central section of the Imperial fault (Mason and others, 1979; Crook and others, this volume), we concentrated on measuring ground deformation in and near the north third of the zone of ground breakage (Sharp and others, this volume).

Beginning on October 27, we made repeated measurements of the line lengths of 54 base lines (fig. 149) extending northwestward from the earlier geodetic network set up in 1970 by the Imperial College, London (Mason and others, 1979). Our new network includes three of the Imperial College bench marks (J33, G33, and G34), and six alinement-array bench marks (here designated HSE1, HSE3, HSW1, HSW3, HSW3′, and HSW4), installed by Harsh (this volume) on either side of the fault at Harris Road (fig. 149). To avoid losing time in establishing this new network, we elected to use concrete nails driven into the road pavement as bench marks rather than more permanent marks, such as those used by Mason and others (1979).

As seen on the map (fig. 149), the network includes both lines that cross the fault and lines completely to the northeast or southwest of the trace. The geometry of the network was influenced largely by the availability of lines of sight across rather flat topography; thus the majority of lines follow roads. Another limitation on the network, imposed by the instrument used, was difficulty in measuring line lengths longer than 3 km.

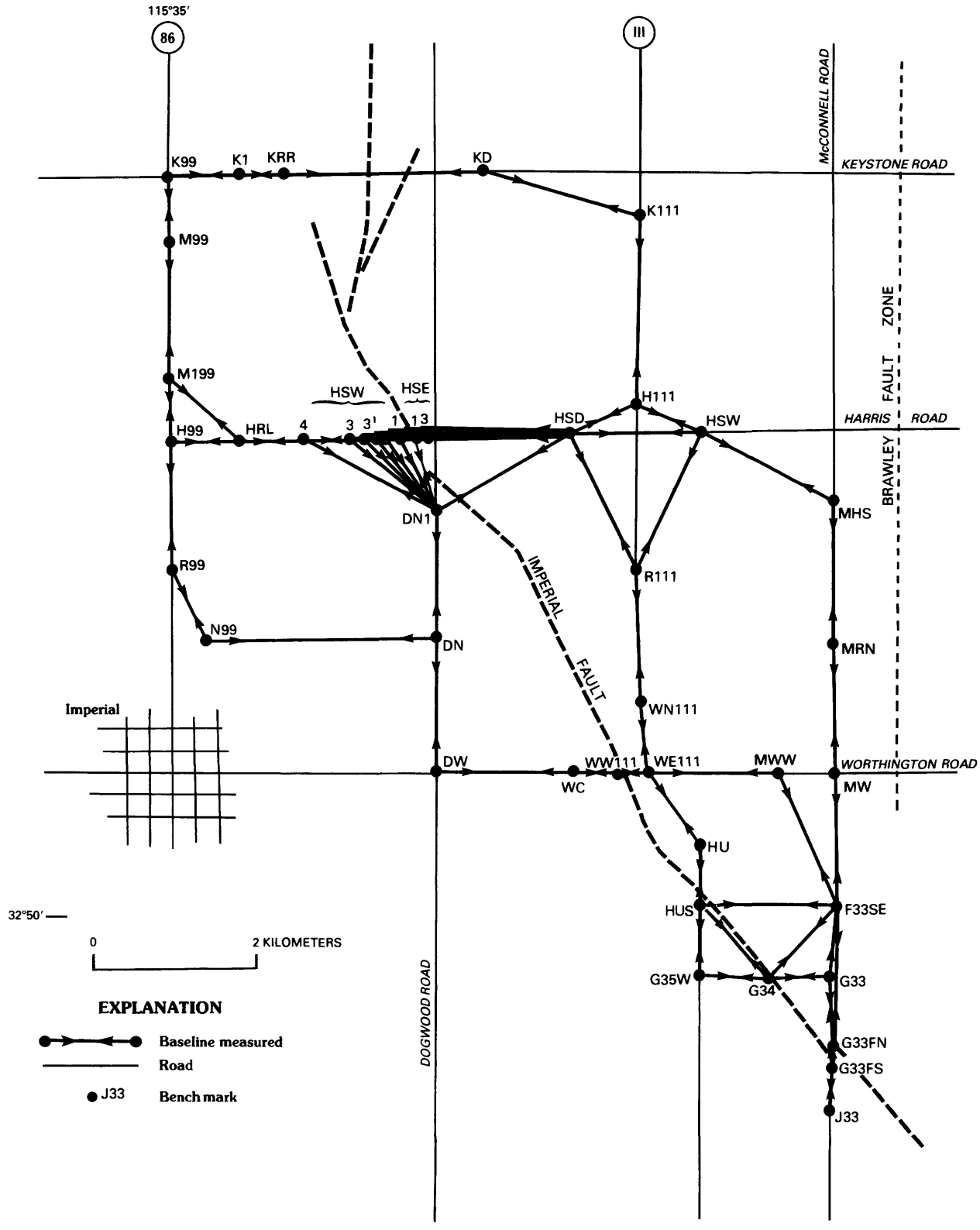

FIGURE 149.—Locations of base lines in geodetic network used to measure surface strain and slip on Imperial fault. Heavy dashed line indicates approximate location of observed trace of Imperial fault; light dashed line indicates Brawley fault zone. Obvious surface ruptures from October 15 earthquake could be observed north and south of Keystone Road.

As discussed below, the large number of lines allowed the determination of fault displacement and strain change as a function of time and position within the network. The capability of measuring deformation within regions of the network is important here because within the network the coseismic fault displacements exhibited spatial gradients to the southeast of Keystone Road of more than 2 mm/km across 10 km of the most obvious surface rupture. In the first 10 days after rupturing, postseismic fault displacements also showed a spatial gradient of more than 1 mm/km across the same rupture zone (Harsh, this volume; Sharp and others, this volume). Therefore, strain in this area should not be expected to be homogeneous.

OBSERVATIONS

Figure 150 plots the changes in line length for each base line in the network during the interval October 27–December 16, 1979. The time scales of these plots are somewhat longer than necessary because we intended to continue our observational program into the first quarter of 1980. Figure 150*A* shows the changes in displacement for only those lines that cross the surface trace of the Imperial fault; all other displacement-time histories are for lines that do not cross the fault. All data have been corrected for the effects of temperature, pressure, and humidity on the atmospheric refractive index (Bomford, 1971), and for shifts in the frequency of the reference oscillator of the instrument due to changes in ambient temperature (Lisowski and Prescott, 1981).

For the base lines that cross the fault, the line-length changes are apparently rapid and generally linear, although the displacement rate seems to decrease somewhat over time. On most of the base lines that do not cross the Imperial fault, changes in line length appear to be more subtle and of varying significance. The multitude of measured lines, however, provide considerable redundancy, and so good estimates of strain change can be made for selected regions of the network. The data from many base lines that do not cross the fault also indicate a standard deviation in the measurements smaller than the 4.5 mm estimated by Lisowski and Prescott (1981). For example, five base lines in our network were measured at least six times. Fitting linear trends to this data set gives estimates of the unbiased standard deviation of the fit of from 2.6 to 3.6 mm. Adding the data from the base lines measured five times gives an average standard deviation of 3.9 mm for fitting either a linear trend or a simple mean to the data. Estimates of the error in the atmospheric-refractive-index correction (Bomford, 1971) are assumed to be one part in 10^6, which is statistically added to the 3.9-mm nominal error.

DISCUSSION

Although the observed fault displacements indicate that inhomogeneous strain change within the survey network is likely, it seemed worthwhile first to analyze the geodetic data in terms of a simple model involving constant fault slip and homogeneous deformation. In this report we elaborate this initial analysis by considering homogeneous deformation within regions of the network, but do not discuss more complex models involving finite faults.

Assuming an infinite fault with uniform slip in a half-space, we can use the observed line-length changes to infer the value of fault slip and the changes in the three horizontal components of strain. The degree of misfit to the resulting solution gives some indication of how useful our observations are likely to be if we were to analyze them in terms of more realistic fault models.

For an assumed homogeneous deformation, the changes in line length ΔL_i are related to the slip rate $\dot{U}$ and the components of the strain-rate tensor $\dot{E}_{ee}$, $\dot{E}_{en}$, and $\dot{E}_{nn}$ by:

$$\Delta L_i = L_{ij} - \bar{L}_i$$

$$= (T_{ij} - \bar{T}_i)\left[\dot{U}\cos\ \alpha_i + L_i(\dot{E}_{ee}\cos^2\ \phi_i + 2\dot{E}_{en}\cos\ \phi_i \sin\ \phi_i + \dot{E}_{nn}\sin^2\ \phi_i)\right],$$

where L_{ij} is the distance on the ith base line measured at time T_{ij}, $\bar{L}_i$ and $\bar{T}_i$ are the average distance and time, respectively, ϕ_i is the angle between the ith base line and the direction east, and α_i is the angle between the fault trace and the ith base line. We use the technique of weighted least squares to determine the model parameters from the data; the weights used are the squares of the reciprocal of the standard measurement error for each data point. In the following discussion we present the results for different spatial and temporal subsets of the data (fig. 151). Because we use a weighted-least-squares technique here, the standard deviation of the fit to the model is dimensionless, and the values less than unity indicate a good fit of the model to the data.

Using the entire data set, we infer the following:

$$\dot{U} = 1.08 \pm 0.08 \text{ mm/d},$$

$$\dot{E}_1 = -0.08 \pm 0.02 \text{ microstrain per day},$$

$$\dot{E}_2 = 0.02 \pm 0.02 \text{ microstrain per day},$$

$$\theta_1 = \text{N. } 89.4° \pm 28.5° \text{ E},$$

and

$$\sigma = 1.00 \text{ mm/mm},$$

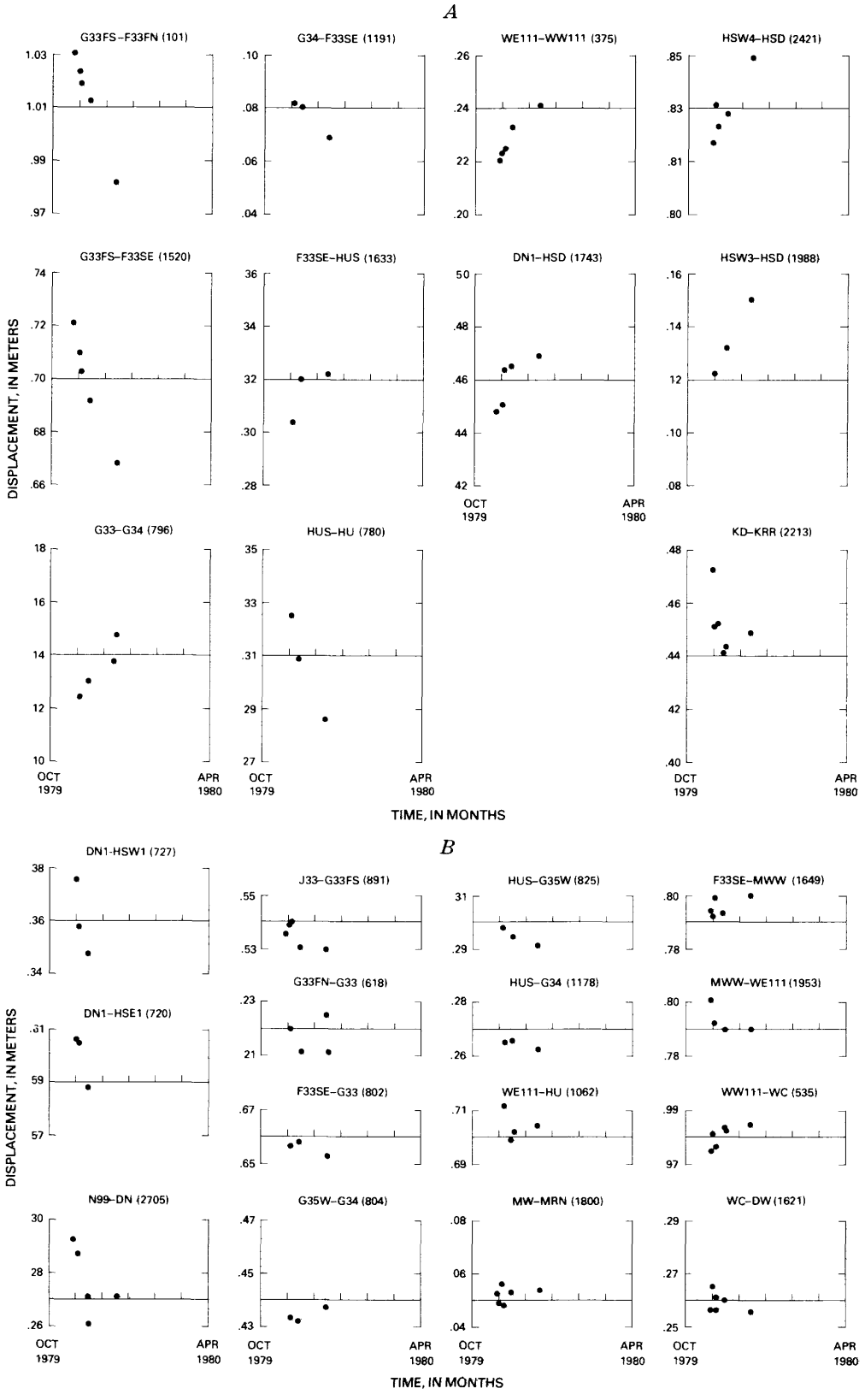

FIGURE 150.—Line length as a function of time for all base lines in geodetic network (see fig. 149 for locations). Each plot represents separate base line; number in parentheses following bench-mark names indicates length of base line (in meters). Time scale starts at October 1, 1979. *A*, Changes in displacement for only those lines that cross surface trace of Imperial fault. *B*, Changes in displacement for lines that do not cross Imperial fault.

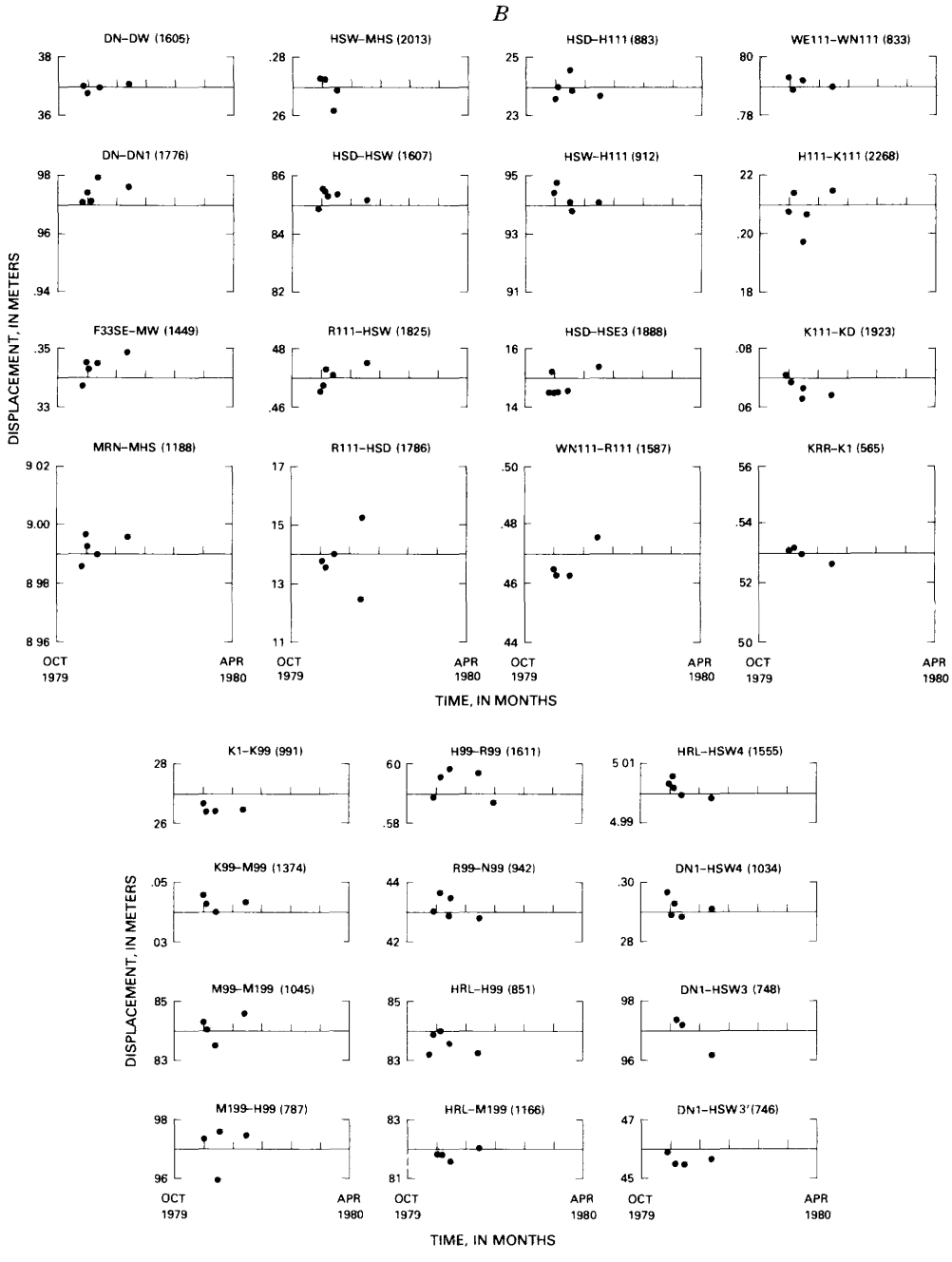

FIGURE 150.—Continued

ALL DATA

SUBSET (MEASUREMENT)	PERIOD		
	10/27–12/13	10/27–11/14	11/12–12/13
$\dot{E}_1$ (μstr/d)	-0.07 ± 0.02	-0.32 ± 0.09	-0.05 ± 0.06
$\dot{E}_2$(μstr/d)	0.02 ± 0.02	0.07 ± 0.11	0.07 ± 0.06
'1' azimuth	N.89° ± 22°E.	N.59° ± 10°W.	N.64° ± 21°E.
$\dot{U}$ (mm/d)	1.08 ± 0.08	1.96 ± 0.29	0.80 ± 0.13
σ(mm/mm)	1.04	0.83	0.79
Number of observations	224	184	119
Vectors			

EASTERN-BLOCK DATA

SUBSET (MEASUREMENT)	PERIOD		
	10/27–12/13	10/27–11/14	11/12–12/13
$\dot{E}_1$ (μstr/d)	−0.06 ± 0.05	−0.27 ± 0.15	−0.00 ± 0.08
$\dot{E}_2$(μstr/d)	0.10 ± 0.05	0.19 ± 0.15	0.11 ± 0.06
'1' azimuth	N.63° ± 14°W.	N.49° ± 9°W.	N.84° ± 45°E.
$\dot{U}$ (mm/d)			
σ(mm/mm)	0.85	0.65	0.85
Number of observations	90	70	45
Vectors			

WESTERN-BLOCK DATA

SUBSET (MEASUREMENT)	PERIOD		
	10/27–12/13	10/27–11/14	11/12–12/13
$\dot{E}_1$ (μstr/d)	−0.11 ± 0.07	−0.41 ± 0.21	−0.06 ± 0.12
$\dot{E}_2$(μstr/d)	0.04 ± 0.07	0.09 ± 0.21	0.12 ± 0.12
'1' azimuth	N.65° ± 20°W.	N.65° ± 19°W.	N.47° ± 15°W.
$\dot{U}$ (mm/d)			
σ(mm/mm)	0.88	0.84	0.62
Number of observations	98	76	49
Vectors			

REGION I DATA

SUBSET (MEASUREMENT)	PERIOD		
	10/27–12/13	10/27–11/14	11/12–12/13
$\dot{E}_1$ (μstr/d)	−0.10 ± 0.08	0.28 ± 0.23	0.08 ± 0.10
$\dot{E}_2$(μstr/d)	0.06 ± 0.08	−0.55 ± 0.23	−0.24 ± 0.10
'1' azimuth	N.46° ± 12°E.	N.50° ± 7°E.	N.58° ± 11°W.
$\dot{U}$ (mm/d)	0.99 ± 0.10	1.75 ± 0.30	0.73 ± 0.14
σ(mm/mm)	1.18	0.91	0.74
Number of observations	110	83	56
Vectors			

REGION II DATA

SUBSET (MEASUREMENT)	PERIOD		
	10/27–12/13	10/27–11/14	11/12–12/13
$\dot{E}_1$ (μstr/d)	−0.10 ± 0.10	−0.11 ± 0.40	−0.04 ± 0.12
$\dot{E}_2$(μstr/d)	0.06 ± 0.10	−0.44 ± 0.41	0.22 ± 0.13
'1' azimuth	N.71° ± 38°E.	N.63° ± 50°W.	N.89° ± 51°E.
$\dot{U}$ (mm/d)			
σ(mm/mm)	0.68	0.61	0.75
Number of observations	34	26	17
Vectors			

REGION III DATA

SUBSET (MEASUREMENT)	PERIOD		
	10/27–12/13	10/27–11/14	11/12–12/13
$\dot{E}_1$ (μstr/d)	−0.07 ± 0.06	0.21 ± 0.18	−0.07 ± 0.10
$\dot{E}_2$(μstr/d)	0.08 ± 0.05	−0.28 ± 0.18	0.13 ± 0.09
'1' azimuth	N.67° ± 16°W.	N.54° ± 13°E.	N.85° ± 30°E.
$\dot{U}$ (mm/d)			
σ(mm/mm)	0.95	0.64	1.07
Number of observations	40	32	21
Vectors			

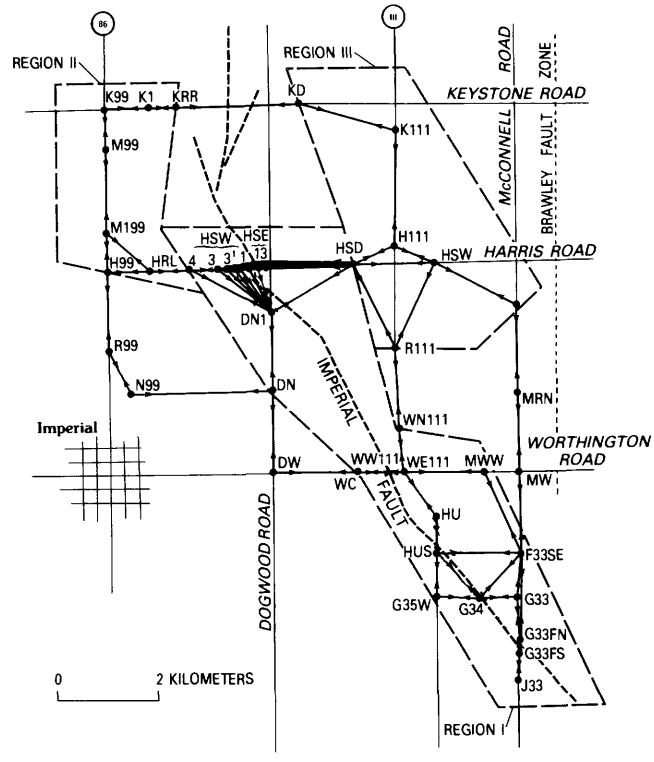

FIGURE 151.—Results of estimating slip and strain rates for different data subsets. U is value of right-lateral slip, and E_1, E_2, and " '1' azimuth" are values of principal strain components and its axis. Vectors indicate azimuth and magnitude of principal strains; direction north points vertically upward on the page. Inset shows locations of regions I, II, and III within network (see fig. 149 for detail). Western and eastern blocks refer to Imperial fault.

where θ_1 is the azimuth of the principal strain rate $\dot{E}_1$, and σ is the standard deviation of the fit of the model to the data. Besides the high rate of fault slip, the major finding from these data is an east-westward contraction at a rate of 0.08 microstrain per day, four times larger than its corresponding estimate of the standard error. We note that the actual direction of contraction is poorly determined. The fit of this model to the data, as indicated by the normalized standard deviation σ, is surprisingly good in view of our simplifying assumptions of uniformity in strain and fault slip in both space and time.

The data from the entire network can be subdivided into two intervals (fig. 151): the first from the initial survey to the survey in mid-November, and the second from mid-November to mid-December. For the first interval the slip rate averaged 1.96 ± 0.29 mm/d, and for the second interval the data indicate a lower slip rate of 0.80 ± 0.13 mm/d. Another significant measurement for the first interval is the contraction rate of 0.32 ± 0.12 microstrain per day along a northwesterly azimuth. The strain rates for the second interval, however, do not differ significantly from zero (fig. 151)—a result to be expected if the rate of deformation was decreasing over time.

Northwest-southeastward contraction also appears to be significant in the areas either to the west or to the east of the Imperial fault (fig. 151) during the first interval. For the entire period of observation, the strain rates in the western block agree well with those inferred from the entire data set. Thus, insignificant strain changes during the second interval and southeast-northwestward contraction during the first interval are evident in both sets of data. Similar conclusions, however, are not substantiated by the data from the eastern block. In contrast to the changes during the first interval, significant strain changes occurred in this block during the second interval. Significant north-southward extension during the second interval, in conjunction with strain changes during the first interval that show nearly pure shear, indicates 0.10 microstrain per day of northeast-southwestward extension over the entire period of observation.

We note that the observation of northwest-southeastward contraction during the first interval in all the data is consistent with strain release due to right-lateral slip on the Imperial fault (Scholz and Fitch, 1969). As pointed out above, problems encountered by using this simple, uniform-strain interpretation may arise as a result of the need to consider: (1) the likely nonuniform distribution of slip; (2) the effect of sympathetic slip on the Brawley fault zone and the Superstition Hills fault to the east and west of the network, respectively; and (3) such geometric effects as the change in fault strike near Harris Road, which may be associated with a substantial vertical component of faulting on this section of the Imperial fault, as observed by Sharp and Lienkaemper (this volume).

In an attempt to determine the spatial variations in strain within the network, we divided the survey area into three smaller regions (inset, fig. 151) to allow internal comparison. As expected, estimates of strain were not so well determined because of the fewer measurements available. Region I consists of all the base lines that cross the Imperial fault south of Keystone Road and those base lines that are within 1.5 km of the fault. Both the inferred slip and strain rates in this region apparently decrease over time, and the strain during the first interval indicates primarily northwest-southeastward contraction. A curious feature is an apparent rotation of the principal strains during the second interval. Region II consists of the base lines on the west side of the Imperial fault near the terminus of the surface rupture. We note a compressional trend, but it is only marginally significant for the first interval, when the slip rate was high. This pattern of strain, in which the estimated strain exceeds the standard deviation, is consistent with simple dislocation models that predict contraction in this northwestern lobe with slip on a right-lateral fault. The significant north-southward extension observed in this region during the second interval is unexplained at this time. Region III consists of the base lines near Harris Road and State Highway 111. Again, significant northwest-southeastward contraction occurred during the first interval, and north-southward extension during the second.

The leveling data of Sharp and Lienkaemper (this volume) indicate that the postseismic fault displacement was mostly dip-slip. Figure 152 plots the relative uplift of the west side of the fault at Harris Road, along with some of our corresponding horizontal measurements. Except for the measurements along base line

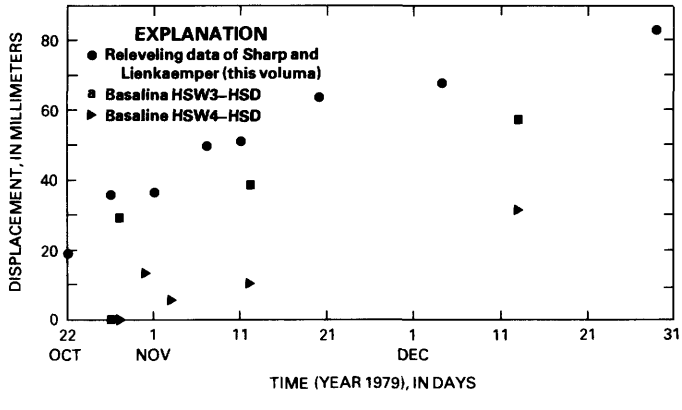

FIGURE 152.—Uplift of western block of Imperial fault relative to eastern block at Harris Road (see fig. 149 for location), from leveling data of Sharp and Lienkaemper (this volume). Horizontal data from our network around Harris Road are also plotted at same scale.

HSW3 to HSD made on October 27, the plot of the vertical and horizontal data (fig.152) seems to indicate a similar history of deformation. We can determine the dip of the Imperial fault near Harris Road, at least in principle, by comparing the vertical and extensional components of the fault-displacement vector. We first attempted to determine the horizontal component of the slip vector from measurements along Harris Road and from bench mark DN1 (fig. 149) crossing the area of interest, but these data were inadequate to estimate both horizontal components. Our data were well suited, however, to estimate the projection of the horizontal-slip vector along Harris Road, which is probably the most significant component in terms of an estimate of the local fault dip because the fault strikes nearly north-south in this locality (Sharp and others, this volume). Accordingly, we compare the line-lengthening rates over the base lines extending from bench mark HSD with the releveling data of Sharp and Lienkaemper (this volume) (fig. 152), to infer an apparent eastward dip of 49°±5° E. which agrees well with field measurements of dip near Harris Road indicating an eastward dip of 59°±8° E. (R. V. Sharp and M. G. Bonilla, oral commun., 1980).

CONCLUSIONS

Postseismic geodetic-strain changes obtained in the area around the north end of the Imperial fault rupture display considerable spatial and temporal complexity. As a first step in analyzing these data, we used a simple model consisting of uniform slip and strain to fit the data. Although many problems remain, the initial fit is surprisingly good and allows two general conclusions to be drawn. (1) Significant postseismic fault displacement can easily be detected with this technique, using all fault-crossing lines; the rate of fault slip decreases over time. (2) Significant changes in strain, observed within about a 3-km zone on either side of the fault, were mainly characterized by a northwest-southeastward compression of 0.3 microstrain per day during the first 2 weeks after initial measurements were made.

ACKNOWLEDGMENTS

The surveys were performed using equipment kindly loaned us by J. C. Savage, W. H. Prescott, Michael Lisowski, and A. G. Lindh, all of the U.S. Geological Survey; R. Estes of the Imperial County Public Works Department; and Mr. Parker of Parker and Riddle, Inc., El Centro, Calif. J. E. Estrem provided field assistance during the initial survey, and P. W. Harsh supplied bench marks and other equipment for the field operations.

REFERENCES CITED

Bomford, Guy, 1971, Geodesy (3d ed.): London, Oxford University Press, 731 p.

Lisowski, Michael, and Prescott, W. H., 1981, Short-range distance measurements along the San Andreas fault system in central California, 1975 to 1979: Seismological Society of America Bulletin, v. 71, no. 5, p. 1607–1624.

Mason, R. G., Brander, J. L., and Bill, M. G., 1979, Mekometer measurements in the Imperial Valley, California, *in* Whitten, G. A., Green, Ronald, and Meade, B. K., eds., Recent crustal movements, 1977: Tectonophysics, v. 52, no. 1–4 (special issue), p. 497–503.

Scholz, C. H., and Fitch, T. J., 1969, Strain accumulation along the San Andreas fault: Journal of Geophysical Research, v. 74, no. 27, p. 6649–6666.

COMPARISON OF 1979 SURFACE FAULTING WITH EARLIER DISPLACEMENTS IN THE IMPERIAL VALLEY

By ROBERT V. SHARP,
U.S. GEOLOGICAL SURVEY

CONTENTS

ABSTRACT

The 1979 surface movements on the Imperial fault and the Brawley fault zone generally followed the traces of historical and prehistoric faulting. Only the north half of the 1940 Imperial fault trace was reactivated, but movement on the Brawley fault zone extended both northward and southward beyond the limits of known earlier surface displacement. Right-lateral offset on the Imperial fault was generally smaller than in 1940, although it may have been larger near Interstate Highway 8. Vertical components of slip may have been greater in 1979 on the Brawley fault zone than during the earthquake swarm of 1975, but evidence for this difference is equivocal. No definite examples of new faulting on either structure are known, but some minor breaks could be new. Although a few photolineaments judged to represent possible fault traces were not activated, nearly all known traces of the 1940 events and Holocene scarps mapped from early aerial photographs were reactivated as far as the southernmost limit of 1979 faulting. Comparison of the ratios of horizontal to vertical components of slip for 1979 with those of 1940 movements on the Imperial fault and with those of 1975 movements on the Brawley fault zone shows that significant changes in the rake angle of slip on fault surfaces can accompany successive slip events on faults.

INTRODUCTION

In the central Imperial Valley, surface faulting related to the October 15, 1979, earthquake occurred along two previously recognized structures—the Imperial fault and the Brawley fault zone (Sharp and others, this volume). Some aspects of the main faulting from the 1979 event can be compared to both prehistoric and earlier historical displacements, in particular the 1940 Imperial Valley earthquake, during which movement occurred on both the Imperial fault and the Brawley fault zone. Although the maximum displacements of the 1979 event are substantially smaller than those of 1940, the comparisons of the locations of traces and of the amount and kind of slip clearly demonstrate a marked similarity of the surface ruptures of the two events.

Opportunities for comparing separate major displacement events in historical time on the same fault structures have been limited. In California, the 1906 displacement on the San Andreas fault extended through a segment of the fault that had moved in 1890, and in the Parkfield area the San Andreas fault moved in 1857, 1901, 1922, 1934, and 1966. These and other examples of multiple historical displacements were summarized by Bonilla (1979). In spite of the number of such events, the profitability of a comparison ultimately rests on the degree to which each event was carefully documented; and many of these historical fault movements, particularly the earlier ones, were not well recorded. What makes the study of 1979 surface faulting in the Imperial Valley especially important is that the faults have previously been recognized as active structures, photographically recorded, mapped in as much detail as existing knowledge permitted, and studied in terms of their earlier historical and prehistoric movements (Ulrich, 1941; Richter, 1958; Brune and Allen, 1967; Allen and others, 1972; Sharp, 1977a, b, 1980; Goulty and others, 1978).

COMPARISONS

The surface faulting associated with the 1979 earthquake can be compared with earlier movement events in several ways, including: the location of traces of rupture, the recognition of previously unbroken fault traces, old fault traces not activated during this event, the length and end points of rupture, the amount and distribution of displacement along the length of the faults, and the ratio of horizontal to vertical components where the displacements were not purely strike-slip.

IMPERIAL FAULT

The Imperial fault, in particular the segment that moved during the 1979 earthquake, has previously displayed intermittent creep on many occasions, including one episode triggered by the distant Borrego Mountain, Calif., earthquake in 1968 (Brune and Allen, 1967; Allen and others, 1972; Goulty and others, 1978). Moreover, the creeping section of the fault is situated where the 1940 surface displacement was significantly less than the maximum displacement and where the fault has generated abundant low-magnitude seismicity since the 1950's (Johnson and Hill, this volume). The 1979 surface movements are distributed over this same post-1940 active segment of the fault.

The surface-rupture length for the 1979 event on the Imperial fault is about 30 km, roughly half that of the 1940 earthquake. Comparison of the north termini of the 1940 and 1979 surface ruptures is more complex, although the south limit of the 1979 break was clearly near the midpoint of the 1940 rupture. The north ends of the breaks for the two events probably were very nearly the same, although the evidence for this conclusion is indirect and is discussed more fully below.

Field observations (J. P. Buwalda, unpub. data, 1940) of the 1940 fault displacement, aerial photographs taken before and after the 1940 earthquake, and mapping of fault-creep locations across present cultural features in the Imperial Valley only partly delineated the trace of the Imperial fault. Because of vigorous agricultural activity in this area, many natural features that reveal details of the fault trace have been and continue to be obliterated. As a consequence, even the most recent pre-1979 attempt to map the fault (Sharp, 1977a) necessarily omitted many of the complexities revealed by the 1979 surface rupture.

RUPTURE TRACES

Brune and Allen (1967) and Allen and others (1972) pointed out that road intercepts of the part of the Imperial fault that moved in 1966, 1968, and 1971 agreed well with the locations noted by J. P. Buwalda for the 1940 rupture. For those segments of the fault that recently have moved by aseismic creep, including the 1977 event reported by Goulty and others (1978) and such earthquake-swarm-associated displacements as the 1966 movement (Brune and Allen, 1967; Johnson and Hill, this volume), the intercepts on all cultural features that cross the fault were documented on maps and photographically recorded (Sharp, 1977a). These features include road pavements, concrete-lined canals, and tracks of a railroad. Within the limits of accuracy that these features could be either photographically compared or located on a 1:24,000-scale topographic map, the traces of all historical movements since 1940 coincide. Figure 153 illustrates a typical offset canal 0.8 km south of County Highway S–80 before and after the 1979 displacement (see pl. 1 for locations of roads); these photographs and other similar ones are the basis for the conclusion that the locations of the 1979 rupture and the earlier traces are the same.

Vertical aerial photographs taken shortly after the 1940 earthquake of the fault trace south of the present position of Interstate Highway 8 can be compared to aerial photographs of the 1979 rupture taken the day after the earthquake. Figure 154 shows that even such small-scale details as the positions of echelon steps in the trace and minor changes in trend were faithfully reproduced from one surface displacement to the next.

Several characteristics of the complexly branched north end of the Imperial fault where it bounds the Mesquite basin deserve comment: (1) there is abundant evidence that most of the 1979 rupture followed preexisting fault traces, even where there was no record of displacement in 1940; (2) the 1940 surface rupture probably extended to the northernmost extremity of the prehistoric Holocene fault traces; and (3) several of the 1940 fault traces near Keystone Road that were shown on earlier maps of the Imperial fault do not exist. Near the Mesquite basin, where the Imperial fault is marked by prominent east-facing scarps, surface rupture was not observed north of Keystone Road in 1940 (J. P. Buwalda, unpub. data, 1940). These scarps, however, which are especially clear on pre-1940 aerial photographs, coincide with the locations of 1979 surface breaks (compare figs. 155*A* and 155*B*).

Movement on the section of the fault between Keystone and Schartz Roads in 1940 is likely, although it was not observed. The fact that the 1979 maximum displacement and earthquake magnitude are smaller than those in 1940, even though the 1979 surface rupture extended to the extremity of the Holocene fault as it was known before the 1979 event (Sharp, 1977a), argues for a high probability that the 1940 surface trace broke similarly. The minimum estimate for the rupture length of the 1940 event consequently should be increased by about 3 km (from about 59 to 62 km) to allow for the omitted probable rupture at the north end.

The multiple branches near Keystone Road shown on earlier maps of the Imperial fault (Allen and others, 1972; Sharp, 1976) indicate some fault traces for which no evidence exists. All but the westernmost fault intersection at Keystone Road shown on the 1972 and 1976 maps should been placed along an unnamed and unpaved east-west road 0.8 km south of Keystone Road to

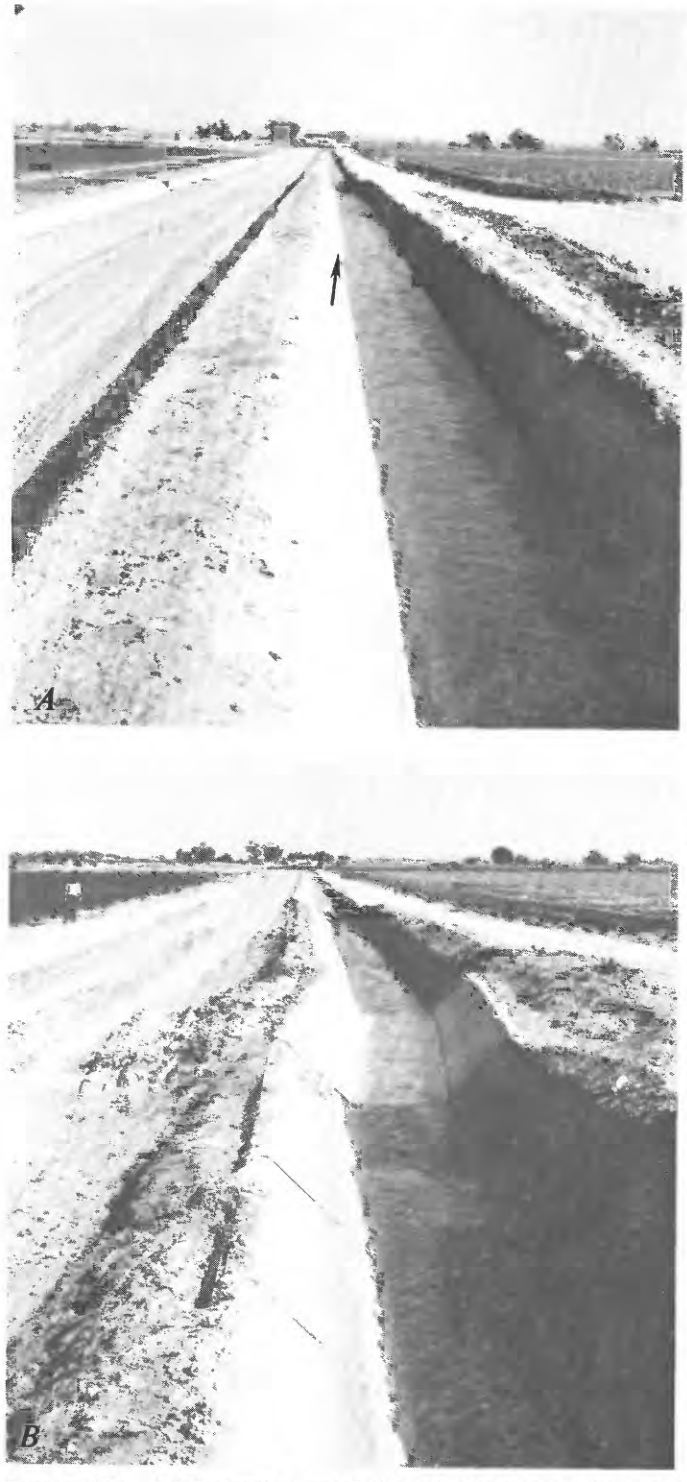

FIGURE 153.—Ash Lateral 15 canal liner. *A*, Alinement of canal in November 1975, showing cumulative offset (arrow) caused by creep events (10± 1 cm of dextral displacement resolved on fault trace). *B*, Alinement of canal on October 26, 1979, after replacement of damaged section of liner. Displacement is about 57 cm, of which probably less than 46 cm is due to coseismic slip and afterslip from October 15 earthquake. Canal is 2.02 m wide. Views eastward.

be consistent with the observations of J. P. Buwalda (unpub. data, 1940). Once relocated, the positions of the main 1940 ruptures in this locality generally agree with those of both the 1979 surface breaks and prehistoric fault traces. Because J. P. Buwalda's observations are the only source of documentation of the 1940 multiple surface breaks near Keystone Road, relocating the features he noted removed the disagreements between the 1940 and 1979 surface ruptures implied by the 1972 and 1976 maps. However, a break noted by him about 180 m east of the railroad 0.8 km south of Keystone Road remains the only documented 1940 break in this area that apparently was not activated during the 1979 event.

The relatively large scale discontinuities in the 1979 surface ruptures between Interstate Highway 8 and Chick Road ¾ km farther south are some of the most interesting and complex features of the Imperial fault. Comparison with the 1940 rupture is difficult because the surface breaks from both events were incompletely delineated on the ground and on aerial photographs. For each event, the traces of the most nearly linear main strands from the north and south define a stepover to the right of about 85 m. The 1979 continuity of a set of subparallel secondary breaks 80 to 180 m southwest of this gap (see pl. 1) could not be confirmed by field checking because of dense crop cover. Although the record of surface rupture in this area is even less complete for the 1940 event, and no data exist for the 1966, 1968, or 1977 movements, the displacements clearly approached zero in 1940 on each main break, and the right stepover between the main breaks apparently formed in much the same way then as in the 1979 event (see Sharp, 1977a). Several of the subsidiary fault traces of the 1979 event have no detectable counterparts on aerial photographs of the 1940 surface rupture. These breaks may represent new faulting near Interstate Highway 8 in 1979, but because ruptures with small displacements cannot easily be detected on aerial photographs, there is no proof that all the 1979 breaks were not actually reactivated older fault strands.

Many secondary and minor branching breaks in the north third of the 1979 surface rupture, where the Imperial fault has a distinct east-facing scarp, are not distinguishable on pre-1940 aerial photographs, even though the ground surface apparently has not been disturbed by farming. Because of sparse documentation of the 1940 rupture in this area, whether these 1979 minor fault strands broke on preexisting structures is indeterminate. Similarly, some of the photolineaments in this area mapped as fault traces by Sharp (1977a) that did not break in 1979 could represent either nonfault

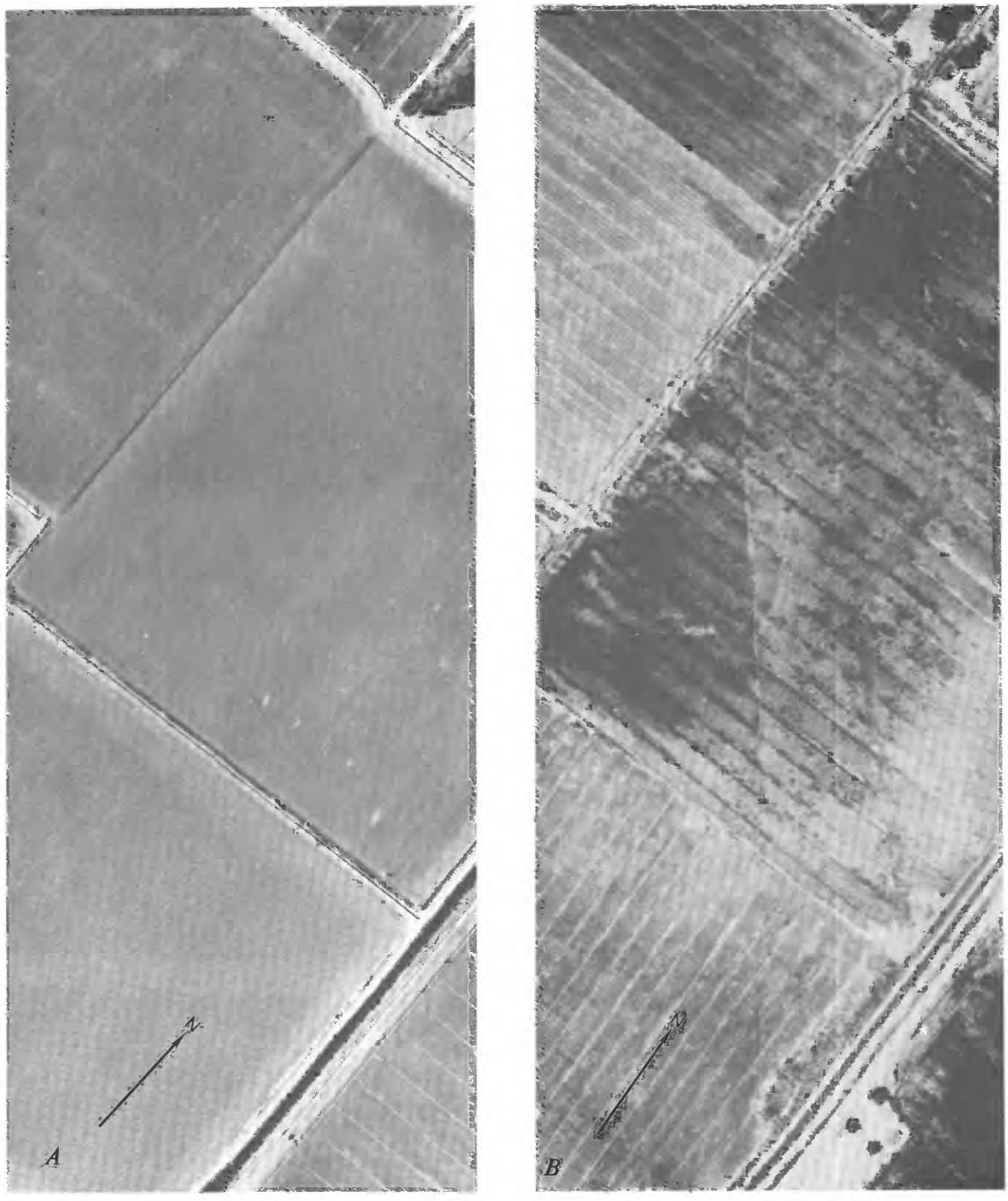

FIGURE 154.—Imperial fault trace west of Anderholt Road. *A*, 1940 fault trace in alfalfa fields as it appeared shortly after earthquake of May 18. Unpaved Anderholt Road cuts diagonally across upper right; dark band west of and parallel to road is Ash Lateral 15 canal. *B*, 1979 fault trace in same locality in newly planted lettuce field (center) and newly plowed but unplanted fields (left and right). Some edges of fields differ from their 1940 positions.

photolineaments or faults quiescent during the 1979 event.

DISTRIBUTION OF DISPLACEMENT

The 1940 and 1979 right-lateral displacements along the length of the Imperial fault can be confidently compared only with regard to major characterisitics. Although afterslip in 1940 was recognized in at least one locality (Richter, 1958), measurements of displacement generally were not repeated after that event (J. P. Buwalda, unpub. data, 1940). In spite of a great abundance of repeated measurements of displacements in the weeks after the 1979 earthquake (see fig. 100 and table 20; Sharp and others, this volume), comparison of these slip data with those recorded for the 1940 event is difficult because offsets of the earlier earthquake were made at different and partly unknown times. Figure 156 presents generalized profiles of displacement as a function of length along the fault for these two events; because of uncertainties, however, only the important differences are emphasized here. The 6-m 1940 maximum lateral displacement was centered south of 1979 surface rupturing, and the offset abruptly diminished northward to probably about 2.5 m at the southeast terminus of the 1979 rupture. Although the zone of largest 1979 right-lateral slip lay within about 6 km of the southeast end point of rupture, displacements in this zone were smaller than those of 1940. That segment of the fault between Barbara Worth Road and Ross Road, however, appears unique in that it apparently was displaced more in 1979 than in 1940, although the evidence is not conclusive. The small 1940 offsets near the location of Interstate Highway 8 correspond to the discontinuity and right stepover between the main strands of the Imperial fault discussed above. Because of possible undetected subsidiary 1940 breaks with small displacements, the 1940 displacement indicated in

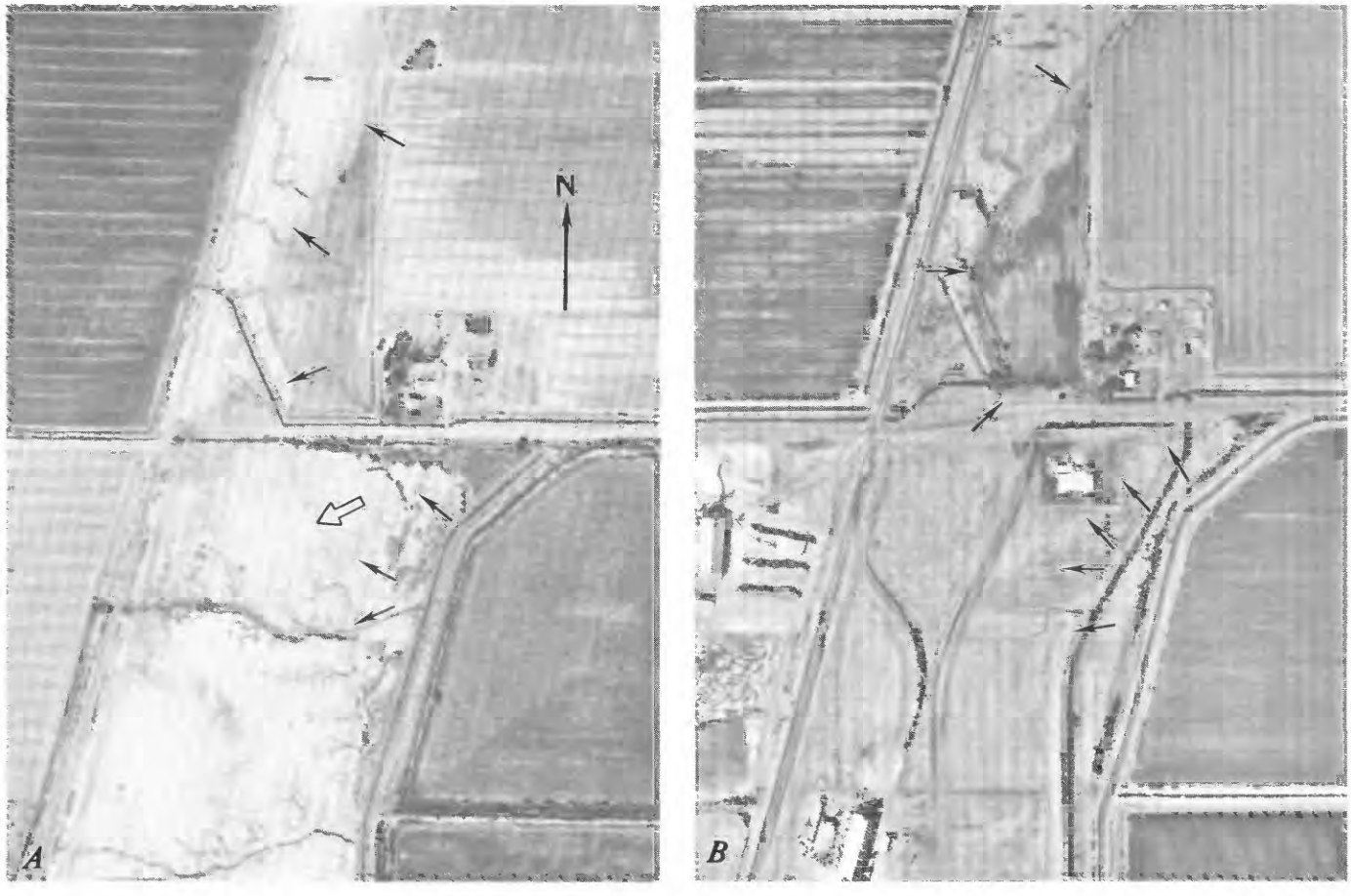

FIGURE 155.—Imperial fault near Carey Road, which cuts horizontally across centers. *A*, Prehistoric traces of Imperial fault as they appeared in 1937. Solid arrows denote traces in several localities; open arrows denote photolineament that may be a fault trace connecting faulting north and south of Carey Road. *B*, View of same locality on October 16, 1979. Solid arrows indicate 1979 surface rupture, which is nearly invisible in this photograph. Photolineament in figure 155*A* is no longer visible, but no new fractures formed along its position. This photolineament represents one possible fault that definitely was not activated in October 15, 1979, earthquake.

figure 4 for this segment of the fault should be taken as a minimum. Northwest of Ross Road, wherever direct comparisons can be made, the lateral displacements of 1979 appear to be mostly smaller than or approximately equal to the 1940 offsets. One peak in the 1979 profile (fig. 156) near McConnell Road projects slightly above linearly fitted lines between the sparse data points of 1940 in the north section; however, to infer that 1940 movements in this locality was actually the smaller of the two events would be unjustified. Considering the quality of the data, probably the best conclusion is that along the northwest two-thirds of the 1979 rupture length, the right-lateral component of slip was somewhat less than that of 1940, and that in both events that component generally diminished toward the northwest.

Richter (1958) noted afterslip following the 1940 earthquake near the United States-Mexican border, but he attempted no systematic documentation. As a conse-

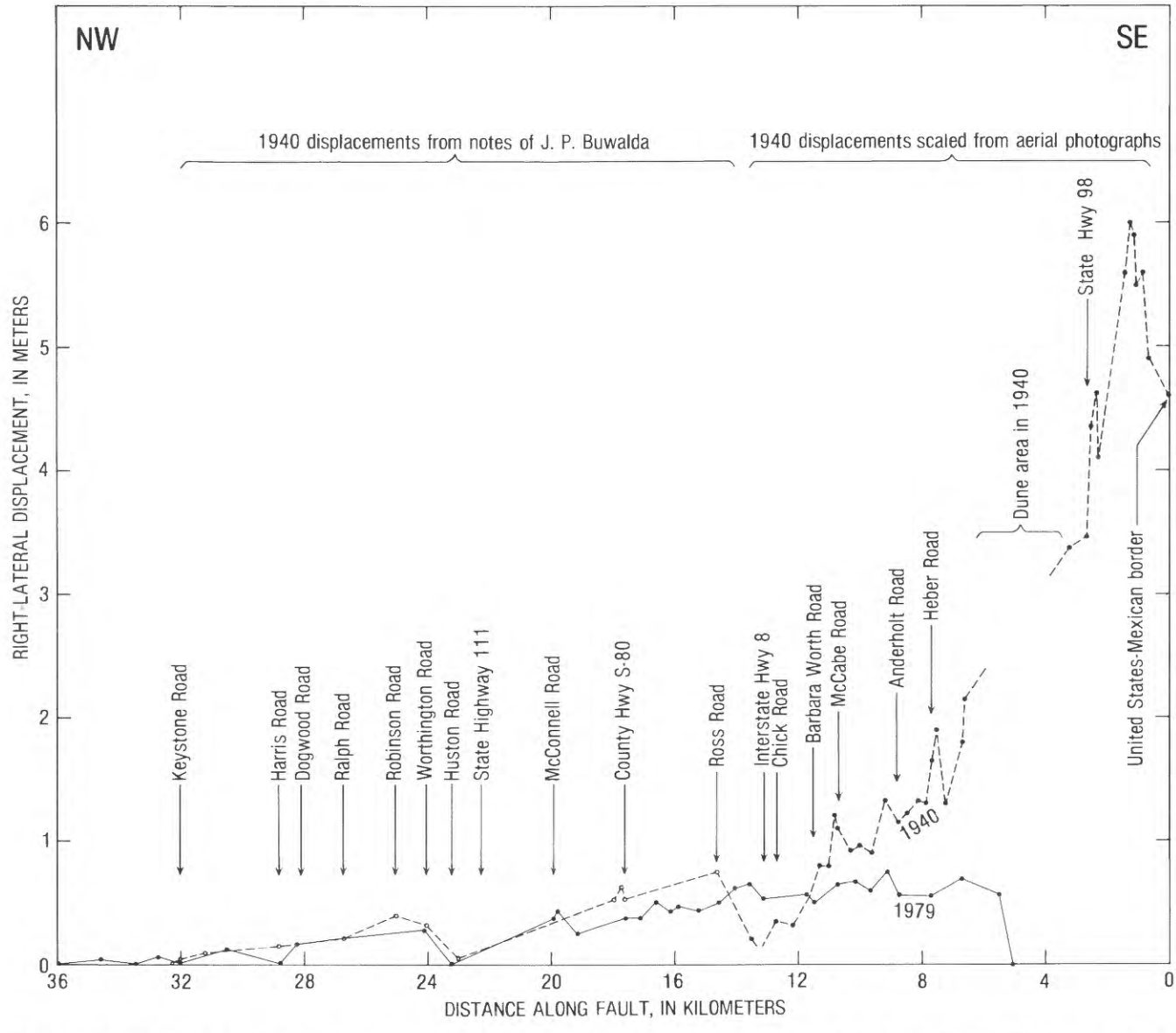

FIGURE 156.—Profiles of right-lateral component of displacement as a function of length along fault for 1940 and 1979 ruptures. Circles, displacements for 1940 event (J. P. Buwalda, unpub. data, 1940); dots, 1940 displacements scaled from vertical aerial photographs. Scaled displacement confirm 5.8-m maximum displacement for 1940 earthquake measured in the field by Richter (1958) and, indeed, indicate slightly larger movements in alfalfa fields not checked in 1940. Many data points in both 1940 and 1979 curves represent averages of many measurements of displacement within a very short distance. Field recording of 1940 movement was made within 15 days of event; 1979 displacement profile is for 20 days after earthquake.

quence, comparison of the history of afterslip from the two events is generally impossible. One exception, the displacement of pavement on County Highway S–80, was discussed as an example of possible afterslip from the 1940 shock by Brune and Allen (1967). During their investigation of small surface displacements on the Imperial fault after a swarm of small earthquakes in 1966, Brune and Allen observed that north-south offset of the Country Highway S–80 pavement was 79 cm (96 cm when recalculated to displacement on the fault), compared with an offset of 46 cm (56 cm of displacement of the fault) measured by J. P. Buwalda (unpub. data, 1940) 6 days after the 1940 earthquake. Brune and Allen proposed that much or even all of the 40 cm of displacement between those dates may have been afterslip from the 1940 event. Afterslip from the 1979 shock (see Cohn and others, this volume; Crook and others, this volume; Harsh, this volume) suggests that this 40 cm of movement falls within the range of expected postearthquake movements that would have accumulated over several years.

RATIO OF DISPLACEMENT COMPONENTS

The ratio of horizontal to vertical components of slip at points on the fault trace is of considerable interest, because this parameter generally has been assumed to be constant over many slip events in several attempts to decipher the past histories of active faults in California from vertical stratigraphic offsets recorded in trenches (for example, Clark and others, 1972). In general, where vertical components of slip on the 1979 Imperial fault rupture were substantial, their sense was the same as that observed in 1940. Many small vertical components were measured in the south half of the 1979 trace, where no record may have been made in 1940 because they were nearly insignificant in comparison with the horizontal components. At Huston and Harris Roads, however, the 1940 records gave ratios of right-slip to vertical component of about 1 to 15–25 and 15 to 25, respectively (J. P. Buwalda, unpub. data, 1940); the 1979 component ratios at the same points on the fault trace are about 0 to 25 and 0–2 to 24, respectively. For these two events, then, the ratios of displacement components were nearly identical at Huston Road and corresponded to a rake angle of about 86° to 90° in the fault surface, but substantially different at Harris Road 5.8 km farther north, where the rake angle changed from 59° or more in 1940 to about 90° in 1979. These comparisons indicate that variation in the ratio of components for the two surface-slip events might be as large at any point on the fault as variations in these ratios at two widely separated points in the same event. Variation in the ratio of slip components for recurrent displacements should be allowed for in future studies of the movement histories of faults and of the paleoseismicity deduced from these histories.

BRAWLEY FAULT ZONE

At least one of the traces of the Brawley fault zone was first identified as a 3-km-long surface rupture of the 1940 earthquake near Harris and Ralph Roads by A. E. Sedgwick (unpub. data, 1940). Although the end points of the rupture were not recorded, the trace was described as trending north-south and bounding the relatively downdropped basin of Mesquite Lake. Surface displacement observed at Keystone Road in 1940 by a local resident (later a superintendent of the County road department) suggests that rupturing along the Brawley fault zone broke the surface for at least 5 km from north to south and that more than one strand in the zone of faulting moved. More extensive faulting may have occurred in 1940 in the Brawley fault zone than was recorded at that time or documented later for 1975 and 1979 movements.

RUPTURE TRACES

Surface rupturing during the Imperial Valley earthquake swarm of January–February 1975 occurred along a 10.4-km-long segment of the Brawley fault zone. The location, distribution, and amount of slip on the surface ruptures from that event are the only measurements that can be compared with those of displacements from the 1979 event.

As along the Imperial fault, the locations of strands of the Brawley fault zone at roads are indistinguishable from those of 1975 (compare Sharp, 1977b, with Sharp and others, this volume, pl. 1). The characteristics of 1979 surface faulting, including the discontinuity of the rupturing, the echelon cracking along some breaks, the single or nearly single cracks on other breaks, and the consistent sense of vertical displacement (downward on the west side) for all ruptures, are also virtually indistinguishable from those of 1975 movements (Sharp, 1976).

The most significant differences between surface faulting from the 1979 and 1975 events are: (1) the number of fault strands involved and their distribution, (2) the total length of rupture, and (3) the appearance of measureable right-lateral components of slip in some localities in 1979. Although changes in elevation along pavements (see Sharp and Lienkaemper, this volume) and canal misalinements generally are the only accurate measures of the vertical and horizontal components of slip, corresponding changes of elevations are unavailable for the 1975 displacements. Leveling surveys along roads crossing the 1975 fault breaks recorded only total deformation since construction of the pavements,

but the 1979 displacements were calculated from leveling surveys in January of that year. Sighting of canal liners showed no evidence of measurable right-lateral shift in 1975 (Sharp, 1976).

The length of 1979 surface breakage along the Brawley fault zone is about 13.1 km, greater by 2.7 km than the rupture of 1975. The difference is due to bilateral extensions of the 1975 traces, probably on the same fault strands, by about 0.9 km northward and 1.8 km southward. The northernmost 1979 breaks extended incipient echelon cracks of 1975 that showed only slight extensional opening in the pavement of McConnell Road (pl. 1). Southward prolongation of surface rupturing was proved by the discovery of discontinuous breaks that start in fields about 100 m south of Worthington Road, the southernmost limit of known faulting in 1975. Lineaments on aerial photographs suggest that this prolongation occurred on the same fault strand that crosses Worthington Road (Sharp, 1977b).

The width of the Brawley fault zone is significantly greater for the 1979 event because of slip along the eastern break, generally less than 1 km east of the known 1975 ruptures (pl. 1). Although faulting along at least part of this eastern break may have occurred in 1975 because its trace was then unknown and consequently unchecked, the pavement of Harris Road was not obviously broken along this strand in 1975. This eastern fault strand may not have slipped in 1975, although lineaments on aerial photographs taken the day after the 1979 earthquake clearly reveal a preexisting structure that has influenced the density of vegetation along its length. Earlier aerial photography does not show this lineament, but the visibility of such features is highly sensitive to the kind of crop and its stage of growth at the time of photography. Although the eastern rupture of the Brawley fault zone may have been quiescent during the 1975 earthquake swarm, it was unquestionably a reactivated part of a preexisting fault during the 1979 event.

A fault rupture for which only scant earlier evidence exists is the break about 24.5 m east of the main western break on Harris Road. Profiles of elevation changes of leveling marks in the pavement show a subtle step in the road surface in that locality between October 1977 and January 1979 (Sharp and Lienkaemper, this volume), although cracking was never detected there before the 1979 earthquake. The leveling data (Sharp and Lienkaemper, this volume, fig. 134*C*) indicate that the present small scarp is almost entirely due to the 1979 event and that earlier movement has only slightly affected the road surface, at least since its paving in August 1970.

DISPLACEMENT COMPONENTS AND THEIR RATIOS

The left-stepping echelon geometry of much of the surface cracking along the Brawley fault zone in 1975 implies that the faulting included an incipient dextral component of slip, although several canal liners crossing the trace were visually straight (Sharp, 1976). A significant difference in the 1979 rupture is that horizontal slip obviously displaced some of the canal liners. Figure 157 shows the canal liner on the north side of Keystone Road after the 1979 earthquake; the right-lateral component of slip on this canal is about 7 cm. In January 1979 this canal was still visually straight (the threshold for detection of offset is probably about 1 cm). The ratio of horizontal to vertical components at Keystone Road for the 1979 slip (about 7 to 9–10) corresponds to a rake angle of slip of 51° or more in the fault surface, although the dip of the fault is unknown. The rake angle of slip at Harris Road about 3.6 km farther south in the Brawley fault zone is 35° or more. Slip rake at the southernmost extremity of rupture in the Brawley fault zone 9.5 km south of Keystone Road is

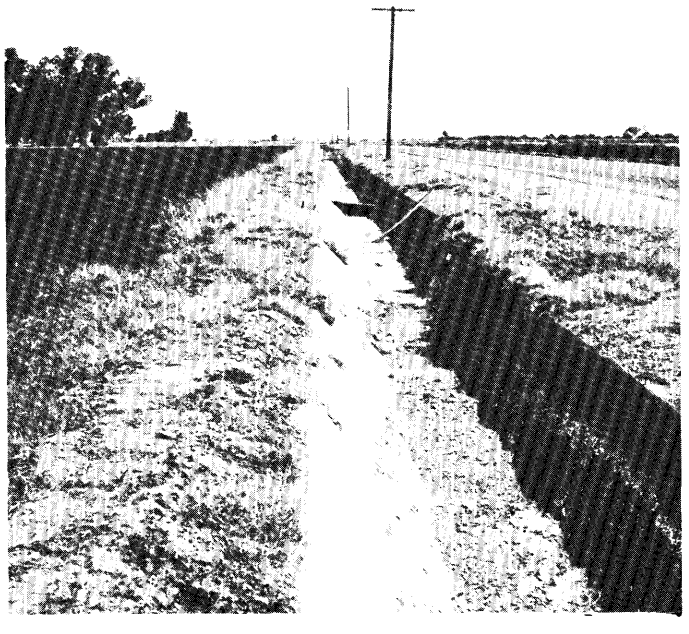

FIGURE 157.—Concrete canal liner on north side of Keystone Road on trace of one strand within Brawley fault zone. About 7 cm of right-lateral misalinement of left side of canal was measured on October 21, 1979. This canal liner had been checked on nearly an annual basis since February 1975 for evidence of horizontal offset; when last checked on January 17, 1979, liner showed no obvious right-lateral displacement. View eastward.

about 36° on a fault surface dipping 87° toward N. 62° W. For the 1975 event, the rake angle of slip at Keystone and Harris Roads was about 90°, that is, purely dip-slip motion, at least at the ground surface.

SUMMARY

Comparison of the 1979 surface faulting with earlier historical and prehistoric fault displacements indicates that preexisting fault strands were reactivated during the October 15 earthquake. Displacements generally, but not everywhere, were smaller for the 1979 earthquake than for the 1940 event. New ruptures along previously unfaulted traces may have occurred west of the north section of the Imperial fault near the Mesquite basin, although similar small breaks at those places could easily have been overlooked during the 1940 earthquake investigation and not detected on aerial photographs. Only one known fault trace of the 1940 earthquake near Keystone Road and one possible prehistoric trace near Carey Road were not reactivated by 1979 surface displacement. The north limit of prehistoric faulting and the 1940 and 1979 surface ruptures probably all lie at about the same point along the Imperial fault; the 1979 break extended southward only about half the total length of the 1940 surface rupture on the Imperial fault.

New surface breaking along preexisting but previously unrecognized fault strands occurred in the Brawley fault zone. Surface rupturing in this fault zone, moreover, extended about 1 km along a trace only partly known from a movement in 1975. To the south, however, the Brawley fault zone extended its rupturing along a prehistoric trace previously identified on aerial photographs.

In some localities on the Imperial fault and in the Brawley fault zone, the ratio of vertical to horizontal components of slip for the 1979 displacement differs substantially from those for other displacements from 1940 to the present. This documentation of changes is the first of its kind known for repeated historical surface-faulting events. Allowance for large changes in slip direction on the surface of a fault during separate movement events is especially important in any interpretation of faulting history based on stratigraphic separations.

REFERENCES CITED

Allen, C. R., Wyss, Max, Brune, J. N., Grantz, Arthur, and Wallace, R. E., 1972, Displacements on the Imperial, Superstition Hills, and San Andreas faults triggered by the Borrego Mountain earthquake, *in* The Borrego Mountain earthquake of April 9, 1968: U.S. Geological Survey Professional Paper 787, p. 87–104.

Bonilla, M. G., 1979, Historic surface faulting—map patterns, relation to subsurface faulting, and relation to preexisting faults, *in* Proceedings of Conference VIII, Analysis of actual fault zones in bedrock: U.S. Geological Survey Open-File Report 79–1239, p. 36–65.

Brune, J. N., and Allen, C. R., 1967, A low-stress-drop, low-magnitude earthquake with surface faulting: The Imperial, California, earthquake of March 4, 1966: Seismological Society of America Bulletin, v. 57, no. 3, p. 501–514.

Clark, M. M., Grantz, Arthur, and Rubin, Meyer, 1972, Holocene activity of the Coyote Creek fault as recorded in sediments of Lake Cahuilla, *in* The Borrego Mountain earthquake of April 9, 1968: U.S. Geological Survey Professional Paper 787, p. 112–130.

Goulty, N. R., Burford, R. O., Allen, C. R., Gilman, Ralph, Johnson, C. E., and Keller, R. P., 1978, Large creep events on the Imperial fault, California: Seismological Society of America Bulletin, v. 68, no. 2, p. 517–521.

Richter, C. F., 1958, Elementary seismology: San Francisco, W. H. Freeman, 768 p.

Sharp, R. V., 1976, Surface faulting in Imperial Valley during the earthquake swarm of January–February, 1975: Seismological Society of America Bulletin, v. 66, no. 4, p. 1145–1154.

——— 1977a, Holocene traces of the Imperial fault in south-central Imperial County, California: U.S. Geological Survey Open-File Report 77-815, 1 p., scale 1:24,000, 5 sheets.

——— 1977b, Map showing Holocene surface expression of the Brawley fault, Imperial County, California: U.S. Geological Survey Miscellaneous Field Studies Map MF–838, scale 1:24,000.

——— 1980, 1940 and prehistoric earthquake displacements on the Imperial fault, Imperial and Mexicali Valleys, California and Mexico, *in* Proceedings of California-Mexico Symposium; human settlements in the San Andreas fault zone: Sacramento, California Seismic Safety Commission, p. 68–81.

Ulrich, F. P., 1941, The Imperial Valley earthquake of 1940: Seismological Society of America Bulletin, v. 31, no. 1, p. 13–31.

LIQUEFACTION AND SECONDARY GROUND FAILURE

By T. Leslie Youd and Gerald F. Wieczorek,
U.S. Geological Survey

CONTENTS

ABSTRACT

Secondary ground effects of the 1979 Imperial Valley earthquake occurred on flatlands (primarily liquefaction and compaction of soil), canal, river, and highway embankments (primarily slumps and lateral spreads), and steep river bluffs and hillsides (primarily earth and rock falls and slides). Effects of the 1979 event were generally less severe than those of the 1940 Imperial Valley earthquake. We present preliminary geotechnical sections for two liquefaction sites where we conducted subsurface investigations. Local geology and proximity to the Imperial fault were the most important factors controlling liquefaction and ground failure during the 1979 event.

INTRODUCTION

The 1979 Imperial Valley earthquake produced strong ground motions, with measured vertical and horizontal accelerations as great as 1.74 and 0.81 g, respectively. Durations of shaking (accelerations above 0.1 g) ranged from 5 to 13 s at several recording stations and averaged about 7 s (Porcella and Matthiessen, 1979). The earthquake caused about $30 million damage, ruptured a 35-km-long segment of the Imperial fault, and generated numerous ground failures in the Imperial Valley and a few in the surrounding hills.

In this chapter, we describe liquefaction, ground failure, and other secondary ground effects generated by the earthquake and its aftershocks at 38 sites in the Imperial Valley. In a concluding discussion we examine the factors controlling liquefaction, ground failure, and other secondary effects. Specific sites are located on the accompanying maps (pl. 4) by number and a symbol indicating the type of ground effect. The sites are listed in the text under three categories based on the general setting: (1) flatlands (sites 1–25), (2) canal, river, and roadway embankments (sites 26–36), and (3) steep river bluffs and hillsides (sites 37, 38).

The surface rupture of the 1979 earthquake is congruent with the northern part of the surface rupture of the 1940 Imperial Valley earthquake (Sharp and others, this volume). Because of this congruence, we compare here the secondary ground effects from these two events.

We define "ground failure" as a permanent ground displacement (horizontal or vertical) capable of damaging constructed works. A differential ground displacement of about 0.1 m is generally required to cause damage to all but the most sensitive works (Youd and Perkins, 1978, p. 436; Youd, 1980). Among the types of ground failures generated by the October 15 earthquake were earth slumps, lateral spreads, ground settlements, earth falls, rock falls, and rock slides. With the exception of ground settlement, these failure types have been defined and described by Varnes (1978). ("Ground settlement" is a vertical displacement of the ground caused by compaction of a sursurface soil layer.) Such secondary ground effects as ground cracks and sand boils, common at many ground-failure sites, were also observed at several sites where no ground failure was evident.

FAILURES ON FLATLANDS

Ground failures on flatlands included lateral spreading and ground settlement, caused by liquefaction or compaction of subsurface sandy sedimentary deposits. Evidence that liquefaction occurred during the earthquake includes the numerous sand boils that erupted (indicative of high pore-water pressures at depth) and the general presence of sandy sediment in the areas where these failures occurred. Damage caused by the failures included disrupted canals and roadways, broken irrigation and drain pipelines, and differential settlements within fields that commonly disrupted irrigation systems.

Sand boils and ground cracks, which were commonly associated with many failure sites on flatlands, also were observed at several sites where no ground failure was evident. Sand boils erupted in straight or curved lines, with or without connecting ground cracks, and in groups with no definite distribution pattern. Spacings between sand boils ranged from coalescing cones to cones several tens of meters apart; cone diameters ranged from a few tenths of a meter to about 10 m. Some sand boils had conical throats; others had almost flat tops. At no site did the eruption of sand and water erode cavities beneath the ground surface, a phenomenon that has been noted in some past earthquakes. The conical shape of most sand boils indicates that they formed subaerially. The oblate shape of a few sand boils in fields and on canal bottoms indicates that they formed subaqueously. At these latter sites the fields and canal bottoms were wet at the time of our visit and were probably flooded at the time of the earthquake.

Liquefaction occurred primarily in two geologic settings: (1) channel, flood-plain, and artificial-fill deposits along the New and Alamo Rivers; and (2) cultivated areas containing sandy subsoil. In the cultivated areas, liquefaction effects were concentrated in an area west of the Alamo River between Holtville, Calif., and the United States-Mexican border, where contours of the land surface and soil surveys show a lobe of higher ground composed of sand dunes and sandy soil (fig. 158). The lobe of higher ground is apparently a delta that extended into ancient Lake Cahuilla. Stratigraphic evidence indicates that Lake Cahuilla last covered this area about 400–300 yr B.P. (Sharp, 1981). North and west of the delta, the soil is derived from clay-rich lakebeds. Other than near active streams, liquefaction did not occur in those lakebed areas.

Aerial photographs of the lobe of higher ground, taken in 1937, show remnant stream channels, levees, and vegetative photolineaments outlining an ancient stream course that extends down the axis of the delta (fig. 159). Since 1937, these remnant features have been nearly obliterated by land leveling and cultivation. Within the delta, several discrete subdeltas are discernible, composed of very sandy sediment that has been reworked, first by the wind to form dunes and subsequently by agriculture. Soil maps of the area (Strahorn and others, 1924) show the extent of the sandy subsoil (pl. 4; fig. 158).

Sand boils were concentrated on the delta and particularly in the filled channel. Ground cracks marked the edge of the channel along several segments. Ground cracks were common in many areas of ground failure and in areas containing sand boils; in fact, small ground cracks provided vents through which many of the sand boils erupted. We saw very few ground cracks on flatlands that were not associated with ground failures or sand boils.

The following descriptions of ground-failure sites (pl. 4) are arranged from south to north; in a final section we discuss the absence of effects near Gadsden, Ariz., an area severely affected by liquefaction during the 1940 Imperial Valley earthquake. In addition to our observations, R. F. Scott and S. G. Muir (written commun., 1979) and T. H. Heaton and others (written commun., 1980) observed sand boils in a few other localities in the Imperial Valley (large dots, pl. 4). The studies by R. F. Scott and S. G. Muir included trenching of a sand boil (see Muir and Scott, this volume).

Site 1.—The southernmost reported cracks and sand boils were in a 500-m-long by 10-m-wide zone that disrupted the pavement on Highway 2 between Sesbania and Casey in northern Mexico. This site is about 14 km south of the United States-Mexican border and 4 km southwest of the Imperial fault. The cracks and sand boils were about 16 km beyond the southeast terminus of surface rupture.

Site 2.—Several ground cracks, a few sand boils, and a ruptured canal lining were reported near Islas

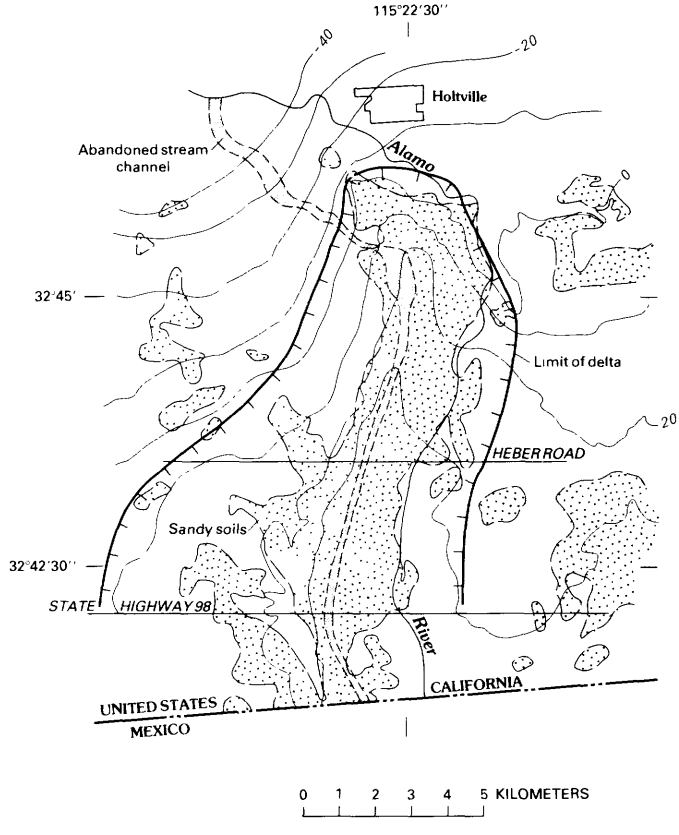

FIGURE 158.—Old delta near Holtville, Calif. Buried stream channel cuts through axis of delta. Sand boils erupted on or very near sandy subsoil, as identified by Strahorn and others (1924). Contour interval, 10 ft.

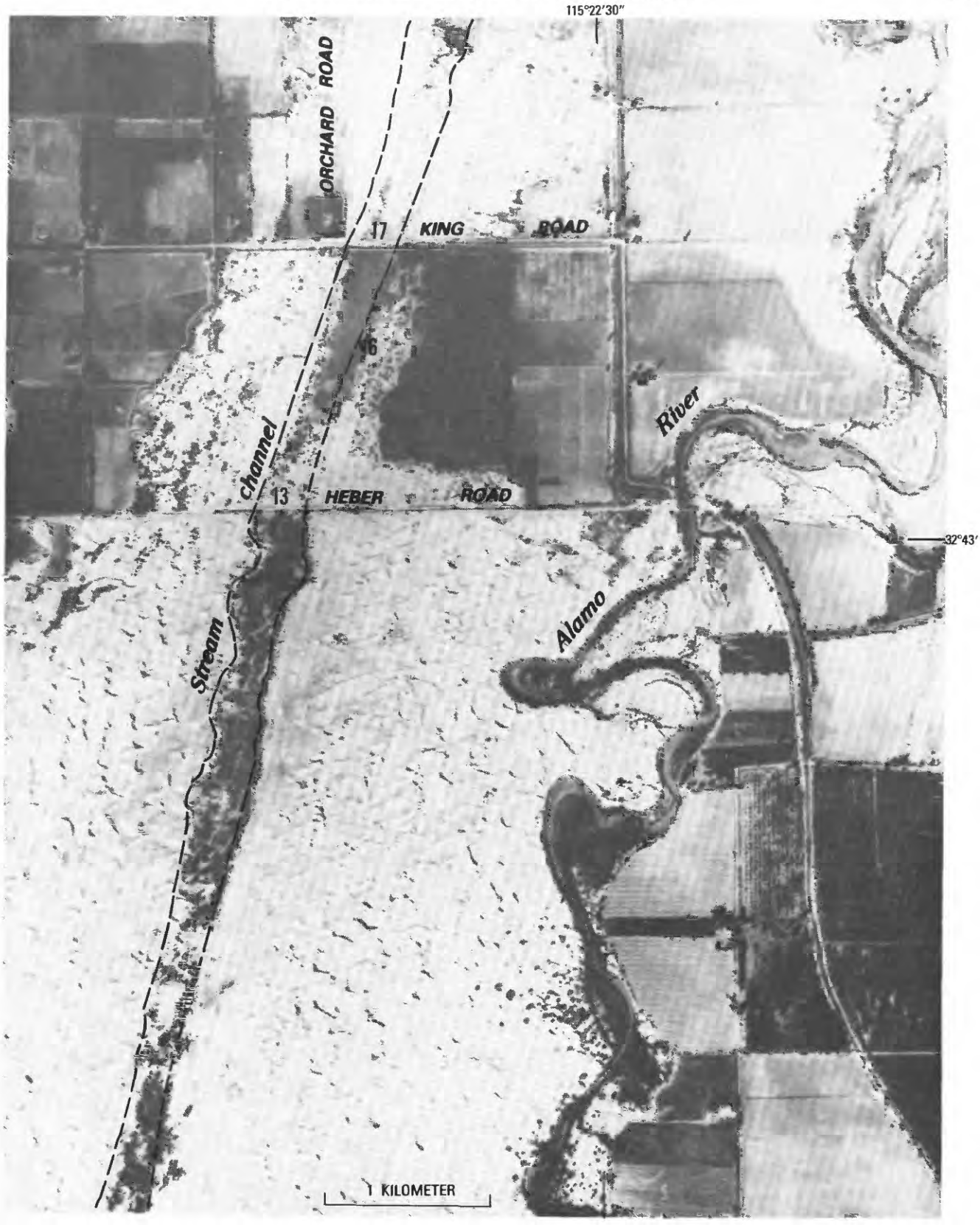

FIGURE 159.—Ancient stream channel south of Holtville, Calif. Numbers refer to sites described in text and shown on plate 4. Aerial photograph from U.S. Agricultural Stabilization and Conservation Service, 1937.

Agrarias, Mexico, 11 km south of the border and 0.2 km northeast of the Imperial fault.

Site 3.—At a site 2.5 km south of the border and 1.1 km southwest of the Imperial fault, a 50-m-wide zone, consisting of several sets of fractures and sand boils, extended 140 m in a generally north-south direction through the interchange of Highway BCN–1 and the road to the Mexicali Airport.

The displacements of several sets of cracks showed both right- and left-lateral movements of as much as 5 cm and vertical movements of from 0 to 3 cm, but no consistent upthrown side. The direction of cracks in this zone ranged from N. 10° W. to N. 25° E.; differences may relate to subsurface sedimentary units. Approximately a half-dozen sand boils, ranging from 0.3 to 1 m in diameter, were observed adjacent to or in line with the fractures (M. G. Bonilla, written commun., 1981).

The zone is near a channel of the Alamo River, and so the observed effects may be attributable to liquefaction of cohesionless sediment associated with the channel and to differential settlements of the channel boundaries. Similar effects were observed and investigated in greater detail at sites 6, 13, and 16, as described below.

Site 4.—At a site 1.5 km south of the border and 0.5 km southwest of the Imperial fault, the head of a small lateral spread intersected a concrete-lined canal, ruptured the canal lining, and displaced the floor of the canal about 20 cm laterally to form a gentle curve (fig. 160). Movement on the lateral spread was toward a nearby 1.5-m-deep depression within which several sand boils erupted.

Site 5.—About 30 sand boils erupted at random in the southwest corner of a field north of the All-American Canal and east of the South Alamo Canal.

Site 6.—A 2-km-long zone of discontinuous surface rupture extended from about 0.5 km north of State Highway 98 to Carr Road 0.8 km north of the border. On State Highway 98, an east-facing scarp about 10 cm high fractured the pavement and continued into a field to the south, where crop rows were shifted as much as 11 cm left laterally. The break died out about 275 m south of the highway; however, a second break on line with the first formed a similar scarp, characterized by small right-lateral displacements, between 425 and 700 m south of State Highway 98. Additional fractures with right-lateral displacements extended northwestward from Carr Road for about 550 m. All these scarps were congruent with the west margin of an old stream channel that previously crossed this area (pl. 4; fig. 158). Several sand boils erupted near the scarp on the north side of State Highway 98. In a field south of the highway, dozens of sand boils erupted on the east side of the scarp (in the old channel), but none erupted to the west. These scarps and sand boils were evidently formed by liquefaction and compaction of the underlying sedimentary deposits, primarily those filling the old channel. Such differential settlement and horizontal displacement are common consequences of liquefaction and compaction.

FIGURE 160.—Canal ruptured and offset by lateral spread at site 4. Maximum horizontal displacement is about 20 cm.

Site 7.—About 20 sand boils erupted at random in a field northwest of the intersection of State Highway 98 and the South Alamo Canal. No major ground cracks or other evidence of ground failure were observed.

Site 8.—About 30 sand boils erupted at random in a field east of the South Alamo Canal and about 1 km north of State Highway 98. There were no indications of ground failure.

Site 9.—About 20 widely spaced sand boils erupted in a 0.4-km-long northeast-trending line with a south terminus about 1 km north of State Highway 98 and 0.3 km east of the South Alamo Canal; this line was not associated with any major or continuous ground cracks. Linearity of the sand boils suggests the presence of a buried stream channel or other feature containing loose sand beneath that area.

Site 10.—About 60 sand boils erupted in an ellipsoidal area within an alfalfa field south of the fault trace, about 1.4 km north of State Highway 98 and 0.7 km east of the South Alamo Canal. The oblate shape of many of these sand boils indicates that they formed subaqueously. The field was wet at the time of our visit (4 days after the earthquake) and may have been flooded when the sand boils erupted. Several small ground cracks were associated with these sand boils.

Site 11.—About 20 sand boils erupted in an 0.6-km-long northeast trending line about 1 km north of State Highway 98 and about 0.2 km east of Bonds Corner Road (fig. 161). Small cracks appeared near the sand boils, but no continuous cracks formed.

Site 12.—A single sand boil erupted about 100 m

from the fault trace at a point about 30 m north of Heber Road and 0.4 km west of the Ash Main Canal. This sand boil was not associated with any other noticeable ground effects.

Site 13.—A lateral spread severely disrupted the pavement on Heber Road 1 km east of Mets Road (figs. 162, 163). The spread shifted the road and a parallel unlined canal about 1.2 m southward toward a 2-m-deep depression in Heber Dunes County Park south of the canal. This depression is the remnant of an old stream channel that passed through the area (pl. 4; figs. 158, 159). The spread was 160 m wide at the road and about 100 m long from the edge of the depression to the northernmost crack in the field north of Heber Road. Arcuate ground cracks and scarps formed around the margins and across the interior of the spread. Along the south edge of the road, scarps as high as 0.9 m formed between blocks of sediment carved out by the spreading movement. Sand boils erupted in several places on the spread, primarily along ground cracks north of the road; a few small sand boils erupted in the field east of the spread along a line parallel to Heber Road. The linearity of this group suggest they formed over a buried drain line.

FIGURE 161.—Line of sand boils at site 11 in field about 1 km north of Bonds Corner. Spacing between sand boils is as much as tens of meters. Some small fissures are associated with individual sand boils, but no fissures are throughgoing. View northeastward.

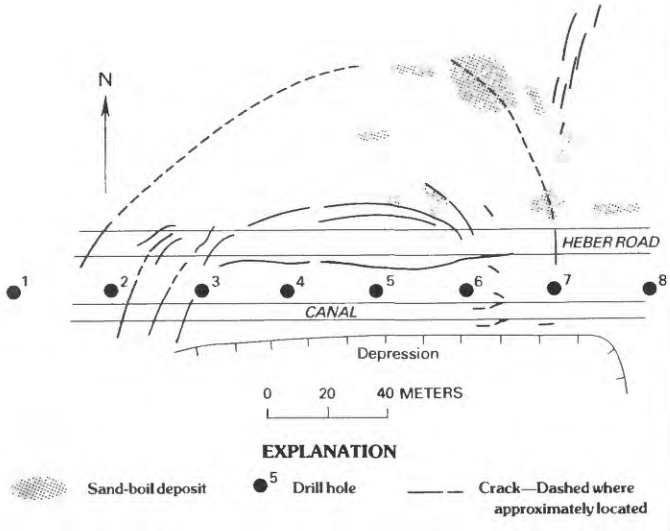

FIGURE 162.—Plan view of lateral spread at site 13 on Heber Road, showing displacements, ground cracks, sand boils, and drilling locations (see fig. 164).

In December 1979 we conducted subsurface investigations along Heber Road to define better the sedimentary profile and soil properties, and to determine which deposits liquefied during the earthquake (Bennett and others, 1981). Our exploration consisted of static-cone-penetration soundings near each drill hole (1–8, fig. 163), followed by continuous sampling of sediment and standard penetration tests in selected drill holes (1, 4, 6, 7). Figure 164 shows a geotechnical section across the line of drill holes. The top 5 m of the section is composed of three distinct units of silty sand: in the western part (drill hole 1), a dense laminar-bedded point-bar deposit; in the central part (drill holes 2–6), very loose natural channel fill in the old stream channel, capped by 1 to 2 m of artificial fill; and in the eastern part (drill holes 7, 8), a loose fluvial-overbank deposit. Our analyses of the liquefaction susceptibility of these three silty-sand units, presented in the section below entitled "Discussion," confirm that the very loose channel fill is highly susceptible to liquefaction. The analyses also indicate that the loose fluvial deposit should have liquefied and that the point-bar sand should have resisted liquefaction. Although a few sand boils erupted in a linear array on the fluvial deposit, possibly over a buried drain, there was no other observable evidence of liquefaction in that unit. There was no evidence of liquefaction in the point-bar sand. Below 5-m depth the section consists of alternating layers of silty clay and sand, probably lakebeds and channel or beach deposits. The sand layers are dense and evidently did not liquefy during the earthquake.

Site 14.—About 20 sand boils erupted at random in fields on both sides of Heber Road west of Keffer Road. The banks of the South Alamo Canal, which runs south of Heber Road, were fissured near these sets of sand boils (site 28).

Site 15.—About 10 sand boils and several ground cracks formed on and adjacent to Heber Road, 0.6 km east of the bridge over the Alamo River. The cracks were

arcuate and apparently formed the head of an incipient lateral spread that shifted slightly northward toward the river. The roadway is on fill over a river meander at this site. Liquefaction of fill, channel, or flood-plain deposits caused these cracks and sand boils to form. Raised welts on the road pavement could reflect additional sand boils erupting beneath the impermeable pavement.

Site 16.—A linear zone of right-stepping ground fissures extended from Heber Road northeastward for 2.4 km. These fissures were characterized by as much as 15 cm of vertical separation, west side down, and locally by small amounts of left-lateral displacement (except at Heber Road, where lateral spreading caused displacements of more than 1 m) (upper left, fig. 163*C*). The breaks were locally discontinuous, and some breaks in thick crop cover were visible only from the air at times of low sun angle. The mapped fractures clearly coincide with the east margin of an ancient stream channel visible in 1937 aerial photographs (pl. 4; figs. 158, 159). Low vertical scarps formed along some fractures where underlying natural and artificial fill in the channel compacted. In the southern part of the fissure zone, the left-lateral slip reflected lateral spreading. Farther north, horizontal displacements were probably caused by local shifting of the soil mass, a phenomenon commonly associated with liquefaction. At Heber Road the scarp was congruent with the east margin of the lateral spread (site 13), and at King Road the scarp merged into the east margin of a zone of ground cracks and sand boils (site 17). Sand boils formed along the scarp in places about 100 m north of Heber Road and about 60 m south of King Road.

Site 17.—Numerous cracks, scarps, and sand boils disturbed the ground surface in a zone several hundred meters long and about 100 m wide centered on King Road, immediately east of its intersection with Orchard Road (fig. 165). The pavement on King Road was fissured within several places in the zone, and the concrete linings of two irrigation canals paralleling the road were fractured, pulled apart, buckled, or overlapped in various places (fig. 166). At the east margin of the zone, the lining of the canal on the north side of the road was fractured and overlapped by 13 cm (fig. 166*D*); in other places, the linings were pulled apart. Thus, it appears that both extensional and compressional ground displacements occurred beneath the canal. A local farmer reported that ground cracks and sand boils also formed in this area during the 1940 Imperial Valley earthquake.

The east and west boundaries of the ground-failure zone are congruent with the banks of an old stream channel that passed through this area. Liquefaction of loose sandy sediment in the channel evidently caused the ground disturbances at this site. These disturbances indicate that a liquefied layer decoupled overlying nonliquefied sedimentary layers from underlying stable ground. Ground cracks then separated the upper sediment into discrete blocks that shifted and jostled against each other in response to shaking. Impacts between blocks, or between blocks and adjacent stable ground, produced such compressional effects as buckled and overlapped canal linings; separation of blocks and differential settlement between them left the open cracks and pulled apart linings and the scarps. Similar ground failures occurred during the November 23, 1977, Caucete, Argentina, earthquake (T. L. Youd and D. K. Keefer, unpub. data, 1982).

Site 18.—A linear trough feature about 5 m wide and 0.13 m deep extended westward from Orchard Road for several hundred meters along a farm lane about 0.8 km north of King Road. Trough boundaries were marked by ground cracks and scarps (fig. 167), and small sand boils

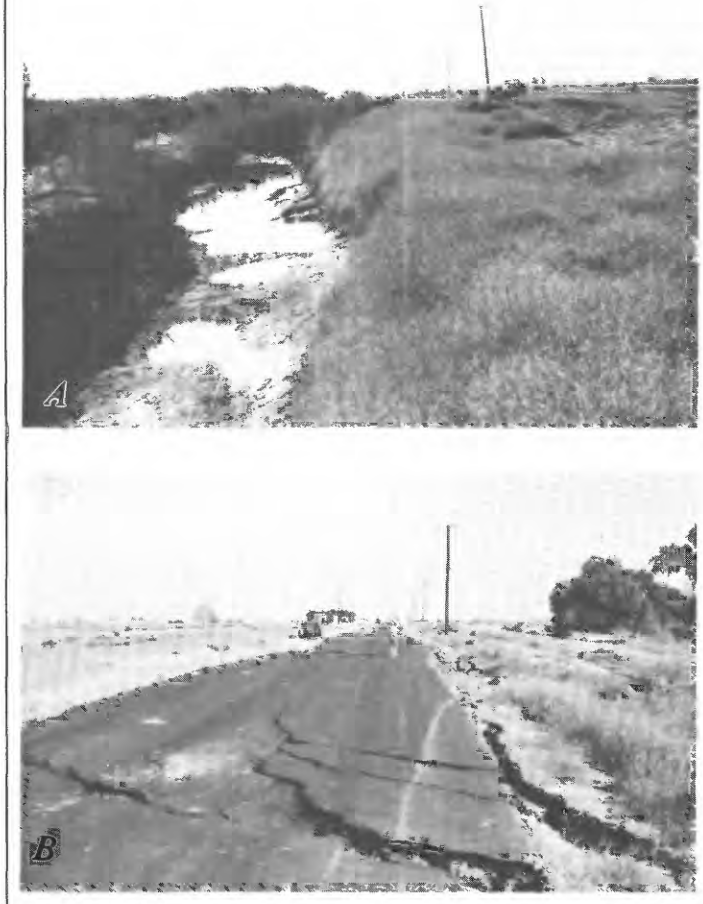

FIGURE 163.—Lateral spread at site 13 on Heber Road, showing associated displacements, fissures, and sand boils (see fig. 162). *A*, Unlined canal, which shifted about 1.2 m to south. View westward. *B*, Pavement on Heber Road, which settled, cracked, and shifted to south by as much as 1.2 m. View eastward. *C*, Sand boils, ground cracks, and displaced road and canal on lateral spread. View eastward. Photograph by Paul Noden.

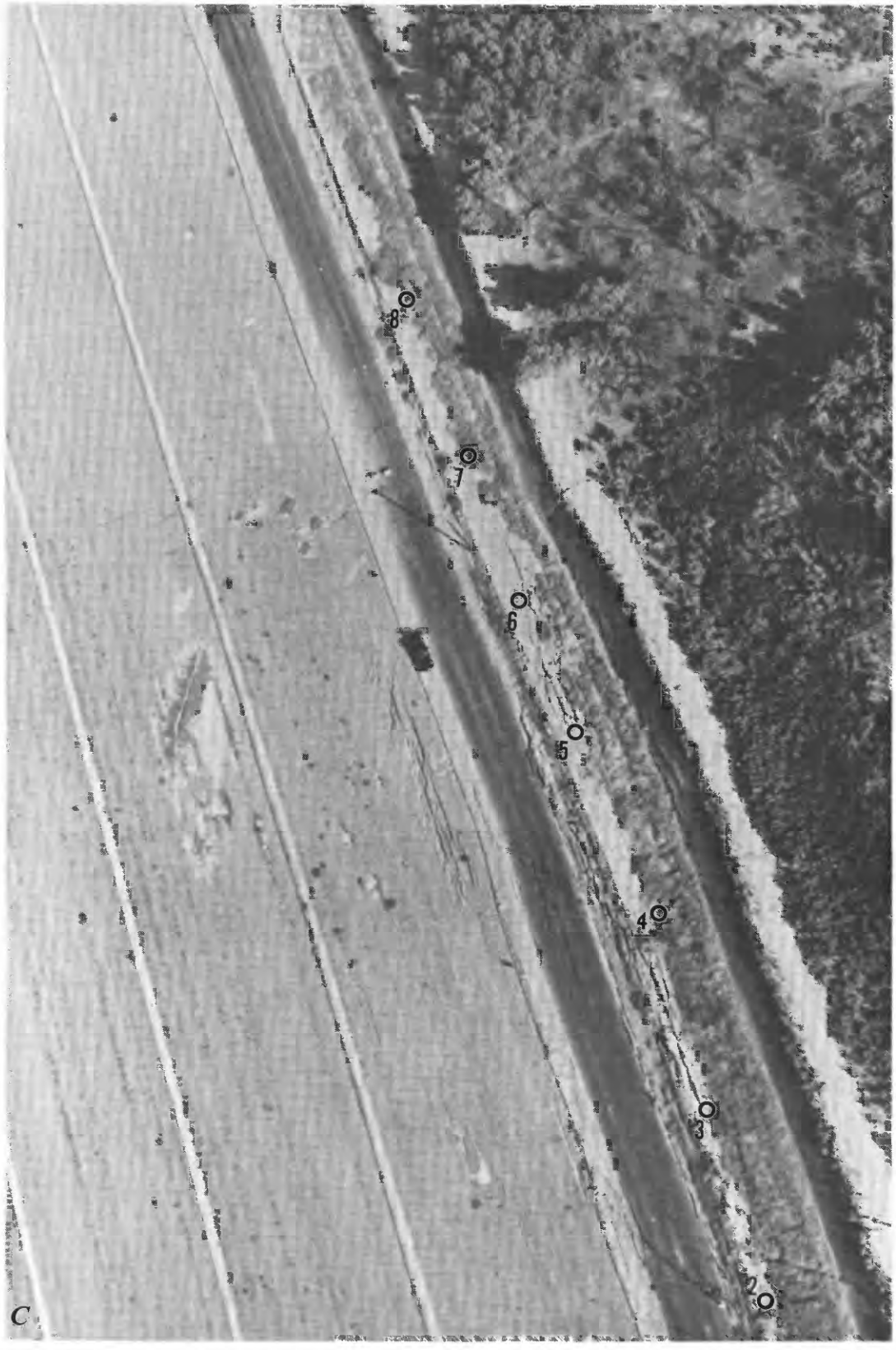

FIGURE 163.—Continued

erupted in many places within it. The trough created a dip several centimeters deep in Orchard Road that was hazardous to fast-moving traffic. Inspection of a manhole near Orchard Road revealed that a drainline about 4 m underground trends westward roughly beneath the centerline of the trough. Compaction and liquefaction of backfill placed over the drainline evidently caused differential settlements, which in turn created the trough and generated the many sand boils within it.

Site 19.—Several large sand boils with coalescing cones, and several smaller sand boils, were alined along a small west-trending 100-m-long fissure about 1 km north of King Road and about 100 m west of Orchard Road.

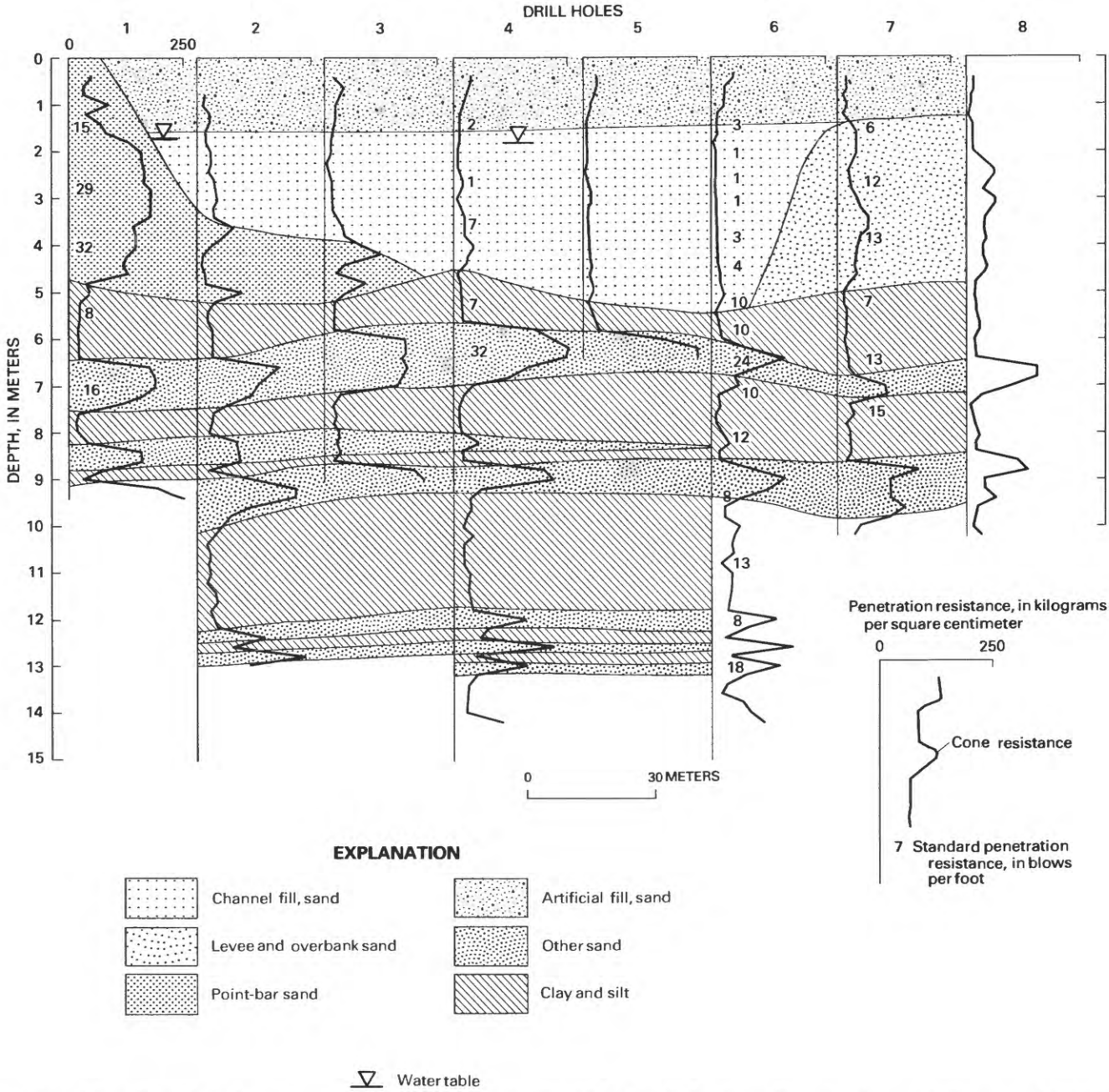

FIGURE 164.—Geotechnical section across lateral spread at site 13 at Heber Road, showing sedimentary layers, static-cone resistances, and standard-penetration resistances. See figure 162 for locations of drill holes. After Bennett and other (1981).

Site 20.—A single sand boil erupted immediately west of the East Highline Canal, 10.4 km east and 0.9 km south of Holtville, Calif. (M. G. Bonilla, oral commun., 1979). Soil in that area, primarily sand and gravel, likely was saturated by seepage from the canal. Liquefaction of that soil generated the sand boil.

Site 21.—About 10 sand boils erupted on part of a golf course just west of Anderholt Road, 0.5 km south of County Highway S–80. The golf course is laid out in lowlands along a small tributary to the Alamo River that follows the course of an old stream channel (fig. 158). About 10 pipes in the course sprinkler system were broken, and two footbridges over a small stream were damaged by compression. The damage to the footbridges indicates that the ground beneath the course shifted at least a few centimeters toward the creek.

Site 22.—About 20 sand boils erupted in a field roughly 50 m behind a slump (site 30) that partly blocked the Barbara Worth Drain south of Zenos Road, about 4 km west of Holtville, Calif. The sand boils probably originated in fill or fluvial sand and silt. The field is in a lowland area, part of a former stream channel (fig. 158), that drains northward into the Alamo River. After the area was leveled for agricultural purposes, the Barbara Worth Drain was excavated to replace the former natural drainage.

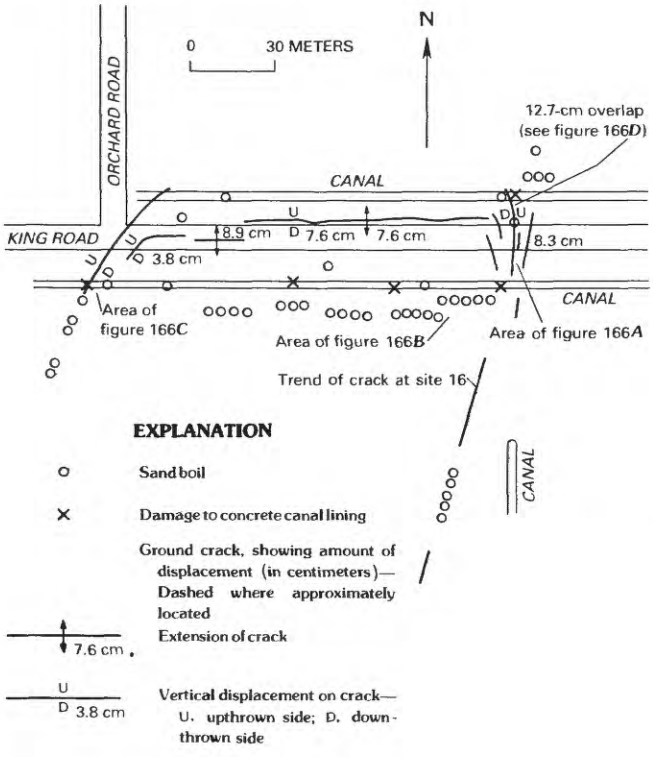

FIGURE 165.—Locations of ground cracks, sand boils, and canal damage at site 17 near intersection of King and Orchard Roads (see fig. 166).

Site 22A.—Fissures developed and as many as a hundred sand boils erupted in fields between the Alamo River and the Redwood Canal at a site 9.7 km northwest of Holtville and approximately 0.8 km west of the river. The sand boils occurred between two continuous fissures, some 10 to 15 m apart, that paralleled each other in an arcuate north-to-south zone approximately 1.8 km long; most of the sand boils were near the eastern fissure. Several shorter, less continuous fissures were scattered between these two major fissures. Vertical displacements across the fissures were as great as 0.35 m, and openings were as great as 0.1 m. Strike-slip displacements were small to negligible.

Ground displacements along the fissures ruptured the concrete linings of four canals; in some places the linings were pulled apart in tension, whereas in others they were buckled in compression. Where the fissures crossed the Graeser Drain, slumping occurred, which necessitated a bulldozer to restore the banks. Ground settlements and displacement disrupted irrigation schemes and fractured tile drains, and required releveling of the fields and replacement of tile drains (J. McKim and W. Flanagan, oral commun., 1981). According to J. McKim, who farmed this area since the 1930's with his father, fissures and sand boils were not observed here after the 1940 Imperial Valley earthquake.

The two continuous fissures mark the edges of a former meander of the Alamo River. The old meander is depicted on aerial photographs by tonal differences in the soil in the fields. Confinement of the sand boils and ground settlement to the area between the continuous fissures indicates that liquefaction and compaction were limited to sediment within the channel. The effects and damage at this site resembled those effects at other sites where former channels were encountered—for example, sites 13 and 16.

Site 23.—Hundreds of sand boils and numerous small (less than 5 cm wide) ground cracks formed in a large graded area along the east side of the New River at the southwest edge of Brawley, Calif. The graded area, called "River Park," contains a rodeo ground, picnic area, stock pasture, and an unpaved parking area. The eruption of sand boils flooded the parking area and also covered parts of the stock pasture and the picnic ground with water and sand (fig. 168). Water continued to seep from a few of the sand boils for 2 weeks after the earthquake. Sand boils erupted preferentially along small ground cracks and around fenceposts and lampposts. Most sand boils were composed of sand, but some, particularly those that came up around the posts, contained silt and sand. A buried concrete drainpipe, 0.4 m in diameter, was ruptured in one place beneath the parking area. All these effects were due to liquefaction of subsurface sediment.

During December 1979, we established an array of borings and made soundings along a line extending westward across River Park, from a bluff on the east to the river on the west (Bennett and others, 1981). A stratigraphic section of the deposits along this line (fig. 169) shows three continuous sedimentary layers crossing the site: an upper layer of sandy silt and silty sand; an intermediate layer of clay and silty clay, containing some sand near the river; and a lower bed of unstratified sand. The cone-penetration data indicate that the upper silty layer and the upper half-meter of the unstratified sand bed are relatively loose. Liquefaction of those layers generated the sand boils; the silty sand-boil deposits came from the upper silty layer, and the coarser deposits from the lower sand bed. The liquefaction susceptibility of these deposits is covered in the section below entitled "Discussion."

In addition to the cracks and sand boils on the graded area of River Park, a slump with displacements as great as 1 m formed along the banks of the New River (site 34). At the top of the bluff, several hundred meters east

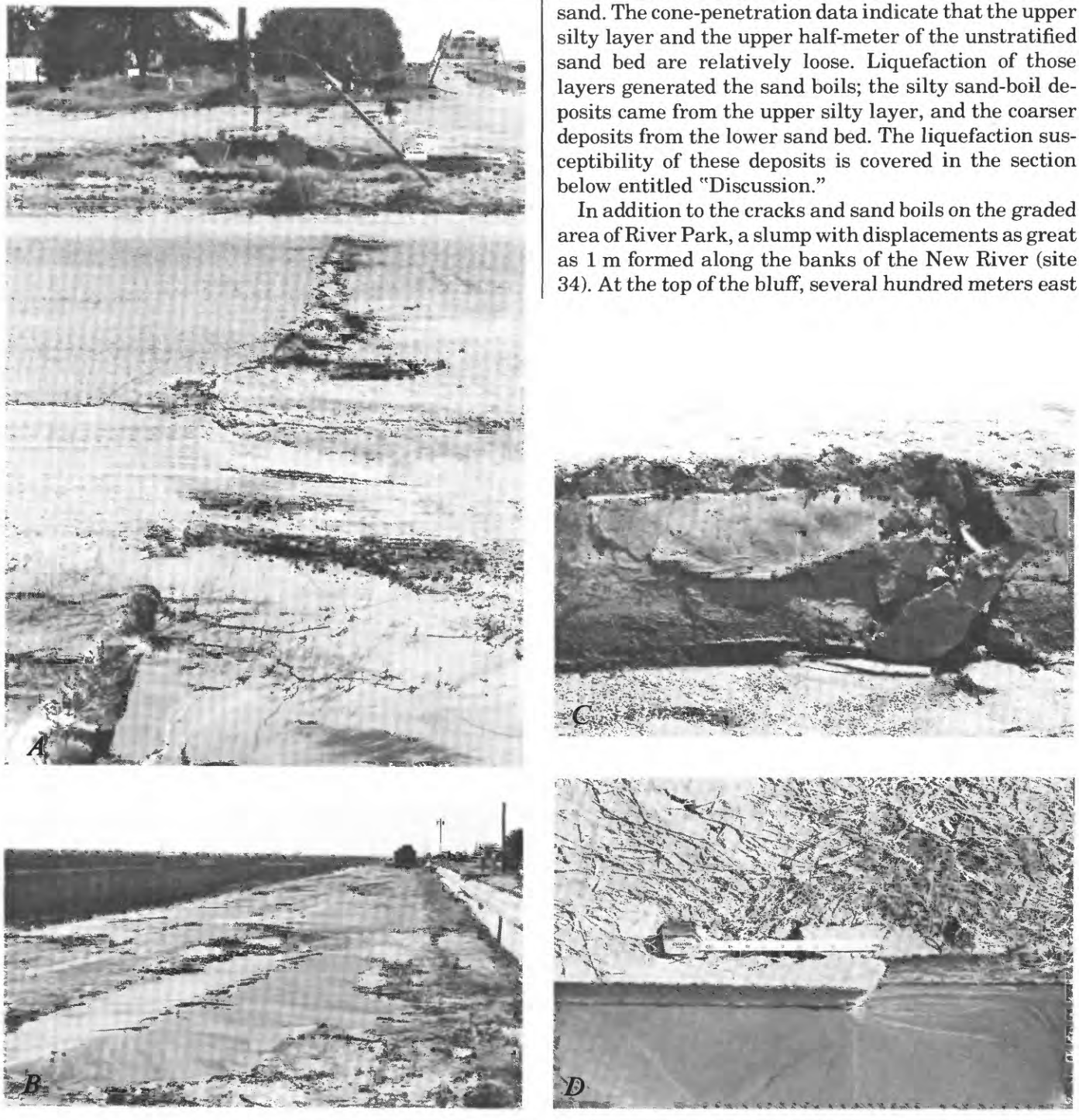

FIGURE 166.—Ground-failure effects at site 17 near intersection of King and Orchard Roads. *A*, Sand boils and scarp in road at east end of disturbed zone. View southward. *B*, Sand boils along canal bank and in field, looking westward from near east end of disturbed zone. *C*, Broken canal lining near west end of disturbed zone. Canal lining is approximately 1 m high. *D*, Overlapped canal lining near east end of disturbed zone. Note sand boil on bottom of canal. Scale in inches.

FIGURE 167.—Scarp at boundary of trough feature at site 18 west of Orchard Road, caused by settlement of fill over buried drainline. Scale in inches.

FIGURE 168.—Site 23 near River Park in Brawley, Calif. *A*, Sand boils in graded parking area (below embankment) and flooded area (darker areas). View northwestward. *B*, Sand boils (white patches) in stock pasture between parking area and New River. View southward.

of the river (site 33), a 120-m-long arcuate slump scarp with a maximum vertical displacement of 13 cm formed.

Site 24.—Several small sand boils erupted in newly placed fill just south of Shank Road and just east of the Alamo River. Liquefaction of fill or the underlying flood-plain deposits generated these sand boils.

Site 24A.—T. H. Heaton, J. G. Anderson, and P. T. German (written commun., 1980) reported:

> A rather sizable pond was apparently created when liquefaction occurred in the New River valley adjacent to the KROP radio transmitter (about 3 km north of Brawley). * * * Numerous sand boils around the margins of the pond were still oozing water on November 2, two weeks after the earthquake. A discontinuous zone of tensional cracking could be found along perhaps 50 percent of the perimeter of this pond, suggesting that the riverbed had subsided. We estimate the dimensions of this pond to be about 50 by 75 m, with a maximum depth probably less than 30 cm. A N. 5° E.-trending linear tensional crack ran from the perimeter of the pond and subparallel to the river bluff. This crack ran up the side of the river bluff. * * * The crack could not be followed into the golf course which lies on the flat land above the bluff, but may have continued into the boundary of a slumped wedge of land with a width of perhaps 1 m and a length of 20 m.

Site 25.—Several ground cracks disrupted a parking lot and an adjacent unpaved picnic area on the east shore of Wiest Lake (fig. 170). The arcuate pattern of some of the cracks indicates incipient lateral spreading toward the lake. Other cracks trended northeast across the highway east of the picnic area. Sand boils erupted in several places along cracks within the picnic area.

Kerry Sieh (written commun., 1979) interviewed a County park ranger who reported that the sand boils at Wiest Lake erupted at three different times: during the main shock, during an aftershock about midnight of the first night (when most of the sand came up), and during an aftershock on the afternoon of October 17, 1979. The fact that the ranger did not notice the crack across the road northeast of the parking lot when he drove through that area the morning after the main shock indicates that this crack may have formed during one of the strong aftershocks. The ranger also stated that several cracks have widened since he first noticed them, and that a few cracks and sand boils appeared in an area of flood plain(?) that had not been graded. The ranger reported that the east shore of Wiest Lake, including the dock area, parking lot, picnic area, and highway, is a wide dike that was constructed of fill dredged from the river to impound the lake. During construction of this dike, the course of the river was moved eastward from beneath the dike to its present position east of the highway.

This information suggests that liquefaction and compaction of fill material, or perhaps of underlying channel or flood-plain deposits, generated the cracks and

sand boils in the parking lot, picnic area, and highway on the west shore of Wiest Lake.

Gadsden, Ariz.—During the 1940 Imperial Valley earthquake, many spectacular effects of liquefaction were observed south of Yuma near Gadsden, Ariz., including eruption of large sand boils, heaving of the bottoms of irrigation and drainage canals, and buckling of bridges and flumes (Sylvester, 1979). Because of this previous history, we reconnoitered the Gadsden area to determine whether similar liquefaction effects were generated by the 1979 earthquake. Interviews with several farmers and a cursory search of the areas most affected by the 1940 event revealed no effects of liquefaction or other ground disturbances from the 1979 main shock.

FAILURES IN EMBANKMENTS

Ground failures in canal, river, and highway embankments consisted of settlements, slumps, incipient slumps, and incipient lateral spreads. The settlements were caused by compaction of subsurface materials, primarily artificial fill; and the slumps, incipient slumps, and incipient lateral spreads were caused by overloading of slopes due to seismically generated inertial forces, by strength loss due to liquefaction, or by a combination of both these processes. The larger slumps

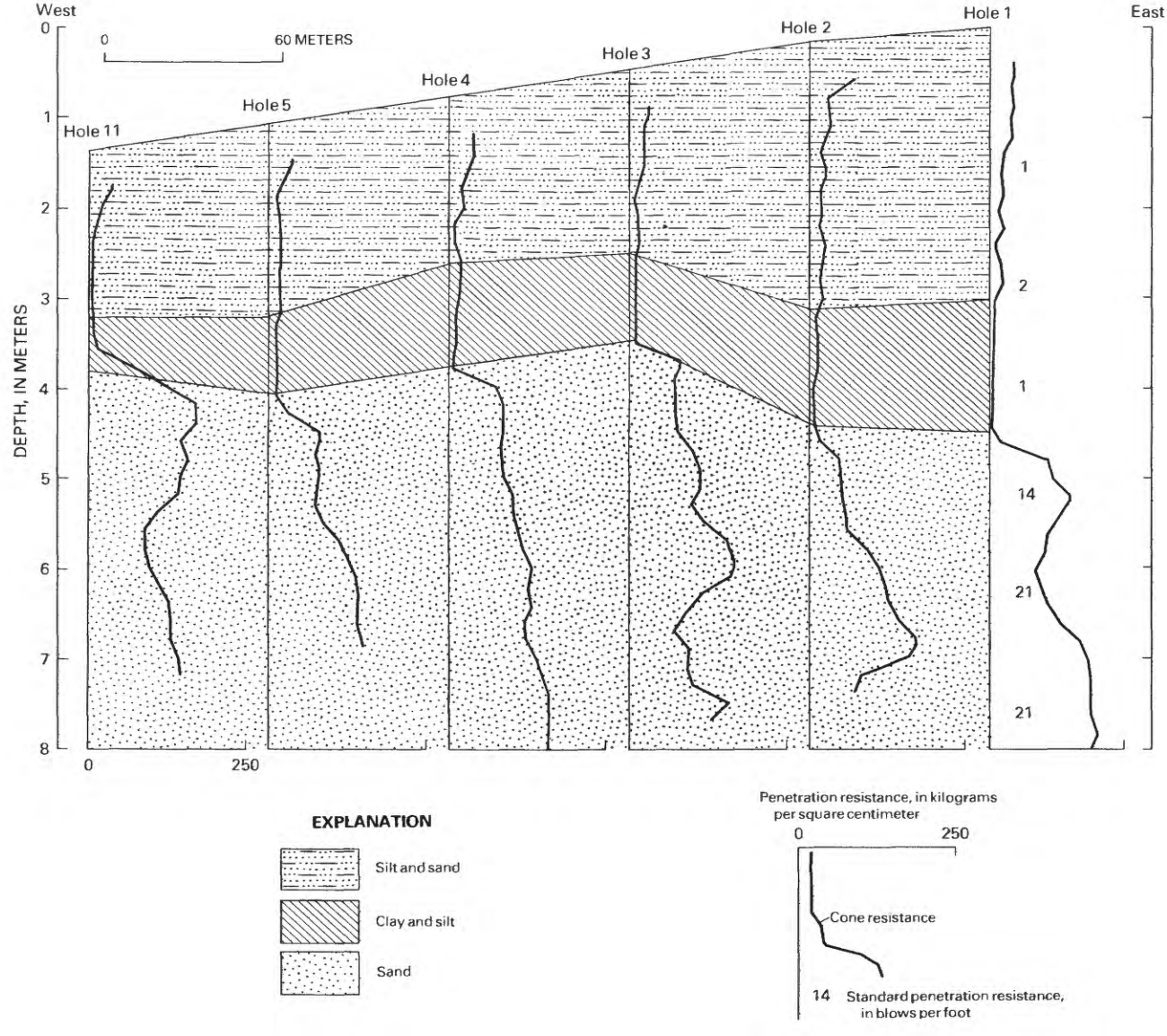

FIGURE 169.—Stratigraphic section at site 23 westward from bluffs, across River Park, to New River, showing sedimentary layers, static-cone resistances, and standard-penetration resistances. Drill holes are numbered 1–5 and 11. After Bennett and others (1981).

so damaged several irrigation canals that extensive regrading of embankments was required; in some places these repairs required reduction or stoppage of flow until repairs could be completed. Settlements, incipient slumps, and incipient lateral spreads were particularly damaging to concrete-lined irrigation canals. These linings, which are generally unreinforced, proved to be highly susceptible to rupture, even for ground displacements of only a few centimeters. To prevent erosion and other damage that might have been caused by leakage through ruptured linings, flow in many damaged sections was halted until the linings were repaired.

Slump displacements of a few tenths of a meter or less in riverbanks, combined with settlements in approach fill, structurally damaged some bridges. On the other hand, several well-constructed bridges sustained little or no damage from slump displacements as great as perhaps 0.15 m. Settlements of 0.15 m in bridge-approach fill halted traffic across several bridges.

FIGURE 170.—Sand boils and ground cracks in unpaved parking area at site 25 near east shore of Wiest Lake. View northeastward.

DAMAGE TO CANALS

Site 26.—The All-American Canal was extensively damaged from settlements, slumps, incipient slumps, and incipient lateral spreads along a 13-km-long section between Drop No. 5 near the Ash Canal and the East Highline Canal (pl. 4). The Imperial Irrigation District estimated total damage to the canal at $982,000 (L. R. McGlocklin, oral commun., 1979). The canal was constructed in the late 1930's by the U.S. Bureau of Reclamation as an unlined earth embankment, using locally available materials.

Waterflow in the canal was 110 m^3/s at the time of the earthquake (4:15 p.m. P.d.t.); by 6 p.m. flow was reduced to 20 m^3/s to prevent a possible breach and to assess damage and estimate needed repairs. The canal was repaired rapidly and flow restored to 116 m^3/s by October 19, only 4 days after the earthquake (L. R. McGlocklin, oral commun., 1979). Repair of the canal was urgent because of the many crops depending on irrigation water from the canal.

This rapid repair prevented any detailed mapping of the embankment damage. An aerial photograph (fig. 171) shows the concentration of damage along a 1.5-km-long section of the canal near the Alamo River. Several types of ground failures damaged the canal. Rotational earth slumps (fig. 172) that threatened to breach the canal required dredging to restore the original capacity of the channel. Incipient slumps or lateral spreads, as well as many undifferentiated fissures, so cracked the embankment that its ability to hold water was in question. Cracks were also observed in compacted fill around structures (fig. 173).

Near the junction of the East Highline Canal with the All-American Canal, water seeped from the south embankment into a pond in an adjacent depression (fig. 172*B*). The hydraulic gates and concrete transition structure of Drop No. 5 were damaged from settlement. Drop No. 5 was similarly damaged in the 1940 Imperial Valley earthquake (Clark, 1940; Sylvester, 1979).

Damage to the All-American Canal extended 10 km east of the Imperial fault, but only 3 km to the west. Intensity differences on opposite sides of the fault, or differences in embankment and foundation materials, probably explain the asymmetric distribution of canal damage. The absence of sand boils near damaged sections of the canal suggests that large-scale liquefaction was not involved in the bank failures. Increased porewater pressures and localized liquefaction, however, probably contributed to failure in some places.

Site 27.—The East Highline Canal east of Holtville, Calif., was damaged by slumping and incipient slumping for approximately 500 m along the east side of the

canal. The embankment was rapidly repaired. Only a few cracks in the bank and some traces of sediment in the channel marked the site of failure 2 days after the earthquake.

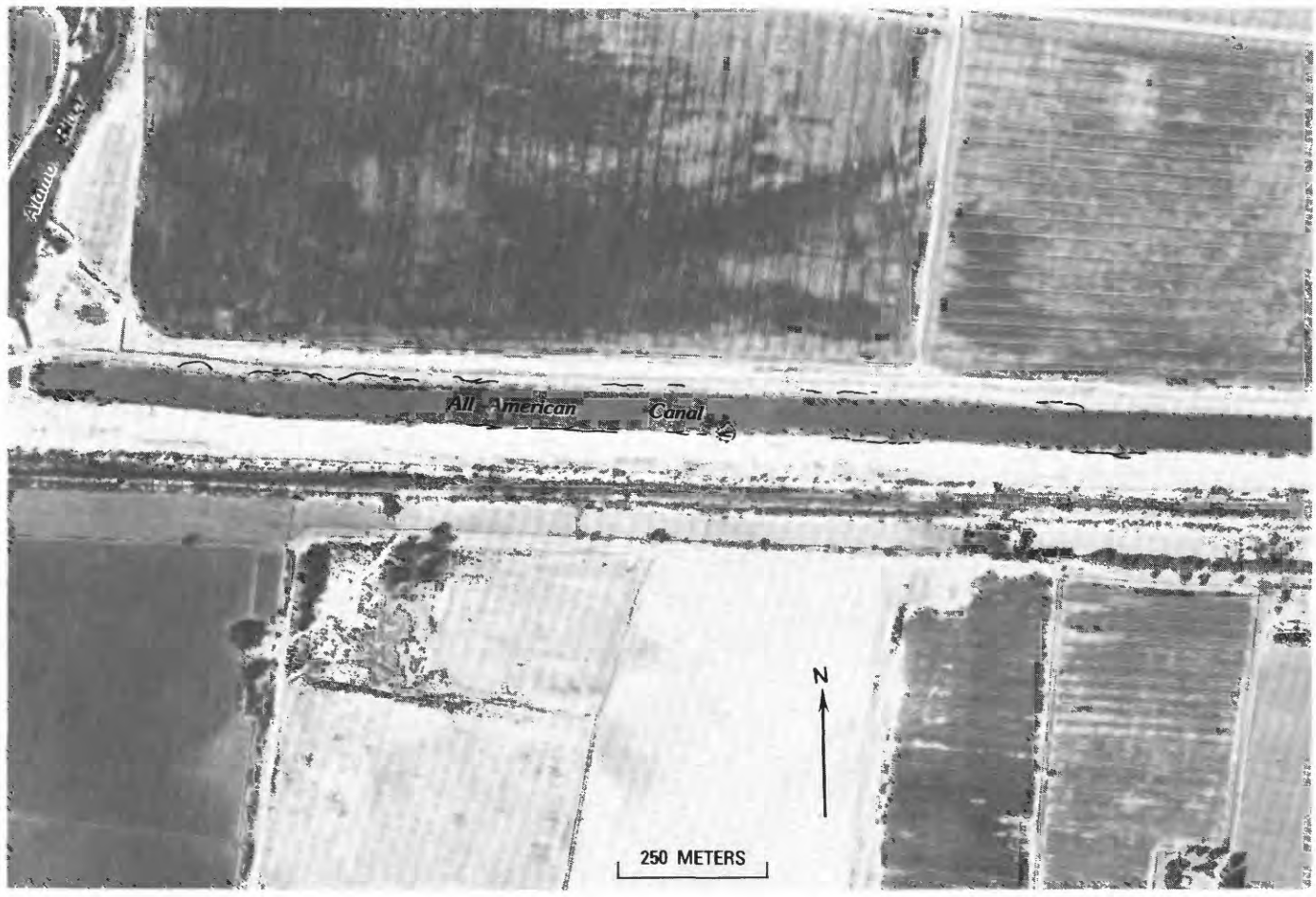

FIGURE 171.—All-American Canal at site 26 east of Alamo River, showing cracks and slumps in embankment. Aerial photograph from I. K. Curtis Services.

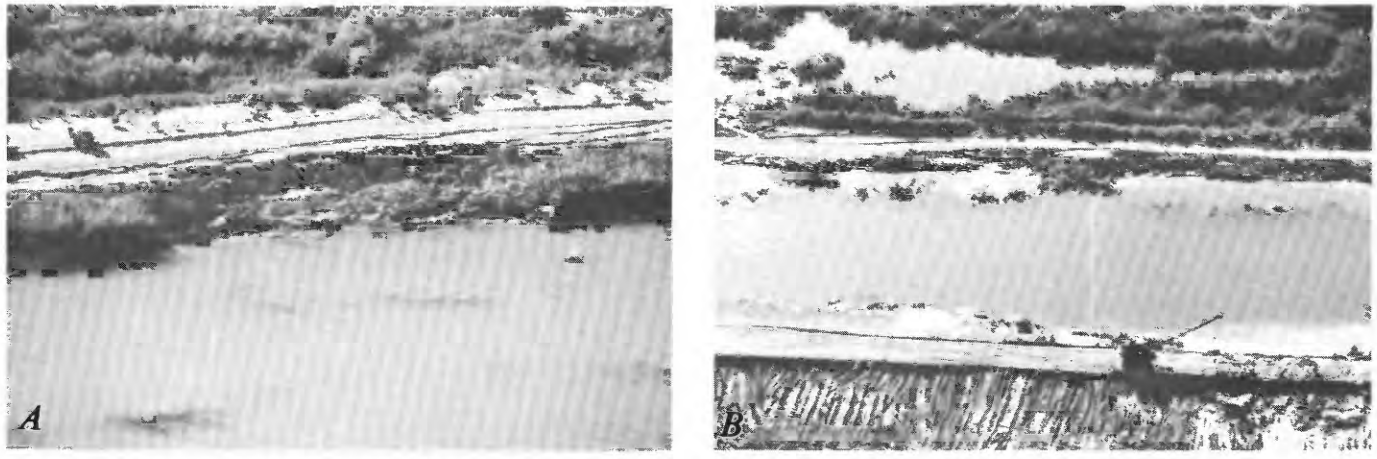

FIGURE 172.—Slumps and cracks in All-American Canal embankments at site 26. *A*, Major slump, showing incipient slump to left and additional cracks behind these two failures. View southward. *B*, Large slumps in canal bank. Bank did not breach, but some water leaked into pond at top. Crane is repairing bank at bottom. View southward.

Site 28.—Near the intersection of Heber and Keffer Roads, cracks riddled the banks of the South Alamo Canal, which parallels Heber Road on the south (fig. 174). Longitudinal cracks in the banks extended for at least 100 m along both sides of the canal. A badly cracked zone approximately 15 m wide extended from the canal to a barrow pit alongside Heber Road. The cracks, which showed from 5 to 10 cm of vertical separation, displayed little, if any, horizontal displacement. Vertical displacement along cracks on the north side of the canal was consistently downward toward the barrow pit and indicated incipient slumping or incipient lateral spreading toward the pit. In contrast, vertical displacement on cracks along the south side of the canal was consistently downward toward the canal.

Site 29.—The east bank of the South Alamo Canal and an adjacent roadway were fissured for 0.5 km from 1.0 km north of State Highway 98 to the right-angle turn south of the sand dunes. The fissures were caused by incipient slumping or lateral spreading toward the canal. The cracks showed as much as 10 cm of opening and vertical separation. Along a stretch roughly 100 m long the cracks crossed the roadway and intersected a concrete-lined irrigation canal to the east; the lining near the base of the canal was ruptured and displaced westward a few centimeters along part of this segment (fig. 175). The lined canal was taken out of service until the cracks could be repaired.

Site 30.—About 4 km west of Holtville, Calif., both banks of the Barbara Worth Drain slumped into the channel in several places between Zenos Road and a right-angle turn 0.4 km south of that road (fig. 176). The slumps cut several meters into the banks, destroyed unpaved farm lanes on both sides of the drain, and partly dammed the channel. Fissures and scarps showing separations as wide as a few tenths of a meter that formed behind and between the slumps indicate incipient failure in these places. These fissures and scarps broke up the pavement on Zenos Road and impeded traffic. About 10 sand boils that erupted about 50 m east of the largest slumps (site 22) indicate that liquefaction may have contributed to these failures. The drain lies in a lowland area that drains northward into the Alamo River. The lowland was leveled for agricultural purposes, and the drain was cut through after the leveling operation. Thus, the banks that slumped are probably composed of uncompacted fill.

Site 31.—About 200 m east of the Alamo River, the banks and part of the shoulder of Worthington Road slumped southward into a drainage ditch paralleling the road (fig. 177). The slump partly blocked the ditch and diverted the flow southward into the opposite bank.

COMPARISON WITH THE 1940 IMPERIAL VALLEY EARTHQUAKE

The 1940 Imperial Valley earthquake caused widespread damage to canals in both the United States and Mexico, extending from Holtville, Calif., in the north to the Solfatara Canal in the south (Clark, 1940; Ulrich, 1941; Sylvester, 1979). Approximately 108 km of the Ash, Holtville Main Drain, All-American, East Highline, Central Main, Alamo, and Solfatara Canals was damaged or destroyed. In Mexico, an 11.7-km section of

FIGURE 173.—Differential settlement and incipient slump near box culvert through embankment of All-American Canal at site 26. View southward.

FIGURE 174.—Cracks in banks of South Alamo Canal at site 28 west of Keffer Road. Displacements across cracks in near bank are consistently downward away from canal; displacements in far bank are consistently downward toward canal. Light patches in field beyond canal are sand boils at site 14. View southeastward.

the Solfatara Canal (pl. 4) was destroyed by bank slumps and heaving of canal bottoms that reduced the embankments from 3 to only 0.3–0.6 m above the canal bottom. Only the Ash, All-American, and East Highline Canals were damaged during the 1979 earthquake. Thus, the 1979 canal damage was only a fraction of that in 1940.

Disruption of the All-American Canal in 1940 included damage to gates and drops, as well as embankment damage. Many of the same sites were damaged in 1979 as in 1940; however, in several places damage was more severe during the 1940 event. During both earthquakes, Drop No. 5 underwent settlement, and embankments showed considerable longitudinal cracking, slumping, and incipient slumping between Drop No. 5 and the East Highline Canal.

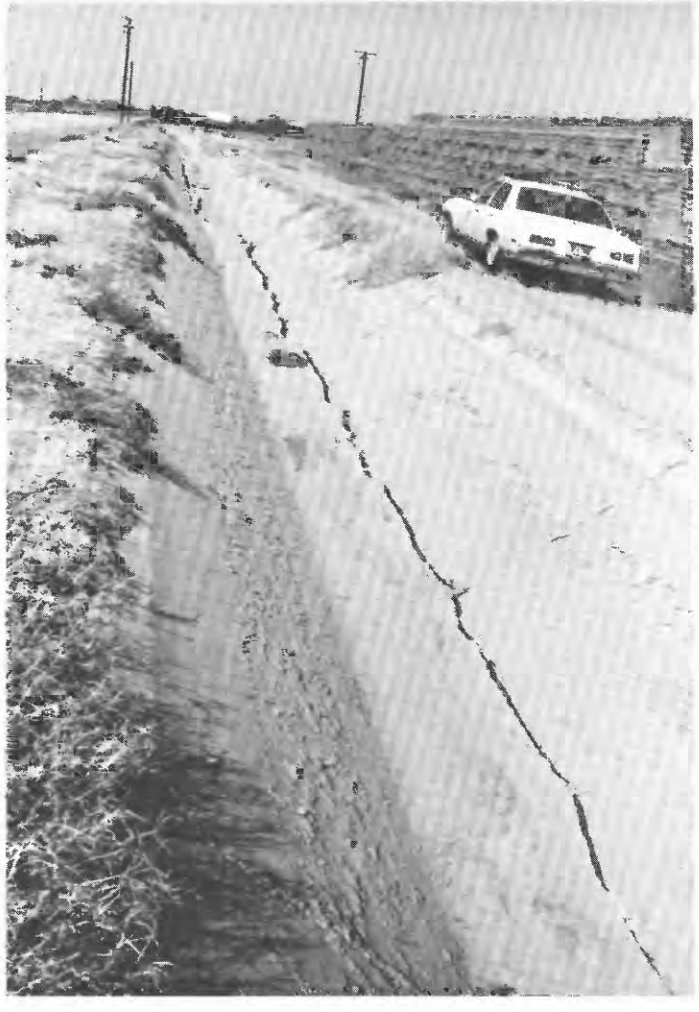

FIGURE 175.—Ruptured canal lining at site 29, caused by a few centimeters of westward lateral ground displacement of left side of canal. Canal was taken out of service until lining could be repaired. New northward.

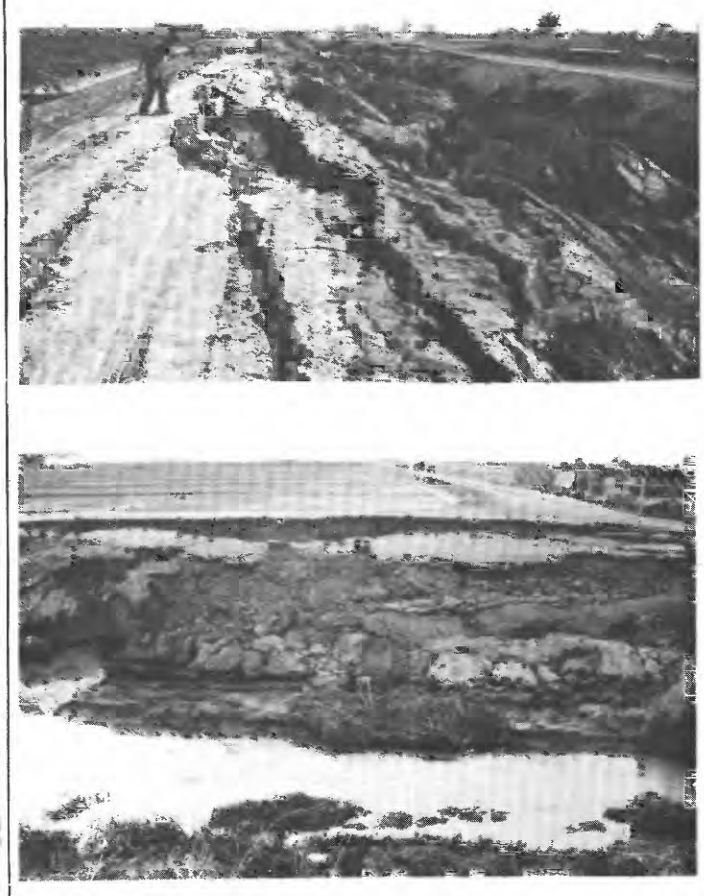

FIGURE 176.—Slumped banks of Barbara Worth Drain at site 30. *A*, Slump in east bank, that destroyed farm lane and blocked drain. View southward. *B*, Slump and scarp in west bank. View westward.

FIGURE 177.—Slumped bank of a drain at site 31 along south side of Worthington Road, about 200 m east of Alamo River. View eastward.

The distribution of canal damage from these two earthquakes appears to be related to the proximity to surface rupture along the fault. In 1940, the surface rupture extended into Mexico as far southward as the Solfatara Canal, whereas that in 1979 extended only as far southward as the South Alamo Canal (pl. 4). Severe canal damage in both earthquakes was limited to areas within about 10 km of the surface rupture.

RIVER AND HIGHWAY EMBANKMENTS

Because most highway-embankment failures (settlements) were in approach fill to bridges spanning rivers, where slumps in banks were also common, we discuss these two failure types together in this section.

New and Alamo Rivers.—Along the New River between Seeley and Rutherford Roads north of Brawley, Calif. (a distance of 34 km), and along the Alamo River between State Highway 98 and Wiest Lake (a distance of 40 km), we observed incipient slump cracks in riverbanks or in nearby flood-plain deposits at each site we examined. These cracks were generally 1 to 10 cm wide and roughly paralleled nearby banks. In a few places the cracks widened to several tenths of a meter, and at one site (34) we observed a well-developed slump. Slumping caused some damage to bridges (described below) and to River Park in Brawley.

Site 32.—The bridge over the New River west of Brawley, Calif., was damaged and had to be closed after the earthquake (fig. 178). The 60-m-long bridge was constructed in 1952 as two parallel concrete structures, each resting on nine sets of cast-in-place concrete piles that extend at least 9 m below the ground surface into fine and very fine sandy soil. A few piles on the west side of the bridge showed some repaired preearthquake damage (cracks), reportedly caused by foundation displacements due to slumping of the west bank. During the earthquake, ground displacements caused by settling and slumping of the approach fill and streambank caused the superstructures of the bridges to rotate counterclockwise in a horizontal plane; this movement cracked and tilted several supporting piles. In spite of these ground and bridge movements, the two decks were virtually undamaged (fig. 178). Repair costs were estimated at $115,000 to realine the bridge, epoxy the cracked piles, and regrade and repave the approaches (California Department of Transportation, 1979).

The earthquake generated a series of cracks in the riverbanks beneath the bridge, and parts of the banks slumped at least 10 cm toward the river. Relative ground settlements as great as 4 cm occurred around the piles; ground movement toward the river caused soil to compress against the upslope side of the piles and pull away from the downslope side (fig. 179). Inundated vegetation near the cracks on the southeast side of the bridge offered additional evidence of downward bank movement.

Ground displacements toward the river pushed against the spans and caused the bridges to rotate horizontally. The west ends of the span shifted 19 cm southward, and the east ends 9 cm northward, relative to the bridge approaches (fig. 180). The west and east approach fills settled 15 and 7.6 cm, respectively, relative to the

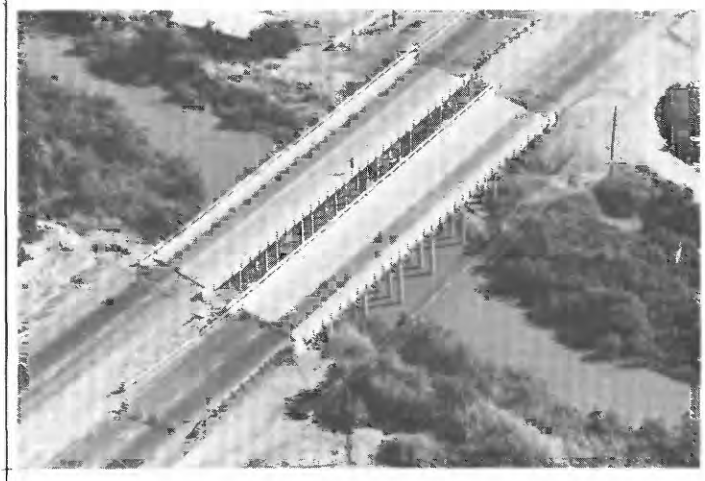

FIGURE 178.—State Highway 86 bridge over New River at site 32 west of Brawley, Calif. Abutment fill settled about 0.15 m, and both ends of bridge and riverbanks slumped about 0.1 m toward stream. Ground displacements caused bridge decks to rotate about 0.3° counterclockwise in a horizontal plane but did not seriously damage structure.

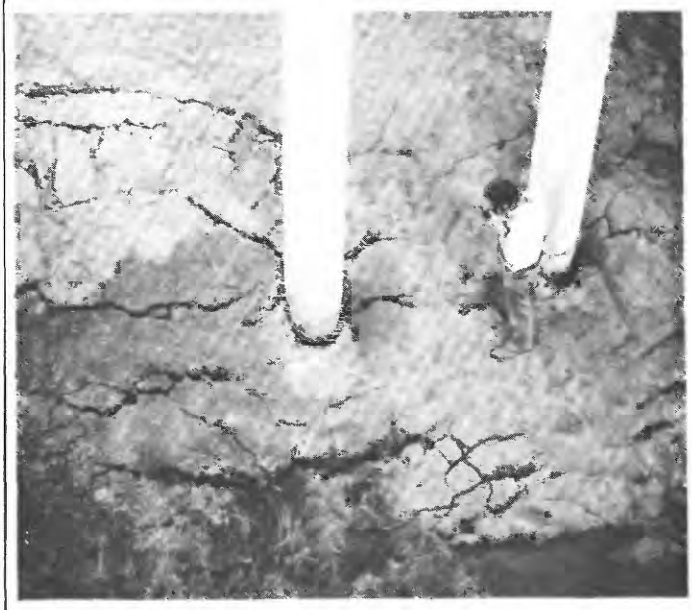

FIGURE 179.—Slumping of riverbank around piles of bridge at site 32. Soil moved 10 cm past stationary piles, gap opened on downslope side, and soil bunched up on upslope side. Cracks in riverbank are typical of those in many localities along New and Alamo Rivers.

abutments (fig. 181). This shifting also damaged the bridge abutments (fig. 181*B*). Piles in bents Nos. 2 and 8 (fig. 180) cracked and spalled near the pile junctions with the bent cap. These two columns tilted 3.2° in the direction of bridge rotation; the other pile columns cracked and tilted somewhat less. Figure 180 presents a plan-view sketch indicating the relative ground and bridge movements. During the 1964 Alaska earthquake, comparable bridge damage was caused by somewhat similar ground displacements (McCulloch and Bonilla, 1970).

The 1940 Imperial Valley earthquake damaged a two-lane timber bridge over the New River in the same location as the present concrete structure. The southeastern section of the old bridge settled noticeably, but the full extent of damages is not known. Cracks paralleled the river south of the bridge; near the bridge these cracks swung away from the river and crossed the highway several meters to the east. These observations suggest that the bridge damage was due to settling and slumping of the approach fill and riverbanks. Similar fissures and slumping was observed in the 1979 earthquake.

Other bridges.—Although we did not comprehensively survey bridge damage in the Imperial Valley, we examined five other river crossings where ground failure occurred along the riverbanks and in embankments near the bridges. At each crossing, pavement cracks indicated settlement of the approach fill or incipient slumping toward the river. Separations on these cracks were primarily vertical or extensional toward the river

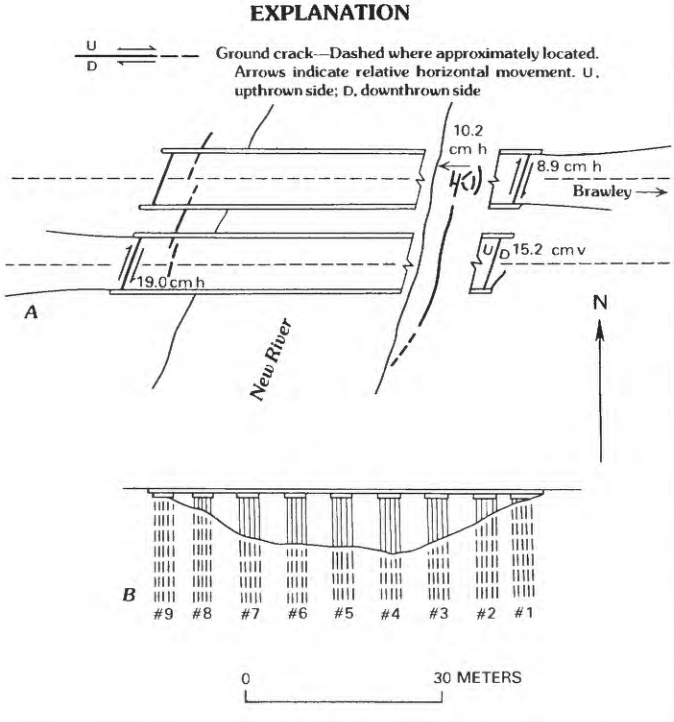

FIGURE 180.—Bridge at site 32 (see fig. 178), showing ground and bridge movements. *A*, Plan view showing relative ground and bridge movements (in centimeters). h, horizontal; v, vertical. *B*, Section of bridge, showing bents numbered 1–9 (see text).

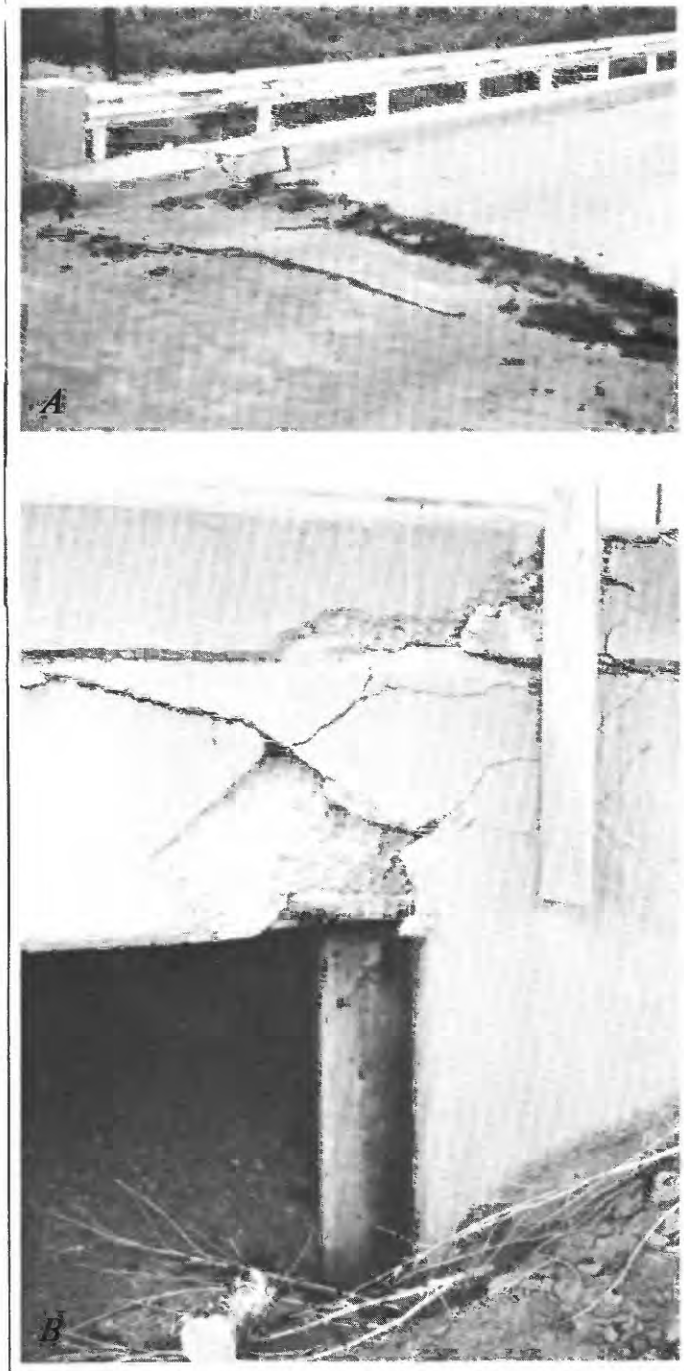

FIGURE 181.—Abutment of bridge at site 32 (see fig. 178). *A*, Vertical separation at abutment, caused by settlement of approach fill. *B*, Damage to abutment-deck connection, caused by differential movement between bridge and abutment.

and resembled cracks observed elsewhere along the river.

Some reparable damage occurred to bridges over the Alamo River at Rutherford Road, State Highway 98, and Keystone Road. This damage included settlements in approach fill, distress to abutment-span connections, cracked piles, and broken timber guardrails. Increased horizontal forces on abutments due to compaction of approach fill, or ground displacement toward the river due to slumping, apparently forced or tilted abutments toward the river. Similar ground displacements were observed at the Worthington Road and Heber Road bridges over the Alamo River; however, the reinforced-concrete bridges in those places resisted the ground movements without distress to structural members.

Although bridge damage caused by ground failure is apparently related to the type and age of the bridge as well as to the amount of displacement, the data reported here are insufficient for any general conclusions regarding the relative importance of these factors.

Site 33.—An arcuate scarp, approximately 13 cm high and 7 cm wide, outlined a 122-m-long incipient earth slump that formed in a sanitary-landfill embankment in the southwestern part of Brawley, Calif. (fig. 182). The embankment extends north-southward along the bluffs of the New River above River Park. Although the scarp was well marked at the top of the embankment and in the slope, we observed no lower boundary or toe of the slump in the heavy undergrowth at the base of the embankment. A waterpipe buried in the embankment was broken, presumably by the slump movement. A trench excavated to repair the pipe revealed the fill to be dry fine silt.

Site 34.—A rotational slump formed in the picnic area of River Park along the New River southwest of Brawley, Calif. The slump scarp ran 30 m along the river and extended 5 m away from the river's edge (fig. 183*A*). The height of the scarp ranged from a maximum of 1.2 m at its north end to near zero at its south end, where the scarp merged into incipient slump cracks that were pervasive along the river in that area. The slump disrupted a grassy picnic area and broke several pipes in a sprinkler system; the picnic area is at the west edge of a graded flood plain on which the park is situated.

The soil exposed in the northern part of the slump scarp is a dark moist organic silt. Behind and south of the scrap, sand boils composed of fine white sand that erupted along several cracks (fig. 183*B*) indicate that liquefaction occurred near the slump. From a subsurface investigation (Bennett and others, 1981), E. L.

FIGURE 182.—Arcuate incipient-slump scarp with 13 cm of vertical separation in embankment at site 33 east of River Park in Brawley, Calif. View southeastward.

FIGURE 183.—Slump and cracks at site 34 in River Park in Brawley, Calif. *A*, Slump near New River, showing 1 m of vertical displacement. View northward. *B*, Sand boils along crack south of slump in figure 183*A*.

Harp (oral commun., 1980) concluded that liquefaction of a sand layer about 3 m deep was the cause of failure.

Site 35.—During the 1968 Borrego Mountain, Calif., earthquake (M=6.4), a 0.4-km-long fissure, with as much as 50 mm of vertical separation, crossed County Highway S–80 about 125 m west of the New River (Castle and Youd, 1972, p. 164). Most of this fissure reopened during the 1979 main shock, although maximum displacement was only about 20 mm and the crack was intermittent to very faint in some segments.

Site 36.—Fissures, common along both the New and Alamo Rivers, also transected the grounds of the Brawley sewage-treatment plant east of the New River about 3.5 km north of Brawley, Calif. The fissures opened as wide as 6 cm where they passed beneath a single-story control building. Ground rupture beneath the building caused at most hairline cracks in the concrete-block exterior walls (fig. 184). The cracks also passed beneath cylindrical concrete filtration tanks but did not noticeably disrupt the tanks. One small leak developed in these tanks that may or may not have been due to ground displacement. We noted additional cracks along the base of the bluffs south of the sewage-treatment plant, and T. H. Heaton and others (written commun., 1980) noted cracks, slumps, and sand boils farther south near the KROP radio tower (site 24*A*).

FIGURE 184.—6-cm-wide crack at site 36 of type common along New and Alamo Rivers. Crack, which passes beneath block building at Brawley sewage-treatment plant, caused no more than hairline cracks in exterior walls of building.

STEEP RIVER BLUFFS AND HILLSIDES

The October 15, 1979, Imperial Valley earthquake and its aftershocks triggered earth falls along steep river bluffs in the Imperial Valley and generated a few scattered rock slides and falls in the nearby mountains. The earth falls occurred along the nearly vertical bluffs of the New and Alamo Rivers, and in several washes near the Salton Sea (pl. 4). With the exception of one earth fall that blocked Fredricks Road north of Brawley, Calif. (site 37), none of these landslides caused significant damage.

Bluffs as high as 6 m composed of poorly consolidated sandy silt bound the flood plains of the New and Alamo Rivers. Small earth falls (most less than 2 m^3 volume) were pervasive along many of these bluffs. For example, a local resident noted that plumes of dust generated by earth falls during the earthquake marked the course of the New River southwest of Brawley. Open cracks immediately behind the bluff faces in many places indicate that tensile fracture occurred in the bluffs. Individual earth falls, and cracks marking the positions of incipient earth falls, are shown on the map (pl. 4). Several larger earth falls (a few hundred cubic meters in volume) along the bluffs of the New River north of Brawley may have been triggered by one of the large aftershocks that struck that area.

We observed only a half-dozen rock slides and falls during aerial and ground reconnaissance of the Cargo Muchacho, Fish Creek, Coyote, and Jacumba Mountains. These landslides were generally small (less than 10 m^3 volume). No rock slides or falls were reported in the Sierra de los Cucapás in Mexico (Francisco Suarez, oral commun., 1979).

Several apparently recent rock slides on mountain fronts observed from the air exhibited fresh rock surfaces in scarps; however, examination on the ground would be necessary to verify whether these landslides were caused by the earthquake. Thus, landslides identified from the air but not verified on the ground are queried on the map (pl. 4).

The sparsity of rock slides and falls in the mountains reflects the areal geology and the distance of the mountains from the source of seismic energy. The mountains are primarily composed of granitic and vol-

canic rocks that have high tensile strength, wide spacing between discontinuities, slight weathering, and very thin residual or colluvial soil.

We observed no rock slides in the few rock slopes within 40 km of the fault rupture, only a few scattered rock slides and falls in mountain fronts between 40 and 65 km from the fault, and no rock slides beyond 65 km from the fault.

Site 37.—The bluff of the New River north of Brawley, Calif., collapsed over a length of 400 m, and Fredricks Road was blocked by 4,000 m^3 of sandy-silt debris. This ground failure was the largest earth fall generated by the 1979 earthquake. The road remained blocked for nearly a month after the shock. The nearly vertical 4- to 6-m-high bluffs above the road are among the highest in the Imperial Valley. This bluff may have been modified during the construction of Fredricks Road.

Site 38.—Two small (less than 1 m^3 volume) rock slides each occurred on an estimated 10-m-high cut slope of fresh jointed gneiss along Interstate Highway 8 at Devils Canyon in the Jacumba Mountains (fig. 185). Joints and foliation intersecting the cut isolated wedge-shaped blocks that slid downslope during the earthquake. These displaced blocks were very hard and showed no signs of weathering. Several additional joints on the cut slope apparently were enlarged during the shaking. We observed no rock slides or falls on natural slopes in the Jacumba Mountains, even though the natural slopes are equally as high and as steep as the cut slopes.

DISCUSSION

Secondary ground effects generated by the 1979 earthquake are consistent with the effects of past earthquakes of similar magnitude and duration. The types of effects produced, their distribution, and the geologic units affected also are all consistent with past observations.

LIQUEFACTION

Effects of liquefaction from the 1979 earthquake include lateral spreads, ground cracks, and sand boils. Such effects are associated with almost every large earthquake. Bearing failures and flow failures—both common consequences of liquefaction—were not observed during this earthquake, owing to flatness of the terrain in the areas where liquefaction occurred (which eliminates the potential for flow failure) and to the absence of tall or heavy structures (which eliminates the potential for bearing failure).

Most liquefaction effects were within 4 km of the fault rupture, and the most distant effects capable of causing damage were about 16 km (site 1) from the rupture, a distance compatible with the data from past events (fig. 186). Sand boils were reported by R. F. Scott and S. G. Muir (written commun., 1979) at a greater distance—35 km northwest of the north terminus of surface rupture—in the channel of San Felipe Creek (pl. 4). These sand boils, however, were not associated with ground displacements capable of causing significant damage.

Generally, liquefaction effects are more abundant near a fault or source of seismic energy and become sporadic with distance from the source. Such a trend was generally observed for this event. Most liquefaction effects occurred within about 4 km of the fault and were

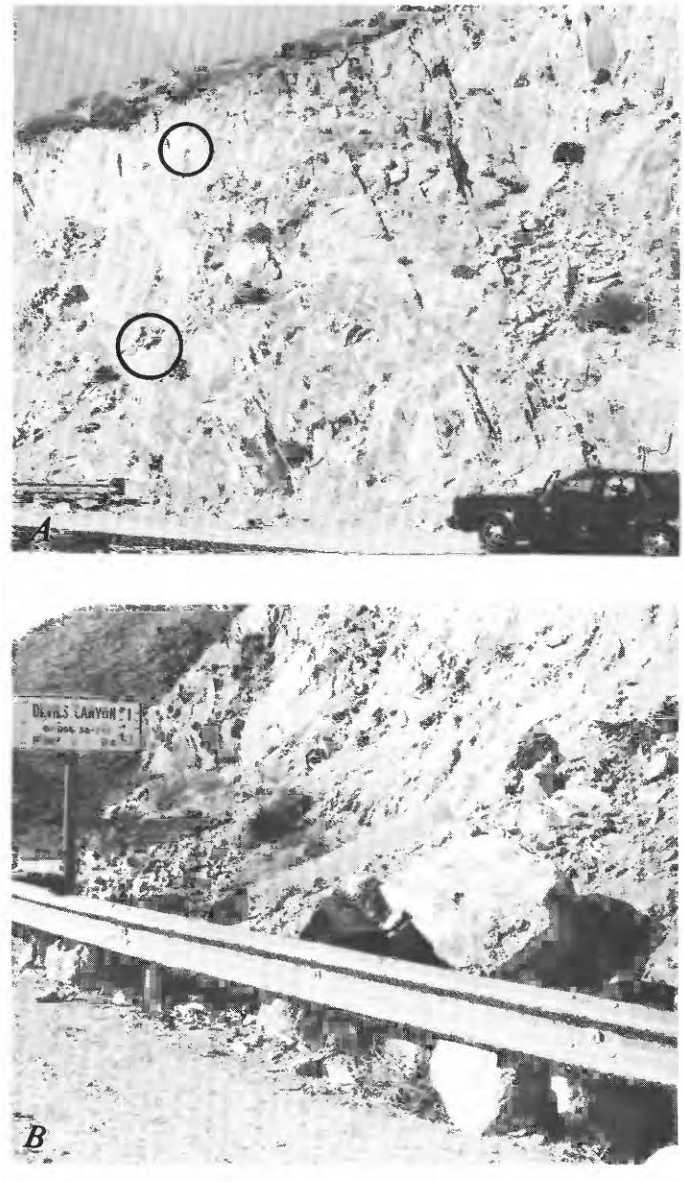

FIGURE 185.—Cut slope at site 38 in Devils Canyon from which small rock slides fell during earthquake. *A*, Debris (lower circle) that fell from fresh scarps above (upper circle). *B*, Debris from rock slides that rolled against guardrail.

sporadic beyond that distance. The distribution of liquefiable sedimentary deposits was also a major control on the distribution of liquefaction effects. Nearly all liquefaction effects occurred either in the area of sandy soil within an old delta (fig. 158) or along rivers where deposits of sand are common. Areas without underlying loose sand deposits were unaffected by liquefaction. In all instances, liquefaction developed in deposits of late Holocene age. For example, the soil on the old delta (fig. 158) is apparently little older than 400 years. These occurrences are consistent with past behavior showing that recently deposited sand is highly susceptible to liquefaction (Youd and Perkins, 1978, p. 441).

Duration of ground shaking is another control on liquefaction. The 5- to 13-s duration of the 1979 event, about normal for an $M=6.6$ earthquake, is marginal for causing liquefaction in many materials. Had the duration been longer, liquefaction effects likely would have been larger and more numerous.

We used data from the geotechnical section (fig. 164) to estimate the liquefaction susceptibility of the soil layers penetrated by soundings and borings along Heber Road (site 13), according to the technique of Seed (1979). Three silty-sand units are in the upper 5 m of the section: dense point-bar sand in the western part (drill hole 1), very loose natural channel fill covered by 1 to 2 m of artificial fill in the central part (drill holes 2–6), and loose overbank or deltaic deposits in the eastern part (drill holes 7, 8). Average standard-penetration blow counts below 2 m (the depth of the water table)

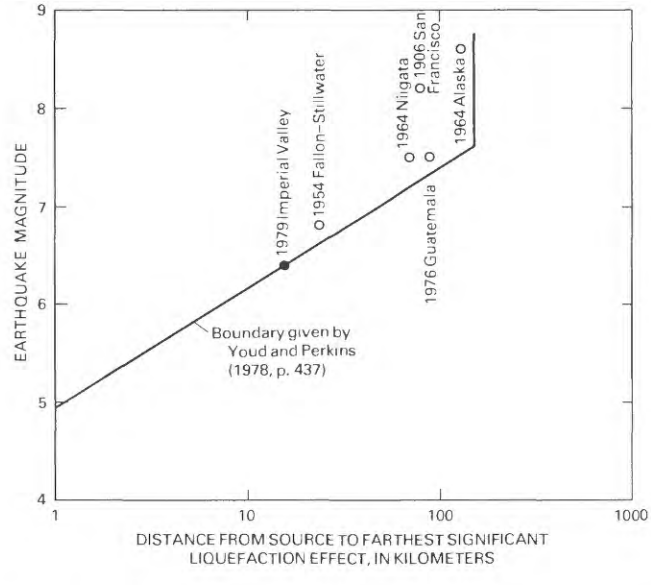

FIGURE 186.—Distance from seismic-energy source (fault rupture) to farthest effect of liquefaction as a function of earthquake magnitude. Distance of 16 km for 1979 Imperial Valley earthquake is consistent with trend of distances for past earthquakes.

were 3, 12, and 33 blows/ft, respectively, in these units. Other parameters needed in our calculation of liquefaction susceptibility include an estimated dry density of 1.6 g/cm^3, a depth of 4 m to the critical layer, and a maximum horizontal acceleration of 0.6 g (conservatively estimated from the strong-motion data of Porcella and Matthiesen, 1979). The equation given by Seed (1979, p. 210) for calculating the cyclic-stress ratio τ_{avg}/σ_0' is:

$$\tau_{avg}/\sigma_0' = 0.65 a_{max}(\sigma_0/\sigma_0')r_d, \quad (1)$$

where a_{max} is the maximum acceleration at the ground surface divided by the acceleration of gravity, σ_0 is the total overburden pressure on the critical layer (0.64 kg/cm^2 here), σ_0' is the effective overburden pressure (0.42 kg/cm^2 here), and r_d is a stress-reduction factor (about 0.95 for a depth of 4 m). Inserting these values into equation 1 yields a cyclic-stress ratio of 0.56 at the 4-m critical depth.

To complete the analysis, we need corrected blow counts. Curves given by Seed (1979, p. 238) indicate a correction factor of 1.4 for an effective overburden pressure of 0.42 kg/cm^2. Applying this factor to the blow counts listed above yields corrected blow counts of 4, 17, and 46 blows/ft for the fill, fluvial deposit, and point-bar sand, respectively. These data, plotted (fig. 187) for a cyclic-stress ratio of 0.56, indicate that for an $M=6.6$ earthquake, both the channel fill and the fluvial deposits should have liquefied, but that the point-bar sand should have resisted liquefaction. A variation by ±50 percent in the cyclic-stress ratio would not change these conclusions. Surface effects at the Heber Road site indicate that widespread liquefaction and large (1.2 m) ground displacements occurred in the area of channel fill. A few sand boils erupted in a linear pattern in the area of the fluvial deposits. These sand boils may have been generated in fill over a buried drainline. No other indications of liquefaction were observed on the overbank deposits, and no liquefaction was evident in the area of the point-bar sand.

We also used the above technique on data from the stratigraphic section (fig. 169) to calculate the liquefaction susceptibility of the deposits at River Park. Parameters estimated for that site include a maximum acceleration of 0.2 g (estimated from a strong-motion record recorded at Brawley Airport), a dry unit weight of 1.6 g/cm^3, critical depths of 2 m for the silty-sand layer and 5 m for the unstratified sandbed, and a water table at the ground surface. From the few standard-penetration data at that site, we estimate a value of 2 blows/ft for the silty sand and a maximum of 14 blows/ft for the upper part of the unstratified sand. Corrected blow counts for these layers are about 4 and 20 blows/ft, respectively.

The calculated cyclic-stress ratio for both layers is 0.25. The plot of this value against the corrected blow counts (fig. 187) shows that the silty sand should have liquefied readily and that liquefaction in the unstratified sand was marginal for an $M=6.6$ earthquake. The cone-penetration data indicate that looser sand lies above the 14-blows/ft level, and so this looser sand layer should also have liquefied readily. As noted above, the textures of the sand-boil deposits at River Park indicate that liquefaction occurred in both the silty-sand and the unstratified-sand layers.

Only limited comparisons are possible between the liquefaction effects from the 1940 and 1979 earthquakes. In 1940, large and spectacular sand boils erupted and several bridges were buckled owing to liquefaction and lateral spreading near Gadsden, Ariz. We observed no liquefaction in that area in 1979. In 1940 the surface rupture extended to a point 38 km west of Gadsden, whereas in 1979 the nearest point on the rupture was 57 km from Gadsden, and thus shaking intensity in 1940 was probably stronger than in 1979. Because little information is available on liquefaction effects in the Imperial Valley from the 1940 earthquake, we have no basis for comparing liquefaction effects in that region.

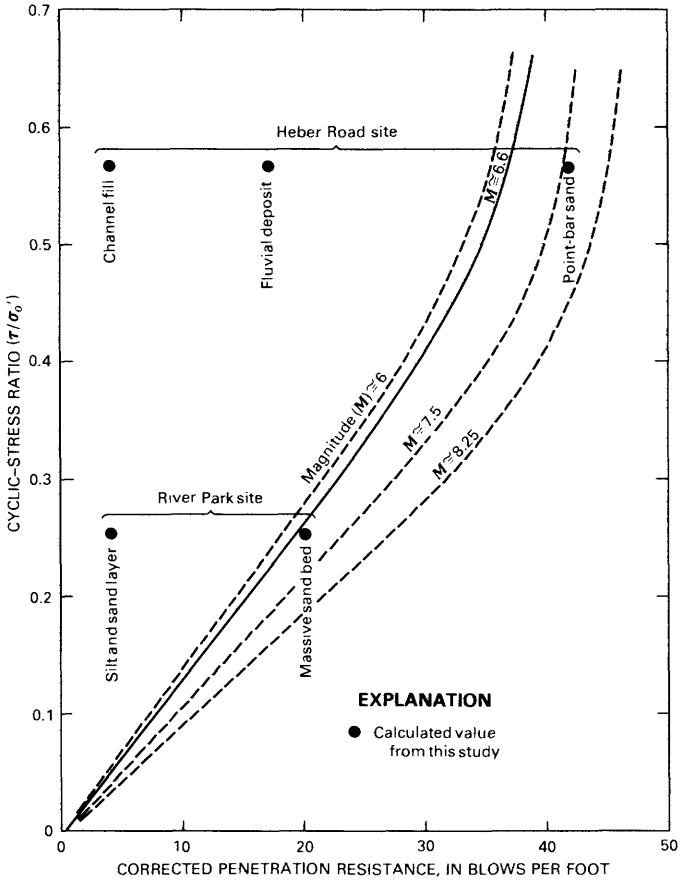

FIGURE 187.—Results from analyses of liquefaction susceptibility for Heber Road and River Park drilling sites (sites 13, 23), plotted on a graph of liquefaction behavior for level ground conditions presented by Seed (1979, p. 237). Solid line represents 1979 Imperial Valley earthquake; dashed lines represent earthquakes of different magnitudes. Cyclic-stress ratio is explained in text.

After the 1968 Borrego Mountain, Calif., earthquake ($M=6.5$), Castle and Youd (1972, p. 167) noted a few sand boils on a terrace along the New River north of Keystone Road southwest of Brawley, Calif. No sand boils erupted in that locality in 1979. In 1968 water was ponded on the ground surface, whereas in 1979 this surface was desiccated. These observations indicate a much lower water table that may explain why no sand boils erupted during the 1979 event.

SLUMPS

Slumping affected canal, highway, and river embankments. Although several canals were seriously damaged by slumps, most of the damage was repaired within a week. Slumps or incipient slumps were pervasive along the banks of the New and Alamo Rivers, and in some places disrupted highway embankments and distressed bridge spans. Slumps, including those in canal banks, were concentrated within 10 km of the surface rupture; the farthest known slump was 15 km away. A similar distribution of canal damage with respect to distance from the fault was observed in the 1940 Imperial Valley earthquake, when canal damage, largely caused by slumping of banks, also was concentrated within 10 km of the fault trace, although the trace was so much longer that a much larger area was affected.

Canal damage caused by slumping of banks was concentrated in an area extending from Holtville, Calif., to the United States-Mexican border in 1979, and from Holtville to the Solfatara Canal in northern Mexico in 1940 (pl. 4). Although this damage was not clearly associated with the occurrence of liquefaction, the soil in the affected areas generally contains sand layers, whereas that in unaffected areas does not (Strahorn and others, 1924).

EARTH FALLS AND ROCK SLIDES

Most earth falls along the bluffs of the New and Alamo Rivers were within 12 km of the surface rupture, although a few were as far away as San Felipe Creek, 35 km from the rupture. These silty bluffs stand in near-vertical slopes under static conditions, and the low tensile strength of the silt makes these bluffs susceptible to failure during earthquake shaking.

The generation of rock slides was controlled by local geology and by distance from the mountain fronts to the

surface rupture. The rocks in the nearby mountains have a low susceptibility to seismically induced landslides because of their high tensile strength, wide spacing between discontinuities, and absence of weathering. The seismic shaking in the mountains was too weak at 40 km or more from the surface rupture to generate more than a few widely scattered rock slides.

ACKNOWLEDGMENTS

Robert V. Sharp, Edwin L. Harp, and John Sarmiento provided information and assistance during this study. Sam Shaler and Michael Bennett conducted subsurface investigations. Our accounts of the sites in Mexico are based on information provided by Francisco Suarez.

REFERENCES CITED

Bennett, M. J., Youd, T. L., Harp, E. L., and Wieczorek, G. F., 1981, Subsurface investigations of liquefaction, Imperial Valley earthquake, California, October 15, 1979: U.S. Geological Survey Open-File Report 81-502, 83 p.

California Department of Transportation, 1979, Supplementary bridge report—bridge No. 58-05R: Unpublished report, 7 p.

Castle, R. O., and Youd, T. L., 1972, Engineering geology, *in* The Borrego Mountain earthquake of April 9, 1968: U.S. Geological Survey Professional Paper 787, p. 158–174.

Clark, T. A., 1940, Report of earthquake damage in Imperial Valley, May 18, 1940: U.S. Bureau of Reclamation, All-American Canal Project report, 40 p.

McCulloch, D. S., and Bonilla, M. G., 1970, Effects of the earthquake of March 27, 1964, on the Alaska Railroad: U.S. Geological Survey Professional Paper 545-D, p. D1–D161.

Porcella, R. L., and Matthiesen, R. B., 1979, Preliminary summary of the U.S. Geological Survey strong-motion records from the October 15, 1979, Imperial Valley earthquake: U.S. Geological Survey Open-File Report 79-1654, 41 p.

Seed, H. B., 1979, Soil liquefaction and cyclic mobility evaluation for level ground during earthquakes: American Society of Civil Engineers Proceedings, Geotechnical Engineering Division Journal, v. 105, no. GT2, p. 201–255.

Sharp, R. V., 1981, Variable rates of late Quaternary strike slip on the San Jacinto fault zone, southern California: Journal of Geophysical Research, v. 86, no. B3, p. 1754–1762.

Strahorn, A. T., Watson, E. B., Kocher, A. E., and Eckmann, E. C., 1924, Soil survey of the El Centro area, California, *in* Field operations of the Bureau of Soils, 1918: Washington, U.S. Government Printing Office, p. 1633–1688.

Sylvester, A. G., 1979, Earthquake damage in Imperial Valley, California, May 18, 1940 as reported by T. A. Clark: Seismological Society of America Bulletin, v. 69, no. 2, p. 547–568.

Ulrich, F. P., 1941, The Imperial Valley earthquakes of 1940: Seismological Society of America Bulletin, v. 31, no. 1, p. 13–32.

Varnes, D. J., 1978, Slope movement types and processes, *in* Schuster, R. L., and Krizek, R. J., Landslides: Analysis and control: Washington, U.S. National Academy of Sciences, National Research Council, Transportation Research Board Special Report 176, p. 11–33.

Youd, T. L., 1980, Ground failure displacement and earthquake damage to buildings: Conference on Civil Engineering and Nuclear Power, 2d, Knoxville, Tenn., 1980, Proceedings, v. 2, p. 7-6-1 to 7-6-26.

Youd, T. L., and Perkins, D. M., 1978, Mapping liquefaction-induced ground failure potential: American Society of Civil Engineers Proceedings, Geotechnical Engineering Division Journal, v. 104, no. GT4, p. 433–466.

EARTHQUAKE-GENERATED SANDBLOWS FORMED DURING THE MAIN SHOCK

By S. G. MUIR and R. F. SCOTT,
CALIFORNIA INSTITUTE OF TECHNOLOGY

CONTENTS

ABSTRACT

In sandblows formed during the main shock, fine-grained lacustrine sand and water traveled upward from a depth of 2 m within a dikelike pathway and were ejected at the surface, where the sand formed cones. Sandblows were reactivated during subsequent aftershocks. The subsurface sandblow features described here resemble sedimentary structures within lacustrine deposits that have been suggested to be sandblow features formed during prehistoric earthquakes.

INTRODUCTION

Sandblows and their deposits form by liquefaction during or shortly after moderate to large ($M \geq 5.5$) earthquakes (Sieh, 1978); their occurrence and distribution have been documented for many historical earthquakes. Structures preserved in Holocene lacustrine deposits, suggested to be subsurface sandblow features formed during prehistoric earthquakes along the San Andreas fault, were described by Sieh (1977, 1978) and Meisling (1979), and similar features in other localities were described by Hesse and Reading (1978) and Lamar and others (1979a, b). We are unaware of any previously described subsurface sandblow features that formed during recent earthquakes except those from the 1971 San Fernando, Calif., earthquake (Scott, 1974).

DESCRIPTION

Sandblows formed during the main shock near the intersection of King and Orchard Roads (fig. 188), approximately 2 km east of the 1940 and 1979 ground ruptures along the Imperial fault. A map depicting the distribution of sandblows and ground-failure phenomena within the study area is presented by Youd and Wieczorek (this volume, pl. 4). Sandblows composed of very well sorted fine sand formed in east-west-oriented rows of vents spaced 50 to 70 cm apart (fig. 189) and in a few isolated cones. According to local residents, the sandblows formed immediately after the main shock. Residents reported that the same occurence and distribution of sandblows were observed during the Imperial Valley main shock of May 18, 1940.

Sandblow vents ranged from 2 to 20 cm in diameter and averaged 5 cm in size. Some sandblow vents apparently collapsed and formed craters in which new vents later formed. The sandblows that were in rows formed cone structures, commonly 2 m in diameter and 10 to 15 cm high; the isolated sandblow cones ranged from 0.2 to 3 m in diameter and reached a height of approximately 10 cm.

A tractor-mounted backhoe was used to excavate a trench 2.5 m deep and 4 m long to investigate the subsurface structure of one isolated sandblow. Fine sand, probably representing a beach deposit of ancient Lake Cahuilla, was transported from a depth of 170 cm upward along a dikelike path 1.0 to 1.5 cm wide and was ejected at the surface to form a cone (fig. 190). This sandblow ejected approximately 0.1 to 0.25 m^3 of sand over an area of 4 m^2. Laminations 1 to 5 mm thick within the dike may represent heavy minerals that segregated into flow bands during sand transport (fig. 191). Truncation of the flow laminations suggests that the sand was transported upward within the dike at least twice along slightly different pathways. Although similar in grain size to the medium-brown (5YR 3/4) source sand, sand within the dike was light olive gray (5YR 6/1). A color contrast between the dike and source sand has also been observed in sandblow features in the lakebed of Kern Lake and in sediment-liquefaction experiments that model sandblows (S. G. Muir, unpub. data, 1980).

The fine-sand dike originated at a depth of 2 m and continued upward to a claybed at a depth of 80 cm. The dike migrated horizontally for several tens of centimeters to a point where it penetrated the claybed at a near-vertical angle, and then continued upward

through fine sand at a low angle until it was 10 cm from the surface (fig. 190). At that point the dike became vertical, and sand was ejected onto the land surface, where it formed a cone. Laminations in the cone of the sandblow, dipping outward from the vent, suggest continuous extrusion of sand from the same vent during formation. Standing water was observed in the trench at a depth of 2 m, and moist sand and clay above 2 m indicated that the ground-water table may actually have been nearer the land surface.

Reactivation of sandblows within the study area apparently occurred during October 15–18, 1979. Evidence of reactivation included incised drainage patterns on sandblow cones, alternating dry and wet cone surfaces, and the presence of vents of several ages within the same cone (fig. 189). A series of time-progressive photographs indicates that no significant amounts of sand were deposited during reactivation periods, but instead a slurry of clay and water was ejected onto the cones and eroded pathways on the cone surfaces. Standing water observed within vents and around the base of sandblows during the morning of October 18, 1979, suggests very recent reactivation.

CONCLUSIONS

1. Excess water produced by liquefaction and fine sand traveled upward along a dikelike pathway through lacustrine deposits, penetrated an overlying clay

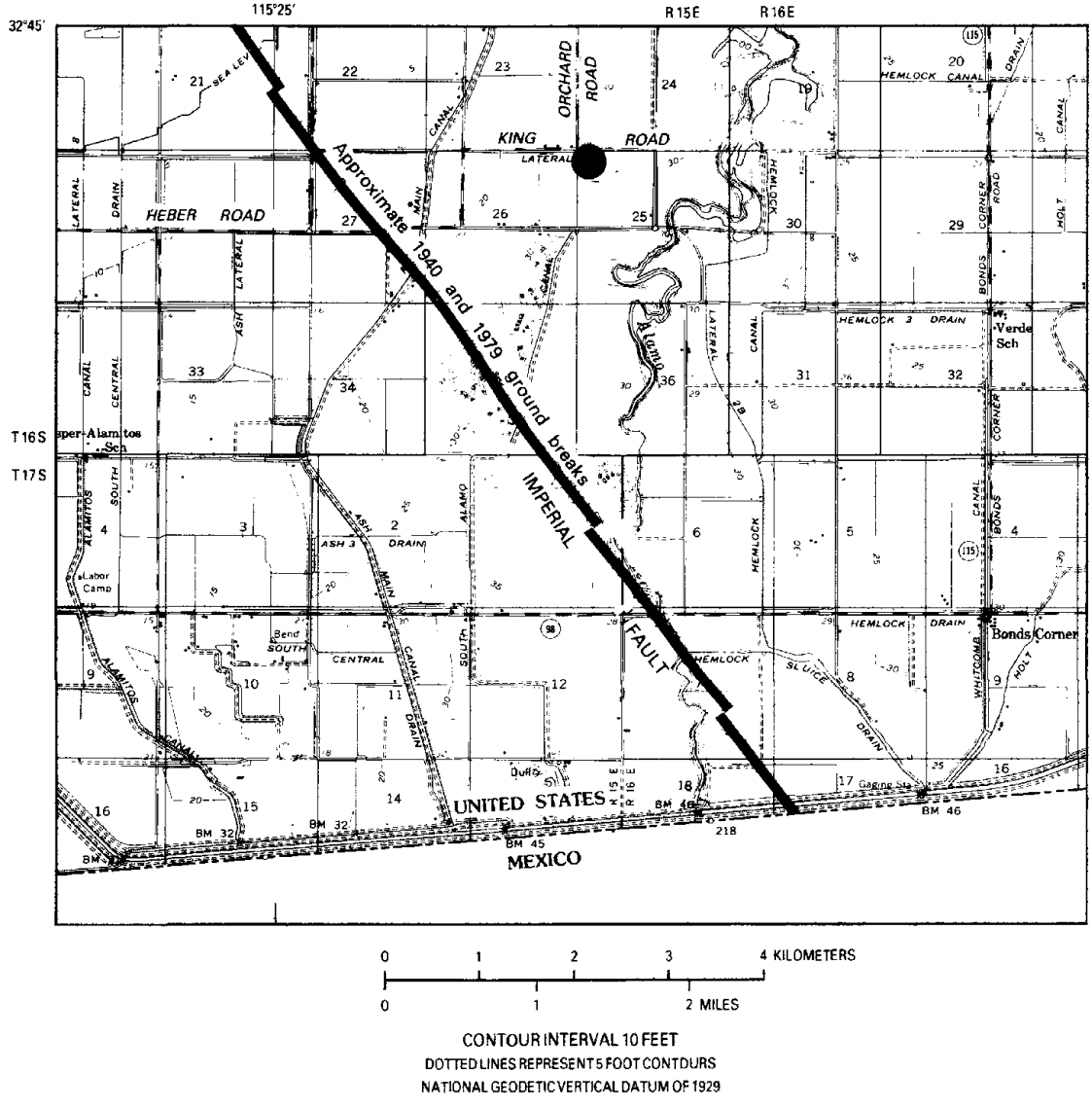

FIGURE 188.—Sandblow study area (dot) and ground rupturing along Imperial fault, southern California. Base from U.S. Geological Survey, Calexico 15-minute quadrangle, 1957.

layer, and continued upward through fine sand until it was ejected onto the ground surface. The source sand and water table were within 2 m of the ground surface.

2. Reactivation of the sandblows by aftershocks involved the same pathways of ejection. Truncation of flow laminations suggests a minimum of one reactivation period.
3. Sedimentary structures similar to those we observed have been documented within lacustrine deposits in other tectonically active areas and may have formed during prehistoric earthquakes.

FIGURE 189.—East-west-oriented sandblows, showing collapsed vents, incised drainage patterns on cones, and formation of secondary cones.

REFERENCES CITED

Hesse, Reinhard, and Reading, H. G., 1978, Subaqueous clastic fissure eruptions and other examples of sedimentary transportation in

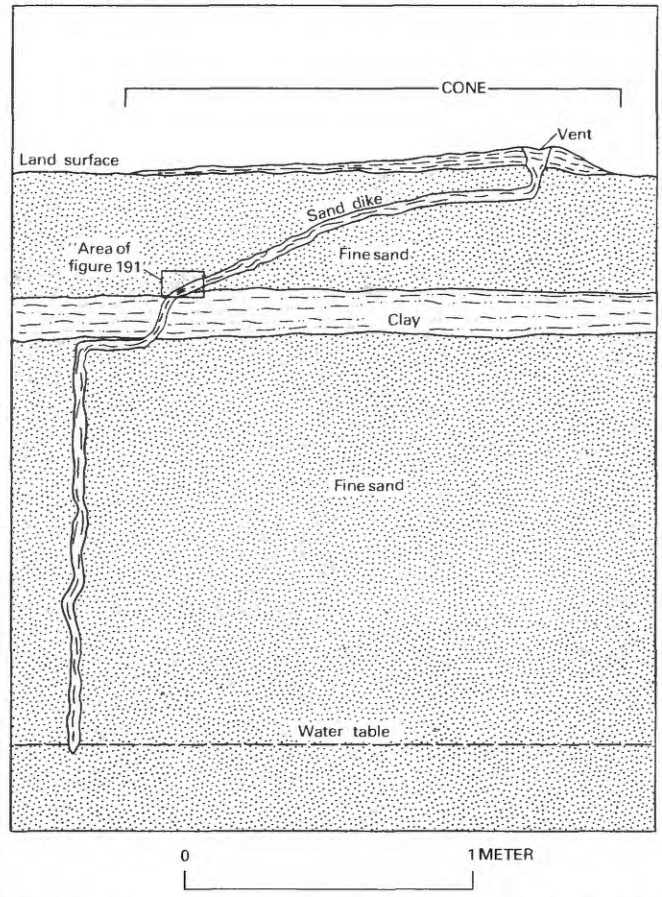

FIGURE 190.—Cross section of sandblow features observed within trench.

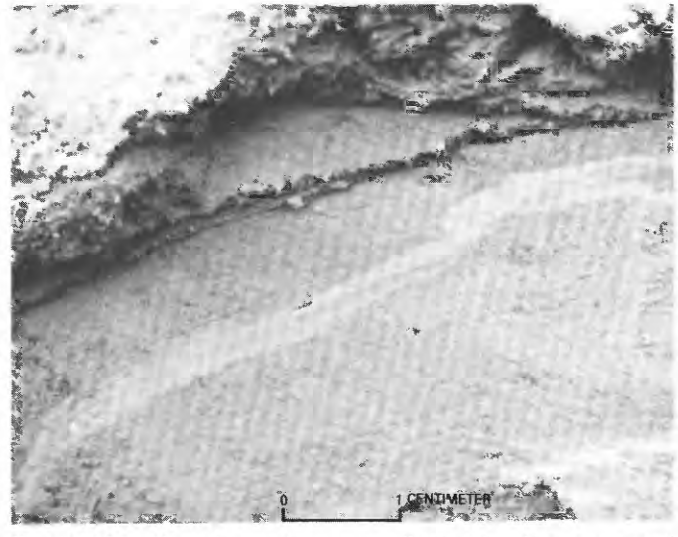

FIGURE 191.—Flow laminations in sandblow dike. Note truncated dark layers along margins.

the lacustrine Horton Bluff Formation (Mississippian), Nova Scotia, Canada, *in* Matter, Albert, and Tucker, M. E., Modern and ancient lake sediments: International Association of Sedimentologists Special Publication 2, p. 241–257.

Lamar, D. L., Muir, S. G., Merifield, P. M., and Reed, W. E., 1979a, Description of earthquake deformed sediments in Kern Lake, Kern County, California: Lamar-Merifield Technical Report 79–1, U.S. Geological Survey Contract 14–08–0001–16791, 44 p.

———1979b, Possible earthquake deformed sediments in Kern Lake, Kern County, California [abs.]: Geological Society of America Abstracts with Programs, v. 11, no. 3, p. 88.

Meisling, K. E., 1979, Possible emplacement history of a sandblow structure at Pallett Creek, California, *in* Abott, P. L., ed., Geological excursions in the southern California area: San Diego, Calif., San Diego State University, Department of Geological Sciences, p. 63–66.

Scott, R. F., 1974, Observations of sandblows: Pasadena, California Institute of Technology report, 24 p.

Sieh, K. E., 1978, Prehistoric large earthquakes produced by slip on the San Andreas fault at Pallett Creek, California: Journal of Geophysical Research, v. 83, no. B8, p. 3907–3939.

———1977, A study of Holocene displacements along the south-central reach of the San Andreas fault: Stanford, Calif., Stanford University, Ph. D. thesis, 219 p.

PRELIMINARY EVALUATION OF THE DISTRIBUTION OF SEISMIC INTENSITIES

By B. G. Reagor, C. W. Stover, S. T. Algermissen, K. V. Steinbrugge, Peter Hubiak, M. G. Hopper, and L. M. Barnhard,
U.S. Geological Survey

CONTENTS

ABSTRACT

The maximum modified Mercalli intensity (MMI) of the 1979 main shock is estimated at VII, although the Imperial County Services Building in El Centro was shaken by an intensity of IX. MMI's of VII were observed in Brawley, Calexico, El Centro, and Imperial, Calif. No study was undertaken in Mexico, but from the available data, the maximum MMI in Mexicali is believed to have been VII. Although the local magnitude and felt areas of the 1940 and 1979 Imperial Valley earthquakes were approximately the same, damage in 1940 was much greater than in 1979, probably because the duration of strong shaking was greater in 1940.

INTRODUCTION

The Imperial Valley is a well-known seismically active area in which at least 14 earthquakes with maximum modified Mercalli intensities (MMI) of VII or higher have occurred since 1906. The Imperial Valley earthquakes have shown a wide range of source characteristics and geologic and engineering effects: multiple ruptures, extensive surface faulting, liquefaction and other types of ground failures, and damage to buildings that vary widely in framing, materials, design, and age.

The 1979 earthquake strongly shook the Imperial Valley. In the United States, the "generally felt" land area was approximately 128,000 km^2. The tremor was felt as far away as Los Angeles, Calif.; Las Vegas, Nev.; Phoenix, Ariz.; and in Mexico. At least 70 people were reported injured as a result of the earthquake in the four California communities of Brawley, Calexico, El Centro, and Imperial.

The heavily damaged Imperial County Services Building in El Centro underwent shaking of intensity IX. An MMI of VII, however, characterizes the general level of damage to buildings, most of which were low rise, and to other structures within the Imperial Valley.

After the earthquake, questionnaires were distributed extensively in the United States to determine the approximate limits of the felt area, and we undertook a field reconnaissance within the epicentral area. This report summarizes the observed or reported earthquake effects and the intensities assigned to those communities where the earthquake was felt.

ISOSEISMAL MAP

Intensity questionnaires were distributed to postmasters and selected Government agencies within 425 km of the epicenter. The returned questionnaires were evaluated according to the MMI scale of 1931 (Wood and Neumann, 1931). The intensities assigned to locations from postmaster canvasses routinely reflect the maximum effects reported. Table 25 lists the rated intensities by State and city. These and other accounts from places where the event was not felt are the basis for the generalized isoseismals shown on the map (fig. 192). The MMI=VII isoseismal encompasses the towns of Brawley, Calexico, El Centro, and Imperial, Calif. An MMI of VII was estimated for Mexicali, Mexico, on the basis of press reports.

There were isolated felt reports from communities in the United States situated outside the contiguous felt area. Felt reports from such metropolitan communities as Las Vegas, Nev., and Phoenix, Ariz., were mostly from people in high-rise buildings.

The configuration of the felt area in the United States remarkably resembles the distribution of intensities

TABLE 25.—*October 15, 1979, earthquake intensities by State and city*

Location	Latitude N.	Longitude W.	MMI
Arizona			
Aguila	33.93°	113.18°	IV
Arlington	33.33°	112.77°	III
Bouse	33.93°	114.00°	IV
Bullhead City	35.12°	114.57°	IV
Chloride	35.40°	114.15°	II
Dateland	32.75°	113.62°	V
Ehrenberg	33.63°	114.50°	IV
Gadsden	32.55°	114.77°	IV
Gila Bend	32.93°	112.70°	II
Kirkland	34.43°	112.72°	III
Lake Havasu City	34.45°	114.37°	III
Mesa	33.41°	111.83°	III
Palo Verde	33.35°	112.68°	IV
Parker	34.15°	114.30°	V
Phoenix	33.50°	112.05°	V
Prescott	34.56°	112.46°	IV
Quartzsite	33.68°	114.23°	IV
Roll	32.75°	113.98°	IV
Salome	33.82°	113.62°	III
San Luis	32.48°	114.77°	V
Sasabe	31.52°	111.52°	III
Silver Bell	32.43°	111.52°	IV
Skull Valley	34.52°	112.67°	IV
Somerton	32.58°	114.73°	IV
Tacna	32.67°	114.00°	V
Wellton	32.65°	114.15°	V
Wendon	33.87°	113.50°	III
Wickenburg	33.98°	112.73°	IV
Wikieup	34.70°	113.60°	III
Yarnell	34.23°	112.75°	IV
Yuma	32.66°	114.65°	VI
California			
Aguanga	33.44°	116.85°	IV
Alhambra	34.14°	118.15°	IV
Alpine	32.83°	116.75°	IV
Amboy	34.55°	115.74°	IV
Anaheim	33.83°	117.91°	IV
Angelus Oaks	34.15°	116.98°	IV
Anza	33.56°	116.68°	IV
Apple Valley	34.50°	117.20°	III
Bard	32.78°	114.56°	IV
Beaumont	33.91°	116.98°	IV
Bellflower	33.90°	118.13°	III
Big Bear City	34.26°	116.84°	V
Blue Jay	34.25°	117.21°	II
Blythe	33.60°	114.61°	III
Bonita	32.65°	117.03°	V
Bonsall	33.28°	117.22°	IV
Boulevard	32.66°	116.26°	IV
Brawley	32.98°	115.51°	VII
Bryn Mawr	34.05°	117.23°	IV
Buena Park	33.88°	118.00°	IV
Burbank	34.18°	118.31°	IV
Cabazon	33.91°	116.78°	V
Calexico	32.67°	115.50°	VII
Calimesa	34.00°	117.06°	IV
Calipatria	33.13°	115.50°	V
Campo	32.60°	116.47°	V
Cardiff-by-the-Sea	33.02°	117.27°	V
Carlsbad	33.15°	117.33°	III
Cathedral City	33.76°	116.46°	IV
China Lake	35.66°	117.67°	V
Chino	34.00°	117.70°	IV
Chula Vista	32.61°	117.08°	V
City of Industry	34.03°	117.95°	IV
Claremont	34.10°	117.71°	III
Coachella	33.66°	116.16°	V
Colton	34.06°	117.33°	III
Corona	33.88°	117.56°	IV
Costa Mesa	33.65°	117.93°	IV
Covina	34.08°	117.90°	IV

TABLE 25.—*October 15, 1979, earthquake intensities by State and city*—Continued

Location	Latitude N.	Longitude W.	MMI
Crestline	34.23°	117.25°	IV
Culver City	34.01°	118.41°	IV
Cypress	33.83°	118.01°	IV
Dana Point	33.45°	117.71°	IV
Del Mar	32.95°	117.26°	IV
Desert Center	33.71°	115.40°	III
Dulzura	32.64°	116.78°	IV
Eagle Mountain	33.85°	115.48°	V
Earp	34.16°	114.29°	V
East Highlands	34.10°	117.16°	IV
El Cajon	32.78°	116.95°	IV
El Centro	32.79°	115.56°	VII
El Monte	34.05°	118.03°	III
El Toro	33.62°	117.69°	III
Encinitas	33.06°	117.28°	V
Escondido	33.10°	117.11°	IV
Etiwanda	34.13°	117.51°	IV
Fallbrook	33.38°	117.25°	IV
Fillmore	34.41°	118.91°	III
Fontana	34.10°	117.46°	III
Forest Falls	34.11°	116.90°	IV
Fountain Valley	33.71°	117.96°	III
Fullerton	33.86°	117.91°	IV
Garden Grove	33.78°	117.93°	IV
Gardena	33.90°	118.28°	III
Glamis	32.99°	115.07°	IV
Green Valley Lake	34.25°	117.08°	III
Hawthorne	33.91°	118.35°	IV
Heber	32.73°	115.53°	VI
Hemet	33.75°	116.96°	V
Highland	34.12°	117.23°	V
Holtville	32.80°	115.40°	VI
Huntington Beach	33.65°	118.00°	V
Idylwild	33.74°	116.71°	IV
Imperial	32.85°	115.55°	VII
Imperial Beach	32.55°	117.11°	IV
Indio	33.71°	116.21°	IV
Jacumba	32.61°	116.18°	V
Joshua Tree	34.13°	116.31°	III
Julian	33.07°	116.60°	V
La Jolla	32.83°	117.28°	IV
La Mesa	32.78°	117.03°	IV
La Puente	34.03°	117.95°	IV
La Quinta	33.67°	116.31°	V
Laguna Beach	33.53°	117.75°	IV
Laguna Niguel	33.50°	117.73°	V
Lake Elsinore	33.68°	117.33°	III
Lakeside	32.82°	116.89°	IV
Lakeview	33.83°	117.11°	III
Lakewood	33.83°	118.13°	IV
Lemon Grove	32.73°	117.03°	IV
Loma Linda	34.05°	117.28°	IV
Long Beach	33.78°	118.18°	III
Los Alamitos	33.81°	118.06°	IV
Los Angeles	34.05°	118.25°	IV
Lucerne Valley	34.42°	116.87°	IV
Lytle Creek	34.26°	117.50°	II
Mecca	33.57°	116.08°	IV
Mentone	34.06°	117.15°	IV
Midway City	33.76°	117.99°	IV
Mira Loma	34.01°	117.53°	III
Mission Viejo	33.59°	117.67°	IV
Montebello	34.00°	118.11°	IV
Moreno	33.93°	117.16°	IV
Morongo Valley	34.05°	116.58°	V
Mount Laguna	32.87°	116.41°	IV
Murrieta	33.55°	117.23°	IV
National City	32.66°	117.11°	IV
Needles	34.83°	114.60°	IV
Nestor	32.55°	117.09°	IV
Newport Beach	33.61°	117.93°	V
Niland	33.24°	115.51°	V
Norwalk	33.90°	118.08°	IV
Oak View	34.40°	119.28°	III

TABLE 25.—*October 15, 1979, earthquake intensities by State and city*—Continued

Location	Latitude N.	Longitude W.	MMI
Oceanside	33.20°	117.38°	III
Ocotillo	33.14°	116.13°	V
Pala	33.36°	117.08°	IV
Palm Desert	33.72°	116.37°	V
Palm Springs	33.81°	116.56°	IV
Palo Verde	33.43°	114.73°	V
Palos Verdes Peninsula	33.80°	118.39°	IV
Paramount	33.90°	118.16°	III
Parker Dam	34.28°	114.14°	IV
Pasadena	34.15°	118.16°	III
Patton	34.13°	117.21°	IV
Perris	33.78°	117.23°	III
Phelan	34.37°	117.59°	III
Pico Rivera	33.97°	118.12°	III
Pine Valley	32.82°	116.53°	IV
Pinon Hills	34.43°	117.64°	III
Plaster City	32.79°	115.85°	IV
Pomona	34.05°	117.71°	III
Potrero	32.61°	116.61°	IV
Poway	32.95°	117.03°	IV
Ramona	33.03°	116.86°	IV
Rancho Mirage	33.72°	116.39°	IV
Rancho Santa Fe	33.01°	117.20°	V
Redlands	34.06°	117.18°	V
Redondo Beach	33.82°	118.38°	IV
Reseda	34.19°	118.57°	III
Rialto	34.10°	117.36°	IV
Ridgecrest	35.63°	117.68°	IV
Ripley	33.52°	114.65°	V
Riverside	33.96°	117.36°	IV
Rosemead	34.10°	118.06°	IV
Running Springs	34.21°	117.17°	III
San Bernardino	34.10°	117.31°	V
San Diego	32.73°	117.16°	V
San Dimas	34.10°	117.83°	IV
San Jacinto	33.78°	116.96°	V
San Luis Rey	33.22°	117.34°	III
San Marcos	33.14°	117.19°	IV
Santa Ana	33.73°	117.85°	III
Santa Ysabel	33.11°	116.67°	IV
Santee	32.81°	116.93°	V
Seeley	32.79°	115.68°	V
Solano Beach	32.99°	117.27°	IV
South Gate	33.95°	118.21°	III
Stanton	33.81°	118.00°	III
Sun City	33.70°	117.28°	III
Sunnymean	33.93°	117.25°	III
Surfside	33.73°	118.08°	IV
Temecula	33.49°	117.15°	V
Thousand Palms	33.81°	116.39°	IV
Torrance	33.83°	118.31°	IV
Trabuco Canyon	33.66°	117.60°	IV
Twentynine Palms	34.13°	116.03°	IV
Valley Center	33.21°	117.07°	IV
Valyermo	34.38°	117.82°	III
Vista	33.20°	117.25°	IV
Warner Springs	33.28°	116.63°	V
Westminster	33.75°	118.00°	IV
Westmorland	33.05°	115.61°	V
White Water	33.90°	116.63°	IV
Whittier	33.98°	118.03°	IV
Wildomar	33.58°	117.23°	V
Wilmington	33.78°	118.27°	IV
Winchester	33.70°	117.10°	V
Winterhaven	32.72°	114.60°	IV
Yorba Linda	33.88°	117.81°	IV
Yucaipa	34.04°	117.04°	V
Nevada			
Las Vegas	36.18°	115.15°	IV

associated with the 1940 Imperial Valley earthquake (M_L=6.5; Kanamori and Jennings, 1978), which was assigned an MMI of X and had a felt area of 156,000 km^2 (Ulrich, 1941).

EARTHQUAKE EFFECTS AND DISTRIBUTION OF DAMAGE

The strength of ground shaking is believed to have been approximately the same in Brawley, Calexico, El Centro, and Imperial, Calif., the four communities in the United States most affected by the main shock and aftershocks. The pattern of damage associated with the 1979 earthquake is complex because many buildings in these four cities have been damaged by earlier earthquakes in the Imperial Valley. The susceptibility of many older buildings to damage in 1979 depended somewhat on their preearthquake conditions. This condition was commonly difficult to evaluate because the older buildings had not been repaired in any uniform manner, and their resistance to damage in 1979 varied greatly. The damage and intensity pattern is further complicated by the northwestward migration of aftershocks. Imperial and Brawley apparently were affected by several strong aftershocks that are known, from interviews with residents, to have caused additional building damage after the main shock. Apparently only minimal additional damage was caused in El Centro and Calexico by aftershocks. Very little damage to single-family dwellings was observed in any of the four cities. Wood-frame stucco dwellings, some as close as 30 m from the Imperial fault rupture, showed very minor damage.

The most heavily damaged modern building was the Imperial County Services Building in El Centro, a six-story reinforced-concrete frame and shear-wall structure designed under the 1967 Uniform Building Code. At the Imperial County Services Building the shaking was assigned an intensity of IX, although the damage to this building is not representative of the level of earthquake damage elsewhere in El Centro. Excluding this building, the most severe damage in Brawley, Calexico, El Centro, and Imperial was generally to low unreinforced-brick buildings and to a few low reinforced-concrete-frame buildings constructed before the 1940 El Centro earthquake. Many of the buildings appreciably damaged in the 1979 earthquake apparently were also damaged in 1940.

Earthquake damage and effects in the Imperial Valley varied greatly in Brawley, Calexico, El Centro, and Imperial. The damage caused by the earthquake and aftershocks consisted of partially collapsed unreinforced-brick walls; isolated instances of cracked or fallen cornices, parapets, and gables; a few damaged chimneys; display windows broken or shattered; plaster

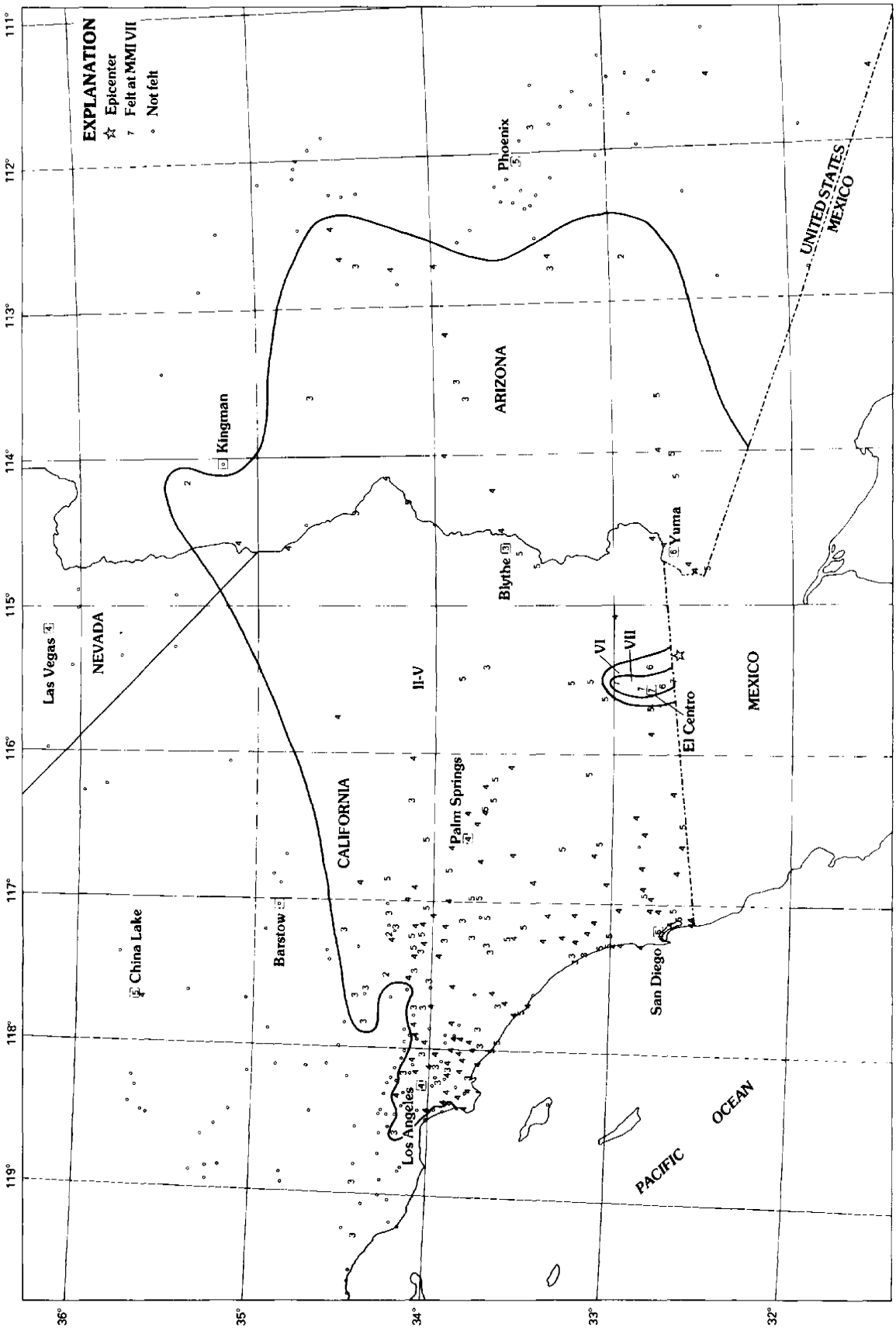

FIGURE 192.—Isoseismal map of 1979 Imperial Valley earthquake.

cracked and fallen; sections of suspended ceiling tiles with framework displaced or fallen; shelves and counters shifted or overturned and merchandise thrown from shelves in many stores; all types of furniture moved, and lighter furniture, bookcases, and table lamps overturned; pictures and mirrors fallen; and a considerable number of glassware, dishes, and small objects fallen and broken. In the older parts of the business districts, porticoes were extensively cracked and their columns damaged.

The reactions of people to the earthquake, especially in the towns, ranged from moderate alarm to great fright. A Federal Aviation Administration employee who was in downtown El Centro at the time of the main shock described the effects of the motion thus: "The ground rose and fell about a foot, and I had to hang onto a parked car for support to stand. Buildings and poles swayed back and forth. A parked car nearby rolled backward when the braking mechanism failed." Several people said that a loud roar preceded the earthquake. Some people felt the quake in moving vehicles. Many people found it hard to stand or walk, and, if sitting, had difficulty rising.

Effects of the earthquake in El Centro, Brawley, Imperial, and Calexico, Calif., and press reports from Mexicali, Mexico, are summarized below.

INTENSITY IX

Although the earthquake damage in El Centro generally indicates an MMI of VII, the Imperial County Services Building (ICSB), on Main Street between Ninth and 11th Streets, underwent shaking of intensity IX. This six-story reinforced-concrete frame and shear-wall structure, completed in 1971 (Rojahn and Ragsdale, 1980), was designed to be earthquake resistant. Though severely damaged, the building did not collapse. The major damage to the building was failure of the four reinforced-concrete support columns on the east side of the building (fig. 193): The concrete at the base of the columns was shattered, and the vertical reinforcing bars were severely bent. Partial collapse of the columns allowed the east end of the building to sag about 30 cm (Rojahn and Ragsdale, 1980). In the upper levels of the building, the south exterior wall was extensively cracked near the window frames. Also, in several places the floors, walls, and ceilings partially separated. Fallen suspended ceiling tiles, damage to interior walls, and office furniture shifted or overturned were some of the effects reported inside the building.

In contrast to this extensive damage to the ICSB, the Sombrero Cafe, across the street and southeast of the building, was not damaged. This single-story cafe is built of concrete blocks with a stucco veneer. Only a few dishes were broken, and potted plants atop a 2.4-m partition were not shaken down. The County Courthouse, across the street and south of the ICSB, had a few plaster cracks in the corners of rooms at the ceiling connection. Cracks appeared at the top of most pillars where they joined the ceiling. Large horizontal cracks occurred in the wallboard in the County Clerk's office. Pictures fell from walls, and flowerpots were toppled.

INTENSITY VII

EL CENTRO

In the older business district of El Centro, most building damage was along Main and State Streets between Fourth and Eighth Streets, and in the 400 and 500 blocks on Broadway. The newer shopping centers along Imperial Avenue and to the west of the older business district appeared to have sustained only minor damage, such as small plaster cracks and some fallen plaster, merchandise damage due to fall from shelves, and displacement and occasional fall of suspended ceiling tiles in places where the framework was slightly bent or hanging down.

Hoffman Music Store (534 Main St.).—The brick-and-stucco-veneer storefront over this building was extensively fractured.

Deluxe Cleaners (119 N. Fifth St.).—This two-story wood-frame and brick building was damaged by partial collapse of the west-facing parapet and by fall of the brick veneer from the second-story walls. The roof over the second story was reported to have collapsed. The upper story had been condemned before the earthquake.

Mayan Hotel (595 State St.).—This two-story steel-frame and brick building with stucco veneer was moderately damaged. Along the length of the east wall, there was about 2.5 cm of separation at the connections of the ceilings and floors. There was also much fallen and cracked plaster from ceilings and walls in all the rooms and in the lobby.

Gio's Mobile Home Estates (Lincoln Ave.).—Many of the nearly 90 mobile homes were damaged when they were shaken from their metal support stands. A concrete-block masonry fence, running east-west, was partly thrown down at the south entrance.

Other effects in and around El Centro.—North of El Centro, an oil tank split 15 cm along a seam near the base at the Southern Pacific Pipe Line tank farm. Underground waterpipes were broken in many places; however, utilities were interrupted for only a short time. Asphalt roads cracked, buckled, and slumped in many places, especially where the fault trace crosses the roadway.

BRAWLEY

Many buildings were damaged in Brawley's business district along Main Street between the 500 and 900

blocks. Further damage was caused by aftershocks that occurred near midnight on October 15. These aftershocks, according to several people, were responsible for additional building damage, window breakage, and the shaking of large quantities of merchandise from store shelves.

McMahan's Furniture Store (500 block).—A crack about 15 m long and 2.5 cm wide opened in the west wall. Concrete columns that supported the balconies were moderately cracked at the ceiling connection. Ceiling tiles were dislodged, and some fell. The dry wall was split, and one section was thrown down from the south wall. The building cornice cracked but did not fall. The east side of a metal sign that covered the upper level of the storefront was shaken down.

Newberry Department Store (500 block).—The west brick wall was knocked away from the roof and partially collapsed; 12 wooden support trusses were broken. Bricks fell from the roof and caused much damage inside the store.

National Department Store (600 block).—The roof collapsed somewhat. Fallen bricks caused dry-wall ceilings to split and fall. The concrete floor in the storage area was cracked in a few places. Metal shelves that were bolted to concrete walls were thrown down.

Fire Station (800 block).—This building was a reinforced-concrete structure with a roof supported by wooden beams. A few beams were reported to be cracked

FIGURE 193.—Partial collapse of four columns along east side of Imperial County Services Building. Photograph by Peter Hubiak.

along their length. In the firehouse living quarters, a metal support bracket for one of the east-west beams was slightly twisted. A metal hose rack bolted to the west wall was thrown down. Roof tiles were dislodged, and some fell. During the main shock, according to one fireman, the trucks inside the garage were shaken so strongly that they nearly touched each other.

Victory Market (900 block).—This one-story building was a steel-frame and brick structure. The northeast corner of the east brick wall partially collapsed. There were open cracks 2.5 to 5 cm wide in the west brick wall in several places. In the middle of the 900 block the portico roof partially collapsed. In this area, according to the owner of the Victory Market, some of the buildings had been condemned before the earthquake.

200 block, G Street.—Several homes were damaged. A stucco-covered chimney on the west side of one house was shifted about 5 cm from the wall. An attached wooden porch roof was shaken down from a wood-frame house across the street to the north. On Third Street, one block south, a few chimneys were broken at the roofline, or else the upper tiers of bricks were thrown down to the west.

New River Bridge (on State Highway 86).—The abutments at each end of the bridge were cracked and chipped to the extent that the reinforcement bars were exposed at bridge level. Many of the support columns were cracked at the bridge-deck connection. The asphalt road settled about 12.5 cm relative to the bridge.

An elevated water tower 2.5 km south of Main Street on Dogwood Road collapsed.

IMPERIAL

Several buildings were damaged in the 100 block of Imperial Avenue in Imperial.

Lydia's Cafe (133 S. Imperial).—This one-story wood-frame and brick structure was damaged by partial collapse of the south wall. Part of the roof was knocked out.

Imperial Hardware Store (125 Imperial).—The rear wall of this brick building was severely cracked, and the top part of the building was pushed to the west.

The police chief reported that in the residential area of Imperial, many stucco homes moved on their foundations and others had lateral cracks near their foundations. A masonry fence supporting a carport partially collapsed. Chimney bricks were loosened. At the police station, the plastered wall between the chief's office and the jail area cracked vertically and opened to a width of 2.5 cm. The police chief stated, "I was in a doctor's office at the time of the initial tremor, and I could not get up out of the chair due to the building moving in all directions at once. A loud roaring sound preceded the earthquake."

CALEXICO

Several buildings were damaged in Calexico in the business district along Second and Third Streets. Many of the storefronts along Second Street exhibited large vertical and horizontal cracks in the stucco walls.

McMahan's Furniture Store (104 E. Second St.).—Partial collapse of the second-story west brick wall and parapet caused the roof of the portico to cave in. The upper story had been condemned before the earthquake.

International Music Store (Third St. and Paulen).—The roof caved in when part of the east brick firewall collapsed.

Other effects in Calexico included fallen chimneys, chimney bricks loosened or slightly displaced, and broken underground pipes.

MEXICALI

The main airport building east of the city was extensively damaged; minor damage occurred to some Government buildings. Walls fell in some houses. Zap's Shoe Store was heavily damaged from bricks falling from the storefront and from shattering of the display windows.

INTENSITIES LOWER THAN VII

Intensity VI.—Large cracks appeared in plaster or stucco interior and exterior walls; foundations cracked; a few windows cracked, and some broke; interior walls separated from ceilings or floors; heavy furniture moved; hanging pictures fell.

Intensity V.—Furniture moved; light furniture overturned; a few windows cracked; small objects were overturned and broken; hanging pictures were knocked out of place; small or fine plaster cracks formed; hanging pictures fell.

Intensity IV.—Windows, doors, and dishes rattled; buildings creaked or trembled strongly; liquid was disturbed in small containers; standing vehicles rocked slightly to moderately; hanging pictures were knocked out of place; small objects moved.

Intensity III.—Hanging objects and pictures swung; buildings trembled slightly.

Intensity II.—Felt.

DISCUSSION

The 1979 Imperial Valley earthquake is here assigned a maximum MMI of VII, although a single building in El Centro, the Imperial County Services Building, underwent shaking of intensity IX. The maximum intensity in Brawley, Imperial, and El Centro, taking into account the effects of aftershocks, was probably near the upper limit of MMI VII. The maximum intensity in Calexico was also VII, although the intensity of

TABLE 26.—*Comparison of the 1940 and 1979 Imperial Valley earthquakes*

Date	M_l	Maximum acceleration at El Centro station 9 (g)	Maximum MMI	Approximate length of faulting (km)	Approximate maximum slip (m)	Duration of shaking $\geq 0.1\,g$ (s)[1]
1940	[2]6.5	[3]0.36	[4]IX	[5]65	[5]5.9	[6]24.9
1979	[7]6.6	[8]0.40	VII	[9]31	[9]0.8	[8]7.4

[1]Bolt (1973).
[2]Kanamori and Jennings (1978).
[3]California Institute of Technology (1976).
[4]Estimated from Ulrich (1941).
[5]Richter (1958).
[6]McGuire and Barnhard (1979).
[7]Seismological Laboratory, California Institute of Technology.
[8]Matthiesen and Porcella (this volume).
[9]Sharp and others (this volume).

ground shaking there probably was slightly less than in Brawley, Imperial, and El Centro.

The 1940 Imperial Valley earthquake (Kanamori and Jennings, 1978) was assigned a maximum MMI of X by Ulrich (1941). To compare the effects of the 1940 and 1979 earthquakes, we here consider the maximum intensity of the 1940 earthquake as IX because the effects characteristic of MMI=X were observed in 1940 in only a few places. Table 26 summarizes our comparison between the 1940 and 1979 earthquakes. Although the maximum horizontal accelerations, at least in El Centro, did not markedly differ in the two earthquakes (table 26), the bracketed duration of shaking of 0.1 g or greater differs by a factor of at least 3. Thus, the differences in the damage (and maximum intensity) and in the areas shaken at intensities VII or higher apparently reflect the greater duration of shaking during the 1940 main shock.

REFERENCES CITED

Bolt, B. A., 1973, Duration of strong ground motion: World Conference on Earthquake Engineering, 5th, Rome, Italy, 1973, Proceedings, v. 1, p. 1304–1313.

California Institute of Technology, 1976, Strong-motion earthquake accelerograms index volume: Pasadena, California Institute of Technology, Earthquake Engineering Research Laboratory Report EERL 76–02, 42 p.

Kanamori, Hiroo, and Jennings, P. C., 1978, Determination of local magnitude from strong-motion accelerograms: Seismological Society of America Bulletin, v. 68, no. 2, p. 471–485.

McGuire, R. K., and Barnhard, T. P., 1979, Four definitions of strong-motion duration: Their predictability and utility for seismic hazard analysis: U.S. Geological Survey Open-File Report 79–1515, 115 p.

Richter, C. F., 1958, Elementary seismology: San Francisco, W. H. Freeman, 768 p.

Rojahn, Christopher, and Ragsdale, J. T., 1980, Strong-motion records from the Imperial County Services Building, El Centro, *in* Leeds, D. J., ed., Imperial County, California, earthquake, October 15, 1979: Berkeley, Calif., Earthquake Engineering Research Institute reconnaissance report, p. 173–184.

Ulrich, F. P., 1941, The Imperial Valley earthquake of 1940: Seismological Society of America Bulletin, v. 31, no. 1, p. 13–31.

Wood, H. O., and Neumann, Frank, 1931, Modified Mercalli intensity scale of 1931: Seismological Society of America Bulletin, v. 21, no. 4, p. 277–283.

SEISMIC-INTENSITY STUDIES IN THE IMPERIAL VALLEY

By ROBERT NASON,
U.S. GEOLOGICAL SURVEY

CONTENTS

ABSTRACT

The seismic-intensity pattern of the earthquake has been investigated in detail, using the seismic disturbance of grocery, liquor, and furniture stores in different towns as a special intensity indicator. The store disturbances indicate that: (1) the seismic disturbance from the main shock was of modified Mercalli intensity (MMI) VII in the central region; (2) the seismic intensity was approximately uniform throughout the central region, except to the north of Brawley, Calif., where it was lower; and (3) the seismic-intensity values determined by the store-disturbance technique correlate well with the peak-acceleration values of instrumental recordings—0.12g for MMI=VI, and 0.25 g for MMI=VII.

INTRODUCTION

The purpose of the investigation reported here was to determine accurate and reliable ratings of seismic intensity in the central region of the 1979 Imperial Valley earthquake. These ratings of seismic intensity can then be compared with the many instrumental recordings of ground motion during this earthquake to ascertain which characteristics of strong ground motion are most important for earthquake damage.

The seismic-intensity ratings of this study are based mainly on the disturbance of items in grocery, liquor, and furniture stores rather than on the damage to buildings. The items in stores generally are more uniform than the construction of buildings and thus constitute a more reliable indicator for comparison from place to place. Most of the data reported here are from grocery and liquor stores, and the rest are from furniture stores and libraries. The damage to buildings and other features of intensity were investigated by Reagor and others (this volume), Real (this volume), and Wosser and others (this volume).

The intensity ratings were compared with the peak accelerations recorded by instruments for the main shock (11 localities) and one aftershock (1 locality). Many of the instruments located in small shelters are effectively free field instruments, considered more reliable than those inside buildings that might distort the signals.

SEISMIC INTENSITY

The seismic-intensity scale is intended to measure the overall strength of earthquake shaking in terms of the severity of disturbance. Which characteristics of the earthquake strong motion are most important for the disturbance and damage is unknown. Accurate determination of local seismic intensities with strong-motion instruments should help to determine which aspects of ground motion are most significant for earthquake damage.

Commonly, seismic-intensity ratings are based mainly on the damage to buildings. The use of buildings necessarily involves an evaluation of their earthquake resistance, and such an evaluation will be unreliable insofar as there are significant differences in the design or materials of different buildings; therefore, other indicators of seismic intensity were sought in this study. For uniformity and reliability, the intensity indicators should be widespread and comparable to each other at each of the different localities.

The disturbance of loose items in grocery, liquor, and furniture stores provides a reliable indicator of the intensity of the ground motion. Loose items in these stores act as accidental "seismoscopes." In addition, store disturbances are already factors in the existing seismic-intensity scales, and so these disturbances can easily be correlated with existing intensity scales.

For this study, I examined grocery, liquor, and furniture stores that had their displays at ground levels in low buildings. The central areas of such stores are away from the walls, and so the results there are not significantly influenced by the variable seismic action of the buildings themselves. Information on the disturbance in the stores was collected by interviewing store personnel in the days after the earthquake. In most localities, several different stores were visited, and the results from individual stores in a given town were generally similar. In addition, the store personnel commonly could describe the disturbances from separate strong aftershocks because the main-shock disturbance was ordinarily cleaned up rapidly.

INTENSITY RATING OF STORE DISTURBANCE

GROCERY AND LIQUOR STORES

The levels of disturbance in grocery and liquor stores, and the equivalent ratings on the modified Mercalli intensity (MMI) scale (Wood and Neumann, 1931; Richter, 1958), are:

1. *No disturbance.*
2. *Light disturbance.*—A few items are shifted in their position or fall onto the floor. MMI=V.
3. *Mild disturbance.*—The fall of items is common in the store, but the store walkways are not blocked. MMI=VI.
4. *Much disturbance.*—The floor is covered with fallen items, and the store walkways are blocked. Estimated MMI=VII.
5. *Great disturbance.*—In addition to the floor being covered with fallen items, most of the shelves and fixtures are shifted sideways on linoleum or concrete floors. Estimated MMI=VIII.

The seismic-intensity ratings for MMI=V and VI are taken directly from the original scale (Wood and Neumann, 1931; Richter, 1958). The estimation of MMI=VII for "much disturbance" is based on the damage in Calexico and El Centro (fig. 194), where the fall of a few parapets was also noted (rated as MMI=VII in the description by Richter, 1958). The estimated MMI=VIII for "great disturbance" in grocery and liquor stores is based on a correlation of the store disturbance in Brawley with much disturbance of furniture in Brawley from an aftershock. The disturbance of furniture in Brawley was much greater than that in Calexico or El Centro, where MMI=VII, and so the disturbance at Brawley is tentatively estimated at MMI=VIII (subject, of course, to future correction).

FURNITURE STORES

The general levels of disturbance in furniture stores are:

1. *No disturbance.*
2. *Mild disturbance.*—Such tall items as lamps, clocks, or tall cabinets are shifted or overturned, and a few heavy shelves are shifted on hard floors, but such heavy furniture as tables and sofas is not shifted on carpeted floors.
3. *Much disturbance.*—Most heavy furniture is shifted on hard floors, and many or most pieces of heavy furniture are shifted on carpeted floors.

The intensity ratings of these levels of disturbance are best determined by careful correlation with other types of damage. For example, in both Calexico and El Centro the disturbance of shelf items and the fall of a

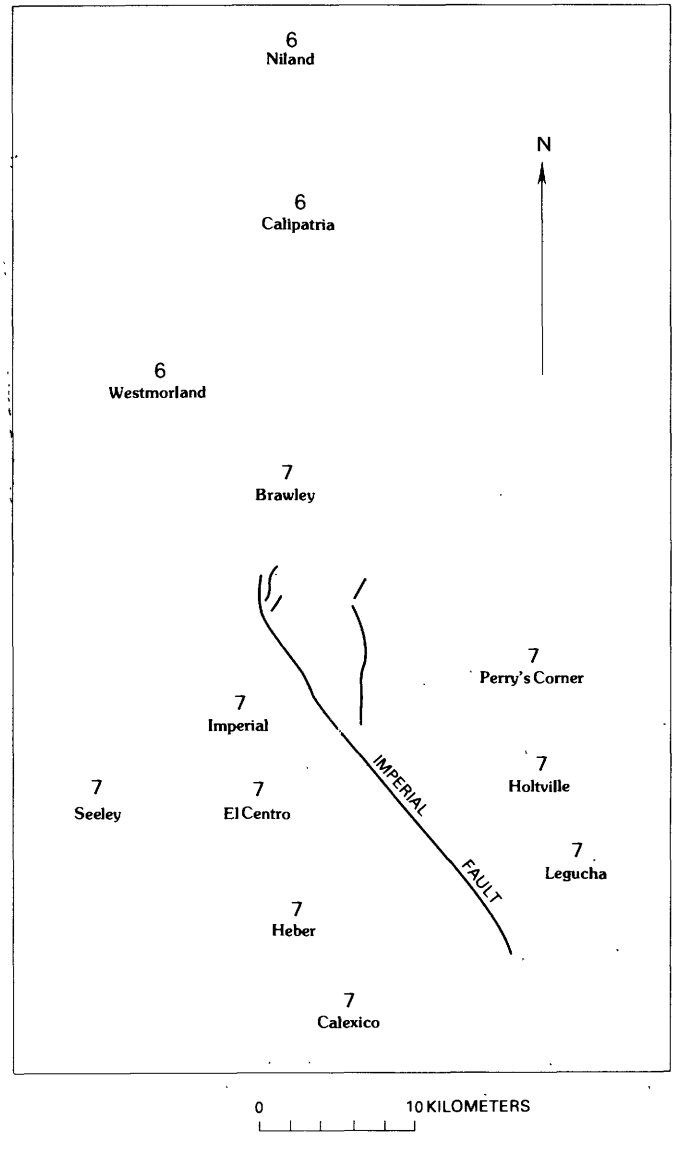

FIGURE 194.—Seismic-intensity ratings of October 15 main shock, using store-disturbance technique for evaluating modified Mercalli intensity. All ratings are at geographic location of communities. Aftershocks not included.

few parapets indicates an MMI of VII. However, there was only mild disturbance of furniture in El Centro, and little or no disturbance of furniture at the furniture store in Calexico, although the store is inside a building from which part of the parapet fell.

This correlation tentatively indicates the following seismic-intensity ratings from furniture disturbance: "no disturbance" is an MMI of VII or less, "some disturbance" is estimated at MMI=VII, and "much disturbance" is estimated at MMI=VIII. These intensity ratings of furniture disturbance are somewhat higher here than those in the current MMI scale, which give a lower rating to the amount of furniture disturbance than is indicated by the correlation. For instance, the description by Richter (1958) correlates the fall of a few parapets at an MMI of VII with much disturbance of furniture, but observations at Calexico indicate very little disturbance of furniture inside a building from which part of the parapet fell.

LIBRARIES

Useful information can also be obtained from the disturbance of books and shelving in libraries. The types of disturbance in a library include the fall of books from shelves, the shifting or fall of unbraced bookshelves, and the shifting or fall of braced or anchored bookshelves. However, because the details of shelving vary widely in different libraries, library disturbances are not so uniform and reliable as store disturbances.

OBSERVATIONS

MAIN SHOCK, CENTRAL AREA

Brawley.—The main shock caused much disturbance in a grocery store and a liquor store, and mild disturbance in a furniture store (the additional disturbance during a strong aftershock is described later). MMI=VII.

Calexico.—There was much disturbance at five grocery stores, but little or no disturbance in a furniture store inside a building from which the parapet fell. MMI=VII.

Calipatria.—There was mild disturbance at a grocery store. MMI=VI.

El Centro.—There was much disturbance in four grocery stores (the stores on the east side of El Centro had approximately the same disturbance as on the west side of El Centro), and mild disturbance at a furniture store near the damaged Imperial County Services Building (such heavy pieces of furniture as tables and sofas were not noticeably shifted on the carpeted floor of the furniture store). At the library, many books fell, several bookcases fell over, and some anchored bookshelves shifted and pulled braces out of the wall. MMI=VII.

Heber.—There was much disturbance at two grocery stores. MMI=VII.

Holtville.—There was much disturbance at two grocery stores and a liquor store, and at the library many books fell, but anchored bookshelves did not shift. MMI=VII.

Imperial.—There was much, perhaps great, disturbance at a grocery store. At the library most of the books fell, and several bolts supporting the bookshelves were broken. MMI=VII or more.

Imperial Valley College.—At the library many books fell, and several bookshelves were overturned. MMI≃VII (the damage resembled that at the El Centro library).

Lechuga Store.—There was much disturbance in a small grocery store. MMI=VII.

Niland.—There was mild disturbance in a grocery store. MMI=VI.

Perry's Corner.—There was much or great disturbance at a small grocery store. MMI=VII or more.

Seeley.—There was much disturbance at two grocery stores. MMI=VII.

Westmorland.—There was mild disturbance at two grocery stores and a liquor store. MMI=VI.

MAIN SHOCK, SURROUNDING REGION

Campo (95 km west of the earthquake fault rupture).—There was light disturbance at the grocery store and no disturbance at the library. MMI=V.

Coachella (100 km northwest of the earthquake fault rupture).—There was light disturbance at a supermarket. MMI=V.

Palm Springs (135 km northwest of the earthquake fault rupture).—There was light disturbance at a few stores and no disturbance at the library. MMI=V.

Yuma (70 km east of the earthquake fault rupture).—There was light disturbance in a few grocery stores and in a liquor store. MMI=V.

AFTERSHOCKS

Brawley (evening of October 15, after 11 p.m. P.s.t.).—There was great disturbance at a grocery store and at a liquor store, and much disturbance in a furniture store. At the library most books fell, and unanchored heavy bookshelves and card catalogs shifted on the concrete floor. MMI≃VIII.

Calexico.—There was no disturbance at grocery stores from aftershocks.

Calipatria.—There was light disturbance of groceries from aftershocks at 4:30 p.m. P.s.t. October 16 and at 3:45 p.m. October 17. MMI=V for each of the aftershocks.

El Centro.—There was light disturbance of groceries from aftershocks during the night of October 15 and at

approximately 4:30 p.m. P.s.t. October 16. MMI=V for each of the aftershocks.

Heber.—There was light disturbance of groceries during the night of October 15. MMI=V.

Holtville.—There was light disturbance of groceries at approximately 3:45 p.m. P.s.t. October 17. MMI=V.

Perry's Corner.—There was mild disturbance of groceries from an aftershock during the night of October 15. MMI=VI.

Seeley.—There was light disturbance of groceries just before midnight on October 15. MMI=V.

Westmorland.—There was light disturbance of groceries from aftershocks during the night of October 15 and at 4:30 p.m. P.s.t. October 16. MMI=V.

COMPARISON OF SEISMIC INTENSITY AND PEAK ACCELERATION

The data on seismic intensities can be compared directly with the measurements from strong-motion instruments in seven localities. The seismic intensities were determined by using only one main criterion, the grocery-store disturbance, which was chosen because it should be highly reliable as an indicator of the seismic shaking in the different places. The grocery-store criterion is well determined at each of the instrument-comparison localities, except at Imperial Valley College, where the comparison with other localities is based on the disturbances in the library.

It is not known which of the characteristics, or parameters, of earthquake strong motion are most important for earthquake disturbance and damage and are thus likely to be related to the seismic intensity. Possibilities include: the average or peak values of particle acceleration, velocity, or displacement; the earthquake duration; the number of cycles above some threshold value; the cumulative energy; or possibly some combination of these parameters. Earthquake shaking of short duration may differ significantly from shaking of long duration.

One parameter commonly used with strong-motion records is the peak-acceleration value (horizontal), which is quickly and easily obtained from the instrumental recordings. Peak accelerations for records of the earthquake, reported by Matthiesen and Porcella (this volume), are listed in table 27 along with seismic-intensity values and are plotted together in figure 195. The acceleration value for El Centro was obtained from a free-field instrument near the Imperial County Services Building.

In localities where the strong-motion instruments did not trigger, the peak acceleration was probably less than 0.01 *g* (Matthiesen and Porcella, this volume). In localities of MMI=IV (Reagor and others, this volume), most strong-motion instruments did not trigger, and so an MMI of IV correlates with a peak acceleration of less than 0.01 *g*.

TABLE 27.—*Correlation of seismic-intensity and peak-acceleration measurements*

[Strong-motion instruments were within 5 km of store-disturbance locations]

Station	Location	Peak acceleration (*g*)
	MMI=V	
5061	Calipatria	[1]0.02
----	Coachella	([2])
C284	Palm Springs	.02
2316	Yuma	.03
	MMI=VI	
5061	Calipatria	0.13
C23	Niland	.10
C900	Westmorland	.11
	MMI=VII	
5060	Brawley	0.22
5053	Calexico	.28
5154	El Centro	.24
5055	Holtville	.26
5028	Imperial Valley College	.52

[1]Aftershock. [2]Not triggered.

In the four localities of MMI=V, the peak accelerations ranged from less than 0.01 *g* (not triggered) to 0.03 *g*. In the three localities of MMI=VI, the peak acceleration values were approximately 0.12 *g* (0.10–0.13 *g*). At MMI=VII, four of the sites had peak acceleration values (horizontal) of approximately 0.25 *g* (0.22–0.28 *g*), and one site had a larger value of 0.52 *g* (Imperial Valley College). Several other instrument sites had peak acceleration values of from 0.3 to 0.8 *g*, but reliable intensity ratings could not be made for them using the store-disturbance technique. It is not known whether the seismic intensity was higher at those sites, but it may not have been, because the seismic intensity at the fault zone itself was only MMI=VII (Real, this volume).

An additional comparison between seismic intensity and instrumental measurements was obtained from the August 6, 1979, Coyote Lake, Calif., earthquake at Gilroy, Calif., where there was only mild disturbance of furniture on the carpeted floor of a furniture store (MMI=VII). At three free-field instrument sites (stations 2, 3, and 4) in the valley 3 km south and 3 km east of Gilroy, the peak (horizontal) acceleration values were 0.26, 0.27, and 0.26 *g*, respectively (Porcella and others, 1979).

1940 EARTHQUAKE DAMAGE

An earthquake of similar body-wave magnitude that occurred along the same segment of the Imperial fault on May 18, 1940, caused significant damage and involved much larger fault slippage than the 1979 earth-

quake—more than 4 m of horizontal fault slip near the United States-Mexican border, and 20 km of fault rupture south of the border where there was no movement during the 1979 earthquake (Richter, 1958). Damage reports on the 1940 earthquake, given here for comparison with the 1979 earthquake, are from the reports by Ulrich (1941), Neumann (1942), Richter (1958), the Los Angeles Times (1940a, b) and the San Diego Union (1940a, b).

Brawley.—"The principal visible damage * * * took place during an aftershock" 1 hour after the main shock (Richter, 1958, p. 489). This aftershock was of magnitude 5.5 (Hileman and others, 1973). "At least half the buildings in Brawley's business district * * * may have to be entirely reconstructed.

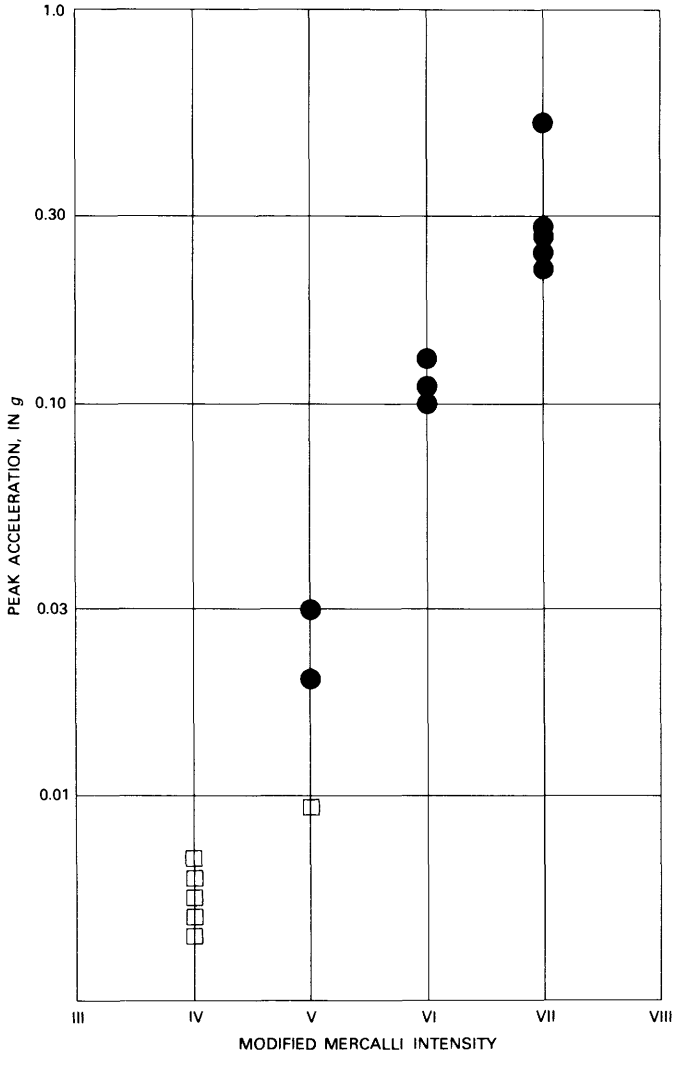

FIGURE 195.—Correlation of seismic-intensity ratings with peak acceleration values. Squares represent data from instruments that did not trigger, for which peak acceleration was probably less than 0.01 *g*. Circles indicate data points listed in table 27.

* * * The shock slipped scores of homes from their foundations and toppled almost every chimney," and the wooden Woodrow Wilson Hotel collapsed (San Diego Union, 1940b). The seismic intensity of the earthquake sequence (main shock plus aftershock) was apparently MMI=IX, although it is not known how much of the damage was from either the main shock or the aftershock.

Calexico.—In Calexico, "one building was damaged appreciably and a number of others showed cracks. * * * Chimneys were twisted and cracked" (Neumann, 1942). The building and chimney damage indicates an MMI of VII.

Calipatria.—That dishes were broken in 1940 indicates an MMI of apparently VI.

El Centro.—"One outer wall of each of three buildings has partly fallen" (Los Angeles Times, 1940a); "in the residential area, chief damage was broken windows and toppled chimneys" (Los Angeles Times, 1940b). Because most damage was to old brick buildings, the MMI was probably VII.

Heber.—That "some chimneys fell; others were twisted" (Neumann, 1942) indicates an MMI of VII.

Holtville.—That "a few walls were thrown down" in the business district and "chimneys * * * were thrown down" (Neumann, 1942) indicates an MMI of VII or VIII.

Imperial.—"About 10 older buildings [were] leveled" (San Diego Union, 1940a). Afterward, an announcement by the city of Imperial that "all its old buildings of soft brick and lime mortar must come down" (Los Angeles Times, 1940b) indicates that many buildings of weak construction had not collapsed in the earthquake. The MMI was either VIII or IX.

Westmorland.—MMI=IV (Neumann, 1942). The seismic intensity in Calipatria and Westmorland, 10 to 20 km north of Brawley, was much lower than in Brawley for the 1940 earthquake, as was also the case for the 1979 earthquake.

CONCLUSIONS

1. Earthquake disturbance in grocery, liquor, and furniture stores provides a reliable and uniform indicator for evaluating the seismic intensity.
2. On the basis of the store-disturbance technique, the MMI for the 1979 main shock was approximately VII everywhere in the central Imperial Valley south of Brawley.
3. The seismic-intensity rating, based on store disturbance near the damaged Imperial County Services Building in El Centro, was MMI=VII.
4. A strong aftershock during the night of October 15 caused greater disturbance at Brawley than the main shock.
5. The instrumentally measured peak accelerations

correlate well with the seismic-intensity ratings of this investigation: an MMI of VII correlates with a peak acceleration of 0.25 g.

6. The seismic-intensity ratings for the 1940 earthquake resemble those for the 1979 earthquake in the southern Imperial Valley, at Calexico and El Centro, even though the fault slippage near Calexico and El Centro was much greater in 1940 than in 1979.
7. The seismic-intensity ratings in the northern Imperial Valley region at Brawley and Imperial were apparently greater during the 1940 earthquake than during the 1979 earthquake. Interestingly, at Brawley the main damage in both 1940 and 1979 occurred during aftershocks.

REFERENCES CITED

Hileman, J. A., Allen, C. R., and Nordquist, J. M., 1973, Seismicity of the southern California region, 1 January 1932 to 31 December 1972: Pasadena, California Institute of Technology, Division of Geological and Planetary Sciences Contribution 2385, 83 p.

Los Angeles Times, 1940a, Quake damage exaggerated, declares El Centro leader: May 20, 1940, p. A.

———1940b, Quake zone acts to solve water crisis: May 21, 1940, p. 1, 10.

Neumann, Frank, 1935, United States earthquakes, 1933: U.S. Coast and Geodetic Survey Serial 579, 82 p.

———1942, United States earthquakes, 1940: U.S. Coast and Geodetic Survey Serial 647, 74 p.

Porcella, R. L., Matthiesen, R. B., McJunkin, R. D., and Ragsdale, J. T., 1979, Compilation of strong-motion records from the August 6, 1979 Coyote Lake earthquake: U.S. Geological Survey Open-File Report 79–385, 71 p.

Richter, C. F., 1958, Elementary seismology: San Francisco, W. H. Freeman, 768 p.

San Diego Union, 1940a, 7 die as quake rocks Imperial: May 19, 1940, p. 1, A.

———1960b, Quake damage $2,500,000; valley faces water shortage: May 20, 1940, p. 1, 2A.

Ulrich, F. P., 1941, The Imperial Valley earthquakes of 1940: Seismological Society of America Bulletin, v. 31, no. 1, p. 13–32.

Wood, H. O., and Neumann, Frank, 1931, Modified Mercalli intensity scale of 1931: Seismological Society of America Bulletin, v. 21, no. 4, p. 277–283.

EFFECTS OF SHAKING ON RESIDENCES NEAR THE IMPERIAL FAULT RUPTURE

By CHARLES R. REAL,
CALIFORNIA DIVISION OF MINES AND GEOLOGY

CONTENTS

ABSTRACT

Examination of four single-story houses and four mobile homes within a few hundred meters of the 1979 Imperial fault rupture showed comparatively little damage from ground shaking relative to buildings a few kilometers from the rupture zone. Except for one mobile-home foundation failure, I observed no other structural damage. Observations of the behavior of contents of the homes suggest that the maximum modified Mercalli intensity (MMI) near the fault did not exceed VII, the value determined for the immediate Imperial Valley region.

INTRODUCTION

To complement the abundant nearfield accelerograms recorded during the main shock, I interviewed the occupants of four single-story houses and four mobile homes within a few hundred meters of the Imperial fault rupture (fig. 196). The examined structures are scattered along the fault trace for 20 km extending from the southern section, where ground displacement was predominantly horizontal, to the north end, where displacement was predominantly vertical.

In view of the strong ground motions recorded (Matthiesen and Porcella, this volume), the moderate size of the main shock, the proximity to the fault rupture, and the serious damage to buildings and structures several kilometers from the fault trace (Wosser and others, this volume), the extent of damage to dwellings near the fault was surprisingly small. The modified Mercalli intensity (MMI; Wood and Neumann, 1931) near the surface fault rupture, on the basis of observed damage and effects of shaking, appears to have been less than VII. This value, which compares well with a maximum MMI of VII determined for most of the area shown on the map (fig. 196) (Nason, this volume; Reagor and others, this volume), points to complexly correlated structural damage, ground shaking, and intensity near the fault rupture. I describe below my observations at seven sites where structure damage was surveyed; all photographs (figs. 197–203) were taken within 5 days of the main shock.

OBSERVATIONS

SITE 1

The first and southernmost site, near Anderholt Road between Bank and Heber Roads southeast of El Centro, Calif., includes a mobile home and a hay-bale stack (figs. 197, 198). The ground rupture passed beneath the west end of the stack and continued northwestward across Anderholt Road (power pole in center of fig. 197*A* is on Anderholt Road). Although the fault rupture passed under the stack, fall of the hay bales was probably caused by shaking. Of all the disrupted hay-bale stacks observed throughout the meizoseismal region, only the end bales toppled down, regardless of the orientation of the stack.

The owners of a mobile home along Anderholt Road about 100 m south (left, fig. 197*B*) of the fault rupture were not present to describe the effects of the earthquake. The unanchored mobile home apparently did not fall from is metal support piers, and there was no visible evidence of any disruption of the coach foundation. Because I visited this site only 2 days after the main shock, it is unlikely that the coach was completely repaired if it had collapsed. Mobile homes damaged by earthquakes commonly remain so for more than a week because of

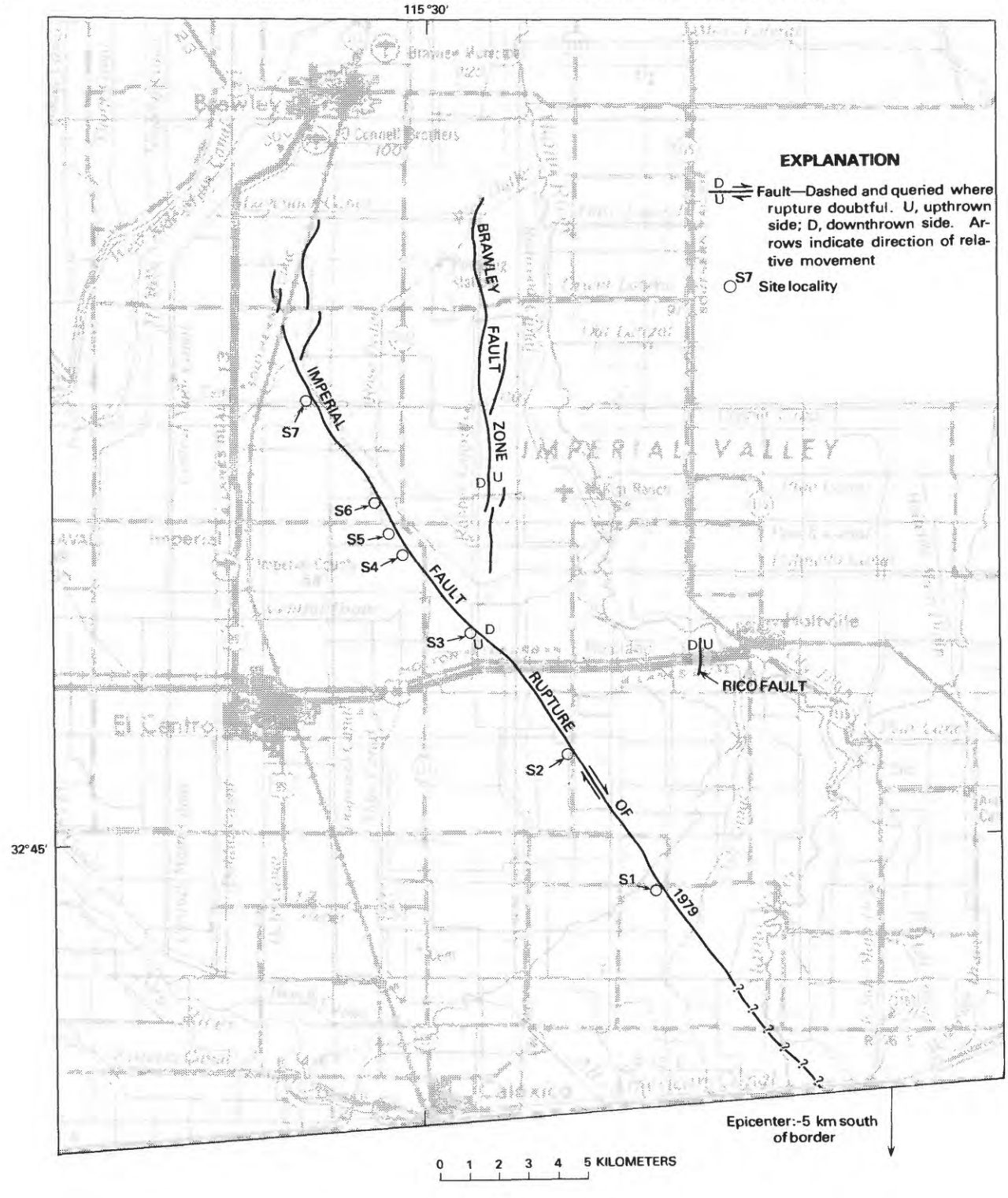

FIGURE 196.—Surface traces of Imperial fault and Brawley fault zone, showing ruptures formed during main shock and sites of residences at which shaking effects were investigated. Faults after Morton (1977), Sharp (1977a, b), and Hart (1979). Base from U.S. Geological Survey, El Centro sheet, 1969.

delays in damage appraisals for insurance claims and arrangements for repair.

A small water tank resting on a raised platform against the right side of the coach remained standing. Such water tanks, which are common throughout the area, consist of a galvanized-steel tank unfastened to a 4- to 5-ft wooden tower that rests on the ground. Commonly the only lateral support is provided by a ½-in. pipe carrying water into the home.

FIGURE 197.—Site 1. *A*, Imperial fault rupture passing beneath west end of hay-bale stack, oriented east-west. *B*, Mobile home still resting on metal piers, only a few tens of meters from surface rupture of Imperial fault.

FIGURE 198.—Site 2. Mobile home resting undisturbed on its foundation. Fault rupture passes across foreground within about 15 m of coach. View southwestward.

SITE 2

Site 2 consists of a mobile home at the corner of Ross and Meloland Roads east of El Centro (figs. 196, 198). Although the ground breakage passed within 20 m of the mobile home, the coach suffered no damage. Inspection of the supporting members indicated that the unit is neither bolted to the ground nor tied down. No signs of relative movement were visible between the metal supporting piers and the coach or the ground surface. The occupants reported that some glassware fell from shelves and the stereo console (about 0.8 m high and 1.5 m long, sitting on 15-cm legs) tipped over. The porch and patio deck of heavy timbers butted against the front side of the coach (not shown in fig. 198) may have added support to the unit, which resisted movement in a north-south direction.

SITE 3

At the home of Mr. and Mrs. Albert Lehmann, about 2 km north of East Evan Hewes Highway and McConnell Road east of El Centro (figs. 196, 199), the surface fault rupture passed directly beneath a wooden chicken coop (fig. 199*A*, 199*B*). The coop was undamaged, but a plastic waterpipe broke where the fault trace passed under it (left of corner of shed, fig. 199*C*). An adjacent shed, about 3 m to the left of the coop (fig. 199*B*), was still resting, apparently undisturbed, on its concrete supporting piers (fig. 199*C*), as was the owners' house, which was less than 10 m from the fault trace (fig. 199*D*). The owners reported no structural damage to the house and no broken windows; a few glass jars fell from a shelf, but large furniture did not shift position.

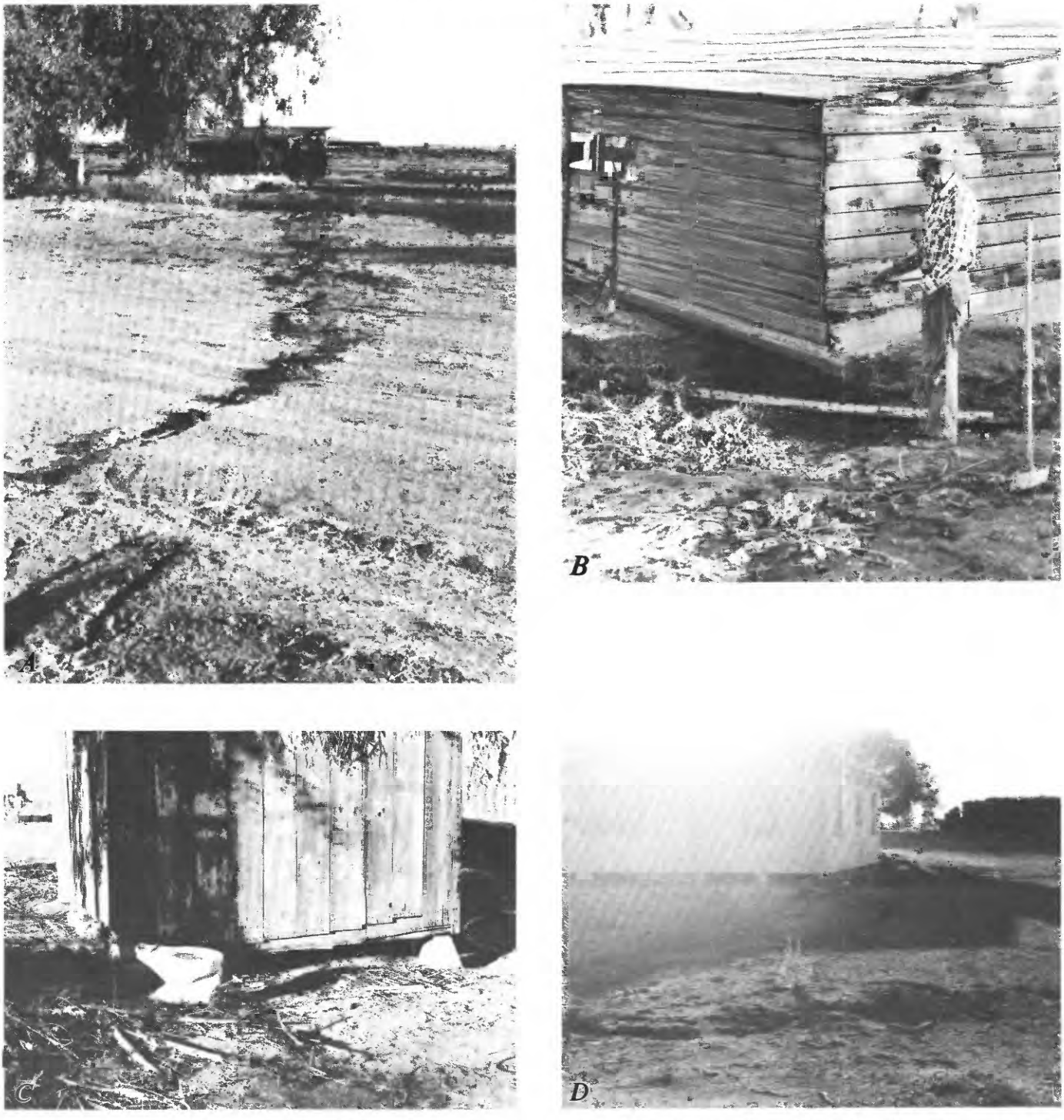

FIGURE 199.—Site 3. *A*, Surface rupture of Imperial fault passing directly beneath undamaged wooden chicken coop. *B*, Broken plastic water pipe where it crosses fault. Fault rupture trends from lower left corner of photograph through a point beneath corner of coop in center. *C*, Small shed adjacent to coop in figure 199*B*, a few meters from fault rupture, resting undisturbed on concrete piers. (Location of toilet bowl was not a consequence of the earthquake.) *D*, Surface trace of Imperial fault (foreground) near undamaged house. Orientation of toppled hay-bale stack (background) is north-south.

The owners reported that about 3 months before the earthquake, a subsurface drainage tile had broken for no apparent reason and allowed water to rise to the surface in a field about 50 m beyond the coop (fig. 198), directly on the trace of the Imperial fault rupture. This observation strongly suggests forecreep before the October 15 main shock.

SITE 4

At site 4 is a wood-frame house with wood siding on Huston Road between Dogwood Road and State Highway 111, east of Imperial, Calif. (figs. 196, 200). Although the surface fault rupture passed within 40 m of the house, the house incurred no structural damage; there were no broken windows, and the stone fireplace was completely intact. However, a separation of about 1 cm that occurred beneath the eaves between the house and the fireplace may have been greater, had the roof not enclosed the chimney. None of the heavy appliances in the house shifted position, although a wooden closet (extreme right, fig. 200*B*) fell over. A ladder leaning against the eaves, and a small water tank resting unfastened on the roof, remained undisturbed throughout the entire series of events. The only noticeable effects of shaking inside the house were that an ironing board fell over and a picture fell from a wall.

SITE 5

At site 5 is a wood-frame house with wood siding and a stucco addition near the intersection of Worthington Road and State Highway 111, due east of Imperial (figs. 196, 201). The surface trace of the Imperial fault passed within 10 m of the house, but there was no visible structural damage; no windows were broken, and no cracks appeared in the foundation or elsewhere in the stucco parts of the building. The occupants could not be contacted for a description of shaking effects inside the house.

SITE 6

At site 6 is a wood-frame house with stucco exterior and concrete-block foundation on Robinson Road, about 1 km west of its intersection with State Highway 111 (figs. 196, 202). The surface rupture of the Imperial fault passed about 300 m to the east of the site. The home exhibited no visible structural damage; no cracks appeared in the plaster exterior (which had recently been painted before the earthquake), and no windows were

FIGURE 200.—Site 4. *A*, Undisturbed residence a few tens of meters from Imperial fault surface rupture. Fault scarp can be seen as a dark line along levee bank through clearing in trees, off left corner of house, just beneath eave. Fault displacement here, as well as at three described sites to north, is predominantly vertical. *B*, Undisturbed wooden ladder, water tank, and large appliances at rear of house in figure 200*A*.

FIGURE 201.—Site 5. *A*, Surface trace of Imperial fault rupture passing within a few meters of wood-and-stucco house that showed no visible signs of damage. *B*, Closeup of house in figure 201*A*.

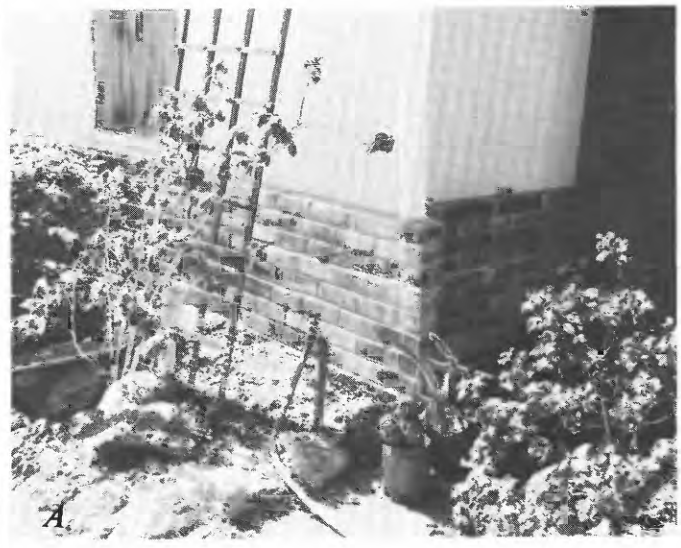

FIGURE 202.—Site 6. *A*, Recently painted plaster walls of house a few hundred meters from surface rupture of Imperial fault, showing no cracks in brick-and-mortar facade. *B*, Undisturbed water tank resting on wooden platform at rear of house in figure 202*A*.

broken. The foundation has a brick-and-mortar facing that was totally undisturbed. Inside the house, a few pieces of furniture moved about 15 cm, but most were unaffected. Some items toppled off shelves, and in the garage one shelf fell over and several cans of paint were spilled onto the floor. A water tank resting unsecured on a raised platform at the rear of the house remained standing and showed no visible signs of movement (fig. 202*B*).

SITE 7

The last and northernmost observation site is about ½ km west of the intersection of Harris and Dogwood Roads, northeast of Imperial (fig. 196). The surface rupture of the Imperial fault passed between two mobile homes that are both within 100 m of the fault trace. The southwestern mobile home on the west side of the fault (fig. 203*A*) was undamaged; the home is bolted down to a concrete foundation with metal straps spaced at 2-m intervals. The owners stated that the home was erected in 1975, when a local ordinance (later repealed) required that mobile homes be anchored. The occupants reported that heavy furniture did not move, although a television on casters tumbled over. One occupant had difficulty getting up from the ground during the earthquake. A waterline a few meters from the fault rupture broke.

The other mobile home, about ½ km to the northeast on the opposite side of the fault, was thrown off its foundation (fig. 203*B*). Although the owners could not be contacted, the interior contents of the coach apparently were considerably disrupted by ground shaking. This was the only mobile home of the four observed within a few hundred meters of the Imperial fault where foundation failure occurred.

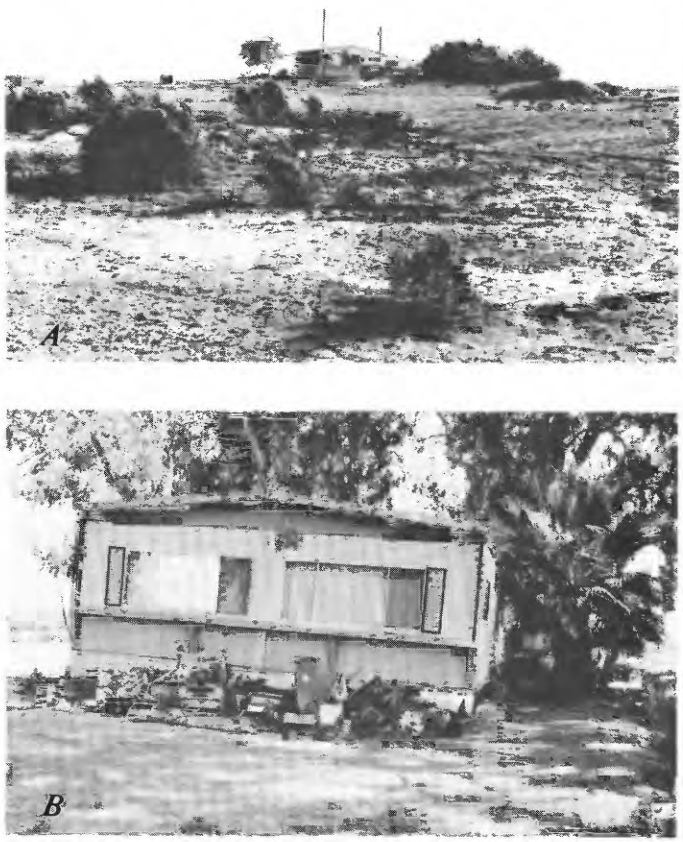

FIGURE 203.—Site 7. *A*, Undisturbed mobile home of a few tens of meters from surface trace of Imperial fault (center). *B*, Mobile home that collapsed on its foundation, situated a few hundred meters from mobile home in figure 203*A* on opposite side of fault.

DISCUSSION

Examination of single-story houses and mobile homes at seven sites within a few hundred meters of the 1979 Imperial fault rupture reveals that little damage was caused by ground shaking near the fault. It is unreasonable to assume that the structures examined had exceptional structural integrity, except for one mobile home that was tied down to a concrete foundation. When as many as 50 to 60 percent of the mobile homes in parks several kilometers from the fault underwent foundation failure, any unanchored coach situated within meters of the ground rupture might not have been expected to remain standing; yet only one of the three unanchored coaches I observed collapsed. The slight disturbance at all seven sites suggests an MMI no higher than VII, possibly even lower.

REFERENCES CITED

Hart, E. W., 1979, Preliminary map of October 1979 fault rupture, Imperial and Brawley faults, Imperial County, California, supp. 1 *to* California Division of Mines and Geology Fault Evaluation Report FER–83: 8 p., scale 1:24,000, 6 sheets.

Morton, P. K., 1977, Geology and mineral resources of Imperial County, California: California Division of Mines and Geology County Report 7, 104 p.

Sharp, R. V., 1977a, Holocene traces of the Imperial fault in south-central Imperial County, California: U.S. Geological Survey Open-File Report 77–815, 1 p., scale 1:24,000, 5 sheets.

—— 1977b, Map showing Holocene surface expression of Brawley fault, Imperial County, California: U.S. Geological Survey Miscellaneous Field Studies Map MF–838, scale 1:24,000.

Wood, H. O., and Neumann, Frank, 1931, Modified Mercalli intensity scale of 1931: Seismological Society of America Bulletin, v. 21, no. 4, p. 277–283.

DAMAGE TO ENGINEERED STRUCTURES IN CALIFORNIA

By THOMAS D. WOSSER, DOMINIC E. CAMPI, and MARIO A. FOVINCI,
H. J. DEGENKOLB & ASSOCIATES;

and

WILLIAM H. SMITH,
AMERICAN IRON AND STEEL INSTITUTE

CONTENTS

ABSTRACT

Damage to engineered structures in the area most strongly affected by the main shock consisted primarily of some parapet damage and veneer loss to one- and two-story buildings, as well as minor architectural damage and occasional cracking; for the most part, the greatest effect appeared to be losses of library racks and shelved items. By far the most significant structural effect observed was the failure of the Imperial County Services Building, a six-story reinforced-concrete office building in El Centro, Calif. Four columns at the east end of the building were badly shattered in the area immediately above the first-floor line; ties opened up and vertical bars buckled, and the columns lost a foot or more of their length. We also observed damage at the Southern Pacific Pipe Lines tank farm, the New River Bridges, the Magma Electric Geothermal Generating Plant, Imperial Valley College, elevated water tanks, KXO radio station, the Imperial County Emergency Services and Fire Department Building at the airport, and the shopping centers and churches in El Centro.

INTRODUCTION

This report on damage from the 1979 Imperial Valley earthquake summarizes our observations during inspections conducted on October 17, 18, and 19, 1979. The principal cities in the affected area of California are El Centro, Calexico, and Brawley (fig. 204). Most commercial buildings in these cities are one- and two-story structures of various ages; although many of them are relatively old and of unreinforced-masonry construction (fig. 205), a representative group are recent structures of relatively modern architectural and structural design (fig. 206). Some parapet damage and veneer loss (fig. 207), as well as minor architectural damage and occasional cracking, occurred, but for the most part the greatest effect appeared to be losses of library racks and shelved items. Although a few buildings were eventually condemned, in general only scattered minor damage afflicted typical commercial construction.

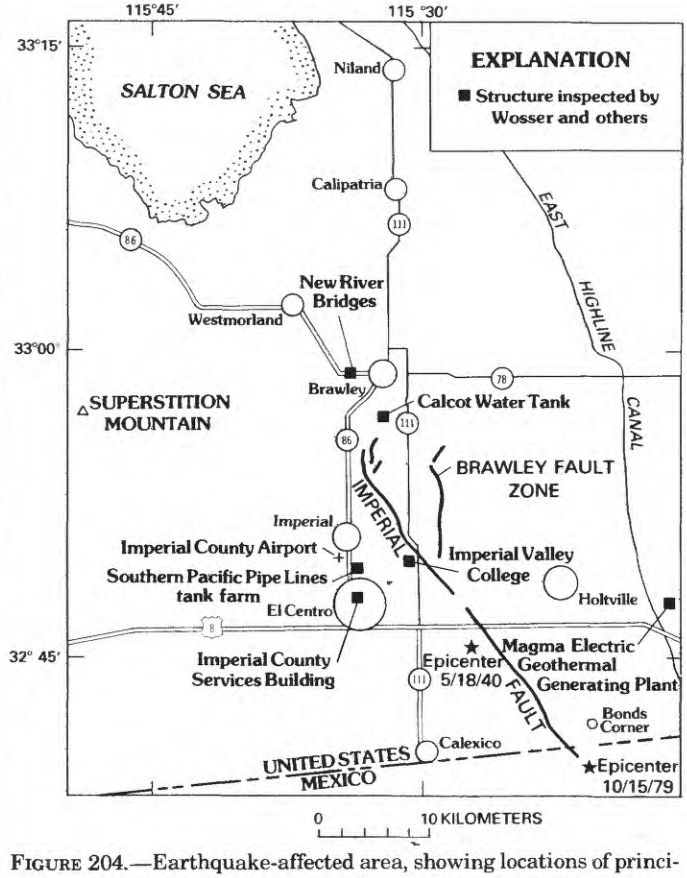

FIGURE 204.—Earthquake-affected area, showing locations of principal cities and structures referred to in this chapter.

FIGURE 205.—U.S. Post Office, El Centro, a typical two-story unreinforced-masonry building.

FIGURE 206.—Typical one-story building of modern structural design, El Centro.

By far the most significant structural effect we observed was the failure of the Imperial County Services Building. We also observed damage at the Southern Pacific Pipe Lines tank farm, the New River Bridges, the Magma Electric Geothermal Generating Plant, Imperial Valley College, elevated water tanks, KXO radio station, the Imperial County Emergency Services and Fire Department Building at the airport, and the shopping centers and churches in El Centro.

IMPERIAL COUNTY SERVICES BUILDING

From the viewpoint of the structural engineer, the story of the Imperial Valley earthquake of 1979 is the story of the Imperial County Services Building in El Centro (fig. 208). This six-story reinforced-concrete structure, designed in 1968, underwent first-story failure of all four columns in the column line at the east end of the building (fig. 209). With this failure, the first story dropped by a foot or more on that line, the endbay framing hinged at the first interior-column line, and a major crack across the building appeared at that line on all floors.

In an area where most older unreinforced-masonry buildings were little damaged, the failure of this structure was dramatic and was well publicized by the press, which frequently referred to this recently constructed "earthquake proof" building. This failure is bound to be the subject of much further study, particularly because the building was equipped with 13 accelerometers, and an additional free-field accelerograph was 100 yd away (Rojahn and Mork, this volume).

The building is supported on a Raymond concrete-pile foundation and is five bays long in an east-west direction by three bays wide in a north-south direction; all

FIGURE 207.—Parapet and veneer damage to older building in El Centro.

bays are 25 ft long (fig. 210). At the east and west ends of the building, the exterior facade above the second floor consists of a reinforced-concrete shear wall placed 5 ft 11 in. outside the first-floor column line (figs. 210, 211). The walls, which run the full width of the building, stop at the second floor and leave open ends in the first story. The two ends differ slightly: the west-end wall has a smoke-tower opening at midlength of the wall on all floors; in addition, in the first story is a shear wall on the center bay of the set-back exterior-column line.

The longitudinal exterior walls, which have a sunscreen-type treatment, are made of a mixture of cast-in-place and precast concrete. The columns are square up to the second floor, above which they are elongate to the outside and taper from 18 to 10 in. wide over a length of 5 ft 10 in. The second-floor slab extends roughly the same distance to form a platform for the sunscreen above, again in a style reflecting a building on stilts. At the other upper floors are exterior horizontal precast slabs between the columns and four vertical precast fins between the slabs.

The building is framed with reinforced-concrete joists, at 36 in. on center in the transverse direction. Typically, the joists are 5½ by 14+3 in. at most floors and 5½ by 14+5 in. at the second floor. This thicker slab at the second floor is probably a recognition of the shear transfer in the diaphragm. Longitudinal framing is made up of a 10-in.-thick by 4-ft-6-in.-deep spandrel section below the floors (except at the second floor) on the exterior-column lines, and 24- by 30-in. girders on the two interior-column lines. Interior columns are 24-in.-square reinforced concrete. Some ductile-concrete details required by the 1967 Uniform Building Code were used in the design, but not throughout. For example, column ties are extended through the girder depths, column bars are spliced at midheight, and continuous top-and-bottom steel was used in the girders. These provisions did not include the current code requirements for special transverse-column-reinforcement full height under discontinuous shear walls.

The earthquake-resistant construction in the longitudinal direction is a moment-resisting frame system; no longitudinal shear walls are included in the building. We understand that longitudinal seismic forces were calculated for a moment-frame building with a K-factor of 0.67, but that the forces in the exterior frames were

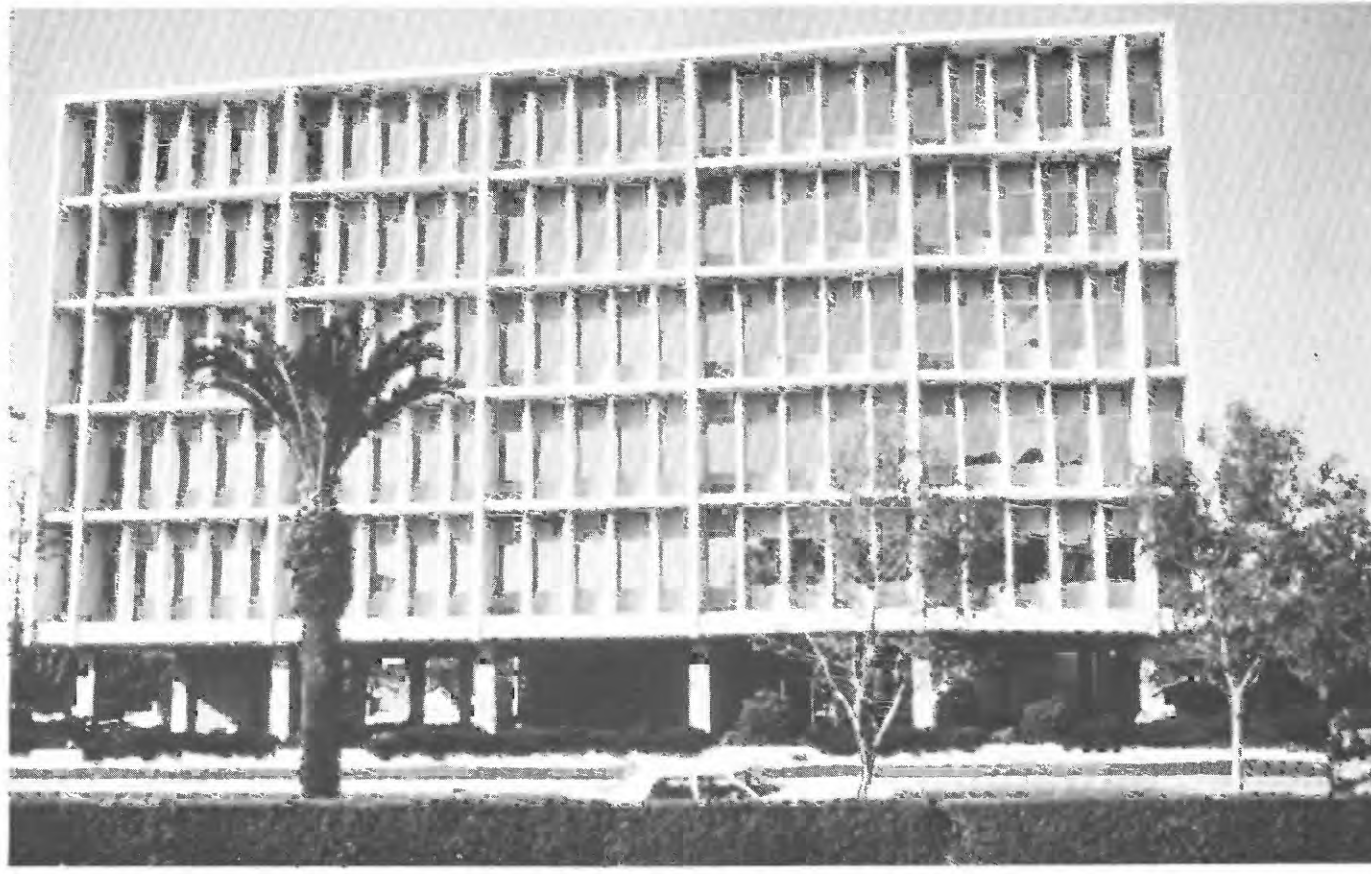

FIGURE 208.—Imperial County Services Building, El Centro. South elevation.

increased by 50 percent to be equivalent to a K-factor of 1.00 because the exterior frames do not have a configuration conforming to ductile-concrete details. In the transverse direction (fig. 211) the exterior walls are the only shear walls above the second floor. Below the second floor, the exterior shear walls are replaced by four 25-ft-long walls within the length of the building (figs. 210, 211). The upper shear walls are 7½ in. thick in the second story and 7 in. thick above, all with a single curtain of steel; in the first story the walls are 12 in. thick with two curtains of steel.

In the columns of interest in the first story, column ties are generally #5-at-2-in. hoop ties with #3-at-2-in. interior ties for the distance within points 2 ft 2 in. above and below the limits of the girder framing. In between, at midheight of the column, all ties are #3 at 12 in. At the first-floor level the pile caps are 2 ft 2 in. below the floorline, and the heavy-tie spacing is within that distance. The minimum ties, #3 at 12 in., start at the first-floor slab line.

All four columns in column line G at the east end of the building were badly shattered in the area immediately above the first-floor line (fig. 209). Ties opened up and vertical bars buckled, and the columns lost a foot or more of their length (fig. 212). Apparently, the columns dropped straight down without leaning in any direction. The settlement of these columns caused hinging of the endbay and yielding of the girders, clearly evident in the expected places. In other parts of the first story, some concrete was spalled from the columns at the first-floor line, but nothing approaching complete failure was visible. Although we did not notice it at the time, J. A. Willis (written commun., 1980) reported typical X cracking of all the first-story columns just above the ground-floor slab due to longitudinal-frame action. He also observed yielding due to

FIGURE 209.—Line of columns that failed at east end of Imperial County Services Building.

longitudinal-frame action in the first story, as well as minor cracking and incipient spalling at the tops of some columns.

In the upper stories we observed no significant structural distress except that from the column failures on line G. No evidence was apparent of any diaphragm cracking or of yielding near the column-girder intersections; neither was there any distress apparent in the cantilever beams that extend beyond the end-column lines to the transverse exterior shear walls. However, subsequent investigations by J. A. Willis and Vitelmo Bertero (oral commun., 1980) have disclosed shear cracks in the floor diaphragms and some longitudinal-frame yielding. The exterior shear walls themselves exhibited diagonal tension cracks related to the exterior columns and reflected minor movement on the horizontal construction joints, but no major distress was apparent in the walls.

The interior of the building was a mess from the standpoint of its contents; papers, files, plants, and so on were everywhere. The ceiling, ceiling light fixtures, and partitions, however, were all in remarkably good condition (fig. 213). Except at a few places in the endbay, almost all doors were operable. The elevator equipment was rigidly anchored to the roof slab and suffered no apparent damage; the elevators were reported to be operable immediately after the earthquake. The air-conditioning equipment on the roof was mounted on vibration isolators without keepers or holddowns; as might have been expected, it was shaken from its supports.

Initially we judged that the four west bays of the building underwent only minor structural damage in the first story. Subsequent observations by J. A. Willis

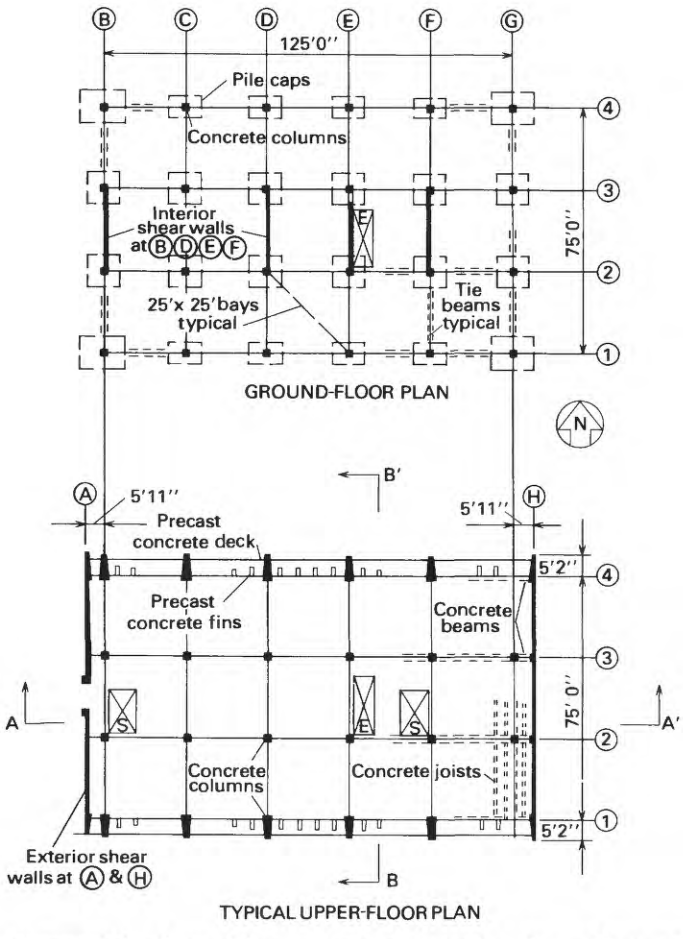

FIGURE 210.—Ground-floor and typical upper-floor plans of Imperial County Services Building. Circled letters identify lines of columns in north-south direction; circled numbers, lines of columns in east-west direction. See figure 211 for cross sections *A–A'* and *B–B'*. S, stairs; E, elevators.

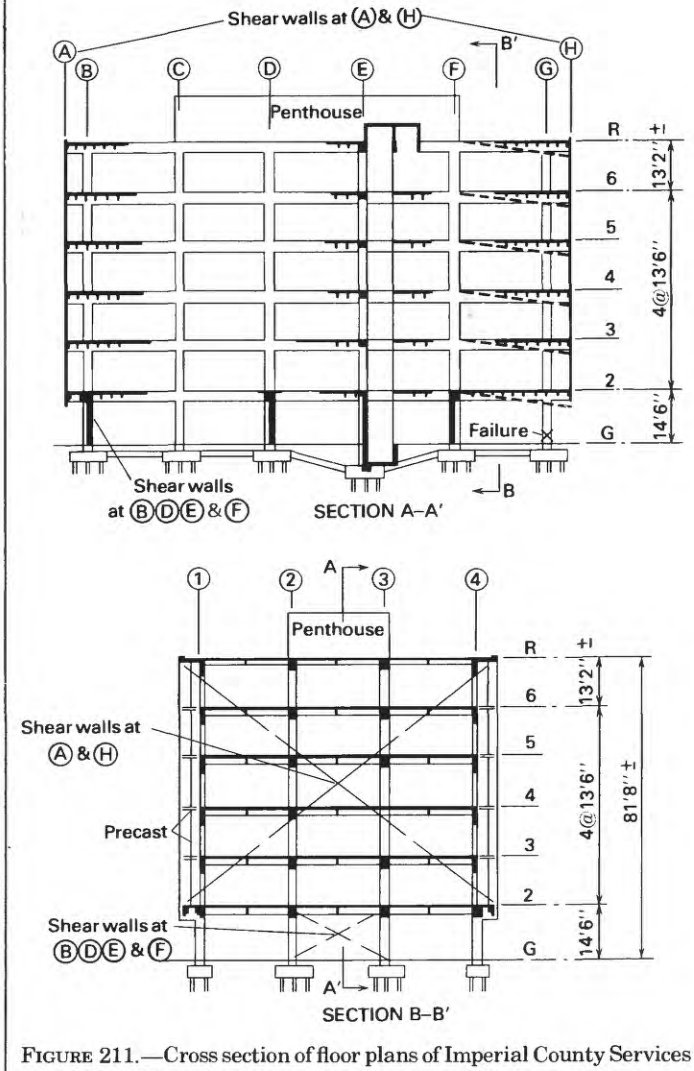

FIGURE 211.—Cross section of floor plans of Imperial County Services Building. Circled letters and numbers same as in figure 210. In cross section *A–A'*, dashed lines between F and H indicate endbay failure.

(written commun., 1980), however, have indicated that distress may have been more significant than originally thought.

We consider that the failure of the first-story columns on line G resulted from extremely high axial loads due to overturning moments in both principal directions of the building, as well as from flexural yielding of the columns due to longitudinal-frame action. This failure occurred near the first-floor line, where column ties were inadequate to prevent buckling of the reinforcing steel or to confine the concrete. Fixity of the column bases by the pile caps apparently resulted in higher bending moments in that place than at the top of the first-story columns. In particular, the corner columns were subjected to high overturning forces from action in both directions, most significantly transversely under the discontinuous upper shear walls. On the basis of a consideration of the forces in both principal directions and on a preliminary column-capacity analysis, these forces may have exceeded the design forces by as much as fourfold or possibly more. Of further significance is the recognized fact that concrete columns creep to the extent that after a relatively short time in service, most of the load is transferred from the concrete to the reinforcing steel, and the steel may be stressed to a level near its yield stress in carrying normal gravity loads. Thus, a sudden significant overload can cause the columns to fail.

FIGURE 212.—Typical column failure, Imperial County Services Building.

The subject of earthquake-induced axial loads must be evaluated further, especially because a significant earthquake imposes forces appreciably larger than those considered by the building code. Current seismic-code requirements are based on the premise that in a major earthquake, the building, or elements of the building, will be stressed beyond the elastic limit and must absorb excess energy in the plastic range. To respond in this manner, a building must be tough; any local failures must be ductile failures that will not lead to collapse, even partial. Clearly, column failures must be avoided.

In developing the code requirements for ductile moment-resisting space frames for reinforced concrete, avoidance of hinging columns and forcing of yielding into the girders were considered essential design features; furthermore, the girder design must allow for yielding without any shear failure. These requirements do more than prevent hinging of the columns; they also set an upper limit on the earthquake-induced axial load that can be transmitted to the columns. At each floor level, that increment of the axial load is determined by the yield moments at the ends of the girders framing into the columns. Thus, the maximum ultimate axial load on columns can be reasonably well determined for ductile moment-resisting space frames.

The same cannot be said, however, for systems similar to the transverse-wall system in the Imperial County Services Building, where shear walls are discontinuous and supported on freestanding columns below. In this type of system, no element will yield, and thus no control exists over the axial load that can be imposed on the column due to the overturning effects of earthquake forces—that is, the system has no ductility. The entire philosophy of earthquake-resistant design is based on the recognition that actual forces may greatly exceed the code forces and that the response of structural elements must enable them to resist those forces. Normally, this result is achieved through ductility of the system; where such ductility is impossible, the members must be designed for a substantially higher

factor of safety. This reasoning clearly applies to the columns supporting a stilt-type building.

SOUTHERN PACIFIC PIPE LINES TANK FARM

At the Southern Pacific Pipe Lines gasoline storage tank farm (fig. 214), east of the Imperial County Airport, damage in the main shock prompted the evacuation of all persons from within a 1-mi radius of the site. This evacuation was ordered because of a leak from a minor rupture in the most severely damaged tank, IP–13. The 11,000-gal-capacity steel tank measures 41 ft in diameter by 49 ft high. The unit utilizes a Weathermaster roof of rigid steel with a floating steel liner; the tank is supported by a concrete-perimeter ringbeam on compacted fill. No direct attachment exists between the tank and perimeter beam. Tank IP–13, which has the largest ratio of height to diameter of all the tanks on the site, was nearly full at the time of the earthquake, as were all the other tanks.

Observed damage to tank IP–13 included an "elephant's foot" at the base of the tank that extended over a 90° arc and bulged out a maximum of 6 in. over a 2-ft height (fig. 215). Directly opposite the bulge was a 4-in.-long rupture where the tank wall is welded to the floorplate. No sliding of the tank relative to its foundation was observed here or at any other tank.

Damage to other tanks included racking damage to an aluminum floating roof on tank IP–16 (48 ft in diameter by 48 ft high). A height of 5 ft of sloshing was measured by plant personnel in a tank with a floating roof. Tank IP–16 also exhibited a small "elephant's foot" and a minor leak in a 1-in.-diameter connecting pipeline.

The ground strap on tank IP–12 (43 ft in diameter by 40 ft high) exhibited evidence of working and pullup that indicated probable rocking at the base. Only tank IP–5 (48 ft in diameter by 48 ft high) and tank IP–4 rest directly on compacted fill with no concrete ringbeam. These tanks settled approximately 2 in. into the fill, and we again noted pullup of the ground straps. Tank IP–4 also exhibited a small "elephant's foot" near the base.

No significant damage to connecting pipes from the tanks was observed. These pipes are fitted with a connection that allows some sliding to accommodate temperature-induced motions.

NEW RIVER BRIDGES

The New River Bridges on State Highway 86 approximately 2 mi west of Brawley, Calif., were the most severely damaged highway structures in the area and had to be closed to traffic until shored. The twin straight parallel two-lane bridges (fig. 216), each supported on

FIGURE 213.—Interior of Imperial County Services Building, showing undamaged ceiling, ceiling light fixtures, and partitions. Such contents as papers, files, and bookshelves, however, were thrown about.

seven interior bents, extend east-westward 198 ft between free-floating abutments; the ends of the bridges are skewed 20°. The bridges are supported on Raymond step-taper piles extending approximately 60 ft below the elevation of the bridge decks. Octagonal concrete columns, each supported on a single pile, extend from 1 ft below grade to a cap at the deck soffit at interior bents.

After the main shock, the bridges were inspected by personnel from the California Department of Transportation (Caltrans) and allowed to remain open. Significant damage to the bridges resulted from the midnight aftershocks of October 15, which were reported by many in the town of Brawley to have been of greater intensity than the main shock in that area.

The earthquake caused the abutments at each end of the bridges to move inward. The total movement at the west abutment of the southern bridge (eastbound lane) was measured by Caltrans to be 14½ in. from its original position. Previous measurements made in 1975 indicated that 7½ in. of movement had taken place by then since construction in 1952. Therefore, approximately 6 in. of additional movement may be attributed to slope movement during the earthquake. Hinging at the tops of the columns on the first interior bents at each end of the bridges, and roadway settlements of 6 to 8 in. behind the abutments, may also be attributed to slope movement.

The superstructure shifted approximately 3 in. northward at the east end (fig. 217) and 8 in. southward at the west end relative to the abutments. Lateral motion caused failure of the lightly reinforced concrete wingwalls that attempt to restrain such motion. Rotational movement of the bridges was probably forced by

FIGURE 215.—Tank IP–13, Southern Pacific Pipe Lines gasoline storage tank farm. Note "elephant's foot" at base of tank.

FIGURE 214.—Southern Pacific Pipe Lines gasoline storage tank farm. View southward.

the skewed ends of the superstructure bearing against the adjacent soil. The superstructure of the bridges had been slated for reworking before the earthquake, owing to the slope problems previously mentioned.

MAGMA ELECTRIC GEOTHERMAL GENERATING PLANT

A recently completed 100-MW geothermal generating plant 8 mi east of Holtville, Calif., was not damaged by the earthquake. The site, which was severely shaken during the main shock, according to the plant superintendent, contains various mechanical equipment, tanks, piping, and large cooling ponds with lined sand embankments (fig. 218).

All pieces of mechanical equipment and the tanks are anchored to their foundations, and the elevated equipment to rigidly braced frames. Anchorage, in general, appeared to be substantial; the superintendent stated that all anchorages were designed to sustain seismically induced forces. Piping is mounted on sliding supports to allow for thermal movements. The runs of piping that we observed generally have bracing at one end in the longitudinal direction and at each end in the transverse direction; the maximum length of these runs is approximately 60 ft. The steel pipe segments are connected by flange bolts.

The large cooling ponds at the site were originally to have had embankments constructed of a sand-cement mixture. At the time of construction, however, cement became scarce, and so it was decided to construct the banks of sand alone. No damage to the embankments was observed.

The new plant is still in the testing phase and was not operating at the time of the earthquake. Subsequent startup has indicated no internal damage to any equipment at the site.

FIGURE 216.—New River Bridges on State Highway 86, showing southern bridge (eastbound lane). View westward.

IMPERIAL VALLEY COLLEGE

The Imperial Valley College campus is approximately 4 mi east of the town of Imperial, Calif., on Aten Road near State Highway 111, northeast of El Centro and very near the Imperial fault. Most structures on the campus are low one-story buildings with reinforced-concrete-block walls and metal deck roofs overhanging the exterior corridors (fig. 219). Interior roof framing was not confirmed. The buildings are of recent construction, probably less than 10 years old. Window openings in the walls, particularly in the classroom buildings, are few and generally small.

Structural damage to the buildings on the campus was minimal or nonexistent. Neither movement nor damage was apparent in the mechanical equipment examined, much of which was unanchored or only nominally anchored. In the gymnasium a pipe trapeze was damaged and a few fluorescent-light fixtures fell, all of which were supported from the steel truss-roof members high above the basketball courts. In the library many unanchored bookcases overturned, and some bookcases with base holddowns had splitting cracks in the wood bases at the anchors. The shelves were unbraced at their tops. Some minor shifting damage also occurred to the ceiling panels below the truss-joist roof in the library. About $15,000 worth of damage to equipment and chemicals in the chemistry laboratories was reported to have been caused by the earthquake, although we did not visit these laboratories. In the administration building, minor floor cracks were visible in a northwest-southeast direction, and the staff indicated that a few flourescent-light fixtures mounted in the ceiling and several bookcases and shelves had come down.

ELEVATED WATER TANKS

Elevated water tanks in the El Centro area sustained minor to moderate damage, with the exception of one

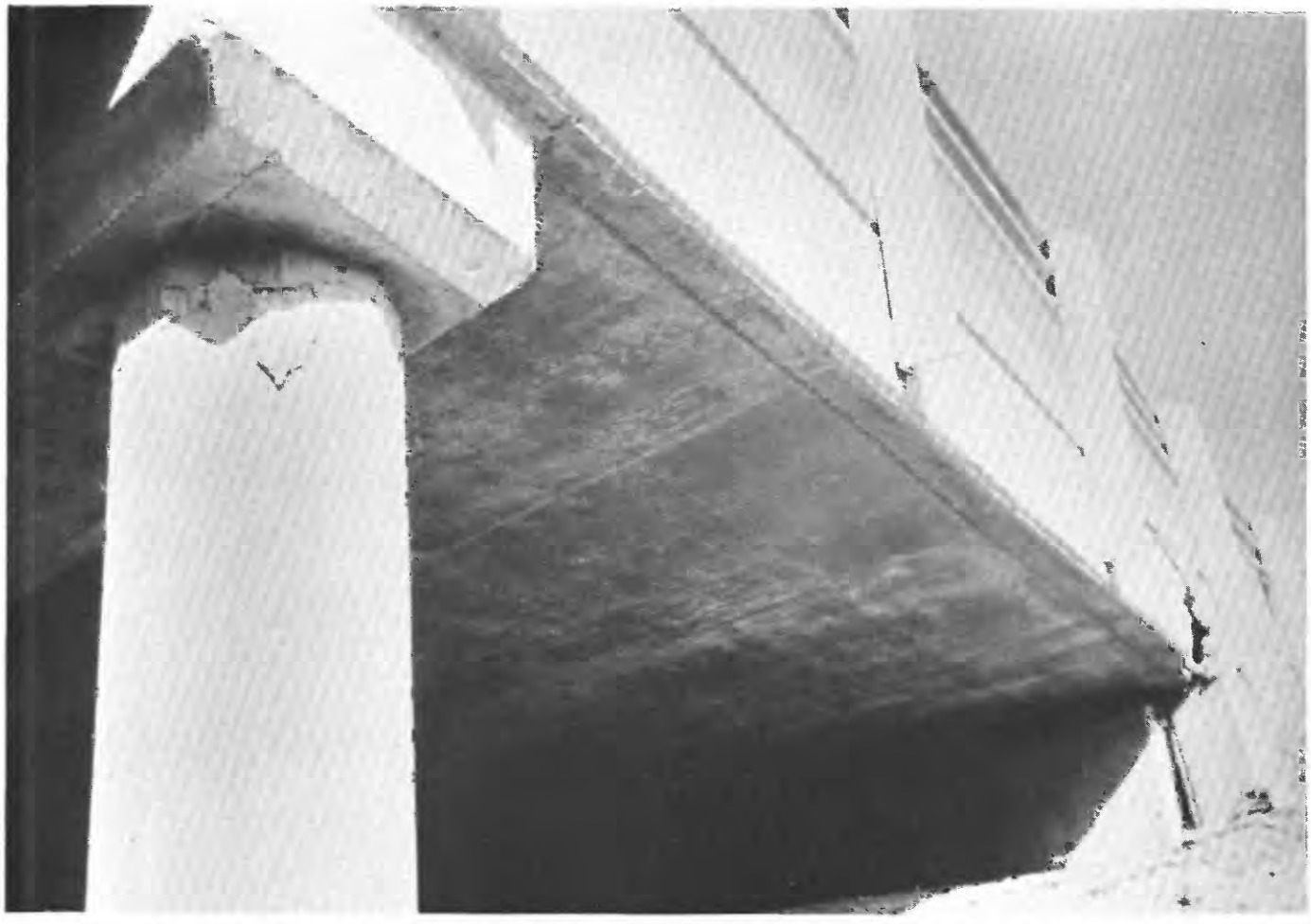

FIGURE 217.—New River Bridges on State Highway 86, showing east end of northern bridge (westbound lane). Note damaged abutment where superstructure shifted to north.

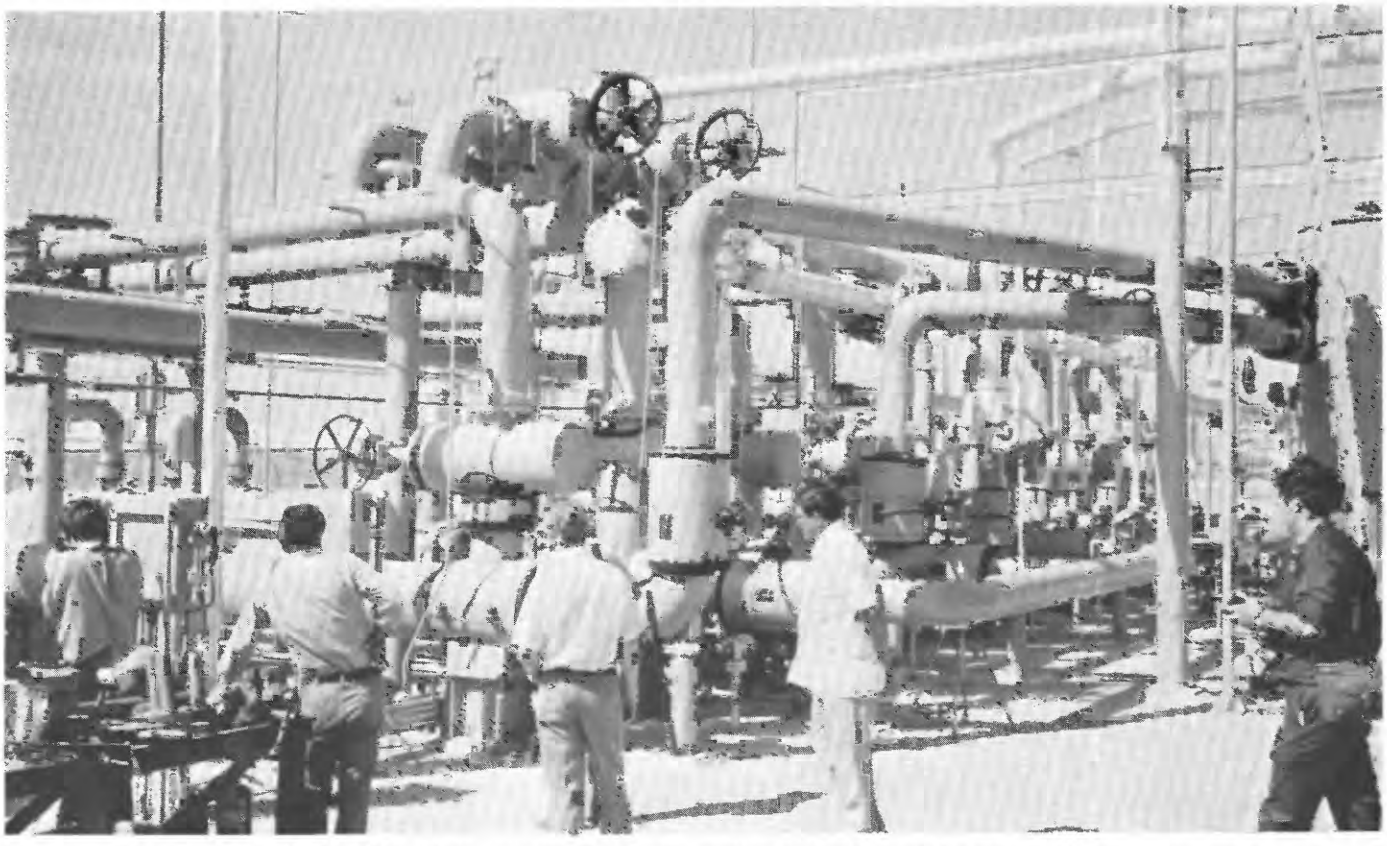

FIGURE 218.—Undamaged piping at Magma Electric Geothermal Generating Plant.

FIGURE 219.—Imperial Valley College. View northwestward.

tank just south of Brawley on Dogwood Road that completely collapsed. This collapsed tank (fig. 220), known as the Calcot Water Tank, was estimated to have been 100 ft tall by 30 ft wide at the base. Its four tubular legs, 21 in. round by ⅜ in. thick, were braced by three tiers of diagonal rods, 2¼ in. round in the bottom tier. Rods had upset threads and turnbuckles at one end, and were welded to two plates at the other to form clevises. Struts were T-shaped 8-in. double channels. Clevises and struts were connected to 1-in. gusset plates welded to the tubular uprights. Diaphragm plates were generally welded into place within the tubes above and below the gusset plates. Some nuts were not fully threaded onto the clevis pins. Welds generally appeared satisfactory.

The tank was filled with water at the time of the main shock. Brash failures occurred in the rods where they were welded to the clevis plates, and the gussets tore from the tube walls in some places from the wall and weld (fig. 221).

Figure 222 shows one example of a typical relatively undamaged tank 2½ mi east of El Centro. The tank was carring a full 100,000 gal at the time of the earthquake. Damage consisted of one broken diagonal bracing rod that tore out the gusset, and one slightly buckled strut.

KXO RADIO STATION

The second tallest building in El Centro is KXO radio station (fig. 223) at the Valley Plaza Shopping Center, three blocks west of the Imperial County Services Building. The structure is a four-story steel frame with lightweight concrete-on-steel deck, 50 by 100 ft in plan, on 50-ft piles, built in 1966. No broken windows were visible. Some horizontal hairline cracks were apparent in the north- and south-facing 50-ft walls, assumed to be nonbearing. No architectural damage was noticeable on the ground floor, although one employee of the radio station stated that some minor tile damage was visible in the third-floor bathrooms. The station was fully functional when power was restored to the building a few hours after the earthquake.

IMPERIAL COUNTY EMERGENCY SERVICES AND FIRE DEPARTMENT BUILDING

The Imperial County Emergency Services and Fire Department Building, 2½ mi north of El Centro at the Imperial County Airport, is housed in a one-story approximately 60 by 120 ft preengineered steel-frame

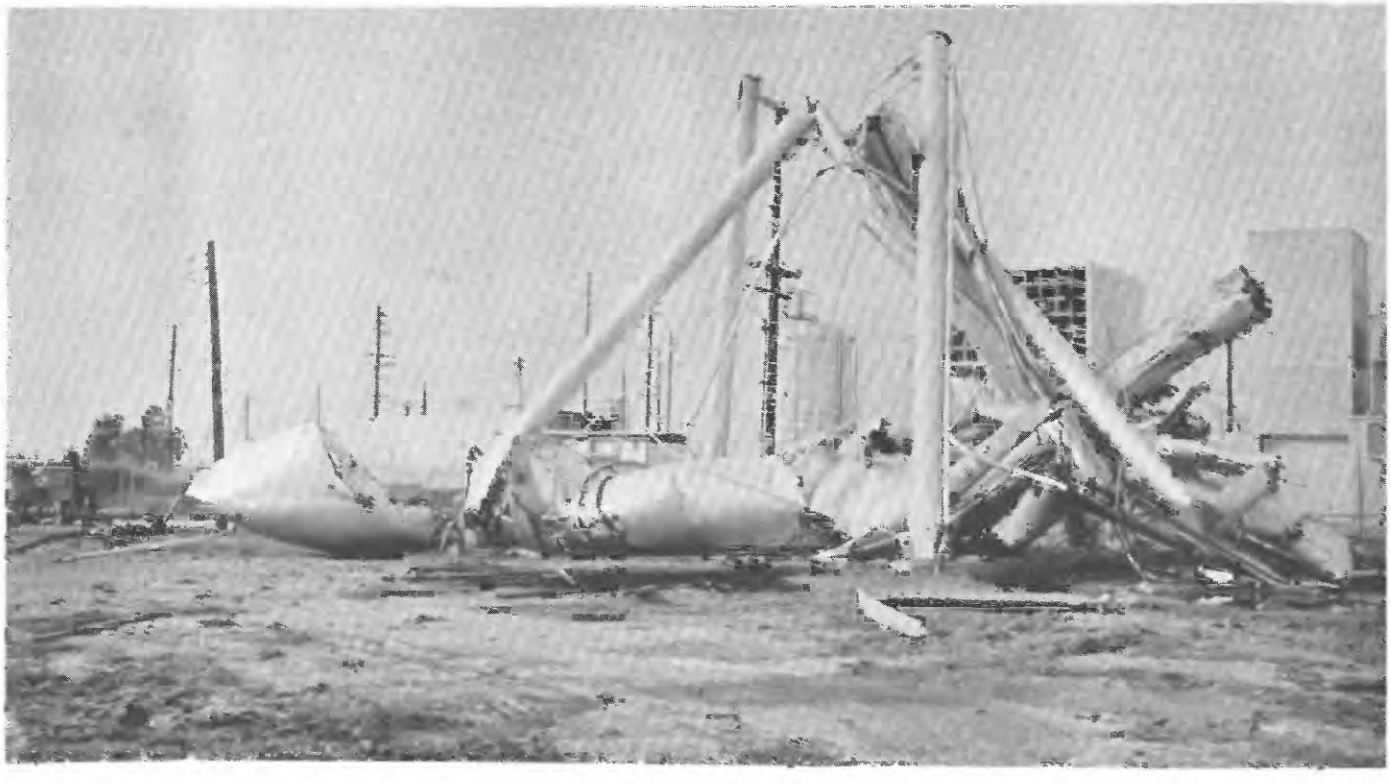

FIGURE 220.—Collapsed Calcot Water Tank.

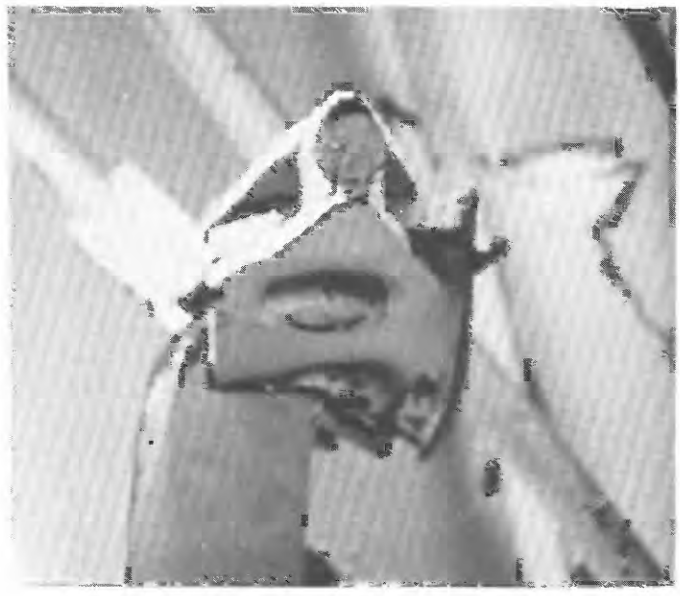

FIGURE 221.—Calcot Water Tank rod failure.

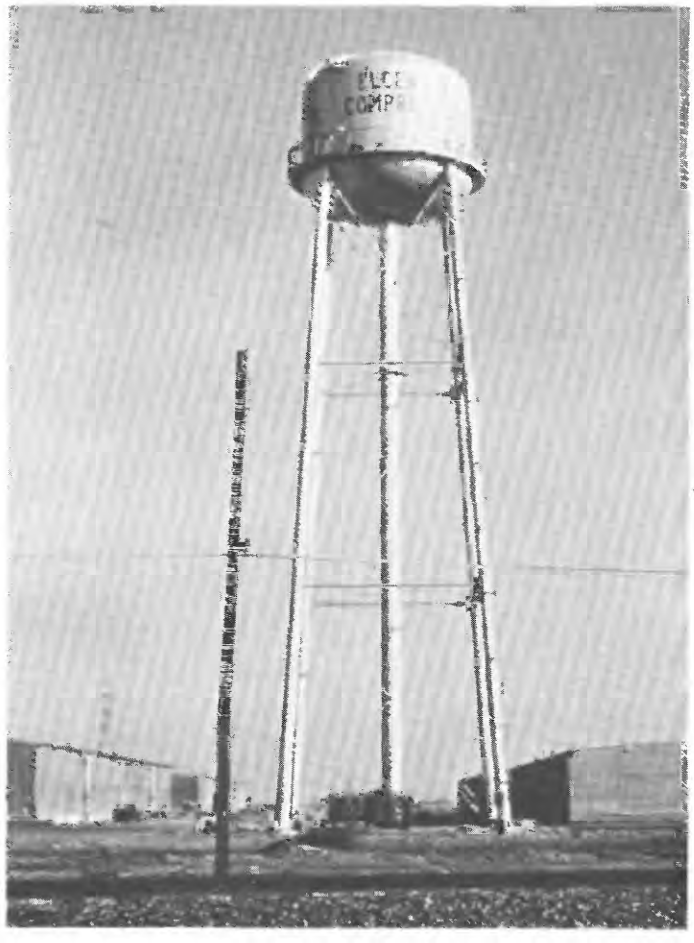

FIGURE 222.—Slightly damaged elevated water tank 2½ mi east of El Centro.

building (fig. 224) divided into three occupancies: garage, office space, and repair shop. No damage to the structure was visible. Many of the lights in the garage and shop, suspended from the frame on small chains, broke after swinging into the ceiling or becoming unhooked. The steel duct system within the shop exhibited considerably less response, according to employees. Sprayed-on-wall insulation in the shop was cracked. Some ceiling tiles and insulation in the office fell. A hairline crack was visible in the garage floor; fire engines were parked in the garage during the earthquake. The office functioned as the County emergency services center after the earthquake.

FIGURE 223.—KXO radio station, El Centro. View northwestward.

FIGURE 224.—Imperial County Emergency Services and Fire Department Building, Imperial County Airport. View northeastward.

SHOPPING CENTERS

Modern shopping centers throughout the area performed well structurally, although in many places contents were thrown to the floor. Within El Centro are several such centers along Imperial Avenue in the northwest sector of the city, including the Valley Plaza (built in 1965), the El Centro Center with Sears (built in 1968), and the K Mart, next to the El Centro Center (built in 1975).

The K Mart is a one-story concrete-block structure with Glu-lam roof construction, suspended ceiling with drop-in light panels, and concrete slab on grade. The building is rectangular in plan, 100 by 285 ft. An occasional ceiling tile was displaced, and a few diagonal hairline cracks appeared in the long east-facing wall and in the slab construction joint. The store was open for business when visited on October 19.

The Sears building is one store in a one-story covered-mall shopping center, 300 by 575 ft in plan. Some architectural damage occurred in the covered-mall walkway between stores. In Sears, several ceiling panels fell down. The Sears building is constructed with tiltup concrete walls, steel-frame roofing, and steel decking, and is equipped with sprinklers throughout. The store was closed Monday after the earthquake but open on Tuesday.

No damage to parking-lot lights or the large shopping-center sign was apparent at the El Centro Center.

In Calexico the sprinkler system in the Fed-Mart was activated by ground shaking, not by fire.

CHURCHES IN EL CENTRO

We made a quick assessment of earthquake-related damage to the churches in El Centro on October 19, 1979. We examined the Church of the Four Square Gospel, the First Church of the Nazarene, Grace Lutheran Church, and the United Methodist Church. All these churches are on Eighth Street south of Main Street near downtown El Centro. Our examination was limited to an observation of the exterior of the buildings, except for the interior of the sanctuary building of the United Methodist Church.

In general, earthquake-related structural damage to these church buildings was minor or nonexistent. No damage was observed at the First Church of the Nazarene, Grace Lutheran Church, or the United Methodist Church. The Church of the Four Square Gospel (fig. 225), an old one-story unreinforced-masonry bearing-wall structure with a wood roof, had some cracking in its entrance stairway, walls, and parapets, and the guy wires for the cross atop the building apparently were elongated owing to the earthquake.

The undamaged structures, of wood, masonry, and tiltup construction, appeared to have been built since 1950. The First Church of the Nazarene (fig. 226) is a low one-story structure of wood or wood-and-masonry construction with a ridge roof. Grace Lutheran Church (fig. 227) is a tall one-story building with a very steep wood ridge roof and heavy stone or stone-veneer walls. A tall square belltower of similar construction joins the building at its southwest corner. The sanctuary building at the United Methodist Church (fig. 228) is a fairly tall rectangular one-story structure with concrete-block and reinforced-concrete tiltup walls and a wood roof. The roof is built in four arched sections, each sloping downward to the south end of the building. Vertical stained-glass windows close up the space between the adjacent roof sections; on the north end (the entrance side) the space between the tall slender tiltup panels is also filled by stained-glass windows. No glass breakage was observed, and the church staff reported that the only known damage was breakage of the wire backstays for the crucifix hung from the sanctuary roof. The other

FIGURE 225.—Church of the Four Square Gospel, El Centro. View eastward.

FIGURE 226.—First Church of the Nazarene, El Centro. View southwestward.

FIGURE 227.—Grace Lutheran Church, El Centro. View northeastward.

FIGURE 228.—United Methodist Church, El Centro. View southwestward.

buildings at the United Methodist Church, of more conventional construction, were apparently undamaged.

In conclusion, behavior of the churches during the earthquake was representative of that of most other one-story structures in the El Centro area. The older churches suffered some damage to unreinforced-masonry walls and parapets, but the newer structures were very minimally damaged, if at all.

ACKNOWLEDGMENTS

We gratefully acknowledge the information and assistance provided by James A. Willis of Blaylock-Willis and Associates, San Diego, Calif.; Vitelmo Bertero of the University of California, Berkeley; D. A. ("Jim") Roberts and Randy Rister of the Imperial County Department of Buildings and Grounds, El Centro; John D. Hess of John D. Hess Testing Corp., El Centro; and David E. Pierson of the Imperial County Department of Public Works, El Centro.

STRONG-MOTION DATA RECORDED IN THE UNITED STATES

By R. L. PORCELLA, R. B. MATTHIESEN, and R. P. MALEY,
U.S. GEOLOGICAL SURVEY

CONTENTS

ABSTRACT

A total of 43 U.S. strong-motion stations within an epicentral distance of 150 km were in operation during the main shock. Maximum horizontal ground accelerations greater than 0.5 *g* were measured at seven stations within 10 km of the Imperial fault rupture; a maximum vertical acceleration of 1.74 *g* recorded at El Centro array station 6 exhibits a duration (peak accelerations greater than 0.1 *g*) of more than 6 s. More than 260 aftershock records were obtained at 21 stations within 30 km of the main-shock surface rupture; this data set contains the most comprehensive collection of close-in accelerograms ever recorded. Because absolute times were recorded on many of the records, detailed studies of the source mechanism and ground-motion characteristics are possible.

INTRODUCTION

In this report we summarize the main-shock and aftershock data from strong-motion instruments (accelerographs and seismoscopes) operated within the United States in the greater Imperial Valley region (fig. 229); our primary purpose is to alert other workers regarding the existence and availability of this data set. Most of the 44 stations that recorded the data are maintained by the U.S. Geological Survey (USGS), 11 by the California Division of Mines and Geology (CDMG), and 3 by different station owners. Additional data from a network of 13 strong-motion accelerographs in Baja California, operated by the Universidad Nacional Autónoma de México (UNAM) in cooperation with the University of California, San Diego (UCSD), and the Secretaría de Asentamientos Humanos y Obras Publicas (SAHOP), are summarized by Brune and others (this volume).

The October 15 main shock triggered all the USGS accelerographs within about 100 km of the epicenter and one as far away as 196 km (Porcella and Matthiesen, 1979a). The strong-motion stations in operation included one 13-station array alined transverse to the Imperial fault and one closely spaced 6-station array. Instruments in the CDMG network that were triggered included those in a six-story building and on an interstate highway overcrossing. The complete strong-motion records, including those from Baja Califonia, make up the most comprehensive close-in ground motion data set ever collected from a single event and are the fruit of several years of planning and execution of a cooperative effort in southern California by the USGS, CDMG, and the Earthquake Engineering Research Laboratory of the California Institute of Technology (CIT), as well as a similar effort in Baja California by UNAM, UCSD, and SAHOP.

DEVELOPMENT OF THE IMPERIAL VALLEY ACCELEROGRAPH NETWORK

A standard U.S. Coast and Geodetic Survey accelerograph was first installed at the site of the Imperial Irrigation District (formerly the Southern Sierra Power Co.) substation on Commercial Avenue in El Centro (sta. 9, fig. 230) in July 1932 as part of a program to gather strong-motion records from seismically active regions of the Western United States. In the early 1970's, the number of accelerograph stations in the Imperial Valley was increased substantially as a result of a reorganization of the nationwide USGS program, the deployment by the CIT of a network of accelerographs along the San Jacinto fault system, the initiation of the CDMG program, and the initial establishment of the UNAM/UCSD network in Baja California. In 1975, the three groups operating networks in southern California (USGS, CDMG, and CIT) combined their efforts and exchanged instrument sites and maintenance responsibility for greater operational efficiency. The USGS became responsible for most of the stations established by the CIT in southern California and most ground stations in the Imperial Valley,

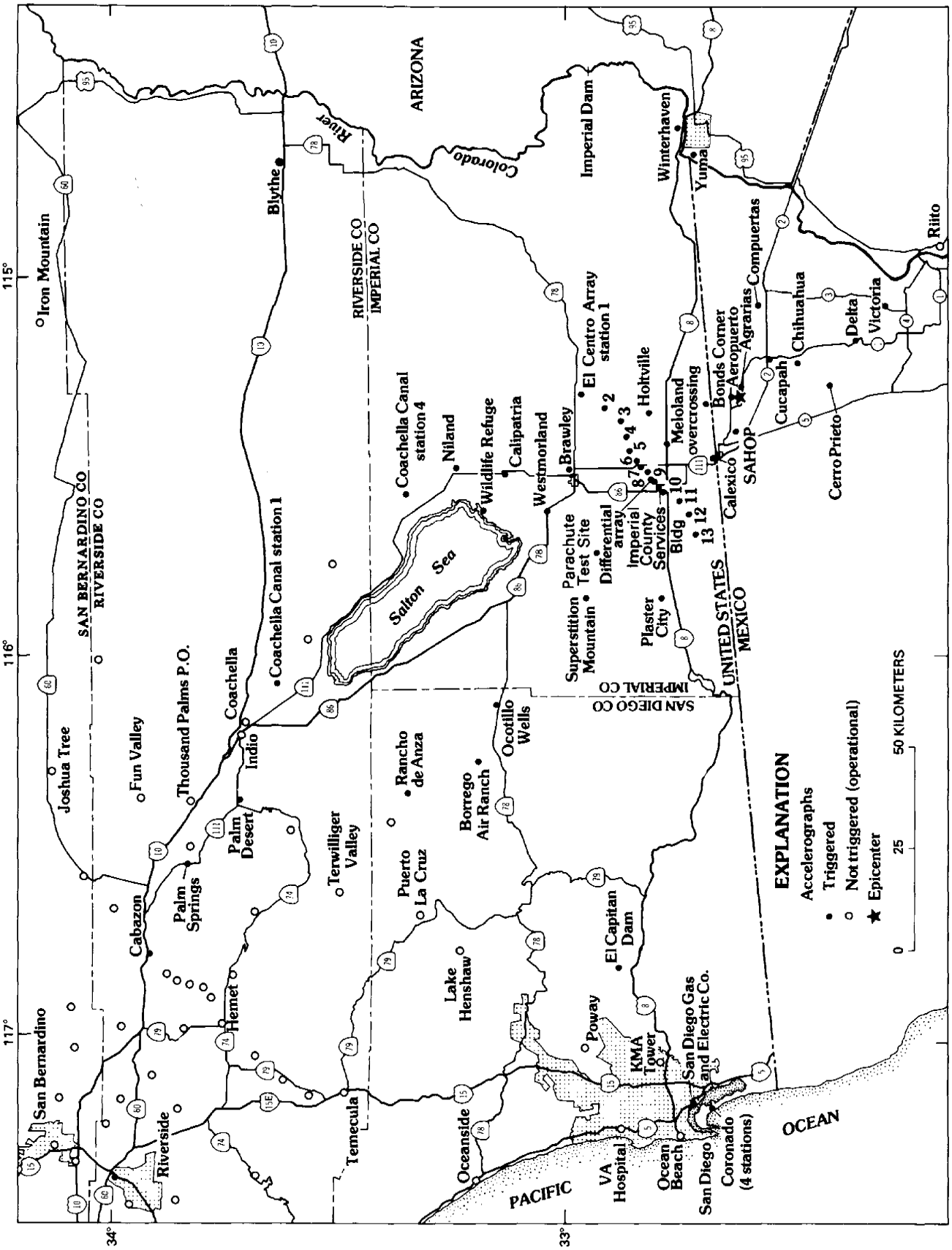

FIGURE 229.—Strong-motion stations in Imperial Valley region that were operational during 1979 earthquake.

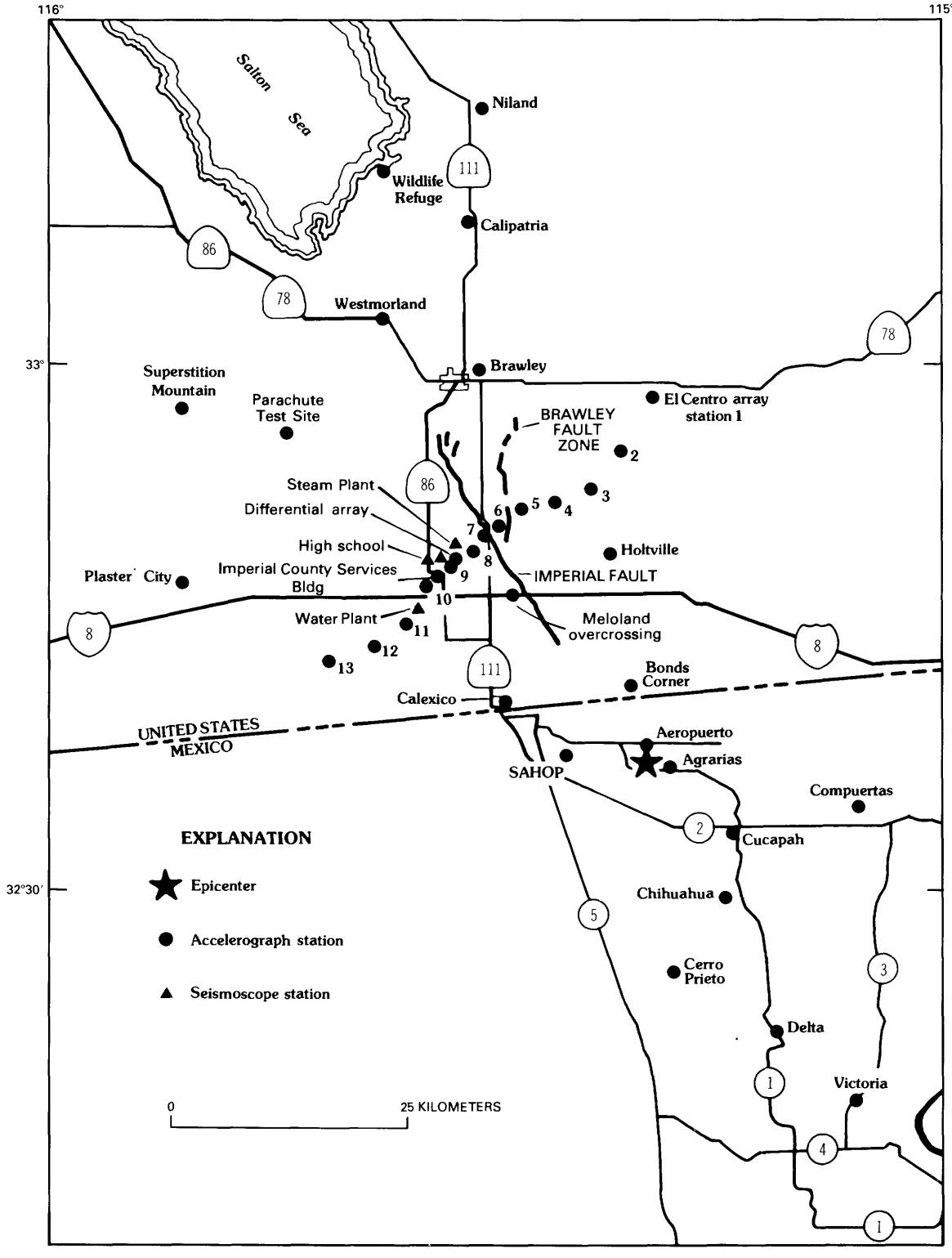

FIGURE 230.—Close-in strong-motion stations that were in operation during 1979 earthquake.

whereas the CDMG became responsible for most stations throughout the remainder of the State. The CDMG retained responsibility for the instruments on structures in the Imperial Valley, although the planning of this instrumentation was conducted in cooperation with the USGS and other organizations (Rojahn and Ragsdale, 1978). The USGS also began a concerted effort to develop specialized ground-motion arrays within the Imperial Valley to fulfill specific research needs required for studies of source mechanism, attenuation of ground motion, and differential ground motions. Figure 230 shows the locations of these arrays and their proximity to the Imperial fault and the Brawley fault zone.

The special-purpose arrays installed in the Imperial Valley region include: (1) the USGS-maintained El Centro array alined transverse to the Imperial fault, (2) the USGS-maintained differential array, and (3) the CDMG-maintained multichannel system at the Imperial County Services Building and at the Meloland Road-Interstate Highway 8 overcrossing (fig. 230). The El Centro array, made up of 13 stations at 3- to 5-km spacings, was established to provide information on the attenuation of motion with distance from the causative fault and to provide information on nearfield motion for the interpretation of source motions. This array extends a total length of 45 km transverse to the 1940 fault trace and contains accelerographs both in small Fiberglass housings (to approximate a free-field condition) and in buildings (including schools and a hospital). The differential array, installed in 1979 in cooperation with the Federal Highway Administration, consists of a 305-m-long array of six triaxial accelerometers at unequal spacings. The primary objective of the array, described by Bycroft (this volume), is to obtain differential ground-displacement data for use in studies of bridges, dams, pipelines, and other extended structures. The purpose of the instrumentation on the Meloland Road-Interstate Highway 8 crossing and in the Imperial County Services Building is to obtain data on the response of such structures at high levels of imput motion. The overcrossing is instrumented with a 26-channel accelerograph system, including 3 channels at a nearby ground site intended to be free field (Rojahn and others, this volume); the six-story Imperial County Services Building contains a 13-channel system, as well as a nearby free-field triaxial accelerograph at ground level (Rojahn and Mork, this volume).

Before the October 15, 1979, earthquake, more than 250 accelerograms had been recovered from the Imperial Valley region, nearly 200 of them since January 1975; these accelerograms contain accelerations as great as 0.3 to 0.5 g from moderate-size (M=4-5) earthquakes. All the records recovered before 1966 were obtained at the Commercial Avenue station, the only station operating in the Imperial Valley during that time. The increases in the number of records and in the peak accelerations reported since 1970 reflect an increase in the number of stations in the region and thus a decrease in the reported epicentral distances. Because of the short durations on many of these accelerograms, the data are of minimal engineering significance; however, many of the records contain useful seismologic information relevant to epicenter determinations, wave propagation, and source-mechanism studies of the Imperial Valley region (Porcella and Matthiesen, 1979b).

MAIN-SHOCK GROUND-MOTION DATA

Figure 229 shows the locations of instruments in the greater Imperial Valley region (including Baja California) that were operational at the time of the October 15 main shock, and table 28 summarizes the ground-motion accelerograph data obtained from stations in the United States during the main shock. The tabular information is listed alphabetically by station for convenience in correlating this information with the station locations.

Of the 24 USGS stations in the Imperial Valley, 21 contain Kinemetrics SMA-1T accelerographs equipped with vertical starters (capable of bringing the instrument into full operation within 0.2 s of the first vertical ground motion greater than 0.01 g) and with radio receivers that record WWVB absolute-time codes on the accelerograms. During the October 15 main shock, these accelerographs typically triggered on an early P-wave arrival, and the absolute trigger time as well as the S-wave arrival minus trigger time ($S-t$) interval could be determined (fig. 231; table 28). Some of the more distant stations were triggered by S-wave arrivals (footnote 1, table 28). To determine the event-origin time, the trigger-delay time (nominally 0.1-0.2 s) and the triggering-wave traveltime must be subtracted from the trigger time; the triggering-wave traveltimes may vary considerably because they depend on the specific source-to-station travel-path geometries. A comparison of epicentral distances and trigger times (a traveltime plot) indicates that at several of the close-in stations, arrivals were delayed as long as 1 s, which is typical of delays recorded at some of the more sensitive seismograph stations in the Imperial Valley region (Ralph Archuleta, oral commun., 1979).

The main-shock accelerograph records from USGS stations within 30 km of the fault rupture (fig. 231) provide valuable insight into the nature of ground shaking during a moderate-magnitude shallow-focus strike-slip earthquake. Of particular significance is the long-period pulse evident in many horizontal compo-

TABLE 28.—*Main-shock accelerograph ground-motion data for U.S. stations in the greater Imperial Valley region*

[Station numbers prefixed with "C" are assigned by CDMG, those with "CT" by CIT, and those without a prefix by USGS (U.S. Geological Survey, 1977). Epicentral distance is measured from station to epicenter at lat 32.64° N., long 115.33° W.; bracketed number denotes distance from station to nearest point on 1979 Imperial fault trace, which is assumed to extend from lat 32.94° N., long 115.54° W., to lat 32.72° N., long 115.40° W. Trigger time is measured in minutes and seconds after 288 d 23 h G.m.t., as determined from WWVB time code. Direction of acceleration is for upward trace deflection on accelerogram; horizontal components are listed as azimuth (in degrees clockwise from north), compass direction (N., S., E., or W.) indicates orientations based on a reference north, and vertical components are listed as "up" or "down." Maximum acceleration is peak value recorded at ground level on one vertical and two orthogonal horizontal components. Duration of acceleration is time between first and last peaks of acceleration greater than 0.10 *g*]

Station identification[1]			Site geology	Epicentral distance (km)	*S-t* interval (s)	Trigger time (G.m.t.)	Acceleration		
Number (data source)	Name and description	Coordinates (lat. °N., long °W.)					Direction	Maximum (*g*)	Duration (s)
C21	Blythe,	33.61, 114.71	Alluvium	122 [108]	(1)	(3)	360°	0.02	---
722	CDF Fire Station,						up	.02	---
(CDMG)	1-story building.						270°	.02	---
5054	Bonds Corner,	32.693, 115.338	Alluvium	6 [7]	2.4	16:57.11	230°	.81	13.2
CT62	Highways 98 and 115,						up	.47	12.0
(USGS)	1-story building.						140°	.66	13.3
5049	Borrego Air Ranch,	33.19, 116.28	Rock	108 [74]	8.2	17:20.06	315°	.04	---
CT29	Borrego Springs,						up	.02	---
(USGS)	1-story building.						225°	.03	---
5060	Brawley Airport,	32.988, 115.509	Alluvium	42 [6]	6.3	17:03.51	315°	.22	2.2
CT39	Brawley,						up	.18	5.2
(USGS)	instrument shelter.						225°	.17	1.8
5073	Cabazon Post Office,	33.92, 116.78	Alluvium	196 [158]	(1)	17:55.95	270°	.01	---
CT52	Cabazon,						up	.02	---
(USGS)	1-story building.						180°	.02	---
5053	Calexico Fire Station	32.669, 115.492	Alluvium	15	3.2	16:58.87	315°	.22	9.5
CT35	Fifth and Mary,						up	.21	8.8
(USGS)	1-story building.						225°	.28	10.8
5061	Calipatria Fire Station,	33.13, 115.52	Alluvium	57	7.4	17:06.55	315°	.09	---
CT40	Calipatria,						up	.07	---
(USGS)	2-story building.						225°	.13	1 peak
5074	Cherry Valley,	33.98, 116.99	---	214 [177]	---	(4)	---	---	---
CT53	Johnson Residence,								
	1-story building.								
5063	Coachella Canal,	33.64, 116.08	Alluvium	131 [92]	(1)	17:23.98	135°	.02	---
CT45	Station 1,						up	.02	---
(USGS)	1-story building.						045°	.03	---
5064	Coachella Cannal,	33.56, 115.95	Alluvium	117 [79]	---	(4)	---	---	---
CT44	Station 2,								
	1-story building.								
5065	Coachella Canal,	33.51, 115.77	Alluvium	105 [67]	---	(4)	---	---	---
CT43	Station 3,								
	1-story building.								
5066	Coachella Canal,	33.36, 115.59	Alluvium	84 [47]	8.5	17:11.44	135°	.14	.5
CT42	Station 4,						up	.04	---
(USGS)	1-story building.						045°	.11	.3
C26	Coachella Citrus,	33.72, 116.16	Alluvium	143 [104]	---	(4)	---	---	---
726	Indio,								
	instrument shelter.								
5046	Collins Valley,	33.42, 116.47	Rock	136 [102]	---	(4)	---	---	---
CT26	Anza Borrego Park,								
	instrument shelter.								
767	Coronado,	32.68, 117.17	Alluvium	172 [155]	(1)	(3)	130°	.01	---
(USGS)	1770 Ava del Mundo,						up	---	---
	16-story building.						040°	.01	---
5117	Coronado,	32.68, 117.17	Alluvium	172 [155]	(1)	(3)	130°	.01	---
(USGS)	1780 Ava del Mundo,						up	.01	---
	17-story building.						040°	.01	---
781	Coronado,	32.68, 117.17	Alluvium	172 [155]	---	(4)	---	---	---
	1820 Ava del Mundo,								
	16-story building.								
5042	Cranston Forest Station,	33.74, 116.84	---	186 [150]	---	(4)	---	---	---
CT21	San Jancinto Valley,								
	1-story building.								
620	Devils Canyon,	34.21, 117.33	---	254 [217]	---	(4)	---	---	---
	San Bernardino,								
	powerplant.								
C243	El Capitan Dam,	32.88, 116.82	Rock	142 [119]	(1)	17:37.8	154°	.02	---
5094	El Capitan Reservoir,						up	.01	---
(CDMG)	earth dam.						064°	.02	---

TABLE 28.—*Main-shock accelerograph ground-motion data for U.S. stations in the greater Imperial Valley region* — Continued

Station identification[1]			Site geology	Epicentral distance (km)	*S-t* interval (s)	Trigger time (G.m.t.)	Acceleration		
Number (data source)	Name and description	Coordinates (lat. °N., long °W.)					Direction	Maximum (g)	Duration (s)
C260	El Centro, Imperial,	32.793, 115.564	Alluvium	27 [8]	5.0	17:00	360°	.35	6
5090	County Services Building,						up	.19	4
(CDMG)	6-story building.						090°	.32	6
C335	El Centro,	32.79, 115.56	Alluvium	27 [8]	5.0	16:59.9	092°	.24	5
5154	Imperial County Center,						up	.27	---
(CDMG)	instrument shelter.						002°	.24	---
5056	El Centro array station 1,	32.960, 115.319	Alluvium	36 [22]	6	17:02.2	230°	.15	3.1
CT38	Borchard Ranches,						up	.10	1 peak
(USGS)	instrument shelter.						140°	.15	4.8
5115	El Centro array station 2,	32.916, 115.366	Alluvium	31 [16]	6	17:01.17	230°	.43	5.7
(USGS)	Keystone Road,						up	.17	9.3
	instrument shelter.						140°	.33	9.2
5057	El Centro array station 3,	32.894, 115.380	Alluvium	29 [13]	5.4	(3)	230°	.22	6.2
CT60	Pine Union School,						up	.15	5.6
(USGS)	1-story building.						140°	.27	6.0
955	El Centro array station 4,	32.864, 115.432	Alluvium	27 [7]	[2]4.8	17:01.77	230°	.38	6.5
(USGS)	2905 Anderson Road,						up	.32	6.7
	instrument shelter.						140°	.61	6.8
952	El Centro array station 5,	32.855, 115.466	Alluvium	27 [4]	5.1	17:01.36	230°	.40	7.6
(USGS)	2801 James Road,						up	.71	5.6
	instrument shelter.						140°	.56	7.4
942	El Centro array station 6,	32.839, 115.487	Alluvium	27 [1]	[2]5	17:01	230°	.45	7.9
C192	551 Huston Road,						up	1.74	6.2
(USGS)	instrument shelter.						140°	.72	11.8
5028	El Centro array station 7,	32.829, 115.504	Alluvium	27 [1]	4.6	(3)	230°	.52	4.9
CT37	Imperial Valley College,						up	.65	5.5
(USGS)	1-story building.						140°	.36	3.7
958	El Centro array station 8,	32.811, 115.532	Alluvium	27 [4]	[2]5	17:00.5	230°	.50	6.9
C193	95 E. Cruickshank Road,						up	.55	5.8
(USGS)	instrument shelter.						140°	.64	6.9
117	El Centro array station 9,	32.794, 115.549	Alluvium	27 [6]	(1)	(3)	down	.38	4.7
(USGS)	302 Commercial Avenue,						360°	.40	7.4
	2-story building.						090°	.27	7.0
412	El Centro array station 10,	32.780, 115.567	Alluvium	27 [9]	4.9	(3)	050°	.20	5.2
(USGS)	Community Hospital,						up	.15	2.2
	1-story building.						320°	.23	5.1
5058	El Centro array station 11,	33.752, 115.594	Alluvium	28 [13]	5.6	17:00.48	230°	.38	6.5
CT34	McCabe School,						up	.16	7.7
(USGS)	1-story building.						140°	.38	7.0
931	El Centro array station 12,	32.718, 115.637	Alluvium	30 [18]	5.2	17:01.50	230°	.11	4.9
C218	907 Brockman Road,						up	.08	---
(USGS)	instrument shelter.						140°	.15	3.8
5059	El Centro array station 13,	32.709, 115.683	Alluvium	34 [22]	5.1	17:02.40	230°	.15	5.0
CT61	Strobel Residence,						up	.06	---
(USGS)	1-story building.						140°	.12	2.4
5165	El Centro differential array,	32.796, 115.535	Alluvium	26 [5]	5	(3)	360°	.51	10.2
(USGS)	Dogwood Road,						up	.93	7.0
	1-story building.						270°	.37	7.0
C336	El Centro, Meloland Road-	32.773, 115.448	Alluvium	18 [1]	(1)	16:59.5	360°	.32	6
5155	Interstate Highway 8						up	.23	4
(CDMG)	overcrossing.						270°	.30	7
5075	Forest Falls,	34.09, 116.92	---	218 [181]	---	(4)	---	---	---
CT54	Mill Creek Canyon,								
	1-story building.								
5069	Fun Valley,	33.93, 116.39	Alluvium	174 [135]	---	(4)	---	---	---
CT48	Reservoir 361,								
	1-story building.								
5040	Gilman Hot Springs,	33.84, 116.99	---	204 [167]	---	(4)	---	---	---
CT19	Massacre Canyon Inn,								
	1-story building.								
C198	Hemet array station A,	33.60, 117.12	Alluvium	198 [164]	---	(4)	---	---	---
5000	Murietta Hot Springs,								
	instrument shelter.								
C199	Hemet array station B,	33.62, 117.10	Rock	197 [1[illegible]	---	(4)	---	---	---
5001	Bergman Ranch,								
	instrument shelter.								

TABLE 28.—*Main-shock accelerograph ground-motion data for U.S. stations in the greater Imperial Valley region*— Continued

Station identification[1]			Site geology	Epicentral distance (km)	S-t interval (s)	Trigger time (G.m.t.)	Acceleration		
Number (data source)	Name and description	Coordinates (lat. °N., long °W.)					Direction	Maximum (g)	Duration (s)
C200 5002	Hemet array station C, Hidden Valley Farms, instrument shelter.	33.68, 117.05	Rock	197 [163]	---	(4)	---	---	---
C201 5003	Hemet array station D, Page Brothers Ranch, instrument shelter.	33.71, 117.06	Alluvium	200 [165]	---	(4)	---	---	---
C331 123	Hemet array station E, 895 Stetson, 1-story building.	33.73, 116.98	Alluvium	195 [160]	---	(4)	---	---	---
C202 5004	Hemet array station F, San Jacinto Valley, 1-story building.	33.76, 116.96	---	196 [160]	---	(4)	---	---	---
C203 5005	Hemet array station G, San Jacinto, 1-story building.	33.78, 116.59	---	172 [135]	---	(4)	---	---	---
C204 5006	Hemet array station H, Soboda, 1-story building.	33.80, 116.88	---	193 [157]	---	(4)	---	---	---
C205 5007	Hemet array station I, Poppet Creek, instrument shelter.	33.83, 116.87	---	195 [160]	---	(4)	---	---	---
C206 5008	Hemet array station J, Silent Valley, instrument shelter.	33.85, 116.85	---	195 [158]	---	(4)	---	---	---
C268 5009	Hemet array station K, Valley High Park, 1-story building.	33.87, 116.83	---	195 [158]	---	(4)	---	---	---
C266 5091	Hemet Library, 510 East Florida, 1-story building.	33.75, 116.97	---	196 [160]	---	(4)	---	---	---
C267 5092	Hemet Valley Hospital, 1116 East Latham, 4-story building.	33.75, 116.96	---	195 [158]	---	(4)	---	---	---
5055 CT36 (USGS)	Holtville, Post Office, 1-story building.	32.812, 115.377	Alluvium	20 [8]	4.1	(3)	315° up 225°	.22 .31 .26	7.5 7.0 6.2
5043 CT22	Hurkey Creek, County Park, 1-story building.	33.67, 116.68	Alluvium	170 [133]	---	(4)	---	---	---
5067 CT46	Indio, Southern California Gas Co., 1-story building.	33.75, 116.21	Alluvium	148 [109]	---	(4)	---	---	---
820	Iron Mountain, MWD Pumping Plant.	34.15, 115.12	---	169 [140]	---	(4)	---	---	---
C170 934	Joshua Tree, 6715 Park Boulevard, 1-story building.	34.13, 116.31	Alluvium	189 [150]	---	(4)	---	---	---
C166 976	Lake Elsinore, Park Maintenance Building, 1-story building.	33.67, 117.37	Alluvium	221 [188]	---	(4)	---	---	---
C167 932	Lake Henshaw, USFS Pump House, 1-story building.	33.23, 116.76	Rock	148 [118]	---	(4)	---	---	---
5071 CT50	Morongo Valley, Fire Station, 1-story building.	34.05, 116.58	---	195 [156]	---	(4)	---	---	---
C23 724 (CDMG)	Niland Fire Station, 8071 Luxor, 1-story building.	33.24, 115.51	Alluvium	69 [33]	5.7	(3)	090° up 360°	.10 .03 .07	2 peaks --- ---
5070 CT49	North Palm Springs, Post Office, 1-story building.	33.92, 116.54	---	181 [143]	---	(4)	---	---	---
C121 898	Ocean Beach, 4711 Voltaire, 1-story building.	32.75, 117.24	Alluvium	179 [160]	---	(4)	---	---	---
C333 5153	Oceanside "B", Airport, 1-story building.	33.22, 117.35	---	199 [171]	---	(4)	---	---	---

TABLE 28.—*Main-shock accelerograph ground-motion data for U.S. stations in the greater Imperial Valley region*—Continued

Station identification[1]			Site geology	Epicentral distance (km)	*S-t* interval (s)	Trigger time (G.m.t.)	Acceleration		
Number (data source)	Name and description	Coordinates (lat. °N., long °W.)					Direction	Maximum (g)	Duration (s)
5050	Ocotillo Wells,	33.14, 116.13	Alluvium	93 [59]	[2]7.5	17:15.68	315°	.05	---
CT30	Burro Bend Cafe,						up	.03	---
(USGS)	1-story building.						225°	.04	---
C284	Palm Desert,	33.76, 116.41	Alluvium	160 [122]	(1)	(3)	N.	.02	---
(CDMG)	Kiewit Building,						up	.01	---
	4-story building.						E.	.03	---
C25	Palm Springs,	33.83, 116.51	Alluvium	172 [134]	---	(4)	---	---	---
725	Airport,								
	instrument shelter.								
C299	Palm Springs,	33.84, 116.54	Alluvium	174 [136]	(1)	(3)	N.	.01	---
(CDMG)	Desert Hospital,						up	.01	---
	4-story building.						W.	.02	---
5051	Parachute Test Site,	32.93, 115.70	Alluvium	47 [15]	7.0	(3)	315°	.20	1.5
CT32	Imler Road,						up	.18	5.2
(USGS)	1-story building.						225°	.11	1.4
803	Perris Dam,	33.85, 117.18	---	218 [183]	---	(4)	---	---	---
	Lake Perris,								
	earth dam.								
5044	Pinon Flat,	33.61, 116.46	Rock	150 [113]	---	(4)	---	---	---
CT23	UCSD Observatory,								
	underground vault.								
C161	Pinto Wye Station,	34.02, 116.02	Alluvium	166 [128]	---	(4)	---	---	---
935	Twentynine Palms,								
	1-story building.								
5052	Plaster City,	32.79, 115.86	Alluvium	52 [31]	[2]5	(3)	135°	.07	---
CT33	storehouse,						up	.03	---
(USGS)	1-story building.						045°	.05	---
C119	Poway,	32.95, 117.06	Alluvium	165 [142]	---	(4)	---	---	---
897	12324 Oak Knoll,								
	1-story building.								
C168	Puerta La Cruz,	33.32, 116.68	Alluvium	147 [114]	---	(4)	---	---	---
933	USFS storage building,								
	1-story building.								
5047	Rancho de Anza,	33.35, 116.40	Alluvium	127 [92]	(1)	17:27.08	135°	.03	---
CT27	Anza Borrego Park,						up	.02	---
(USGS)	instrument shelter.						045°	.02	---
5037	Reche Canyon,	34.01, 117.22	---	232 [196]	---	(4)	---	---	---
CT16	Olive Dell Ranch,								
	1-story building.								
C123	Riverside Airport,	33.95, 117.44	Alluvium	244 [209]	---	(4)	---	---	---
900	maintenance Shop,								
	1-story building.								
C312	Riverside County	33.98, 117.37	---	241 [205]	(1)	(3)	E.	.01	---
(CDMG)	Administration Building,						up	.01	---
	13-story building.						N.	.01	---
C118	Sage,	33.58, 116.93	Alluvium	182 [147]	---	(4)	---	---	---
901	3738 Sage Street,								
	1-story building.								
5062	Salton Sea	33.18, 115.62	Alluvium	66 [28]	[2]3.5	17:11.39	315°	.06	---
CT41	Wildlife Refuge,						up	.03	---
(USGS)	1-story building.						225°	.06	---
C300	San Diego,	32.72, 117.16	Alluvium	171 [153]	(1)	(3)	090°	.01	---
275	SDGE Office Building,						up	.01	---
(CDMG)	22-story building.						360°	.01	---
C27	San Diego,	32.79, 117.06	Rock	162 [143]	---	(4)	---	---	---
727	KMA Radio Tower,								
	instrument shelter.								
639	San Siego VA Hospital,	32.87, 117.23	Rock	179 [158]	---	(4)	---	---	---
	La Jolla, Building 2,								
	2-story building.								
C178	Steephole Pass,	34.23, 115.72	Rock	180 [144]	---	(4)	---	---	---
946	instrument shelter.								

TABLE 28.—*Main-shock accelerograph ground-motion data for U.S. stations in the greater Imperial Valley region* — Continued

Station identification[1]			Site geology	Epicentral distance (km)	S-t interval (s)	Trigger time (G.m.t.)	Acceleration		
Number (data source)	Name and description	Coordinates (lat. °N., long °W.)					Direction	Maximum (g)	Duration (s)
720	Skinner Dam, Murrieta Hot Springs, earth dam.	33.58, 117.07	---	193[159]	---	(4)	---	---	---
286	Superstition Mountain,	32.955, 115.823	Rock	58[26]	[2]7.2	17:06.76	135°	.21	1.1
CT31	USN Camera Site						up	.09	---
(USGS)	1-story building.						045°	.12	.6
C172	Temecula,	33.50, 117.15	Alluvium	194[162]	---	(4)	---	---	---
947	CDF Fire Station, 1-story building.								
5045	Terwilliger Valley,	33.48, 116.59	Rock	150[114]	---	(4)	---	---	---
CT25	Snodgrass residence, instrument shelter.								
5068	Thousand Palms,	33.82, 116.40	Alluvium	164[126]	---	(4)	---	---	---
CT47	Post Office, 1-story building.								
C369	Westmorland	33.04, 115.62	Alluvium	52[13]	5.4	(3)	180°	.11	1 peak
(CDMG)	Fire Station, 2-story building.						up	.09	---
							090°	.08	---
5072	White Water Canyon,	33.99, 116.66	---	194[156]	---	(4)	---	---	---
CT51	trout farm, 1-story building.								
C22	Winterhaven	32.74, 114.64	Alluvium	65[71]	(1)	(3)	270°	.07	---
723	Sheriff's Substation,						up	.02	---
(CDMG)	1-story building.						180°	.05	---
2316	Yuma, Ariz.,	32.73, 114.70	Alluvium	60[65]	(1)	17:11.34	090°	.03	---
(USGS)	Strand Avenue, instrument shelter.						up	.02	---
							360°	.03	---

[1]Instrument triggered by S wave, or S-wave arrival unidentifiable.
[2]Questionable.
[3]WWVB time code illegible, or instrument not equipped with a radio receiver.
[4]Ground-level instrument did not trigger.

nents on the records from stations within 10 km of the fault; these acceleration pulses produce significant changes in velocity and displacement (Brady and others, this volume). For distances greater than 10 km from the fault trace, the peak-acceleration values are consistent with those recorded during previous events of this magnitude, but the main-shock data provide significant new information on the motions within 15 km of the fault trace (Boore and Porcella, this volume). Of additional importance relative to the close-in stations is the observation that many of the vertical accelerations are greater than the corresponding horizontal accelerations, in contrast to observations obtained at more distant stations during previous events (Maley and Cloud, 1973; Newmark Consulting Engineering Services, 1973).

The main-shock accelerograph data include one accelerogram recorded at the Commercial Avenue station, the same site where the well-known accelerogram of the May 18, 1940, earthquake was recorded (Neumann, 1942). For many years this 1940 El Centro record has been used worldwide in earthquake-engineering studies as representative of ground motion from a strong local earthquake. Because all three component traces on the 1940 accelerograph record went off scale (6-in. photographic paper was used at the time), it is of some interest to compare the 1940 record with the 1979 record from a similar instrument (one that records on 12-in. photographic paper) at the same site (El Centro array sta. 9, fig. 230).

Figure 232 presents these two records to the same scale. The component traces of the 1940 record were plotted from a digitized version that includes those parts extrapolated beyond the limits of the original record, whereas the 1979 record, which did not go off scale, was carefully traced to remove two displacement traces and to separate the three acceleration traces. A comparison of the two records shows more similarities than differences; although the reported values of peak acceleration on the 1979 record are higher than those reported for the 1940 record, this relation may be artifactual because the peak accelerations on the 1940 record could not be accurately ascertained. On the other hand, the high accelerations on the 1940 record

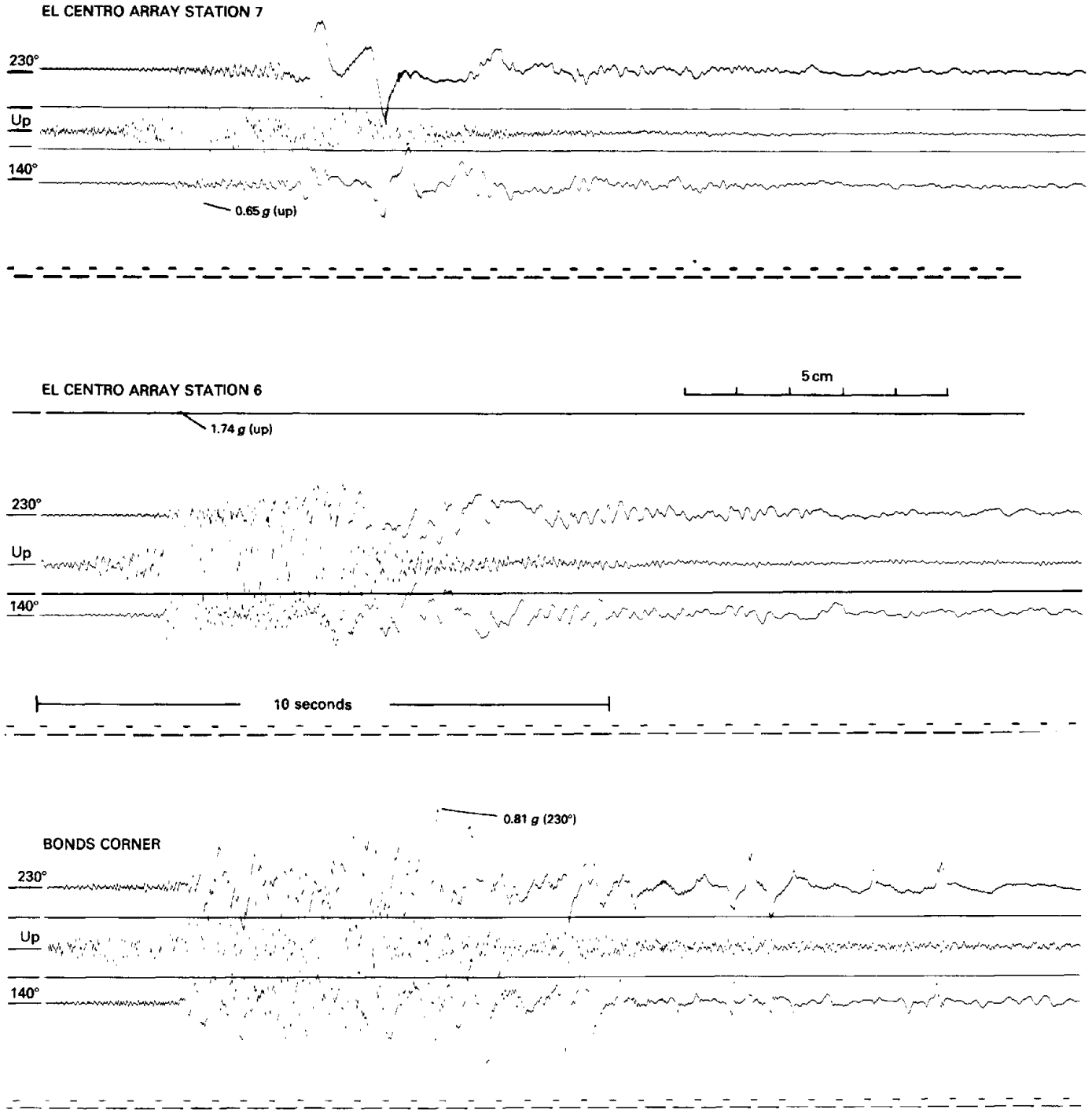

FIGURE 231.—USGS accelerograms from stations within 30 km of fault rupture of 1979 earthquake (array station 9 accelerogram is shown in fig. 232), showing peak accelerations. Solid horizontal lines are zero reference traces. Poor quality of some data traces is due to high-frequency high-amplitude motion recorded on photo-optical accelerographs.

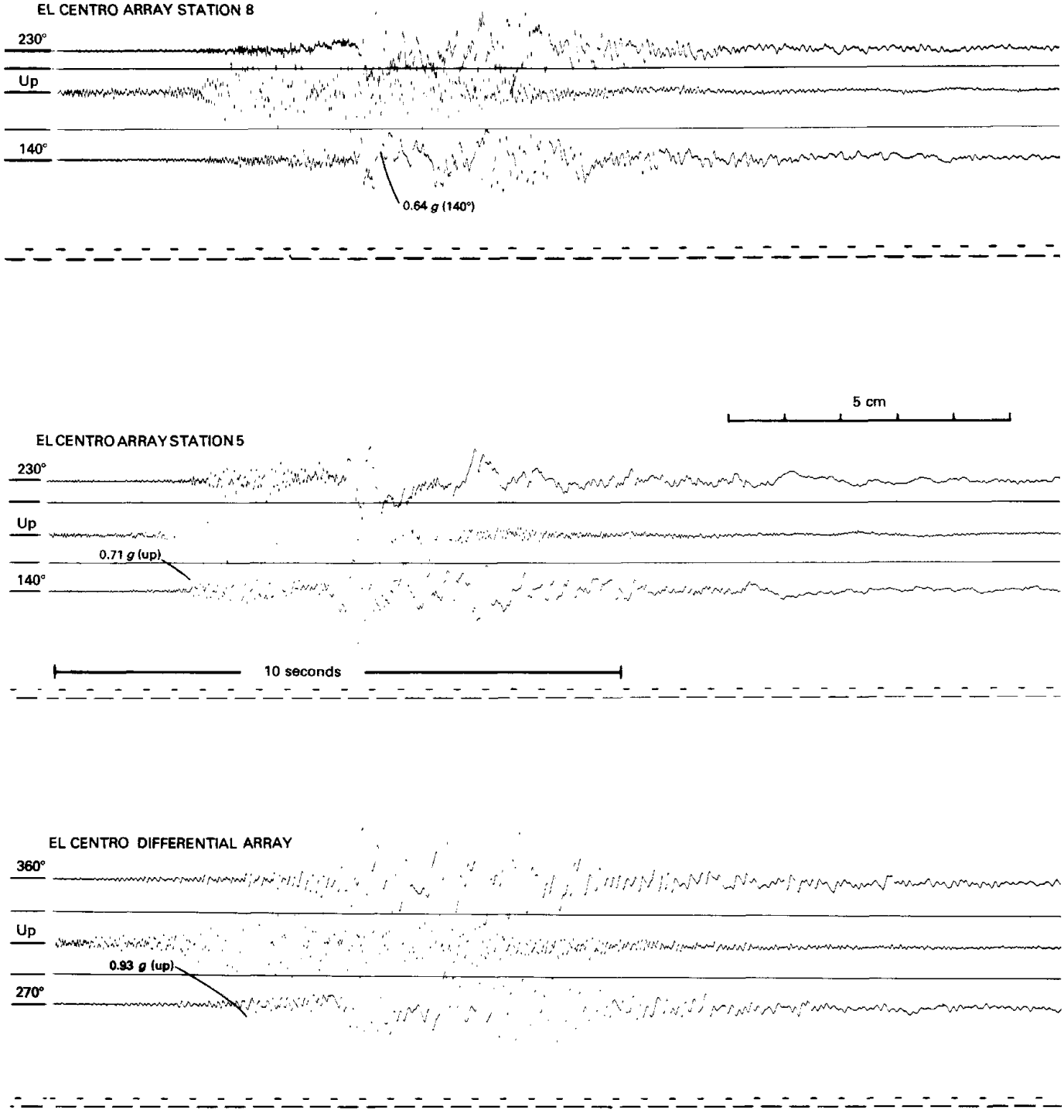

FIGURE 231.—Continued.

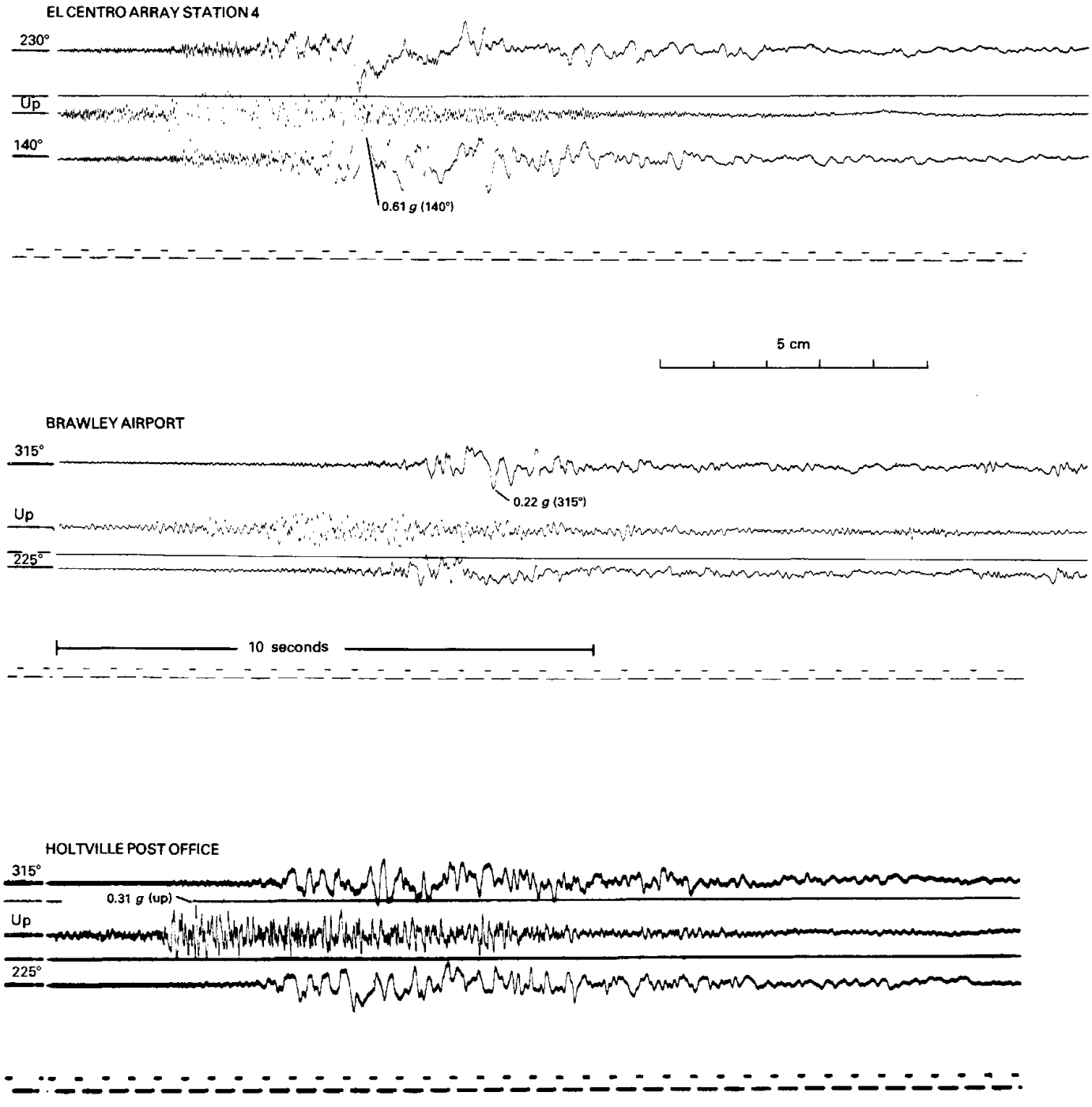

FIGURE 231.—Continued.

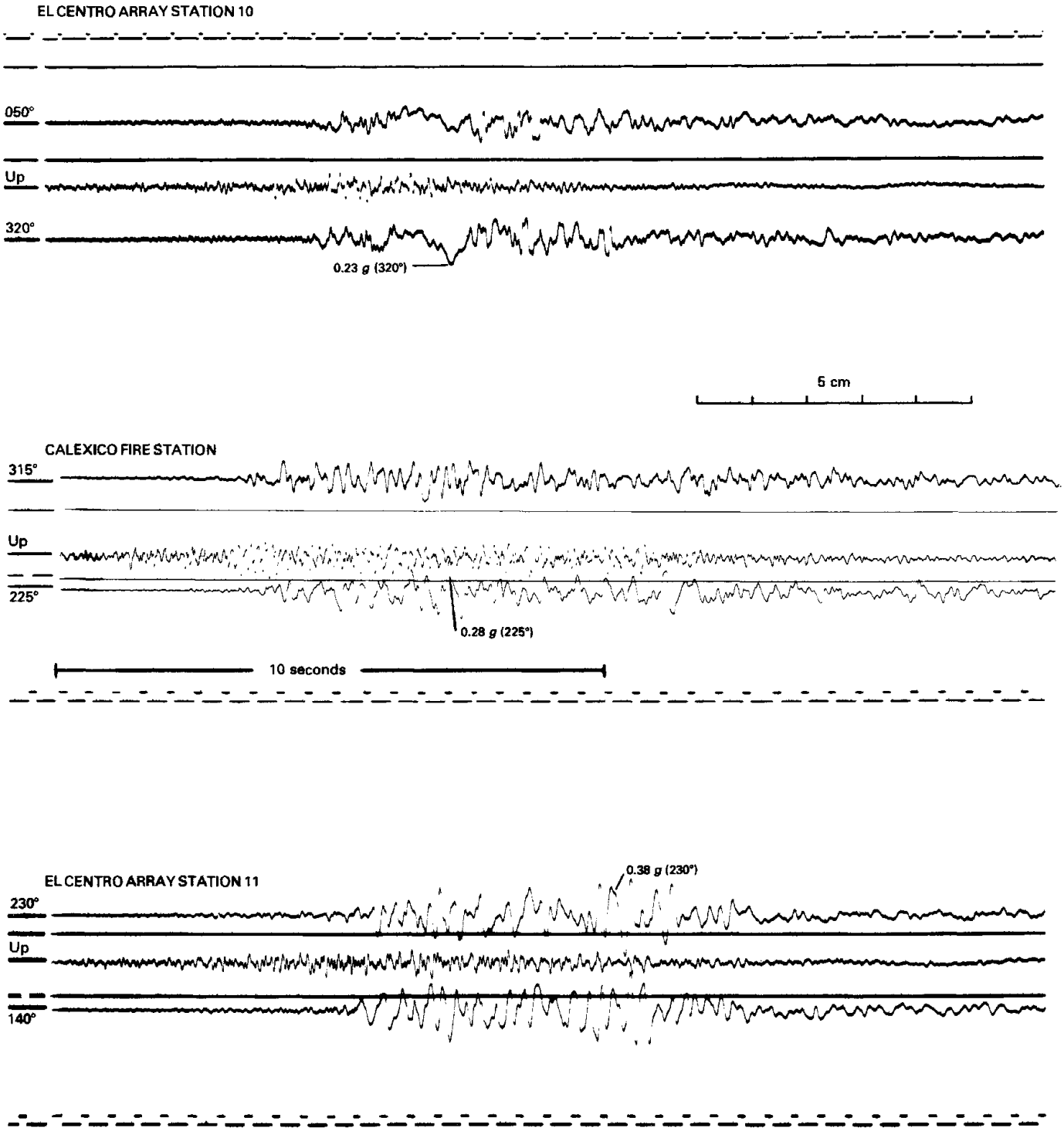

FIGURE 231.—Continued.

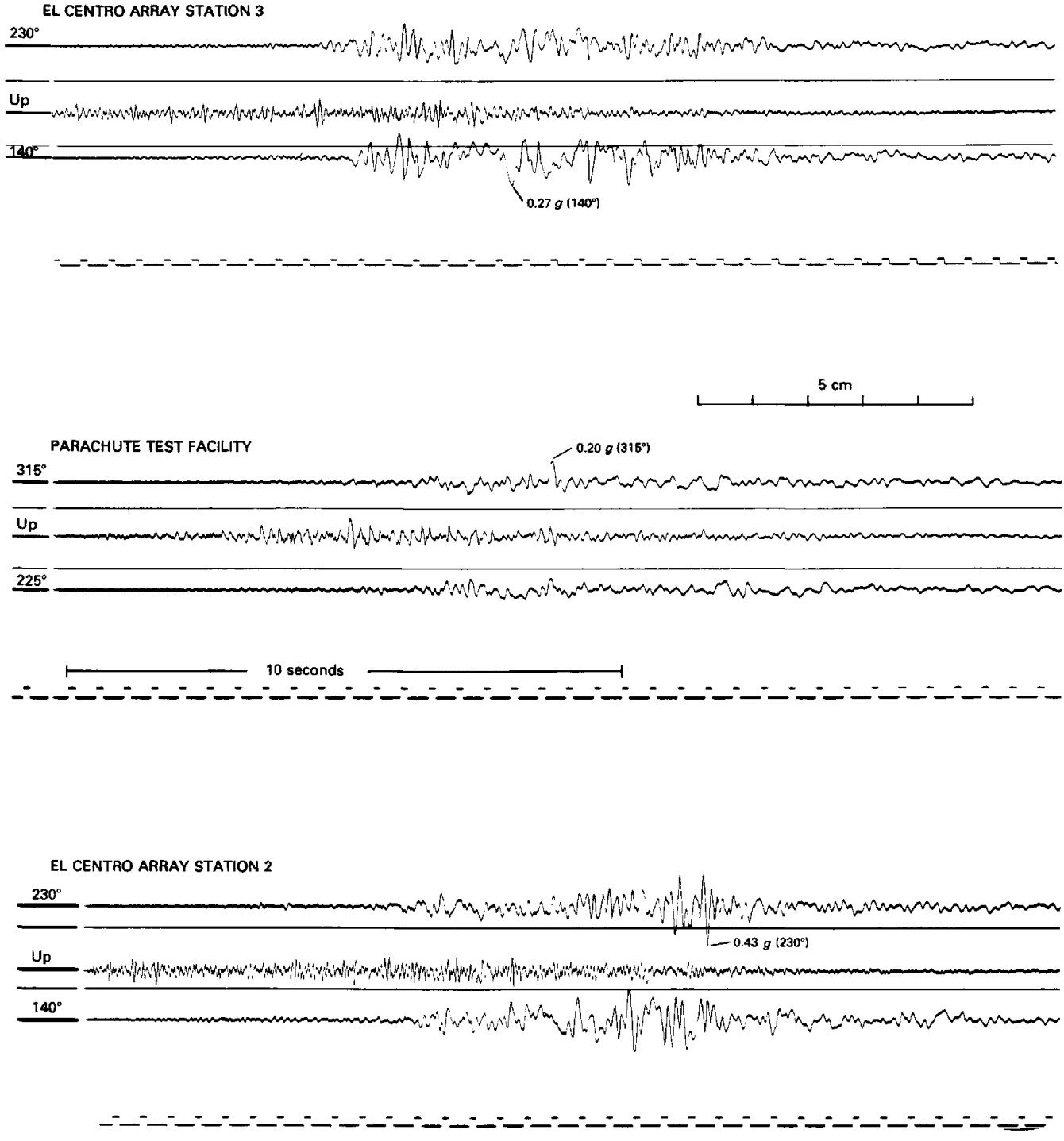

FIGURE 231.—Continued.

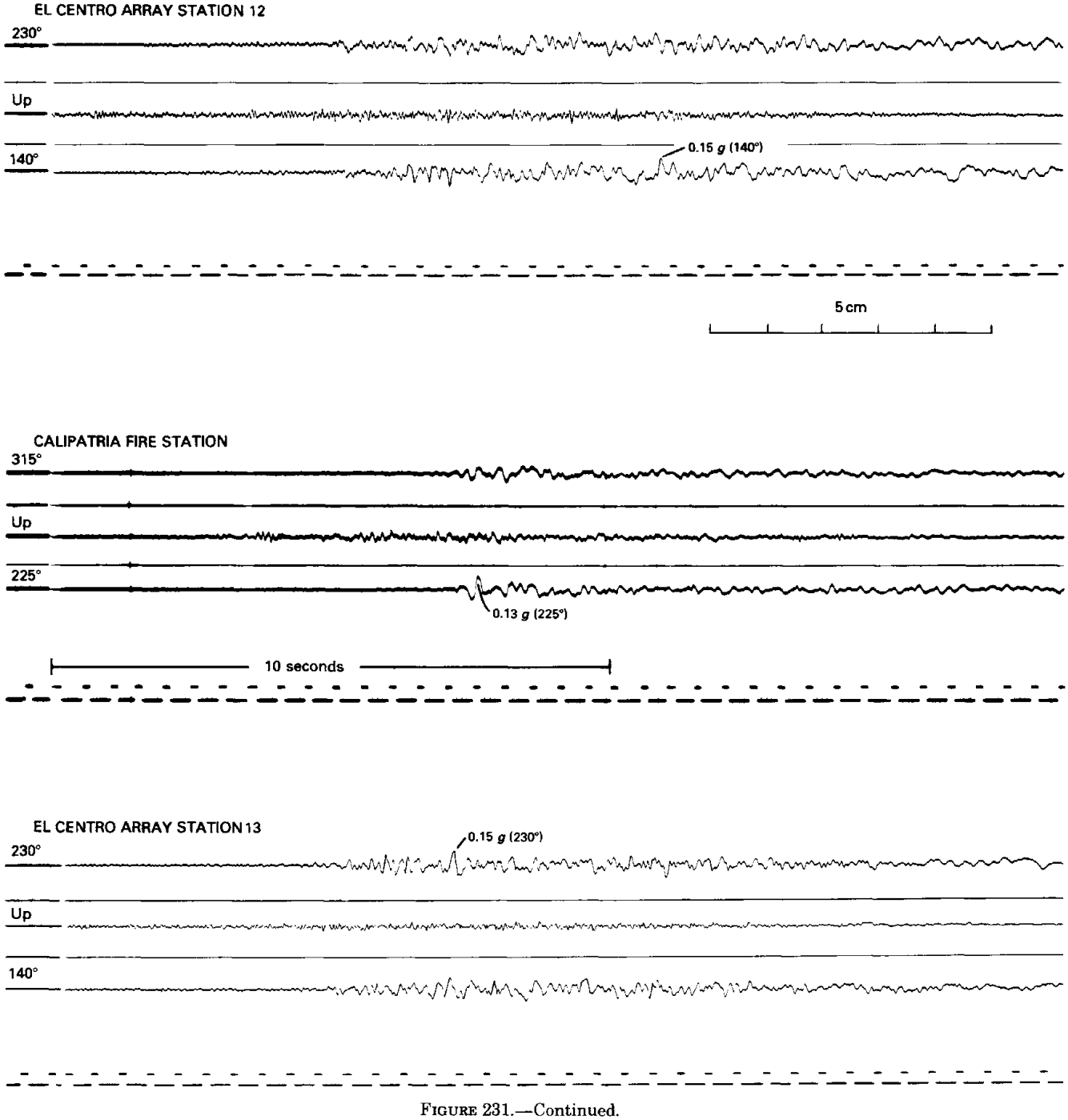

FIGURE 231.—Continued.

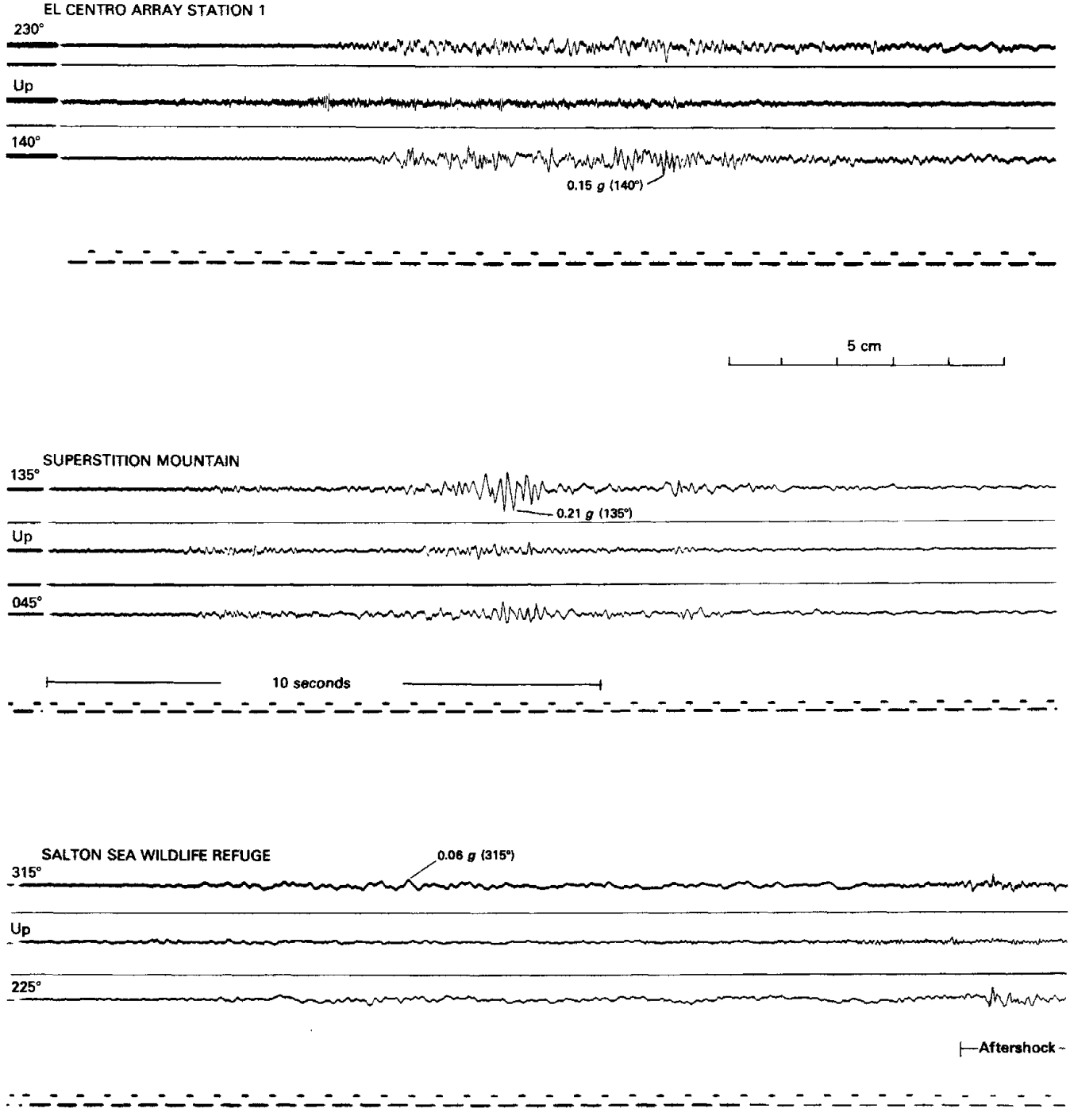

FIGURE 231.—Continued.

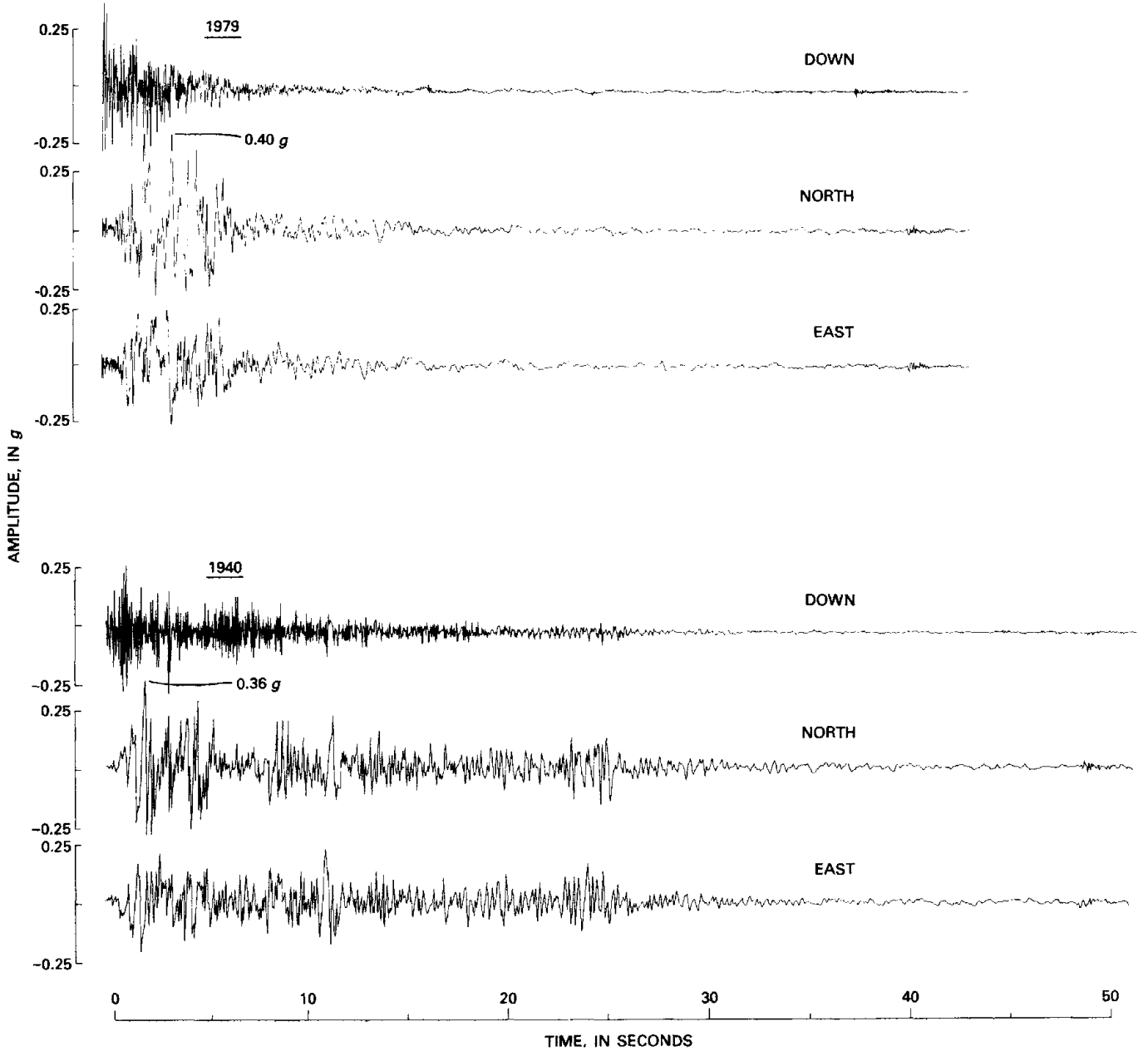

FIGURE 232.—Accelerograms from El Centro array station 9 (Commercial Ave.) for Imperial Valley earthquakes of October 15, 1979, and May 18, 1940, showing peak accelerations.

last for a longer time; this longer duration of high accelerations is consistent with the interpretation that the 1940 event was a multiple event in which five or more earthquakes occurred within seconds of one another (Trifunac and Brune, 1970). A preliminary interpretation of the 1979 records suggests that this earthquake also was a multiple event in which most of the accelerographs were triggered by motion from the reported hypocenter but most of the energy came from a later (2-3 s) event associated with the surface faulting (T. C. Hanks, oral commun., 1979). This interpretation and others regarding the influence of the direction of rupture propagation on the values of acceleration (Brune and others, this volume) are tentative and require further substantiation as these records and other seismologic data are studied in greater detail.

The October 15 main shock was also recorded by five seismoscopes, four of which (fig. 233; table 29) were in the Imperial Valley (fig. 230) and the fifth at the Imperial Dam, northeast of Yuma, Ariz. (fig. 229). One of the Imperial Valley seismoscopes is at the original El Centro accelerograph station on Commercial Avenue, and another is within 1 km of the El Centro differential array (fig. 230).

MAIN-SHOCK DATA FROM INSTRUMENTED STRUCTURES

The main shock was recorded by accelerograph systems at eight buildings, one bridge, and one dam. The summary of data from instrumented structures (table 30) indicates that only the records from the Imperial County Services Building in El Centro (peak acceleration, 0.59 *g*) and the Meloland Road-Interstate Highway 8 overcrossing (peak acceleration, 0.51 *g*) are appropriate for structural-response studies because of the high amplitudes and long durations of recorded motion (Rojahn and Mork, this volume; Rojahn and Ragsdale, this volume). The other structures, which were farther than 140 km from the October 15 main shock, recorded substantially lower levels of motion.

TABLE 29.—*Main-shock seismoscope data*

[Epicentral distance is measured from station to epicenter at lat 32.64° N., long 115.33° W.; bracketed number denotes distance from station to nearest point on 1979 Imperial fault trace, which is assumed to extend from lat 32.94° N., long 115.54° W., to lat 32.72° N., long 115.40° W. S_v, relative-velocity response-spectrum ordinate; S_d, relative-displacement response-spectrum ordinate (Hudson and Cloud, 1967)]

Station name (data source)	Coordinates (lat °N., long °W.)	Epicentral distance (km)	S_v (cm/s)	S_d (cm)
El Centro High School (USGS)	32.79 115.56	27 [8]	29.7	3.5
El Centro Steam Plant (USGS)	32.80 115.54	26 [5]	55.1	6.6
El Centro Substation[1] (USGS)	32.794 115.549	27 [6]	53.3	6.4
El Centro Water Plant (USGS)	32.77 115.56	26 [10]	34.3	4.1
Imperial Dam (USGS)	32.88 114.47	85 [89]	8.1	1.0

[1]Same site as accelerograph station 117, El Centro array station 9.

AFTERSHOCK GROUND-MOTION DATA

The USGS Imperial Valley accelerograph network recorded 82 identifiable aftershocks at 21 stations during the first week after the October 15 main shock; 14 of these aftershocks were recorded at 3 or more stations. This data set contains more than 150 records that can be used for epicenter and magnitude determinations, as well as in source-mechanism and ground-motion-attenuation studies (table 31). In all, 21 stations within 30 km of the main-shock surface rupture produced more than 260 aftershock records, approximately 50 of which contain peak accelerations greater than 0.1 *g* (table 32). Additional data were recorded at temporary stations installed by the University of Southern California (Anderson and Heaton, this volume) and by the USGS (Boore and Fletcher, this volume).

Only 2 of the 21 stations that recorded aftershocks do not have WWVB time capabililty; however, only 44 percent of the nearly 250 records recovered at stations with WWVB receivers contain good-quality time-code traces. This problem is evident on the records from El Centro array stations 6 and 7, the differential array, Holtville, and the Parachute Test Site, where significant numbers of time-code traces that cannot be positively correlated with an event were obtained (table 32).

The reported numbers of aftershocks recorded at several stations require some clarification. The Brawley Airport station recorded 40 aftershocks (although the instrument actually was triggered only 26 times), but the instrument ran out of film within 4 hours after the main shock (see table 32). The airport manager noted that the accelerograph counter (which is tripped once each time the trigger is actuated) indicated 19 triggerings approximately 2 hours after the main shock and 77 triggerings approximately 18 hours after the main shock (Ken Bemis, oral commun., 1979); the counter indicated 89 triggerings at 1545 G.m.t. October 17 when the record was recovered from the station. El Centro array station 6, situated between the Brawley and Imperial fault traces (fig. 230), recorded 38 aftershocks (16 triggerings) before the accelerograph ran out of film. Because of intermittent operation of the WWVB time-code generator, the time at which the film supply was exhausted cannot be determined; a new supply of film was installed approximately 24 hours after the main shock, at which time the counter indicated 39 triggerings. Other stations at which the film supply ran out so that some triggerings were not recorded include: El Centro array station 8, four unrecorded triggerings; El Centro array station 12, two unrecorded triggerings; and Calipatria Fire Station, eight unrecorded triggerings (see table 32).

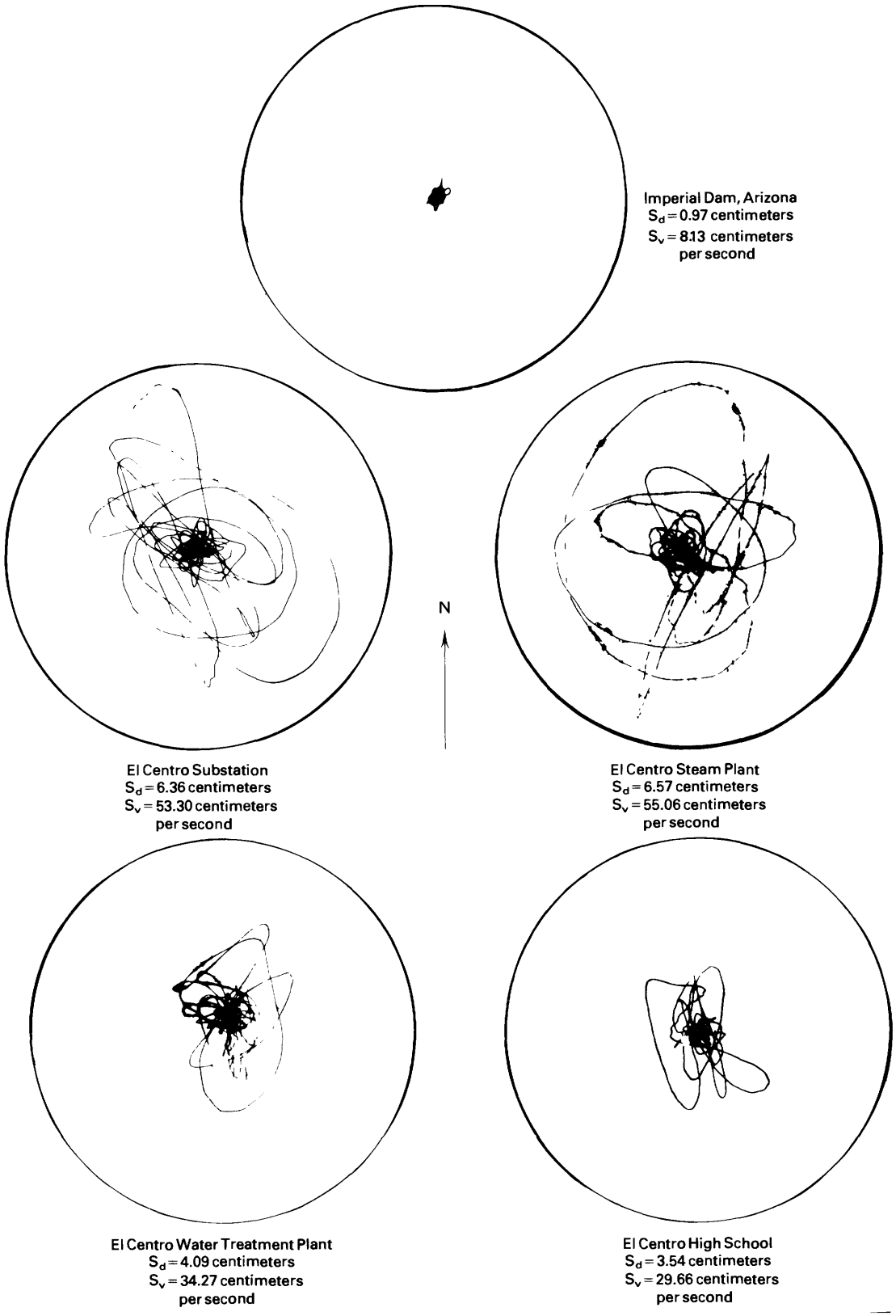

FIGURE 233.—USGS seismoscope records from 1979 Imperial Valley earthquake. See table 29 for other data and explanation of S_d and S_v.

TABLE 30.—*Main-shock accelerograph data from instrumented structures*

[Station numbers prefixed with "C" are assigned by CDMG, and those without a prefix by USGS (U.S. Geological Survey, 1977). Epicentral distance is measured from station to epicenter at lat 32.64° N., long 115.33° W.; bracketed number denotes distance from station to nearest point on 1979 Imperial fault trace, which is assumed to extend from lat 32.94° N., long 115.54° W., to lat 32.72° N., long 115.40° W. Only peak values of horizontal acceleration are given because any brief summary of structural-response data is necessarily incomplete]

Station identification		Epicentral distance (km)	Structure type/size	Acceleration	
No.	Name (data source)			Location	Maximum (g)
767	Coronado, 1770 Ava del Mundo (owner)	172 [155]	16-story building.	Basement	0.01
				7th floor	.02
				Roof	.04
5117	Coronado, 1780 Ava del Mundo (owner)	172 [155]	17-story building.	Basement	.01
				8th floor	.01
				Roof	.03
781	Coronado, 1820 Ava del Mundo (owner)	172 [155]	16-story building.	Basement	---
				9th floor	---
				Roof	.03
C243 5094	El Capitan Dam, El Capitan Reservoir (CDMG)	142 [119]	Earth dam	Abutment	.02
				Crest	.07
C260 5090	El Centro, Imperial County Services Building (CDMG)	27 [8]	6-story building.	Ground	.35
				2d floor	.35
				Roof	.59
C336 5155	El Centro, Meloland Road-Interstate Highway 8 overcrossing (CDMG)	18 [1]	Freeway overpass.	Ground	.32
				Abutment	.49
				Deck	.51
C284	Palm Desert, Kiewit Building	160 [122]	4-story building.	Ground	.03
				Roof	.05
C299	Palm Springs, Desert Hospital (CDMG)	174 [136]	4-story building.	Ground	.02
				Roof	.05
C312	Riverside County Administration Building	241 [205]	13-story building.	Basement	.01
				Roof	.03
C300 275	San Diego Gas & Electric office building	171 [153]	22-story building.	Basement	.01
				Roof	.03

TABLE 31.—*Aftershocks recorded at USGS accelerograph stations*

[Approximate trigger time is an average for corresponding stations in columns; event-origin time is equal to trigger time minus trigger-delay time and triggering-wave traveltime. Station abbreviations: BC, Bonds Corner; BR, Brawley Airport; CX, Calexico Fire Station; CP, Calipatria Fire Station; DA, El Centro differential array; HV, Holtville Post Office; PT, Parachute Test Site; SS, Salton Sea Wildlife Refuge; SM, Superstition Mountain. "×" indicates that accelerogram contains WWVB time code; "×" in parentheses indicates that a record-event correlation is questionable; dashes indicate that a record-event correlation cannot be made because either a time code is not on accelerogram or the accelerograph did not trigger]

Approximate trigger time (G.m.t.)	BC	BR	CX	CP	El Centro array station													DA	HV	PT	SS	SM
					1	2	3	4	5	6	7	8	9	10	11	12	13					
288/23:17:28	---	×	---	---	---	---	---	---	---	---	---	---	---	---	---	---	---	---	---	---	×	---
23:17:37	---	×	---	---	---	---	---	---	×	×	---	×	---	---	---	---	---	---	---	---	---	---
23:17:41	---	---	---	---	---	---	---	---	×	×	(×)	×	(×)	---	---	---	---	(×)	---	---	---	---
23:17:47	---	×	---	---	---	---	---	---	---	---	---	---	---	---	---	---	---	---	---	---	---	---
23:18:03	---	×	×	---	---	---	---	---	---	---	---	---	---	---	---	---	---	---	---	---	---	---
23:18:21	---	---	---	---	---	---	---	---	×	×	(×)	×	(×)	---	---	---	---	(×)	---	---	---	---
23:18:42	×	---	---	---	---	---	---	---	---	×	(×)	×	(×)	---	---	---	---	(×)	(×)	---	---	---
23:18:57	---	---	---	---	---	---	---	---	---	×	---	---	---	---	---	---	---	---	---	---	---	---
23:19:01	---	---	---	---	---	---	---	---	---	×	---	---	---	---	---	---	---	---	---	---	---	---
23:19:20	---	---	---	---	---	---	---	---	---	×	---	---	---	---	---	---	---	---	---	---	---	---
23:19:35	×	×	×	---	×	×	×	×	×	×	(×)	×	(×)	(×)	×	---	---	(×)	(×)	---	---	---
23:19:57	---	---	---	---	---	---	---	---	---	---	---	---	(×)	---	---	---	---	---	---	---	---	---
23:20:30	---	×	---	---	---	---	---	---	---	---	---	---	---	---	---	---	---	---	---	---	---	---
23:20:36	---	×	---	---	---	---	---	---	---	---	---	---	---	---	---	---	---	---	---	---	---	---
23:21:52	---	---	×	---	---	---	---	---	---	---	---	---	---	---	---	---	---	---	---	---	---	---
23:25:56	---	×	---	---	---	---	---	---	---	---	---	×	---	---	---	---	---	---	---	---	---	---
23:28:20	---	×	---	---	---	---	---	---	---	---	---	---	---	---	---	---	---	---	---	---	---	---

TABLE 31.—*Aftershocks recorded at USGS accelerograph stations*— Continued

Approximate trigger time (G.m.t.)	BC	BR	CX	CP	El Centro array station													DA	HV	PT	SS	SM
					1	2	3	4	5	6	7	8	9	10	11	12	13					
23:32:31 _____	---	×	---	---	---	---	---	---	---	---	---	---	---	---	---	---	---	---	---	---	---	---
23:53:07 _____	---	×	---	---	---	---	---	---	---	---	---	---	---	---	---	---	---	---	---	---	---	---
23:55:07 _____	---	×	---	---	---	---	---	---	×	(×)	---	---	---	---	---	---	---	---	---	---	---	---
23:56:32 _____	---	---	---	---	---	---	---	---	---	×	---	---	---	---	---	---	---	---	---	---	---	---
23:56:54 _____	---	---	---	---	---	---	---	---	---	(×)	---	---	---	---	---	---	---	---	---	---	---	---
23:57:05 _____	---	---	---	---	---	---	---	---	---	(×)	---	---	---	---	---	---	---	---	---	---	---	---
289/00:02:44 _____	---	×	---	---	---	---	---	---	---	---	---	---	---	---	---	---	---	---	---	---	---	---
00:22:16 _____	---	×	---	×	---	(×)	---	---	---	---	---	---	---	---	---	---	---	---	---	---	---	---
00:22:34 _____	---	×	---	---	---	---	---	---	---	---	---	---	---	---	---	---	---	---	---	---	---	---
00:27:58 _____	---	×	---	×	---	---	---	---	---	---	---	---	---	---	---	---	---	---	---	---	---	---
00:28:04 _____	---	×	---	---	---	---	---	---	---	---	---	---	---	---	---	---	---	---	---	---	---	---
00:30:03 _____	---	×	---	---	---	---	---	---	---	---	---	---	---	---	---	---	---	---	---	---	---	---
00:51:02 _____	---	×	---	---	---	---	---	---	---	---	---	---	---	---	---	---	---	---	---	---	---	---
01:00:16 _____	---	---	---	---	---	---	---	---	×	---	---	---	---	---	---	---	---	---	---	---	---	---
01:00:31 _____	---	---	---	---	---	---	---	---	×	---	---	---	---	---	---	---	---	---	---	---	---	---
01:07:14 _____	---	×	---	---	---	---	---	---	---	---	---	---	---	---	---	---	---	---	---	---	---	---
01:14:25 _____	---	×	---	×	---	---	---	---	×	---	---	---	---	---	---	---	---	---	---	---	---	---
01:39:06 _____	---	×	---	---	---	---	---	---	---	---	---	---	---	---	---	---	---	---	---	---	---	---
01:41:36 _____	---	×	---	---	---	---	---	---	---	---	---	---	---	---	---	---	---	---	---	---	---	---
01:42:09 _____	---	×	---	---	---	---	---	---	---	---	---	---	---	---	---	---	---	---	---	---	---	---
01:42:41 _____	---	×	---	---	---	---	---	---	---	---	---	---	---	---	---	---	---	---	---	---	---	---
02:00:08 _____	---	×	---	---	---	---	---	---	---	---	---	---	---	---	---	---	---	---	---	---	---	---
02:00:23 _____	---	×	---	---	---	---	---	---	---	---	---	---	---	---	---	---	---	---	---	---	---	---
02:36:37 _____	---	×	---	---	---	---	---	---	---	---	---	---	---	---	---	---	---	---	---	---	---	---
03:10:49 _____	---	×	---	×	---	---	---	---	---	---	---	---	---	---	---	---	---	---	---	---	---	---
03:39:39 _____	---	---	---	×	---	---	---	---	---	---	---	---	---	---	---	---	---	---	---	---	---	×
04:25:32 _____	---	---	---	---	---	---	---	---	×	---	---	---	---	---	---	---	---	---	---	---	---	---
04:32:58 _____	---	---	---	×	---	---	---	---	---	---	---	---	---	---	---	---	---	---	---	---	---	---
05:17:12 _____	---	---	---	---	---	---	---	---	---	---	---	×	---	---	---	---	---	---	---	---	---	---
05:49:15 _____	×	---	×	×	(×)	×	---	×	×	---	---	×	---	---	×	---	---	---	---	---	---	---
05:50:25 _____	---	---	---	---	---	---	---	---	---	---	---	×	---	---	---	---	---	---	---	---	---	---
06:04:42 _____	---	---	---	---	---	---	---	---	×	---	---	×	---	---	---	---	---	---	---	---	---	---
06:05:17 _____	---	---	---	---	---	---	---	---	---	---	---	×	---	---	---	---	---	---	---	---	---	---
06:13:53 _____	---	---	---	---	---	---	---	---	×	---	---	---	---	---	---	---	---	---	---	---	---	---
06:19:02 _____	---	---	---	---	---	---	---	---	---	---	---	---	---	---	---	---	---	---	---	---	×	---
06:19:53 _____	×	---	---	×	×	×	---	×	×	---	---	×	---	---	×	---	---	---	---	---	×	---
06:55:28 _____	---	---	---	×	---	---	---	---	---	---	---	---	---	---	---	---	---	---	---	---	---	---
06:58:48 _____	---	---	×	×	×	×	---	×	×	---	---	(×)	---	---	×	---	(×)	---	---	---	×	---
07:23:27 _____	---	---	---	---	---	---	---	---	×	---	---	---	---	---	---	---	---	---	---	---	---	---
09:33:55 _____	---	---	---	---	---	---	---	---	×	---	---	---	---	---	---	---	---	---	---	---	---	---
09:36:48 _____	---	---	---	---	---	---	---	---	×	---	---	---	---	---	---	---	---	---	---	---	---	---
09:37:09 _____	---	---	---	---	---	---	---	---	×	---	---	---	---	---	---	---	---	---	---	---	---	---
11:47:02 _____	---	---	×	---	---	×	---	×	---	---	---	---	---	---	---	---	---	---	---	---	---	---
12:01:53 _____	---	---	---	---	---	×	---	---	×	---	---	---	---	---	---	---	---	---	---	---	---	---
17:22:58 _____	---	---	---	---	---	---	---	---	×	---	---	---	---	---	---	---	---	---	---	---	---	---
23:16:38 _____	---	---	---	---	×	×	---	---	---	---	---	---	---	---	---	---	---	---	---	---	×	---
290/08:38:56 _____	---	---	---	---	×	---	---	---	---	---	---	---	---	---	---	---	---	---	---	---	---	---
09:17:24 _____	---	---	---	---	---	---	---	---	---	---	---	---	---	---	---	---	---	---	---	---	×	---
11:47:56 _____	---	---	---	---	---	---	---	---	---	×	---	---	---	---	---	---	---	---	---	---	---	---
16:17:38 _____	---	×	---	---	---	---	---	---	---	---	---	---	---	---	---	---	---	---	---	---	---	---
19:03:05 _____	---	×	---	---	---	---	---	---	---	---	---	---	---	---	---	---	---	---	---	---	---	---
19:14:41 _____	---	×	---	---	---	---	---	---	---	---	---	---	---	---	---	---	---	---	---	---	---	---
22:45:40 _____	---	×	---	---	×	×	---	---	---	---	---	---	---	---	---	---	---	---	---	---	---	---
22:45:56 _____	---	×	---	---	---	---	---	---	---	---	---	---	---	---	---	---	---	---	---	---	---	---
22:47:08 _____	---	×	---	---	---	---	---	---	---	---	---	---	---	---	---	---	---	---	---	---	---	---
22:47:13 _____	---	×	---	---	---	---	---	---	---	---	---	---	---	---	---	---	---	---	---	---	---	---
291/00:29:13 _____	---	---	---	---	---	---	---	---	---	---	---	---	---	---	---	---	---	---	---	---	×	---
02:14:50 _____	---	---	---	---	---	---	---	---	---	---	---	---	---	---	---	---	---	---	---	---	×	---
02:19:14 _____	---	×	---	---	---	---	---	---	---	---	---	---	---	---	---	---	---	---	---	---	---	---
12:42:24 _____	---	×	---	---	---	---	---	---	---	---	---	---	---	---	---	---	---	---	---	---	---	---
12:56:21 _____	---	×	---	---	---	---	---	---	---	---	---	---	---	---	---	---	---	---	---	---	---	---
13:20:29 _____	---	---	---	---	---	---	---	---	---	×	---	---	---	---	---	---	---	---	---	---	---	---
16:24:40 _____	---	---	---	---	---	---	---	---	---	×	---	---	---	---	---	---	---	---	---	---	---	---
293/14:52:57 _____	---	---	---	---	---	---	---	---	---	×	---	---	---	---	---	---	---	---	---	---	---	---
294/18:18:00 _____	---	---	---	---	---	---	---	---	---	×	---	---	---	---	---	---	---	---	---	---	---	---

TABLE 32.—*Summary of USGS accelerograph aftershock data*

[Trigger time in parentheses was determined by correlating the record with one from a nearby station and therefore is questionable; dash indicates that either the accelerograph does not contain a WWVB radio receiver or the WWVB time code was not adequately recorded for acceptable correlation with an event. Event-origin time is equal to trigger time minus trigger-delay time and triggering-wave traveltime. Direction of acceleration is for upward trace deflection on accelerogram; horizontal components are listed as azimuth (in degrees clockwise from north); vertical components are listed as "up" or "down." Maximum acceleration is peak value recorded at ground level on one vertical and two orthogonal horizontal components. Duration of acceleration is time between first and last peaks of acceleration greater than 0.10 g]

Trigger time (G.m.t.)	S-t interval (s)	Acceleration		
		Direction	Maximum (g)	Duration (s)
Bonds Corner, Highways 98 and 115				
288/23:18:49	(1)	230°	0.029	---
		up	.012	---
		140°	.029	---
288/23:19:33	[2]3.1	230°	.129	1 peak
		up	.052	---
		140°	.074	---
289/05:49:26	(1)	230°	.023	---
		up	.012	---
		140°	.023	---
289/06:20:03	(1)	230°	.029	---
		up	.012	---
		140°	.046	---
Brawley Airport				
288/23:17:28	[2]2.8	315°	0.017	---
		up	.016	---
		225°	.011	---
288/23:17:38	[2]2.8	315°	.006	---
		up	.016	---
		225°	.006	---
288/23:17:47	[2]2.3	315°	.006	---
		up	.011	---
		225°	.006	---
288/23:18:05	[2]2.4	315°	.011	---
		up	.016	---
		225°	.011	---
288/23:19:35	4.3	315°	.057	---
		up	.043	---
		225°	.045	---
288/23:20:30	[2]2.1	315°	.023	---
		up	.011	---
		225°	.023	---
288/23:20:36	[2]2.3	315°	.017	---
		up	.016	---
		225°	.017	---
288/23:25:58	0.8	315°	.023	---
		up	.011	---
		225°	.017	---
288/23:28:20	2.2	315°	.017	---
		up	.011	---
		225°	.011	---
288/23:32:31	2.2	315°	.023	---
		up	.016	---
		225°	.023	---
288/23:53:07	1.9	315°	.080	---
		up	.027	---
		225°	.056	---
288/23:55:07	2.5	315°	.074	---
		up	.027	---
		225°	.062	---
289/00:02:44	1.7	315°	.040	---
		up	.016	---
		225°	.056	---
289/00:22:16	2.1	315°	.170	.1
		up	.096	---
		225°	.169	.1
289/00:22:34	[2]2.3	315°	.023	---
		up	.005	---
		225°	.011	---
289/00:27:55	2.1	315°	.028	---
		up	.032	---
		225°	.034	---
289/00:28:04	[2]2.2	315°	.011	---
		up	.016	---
		225°	.011	---
289/00:30:03	2.1	315°	.028	---
		up	.016	---
		225°	.023	---
289/00:51:02	(1)	315°	.017	---
		up	.011	---
		225°	.034	---
-----------	2.6	315°	.085	---
		up	.032	---
		225°	.090	---
289/01:07:14	2.2	315°	.028	---
		up	.027	---
		225°	.028	---
289/01:14:24	2.4	315°	.102	1 peak
		up	.053	---
		225°	.079	---
289/01:39:06	2.6	315°	.080	---
		up	.027	---
		225°	.028	---
289/01:41:36	2.2	315°	.023	---
		up	.005	---
		225°	.017	---
289/01:42:09	[2]2.2	315°	.051	---
		up	.027	---
		225°	.028	---
289/01:42:41	[2]2.0	315°	.011	---
		up	.005	---
		225°	.011	---

TABLE 32.—*Summary of USGS accelerograph aftershock data* — Continued

Trigger time (G.m.t.)	S-t interval (s)	Acceleration		
		Direction	Maximum (g)	Duration (s)
289/02:00:08	2.0	315°	.034	---
		up	.011	---
		225°	.023	---
289/02:00:23	[2]2.4	315°	.011	---
		up	.005	---
		225°	.006	---
289/02:36:37	2.4	315°	.045	---
		up	.016	---
		225°	.034	---
289/03:10:49	2.1	315°	.176	.3
		up	.101	1 peak
		225°	.164	.3
Note: Film supply ran out during this event; new film supply installed at approximately 290/15:45 (65 unrecorded triggerings during this interval, including 2 during film installation).				
290/16:17:38	2.1	315°	.017	---
		up	.011	---
		225°	.011	---
290/19:03:05	1.3	315°	.068	---
		up	.037	---
		225°	.090	---
290/19:14:41	2.6	315°	.034	---
		up	.016	---
		225°	.040	---
290/22:45:35	1.7	315°	.273	.9
		up	.160	1.5
		225°	.266	1.2
290/22:45:56	[2]1.8	315°	.097	---
		up	.101	1 peak
		225°	.198	.2
290/22:47:08	[2]1.9	315°	.057	---
		up	.043	---
		225°	.073	---
290/22:47:13	[2]1.9	315°	.057	---
		up	.027	---
		225°	.051	---
291/02:19:14	1.5	315°	.034	---
		up	.021	---
		225°	.068	---
291/12:42:24	1.4	315°	.176	.1
		up	.037	---
		225°	.119	.1
291/14:56:21	1.8	315°	.028	---
		up	.027	---
		225°	.028	---
Calexico Fire Station				
288/23:18:03	[2]1.9	315°	0.011	---
		up	.006	---
		225°	.010	---
288/23:19:33	2.9	315°	.071	---
		up	.034	---
		225°	.097	---
288/23:21:52	3.7	315°	.005	---
		up	.006	---
		225°	.005	---
289/05:49:18	3.7	315°	.016	---
		up	.011	---
		225°	.015	---
289/06:58:51	5.5	315°	.033	---
		up	.022	---
		225°	.026	---
289/11:47:02	([1])	315°	.005	---
		up	.011	---
		225°	.010	---
Calipatria Fire Station				
289/00:22:19	([1])	315°	0.005	---
		up	.027	---
		225°	.011	---
289/00:27:58	([1])	315°	.005	---
		up	.022	---
		225°	.006	---
289/01:14:27	4.1	315°	.022	---
		up	.022	---
		225°	.017	---
289/03:10:52	4.2	315°	.016	---
		up	.022	---
		225°	.011	---
289/03:39:39	4.1	315°	.022	---
		up	.043	---
		225°	.028	---
289/04:32:58	([1])	315°	.005	---
		up	.011	---
		225°	.006	---
289/05:49:15	4.3	315°	.022	---
		up	.038	---
		225°	.028	---
289/06:19:53	4.4	315°	.032	---
		up	.081	---
		225°	.039	---
289/06:55:28	3.5	315°	.016	---
		up	.016	---
		225°	.034	---
289/06:58:47	3.6	315°	.124	.6
		up	.177	2.5
		225°	.168	1.5
.....	([1])	315°	.016	---
		up	.005	---
		225°	.010	---

TABLE 32.—*Summary of USGS accelerograph aftershock data* —Continued

Trigger time (G.m.t.)	S-t interval (s)	Acceleration		
		Direction	Maximum (g)	Duration (s)
Note: Film supply ran out during this event; new film supply installed at approximately 291/23:30 (8 unrecorded triggerings during this interval).				
El Centro array station 1, Borchard Ranch				
288/23:19:35	4.0	230°	0.060	---
		up	.033	---
		140°	.033	---
(289/05:49:20)	(1)	230°	.027	---
		up	.017	---
		140°	.027	---
289/06:19:53	3.3	230°	.043	---
		up	.055	---
		140°	.049	---
289/06:58:48	3.8	230°	.114	1 peak
		up	.066	---
		140°	.093	---
289/23:16:38	0.9	230°	.054	---
		up	.022	---
		140°	.038	---
290/08:38:56	(1)	230°	.082	---
		up	.033	---
		140°	.066	---
290/22:45:40	1.4	230°	.054	---
		up	.017	---
		140°	.038	---
El Centro array station 2, Keystone Road				
288/23:19:34	3.6	230°	0.089	---
		up	.054	---
		140°	.154	1 peak
(289/00:22:18)	3.3	230°	.018	---
		up	.016	---
		140°	.017	---
289/05:49:15	2.5	230°	.089	---
		up	.048	---
		140°	.086	---
289/06:19:53	3.5	230°	.083	---
		up	.065	---
		140°	.080	---
289/06:58:48	4.0	230°	.113	1 peak
		up	.151	.1
		140°	.091	---
289/11:47:00	3.8	230°	.024	---
		up	.027	---
		140°	.017	---
289/12:01:53	(1)	230°	.101	1 peak
		up	.016	---
		140°	.046	---
289/23:16:36	3.2	230°	.137	.2
		up	.027	---
		140°	.069	---
290/22:45:40	1.7	230°	.089	---
		up	.022	---
		140°	.057	---
El Centro array station 3, Pine Union School				
288/23:19:33	3.5	230°	0.103	1 peak
		up	.039	---
		140°	.147	.4
.....	2.8	230°	.054	---
		up	.022	---
		140°	.071	---
.....	3.4	230°	.043	---
		up	.022	---
		140°	.033	---
.....	4.0	230°	.120	1 peak
		up	.067	---
		140°	.130	1 peak
.....	3.6	230°	.022	---
		up	.006	---
		140°	.011	---
.....	3.3	230°	.043	---
		up	.017	---
		140°	.038	---
.....	3.2	230°	.054	---
		up	.017	---
		140°	.049	---
.....	2.8	230°	.190	1 peak
		up	.034	---
		140°	.054	---
El Centro array station 4, Anderson Road				
288/23:19:33	3.1	230°	0.168	0.7
		up	.079	---
		140°	.237	.5
289/05:49:15	2.7	230°	.053	---
		up	.045	---
		140°	.047	---
289/06:19:59	(1)	230°	.032	---
		up	.022	---
		140°	.026	---
289/06:58:50	1.4	230°	.063	---
		up	.039	---
		140°	.032	---
289/11:47:03	(1)	230°	.021	---
		up	.017	---
		140°	.021	---
El Centro array station 5, James Road				
288/23:17:37	[2]2.4	230°	0.054	---
		up	.058	---
		140°	.059	---

TABLE 32.—*Summary of USGS accelerograph aftershock data* —Continued

Trigger time (G.m.t.)	S-t interval (s)	Acceleration		
		Direction	Maximum (g)	Duration (s)
288/23:17:42	[2]2.5	230°	.042	---
		up	.035	---
		140°	.041	---
288/23:18:21	[2]2.7	230°	.048	---
		up	.023	---
		140°	.047	---
288/23:19:33	3.2	230°	.286	.2
		up	.117	1 peak
		140°	.235	.3
288/23:55:07	2.9	230°	.060	---
		up	.041	---
		140°	.059	---
289/01:00:16	2.9	230°	.101	1 peak
		up	.041	---
		140°	.147	.3
289/01:00:31	[2]2.9	230°	.030	---
		up	.018	---
		140°	.029	---
289/01:14:25	2.7	230°	.083	---
		up	.035	---
		140°	.059	---
289/04:25:32	([1])	230°	.196	.3
		up	.029	---
		140°	.200	.2
289/05:49:13	3.3	230°	.143	1.8
		up	.058	---
		140°	.171	1.0
289/06:04:42	2.7	230°	.048	---
		up	.018	---
		140°	.041	---
289/06:13:53	2.6	230°	.077	---
		up	.023	---
		140°	.053	---
289/06:19:53	2.1	230°	.095	---
		up	.029	---
		140°	.094	---
289/06:58:48	3.6	230°	.161	1.4
		up	.053	---
		140°	.118	1.2
289/07:23:27	2.7	230°	.048	---
		up	.053	---
		140°	.073	---
289/09:33:55	2.7	230°	.042	---
		up	.018	---
		140°	.047	---
289/09:36:48	([1])	230°	.077	---
		up	.018	---
		140°	.047	---
289/09:37:09	[2]2.7	230°	.030	---
		up	.018	---
		140°	.035	---
289/12:01:47	2.3	230°	.137	.1
		up	.041	---
		140°	.153	.4
289/17:22:58	2.5	230°	.119	1 peak
		up	.047	---
		140°	.076	---
El Centro array station 6, Huston Road				
288/23:17:37	[2]2.3	230°	0.043	---
		up	.046	---
		140°	.051	---
288/23:17:41	[2]2.6	230°	.097	---
		up	.143	.1
		140°	.085	---
288/23:18:21	[2]2.6	230°	.102	1 peak
		up	.051	---
		140°	.079	---
288/23:18:42	[2]2.6	230°	.167	.2
		up	.069	---
		140°	.113	1 peak
288/23:18:57	[2]2.4	230°	.022	---
		up	.029	---
		140°	.034	---
288/23:19:01	[2]2.8	230°	.016	---
		up	.011	---
		140°	.006	---
288/23:19:20	[2]2.8	230°	.011	---
		up	.011	---
		140°	.006	---
288/23:19:32	[2]2.9	230°	.263	1.3
		up	.080	---
		140°	.175	.3
.....	2.4	230°	.048	---
		up	.017	---
		140°	.023	---
.....	[2]3.0	230°	.022	---
		up	.011	---
		140°	.011	---
.....	[2]2.4	230°	.022	---
		up	.011	---
		140°	.028	---
.....	2.5	230°	.022	---
		up	.029	---
		140°	.023	---
.....	[2]2.5	230°	.070	---
		up	.023	---
		140°	.040	---
.....	[2]3.0	230°	.032	---
		up	.006	---
		140°	.023	---

TABLE 32.—*Summary of USGS accelerograph aftershock data* — Continued

Trigger time (G.m.t.)	S-t interval (s)	Acceleration		
		Direction	Maximum (g)	Duration (s)
.....	2.9	230°	.043	---
		up	.023	---
		140°	.034	---
.....	2.2	230°	.059	---
		up	.034	---
		140°	.034	---
.....	[2]2.0	230°	.016	---
		up	.006	---
		140°	.011	---
.....	[2]3.0	230°	.016	---
		up	.017	---
		140°	.028	---
.....	2.6	230°	.011	---
		up	.023	---
		140°	.011	---
.....	[2]3.2	230°	.054	---
		up	.017	---
		140°	.040	---
(288/23:55:07)	2.7	230°	.124	.5
		up	.040	---
		140°	.079	---
(288/23:56:32)	2.2	230°	.054	---
		up	.017	---
		140°	.028	---
(288/23:56:54)	[2]2.0	230°	.016	---
		up	.011	---
		140°	.023	---
(288/23:57:05)	[2]2.8	230°	.005	---
		up	.011	---
		140°	.006	---
.....	2.9	230°	.075	---
		up	.034	---
		140°	.040	---
.....	[2]2.9	230°	.027	---
		up	.011	---
		140°	.017	---
.....	2.7	230°	.048	---
		up	.034	---
		140°	.023	---
.....	[2]2.9	230°	.102	1 peak
		up	.040	---
		140°	.068	---
.....	[2]3.0	230°	.183	.6
		up	.057	---
		140°	.169	1 peak
.....	[2]3.0	230°	.054	---
		up	.023	---
		140°	.034	---
.....	2.9	230°	.043	---
		up	.029	---
		140°	.028	---
.....	3.0	230°	.188	.7
		up	.069	---
		140°	.175	.4
.....	[2]3.3	230°	.032	---
		up	.011	---
		140°	.028	---
.....	2.8	230°	.081	---
		up	.017	---
		140°	.045	---
.....	3.1	230°	.038	---
		up	.011	---
		140°	.034	---
.....	1.0	230°	.070	---
		up	.029	---
		140°	.068	---
.....	2.9	230°	.032	---
		up	.023	---
		140°	.040	---
.....	2.9	230°	.027	---
		up	.017	---
		140°	.028	---

Note: Film supply ran out during this event; new film supply installed at approximately 290/06:00 (23 unrecorded triggerings during this interval).

290/11:57:56	1.9	230°	.043	---
		up	.017	---
		140°	.119	1 peak
290/13:20:29	2.7	230°	.022	---
		up	.017	---
		140°	.023	---
291/16:24:40	2.7	230°	.027	---
		up	.011	---
		140°	.011	---
293/14:52:57	2.6	230°	.086	---
		up	.023	---
		140°	.085	---
294/18:18:00	3.0	230°	.016	---
		up	.023	---
		140°	.028	---

El Centro array station 7, Imperial Valley College

(288/23:17:40)	[2]2.1	230°	0.043	---
		up	.038	---
		140°	.042	---
(288/23:18:19)	[2]2.1	230°	.033	---
		up	.016	---
		140°	.047	---

TABLE 32.—*Summary of USGS accelerograph aftershock data* —Continued

Trigger time (G.m.t.)	S-t interval (s)	Acceleration		
		Direction	Maximum (g)	Duration (s)
(288/23:18:40)	[2]2.1	230°	.027	---
		up	.011	---
		140°	.021	---
(288/23:19:35)	2.6	230°	.230	.4
		up	.086	---
		140°	.147	.3
.....	2.1	230°	.118	1 peak
		up	.032	---
		140°	.079	---
.....	1.8	230°	.080	---
		up	.038	---
		140°	.084	---
.....	2.2	230°	.059	---
		up	.022	---
		140°	.058	---
.....	2.7	230°	.048	---
		up	.027	---
		140°	.053	---
.....	([1])	230°	.037	---
		up	.016	---
		140°	.026	---
.....	2.5	230°	.193	.8
		up	.038	---
		140°	.111	.4
.....	[2]2.7	230°	.080	---
		up	.022	---
		140°	.063	---
.....	1.9	230°	.080	---
		up	.027	---
		140°	.068	---
.....	2.2	230°	.131	.7
		up	.072	---
		140°	.117	1 peak
.....	[2]2.7	230°	.026	---
		up	.021	---
		140°	.017	---
.....	2.9	230°	.047	---
		up	.036	---
		140°	.028	---
289/05:17:12	2.5	230°	.010	---
		up	.015	---
		140°	.022	---
289/05:49:14	2.7	230°	.141	1.2
		up	.046	---
		140°	.100	1 peak
289/05:50:25	[2]3.0	230°	.010	---
		up	.010	---
		140°	.006	---
289/06:04:42	2.7	230°	.047	---
		up	.026	---
		140°	.033	---
289/06:05:17	[2]3.0	230°	.010	---
		up	.010	---
		140°	.011	---
289/06:19:53	3.0	230°	.068	---
		up	.031	---
		140°	.050	---
(289/06:58:49)	3.0	230°	.052	---
		up	.031	---
		140°	.067	---

Note: Film supply ran out during this event; new film supply installed at approximately 289/23:00 (4 unrecorded triggerings during this interval).

El Centro array station 8, Cruickshank Road

288/23:17:38	[2]2.2	230°	0.021	---
		up	.026	---
		140°	.044	---
288/23:17:42	[2]2.3	230°	.026	---
		up	.015	---
		140°	.078	---
288/23:18:21	[2]2.3	230°	.026	---
		up	.010	---
		140°	.028	---
288/23:18:43	2.0	230°	.042	---
		up	.015	---
		140°	.039	---
288/23:19:33	[2]2.7	230°	.157	.2
		up	.056	---
		140°	.128	.8
288/23:25:56	2.8	230°	.026	---
		up	.026	---
		140°	.022	---

El Centro array station 9, Commercial Avenue

(288/23:17:41)	3.0	down	0.023	---
		360°	.019	---
		090°	.020	---
(288/23:18:20)	2.8	down	.016	---
		360°	.007	---
		090°	.012	---
(288/23:18:41)	2.9	down	.008	---
		360°	.030	---
		090°	.035	---
(288/23:19:30)	[2]3.6	down	.078	---
		360°	.086	---
		090°	.133	.6
(288/23:19:57)	[2]3.6	down	0.004	---
		360°	.007	---
		090°	.004	---
.....	([1])	down	.002	---
		360°	.006	---
		090°	.014	---

TABLE 32.—*Summary of USGS accelerograph aftershock data* — Continued

Trigger time (G.m.t.)	S-t interval (s)	Acceleration		
		Direction	Maximum (g)	Duration (s)
.....	(1)	down	.010	---
		360°	.022	---
		090°	.031	---
.....	(1)	down	.002	---
		360°	.010	---
		090°	.012	---
.....	(1)	down	.010	---
		360°	.013	---
		090°	.023	---
.....	(1)	down	.002	---
		360°	.007	---
		090°	.010	---
El Centro array station 10, Community Hospital				
(288/23:19:35)	2.7	050°	0.055	---
		up	.026	---
		320°	.051	---
.....	1.3	050°	.016	---
		up	.016	---
		320°	.027	---
.....	1.3	050°	.011	---
		up	.011	---
		320°	.011	---
.....	[2]2.7	050°	.011	---
		up	.005	---
		320°	.010	---
.....	2.3	050°	.038	---
		up	.047	---
		320°	.036	---
.....	1.5	050°	.033	---
		up	.021	---
		320°	.036	---
.....	(1)	050°	.033	---
		up	.021	---
		320°	.046	---
.....	0.9	050°	.027	---
		up	.021	---
		320°	.041	---
El Centro array station 11, McCabe School				
288/23:19:33	3.4	230°	0.192	0.5
		up	.063	---
		140°	.098	---
289/05:49:18	1.6	230°	.026	---
		up	.016	---
		140°	.027	---
289/06:19:57	1.6	230°	.047	---
		up	.016	---
		140°	.043	---
289/06:58:50	4.4	230°	.036	---
		up	.026	---
		140°	.033	---
El Centro array station 12, Brockman Road				
Note: Film supply ran out during main event; new film supply installed at approximately 289/22:00 (2 unrecorded triggerings during this interval).				
El Centro array station 1, Strobel residence				
(289/06:58:59)	(1)	230°	0.022	---
		up	.022	---
		140°	.022	---
El Cntro differential array, Dogwood Road				
(288/23:17:41)	[2]2.5	360°	0.047	---
		up	.016	---
		270°	.045	---
(288/23:18:20)	[2]2.4	360°	.021	---
		up	.016	---
		270°	.028	---
(288/23:18:42)	2.1	360°	.047	---
		up	.022	---
		270°	.051	---
(288/23:19:35)	[2]2.8	360°	.146	.9
		up	.103	1 peak
		270°	.147	.5
.....	2.2	360°	.021	---
		up	.016	---
		270°	.011	---
.....	[2]1.8	360°	.036	---
		up	.022	---
		270°	.028	---
.....	2.9	360°	.010	---
		up	.022	---
		270°	.028	---
.....	2.8	360°	.047	---
		up	.049	---
		270°	.045	---
.....	2.6	360°	.010	---
		up	.011	---
		270°	.011	---
.....	[2]2.8	360°	.016	---
		up	.022	---
		270°	.011	---
.....	[2]3.1	360°	.010	---
		up	.022	---
		270°	.011	---
.....	2.2	360°	.068	---
		up	.043	---
		270°	.107	1 peak
.....	3.0	360°	.068	---
		up	.027	---
		270°	.073	---

TABLE 32.—*Summary of USGS accelerograph aftershock data* —Continued

Trigger time (G.m.t.)	S-t interval (s)	Acceleration		
		Direction	Maximum (g)	Duration (s)
.....	3.7	360°	.089	---
		up	.049	---
		270°	.102	1 peak
.....	3.0	360°	.083	---
		up	.027	---
		270°	.079	---
.....	3.0	360°	.120	.1
		up	.119	.3
		270°	.107	1 peak
.....	[2]3.1	360°	.036	---
		up	.022	---
		270°	.023	---
.....	2.7	360°	.010	---
		up	.022	---
		270°	.011	---
.....	2.8	360°	.005	---
		up	.005	---
		270°	.006	---
.....	2.7	360°	.021	---
		up	.016	---
		270°	.017	---
.....	3.0	360°	.026	---
		up	.038	---
		270°	.062	---
.....	2.8	360°	.016	---
		up	.038	---
		270°	.017	---
.....	2.6	360°	.010	---
		up	.005	---
		270°	.011	---
Holtville Post Office				
(288/23:18:43)	2.5	315°	0.026	---
		up	.011	---
		225°	.037	---
(288/23:19:33)	[2]2.7	315°	.264	.3
		up	.042	---
		225°	.116	.4
.....	3.6	315°	.016	---
		up	.011	---
		225°	.016	---
.....	4.1	315°	.016	---
		up	.011	---
		225°	.016	---
.....	3.0	315°	.026	---
		up	.026	---
		225°	.037	---
.....	4.0	315°	.047	---
		up	.042	---
		225°	.048	---
.....	4.4	315°	.047	---
		up	.032	---
		225°	.058	---
.....	([1])	315°	.026	---
		up	.021	---
		225°	.021	---
Parachute Test Site				
.....	4.5	315°	0.042	---
		up	.025	---
		225°	.048	---
.....	([1])	315°	.005	---
		up	.010	---
		225°	.005	---
.....	1.1	315°	.016	---
		up	.025	---
		225°	.021	---
.....	2.9	315°	.011	---
		up	.010	---
		225°	.011	---
.....	3.0	315°	.016	---
		up	.015	---
		225°	.021	---
.....	2.7	315°	.068	---
		up	.051	---
		225°	.063	---
.....	([1])	315°	.021	---
		up	.015	---
		225°	.021	---
.....	2.1	315°	.026	---
		up	.040	---
		225°	.021	---
.....	2.9	315°	.047	---
		up	.051	---
		225°	.063	---
.....	1.1	315°	.042	---
		up	.015	---
		225°	.026	---
.....	2.7	315°	.147	2.5
		up	.076	---
		225°	.116	2.5
.....	[2]2.6	315°	.011	---
		up	.020	---
		225°	.016	---
.....	([1])	315°	.016	---
		up	.010	---
		225°	.021	---
.....	([1])	315°	.005	---
		up	.015	---
		225°	.005	---

TABLE 32.—*Summary of USGS accelerograph aftershock data* —Continued

Trigger time (G.m.t.)	*S-t* interval (s)	Acceleration		
		Direction	Maximum (*g*)	Duration (s)
.....	(1)	315°	.011	---
		up	.010	---
		225°	.005	---
.....	2.2	315°	.032	---
		up	.020	---
		225°	.026	---
.....	(1)	315°	.021	---
		up	.015	---
		225°	.021	---
.....	3.4	315°	.074	---
		up	.035	---
		225°	.112	1 peak
Salton Sea Wildlife Refuge				
288/23:17:26	.7	315°	0.103	1 peak
		up	.060	---
		225°	.115	1 peak
289/06:19:02	1.4	315°	.103	1 peak
		up	.076	---
		225°	.098	---
289/06:19:55	[2]3.9	315°	.022	---
		up	.011	---
		225°	.016	---
289/06:58:48	3.1	315°	.082	---
		up	.038	---
		225°	.071	---
289/23:16:41	(1)	315°	.016	---
		up	.011	---
		225°	.016	---
290/09:17:24	1.4	315°	.027	---
		up	.043	---
		225°	.049	---
290/22:45:40	.7	315°	.027	---
		up	.011	---
		225°	.022	---
291/00:29:49	1.3	315°	.016	---
		up	.011	---
		225°	.027	---
291/02:14:50	1.6	315°	.016	---
		up	.011	---
		225°	.022	---
Superstition Mountain, U.S. Air Force camera site				
289/03:39:44	(1)	135°	0.021	---
		up	.011	---
		045°	.020	---
289/06:58:49	2.4	135°	.031	---
		up	.021	---
		045°	.025	---

[1] *S-t* time not determined, ordinarily because instrument triggered late.
[2] *S*-wave arrival minus *P*-wave arrival time (*S-P*).

ACKNOWLEDGMENTS

We acknowledge the cooperation of individuals and organizations in the Imperial Valley, Calif., who have permitted strong-motion instruments to be installed on their property. In particular, we acknowledge the cooperation of Tom Wootton and John Ragsdale of the California Division of Mines and Geology, and the Coronado, Calif., building owners for making available summary information from their stations. We also thank John Nielson, who has been primarily responsible for maintaining the USGS instruments in the Imperial Valley; Ed Etheredge, who directed recovery of the records and spent many hours carefully developing them; Leroy Foote, Dennis Johnson, and Arnie Acosta for their efforts in recovering records; Chuck Knudson for recovery and analysis of the seismoscope records; and Barry Silverstein for assistance in verifying information about the stations.

REFERENCES CITED

Hudson, D. E., and Cloud, W. K., 1967, An analysis of seismoscope data from the Parkfield earthquake of June 27, 1966: Seismological Society of America Bulletin, v. 57, no. 6, p. 1143-1159.

Maley, R. P., and Cloud, W. K., 1973, Strong-motion accelerograph records, *in* Benfer, N. A., and Coffman, J. L., eds., San Fernando, California, earthquake of February 9, 1971: Washington, U.S. Department of Commerce, National Oceanic and Atmospheric Administration, Environmental Research Laboratories, v. 3, p. 325-348.

Neuman, Frank, 1942, United States earthquakes— 1940: U.S. Department of Commerce, Coast and Geodetic Survey Serial 647, 74 p.

Newmark Consulting Engineering Services, 1973, A study of vertical and horizontal earthquake spectra: U.S. Atomic Energy Commission Report WASH-1255, UC-11, 151 p.

Porcella, R. L., and Matthiesen, R. B., 1979a, Preliminary summary of the U.S. Geological Survey strong-motion records from the October 15, 1979 Imperial Valley earthquake: U.S. Geological Survey Open-File Report 79-1654, 41 p.

—— 1979b, Strong-motion instrumentation in the Imperial Valley, California, *in* Los Asentamientos Humanos en la Falla de San Andreas: Instituto Tecnologico Regional de Tijuana Symposium, Baja California, 1979, Proceedings, p. 122-134.

Rojahn, Christopher, and Ragsdale, J. D., 1978, Building instrumentation phase of the California Strong-Motion Instrumentation Program: Structural Engineers Association of California Annual Convention, 48th, Lake Tahoe, Calif., 1978, Proceedings, p. 21-39.

Trifunac, M. D., and Brune, J. N., 1970, Complexity of energy release during the Imperial Valley, California, earthquake of 1940: Seismological Society of America Bulletin, v. 60, no. 1, p. 137-160.

U.S. Geological Survey, 1977, Western Hemisphere strong-motion accelerograph station list— 1976: Open-File Report 77-374, 112 p.

Wootton, T. M., Wells, W. M., and Power, J. H., 1976, Second report on the strong-motion instrumentation program: California Division of Mines and Geology Special Publication 48, 39 p.

STRONG-MOTION DATA RECORDED IN MEXICO DURING THE MAIN SHOCK

By JAMES N. BRUNE, FRANK L. VERNON III, and RICHARD S. SIMONS,
SCRIPPS INSTITUTION OF OCEANOGRAPHY;

and

JORGE PRINCE and ENRIQUE MENA,
INSTITUTO DE INGENIERÍA, UNIVERSIDAD NACIONAL AUTÓNOMA DE MÉXICO

CONTENTS

ABSTRACT

Seismic signals from the 1979 Imperial Valley earthquake were recorded at nine strong-motion stations in the northern Baja California array operated jointly by U.S. and Mexican research interests. Seven of these stations were occupied by three-component digitally recording accelerographs, and the other two by three-component film-recording accelerographs. In this report, we summarize the peak accelerations and velocities observed for all components and, where possible, the *P*- and *S*-wave arrival times. Four of the stations lacked absolute timing, and one station triggered on the *S* wave rather than the *P* wave. Near the United States-Mexican border, most instruments recorded peak horizontal accelerations of about 0.3 *g*; the minimum was 0.17 *g* at the farthest station. The general pattern of strong motion shows considerable complexity.

From each digital station we present playbacks of the three-component accelerograms, as well as integrations of the acceleration records (without instrument correction) to show velocity and displacement. To determine local magnitude, we converted the digital horizontal strong-motion records into equivalent Wood-Anderson seismograms, using a deconvolution-convolution technique. The average magnitude of 6.3 from this data set is somewhat lower than that determined from stations to the northwest (6.6) and suggests some focusing of energy to the northwest.

INTRODUCTION

The Imperial Valley earthquake of October 15, 1979, provided a wealth of strong-motion data, both north and south of the United States-Mexican border. Most important, relative to the data presented here, was that the earthquake was surrounded by instruments both in the direction of rupture propagation (northwestward in the Imperial Valley) and in the direction away from rupture propagation (southeastward to our array in Baja California, Mexico). In addition, recording of the event by many digital instruments (seven in our own array) allows, for the first time, a detailed comparison of the performance of digital and conventional accelerographs.

PRELIMINARY DESCRIPTION OF DATA

The northern Baja California strong-motion array was installed as a cooperative United States-Mexican project. Initially, 16 SMA–1 film-recording instruments were installed (Prince and others, 1977). Before the 1979 Imperial Valley earthquake, strong-motion records were obtained from the Mesa de Andrade, Mexico, earthquake of December 7, 1976, and the Victoria, Mexico, earthquake swarm of March 1978. We subsequently replaced several of the SMA–1 instruments with 10 digital accelerographs of the two kinds then available (Terra Technology and Kinemetrics) and deployed a crossarray of stations to study attenuation of strong motion perpendicular to the fault. At the time of the October 15, 1979, earthquake, most of these digital instruments were in operation (two had been temporarily diverted to record possible aftershocks of the March 14, 1979, Petatlán, Mexico, earthquake), and most of the piers in the crossarray were instrumentally equipped. Figure 234 shows the part of the array in the Mexicali Valley. Aside from instruments in the regular array, one instrument operated by UNAM and the Secretaría de Asentamientos Humanos y Obras Publicas (SAHOP) was temporarily at the private residence of Alfonso Flores in Mexicali.

Most of the instruments performed well, although no radio time was recorded on any of the Kinemetrics in-

struments (two digital and two SMA–1, all relying on WWVB radio for time). One Terra Technology DCA 310 digital instrument malfunctioned, and we have not been able to read the cassette tape from it; another Terra Technology instrument had unexplained erratic low-bit behavior. One channel of one of the Kinemetrics digital recorders also failed.

One presumably erroneous recording of a high-frequency vertical acceleration was obtained from station Agrarias (approximately 0.8 g at frequencies of about 30 Hz). Inspection of this instrument after the earthquake revealed that a mounting bolt was loose on the accelerometer package. This circumstance likely caused the anomalously high frequencies recorded: one corner of the accelerometer package could be slightly oscillated vertically with a finger. The package could not be moved horizontally, however, and thus we believe that aside from the high-frequency crosscoupling (which can be filtered out), the horizontal records should be reliable, especially for velocity and displacement. In all, for the main event we obtained nine records (five Terra Technology DCA 310, two Kinemetrics digital DSA–1, and two Kinemetrics photographic SMA–1). Table 33 lists the locations, orientations, and peak accelerations for these records.

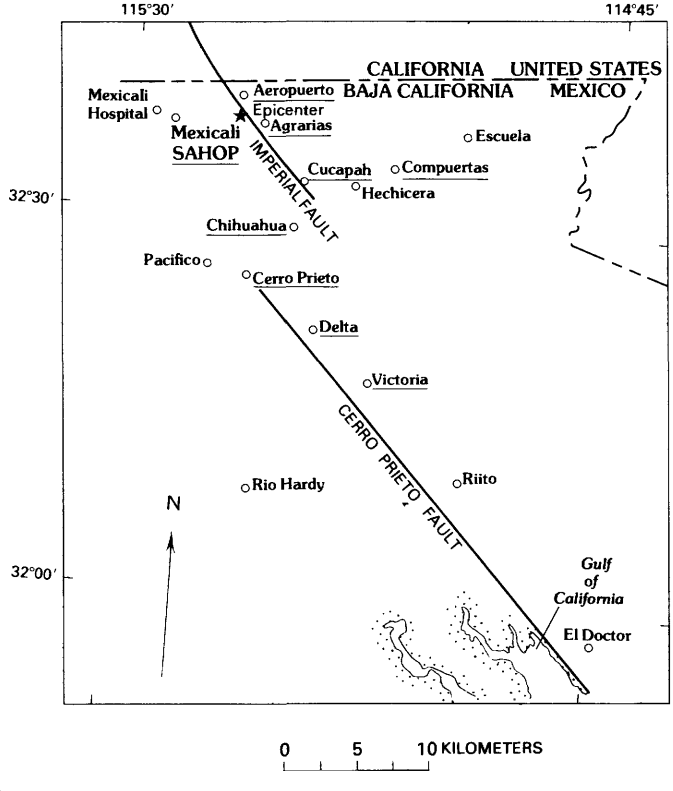

FIGURE 234.—Locations of strong-motion stations in Mexicali Valley, Baja California. Stations underlined are those from which usable records were obtained for 1979 Imperial Valley earthquake.

Near the border, most instruments recorded peak horizontal accelerations of about 0.3g, with a minimum of 0.17g at the farthest station. The station Cerro Prieto record is of special interest because it was the only record obtained on solid rock south of the border. The stations on solid rock north of the border that recorded this earthquake were farther away and recorded considerably lower accelerations (Matthiesen and Porcella, this volume). Cerro Prieto is a massive volcanic cone emplaced through the thick sedimentary deposits of the Mexicali Valley. Although its higher rigidity would normally be expected to reduce surface accelerations, because the cone is connected to the basement beneath the deposits we might expect it to transmit high-frequency energy to the surface more efficiently than the deposits and thus tend to increase the accelerations. The peak acceleration recorded at station Cerro Prieto is somewhat lower than that for nearby stations in the deposits, although its predominant frequency appears to be higher.

Figure 235 plots peak acceleration as a function of distance from the intersection of the Imperial fault with the United States-Mexican border, including data from several stations north of the border (Matthiesen and Porcella, this volume). The accelerations to the southeast are high, out to fairly large distances; that is, they do not show any sharp falloff with distance near the epicenter. The high acceleration observed at station Delta, at a distance of 33 km, is particularly surprising.

Figure 236 shows the (unprocessed) three-component acceleration records obtained from the digital accelerographs. We note that the instrument at station Compuertas triggered on the S wave but not the P wave.

Figure 237 presents the results of a preliminary integration of the acceleration records to obtain particle velocities and displacements for a few stations, according to the procedure of Trifunac and Lee (1973). These records have not been corrected for instrument response at high frequencies. The high-pass filter for these integrations has a corner frequency of 0.6 Hz. The peak values of velocity for these stations are given in figure 237 and listed in table 33. The results for displacement are affected by the relatively high frequency of the high-pass filter and should not be taken as the true values for ground displacement. The displacement results were only meant as preliminary values to be available immediately after the earthquake.

ARRIVAL TIMES

Because the digital strong-motion instruments had a delayed recording of 1.6 s, we can accurately read the onsets of P waves as well as of S waves. We have interpreted arrival times as indicated on the records (dots, fig. 236); these values are listed in table 33.

TABLE 33.—*Summary of strong-motion data recorded in Mexico during the main shock*

[Station numbers are those assigned by the U.S. Geological Survey (1977). Epicentral distance is measured from epicenter at lat 32.63° N., long 115.34° W. Instruments: KN, Kinemetrics Digital Recorder; SM, Kinemtrics SMA-1 Film Recorder; TT, Terra Technology Digital Recorder. $S-P$ interval is equal to S-wave arrival time minus P-wave arrival time; values in parentheses are equal to S-wave arrival time minus trigger time. P-wave arrival time is measured in minutes and seconds after 288 d 23 h G.m.t., as determined from internal clock synchronized with radio WWVB time code. Direction of acceleration is that for upward trace deflection on accelerogram; horizontal components are listed as azimuth (in degrees clockwise from north), and vertical components as "up" or "down"]

Station identification			Epicentral distance (km)	Instrument	$S-P$ interval (s)	P-wave arrival time	Acceleration		Velocity (cm/s)	Local magnitude (M_L)
No.	Name (data source)	Coordinates (lat °N., long °W.)					Direction	Max (g)		
6616	Aeropuerto (UNAM/UCSD)	32.651, 115.332	2	SM	(1.2)	[1]	045°	0.316	[2]	[2]
							up	.179	----	----
							315°	.240	----	----
6618	Agrarias (UNAM/UCSD)	32.621, 115.301	4	TT	1.7	16:56.88	183°	[3].280	29.8	6.12
							down	----	10.0	----
							0.93°	[3].227	33.6	6.16
6604	Cerro Prieto (UNAM/UCSD)	32.420, 115.301	24	TT	[4]	16:58.84	057°	.149	14.5	6.45
							down	.198	5.74	----
							327°	.167	11.9	6.13
6621	Chihuahua (UNAM/UCSD)	32.484, 115.240	19	TT	2.3	16:59.32	192°	.267	21.4	6.29
							down	.215	4.95	----
							102°	.263	33.3	6.44
6622	Compuertas (UNAM/UCSD)	32.572, 115.083	23	TT	[4]	[1]	195°	.188	14.5	6.18
							down	.066	2.97	----
							105°	.149	10.22	5.82
6617	Cucapah (UNAM/UCSD)	32.545, 115.235	14	KN	[4]	[1]	085°	.310	34.6	6.25
							up	.115	2.92	----
							355°	----	----	----
6605	Delta (UNAM/UCSD)	32.356, 115.195	33	TT	[4]	17:01.39	172°	.349	31.9	6.91
							down	.152	4.92	----
							082°	.235	22.10	6.80
6619	Mexicali SAHOP[5] (SAHOP/UNAM)	32.618, 115.428	13	SM	(2.7)	[1]	000°	.311	[2]	[2]
							up	.332	----	----
							090°	.459	----	----
6610	Victoria (UNAM/UCSD)	32.289, 115.103	44	KN	[4]	[1]	075°	.122	5.64	6.34
							up	.056	1.34	----
							345°	.163	8.28	6.56
Average										6.34

[1]No absolute timing at station.
[2]Film recorders; therefore, acceleration traces could not be readily integrated for velocity or deconvolved-convolved for magnitude.
[3]Questionable.
[4]$S-t$ or $S-P$ interval is questionable.
[5]This station was temporarily located at the Flores residence in Mexicali, approximately 1 km east of the normal station Mexicali SAHOP (No. 6619); coordinates listed here are those of the Flores residence.

MAGNITUDES

Because no Wood-Anderson recordings are available southeast of the epicenter, determinations of the local magnitude M_L, based primarily on records from stations to the northwest, could be seriously biased, especially if the rupture propagation focused energy toward the northwest. To remedy this situation partially, we converted the digital strong-motion records from the northern Baja California array into Wood-Anderson equivalent records, using the deconvolution-convolution technique suggested by Kanamori and Jennings (1978). We then computed magnitudes from these mock-Wood-Anderson records, using the standard tables; these values are listed in table 33. The average magnitude from this data set is 6.34; the only solid-rock recording, from station Cerro Prieto, gave a comparable value of 6.2. These magnitudes are somewhat lower than the average magnitude determined to the northwest (6.6; Espinosa, this volume) and suggest some focusing of energy to the northwest. Thus, the magnitude that we would have obtained from a uniform sampling of Wood-Anderson records at all azimuths would probably have been about 6.5.

CONCLUSION

The strong-motion records for the Imperial Valley earthquake obtained from stations in Mexico, combined with the numerous records obtained north of the border, provide relatively complete azimuthal coverage, that is, both in the direction of rupture propagation (northwestward) and in the opposite direction. Both the accelerations and velocities are generally higher along the fault to the northwest in the Imperial Valley; however,

the pattern of strong motion shows a considerable complexity, not explainable by a simple propagating point source, that may be due to nonuniform displacement along the fault rupture or to structural inhomogeneities. The local magnitude estimated from the strong-motion records is 6.3, somewhat lower than the average magnitude determined from stations to the northwest. Because the data for this earthquake are so extensive, we anticipate that further study will lead to a better understanding of the rupture propagation for this earthquake than has been possible for any previous earthquake.

ACKNOWLEDGMENTS

The installation and operation of the Baja California strong-motion array was supported by U.S. funding provided by Research Applied to National Needs (RANN) and Applied Science and Research Applications (ASRA) under National Science Foundation Grants NSF RANN ENV 75–02939 and NSF ASRA PFR 77–23829, and by Mexican funding provided by the Consejo Nacional de Ciencia y Technología (CONACYT) and the Instituto de Ingeniería, Universidad Nacional Autónoma de México (UNAM). The deconvolution-convolution program was written by Alejandro Nava.

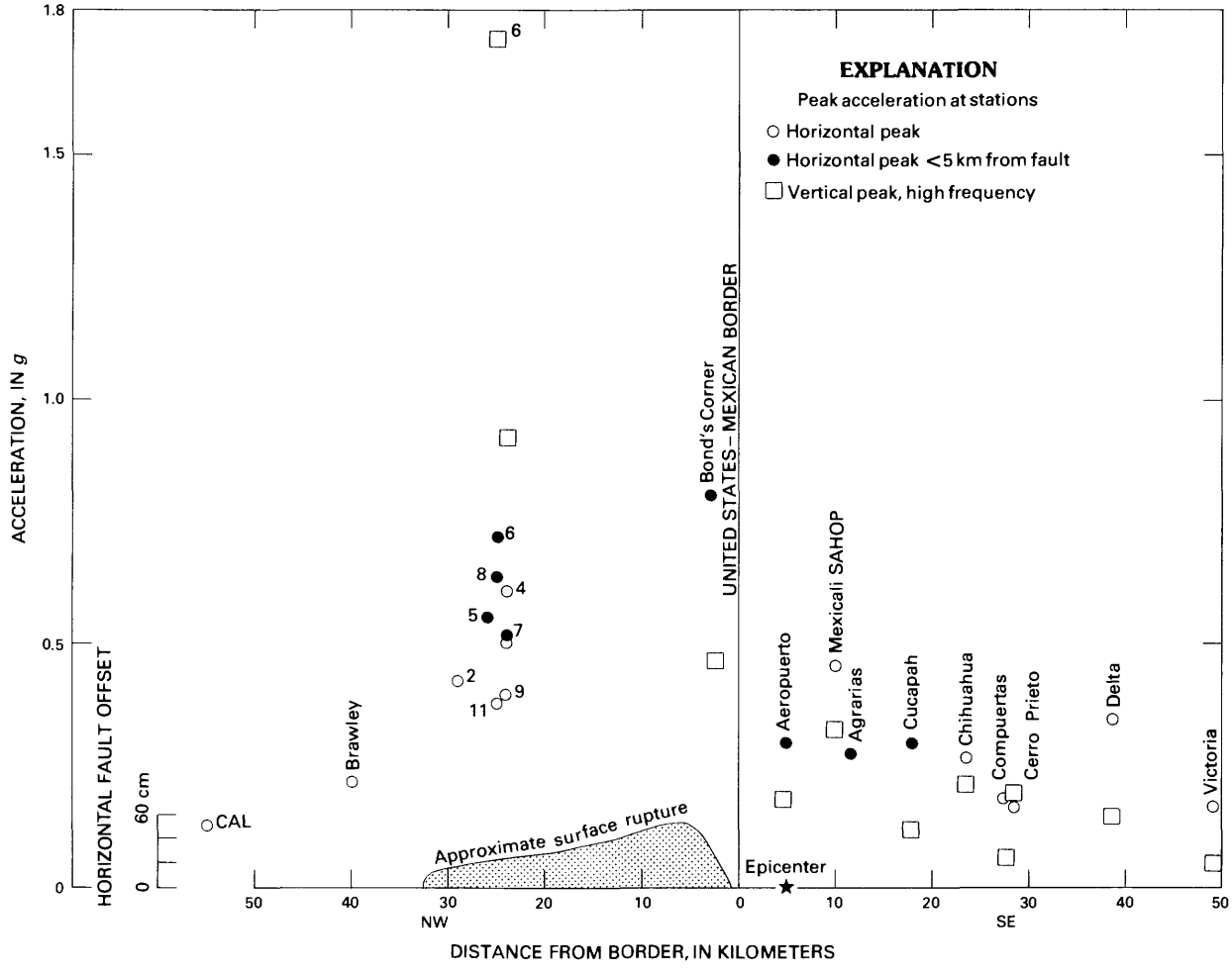

FIGURE 235.—Peak acceleration from 1979 Imperial Valley earthquake as a function of distance from point of intersection of Imperial fault with United States-Mexican border. Numbers refer to stations in U.S. Geological Survey Imperial Valley array.

REFERENCES CITED

Kanamori, Hiroo, and Jennings, P. C., 1978, Determination of local magnitude, M_L, from strong-motion accelerograms: Seismological Society of America Bulletin, v. 68, no. 2, p. 471–485.

Prince, Jorge, Brune, J. N., Reyes, Alfonso, Nava, Alejandro, 1977, Strong-motion instrumentation of northern Baja California [abs.]: Geological Society of America Abstracts with Programs, v. 9, no. 4, p. 484.

Trifunac, M. D., and Lee, V., 1973, Routine computer processing of strong-motion accelerograms: Pasadena, California Institute of Technology, Earthquake Engineering Research Laboratory Report EERL 73–03, 360 p.

U.S. Geological Survey, 1977, Western Hemisphere strong-motion accelerograph station list—1976: U.S. Geological Survey Open-File Report 77–374, 112 p.

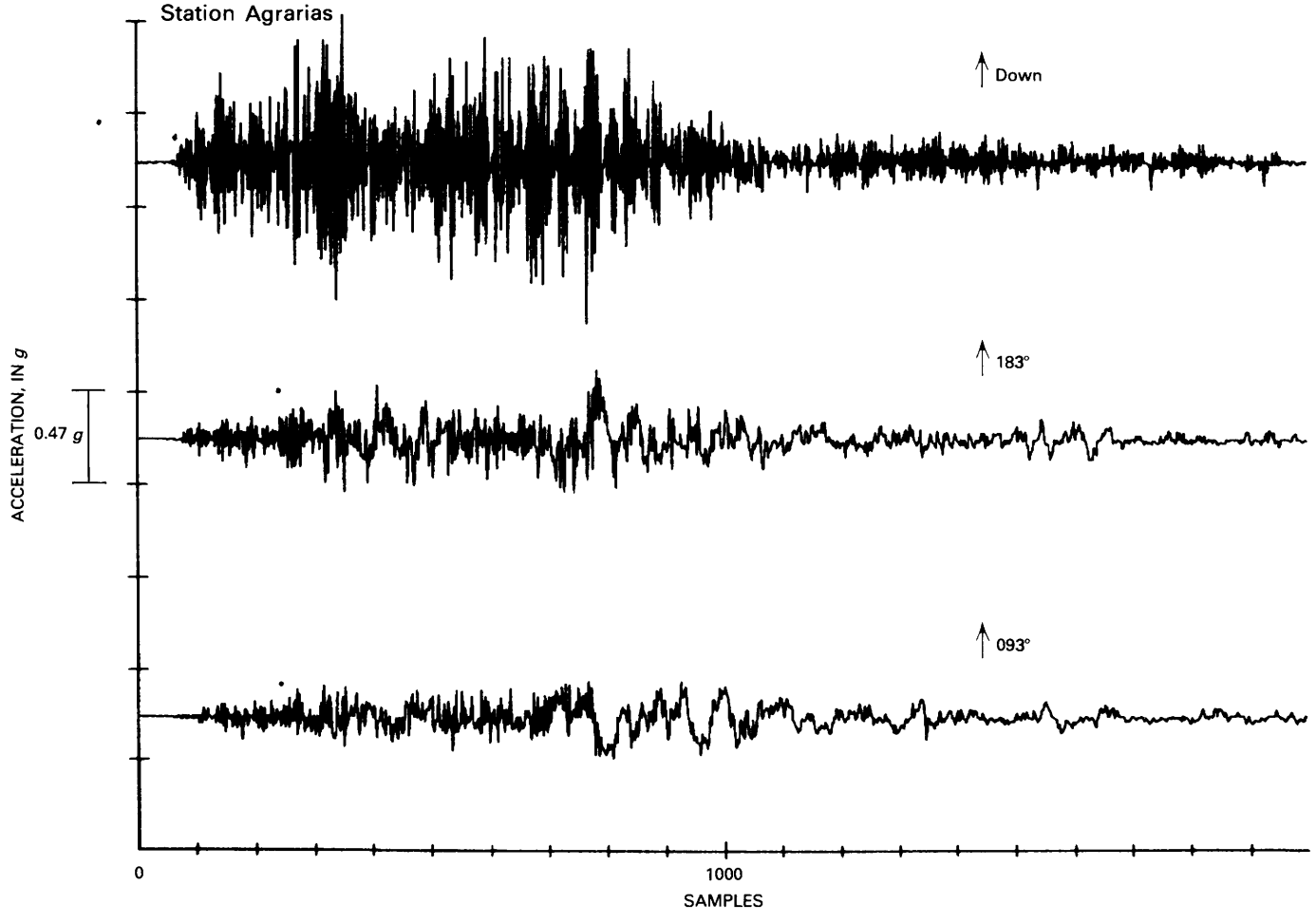

FIGURE 236.—Strong-motion records for October 15 main shock (see fig. 234 for locations of stations). Dots indicate interpreted arrival times. Each tick on horizontal axis equals 1 s.

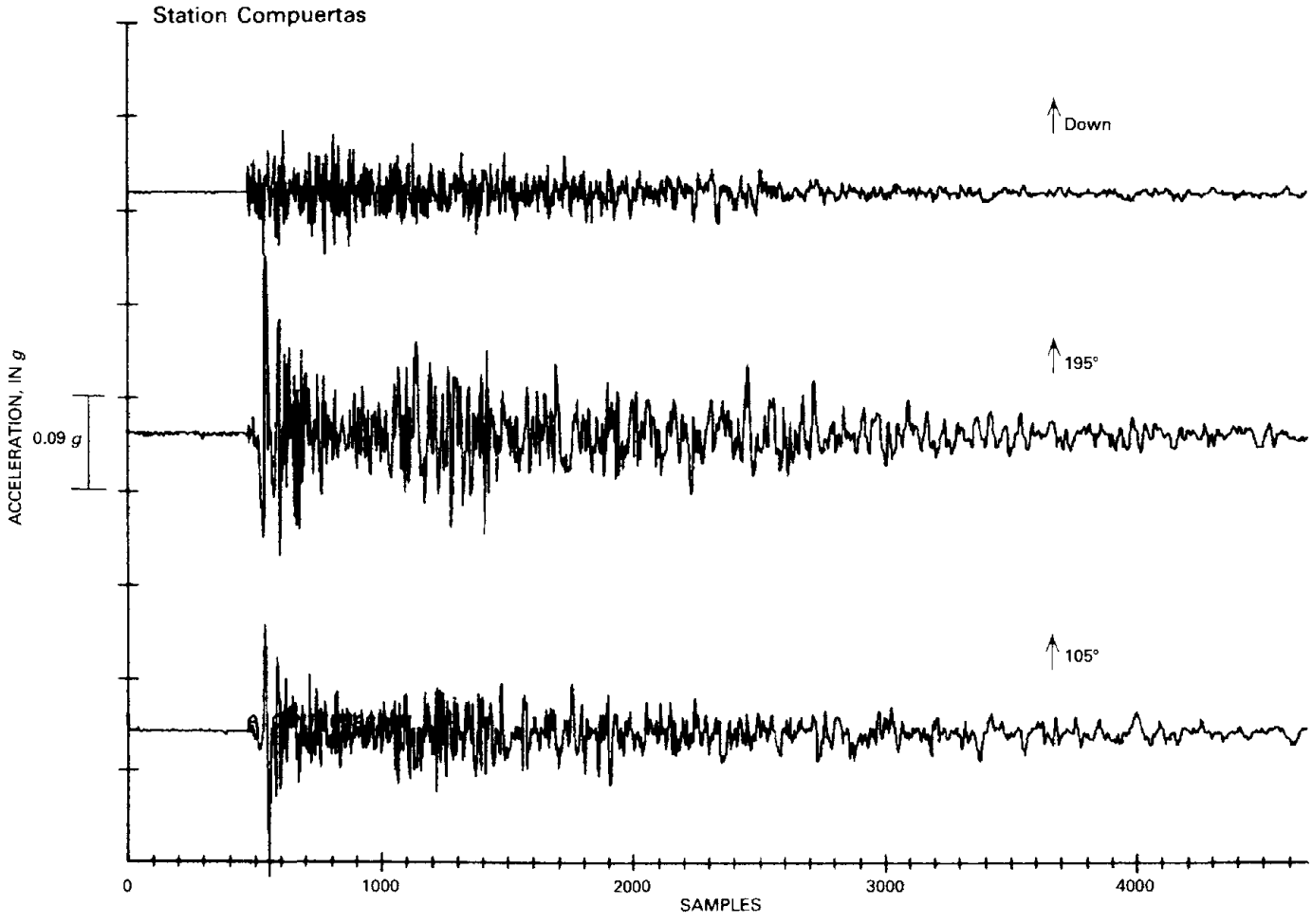

FIGURE 236.—Continued

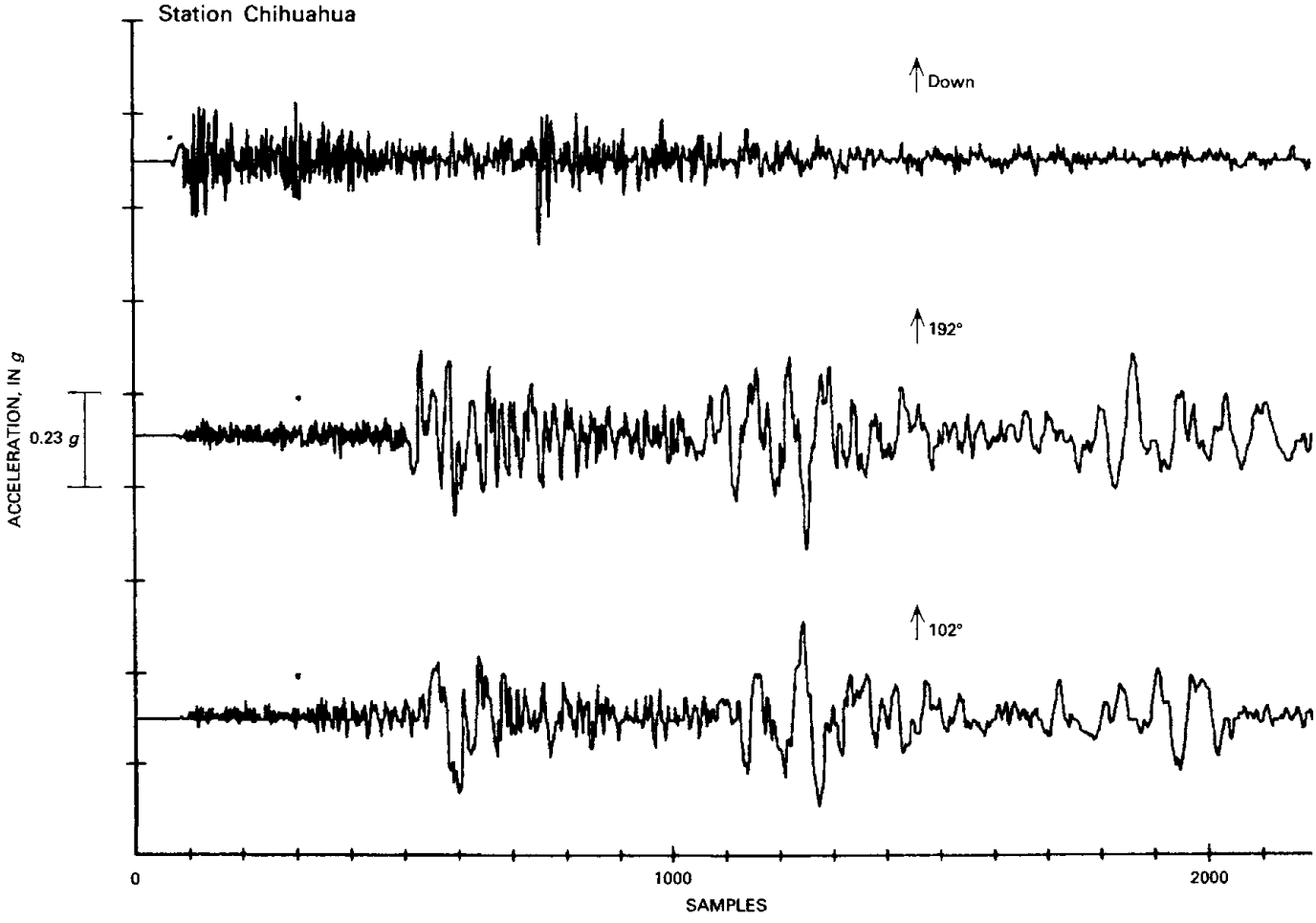

FIGURE 236.—Continued

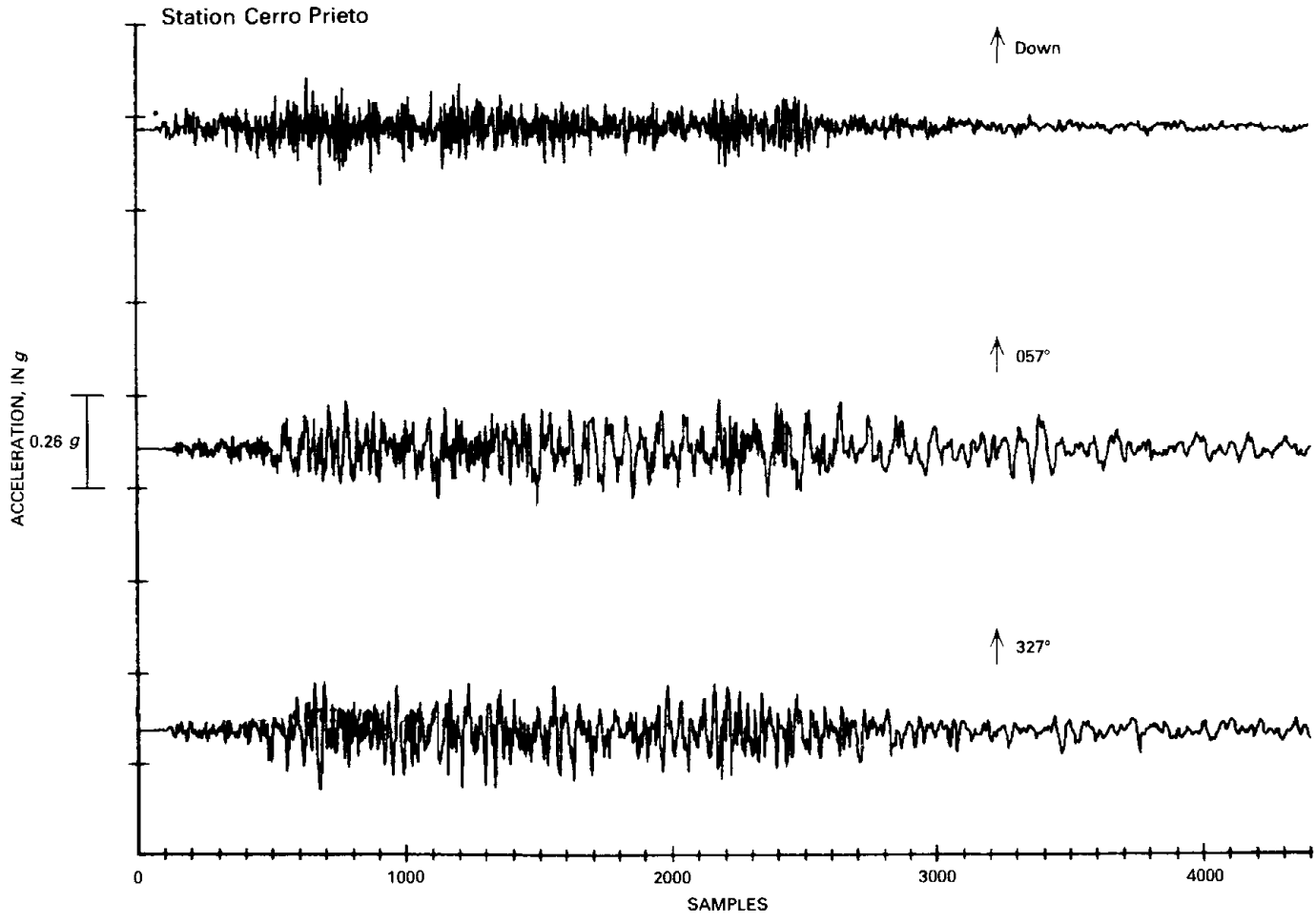

FIGURE 236.—Continued

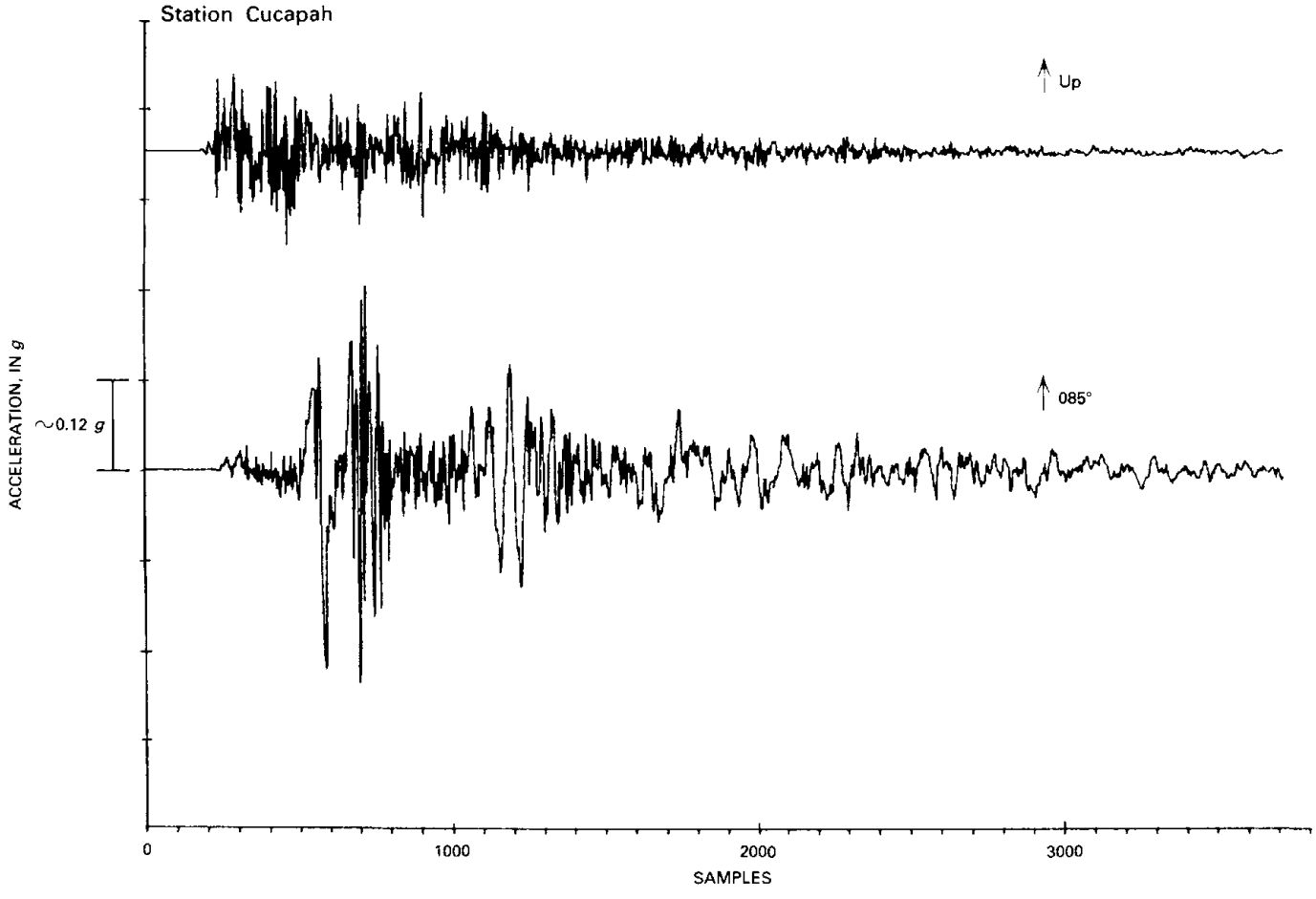

FIGURE 236.—Continued

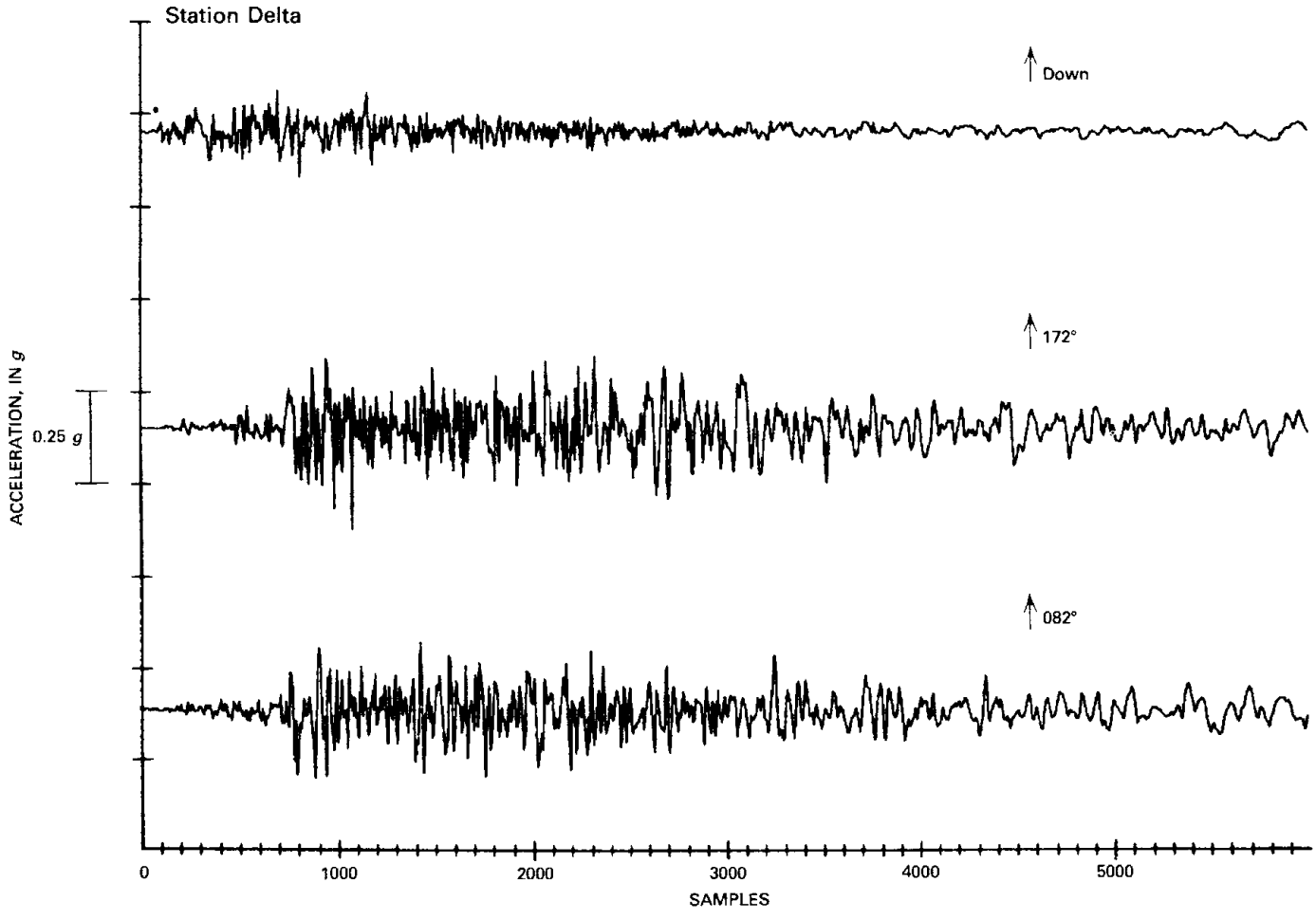

FIGURE 236.—Continued

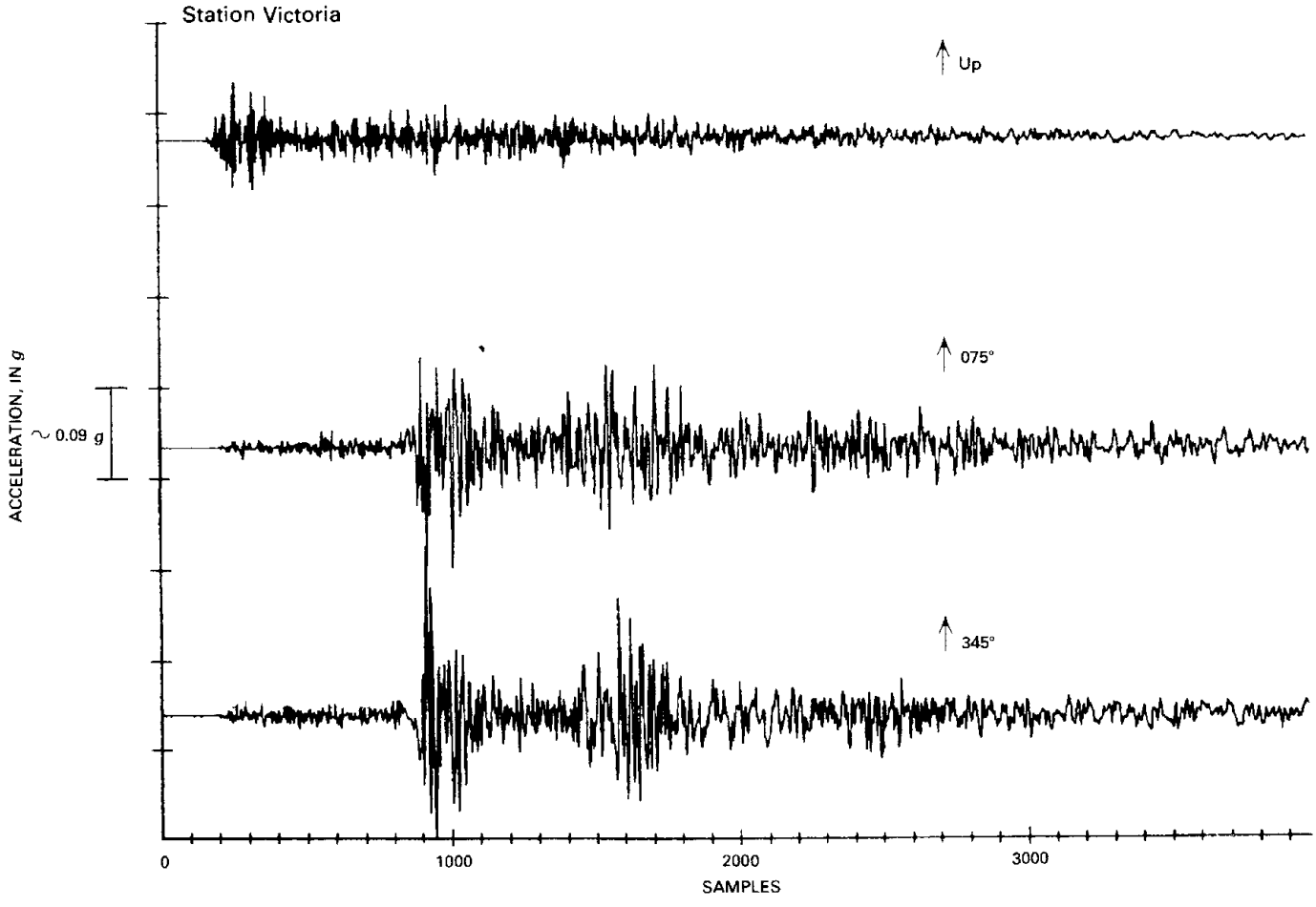

FIGURE 236.—Continued

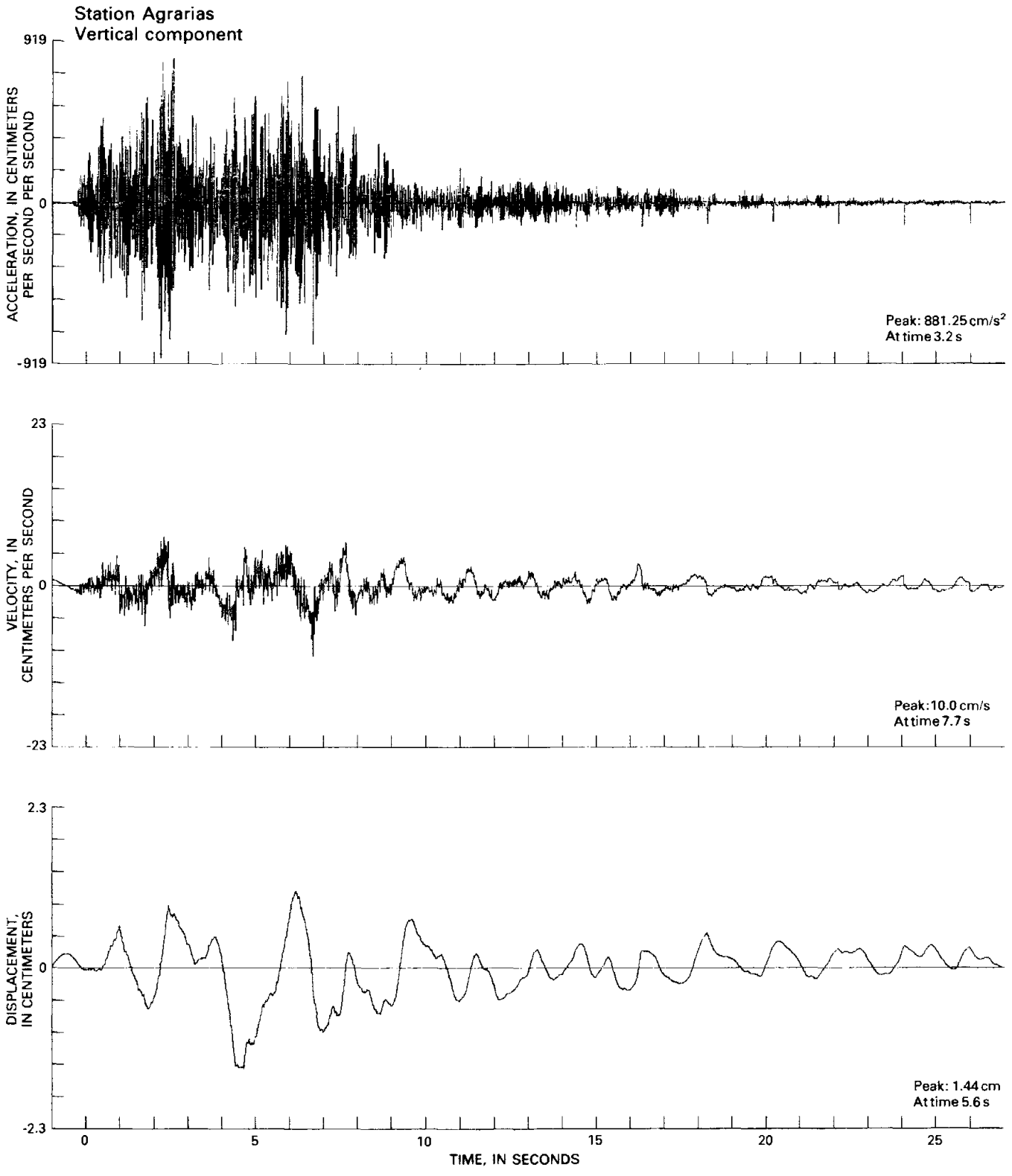

FIGURE 237.—Acceleration, velocity, and displacement (not corrected for instrument response) from 1979 Imperial Valley earthquake at seven stations (see fig. 234 for locations).

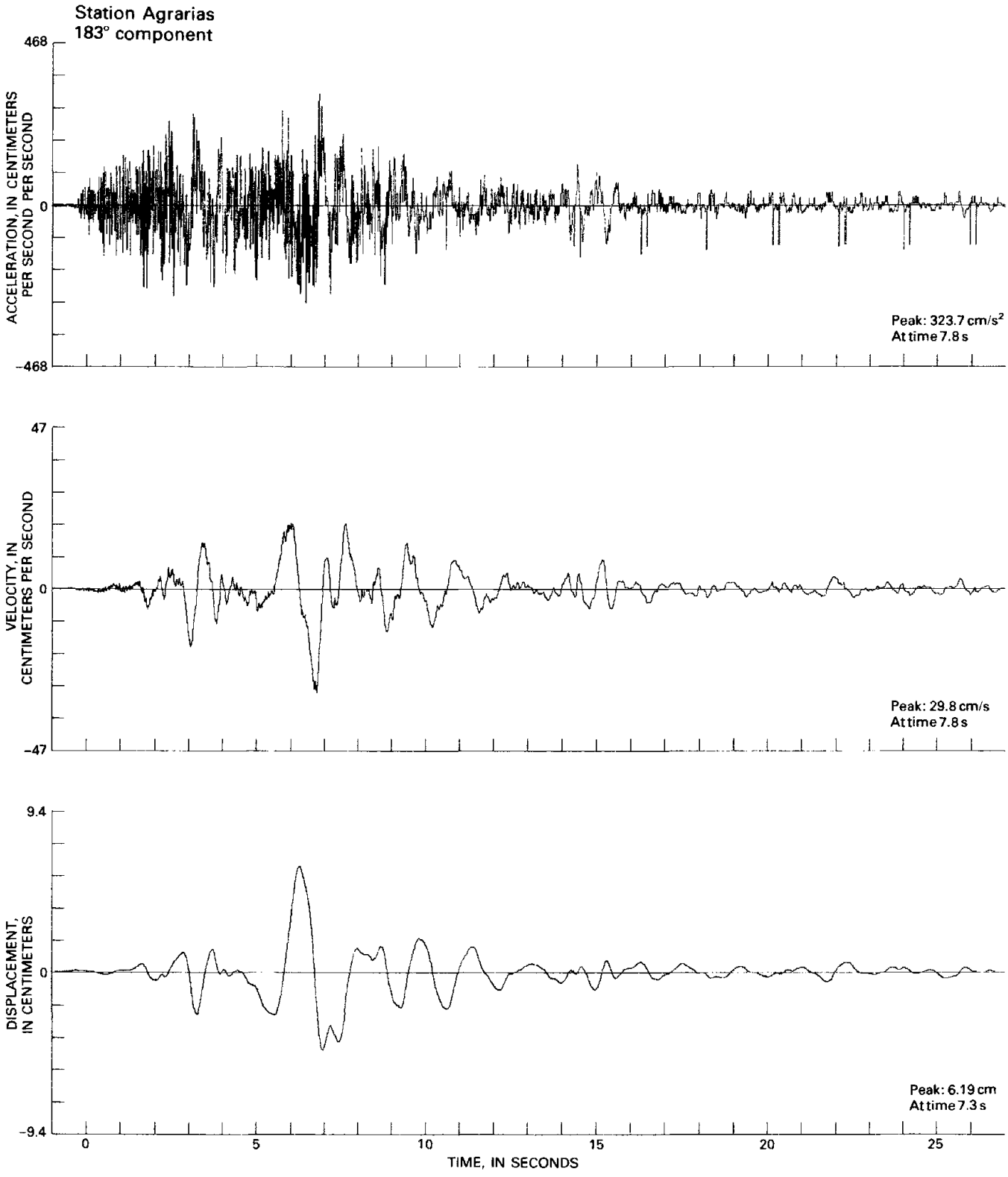

FIGURE 237.—Continued

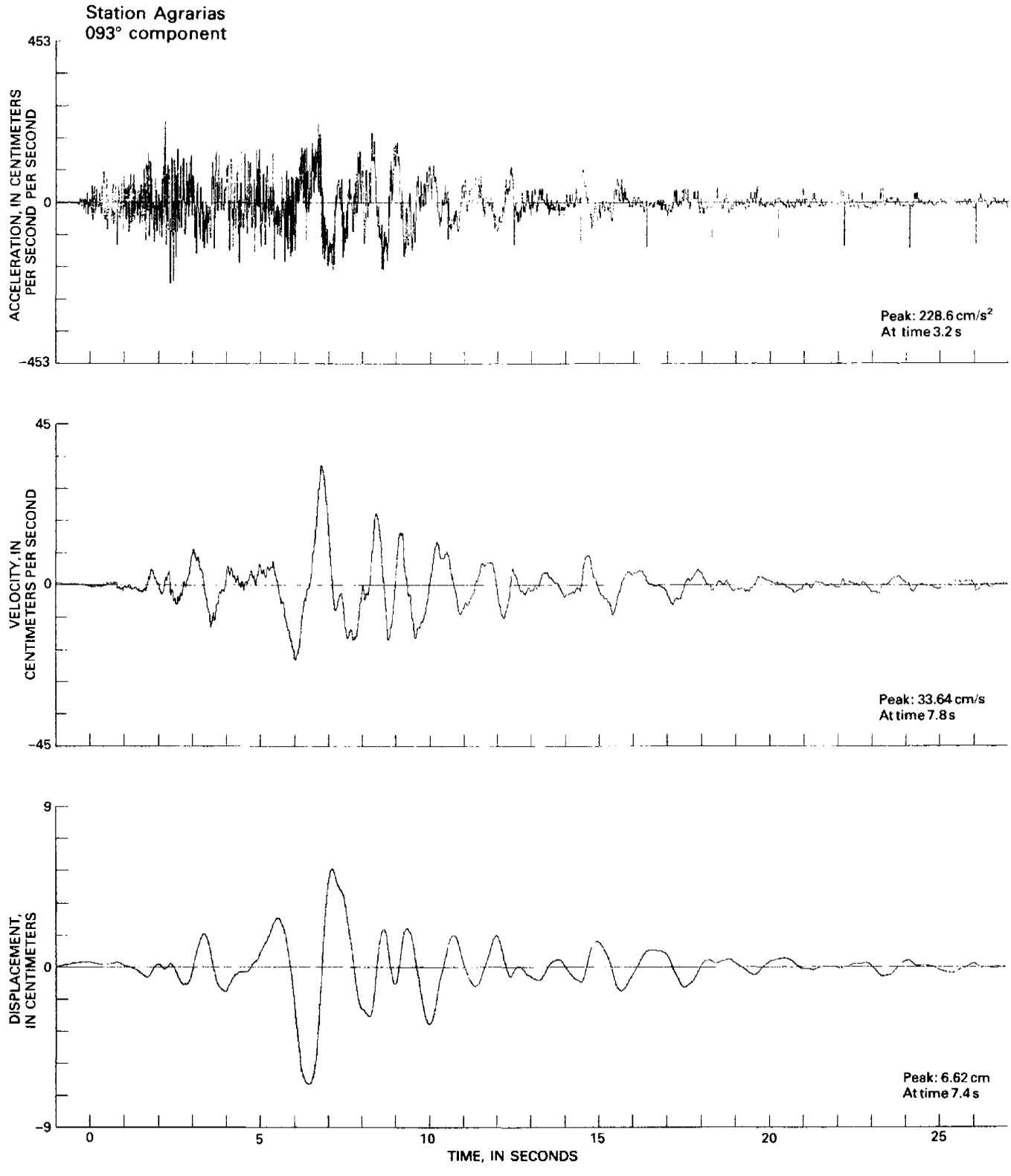

FIGURE 237.—Continued

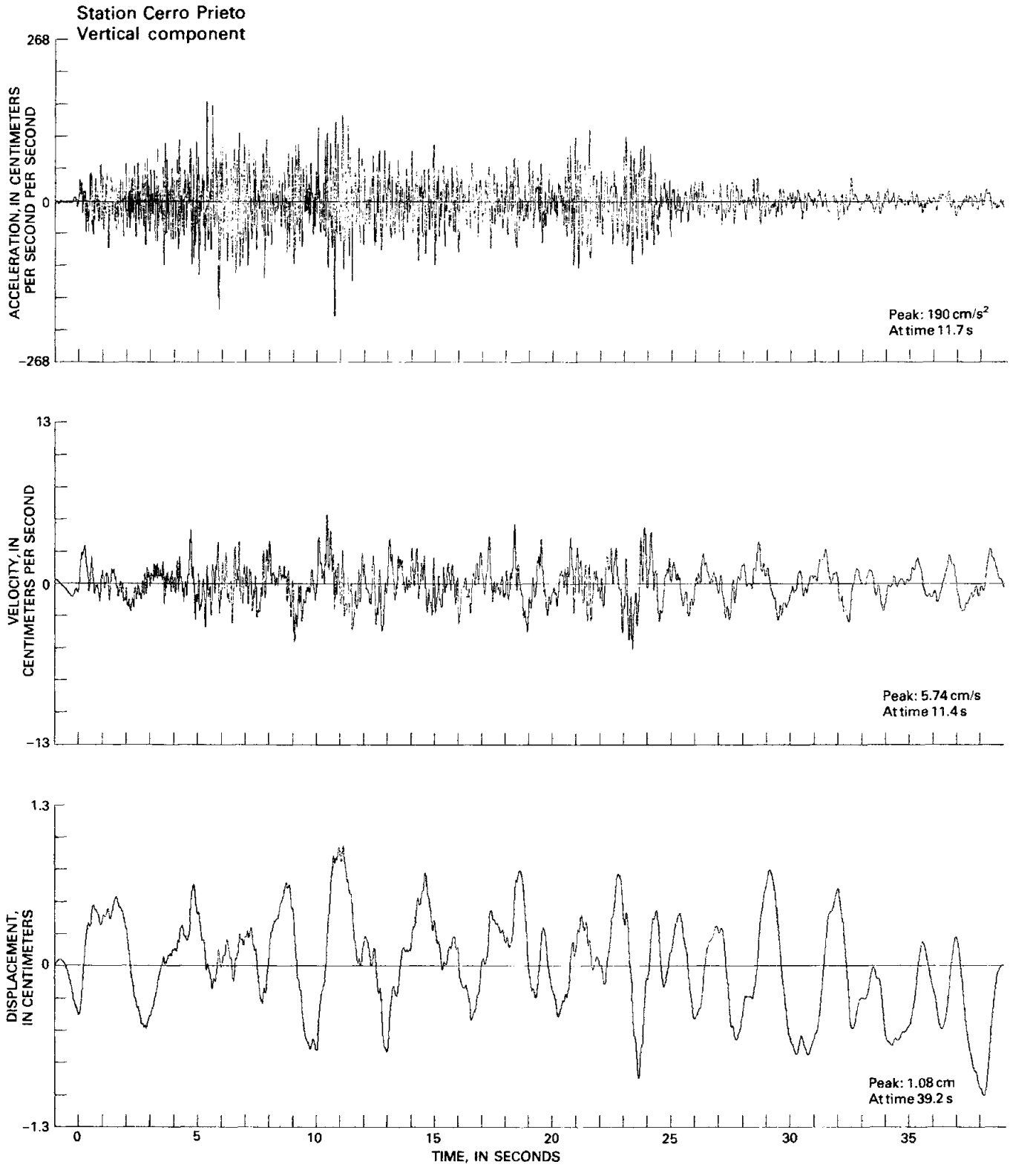

FIGURE 237.—Continued

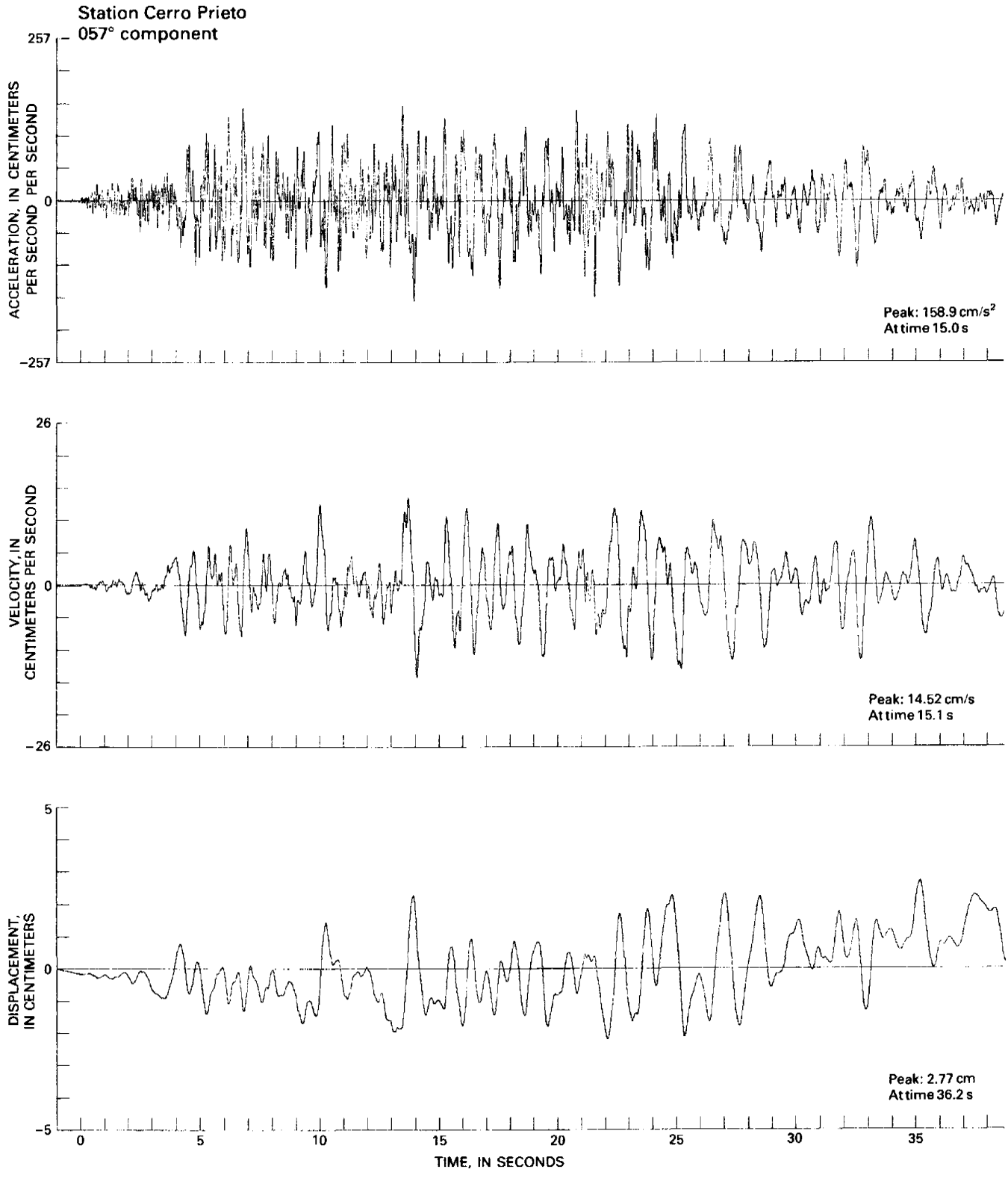

FIGURE 237.—Continued

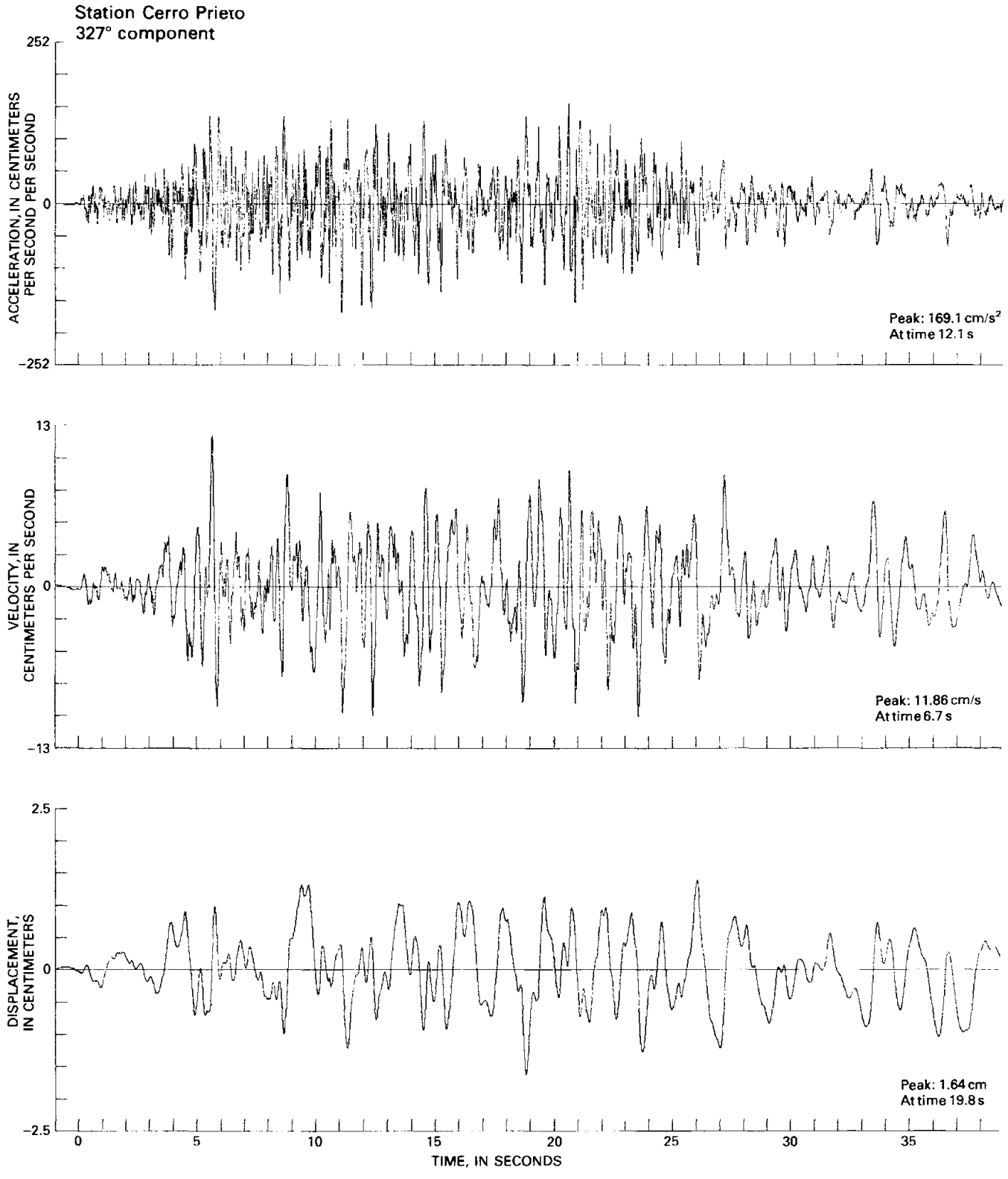

FIGURE 237.—Continued

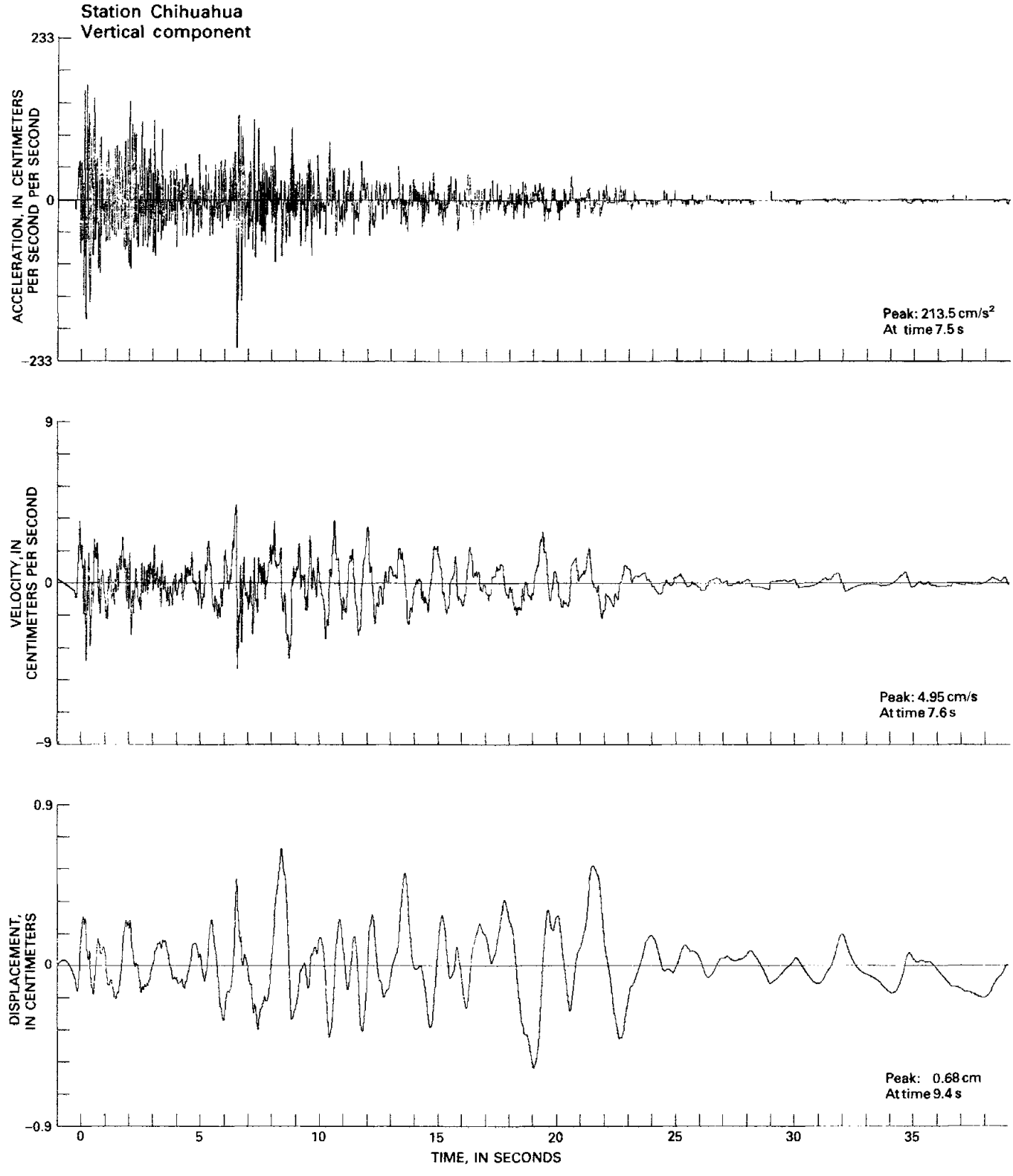

FIGURE 237.—Continued

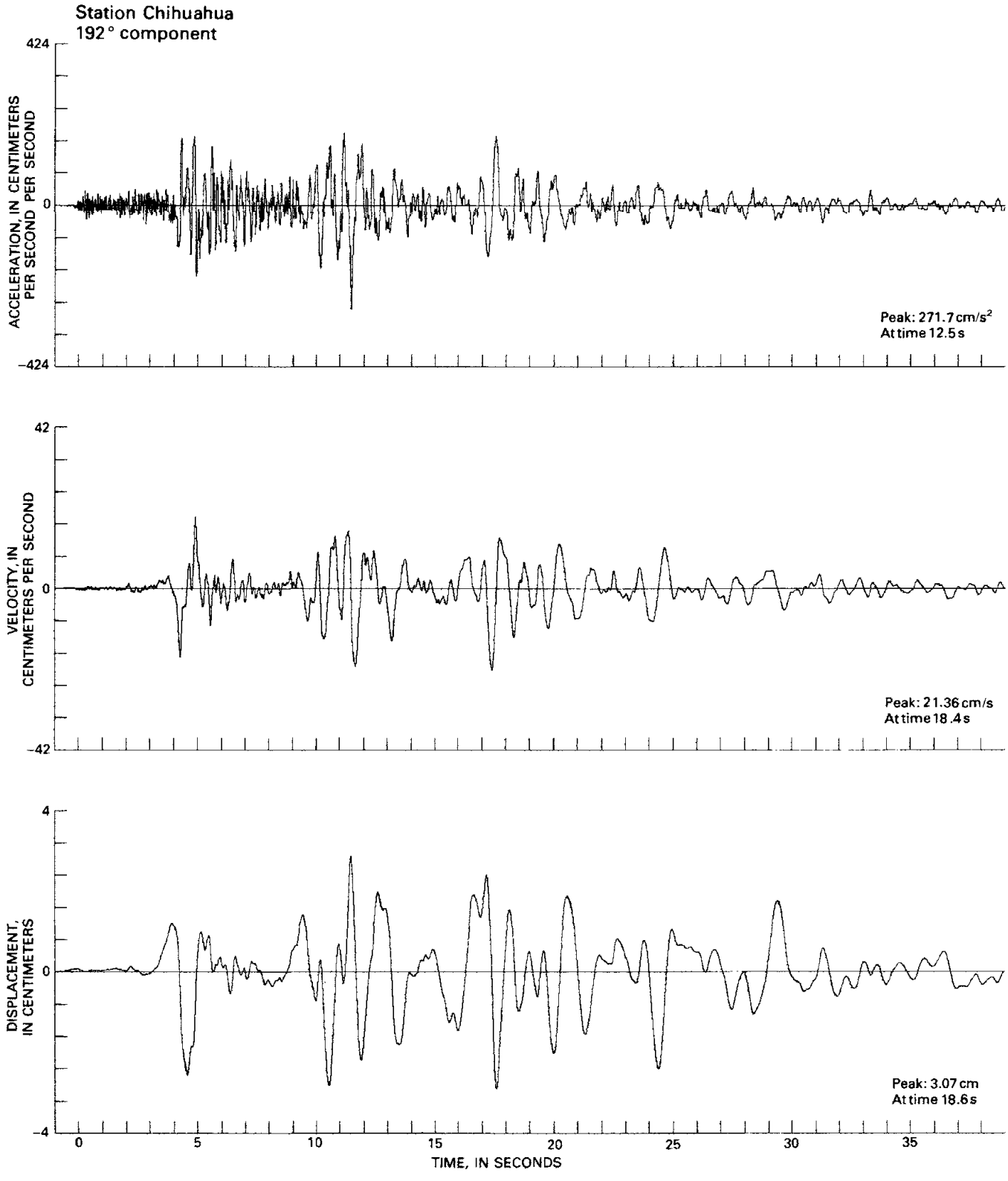

FIGURE 237.—Continued

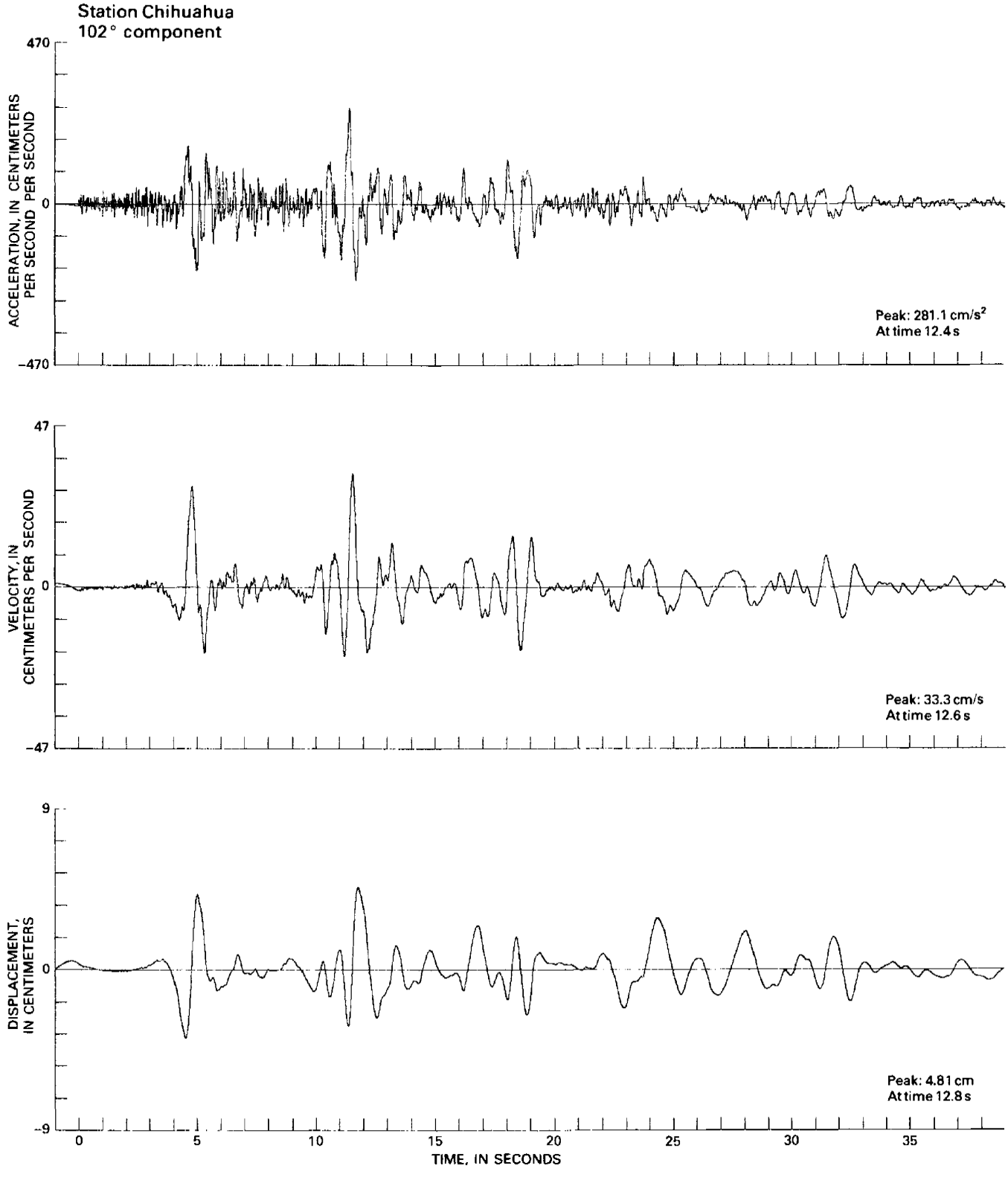

FIGURE 237.—Continued

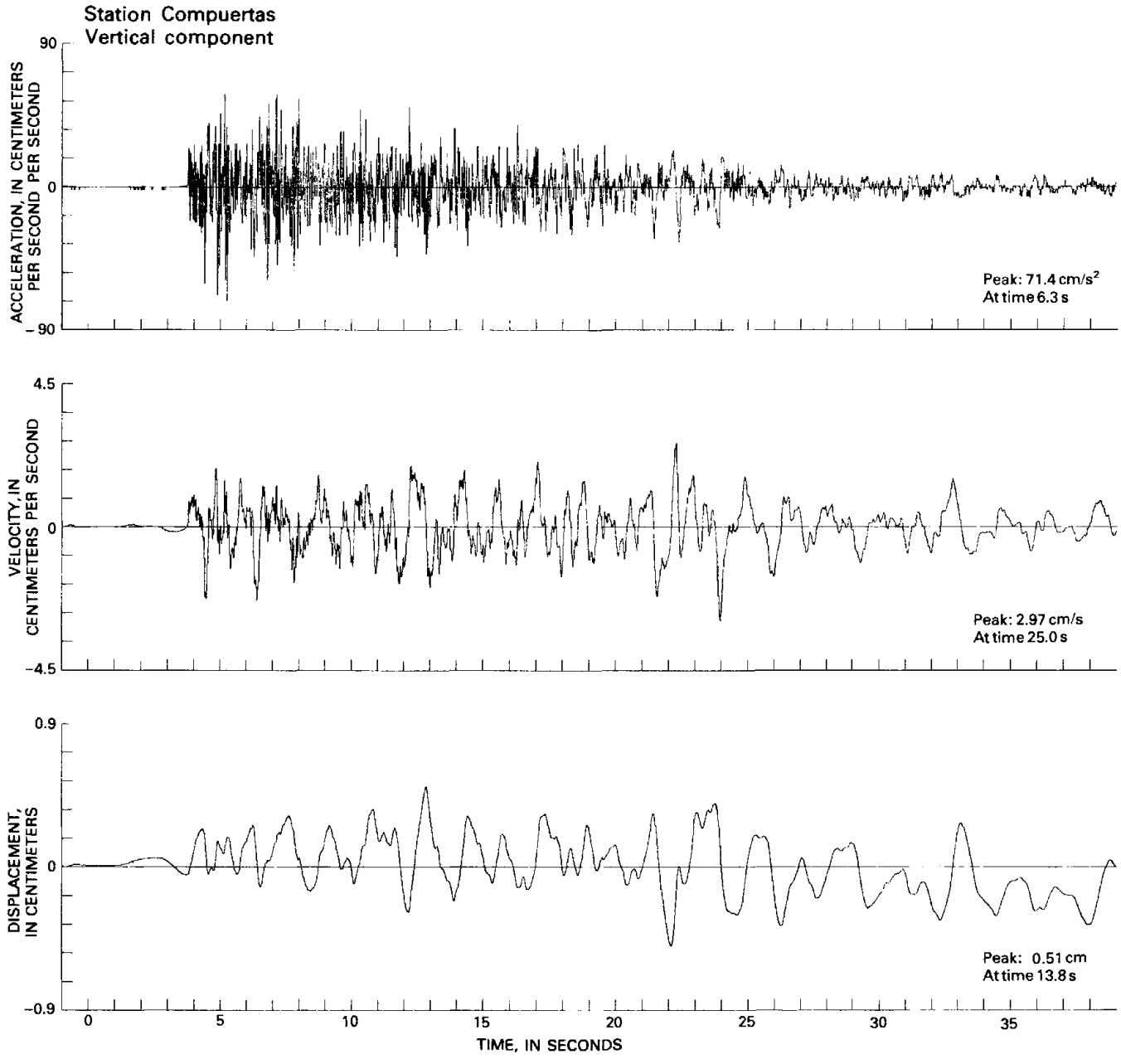

FIGURE 237.—Continued

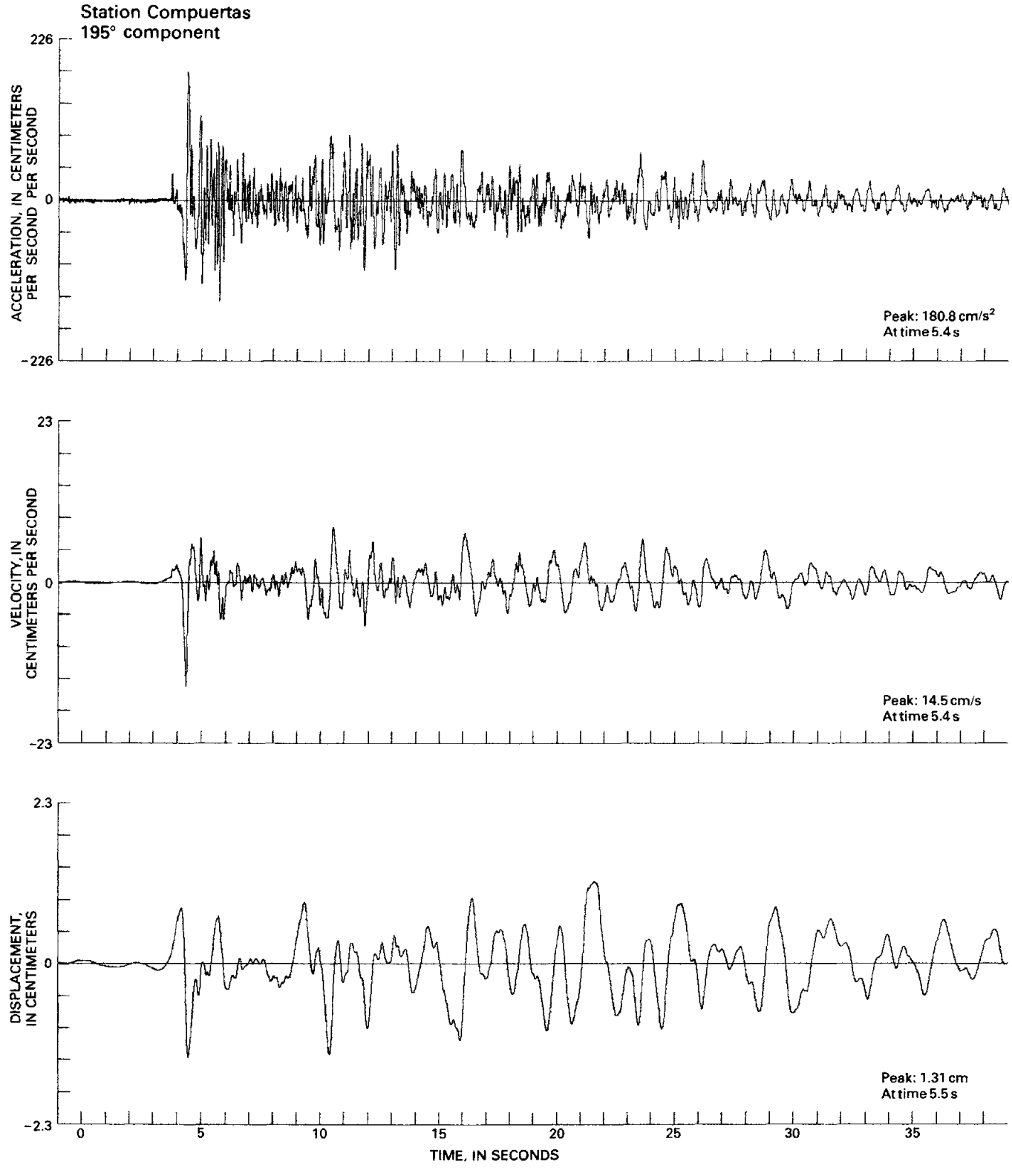

FIGURE 237.—Continued

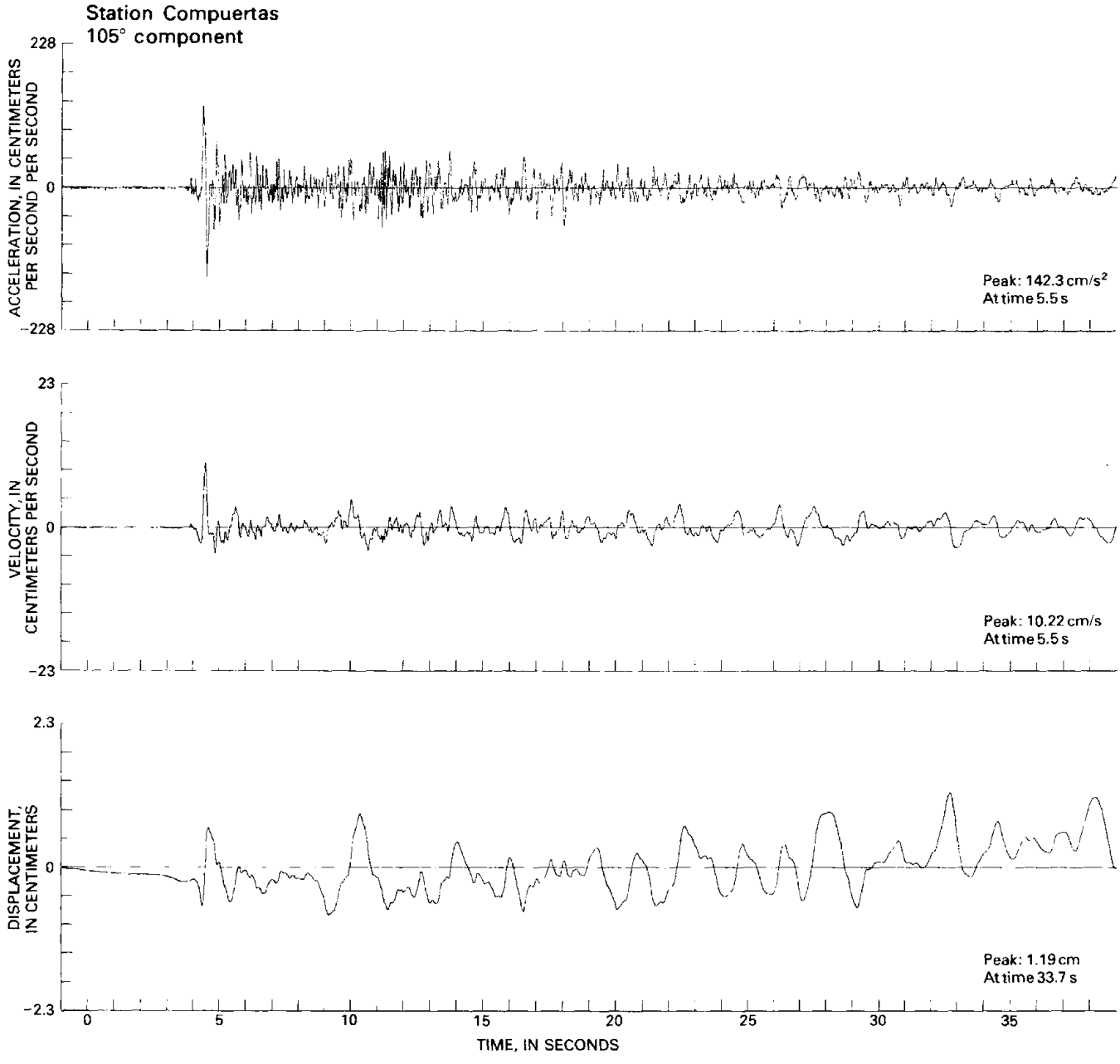

FIGURE 237.—Continued

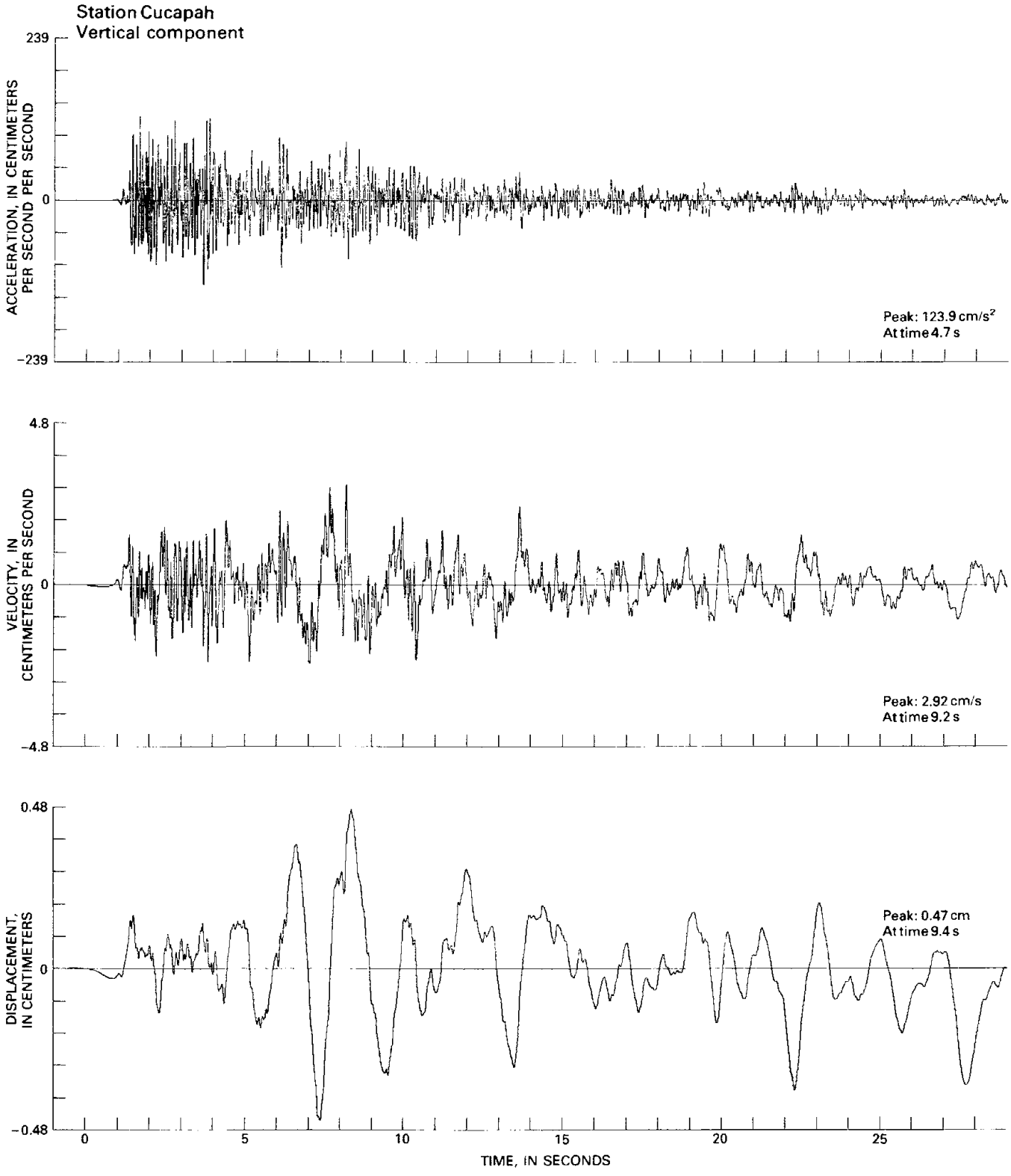

FIGURE 237.—Continued

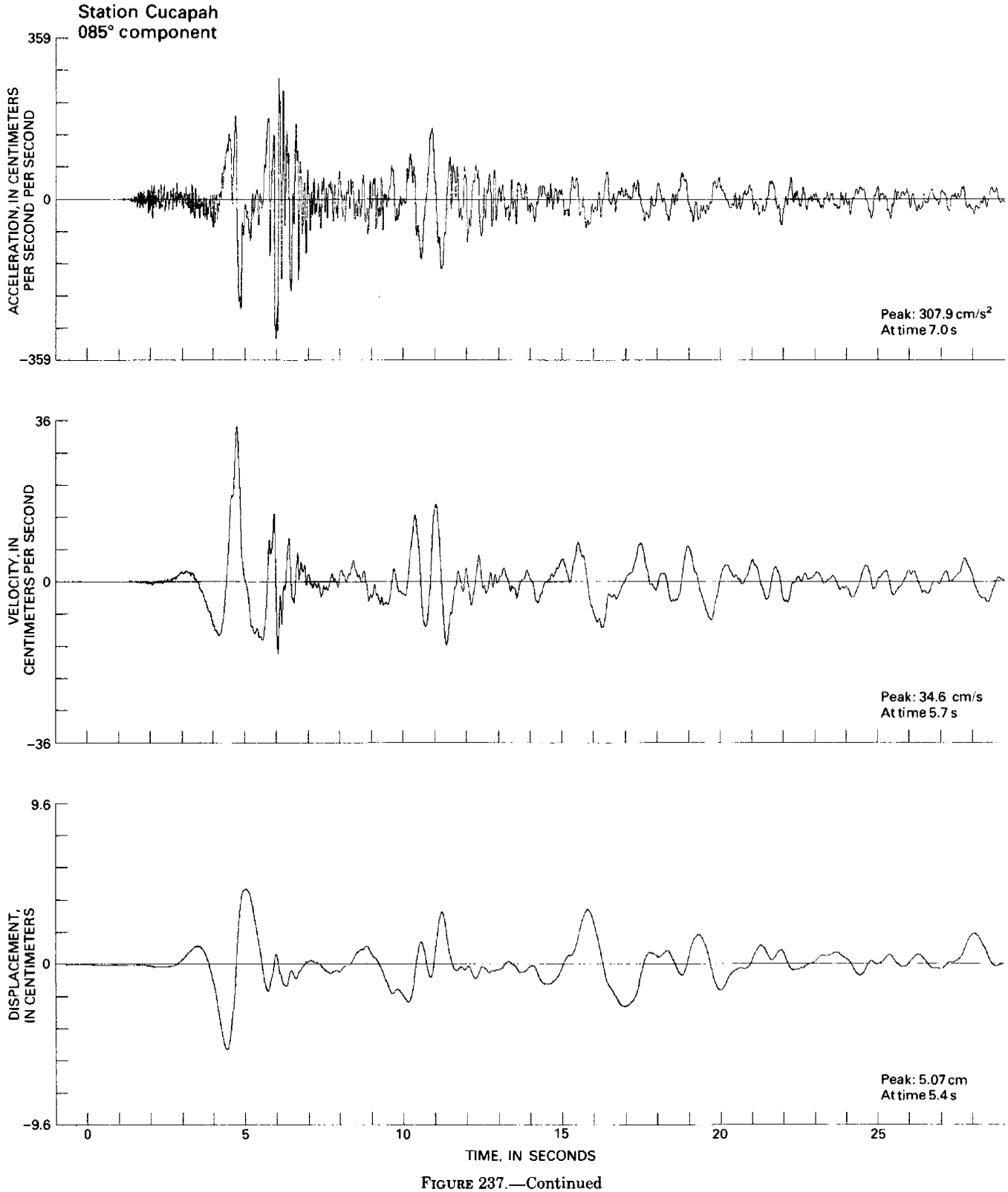

FIGURE 237.—Continued

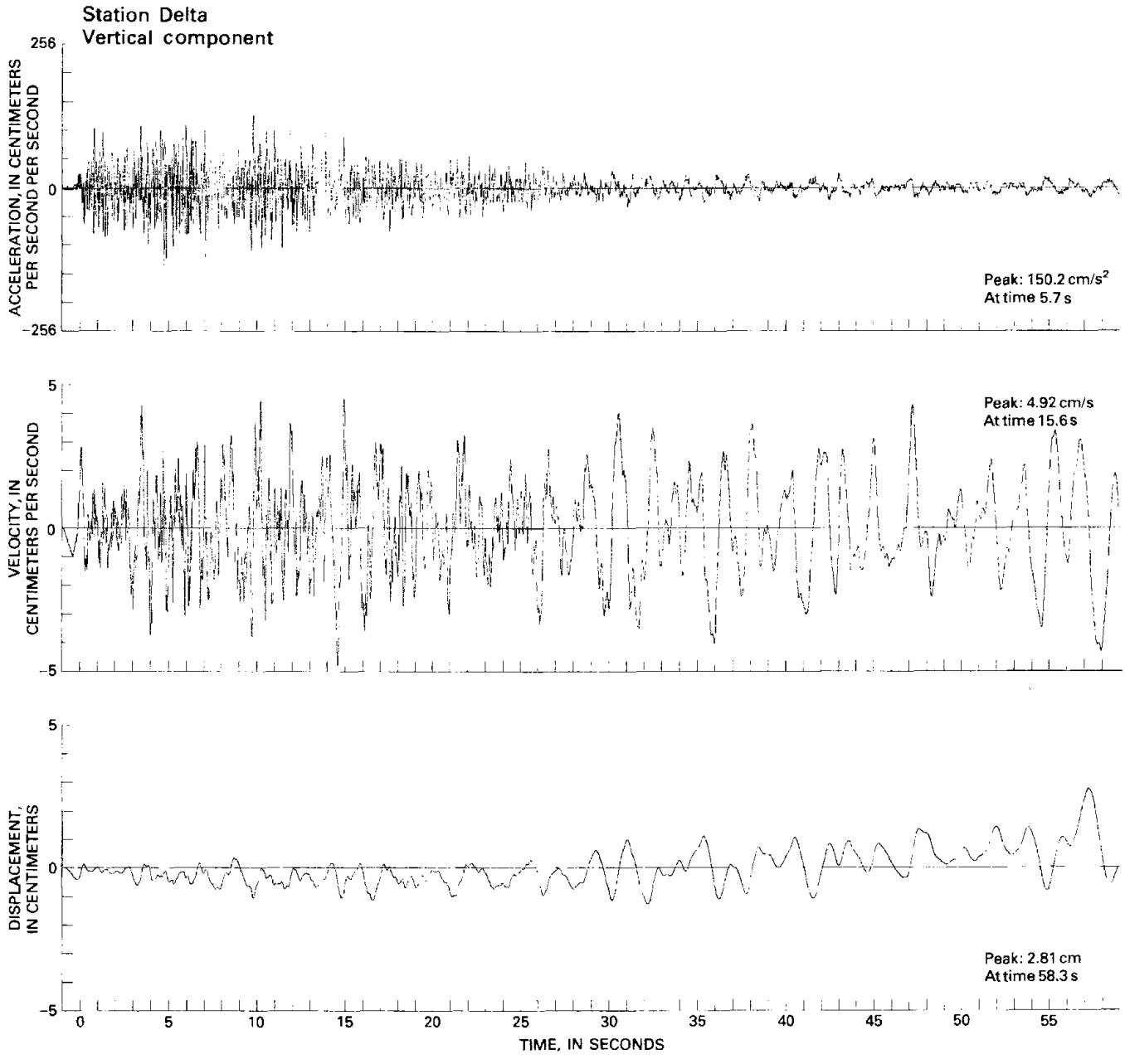

FIGURE 237.—Continued

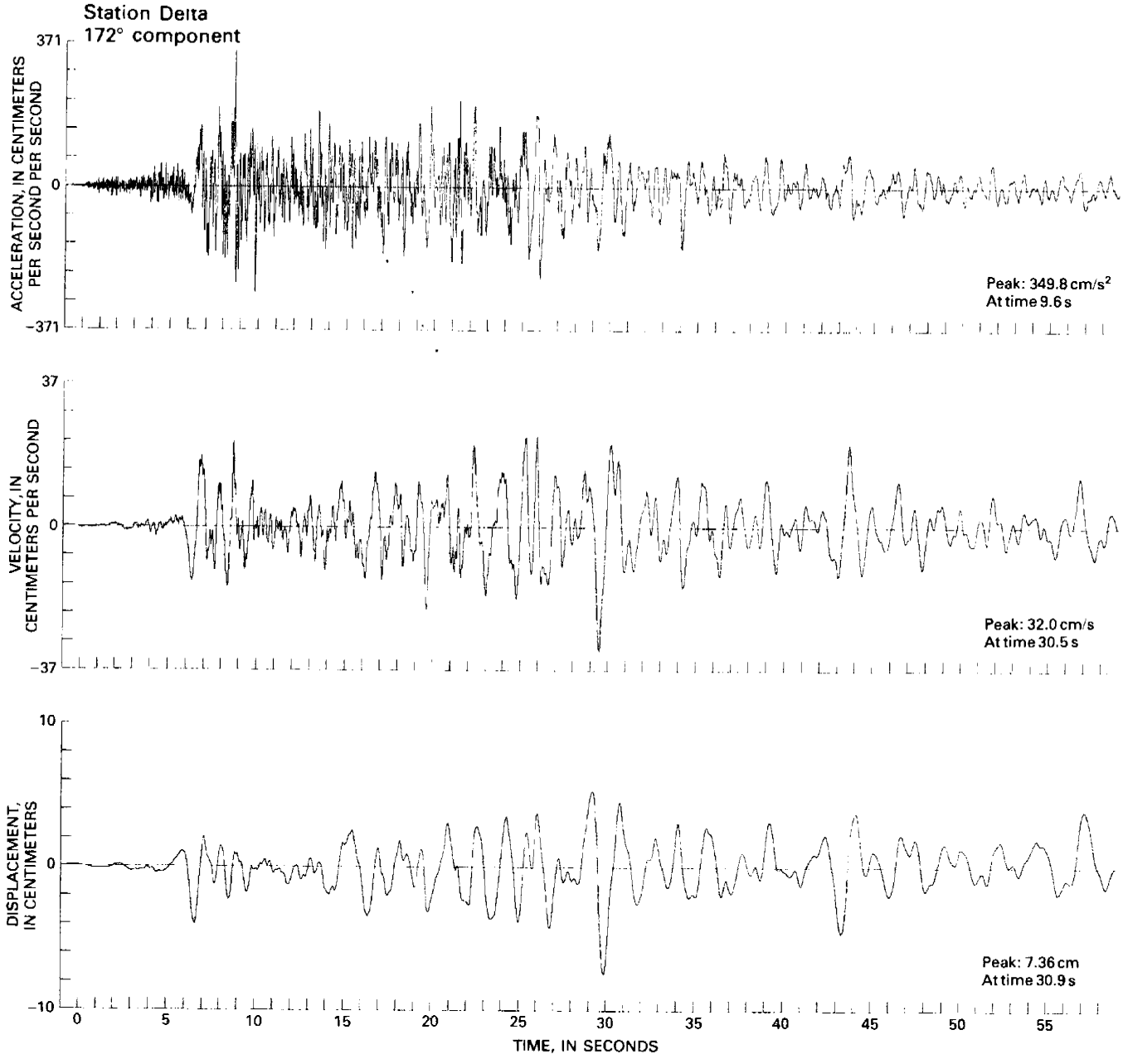

FIGURE 237.—Continued

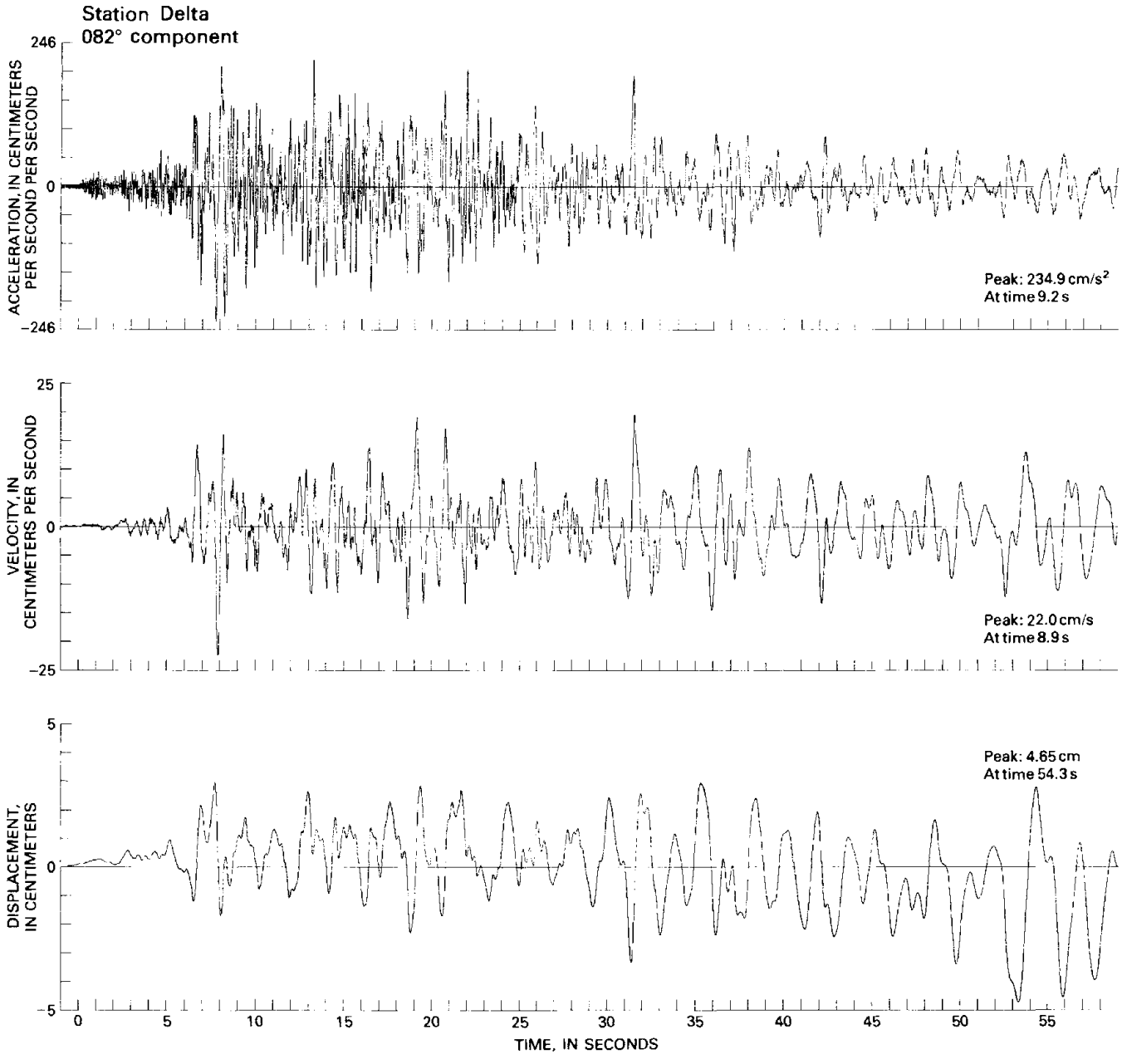

FIGURE 237.—Continued

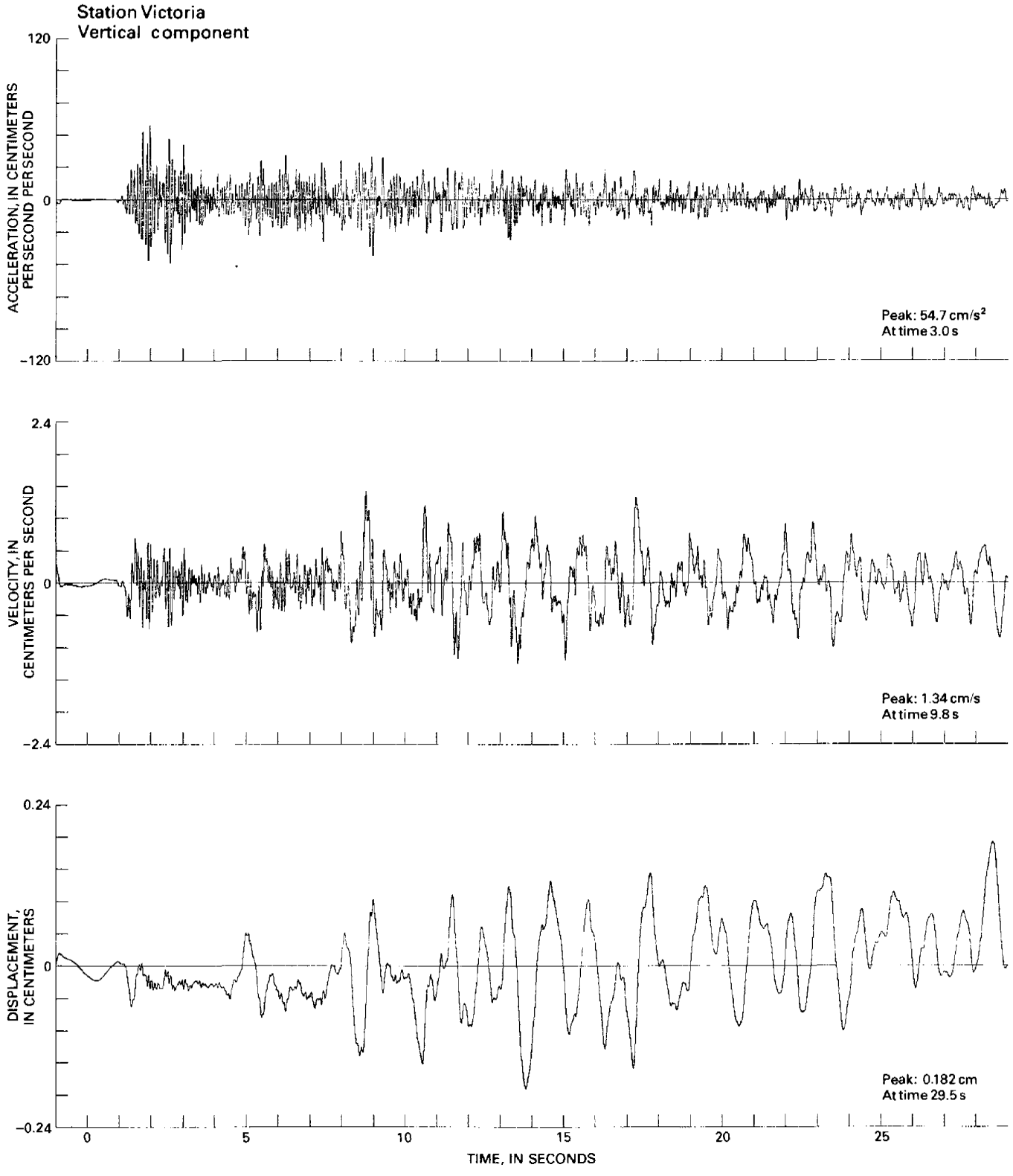

FIGURE 237.—Continued

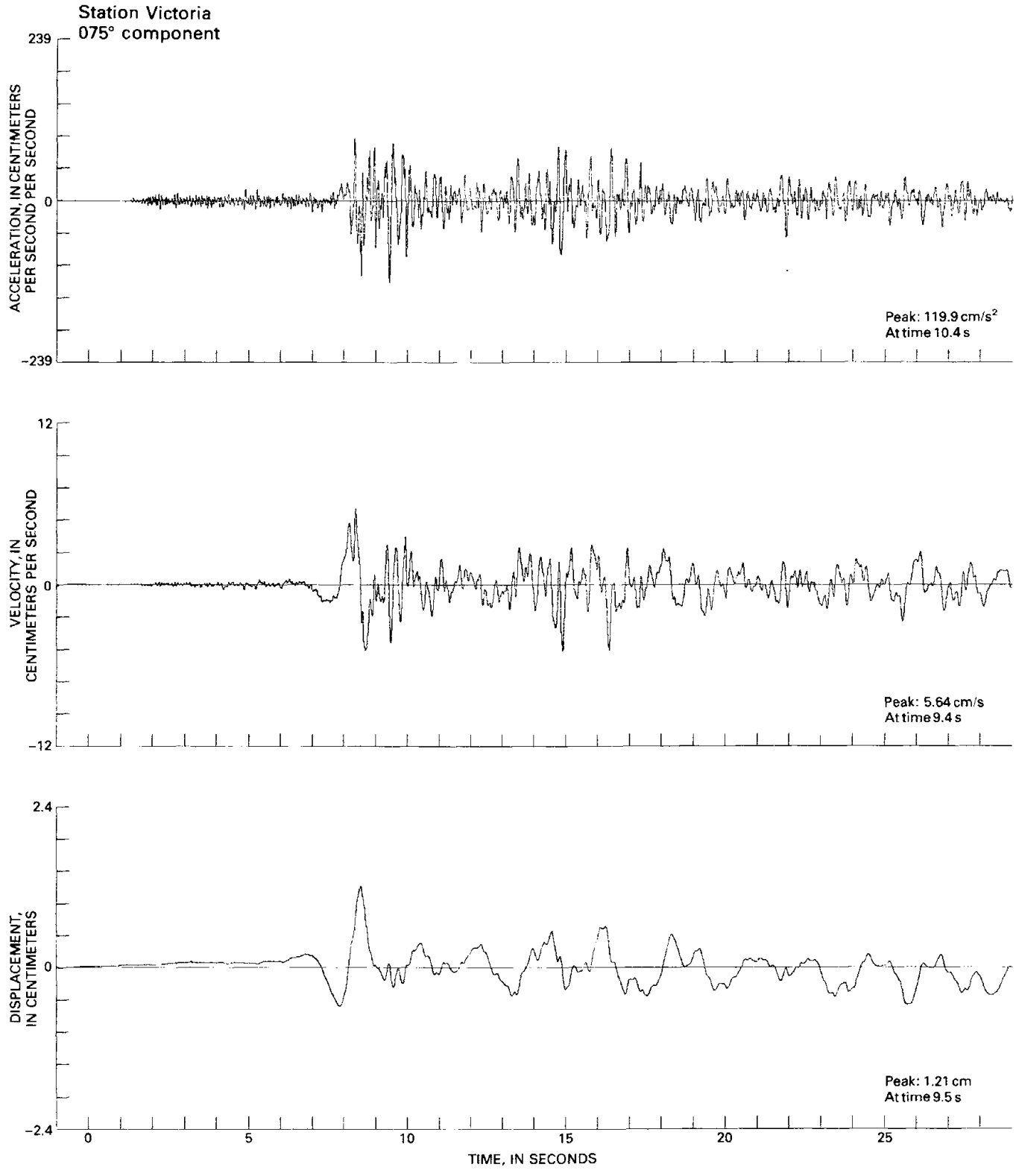

FIGURE 237.—Continued

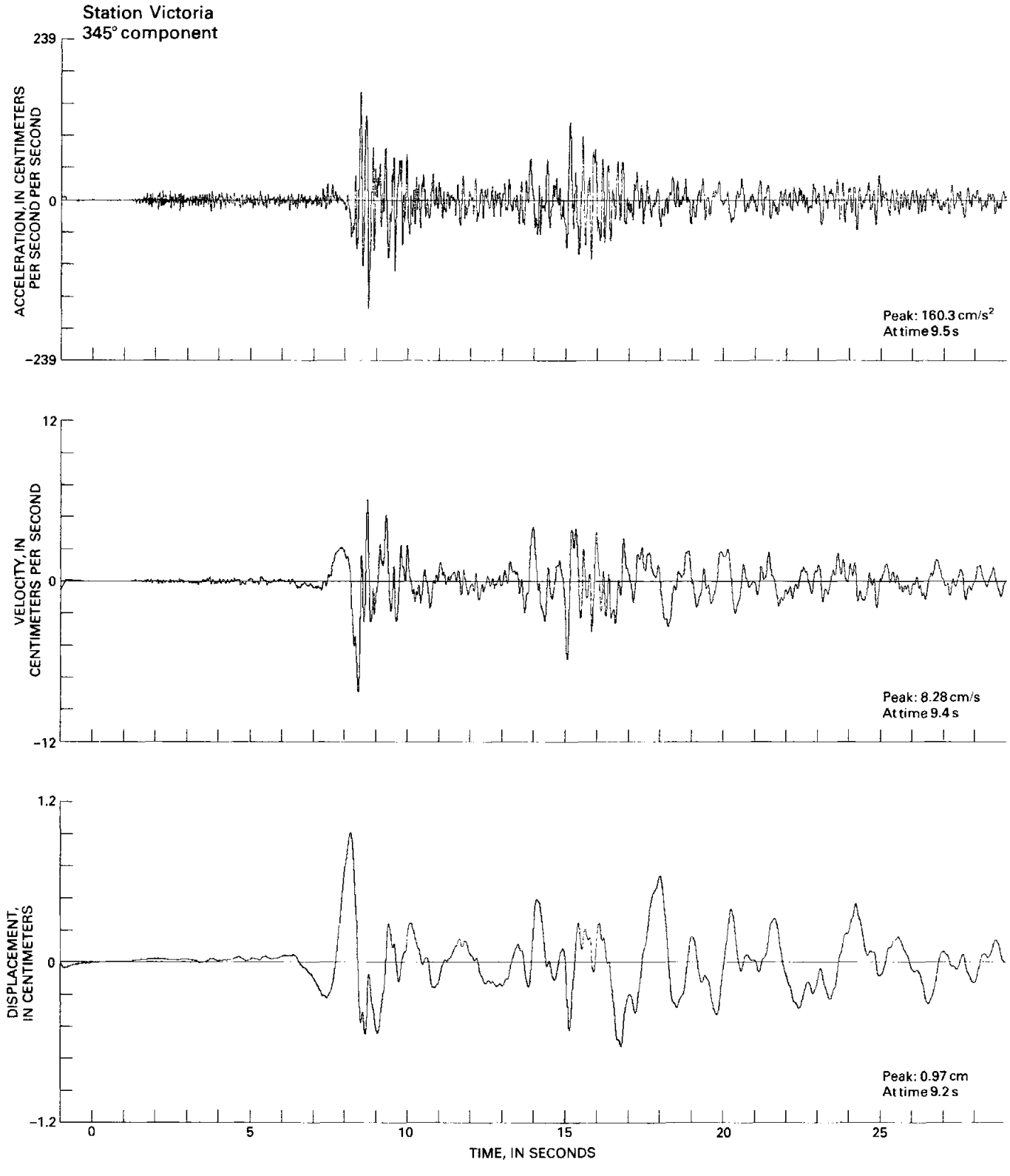

FIGURE 237.—Continued

EL CENTRO DIFFERENTIAL GROUND MOTION ARRAY

By G. N. BYCROFT
U.S. GEOLOGICAL SURVEY

CONTENTS

ABSTRACT

Differential ground motions due to horizontally propagating seismic surface waves are important in determining the stresses in such extended structures as large mat foundations for nuclear power stations, dams, bridges, and pipelines. This report discusses the design of an array to measure these differential ground motions and describes one such array, recently installed at El Centro, Calif. The records from the October 15, 1979, Imperial Valley earthquake are also presented.

INTRODUCTION

Aseismic design has generally assumed that all points on the ground move in unison with the free-field motion over a region that is larger than the foundation of the structure. This assumption is based on the notion that seismic waves are substantially propagated in high-wave-velocity basement rock and transmitted vertically to the region of interest through lower velocity layers. However, surface waves propagating horizontally through surface layers may have wavelengths along the surface of approximately the dimensions of a large structure (Luco, 1969; Trifunac, 1972; Wong and Trifunac, 1974; Bycroft, 1980). The foundation of the structure would then undergo differential motions that would cause additional strains to be superimposed on those due to inertial loading. Thus, adjacent bridge piers would move relative to each other and cause substantial stresses in the piers and the bridge decking. Structures built on spread footings, dams, and pipelines would be similarly affected. A large relatively rigid raft foundation, such as may be used for a nuclear power station, would move less than the free-field motion (Bycroft, 1980), and so the input to structures on such a foundation would be attenuated; the input motion to such structures would differ from the free-field motion.

To study such motion, differential ground motions must be measured, and methods of utilizing this information in aseismic design must be developed. The measurement of free-field ground motion is relatively straightforward in that no spatial parameter is involved. For differential ground motions, however, surface waves may propagate at wavelengths comparable to the size of the foundation, and so a spatial array of instruments is needed. If expense were no consideration, a fully three dimensional array comprising many instruments could be built. Initially, it would appear more advantageous to divide these instruments among several simpler arrays in different suitable regions that should, of course, be of high seismicity both in amplitude and occurrence. To detect surface waves of significant amplitude, regions of large contrast in wave velocity between the surface and underlying layers must be selected. The upper layer should be of as low a velocity as possible, so that the wavelengths are as short as possible. Furthermore, the selected region should be flat, homogeneous, and secure; power should be readily available; and the regional velocity profile should be known.

The simplest array that would give useful information appears to be one comprising several instruments along a straight line. This line should point toward the epicenter of an imminent large earthquake to measure the maximum amplitudes of the incident transverse surface waves. It is difficult, however, to predict such an orientation, and so the best that can be done is to point the array toward a general region of recent activity. If enough instruments are available, an additional perpendicular array would be advantageous.

The differential motion between any two points is a function of wavelength and of the magnitude of the component of that wavelength in the ground motion. Thus, the difference in motion between points at varying distances apart must be measured. If n instruments are to be used, there are $n(n-1)/2$ pairs of points whose distances apart may be arranged to be different. The instruments should be so placed along the line of the array that these distances increase reasonably uniformly from smallest to largest, assuming that the region is uniform over an area somewhat larger than that of the array. The length of the array should be deter-

mined largely by the size of the largest structures envisaged.

EL CENTRO DIFFERENTIAL ARRAY

Such an array, funded jointly by the Federal Highway Administration and the U.S. Geological Survey, was recently installed at El Centro, Calif., in time to record the earthquake of October 15, 1979. The Imperial Valley Irrigation District permitted the array to be placed in a large vacant area near El Centro steam station 4 (Matthiesen and Porcella, this volume) that is secured by a cyclone fence and meets the other requirements discussed above. Figure 238 shows the structure, and table 34 the velocity profile, of the region; figure 239 shows the location of the array with respect to local faults. Because faults surround the area, no particular orientation appeared optimal, and so the array was laid south to north along the inside of the fence running along Dogwood Road (fig. 240). This area is remote from the powerplant, and so interactional effects should be negligible. The six instruments were placed at distances of 0, 60, 180, 420, 700, and 1,000 ft and numbered 1 through 6, respectively; these spacings give distances between any two instruments of 60, 120, 180, 240, 280, 300, 360, 420, 520, 580, 640, 700, 820, 940, and 1,000 ft.

The sensors are triaxial downhole force-balance accelerometers manufactured by the Terra Technology Corp., Seattle, Wash. The sensors were placed in 5-in.-diameter holes 4 ft deep, tamped in with 2 to 3 mm of coarse sand, and connected by wiring laid in conduit to DCA-300 recorders in an air-conditioned building at the south end of the array. The analog signal from the sensors is digitized at intervals of 0.01 s and stored on magnetic tape. The system continually remembers events as long as 1.5 s before triggering, and thus permits a record of the events that precede triggering. The six instruments are triggered from an SMA-1 seismometer and have a common clock. The radio WWVB time signal is also recorded on the tape.

TABLE 34.—*Low-strain shear-wave velocities from El Centro differential ground motion array*

[Shear-wave velocities were obtained from field downhole geophysical measurements at strain levels of approximately 10^{-4} percent (Shannon & Wilson, Inc., and Agbabian Associates, 1976)]

Test-depth interval (ft)	Test-depth interval (m)	Average shear-wave velocity (ft/s)	Average shear-wave velocity (m/s)
0–16	0–4.9	400	122
16–32	4.9–9.8	550	168
32–72	9.8–21.9	700	213
72–116	21.9–35.4	850	259
116–225	35.4–68.6	1,000	305
225–271	68.6–82.6	1,150	351
271–344	82.6–104.9	1,320	402
344–390	104.9–118.9	1,450	442

The installation of this array had been delayed by many factors but, fortuitously, was completed about 2 weeks before the October 15 earthquake. There were several malfunctions associated with this event. Instrument 6 was out of tape, owing to some unknown

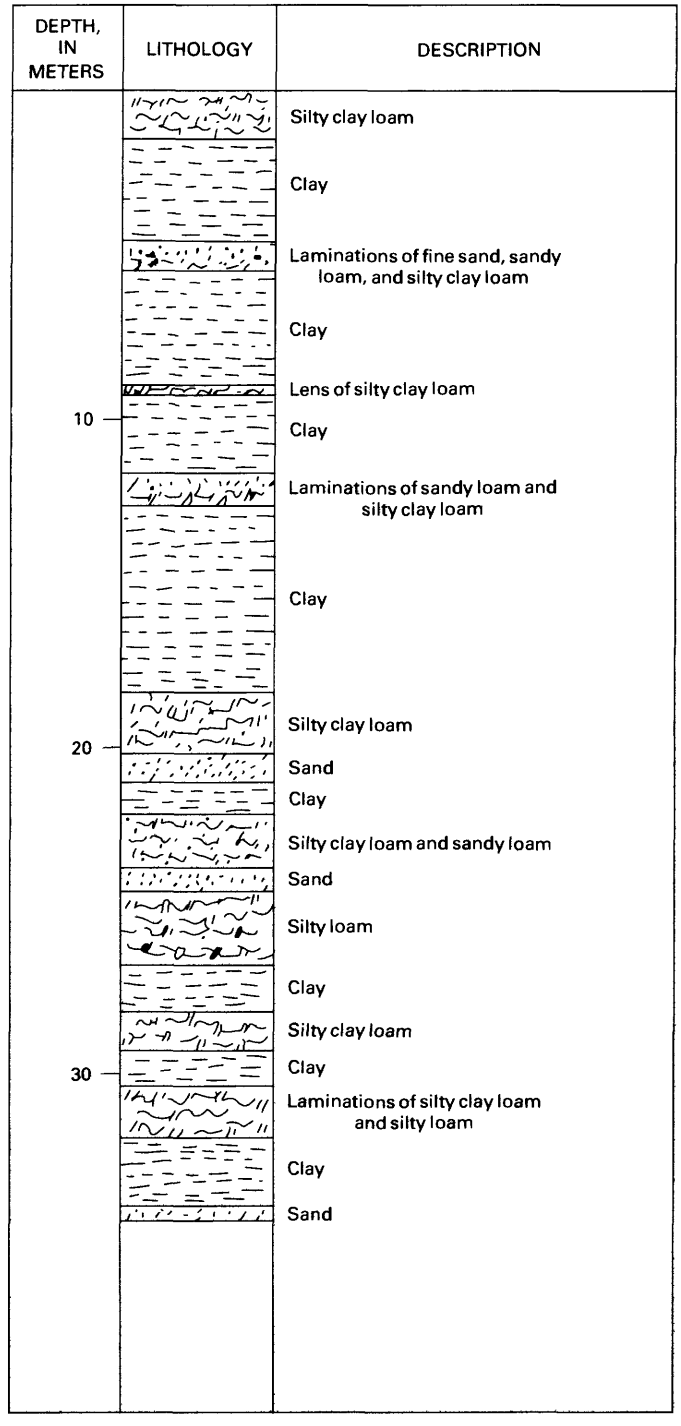

FIGURE 238.—Geologic structure at El Centro differential ground motion array (Hansen and others, 1973).

extraneous triggering before the main shock, and several records contain noise. The instruments were not synchronized in time as planned, and the time signal was not recorded owing to a receiver problem. Consequently, common time was lost.

Analog printouts of the tapes from the five stations (fig. 241) are nearly identical in shape. The maximum acceleration of 0.67 g occurred at stations 1 and 2 in the unusual event early in the vertical component; station 5, however, recorded this event at a maximum of 0.33 g. The corresponding maximum acceleration in the horizontal directions differ from each other by 20 percent. Terra Technology Corp. has translated the tapes into a computer-compatible tape and has established common time from a distinct P-wave arrival from an aftershock 2.5 min after the main event. Tentative values of the velocities, displacements, and differential displacements have been obtained by suitable corrections and double integration of the accelerograms.

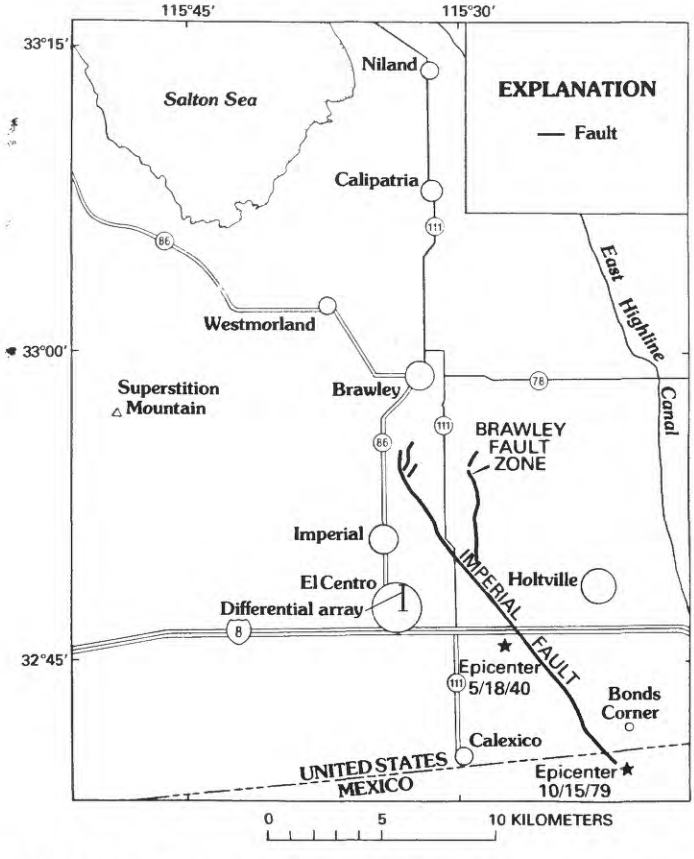

FIGURE 239.—Location of El Centro differential ground motion array (lat 32°47'46" N., long 115°32'06" W.). Array runs north-south.

REFERENCES CITED

Bycroft, G. N., 1980, Soil foundation interaction and differential ground motions: Journal of Earthquake Engineering and Structural Dynamics, v. 8, no. 5, p. 397–404.

Hansen, W. R., Weiss, R. B., Idress, I. M., and Cluff, L. S., 1973, Geotechnical data compilation for selected strong-motion sites: Oakland, Calif., Woodward-Lundgren Associates report, 411 p.

Luco, J. E., 1969, Dynamic interaction of a shear wall with the soil: American Society of Civil Engineers Proceedings, Engineering Mechanics Division Journal, v. 95, no. EM2, p. 333–346.

Shannon & Wilson, Inc., and Agbabian Associates, 1976, Geotechnical and strong-motion earthquake data from U.S. accelerograph stations: U.S. Nuclear Regulatory Commission Report NUREG–0029, v. 1.

Trifunac, M. D., 1972, Interaction of a shear wall with the soil for incident plane *SH* waves: Seismological Society of America Bulletin, v. 62, no. 1, p. 63–83.

Wong, H. L., and Trifunac, M. D., 1974, Interaction of a shear wall with the soil for incident plane *SH* waves: Elliptical rigid foundation: Seismological Society of America Bulletin, v. 64, no. 6, p. 1825–1842.

FIGURE 240.—El Centro differential ground-motion array site. Recording house is shown in right center. Black box adjacent to house (to left) is station 1; remainder of array extends northward (into background).

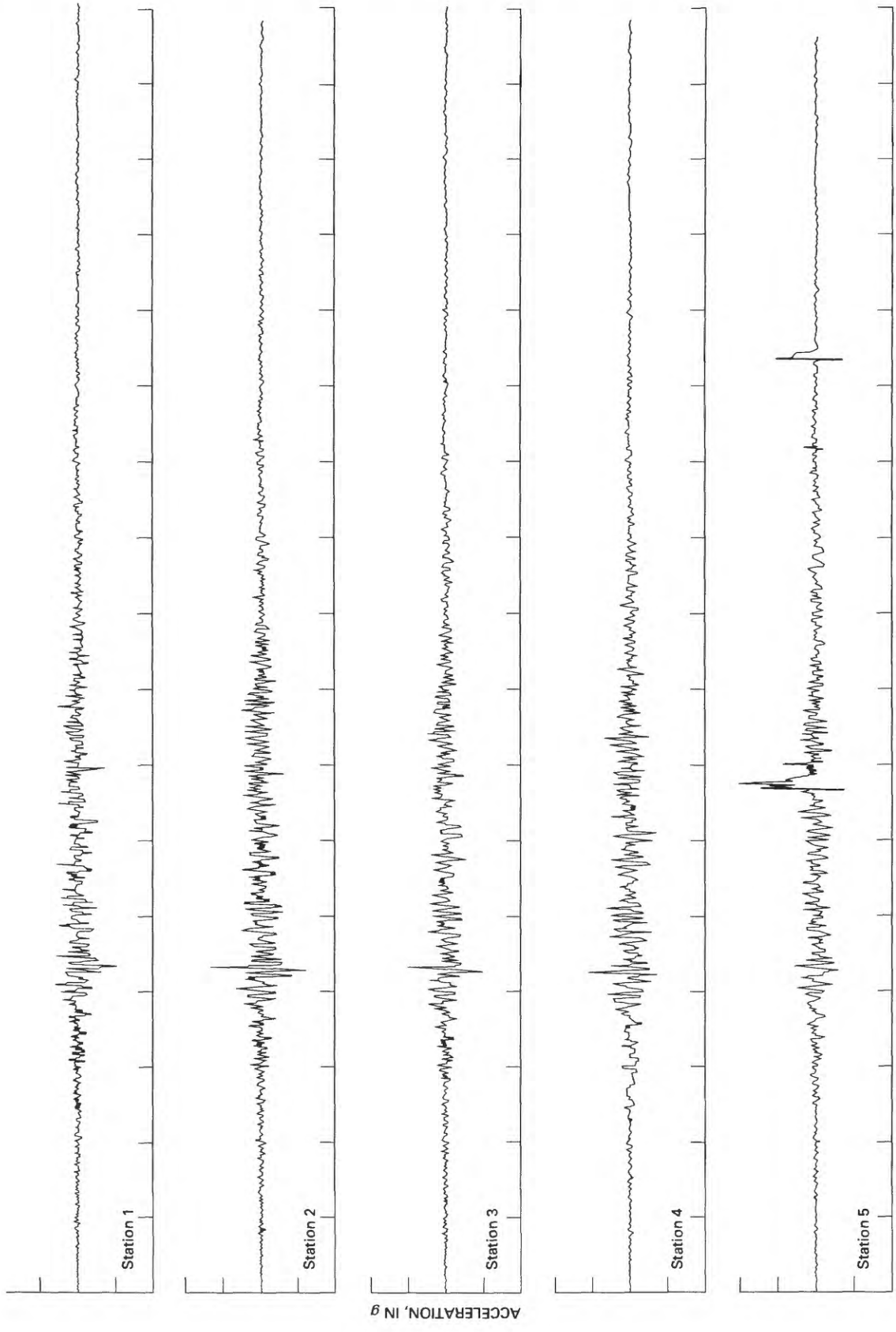

FIGURE 241.—Accelerations at El Centro differential ground motion array from 1979 Imperial Valley earthquake. Each tick on vertical axis equals 0.5 *g*; each tick on horizontal axis equals 1 s. *A*, Vertical acceleration. *B*, East-west acceleration. *C*, North-south acceleration.

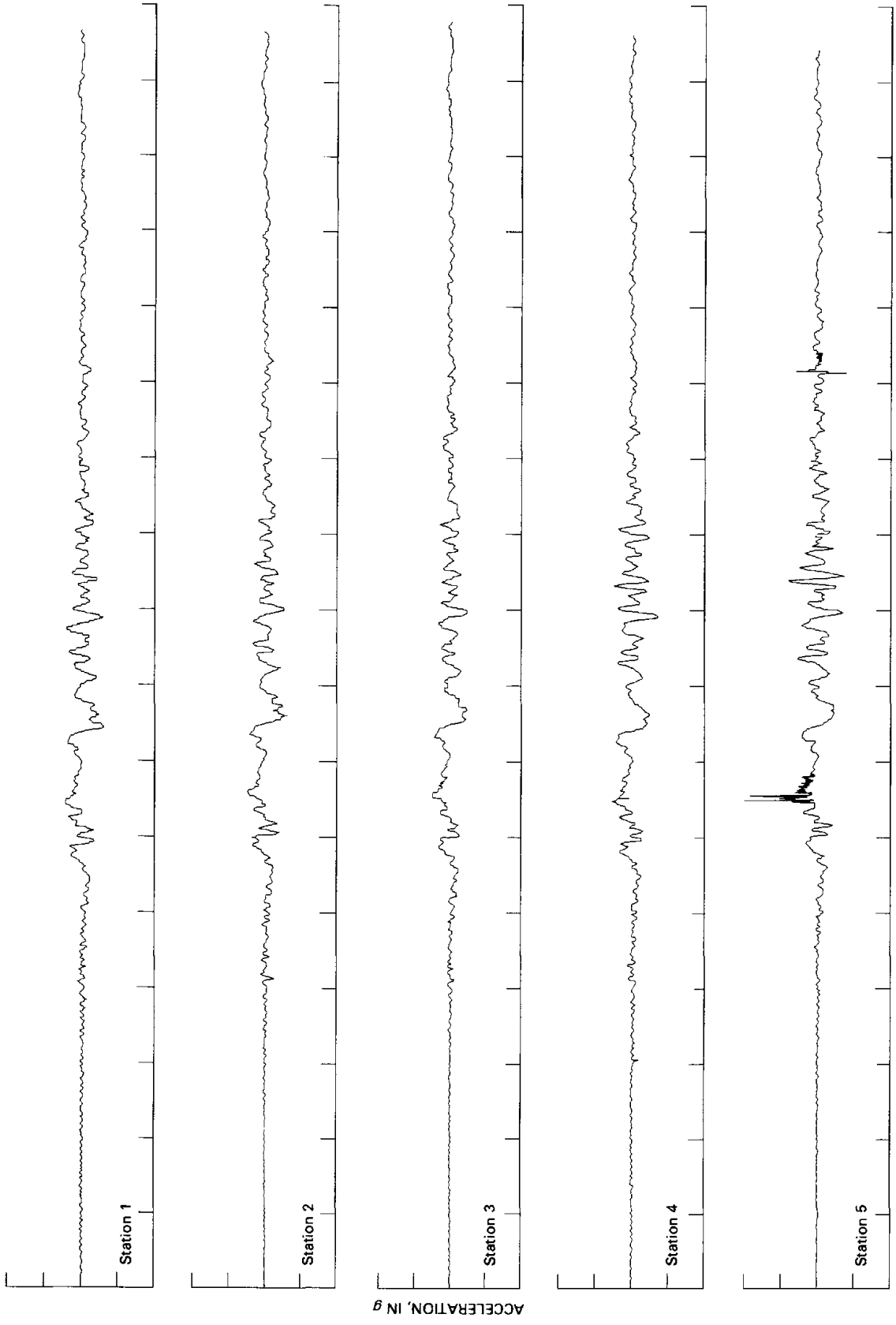

FIGURE 241.—Continued

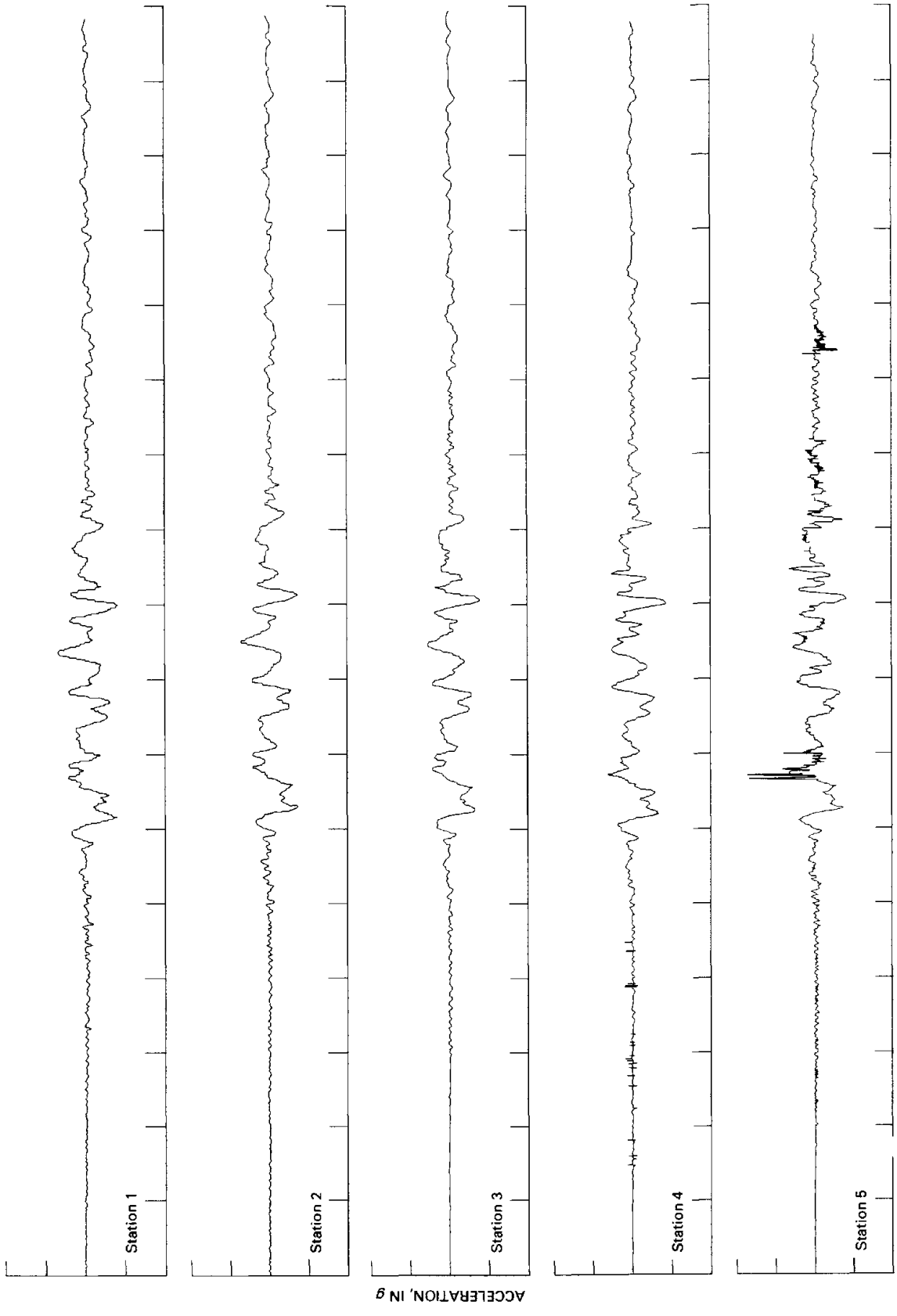

FIGURE 241.—Continued

AN ANALYSIS OF STRONG-MOTION DATA FROM A SEVERELY DAMAGED STRUCTURE— THE IMPERIAL COUNTY SERVICES BUILDING, EL CENTRO, CALIFORNIA

By CHRISTOPHER ROJAHN and P. N. MORK,
U.S. GEOLOGICAL SURVEY

CONTENTS

ABSTRACT

The Imperial County Services Building, a six-story reinforced-concrete frame and shear-wall office building situated 7.6 km southwest of the Imperial fault trace in El Centro, Calif., sustained significant structural damage during the October 15 main shock. Strong-motion instrumentation at the site, installed and maintained by the California Division of Mines and Geology, consisted of a 13-channel remote-accelerometer central-recording accelerograph system in the building and a triaxial accelerograph located at ground level approximately 100 m to the east. Several features of the main-shock accelerogram recovered from the building, including abrupt changes in frequency content and bursts of high-frequency motion, provide important information on the mechanism of structural failure. A comparison of the main-shock motions recorded at the base of the building with those recorded at the adjacent ground site (intended to be free field) indicates that the motion recorded at the ground floor of the building incorporates to a significant extent the response of the building-soil-foundation system. The acceleration data also show that the building's fundamental periods changed significantly during the earthquake. A preliminary relative-displacement analysis indicates that the east-west interstory displacement between the second and ground floors was approximately 6.2 cm when the columns began to collapse.

INTRODUCTION

The Imperial County Services Building, a six-story reinforced-concrete frame and shear-wall building in downtown El Centro, Calif., 7.6 km southwest of the nearest point on the Imperial fault and 27 km northwest of the main-shock epicenter (fig. 242), sustained significant structural damage during the October 15, 1979, earthquake. Strong-motion instrumentation at the site consisted of a 13-channel accelerograph system in the building and a triaxial accelerograph at ground level approximately 100 m east of the building. Both instruments, installed and maintained by the California Division of Mines and Geology (CDMG), triggered and functioned properly during the earthquake.

The accelerograms recovered from the building are of great interest, not only because this is the first time an extensively instrumented building has sustained significant earthquake-induced structural damage, but also because the time and mechanism of damage can be inferred from the recorded data. The records, therefore, provide important information on forces, dynamic properties, and relative motions before, during, and after the time when damage was occurring. In conjunction with the records from the adjacent ground site, the building records also provide important insight into the extent to which the building and its foundation system influenced the motion recorded at the ground floor of the building.

BUILDING DESCRIPTION

The Imperial County Services Building (fig. 243), which served as an office building for Imperial County, was at 940 Main Street, El Centro, at lat 32.792° N., long 115.564° W. It was designed in 1968 (using the 1967 edition of the Uniform Building Code) and was completed in 1971 at a construction cost of $1.87 million (Randy Rister, oral commun., 1979). The building was 41.71 by 25.92 m (136 ft 10 in. by 85 ft 4 in.) in plan and

founded on a Raymond step-taper concrete-pile foundation. The piles, which are interconnected with reinforced-concrete link beams, extend 14 to 18 m into the alluvial foundation material, composed primarily of sand with interbeds of clay (based on logs from four 12- to 18-m-deep soil borings at the site).

The building's structural system and major architectural features are described in detail by Wosser and others (this volume). Vertical loads are carried by reinforced-concrete floor slabs supported by reinforced-concrete pan joists spanning in the north-south direction; the joists are supported by four longitudinal five-bay reinforced-concrete frames at 7.6 m (25 ft) on center. Lateral loads are resisted by the four reinforced-concrete frames in the east-west direction and by reinforced-concrete shear walls in the north-south direction. The shear walls are discontinuous at the second floor. Below the second floor the shear walls are placed along three interior lines and at the west end; above the second floor they are at the east and west ends of the building only. The design requires that lateral loads at the east end of the building be transferred from the upper-story east-end shear wall to the closest interior first-story shear wall (approximately 9.4 m to the west) through the second-floor diaphragm. It also requires that overturning at the east end of the building be resisted in the first story by a row of four reinforced-concrete columns approximately 2 m west of the upper-story east-end shear wall.

EARTHQUAKE DAMAGE

As described in the report by Wosser and others (this volume), the most significant damage to the Imperial County Services Building was the partial collapse just above ground level of the four reinforced-concrete columns along the building's east end (figs. 244, 245). Concrete at the base of each column was badly shattered, vertical reinforcing bars were severely buckled, and horizontal tie bars were widely splayed. On the basis of measurements by the Imperial County Department of Buildings and Grounds, the columns were shortened by approximately 23 cm (9 in.) during the main shock and

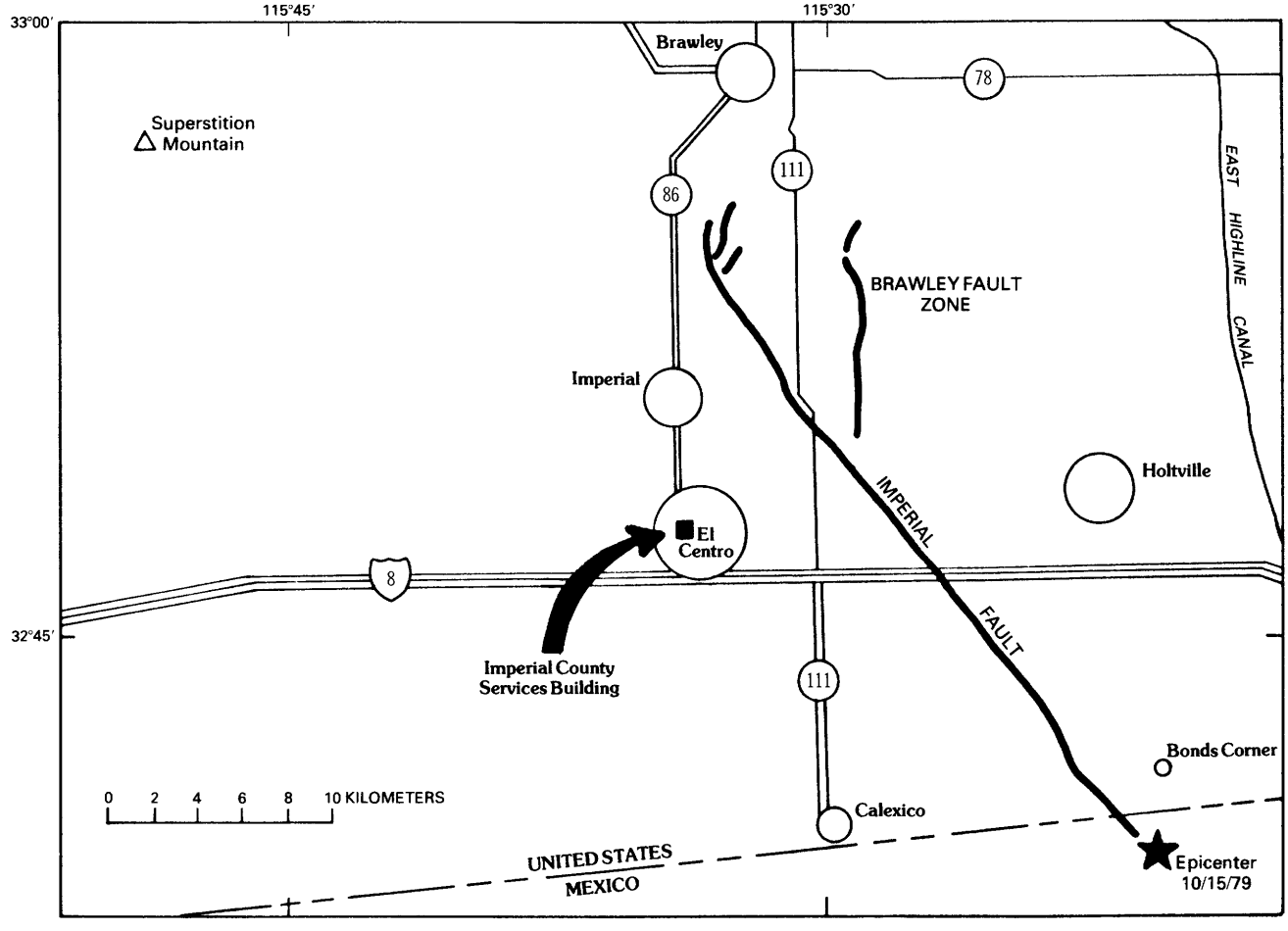

FIGURE 242.—Location of Imperial County Services Building relative to Imperial fault trace and October 15 main-shock epicenter.

FIGURE 243.—Imperial County Services Building, El Centro, Calif. View northwestward.

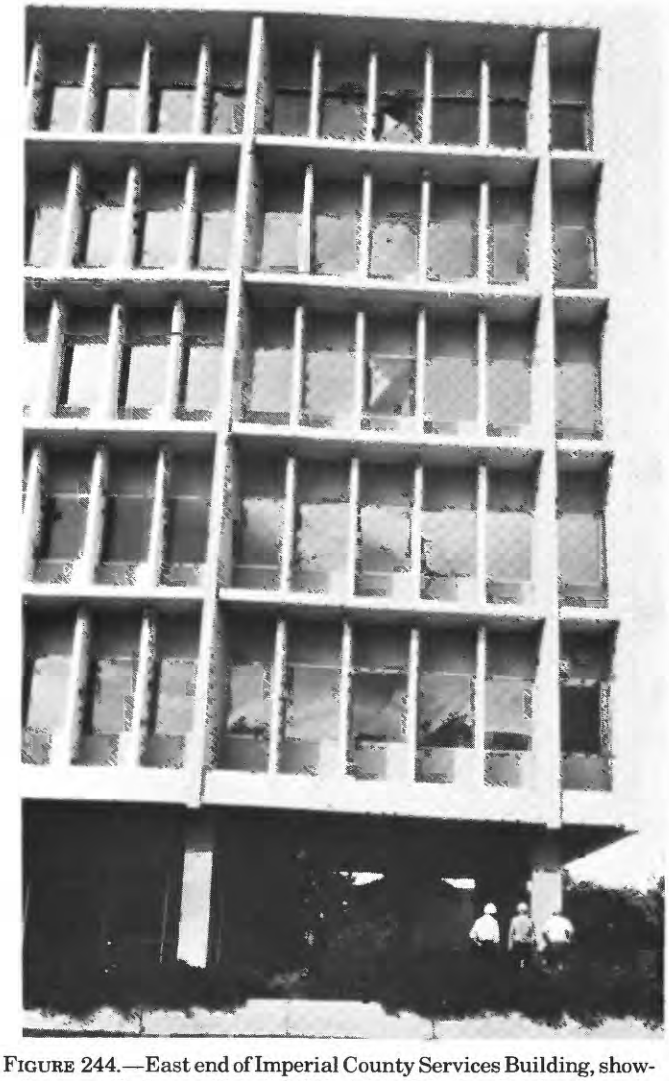

FIGURE 244.—East end of Imperial County Services Building, showing row of columns (far right) that failed during October 15 main shock. View northward.

by approximately 7½ cm (3 in.) more during the strongest aftershock (Randy Rister, oral commun., 1979). Less significant damage elsewhere in the building included minor cracking in all columns beneath the second floor (just beneath the beams), minor cracking or spalling at the base of most columns (just above ground level), and a north-south line of severe cracking (fig. 246) in all upper-story floor slabs just to the east of the first interior row of columns (from the east end). The pattern of column damage suggests frame yielding in the longitudinal (east-west) direction and axial-force failure due to north-south overturning of the east-end shear wall; the floor-slab cracks were due to settlement of the structure at the east end.

FIGURE 245.—One of four damaged reinforced-concrete columns along east end of Imperial County Services Building between ground and second floors. Damage to other three columns was similar.

STRONG-MOTION INSTRUMENTATION

The building was originally selected for instrumentation under the California Strong-Motion Instrumentation Program because of its structural characteristics, size, and location in a known highly active seismic area (Rojahn and Ragsdale, 1980a). It was initially instrumented in May 1976 with a nine-channel Kinemetrics CRA–1 accelerograph system that was placed in accordance with recommendations by the following three groups: the Instrumentation Subcommittee of the Structural Engineers Association of Southern California (SEAOSC); the California Seismic Safety Commission's Subcommittee on Instrumentation for Buildings; and a site-visitation committee composed of personnel representing the various organizations interested in the project (first author, CDMG and SEAOSC representatives, building owner, and design engineer).

The original nine-channel system was triggered by the November 4, 1976, Imperial Valley M_L=4.9 earthquake, the epicenter of which was located approximately 32 km north of the Imperial County Services Building (Porcella and Nielson, 1977). After a review of the November 4 strong-motion record and on the basis of the first author's recommendations, the system was upgraded to its present 13-channel configuration, and a triaxial Kinemetrics SMA–1 accelerograph was added at ground level (intended to be a free-field site) approximately 100 m east of the building. The revised system was installed in May 1978 under the supervision of J. T. Ragsdale and on the basis of building strong-motion instrumentation guidelines developed by the U.S. Geological Survey (Rojahn and Matthiesen, 1977). The instrumentation is maintained by the CDMG Office of Strong-Motion Studies.

The SMA–1 accelerograph at the ground-level site east of the building (hereafter referred to as the free-field site) is in a standard Fiberglass instrument shelter (fig. 247) founded on a small reinforced-concrete pad. The three-component accelerograph is battery powered, is triggered by vertical motion that equals or exceeds 0.01 g, and records analog signals on 70-mm light-sensitive film. The 1-g accelerometers have a natural frequency of approximately 25 Hz and thus respond to frequency components nominally within the range 0–25 Hz. Real time is provided on each record by a radio

FIGURE 246.—North-south-trending crack in sixth floor just east of first interior row of columns (from east face).

FIGURE 247.—Fiberglass instrument shelter (foreground) housing SMA–1 accelerograph east of Imperial County Services Building (background). Note solar cells mounted on pole adjacent to shelter; these cells provide current for accelerograph's battery charger.

WWVB time-code receiver and time-tick generator system.

The site for the SMA–1 accelerograph was selected on the basis of a distance (from the instrumented structure) criterion suggested by R. B. Matthiesen (oral commun., 1976), as well as because of its proximity to other buildings. This criterion specifies that sites intended to be free field should be at a distance from the instrumented structure equal to 1 to 1½ times the estimated wavelength of a shear wave (at the surface) having a period equal to the fundamental period of the instrumented structure.

The 13-channel CRA–1 system in the building consisted of nine FBA–1 single-axis force-balance accelerometers in various places throughout the upper stories; an east-west HS–0 horizontal starter at roof level; and one FBA–3 triaxial force-balance accelerometer package, one FBA–1 accelerometer, one 13-channel central recording unit, and a VS–1 vertical starter at ground level. The FBA accelerometers, which have a natural frequency of approximately 50 Hz, were connected by low-voltage data cable to the central recording unit. This unit is battery powered, is triggered by horizontal or vertical motion that equals or exceeds 0.01 *g*, and records on 178-mm (7 in.) light-sensitive film. The system is designed to record acceleration with frequency components nominally within the range 0–50 Hz and with maximum amplitudes of 1 *g*. Real time is provided by a WWVB radio receiver and a time-tick generator system; the recorder was not connected to the SMA–1 accelerograph east of the building.

The FBA accelerometers (fig. 248) were placed to provide information on overall building response as well as input ground motion. The primary purpose of the three north-south-oriented accelerometers at the roof and second floor (accelerometers 1–3, 7–9, fig. 248) is to obtain and isolate north-south translational, torsional, and inplane floor-bending response. In conjunction with the north-south-oriented accelerometers at ground level (accelerometers 10, 11), these accelerometers provide translational- and torsional-response, mode-shape, and ground-to-second-floor interstory-motion information. Similarly, the accelerometers at the ground floor, second floor, fourth floor, and roof in the more flexible

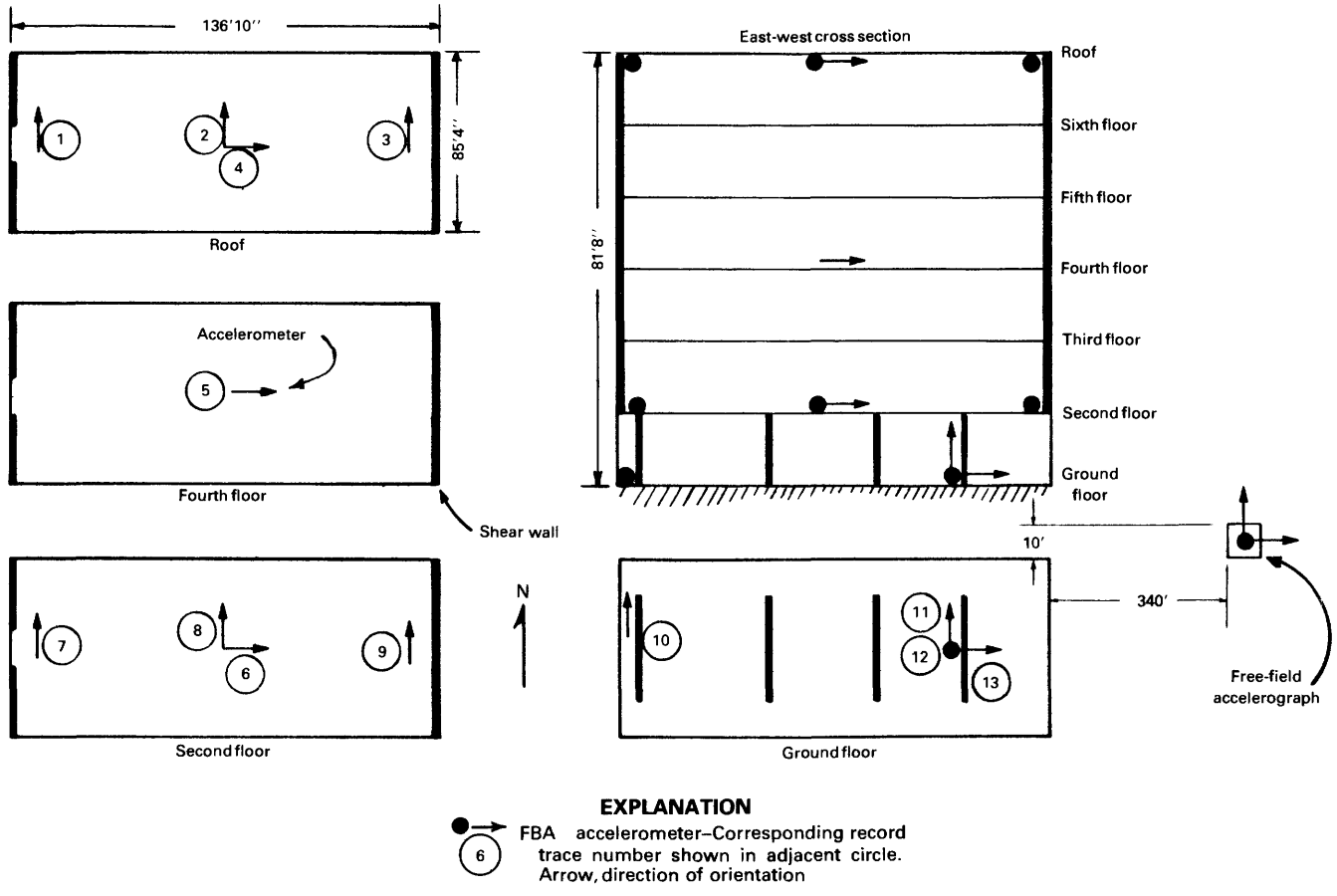

FIGURE 248.—Locations of FBA accelerometers (arrows with numbers) and SMA–1 accelerograph at Imperial County Services Building and adjacent free-field site (after Rojahn and Ragsdale, 1980b). Arrows denote direction of positive acceleration on trace.

east-west (frame) direction (accelerometers 4–6, 13) provide east-west translational-response, mode-shape, and interstory-motion information. The two north-south-oriented accelerometers at ground level (accelerometers 10, 11) are intended to identify collectively the extent to which differential horizontal ground motion has occurred, and the vertical accelerometer at ground level (accelerometer 12) provides information on vertical motion. There are no vertically oriented accelerometers above ground level.

OCTOBER 15 ACCELEROGRAMS

Both the 13-channel accelerograph system in the building and the triaxial SMA–1 accelerograph at the free-field site to the east provided complete high-quality strong-motion accelerograms (figs. 249, 250) of the October 15 earthquake. Peak accelerations (as read from the original accelerogram) at the ground floor near the center of the building were 0.29, 0.19, and 0.32 *g*, respectively, for the north (002°), up, and east (092°) components (traces 11, 12, 13, fig. 249). Peak north-south

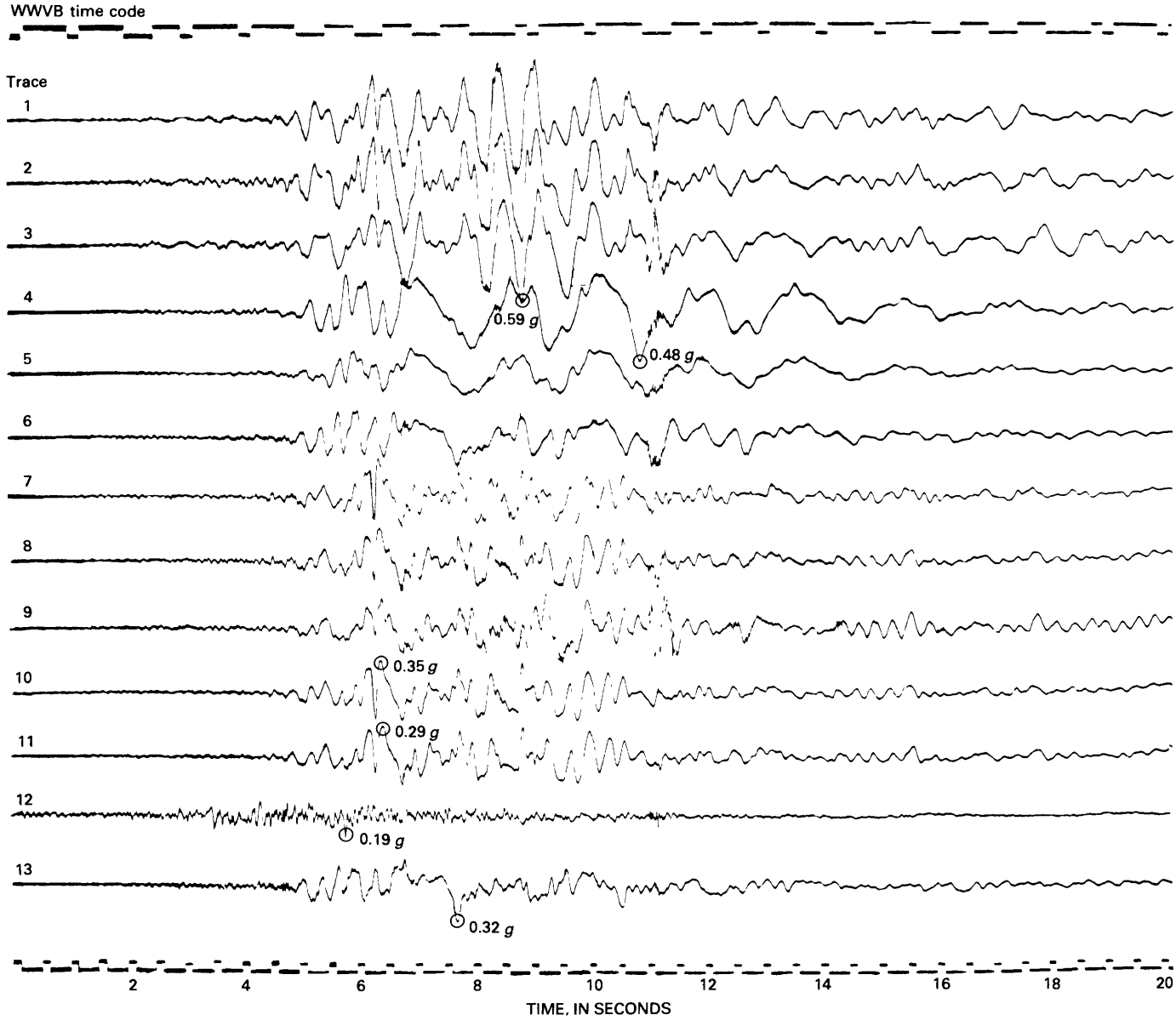

FIGURE 249.—Part of CRA–1 strong-motion accelerogram recorded on October 15, 1979, in Imperial County Services Building. Total record length was 90 s (Porter, this volume). Trace numbers at start of record (left of traces) correspond to accelerometer numbers in figure 248.

acceleration at the west end at the ground floor (trace 10, fig. 249) was 0.35 g, slightly higher than near the center of the building (trace 11), although both components were nearly identical in signature. At the free-field site to the east, peak accelerations were 0.24, 0.27, and 0.24 g, respectively, for the 002°, up, and 092° components (fig. 250). The maximum durations of motion between the first and last peaks equal to or greater than 0.1 g were approximately 4 and 6 s for the vertical and horizontal components, respectively. In terms of frequency content, perhaps the most notable feature of these records is the long-period acceleration pulse in the east-west component at the building's ground floor (trace 13, fig. 249) between seconds 6 and 8. At that point, the acceleration remained positive and relatively high in amplitude (maximum acceleration, 0.26 g) for approximately 1 s and apparently generated large velocity and displacement pulses.

Among the most notable features of the acceleration traces in the upper stories of the building (traces 1–9, fig. 249) are the following: (1) peak roof-level accelerations of approximately 0.59 g at 8.9 s and 0.48 g at 10.9 s in the north-south and east-west directions (traces 3, 4, fig. 249), respectively; (2) abrupt occurrence of long-period motion in the east-west components at the roof, fourth floor, and second floor at 6.8 s (traces 4–6, fig. 249); (3) bursts of low-amplitude high-frequency (approx 50 Hz) motion at various times in all upper-story records at and after 6.8 s; (4) a 0.5-s-long burst of high-amplitude high-frequency (approx 50 Hz) motion near 11 s in the north-south direction on the second floor (trace 9, fig. 249) directly above the columns that failed; and (5) continuation of high-amplitude motion in the upper-story components after the high-amplitude ground motions had subsided (after 11 s). Most of these features denote critical times in the performance of the building and are discussed later.

COMPARISON OF FREE-FIELD AND BUILDING GROUND-FLOOR MOTIONS

The signatures of corresponding components of motion recorded at the free-field site and at the ground floor of the building differ significantly (fig. 251). Vertical motion at the free-field site is generally higher in amplitude than at the ground floor, whereas for the horizontal motion the opposite is true. A comparison of corrected acceleration, velocity, and displacement peak amplitudes on the two records (Porter, this volume) indicates that the differences are most noticeable in acceleration (table 35). The maximum vertical acceleration at the free-field site (0.24 g), for example, is approximately 30 percent higher than at the ground floor (0.18 g); corresponding differences in velocity and displacement for the same component are approximately 5 and 15 percent, respectively. The trend is even more striking for the horizontal components. In the case of the 002° component, the maximum acceleration at the west end of the ground floor (0.34 g) is approximately 60 percent higher than at the free-field site (0.21 g); corresponding differences in velocity and displacement, however, are substantially smaller (approx 20 and 5 percent, respectively). Corresponding differences for the 092° component are similar.

There are also significant differences in the frequency content of the two records. The horizontal motions recorded at the ground floor contain relatively high amplitude low-frequency (approx 3–4 Hz) components that do not exist in the free-field motion. These frequencies correspond to those of the second mode of building response in both directions (note that the motions at the ground and second floor in fig. 249 are 180° out of phase with that at the roof). This difference in horizontal motion is most noticeable in the 002° (north) component, the direction in which lateral forces are resisted by the shear walls. The difference in motion is evidently re-

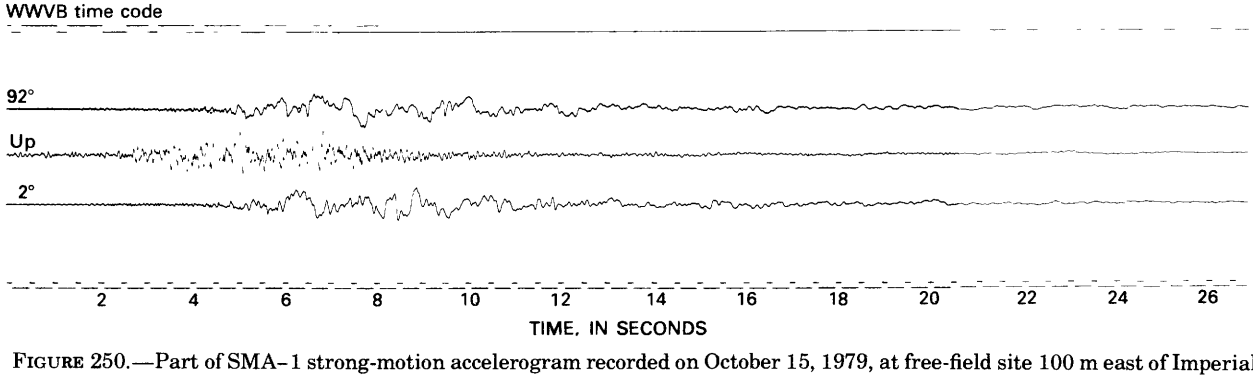

FIGURE 250.—Part of SMA–1 strong-motion accelerogram recorded on October 15, 1979, at free-field site 100 m east of Imperial County Services Building. Direction of positive acceleration is given at beginning of trace.

lated to the fact that the building is founded on piles and suggests that the effective base of the building is below ground level (in other words, ground level is effectively above the base of the structural system).

EVIDENCE OF DAMAGE INITIATION AND SUBSEQUENT COLUMN COLLAPSE IN THE OCTOBER 15 BUILDING ACCELEROGRAM

Various features of the main-shock accelerogram recovered from the building (fig. 249) provide important information on the mechanism of structural failure. These features are clearly evident in a twofold enlargement of the original record (fig. 252) but are not apparent in the plots of corrected digitized data (Porter, this volume). The first major feature, an abrupt change in frequency content in the upper-story east-west components, occurs at 6.8 s (traces 4 [shaded area A]–6, fig. 252). At that time the predominant period of vibration in all three components abruptly lengthens to approxi-

TABLE 35.—*Comparison of free-field and ground-floor motions*

Component	Maximum acceleration (g)		Maximum velocity (cm/s)		Maximum displacement (cm)	
	Free field	Ground floor	Free field	Ground floor	Free field	Ground floor
[1]002°	0.21	0.34	36.2	43.3	16.4	16.0
Up	.24	.18	17.4	16.2	8.0	7.0
092°	.24	.33	64.4	64.6	28.2	27.4

[1]Trace 10, figure 249.

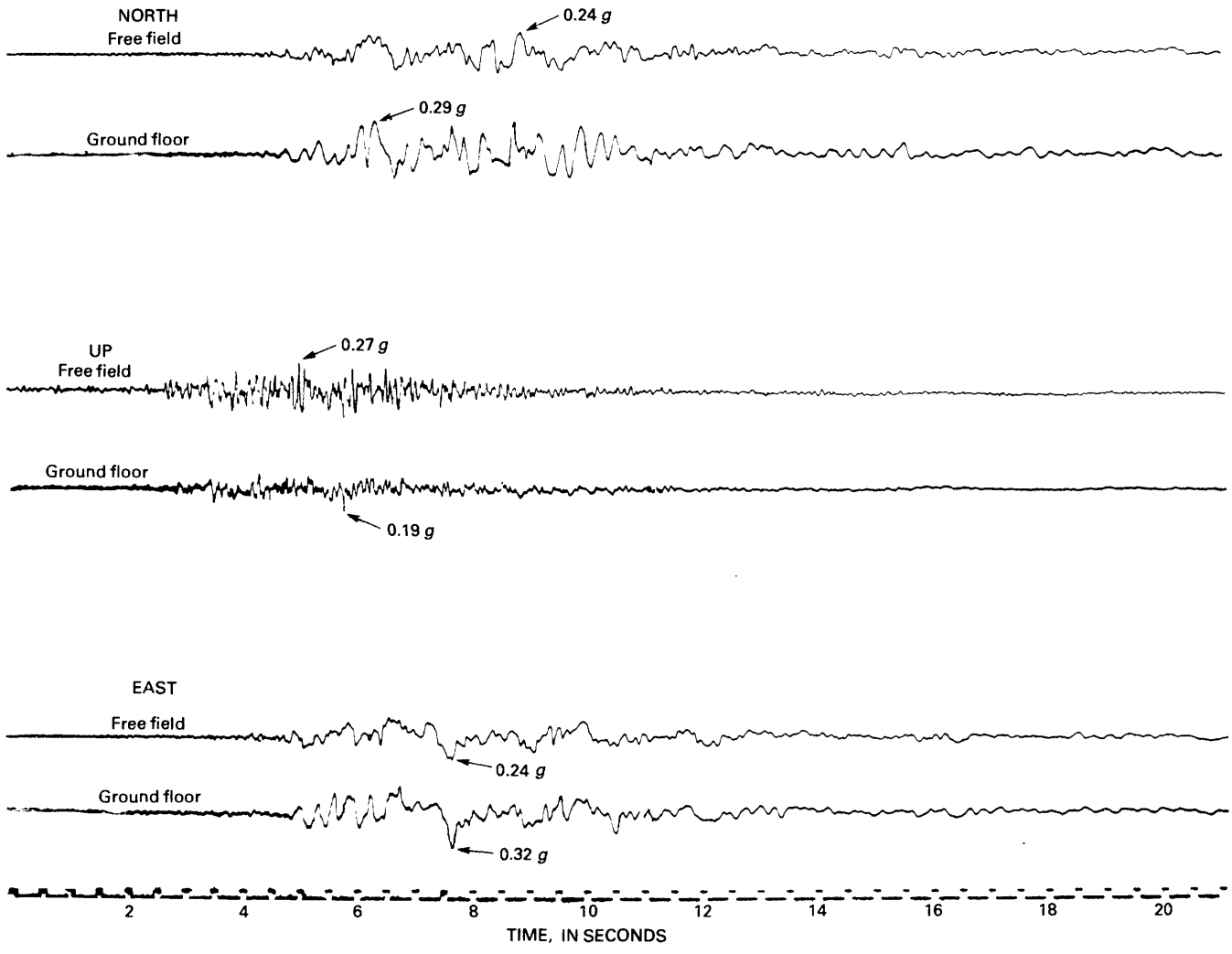

FIGURE 251.—October 15 acceleration time histories recorded at Imperial County Services Building and adjacent free-field site.

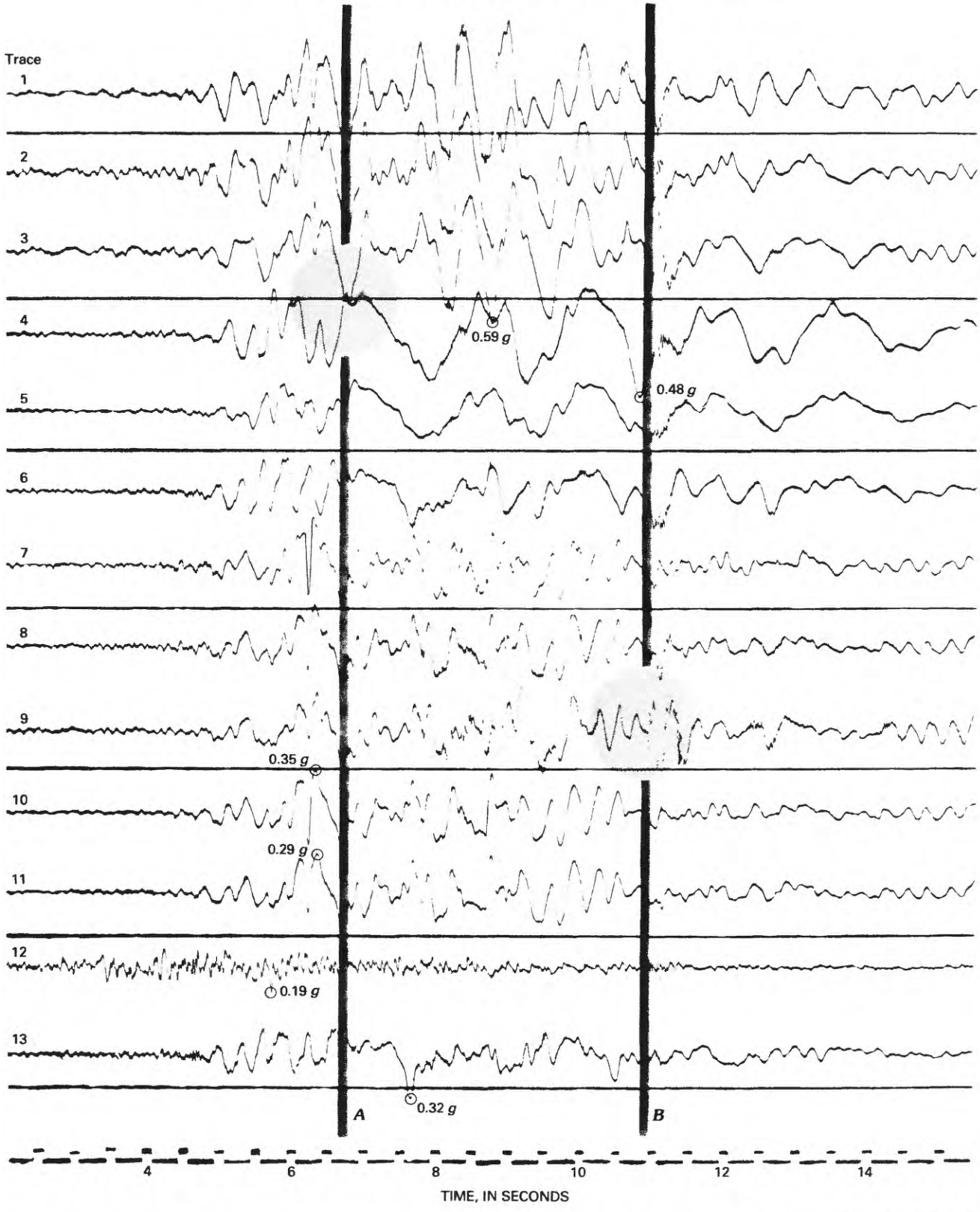

FIGURE 252.—Enlargement of critical portion of October 15 accelerogram recorded in Imperial County Services Building. Shaded circles denote features discussed in text. A and B, times at which damage was initiated and columns began to collapse, respectively.

mately 1.6 s (average value for first 2½ cycles after 6.8 s). This period elongation, which occurs during the long-period acceleration pulse in the east-west component at ground level (maximum pulse acceleration, 0.24 *g* [uncor]), denotes a sudden decrease in the stiffness of the east-west reinforced-concrete frames. We therefore interpret this feature as the time when damage was initiated. Immediately after 6.8 s, bursts of low-amplitude high-frequency motion begin to appear in all upper-story components (especially traces 4, 6, 9, fig. 252). These bursts probably reflect the continuation of damage.

The second major feature, a 0.5-s-long burst of high-amplitude high-frequency (approx 50 Hz) motion, occurs at 11.0 s in trace 9 (shaded circle B, fig. 252), which is the acceleration time history of the north-south component at the second floor directly above the columns that failed. We interpret this feature to denote the time when the columns along the building's east face collapsed. At the same time, the frequency content of the north-south-component time histories recorded at both ends of the roof changed (traces 1, 3, fig. 252). Before 11.0 s the frequency of these two traces is roughly equivalent—that is, both ends of the roof are vibrating in phase—but after 11.5 s their frequencies are no longer the same. The predominant frequency at the west end of the roof after 11.5 s (trace 1, fig. 252) is approximately 1.7 Hz, whereas that at the east end of the roof (trace 3) is approximately 0.8 Hz. Corresponding predominant periods for the two components are 0.6 s (west end) and 1.2 s (east end). These data imply that the stiffness characteristics of the building in the north-south direction at the east and west ends were altered substantially between 11.0 and 11.5 s; and because the columns collapsed at the east end, this sudden difference in stiffness must denote that collapse.

GROUND-SHAKING AMPLITUDES BEFORE DAMAGE INITIATION AND COLUMN COLLAPSE

Because the intensity of ground shaking and the building response before and during the times of damage initiation and column collapse are of great importance, and because there is little documentation on the subject, it is of interest to examine selected time histories of ground motion and building response for these critical moments. Our discussion here is limited to the recorded acceleration and calculated velocity time histories (Porter, this volume) and excludes calculated displacement time histories because of the uncertain effect of record processing on displacements obtained from doubly integrated accelerograms. For brevity, we also limit our discussion to ground-floor and roof-level records (components relevant to response-spectra studies).

The acceleration and velocity time histories for the three ground-level components recorded near the east end of the building (traces 11–13, fig. 252; fig. 253) indicate that damage was initiated (at 6.8 s) approximately 2 s after the onset of high-amplitude horizontal motion and that the columns began to collapse (at 11.0 s) 4 s later, near the end of these high-amplitude motions, that is, just after the strongest motions had subsided. When damage was initiated, for example, ground accelerations in the north-south, vertical, and east-west directions were approximately 0.26, 0.12, and 0.24 *g*, respectively, whereas when the columns began to collapse they were approximately 0.07, 0.02, and 0.03 *g*, respectively. More significant, perhaps, is the evidence that damage was initiated during the long-period (greater than 1 s) acceleration pulse in the east-west direction (trace 13, fig. 252) and that it immediately followed the maximum ground velocity of 42.4 cm/s in the north-south direction (fig. 253). It is also noteworthy that (1) the maximum east-west velocity of 64.6 cm/s occurred approximately 1 s after damage was initiated and 3 s before the columns began to collapse, and (2) peak velocities exceeded 40 cm/s on two occasions (once in the east-west and once in the north-south direction) before damage was initiated and on four occasions before the columns began to collapse (table 36). These observations, particularly those regarding the number of velocity peaks greater than 40 cm/s and the times of occurrence of the long-period acceleration pulse and maximum-velocity amplitudes, should assist in specifying the ground motions that may be damaging to structures having dynamic properties similar to those of the

TABLE 36.—*Peak ground-floor velocities before column collapse*

Peak number	Time after triggering (s)	Amplitude (cm/s)
East component (accelerometer 13)[1]		
1	5.60	−40.3
(Damage initiation)	6.8	----
2	7.54	[2]64.6
3	9.30	−31.4
4	10.32	26.6
(Column collapse)	11.0	----
North component (accelerometer 11)[1]		
1	5.94	−29.4
2	6.62	[2]42.4
(Damage initiation)	6.8	----
3	7.20	−9.7
4	8.01	28.6
5	8.80	−18.5
6	9.38	22.2
7	9.91	−42.0
8	11.0	12.9
(Column collapse)	11.0	----

[1]See figure 248.
[2]Maximum-component amplitude.

Imperial County Services Building. The data also suggest that, had the high-amplitude ground shaking lasted longer, as it did during the 1940 Imperial Valley earthquake (Espinosa, this volume; Matthiesen and Porcella, this volume) the columns would have collapsed during (not after) these strong motions, and the resulting damage might have been far more severe.

The acceleration and velocity time histories for the roof-level components (traces 1–4, fig. 252; fig. 254) indicate that damage was initiated (at 6.8 s) approximately 2 s after the onset of high-amplitude horizontal motions, as was the case at ground level. The plots also indicate that the columns began to collapse at 11.0 s near the end of high-amplitude response in the north-south direction, whereas in the east-west direction the response level remained high for several seconds after column collapse. In addition, the data indicate that: (1) when damage was initiated (6.8 s), peak east-west and north-south accelerations were approximately 0.28 and 0.44 *g* (average for traces 1–3), respectively; (2) the maximum east-west acceleration (0.48 *g*) occurred just before the columns began to collapse (11.0 s); (3) the maximum north-south acceleration (0.59 *g*) occurred midway between damage initiation and column collapse; (4) the building underwent roof-level torsional response approximately 1.3 s before the columns began to collapse (at 9.7 s the north-south acceleration at the east end of the building was approximately 0.53 *g*, whereas at the west end it was 0.26 *g*); (5) both the east-west and north-south (trace 3, east end) peak-velocity responses exceeded 40 cm/s on one occasion before damage was initiated and on six occasions before

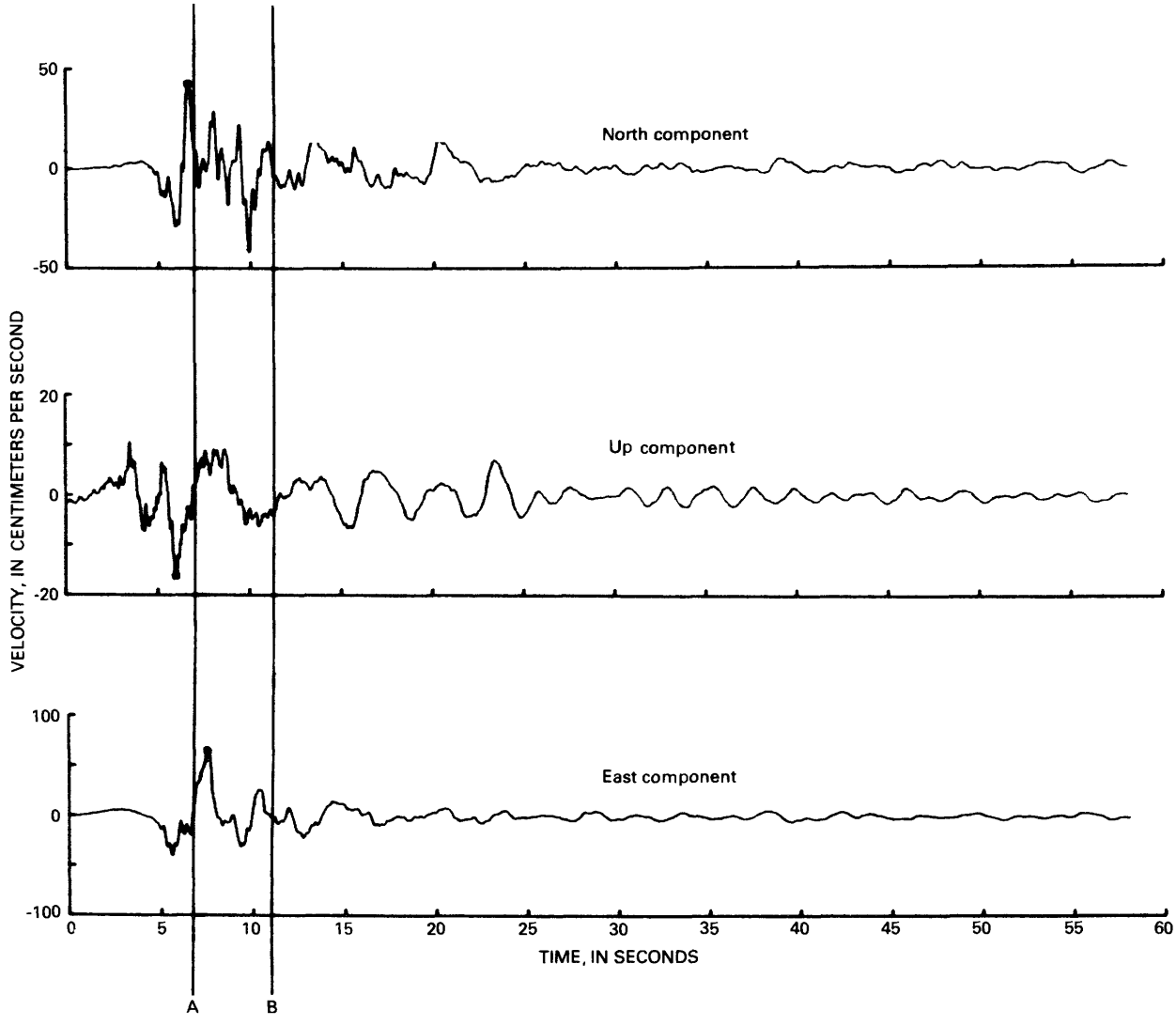

FIGURE 253.—Velocity time histories for north, up, and east components (accelerometer 11) recorded at ground level (after Porter, this volume). A and B are same as in figure 252.

column collapse (table 37); (6) peak north-south (trace 3, east end) velocity response exceeded 60 cm/s on one occasion before column collapse (table 37); and (7) peak east-west velocity response exceeded 80 cm/s on three occasions before column collapse (table 37). These latter observations provide information on the number of cycles of motion (each peak corresponds to half a cycle) above various response thresholds before damage initiation and column collapse; they should, therefore, aid interpretation of the velocity-response-envelope spectra (Perez, 1973) obtained from other sites during other earthquakes. In general, the above observations should

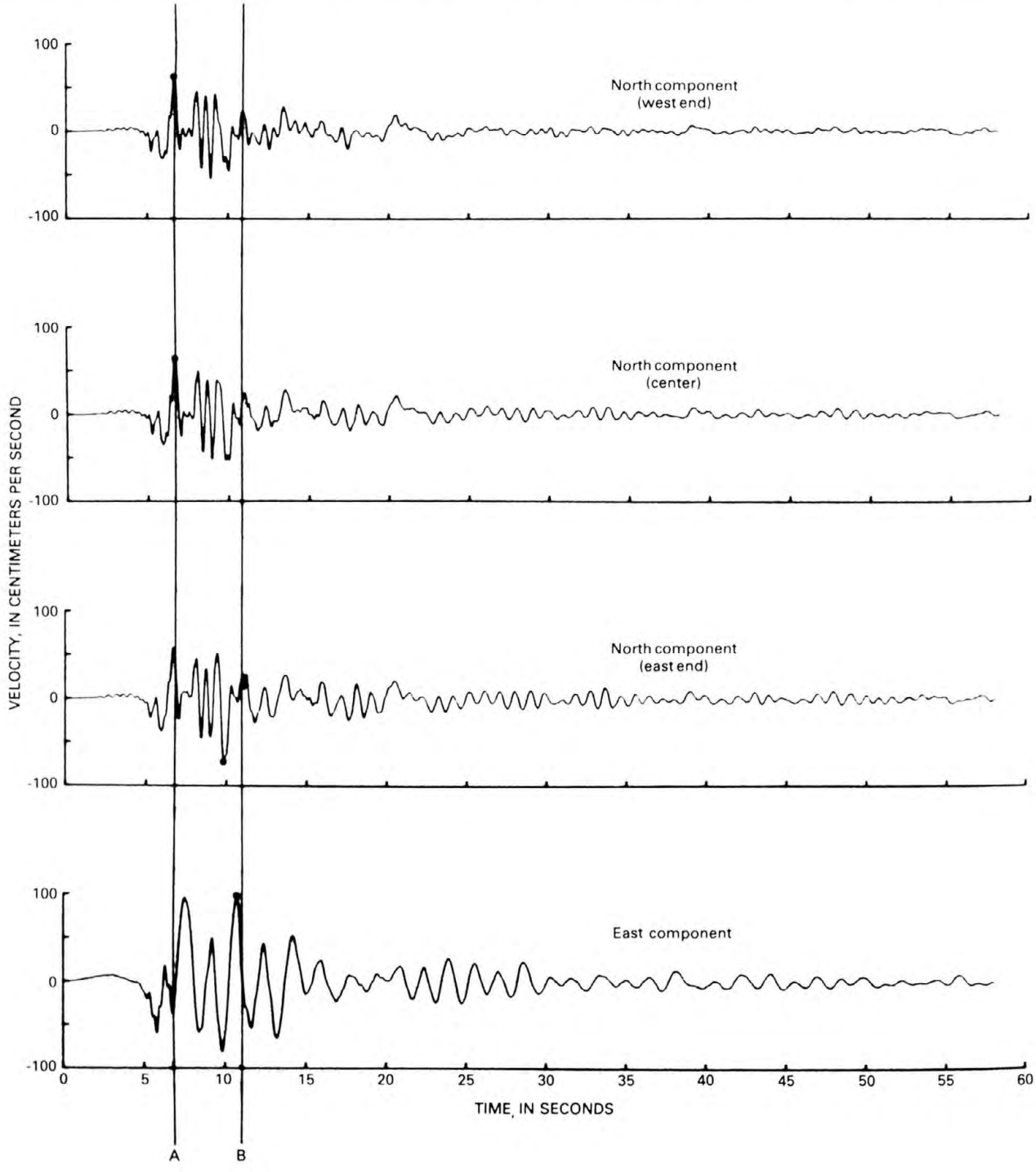

FIGURE 254.—Velocity time histories for north and east components recorded at roof level (after Porter, this volume). A and B are same as in figure 252.

TABLE 37.—*Peak roof-level velocities before column collapse*

Peak number	Time after triggering (s)	Amplitude (cm/s)
East component (accelerometer 4)[1]		
1	5.70	59.5
2	6.28	18.0
3	6.76	−38.0
(Damage initiation)	6.8	----
4	7.49	95.9
5	8.40	−58.9
6	9.18	49.8
7	9.84	−81.0
8	10.72	[2]98.1
(Column collapse)	11.0	----
North component (accelerometer 3)[1]		
1	5.96	−37.8
2	6.70	58.5
(Damage initiation)	6.8	----
3	7.06	−23.9
4	8.13	46.4
5	8.43	−45.9
6	8.74	35.1
7	8.99	−43.8
8	9.42	52.5
9	9.84	[2]−72.5
10	10.31	15.9
11	10.68	−4.3
(Column collapse)	11.0	----

[1]See figure 248.
[2]Maximum-component amplitude.

also help in determining the response levels at which damage can be expected in structures with dynamic properties similar to those of the Imperial County Services Building.

BUILDING FUNDAMENTAL-PERIOD CHANGES

Preearthquake ambient-vibration data and the October 15 accelerogram recovered from the building indicate that the building's fundamental period in both principal directions changed over time and with the strength of ground shaking. Results from an ambient vibration study conducted in spring 1979 (Pardoen, 1979) indicate that the fundamental periods in the north-south and east-west directions under ambient conditions were 0.45 and 0.65 s, respectively. The October 15 accelerogram (fig. 252), on the other hand, indicates that these periods were substantially longer during earthquake excitation and that they fluctuated during the earthquake. During the initial strong ground shaking but before damage was initiated (between 5.0 and 6.8 s), the east-west fundamental period is estimated to be approximately 1.0 s (we were unable to infer from the original accelerogram the north-south fundamental period during this time). After damage was initiated but before column collapse (between 6.8 and 11.0 s) the north-south fundamental period steadily lengthens from about 0.6 to 0.8 s (traces 1–3, fig. 252), whereas the east-west fundamental period is about 1.6 s (trace 4, fig. 252). After column collapse and until the amplitudes of building response subside (after 11.5 s), the fundamental period in the east-west direction is estimated at 1.7 s, and that in the north-south direction is no longer consistent throughout the length of the building. During this time, as indicated earlier in this chapter, the north-south fundamental period at the west end of the building is estimated to be about 0.6 s, and that at the east end 1.2 s.

A comparison of the preearthquake and earthquake periods (table 38) indicates that: (1) during the initial strong ground shaking but before damage was initiated, the building's east-west fundamental period increased by approximately 50 percent relative to that under ambient conditions; (2) after damage was initiated but before column collapse, the east-west fundamental period increased from that under ambient conditions by approximately 150 percent, and the north-south fundamental period increased over time by approximately 30 to 80 percent; and (3) during the final excursions of high-amplitude building response after column collapse, the east-west fundamental period increased by about 160 percent, and the north-south fundamental periods by about 30 and 170 percent at the west and east ends of the building, respectively.

TABLE 38.—*Fundamental periods of the Imperial County Services Building*

Measurement date and type	North-south direction (s)	East-west direction (s)
Spring 1979:		
Ambient (Pardoen, 1979)	0.45	0.65
October 15, 1979, earthquake:		
Before damage was initiated (during high-amplitude ground shaking)	[1]	1.0
After damage was initiated but before column collapse	0.6–0.8	1.6
After column collapse (during high-amplitude building response)	.6 (west end) 1.2 (east end)	1.7

[1]Not inferable from original accelerogram.

PRELIMINARY RELATIVE-DISPLACEMENT ANALYSIS

Our analysis of the building accelerogram also includes computing and interpreting the relative-displacement time histories that are obtained by differencing the displacement time histories of various acceleration traces (fig. 249). We refer to this relative-displacement analysis as a preliminary effort to stress that uncertainties are introduced when displacements are obtained by doubly integrating accelerograms. We believe that we have minimized the uncertainties by differencing and careful filtering.

Rather than using the corrected displacement time histories computed by the CDMG (Porter, this volume), we elected to process the uncorrected acceleration data by using different Ormsby-filter limits (Ormsby, 1961). These filter limits were selected on the basis of recent studies by Hanks (1975) and Basili and Brady (1978) which suggested that the uncertainties in displacements calculated by using the Ormsby filter (Trifunac and Lee, 1973; U.S. Geological Survey, 1976) increase with the period. Therefore, we chose limits to exclude most components of motion with periods longer than the longest fundamental period of the building observed in the original accelerogram (1.7 s). The resulting filter had a gain of unity between the frequencies 0.5–23 Hz, and fell linearly to zero from 0.50 to 0.10 Hz and from 23 to 25 Hz. In terms of period, removal of the long-period content commenced at 2 s and was complete at 10 s.

The time history of north-south differential motion at the ground floor (fig. 255), computed by differencing the displacement time histories for traces 10 and 11 (fig. 249), indicates that the maximum differential motion between the west and east ends of the building (accelerometers 10, 11, fig. 248) was approximately 0.6 cm. Because accelerometers 10 and 11 are 30 m apart, these data suggest that the maximum horizontal shear strain at the ground floor was 0.6 cm/30 m, or about 2×10^{-4}. Because the cyclic relative motion is similar in frequency content to that of the upper-story north-south components, the extent of relative motion is probably influenced, to a large degree, by the structure itself.

East-west relative-displacement time histories, computed by differencing the east-west displacement time histories for the various floor levels, provide insight into the overall extent of building response. Roof minus ground-floor, fourth-floor minus ground-floor, and second-floor minus ground-floor east-west relative-displacement data (fig. 256), computed by differencing the displacement time histories for traces 4 and 13, 5 and 13, and 6 and 13 (figs. 248, 249), respectively, suggest that the east-west relative displacements between the second and ground floors (hereafter referred to as the first story) were substantially larger than those between any other adjacent floors (table 39). More specifically, these data suggest that the maximum interstory displacement was approximately 2 cm (average value) in the fourth, fifth, and sixth stories, approximately 3 cm in the second and third stories, and approximately 8 cm in the first story.

North-south relative-displacement time histories, computed by differencing the north-south displacement time histories for various places (west end, center, and east end) at the roof, second floor, and ground floor (fig. 257; table 40), suggest that interstory motion in the north-south direction was substantially less than in the east-west direction (fig. 256; table 39). Between the roof and ground floor at the east end of the building, for example, the maximum north-south relative displacement was about 9 cm, whereas in the east-west direction it was approximately 20 cm. These data also suggest that the north-south relative displacements between the second and ground floors at the east end of the building (maximum amplitude, 2.7 cm; fig. 257), where

TABLE 39.—*Selected east-west relative horizontal displacements*
[Damage was initiated at 6.8 s; columns began to collapse at 11.0 s. All displacements in centimeters]

Time after triggering (s)	2d floor minus ground floor	4th floor minus 2d floor	Roof minus 4th floor
6.8	1.1	0.6	0.4
9.4	5.1	5.9	[1]5.8
10.3	−7.4	[1]−6.3	−5.8
11.0	6.2	5.8	5.2
11.1	[1]7.7	4.4	3.9

[1]Maximum.

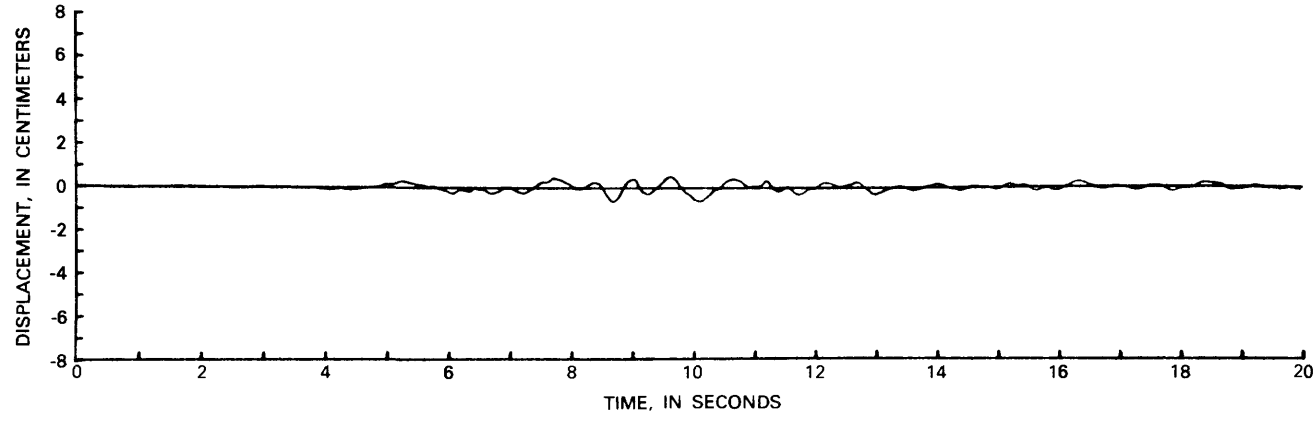

FIGURE 255.—Time history of north-south relative displacement at ground level, computed by differencing displacement time histories for acceleration traces 10 and 11 (fig. 249).

TABLE 40.—*Selected north-south relative horizontal displacements*
[Damage was initiated at 6.8 s; columns began to collapse at 11.0 s. All displacements in centimeters]

Time after triggering (s)	2d floor minus ground floor			Roof minus 2d floor		
	West end	Center	East end	West end	Center	East end
6.8	−0.1	0.1	0.9	1.6	1.6	0.4
8.8	.7	.4	1.6	[1]4.3	4.7	1.7
9.1	[1]−1.1	−.4	−1.0	−3.2	−3.5	2.4
9.2	−.7	−.3	−1.9	−3.4	[1]−4.9	−3.8
9.7	.2	.5	[1]2.7	2.3	4.8	[1]5.9
11.0	.6	.3	−.4	.0	−1.2	−.4
11.2	.5	[1].7	2.1	1.4	−.2	−1.4

[1]Maximum.

the columns collapsed, were substantially larger than at the center and west end (maximum amplitudes, 0.7 and 1.1 cm, respectively; fig. 257). These data imply, then, that the row of columns at the east end of the building underwent larger north-south relative displacements between the ground and second floors than did any other north-south row of columns in the first story. These data also imply that that part of the second-floor diaphragm between the east end of the building and the easternmost first-story shear wall (9.4 m to the west) did not remain rigid in its own plane but rather sustained relatively large north-south bending or shear distortions. These diaphragm distortions are clearly evident in figure 258, which plots the time histories of north-south relative displacements between the center and east end (maximum amplitude, 2 cm) and between the center and west end (maximum amplitude, 1 cm) of the second-floor diaphragm.

Superposition of the north-south and east-west time histories of relative displacement at the east end between the second and ground floors (fig. 259) provides insight into the two-dimensional horizontal motion there before, during, and after the beginning of damage and the collapse of the columns. This plot indicates that: (1) at the time when damage was initiated, the amplitudes of north-south and east-west relative displacement between the second and ground floors were approximately 0.9 and 1.1 cm, respectively; (2) the

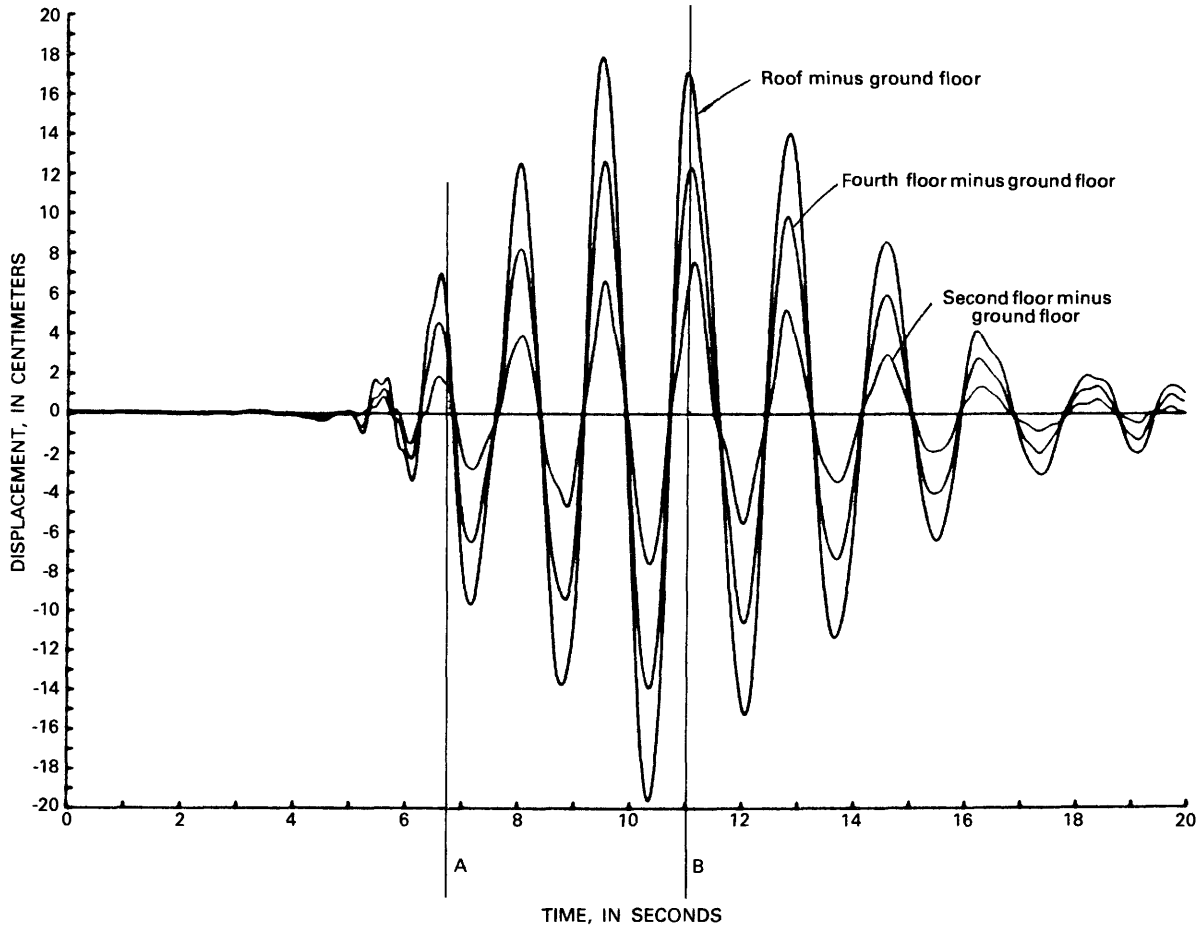

FIGURE 256.—Time history of east-west relative displacement between roof and ground floor (difference of data from accelerometers 4 and 13), between fourth and ground floors (difference of data from accelerometers 5 and 13), and between second and ground floors (difference of data from accelerometers 6 and 13). A and B are same as in figure 252.

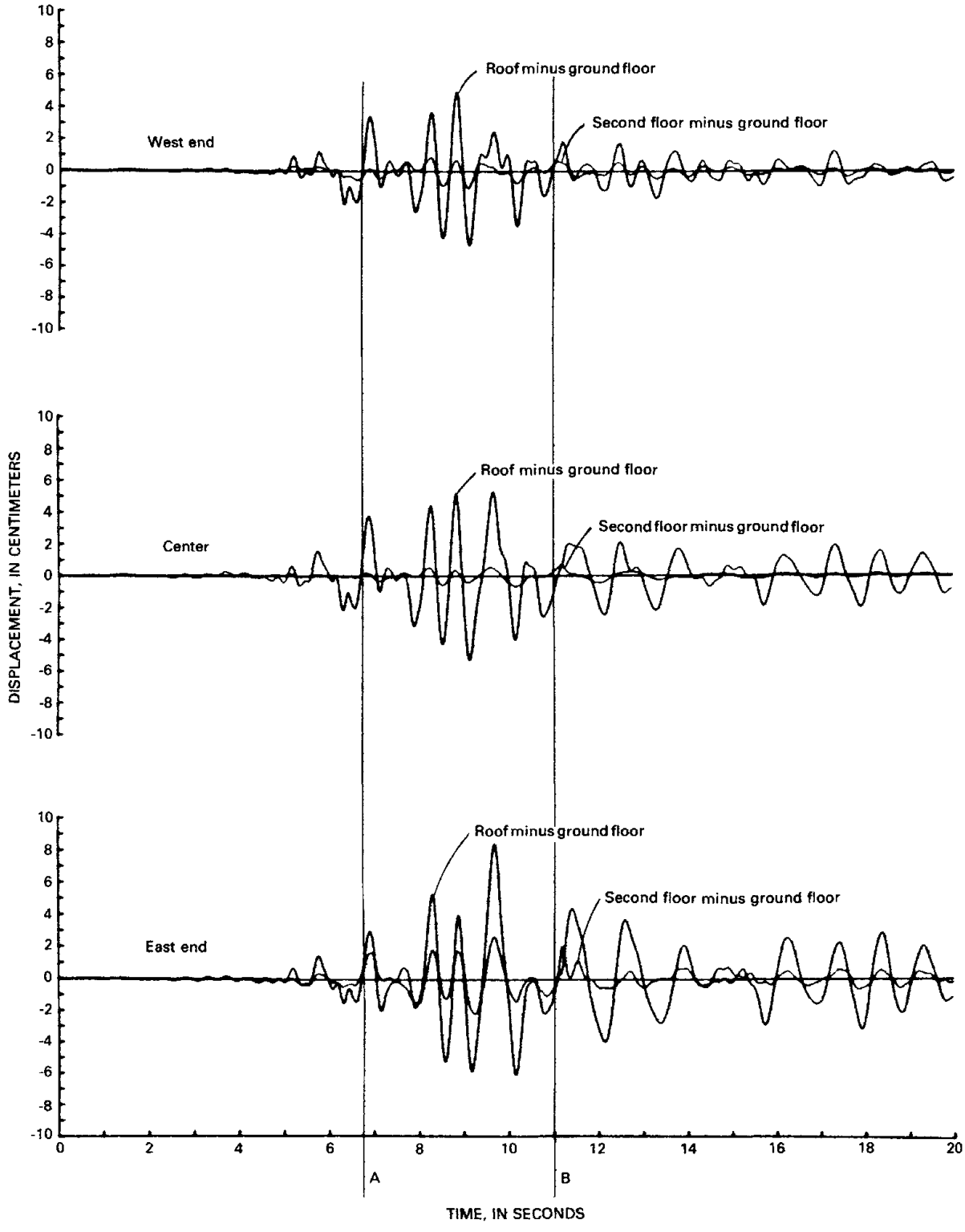

FIGURE 257.—Time histories of north-south relative displacement between roof and ground floor and between second and ground floors at west end (difference of data from accelerometers 1 and 10, and 7 and 10), center (difference of data from accelerometers 2 and 11, and 8 and 11), and east end (difference of data from accelerometers 3 and 11, and 9 and 11) of building. A and B are same as in figure 252.

maximum north-south first-story relative displacement of approximately 2.7 cm occurred about 1.3 s before the columns began to collapse; (3) the columns apparently began to collapse when the east-west relative displacement was approximately 6.2 cm, or 81 percent of the maximum displacement (7.7 cm) that occurred approximately 0.1 s later; and (4) the north-south first-story relative displacement was relatively small (0.4 cm) when the columns began to collapse. Also, the amplitude of north-south relative displacement between the roof and ground floor at the east end (fig. 257) when the columns began to collapse was small (0.8 cm); in other words, at the time of column collapse, the building was alined nearly vertical in a north-south direction.

SUMMARY AND CONCLUSIONS

The October 15 accelerograms recovered from the structurally damaged Imperial County Services Building and adjacent free-field site constitute a valuable data set for earthquake engineering studies. The 13-channel remote-accelerometer central-recording

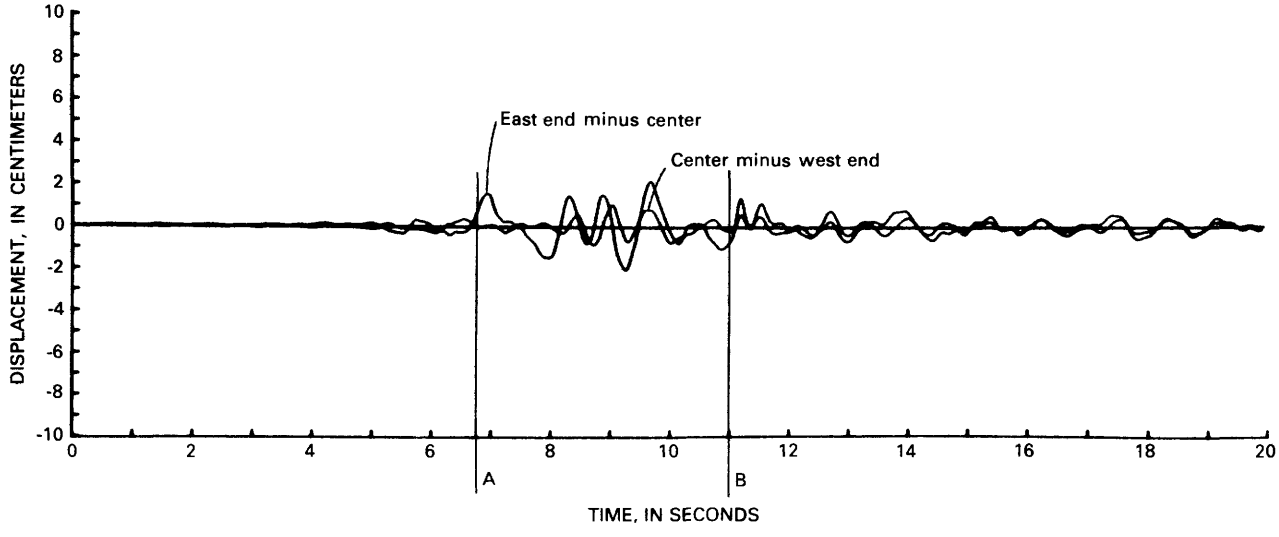

FIGURE 258.—Time histories of north-south relative displacement between center and east end of second-floor diaphragm (difference of data from accelerometers 8 and 9) and between center and west end of second-floor diaphragm (difference of data from accelerometers 7 and 8). A and B are same as in figure 252.

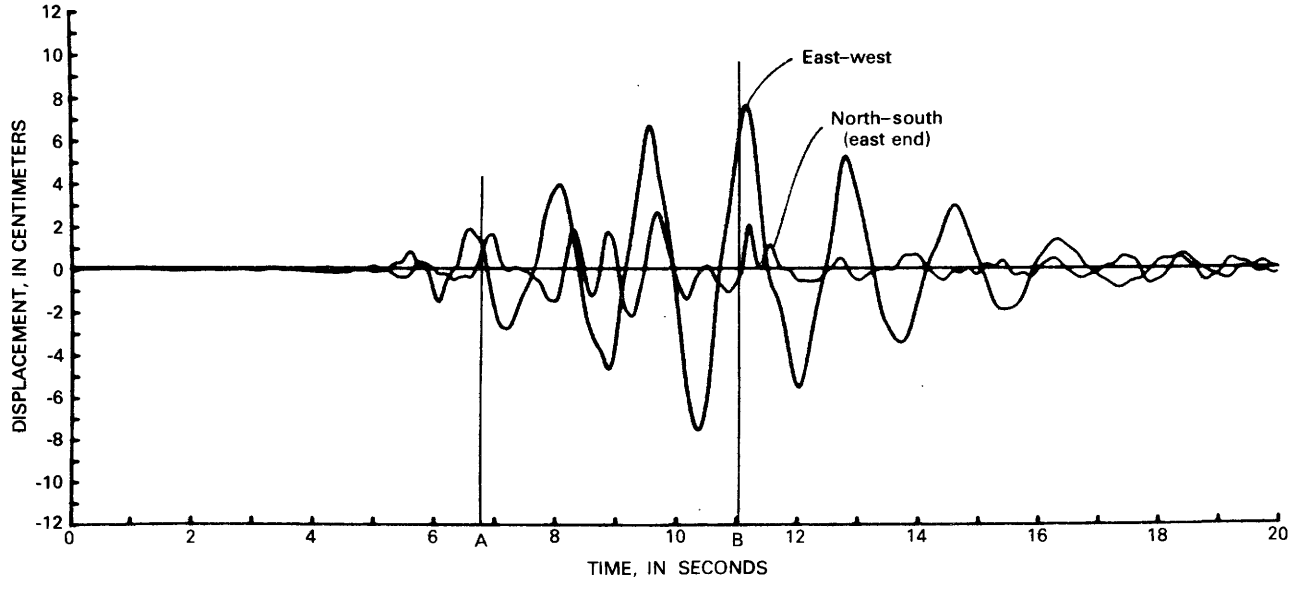

FIGURE 259.—Time history of east-west and north-south relative displacement between ground and second floors (difference of data from accelerometers 6 and 13, and 9 and 11). A and B are same as in figure 252.

CRA–1 accelerograph system in the building performed excellently and provided a 90-s-long accelerogram in analog form that is of great interest, primarily because the time and mechanism of damage, as well as the associated ground shaking and structural response, can be inferred from the recorded data.

The accelerograms from the building and adjacent free-field site indicate that the motion recorded at the ground floor of the building incorporates, to some significant extent, building-soil-foundation system response. More specifically, the data suggest that the effective base of the building, founded on piles, is below the ground floor. The records also show that the maximum horizontal acceleration recorded at the ground floor was approximately 60 percent higher than at the free-field site. Corresponding increases in velocity and displacement, however, were substantially less.

Features of the building accelerogram that provide insight into the mechanism of structural damage include abrupt changes in frequency content in the upper-story north-south and east-west components, as well as bursts of high-frequency motion. These features suggest that damage was initiated 6.8 s after the instrument was triggered and that the four columns along the building's east face began to collapse 4.2 s later, or 11.0 s after triggering.

The recorded acceleration data and calculated velocity time histories (Porter, this volume) indicate that damage was initiated approximately 2 s after the onset of strong ground motion during a long-period acceleration pulse in the east-west direction, and that it immediately followed the maximum ground velocity of 42.4 cm/s in the north-south direction. The columns began to collapse immediately after the strong ground motions. Before damage initiation, peak horizontal ground velocity exceeded 40 cm/s on two occasions (once in each direction), and before column collapse on four occasions (twice in each direction). Also before column collapse, roof-level peak velocity exceeded 40 cm/s on 12 occasions (6 in each direction), 60 cm/s on 4 occasions (once in the north-south direction and 3 times in the east-west direction), and 80 cm/s on 3 occasions (all in the east-west direction). The roof-level data also indicate that the peak east-west and north-south accelerations when damage was initiated were approximately 0.28 and 0.44 g, respectively; that the maximum east-west acceleration (0.48 g) occurred just before the columns began to collapse; that the maximum north-south acceleration (0.59 g) occurred approximately 2 s before the columns began to collapse; and that the roof underwent torsional response approximately 1.3 s before the columns began to collapse.

The original accelerogram also suggests that the building's fundamental period in both principal directions changed significantly during the earthquake. During strong ground shaking but before damage was initiated, for example, the fundamental period in the east-west direction (the direction in which lateral forces are resisted by frame action) was approximately 1.0 s, or 50 percent longer than that measured under ambient conditions (0.65 s) in spring 1979. After damage was initiated and before column collapse, this period was approximately 1.6 s, or approximately 150 percent longer than the ambient period; and during the final excursions of high-amplitude building response after column collapse, approximately 1.7 s, or 160 percent longer. Corresponding increases in the fundamental period in the north-south direction (the direction in which lateral forces are resisted by shear walls) were generally smaller, with one exception: after column collapse, the fundamental period in the north-south direction at the east end of the building was approximately 1.2 s, or 170 percent longer than that measured under ambient conditions (0.45 s). At the west end during the same interval it was approximately 0.6 s, or 30 percent longer.

Results of a preliminary relative-displacement analysis, based on data corrected by using specially selected Ormsby-filter limits, suggests that the north-south differential motion between two points 30 m apart at ground level was small (max 0.6 cm, which corresponds to a shear strain of 2×10^{-4}), that the four columns at the east end of the building sustained larger relative displacements between the second and ground floors in the north-south direction (2.7 cm) than did any other north-south row of first-story columns, and that the large interstory displacements (max 7.7 cm) between the second and ground floors in the east-west direction played a key role in the column-collapse mechanism. When damage was initiated (at 6.8 s), the maximum north-south and east-west first-story relative displacements at the east end of the building were approximately 0.9 and 1.2 cm, respectively. When the columns began to collapse (at 11.0 s), the east-west first-story relative displacement was approximately 6.2 cm, or 15 times that in the north-south direction at the east end (0.4 cm). The relative-displacement data also indicate that the building was alined nearly vertical in the north-south direction when the columns began to collapse. This orientation implies that axial loads due to north-south overturning moments played only a minor role in the actual collapse that began at 11.0 s, whereas stresses due to large east-west interstory displacements played a major role. Before column collapse, however, the large north-south relative displacements (max 8.5 cm) between the roof and ground floor suggest that north-south overturning moments played a more significant role. Collectively, the relative-displacement

data suggest that, from 6.8 to 11.0 s, stresses in the east-end first-story columns were higher than in any other row, presumably because these columns underwent the largest axial strains (from north-south and east-west overturning moments) as well as the largest flexural stresses (from north-south interstory displacements), in addition to the flexural stresses (due to east-west frame action) that affected all the first-story columns about equally. In short, the relative-displacement data suggest that north-south overturning moments and north-south relative displacements between the second and ground floors played a significant role during damage initiation and the continuation of yielding before column collapse (in weakening the east row of first-story columns), but that collapse was primarily caused by stresses due to large east-west interstory displacements—that is, by a combination of east-west flexural stresses and east-west overturning-moment axial stresses.

ACKNOWLEDGMENTS

Many people were involved in obtaining these data. We are particularly grateful to J. T. Ragsdale and the technicians from the CDMG Office of Strong-Motion Studies, who installed and maintained the equipment; to Randy Rister of the Imperial County Department of Buildings and Grounds, for his continued support and interest in the project; to the other members of the California Seismic Safety Commission's Subcommittee on Instrumentation for Buildings (William E. Gates, Gary C. Hart, Kenneth K. Honda, John F. Meehan, Chris D. Poland, John O. Robb, Roland L. Sharpe, and James L. Stratta), who advise and actively support the building-instrumentation phase of the California Strong-Motion Instrumentation Program; to the SEAOSC Instrumentation Subcommittee, for their role in selecting and instrumenting the building; to A. G. Brady and R. B. Matthiesen of the U.S. Geological Survey, for their helpful suggestions; and to Richard P. Maley of the U.S. Geological Survey, who initially recommended the building for instrumentation. This research was supported by National Science Foundation Grant CA-114.

REFERENCES CITED

Basili, M., and Brady, A. G., 1978, Low frequency filtering and the selection of limits for accelerogram corrections: European Conference on Earthquake Engineering, 6th, Dubrovnik, Yugoslavia, 1978, Proceedings, p. 251–258.

Hanks, T. C., 1975, Strong ground motion of the San Fernando, California, earthquake—ground displacements: Seismological Society of America Bulletin, v. 65, no. 1, p. 193–225.

Ormsby, J. F. A., 1961, Design of numerical filters with applications to missile data processing: Association for Computer Machinery Journal, v. 8, p. 440–466.

Pardoen, G. C., 1979, Imperial County Services Building ambient vibration test results: Christchurch, New Zealand, University of Canterbury Report 79–14, 21 p.

Perez, Virgilio, 1973, Velocity response envelope spectrum as a function of time, *in* Benfer, N. A., Coffman, J. L., and Bernick, J. R., eds., San Fernando, California, earthquake of February 9, 1971: Washington, U.S. Department of Commerce, National Oceanic and Atmospheric Administration, Environmental Research Laboratories, v. 3, p. 393–401.

Porcella, R. L., and Nielsen, J. D., 1977, Preliminary report on the Calipatria, California, earthquake swarm: November, 1976, *in* Porcella, R. L., ed., Seismic engineering program report, October–December 1976: U.S. Geological Survey Circular 736–D, p. 1–3.

Rojahn, Christopher, and Matthiesen, R. B., 1977, Earthquake response and instrumentation of buildings: American Society of Civil Engineers Proceedings, Technical Councils of ASCE Journal, v. 103, no. TC1, p. 1–12.

Rojahn, Christopher, and Ragsdale, J. T., 1980a, Building instrumentation phase of the California Strong-Motion Instrumentation Program: Structural Engineers Association of California Annual Convention, Lake Tahoe, Calif., 1978, Proceedings, p. 21–39.

———1980b, Strong-motion records from the Imperial County Services Building, El Centro, *in* Leeds, D. J., ed., Imperial County, California, earthquake, October 15, 1979: Berkeley, Calif., Earthquake Engineering Research Institute reconnaissance report, p. 173–184.

Trifunac, M. D., and Lee, V. W., 1973, Routine computer processing of strong-motion accelerograms: Pasadena, California Institute of Technology, Earthquake Engineering Research Laboratory Report EERL 73–03, 360 p.

U.S. Geological Survey, 1976, Strong-motion earthquake accelerograms, digitization and analysis, 1971 records: Open-File Report 76–609, 135 p.

MAIN-SHOCK STRONG-MOTION RECORDS FROM THE MELOLAND ROAD-INTERSTATE HIGHWAY 8 OVERCROSSING

By CHRISTOPHER ROJAHN,
U.S. GEOLOGICAL SURVEY;

J. T. RAGSDALE,
CALIFORNIA DIVISION OF MINES AND GEOLOGY;

J. D. RAGGETT,
J. D. RAGGETT & ASSOCIATES, INC.;

and

J. H. GATES,
CALIFORNIA DEPARTMENT OF TRANSPORTATION

CONTENTS

ABSTRACT

At the time of the October 15 main shock, the Meloland Road-Interstate Highway 8 overcrossing, a continuous two-span reinforced-concrete bridge 0.5 km southwest of the Imperial fault, was instrumented with two 13-channel remote-accelerometer central-recording accelerograph systems. Although the film transport in one of the two recorders malfunctioned during the earthquake, these instruments provided an important and usable data set. Peak accelerations in the north-south, vertical, and east-west directions at the base of the bridge's central support column were 0.28, 0.17, and 0.33 g, respectively, whereas those at an adjacent free-field site were 0.32, 0.23, and 0.30 g, respectively. Peak accelerations recorded on embankment sites adjacent to each abutment were substantially higher than those recorded at the base of the bridge's central support column; these data suggest that the structure itself altered the motion at the embankment sites. Other important features of the records include (1) an acceleration pulse 1 s long occurring in the east-west components at the free-field, column-base, and embankment sites; and (2) strong evidence of modal response of the bridge during and after the period of strongest ground shaking. The bridge did not sustain any significant structural damage during the earthquake.

INTRODUCTION

The Meloland Road-Interstate Highway 8 overcrossing, a continuous two-span reinforced-concrete bridge, is 0.5 km southwest of the Imperial fault and 18 km northwest of the epicenter of the October 15 main shock (fig. 260). The bridge and three adjacent ground sites were instrumented with two 13-channel accelerograph systems installed and maintained by the California Division of Mines and Geology (CDMG). Although the bridge did not sustain any significant structural damage during the earthquake, the strong-motion records from the bridge constitute an important data set. This is the first time that strong-motion data have been obtained from an extensively instrumented structure situated less than 1 km from the surface-rupture zone of a damaging earthquake.

The overcrossing (bridge No. 58–215) was designed in 1968–69 by the California Department of Transportation, using 1968 California Division of Highways criteria. The seismic-design portion of these criteria is based, in part, on the lateral-force requirements for buildings of the Structural Engineers Association of California.

The bridge is a continuous two-span cast-in-place reinforced-concrete box girder with 104-ft spans (fig. 261) carrying two lanes of local traffic over Interstate Highway 8. The bridge superstructure, which weighs

about 7,100 lb per linear foot, is supported by an abutment at each end and a single column at the center of plan (fig. 262). The central support column is a 5-ft-diameter reinforced-concrete column resting on a 15-ft-square stepped 25-pile footing. The column is reinforced with 18 #18 bars confined by #5 spiral bars at 5-in. pitch. The bridge abutments are poured monolithic with the superstructure. Each 18-in. abutment wall, which is nominally reinforced with #7 bars at 12 in. vertically and #4 bars at 18 in. horizontally, is about 5 ft high and rests on a 3- by 1.5-ft seven-pile footing. The piles are 45-ton timber piles that extend 40 to 45 ft into the alluvial foundation material. Logs from three soil borings at the site indicate that the foundation material consists of soft to stiff silty clay.

Although the bridge did not sustain any significant earthquake-induced structural damage, there was evidence of relative motion between the abutments and the surrounding fill material. An airspace approximately a centimeter wide was observed between the south abutment's north face and adjacent fill material. There was similar evidence of relative motion along the south face of the north abutment.

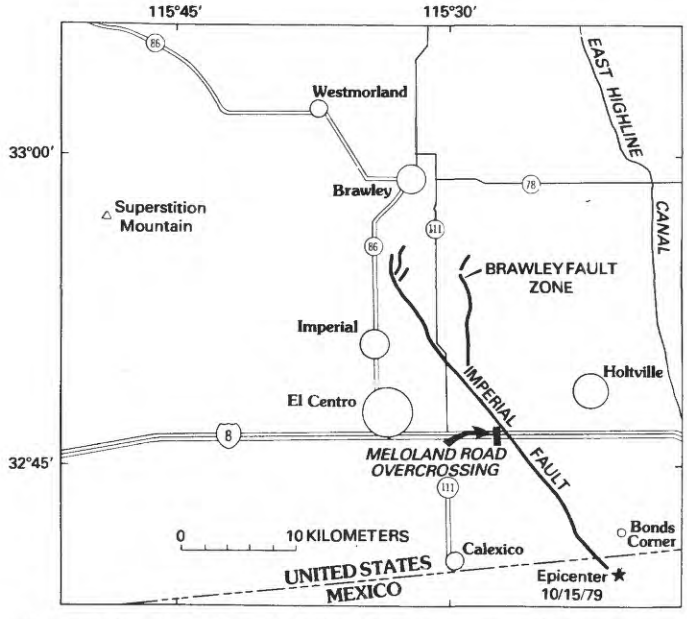

FIGURE 260.—Location of Meloland Road-Interstate Highway 8 overcrossing relative to Imperial fault and October 15 main-shock epicenter.

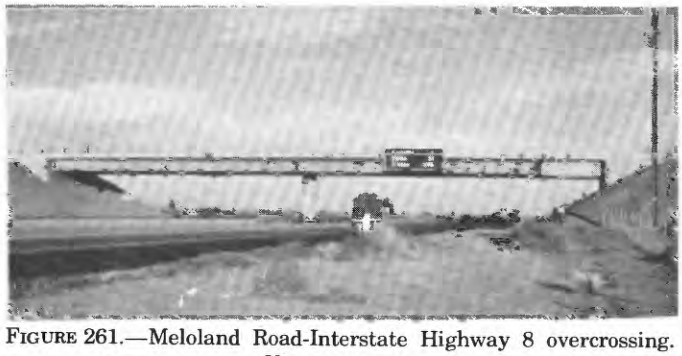

FIGURE 261.—Meloland Road-Interstate Highway 8 overcrossing. View eastward.

STRONG-MOTION INSTRUMENTATION

The bridge was originally selected for instrumentation under the California Strong-Motion Instrumentation Program because of its structural characteristics, size, and location in a known highly active seismic area. It was instrumented in November 1978 with two 13-channel Kinemetrics CRA–1 remote-accelerometer central-recording accelerograph systems that were installed in accordance with the recommendations of the following two groups: the California Seismic Safety Commission, Subcommittee on Instrumentation for Transportation and Other Lifeline Facilities; and an ad hoc site-visitation committee composed of J. D. Raggett and J. H. Gates. The system, installed under the supervision of J. T. Ragsdale, is consistent with the bridge strong-motion instrumentation guidelines and data-analysis procedures developed by the U.S. Geological Survey (Raggett and Rojahn, 1978). The instruments are maintained by the CDMG Office of Strong-Motion Studies.

Instrumentation at the site consists of fourteen FBA–1 single-axis packages and one FBA–3 triaxial package of force-balance accelerometers on the bridge structure, two FBA–3 accelerometer packages on embankments adjacent to each abutment, one FBA–3 accelerometer package at a ground site intended to be free field, and two 13-channel central recording units and one VS–1 vertical starter at ground level beneath the bridge (fig. 262). The FBA accelerometers have a natural frequency of approximately 50 Hz and are connected by low-voltage data cable to the central recording units. The battery-powered recording units are triggered by vertical motion that equals or exceeds 0.01 g, record on 7-in. (178 mm) light-sensitive film, and are designed to register accelerations with frequency components nominally within the range 0–50 Hz with maximum amplitudes of 1 g. Real time is provided by a WWVB radio receiver and time-tick generator system; the recorders are interconnected for common timing.

The 13-channel recording units are housed in two Fiberglass instrument shelters adjacent to the bridge's central support column; the two FBA–3 accelerometer packages on the embankments and the free-field FBA–3 accelerometer package are housed in ground vaults just beneath the surface. The embankment sites are intended to record ground motion on the fill material

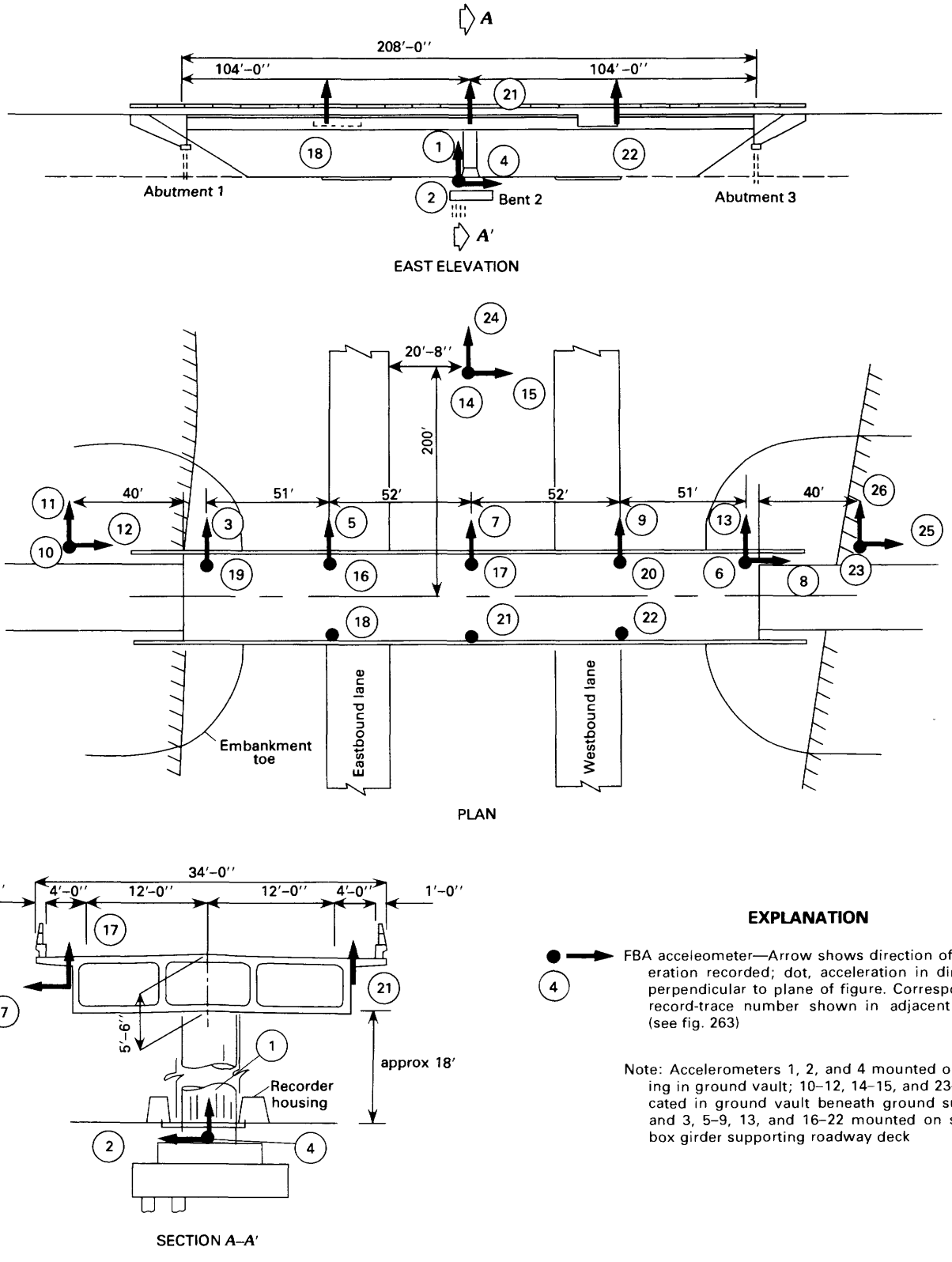

FIGURE 262.—Elevation, plan, and section of Meloland Road-Interstate Highway 8 overcrossing, showing location and orientation of FBA accelerometers.

adjacent to each abutment; they are not intended to be free-field sites.

The FBA accelerometer locations on the bridge structure (fig. 262) were selected to provide information on overall bridge response as well as base input motion. The primary purpose of the five east-west-oriented accelerometers and one north-south-oriented accelerometer on the bridge superstructure (accelerometers 3, 5, 7–9, 13) was to obtain and isolate east-west translational, north-south translational, torsional (about a

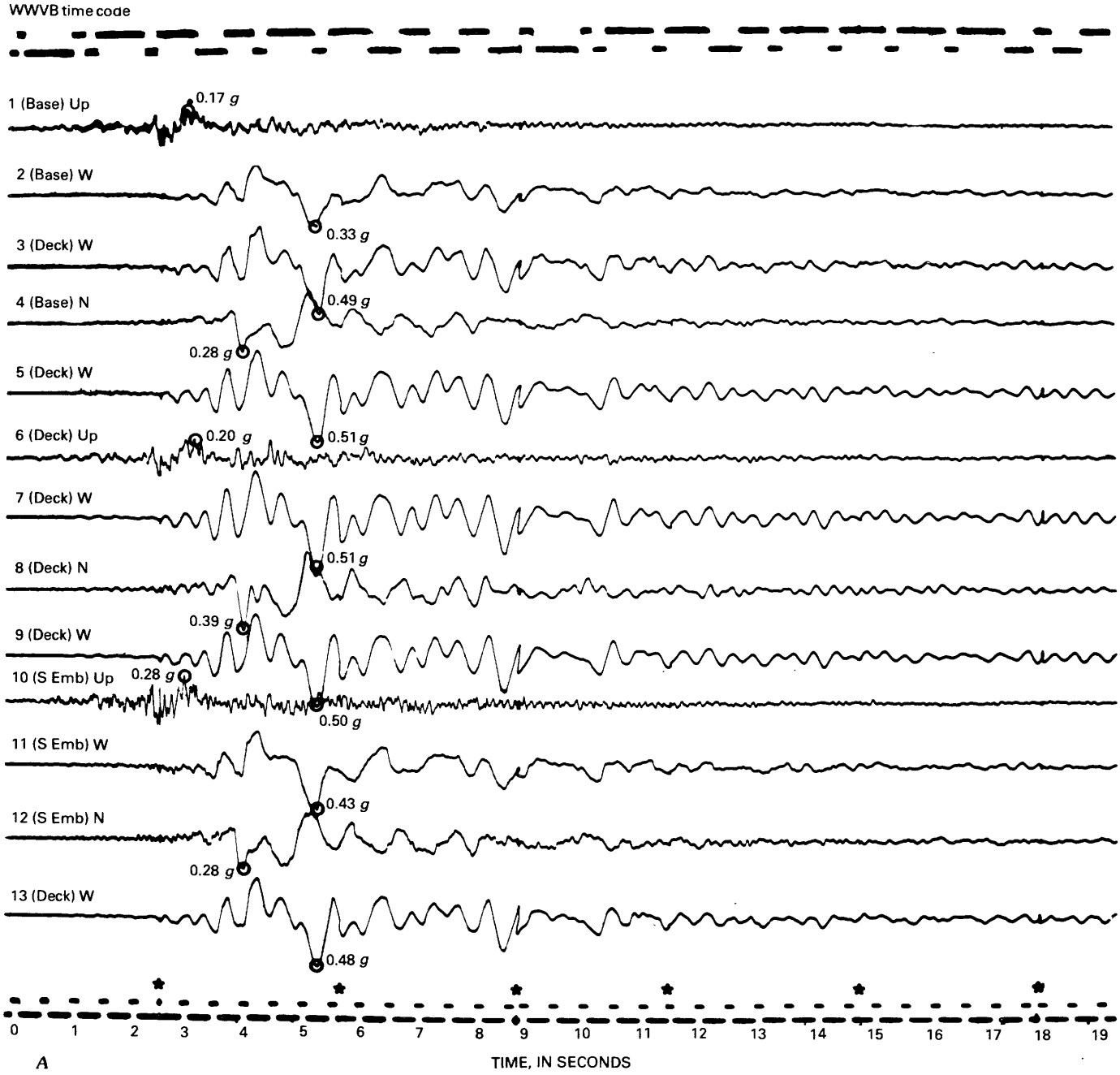

FIGURE 263.—First 19 s of October 15 strong-motion accelerogram recorded at Meloland Road-Interstate Highway 8 overcrossing (CDMG station 336, lat 32°46′23″ N., long 115°26′53″ W.). N (north), W (west), or up (vertical) in trace identification denotes direction of positive acceleration. Circle indicates maximum acceleration for each trace. Accelerometer locations (1–26) are shown in figure 262. *A*, Master recorder. Asterisks denote times at which recorder film-transport system stalled, characterized by overtracing. *B*, Slave recorder.

vertical axis), and inplane bending response of the roadway deck. In conjunction with the accelerometers on the footing of the central support column (accelerometers 2, 4), these accelerometers provide information on overall east-west and north-south modal response as well as relative motion between the base of the central support column and the bridge superstructure. The vertically oriented accelerometers on the roadway deck (accelerometers 6, 16–22) and on the footing of the central support column (accelerometer 1) provide information on vertical flexure (bending) of the roadway deck as well as twisting of the bridge deck about the roadway centerline.

EARTHQUAKE ACCELEROGRAMS

Although both accelerograph systems operated during the October 15, 1979, earthquake, the record from one system was spoiled to a limited but significant ex-

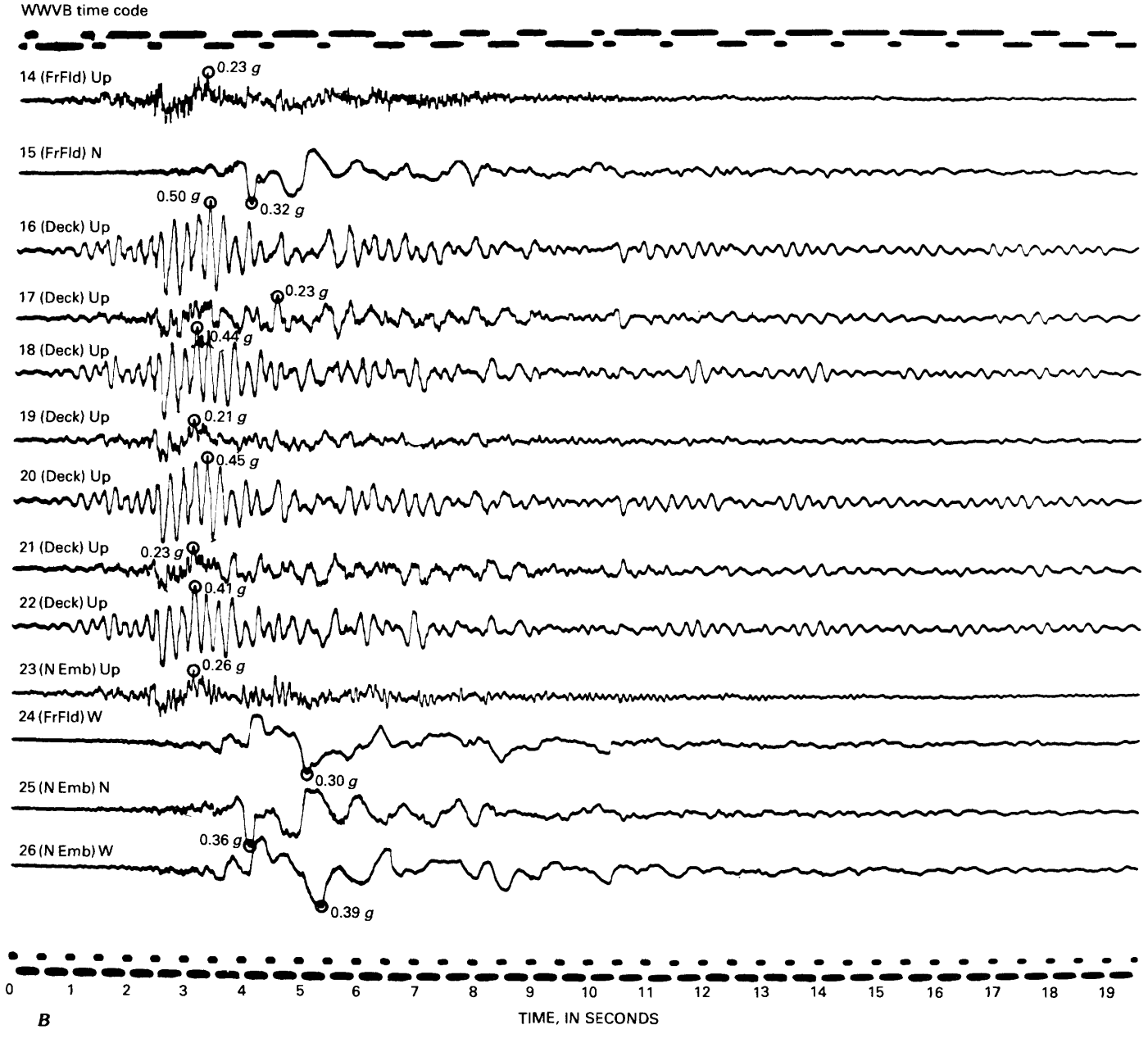

FIGURE 263.—Continued

tent because the recorder film transport stalled during the earthquake. The malfunction occurred at intervals of roughly 3 s during the first 30 s of operation and is characterized by overtracing on the record (fig. 263*A*). The CDMG hopes to extract from this record a reasonably accurate facsimile of the actual waveforms (L. D. Porter, oral commun., 1980); waveforms from corresponding channels on the other 13-channel record (fig. 263*B*) will then be used to evaluate and improve the restored data. The fact that corresponding components at the two embankment sites (traces 10–12, fig. 263*A*; traces 23, 25, 26, fig. 263*B*) were not recorded on the same system should help in this regard. In its original state, the flawed record (fig. 263*A*) provides peak-acceleration data and frequency characteristics as well as an overall sense of the strong motion at the site.

Peak accelerations at the free-field site 60 m west of the bridge were 0.32, 0.23, and 0.30 *g*, respectively, for the north-south, vertical, and east-west components (traces 15, 14, and 24, respectively, fig. 263). The maximum durations of motion between the first and last peak equal to or greater than 0.1 *g* were approximately 4 and 7 s for the vertical and horizontal components, respectively. In terms of frequency content, perhaps the most notable feature of these records is the long-period acceleration pulse occurring in the east-west component between seconds 4 and 6. At that point, the acceleration remained positive and relatively large in amplitude (maximum acceleration, 0.27 *g*) for approximately 1 s and no doubt generated large velocity and displacement pulses.

Peak accelerations at the base of the bridge's central support column were 0.28, 0.17, and 0.33 *g*, respectively, for the north-south, vertical, and east-west components (traces 4, 1, and 2, respectively, fig. 263). Although the peak values for the horizontal components differed slightly from those recorded at the free-field site, the signatures of corresponding components are generally the same; however, the signatures of the vertical components at these sites (traces 1, 14, fig. 263) differ significantly. Peak vertical accelerations are similar, but high-frequency motions in the free-field record are substantially larger in amplitude than their counterparts in the column-base record.

Corresponding motions recorded on the embankment sites adjacent to each abutment differ somewhat from those recorded at the base of the bridge's central support column. In general, the waveforms are the same: the east-west components (traces 11, 26, fig. 263) contain the approximately 1 s long acceleration pulse between seconds 2 and 4 that is apparent in the column-base record. The records differ in that peak accelerations recorded at the embankment sites are generally higher than those recorded at the base of the central support column. In the east-west direction, peak accelerations at the north and south embankment sites (0.39 and 0.43 *g*, respectively) are 18 and 30 percent higher than that recorded at the base of the central support column (0.33 *g*). In the north-south direction (traces 12, 25, fig. 263), where peak column-base motion is 0.28 *g*, these peak accelerations are equal and 29 percent higher; and in the vertical direction (traces 10, 23, fig. 263), where peak column-base motion is 0.17 *g*, they are 53 and 65 percent higher. These data suggest that the embankment motion near each abutment was strongly affected by the embankment itself. This effect is no surprise, considering that the embankments are of fill material and the abutments are massive stiff structures supported by piles.

Among the most notable features of the acceleration time histories recorded on the bridge deck are: (1) a dominant frequency of approximately 2.3 Hz in the east-west components (traces 3, 5, 7, 9, 13, fig. 263), with highest amplitudes of motion occurring between seconds 3 and 9; (2) a dominant frequency of approximately 4.5 Hz in the midspan vertical components (traces 16, 18, 20, 22, fig. 263), with highest amplitudes of motion occurring between seconds 2 and 4; (3) peak accelerations of 0.39 and 0.51 *g*, respectively, in the north-south and east-west directions (traces 8, 7, fig. 263); (4) peak vertical accelerations of 0.50 and 0.23 *g*, respectively, at midspan and above the central support column (traces 16, 21, fig. 263); and (5) a continuation of relatively large amplitude lateral (east-west) and vertical deck motions after the period of strongest ground shaking ended, that is, after approximately second 9.

We also note the coherence of waveforms in several groups of traces from comparable locations and components (compare traces 16, 18, 20, and 22; 17 and 21; 19 and 6; 3, 5, 7, 9, and 13; 11 and 26). The waveform similarities within each of these groups reflect symmetry in the structure and in the placement of accelerometers. The striking differences in waveforms between groups, however, reflect the large-amplitude modal response of the bridge during and after the time of strongest ground shaking. Between seconds 2 and 4, for example, the vertical-component time histories recorded at the center of each span (traces 16, 18, 20, 22, fig. 263) contain high-amplitude cyclic motion at a frequency of approximately 4.5 Hz (vertical-deck modal response) that does not occur in the vertical-deck components recorded adjacent to the central support column and near the abutments (traces 6, 17, 21, 19, fig. 263). Similarly, between seconds 3 and 6, the east-west-component time histories recorded on the roadway deck (traces 3, 5, 7, 9, 13, fig. 263) contain approximately 2.3 Hz cyclic motion (lateral-deck modal response) that does not occur in corresponding-component time histories

recorded at the north and south embankment sites (traces 11, 26, fig. 263). In both time histories, the cyclic motion (deck response) continued at smaller amplitudes after the period of strongest ground shaking had ended. In addition, deck rotation about a horizontal axis parallel to the roadway centerline is evident in the vertical-deck components recorded adjacent to the central support column (traces 17, 21, fig. 263) because, starting near second 5 and continuing through second 19, the two motions are 180° out of phase.

ACKNOWLEDGMENTS

Among the many people who assisted us in obtaining these data, we are particularly grateful to the technicians from the CDMG Office of Strong-Motion Studies, who installed and maintained the equipment; and to the members of the California Seismic Safety Commission, Subcommittee on Instrumentation for Transportation and Other Lifeline Facilities (Robert C. Cassano, L. Dale Mills, John Canestro, Mary W. Henderson, and Tom M. Wootton), who advise and actively support the bridge-instrumentation phase of the California Strong-Motion Instrumentation Program.

REFERENCE CITED

Raggett, J. D., and Rojahn, Christopher, 1978, Use and interpretation of strong-motion records from highway bridges: Federal Highway Administration Report FHWA-RD-78-158, 168 p.

DIGITIZATION AND PROCESSING OF MAIN-SHOCK GROUND-MOTION DATA FROM THE U.S. GEOLOGICAL SURVEY ACCELEROGRAPH NETWORK

By A. G. BRADY, VIRGILIO PEREZ, and P. N. MORK,
U.S. GEOLOGICAL SURVEY

CONTENTS

ABSTRACT

The 1979 Imperial Valley earthquake has increased substantially the number of significant strong-motion accelerograms available for studies of motion close to the causative fault of a moderate earthquake. Scaled peak accelerations reach a maximum of 1.74 g, recorded vertically within 1 km of the fault; seven accelerograms within 7 km of the fault recorded horizontal accelerations greater than 0.5 g. Of 30 main-shock accelerogram recordings from the U.S. Geological Survey network, we chose 22 for digitization from stations that were nearer than approximately 30 km from the Imperial fault.

Preliminary testing for appropriate values of high-frequency cutoff, interpolation density, and long-period limits was required for the special circumstances evident in this family of recordings, to achieve the maximum signal-to-noise ratio at long periods and to reproduce as accurately as possible the peaks in acceleration. As a result, the filter used in correcting the data had a gain of unity between 0.17 and 23 Hz, fell linearly to zero from 0.17 to 0.03 Hz at the low-frequency end, and from 23 to 25 Hz at the high-frequency end. We include here plots of the time histories of corrected acceleration, velocity, and displacement, displayed at 0.01-s intervals, and the response and Fourier spectra for selected components. We briefly note a strong coherence of the displacement pulses on the horizontal components, which confirms the overall accuracy of our processing techniques.

INTRODUCTION

Among the first strong-motion accelerographs installed during the early 1930's by the Seismological Field Survey was one instrument at the Southern Sierra Power Co. terminal station at 302 Commercial Avenue, El Centro, Calif. This strong-motion station, subsequently known as the Imperial Valley Irrigation District substation, has since that time been occupied by a standard accelerograph, while a U.S. Geological Survey (USGS) network of newer 70-mm-film recorders has been expanded throughout the Imperial Valley. The seismicity of this part of California, and the accompanying records recovered from the El Centro station since the 1930's, have resulted in the placement of recorders throughout the Imperial Valley, including the El Centro array transverse to the Imperial fault, a differential-ground-motion array of digital recorders (Bycroft, this volume) in El Centro, and instruments in several towns from the United States-Mexican border northward to the Salton Sea (Matthiesen and Porcella, this volume). The main-shock records of the 1979 earthquake provided by the 70-mm-film recorders are the subject of this report. These recorders consist of three accelerometers, two in the horizontal and one in the vertical direction. The three traces are written on photographic film, together with at least one reference trace and a time-mark trace giving half-second time intervals after triggering. All recorders have WWVB radio receivers for the recovery of absolute time and are designed to run for at least 60 s after triggering to allow the complete time code to be recorded.

Of the 30 main-shock records obtained from the USGS network (Matthiesen and Porcella, this volume), we chose 22 for digitization that were from stations less than approximately 30 km from the 1940 Imperial fault trace. Peak accelerations beyond this distance reached no more than 0.05 g except on the record from Coachella Canal station 4, which showed a typical soil-structure interaction (Porcella and Matthiesen, 1979) and is included in this report. Two records from stations within this 30-km distance were not included owing to expected difficulties in digitization and processing (El Centro array station 9) or to less than 0.05 g peak acceleration (Salton Sea Wildlife Refuge). The 22 records processed were from the following stations (see fig. 264, based on Matthiesen and Porcella, this volume): El Centro array stations 1 through 8 and 10 through 13, Bonds Corner, El Centro differential array, Brawley, Holtville, Calexico, Parachute Test Site, Calipatria, Superstition Mountain, Plaster City, and Coachella Canal station 4.

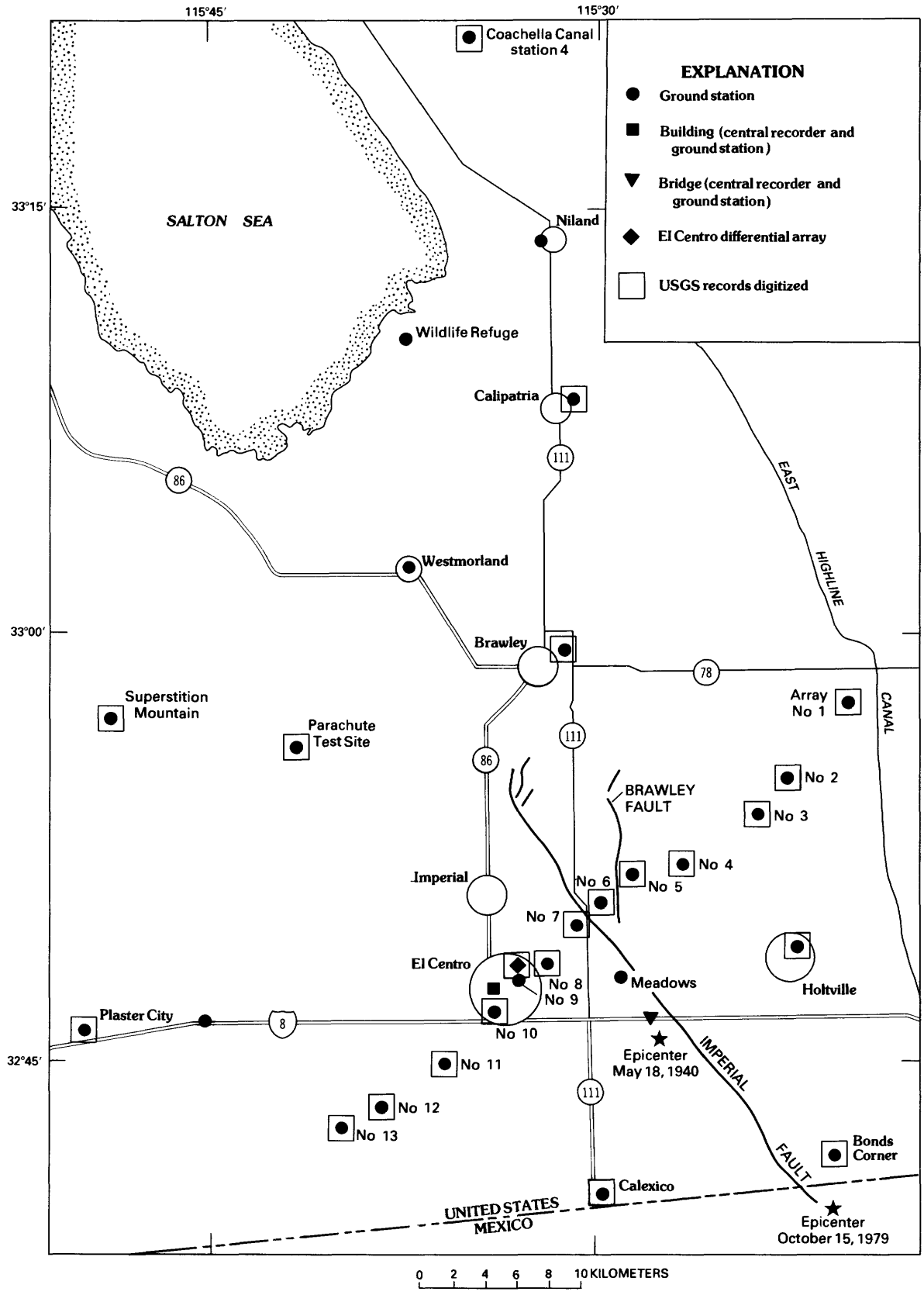

FIGURE 264.—Strong-motion stations in Imperial Valley, Calif. (from Porcella and Matthiesen, 1979).

In the following sections we describe in some detail the special circumstances that contributed to our digitizing and processing decisions with regard to this set of 70-mm-film recordings. Records were digitized on a laser-operated trace-following automatic scanner. The maximum duration processed for this report was 40 s, initially digitized in approximately 10 s frames. We also report difficulties with faint traces in the first 10 s of several records close to the fault, as well as confirmation of the quality of the reassembly of adjacent frames of digitized data.

Before processing the digitized data, we tested the records with regard to the choice of proper parameters for the data-correction procedures: the long-period limit (finally chosen as 6 s), the high-frequency limit (a reasonably standard 23 Hz), and the sampling frequency (finally chosen at 100 samples/s). The resulting processed data, originally provided on two seven-track magnetic tapes containing 11 records each, are available from the Environmental Data and Information Service, U.S. National Oceanic and Atmospheric Administration, Boulder, CO 80302; the computer plots were presented by Brady and others (1980). The reader is also referred to the other chapters in this volume and to the preliminary report by Porcella and Matthiesen (1979).

DIGITIZATION PROCEDURES

Contact prints prepared from the original records were processed on a trace-following automatic digitizer capable of averaging 600 points/s at unequal time intervals. Operator intervention is required for decisions at trace intercepts, and for selecting visually located points when the trace is too pale for automatic detection. The frame size of the equipment limits the record duration scanned at one setup to approximately 11½ cm, corresponding to 11½ s of elapsed time. Vertical butting lines are scribed on the prints at 9½-cm spacing to allow a 1-cm overlay at each edge of the frame, and these lines are digitized with each frame's data to facilitate the reassembly of records longer than one frame.

On many of the main-shock accelerograms an aftershock arrival occurs between 35 and 40 s after triggering. To avoid confusion between the displacements from this aftershock and the noise from processing the extremities of the main shock, the processing described in the following sections has been carried out on nearly all records for 36 s contained in four frames of digitizing. Three of the records, from stations most distant (farther than 25 km) from the fault trace—Superstition Mountain, Plaster City, and Coachella Canal station 4—have been digitized for less than 30 s. At these distances, the acceleration amplitudes are as low as 0.02 g at the end of the digitized duration.

The quality of the reassembly procedures, as outlined by Porter and others (1978), was verified by checking the consistency of location of the intersections of butting lines with reference traces when these intersections were repetitively digitized on successive frames. In addition, subsequent Fourier analysis indicated no abnormal content at a period of 9½ s, the existence of which would have been the first indication not only of faulty reassembly but also of optical distortion within the digitizing system.

The preliminary computer run that reassembles the traces from the individual digitizing of each frame also carries out some elementary Hanning smoothing (Blackman and Tukey, 1958) and removal of points to reduce the average density to approximately 125 points/s. All local peaks are retained during this step, including the maximum digitized peak. An exception is when manual intervention is required during digitization, when individual points are chosen by the operator that are so widely separated in the y-direction that elementary Hanning smoothing clips them. Points at this reduced density are transferred to the stage 1 processing for uncorrected data (Hudson, 1976) and for subsequent processing according to current USGS practice (Basili and Brady, 1978).

CONVERSION TO CORRECTED ACCELERATIONS

Correction of the basic acceleration ordinates derived, as described in the preceding section, from the film record involves the removal by filtering of high-frequency noise, the removal by filtering of long-period noise, the selection of a sampling frequency compatible with the high-frequency filter, and an instrument correction to take account of the dynamic characteristics of the transducer. Selection of the filter corners and of the interpolation rate is discussed below; the instrument correction is standard mathematical procedure for a viscously damped single-degree-of-freedom oscillator (see, for example, Trifunac, 1962).

Major efforts have been exerted in data processing since the California Institute of Technology (CIT) project with the 1971 San Fernando, Calif., earthquake accelerograms was completed (Trifunac and Lee, 1973; Hudson 1976). We particularly emphasize the selection of the long-period limit, beyond which all Fourier content is removed (Basili and Brady, 1978; Trifunac and Lee, 1978; Fletcher and others, 1980), and the details of the filtering procedures.

Several factors have influenced selection of the long-period limit for the Ormsby filter used in processing the Imperial Valley digitized data. We restrict our discussion to the close-in records, that is, those within approximately 10 km of the nearest point on the 1979 fault trace (fig. 264; see Matthiesen and Porcella, this volume).

The stations at Calexico and Holtville, and El Centro array stations 3 and 11 (fig. 264), are approximately equidistant from each end of the fault rupture. The strong-motion duration (time span between the first and last peak greater than $0.10g$) on the records from these stations of from 5.7 to 10.8 s (Porcella and Matthiesen, 1979) indicates that we should attempt to force the long-period limit out to 6 s. The record length of 36 s provides an upper bound to termination of the cutoff ramp in the period domain. The corresponding ramp in the frequency domain is therefore between 0.03 and 0.17 Hz. An Ormsby filter with this ramp (Df=0.14 Hz) requires a filter-weighting-function length L of 14 s (that is, $2/Df$), a large fraction of the record length of 36 s. Thus, particularly for those records with maximum amplitudes occurring as early as 3 s after triggering, we might expect that processing noise becomes predominant as the 6-s long-period limit is approached.

A series of test runs was performed on the El Centro array station 7 record, recovered at ground level from a one-story building at Imperial Valley College in El Centro, Calif., to investigate the effect of varying the long-period filter parameters. The long-period limit (cutoff period, T_c) was varied from 3.7 to 6 s, as indicated in table 41, which also lists additional details of the filter parameters applied to the three components on this record. For this preliminary test we interpolated the data at 50 points/s and filtered them to remove high (above 23 Hz) frequencies. The ramp in the frequency domain lies between f_t and f_c, the termination and cutoff frequency, respectively, and in the time domain (where the ramp falls off hyperbolically) between T_c and T_t, the cutoff and termination period, respectively. As we attempted to lengthen the cutoff period T_c to examine longer period content, we were forced into greater lengths L of the filter weighting function. The test-run plots (fig. 265) show the effects of these longer filters. Taking into account the scale changes on the individual plots and our past experience with the details of this type of filter adjustment, we assume that, so far as the first 5 s of record is concerned, the first two components (230° and up) have not been impaired from lengthening the cutoff period, whereas the 140° component shows some additional motion arising either directly from filter processing or from the additional entry of further long-period signal contaminated to some extent by noise.

TABLE 41.—*Low-frequency-filter parameters for three processing schemes applied to the main-shock records from El Centro array station 7 during test runs*

[Df, filter ramp (f_c–f_t); L, weighting-function length ($2/Df$)]

Scheme	Frequency		Period		Df (Hz)	L (s)
	Termination f_t	Cutoff f_c	Cutoff T_c	Termination T_t		
1	0.07	0.27	3.7	14	0.20	10
2	.03	.20	5	33	.17	12
3	.03	.17	6	33	.14	14

Before we can conclude that the 6-s filter is satisfactory, the following additional comments on the appearance of the time histories in figure 265 are required. First, the 230° component on the original recorded accelerogram exhibits a pronounced trend of increasing acceleration amplitude, in the negative direction, within the first 4½ s. This trend is transmitted through integration to the velocity and displacement, which also exhibit a rather pronounced motion in this direction. Our previous experience with such behavior in corrected displacement time histories leads us to conclude that the signal-to-noise ratio in the processed data is insufficiently high and that these apparently excessive displacement amplitudes before the arrival of the shear wave are spurious. The appearance here of motion in the original accelerogram before any processing confirms, however, that the displacements during the first 5 s are based on a visible signal in the accelerogram, even though they change with application of the various filters.

Second, the 4.75-s oscillations evident in the vertical components of displacement, from 5 s into the record until the end, are visible also in the recorded acceleration. The amplitudes of these acceleration oscillations correspond to those evident in displacement with 5- and 6-s long-period filters (figs. 265*E* and 265*F*, respectively). The 3.7-s filter, however, theoretically reduces the content of a 4.75-s Fourier component by 30 percent, and this reduction is evident in the displacement (see fig. 265*D*). Thus, these oscillations reflect true ground motion and not processing noise.

Third, the 140° components (figs. 265*G*–265*I*) exhibit a characteristically worsening noise problem during the first 5 s as the filter-window length is increased. The 6-s filter (fig. 265*I*) extends 7 s on each side of its midpoint (L=14 s, table 41), well into the high-amplitude accelerations, and the resulting displacements cause some concern about forcing the long-period limit to 6 s.

As a result of these preliminary tests, we processed a selection of 11 close-in records according to scheme 3 of table 41 to ascertain whether a search for 6-s content was justified in light of the displacement distortions that could be expected on some components (for example, the 140° components above), owing to mismatching of filter properties with record characteristics and to processing noise. Because the results were encouraging, we elected to utilize the filter parameters of scheme 3 and proceeded with further elementary testing at the high end of the frequency range of interest to determine whether frequencies of greater than 25 Hz should be

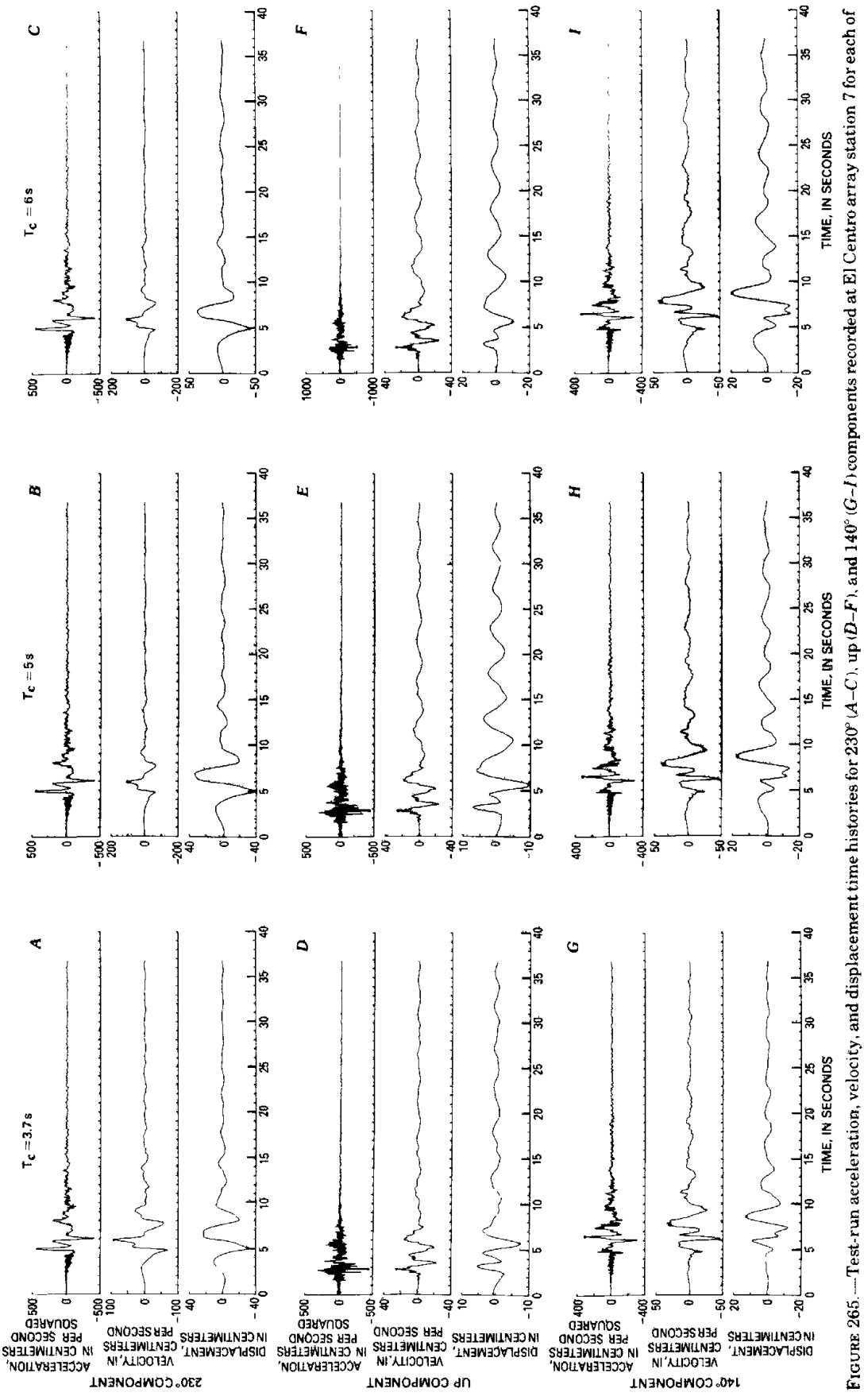

FIGURE 265.—Test-run acceleration, velocity, and displacement time histories for 230° (*A–C*), up (*D–F*), and 140° (*G–I*) components recorded at El Centro array station 7 for each of three cutoff periods T_c.

TABLE 42.—*Peak accelerations for several main-shock records at consecutive stages of processing*

Station	Component	Peak acceleration (*g*)	Uncorrected acceleration (*g*)	Corrected acceleration (cm/s² (*g*))	
				50 points/s	100 points/s
El Centro array station 7	230°	0.52	0.47	450.7 (0.46)	453.6 (0.46)
	up	.65	.63	431.2 (0.44)	503.6 (0.51)
El Centro array station 6	230°	.45	.44	422.7 (0.43)	428.1 (0.44)
	up	1.74	1.70	1,566.5 (1.60)	1,662.7 (1.69)
Bonds Corner	230°	.81	.78	766.0 (0.78)	770.4 (0.79)
	up	.47	.44	318.6 (0.32)	347.7 (0.35)
El Centro array station 8	230°	.50	.48	436.0 (0.44)	457.4 (0.47)
	up	.55	.48	339.3 (0.35)	405.9 (0.41)

included in the corrected data.

Until peak ground acceleration loses some of its current importance in structural design and earthquake research, an explanatory note is required to discuss the apparent discrepancies between the peak-acceleration values at different stages of processing. Table 42 lists these values for components transverse to the fault and vertically upward on four close-in records: El Centro array stations 6 through 8, and Bonds Corner. The peak accelerations, scaled from the original recordings, were reported earlier by Porcella and Matthiesen (1979). The uncorrected accelerations were obtained from automatic digitization, although some peaks were manually inserted by the operator at the correct locations because very faint traces caused automatic trace following to fail. The differences between these two sets of peaks can be attributed to subjective or instrumental variations in the treatment of details of the records and to occasional partial loss of a lone manually digitized peak. In general, the automatic digitizer produces peak values a few percent lower than the original scaled peaks. The corrected accelerations (table 42) are the peak values after correction for instrument characteristics and low- and high-frequency filtering. Here, the low-frequency filter has a ramp of from 0.03 to 0.17 Hz, and the high-frequency filter of from 23 to 25 Hz.

The peak values are lost, without exception, by as much as 30 percent, as reported by Hudson (1976) for the CIT processing program. Possible causes for these losses are: (1) interpolation at too low a time interval, (2) high-frequency filtering out of the high frequencies that contain the peak accelerations, and (3) application of the instrument correction. Causes 2 and 3 can be mostly eliminated by noting on the original records that the maximum frequencies present during recording of the peak values are within the range 15–20 Hz and that the natural instrumental frequency lies between 25 and 27 Hz. The interpolation density is probably more important in improving the relation between corrected and uncorrected peaks, whether this improvement is warranted or not, as shown by interpolation at 100 points/s, which recovers more of the scaled peaks (table 42).

Details of the highest peak value (up component on El Centro array station 6 record), scaled at 1.74 *g*, are shown in figure 266, which plots the uncorrected and corrected points for a few hundredths of a second on either side of the critical peak. The 23-Hz filter has smoothed the uncorrected points and eliminated the 1.74 *g* peak, and thus allows a different peak to assume the role of the corrected peak. The effects of interpolation at 100 points/s is evident, as well as the phase lag of the instrumental recording (nominally one-fourth the instrumental free period; here, 0.039/4=9.75 ms). Owing to these interpolation tests, the outputs for corrected acceleration, velocity, and displacement are given at equal intervals of 0.01 s.

Table 43 verifies the minor role that the inclusion of high (greater than 25 Hz) frequencies plays in the recovery of scaled maximum peak values during application of the correction procedures to this data set and lists the peak acceleration, velocity, and displacement after high-frequency filtering at 35 and 50 Hz for two components with particularly severe peak-value losses during correction (up component on Bonds Corner records and 230° component on El Centro array station 8 [Cruickshank Road] record). The time spacing was 0.01 s for this

TABLE 43.—*Comparison of peak acceleration, velocity, and displacement for different filters applied to main-shock components with severe peak-value loss during correction*

Station and component	Peak value	High-frequency filter (ramp)		
		25 Hz (23–25 Hz)	35 Hz (33–35 Hz)	50 Hz (48–50 Hz)
Bonds Corner, up...	Acceleration (cm/s²)	347.7	340.6	337.4
	Velocity (cm/s)	12.17	12.15	12.15
	Displacement (cm)	2.46	2.46	2.46
El Centro array station 8, 230°.	Acceleration (cm/s²)	457.4	462.1	459.1
	Velocity (cm/s)	47.71	47.72	47.72
	Displacement (cm)	29.34	29.34	29.34

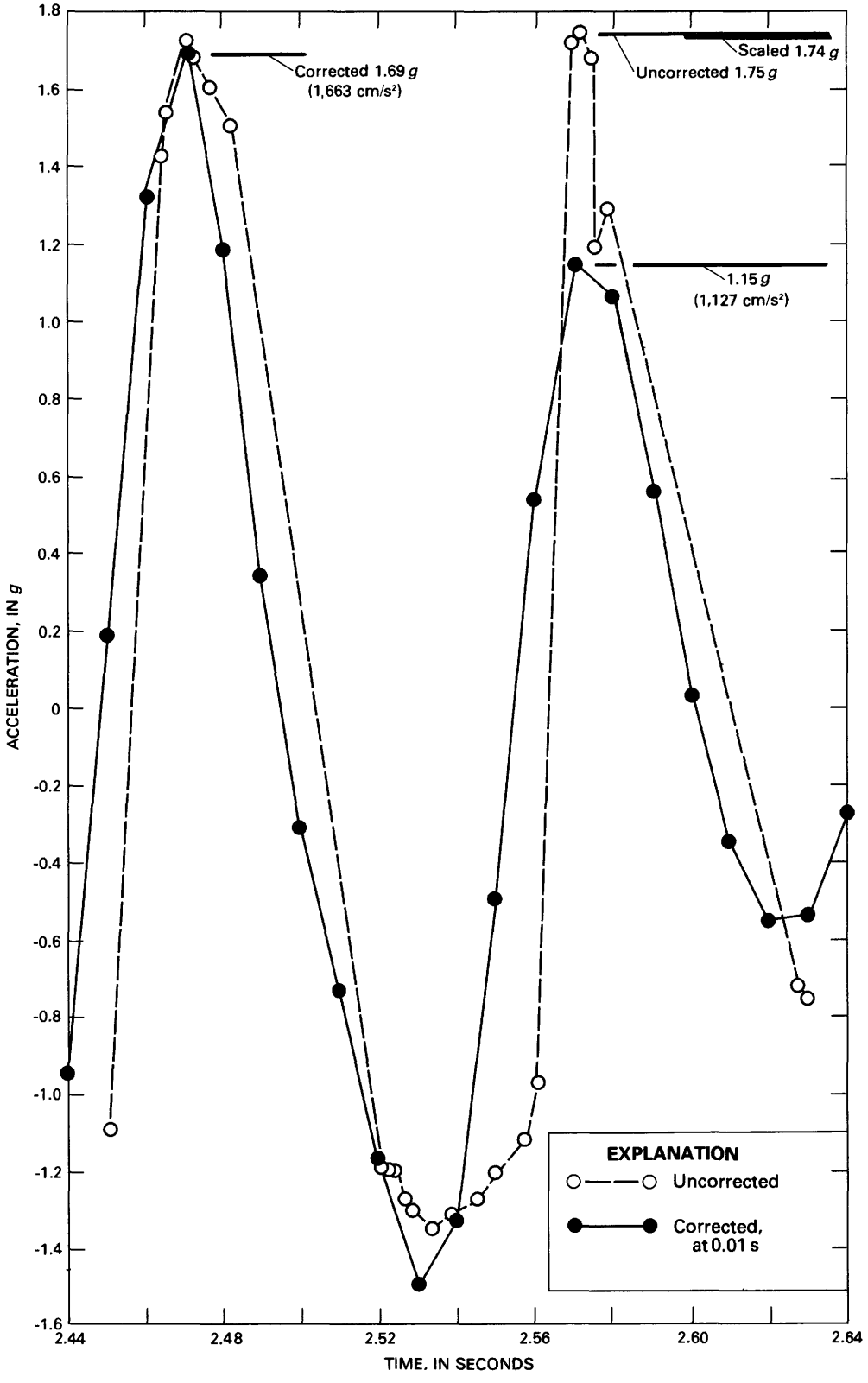

FIGURE 266.—Details of peak values of up components on main-shock accelerogram from El Centro array station 6.

test, and so the 50-Hz results are meaningful, although the actual filtering step was performed at twice this density. Table 43 indicates that for these components there is no advantage in raising the high-frequency limit beyond 25 Hz solely to recover the scaled maximum peak accelerations. This result is to be expected if the peak occurs during oscillations at a frequency considerably lower than 25 Hz, as on many records of this event, although these records may still contain information of very low amplitudes at frequencies higher than 25 Hz. Thus we will generally continue to use a high-frequency filter with a ramp of from 23 to 25 Hz. We can subsequently investigate frequencies higher than 23 Hz, if required, from the uncorrected data.

REPRESENTATIVE SAMPLES OF ROUTINE PROCESSING

We present here a representative sample of the corrected acceleration, velocity, and displacement time histories, the response spectrum on tripartite axes, and the Fourier spectrum on log-log axes, calculated by the fast Fourier transform (FFT) algorithm. The sampling rate is 100 points/s, and the data is band passed with ramps of from 0.03 to 0.17 Hz and from 23 to 25 Hz. We consider three groups of specific components from records either close to the fault or within El Centro: (1) the vertical components on the records from Bonds Corner and El Centro array stations 6 and 7, (2) the component transverse to the fault on the records from El Centro array stations 6 and 7, and (3) the component transverse to the fault on the records from El Centro array stations 8 and 10 and the El Centro differential array.

Plots of the processing of the vertical components of ground acceleration at the three stations closest to the fault—that is, Bonds corner (6 km epicentral distance, within 3 km of the fault) and El Centro array stations 6 (Huston Road) and 7 (Imperial Valley College) (within 1 km on either side of the fault)—are included in figures 267 (corrected time-history data), 268 (response spectra) and 269 (Fourier spectra). This first group of components includes the El Centro array station 6 component with a scaled peak of 1.74 g. These plots indicate the presence of high-frequency energy, particularly between 10 and 20 Hz. The acceleration plots are not designed to show this feature particularly clearly because the entire record (almost 40 s) is plotted on only one section of the time axis. Nonetheless, the arrival of the high-amplitude packet at El Centro array stations 6 and 7 approximately 2.5 s after triggering is particularly apparent. The long-period content of vertical motion discussed above is evident in the displacement at all three sites and has a period at El Centro array stations 6 and 7 of approximately 4.75 s. (figs. 268*B*, 268*C*).

The second group of components (figs. 270–272) consists of high-amplitude horizontal accelerations from stations close to the fault, as portrayed on the records from El Centro array stations 6 and 7. The absence of high-frequency ripple on the El Centro array station 7 record between 4.5 and 7.5 s after triggering is reflected in the spectral plots. None of the other records, in a direction transverse to the fault, were as free of high-frequency content as the El Centro array station 7 record during the large-amplitude accelerations.

The third group of components (figs. 273–275) are those from records at three USGS-operated stations that are closest to the Imperial County Services Building in El Centro (see Rojahn and Mork, this volume): El Centro array station 8 (95 E. Cruickshank, approximately 4 km northeast of the building), the El Centro differential array (Dogwood Rd.; a film recorder placed near the recorders of the digital array, approx 3 km east of the building), and El Centro array station 10 (Community Hospital at Imperial and Ross Rds., approx 1.5 km S. of the building). Taking into account the 180° difference in direction at El Centro array stations 8 and 10, the displacement pulse associated with the transverse shear-wave arrival is remarkably coherent across this section of the city and has a peak displacement within a few centimeters of the average of 30 cm. However, falling off of the peak acceleration from 457.4 to 168.2 cm/s^2 indicates an attenuation of the high-frequency content (though present to the extent expected for stations this close to the causative fault) from El Centro array station 8 to 10. The response and Fourier amplitude spectra for El Centro array stations 8 and 10 (figs. 274, 275) show clearly the consistent level of long-period (for example, longer than 1 s) content and the gradual decay of high-frequency (between 3 and 10 Hz) content.

EL CENTRO ARRAY CALCULATED GROUND DISPLACEMENT

The records from the 13 stations in the El Centro array provide an opportunity to check the long-period performance of the processing described here. We exclude the record from El Centro array station 9, not yet digitized, and add that from the film recorder stationed next to the digital recorders of the differential array (see Matthiesen and Porcella, this volume, and Bycroft, this volume). All except the differential-array instrument are alined approximately parallel and transverse to the Imperial fault. All the records show an exceptionally clear transverse-displacement pulse, identified as the direct S wave in the southwest direction, with a maximum peak-to-peak amplitude, at El Centro array station 6 within 1 km of the fault, of 88 cm and a period of 3.6 s. Figure 276 plots the transverse-displacement

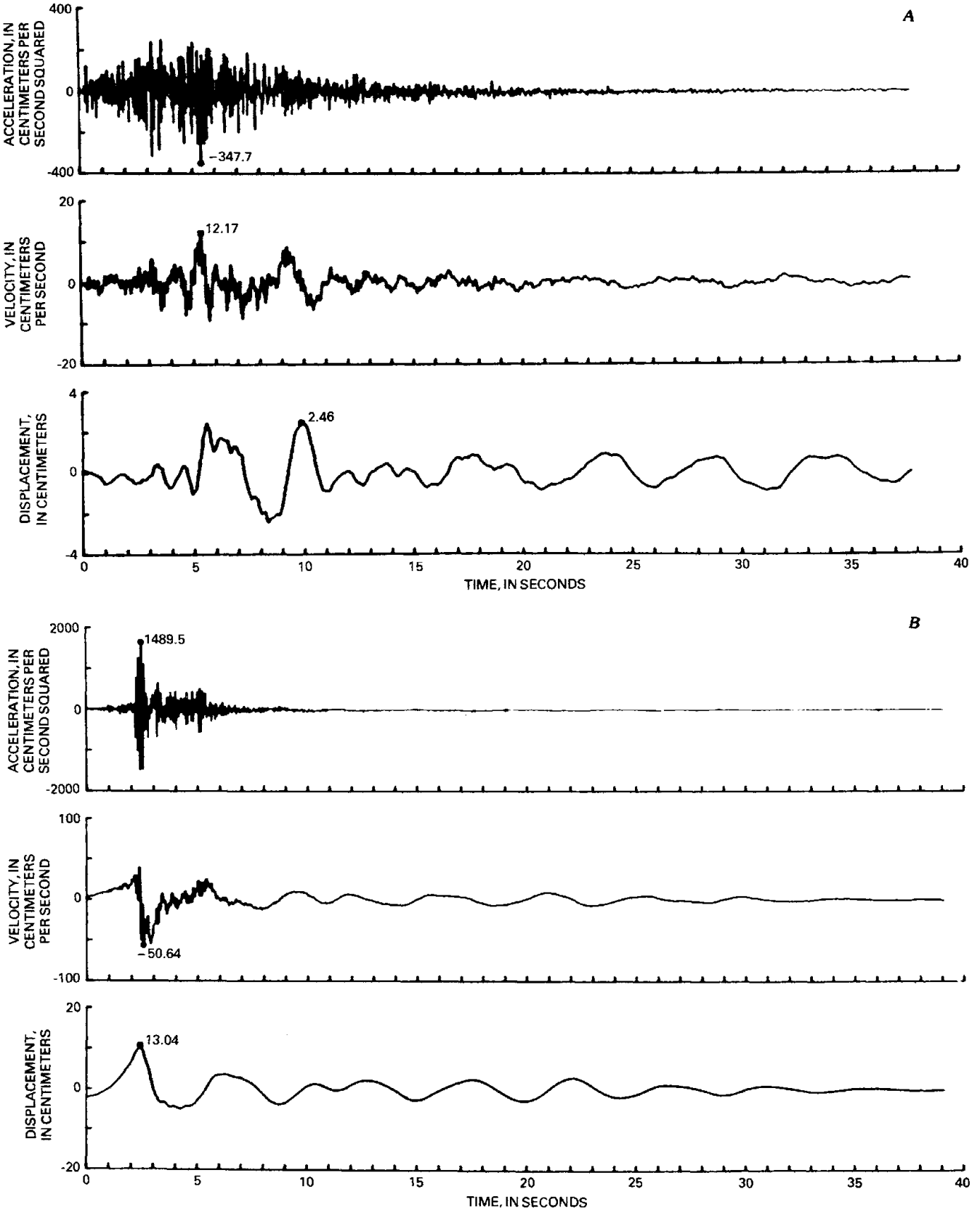

FIGURE 267.—Corrected main-shock acceleration, velocity, and displacement time histories for vertical components at Bonds Corner (*A*) and El Centro array stations 6 (*B*) and 7 (*C*). Dot shows peak value.

time histories for nine records containing the WWVB time code, adjusted in the time direction such that all records are synchronized to the WWVB time code (see table 44). The displacement scales remain unchanged from those used on the plots of corrected acceleration, velocity, and displacement time history (figs. 270*A*, 273*A*). From a value of 88 cm at El Centro array station 6, the peak-to-peak amplitude falls off until at stations 1 and 13, 22 km on either side of the fault, the pulse measures 4 and 3 cm, respectively.

TABLE 44.—*Main-shock WWVB trigger times for nine stations in the El Centro array*

[Arrival time is in minutes and seconds after 288d 23h G.m.t.]

El Centro array station	Arrival time
1	17:02.24
2	17:01.18
4	17:01.78
5	17:01.39
6	17:01.40
8	17:00.62
11	17:00.48
12	17:01.48
13	17:02.45

We can confidently identify the *S*-wave pulse on these nine records and its arrival times at the various stations in the El Centro array. This pulse's ground motion in the 230° direction (approx SW.) begins at 17:05.0 at station 8, at 17:06.1 at station 6 on the other side of the fault, and as late as 17:07.4 at station 1, 22 km northeast of the fault. The displacement record both before and after the *S*-wave passage is surprisingly coherent along the entire array. All stations show the preliminary motion to the northeast (downward in fig. 276), as was expected from the original accelerograms on which the motion was first noted. Stations more distant from the fault indicate some signal-to-noise problems, although the oscillatory motion, with a 4.75-s period, is evidently associated with conspicuous vertical motions (fig. 267*C*) with the same period.

CONCLUSIONS

From tests on the high-frequency content of the October 15, 1979, earthquake accelerograms, we have applied a high-frequency limit of 23 Hz and a final sampling rate of 100 points/s. The long-period limit was chosen at 6 s, and the rolloff termination at 33 s. The processed length of the records generally is approximately 36 s.

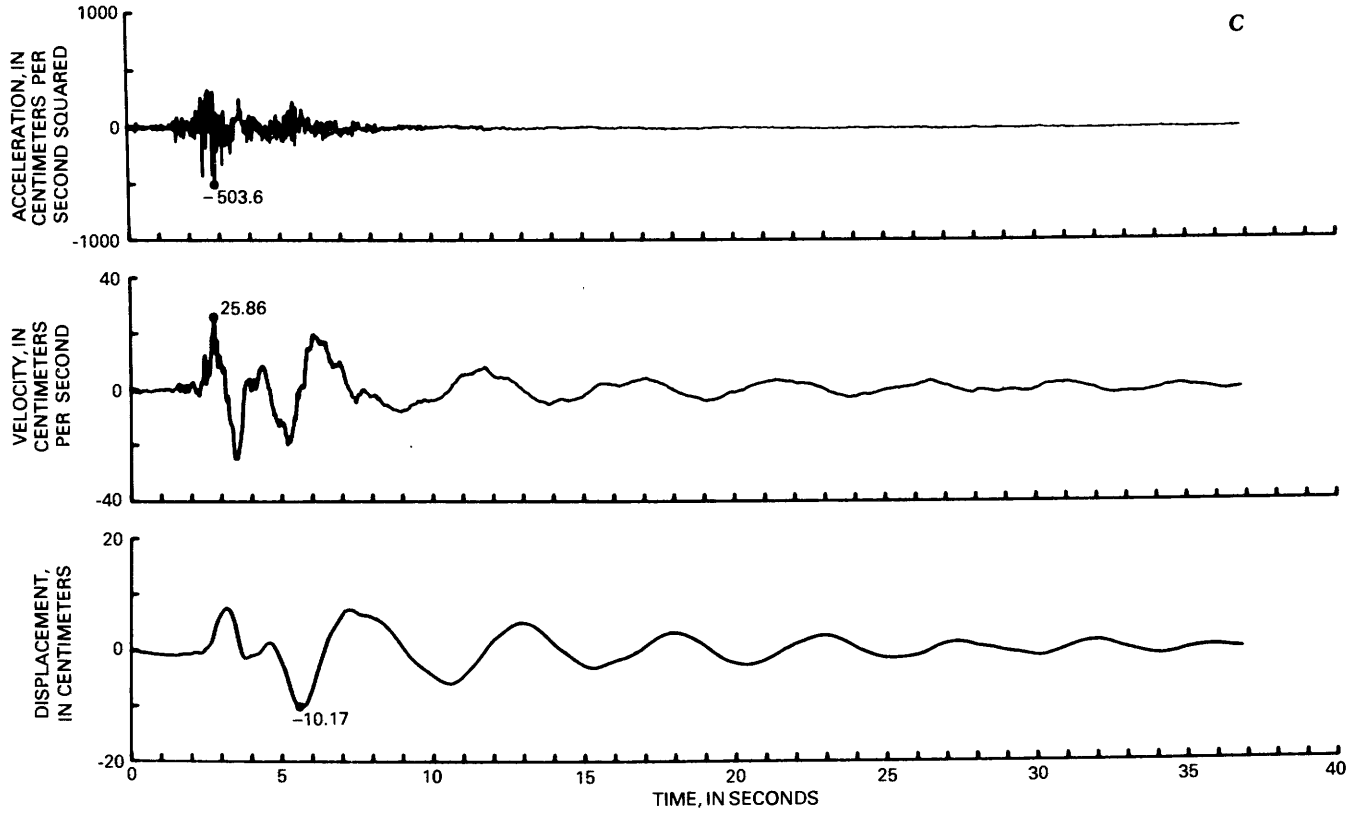

FIGURE 267.—Continued

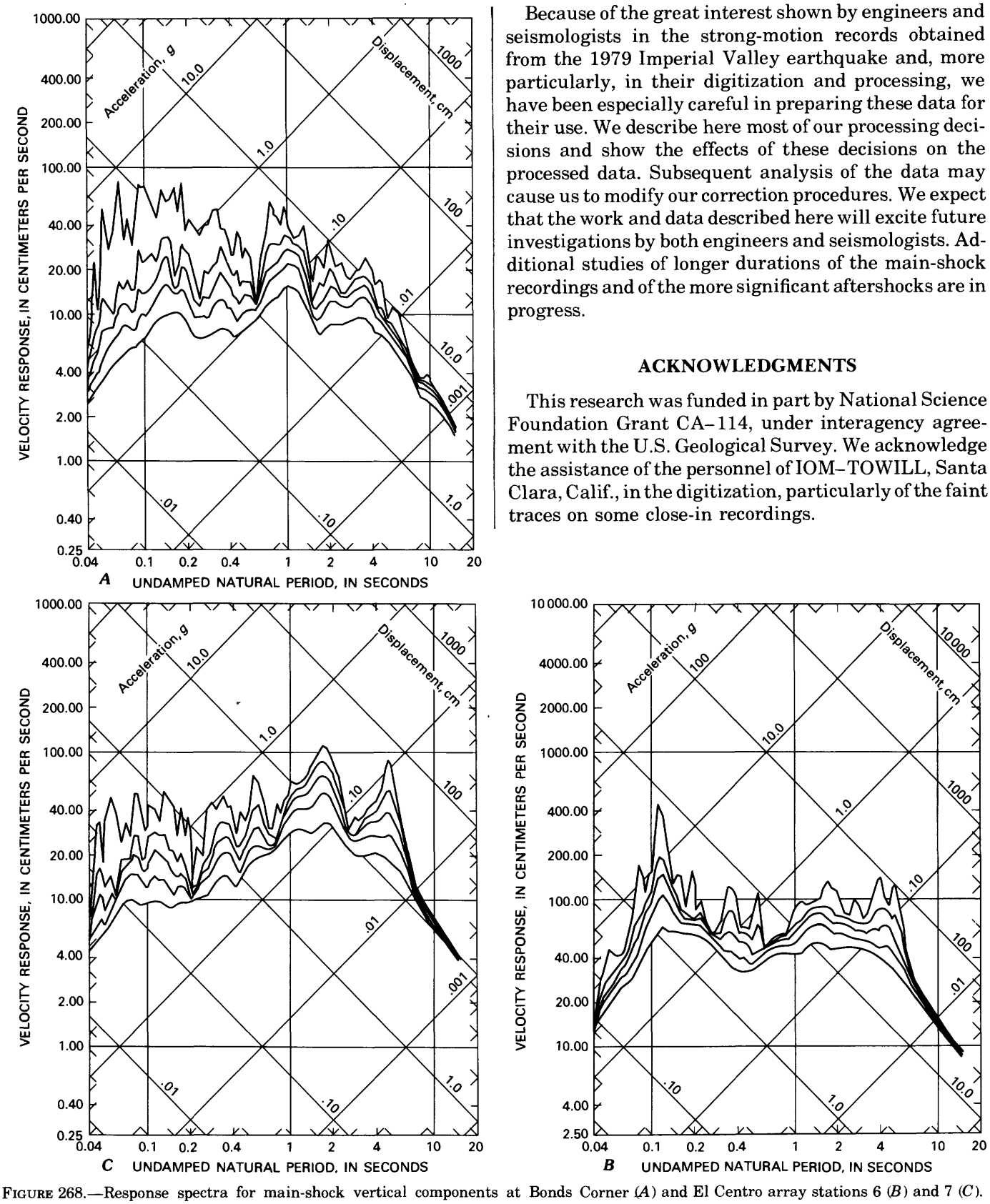

FIGURE 268.—Response spectra for main-shock vertical components at Bonds Corner (*A*) and El Centro array stations 6 (*B*) and 7 (*C*).

Because of the great interest shown by engineers and seismologists in the strong-motion records obtained from the 1979 Imperial Valley earthquake and, more particularly, in their digitization and processing, we have been especially careful in preparing these data for their use. We describe here most of our processing decisions and show the effects of these decisions on the processed data. Subsequent analysis of the data may cause us to modify our correction procedures. We expect that the work and data described here will excite future investigations by both engineers and seismologists. Additional studies of longer durations of the main-shock recordings and of the more significant aftershocks are in progress.

ACKNOWLEDGMENTS

This research was funded in part by National Science Foundation Grant CA–114, under interagency agreement with the U.S. Geological Survey. We acknowledge the assistance of the personnel of IOM–TOWILL, Santa Clara, Calif., in the digitization, particularly of the faint traces on some close-in recordings.

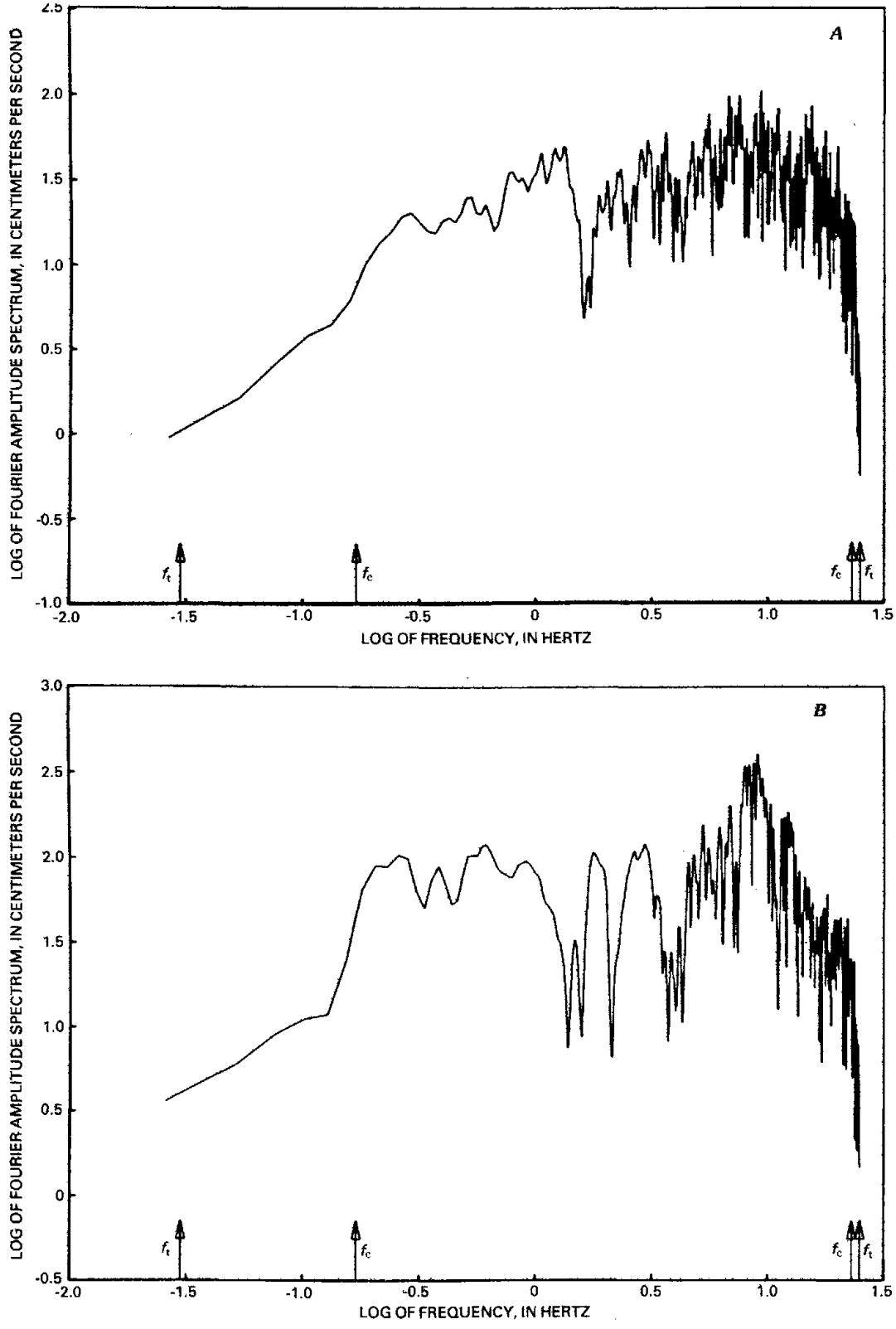

FIGURE 269.—Fourier amplitude spectra for main-shock vertical components at Bonds Corner (*A*) and El Centro array stations 6 (*B*) and 7 (*C*). Cutoff and termination frequencies, f_c and f_t, respectively, indicated by arrows.

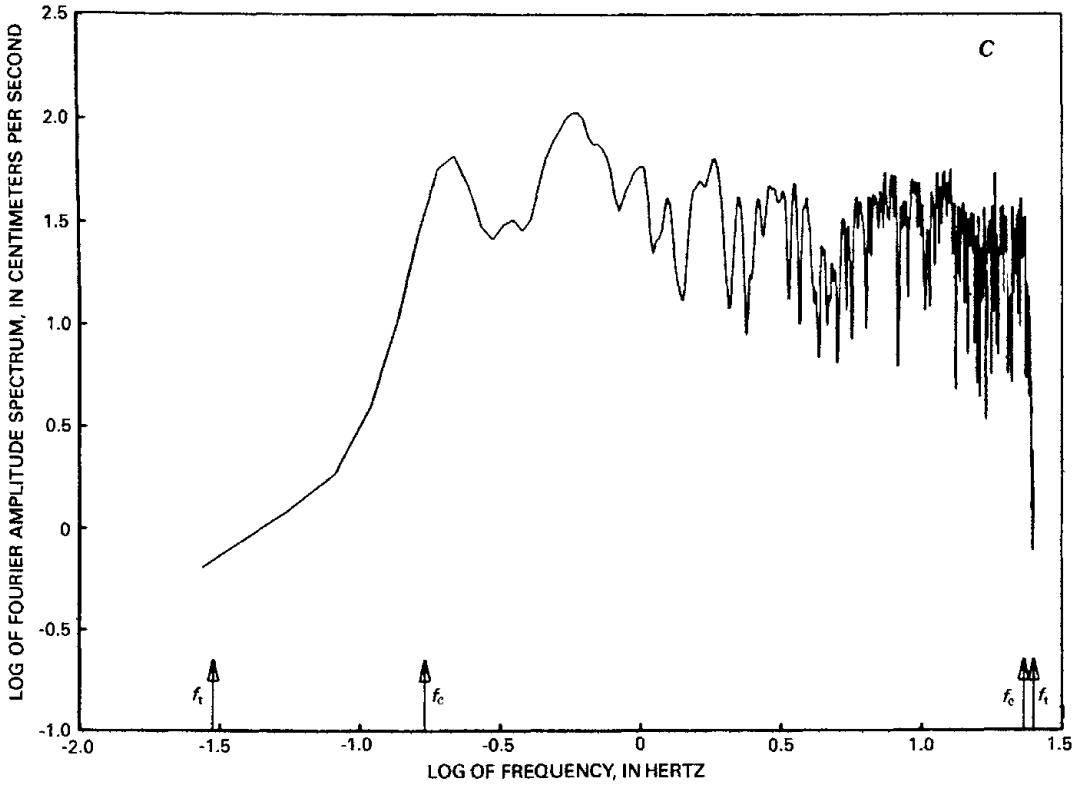

FIGURE 269.—Continued

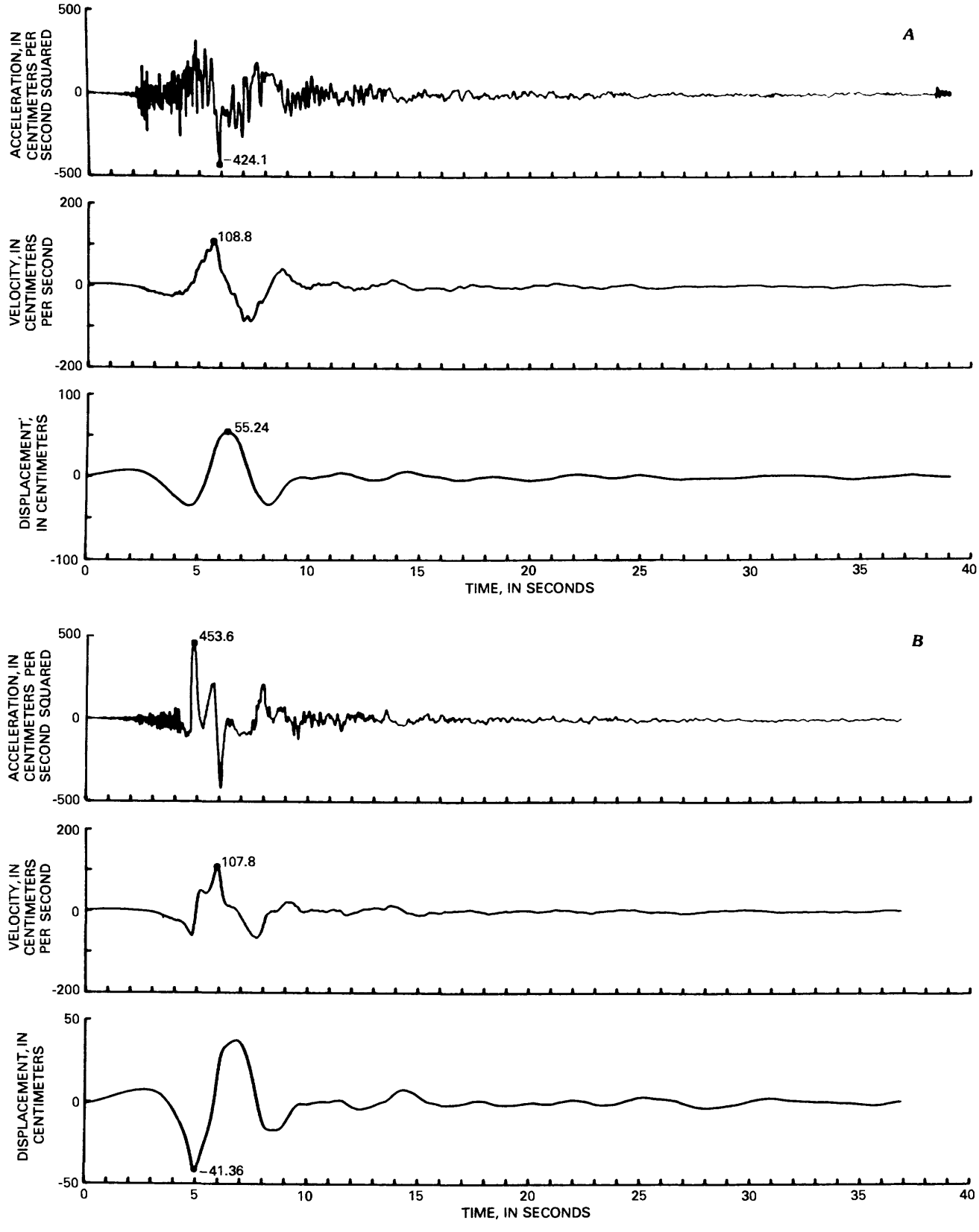

FIGURE 270.—Corrected main-shock acceleration, velocity, and displacement time histories for components transverse to fault at El Centro array stations 6 (*A*) and 7 (*B*). Dot shows peak value.

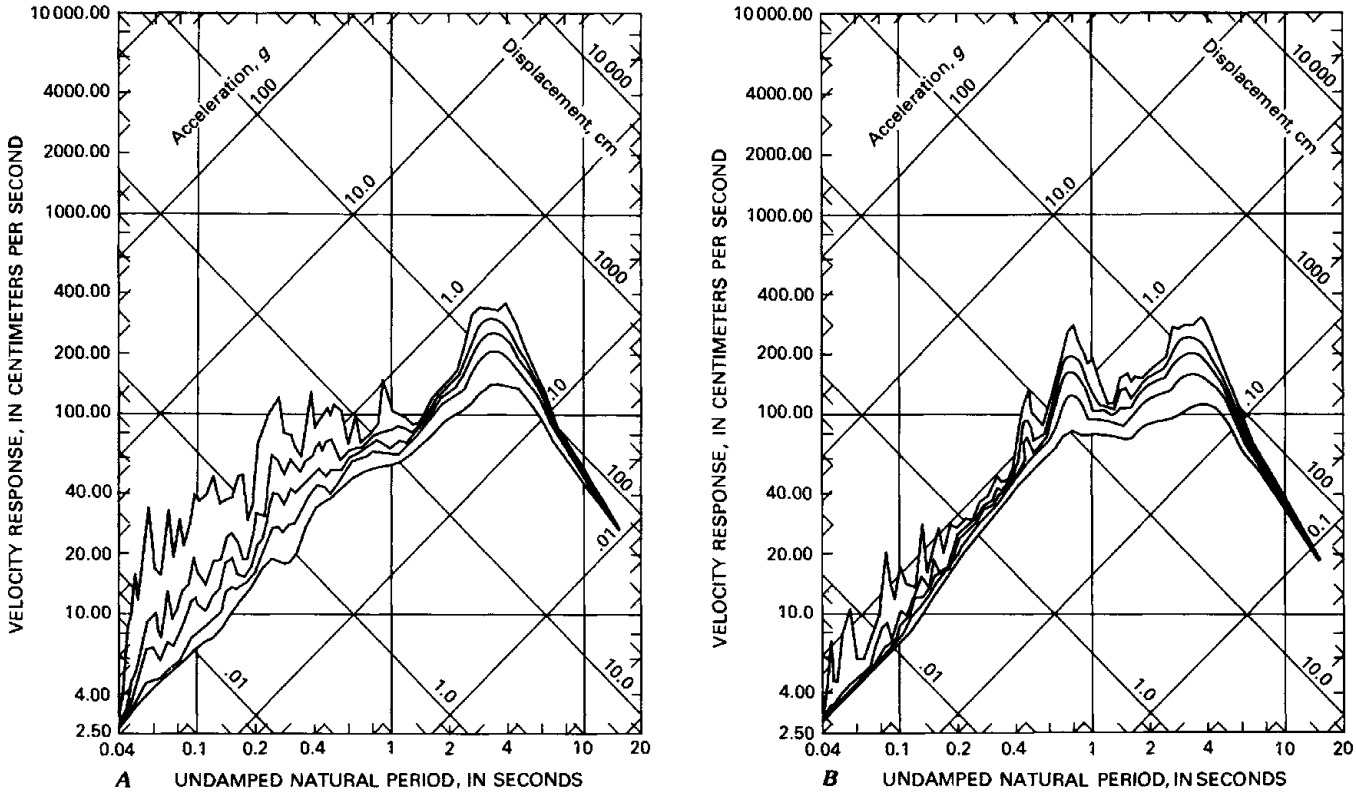

FIGURE 271.—Response spectra for main-shock components transverse to fault (230° direction) at El Centro array stations 6 (*A*) and 7 (*B*).

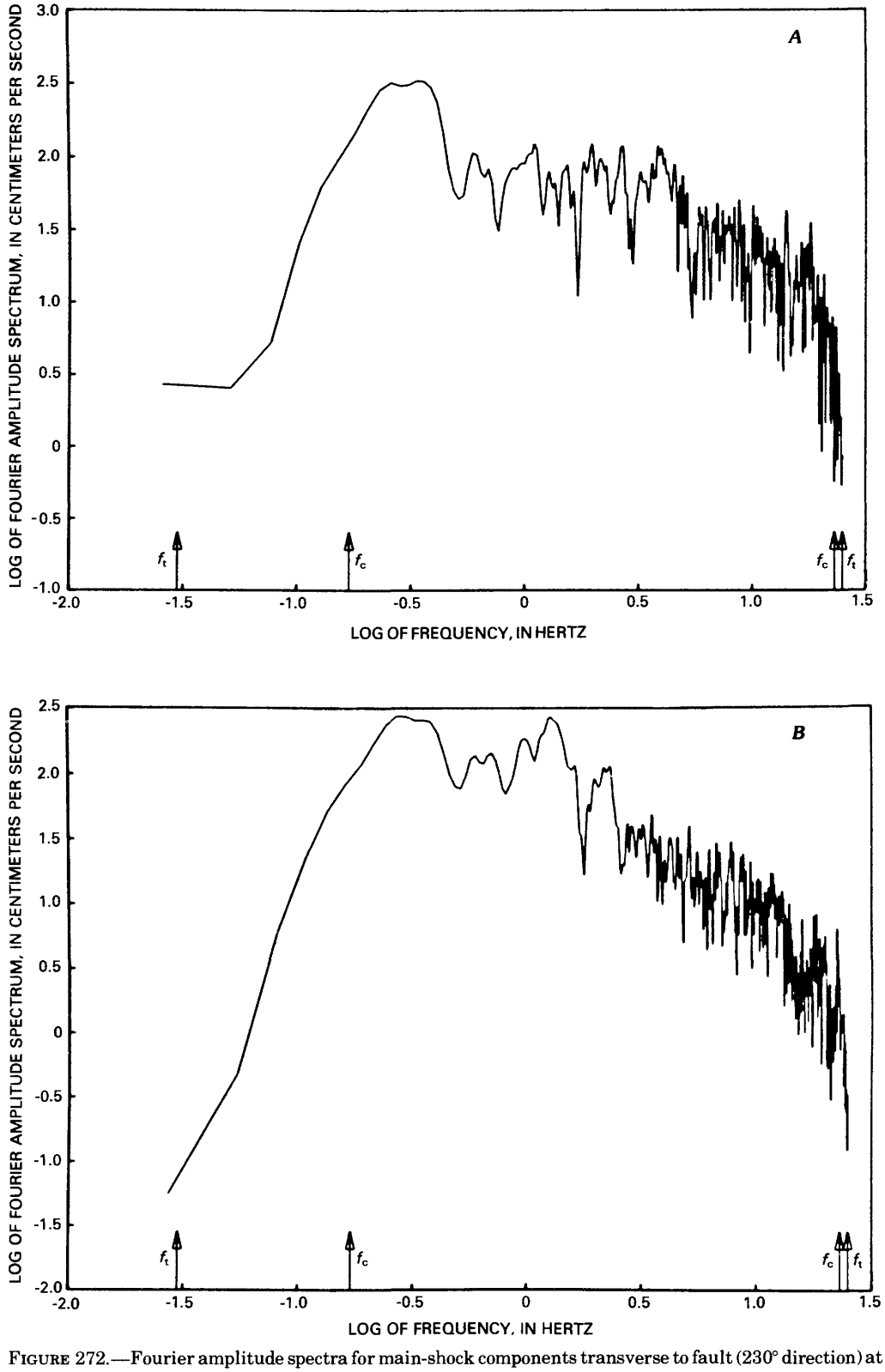

FIGURE 272.—Fourier amplitude spectra for main-shock components transverse to fault (230° direction) at El Centro array stations 6 (*A*) and 7 (*B*). Cutoff and termination frequencies, f_c and f_t, respectively, are indicated by arrows.

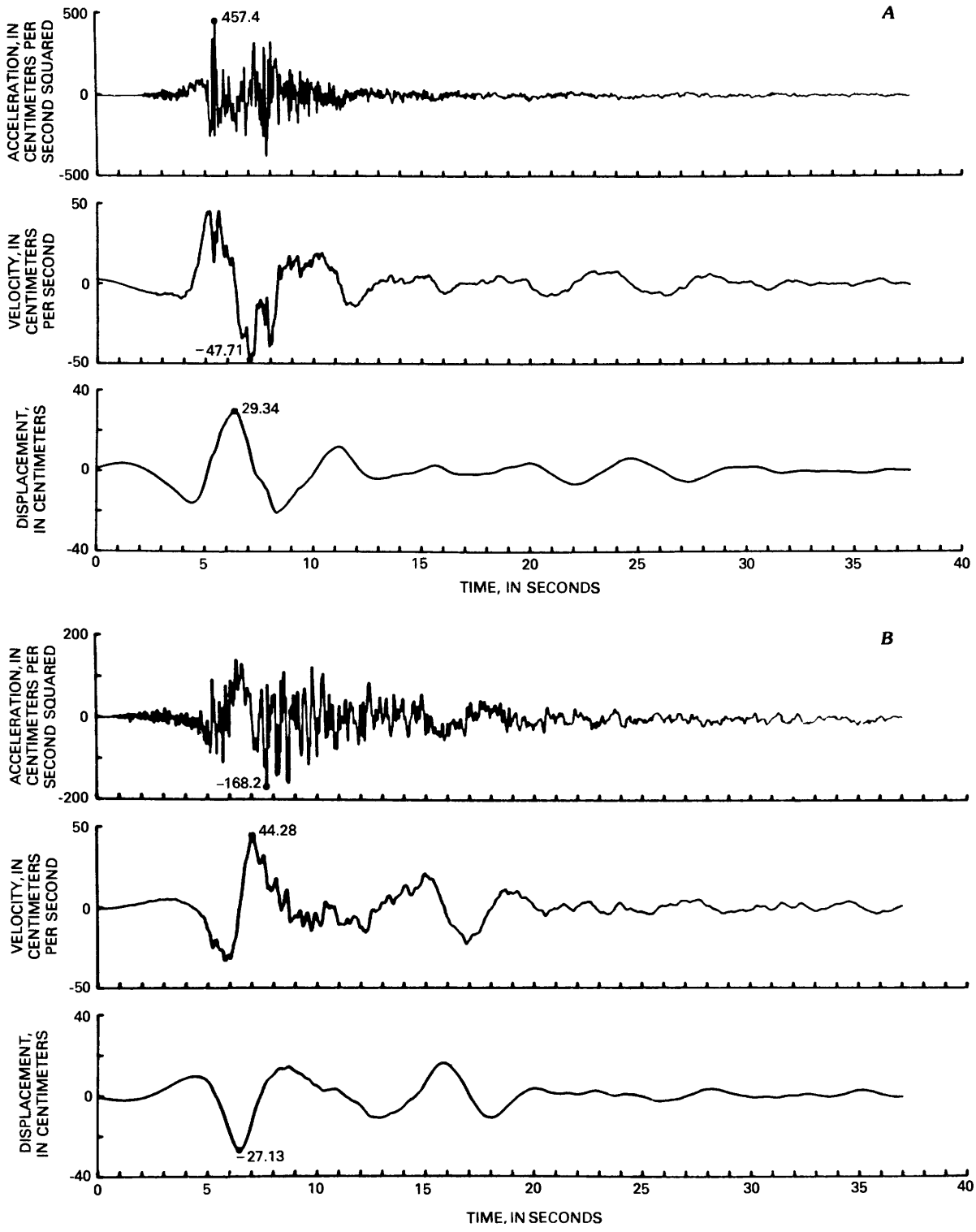

FIGURE 273.—Corrected main-shock acceleration, velocity, and displacement time histories for components transverse to fault at El Centro array stations 8 (230° direction, *A*) and 10 (50° direction, *B*), and for west component on El Centro differential array (*C*). Dot shows peak value.

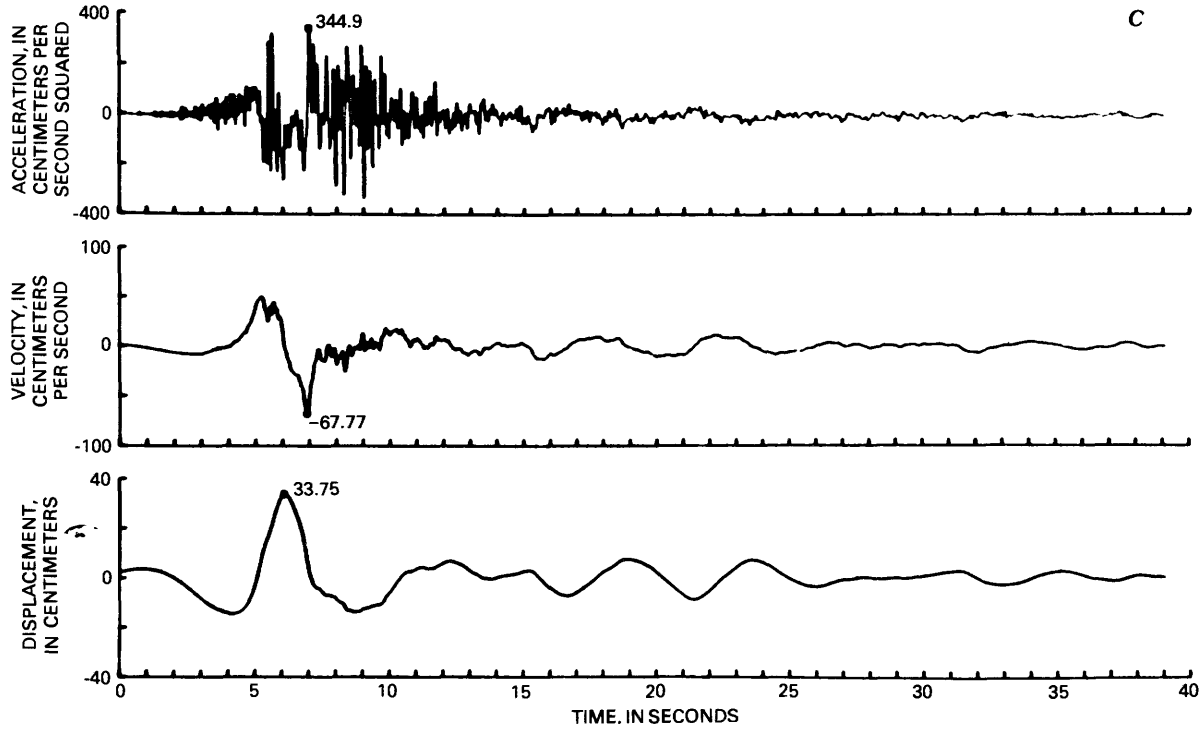

FIGURE 273.—Continued

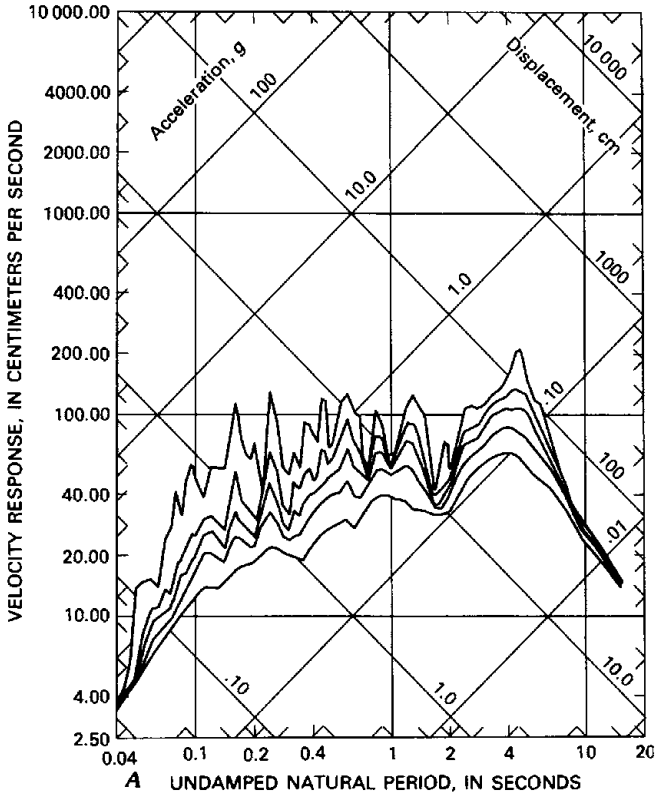

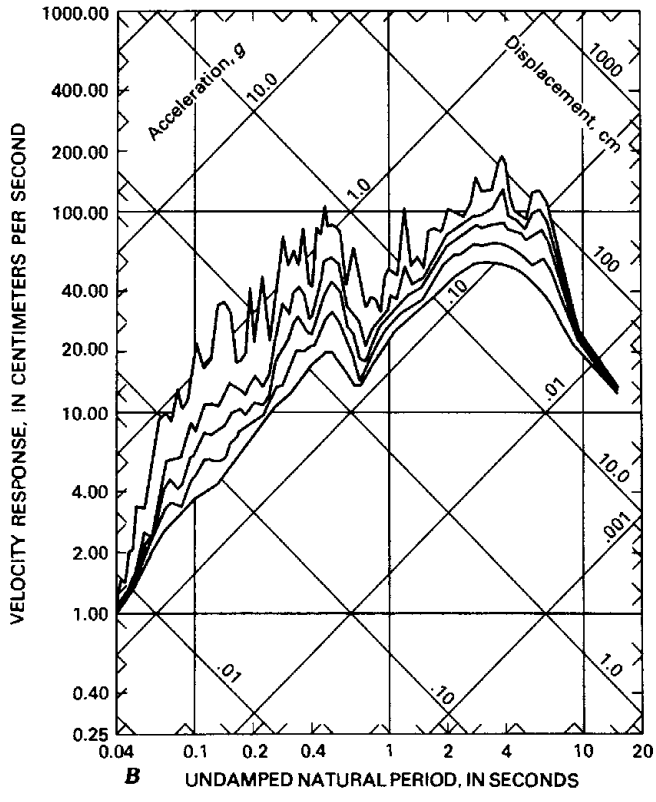

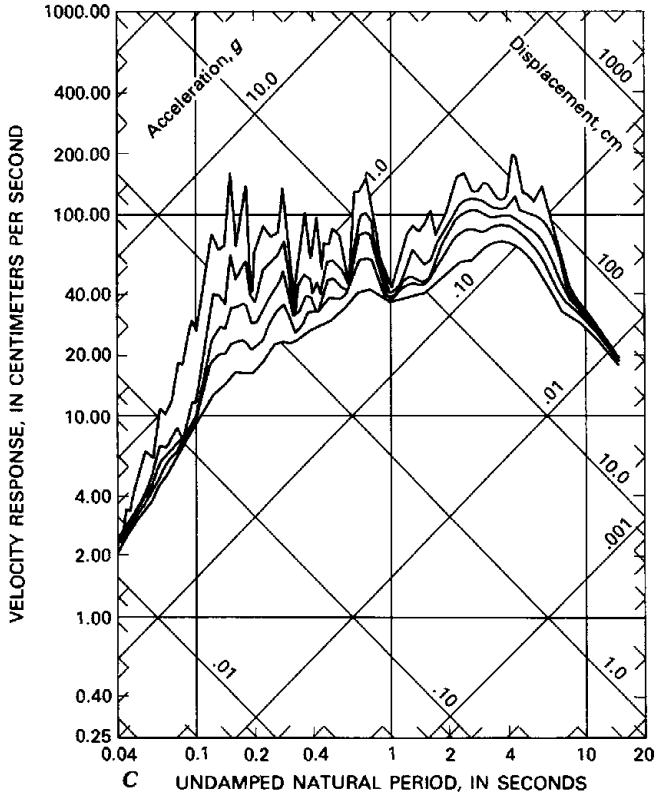

FIGURE 274.—Response spectra for main-shock components transverse to fault at El Centro array stations 8 (230°direction, *A*) and 10 (50° direction, *B*), and for west component on El Centro differential array (*C*).

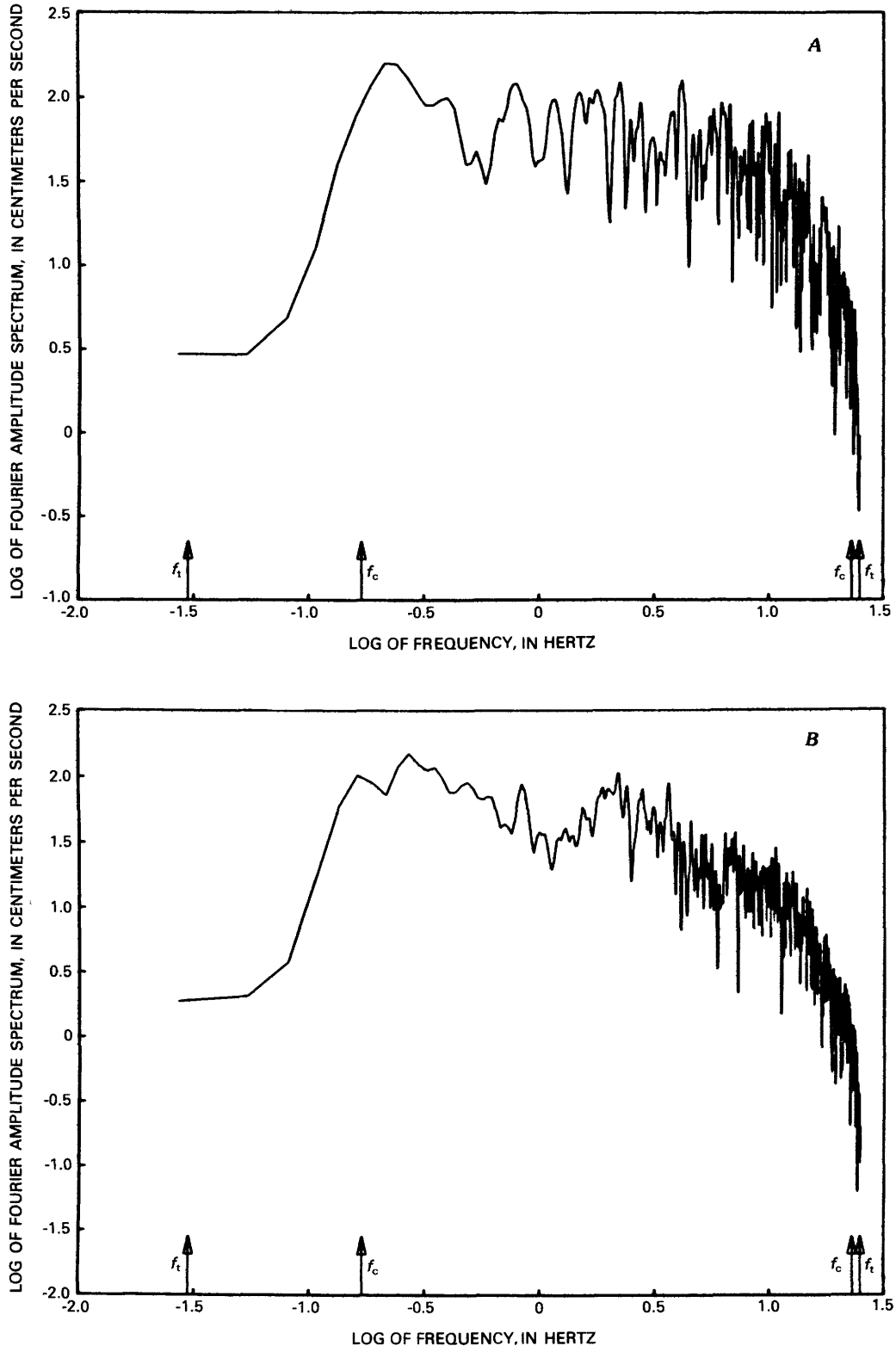

FIGURE 275.—Fourier amplitude spectra for main-shock components transverse to fault at El Centro array stations 8 (230° direction, *A*) and 10 (50° direction, *B*), and for west component on El Centro differential array (*C*). Cutoff and termination frequencies, f_c and f_t, respectively, are indicated by arrows.

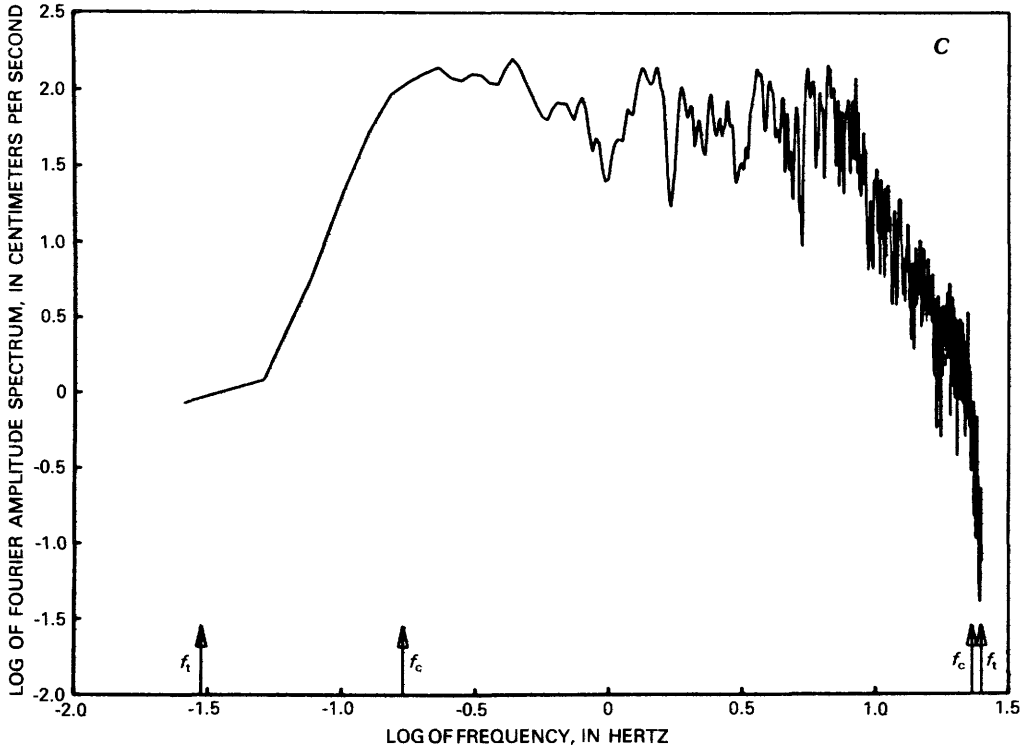

FIGURE 275.—Continued

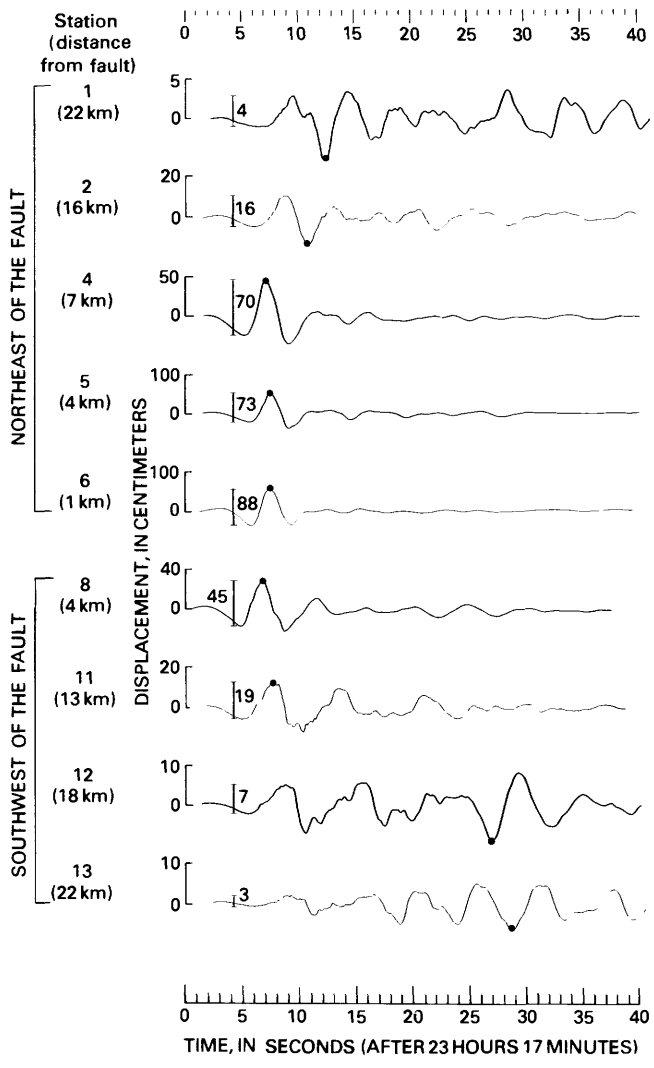

FIGURE 276.—Main-shock ground displacement transverse to Imperial fault trace (230° direction) on El Centro array. Dot shows peak value; vertical bar indicates peak-to-peak amplitude of shear wave.

REFERENCES CITED

Basili, M., and Brady, A. G., 1978, Low frequency filtering and the selection of limits for accelerogram corrections: European Conference on Earthquake Engineering, 6th, Dubrovnik, Yugoslavia, 1978, Proceedings, p. 251–258.

Blackman, R. B., and Tukey, J. W., 1958, The measurement of power spectra: New York, Dover, 190 p.

Brady, A. G., Perez, Virgilio, and Mork, P. N., 1980, The Imperial Valley earthquake, October 15, 1979: Digitization and processing of accelerograph records: U.S. Geological Survey Open-File Report 80–703, 309 p.

Fletcher, J. B., Brady, A. G., and Hanks, T. C., 1980, Strong-motion accelerograms of the Oroville, California, aftershocks: Data processing and the aftershock of 0350 August 6, 1975: Seismological Society of America Bulletin, v. 70, no. 1, p. 243–267.

Hudson, D. E., 1976, Strong-motion earthquake accelerograms index volume: Pasadena, California Institute of Technology, Earthquake Engineering Research Laboratory Report EERL 76–02, 72 p.

Porcella, R. L., and Matthiesen, R. B., 1979, Preliminary summary of the U.S. Geological Survey strong-motion records from the October 15, 1979 Imperial Valley earthquake: U.S. Geological Survey Open-File Report 79–1654, 41 p.

Porter, L. D., Brady, A. G., and Roseman, W. R., 1978, Computer reassembly of multiframe accelerograms [abs.]: Earthquake Notes, v. 49, no. 4, p. 13.

Trifunac, M. D., 1972, A note on correction of strong-motion accelerograms for instrument response: Seismological Society of America Bulletin, v. 62, no. 1, p. 401–409.

Trifunac, M. D., and Lee, V. W., 1973, Routine computer processing of strong-motion accelerograms: Pasadena, California Institute of Technology, Earthquake Engineering Research Laboratory Report EERL 73–03, 360 p.

——— 1978, Uniformly processed strong earthquake ground accelerations in the western U.S.A. for the period from 1933 to 1971: Corrected acceleration, velocity and displacement curves: Los Angeles, University of Southern California Report CE78–01, 220 p.

DATA-PROCESSING PROCEDURES FOR MAIN-SHOCK MOTIONS RECORDED BY THE CALIFORNIA DIVISION OF MINES AND GEOLOGY STRONG-MOTION NETWORK

By L. D. PORTER,
CALIFORNIA DIVISION OF MINES AND GEOLOGY

CONTENTS

ABSTRACT

Six main-shock records from the California Division of Mines and Geology strong-motion network have been digitized. These records were obtained from four sites—two ground stations and two intensively instrumented structures with associated free-field accelerographs—for a total of 48 traces. Five records have been processed as of early 1980; the sixth will require special procedures to remove effects of an instrument malfunction. Computer-drawn graphics of the processed data, showing the corrected time histories of 19 traces, response spectra for the ground-level horizontal and vertical components, and velocity-response-envelope spectra (VRES) and duration spectra for the horizontal ground-level components, are presented here.

INTRODUCTION

This preliminary report summarizes the procedures by which the California Division of Mines and Geology (CDMG) is processing the strong-motion data from the 1979 Imperial Valley earthquake. Computer-drawn graphics are also presented for highlights of the results obtained so far. The geophysical and engineering significance of this data set calls for corresponding significant changes in the processing procedures required for densely digitized multichannel (13 channel) records of long duration. Although the bulk of the CDMG data-processing system is based on source programs supplied by the U.S. Geological Survey (USGS), extensive modifications have been necessary to analyze these accelerograms. By early 1980, two-thirds of the CDMG data from the main shock had been completely processed in a standardized manner. One digitized multichannel record, however, will need special treatment to remove defects caused by an instrument malfunction.

Although the earthquake was of only moderate magnitude (M=6.5), the resulting strong-motion data set is one of the most important obtained to date, especially because the data include the first recording of the response of a well-instrumented building, the Imperial County Services Building in El Centro, Calif., that sustained structural failure during an earthquake. The content and completeness of these data are the reward for the years of attention and planning that went into the development of several networks operating in the Imperial Valley (Matthiesen and Porcella, this volume).

SITES INSTRUMENTED AND RECORDS RECOVERED

The main shock triggered 13 CDMG stations at distances ranging from 18 to 241 km from the epicenter (table 45). Six records from four stations (fig. 277) have peak amplitudes of more than 0.05 g and thus warrant digital processing. Two records (fig. 278) that showed peak accelerations of approximately 0.10 g are from ground-level stations—Westmorland Fire Station and Niland Fire Station—at epicentral distances of 52 and 69 km, respectively. The remaining two stations—the Imperial County Services Building and the Meloland Road-Interstate Highway 8 overcrossing—are in and near El Centro, Calif.; both are well-instrumented structures situated near the fault and epicenter, and both registered peak ground-level accelerations of 0.25 g or greater.

The Imperial County Services Building, which sustained severe structural damage during the earth-

TABLE 45.—*Main-shock accelerograph data from the CDMG strong-motion network*

[Epicentral distance is measured from station to epicenter at lat 32.64° N., long 115.33° W.; number in brackets denotes distance from station nearest point on 1979 Imperial fault trace, which is assumed to extend from lat 32.94° N., long 115.54° W., to lat 32.72° N., long 115.40° W. Direction of acceleration is for upward trace deflection on accelerogram; horizontal components are listed as azimuth (in degrees clockwise from north), vertical components as "up" or "down." Maximum acceleration is for uncorrected peak recorded at ground or basement level, or on abutment. Duration of acceleration is time between first and last peaks greater than 0.10 *g*]

No.	Station	Coordinates (lat °N., long °W.)	Epicentral distance (km)	Site geology	Structure type/size	Instrument location(s)	Acceleration		
							Direction	Maximum (g)	Duration (s)
336	El Centro, Meloland Rd.-Interstate Highway 8 overcrossing	32.77, 115.45	18 [0.5]	Alluvium	Freeway overpass.	Ground, deck, embankments, abutments.	360°	0.32	7
							up	.23	---
							270°	.30	---
260	El Centro, Imperial County Services Building	32.79, 115.56	27 [8]	do	6-story building.	Ground, 2d, and 4th floors, roof.	360°	.35	6
							up	.19	---
							090°	.32	---
335	El Centro, Imperial County Center	32.79, 115.56	27 [8]	do	T-hut.	Ground	092°	.24	5
							up	.27	---
							002°	.24	---
369	Westmorland Fire Station	33.04, 115.62	52 [13]	do	1-story building.	do	180°	.11	1 peak
							up	.09	---
							090°	.08	---
22	Winterhaven, Sheriffs Substation	33.74, 114.64	65 [71]	do	do	do	270°	.07	---
							up	.02	---
							180°	.05	---
23	Niland Fire Station	33.24, 115.51	69 [33]	do	do	do	090°	.10	2 peaks
							up	.03	---
							360°	.07	---
21	Blythe Fire Station	33.61, 114.71	122 [108]	do	do	do	360°	.02	---
							up	.02	---
							270°	.02	---
243	El Capitan Dam	32.88, 116.82	142 [119]	Granite	Earth dam	Left abutment, center and left crest.	154°	.02	---
							up	.01	---
							064°	.02	---
284	Palm Desert, Kiewit Bldg	33.76, 116.41	160 [122]	Alluvium	4-story building.	Ground, 2d floor, roof.	360°	.02	---
							up	.01	---
							090°	.03	---
300	San Diego, Gas & Electric Building	32.72, 117.16	171 [153]	do	22-story building.	Basement, 3d 12th, and 20th floors, roof.	090°	.01	---
							up	.01	---
							360°	.01	---
299	Palm Springs, Desert Hospital	33.84, 116.54	174 [136]	do	4-story building.	Basement, 2d floor, roof.	360°	.01	---
							up	.01	---
							090°	.02	---
331	Hemet, Stetson/Palm Fire Station	33.73, 116.98	195 [160]	do	1-story building.	Ground.	360°	.01	---
							up	.01	---
							270°	.01	---
312	Riverside, County Administration Building	33.98, 117.37	241 [205]	do	13-story building.	Basement 3d and 7th floors, roof.	119°	.01	---
							up	.01	---
							029°	.01	---

quake, is instrumented with a 13-channel central-recording accelerograph system; an adjacent isolated triaxial free-field accelerograph is at ground level approximately 100 m to the east. Instrument locations and the main-shock records are described in detail by Rojahn and Mork (this volume); damage to the building is described by Wosser and others (this volume). The 13-channel building record and 3-channel free-field record do not have common timing, but both contain radio WWVB time codes. The code is clearly visible on the building record; that for the free-field station record, however, can be deciphered only with difficulty. This record pair is of great interest because it is the first data set of its type ever recorded during damaging levels of motion, because of the insight that it provides into the failure mechanism of the building (Rojahn and Mork, this volume), and because of the proximity of the recording sites to the epicenter and the Imperial fault (27 and 8 km, respectively).

The Meloland Road-Interstate Highway 8 overcrossing, which sustained no observable structural damage during the main shock, is instrumented with two 13-channel central-recording accelerograph systems. Bridge-construction details, instrument locations, and the main-shock records are described in detail by Rojahn and others (this volume). The data include 3 channels from a free-field site approximately 60 m west of the bridge, 6 channels from two embankment (non-free field) sites adjacent to the bridge abutments, and 17 channels from on and beneath the bridge. Both 13-channel recorders recorded the main shock as well as the WWVB time code, but the film transport of one stalled briefly 10 times, and so a total of about 1 s of data was lost. The overcrossing records have received immediate attention, not only because of their importance for structural-response studies, but also owing to extreme closeness of the station (0.5 km) to the Imperial fault surface rupture. In fact, the Meloland Road-Interstate Highway 8 overcrossing is the closest station in the Imperial Valley to the fault, and so its free-field record should provide valuable information for studies of rupture propagation and other seismologic studies.

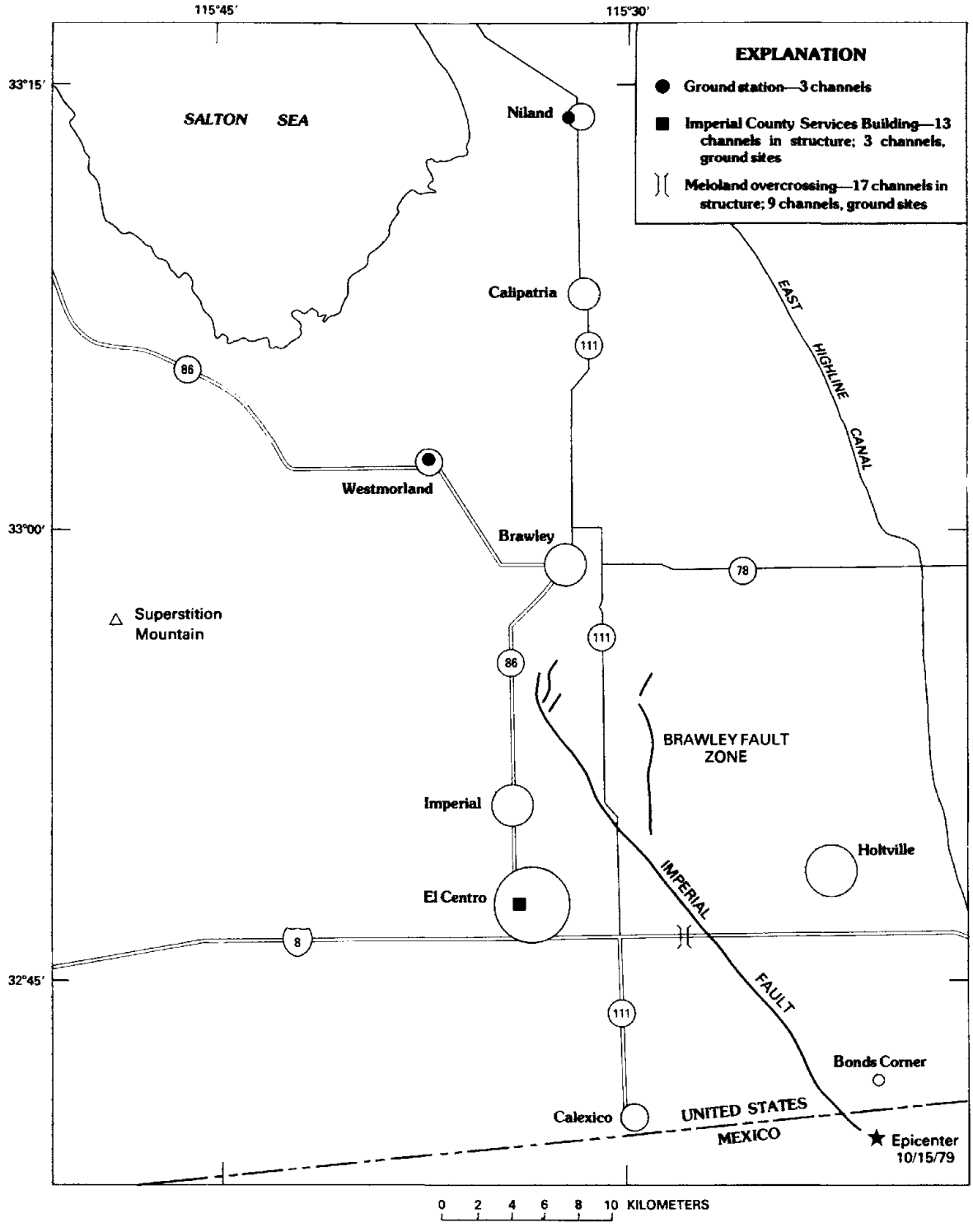

FIGURE 277.—Strong-motion stations in CDMG network for which records of October 15 main shock have been digitized.

Between them, the two overcrossing station records contain 26 data channels, more than half the total CDMG network channel count for the main shock.

DIGITIZATION AND REASSEMBLY

The seismograms were digitized from first-quality contact-positive copies of the seismograph film records. Using the techniques developed for the 1978 Santa Barbara, Calif., earthquake (Porter and others, 1979b, v. 1, p. 5-11), the records were digitized in overlapping segments by an automatic line-following system. After digitization, a computer program (L. D. Porter and others, unpub. data, 1980) was used to reassemble the segments (frames) into a complete numerical version of the original accelerogram.

To accommodate the high-frequency signal content of the Imperial Valley records, the digitizer was set to extract about 625 points from each second of the record. This density of data points represents approximately a 20-percent increase over the density required in the analysis of smaller shocks, such as the 1978 Santa Barbara and 1979 Coyote Lake, Calif., earthquakes. The processing steps used during smoothing, decimation, and reassembly were set to yield a final data density of about 135 points/s, nearly a threefold increase over that associated with hand-digitizing methods (Hudson, 1979). The accelerogram durations for the CDMG network records average about 58 s; the longest, the Imperial County Services Building record, is 90 s.

Reassembly (Porter and others, 1979a) was carried out in one, sometimes two, steps. First, the accelerogram frames were joined together into horizontal panels. The panel height (8 cm) is sufficient to cover a 70-mm triaxial film record, or three or four data traces on a 178-mm (7 in.) film record from a central-recording system, such as those at the Imperial County Services Building and Meloland Road-Interstate Highway 8 overcrossing stations. For the multichannel records, a second step is necessary, by which the panels are vertically reassembled by synchronizing the first frame (approx 9 s) of each panel. For a record length of 60 s, typical of those from the Imperial Valley main shock, the panels are synchronized to within 0.01 s or less over their entire lengths. For the 13-channel re-

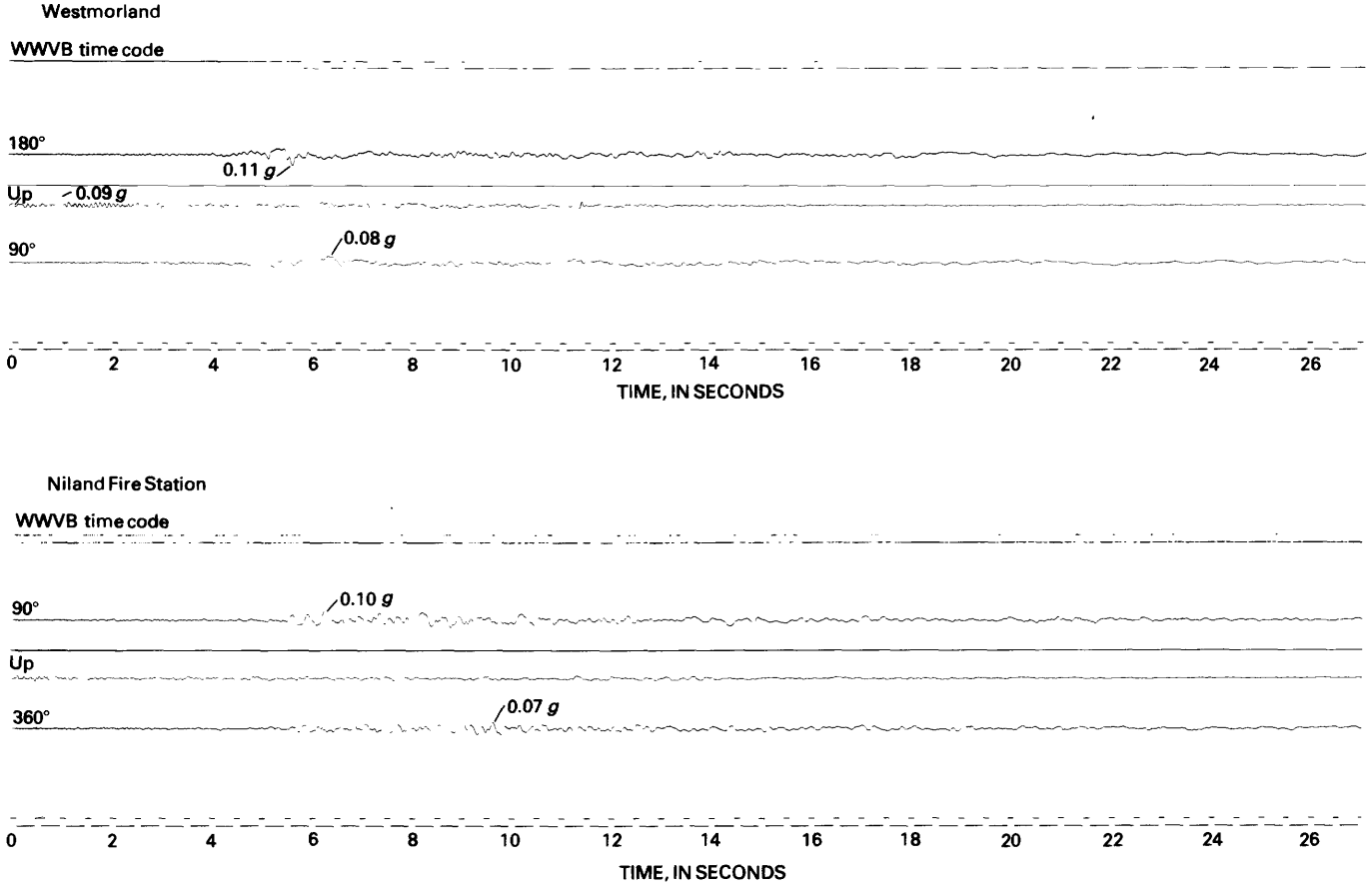

FIGURE 278.—Accelerograms of October 15 main shock from CDMG ground-level stations at Westmorland and Niland, Calif. Direction of case acceleration for upward trace deflection is given at beginning of trace, and measured peak acceleration to right.

cords, panel 1 contains traces 1 through 3; panel 2, traces 4 through 7; panel 3, traces 8 through 11; and panel 4, traces 12 and 13.

STANDARDIZED PROCESSING

The accelerograms from the main shock were processed with the aid of a standardized package maintained at the Lawrence Berkeley Laboratory of the University of California. Most of the source programs in this package are based on those used by the U.S. Geological Survey (1976), which in part are derived from earlier procedures developed at the California Institute of Technology (Trifunac and Lee, 1973). A review of the signal content of the Imperial Valley data shows that three important changes in processing procedures were necessary: (1) the use of angular sensitivities where desirable, especially for the records from the 13-channel central recording systems; (2) a doubling of the density for the corrected data from the usual value to 100 points/s; and (3) an extension of the maximum processable record length to 60 s and, for one record, to 90 s.

The first modification, introduced for the 1978 Santa Barbara earthquake, calibrates the accelerometer sensitivities in terms of angular deflection of the galvanometer rather than trace excursions on the film (L. D. Porter and others, unpub. data, 1980). This approach takes into account an effect that is particularly noticeable for the central recording systems, in which most of the galvanometers exhibit different sensitivities for positive and negative tilt tests. Although the correction affects the peak amplitudes by less than 5 percent, it allows more consistent and accurate handling of the data. This method of calibration was used for the Imperial County Services Building station record, and the sensitivities were taken from postevent tilt tests.

The second and third modifications represent requirements developed specifically for handling film accelerograms from the main shock. The enhanced data density acknowledges the importance of this record collection and more fully exploits the high-quality output available from the line-following digitizer. The extension of the maximum processable record length avoids any truncation of the data.

The numerical filters used in calculating the corrected time histories and spectra were selected on the basis of a series of investigations on low-frequency filtering for accelerograms (Basili and Brady, 1978). For the main shock these settings remove all frequencies below 0.03 Hz and above 25 Hz and filter progressively less within these limits, so that frequencies between 0.17 and 23 Hz are untouched. Almost all the main-shock data processed by the CDMG and USGS were filtered using these settings.

CORRECTED TIME HISTORIES

By early 1980, 35 channels of corrected data were available form the CDMG network. Corrected acceleration, velocity, and displacement time histories for 19 ground-level components are included here in the order of increasing epicentral distance. Figure 279 shows the time histories and instrumentation scheme for the Meloland Road-Interstate Highway 8 overcrossing station (Rojahn and others, this volume), figure 280 the time histories and instrumentation scheme for the Imperial County Services Building station (Rojahn and Ragsdale, 1980), and figures 281 and 282 the time histories for Westmorland Fire Station and Niland Fire Station, respectively.

Significant features of the Meloland Road-Interstate Highway 8 overcrossing and the Imperial County Services Building records are described elsewhere (Rojahn and Mork, this volume; Rojahn and others, this volume); the Westmorland and Niland records have not yet been interpreted. Because this data set includes records from only four stations, the free-field data from the CDMG network should be incorporated into and compared with those from the USGS network (Brady and others, this volume; Bycroft, this volume) and the northern Baja California array (Brune and other, this volume) to obtain a more complete picture of the ground-motion measurements and their corrected time histories for the entire southern California region.

RESPONSE SPECTRA

Plots of response spectra compiled from ground-level data from the four CDMG stations provide important information on the ground motion at the structures involved, as well as insight into the interaction of soil, foundation, and structure (at the Imperial County Services Building and Meloland Road-Interstate Highway 8 overcrossing). Figure 283 shows response-spectra plots for six channels from the Meloland Road-Interstate Highway 8 overcrossing station, figure 284 for seven from the Imperial County Services Building station, and figures 285 and 286 for six from the ground-level stations at Westmorland and Niland, respectively.

VELOCITY-RESPONSE-ENVELOPE AND DURATION SPECTRA

The velocity-response-envelope spectrum (VRES) is a spectral plot showing when and how long response exceeds a given level; the duration spectrum of the velocity response envelope shows the total time (duration) that response exceeds the given levels. For the 1971 San Fernando, Calif., earthquake, Perez (1973) suggested that the VRES and duration spectral plots provide a more accurate index of earthquake-induced damage than does peak acceleration. To provide more

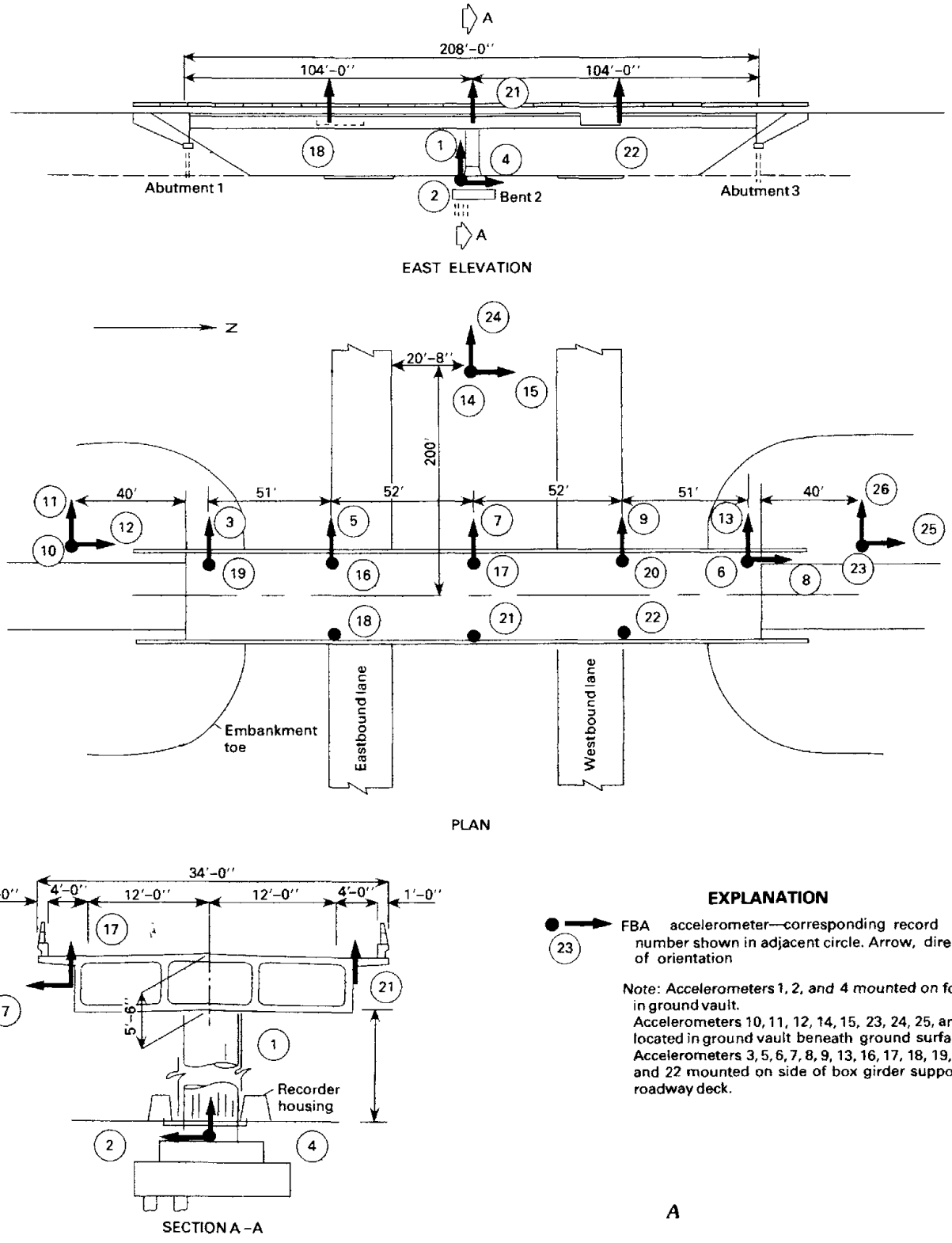

FIGURE 279.—Accelerometer locations (Rojahn and others, this volume) (*A*) and corrected acceleration, velocity, and displacement time histories of October 15 main-shock free-field data (*B*) and north-embankment data (*C*) from Meloland Road-Interstate Highway 8 overcrossing station. Peak values and locations (dots) are given. Time-history data are plotted at equal time increments of 0.01 s. Accelerogram is band passed with ramps of 0.030–0.170 and 23.0–25.0 Hz.

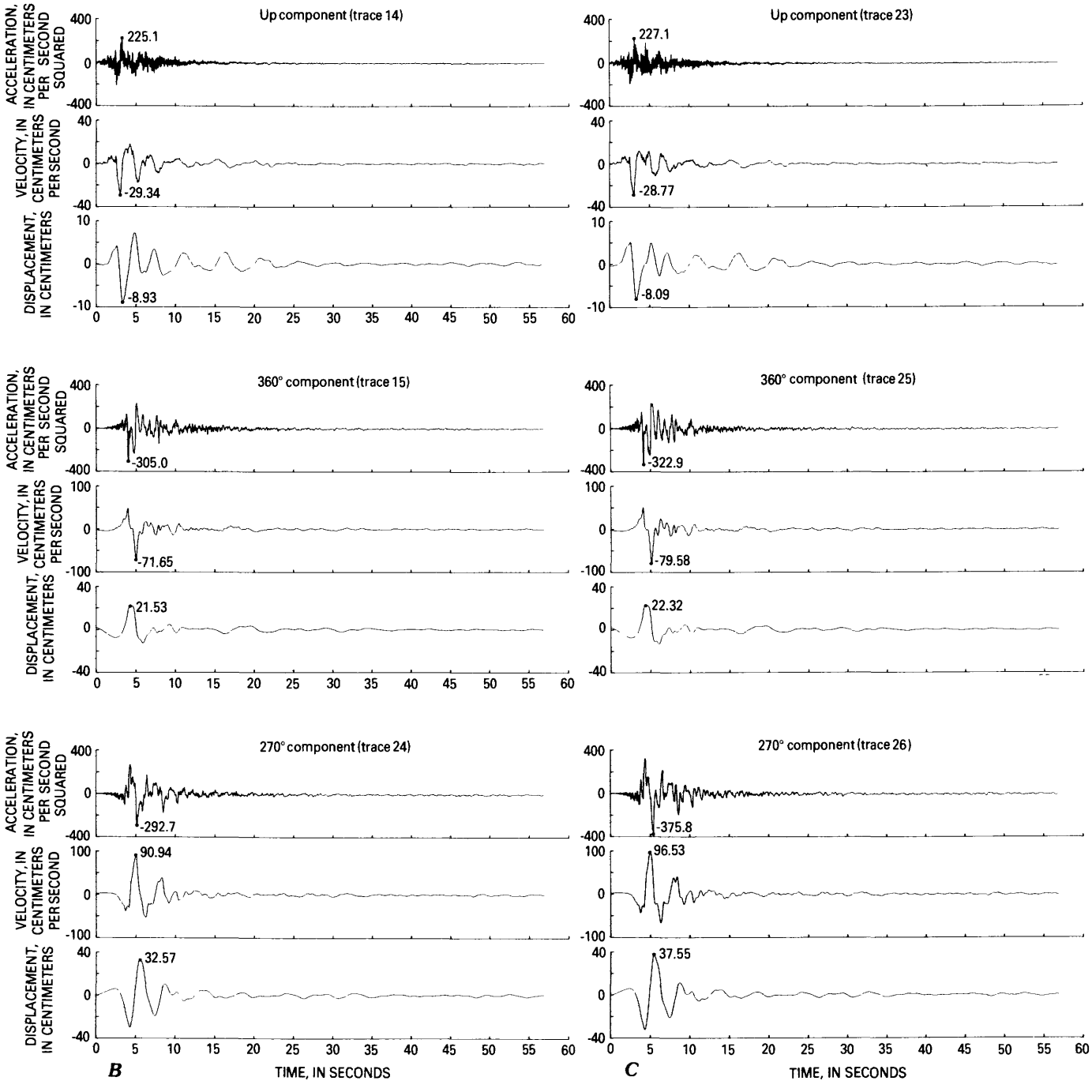

FIGURE 279.—Continued

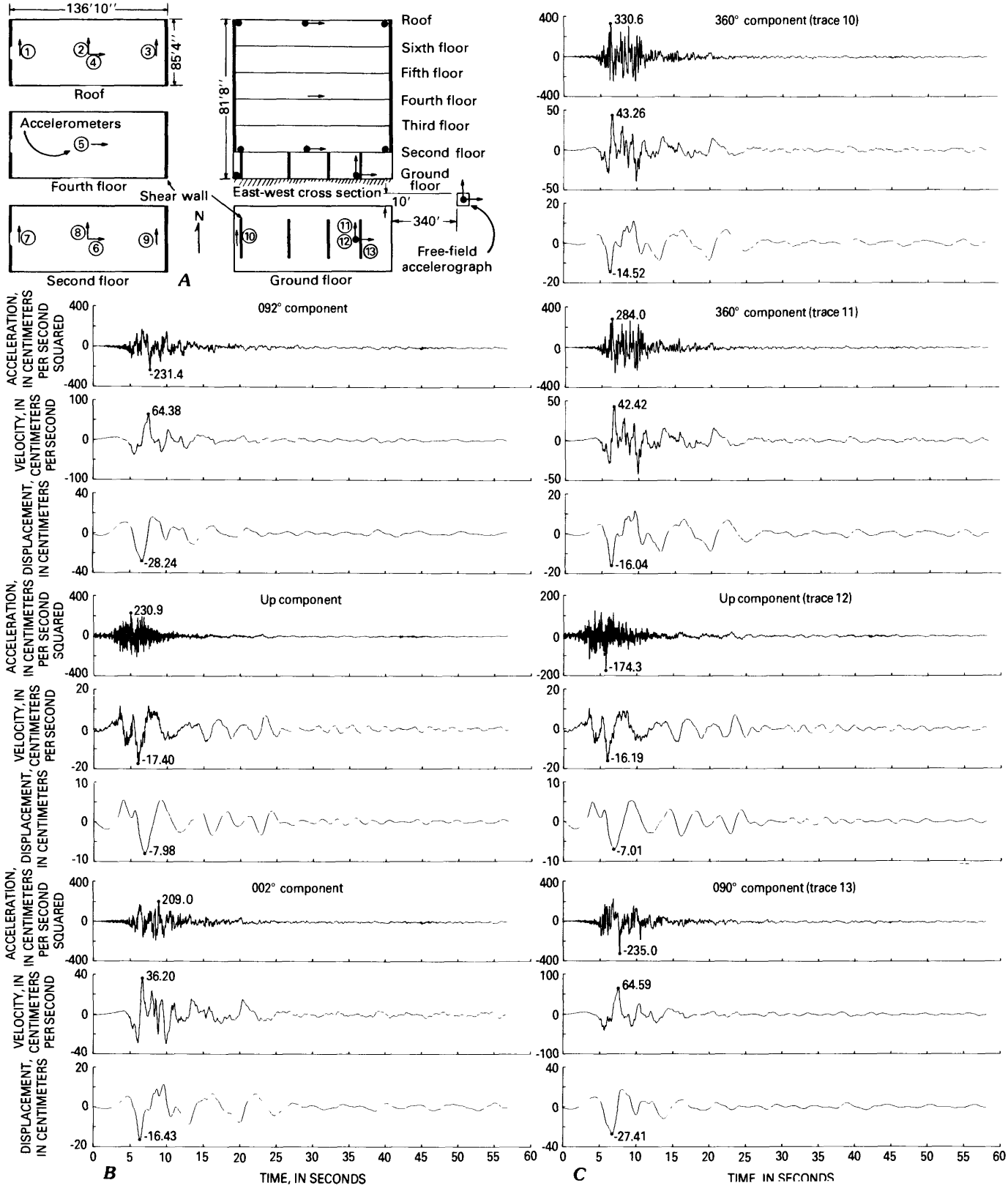

FIGURE 280.—Accelerometer locations for Imperial County Services Building and adjacent free-field site (after Rojahn and Ragsdale, 1980) (see fig. 279*A* for explanation) (*A*); corrected acceleration, velocity, and displacement time histories of October 15 main-shock free-field data (*B*); and ground-floor data from Imperial County Services Building station (*C*). Peak values and locations (dots) are given; time-history data are plotted at equal time increments of 0.01 s. Accelerogram is band passed with ramps of 0.030–0.170 and 23.0–25.0 Hz.

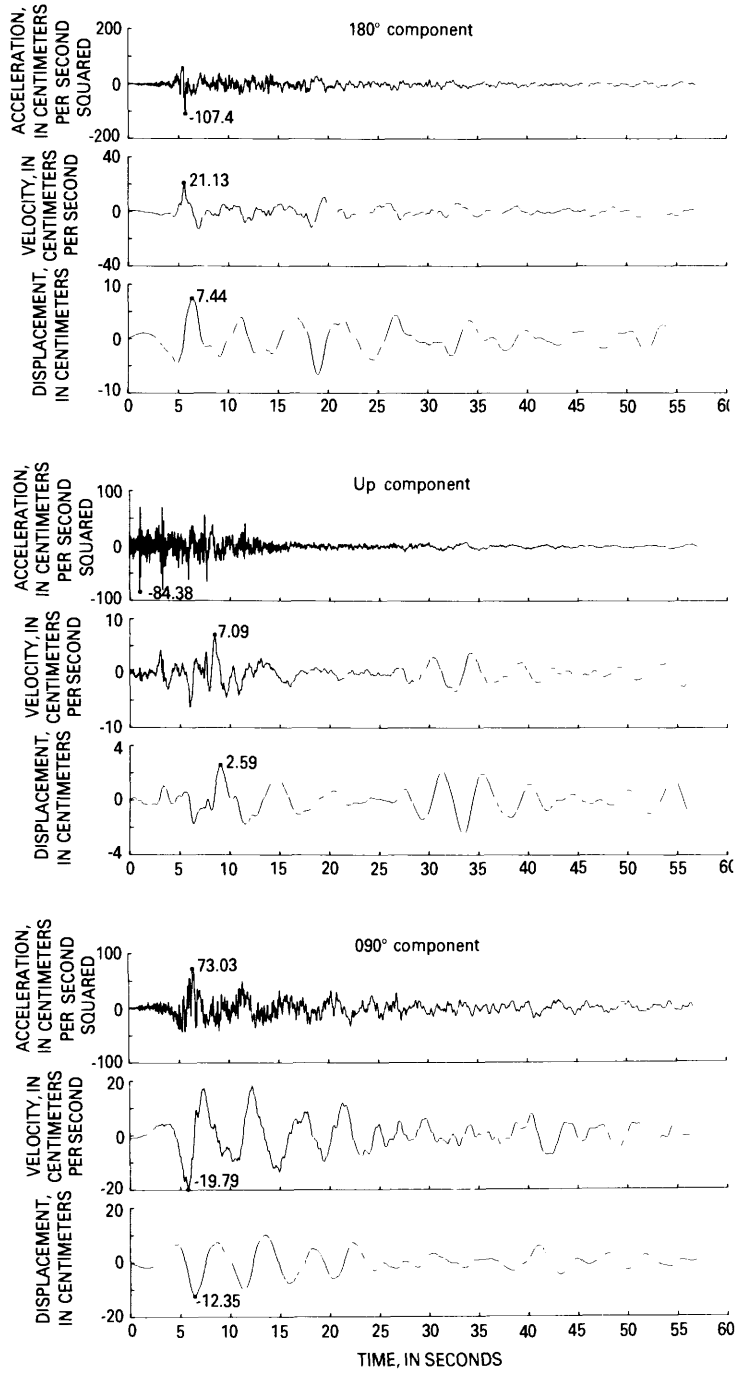

FIGURE 281.—Corrected acceleration, velocity, and displacement time histories of October 15 main-shock data from Westmorland ground-level station. Peak values and locations (dots) are given. Data are plotted at equal time increments of 0.01 s. Accelerogram is band passed with ramps of 0.030–0.170 and 23.0–25.0 Hz.

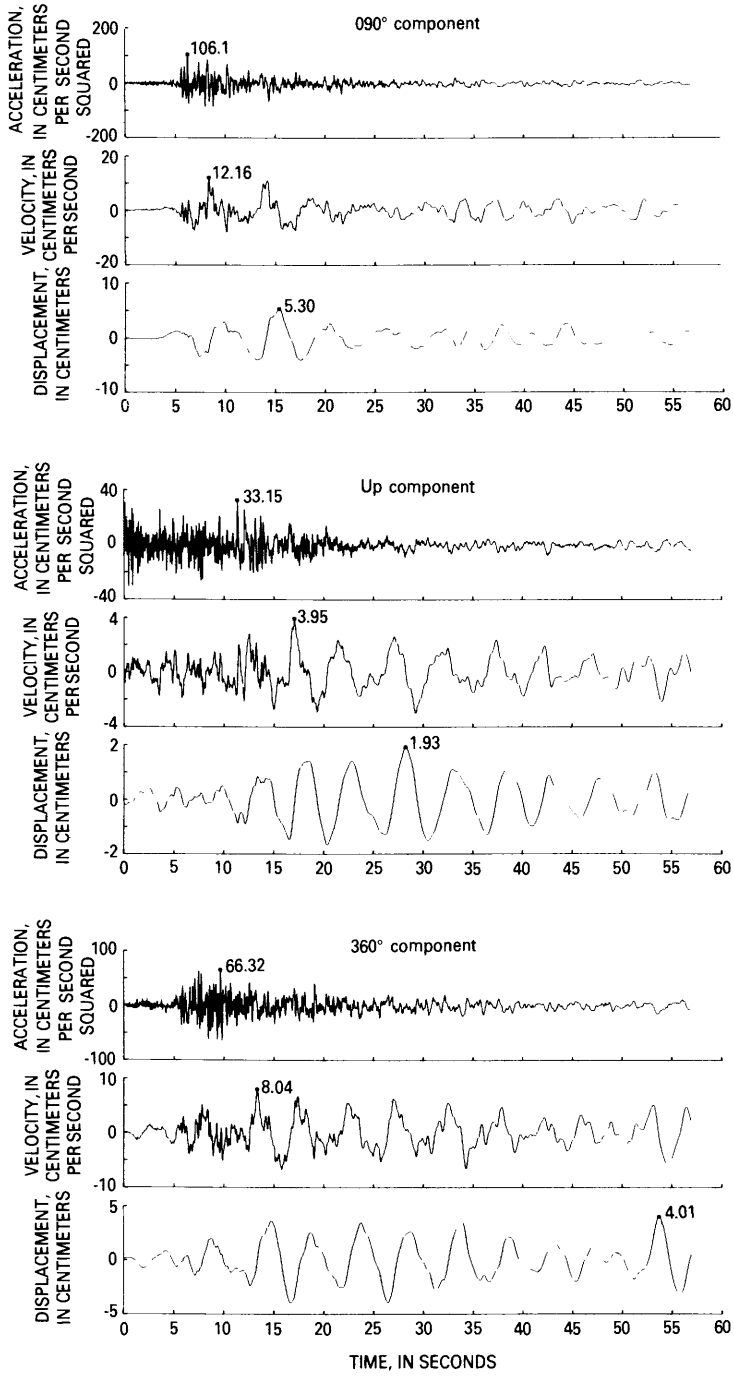

FIGURE 282.—Corrected acceleration, velocity, and displacement time histories of October 15 main-shock data from Niland ground-level station. Peak values and locations (dots) are given. Data are plotted at equal time increments of 0.01 s. Accelerogram is band passed with ramps of 0.030–0.170 and 23.0–25.0 Hz.

information on the main-shock data, these plots for 5 percent of critical damping are shown for the horizontal ground and free-field components recorded at the four CDMG stations (figs. 287-290).

ACKNOWLEDGMENTS

The California Division of Mines and Geology acknowledges the cooperation of the U.S. Geological Survey in providing access to their computer programs at the Lawrence Berkeley Laboratory of the University of California. I thank A. Gerald Brady and Virgilio Perez for their assistance and instruction in the use of these programs, and Peter N. Mork for his help in processing the data from the Imperial County Services Building station.

REFERENCES CITED

Basili, M., and Brady, A. G., 1978, Low-frequency filtering and the selection of limits for accelerogram corrections: European Conference on Earthquake Engineering, 6th, Dubrovnik, Yugoslavia, 1978, Proceedings, p. 251-258.

Hudson, D. E., 1979, Reading and interpreting strong-motion accelerograms: Berkeley, Calif., Earthquake Engineering Research Institute, 112 p.

Perez, Virgilio, 1973, Velocity response envelope spectrum as a function of time, *in* Benfer, N. A., and Coffman, J. L., eds., San Fernando, California, earthquake of February 9, 1971: Washington, U.S. Department of Commerce, National Oceanic and Atmospheric Administration, Environmental Research Laboratories, v. 3, p. 393-401.

Porter, L. D., Brady, A. G., and Roseman, W. R., 1979a, Computer reassembly of multiframe accelerogram [abs.]: Earthquake Notes, v. 49, no. 4, p. 13.

Porter, L. D., Ragsdale, J. T., and McJunkin, R. D., 1979b, Processed data from the strong-motion records of the Santa Barbara earthquake of 13 August 1978: Final results, 1979: California Division of Mines and Geology Special Report 144, 3 v.

Rojahn, Christopher, and Ragsdale, J. T., 1980, Strong-motion records from the Imperial County Services Building, El Centro, *in* Leeds, D. J., ed., Imperial County, California, earthquake, October 15, 1979: Berkeley, Calif., Earthquake Engineering Research Institute reconnaissance report, p. 173-184.

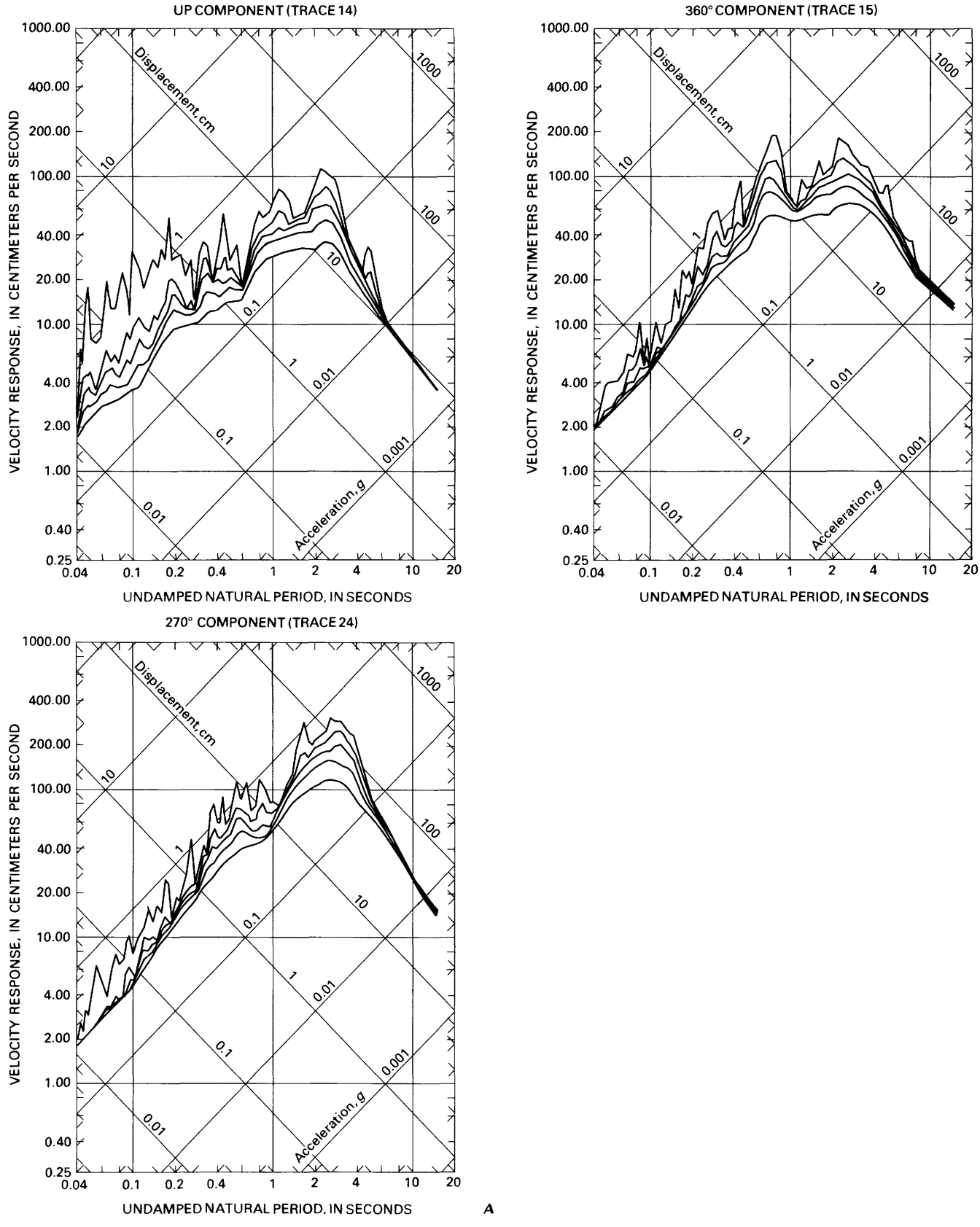

FIGURE 283.—Response spectra of October 15 main-shock free-field data (traces 14, 15, 24) (*A*) and north-embankment data (traces 23, 25, 26) (*B*) from Meloland Road-Interstate Highway 8 overcrossing station. Accelerometer locations (trace numbers) are shown in Rojahn and others (this volume). Response spectra is for damping values of 0, 2, 5, 10, and 20 percent of critical for all graphs.

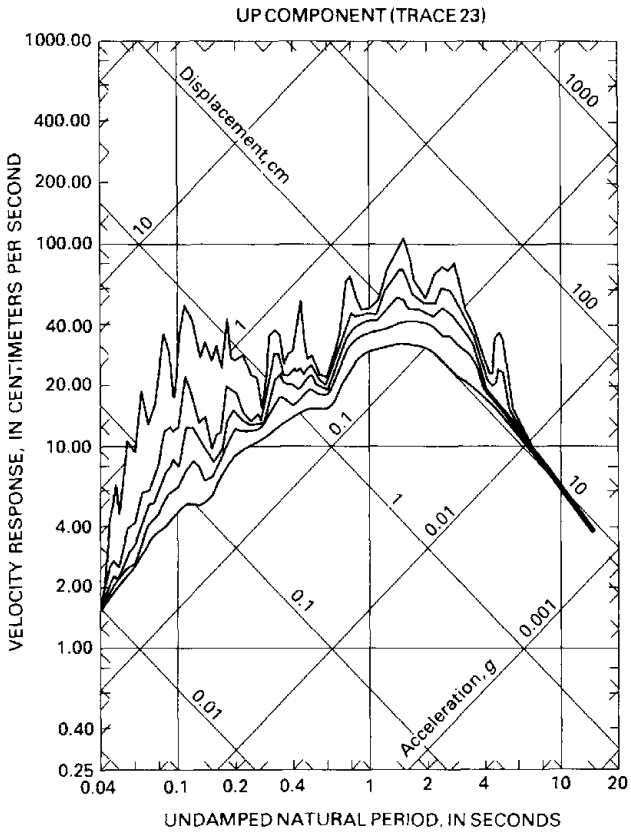

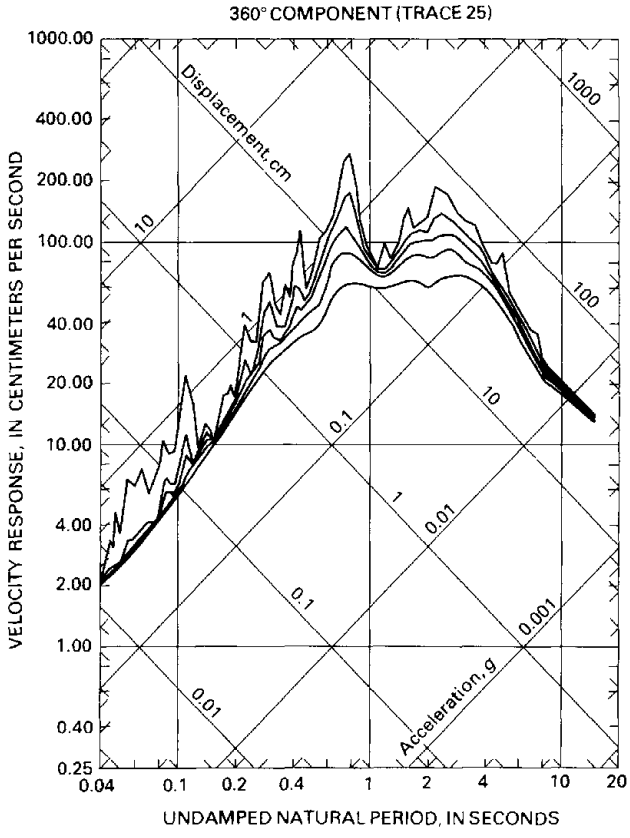

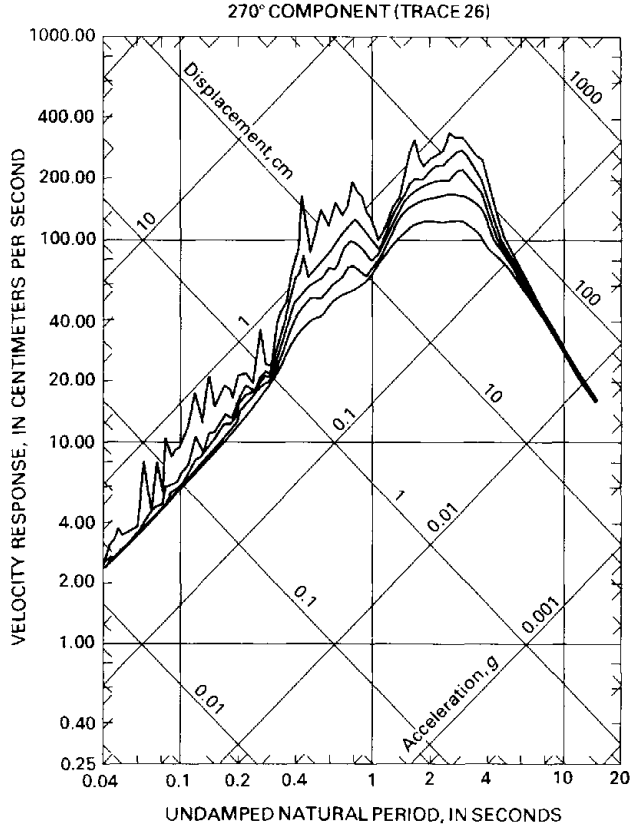

B

FIGURE 283.—Continued

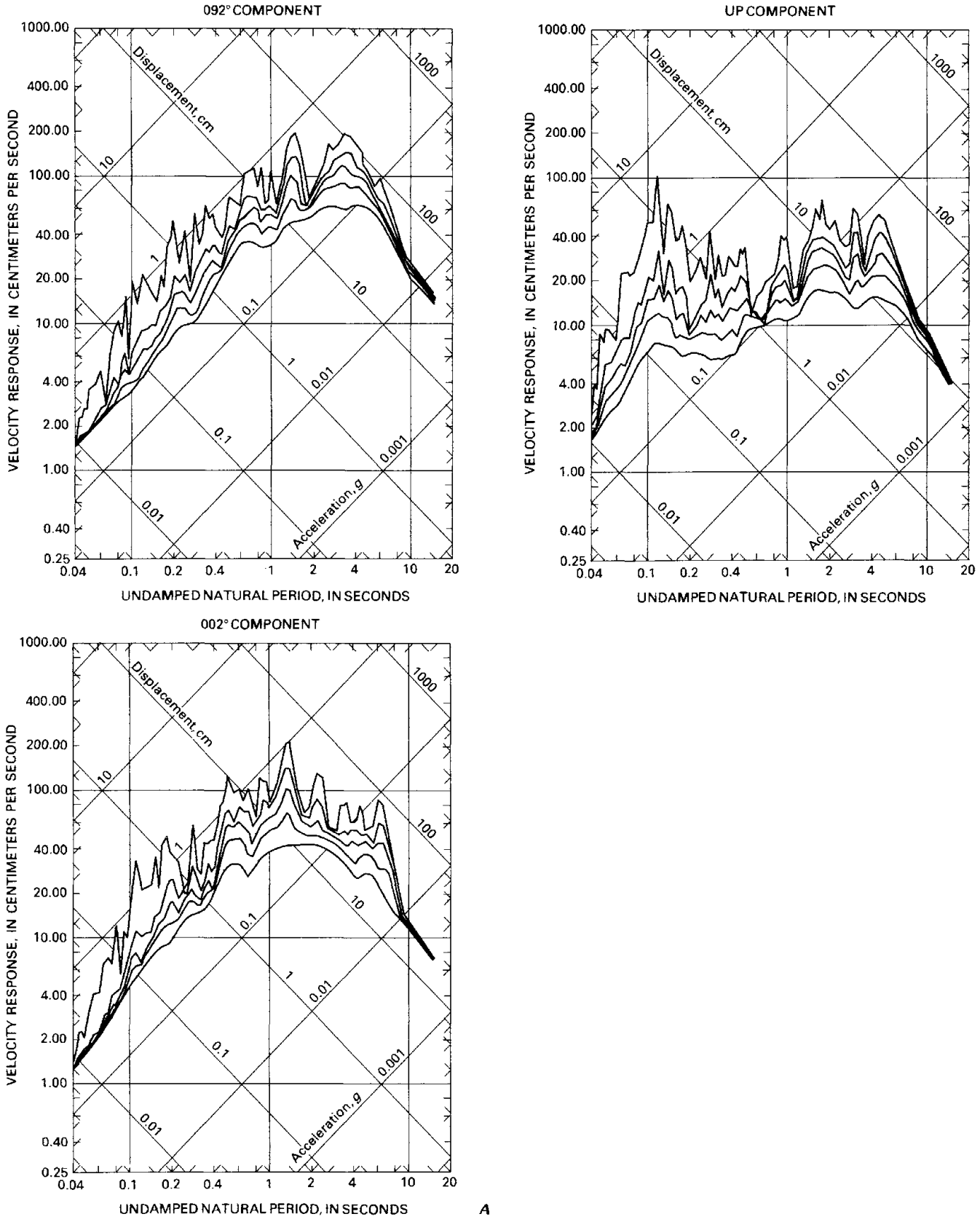

A

FIGURE 284.—Response spectra of October 15 main-shock data from Imperial County Services Building station. *A*, Free field. *B*, Ground floor (traces 10–13). Accelerometer locations (trace numbers) are shown in figure 280*A*. Response spectra is for damping values of 0, 2, 5, 10, and 20 percent of critical for all graphs.

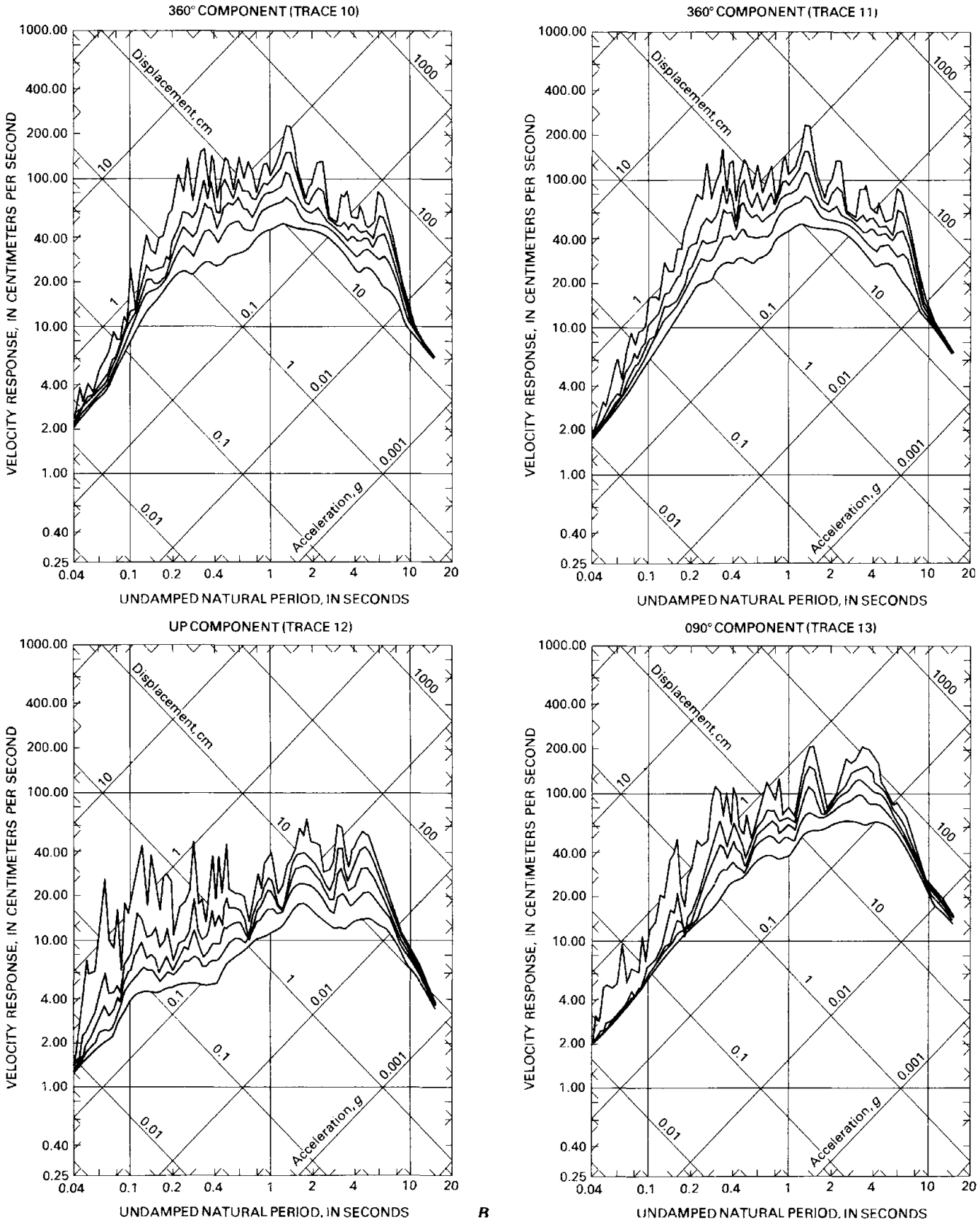

B

FIGURE 284.—Continued

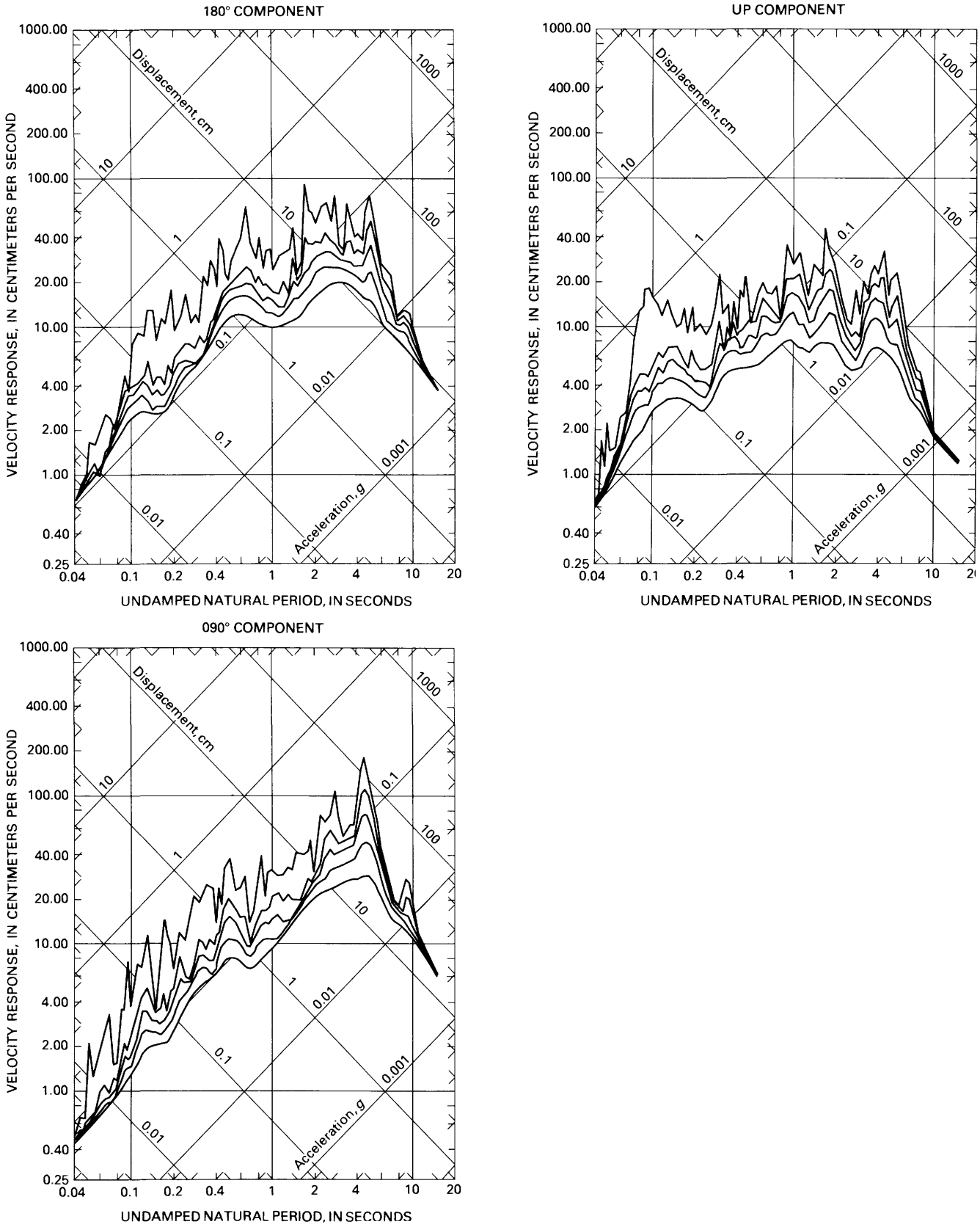

FIGURE 285.—Response spectra of October 15 main-shock data from Westmorland ground-level station. Response spectra is for damping values of 0, 2, 5, 10, and 20 percent of critical for all graphs.

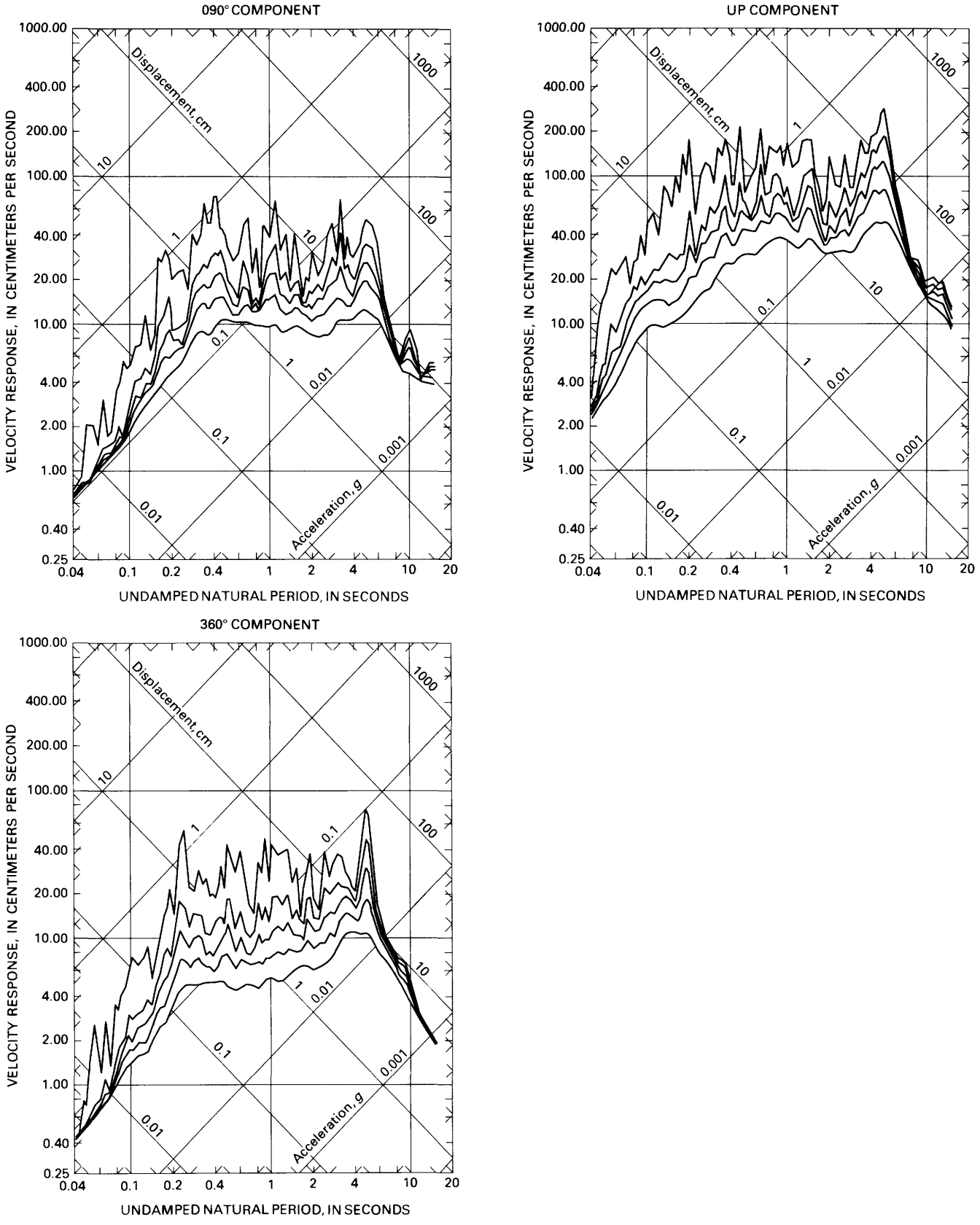

FIGURE 286.—Response spectra of October 15 main-shock data from Niland ground-level station. Response spectra is for damping values of 0, 2, 5, 10, and 20 percent of critical for all graphs.

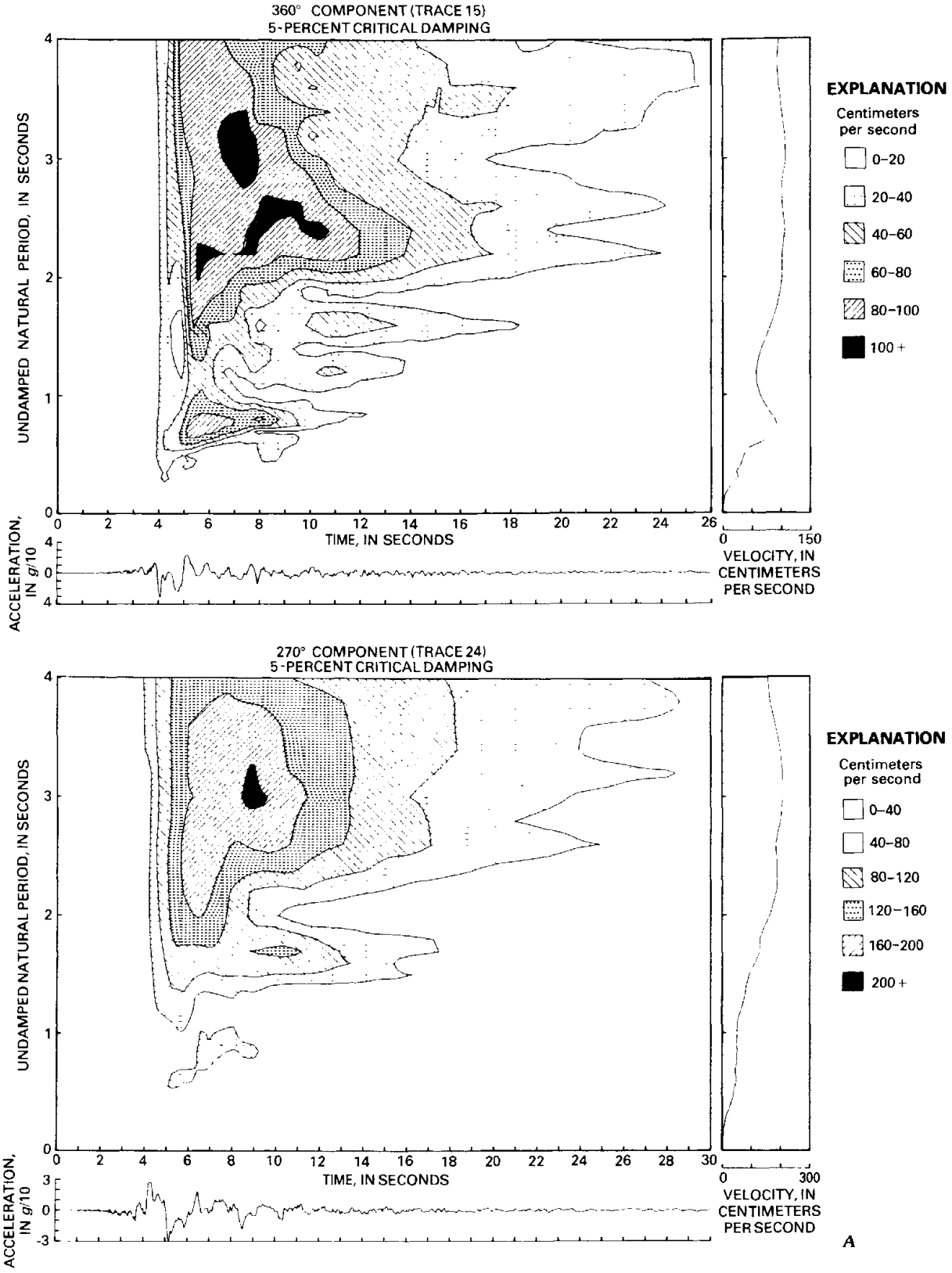

FIGURE 287.—VRES (*A*) and duration spectra of velocity response envelope (*B*) for October 15 main-shock free-field horizontal components recorded at Meloland Road-Interstate Highway 8 overcrossing station.

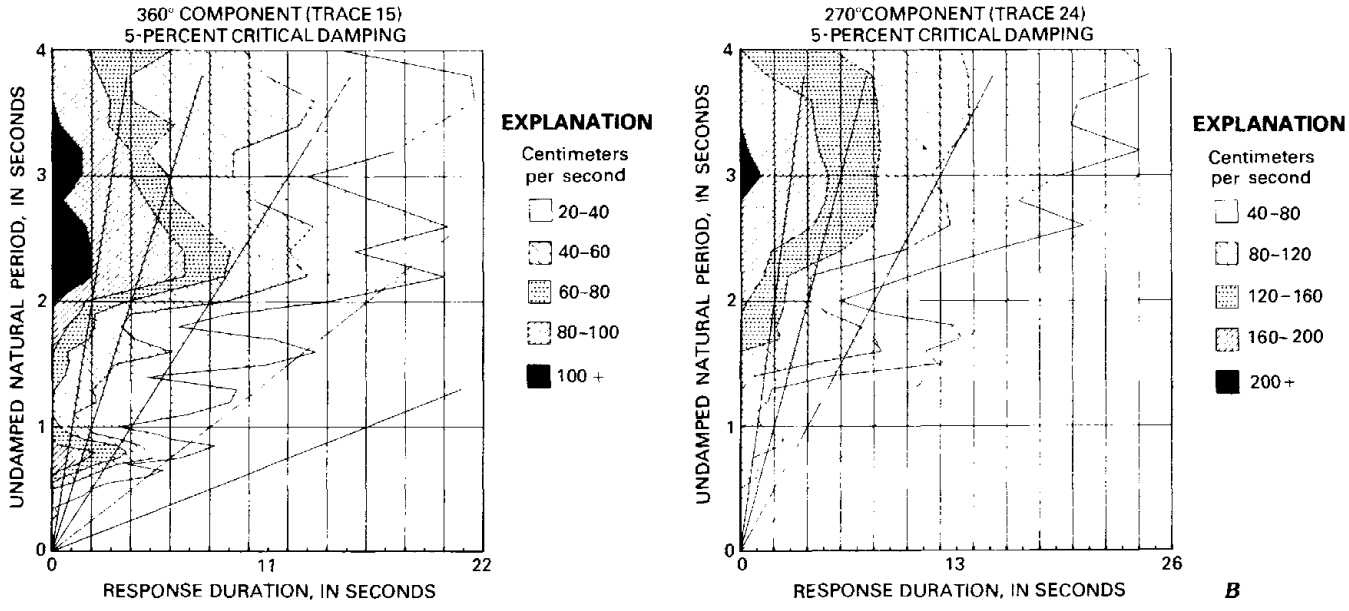

FIGURE 287.—Continued

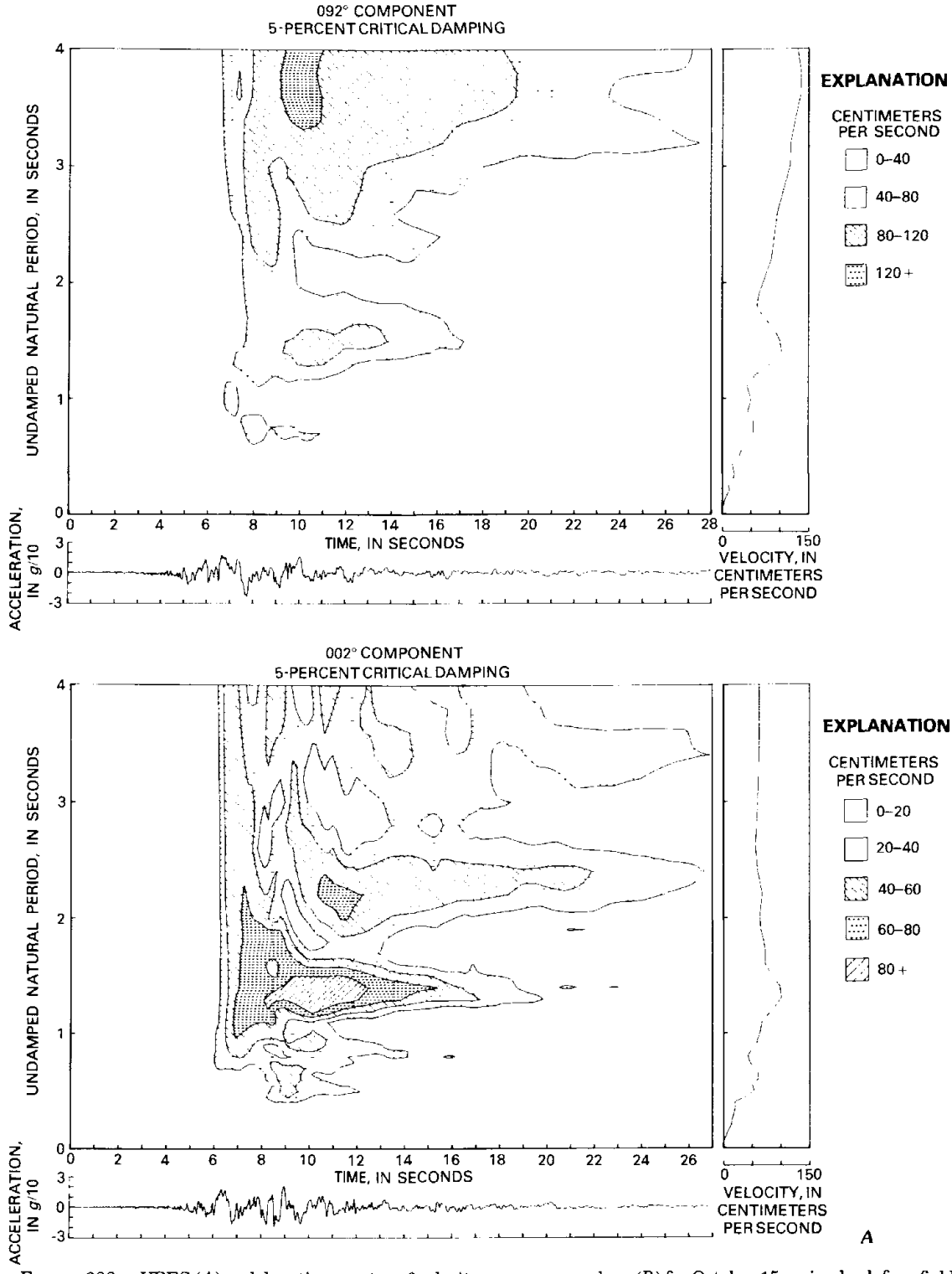

FIGURE 288.—VRES (*A*) and duration spectra of velocity response envelope (*B*) for October 15 main-shock free-field horizontal components recorded at Imperial County Services Building station.

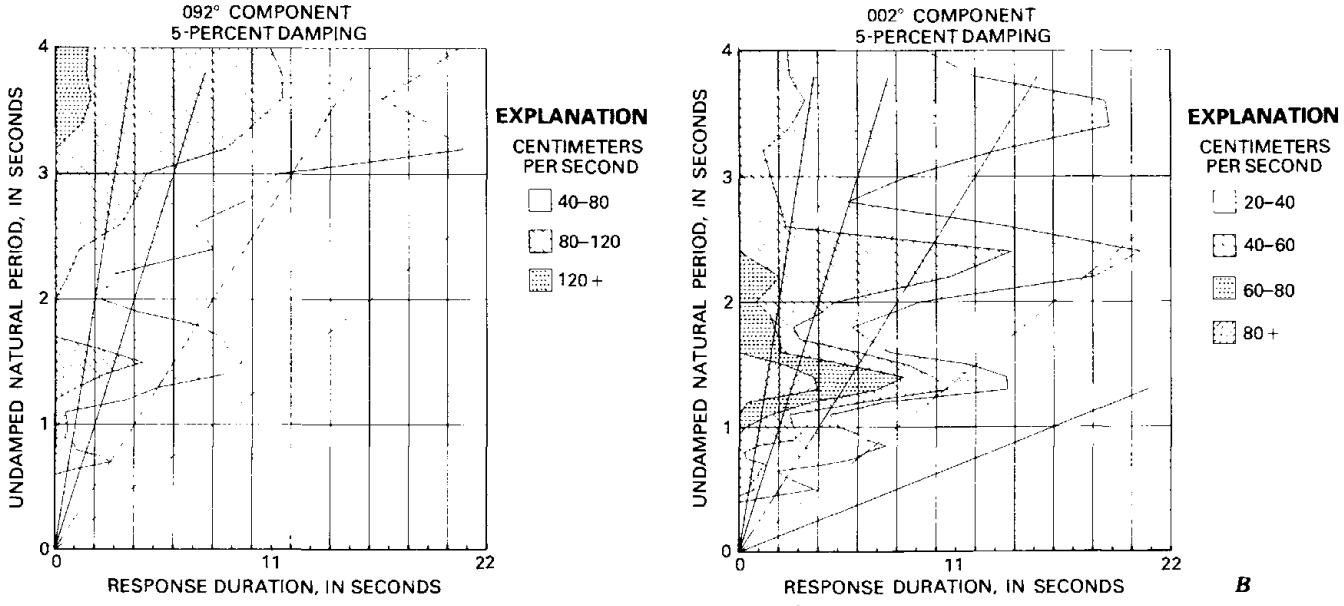

FIGURE 288.—Continued

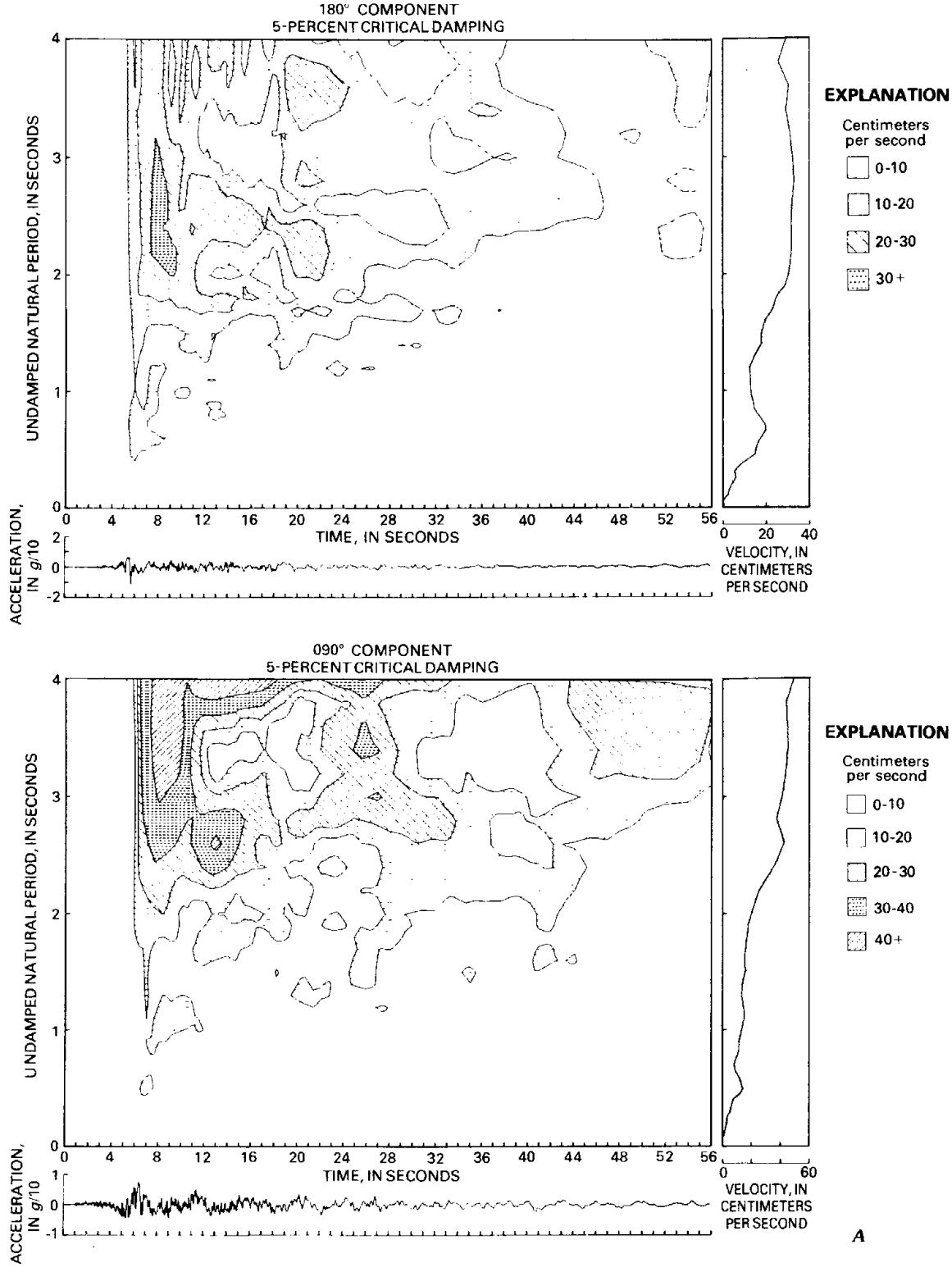

FIGURE 289.—VRES (*A*) and duration spectra of velocity response envelope (*B*) for October 15 main-shock horizontal components recorded at Westmorland ground-level station.

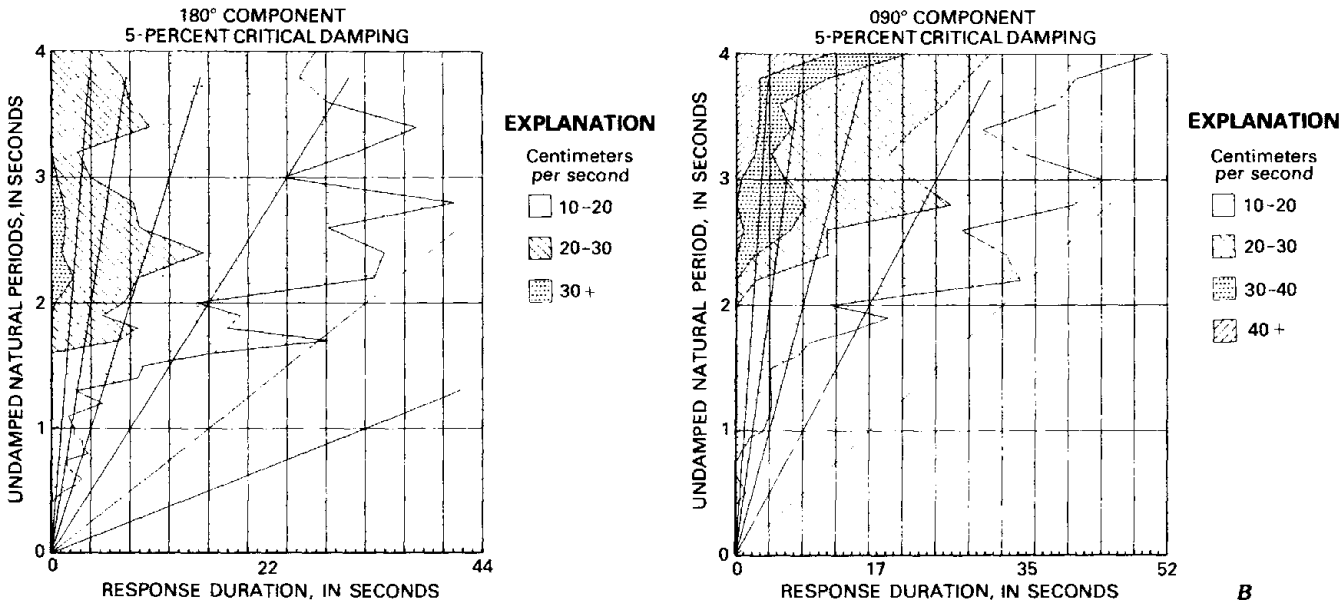

FIGURE 289.—Continued

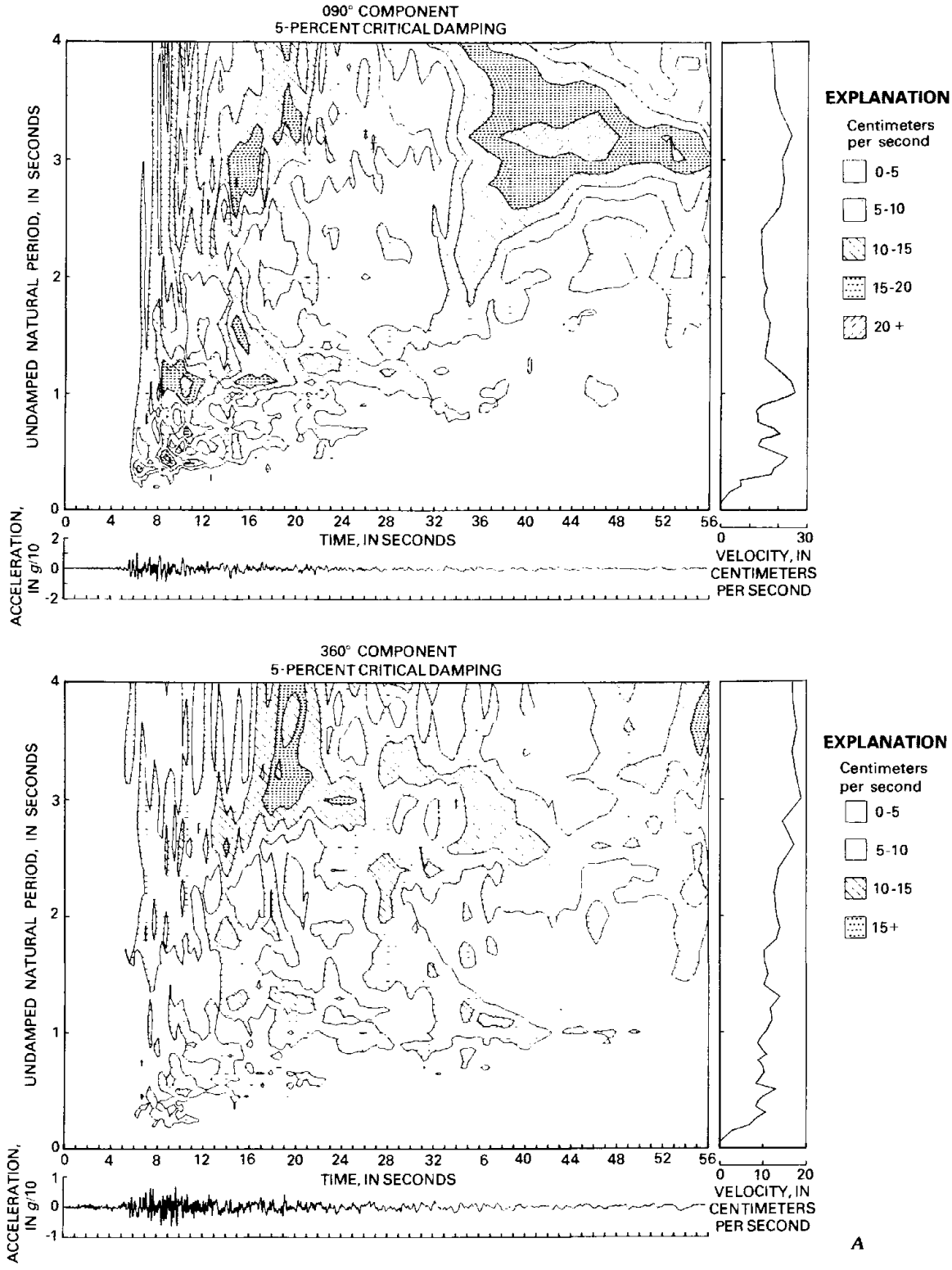

FIGURE 290.—VRES (*A*) and duration spectra of velocity response envelope (*B*) for October 15 main-shock horizontal components recorded at Niland ground-level station.

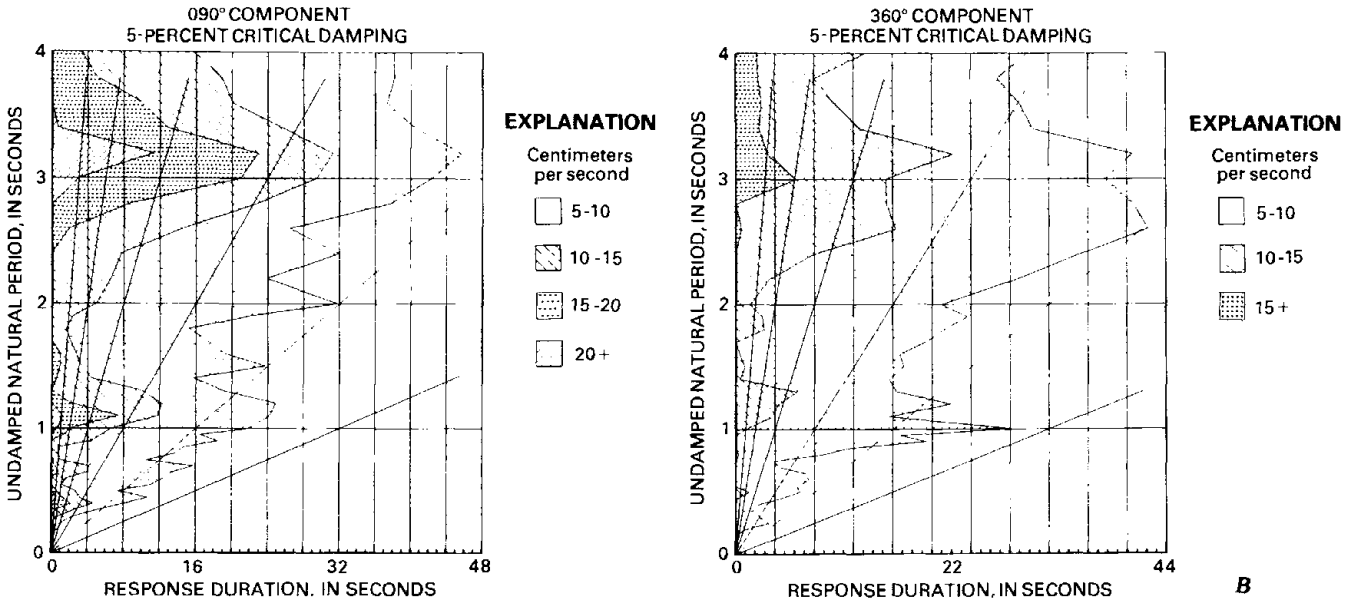

FIGURE 290.—Continued

M_L AND M_0 DETERMINATION FROM STRONG-MOTION ACCELEROGRAMS, AND EXPECTED-INTENSITY DISTRIBUTION

By A. F. ESPINOSA,
U.S. GEOLOGICAL SURVEY

CONTENTS

ABSTRACT

Generalized empirical relations derived to determine the local magnitude M_L and the seismic moment M_0 from strong-motion records in the Western United States yield for the 1979 Imperial Valley earthquake an M_L of 6.6, in excellent agreement with that obtained by the California Institute of Technology, and an M_0 of 1.1×10^{26} dyne-cm (11×10^{18} N·m), similar to the seismic moment for the 1940 Imperial Valley earthquake. Simulated modified Mercalli intensities (MMI's) for the 1979 event, using point and line sources, are much higher than those observed in the field. The observed isoseismals for the 1979 earthquake, relative to those for the 1940 event, are low. This difference is thought to be due to: (1) lower frequency content in the 1979 earthquake records, (2) shorter duration of the 1979 strong ground motion, and (3) less energy released during the first 15 s of the 1979 event. The observed horizontal accelerations agree fairly well with the expected ground accelerations calculated from an empirical attenuation law.

INTRODUCTION

The intensity and effect of ground motion depend on such earthquake-source parameters as magnitude, seismic moment, dimensions of the fault, distance to the fault rupture, and preferential direction of the slip surface (bilateral or unilateral). Furthermore, the composition of surficial geologic materials appears to influence ground shaking a great deal (Espinosa and Algermissen, 1972; Borcherdt, 1975). Therefore, one of the problems of estimating in advance the intensity of ground shaking at a point is the determination of the attenuation function for the surficial geology of the region under study.

The local magnitude M_L, a parameter developed by C. F. Richter, and the seismic moment M_0 are two measures of the size of an earthquake; both have a direct application to strong-motion and engineering seismology studies. The M_L determination, performed at short distances, takes into consideration some of the body-wave frequencies of interest to engineering, architecture, and earthquake-hazard reduction; M_L is more related to the intensity of ground shaking—and hence to damage—than the teleseismically determined magnitudes m_b and M_S. M_0 is an earthquake-source parameter that measures the size of an event and is free of the saturation level found in the magnitude scale for larger earthquakes. A newly developed procedure (Kanamori and Jennings, 1978; Espinosa, 1979, 1980) allows the evaluation of M_L from the accelerograms of moderate and larger earthquakes recorded at short epicentral distances; another newly developed procedure (A. F. Espinosa, unpub. data, 1980) allows the evaluation of M_0 from such accelerograms. A determination of the size of the October 15, 1979, earthquake in terms of M_L and M_0 is part of the subject of this report.

This report also includes an evaluation of the expected intensity of ground shaking on the modified Mercalli intensity (MMI) scale, taking into consideration the response of the generalized surficial geologic units in the area; these estimated intensities are then compared to the intensity ratings obtained in the field. A comparison of the 1940 and 1979 strong-motion accelerograms recorded at the same site in El Centro, Calif., is used to facilitate the investigation.

DETERMINATION OF M_L

The local magnitude M_L of the October 15, 1979, earthquake was determined from the maximum horizontal acceleration recorded at 30 U.S. Geological Survey accelerograph stations in the Imperial Valley (Porcella and others, this volume) and at 7 accelerograph stations in northern Mexico (Brune and others,

this volume). The M_L values, determined by means of the empirical scale law (Espinosa, 1980), are given by

$$M_L = 2.96 + \log_{10} \text{Acc} + 0.11\ (\log_{10} \Delta) + 0.5(\log_{10} \Delta)^2,$$

where Acc is the maximum horizontal ground acceleration and Δ is the epicentral distance (table 46). The magnitudes, plotted in figure 291, are not the mean M_L's but rather the M_L values that correspond to the maximum horizontal acceleration on each component of motion at a given station (table 46), denoted M_L (Acc). When the maximum horizontal ground accelerations from the 1979 earthquake recorded at each station (table 46) are compared with the expected mean horizontal-acceleration attenuation curves (Espinosa, 1980), the data agree fairly well—within ± 0.3 magnitude unit (fig. 291).

Using data from the U.S. Geological Survey network only, the mean local magnitude M_L (Acc) for the 1979 Imperial Valley earthquake is 6.66 ± 0.26, averaged over 60 horizontal components in the epicentral-distance range of about 6 to 196 km (Porcella and Matthiesen, 1979). The M_L values determined by the Pasadena and Berkeley seismologic laboratories from Wood-Anderson recordings are 6.6 and 7.0, respectively. If, instead of using the epicentral distance, we use the distance to the nearest point on the 1940 Imperial fault trace, we obtain, for this data set, a lower grand average M_L (Acc) of 6.11 ± 0.29. This value resembles that determined for the 1966 Parkfield, Calif., earthquake (Kanamori and Jennings, 1978; Espinosa, 1979).

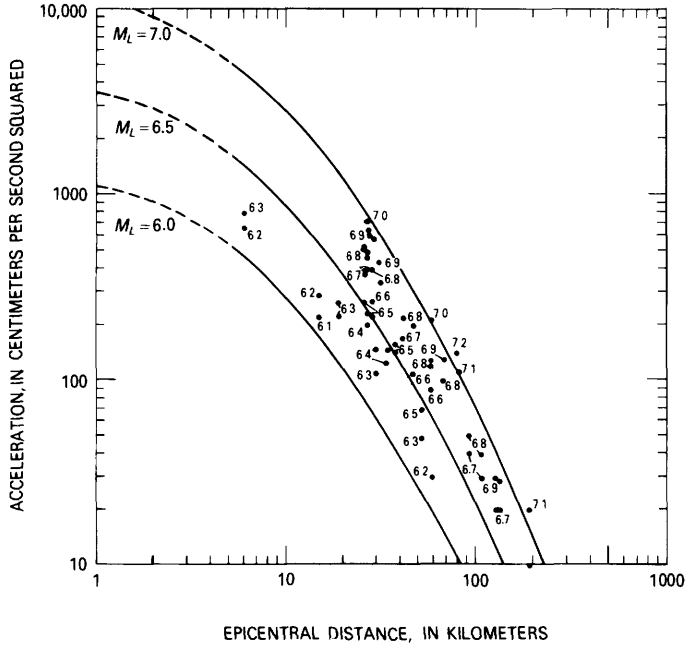

FIGURE 291.—Maximum acceleration from each horizontal component as a function of epicentral distance (see table 46). Numerals are M_L (Acc) (mean local magnitude) values. Solid lines, expected mean-attenuation values from empirical relation of Espinosa (1980); dashed lines, estimated extensions of curves.

Assuming that equation 1 is applicable to northern Mexico, the mean M_L is calculated to be 6.61 ± 0.27. This value is more representative of the size of the 1979 Imperial Valley earthquake because the data used cover a wider azimuthal distribution.

DETERMINATION OF M_0

The seismic moment M_0 for the 1940 Imperial Valley earthquake was determined to be 3.0×10^{26} dyne-cm (30×10^{18} N·m) (Hanks and others, 1975). Using strong-motion horizontal accelerations at short distances, M_0 for the 1979 earthquake may be computed from the empirically derived relation (A. F. Espinosa, unpub. data, 1980), which excluded the 1979 strong-motion data:

$$M_0 = 1.62 \times 10^{21} \text{Acc} \cdot \Delta^{1.6}, \quad (2)$$

where Acc is the maximum horizontal acceleration and Δ is the epicentral distance. The average value of M_0 computed from the tabulated strong-motion data (table 46) is 1.1×10^{26} dyne-cm (11×10^{18} N·m). Thus, the 1940 and 1979 M_0 values are in fairly good agreement.

COMPARISON OF 1940 AND 1979 ACCELEROGRAMS

The Imperial Valley earthquake of May 18, 1940, which had an M_L of 6.5 (Kanamori and Jennings, 1978, app. 1) or 6.4 (Trifunac and Brune, 1970; Espinosa, 1980), was recorded at an epicentral distance of 21 km at El Centro array station 9, where the maximum reported accelerations on the east and north components were 210 and 342 cm/s^2, respectively (fig. 292*A*). The same station recorded the 1979 earthquake and showed similar horizontal accelerations of 265 and 392 cm/s^2 (fig. 292*B*; table 46). When the tracings of the accelerograms from El Centro array station 9 (Porcella and Matthiesen, 1979, p. 18) are compared with those for the 1940 earthquake, the richness of high-frequency energy is apparent on the vertical component of motion (fig. 293) from both earthquakes. The time interval displayed in this figure is 25 s. Significant ground motion in the 1940 event evidently lasted much longer than in 1979, when the vertical component amplitudes decayed almost exponentially to a low level of ground motion after about 11 s from the triggering time. When the horizontal components of the 1940 accelerogram at El Centro array station 9 (fig. 292*A*) are compared with those of the 1979 accelerogram (fig. 292*B*), it is also evident that (1) the 1979 event was as complex as the 1940 multiple rupture, and (2) the energy released during the first 15 s in the 1979 event was less than in the 1940 event, as described by Trifunac and Brune (1970).

TABLE 46.—*Local magnitude (M_L) determined from the maximum horizontal acceleration measured on strong-motion instruments for the 1979 Imperial Valley earthquake*

[Station code, name, latitude, and longitude from U.S. Geological Survey (1976). Epicentral distance, orientation, and acceleration from Porcella and Matthiesen (1979). Numbers in parentheses are distances to nearest point on 1940 Imperial fault trace (Porcella and Matthiesen, 1979); epicentral distances for station codes 6600 and higher art from Brune and others (this volume)]

Code	Station	Lat N.	Long W.	Epicentral distance (km)	Orientation	Acceleration (cm/s²)	M_L (Acc)
5028	El Centro array station 7	32.83°	115.50°	26 (1)	230°	509.6	6.82
					140°	352.8	6.66
942	El Centro array station 6	32.84°	115.49°	27 (1)	230°	441.0	6.79
					140°	705.6	6.99
5054	Bonds Corner	32.69°	115.34°	6 (3)	230°	793.8	6.25
					140°	646.8	6.16
958	El Centro array station 8	32.81°	115.53°	27 (4)	230°	490.0	6.83
					140°	627.2	6.94
952	El Centro array station 5	32.86°	115.47°	28 (4)	230°	392.0	6.76
					140°	548.0	6.91
5165	El Centro differential array	32.80°	115.54°	26 (5)	360°	499.8	6.82
					270°	362.6	6.68
117	El Centro array station 9	32.79°	115.55°	26 (6)	360°	392.0	6.71
					90°	264.6	6.54
955	El Centro array station 4	32.86°	115.43°	26 (7)	230°	372.4	6.69
					140°	597.8	6.89
5060	Brawley Airport	32.99°	115.51°	42 (7)	315°	215.6	6.79
					225°	166.6	6.68
5055	Holtville	32.81°	115.38°	19 (8)	315°	215.6	6.25
					225°	254.8	6.32
412	El Centro array station 10	32.78°	115.57°	27 (9)	50°	196.0	6.43
					320°	225.4	6.49
5053	Calexico Fire Station	32.67°	115.49°	15 (11)	315°	215.6	6.11
					225°	274.4	6.22
5058	El Centro array station 11	32.75°	115.59°	27 (13)	230°	372.4	6.71
					140°	372.4	6.71
5057	El Centro array station 3	32.89°	115.38°	28 (13)	230°	215.6	6.50
					140°	264.6	6.59
5051	Parachute Test Site	32.93°	115.70°	47 (15)	315°	196.0	6.83
					225°	107.8	6.57
5115	El Centro array station 2	32.92°	115.37°	31 (16)	230°	421.4	6.86
					140°	323.4	6.75
931	El Centro array station 12	32.72°	115.64°	30 (18)	230°	107.8	6.25
					140°	147.0	6.38
5061	Calipatria Fire Station	33.13°	115.52°	57 (21)	315°	88.2	6.64
					225°	127.4	6.80
5059	El Centro array station 13	32.71°	115.68°	34 (22)	230°	147.0	6.47
					140°	117.6	6.37
5056	El Centro array station 1	32.96°	115.32°	37 (22)	230°	147.0	6.53
					140°	147.0	6.53
286	Superstition Mountain	32.95°	115.82°	57 (26)	135°	205.8	7.01
					45°	117.6	6.77
5062	Salton Sea	33.18°	115.62°	66 (28)	315°	98.0	6.81
					225°	127.4	6.92
5052	Plaster City	32.79°	115.86°	52 (31)	135°	68.6	6.46
					45°	49.0	6.31
5066	Coachella Canal station 4	33.36°	115.59°	84 (47)	135°	137.2	7.16
					45°	107.8	7.06
5050	Ocotillo Wells	33.14°	116.13°	93 (59)	315°	49.0	6.80
					225°	39.2	6.71
2316	Yuma	32.73°	114.70°	60 (61)	90°	29.4	6.20
					360°	29.4	6.20
5049	Borrego Air Ranch	33.19°	116.28°	108 (74)	315°	39.2	6.84
					225°	29.4	6.72
5047	Rancho de Anza	33.35°	116.40°	127 (92)	135°	29.4	6.87
					45°	19.6	6.70
5063	Coachella Canal station 1	33.64°	116.08°	131 (92)	135°	19.6	6.73
					45°	29.4	6.90
5073	Cabazon	33.92°	116.78°	196 (158)	270°	9.8	6.83
					180°	19.6	7.13
6604	Cerro Prieto	32.42°	115.30°	24	237°	146.0	6.23
					147°	163.7	6.28
6621	Chihuahua	32.49°	115.24°	19	12°	261.7	6.34
					282°	257.7	6.33
6622	Compuertas	32.58°	115.09°	23	15°	184.2	6.30
					285°	146.0	6.20
6617	Cucapah	32.55°	115.23°	14	85°	303.8	6.23
6605	Delta	32.36°	115.19°	33	352°	342.0	6.81
					262°	230.3	6.64
6619	Mexicali SAHOP	32.62°	115.42°	13	0°	304.8	6.19
					90°	449.8	6.36
6610	Victoria	32.29°	115.10°	44	75°	119.6	6.57
					345°	159.7	6.69
Mean M_L using U.S. stations							6.66± 0.26
Mean M_L using U.S. and Mexican stations							6.61± 0.27

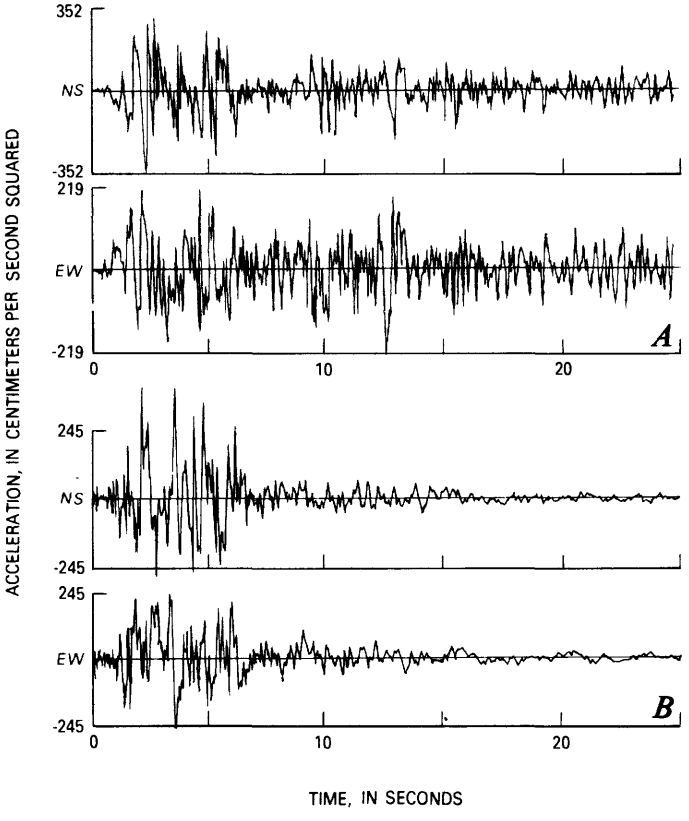

FIGURE 292.—Horizontal accelerograms of two Imperial Valley earthquakes. *A*, Digital playback of horizontal accelerograms of 1940 earthquake recorded at El Centro array station 9. *B*, Tracing of horizontal accelerograms of 1979 earthquake recorded at El Centro array station 9.

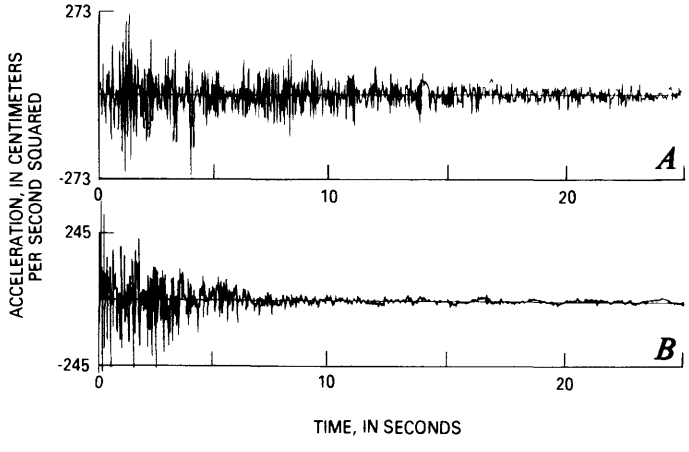

FIGURE 293.—Vertical accelerograms of two Imperial Valley earthquakes. *A*, Digital playback of vertical accelerogram of 1940 earthquake recorded at El Centro array station 9. *B*, Tracing of vertical accelerogram of 1979 earthquake recorded at El Centro array station 9.

EXPECTED INTENSITIES

In several recent reports (Evernden, 1975; Espinosa, 1977; Espinosa and López-Arroyo, 1977) a procedure has been proposed to derive the seismic intensity at a point for a given-size (local magnitude) earthquake. In some of these reports, empirical relations have been derived from records of earthquakes in California that allow extension of this procedure to estimate the MMI distribution, using the underlying geologic units as an additional variable. The predicted isoseismal for a given source (point or a fault of finite length) are evaluated at the same points where observational data (Reagor and others, this volume) were obtained from the 1979 Imperial Valley earthquake. The geologic units are those on the "Geologic Map of California" (U.S. Geological Survey and California Division of Mines and Geology, 1966). The 11 geologic units on this map are grouped into four general categories: (1) Precambrian rocks of all types, pre-Cenozoic metamorphic rocks, Mesozoic granitic rocks, and Mesozoic ultramafic rocks; (2) late Mesozoic eugeosynclinal rocks, Mesozoic sedimentary and volcanic rocks, and Paleozoic sedimentary and volcanic rocks, in places strongly metamorphosed; (3) Cenozoic marine sedimentary rocks, Cenozoic volcanic rocks, and late Mesozoic shelf and slope sedimentary rocks; and (4) Cenozoic nonmarine sedimentary rocks and alluvial deposits. Although these four categories are quite general, their purpose is to characterize the geologic units by their seismic responses. The seismic-response value is subtracted from the predicted MMI at the site under consideration. The seismic-response values used are: for category 1, 2.59; for category 2, 1.58; for category 3, 1.0; and for category 4, 0 (Espinosa and López-Arroyo, 1977). The procedure to predict MMI ratings at a point (Espinosa, 1977) is rather straightforward. This procedure has been tested using data on the 1952 Kern County, Calif., earthquake with satisfactory results. Similar techniques have been developed in the U.S.S.R. (see Medvedev, 1962).

Figure 294 displays the predicted isoseismals for the 1979 Imperial Valley earthquake, showing both the MMI values predicted using the epicentral location (lat 32.64° N., long 115.33° W.) as the source of energy release (fig. 294*A*) and the MMI values predicted using the total length of the mapped fault (approx 30 km; Sharp and others, this volume) as the source of energy release (fig. 294*B*). The fault is assumed to extend from lat 32.71° N., long 115.39° W., to lat 32.94° N., long 115.54° W. These two maps show that the expected MMI ratings for the 1979 event are far higher than those observed in the field (Reagor and others, this volume).

The overall distribution of expected intensities (fig. 294) generally agrees with the observed isoseismal shapes; the MMI values, however, do not. Some of the closed contours for an MMI of III agree with observations in the field.

There are several possible explanations for the discrepancy between expected and observed intensity values. (1) The model used does not apply to this area because the intensity attenuation is quite different

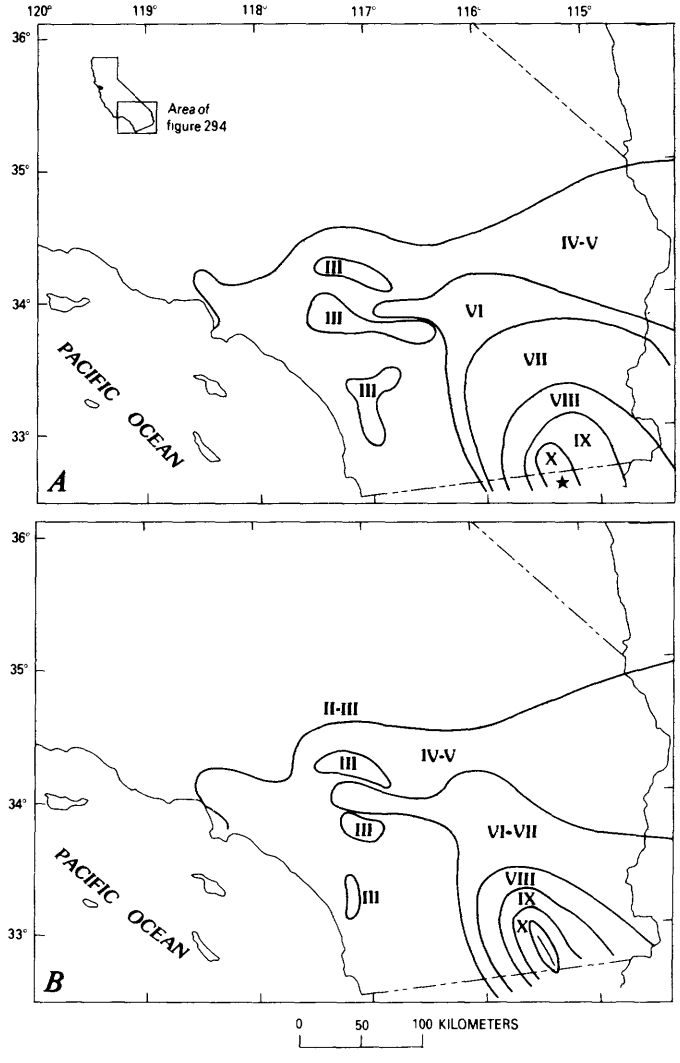

FIGURE 294.—Predicted isoseismal distribution and MMI values of 1979 Imperial Valley earthquake, evaluated using a geologic-unit correction factor. Geologic units are those shown on "Geologic Map of California" (U.S. Geological Survey and California Division of Mines and Geology, 1966). *A*, Distribution based on epicentral location (star). *B*, Distribution based on mapped surface rupture (Sharp and others, this volume). Diagonal line represents length of fault (31 km).

there from that in other areas of California. (2) The categories of geologic units are too general and may increase the predicted intensities by half an intensity unit or more. (3) The length of faulting used may be too great and may yield an overestimation of the MMI distribution. (4) The duration of strong shaking for this event was shorter than that for an event of similar size, such as the 1940 Imperial Valley earthquake (figs. 292, 293). The duration of shaking will affect the damage sustained at short distances from the region of energy release and thus will affect the overall intensity ratings.

In comparison with the 1940 Imperial Valley earthquake (M_L=6.5), the 1979 event (M_L=6.61) caused less damage and thus had lower intensities. In addition to the longer duration of shaking in the 1940 event, other possible reasons for this difference may be that (1) lower frequencies were excited in the horizontal components of ground motion during the 1979 event, and (2) more energy was released in the first 15 s of ground shaking during the 1940 event. The predicted isoseismals for the 1979 earthquake (fig. 294) and for the 1940 earthquake (Neumann, 1942) generally agree in their pattern distribution and in the MMI ratings assigned to the isoseismals.

CONCLUSIONS

(1) The observed horizontal peak ground accelerations from the 1979 event agree fairly well with the ground-level accelerations expected for a similar-size event, derived from an empirical attenuation law for the Western United States. (2) The M_L of 6.61 determined from the peak horizontal accelerations agrees with the M_L of 6.6 determined from Wood-Anderson recordings at the California Institute of Technology. (3) The M_0 of 1.1×10^{26} dyne-cm (11×10^{18} N·m) determined using the strong-motion records agrees fairly well with the M_0 of 3.0×10^{26} dyne-cm (30×10^{18} N·m) for the 1940 event (M_L=6.5). (4) The reasons for the low intensities—and, therefore, absence of damage—in the 1979 event, in contrast to the 1940 event, are believed to be: (a) lower frequency content in the earthquake signature, (b) shorter duration of strong ground shaking, and (c) less energy released in the "possible multiple earthquake" occurrence during the first 15 s.

REFERENCES CITED

Borcherdt, R. D., ed., 1975, Studies for seismic zonation of the San Francisco Bay region: U.S. Geological Survey Professional Paper 941-A, p. A1-A102.

Espinosa, A. F., 1977, Particle-velocity attenuation relations: San Fernando earthquake of February 9, 1971: Seismological Society of America Bulletin, v. 67, no. 4, p. 1195-1214.

———1979, Horizontal particle velocity and its relation to magnitude in the Western United States: Seismological Society of America Bulletin, v. 69, no. 6, p. 2037–2061.

———1980, Attenuation of strong horizontal ground accelerations in the Western United States and their relation to M_L: Seismological Society of America Bulletin, v. 70, no. 2, p. 583–616.

Espinosa, A.F., and Algermissen, S. T., 1972, A study of soil amplification factors in earthquake damage areas, Caracas, Venezuela: National Oceanic and Atmospheric Administration Technical Report ERL 280–ESL 31, 201 p.

Espinosa, A.F., and López-Arroyo, A., 1977, Earthquake instrumental intensity from strong ground motion records; San Fernando earthquake: World Conference on Earthquake Engineering, 6th, New Dehli, India, 1977, Proceedings, v. 1, p. 367–373.

Evernden, J. F., 1975, Seismic intensities, "size" of earthquakes and related phenomena: Seismological Society of America Bulletin, v. 65, no. 5, p. 1287–1313.

Hanks, T. C., Hileman, J. A., and Thatcher, Wayne, 1975, Seismic moments of the larger earthquakes of the Southern California region: Geological Society of America Bulletin, v. 86, no. 8, p. 1131–1139.

Kanamori, Hiroo, and Jennings, P. C., 1978, Determination of local magnitude, M_L, from strong-motion accelerograms: Seismological Society of America Bulletin, v. 68, no. 2, p. 471–485.

Medvedev, S. V., 1962, Engineering seismology: Moscow, U.S.S.R. Academy of Sciences, 260 p.

Neumann, Frank, 1942, United States earthquakes, 1940: U.S. Coast and Geodetic Survey Serial 647, 74 p.

Porcella, R. L., and Matthiesen, R. B., 1979, Preliminary summary of the U.S. Geological Survey strong-motion records from the October 15, 1979 Imperial Valley earthquake: U.S. Geological Survey Open-File Report 79–1654, 41 p.

Trifunac, M. D., and Brune, J. N., 1970, Complexity of energy release during the Imperial Valley, California, earthquake of 1940: Seismological Society of America Bulletin, v. 60, no. 1, p. 137–160.

U.S. Geological Survey, 1977, Western Hemisphere strong-motion accelerograph station list—1976: Open-File Report 77–374, 112 p.

U.S. Geological Survey and California Division of Mines and Geology, compilers, 1966, Geologic map of California: U.S. Geological Survey Miscellaneous Geologic Investigations Map I–512, scale 1:2,500,000.

PEAK HORIZONTAL GROUND MOTIONS FROM THE MAIN SHOCK: COMPARISON WITH DATA FROM PREVIOUS EARTHQUAKES

By D. M. BOORE and R. L. PORCELLA,
U.S. GEOLOGICAL SURVEY

CONTENTS

ABSTRACT

The peak horizontal ground motions from the 1979 Imperial Valley earthquake at distances greater than about 15 km from the fault surface agree excellently with values from previous earthquakes of similar magnitude: 71 percent of the new peak-acceleration data fall within the 70-percent prediction intervals defined by the previous data. The peak velocities and displacements are predicted almost as well. The primary significance of these new data is that they include records at distances less than 10 km, where few data are available from previous earthquakes. An understanding of the full implications of the new data for general attenuation relations between peak ground motion and distance to the fault surface awaits further study of the effects on the recorded motions of fault propagation, radiation pattern, and geologic structure.

INTRODUCTION

The strong-motion recordings from the 1979 Imperial Valley earthquake form the most valuable data set available for studies of ground motion close to a fault: numerous recordings were made at close distances to the fault; absolute timing is available on many of the records; and detailed correlative studies that will be invaluable for further analysis of the data, such as studies of geologic structure, aftershock locations, and ground deformation around the fault, are now or will soon be available. These strong-motion data should be the subject of numerous detailed investigations for the next few years. It seems useful at this time, however, to put the new data into perspective by seeing how one measure of the strong motion—peak horizontal ground motion—compares with that from previous earthquakes.

DATA ANALYSIS

In a convenient summary of previous earthquake records by Boore and others (1978, 1980), data from western North America were divided into various magnitude classes (using local Richter magnitudes where available) and then subdivided according to whether they were recorded at the base of buildings two stories high or lower, at dam abutments, or at the base of buildings higher than two stories. For the regression curves, the largest motion from the two horizontal components at a given site was plotted against the closest distance to the fault surface on a log-log plot, and a straight line was fitted to the data over a distance interval for which a significant number of data were available. For the magnitude class 6.0–6.4 this distance was 15 to 55 km. Only two data points were available at closer distances, and at greater distances some bias may have been present because not all instruments were triggered. The 1971 San Fernando, Calif., earthquake, with combined thrusting and strike-slip-fault slip, provided most of the data. Figure 295 compares the data from the 1979 Imperial Valley earthquake with the best-fit straight line and confidence limits for previous earthquakes in the magnitude class 6.0–6.4 (Boore and others, 1980).

Table 47 lists the main-shock ground-motion data for the 1979 Imperial Valley earthquake. For accelerations less than $0.10\,g$ we retained two significant digits after scaling peak horizontal accelerations from the original records. These records are from buildings lower than three stories; three records are from two-story buildings; and the rest are from single-story buildings or small instrument shelters, including the Meloland Road-Interstate Highway 8 overcrossing site, a free-field installation on the median strip 61 m from the overcrossing, and the Imperial County Center record, obtained from a free-field instrument shelter approximately 100 m east of the six-story Imperial County Services Building in El Centro, Calif. The peak-velocity and displacement data are from Brady and others (this volume); data from several of the more distant stations

were not available at the time of this writing.

The distances listed in table 47 required some interpretation on our part. The location of the 1979 rupture surface is uncertain at the south end of the fault, where no ground breakage was near the epicenter, and at the north end, where the surface trace of the Imperial fault splays into several segments. Furthermore, the Brawley fault zone showed surface slip, and although its contribution to the accelerograms has not yet been determined, we assume that it played a minor role in the horizontal ground motions. We adopted the following procedure in measuring distances: we used the point on the surface trace of the 1979 Imperial fault rupture nearest the station, unless that point was at the north or south end of the rupture. If it was at the north end, we measured the station distance from a point on the surface at lat 32°55′ N., long 115°32.5′ W.; if it was at the south end (involving primarily the distances to stations in Mexico), we assumed the slipped surface of the fault to be 5 km below the surface trace of the 1940 fault rupture (except for Bonds Corner, where the slipped surface was assumed to be at 3-km depth).

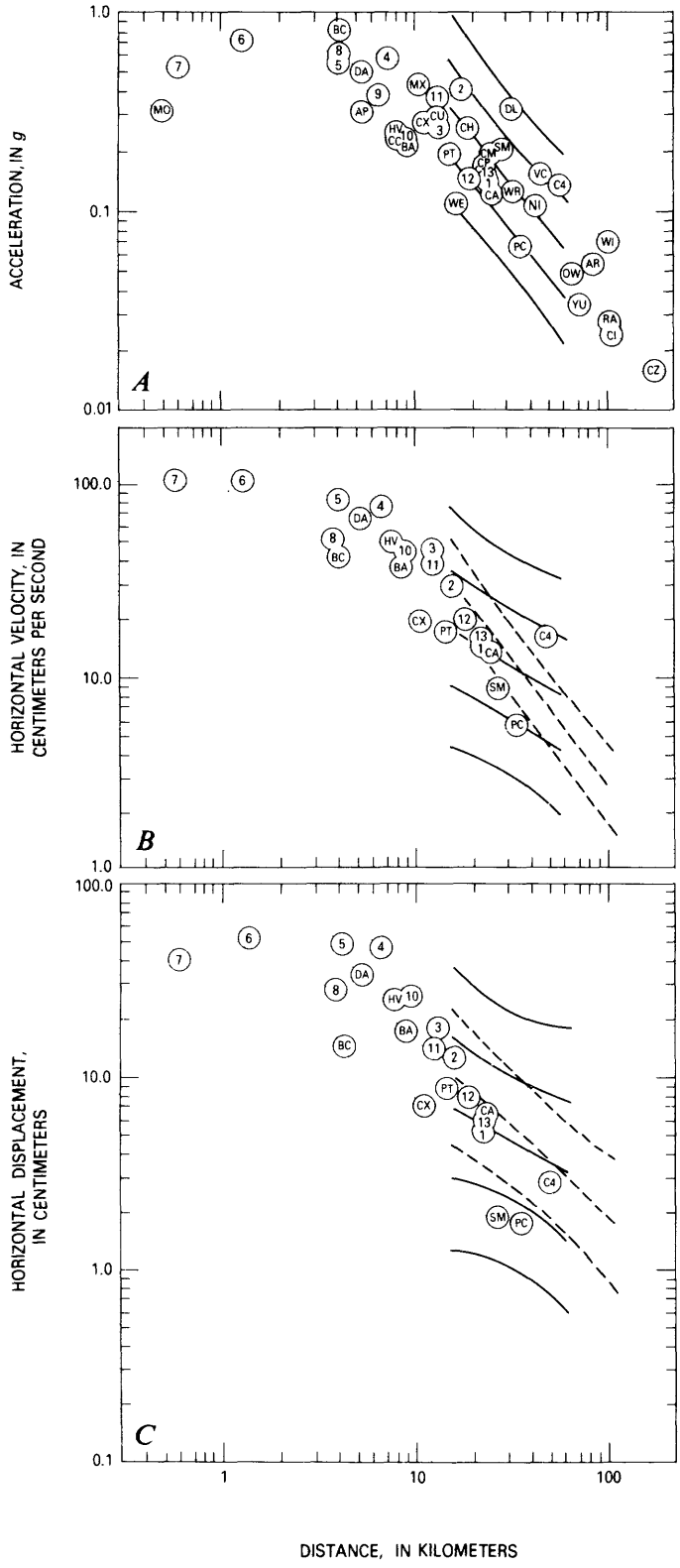

FIGURE 295.—October 15 main-shock peak horizontal ground motions as a function of closest distance to slipped part of fault surface, in comparison with data from previous earthquakes of similar magnitude. See table 47 for station data and explanation of symbols. Curves are regression lines from Boore and others (1978, 1980); mean regression line is bounded by 70- and 95-percent prediction intervals (for example, 70 percent of data points should fall within 70-percent prediction interval). Mean regression line and prediction bounds for soil-site data from 1971 San Fernando, Calif., earthquake almost coincide with curves shown and have been omitted for clarity. Dashed lines in figures 295*B* and 295*C* are mean regression lines and 70-percent prediction bounds for soil-site data from 1971 San Fernando, Calif., earthquake (Boore and others, 1978). *A*, Peak horizontal acceleration. *B*, Peak horizontal velocity. *C*, Peak horizontal displacement.

DISCUSSION

The agreement between previous data, as summarized by the regression lines, and the ground motions from the 1979 Imperial Valley earthquake is excellent (see fig. 295*A*): for peak acceleration, 12 of the 17 values from the 1979 earthquake (71 percent) fall within the 70-percent prediction intervals, and all fall within the 95-percent prediction intervals. The comparison is also good for the peak-velocity and displacement data (figs. 295*B*, 295*C*). As discussed by Boore and others (1978), the slopes of the regression lines fitting the velocity and displacement data are not well determined because nontriggering of instruments (for one of the earthquakes providing data) limited the distance range used in the regression analysis. The mean regression line and 70-percent prediction intervals determined from data for soil sites in the 1971 San Fernando, Calif., earthquake are shown for comparison (dashed lines, figs. 295*B*, 295*C*); the slopes of these lines agree with the data better than do those of the solid lines. A more detailed comparison with the regression estimates for

TABLE 47.—*Main-shock ground-motion data*

[Station owners: USGS, U.S. Geological Survey; CDMG, California Division of Mines and Geology; UNAM, Universidad Nacional Autónoma de México; UCSD, University of California, San Diego. Distance is measured from station to slipped surface at Imperial fault (see text); numbers in brackets are distances to Brawley fault zone. Acceleration, velocity, and displacement are for peak horizontal motion on one of two orthogonal horizontal components; vertical peak acceleration was larger at several stations (data from Porcella and Matthiesen, 1979; Brune and others, this volume; and Porcella and others, this volume)]

Code	Station	Distance (km)	Acceleration (g)	Velocity (cm/s)	Displacement (cm)
	USGS stations				
7	El Centro station 7	0.6	0.52	110	41
6	El Centro station 6	1.3 [1.0]	.72	110	55
8	El Centro station 8	3.8	.64	53	29
5	El Centro station 5	4.0 [1.0]	.56	87	52
BC	Bonds Corner	4.0	.81	44	15
DA	El Centro differential array	5.1	.51	68	34
9	El Centro station 9	6.2	.40	--	--
4	El Centro station 4	6.8 [4.1]	.61	78	48
HV	Holtville Post Office	7.5	.26	48	25
BA	Brawley Airport	8.5 [3.6]	.22	37	19
10	El Centro station 10	8.5	.23	44	27
CX	Calexico Fire Station	10.6	.28	19	7.0
11	El Centro station 11	12.6	.38	39	14
3	El Centro station 3	12.7 [9.4]	.27	46	18
PT	Parachute Test Site	14	.20	17	9.2
2	El Centro station 2	16 [11]	.43	31	13
12	El Centro station 12	18	.15	19	8.4
1	El Centro station 1	22 [15]	.15	15	5.5
13	El Centro station 13	22	.15	15	6.0
CA	Calipatria Fire Station	23	.13	15	6.9
SM	Superstition Mountain	26	.21	9.0	1.9
WR	Salton Sea Wildlife Refuge	29	.13	--	--
PC	Plaster City	32	.066	5.8	1.8
C4	Coachella Canal station 4	49	.14	16	3.1
OW	Ocotillo Wells	60	.049	--	--
YU	Yuma	64	.034	--	--
AR	Borrego Air Ranch	75	.043	--	--
RA	Rancho de Anza	93	.027	--	--
C1	Coachella Canal station 1	94	.025	--	--
CZ	Cabazon Post Office	160	.016	--	--
	CDMG stations				
MO	Meloland Road-Interstate Highway overcrossing	.8	.32	--	--
CC	El Centro, Imperial County Center	7.6	.24	--	--
WE	Westmorland	15	.11	--	--
NI	Niland	36	.10	--	--
WI	Winterhaven	86	.05	--	--
	UNAM and UCSD stations				
AP	Aeropuerto	5.0	.32	--	--
MX	Mexicali SAHOP	9.7	.46	--	--
CH	Chihuahua	17	.27	--	--
CU	Cucapah	12.7	.31	--	--
CP	Cerro Prieto	22	.17	--	--
CM	Compuertas	23	.19	--	--
DL	Delta	29	.35	--	--
VC	Victoria	42	.16	--	--

peak velocities and displacements awaits the integration of accelerograms at distances greater than about 25 km.

We have 19 data points for distances within 15 km of the slip surface, in comparison with only 2 points in the data set analyzed by Boore and others (1978, 1980). Because the new peak-acceleration data fall below an inward extrapolation of the mean regression line, a single power-law relation between peak horizontal ground acceleration and distance is inappropriate. This result, however, is not unexpected; many workers concerned with attenuation laws have postulated a flattening of the curves at close distances. We may now have enough data to draw quantitative conclusions about the shape of the curve. Before assigning any universality to the attenuation curve derived from the new data, however, the effects on the recorded motions of fault propagation, radiation pattern (which may explain the low value at the Meloland Road-Interstate Highway 8 overcrossing; MO, fig. 295*A*), and geologic structure must be understood.

ACKNOWLEDGMENTS

We thank Jim Brune for permission to use the Universidad Nacional Autónoma de México/University of California, San Diego, data in advance of publication in this volume, and Tom Wootton for providing the California Division of Mines and Geology data listed in table 47.

REFERENCES CITED

Boore, D. M., Joyner, W. B., Oliver, A. A., III, and Page, R. A., 1978, Estimation of ground motion parameters: U.S. Geological Survey Circular 795, 43 p.

———1980, Peak acceleration, velocity, and displacement from strong-motion records: Seismological Society of America Bulletin, v. 70, no. 1, p. 305–321.

Porcella, R. L., and Matthiesen, R. B., 1979, Preliminary summary of the U.S. Geological Survey strong-motion records from the October 15, 1979 Imperial Valley earthquake: U.S. Geological Survey Open-File Report 79–1654, 41 p.

AFTERSHOCK ACCELEROGRAMS RECORDED ON A TEMPORARY ARRAY

By J. G. ANDERSON,
SCRIPPS INSTITUTION OF OCEANOGRAPHY;

and

T. H. HEATON,
CALIFORNIA INSTITUTE OF TECHNOLOGY

CONTENTS

ABSTRACT

We recovered 52 timed analog accelerograms from 25 aftershocks of the 1979 Imperial Valley earthquake, between 3:33 p.m. P.d.t. October 16 and 5:43 a.m. October 31. The largest aftershock that we recorded (M_L=4.9) occurred at 4:16 p.m. October 16. This aftershock triggered eight accelerographs; preliminary estimates of epicentral distance range from 7 to 35 km. The data from this aftershock may be useful for study of both source and wave-propagation phenomena in the Imperial Valley.

INSTRUMENTATION

In the evening hours after the October 15, 1979, earthquake, a field crew was organized. Beginning early the next morning, they installed 10 accelerographs along the Imperial fault from north of Brawley, Calif., to the United States-Mexican border, with the object of recording aftershocks. The accelerographs (Kinemetrics model SMA-1) record three components of acceleration on 70-mm film, in the amplitude range of less than 0.01 to more than 1 g and in the frequency band 0 to about 25 Hz. These instruments were slated to be installed in the Los Angeles area as part of a network being established there by the University of Southern California and the California Division of Mines and Geology.

Each instrument has an internal clock (Kinemetrics TCG-1) that generates a time code to be recorded on the film. The clocks have a temperature-compensated crystal oscillator with a frequency stability of $\pm 3 \times 10^{-7}$ in the temperature range 0°-50°C; this stability implies a daily drift of less than 26 ms, provided the crystal frequency is set properly. The clocks tended to drift much less than this limit. Clocks were corrected in the laboratory before instrument deployment, at the time of installation on October 16, at most stations on October 17, and at the time the instruments were recovered on November 1 or 2. There is no reason to suspect an uncertainty of greater than 10 ms in the clock corrections interpolated to the occurrence times of aftershocks. Table 48 lists the locations, elevations, and orientations of the accelerograph installations (see fig. 296), as well as the sensor characteristics for each accelerometer.

RECOVERED DATA

One or more of the accelerographs were triggered by at least 25 aftershocks with preliminary local magnitudes estimated at from less than 3.0 to 4.9. Because of clock problems, the times of 5 of the 52 total triggerings are uncertain. Triggering times and S-wave arrival times for the remaining 47 records (table 49) were read directly from the film accelerograms. In addition to these data, table 49 lists the stations that recorded the aftershocks and the peak accelerations recorded for each aftershock. These peak accelerations, obtained from the maximum trace amplitudes, have not been corrected for the response of the accelerometers. Figure 297 illustrates the spatial relation between the preliminary aftershock locations and the accelerographs that recorded them. About 75 percent of the triggerings occurred on the three northernmost accelerographs (stations 3689, 3692, 3698, fig. 296); the two southernmost stations (3695, 3696) did not record any aftershocks. This pattern is consistent with the distribution of the aftershock sequence, in which most of the later aftershocks occurred north of Brawley, Calif. (Johnson and Hutton, this volume).

TABLE 48.—*Temporary accelerograph sites*

[Location is within ±0.003°. Sensor orientation is direction of ground motion that causes positive trace motion on the film; upward ground acceleration causes positive trace motion on the vertical component. Accelerograph characteristics were supplied by Kinemetrics; damping is 60 percent of critical on all instruments]

Site	Station	Location		Elevation (ft)	Sensor orientation (azimuth)		Accelerograph characteristics		
		Latitude N.	Longitude W.		Longitudinal	Transverse	Axis	Sensitivity (mm/g)	Natural frequency (Hz)
Del Rio Country Club	3698	33.0095°	115.5207°	−145	081°	351°	Long.	18.9	25.8
							Vert.	18.8	25.6
							Trans.	18.3	25.7
Brawley Airport	3689	32.9914°	115.5167°	−130	250°	160°	Long.	18.7	25.0
							Vert.	18.6	24.8
							Trans.	19.0	24.9
Sam Etchegaray Livestock Co.	3692	32.9816°	115.4743°	−135	338°	248°	Long.	18.5	24.5
							Vert.	18.5	25.5
							Trans.	17.4	26.4
Doyle McDuffy home	3681	32.9133°	115.4920°	−132	334°	244°	Long.	19.7	24.2
							Vert.	18.2	25.7
							Trans.	17.5	26.3
Memory Gardens Cemetery	3693	32.8919°	115.5676°	−80	095°	005°	Long.	19.6	24.2
							Vert.	18.0	25.6
							Trans.	19.3	24.7
Sharon Fox home	3678	32.8437°	115.4996°	−100	357°	267°	Long.	18.1	26.1
							Vert.	19.4	25.6
							Trans.	18.3	25.8
University of California Field Station	3697	32.8044°	115.4467°	−55	000°	270°	Long.	18.9	24.9
							Vert.	19.4	25.2
							Trans.	17.6	26.0
McGrew Farm	3688	32.7769°	115.4448°	−25	356°	266°	Long.	19.5	24.3
							Vert.	17.6	25.8
							Trans.	17.0	27.2
Jasper Road	3695	32.7090°	115.4244°	15	180°	090°	Long.	18.1	26.3
							Vert.	18.7	25.3
							Trans.	19.3	25.2
Tuttle Ranch	3696	32.6940°	115.3745°	25	100°	010°	Long.	17.8	26.2
							Vert.	18.2	25.4
							Trans.	17.1	26.9

Station 3698 did not record any events between 4:16 p.m. P.d.t. October 16 and 1:33 p.m. the next day because the film jammed. The vertical component of the station 3692 instrument was knocked badly out of alinement on the trip to the Imperial Valley or during installation and, therefore, did not record any data. Stations 3688, 3693, 3695, and 3696 were not on battery chargers, and the batteries were drained when those instruments were recovered on November 2.

The largest aftershock recorded was an $M_L = 4.9$ event that occurred at 4:16 p.m. P.d.t. October 16; this aftershock triggered the eight northernmost accelerographs. The preliminary epicentral location is 7½ km north-northwest of station 3698, at a depth of 5 km. This event is characterized by strong relatively long period accelerations on the horizontal components of the three northernmost stations, and by high-frequency shaking on the vertical components. At stations 3689 and 3698, near-field effects are clearly visible on the horizontal components before the arrival of the *S* wave (fig. 298). These records may be useful for studies of wave propagation and attenuation along the fault zone.

Several accelerograms in figure 298 have been digitized on the automatic digitizer at the University of Southern California and integrated according to the accelerogram-processing techniques of Trifunac and Lee (1973). Figure 299 shows the results for the three northernmost stations. This processing is not optimal for all these records because long-period ringing from the filter may be present on some processed displacement traces, and nearfield permanent displacements are removed by the baseline correction. The peak accelerations on these digitized and processed records are smaller than those listed in table 49 for all stations, and for the vertical component at station 3689 the reduction is large—from 0.63 to 0.26*g*. This effect, which has been

noticed before (California Institute of Technology, 1976), results from sampling the data at too large a time interval to define the high-frequency peaks adequately. The solitary large peak on the station 3689 record (fig. 298) has a duration of 0.03 s between adjacent zero crossings and was sampled at 0.02-s intervals, and so it is not surprising that the digitized peak is greatly reduced.

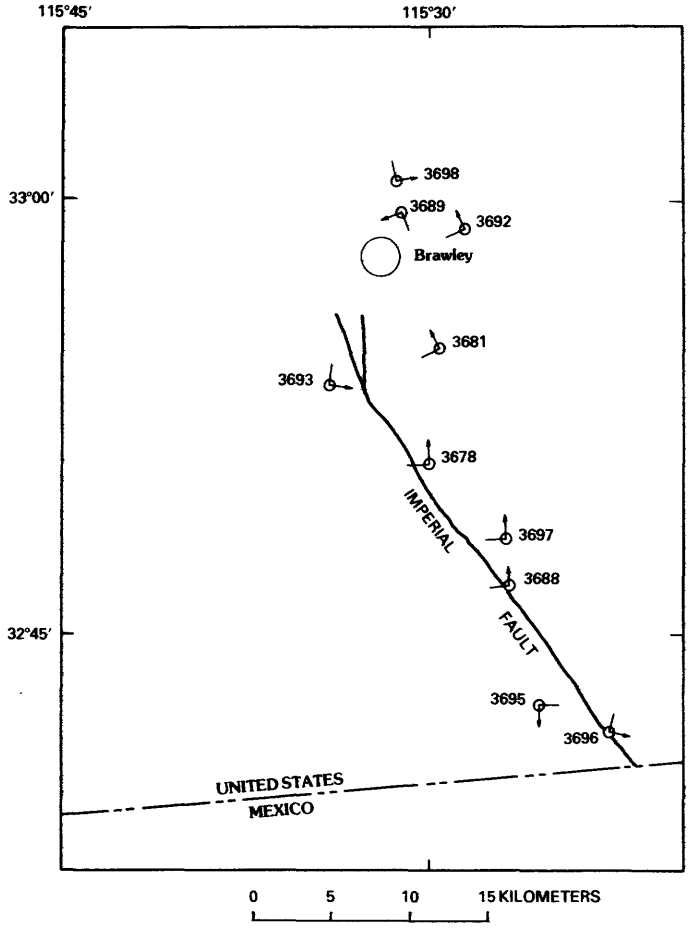

FIGURE 296.—Locations of temporary strong-motion accelerometer stations (see table 48). Arrows show direction of ground acceleration that causes positive amplitudes of recorded motion on longitudinal component of accelerometer; lines without arrows denote direction of positive motion on transverse component. Location of Imperial fault after Strand (1962).

Horizontal velocities and displacements on these records have relatively simple S-wave pulses that probably are dominantly controlled by the physics of the source for this particular aftershock.

ACKNOWLEDGMENTS

Several persons and institutions readily cooperated to help install the accelerographs quickly after the earthquake. These included A. Amini and B. Westermo of the University of Southern California, D. Helmberger of the California Institute of Technology, D. Halverson of Kinemetrics, Inc., and D. Hadley of Sierra Geophysics. Without their prompt response, this project would not have been possible. We also thank the following persons and institutes for allowing us to install an accelerograph on their property: Del Rio Country Club, Brawley Airport, Sam Etchegaray Livestock Co., the University of California Field Station, D. McDuffy, S. Fox, E. McGrew, and the California Institute of Technology. V. W. Lee, M. D. Trifunac, and M. Dravinski helped to digitize and process the accelerograms. The Los Angeles accelerograph network is supported by National Science Foundation Grant PFR 78–06926.

REFERENCES CITED

California Institute of Technology, 1976, Strong-motion earthquake accelerograms index volume: Pasadena, California Institute of Technology, Earthquake Engineering Research Laboratory Report EERL 76–02, 42 p.

Kinemetrics, Inc., 1977, Operating instructions for the time code generator, TCG–1: Pasadena, Calif., 14 p.

Strand, R. G., compiler, 1962, San Diego-El Centro sheet *of* Geologic map of California: California Division of Mines and Geology, scale 1:250,000.

Trifunac, M. D., and Lee, V. W., 1973, Routine computer processing of strong-motion accelerograms: Pasadena, California Institute of Technology, Earthquake Engineering Research Laboratory Report EERL 73–03, 360 p.

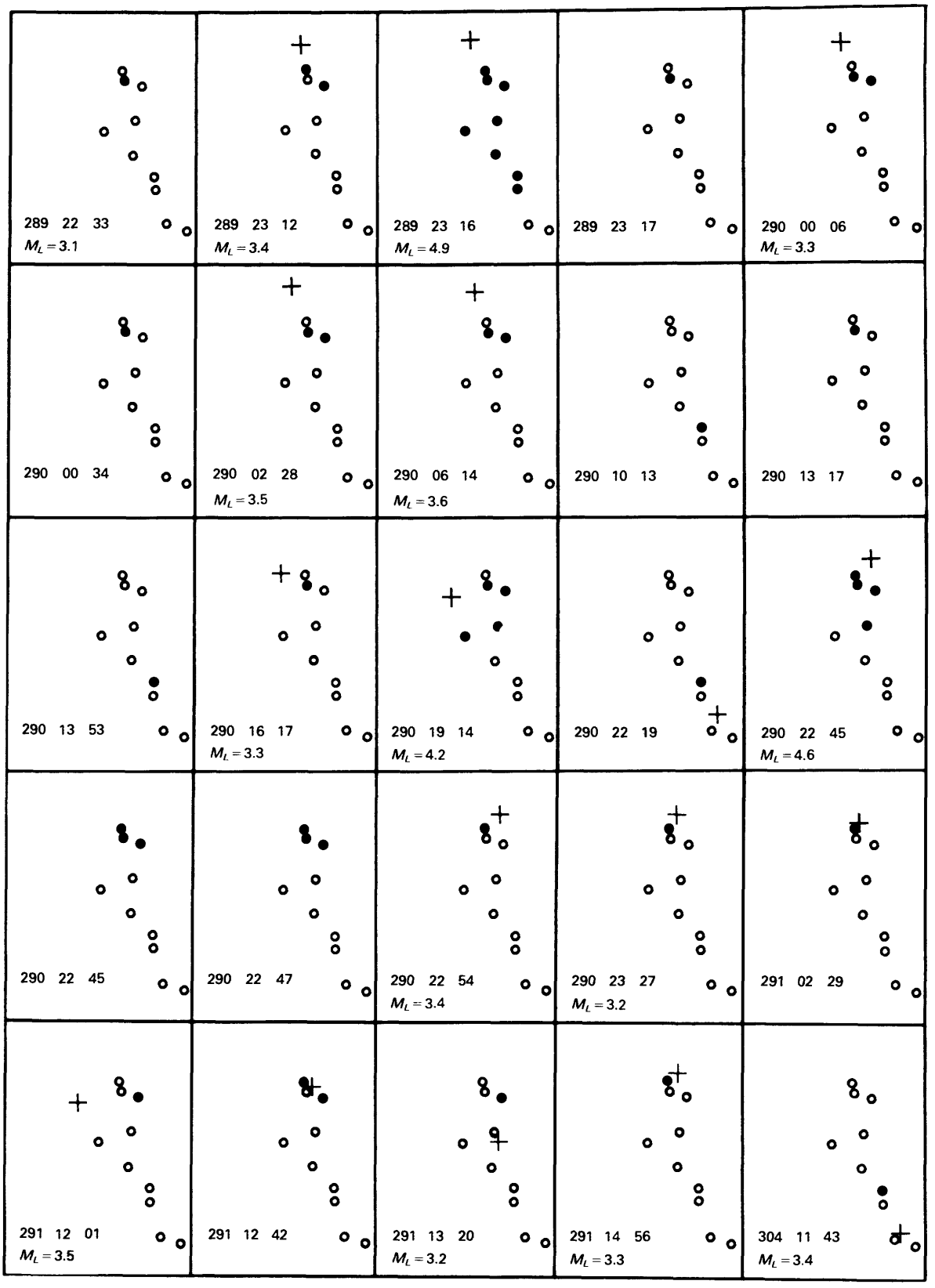

FIGURE 297.—Summary of strong-motion data recorded at temporary accelerometer stations (see table 49). Each frame is a simplified map representing one aftershock. Stations (see fig. 296 for locations) are shown as either circles (no record) or dots (record), and preliminary epicentral locations, where available, as crosses. Julian day, hour, and minute (G.m.t.) of aftershock is given in lower left corner, and preliminary local-magnitude estimates are given for events of $M_L \geq 3$.

TABLE 49.—*Summary of aftershock accelerograms*

[Time of event is Julian day (Jan 1=1, Oct. 15=289) and Greenwich mean (G.m.t.); for Pacific time, subtract 8 hours (P.s.t.) or 7 hours (P.d.t.). Locations were determined without use of *S*-wave arrival times listed for these accelerometers. Depth measurements are particularly unreliable (C. E. Johnson, oral commun., 1979). See table 48 for azimuthal directions of horizontal components of peak accelerations]

Event					Location (lat, long)	Depth (km)	Magnitude	Station	Preliminary epicentral distance (km)	Peak accelerations (*g*)		
Day	Hr	Min	Second							Longitudinal	Vertical	Transverse
			Trigger	*S* arrival								
289	22	33	59.53	61.50	----	----	3.1	3689	----	0.02	0.03	0.02
289	23	12	38.36	39.19	33°4.32′ N.,	1.8	3.4	3698	7.0	.05	.03	.02
			38.46	40.75	115°31.94′ W.			3692	11.5	.03	----	.06
289	23	16	33.16	34.46	33°4.48′ N.,	5.0	4.9	3698	7.8	.30	.26	.16
			34.21	34.94	115°33.26′ W.			3689	10.0	.29	.63	.22
			33.71	36.22				3692	12.8	.41	----	.29
			35.68	38.14				3681	19.0	.06	.04	.05
			36.07	39.32				3693	20.3	.10	.03	.12
			36.92	40.63				3678	26.0	.09	.04	.07
			40.84	42.47				3697	32.0	.08	.01	.05
			44.74	(1)				3688	35.0	.04	.02	.02
289	23	17	29.81	31.49	----	----	----	3689	----	.09	.05	.02
290	00	06	23.70	25.44	33°3.80′ N.,	6.3	3.3	3689	8.8	.04	.06	.03
			24.26	26.56	115°32.75′ W.			3692	11.3	.07	----	.09
290	00	34	6.41	8.46	----	----	----	3689	----	.02	.04	.02
290	02	28	20.44	22.24	33°4.77′ N.,	5.0	3.5	3689	10.3	.05	.07	.08
			20.92	23.35	115°33.16′ W.			3692	13.0	.05	----	.03
290	06	14	3.87	5.60	33°4.31′ N.,	5.6	3.6	3689	9.8	.06	.05	.05
			4.31	6.61	115°33.04′ W.			3692	12.8	.08	----	.07
290	10	13	19.27	12.37	----	----	----	3697	----	.11	.06	.11
290	13	17	20.56	22.68	----	----	----	3689	----	.03	.01	.02
290	13	53	47.31	50.04	----	----	----	3697	----	.02	.02	.02
290	16	17	39.02	41.07	33°1.13′ N.,	6.2	3.3	3689	5.8	.02	.01	.02
					115°34.26′ W.							
290	19	14	41.41	44.08	33°58.32′ N.,	4.7	4.2	3689	8.5	.10	.02	.05
			41.62	44.91	115°36.36′ W.			3692	12.5	.05	----	.05
			40.91	43.65				3681	12.5	.06	.05	.06
			40.09	42.03				3693	9.8	.25	.08	.39
290	22	19	47.60	50.67	32°44.47′ N.,	17.8	----	3697	7.5	.02	.02	.02
					115°24.83′ W.							
290	22	45	35.14	36.37	33°2.73′ N.,	3.9	4.6	3698	5.0	.11	.15	.09
			35.41	37.18	115°29.40′ W.			3689	6.8	.21	.22	.13
			35.66	38.06				3692	7.3	.16	----	.18
			39.71	40.41				3681	14.8	.03	.02	.03
290	22	45	56.44	57.60	----	----	----	3698	----	.05	.03	.05
			56.46	58.22				3689	----	.12	.15	.10
			57.03	59.23				3692	----	.10	----	.09
290	22	47	7.86	9.16	----	----	----	3698	----	.03	.04	.03
			8.50	9.95				3689	----	.05	.04	.04
			8.88	10.66				3692	----	.04	----	.05
290	22	54	21.80	23.13	33°2.58′ N.,	4.8	3.4	3698	4.5	.01	.02	.02
					115°29.39′ W.							
290	23	27	32.82	33.80	33°2.52′ N.,	7.1	3.2	3698	4.0	.03	.02	.02
					115°30.19′ W.							
291	02	29	14.45	15.72	33°1.21′ N.,	5.0	----	3698	1.3	.04	.04	.04
					115°31.08′ W.							
291	12	01	15.17	16.33	32°58.25′ N.,	15.3	3.5	3692	13.5	.02	----	.01
					115°36.99′ W.							
291	12	42	24.78	25.90	33°0.40′ N.,	5.1	----	3698	2.5	.02	.03	.01
			25.22	27.34	115°29.75′ W.			3692	3.5	.09	----	.13
291	13	20	29.81	32.89	32°54.17′ N.,	5.0	3.2	3692	9.0	.02	----	.02
					115°29.48′ W.							
291	14	56	21.04	22.37	33°2.19′ N.,	5.1	3.3	3698	4.3	.03	.03	.03
					115°29.59′ W.							
304	11	43	49.66	52.78	32°43.35′ N.,	17.4	3.4	3697	9.5	.03	.04	.06
					115°24.80′ W.							
For the following events, the clocks did not work properly:												
291	02	29?	----	----	----	----	----	3689	----	.09	.04	.05
or	12	01?										
291	12	42?	----	----	----	----	----	3689	----	.09	.05	.07
291	13	20?	----	----	----	----	----	3689	----	.03	.03	.02
or	14	56?										
		?	----	----	----	----	----	3678	----	.04	.02	.04
		?	----	----	----	----	----	3678	----	.03	.03	.04

[1]Triggered during *S*-wave arrival.

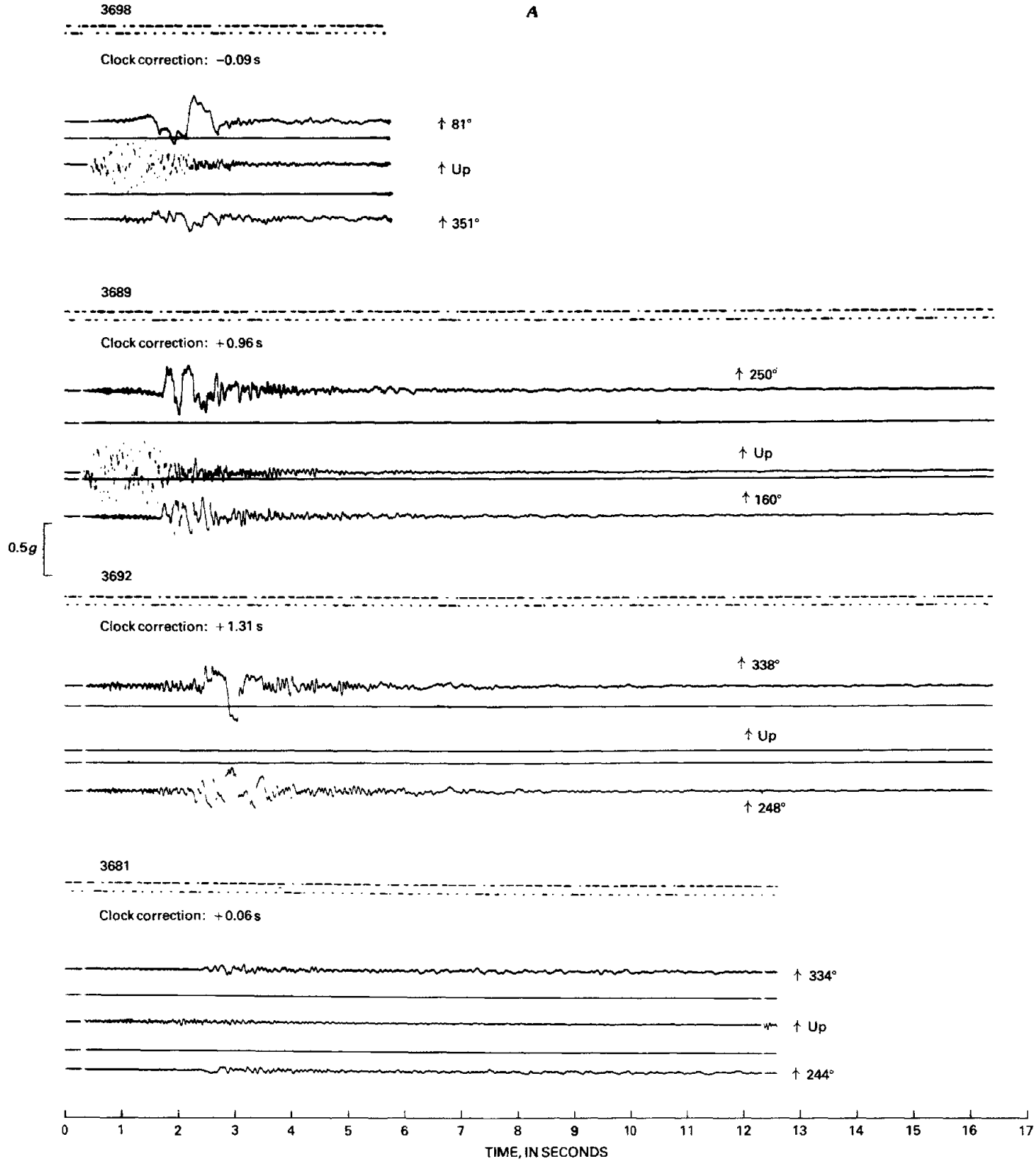

FIGURE 298.—Original accelerograms from M_L=4.9 aftershock of October 16, 1979. Records are shown from north (top) to south (bottom) in order of increasing epicentral distance. Time trace at tip of each record gives a code with 5 (downward) pulses per second; code is interpreted as in Kinemetrics, Inc. (1977). Clock corrections at time of aftershock are also shown. Numbers to right on each trace indicate longitudinal, vertical, and transverse azimuths from top to bottom, respectively. *A*, Northern four records. *B*, Southern four records.

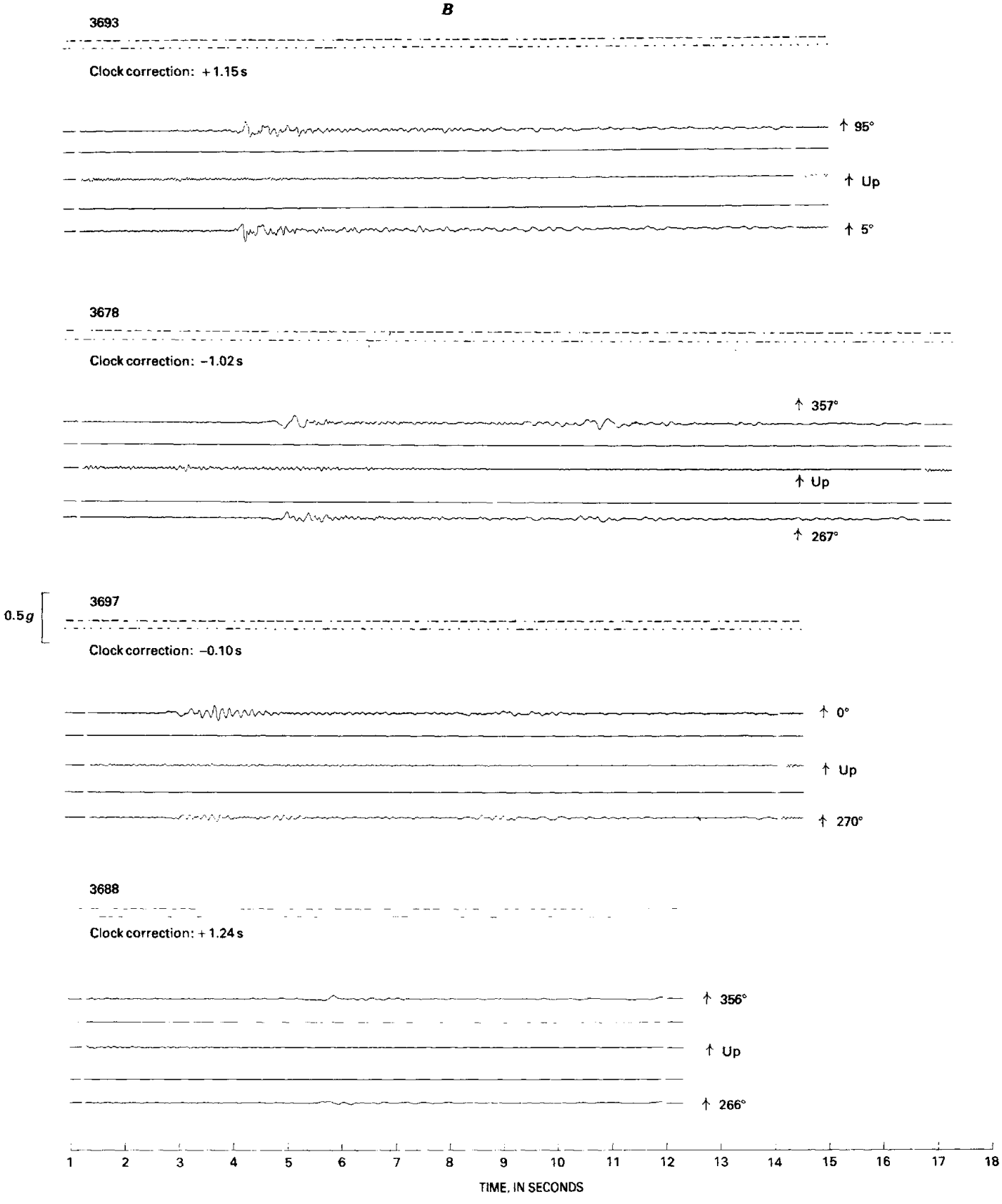

FIGURE 298.—Continued

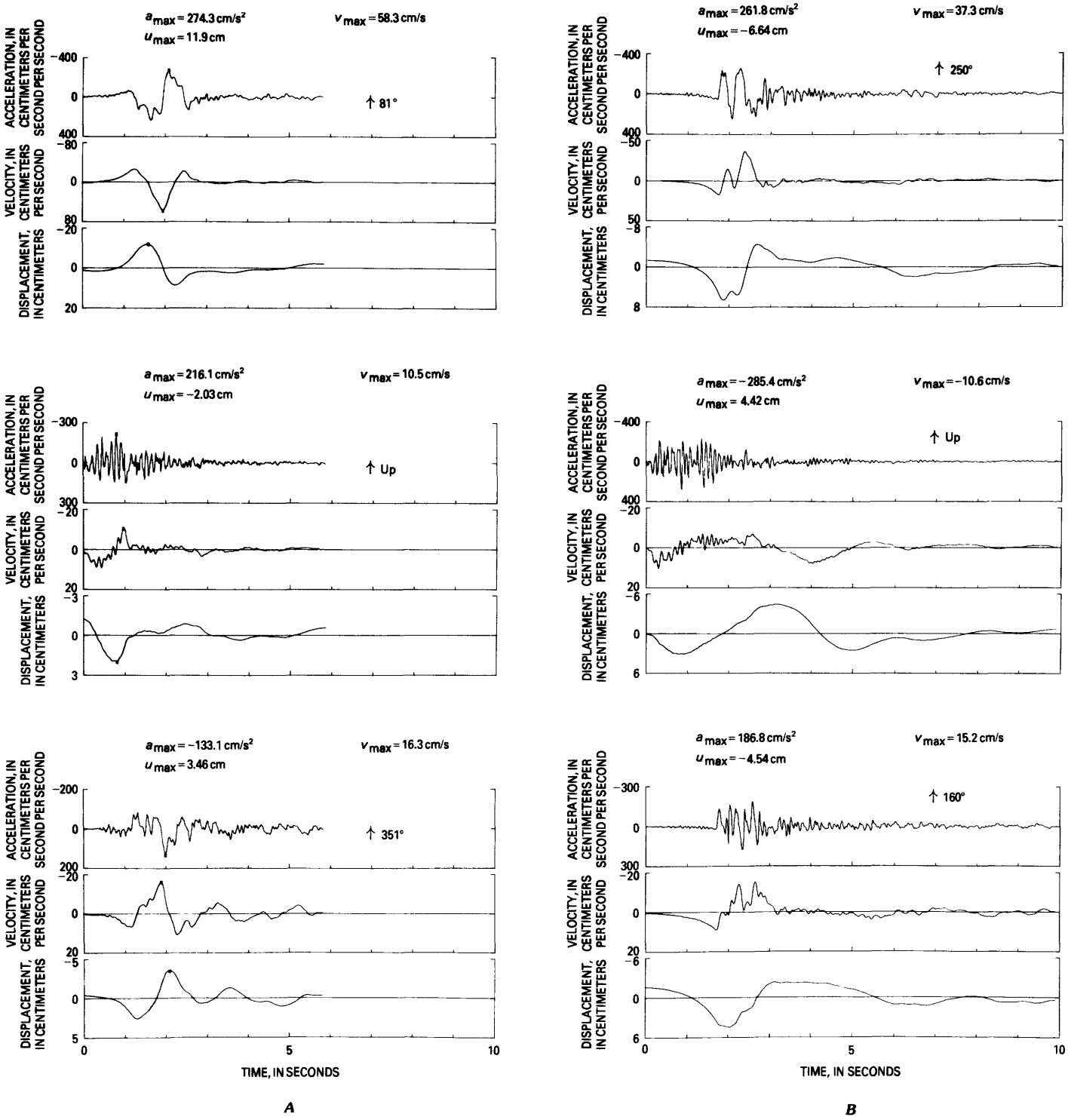

FIGURE 299.—Digitized, baseline-corrected, and integrated accelerograms from three stations closest to epicenter of M_L=4.9 aftershock of October 16, 1979: 3698 (*A*), 3689 (*B*), and 3692 (*C*). Only first 10 s of digitized record is shown; numbers to right on each graph indicate longitudinal, vertical, and transverse azimuths from top to bottom, respectively. a_{max}, maximum acceleration; u_{max}, maximum displacement; v_{max}, maximum velocity.

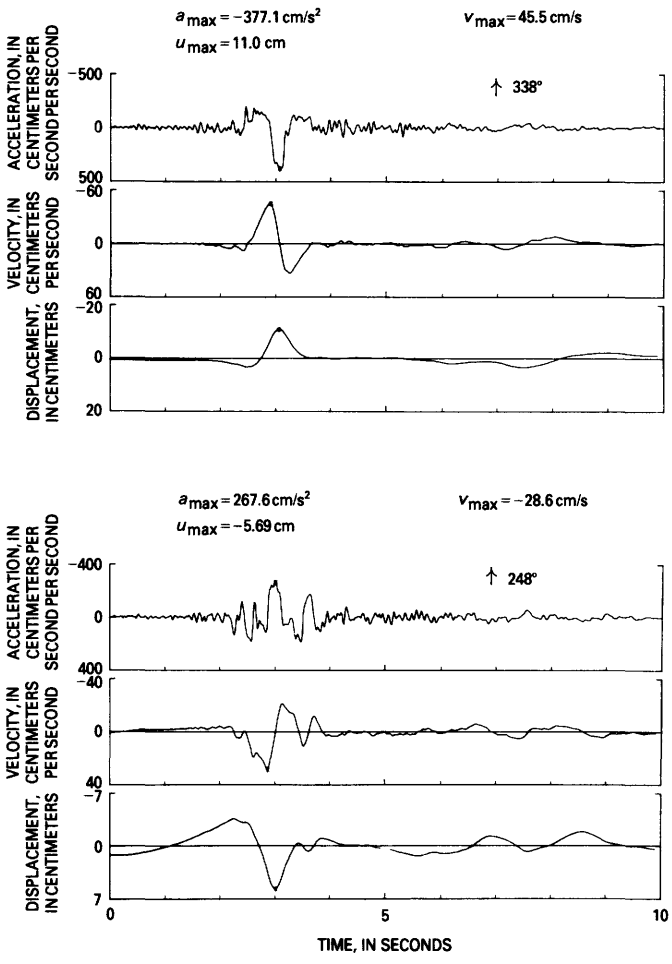

C

FIGURE 299.—Continued